

P N76-71920

# Sonic and Vibration Environments for Ground Facilities.....

## ... a Design Manual

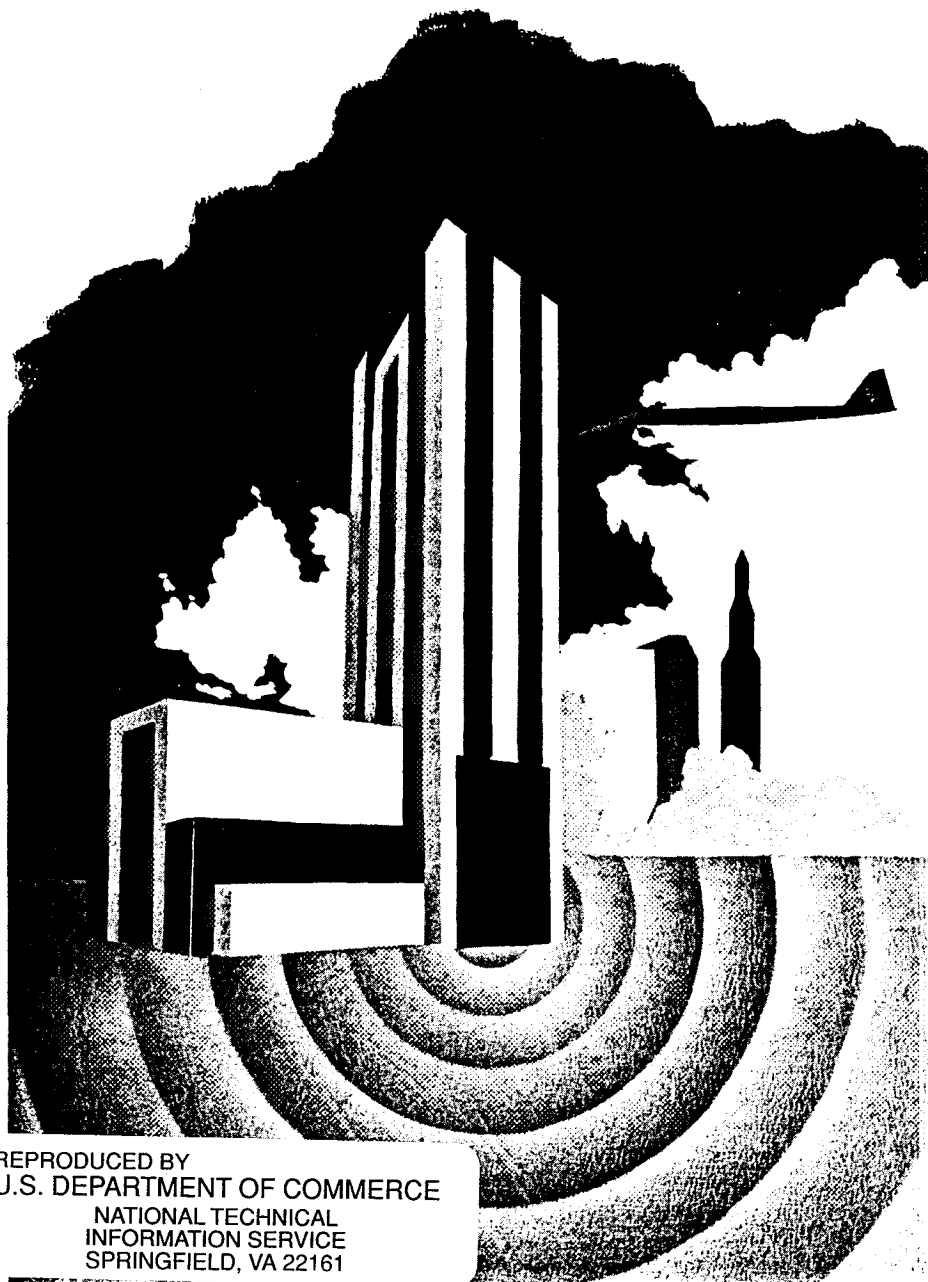


NATIONAL AERONAUTICS  
AND SPACE ADMINISTRATION

PREPARED FOR

GEORGE C. MARSHALL  
SPACE FLIGHT CENTER  
HUNTSVILLE, ALABAMA

NAS8-11217



**WYLE LABORATORIES**

REPRODUCED BY  
U.S. DEPARTMENT OF COMMERCE  
NATIONAL TECHNICAL  
INFORMATION SERVICE  
SPRINGFIELD, VA 22161

WYLE LABORATORIES - RESEARCH STAFF  
REPORT NUMBER WR 68-2

SONIC AND VIBRATION  
ENVIRONMENTS FOR GROUND  
FACILITIES - A DESIGN MANUAL

By

Wyle Laboratories Research Staff

Submitted Under NASA Contract NAS8-11217

Editor and Principal Author - L. C. Sutherland

Date: March 1968

COPY NO: \_\_\_\_\_

**WYLE LABORATORIES**  
RESEARCH STAFF  
Huntsville Facility Huntsville, Alabama



## TABLE OF CONTENTS

	Chapter
INTRODUCTION	1
TERMINOLOGY	2
FUNDAMENTALS OF VIBRATION	3
FUNDAMENTALS OF ACOUSTICS	4
SONIC AND VIBRATION CONTROL PLANNING	5
SOURCE CHARACTERISTICS	6
PROPAGATION OF SONIC PRESSURE WAVES AND GROUND VIBRATION	7
ACOUSTIC AND BLAST LOADS ON BUILDINGS	8
ARCHITECTURAL ACOUSTICS AND VIBRATION CONTROL FOR GROUND FACILITIES	9
EFFECTS OF NOISE, VIBRATION AND BLAST ON PERSONNEL	10
VIBRO-ACOUSTIC CONTROL FOR EQUIPMENT	11
CONVERSION TABLES AND MATERIAL PROPERTIES	12

## CHAPTER 1

### INTRODUCTION

This manual provides a comprehensive engineering guide for the evaluation of acoustic, vibration and blast environments in the design and siting of ground facilities for the launch and testing of rocket vehicles. The manual also includes related material covering dynamic loads due to sonic booms.

Since the advent of rocket vehicle testing and development, facility designers have been faced with a new set of design problems created by the intense acoustic noise from rocket exhausts and the potential blast hazards associated with an accidental explosion of rocket propellants. These problems cover a broad area ranging from

- A requirement for structural design concepts to withstand intense acoustic or potential propellant blast loads to
- Detailed studies of land purchase requirements to insure that unacceptable noise or blast environments are not imposed on adjacent communities.

The design or evaluation effort required for the solution of these problems has generally increased as rocket boosters with increasingly greater thrust have been developed. As illustrated in Figure 1.1, the trend in thrust of existing and proposed rocket boosters points to a further increase in the severity of these facility design problems over the next 15 years. Lead time required for their solution will also tend to increase. Thus, the objective of this manual has been to place within one cover, a comprehensive design guide for the benefit of planners, architects, building and equipment designers, and engineering specialist who must solve these problems in the future.

The existing facilities now in use at rocket testing and launch sites have been operated successfully for many years. However, the real impact of frequent exposure of ground facility complexes to routine launches from boosters in the thrust range of the Apollo/Saturn V system, for example, has yet to be experienced. As indicated in Figure 1.2, this type of routine exposure may eventually reach launch rates which exceed current rates of full scale ground testing.

The specific type of design problems encountered due to the dynamic environments created by large rocket boosters will frequently call for special construction techniques and unique design specifications. Such special design requirements are not readily solved by routine or standard methods. As a result, any attempt to establish standard building design concepts for the type of dynamic loads involved, along with realistic cost estimates, would be impractical.

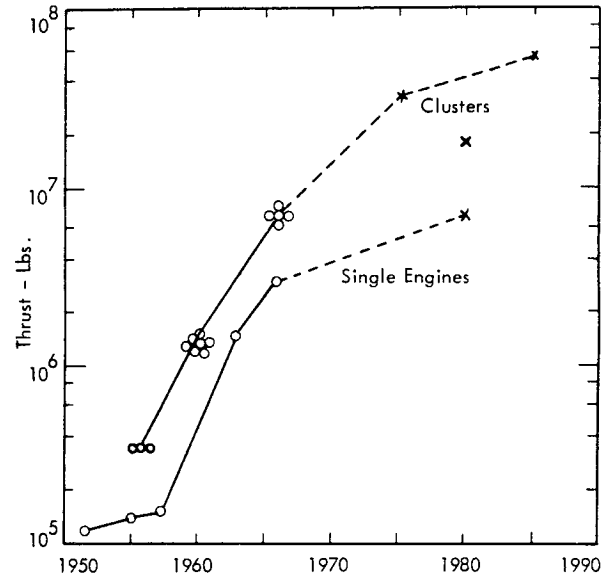


FIGURE 1.1 Trend in Thrust of Booster Engines

Rather, the objective has been to provide the basic background data, theory or empirical procedures upon which specific design studies can be based.

To imply that this manual is only usable for engineering design of major rocket testing facilities would detract from the potential value of much of the basic engineering data, design criteria, and analytical background presented. It is felt, therefore, that the manual may have value for lesser, and often just as important, sonic and vibration problems faced by the engineering specialist or designer. The design of test facilities for any relatively small sources of sonic or vibration loads can, if not properly handled, be just as much a problem as for the larger and more obvious sources.

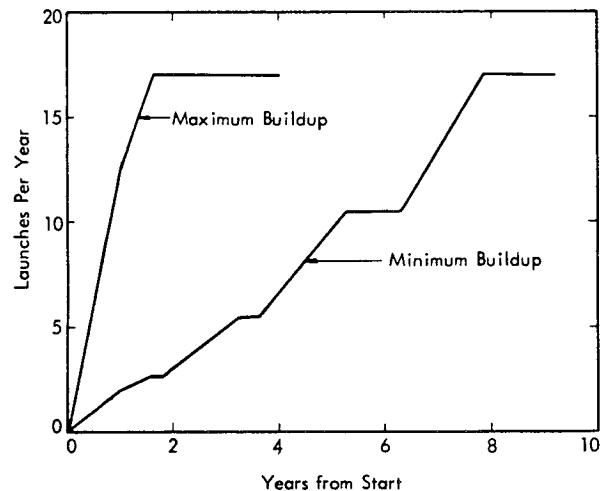


FIGURE 1.2 Projected Apollo/Saturn V Launch Rate for Lunar Exploration

### Organization of the Manual

The major chapters of the manual may be grouped into four basic areas:

- Fundamentals
  - Terminology - Chapter 2
  - Vibration - Chapter 3
  - Acoustics - Chapter 4
- System Concepts and Criteria - Chapter 5
- Source-Transmission-Receiver
  - Source Definition - Chapter 6
  - Propagation - Chapter 7
  - Loads on Buildings - Chapter 8
- Detailed Effects on Receivers
  - Internal Environmental Control - Chapter 9
  - Effects on Personnel - Chapter 10
  - Effects on Equipment - Chapter 11

A set of conversion charts for units and a comprehensive set of data on dynamic, static, and acoustic properties of building materials is presented in Chapter 12.

The organization outlined above has been selected for maximum convenience of the reader who is concerned with a particular facet of the wide variety of problems encountered.

It would be impossible to present under one cover full details covering all of the problems encountered in this manual. However, every effort has been made to adjust the depth of coverage according to the degree of relative importance for each of the areas considered. Without the benefit of the published books, reports, and articles in this field, the material presented in this manual could never have been compiled. It is hoped that the reader will find the contents useful or may be guided by the references to further details which could not be included.

**CHAPTER 1**  
**INTRODUCTION**

**CHAPTER 2**  
**TERMINOLOGY**

## CHAPTER 2

### TERMINOLOGY

Definitions of terms which are used frequently in this manual are assembled here. Many of these definitions are selected from the American Standard Terminology, (Z24, 1-1951) and Technical Documentary Report "Study of Liquid Propellant Blast Hazards" Number AFRPL-TR-65-144 with modifications as necessary for the sake of brevity or for consistency with the usage employed in this manual.

#### ABSORPTION COEFFICIENT (ACOUSTICAL ABSORPTIVITY), $\alpha$

The ratio of the sound energy absorbed by a surface to the sound energy incident upon the surface. The absorption coefficient is a function of both angle of incidence and frequency. The values normally given in tables of absorption coefficients, such as in Chapter 12, are obtained by averaging over all angles of incidence.

#### ACOUSTIC IMPEDANCE

The ratio of the sound pressure on a surface to the flux (volume velocity, or linear velocity multiplied by the area) through the surface. The acoustic impedance may be expressed in terms of mechanical impedance divided by the square of the area of the surface considered. Acoustic Impedance is a complex quantity. The real component is called Acoustic Resistance. The imaginary component is Acoustic Reactance.

#### ACOUSTIC MOBILITY

The ratio of acceleration of a structure under acoustic excitation to the acoustic driving pressure over the same frequency band, expressed in g's/psi. Also expressed in logarithm form as 10 times the log to the base 10 of the square of the ratio of acceleration to sound pressure in dB re: g per psi.

#### ACOUSTIC REFRACTION

The process by which the direction of sound propagation is changed because of spatial variation of the wave velocity in the medium.

#### ACOUSTIC SCATTERING

The irregular and diffuse reflection, refraction, or diffraction of a sound in many directions.

#### AMBIENT NOISE

The residual noise associated with a given environment.

#### ANGULAR FREQUENCY, $\omega$

Frequency in radians per unit time, usually radians per second. Circular frequency multiplied by  $2\pi$ .

#### ANTINODES

A point, line, or surface in a vibrating body at which the amplitude of motion, relative to that at a node, is a maximum.

#### ANTIRESONANCE

The opposite of resonance. (See definition for resonance)

#### ARCHING EFFECT OF SOIL

The transfer of pressure from a yielding mass of soil onto adjoining stationary parts.

#### AUTOCORRELATION FUNCTION

The mean-square value,  $R(\tau)$  of the product  $x(t) \cdot x(t - \tau)$ , where  $x(t)$  is a time-varying quantity,  $t$  is time, and  $\tau$  is an elapsed time quantity.

#### BAND PRESSURE LEVEL

The effective sound pressure level for the sound energy contained within a band of frequencies. The width of the band and the reference pressure must be specified. The width of the band may be indicated by the use of a qualifying adjective: e.g., octave-band (sound pressure) level, third-octave band level, etc. For random noise, the standard deviation of the band pressure level will not exceed 1 dB if the product of the bandwidth in cycles per second by the integration time in seconds exceeds 20.

#### BLAST SCALING LAWS

Scaling laws formulated from the general laws of similitude relating blast and environmental parameters. The most common blast scaling laws (termed "cube root scaling") relate blast wave parameters (e.g., blast pressure  $P$ , positive-phase impulse  $I$ , and positive-phase duration  $t^+$ ) to distance from an explosion  $d$ , and explosion weight  $W$ , as follows:

$$P = f(d/W^{1/3}) = f(\lambda)$$
$$I/W^{1/3} = h(d/W^{1/3}) = h(\lambda)$$
$$t^+/W^{1/3} = g(d/W^{1/3}) = g(\lambda)$$

The quantities  $d/W^{1/3}$  and  $t^+/W^{1/3}$  are commonly referred to as scaled distance and scaled duration, respectively.

#### BLAST WAVE

A pressure pulse (or wave) in air, propagated continuously from an explosion characterized by an initial rapid rise of pressure above ambient values (see Shock Wave).

#### BOUNDARY LAYER

The layer of fluid on a body where the velocity rises rapidly from zero to the free stream value.

#### CHARACTERISTIC IMPEDANCE

The ratio of the effective sound pressure at a given point to the effective particle velocity at that point in a free plane progressive sound wave. The characteristic impedance is equal to the product of the density by the speed of sound in the medium, i.e.,  $(\rho c)$ .

#### COMPLETE-REVERSAL LOAD

Loading applied in a cyclic manner with equal absolute magnitudes of maximum and minimum load.

#### COMPLIANCE

The reciprocal of stiffness.

**COMPOSITE NOISE RATING, CNR**

A numerical subjective scale of noise which takes account of factors that influence community reaction.

**COMPRESSIONAL WAVE**

A wave in an elastic medium which causes an element of the medium to change its volume without undergoing rotation.

**COULOMB DAMPING (DRY FRICTION DAMPING)**

The dissipation of energy that occurs when a particle in a vibrating system is resisted by a force whose magnitude is a constant independent of displacement and velocity, and whose direction is opposite to the direction of the velocity of the particle.

**COUPLED MODES**

Modes of vibration which mutually influence one another because of energy transfer from one mode to the other.

**COVER DEPTH**

Depth of earth fill which covers a structure.

**CRITICAL DAMPING**

The minimum viscous damping that will allow a displaced system to return to its initial position without oscillation.

**CRITICAL SPEED**

The rotating speed of a system which corresponds to a resonant frequency of the system.

**CROSS CORRELATION FUNCTION**

The mean-square value of the product  $x(t) \cdot y(t - \tau)$ , where  $t$  is time,  $\tau$  is an elapsed time quantity,  $x(t)$  and  $y(t)$  are two randomly varying quantities.

**CYLINDRICAL WAVE**

A wave in which the wave fronts are coaxial cylinders.

**DAMAGE-RISK CRITERION**

The maximum sound pressure levels of a noise, as a function of frequency, to which people should be exposed if risk of hearing loss is to be avoided. This criterion includes a specification of the time of exposure, amount of hearing loss considered significant, and the percentage of the population to be protected.

**DAMPING RATIO (CRITICAL DAMPING RATIO)**

For a system with viscous damping, the ratio of actual damping coefficient to the critical damping coefficient.

**DECIBEL, dB**

A unit of level which denotes the ratio between two quantities that are proportional to power; the number of decibels corresponding to the ratio of two amounts of power is 10 times the logarithm to the base 10 of this ratio. In many sound fields, the sound-pressure ratios are not proportional to the square root of the corresponding power ratios, so that strictly speaking the term decibel should not be used in such cases; however, it is common practice to extend the use of the unit to these cases (see, for example, Sound Pressure Level).

**DEGREES OF FREEDOM**

The minimum number of independent coordinates required to define completely the position of a system at any given instant.

**DIRECTIVITY FACTOR**

The ratio of the sound pressure squared, at some fixed distance and specified direction, to the mean-square sound pressure at the same distance averaged over all directions from a sound source. The distance must be great enough so that the sound appears to diverge spherically from the effective acoustic center of the sources.

**DIRECTIVITY INDEX**

Ten times the logarithm to the base 10 of the directivity factor.

**DIFFRACTED WAVE**

A wave whose front has been changed in direction by an obstacle or other nonhomogeneity in a medium, other than by reflection or refraction.

**DIFFUSE SOUND FIELD (RANDOM-INCIDENCE SOUND FIELD)**

A sound field such that the sound pressure level is everywhere the same, and all directions of energy flux are equally probable.

**DURATION OF POSITIVE PHASE**

The time duration of the positive portion of a blast wave at a fixed point.

**EFFECTIVE DURATION OF SHOCK**

The time duration, in seconds, corresponding to a triangular pressure-time representation having the same positive impulse as the actual blast shock.

**EFFECTIVE SOUND PRESSURE (ROOT-MEAN-SQUARE SOUND PRESSURE),  $p$** 

The root-mean-square value of the instantaneous sound pressures, over a time interval at a point under consideration. The interval must be long enough to make the value obtained essentially independent of small changes in the length of the interval. The term "effective sound pressure" is frequently shortened to "sound pressure."

**ENDURANCE LIMIT**

The maximum value of the stress that may be repeated an indefinite number of times without causing failure.

**EXPLOSIVE YIELD (EQUIVALENT TNT YIELD)**

The amount of TNT which if put at the position of the propellant explosion would produce the same value of a particular shock wave parameter at the same distance as for the propellant explosion.

**EQUIVALENT VISCOUS DAMPING**

A value of viscous damping assumed for the purpose of analysis of a vibratory motion, such that the dissipation of energy per cycle at resonance is the same for either the assumed or actual damping force.

**FAR FIELD**

The part of a sound or blast field where the pressure waves propagate like plane waves and it can be assumed that all the energy originates at a point.

**FORCED OSCILLATION (FORCED VIBRATION)**

The oscillation of a system is forced if the response is imposed by the excitation. If the excitation is periodic, the oscillation is steady-state.

**FREE FIELD GROUND MOTION**

Ground motion in a homogeneous soil medium.

**FREE OSCILLATION (FREE VIBRATION)**

The oscillation of some physical quantity of a system when there are no externally applied driving forces.

**FREE PROGRESSIVE WAVE (FREE WAVE)**

A wave in a medium free from boundary effects.

**FREQUENCY**

The reciprocal of the period of a periodic function. The unit is the cycle per second or Hertz (Hz).

**FUNDAMENTAL FREQUENCY**

The reciprocal of the shortest period during which a periodic quantity exactly reproduces itself.

**FUNDAMENTAL MODE OF VIBRATION**

The mode of vibration of a system having the lowest frequency.

**GAUSSIAN DISTRIBUTION (OR NORMAL DISTRIBUTION)**

The first-order probability distribution of a normal or Gaussian process described by the following probability density function

$$p(x) = \frac{1}{\sqrt{2\pi}\sigma} \exp\left[-(x-m)^2/2\sigma^2\right]$$

where  $m$  is the mean and  $\sigma$  is the standard deviation of the distribution.

**HEIGHT OF BURST**

The height above the earth's surface at which an explosive charge is detonated in the air.

**HYSTERESIS DAMPING (OR STRUCTURAL DAMPING)**

The dissipation of energy under cyclic deformation of a material. The amount of energy dissipation is proportional to the stress-strain hysteresis loop for the material.

**IMPEDANCE**

An impedance is the complex ratio of a force-like quantity (force, pressure, voltage) to a related velocity-like quantity (velocity, volume velocity, or current).

**IMPULSE (PER UNIT AREA)**

The integral, with respect to time, of the overpressure in a blast wave at a given point.

**INFRASONIC FREQUENCY (SUBAUDIBLE FREQUENCY)**

A frequency lying below the audio-frequency range.

**INTENSITY LEVEL (SOUND-ENERGY FLUX-DENSITY LEVEL)**

Ten times the logarithm to the base 10 of the ratio of the intensity of a sound to the reference intensity. A commonly used reference is  $10^{-16}$  watt per square centimeters in a specified direction.

**LATERAL STRESS COEFFICIENT**

The ratio of lateral (horizontal) to vertical stresses.

**LOAD FACTOR,  $K_L$** 

The factor by which the total load applied on a structural element is multiplied to obtain the equivalent concentrated load for the equivalent single-degree-of-freedom system.

**LOAD-MASS FACTOR,  $K_{LM}$** 

A factor which is formed by combining the load factor and the mass factor, namely

$$K_{LM} = K_M/K_L$$

**LOUDNESS**

The subject measure of sound intensity. Loudness depends primarily upon the sound pressure of the stimulus but it also depends upon the frequency and waveform of the stimulus.

**LOUDNESS LEVEL**

The level, in phons, of a sound numerically equal to the sound pressure level in decibels, relative to 0.0002 microbar, of a pure tone of frequency 1,000 Hz., consisting of a plane progressive sound wave coming from directly in front of the observer, which is judged by observers to be equivalent in loudness.

**MACH REGION**

The region on the ground at which a Mach stem has formed as the result of an explosion in air.

**MACH STEM (MACH FRONT)**

The shock front formed by the fusion of the incident and reflected shock fronts from an explosion.

**MASS FACTOR,  $K_M$** 

The factor by which the total distributed mass of an element is multiplied to obtain the equivalent lumped mass of the equivalent single-degree-of-freedom system.

**MATERIAL DAMPING**

The process of energy dissipation in a material under dynamic stress.

**MECHANICAL IMPEDANCE**

The complex ratio of force to velocity during simple harmonic motion. The real part is called mechanical resistance; the imaginary part is called mechanical reactance. If acceleration or displacement is used in lieu of velocity, the impedance is called acceleration or displacement impedance. The corresponding real parts become the dynamic mass or stiffness, respectively.

**MICROBAR ( $\mu$  BAR)**

A unit of pressure equal to one dyne per square centimeter.



**MODAL NUMBER**

In general, a vibratory system can be analyzed in terms of its normal modes. The modes may be arranged in a discrete sequence associated with a set of ordered integers which are called modal numbers.

**MODAL SHAPE**

One of the characteristic shapes of a vibrating body or system. It corresponds to a normal mode of vibration.

**MODULUS OF RUPTURE**

The stress computed by the bending stress formula  $Mc/I$ , when  $M$  is the maximum bending moment in a beam loaded to rupture.

**NATURAL FREQUENCY,  $f_n$** 

The frequency of free oscillation of a system. In a damped system, the natural frequency is a quasi-frequency in that the motion is not periodic but is generally taken as the frequency at which the velocity reverses sign. For a multi-degree-of-freedom system, the natural frequencies are the frequencies of vibration in normal modes.

**NEAR FIELD**

That part of a sound or blast field in the immediate vicinity of the source where its relative dimensions cannot be considered to approximate a point.

**NEPERS**

A natural logarithmic unit corresponding to a reduction in amplitude to  $1/e$  of the initial or reference value.

**NODES**

The points, lines, or surfaces in a standing-wave system where some characteristic of the wave field has essentially zero amplitude.

**NOISE REDUCTION**

The sound pressure level outside an area minus the sound pressure level inside the area, both being measured over the same frequency band.

**NORMAL MODE OF VIBRATION**

In an undamped multi-degree-of-freedom system, the pattern of motion assumed by the system in which the motion of every particle is simple harmonic with the same period and phase. Vibration in a normal mode thus occurs at a natural frequency of the system. In general, any composite motion of a system is analyzable into a summation of normal modes. (The terms natural mode, characteristic mode, and eigen mode are synonymous with normal mode).

**NOYS**

The unit of perceived noisiness.

**OCTAVE**

The interval between two frequencies having a ratio of two.

**ONE-THIRD OCTAVE**

The interval between two frequencies having a ratio of the cube root of two.

**OVERPRESSURE**

The transient pressure in excess of the atmospheric pressure.

**PARTICIPATION FACTOR**

The fractional contribution of a normal mode of a beam or plate to the maximum static stress due to a uniform static pressure load.

**PEAK-TO-PEAK VALUE**

The algebraic difference between the extremes of an oscillating quantity.

**PERCEIVED NOISE LEVEL, PNL**

A rating of a given noise expressed in PNdB which is equal to the sound pressure level, in dB, of an octave band of white noise centered at a frequency of 1,000 Hz. which is judged to be equally noisy.

**PRECIEVED NOISE LEVEL, PNL**

A rating of a given noise expressed in PNdB which is equal to the sound pressure level, in dB, re: 0.002  $\mu$ bar of an octave band of white noise centered at a frequency of 1,000 Hz which is judged to be equally noisy.

**PHON**

The unit of loudness level.

**PLANE WAVE**

A wave in which the wave fronts are parallel planes normal to the direction of propagation.

**POWER SPECTRUM LEVEL**

The power level for the acoustic power contained in a band 1 Hz. wide, centered at a specified frequency.

**PRESBYCUSIS**

The normal loss of hearing associated with increasing age.

**PRESSURE SPECTRUM LEVEL**

The effective sound pressure level for the sound energy contained within a band 1 Hz. wide, centered at a specified frequency.

**PURE TONE**

A sound wave, the instantaneous sound pressure of which is a simple sinusoidal function of time.

**RANDOM NOISE (RANDOM FUNCTION)**

A fluctuating quantity (such as sound pressure) whose instantaneous amplitude is, as a function of time, not known, but its mean is predictable.

**RAYLEIGH DISTRIBUTION**

The probability distribution of the peaks of a narrow band of random Gaussian noise.

**REFLECTED PRESSURE**

The total pressure at the instant when the front of a blast wave in air strikes the surface of an object or structure.

**RESIDUAL MOTION**

Residual motion is the free vibration of a system after the external excitation force ceases.

**RESISTANCE FACTOR**

The factor by which the resistance of a structural element must be multiplied to obtain the resistance of the equivalent single-degree-of-freedom system.

**RESONANCE**

A condition under forced vibration when any small increase or decrease in the frequency of excitation causes a decrease in the response of the system.

**RESONANT FREQUENCY**

A resonant frequency is a frequency at which resonance exists.

**REVERBERATION**

Persistence of sound at a given point after direct reception from the source has stopped.

**REVERBERATION TIME**

The time required for the average sound pressure level, originally in a steady state, to decrease 60 dB after the source is stopped.

**ROOT-MEAN-SQUARE SOUND PRESSURE**

(See Effective Sound Pressure).

**SABIN (SQUARE-FOOT UNIT OF ABSORPTION)**

A measure of the sound absorption of a surface; it is the equivalent of 1 square foot of perfectly absorptive surface.

**SABINE ABSORPTION**

The Sabine absorption in a room is the sound absorption ( $\alpha$ ) defined by the Sabine reverberation-time equation

$$T_{60} = 0.049 \frac{V}{\alpha}$$

where  $T_{60}$  is the reverberation time in seconds,  $V$  is the volume of the room in cubic feet, and  $\alpha$  is the total (Sabine) absorption in sabins (square-foot units).

**SCALED DISTANCE**

The ground distance between the center of an explosion and point of measurement divided by the cube root of the equivalent weight of TNT.

**SEISMIC VELOCITY CORRECTION FACTORS**

The correction factors used to obtain stresses and motions for the transeismic and subseismic conditions.

**SHOCK WAVE**

A continuously propagated pressure pulse (or wave) in the surrounding medium, which may be air, water, or earth, initiated by the expansion of the hot gases produced in an explosion. A shock wave in air is referred to as a blast wave.

**SHOCK SPECTRUM ENVELOPE**

The maximum response spectra of a system relative to the support subjected to a shock input.

**SIMPLE HARMONIC MOTION**

Motion in which the relationship between time  $t$  and displacement  $x$  can be expressed in the form  $x = A \sin(\omega t + \phi)$ ,

where  $A$  is the amplitude,  $\omega$  the angular frequency, and  $\phi$  the phase angle.

**SIMPLE SOUND SOURCE**

A source which radiates sound uniformly in all directions under free-field conditions.

**SONE**

A unit of loudness.

**SOUND ENERGY DENSITY**

The sound energy contained in a given infinitesimal part of the medium divided by the volume of that part of the medium. The commonly used unit is the erg per cubic centimeter.

**SOUND INTENSITY (SOUND ENERGY FLUX DENSITY)**

The average rate of sound energy transmitted in a specified direction through a unit area normal to this direction at the point considered.

**SOUND POWER**

The total sound energy radiated by a source per unit of time.

**SOUND POWER LEVEL**

The level in decibels equal to 10 times the logarithm to the base 10 of the ratio of the sound power radiated by a source to a reference power. Throughout this manual, the reference power is  $10^{-13}$  watts.

**SOUND PRESSURE LEVEL**

The level in decibels equal to 20 times the logarithm to the base 10 of the ratio of the pressure of this sound to the reference pressure. The reference pressure employed throughout this manual is 0.0002 microbar. In many sound fields the sound-pressure ratios are not proportional to the square root of corresponding power ratios and hence cannot be expressed in decibels in the strict sense; however, it is common practice to extend the use of the decibel to these cases.

**SOUND PRESSURE SPECTRUM LEVEL**

(See Pressure Spectrum Level).

**SOUND TRANSMISSION COEFFICIENT**

(See Transmission Coefficient).

**SOUND TRANSMISSION LOSS**

A quantity expressed in decibels equal to 10 times the logarithm of the ratio of sound power incident on a surface to the sound power transmitted through the surface.

**SPECIFIC ACOUSTIC IMPEDANCE (UNIT-AREA ACOUSTIC IMPEDANCE)**

The complex ratio of sound pressure to particle velocity.

**SPECIFIC ACOUSTIC REACTANCE**

The imaginary component of the specific acoustic impedance.

**SPECIFIC ACOUSTIC RESISTANCE**

The real component of the specific acoustic impedance.

**SPECTRUM**

A description of the resolution of a time function into sinusoidal frequency components of different frequency and (usually) different amplitude and phase.

**SPEECH INTERFERENCE LEVEL, SIL**

The average, in decibels, of the sound pressure levels of the noise in the three octave bands of frequency 600-1200, 1200-2400, and 2400-4800 Hz.

**SPHERICAL WAVE**

A wave in which the wave fronts are concentric spheres.

**STANDING WAVES**

Periodic waves having a fixed distribution in space which is the result of interference of progressive waves of the same frequency and kind. Such waves are characterized by the existence of nodes or partial nodes and anti-nodes that are fixed in space.

**TERMINAL YIELD**

The value of the explosive yield in the region where the explosive yield becomes independent of distance from the explosion or the shock wave parameter used in the calculation.

**THRESHOLD OF AUDIBILITY (THRESHOLD OF DETECTABILITY)**

The minimum effective sound pressure of the signal capable of evoking an auditory sensation.

**THRESHOLD OF FEELING (OR DISCOMFORT, TICKLE, OR PAIN)**

The minimum effective sound pressure for which there is the sensation of feeling (or discomfort, tickle, or pain).

**TRANSMISSION COEFFICIENT**

The fraction of incident sound power transmitted through a partition at a specified angle of incidence.

**TRANSMISSION LOSS**

The reduction in the magnitude of some characteristic of a signal, between two stated points in a transmission system, (see Sound Transmission Loss).

**TRIPLE POINT**

The intersection of the incident, reflected, and fused (or Mach) shock fronts accompanying an air burst. The height of the triple point above the surface, i.e., the height of the Mach stem, increases with increasing distance from a given explosion, (see Mach Stem).

**VERTICAL ATTENUATION FACTOR**

The ratio of surface motion (or stress) to subsurface motion (or stress) due to propellant explosions.

**VISCOUS DAMPING**

The dissipation of energy that occurs when a particle in a vibrating system is resisted by a force that has a magnitude proportional to the magnitude of the velocity of the particle and direction opposite to the direction of the particle.

**WATER CONTENT**

The ratio of weight of water to weight of solid matter in a soil.

**WHITE NOISE**

White noise is noise of a statistically random nature having equal energy per unit frequency bandwidth over a specified total frequency band.

## FOREWORD

This manual is the result of over three years of planning, experiments, research and production. The work was performed under the auspices of Mr. J. Farrow, Chief, Acoustics and Vibration Branch, Propulsion and Vehicle Engineering, Marshall Space Flight Center, NASA, with Mr. R. Jewell, Chief, Advanced Research Section, as Technical Monitor.

The Editor gratefully acknowledges the participation of the members of the Wyle Research Staff, particularly the following individuals whose contributions and prime responsibilities in the areas noted made this manual possible.

• Fundamentals of Acoustics	(Chapter 4)	E. Cuadra
• Sonic and Vibration Control Systems Concepts	(Chapter 5)	E. Cuadra
• Rocket Noise Sources	(Chapter 6)	R. Potter
• Propellant Blast Parameters	(Chapter 6)	F. Bracco
• Sonic Boom Environments	(Chapter 6)	E. Cuadra
• Attenuation of Rocket Noise	(Chapter 7)	R. Potter
• Acoustic Fatigue	(Chapter 8)	R. Barrett
• Propellant Blast Loads and Design Criteria	(Chapter 8)	V. Conticelli
• Architectural Acoustics	(Chapter 9)	B. Sharp
• Noise and Vibration Effects on Personnel	(Chapter 10)	J. Ollerhead
• Design Charts and Material Properties	(Chapter 12)	G. Chan

To K. McK. Eldred, Wyle Director of Research, for his many helpful discussions and guidance, to R. White, Senior Staff Advisor, for his assistance, and to J. Bowman, Assistant Director of Research, for his invaluable support during the completion of this manual, the editor is particularly grateful.

A special thanks goes to Joe Matzkiw, Technical Illustrator, and Mary King, Ann Philo, and Buelah Miller, Technical Typists, for their personal touch in the final quality of the production of this manual.

L. C. Sutherland  
Director of Research Staff  
Wyle Huntsville

**CHAPTER 3**  
**FUNDAMENTALS OF VIBRATION**

TABLE OF CONTENTS

<u>SECTION</u>		<u>PAGE</u>
3.1	<u>INTRODUCTION</u> . . . . .	3-1
3.2	<u>STRUCTURAL VIBRATION – SOME FUNDAMENTALS</u> . . . . .	3-1
3.2.1	DYNAMICS OF THE SINGLE DEGREE-OF-FREEDOM SYSTEM WITH VISCOUS DAMPING . .	3-3
3.2.1.1	General Solution to the Equation of Motion . . . . .	3-3
3.2.1.2	Transient Response . . . . .	3-4
3.2.1.3	Alternate General Solution . . . . .	3-4
3.2.1.4	Steady State Response to a Sinusoidal Input . . . . .	3-6
3.2.1.5	Force and Motion Transmissibility . . . . .	3-7
3.2.1.6	Summary of Transfer Functions for Single Degree-of-Freedom System to Sinusoidal Excitation . . . . .	3-8
3.2.2	RESPONSE OF THE SINGLE DEGREE-OF-FREEDOM SYSTEM TO TRANSIENT INPUTS . . . . .	3-8
3.2.2.1	Superposition Principle . . . . .	3-10
3.2.2.2	Response to Triangular Pulse . . . . .	3-10
3.2.2.3	Acceleration Response to Triangular Pulse . . . . .	3-12
3.2.2.4	Alternate Methods of Defining Transient Response . . . . .	3-14
3.2.2.5	Application of Fourier Transform . . . . .	3-14
3.2.2.6	Application of Laplace Transform . . . . .	3-17
3.2.2.7	Relationship Between Fourier Spectrum and Residual Shock Spectrum . . . . .	3-18
3.2.2.8	Shock Response Spectrum of Sonic Boom N-Wave . . . . .	3-20
3.2.2.9	Transient Response to Other Types of Pulses . . . . .	3-24
3.2.3	RESPONSE OF LINEAR SINGLE DEGREE-OF-FREEDOM SYSTEMS TO RANDOM EXCITATION . . . . .	3-25
3.2.3.1	Characteristics of Random Noise . . . . .	3-25
3.2.3.2	Basic Parameters of Random Noise . . . . .	3-26
3.2.3.3	Mean Value . . . . .	3-27
3.2.3.4	Mean Square Value . . . . .	3-27
3.2.3.5	Power Spectral Density . . . . .	3-28
3.2.3.6	Application of Power Spectral Density Data for Defining Random Response of a Single Degree-of-Freedom System . . . . .	3-30
3.2.3.7	Statistics of Random Noise . . . . .	3-31
3.2.3.8	Occurrence Rate for Zero Crossings and Maxima . . . . .	3-36
3.2.3.9	Probability of Simultaneous Occurrence of Peak Responses for Two Different Systems . . . . .	3-37
3.2.3.10	Derivation of Response of Single Degree-of-Freedom System to Random Excitation – A Brief Summary . . . . .	3-37
3.2.3.11	Engineering Methods for Analyzing Random Response . . . . .	3-41
3.3	<u>VIBRATION RESPONSE OF COMPLEX STRUCTURE</u> . . . . .	3-48
3.3.1	METHOD OF VIBRATION ANALYSIS FOR COMPLEX STRUCTURE . . . . .	3-48
3.3.1.1	Application of Digital Computer Techniques . . . . .	3-49
3.3.1.2	Objectives of Dynamic Analysis . . . . .	3-49
3.3.2	CLASSICAL NORMAL MODE ANALYSIS FOR LUMPED PARAMETER SYSTEMS . . . . .	3-50
3.3.2.1	Equations of Motion for Two Degree-of-Freedom System . . . . .	3-50
3.3.2.2	Normal Mode Solution for Two Degree-of-Freedom System . . . . .	3-51
3.3.2.3	Free Vibration Response of Symmetrical Two Degree-of-Freedom System . . . . .	3-52
3.3.2.4	Energy, Generalized Mass and Stiffness of Two Degree-of-Freedom System . . . . .	3-54
3.3.2.5	Generalized Mass and Stiffness for N Degree-of-Freedom System . . . . .	3-55
3.3.2.6	Dynamically and Statically Coupled Systems . . . . .	3-56
3.3.2.7	Orthogonality of Normal Modes . . . . .	3-58
3.3.2.8	Application of Lagrange's Equation . . . . .	3-58
3.3.2.9	Free Vibration Response of N Degree-of-Freedom System . . . . .	3-59

TABLE OF CONTENTS (CONTINUED)

<u>SECTION</u>		<u>PAGE</u>
3.3.3	FORCED VIBRATION RESPONSE OF LUMPED PARAMETER SYSTEMS . . . . .	3-62
3.3.3.1	Generalized Force and Generalized Damping . . . . .	3-62
3.3.3.2	General Form of Solutions for Various Types of Excitation . . . . .	3-64
3.3.3.3	Response of Lumped Parameter Systems to Transient Loads . . . . .	3-66
3.3.3.4	Response of Two Degree-of-Freedom System to Triangular Shock Load . . . . .	3-67
3.3.3.5	Response of Lumped Parameter Systems to Sinusoidal Loads . . . . .	3-70
3.3.3.6	Summation of Multiple Sinusoidal Responses . . . . .	3-72
3.3.3.7	Response to Steady State and Transient Periodic Excitation . . . . .	3-80
3.3.3.8	Example of Response of Two Degree-of-Freedom System to Sinusoidal Excitation . . . . .	3-81
3.3.3.9	Response of Lumped Parameter Systems to Random Excitation . . . . .	3-86
3.3.3.10	Joint Acceptance for Random Loads . . . . .	3-88
3.3.3.11	Cross-Correlation Functions and Cross-Power Spectral Density . . . . .	3-90
3.3.3.12	Summary of Terminology for Random Loads . . . . .	3-93
3.3.4	MATRIX METHODS FOR NORMAL MODE ANALYSIS OF LUMPED PARAMETER SYSTEMS . . . . .	3-95
3.3.4.1	Matrix Definitions . . . . .	3-95
3.3.4.2	Matrix Operations . . . . .	3-96
3.3.4.3	Matrix Solution of Equations of Motion . . . . .	3-98
3.3.4.4	Example of Matrix Iteration Methods . . . . .	3-102
3.3.4.5	Upper and Lower Bounds for Natural Frequencies . . . . .	3-104
3.3.4.6	Normal Mode Response in Matrix Form . . . . .	3-105
3.3.5	RESPONSE OF STRUCTURE WITH DISTRIBUTED MASS AND STIFFNESS . . . . .	3-107
3.3.5.1	Free and Forced Undamped Vibration of Continuous Structure . . . . .	3-108
3.3.5.2	Longitudinal Vibration of Bars . . . . .	3-114
3.3.5.3	Torsional Vibration of Bars . . . . .	3-120
3.3.5.4	Lateral Vibration of Beams . . . . .	3-122
3.3.5.5	Effect of Mass and Stiffness Loads on Lateral Vibration of Beams . . . . .	3-130
3.3.5.6	Lateral Vibration of Plates . . . . .	3-134
3.3.5.7	Natural Frequencies for Plates with Non-Ideal Boundary Conditions . . . . .	3-139
3.3.5.8	Natural Frequencies of Non-Homogeneous Plates . . . . .	3-140
3.3.5.9	Normal Modes of Mass and Stiffness Loaded Plates . . . . .	3-142
3.3.6	FORCED RESPONSE OF BEAMS AND PLATES TO LATERAL LOADS . . . . .	3-143
3.3.6.1	Normal Mode Solution for a Uniform Static Load . . . . .	3-143
3.3.6.2	Response of Beams and Plates for Sinusoidal Loads . . . . .	3-146
3.3.6.3	Response of a Beam to a Traveling Step Load . . . . .	3-151
3.3.6.4	Response of a Beam to Motion of Its Supports . . . . .	3-153
3.3.6.5	Reaction Forces at Boundaries of Beams and Plates . . . . .	3-155
3.3.6.6	Dynamic Stress at Resonance of Vibrating Structure . . . . .	3-157
3.3.7	DAMPING OF CONTINUOUS STRUCTURE . . . . .	3-158
3.3.7.1	Types of Damping . . . . .	3-158
3.3.7.2	Propagation of Damped Longitudinal and Flexural Waves in Structure . . . . .	3-161
3.4	<u>VIBRATION DESIGN TABLES</u> . . . . .	3-163
	REFERENCES . . . . .	3-189

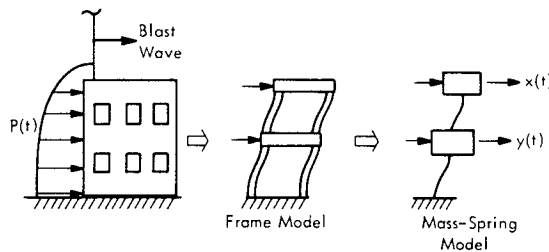
## CHAPTER 3

### FUNDAMENTALS OF VIBRATION

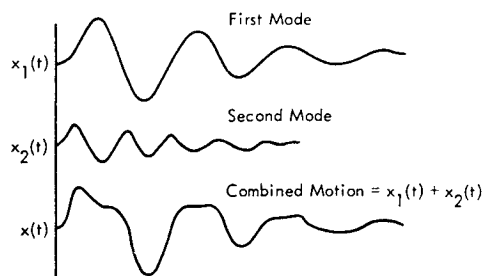
#### 3.1 INTRODUCTION

The sonic environments, considered in this manual, represent a source of dynamic loading on structure. These loads vary both in position on the structure and in time. The net result of such dynamic loading is to cause a complex vibratory motion of the structure in response to the non-uniform time varying load.

The development of a simplified analytical model is a basic prerequisite for predicting this dynamic response in a straightforward manner. For example, as illustrated in Figure 3.1a, the deflection time history of a frame building, when exposed to a blast wave, can be approximated by the response of the equivalent dynamic model shown at the right. This consists of a system of lumped masses representing the floors of the building connected by massless springs which simulate the lateral stiffness of the supporting columns. Furthermore, it will be shown later how the motion,  $x(t)$ , of any one element of this simplified model can be broken down into various components, each with its own characteristic period of vibration. This concept is illustrated in Figure 3.1b.



a) Simplified Analysis Model



b) Time History of One Mass

FIGURE 3.1 Equivalent Dynamic Model of Building Exposed to Blast Load and Composite Time History of One Mass Showing Summation of Normal Modes of Vibration

Therefore, the first part of this chapter starts with a brief review of the fundamentals of vibration response of simple mass spring systems to different types of dynamic loads. These encompass the transient loads due to blast or sonic boom as well as the continuous random-type of loads characteristics of rocket engine noise. The discussion on response to random excitation includes a brief introductory review of the general characteristics of random vibration.

Following this treatment of the single degree of freedom system, methods for the analysis of more complex structure are considered. This begins with a review of classical methods for analyzing the response of lumped mass-spring systems, such as illustrated in Figure 3.1a. Application of the analysis methods are illustrated by examples. This is followed by a discussion of the free and forced vibration characteristics of continuous structural elements such as beams and plates. A number of basic vibration design charts for the stiffness and natural frequencies of vibrating systems are included at the end of this chapter.

The objective of this chapter has been to provide, within this manual, one basic reference source of practical methods for analyzing response of ground structure to sonic loads. The methods are outlined in detail and provide the foundation for the design tools developed in subsequent chapters. The reader is referred to the extensive literature for a more thorough development of structural vibration theory. In particular, References 3.1 - 3.5 provide an extensive coverage of vibration theory. Additional background relating vibration and acoustics is provided in References 3.6 - 3.9.

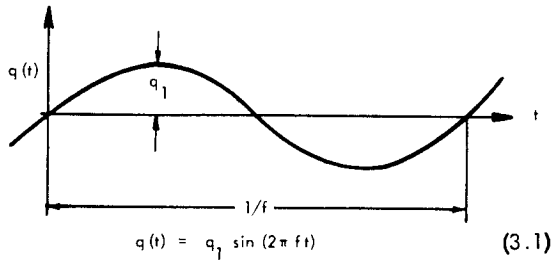
#### 3.2 STRUCTURAL VIBRATION - SOME FUNDAMENTALS

Under pure static loading, a linear structure stores the work done on it by external forces in the form of elastic energy. For structure loaded beyond its yield point, additional energy is stored in the form of plastic energy which can not be recovered. For the most part, this manual will consider only linear elastic structures.

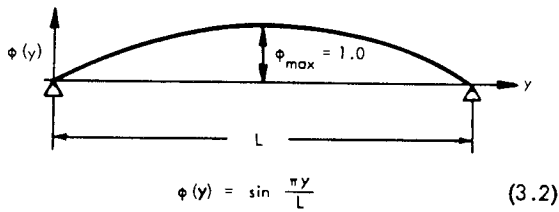
If the static load is applied suddenly or is changed in a cyclic manner, then some of the work done by the external forces on the structure is expended in the form of kinetic energy, - the energy of motion. Thus, a structure which is displaced initially from its equilibrium position and then released, will spring back releasing the stored elastic energy in the form of kinetic energy. If allowed to continue, the structure will thus oscillate back and forth about its equilibrium position with a continual flow of energy from elastic to kinetic and visa versa. The frequency of this oscillation is called a natural frequency. If an external driving force is applied to the system at this same frequency, the amplitude of vibration will increase to a maximum resonant response amplitude limited only by losses in energy due to damping or by nonlinearities in the system.



For a structure which may be represented by a simple lumped mass on a single linear spring, this vibration takes its simplest form - simple harmonic motion or sinusoidal motion, which is illustrated in Figure 3.2a. This shows the time history of the displacement  $q(t)$  of the center of a pinned-pinned beam vibrating at its fundamental resonance frequency. The fundamental frequency is the lowest frequency of vibration for which a system will vibrate freely without excitation by external forces.



a) Simple Harmonic Motion (Time Variable)



b) Mode Shape (Space Variable)

FIGURE 3.2 Sinusoidal Time History (a) and Mode Shape (b) of Simply Supported Beam Vibrating in its Fundamental Mode

The motion of the center of the beam is completely defined by its peak amplitude  $q_0$ , its frequency of vibration,  $f$ , and time  $t$  in equation 3.2 in Figure 3.2b.

To describe the motion at all points along the beam, an additional term is required - the mode shape,  $\phi(y)$  - the variation in the shape of the beam along its length given by Equation 3.2 in Figure 3.2b. Thus, for this mode of vibration, the displacement  $x(y,t)$  at any point  $y$  at time  $t$  is the product

$$x(y,t) = \phi(y) \cdot q(t) \tag{3.3}$$

Since only one time variable is required, this mode of vibration is equivalent to a single degree-of-freedom system - that is, the amplitude of a fixed reference point is completely described by only one time variable,  $q(t)$ .

However, for the simple beam in Figure 3.2 and for all types of structure, higher modes of vibration can occur, each with its own natural frequency of vibration  $f_n$ . These are called the normal modes of vibration. In general, the motion of any linear structure can be described by the summation of the motion of its normal modes, each of which can be treated as a single degree-of-freedom system. Thus, the general expression for motion at any point at time  $t$  of a structure may be given by the summation

$$x(y,t) = \sum_{n=1}^N \phi_n(y) q_n(t) \tag{3.4}$$

where  $\phi_n(y)$  = Mode shape for  $n$ th normal mode

$q_n(t)$  = Time variation (called generalized coordinate) of  $n$ th normal mode.

Except for coupling of energy between modes through damping forces, each mode responds independently of the response of other modes. Therefore, a basic understanding of the single degree-of-freedom system is fundamental to the analysis of any structure, no matter how complex.

For most structural dynamic problems, the lower order modes (the first two to four modes in the order of their natural frequencies) exhibit the greatest response, and generally, the response amplitudes decrease monotonically with increasing resonance frequency of the modes. This is due to the fact that the effective force driving the higher order modes falls off rapidly with the order of the modes.

This is a fortunate circumstance since internal dynamic loads in a structure increase with the order of the modes when each mode has the same deflection amplitude. The rapid decrease in amplitude of the effective driving force generally overrides the increasing load factor with frequency, so that internal loads also decrease with increasing frequency for most actual external loadings.

Complex structures, which have a large number of very complex modal patterns, are difficult to analyze in detail; however, advantage can be taken of the fact that only the lower simpler type modes need to be considered. Thus, one efficient technique for computing or estimating response of most structural systems is to estimate the resonance frequencies and mode shapes of the first few modes, find the response of each mode using a single degree of freedom model for each mode, and then add up the individual modal responses to obtain the total response. This method is not limited to dynamic deflections, but can be used to obtain dynamic velocities, accelerations, strains, stresses, reaction loads, etc.

One important exception to this predominant influence of lower order modes lies in the area of sound transmission through structure. In this case, the broad frequency range of the human ear requires that many modes be considered in the analysis. This topic is treated separately in Chapter 9.

Because of the importance of the single degree-of-freedom system, it is natural to open this section with a discussion of the response of such a system by various forms of excitation.

Following this, it is shown how more complex systems can be treated as a set of single degree-of-freedom modal systems, and how the effective single degree-of-freedom properties for a given mode are obtained from the properties of the complex structure.

Finally, a series of tabulations and equations for computing resonance frequencies of various structural systems are presented as a convenient reference for the reader.

### 3.2.1 DYNAMICS OF THE SINGLE DEGREE-OF-FREEDOM SYSTEM WITH VISCOUS DAMPING

The forced response of a damped single degree-of-freedom system can be represented by a force  $P(t)$  applied to a single mass  $m$ , a single spring of stiffness  $k$ , and a damping element or dashpot having a damping constant  $c$ . These elements are arranged in the form shown in Figure 3.3. The response displacement of the mass is  $x(t)$  and the force transmitted to the fixed-base is  $P_T(t)$ .

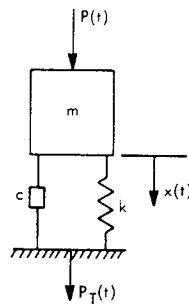


FIGURE 3.3 Single Degree-of-Freedom System

It is desirable to review the response of this system to single frequency steady-state forces, transient force pulses, and random forces, since all of these types of forces are encountered in the sonic environment considered in this manual.

From consideration of the dynamic balance of forces acting on the mass, its equation of motion can be derived. This is stated in two forms below.

#### EQUATION OF MOTION

$$m \ddot{x}(t) + c \dot{x}(t) + k x(t) = P(t) \quad (3.5)$$

where

$x(t)$  = Displacement of mass

$\dot{x}(t)$  = Velocity of mass

$\ddot{x}(t)$  = Acceleration of mass

#### ALTERNATE FORM OF EQUATION OF MOTION

$$\ddot{x}(t) + 2\delta\omega_o \dot{x}(t) + \omega_o^2 x(t) = \omega_o^2 \frac{P(t)}{k} \quad (3.6)$$

where

$\delta = c/c_c =$  Critical damping ratio

$c_c = 2\sqrt{mk} =$  Critical damping constant

$\omega_o = \sqrt{k/m} =$  Undamped natural frequency

##### 3.2.1.1 General Solution to the Equation of Motion

The general solution of Equation 3.6 for an arbitrary input  $P(t)$  may be expressed as the sum of two parts:  $x_1(t)$  - the transient solution due only to the initial conditions, and  $x_2(t)$ , the forced response, so that the general solution for the displacement response  $x(t)$  is

$$x(t) = x_1(t) + x_2(t) \quad (3.7)$$

The transient solution  $x_1(t)$  is

$$x(t)_1 = \frac{e^{-\delta\omega_o t}}{\sqrt{1-\delta^2}} \left[ x(0) \cos(\omega_d t - \theta_1) + \frac{\dot{x}(0)}{\omega_o} \sin \omega_d t \right] \quad (3.8)$$

where

$$\theta_1 = \tan^{-1} \delta / \sqrt{1-\delta^2}$$

$$\omega_d = \omega_o \sqrt{1-\delta^2} \quad \text{Damped natural frequency - radians/sec.}$$

$$\omega_o = 2\pi f_o \quad \text{Undamped natural frequency - radians/sec.}$$

$$f_o = \text{Undamped natural frequency - Hz}$$

$$x(0) = \text{Initial displacement}$$

$$\dot{x}(0) = \text{Initial velocity}$$

The forced response solution  $x_2(t)$  is

$$x_2(t) = \int_{\tau=0}^t h(t-\tau) \cdot P(\tau) \cdot d\tau \quad (3.9)$$

which is the convolution integral for forced response and  $h(t)$  is the response of a single degree-of-freedom system to a unit impulse at time  $t = 0$  and is given by

$$h(t) = \frac{1}{m\omega_d} \left[ e^{-\delta\omega_o t} \sin \omega_d t \right] \quad (3.10)$$

The convolution or Duhamel integral solution, is based on treating the input  $P(t)$  as the sum of a series of very short impulses with a magnitude  $P(\tau)$  at any time  $\tau < t$ . The response at time  $t$  is then the sum of the responses, to a unit impulse, given by Equation 3.10.

For the special case where the input itself is a force impulse  $I$  equal to

$$I = \int_0^{t \rightarrow 0} P(t) dt \tag{3.11}$$

then the forced response is simply equal to

$$x_2(t) = I h(t) \tag{3.12}$$

where  $h(t)$  is given by Equation 3.10. By comparing Equation 3.10 with 3.8, it becomes apparent that the forced response to a unit impulse could be described equally well as the transient response to an initial velocity  $\dot{x}(0)=I/m$ . This is a useful concept when dealing with the response of systems to very short duration forces.

### 3.2.1.2 Transient Response

The transient solution (Equation 3.8) is called "transient" because of the presence of the exponential damping factor  $\exp(-\delta \omega_o t)$ , which causes this motion to be damped out with time. The forced response solution, (Equation 3.9) may also include similar transient terms due to initial application of the excitation.

In both cases, they consist of decaying oscillations at the damped natural frequency,  $\omega_d$ . If no forced excitation is present, the system will come to rest. If a forced excitation is present, the system will continue to vibrate but eventually, only at the frequencies present in the excitation. Examples of such transient oscillations are shown in Figure 3.4. Part a) shows the decaying oscillatory response of a simple damped mass-spring system to an initial velocity (or an equivalent impulse) applied to the mass. Part b) shows the initial transient response due to application of a sinusoidal excitation of frequency  $\omega$  starting at time  $t = 0$ . In this case, the initial transient response is the summation of motion at the damped natural frequency  $\omega_d$  and the forcing frequency  $\omega$ . The former decays rapidly, however, leaving only the steady-state response at the forcing frequency  $\omega$ .

The envelope of the decaying transient response, shown in Figure 3.4a, is described by

$$x(t)|_{\max} = x_{\max}(t \rightarrow 0) \cdot e^{-\delta \omega_o t} \tag{3.13}$$

The rate of decrease of this envelope from one peak to another is a convenient measure for the amount of damping. Between any two successive peaks, this envelope will decrease by a constant factor for linear damping. Thus, a useful term to describe this decay is the natural logarithm of the ratio of two successive peaks which are separated by the period  $t_o = 2\pi/\omega_d$ . This quantity is called the log decrement and is readily shown to be

$$\Delta = \log_e \frac{x(t_{n \max})}{x(t_{n \max} + t_o)} = \frac{2\pi \delta}{\sqrt{1 - \delta^2}} \tag{3.14}$$

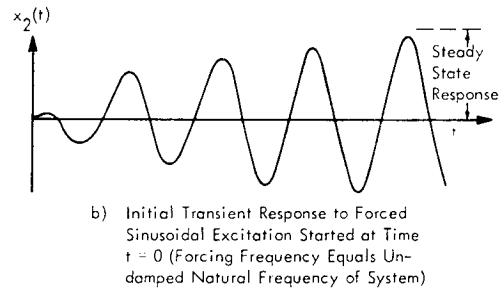
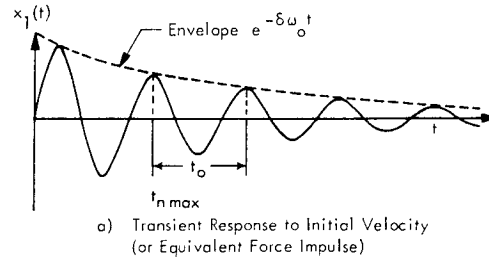


FIGURE 3.4 Transient Responses of a Single Degree-of-Freedom System Due to a) Initial Conditions and b) Initiation of Excitation.

### 3.2.1.3 Alternate General Solution

It is convenient to use another form for the solution of the equation of motion which separates the initial transients from the steady state response. This is given by the more familiar classical form as

$$x(t) = e^{-\delta \omega_o t} [A \cos \omega_d t + B \sin \omega_d t] + x_p(t) \tag{3.15}$$

where

$A, B$  = Constants to be defined by initial displacement and velocity of system and initial value of steady state solution,  $x_p(t = 0)$

$x_p(t)$  = Particular integral or steady state response

The "particular integral" is the function which satisfies the equation of motion. The remaining part of the solution is the "complementary function" which defines the transient response due to an initial displacement  $x(0)$  and/or an initial velocity  $\dot{x}(0)$  of the mass as well as the initial transients due to the initial application of the excitation.

Thus, several choices are available for solution of the basic equations of motion given by Equation 3.5 or 3.6.

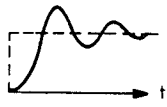
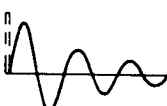
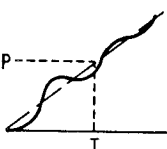
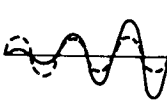
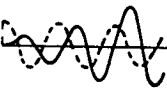
Choice of one particular solution will be based on the particular problem.

- To determine the response for a finite initial displacement and/or velocity only, use Eq. 3.8
- To determine the total response (including initial transients) to a forcing function, use Eq. 3.9
- To determine the steady-state response to a forcing function, use only the particular integral part of Eq. 3.15

Using either Equations 3.7 or 3.15, the following general solutions are obtained for the forced displacement response of a damped system initially at rest. Five types of forcing functions are shown which form the basic building blocks for more complicated types of input. When it is necessary to account for an initial displacement or velocity, Equation 3.8 is added to the response indicated in the following tabulation. The steady state response part of  $x(t)$  in this tabulation is recognized by the absence of any exponential damping term.

TABLE 3.1

FORCED RESPONSE OF SINGLE DEGREE-OF-FREEDOM SYSTEM SHOWN IN FIGURE 3.3

EXCITATION $P(t)$ , (---)	TIME HISTORY	RESPONSE $x(t)$ (—)
STEP $P$		$\frac{P}{k} \left[ 1 - \frac{e^{-\delta\omega_0 t}}{\sqrt{1-\delta^2}} \cos(\omega_d t - \theta_1) \right]$ (3.16)
IMPULSE $I = \int P(t) dt = \dot{x}_0 m$		$\frac{I}{\omega_d m} \left[ e^{-\delta\omega_0 t} \sin \omega_d t \right]$ (3.17)
RAMP $\frac{Pt}{T}$		$\frac{P}{k} \left[ \frac{t}{T} - \frac{2\delta}{\omega_0 T} - \frac{e^{-\delta\omega_0 t}}{\omega_0 T \sqrt{1-\delta^2}} \sin(\omega_d t - \theta_2) \right]$ (3.18)
SINE $P \sin \omega t$		$\frac{P}{k} H(\omega) \left[ \sin(\omega t - \theta_3) - \frac{(\omega/\omega_0) e^{-\delta\omega_0 t}}{\sqrt{1-\delta^2}} \sin(\omega_d t - \theta_4) \right]$ (3.19)
COSINE $P \cos \omega t$		$\frac{P}{k} H(\omega) \left[ \cos(\omega t - \theta_3) - \frac{e^{-\delta\omega_0 t}}{\sqrt{1-\delta^2}} \cos(\omega_d t - \theta_5) \right]$ (3.20)

$$\theta_1 = \tan^{-1} \frac{\delta}{\sqrt{1-\delta^2}} \approx \delta \text{ radians } (\delta < 0.2)$$

$$\theta_4 = \tan^{-1} \frac{2\delta \sqrt{1-\delta^2}}{1 - 2\delta^2 - (\omega/\omega_0)^2}$$

$$\theta_2 = \tan^{-1} \frac{2\delta \sqrt{1-\delta^2}}{1 - 2\delta^2} \approx 2\delta \text{ radians } (\delta < 0.2)$$

$$\theta_5 = \tan^{-1} \frac{\delta [1 + (\omega/\omega_0)^2]}{\sqrt{1-\delta^2} [1 - (\omega/\omega_0)^2]}$$

$$\theta_3 = \tan^{-1} \frac{2\delta \omega/\omega_0}{1 - (\omega/\omega_0)^2}$$

$$H(\omega) = \left[ (1 - (\omega/\omega_0)^2)^2 + (2\delta \omega/\omega_0)^2 \right]^{-1/2}$$

The last two solutions in Table 3.1 make use of one or more of the following transformations which provide a useful alternate form for the solutions to the equation of motion. Note the particular form chosen is based on the input.

$$\begin{aligned}
 A \cos \omega t + B \sin \omega t &= \sqrt{A^2 + B^2} \left\{ \begin{array}{l} \sin(\omega t + \theta_1) \\ \text{or} \\ \cos(\omega t - \theta_2) \end{array} \right\} \\
 -A \cos \omega t + B \sin \omega t &= \sqrt{A^2 + B^2} \left\{ \begin{array}{l} \sin(\omega t - \theta_1) \\ \text{or} \\ -\cos(\omega t + \theta_2) \end{array} \right\} \\
 A \cos \omega t - B \sin \omega t &= \sqrt{A^2 + B^2} \left\{ \begin{array}{l} -\sin(\omega t - \theta_1) \\ \text{or} \\ \cos(\omega t + \theta_2) \end{array} \right\}
 \end{aligned} \tag{3.21}$$

where

$$\theta_1 = \tan^{-1} A/B$$

$$\theta_2 = \tan^{-1} B/A$$

and A, B are positive real quantities.

### 3.2.1.4 Steady State Response to a Sinusoidal Input

The simplest form of steady state input is a sinusoidal force. The steady state response to such an input, with an amplitude P and frequency  $\omega$  is given by the first term in Equations 3.19 or 3.20. The second term, representing the transient response to the initial application of the load, decays rapidly. Thus, if the input to the mass, in Figure 3.3, is a force given by

$$P(t) = P \cos \omega t$$

the steady state response is obtained from Equation 3.20 as

$$x(t) = \frac{P}{k} \frac{\cos(\omega t - \theta_3)}{\left[ (1 - (\omega/\omega_0)^2)^2 + (2\delta\omega/\omega_0)^2 \right]^{1/2}}$$

Ordinarily, only the amplitude of  $x(t)$  is of concern for vibration design. If this is identified by the frequency of excitation,  $\omega$ , and the amplitude of the driving force is similarly identified, then the amplitude of the displacement response  $x(\omega)$  is:

$$x(\omega) = \frac{P(\omega)}{k} H(\omega) \tag{3.22}$$

where  $H(\omega)$  has an absolute value given by

$$H(\omega) = \left[ (1 - (\omega/\omega_0)^2)^2 + (2\delta\omega/\omega_0)^2 \right]^{-1/2} \tag{3.23}$$

The phase angle  $\theta_3$  or  $\theta(\omega)$  between the input and response is

$$\theta(\omega) = \tan^{-1} \frac{2\delta\omega/\omega_0}{1 - (\omega/\omega_0)^2}$$

The quantity  $H(\omega)$ , called the dynamic magnification factor and the phase angle  $\theta(\omega)$ , are plotted on Figure 3.5 for a few values of the damping ratio  $\delta$ .

The maximum value of  $H(\omega)$  occurs at the resonance frequency  $\omega_r = \omega_0 \sqrt{1 - 2\delta^2}$  which is very nearly equal to the natural frequency  $\omega_0$  for the usual amount of damping so that for practical purposes,

$$H(\omega)_{\max} \approx 1/2\delta = Q \tag{3.24}$$

where Q = resonant amplification factor.

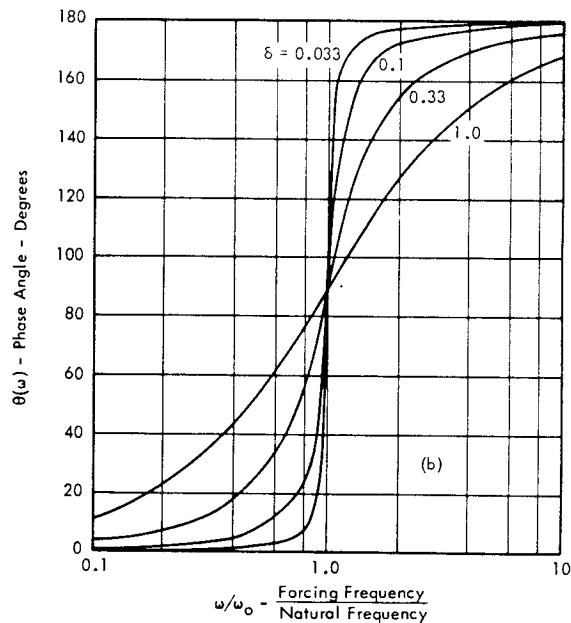
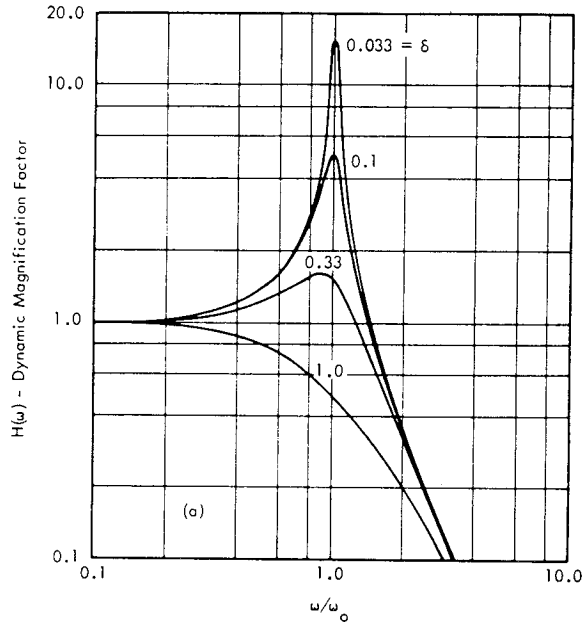


FIGURE 3.5 Dynamic Magnification Factor (a) and Phase Angle (b) for Response of Single Degree of Freedom System to Sinusoidal Input

Note that the displacement response amplitude can be given as

$$\frac{x(\omega)}{x_s} = H(\omega) \quad (3.25)$$

where  $x_s$  is the static displacement that corresponds to a static load  $P$  equal to the amplitude  $P(\omega)$  of the sinusoidal force at the frequency  $\omega$ .

For analysis of acoustic response of structure, it will be convenient to define the acceleration amplitude response  $a(\omega)$  of the structure relative to the driving force  $P(\omega)$ . For acceleration in "g" units, this ratio is

$$\frac{a(\omega)}{P(\omega)} = \frac{\omega^2 x(\omega)}{g P(\omega)} = \frac{1}{g} \left(\frac{\omega}{\omega_0}\right)^2 \frac{H(\omega)}{m} \quad (3.26)$$

Since the total weight  $W$  is equal to  $mg$ , a convenient non-dimensional form of the above is

$$\frac{a(\omega) \cdot W}{P(\omega)} = \left(\frac{\omega}{\omega_0}\right)^2 H(\omega) \quad (3.27)$$

The various relationships given by Equations 3.22 - 3.27 will be utilized frequently throughout this manual. For Equation 3.27, if the force is specified as a force per unit area or pressure  $p(\omega)$ , then  $W$  may be considered to be the weight per unit area,  $w$ . It will also be convenient to substitute frequency in Hz ( $f$ ) for frequency in radians ( $\omega$ ). This will not change the value of  $H(\omega)$  since it is only a function of a frequency ratio and damping.

### 3.2.1.5 Force and Motion Transmissibility

The single degree-of-freedom system in Figure 3.3 has been analyzed, so far, only in terms of the absolute displacement  $x(t)$  of the mass for a force  $P(t)$  applied to the mass. Clearly, the velocity and acceleration response to this same excitation can also be determined by differentiating the displacement response equations - once to obtain the velocity response and twice to obtain the acceleration response. All three response relationships will be shown, later on, to be applicable for analyzing the stress, sound transmission and inertial loads of a wall due to excitation by acoustic pressures.

However, there is another response function which is desired for the simple damped mass-spring system in Figure 3.3. This is the force  $P_T(t)$  transmitted through the system to its foundation. This force is developed by the displacement of the spring and the velocity of the viscous damper and can be expressed by

$$P_T(t) = c\dot{x}(t) + kx(t) \quad (3.28)$$

Restricting consideration to steady state sinusoidal excitation only, then by substituting Equation 3.19 in the above expression, and utilizing the definitions for  $H(\omega)$

from Equation 3.23 and  $\delta$  from Equation 3.6, and the transformations in Equation 3.21, the ratio of the magnitudes of the transmitted force  $P_T(\omega)$  to the driving force  $P(\omega)$  is given by:

$$T(\omega) = \frac{P_T(\omega)}{P(\omega)} = \sqrt{\frac{1 + (2\delta\omega/\omega_0)^2}{(1 - (\omega/\omega_0)^2)^2 + (2\delta\omega/\omega_0)^2}} \quad (3.29)$$

This ratio is called the force transmissibility of the system. It can be applied to the determination of reaction loads at the supports of a wall under acoustic excitation.

### Excitation of Foundation

Consider now the response of the same damped spring-mass system to an excitation of its foundation as illustrated in Figure 3.6. This is a simplified model of a vibration isolation system or a similar configuration involving excitation of a flexibly mounted mass through its foundation.

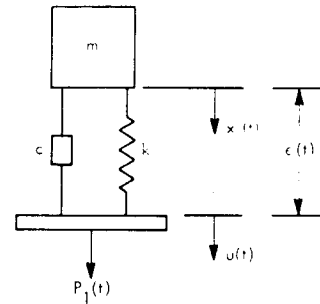


FIGURE 3.6 Single Degree-of-Freedom System with Excitation at Foundation

Several response variables are of interest. The most obvious is the motion of the mass for a given motion of the foundation. The equation of motion, in this case, becomes

$$m\ddot{x}(t) + c\dot{x}(t) + kx(t) = c\dot{u}(t) + ku(t) \quad (3.30)$$

where

$u(t), \dot{u}(t)$  = displacement and velocity, respectively, of the foundation.

The steady state (or particular integral) solution for this equation is well known (e.g. - References 3.1, 3.3, 3.6). It can be used to show that the motion transmissibility, or ratio of magnitudes of the mass displacement, velocity or acceleration to the corresponding motion variable for the foundation is exactly equal to the expression in Equation 3.29 for the force transmissibility. Thus, the ratio of steady state response/input amplitudes is

$$\frac{x(\omega)}{u(\omega)} = \frac{\dot{x}(\omega)}{\dot{u}(\omega)} = \frac{\ddot{x}(\omega)}{\ddot{u}(\omega)} = T(\omega) \quad (\text{See Equation 3.29})$$

This transmissibility,  $T(\omega)$ , is plotted in Figure 3.7 as a function of the relative frequency  $\omega/\omega_0$ . Note that this function is significantly different from the dynamic magnification factor,  $H(\omega)$  in Figure 3.5(a). For low damping, the transmissibility has essentially the same magnitude as  $H(\omega)$  when  $\omega/\omega_0 = 1$  so that the maximum value is

$$T(\omega) \Big|_{\max} \approx 1/2\delta = Q \quad (3.31)$$

where  $Q$  = resonant amplification factor.

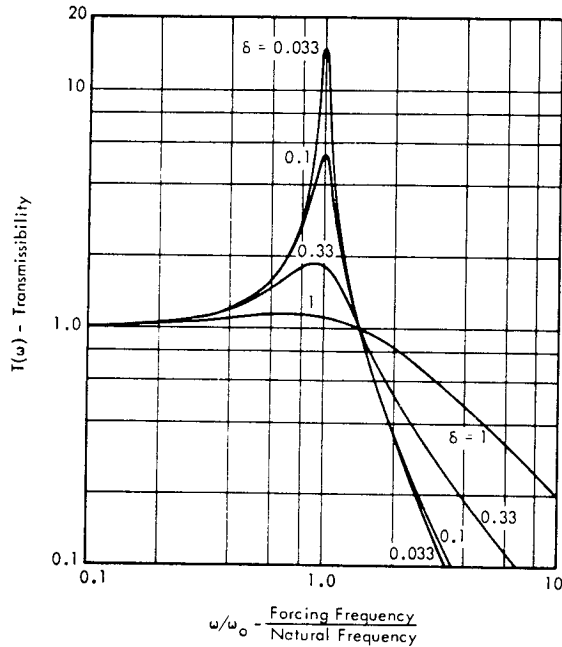


FIGURE 3.7 Force or Motion Transmissibility of a Linear Viscous Damped Single Degree-of-Freedom System

However, above resonance, the transmissibility curve has a very different shape. It passes through 1.0 at  $\omega/\omega_0 = \sqrt{2}$  and decreases above this frequency at a rate which depends on damping. For high damping ( $\delta \rightarrow 1$ ), the decrease is roughly proportional to  $1/\omega$  instead of  $1/\omega^2$  as in Figure 3.5(a). Further theoretical and practical aspects of vibration isolation are given in Chapters 9 and 11.

3.2.1.6 Summary of Transfer Functions for Single Degree-of-Freedom System to Sinusoidal Excitation

Fortunately, the two basic functions,  $H(\omega)$ , given by Equation 3.23, and  $T(\omega)$ , given by Equation 3.29, form the basis for all other sinusoidal transfer functions of interest for the single degree-of-freedom system driven by a force at its mass or by a motion or force at its foundation. The steady state transfer functions of practical significance are briefly summarized in Figure 3.9 in a matrix of input-response relationships which depend upon the relative frequency parameter  $\omega/\omega_0$  and the critical damping ratio

$\delta$ . The matrix includes a definition of the relationship between the relative displacement of the spring and damper (a measure of the stress in a support structure) and the input excitation to the foundation. In this case, the equation of motion of the system can be expressed as

$$m\ddot{\epsilon}(t) + c\dot{\epsilon}(t) + k\epsilon(t) = -m\ddot{u}(t) \quad (3.32)$$

where

$\epsilon(t)$  = the relative displacement of the spring

and

$\ddot{u}(t)$  = the absolute acceleration of the foundation.

For those transfer functions which exhibit a resonant peak, the maximum value of the frequency-dependent part of functions is equal to  $1/2\delta \approx Q$  at resonance, for the degree of damping normally encountered in vibration design ( $Q > 3$ ). However, the change in these transfer functions, above or below resonance, varies widely, depending on the particular input-output variables involved.

3.2.2 RESPONSE OF THE SINGLE DEGREE-OF-FREEDOM SYSTEM TO TRANSIENT INPUTS

The next type of excitation to be considered will be the transient inputs which simulate structural loads imposed by explosions and sonic boom overpressures. These types of loads can be approximated by relatively simple transient pulses without a large number of oscillations such as occur for earthquake loads on buildings. This usually makes it possible to neglect the effects of damping on the response of a simple mass-spring system to such loads.

The significance of damping on the transient response of a simple mass-spring system is illustrated in Figure 3.8. This shows the maximum dynamic response  $x_{\max}$ , with damping, relative to the undamped response for two extreme forms of a transient input - an impulse and a unit step input. For typical critical damping ratios of .02 - .1, the maximum damped response is within 80 percent of the undamped response.

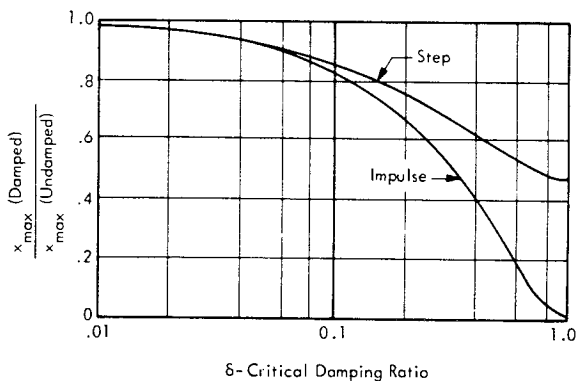


FIGURE 3.8 Relative Effect of Damping on Maximum Response of Single Degree-of-Freedom System to Step Input and Impulse Input

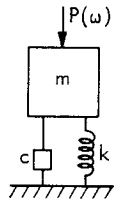
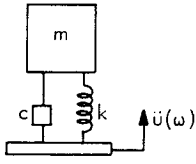
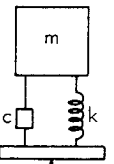
INPUT →		Force Input to Mass	Acceleration Input to Base	Force Input to Base
RESPONSE ↓				
MULTIPLY INPUT →				
BY ↙				
TO OBTAIN ↓				
a(omega)  ↘				
Absolute Motion of Mass	$x(\omega)$ $\dot{x}(\omega)$ $\ddot{x}(\omega)$	$H(\omega)/k$ $(\omega/\omega_o)H(\omega)/\omega_o m$ $-(\omega/\omega_o)^2 H(\omega)/m$	$T(\omega)/\omega^2$ $T(\omega)/\omega$ $T(\omega)$	$(\omega_o/\omega)^2/k$ $1/\omega m$ $1/m$
Absolute Motion of Base	$u(\omega)$ $\ddot{u}(\omega)$	NA NA	$1/\omega^2$ 1	$(\omega_o/\omega)^2/T(\omega) \cdot k$ $1/T(\omega) \cdot m$
Relative Motion of Spring-Damper	$\epsilon(\omega)$	$H(\omega)/k$	$H(\omega)/\omega_o^2$	$H(\omega)/T(\omega) \cdot k$
Force Trans. to Base	$P_T(\omega)$	$T(\omega)$	NA	NA
Legend: $\omega_o = \sqrt{k/m}$ , $\delta = c/2\omega_o m$ $H(\omega) = 1/\sqrt{[1 - (\omega/\omega_o)^2]^2 + (2\delta\omega/\omega_o)^2}$ <sup>1/2</sup> $T(\omega) = [1 + (2\delta\omega/\omega_o)^2]$ <sup>1/2</sup> · H(ω) NA - Not Applicable $H(\omega) _{\max} = 1/2\delta \sqrt{1 - \delta^2}$ at $\omega = \omega_o \sqrt{1 - 2\delta^2}$ $T(\omega) _{\max} \approx \sqrt{1 + 4\delta^2/25}$ at $\omega = \omega_o \sqrt{1 + 8\delta^2/25}$ For $\delta < 0.3$ $H(\omega) _{\max} \approx T(\omega) _{\max} \approx 1/2\delta = Q$				

FIGURE 3.9 Summary of Absolute Value of Steady State Sinusoidal Transfer Functions |a(ω)| for Sinusoidal Excitation of Single Degree-of-Freedom System. Amplitude of Response Variable is equal to Amplitude of Input Variable Times |a(ω)|. (The complex value of H(ω) will be identified in subsequent sections by H(f).)

Resonance Frequency and Natural Frequency

As shown in the legend in Figure 3.9, the maximum value of the dynamic magnification factor,  $H(\omega)|_{\max}$  occurs at the resonance frequency  $\omega_r = \omega_o \sqrt{1 - 2\delta^2}$ . A slightly different resonance frequency is shown for the maximum value of the transmissibility  $T(\omega)|_{\max}$ .

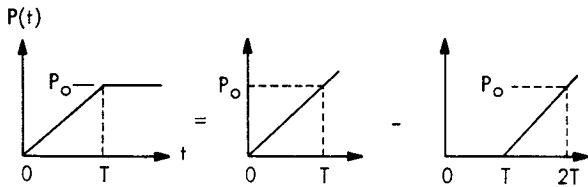
For other input-response combinations given in Figure 3.9, similar resonant frequencies can be defined. However, for the usual amounts of damping, these various resonance fre-

quencies are practically the same as the undamped natural frequency  $\omega_o$  or the damped natural frequency  $\omega_d = \omega_o \sqrt{1 - \delta^2}$ . Throughout the rest of this manual, therefore, these minor differences in frequency will be ignored and the term resonance frequency will be used freely to identify the true resonance frequency where the response is a maximum, or the natural frequency. It will be specified, as convenience dictates, in terms of rad/sec ( $\omega_o$ ) or Hz ( $f_o = \omega_o/2\pi$ ). Similarly, the maximum value of the nondimensional response function (i.e. -- H(ω), T(ω), etc.) will be assumed to be equal to 1/2δ or Q.



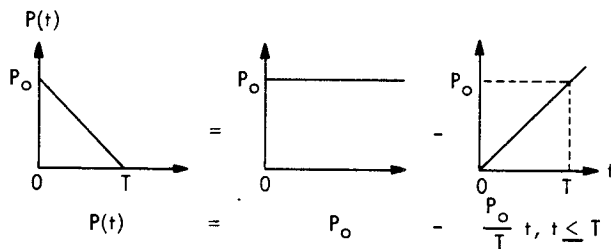
3.2.2.1 Superposition Principle

For a linear system, the response to the sum of a series of inputs is the sum of the responses to each input. If necessary, one or more of the inputs may be delayed to make up the overall input. For example, a ramp step input with a rise time  $T$  may be defined by a positive ramp starting at time  $t = 0$  minus a ramp with the same slope starting at time  $t = T$ , as shown in the following diagram.



The response to the delayed ramp is obtained by replacing  $t$  by  $(t - T)$  in the response equation for the ramp and then adding to this the response due to the first ramp input which starts at  $t = 0$ .

For the triangular pulse, the input, during the time  $0 < t < T$ , may be described as shown below.



3.2.2.2 Response to Triangular Pulse

It will be shown subsequently that a simple triangular pulse with an instantaneous rise is a useful approximation for a blast overpressure pulse. Response to this type of pulse is therefore discussed in some detail.

The forced response to the step input minus the forced response to the ramp input defines the forced response for the triangular pulse during the duration of the pulse. Therefore, subtracting Equation (3.17) from (3.16), the forced response for the damped system can be expressed as

$$\frac{x(t)}{x_s} = 1 - \frac{t}{T} + \frac{2\delta}{\omega_o T} - \frac{e^{-\delta\omega_o t}}{\omega_o T} \beta \cos(\omega_d t - \phi) \quad (3.33)$$

where

$$\beta = \left[ \frac{1 + 2\delta\omega_o T + (\omega_o T)^2}{1 - \delta^2} \right]^{1/2}$$

$$\phi = \tan^{-1} \frac{2\delta^2 + \delta\omega_o T - 1}{(\omega_o T + 2\delta)\sqrt{1 - \delta^2}}$$

and  $x_s = P_o/k$  = static response of system to a static load equal to the maximum value  $P_o$ .

For an undamped system, this reduces to

$$\frac{x(t)}{x_s} = 1 - \frac{t}{T} + \sqrt{1 + (1/\omega_o T)^2} \sin(\omega_o t - \tan^{-1} \omega_o T) \quad (3.34)$$

Following the end of the triangular pulse, the mass-spring system is free to vibrate at its natural frequency. Providing the duration of the pulse is not much greater than the period of the mass-spring system, damping will not significantly influence the magnitude of the first peak reached during this period of free oscillation called the residual response region.

Residual Response To Triangular Pulse

The displacement and velocity at the end of the forced excitation is given by Equations 3.33 or 3.34 for  $t = T$ . Applying these values as initial conditions for the residual or free vibration, and using Equation 3.8, with  $\delta = 0$ , the residual response for the undamped system can be reduced to

$$\frac{x_r(t)}{x_s} = x(T) \cos \omega_o (t - T) + \frac{\dot{x}(T)}{\omega_o} \sin \omega_o (t - T)$$

or, for  $t \geq T$ ,

$$\frac{x_r(t)}{x_s} = \left[ 1 - \frac{2 \sin \omega_o T}{\omega_o T} + \frac{\sin^2 \omega_o T/2}{(\omega_o T/2)^2} \right]^{1/2} \sin(\omega_o t - \theta) \quad (3.35)$$

$$\theta = \tan^{-1} \frac{\omega_o T - \sin \omega_o T}{1 - \cos \omega_o T}$$

Equations 3.34 and 3.35 can now be used to determine an envelope of the peak response to the triangular pulse regardless of when the peaks occur. This envelope of maxima provides a suitable basis for designing structure to this type of transient load.

Maximum Amplitude of Forced Response

Consider only the undamped case. As shown in Figure (3.8), usual values of damping have a minor effect on the peak response to simple transient inputs.

The maximum amplitude occurs when the velocity is zero. Differentiating Equation 3.34 and setting it to zero,

$$\frac{\dot{x}(t)}{x_s} = -\frac{1}{T} \left[ 1 - \cos \omega_o t - \omega_o T \sin \omega_o t \right] = 0$$

or  $\sin \frac{\omega_o t}{2} \left[ \sin \frac{\omega_o t}{2} - \omega_o T \cos \frac{\omega_o t}{2} \right] = 0$

This has two roots for positive and negative peaks given by

$$\left. \begin{aligned} \omega_o t_{\max} &= 2 \tan^{-1} \omega_o T \\ \omega_o t_{\min} &= 2\pi n, \quad n = 1, 2, \text{ etc.} \end{aligned} \right\} (3.36)$$

Substituting these back into Equation 3.34, the maximum and minimum instantaneous values of the forced response are defined by

$$\frac{x_{\max}}{x_s} = +2 \left[ 1 - (\tan^{-1} \omega_o T) / \omega_o T \right] \quad (3.37a)$$

$$\frac{x_{\min}}{x_s} = -2\pi n / \omega_o T \quad (3.37b)$$

In this case, the absolute value of the negative peaks will be always less than the positive peaks for all values of  $\omega_o T$ .

Maximum Amplitude of Residual Response

The amplitude of the residual response is already given by Equation (3.35). The time of maximum residual response is found, in the same manner as above, to be:

$$\omega_o t_{\max} = \tan^{-1} \frac{\cos \omega_o T - 1}{\omega_o T - \sin \omega_o T} \geq \omega_o T \quad (3.38)$$

Displacement Shock Spectrum for Triangular Pulse

The combined envelope of the maximum response amplitudes of the simple mass-spring system during both the forced and free vibration phases is called the shock spectrum. This envelope, normalized by the static response  $x_s$ , is illustrated in Figure 3.10 for the undamped system and is based on Equations 3.35, 3.37, and 3.38. The time of occurrence for positive peaks during the forced and free response is shown in Figure 3.11. As indicated by these figures, the maximum forced response during the pulse is equal to or greater than the residual response for all values of relative response greater than 1. This is not a general rule, however, for all pulse shapes.

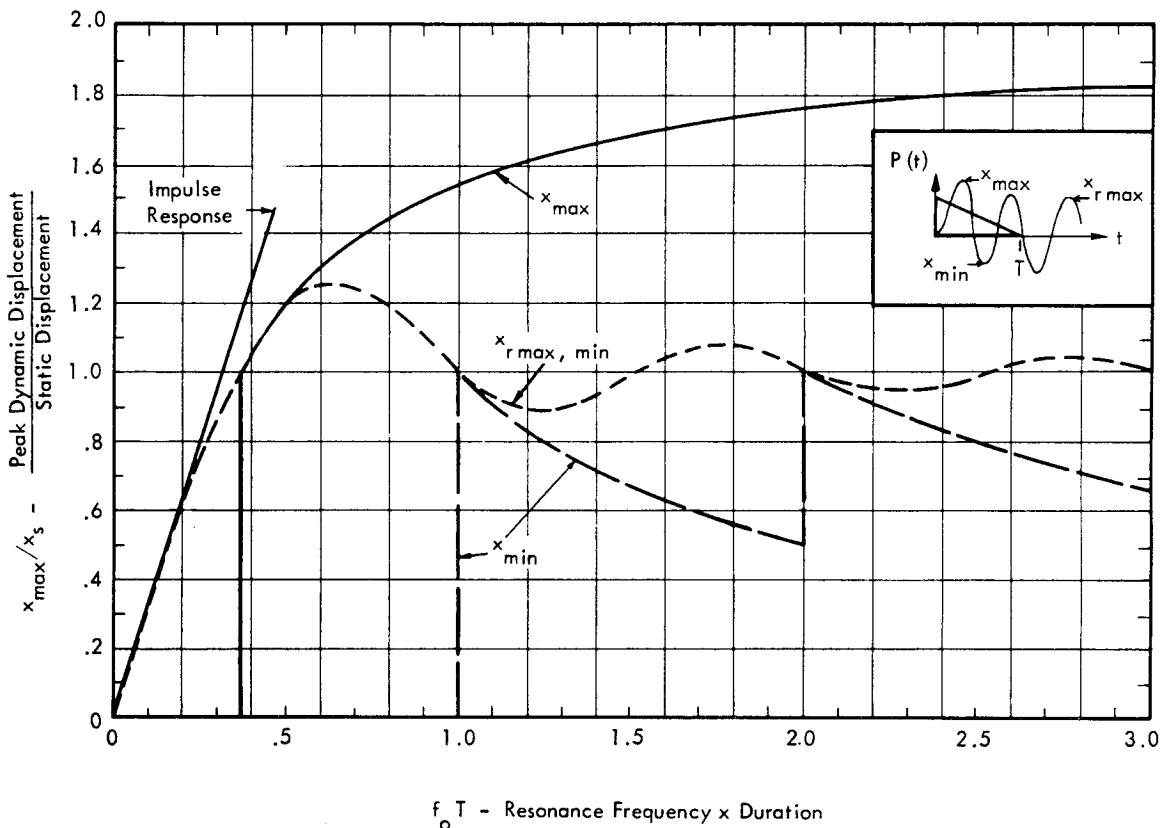


FIGURE 3.10 Normalized Shock Spectra for Triangular Pulse For Simulation of Blast Loading

This shock response spectra, normalized by the static response, provides the basic dynamic load factor for this pulse shape and is widely used for blast load analysis.

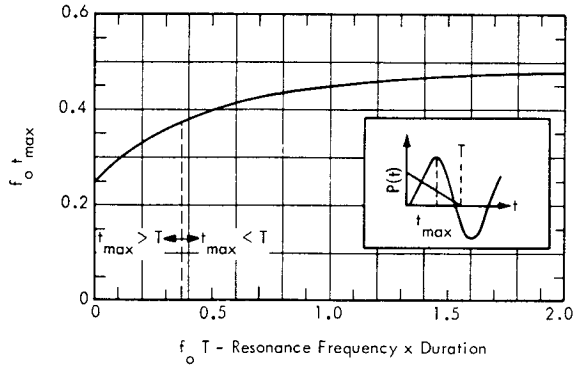


FIGURE 3.11 Time of Occurrence of Maximum Positive Response to Triangular Pulse Multiplied by the Resonance Frequency,  $f_o$ , of the Mass-Spring System

Approximation of Shock Response by Impulse Response

For shock inputs with a duration less than one-fourth the natural period of the system being excited, the input may be approximated by an impulse with the same total impulse as the actual shock. For the triangular pulse, the impulse,  $I$ , is

$$I = \int P(t) dt = P_o T/2$$

The response to this impulse, or to any impulse  $I$  which has only a positive phase (i.e. - load is always positive), is purely a residual or free vibration response with a maximum amplitude given by

$$x_{r \max} = \frac{I}{\omega_o m} = \frac{I \omega_o}{k}$$

For the triangular pulse,  $I$  is equal to  $P_o T/2$ , so that the maximum response, relative to the static response,  $x_s = P_o/k$ , is

$$\frac{x_{r \max}}{x_s} = \frac{\omega_o T}{2} = \pi f_o T \tag{3.39}$$

This impulse response is shown on Figure 3.10, and as expected, agrees very closely with the true shock spectra for the product of resonance frequency times duration of the pulse less than 0.25. This is the approximate upper bound of validity for the impulse response approximation for all pulse shapes with a positive phase only.

3.2.2.3 Acceleration Response to Triangular Pulse

The displacement response to a triangular pulse provides a basic design tool for analyzing dynamic stress in structures loaded by blast waves. It is also desirable to define the acceleration response to this type of load since acceleration or inertial loads on secondary structure or equipment attached to a blast-loaded wall can also represent a significant dynamic load problem.

For steady state sinusoidal excitation of a linear system, the peak acceleration response is simply equal to  $-(2\pi f_o)^2$  or  $-\omega_o^2$  times the peak displacement response. However, for transient loads, this is no longer valid during the time the load is acting.

Maximum Acceleration Response During Forced Response

During the forced excitation by a triangular pulse, the acceleration  $\ddot{x}(t)$ , is equal to the second derivation of the displacement time history given by Equation 3.34. After simplification by using the transformations given in Equation 3.21, the result can be given in non-dimensional form as

$$\frac{\ddot{x}(t)}{\omega_o^2 x_s} = - \left[ \frac{\sqrt{1 + (\omega_o T)^2}}{\omega_o T} \right] \sin(\omega_o t - \phi) \tag{3.40}$$

where

$$\phi = \tan^{-1} \omega_o T$$

The time history of acceleration computed by this expression is compared in Figure 3.12 with the time history of the displacement response for the case of  $\omega_o T = 4\pi$  or  $f_o T = 2$ . The time scale is normalized by the duration of

the pulse. The normalizing factor in Equation 3.40 is the product of the square of the resonance frequency  $\omega_o$  and the static displacement  $x_s$ . The latter is the displacement which would occur for steady application of the peak value of the load. The reason for choosing this pseudo-acceleration to normalize the acceleration response is clarified by noting, in Figure 3.12, that the initial acceleration, at  $t = 0$ , is just equal to this parameter or  $\ddot{x}(0)/\omega_o^2 x_s = 1$ . This is also readily apparent by examining the basic equation of motion of the system (Equation 3.5) at time 0. If the system starts at rest, then this equation reduces to

$$\ddot{x}(0) = \frac{P(0)}{m} = \omega_o^2 x_s \text{ for } t = 0 \quad (3.41)$$

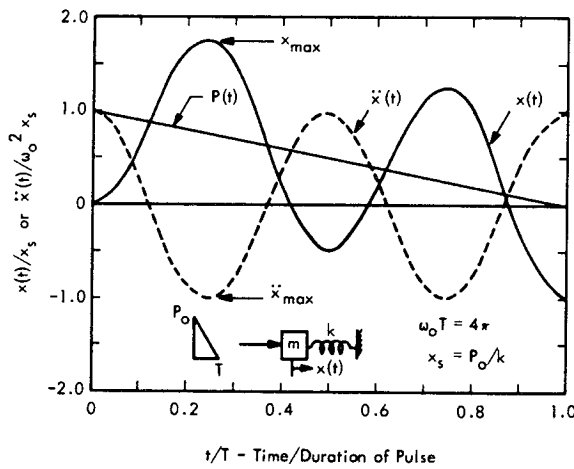


FIGURE 3.12 Comparison of Displacement and Acceleration Forced Response of an Undamped Spring-Mass System to a Triangular Pulse

As shown in Figure 3.12, the next peak acceleration after  $t = 0$  is a minimum and, for the case chosen, has a magnitude only slightly greater (by 0.3 percent) than the initial acceleration. The envelope of the maximum acceleration response during the forced motion for any value of the parameter  $\omega_o T = 2\pi f_o T$ , is given by the term in brackets in Equation 3.40 which is simply the amplitude of the sinusoidal acceleration. The time of occurrence  $t_{max}$  of an acceleration peak during the forced response period can be expressed as

$$f_o t_{max} = \frac{1}{4} + \frac{\tan^{-1} \omega_o T}{2\pi} \quad (3.42)$$

However,  $t_{max}$  can not exceed  $T$  if the acceleration peak is to occur during the forced response period. Thus, negative acceleration peaks are not possible for  $f_o T < 0.45$ .

When this limiting value is inserted in the term in brackets in Equation 3.40, it is found that the maximum value of

an acceleration peak (actually a negative acceleration peak) that can occur during the forced response period is

$$x_{max}|_{max} = 1.06 \omega_o^2 x_s |_{f_o T = 0.45} \quad (3.43)$$

Maximum Acceleration During Residual Response

During the residual response period of free vibration, the motion is purely sinusoidal and the acceleration  $\ddot{x}_r(t)$  is now equal to  $-\omega_o^2 x_r(t)$  where  $x_r(t)$  is the residual displacement response specified by Equation 3.35. The envelope of the maximum acceleration following the pulse, when normalized by  $\omega_o^2 x_s$ , is the same as the envelope of the normalized residual displacement response or

$$\frac{\ddot{x}_{rmax}}{\omega_o^2 x_s} = \frac{x_{rmax}}{x_s} \quad (3.44)$$

Acceleration Shock Spectrum for Triangular Pulse

Based on the concepts outlined above, the envelope of maximum acceleration response to a triangular pulse may be constructed by superimposing the envelopes of maximum acceleration for both the forced and residual response periods. The result, shown in Figure 3.13, indicates that the maximum possible acceleration occurs during the residual response period for  $f_o T = 0.625$  and is equal to  $1.26 \omega_o^2 x_s$ .

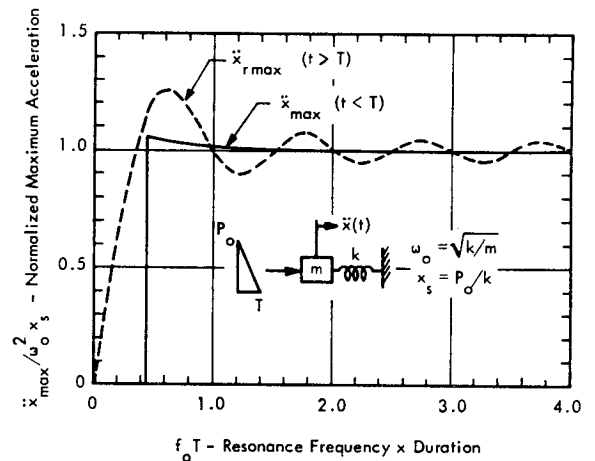


FIGURE 3.13 Acceleration Shock Spectrum for a Triangular Pulse Applied to Mass of Undamped Mass-Spring System

The time of occurrence of the maximum negative acceleration during the forced response period, given by Equation 3.42, is slightly greater than the time of maximum positive displacement as shown in Figure 3.11. The difference is less than 5 percent, however, for  $f_o T > 1$ . During the residual response period, the displacement and acceleration peaks occur simultaneously, but again, with opposite sign. Therefore, Figure 3.11 may be used to define the time of occurrence of maximum negative acceleration peaks with negligible error. The time of occurrence of either the peak displacement or acceleration response can be useful for two purposes: 1) to correct the undamped shock spectrum for damping effects and 2) evaluate the effect of loading rate on failure loads on structure. This latter effect will be discussed in Chapter 5.

A correction for the effect of damping can be carried out by reducing the oscillatory part of the transient response by the exponential damping term,  $e^{-2\pi \delta f_o t_{max}}$ , where  $\delta$  is the damping ratio and  $f_o t_{max}$  is the normalized time of maximum response given by Figure 3.11. Consider, however, the comparison in Figure 3.14 of the damped displacement shock spectrum for the triangular pulse carried out by 1) an exact analysis and 2) by simply applying the damping correction factor indicated in Figure 3.9. This indicates that the latter provides a sufficiently accurate correction for the effect of damping and also shows that the correction, itself, is small for this type of shock pulse thus justifying the use of an undamped system for the shock spectrum analysis.

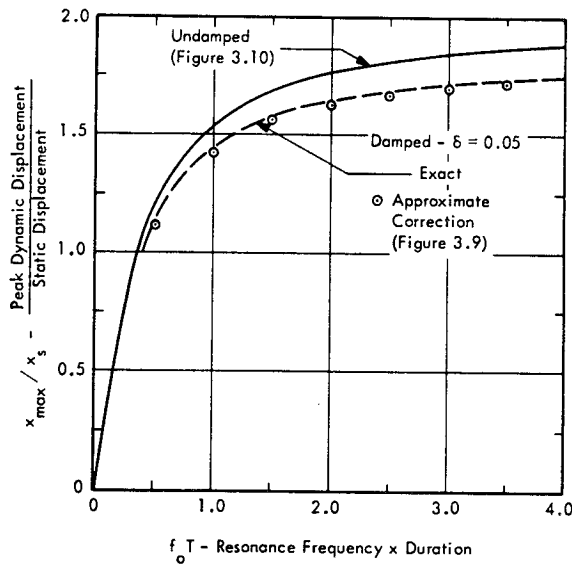


FIGURE 3.14 Comparison of Undamped and Damped Displacement Shock Spectrum for Triangular Pulse Applied to Mass of Single Degree-of-Freedom System.

3.2.2.4 Alternate Methods of Defining Transient Response

Other methods for solution of transient response problems which are frequently employed are:

- Fourier Transform Method
- Laplace Transform Method
- Numerical Integration Method
- Phase-Plane Graphical Method
- Electrical Analog Computer Method

An example of the application of the first two methods, which are related, will be given in the next section. Application of the numerical integration method is made in Section 2 of Chapter 8 for the analysis of the response of complex building structure to blast loads. The phase-plane graphical method provides a useful method for analysis of the response of simple mass-spring systems to complex shock inputs which can not be readily described analytically. Most of the transient sonic loads considered in this manual do not fall in this category since idealized models for the pressure time history are assumed. For the one exception in Chapter 8, where analysis of more complex shock inputs is carried out, the structural system is too complex for efficient utilization of graphical methods. In this case, numerical integration methods are used to solve the equations of motion of the system. For a more complete discussion of application these various methods, the reader is referred to standard texts on vibration theory. Chapters 8, 23, 28 and 29 of Reference 3.1 are particularly useful.

3.2.2.5 Application of Fourier Transform

The pressure time history of a blast, as observed at a remote distance, can be approximated more accurately than by the triangular pulse, by the classical expression for a blast wave equal to

$$P(t) = P_o \left[ 1 - t/T \right] e^{-t/T} \tag{3.45}$$

where  $T$  is the characteristic duration for the blast pressure pulse as shown in Figure 3.15. However, the following analysis will show that the shock spectra for a triangular

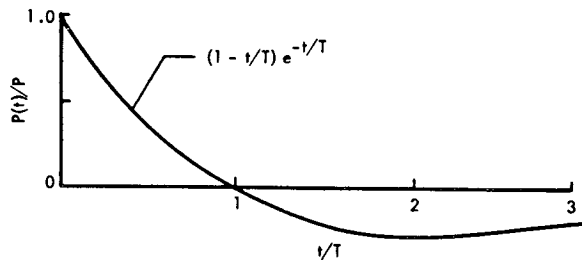


FIGURE 3.15 Classical Definition of Blast Wave Shock Pulse

pulse is, in fact, sufficiently accurate for many blast design problems. The analysis is used to illustrate application of the Fourier and Laplace Transform methods to shock or transient response problems.

Fourier Series and Fourier Spectrum

Any physical event which can be described by a repetitive or periodic function of time  $f(t)$  can also be described by the summation of an infinite series of sine and cosine terms each of which have a frequency  $n\omega_o$  equal to an integral multiple  $n$  of the basic repetition frequency,  $\omega_o$ . This series is known as the Fourier Series and can be expressed in the form

$$f(t) = \frac{a_o}{2} + \sum_{n=1}^{\infty} [a_n \cos n\omega_o t + b_n \sin n\omega_o t] \tag{3.46}$$

The first term  $a_o/2$  is the mean value of the function  $f(t)$ . The constants  $a_n$  and  $b_n$  are the Fourier coefficients which define the amplitude of the  $n$ -th cosine and sine terms and are given by

$$a_n = \frac{2}{t_o} \int_{-t_o/2}^{+t_o/2} f(t) \cos n\omega_o t dt \tag{3.47}$$

$$b_n = \frac{2}{t_o} \int_{-t_o/2}^{+t_o/2} f(t) \sin n\omega_o t dt$$

$n=0, 1, 2, \dots$

$$t_o = 2\pi/\omega_o = \text{period of cyclic event}$$

Note that the first term  $a_o/2$ , can also be determined from the first integral in Equation 3.47 since for  $n = 0$ , the latter reduces to the equation for the mean value

$$\frac{a_o}{2} = \frac{1}{t_o} \int_{-t_o/2}^{+t_o/2} f(t) dt$$

The sine and cosine terms of the same frequency can be combined so that the  $n$ th discrete frequency component of this series can be specified by its amplitude  $C(n\omega_o)$  and phase  $\gamma(n\omega_o)$ , in the form

$$f_n(t) = C(n\omega_o) \cos [n\omega_o t - \gamma(n\omega_o)] \tag{3.48}$$

where  $C(n\omega_o) = \sqrt{a_n^2 + b_n^2}$

and  $\gamma(n\omega_o) = \tan^{-1} b_n/a_n$

The frequency interval between any two of these terms is simply the basic repetition frequency  $\omega_o/2\pi = 1/t_o$ . Note also that each of these frequency components represents a steady state sinusoidal excitation.

When the event happens only once, as for a single transient, the period  $t_o$  approaches infinity or, conversely, the repetition frequency  $\omega_o$  approaches zero. In such a case, the transient can be considered as a "series" where the frequency interval between components,  $1/t_o$ , approaches the differentially small quantity  $d\omega/2\pi$  and the discrete frequency  $n\omega_o$  becomes the continuous frequency variable  $\omega$ . If Equation 3.47 is substituted in Equation 3.46 for the terms  $a_n$  and  $b_n$  and the limiting conditions that  $1/t_o \rightarrow d\omega/2\pi$ ,  $n\omega_o \rightarrow \omega$ , and  $t_o \rightarrow \infty$  are applied, the series becomes an integral which can be expressed in the form

$$f(t) = \frac{1}{\pi} \int_0^{\infty} [A(\omega) \cos \omega t + B(\omega) \sin \omega t] d\omega \tag{3.49}$$

where the terms  $A(\omega)$  and  $B(\omega)$  now define the amplitude of the continuous distribution of spectral components and are given by

$$A(\omega) = \int_{-\infty}^{+\infty} f(t) \cos \omega t dt \tag{3.50}$$

$$B(\omega) = \int_{-\infty}^{+\infty} f(t) \sin \omega t dt$$

Although the integration limits are shown as  $\pm$  infinity in this equation, the actual duration of the transient is used for the limits in any given case. As before, the amplitude and phase angle of this spectrum, called the Fourier spectrum, are given by

$$|F(\omega)| = \sqrt{[A(\omega)]^2 + [B(\omega)]^2} \tag{3.51}$$

$$\theta(\omega) = \tan^{-1} B(\omega)/A(\omega)$$

The similarity between Equations 3.46 - 3.48 for the Fourier series and Equations 3.49 - 3.51 for the Fourier spectrum is clear and helps to provide a clearer understanding of the physical significance of the Fourier spectrum. The essential difference between the Fourier series and the Fourier spectrum lies in the discrete frequency content of the former versus the continuous frequency spectrum of the latter. This is illustrated in Figure 3.16 for a continuous and single sawtooth or N wave. In both cases, however, the frequency components correspond to steady-state sinusoidal components which extend from  $t = -\infty$  to  $t = +\infty$ .

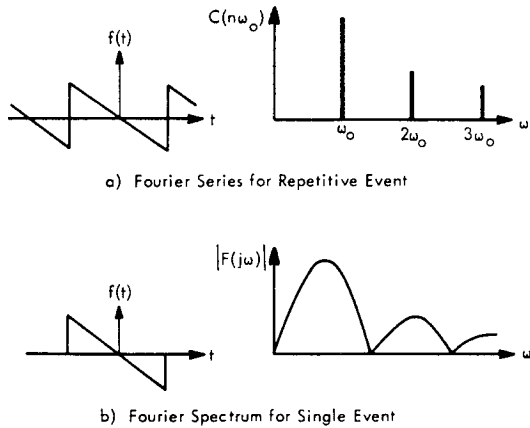


FIGURE 3.16 Comparison of Time History and Frequency Spectrum of Repetitive and Single Sawtooth Wave

A more conventional form of Equations 3.50 and 3.51 is based on the use of complex vector notation to represent the amplitude and phase of the frequency spectrum (References 3.10 and 3.11). Thus, Equation 3.51 becomes

$$F(j\omega) = A(\omega) - j B(\omega) = |F(j\omega)| e^{-j \gamma(\omega)} \quad (3.52)$$

where  $j = \sqrt{-1}$ , the imaginary unit vector and  $|F(j\omega)| = \text{absolute value of } F(j\omega)$ .

The Fourier spectrum is then given in the usual complex form, known as the Fourier Transform, by

$$F(j\omega) = \int_{-\infty}^{+\infty} f(t) e^{-j\omega t} dt \quad (3.53)$$

Equation 3.50 provides equivalent results, however, and was stated first to introduce the Fourier spectrum in a form closely comparable to the well-known Fourier Series without resort to complex vector notation.

Equation 3.49, in complex notation, is the Fourier Integral given by

$$f(t) = \frac{1}{2\pi} \int_{-\infty}^{+\infty} F(j\omega) e^{j\omega t} d\omega \quad (3.54a)$$

or, in a form which avoids the integration over physically meaningless negative frequencies,

$$f(t) = \text{Real Part of} \left[ \frac{1}{\pi} \int_0^{\infty} F(j\omega) e^{j\omega t} d\omega \right] \quad (3.54b)$$

It should be emphasized that Equations 3.54 and 3.49 give identical results. The real part of the product of the

complex quantities  $F(j\omega)$  and  $e^{j\omega t}$  in Equation 3.54 integrate to give the same real value of  $f(t)$  given by the trigonometric form in Equation 3.49.

Now that it has been established that a single transient excitation can be represented by a continuous spectrum of steady state sinusoidal frequency components, one might intuitively expect that solutions for the steady state response of a system can be used to determine the transient response through application of the Fourier transform. This is indeed the case and represents the principal strength of this method.

The primary applications of the Fourier transform or Fourier spectrum to transient response problems can be stated as follows.

- The Fourier spectrum  $R(j\omega)$  of the response of a linear system to any input excitation  $P(t)$  is equal to the product of the Fourier spectrum of the input  $P(j\omega)$  and the complex sinusoidal transfer function  $a(\omega)$  for the system.
- The time history corresponding to this response spectrum can be determined by taking the inverse Fourier transform of  $R(j\omega)$ .
- The Fourier spectrum of a shock pulse can be used to define the residual shock spectrum of an undamped single degree-of-freedom system to this pulse. This provides a simple and useful tool for engineering evaluation of shock response problems.

These three concepts will be illustrated by the following analysis of response to a classical blast wave.

Application of Fourier Spectrum to Classical Blast Wave

The first concept stated above may be expressed by

$$R(j\omega) = P(j\omega) \cdot a(\omega) = |P(j\omega)| |a(\omega)| e^{-j \gamma(\omega)} \quad (3.55)$$

where

$$P(j\omega) = |P(j\omega)| e^{-j \beta(\omega)} \text{ - complex value of Fourier Spectrum of excitation}$$

and

$$a(\omega) = |a(\omega)| e^{-j \theta(\omega)} \text{ - complex value of sinusoidal transfer function}$$

$$\gamma(\omega) = \beta(\omega) + \theta(\omega) \text{ - sum of phase angles of } P(j\omega) \text{ and } a(\omega), \text{ respectively.}$$

For a classical blast wave, the Fourier spectrum can be found by substituting the expression for the time history of the pulse  $P(t)$  given by Equation 3.45 into Equation 3.50 or 3.53. The absolute value of the resulting Fourier spectrum is

$$|P(j\omega)| = \frac{P_0}{\omega} \frac{(\omega T)^2}{1 + (\omega T)^2} \quad (3.56)$$

If the blast pulse is assumed to represent the input force to the mass of a single degree-of-freedom system, then  $P(j\omega)$  is the Fourier spectrum of this excitation. According to Equation 3.55, the Fourier spectrum of the displacement response of the mass is the product of  $P(j\omega)$  and the steady state transfer function  $\alpha(\omega)$ . The latter, in this case, can be considered as the steady state displacement response of the mass for a sinusoidal excitation. The absolute value of this sinusoidal transfer function has already been given earlier in Figure 3.9. (The complex value of  $\alpha(\omega)$  will also be required in this analysis and may be specified by  $|\alpha(\omega)| \exp[-j\theta(\omega)] = |\alpha(\omega)| [\cos \theta(\omega) - j \sin \theta(\omega)]$  where  $\theta(\omega)$  is the phase angle for the sinusoidal transfer functions given in Figure 3.8.) Thus, the absolute value of the Fourier spectrum of the displacement response of the mass to the classical blast wave pulse is

$$|X(j\omega)| = |R(j\omega)| = \frac{P_0}{k} \frac{(\omega T)^2 / [1 + (\omega T)^2]}{\left[ \left(1 - (\omega/\omega_0)^2\right)^2 + (2\delta\omega/\omega_0)^2 \right]^{1/2}} \quad (3.57)$$

The Fourier spectrum of the response to this pulse can be plotted for a given value of the damping constant  $\delta$ , and resonant frequency  $\omega_0$  of the single degree of freedom system, and for a particular duration  $T$  of the blast wave. Such a plot is shown in Figure 3.17 for the case  $\delta = 0.1$ ,  $\omega_0 T = 2$ . The broad peak, at an angular frequency  $\omega = 1/T$ , corresponds to the maximum value of the frequency spectrum of the input blast wave, while the sharp peak at  $\omega = 2/T$  corresponds to the resonance peak of the frequency response for the mass-spring system.

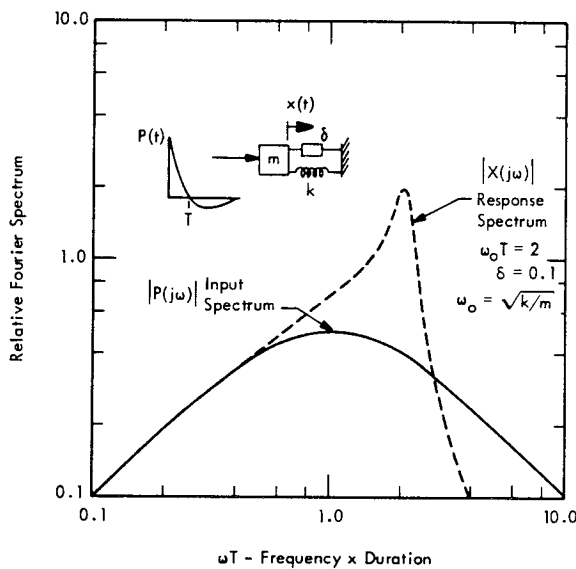


FIGURE 3.17 Fourier Spectrum of Classical Blast Wave and Displacement Response of a Single Degree-of-Freedom System

While such a plot can be helpful to illustrate the general nature of the frequency content of the response, it does not provide any indication of the actual time history or peak value of the response. This leads to consideration of the second point made earlier on application of the Fourier transform.

### 3.2.2.6 Application of Laplace Transform

If the complex form of the Fourier spectrum of the response, in Equation 3.57, is substituted into Equation 3.54, the required integration can be carried out to determine the time history of the displacement response. However, this integration is more readily accomplished by utilizing the Laplace Transform. The Laplace Transform  $F(s)$  of a function of time  $f(t)$  is given by (References 3.10, 3.12, and 3.13).

$$F(s) = \int_0^{\infty} f(t) e^{-st} dt \quad (3.58)$$

where  $s =$  complex Laplace variable  $= a + j\omega$ .

Comparing Equation 3.58 with the Fourier Transform given by Equation 3.53, it is clear that the two are identical providing: 1) the time function  $f(t)$  is zero for  $t < 0$ , and 2) the quantity  $a$  in the Laplace variable approaches zero. These conditions are, in fact, met in the solution of most engineering problems involving transients. Thus, for practical problems, the Fourier and Laplace Transforms yield identical results. However, the Laplace Transform has the advantage of more extensive usage and solutions for the Laplace Transform and its inverse are well known (References 3.1, 3.12 - 3.14).

To find the response time history to the classical blast wave, the Fourier spectrum for the response must first be given in complex form. This complex form, comparable to the absolute magnitude given in Equation 3.57, is

$$X(j\omega) = \frac{P_0}{k} \left[ \frac{j\omega T^2}{(1+j\omega T)^2} \right] \cdot \left[ \frac{1}{1 - (\omega/\omega_0)^2 + j2\delta\omega/\omega_0} \right] \quad (3.59)$$

The complex frequency  $j\omega$  in this equation is then replaced with the Laplace variable  $s$  using the transformation

$$s \rightarrow j\omega$$

The resulting algebraic expression in  $s$  is the Laplace Transform of the displacement response to the blast wave and has the form

$$X(s) = \frac{s \omega_0^2 P_0 / k}{\left(\frac{1}{T} + s\right)^2 (s^2 + 2\delta\omega_0 s + \omega_0^2)} \quad (3.60)$$

The inverse Laplace Transform, which defines the response time function  $x(t)$  corresponding to this Laplace Transform  $X(s)$ , is found in the literature (References 3.12 - 3.14) and can be shown to be



$$\frac{x(t)}{x_s} = \frac{(\omega_o T)^2}{D} \left\{ \left[ \frac{(\omega_o T)^2 - 1}{D} - \frac{t}{T} \right] e^{-t/T} + \frac{e^{-\delta \omega_o t}}{\sqrt{1-\delta^2}} \sin(\omega_o \sqrt{1-\delta^2} t + \psi) \right\} \quad (3.61)$$

where

$$D = (\omega_o T)^2 - 2\delta\omega_o T + 1$$

$$\psi = \tan^{-1} \frac{1-\delta^2}{-\delta^2} - 2 \tan^{-1} \frac{\omega_o T \sqrt{1-\delta^2}}{1-\delta\omega_o T}$$

$x(t)$  = dynamic displacement of mass at time  $t$

$x_s$  = static displacement of mass to peak pressure  $P_o$  of the blast wave.

Thus, by carrying out a simple integration to obtain the Fourier spectrum of the input using Equation 3.53, and employing the sinusoidal transfer function  $\alpha(\omega)$  for the system, then, with the aid of Laplace Transform tables, a solution to the response of a single degree-of-freedom system is obtained without resorting to the classical methods for determining the transient response.

A typical time history of the displacement response, given by Equation 3.61, is shown in Figure 3.18 for the case,  $f_o T = \omega_o T/2\pi = 0.5$  and  $\delta = 0$  (no damping). The graph is normalized by plotting the dynamic displacement relative to the peak pressure static displacement  $x_s$  and by using a time scale divided by the positive phase duration  $T$  of the classical blast wave. The peak displacement response obtained in this manner for the classical blast wave will be compared in the next section to the displacement shock spectra for the triangular blast pulse model analyzed in Section 3.2.2.2. First, however, it is desirable to consider the final point regarding application of the Fourier spectrum to transient response problems.

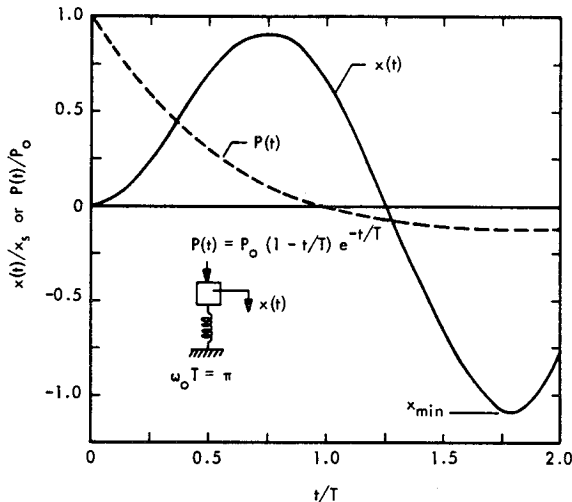


FIGURE 3.18 Typical Response of an Undamped Mass-Spring System to Excitation by a Classical Blast Wave Shock Pulse

### 3.2.2.7 Relationship Between Fourier Spectrum and Residual Shock Spectrum

A useful relationship exists between the Fourier spectrum of a transient excitation and the residual shock response spectrum of an undamped system for this transient excitation (Reference 3.1 - pp. 23-23). For a transient force excitation of the mass of a fixed-base mass-spring system, such as in Figure 3.3., this relationship can be expressed by the equation

$$\frac{\omega_o \cdot |P(j\omega_o)|}{P_o} = \frac{x_r \max}{x_s} \quad (3.62)$$

The left-hand side is the product of the mass-spring resonance frequency  $\omega_o$ , and the absolute value of the Fourier spectrum of the transient force at this frequency, normalized by its peak value  $P_o$ . This quantity is equal to the maximum residual displacement  $x_r \max$  of the mass normalized by the static displacement  $x_s$  to this peak force.

This relationship is illustrated in Figure 3.19 for a triangular shock pulse excitation. For verification, the time history for this pulse is inserted in the equation for the Fourier spectrum and normalized according to Equation 3.62. The left-hand side of this equation then becomes

$$\frac{\omega_o |P(j\omega_o)|}{P_o} = \omega_o \left| \int_0^T (1-t/T) e^{-j\omega t} dt \right|_{\omega = \omega_o}$$

$$= \left[ 1 - \frac{2}{\omega_o T} \sin \omega_o T + \frac{\sin^2 \omega_o T/2}{(\omega_o T/2)^2} \right]^{1/2} \quad (3.63)$$

The right side of Equation 3.63, in this case, is the residual displacement shock spectrum for this type of pulse. This can be verified by noting the identity of Equation 3.63 with the amplitude term in Equation 3.35.

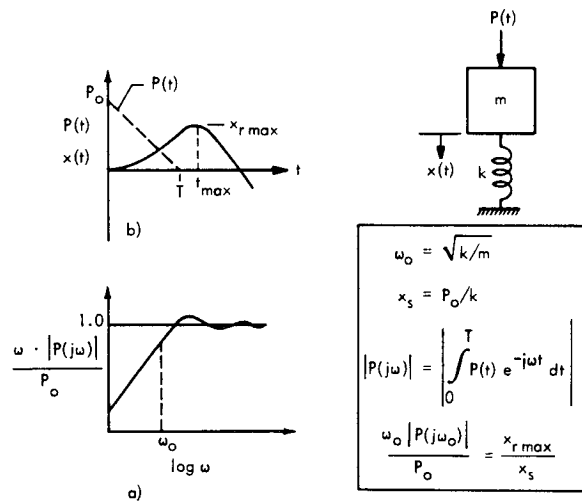


FIGURE 3.19 Relationship Between a) Normalized Fourier Spectrum of Transient Excitation and b) Residual ( $t_{\max} > T$ ) Displacement Shock Response of Undamped Mass-Spring System to a Triangular Shock Pulse

Comparison of Classical and Triangular Blast Pulse Response

This concept can also be applied to the classical blast wave. The only difference is that a clearly defined residual response does not exist for this pulse shape since its duration, theoretically, is infinite. However, validity of Equation 3.62 can be checked by comparison with the computed time history for this pulse given in the preceding section.

The normalized Fourier spectrum for the classical blast is found from Equation 3.56. This is inserted in Equation 3.62 and  $\omega$  set equal to  $\omega_0$  to give

$$\frac{\omega_0 |P(j\omega_0)|}{P_0} = \frac{(\omega_0 T)^2}{1 + (\omega_0 T)^2} \quad (3.64)$$

This expression is plotted in Figure 3.20 along with the maximum and minimum response values computed from Equation 3.61 for several values of the parameter  $f_0 T$ .

The overall shock spectrum (both residual and forced) for the triangular pulse is also plotted in Figure 3.20. A log scale has been used to emphasize the response for small values of  $f_0 T$ . Three conclusions can be drawn from this figure.

- The computed maximum response to the classical blast wave is closely described by the normalized Fourier spectrum for this pulse for values of  $f_0 T$  less than 0.5. In other words, in this low range of  $f_0 T$ , the response of the system is essentially "residual" and the shock spectrum is predicted by the normalized Fourier spectrum as expected.
- For  $f_0 T$  less than 0.1, the response to the classical blast wave decreases more rapidly than for the triangular pulse. This is also expected since the impulse response of the system should be the controlling factor in this region. The classical blast wave has a net zero impulse in contrast to the finite positive impulse for the triangular pulse so that a different response is expected. In fact, it can be shown that for a shock pulse with a net impulse of zero, the shock response spectrum is expected to vary with the square of the product  $f_0 T$  for  $f_0 T \ll 1$  where  $T$  is a characteristic duration of the pulse. This trend is observed for the classical blast wave.
- For values of  $f_0 T > 0.5$ , the shock response spectrum, or envelope of maximum response, for the classical blast wave is apparently closely approximated by the shock spectrum for the triangular pulse. Thus, the latter provides a suitable design envelope for the response to a real blast wave.

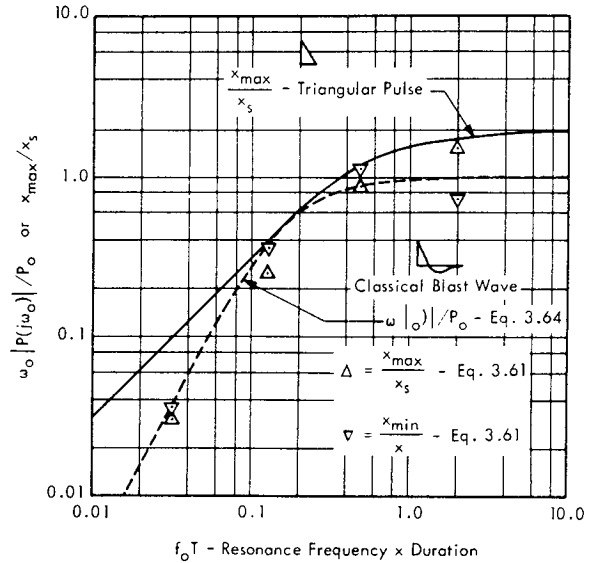


FIGURE 3.20 Comparison of Normalized Fourier Spectrum and Computed Maximum Displacement Response Values for Classical Blast with Displacement Shock Response Spectrum for Triangular Pulse. Excitation Applied to Mass of Undamped Fixed-Base Mass-Spring System.

General Relationship Between Fourier Spectrum and Residual Response

The relationship between the Fourier spectrum and the residual shock response spectrum can be generalized to cover other forms of inputs and corresponding responses of an undamped mass-spring system. The general form of Equation 3.62 is (Reference 3.15)

$$\frac{R_{rmax}}{I_{max}} = \frac{\omega_0 |l(j\omega_0)|}{I_{max}} \quad (3.65)$$

$R_{rmax}$  represents the generalized residual shock response spectrum to a generalized excitation  $l(t)$  whose Fourier spectrum is  $l(j\omega_0)$  and maximum value is  $I_{max}$ . Several specific forms of  $l(t)$  and the corresponding response and Fourier spectrum parameters in Equation 3.65 are listed in Table 3.2. As an example, refer to the third row in the table. For a base displacement  $u(t)$  of an undamped system, the maximum residual displacement of the mass  $x_{rmax}$ , normalized by  $U_{max}$ , is equal to  $\omega_0 |U(j\omega_0)| / U_{max}$  which is the absolute value of the Fourier spectrum of  $u(t)$  multiplied by  $\omega_0$  and divided by the maximum value of  $u(t)$ .

Application of Fourier Spectrum to Step-Type Transient Excitation

Estimating the dynamic forces on rocket test stands during a static firing is another useful application of this concept. During rocket ignition, the transient and steady state thrust forces imposed on the test stand will have the general form illustrated in Figure 3.21a. The initial transient lasts for a time  $T$  followed by a static force  $P_{max}$ . The simulation

TABLE 3.2

RELATIONSHIP BETWEEN NORMALIZED FOURIER SPECTRUM OF TRANSIENT EXCITATION AND CORRESPONDING RESIDUAL RESPONSE SHOCK SPECTRUM FOR VARIOUS EXCITATION-RESPONSE VARIABLES FOR AN UNDAMPED SINGLE DEGREE OF FREEDOM SYSTEM<sup>(1)</sup>

System	Excitation $I(t)$	Non-Dimensional Fourier Spectrum $\omega_o  I(j\omega_o)  / I_{max}$	Residual Response Shock Spectrum $R_{rmax} / I_{max}$	Response $R(t)$	
Fixed Base (Figure 3.3)	Force on Mass - $P(t)/k$	$\omega_o  P(j\omega_o)  / P_{max}$	$x_{rmax} / x_s$ <sup>(2)</sup>	$x(t)$ - Displ. of Mass	
	Force on Mass - $P(t)$	$\omega_o  P(j\omega_o)  / P_{max}$	$P_{Tmax} / P_{max}$	$P_T(t)$ - Transmitted Force	
Moving Base (Figure 3.6)	Base Displ. - $u(t)$	$\omega_o  U(j\omega_o)  / U_{max}$	$x_{rmax} / U_{max}$	$x(t)$ - Displ. of Mass	
	Base Acceleration	$\ddot{u}(t)$	$\omega_o  \dot{U}(j\omega_o)  / \dot{U}_{max}$	$\ddot{x}_{rmax} / \dot{U}_{max}$	$\ddot{x}(t)$ - Accel. of Mass
		$-\ddot{u}(t) / \omega_o^2$		$\omega_o^2 \epsilon_{rmax} / \dot{U}_{max}$	$\epsilon(t)$ - Relative Displ. of Spring
	$m\ddot{u}(t)$		$P_{I max} / m\dot{U}_{max}$	$P_I(t)$ - Dynamic Reaction Force on Base	

(1) Undamped Natural Frequency of System =  $\omega_o$  - rad/sec.

(2)  $x_s = P_{max} / k$  = Static Displacement to Maximum Input,  $P_{max}$ .

of the dynamic reaction to this transient force can be made by treating the thrust stand and rocket, as a lumped mass on a spring, where the thrust force is applied to the mass. The maximum displacement of the spring, analogous to the maximum stress in the load carrying structure of the test stand, can be shown to consist of the residual response  $x_{rmax}$  plus the static response as shown in Figure 3.21b. Thus, the maximum displacement,  $x_{max}$ , relative to the steady state displacement  $x_s$  is simply

$$\frac{x_{max}}{x_s} = \frac{\omega_o |P(j\omega_o)|}{P_{max}} + 1 \quad (3.66)$$

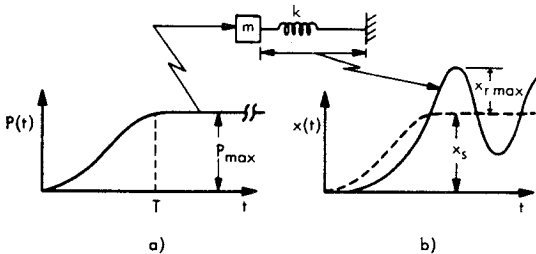


FIGURE 3.21 a) Typical Thrust Transient, and b) Simplified Model of Dynamic Reaction of Static Test Stand for Ignition of Rocket Engine.  $x_s$  is Static Deflection =  $P_{max} / k$ , and  $x_{rmax}$  is Maximum Transient Overshoot.

In other words, the normalized Fourier spectrum of the thrust transient (evaluated at the natural frequency  $\omega_o$  of the mass spring system), added to unity, defines the maximum relative dynamic response of this step-type transient. This is a general result applicable to any normal step-type transient excitation which can be described by the second column in Table 3.2. It is based on the fact that for this type of transient, the maximum transient response occurs during the residual response period after the end of the initial transient of the excitation (Reference 3.1).

The discussion of the Fourier and Laplace Transforms methods in these last three sections has only touched on some of the more useful applications of these powerful methods for solution of transient response problems. For a more complete discussion of their applications and limitations, the reader is referred to the literature (References 3.1, 3.11 and 3.13).

### 3.2.2.8 Shock Response Spectrum of Sonic Boom N-Wave

The other transient sonic load considered in this manual is the sonic boom. A close simulation of the pressure-time history of a sonic boom is given by the N-shaped transient pulse shown in Figure 3.22. Using the same analytical methods covered in Section 3.2.2.2, it can be shown that the deflection-time history of an undamped mass-spring to such a transient force during the forced response period is

$$\frac{x(t)}{x_s} = 1 - t/T + \sqrt{1 + (1/\omega_0 T)^2} \sin(\omega_0 t - \theta) \quad t \leq 2T \quad (3.67)$$

where

$$\theta = \tan^{-1} \omega_0 T$$

$$\omega_0 = 2\pi f_0 = \text{undamped natural frequency} - \text{rad/sec}$$

$$x_s = P_0/k = \text{static deflection to peak pressure.}$$

This is the same equation which defines the forced response for the triangular pulse. For the N-wave, it is applicable for  $t \leq 2T$  instead of  $t \leq T$ , as for the triangular wave.

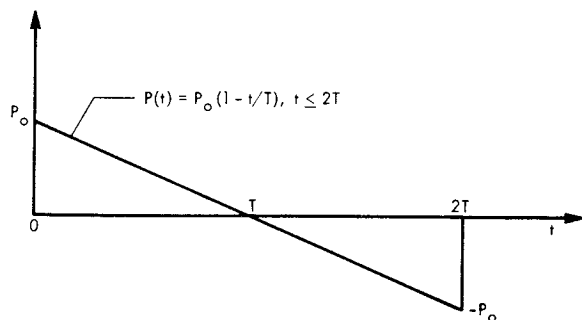


FIGURE 3.22 Pressure Time-History of N-Wave Simulating a Sonic Boom

The residual or free vibration period after the pulse can be determined by using Equation 3.8 with Equation 3.67 to define the residual vibration in terms of its initial displacement and velocity. The resulting expression is

$$\frac{x_r(t)}{x_s} = 2 \left[ \frac{\sin \omega_0 T}{\omega_0 T} - \cos \omega_0 T \right] \cos \omega_0(t-T) \quad (3.68)$$

A typical time history of the response predicted by Equations 3.67 and 3.68 is shown in Figure 3.23 for the case  $f_0 T = 0.5$ . Similar expressions can also be derived for the damped response and results are shown in Figure 3.23 for a damped mass spring system with a dynamic magnification factor,  $Q$ , of 5 and 20.

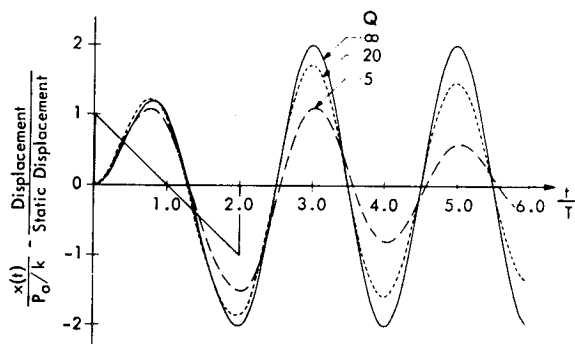


FIGURE 3.23 Displacement Response of Undamped and Damped Single Degree-of-Freedom System to an N-Wave when Natural Frequency  $f_0$ , times Duration of Positive Phase  $T$ , is 0.5

Displacement Shock Spectrum for N-Wave

The displacement shock spectrum for the undamped system is given by the following expressions which define the magnitude of the peak positive and negative displacement during the forced and residual vibration period.

FORCED VIBRATION

$$\frac{x_{\max}}{x_s} = 2 \left[ 1 - \frac{\tan^{-1} \omega_0 T}{\omega_0 T} \right] \quad t < 2T$$

$$\frac{x_{\min}}{x_s} = - \frac{2\pi n}{\omega_0 T} \quad t < 2T \quad (3.69)$$

RESIDUAL VIBRATION

$$\frac{x_{r \max, \min}}{x_s} = 2 \left[ \frac{\sin \omega_0 T}{\omega_0 T} - \cos \omega_0 T \right] \quad t > 2T$$

The displacement shock spectrum for the undamped system is the envelope of the upper bound of these expressions as illustrated in Figure 3.24. The shock spectrum for the N-wave has the complex shape indicated due to the predominance of peak responses during different periods of the excitation. In contrast to the shock spectrum for the triangular blast pulse, the residual response controls the upper limit for the shock spectrum of the undamped system. However, as shown in Figure 3.23, damping reduces this residual response appreciably so that for more practical representation, the shock spectrum for the N-wave should include the effects of damping. Such a "damped" shock spectrum is shown in Figure 3.25, along with the envelope for no damping from Figure 3.24. For values of the parameter  $f_0 T$  greater than about 0.7, the maximum displacement of a system with a typical  $Q$  of 5 to 20, will be primarily determined by the envelope of the positive displacement during the forced response period.

The displacement response of a damped system to an N-wave during this period ( $t < 2T$ ) is given by

$$\frac{x(t)}{x_s} = 1 - \frac{t}{T} + \frac{2\delta}{\omega_0 T} - \frac{e^{-\delta \omega_0 t}}{\omega_0 T} \beta \cos(\omega_d t - \phi) \quad (3.70)$$

where

$$\beta = \left\{ [1 + 2\delta \omega_0 T + (\omega_0 T)^2] / [1 - \delta^2] \right\}^{1/2}$$

$$\omega_d = \omega_0 \sqrt{1 - \delta^2} - \text{damped natural frequency}$$

$$\phi = \tan^{-1} [2\delta^2 + \delta \omega_0 T - 1] / [(\omega_0 T + 2\delta) \sqrt{1 - \delta^2}] .$$

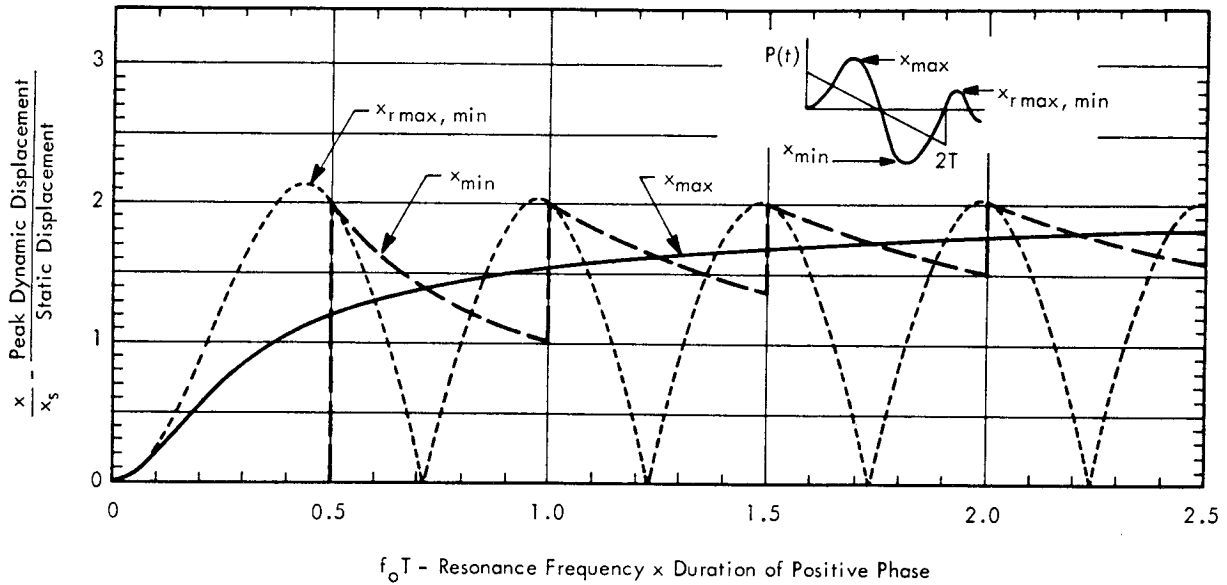


FIGURE 3.24 Normalized Displacement Shock Spectrum for Ideal Sonic Boom N-Wave Excitation of Undamped Mass-Spring System

The residual response can be determined from this equation by the same method as for the undamped case by using Equation 3.8. The shock spectrum for the damped cases were obtained directly from peak values of the response time histories which were calculated with a digital computer using the Duhamel integral approach (see Equation 3.9). This is a common procedure for establishing the shock spectrum of more complex shock pulses, particularly when damping is to be accounted for. Direct analytical solution becomes very cumbersome in such cases.

Time of Maximum Displacement

The time at which the maximum displacement response occurs for an N-wave shock load is a complex function of the parameter  $f_0 T$  and the damping of the system. However, the following relationships may be used for estimating the initial rate of loading of a structure by an ideal N-wave and for estimating the time of occurrence of the maximum response.

For  $f_0 T < 0.5$

The first peak is positive (in the direction of the load) and occurs at a time given by

$$f_0 t_{max} = \frac{1}{\pi} \tan^{-1} \omega_0 T \quad (3.71)$$

For very small values of  $f_0 T$  less than 0.1, the first peak occurs very close to the end of the N-wave or  $t_{max} \approx 2T$ . The highest peak response is the subsequent negative peak and occurs after the end of the pulse during the residual response period at a time given by

$$f_0 t_{rmin} = \frac{1}{2} + f_0 T \quad (3.72)$$

For  $f_0 T \approx 0.5 - 0.7$

The first peak is positive and Equation 3.71 applies. The maximum response is the following negative peak which occurs before the end of the N-wave at a time given by

$$f_0 t_{min} \approx 1 \quad (3.73)$$

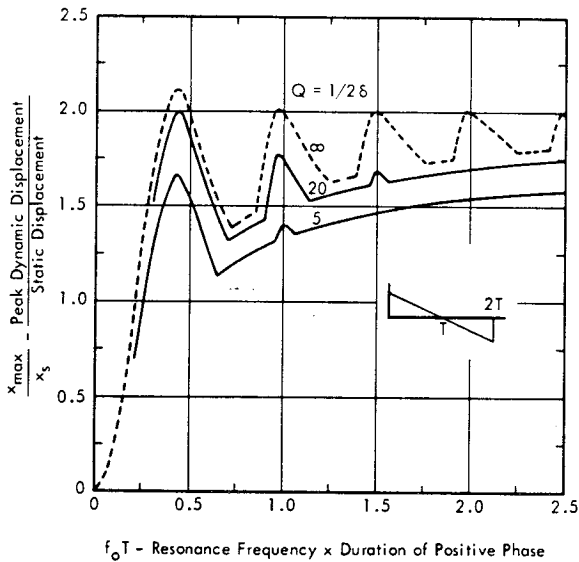


FIGURE 3.25 Normalized Displacement Shock Spectrum for Ideal Sonic Boom N-Wave Excitation of Damped and Undamped Mass-Spring System

For  $f_o T \approx 0.7 - 0.85$

Equation 3.71 still applies to the first positive peak response which is also the maximum response.

For  $f_o T \approx 0.85 - 1.0$

Again, Equation 3.71 applies to the first peak response but the maximum response, for low damping, is the second positive peak which occurs during the residual response period at a time given by

$$f_o t_{rmax} = 1 + f_o T \quad (3.74)$$

For  $f_o T \approx 1.0 - 1.2$

Following the first peak specified by Equation 3.71, the maximum response will be a negative peak occurring just prior to the end of N-wave at a time given by

$$f_o t_{min} = 2 \quad (3.75)$$

For  $f_o T > 1.2$

With the usual amounts of damping, the first positive peak will usually predominate for values of  $f_o T > 1.2$ . In this case, the time of occurrence of the peak, given by Equation 3.71, is approximately equal to  $f_o t_{max} \approx 1/2$ .

Acceleration Shock Spectrum for N-Wave

As previously discussed for the blast wave, the acceleration response to a sonic load is useful for evaluating dynamic loads on equipment attached to walls or roofs which are loaded by a transient pressure load. The acceleration response of an undamped system to an N-wave, during the forced response period, is given by the equation which also defines the forced response to the triangular pulse. This is

$$\frac{\ddot{x}(t)}{\omega_o^2 x_s} = - \sqrt{1 + (1/\omega_o T)^2} \sin(\omega_o t - \tan^{-1} \omega_o T)_{t < 2T} \quad (3.76)$$

The normalizing factor  $\omega_o^2 x_s$  is also the same initial acceleration of the mass due to the suddenly applied force  $P_o$  and is equal to  $\omega_o^2$  times the static deflection to a steady force with a magnitude equal to the initial peak force. During the free vibration period, the acceleration amplitude is determined directly from the residual displacement amplitude or

$$\frac{\ddot{x}_{rmax}}{\omega_o^2 x_s} = \frac{\omega_o^2 x_{rmax}}{\omega_o^2 x_s} = \frac{x_{rmax}}{x_s} \quad (3.77)$$

Therefore, the normalized acceleration shock spectrum is the envelope of the amplitude term in Equation 3.76 and the normalized residual displacement shock spectrum in Figure 3.24. The resulting envelope is shown by the upper bound labeled "undamped", in Figure 3.26. The effect of

damping on the acceleration shock spectrum has also been analyzed in the same manner as for the displacement shock spectrum. The shaded region in Figure 3.26 encompasses the acceleration shock spectrum for damped systems with a Q ranging from 5 to 20. The complex shape of this figure is the result of several factors.

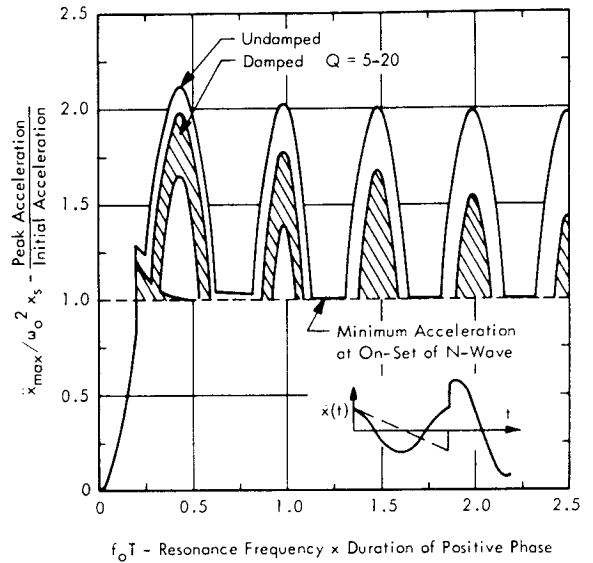


FIGURE 3.26 Acceleration Shock Spectrum for Response of Damped and Undamped Mass-Spring System to Ideal Sonic Boom N-Wave Pulse Applied to Mass

- The small "hook" in the envelope at the left side for  $f_o T \approx 0.2$  is the limiting acceleration that can occur during the period of the N-wave as specified by Equation 3.76. The peak cannot occur for  $f_o T$  less than 0.2.
- The major peaks in the spectrum, at values of  $f_o T$  approximately equal to integral multiples of  $1/2$ , correspond to cases for which the acceleration response at the end of the pulse is just in-phase with the positive-going "jump" at the termination of the pulse. As shown by the insert in Figure 3.26, the time history of the acceleration, in this case, undergoes a similar jump at this point causing a much higher peak acceleration during the residual vibration period. This frequency-sensitive characteristic of the acceleration shock spectrum for the N-wave is very different than the corresponding spectrum for the triangular blast pulse.
- The theoretical minimum acceleration that will occur is the initial value given by the quantity  $\omega_o^2 x_s$ . This value is theoretically independent of damping and may be considered a minimum design value for sonic boom acceleration loads on structure. The maximum value will depend on damping and on the parameter  $f_o T$ , ranging, for practical cases, from 1 to 2 times the minimum initial acceleration.

Further practical aspects of sonic boom loads are discussed in Chapter 8 along with a consideration of the response of actual structure to this type of load.

Since the acceleration shock spectrum is dominated by the peak response during the residual response period, it can be recognized from the discussion in Section 3.2.2.7 that the Fourier Spectrum can be used to define the upper bound of the undamped acceleration shock spectrum for pulse shapes similar to the ideal N-wave. This is, in fact, a characteristic of pulse shapes with an instantaneous change in level at the end of the pulse.

3.2.2.9 Transient Response to Other Types of Pulses

The discussion of response to transient sonic loads characteristic of explosions and sonic booms has been limited to idealized versions of these transient loads. Much more complex load time histories will occur, for example, when diffraction effects are included for loads impinging on finite size buildings. This subject is considered in more detail in Chapter 8. However, the more complex forms of these sonic loads can frequently be approximated by the simpler pulse shapes analyzed in this chapter so that the shock spectrum given for these idealized versions provide a valuable method for simplified design analysis.

Response to the triangular pulse and N-wave, or full cycle triangular pulse, have already been analyzed in the preceding sections. Two other useful pulse shapes for transient load analysis are the rectangular and sinusoidal pulses. The undamped displacement shock spectrum for the single and full cycle version of each of these two shapes is shown in Figures 3.27 and 3.28, respectively. The same normalizing factor  $x_s$ , for the displacement, is applied again. For the full cycle pulses, the maximum response is 4 and 3.26 times the static displacement for the rectangular and sinusoidal pulses, respectively. This contrasts with a factor of 2.12 for the N-wave (or full cycle triangular wave) as shown in Figure 3.24.

For the full cycle rectangular pulse, the response spectrum is highest during both the residual and forced motion period for odd multiples of  $0.5 f_0 T$  while for the full cycle sinusoidal pulse, only one significant peak occurs in the response spectrum at a value of  $f_0 T$  equal to about 0.57. For both the rectangular and sinusoidal pulses, the residual response spectrum is greater than the forced response spectrum for values of  $f_0 T$  less than 0.5.

The shock spectra shown in Figures 3.27 and 3.28 are based on the following equations derived in the same manner as for the triangular pulse. In the following, a maximum may be either positive or negative.

Single Rectangular Pulse

Forced Response,  $t \leq T$

$$\frac{x_{\max}}{x_s} = 2, \quad f_0 T \geq 0.5 \quad (3.78)$$

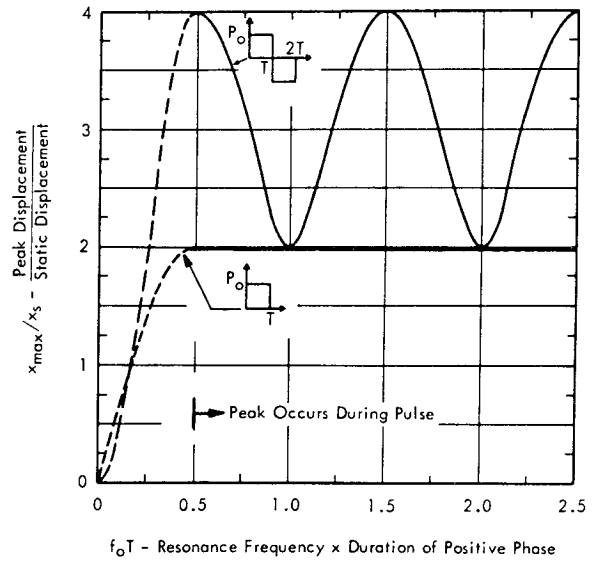


FIGURE 3.27 Displacement Shock Spectrum Envelope for Single and Full Cycle Rectangular Pulse Excitation of Undamped Mass-Spring System when Excitation is Applied to Mass

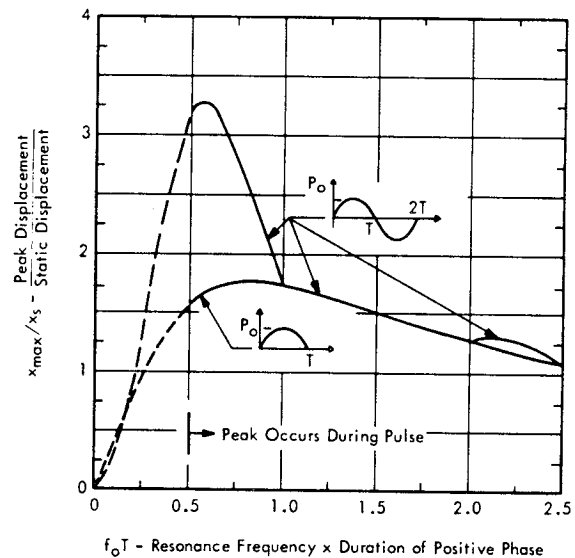


FIGURE 3.28 Displacement Shock Spectrum Envelope for Single and Full Cycle Sinusoidal Pulse Excitation of Undamped Mass-Spring System when Excitation is Applied to Mass

Residual Response,  $t \geq T$

$$\frac{x_r \max}{x_s} = 2 \sin \pi f_0 T \quad (3.79)$$

Full Rectangular PulseForced Response,  $t \leq 2T$ 

$$\frac{x_{\max}}{x_s} = -\left[\sqrt{5 - 4 \cos 2\pi f_o T} + 1\right], \quad f_o T \geq 0.5 \quad (3.80)$$

Residual Response,  $t \geq 2T$ 

$$\frac{x_{r \max}}{x_s} = \left[2 \sin \pi f_o T\right]^2 \quad (3.81)$$

Half-Cycle Sinusoidal PulseForced Response,  $t \leq T$ 

$$\frac{x_{\max}}{x_s} = \frac{\sin \left[2\pi n / (1 + 2f_o T)\right]}{1 - (1/2 f_o T)}, \quad \left. \begin{array}{l} f_o T > 1/2 \\ n = 1, 2, 3, \dots \end{array} \right\} \quad (3.82)$$

$$= \pi/2, \quad f_o T = 1/2$$

Residual Response,  $t \geq T$ 

$$\frac{x_{r \max}}{x_s} = \frac{4 f_o T}{1 - (2 f_o T)^2} \left[ \cos \pi f_o T \right] \quad (3.83)$$

Full Cycle Sinusoidal PulseForced Response,  $t \leq 2T$ 

$$\text{Same as Equation 3.82, except } \left| \frac{x_{\max}}{x_s} \right| = \pi \text{ for } f_o T = \frac{1}{2}$$

Residual Response,  $t \leq 2T$ 

$$\frac{x_{r \max}}{x_s} = \frac{8 f_o T}{1 - (2 f_o T)^2} \left[ \sin \pi f_o T \right] \left[ \cos \pi f_o T \right] \quad (3.84)$$

For a more thorough treatment of the shock spectrum of other types of idealized pulse shapes, the reader is referred to Chapter 8 of Reference 3.1. A presentation of graphical and numerical methods for evaluating the Fourier spectrum of more complex transient excitations is covered in Chapter 23 of Reference 3.1. As indicated in Section 3.2.2.7 and 3.2.2.8, the Fourier spectrum of a shock pulse can provide useful information about the shock spectrum and is a valuable analytical tool for transient response analysis.

### 3.2.3 RESPONSE OF LINEAR SINGLE DEGREE-OF-FREEDOM SYSTEMS TO RANDOM EXCITATION

The type of excitation considered so far may be classified as deterministic; that is, its magnitude can be described exactly at any point in time. However, the other source of sonic loading considered in this manual is noise generated by rocket engines. Its magnitude can only be

defined statistically; that is, an exact magnitude cannot be predicted at any given instant. This type of excitation is called random and the noise generated by rockets which produce this type of excitation is called random acoustic noise or simply, random noise.

Although numerous publications now exist on response of systems to random excitation, this relatively new field is not treated in most of the existing classical texts on vibration theory. Most of the basic literature in the field has been published since 1954. This section, then, attempts to provide a minimum background on random response theory for convenient reference within this manual. For a more thorough treatment of random noise theory, References 3.1 (Chapter 11), 3.2 (Chapter 10), 3.3, 3.16, 3.17 and 3.18, listed in approximate ascending order of detail, provide a basic background of the subject. Response of structure to random excitation is also covered extensively in References 3.19 - 3.21.

Practical methods for analyzing the response of systems to random loads can be related to the more familiar concepts of sinusoidal response. Before developing this, however, some of the basic characteristics of random noise will be considered along with definitions of basic terminology and a discussion of measurement of random noise. The application of the random noise parameters to response predictions is then briefly outlined followed by material on the statistical parameters of random noise. Finally, the basic equations for response to random noise are derived followed by a discussion of practical engineering methods for solving random response problems for a single degree-of-freedom system.

#### 3.2.3.1 Characteristics of Random Noise

Random noise may be visualized as the sum of a large number of steady state sinusoidal components whose frequencies are not harmonically related to each other and whose relative phases vary randomly with time.

#### Summation of Sinusoidal Components

Consider, for example, just two such components,  $x_1(t)$  and  $x_2(t)$ , shown in Figures 3.29 a) and b), whose amplitudes are equal but which have different frequencies  $\omega_1$  and  $\omega_2$  where  $\omega_2$  is only slightly higher than  $\omega_1$ . Neglecting any phase difference, the time history of the sum of these two components will then be

$$x(t) = x_1(t) + x_2(t) = x_o \sin \omega_1 t + x_o \sin \omega_2 t \quad (3.85)$$

This summation can also be expressed as the product of two new sinusoidal components as

$$x(t) = 2x_o \left[ \cos \left( \frac{\omega_1 - \omega_2}{2} t \right) \right] \sin \left( \frac{\omega_1 + \omega_2}{2} t \right) \quad (3.86)$$

Thus, as illustrated in Figure 3.29 c), the instantaneous value of these two components looks like a single sinusoidal component with a frequency equal to the average frequency  $(\omega_1 + \omega_2)/2$  of the two but with an amplitude modulation which varies with a frequency equal to  $1/2$  the difference



frequency ( $\omega_2 - \omega_1$ ) between the two components. However, the effective frequency of the envelope of the amplitude peaks is twice the modulation frequency and is, therefore, simply the difference frequency ( $\omega_2 - \omega_1$ ). Although this time history of two sinusoids is complex, it is completely predictable. Consider, now, what happens when additional sinusoidal components are added.

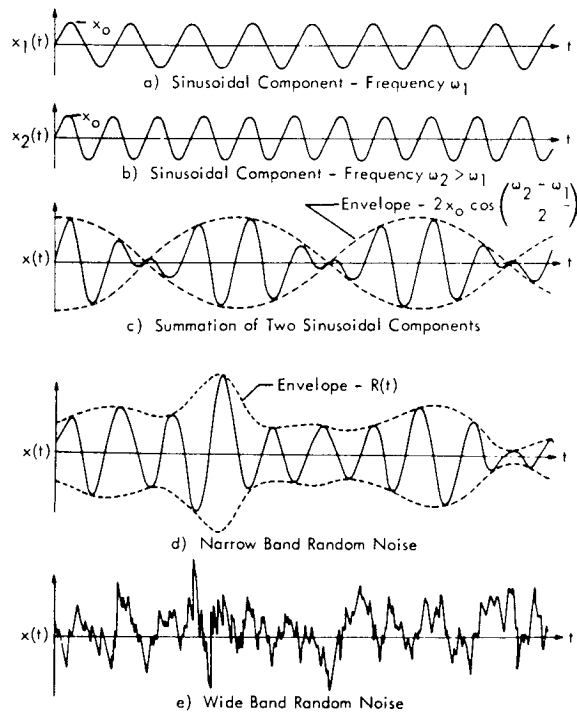


FIGURE 3.29 Time History of Instantaneous Magnitude of: (a,b) Two Sinusoidal Components with Frequency  $\omega_1$  and  $\omega_2$ ; c) Their Summation; d) Narrow Band, Random Noise with a Frequency Spectrum from  $\omega_1$  to  $\omega_2$  and e) Wide Band Random Noise with a Wide Range of Frequencies

### Narrow Band and Wide Band Random Noise

If many more sinusoidal frequency components are added with frequencies between  $\omega_1$  and  $\omega_2$  and with randomly varying phases, and the amplitudes of each component correspondingly reduced, a time history characteristic of narrow band random noise is obtained as illustrated in Figure 3.29 d). Thus, narrow band random noise may be considered to be the summation of an infinite number of infinitesimally small randomly phased sinusoidal components with frequencies continuously distributed over a narrow frequency interval  $\omega_2 - \omega_1$ . The time history of this noise is similar to the summation of two closely spaced sinusoids in two respects.

- Narrow band random noise has an average frequency which is approximately equal to the average of its upper and lower bounding frequencies.

- The envelope of the peaks in a narrow band of noise has a randomly varying amplitude but an average frequency approximately equal to the difference between its upper and lower bounding frequencies.

The similarity stops here, however, since the envelope of the narrow band of noise, indicated in Figure 3.29 d) by the variable  $R(t)$ , can only be defined statistically. Such a time history is typical of the response time history of a single degree-of-freedom system excited by random noise.

As the frequency bandwidth of the random noise is increased, so that more and more components of different frequencies are added, a time history characteristic of wide band noise is achieved, as shown in Figure 3.29 e). The time history no longer has a readily discernible "average frequency" or a clearly defined envelope and is only definable by statistical means. Such a time history is typical of the acoustic noise generated by a rocket engine exhaust.

### 3.2.3.2 Basic Parameters of Random Noise

The variables which can be used to describe random noise which are of primary practical importance to the structural engineer or equipment designer concerned with design of rocket testing facilities are:

- Time average value of the random noise
- Root mean square (rms) value
- Power spectral density
- Peak magnitude
- Number of peaks per second
- Number of zero crossing per second
- Probability of simultaneous occurrence of peak responses of two separate systems

Many other variables are significant for a thorough analysis of random processes; these are not considered in this manual and the reader is referred to the literature cited in 3.2.3 for further details. Before defining the variables listed, it is important to emphasize again that they can only be defined statistically and by the methods discussed which are valid only when the random phenomena is stationary.

### Stationary and Ergodic Random Processes

A stationary random time history is one which has the same statistical properties regardless of the time at which they are measured. This is analogous to the constant parameters of a steady-state vibration - one which has the same magnitude and spectral content for all time.

It is also frequently assumed that random excitation and response processes are ergodic. This term can best be defined by an example. Assume that the acceleration of a particular point on a rocket test stand has been measured

for a very large number of test firings of the same rocket motor. Assume the time histories of these measurements are assembled, as shown in Figure 3.30, and statistical properties of the instantaneous acceleration at the same instant of time following rocket ignition, are obtained over the ensemble of measurements. The vibration records represent an ergodic random process if the same statistical properties are obtained when only one time history is sampled over a long period of time. Thus, a very long time sample from one occurrence of an ergodic random process is a valid measurement of the statistical properties for a theoretically infinite number of repeated occurrences, either past or future, of the same process. The practical importance of the assumption is clear. Without the ability to anticipate random loads for future occurrences of the same process from an analysis of the random variable for one occurrence, the process of designing for random loads would become enormously complex. The key to an ergodic process is the assumption of "the same event or process." Thus, in the above example, a significant change in the noise characteristics of the rocket motor, or in the dynamics of the test stand would invalidate this assumption so that a new measurement would be required to define the new random process.

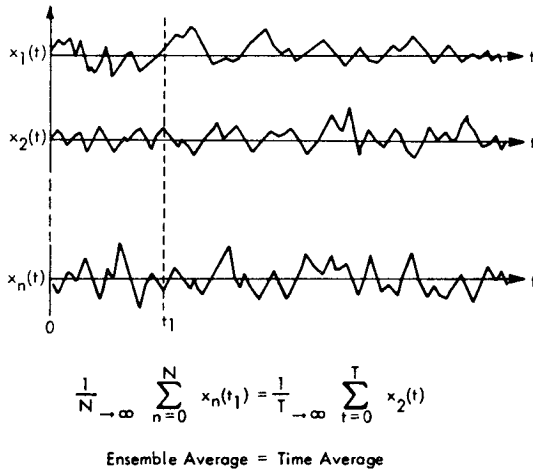


FIGURE 3.30 Illustration of Ensemble of Vibration Records from Repeated Occurrences of the Same Type of Event to Illustrate an Ergodic Random Process

Finally, it should be clear from the preceding discussion that a single random time history can be stationary without being ergodic but an ergodic process is always, inherently, stationary. The random noise variables to be defined in the following assume a stationary random process.

3.2.3.3 Mean Value

The long time average or mean value of random vibration or random acoustic noise is normally zero. This can be seen in Figures 3.29 and 3.30 since for each of the time histories, the areas above and below the  $x = 0$  line (abscissa axis) will be equal over a long period of time.

3.2.3.4 Mean Square Value

Since the instantaneous power or energy in vibrating systems is proportional to the square of the instantaneous vibration amplitude, the long time average or mean value of the square of this instantaneous amplitude is a physically meaningful measure of vibration intensity. This average is called the mean square value  $\overline{x^2}$  and is equal to

$$\overline{x^2} = \lim_{T \rightarrow \infty} \frac{1}{T} \int_0^T x^2(t) dt \tag{3.87}$$

For a zero mean value, the square root of  $\overline{x^2}$  is called the root mean square (rms) value of  $x(t)$  where  $x(t)$  is any time varying quantity such as displacement, velocity, stress, force, etc.

If  $x(t)$  is a complex time history made up of the sum of many discrete sinusoidal components, the square of the instantaneous value of their summation will be the sum of self squared terms and cross product terms in the form

$$\begin{aligned} x^2(t) &= \left[ x_1 \sin \omega_1 t + x_2 \sin \omega_2 t + \dots \right]^2 \\ &= x_1^2 \sin^2 \omega_1 t + x_2^2 \sin^2 \omega_2 t + \dots \\ &\quad + 2x_1 x_2 \sin \omega_1 t \sin \omega_2 t + \dots \end{aligned} \tag{3.88}$$

When this is inserted in Equation 3.86 and the integration carried out term by term, the cross terms drop out and the mean square value of  $x(t)$  becomes

$$\begin{aligned} \overline{x^2} &= \frac{x_1^2}{2} + \frac{x_2^2}{2} + \dots \\ &= \frac{1}{2} \sum_{n=1}^{\infty} x_n^2(\omega_n) \end{aligned} \tag{3.89}$$

where  $x_n$  is the amplitude of the  $n$ th component with a frequency  $\omega_n$ . This simple result is obtained by utilizing the basic expression for the time average value of the product of two sinusoidal components which is

$$\begin{aligned} \frac{1}{T} \int_0^T \sin \omega_1 t \sin \omega_2 t dt &= \frac{1}{2T} \int_0^T \left[ \cos(\omega_2 - \omega_1) t \right. \\ &\quad \left. - \cos(\omega_1 + \omega_2) t \right] dt = \begin{cases} 1/2, & \omega_1 = \omega_2 \\ 0, & \omega_1 \neq \omega_2 \end{cases} \end{aligned} \tag{3.90}$$

Equation 3.90 is valid providing the averaging time  $T$  is an integral multiple of the period of the lowest frequency component or many times larger than this period. For the case  $\omega_1 \neq \omega_2$ , the effective period of the product  $\sin \omega_1 t \sin \omega_2 t$  is the period of the difference frequency  $(\omega_2 - \omega_1)$ .

3.2.3.5 Power Spectral Density

For random noise, instead of the summation of discrete sinusoidal components used in Equation 3.89 to obtain a mean square value of a complex time history, a continuous integral is required to "sum up" the mean square values of the infinitesimally small components which make up a random noise signal. However, discrete frequency components are no longer truly identifiable at any given frequency. Therefore, to establish some measure of the spectral intensity or power of the random noise, the concept of Power Spectral Density is used. For now, let this be defined as the mean square value of all the vanishingly small sinusoidal components with frequencies within a one cycle per second (one hertz) bandwidth centered on a frequency  $f$ . It will be identified by the symbol  $W(f)$ . (Circular frequency is used in this case to be consistent with engineering and measurement practice.) The units of power spectral density are the square of the linear time variable,  $x(t)$  (i.e. -- acceleration, displacement, force, pressure, etc.) per unit Hertz. The factor of 2 involved in Equation 3.89 for discrete components is absorbed in the mathematical definition of  $W(f)$  so that for a continuous frequency distribution from 0 to  $\infty$ , the mean square value of the random noise signal is equal to the integral

$$\overline{x^2} = \int_0^{\infty} W(f) \cdot df \quad (3.91)$$

Thus, as shown in Figure 3.31a, a plot of the power spectral density  $W(f)$  of a random time history is a continuous curve and, at a frequency  $f_0$ , the power spectral density is represented by the average height of a rectangle of unit width centered about the frequency  $f_0$ . Figure 3.31a shows a typical spectrum for a wide band and a narrow band of noise. For the latter, the bandwidth  $\Delta f$  is much less than the center frequency  $f_0$ . In either case, the mean square value of the random variable  $x(t)$  is simply the area under the frequency spectrum plot  $W(f)$  times the graphical scale factor and the rms value is the square root of this scaled area. (It is necessary, of course, that the plot be constructed with linear scales for both  $W(f)$  and  $f$ .)

With this simplified explanation of power spectral density as a background, it is desirable to examine this very important parameter more carefully, for it is a basic variable to be used for quantifying response of structure to random noise. It is also necessary for defining the magnitude of a random noise signal in terms of a measurable frequency spectrum instead of using the statistically uncertain time history.

Spectral Density Measurement Techniques

Consider first, then, the method of measuring the power spectral density of a random variable. Three techniques which are in current use are:

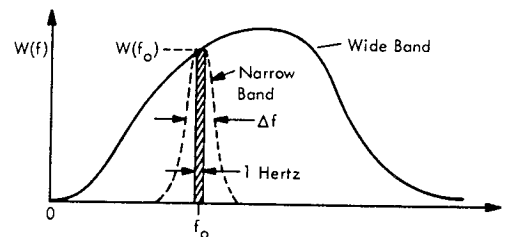
- Direct analysis of continuous random noise by an analog spectrum analyzer
- Analysis of a tape recorded finite length sample by an analog spectrum analyzer

- Digital filtering and analysis of a finite length sample by a computer

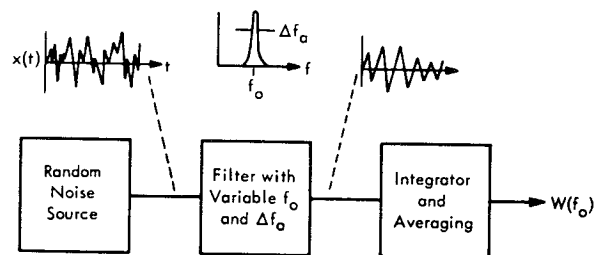
For stationary random noise, all three methods will, theoretically, produce equivalent results. However, the methods introduce similar inherent errors in the measurement of a power spectral density which should be recognized when using measured data for design purposes. These errors are due to:

- Inadequate frequency discrimination of spectrum analyzer
- Finite duration of data sample
- Finite overall frequency bandwidth of analysis

Error Due to Inadequate Frequency Resolution



a) Wide Band and Narrow Band Spectra



b) Spectral Analysis of Random Noise

FIGURE 3.31 a) Typical Power Spectral Density Plots of Random Noise, and b) Simplified Block Diagram of Spectrum Analyzer with Illustration of Time History of Raw and Filtered Data Before and After Passing Through Selective Filter of Analyzer

Frequency discrimination of the spectral analysis of a random signal is fixed by the frequency selectivity or filter bandwidth of the analyzer. This filtering process is illustrated in the simplified diagram in Figure 3.31b where the filter bandwidth is identified as  $\Delta f_0$ . It is normally defined as the interval between the frequencies for which the filter power transmission is 1/2 of its maximum value. The filter itself can consist of frequency selective electronic analog circuits (Reference 3.1 - Chapter 22) or can be simulated by digital analysis on a computer (Reference 3.22). In the case of the analog spectrum analyzer, the output of the filter is a narrow band of noise with a bandwidth  $\Delta f_0$  which is passed through additional circuitry which determines the mean square value of the filtered signal. Digital analysis

accomplishes the same result through computer processing. This mean square value is then divided by the effective bandwidth  $\Delta f_a$  of the analyzer to obtain an observed power spectral density  $W_o(f)$  which may be defined as

$$W_o(f) = \frac{1}{\Delta f_a} \left[ \int_{f - \Delta f_a/2}^{f + \Delta f_a/2} W(f) df \right] \quad (3.92)$$

For a very long time sample of the random noise, as the analyzer filter bandwidth approaches zero, the observed power spectral density would approach the true value  $W(f)$ . Clearly, when the latter changes rapidly within the filter bandwidth  $\Delta f_a$ , the observed value of  $W(f)$  will not be an accurate estimate of the true value. Therefore, the first requirement for accurate measurement of the power spectral density of a random noise signal is that the analyzer bandwidth,  $\Delta f_a$ , should be appreciably less than the narrowest bandwidth  $\Delta f$  of any narrow band noise "spikes" in the true power spectrum. The analyzer bandwidth should be 1/4 to 1/5 of the narrowest bandwidth of noise to be analyzed. The rate of attenuation of the analyzer filter outside its frequency passband influences its effective bandwidth and should be as high as possible.

Error Due to Inadequate Time Sample

The measured duration of a random data sample is necessarily limited to a finite value of time  $T$ . This is the primary source of error in the measurement of a random noise signal. The error is due to fluctuation in the output of the analyzing filter, which is a narrow band of noise. As shown earlier in Figure 3.29, the envelope of this type of random noise varies with a frequency approximately equal to the bandwidth  $\Delta f_a$  of the analyzing filter. This assumes that the latter is less than the actual bandwidth of the noise being analyzed. The magnitude of this envelope fluctuates randomly so that to obtain an accurate measurement of the power spectral density, the analyzer must integrate the instantaneous mean square output of the filter over an averaging time  $T$  which is large relative to the period ( $\sim 1/\Delta f_a$ ) of the envelope fluctuation. Thus, the product  $T\Delta f_a$  must be large for accurate spectrum measurements of random noise.

The fluctuation of the envelope of a band of noise has been analyzed in detail in References 3.18 and 3.23. It is shown that for a spectral density measurement with an ideal "rectangular" filter, the ratio of the standard deviation  $\sigma_w$  of the spectral measurement to the true value  $W(f)$ , is

$$\frac{\sigma_w}{W(f)} = \sqrt{\frac{2}{2T\Delta f_a}} \quad (3.93)$$

where

$T$  = duration of the data sample or averaging time, whichever is less

$\Delta f_a$  = bandwidth of ideal filter.

The quantity  $2T\Delta f_a$  is commonly identified as the degrees of freedom for spectral analysis of random noise. Thus, as indicated qualitatively, this product is the controlling parameter which determines accuracy of spectral density measurements.

The statistical variation in random noise spectrum measurements is illustrated more clearly in Figure 3.32. This shows the upper and lower bounds of the deviation of a measured spectrum from the true value as a function of the degrees of freedom. For example, if the spectral density of 5-second samples of random noise are measured using an effective filter bandwidth of 2 Hz, the degrees of freedom will be 20 so that 80 percent of the measured spectra will fall within a range of 0.62 to 1.42 times the true value and 95 percent of the data will fall within a range of 0.48 to 1.71 times the true value. For this case, 50 percent of the data would fall below 0.96 times the true value. (For practical purposes, the effective bandwidth of the filter  $\Delta f_a$  may be considered to be approximately equal to the width of an equivalent ideal "rectangular" filter, with zero transmission outside its passband, which transmits the same power as the actual filter. For an exact definition of the equivalent bandwidth, refer to Reference 3.18.)

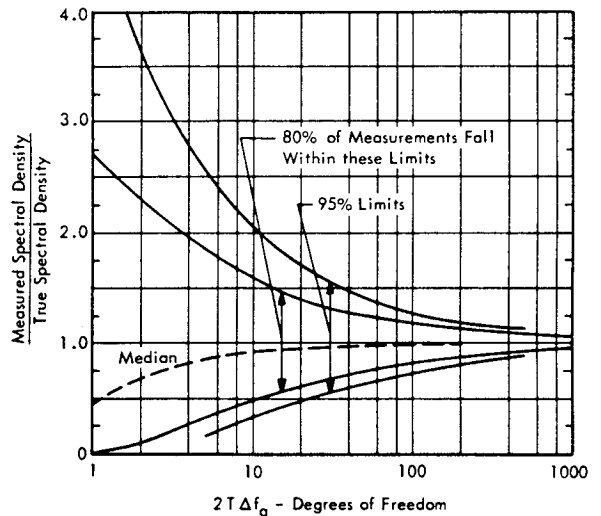


FIGURE 3.32 Statistical Variation in Measured Spectral Density as a Function of Degrees of Freedom. [  $T$  = Sample Length - sec,  $\Delta f_a$  = Effective Bandwidth of Analyzing Filter - Hz ]. [ From Reference 3.23 ]

The variation in random noise transmitted through a simple resonant filter, corresponding to a single degree-of-freedom system, has also been analyzed and is reported in Reference 3.24. The statistical variation in the average noise power transmitted through such a filter is essentially the same as shown in Figure 3.32 for  $2T\Delta f_a \geq 20$ .

To summarize, power spectrum measurement errors, due to a finite averaging time, can be reduced to an acceptable level if the product  $2T\Delta f_a$  exceeds 100 where  $T$  is the sample length or averaging time, whichever is less, and  $\Delta f_a$  is the effective bandwidth of the filter.

Error Due to Inadequate Overall Frequency Range

The final source of error in spectral density measurements to be considered is concerned with limitations in the frequency range of the spectrum analyzer. The variation of random noise spectra with frequency can vary widely. At one extreme, random noise spectra may closely approximate a so-called white noise, namely, a random noise with a constant power spectral density at all frequencies. For example, in the low frequency range, the spectral density of the fluctuating pressures near a rocket exhaust will vary slowly with frequency. On the other hand, structural systems subjected to random loads will tend to show a very ragged vibration response spectrum with high spectral densities at very high frequencies.

In either case, inadequate definition of the true spectra, due to a limited frequency range of the spectrum analyzer, must be avoided to ensure accurate measurement of structural or equipment loads. The increased low frequency energy of large rocket boosters, coupled with the increasing significance of acoustically-generated structural loads at these frequencies will often make it necessary to analyze random noise down to 1 Hz. Adequate frequency resolution is also important in this low frequency range in order to clearly define the true value of resonant peaks in the spectrum. At high frequencies, elimination of part of the true spectrum, due to analyzer frequency limitations, may eliminate significant information about the shock or acceleration loads. Fortunately, by using such techniques as playing back a tape recording of the data at higher or lower speeds, data can be brought within the measurement range of conventional spectrum analyzers. Digital computer processing of data also provides a flexible means of spectrum analysis which can provide any reasonable frequency resolution or effective filter bandwidth desired (Reference 3.22).

By now, the significance of sources of error or random noise measurements should be clear. Without some knowledge of the variation inherent in measurement of random loads, a structural or facility designer is handicapped when reasonable design safety factors must be defined.

3.2.3.6 Application of Power Spectral Density Data for Defining Random Response of a Single Degree-of-Freedom System

It has already been established that random noise may be considered to be the summation of a large number of vanishingly small sinusoidal components with random phases. As indicated earlier by Equation 3.91, the power spectral density  $W(f)$  of such a random noise at a frequency  $f$  is equivalent to the mean square value of these sinusoidal components within a one cycle per second bandwidth centered around the frequency  $f$ . Since all sinusoidal components within this band of noise have essentially the same frequency, the sinusoidal response functions discussed in Section 3.2.1.4 and summarized in Figure 3.9 should be applicable for defining the response to each of the hypothetical sinusoidal components in this one-cycle-per-second (one Hertz) frequency band. It has also been shown, by Equation 3.89, that the mean square value of the sum of

these sinusoidal components (i.e. -- the power spectral density) is equal to the sum of the mean square value of each component. Thus, at a given frequency  $f$ , the power spectral density of the response  $W_x(f)$  of a linear single degree of freedom system to random excitation is simply equal to the product of the power spectral density of the excitation  $W_p(f)$  and the square of the absolute value of the sinusoidal transfer function  $|a(f)|^2$  at this same frequency or

$$W_x(f) = W_p(f) \cdot |a(f)|^2 \quad (3.94)$$

The absolute value of the transfer function,  $|a(f)|$  is the ratio of the amplitude of the sinusoidal response of the single degree of freedom system to the amplitude of a sinusoidal excitation at a frequency  $f$ . In general, it will be the product of a nondimensional response function that varies with frequency, and a constant which relates the form of the input to the response. Consider the example shown in Figure 3.33a. When the mass of a fixed-base mass spring system is excited by a sinusoidal force  $P(t)$ , the Sinusoidal Transfer Function  $a(f)$  is equal to  $H(f)/k$  where  $k$  is the spring constant and  $H(f)$  is the Frequency Response Function. For this case, the absolute value of  $H(f)$  is the Dynamic Magnification Factor  $H(\omega)$  given by Equation 3.23, page 3-6.

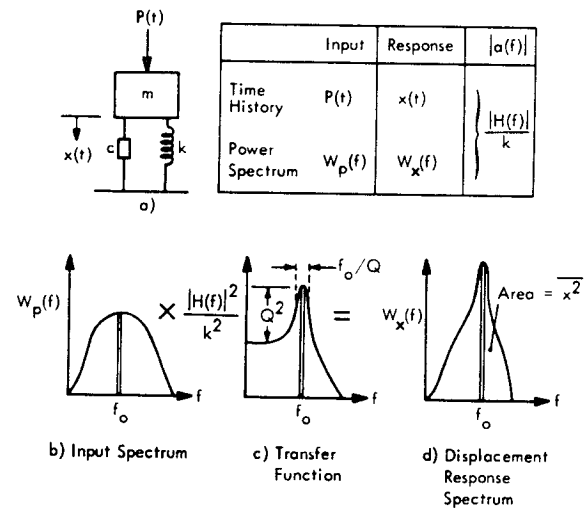


FIGURE 3.33 Power Spectral Density of Displacement Response of a Damped Fixed-Base Mass Spring System to a Wide-Band Random Force Excitation of Mass

As illustrated in Figure 3.33 b-d, for a random force excitation of the mass, the power spectral density  $W_x(f)$  of the displacement response  $x(t)$  is equal to the product of the power spectral density  $W_p(f)$  of the input force  $P(t)$  and the square of  $|H(f)|/k$ . The narrow rectangle at the frequency  $f_0$  shown in each figure corresponds to the input spectral density, square of the response function and the response spectral density, respectively, at the resonance frequency of the mass-spring system.

For the general case, the mean square response of a single degree of freedom system to random excitation is obtained by combining Equations 3.91 and 3.94 to give

$$\overline{x^2} = \int_0^{\infty} W_x(f) df = \int_0^{\infty} W_p(f) |a(f)|^2 df \quad (3.95)$$

For the example in Figure 3.33, this is equivalent to the area under the response spectral density curve in part d. For this case, with a constant power spectral density input  $W_p(f)$  (i.e. -- white noise), this area can be defined by a closed solution for the integral in Equation 3.95 so that the mean square displacement of the mass is

$$\overline{x^2} = \frac{\pi}{2} \frac{W_p(f_o) f_o Q}{k^2} \quad (3.96)$$

where

$f_o$  = resonant frequency

$Q$  = resonant amplification factor.

It will be shown subsequently that an equation of this same form can be used, in most practical cases, for defining the mean square value of any resonant response variable of a linear single degree-of-freedom system to a random excitation with a constant spectral density  $W_p(f_o)$  in the vicinity of the resonance frequency. The only difference will be in the units of the input and response and the proportionality constant (i.e. -- the spring constant  $k$  in the above example) which relates these units. This basic expression takes on a clearer physical meaning if recast in the form

$$\overline{x^2} = \left[ W_p(f_o) \cdot \frac{\pi f_o}{2 Q} \right] \left[ Q^2 \right] \left[ \frac{1}{k^2} \right] \quad (3.97)$$

The first bracketed term in Equation 3.97 is the product of the input spectral density at the resonance frequency  $f_o$ , and an effective resonant bandwidth. This term is simply the effective mean square value of the excitation. As shown in Figure 3.33c and by the above equation, this effective bandwidth is equal to the so-called half-power bandwidth  $f_o/Q$  of the resonant system times a correction factor  $\pi/2$  which accounts for response outside this bandwidth. The second term in brackets in Equation 3.97 is the square of the maximum value of the dynamic magnification factor for sinusoidal excitation. Finally, the third term is, again, the proportionality factor relating in this case, (force)<sup>2</sup> to (displacement)<sup>2</sup>.

For a sinusoidal excitation,  $P_o \sin \omega t$ , of the same system at resonance, the mean square response would be defined by the same equation if the first term  $\left[ W_p(f_o) \pi f_o / 2 Q \right]$  were replaced with the square of the amplitude  $P_o^2$  of the sinusoidal input. Note that while the "sinusoidal" input components for either random or sinusoidal excitation are amplified by the square of the dynamic magnification

factor,  $Q^2$ , the mean square response for random excitation increases by  $Q$  instead of  $Q^2$  since the effective mean square value of the random excitation decreases inversely with  $Q$ .

Equations 3.94-3.96 constitute the basic relationships for engineering calculations of the response of single degree of freedom systems to random excitation. They form the foundation for analyzing response of more complex multi-degree systems to random excitation. Lengthy derivations have been omitted at this point in order to emphasize the physical significance of these expressions and illustrate the application of power spectral density for defining the response of simple systems to random excitation. Before reviewing the basic steps in the derivation, it is desirable to consider the statistical variation in the instantaneous and peak value of a random response.

### 3.2.3.7 Statistics of Random Noise

The statistical variation in the long-time average of the mean square value of a random variable and design application of this value has been considered in the last two sections. However, the design of structures to random excitation must also include consideration of the short time variation in the random response. Specifically, it is necessary to determine the probable value of an instantaneous peak response for a given mean square response. It will be shown, for example, that for a stationary narrow band of random noise, the instantaneous peak value of the noise will exceed three times the root mean square value 1.1 percent of the time.

#### Statistics of Instantaneous Amplitude of Random Noise

If the instantaneous value of a time varying quantity  $x(t)$  is sampled continuously or at repeated uniform intervals for a long period of time, the proportion of time or number of samples for which the observed value is equal to or less than an arbitrary fixed value  $x_1$  is called the cumulative probability distribution or simply distribution function identified as  $P(x \leq x_1)$ . If this sampling process is carried out on a narrow band of random noise with a zero mean value, such as shown in Figure 3.29d, as the number of samples approaches infinity, this cumulative probability approaches the smooth S-shaped curve shown in Figure 3.34. For this figure, the abscissa is the value of the threshold level  $x_1$  normalized by the root mean square (or standard deviation) of  $x(t)$ . The rate of change of the cumulative probability distribution, as a function of the threshold level  $x_1$ , is called the probability density defined as

$$p(x) = \frac{dP(x \leq x_1)}{dx_1} \quad (3.98)$$

For a narrow band of random noise, this probability density has the well-known bell shaped curve, also shown in Figure 3.34, which corresponds to a Gaussian or normal probability distribution. Its probability density is given by

$$p(x_1) = \frac{1}{\sigma \sqrt{2\pi}} e^{-x_1^2/2\sigma^2} \quad (3.99)$$

where

$$\sigma = \text{root mean square(rms) value of } x(t) \\ = \sqrt{\overline{x^2}}$$

This can be expressed in the nondimensional form plotted in Figure 3.34 by multiplying both sides by  $\sigma$  to give

$$\sigma p(x_1) = p\left(\frac{x_1}{\sigma}\right) = \frac{1}{\sqrt{2\pi}} e^{-x_1^2/2\sigma^2} \quad (3.100)$$

Thus, to convert the normalized plot of probability density in Figure 3.34 to a plot for a specific value of  $\sigma$ , the ordinate scale is divided by  $\sigma$  and the abscissa multiplied by  $\sigma$ .

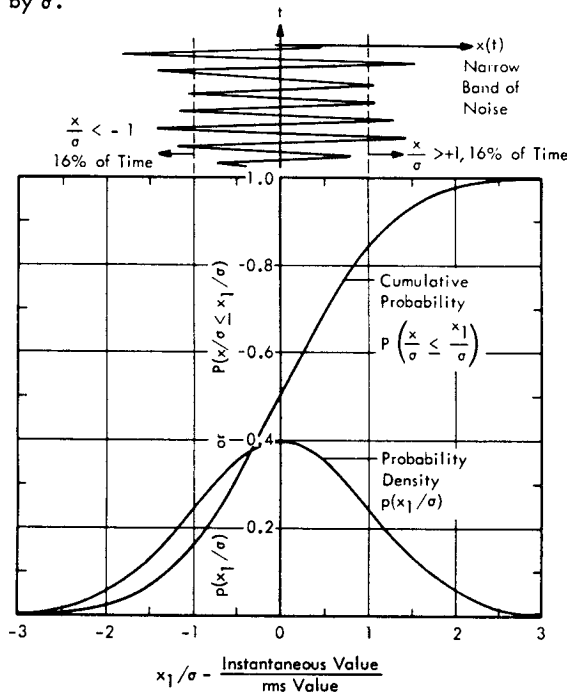


FIGURE 3.34 Normalized Cumulative Probability and Probability Density for Instantaneous Value of Narrow Band of Random Gaussian Noise

The probability that the instantaneous value of  $x$  will fall within a small interval  $x_1$  to  $x_1 + \Delta x$  is equal to the probability density times this interval  $\Delta x$  or

$$p(x_1) \Delta x = \frac{\Delta x}{\sigma \sqrt{2\pi}} e^{-x_1^2/2\sigma^2} \quad (3.101)$$

Thus, the cumulative probability that  $x$  will fall between  $-\infty$  and  $x_1$  can be expressed in the nondimensional form plotted in Figure 3.34, as the integral

$$P\left(\frac{x}{\sigma} \leq \frac{x_1}{\sigma}\right) = \frac{1}{\sqrt{2\pi}} \int_{-\infty}^{x_1/\sigma} e^{-x^2/2\sigma^2} d(x/\sigma) \quad (3.102)$$

In this case, normalizing only involves the independent variable  $x/\sigma$  since the integral is inherently nondimensional. Tabulations of Equations 3.100 and 3.102 are commonly available in the literature (e.g., Reference 3.25). Typical numerical values from these probability curves for the instantaneous value of narrow band random noise are:

- The most probable value of  $x(t)$  is zero if the mean value of  $x(t)$  is zero.
- The instantaneous value of  $x(t)$  exceeds  $\pm\sigma$  about 32 percent of the time,  $\pm 2\sigma$  about 4.6 percent, and  $\pm 3\sigma$  about 0.26 percent of the time.
- Fifty percent of the time, the instantaneous value falls between  $\pm 0.68\sigma$ .
- The average absolute value  $|\overline{x(t)}|$  is  $0.798\sigma$ .
- The area under the normalized probability density curve is unity.

There are two characteristics of Gaussian noise which are very important for defining statistical variation of random structural loads. 1) The summation of a large number of random signals, each of which may not necessarily be Gaussian, tends to have a Gaussian distribution. 2) If a wide band random noise, even a non-Gaussian noise, is passed through a narrow band linear filter such as a structural resonance, the response of the filter will be a narrow band of noise which tends to have a Gaussian distribution. These characteristics can be attributed to the central limit theorem (Reference 3.26). The one significant deviation from a Gaussian distribution in the response of a structure to random excitation occurs when the structure is nonlinear.

The basic conclusion to be drawn regarding the instantaneous amplitude distribution of narrow band random noise is that its statistical variation is defined completely in terms of its rms value or  $\sigma$ . This assumes the noise has a zero mean value and a Gaussian distribution.

If the noise  $x(t)$  has a finite mean value  $\bar{x}$ , then the rms value (or standard deviation) of the fluctuating portion,  $\sigma$ , is

$$\sigma = \left[ \overline{x^2} - (\bar{x})^2 \right]^{1/2} \quad (3.103)$$

where

$$\overline{x^2} = \text{mean square value of } x(t)$$

$$(\bar{x})^2 = \text{square of the mean value.}$$

As shown in Figure 3.35, the Gaussian distribution of the fluctuating portion is then centered about the mean value  $\bar{x}$ . The mean square value,  $\overline{x^2}$  can theoretically be determined by integration of the spectral density of the noise, as discussed in the previous section (see Figure 3.33). However, frequency bandwidth limitations of conventional analog spectrum analyzers will usually reject any mean value of the random signal so that only the rms value  $\sigma$  of the fluctuating portion is normally measured by the spectral analysis.

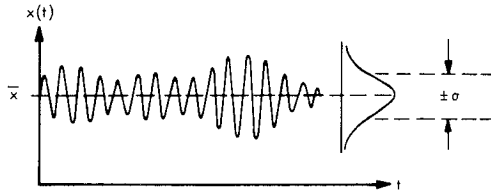


FIGURE 3.35 Gaussian Distribution of a Narrow Band of Random Noise with a Finite Mean Value  $\bar{x}$

For wide band noise, the statistical variation of the instantaneous amplitude also tends to follow the Gaussian distribution shown in Figure 3.34. However, as indicated earlier, a summation of random processes, which individually may be non-Gaussian, tends to have a Gaussian distribution. Therefore, a Gaussian distribution of the overall wide band noise is not a reliable indication of non-linear or non-Gaussian processes within the overall noise. Thus, a wide band random noise should be first passed through a narrow band filter to evaluate its statistical distribution of instantaneous amplitudes. Additional details on methods for analyzing the amplitude distribution of a random signal are given in Reference 3.1 - Chapter 22.

Statistics of Peak Amplitude of Random Noise

Current methods for predicting fatigue life of structure under random loads are based on the statistical distribution of the envelope of the instantaneous peak amplitudes of the random loads. This distribution is also significant for evaluating "rattle space" requirements for equipment subjected to random vibration. Adequate clearance space is needed, in this case, to insure that the vibrating equipment does not momentarily impact a hard surface resulting in high shock loads.

Peak Distribution of Narrow Band Random Noise

For a narrow band of Gaussian noise, the time varying envelope  $R(t)$  of the positive or negative peak amplitude of  $x(t)$ , such as shown in Figure 3.29, page 3.26, is a random variable with a Rayleigh distribution. The cumulative probability that the instantaneous value of the envelope  $R(t)$ , relative to the rms value  $\sigma$  of  $x(t)$ , will be equal to or less than an arbitrary value  $R_1/\sigma$  is given by

$$P\left(\frac{R}{\sigma} \leq \frac{R_1}{\sigma}\right) = 1 - e^{-R_1^2/2\sigma^2} \quad (3.104)$$

The complement of this distribution, plotted in Figure 3.36, is the cumulative probability that  $R/\sigma$  will be greater than  $R_1/\sigma$  which is

$$P\left(\frac{R}{\sigma} > \frac{R_1}{\sigma}\right) = e^{-R_1^2/2\sigma^2} \quad (3.105)$$

The rate of change of this distribution function as a function of  $R_1$  is the Rayleigh probability density and is given by

$$p(R_1) = \frac{R_1}{\sigma^2} e^{-R_1^2/2\sigma^2} \quad (3.106)$$

which can be normalized, as for the Gaussian probability density, to the form

$$\sigma p(R_1) = p(R_1/\sigma) = \frac{R_1}{\sigma} e^{-R_1^2/2\sigma^2} \quad (3.107)$$

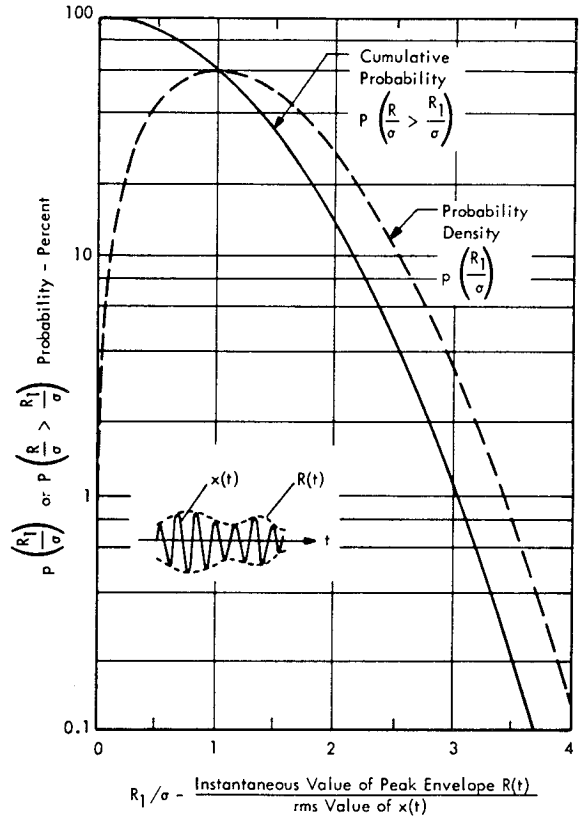


FIGURE 3.36 Normalized Cumulative Probability and Probability Density of Rayleigh Distribution of the Envelope of Peak Values of Narrow Band Random Gaussian Noise

This is the form shown in Figure 3.36. The log scale used for the ordinate in this figure provides a clearer definition of the peak distribution for application to design problems.

The main features of the Rayleigh distribution for peaks of a narrow band of random noise are:

- The envelope of the peaks of a narrow band of random Gaussian noise exceeds  $\pm\sigma$  about 61 percent of the time;  $\pm 2\sigma$ , 13.5 percent of the time; and  $\pm 3\sigma$ , 1.1 percent of the time.
- Fifty percent of the time, the peaks will exceed  $1.18\sigma$ .



- The average value of the envelope of the peaks of a random noise is  $\sqrt{\pi/2} \sigma$  or  $1.25 \sigma$  (Reference 3.2). In other words, the average of the instantaneous peak values of a narrow band of random Gaussian noise is 1.25 times the rms value of the random noise.

As an example, if a single degree-of-freedom system under random excitation has a mean square displacement response of  $0.25 \text{ inch}^2$ , the rms displacement will be  $\sqrt{0.25} = 0.5 \text{ inch}$ . The average peak response will be  $(1.25)(0.5) = 0.625 \text{ inch}$  but about 1 percent of the time, peak responses greater than  $3 \times 0.5 = 1.5 \text{ inches}$  would occur.

One additional feature of the variation in peaks in a narrow band of noise can be defined. As shown in the insert in Figure 3.36, within a single peak of the time varying envelope  $R(t)$ , several individual peaks of the random noise itself  $x(t)$  can occur. This grouping or "clumping" of individual peaks of the noise within any one envelope peak has been analyzed in detail in Reference 3.27. It is shown that for a linear single degree of freedom system with a resonant amplification factor  $Q$  and an rms random response  $\sigma$ , the average number  $\bar{n}_p$  of individual peak responses within a single envelope peak or "clump" which exceed a level  $R_1$  is given by the simple relationship

$$\bar{n}_p = \frac{\sigma}{R_1} \sqrt{Q/\pi} \quad (3.108)$$

Thus, for a  $Q$  of 28, there will be, on the average, just one peak of  $x(t)$  within a peak of the envelope  $R(t)$  which exceeds 3 times the rms value  $\sigma$  of  $x(t)$ . A  $Q$  of 28 is representative for typical structure and equipment with relatively low damping. Thus, a typical  $3\sigma$  peak of the response envelope of a lightly damped resonant system can be expected to show only 1 instantaneous peak of the random response for each envelope peak.

The average rate of occurrence  $f_R$  for which envelope peaks exceed a level  $R_1/\sigma$  is also shown in Reference 3.27 to be

$$f_R = f_o \sqrt{\frac{\pi}{Q}} \frac{R_1}{\sigma} e^{-R_1^2/2 \sigma^2} \quad (3.109)$$

where

$f_o$  = resonant frequency of single degree of freedom system.

Note the similarity to Equation 3.107 for the normalized Rayleigh probability density. Thus, the average rate of occurrence of the envelope peaks relative to the resonance frequency ( $f_R/f_o$ ) is equal to  $\sqrt{\pi/Q}$  times the numerical value of the normalized probability density plotted in Figure 3.36.

The average number of individual peaks per second  $f_p$  which exceed  $R_1/\sigma$  is simply the product of Equations 3.108 and 3.109 which is

$$f_p = f_o e^{-R_1^2/2 \sigma^2} \quad (3.110)$$

As expected, this is the same as the cumulative probability of the envelope (Equation 3.105) multiplied by the average frequency  $f_o$  of the narrow band of noise.

#### Peak Distribution of Wide Band Random Noise

For wide band random noise, the simple relationships outlined above are no longer valid. The time history of a typical wide band random noise, shown earlier in Figure 3.29, page 3-26 is much more complex than the fluctuating sinusoidal time history of a narrow band of noise. Specifically, wide band noise can have several positive peaks and troughs between two successive times when the random signal is zero. This contrasts with the cyclic nature of narrow band noise where each zero crossing is followed by either a positive or negative peak.

Although no closed solution is available for describing the peak distribution for a general wide band noise, two approximations are often used. The first approximation assumes that the peaks of the wide band noise have a Gaussian distribution with the same cumulative probability and probability density as shown in Figure 3.34. This is increasingly true as the bandwidth of the noise increases and the number of peaks between consecutive zero crossings increases (References 3.2 and 3.18).

The other approximation provides a closed solution for the distribution of peaks of a white noise passed through an ideal low-pass filter with a high cutoff frequency (Reference 3.18). This is an idealization of a wide band noise spectrum that contains a wide range of frequencies. For this case, the cumulative distribution of positive peaks greater than a level  $x_1$  normalized by the rms value  $\sigma$  is shown in Figure 3.37. The curve is based on the theory in Reference 3.18. For comparison, the Gaussian distribution for positive peaks is also shown. Finally, the cumulative Rayleigh distribution from Equation 3.105 is given in Figure 3.37. This demonstrates that for  $x_1/\sigma$  greater than one, the Rayleigh distribution is also a very good approximation for the distribution of peaks of this idealized model of wide band random noise. The following will verify that the Rayleigh distribution does, in fact, provide a suitable analytical model for peak distribution of both narrow band and wide band Gaussian random noise.

#### Experimental Data on Peak Distribution of Random Noise

Experimental measurements of the peak distribution of random noise data are frequently carried out to provide useful design data for statistical evaluation of structural loads. Some typical examples of such data are shown in Figure 3.38. These represent the peak distributions of narrow band and wide band samples of random acoustic noise generated by a high speed air jet and a large rocket booster (Reference 3.28). For presentation and evaluation of such data, it is convenient to construct the scales in such a way that the theoretical Rayleigh distribution can be shown as a straight line. This is accomplished by taking the logarithm, to the base 10, of both sides of Equation 3.105.

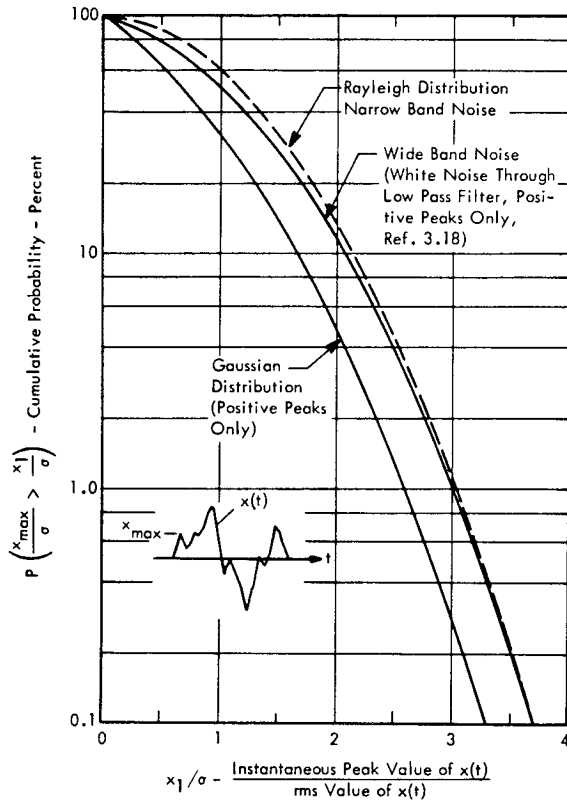


FIGURE 3.37 Normalized Cumulative Probability of Exceedance for Peak Values of Wide Band Random Gaussian Noise

The resulting expression, shown in Figure 3.38, is linear if the cumulative probability is plotted on a log scale and the peak to rms ratio is plotted on a squared scale. As shown in the figure, the experimental data for wide band rocket noise and narrow band air jet noise agree very well with the Rayleigh distribution while the narrow band sample of the same rocket noise data shows a greater deviation

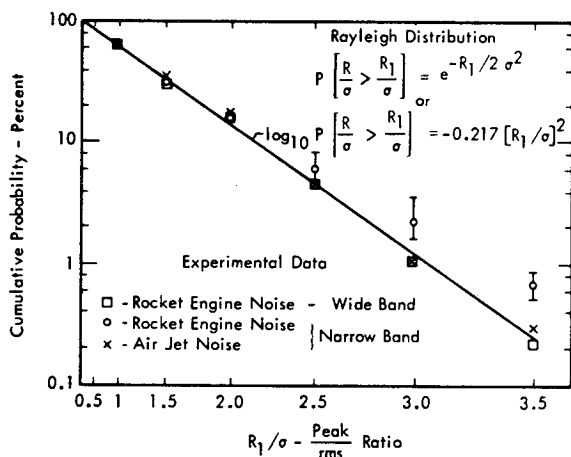


FIGURE 3.38 Experimental Data on Cumulative Probability of Peak Distribution of Random Acoustic Noise (From Ref. 3.27)

from theory. This represents an example of the phenomena discussed earlier of the lack of sensitivity of wide band noise peak distribution data to non-Gaussian random processes. In the case of the rocket noise data plotted in Figure 3.38, non-Gaussian characteristics were observed only when the data was first passed through a filter.

Peak Distribution of Combined Random and Sinusoidal Variables

Although sinusoidal excitation sources are not of primary concern for this manual, vibration of ground equipment located near rotating machinery or other cyclic vibration sources can result in significant combined sinusoidal and random vibration excitation. The statistical distribution for this type of excitation will be significantly different than for random excitation. In fact, identification of this difference is often utilized to verify the presence of a sinusoidal component in a random signal.

When a sinusoidal component is added to a narrow band of random noise centered about the frequency of the sine component, the cumulative distribution of the envelope of the instantaneous peaks takes the form shown in Figure 3.39 (Reference 3.18). In this case, the abscissa axis is the exceedance level  $R_1$  for the envelope divided by the rms value of the combined random and sine components. The distribution is shown for several values of the ratio of the peak amplitude  $A$  of the sinusoid to the rms value  $\sigma_n$  of the narrow band of noise. For random noise only,  $A/\sigma_n=0$ , and the peak distribution is the Rayleigh distribution. For a sinusoid only,  $A/\sigma_n = \infty$  and the distribution is a vertical line at  $R_1/\sigma_0=1.414$  which is simply the peak to rms ratio of a sinusoid. Significant deviation from the Rayleigh distribution does not occur for the combined signal until the peak amplitude of the sinusoid exceeds the rms value of the noise ( $A/\sigma_n > 1$ ).

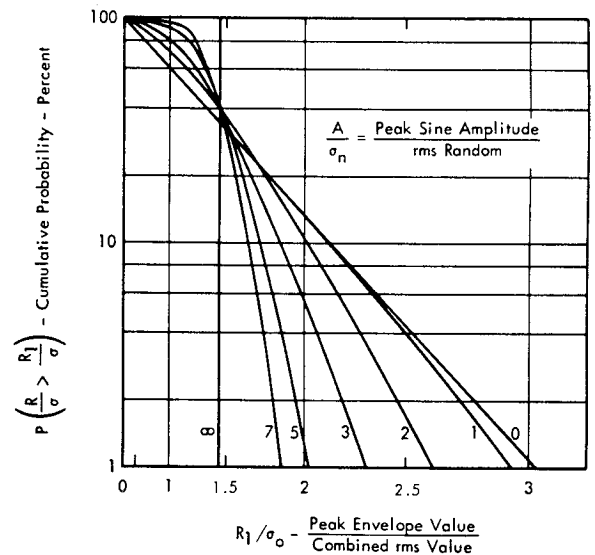


FIGURE 3.39 Normalized Cumulative Probability of Exceedance for Envelope of Combined Narrow Band Random Noise and Sinusoidal Component within the Same Band (Reference 3.18). The combined rms value  $\sigma_0$  is  $\sqrt{\sigma_n^2 + A^2/2}$ .

### Moments of Random Noise

The terminology and definitions employed so far to describe a random noise have covered the more commonly used terms. Useful characteristics of random noise can also be described in terms of its moments. These are defined by the general equation

$$\text{nth Moment} = \int_{-\infty}^{+\infty} x^n p(x) dx \quad (3.111)$$

where  $p(x)$  is the probability density of the random variable  $x$ . The mean value of a random variable,  $\bar{x}$ , is given by the first moment where  $n = 1$ . For stationary random noise and  $n = 1$ , it can be shown that Equation 3.111 is equivalent to the usual expression for the mean value

$$\bar{x} = \lim_{T \rightarrow \infty} \frac{1}{2T} \int_{-T}^{+T} x(t) dt \quad (3.112)$$

The mean square value  $\overline{x^2}$  is given by the second moment so that, for stationary random noise,

$$\overline{x^2} = \int_{-\infty}^{+\infty} x^2 p(x) dx = \lim_{T \rightarrow \infty} \frac{1}{2T} \int_{-T}^{+T} x^2(t) dt \quad (3.113)$$

When this moment is computed about the mean value  $\bar{x}$ , the result is called the variance which is the square of the rms value given by

$$\sigma^2 = \int_{-\infty}^{+\infty} (x - \bar{x})^2 p(x) dx = \overline{x^2} - (\bar{x})^2 \quad (3.114)$$

The next two higher order moments are frequently computed when making a digital analysis of random data. When taken about the mean value, and normalized by  $\sigma$ , these are: (Reference 3.22)

$$(n = 3) \text{ Skewness} = \frac{1}{\sigma^3} \int_{-\infty}^{+\infty} (x - \bar{x})^3 p(x) dx \quad (3.115)$$

For random noise with a Gaussian or normal distribution, the skewness is equal to zero.

$$(n = 4) \text{ Kurtosis} = \frac{1}{\sigma^4} \int_{-\infty}^{+\infty} (x - \bar{x})^4 p(x) dx \quad (3.116)$$

The kurtosis is equal to 3 for random noise with a Gaussian distribution.

### 3.2.3.8 Occurrence Rate for Zero Crossings and Maxima

The fatigue damage of a structure subjected to a varying load depends on the number of times the random load reverses direction (crosses zero) and the number of maxima of the load in a given period of time. For narrow band random noise, these are approximately equal to the average frequency of the band. For wide band noise, or the summation of resonant responses due to random excitation over a wide range of frequencies, an average frequency is no longer apparent. However, for a random Gaussian noise, it has been shown in Reference 3.18 that the average number of zero crossings per second with a positive slope,  $N_o^+$ , is related to the power spectral density  $W(f)$  by

$$N_o^+ = \left[ \int_0^{\infty} f^2 W(f) \cdot df \right]^{1/2} \cdot [\overline{x^2}]^{-1/2} \quad (3.117)$$

where  $\overline{x^2}$  is the mean square value of  $x(t)$  given by Equation 3.113.

It is also shown that the average number of maxima expected per second  $M$  in a wide band random noise is given by

$$M = \left[ \int_0^{\infty} f^4 W(f) df \right]^{1/2} \cdot \left[ \int_0^{\infty} f^2 W(f) df \right]^{-1/2} \quad (3.118)$$

For a constant spectral density over a bandwidth  $f_b - f_a$ , these two expressions reduce to

$$N_o^+ = \left[ \frac{1}{3} \frac{f_b^3 - f_a^3}{f_b - f_a} \right]^{1/2} \quad (3.119)$$

$$M = \left[ \frac{3}{5} \frac{f_b^5 - f_a^5}{f_b^3 - f_a^3} \right]^{1/2} \quad (3.120)$$

If these expressions are divided by the average frequency of the band  $(f_a + f_b)/2$ , a nondimensional value for frequency of occurrence is obtained as shown in Figure 3.40. The figure shows that the average zero crossing frequency (for a positive slope) is approximately equal to the average frequency of the band. This is simply an extension of the same result noted for a narrow band of noise. However, the average frequency of occurrence for the maxima  $M$  varies from 0 to 55 percent higher than the average frequency of the band, indicating more than 1 maxima for each positive-going zero crossing which is characteristic of wide band noise. The average number of maxima between each successive zero crossing is given by the ratio  $M/N_o^+$  which approaches a value of 1.34 for very wide band noise (i.e.  $f_b/f_a \gg 1$ ).

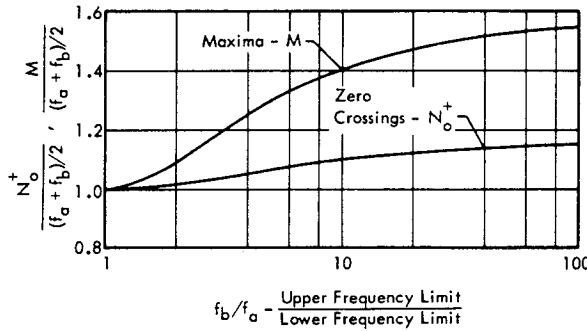


FIGURE 3.40 Average Frequency of Occurrence for Zero Crossings, with Positive Slope  $N_o^+$  and Maxima  $M$  Normalized by Average Frequency of Band of White Noise with Bandwidth  $f_b - f_a$  (From Reference 3.18).

As an example, for a band of white noise from 500 hertz to 5000 hertz, the average frequency is  $(5000 + 500)/2 = 2750$  hertz. According to Figure 3.40, for  $f_b/f_a = 5000/500 = 10$ , the average rate of occurrence of zero crossings with a positive slope would be  $(1.1)(2750) = 3025$  per sec and the average rate of occurrence of maxima would be  $(1.4)(2750) = 3850$  per sec.

3.2.3.9 Probability of Simultaneous Occurrence of Peak Responses for Two Different Systems

If two vibration-isolated equipment packages are located close together, it is possible for the packages to impact each other due to the simultaneous occurrence of peak responses of each package. To avoid this situation, adequate clearance or "rattle space" must be provided. If the excitation to the vibration isolated packages is random, and the packages vibrate completely independently of each other, the probability of impact can be readily determined. This determination is made by considering the joint probability of two random events. For example, consider the situation illustrated in Figure 3.41. The distance  $d$  represents a nominal separation distance of two equipment packages whose motions are defined by  $x(t)$  and  $y(t)$ , respectively, and  $x_1$  represents an arbitrary impact point which lies somewhere between 0 and  $d$ . Providing  $x(t)$  and  $y(t)$  are completely independent of each other, then the cumulative joint probability that the instantaneous sum  $x(t) + y(t)$  will exceed  $d$  can be given by the product of the probabilities that  $x(t)$  will exceed  $x_1$  and  $y(t)$  will exceed  $y_1 = d - x_1$ . The resulting expression can be put into non-dimensional form by normalizing each term by the rms values  $\sigma_x$  and  $\sigma_y$  of  $x(t)$  and  $y(t)$ , respectively, to give

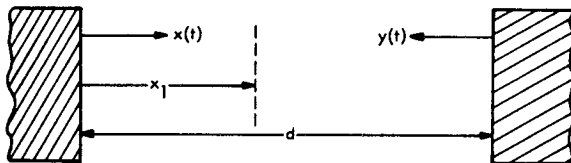


FIGURE 3.41 Illustration of Problem in Joint Probability - The Impact of Two Randomly Vibrating Equipment Packages at a Point  $x_1$  when the Nominal Separation Distance is  $d$ .

$$P [(x + y) > d] = P \left[ \frac{x}{\sigma_x} > \frac{x_1}{\sigma_x} \right] \cdot P \left[ \frac{y}{\sigma_y} > \frac{y_1}{\sigma_y} \right] \quad (3.121)$$

If the vibration response of the packages is a narrow band random variable with a Gaussian distribution, then the distribution of the envelope of the peak responses will follow the Rayleigh distribution given by Equation 3.105 and plotted in Figure 3.36. Thus, the cumulative joint probability is

$$P [(x + y) > d] = e^{-x_1^2/2\sigma_x^2} \cdot e^{-y_1^2/2\sigma_y^2} \quad (3.122)$$

However, the sum of  $x_1 + y_1$  must be equal to the separation distance  $d$ . Utilizing this fact to eliminate  $y_1$  from this equation and then by finding the value of  $x_1$  which gives the highest probability of impact for a given value of  $d$ ,  $\sigma_x$  and  $\sigma_y$ , the cumulative probability of impact can be reduced to the equation

$$P [(x + y) > d] = e^{-d/2 (\sigma_x^2 + \sigma_y^2)} \quad (3.123)$$

This simple result could have been written down directly by recognizing that there is in reality only one random variable in question which is the sum of the displacements,  $x(t) + y(t)$  which must equal  $d$  for impact to occur. The mean square value of this random variable will simply be  $\sigma_x^2 + \sigma_y^2$  since it was assumed that  $x(t)$  and  $y(t)$  were totally independent of each other. When this is no longer true,  $x(t)$  and  $y(t)$  are related to each other, and it is necessary to evaluate their covariance defined as the long time average of their product  $[x(t) \cdot y(t)]$ . Methods for solving this more complex problem are given in Chapter 2 of Reference 3.3.

3.2.3.10 Derivation of Response of Single Degree-of-Freedom System to Random Excitation - A Brief Summary

To complete this discussion of random excitation, a brief review is presented of the key steps which lead to the equations given earlier (Equations 3.94, 3.95 and 3.96) for the response of linear systems to random excitation. A single degree-of-freedom system is used as an example. Methods for handling the multiple degree-of-freedom system will be covered subsequently. The derivation is outlined in abbreviated form with a minimum of intermediate steps and is provided for reference purposes only. The literature cited at the beginning of Section 3.2.3 provides a more complete discussion. Reference 3.3 is particularly useful in this regard.

1) Following this derivation, the last section on random response outlines some of the more commonly used engineering methods for analyzing random loads.

2) Throughout this derivation, complex quantities are used for convenience in notation and for consistency with common practice. The quantity  $j$  is equal to  $\sqrt{-1}$  and the quantity

$e^{j\omega t}$  or  $\exp(j\omega t)$  represents the complex form of a sinusoidal function and is equivalent to a vector of unit length rotating counterclockwise with an angular velocity  $\omega$ . It has real and imaginary components which are given by the transformation

$$e^{j\omega t} = \cos \omega t + j \sin \omega t$$

Its complex conjugate is equivalent to a vector rotating in the opposite direction expressed by

$$e^{-j\omega t} = \cos \omega t - j \sin \omega t$$

Note also that the absolute value of this rotating vector, in other words, its magnitude without regard to phase, is given by the square root of the product of the vector and its complex conjugate or

$$\begin{aligned} |e^{j\omega t}| &= \sqrt{e^{j\omega t} \cdot e^{-j\omega t}} \\ &= \sqrt{(\cos \omega t + j \sin \omega t)(\cos \omega t - j \sin \omega t)} \\ &= \sqrt{\cos^2 \omega t + \sin^2 \omega t} \\ &= 1 \end{aligned}$$

#### Relationship Between Power Spectral Density and Fourier Spectrum of Random Noise

Any time history  $x(t)$  of finite length can be described in terms of a Fourier spectrum. These two variables are related by the Fourier Transform pair which are, in complex form, equal to

$$\begin{array}{l} \text{Fourier Integral} \\ \text{(Inverse Transform)} \end{array} \quad x(t) = \frac{1}{2\pi} \int_{-\infty}^{+\infty} F(j\omega) e^{j\omega t} d\omega \quad (3.124)$$

$$\begin{array}{l} \text{Fourier Transform} \\ \text{(Fourier Spectrum)} \end{array} \quad F(j\omega) = \int_{-\infty}^{+\infty} x(t) e^{-j\omega t} dt \quad (3.125)$$

where  $\omega$  = angular frequency - rad/sec. The second integral is finite only if  $x(t)$  is zero at  $\pm\infty$  so for application to random noise, it is necessary to consider a finite sample of noise of length  $T$  and then allow  $T$  to become very large. With this change, and converting to frequency in Hertz,  $f = \omega/2\pi$ , these equations become

$$x(t) = \int_{-\infty}^{+\infty} F(jf) e^{j2\pi ft} df \quad (3.126)$$

$$F(jf) = \lim_{T \rightarrow \infty} \int_{-T/2}^{+T/2} x(t) e^{-j2\pi ft} dt \quad (3.127)$$

Note that  $F(jf)$  is equal to  $F(j\omega)$  since Equations 3.125 and 3.127 are identical.

#### Mean Square Value

The mean square value of  $x(t)$  is given by

$$\overline{x^2} = \lim_{T \rightarrow \infty} \frac{1}{T} \int_{-T/2}^{+T/2} x(t) \cdot x(t) \cdot dt \quad (3.128)$$

(The limiting process of  $T \rightarrow \infty$  will be understood in the remaining equations.)

By substituting Equation 3.126 for one of the  $x(t)$ 's, this is

$$\overline{x^2} = \frac{1}{T} \int_{-T/2}^{+T/2} x(t) \left[ \int_{-\infty}^{+\infty} F(jf) e^{j2\pi ft} df \right] dt \quad (3.129)$$

Since  $F(jf)$  and  $x(t)$  are continuous in their respective intervals, the order of integration can be changed. Also by recognizing that the complex conjugate (complex quantity with opposite sign for imaginary term) of  $F(jf)$  is

$$F^*(jf) = \int_{-T/2}^{+T/2} x(t) e^{j2\pi ft} dt \quad (3.130)$$

Equation 3.129 becomes

$$\overline{x^2} = \frac{1}{T} \int_{-\infty}^{+\infty} F(jf) \cdot F^*(jf) df \quad (3.131a)$$

Since  $F(jf) \cdot F^*(jf)$  is the square of the absolute value of  $F(jf)$  and is symmetrical about  $f = 0$ , this reduces to

$$\overline{x^2} = \frac{2}{T} \int_0^{\infty} |F(jf)|^2 df \quad (3.131b)$$

The power spectral density  $W(f)$  of  $x(t)$  is defined so that the mean square value  $\overline{x^2}$  is

$$\overline{x^2} = \int_0^{\infty} W(f) df \quad (3.131c)$$

Therefore, by equating these two expressions, the desired relationship sought between the power spectral density and the Fourier spectrum is

$$W(f) = \frac{2}{T} |F(jf)|^2 \quad (3.132)$$

#### Autocorrelation Function

A quantity called the autocorrelation function  $R(\tau)$  will be

useful for evaluating response to random noise. This function is defined as the time average product of  $x(t)$  and the same variable delayed by a time  $\tau$ , or  $x(t + \tau)$ , so that  $R(\tau)$  is

$$R(\tau) = \frac{1}{T} \int_{-T/2}^{+T/2} x(t) x(t + \tau) dt \quad (3.133)$$

For stationary random noise, this time average product of  $x(t)$  and its delayed value  $x(t + \tau)$  is independent of the absolute time  $t$ . Hence,  $R(\tau)$  depends only on the time delay  $\tau$  and is a measure of the similarity or coherence between  $x(t)$  and its delayed value. In other words, it depends on how rapidly  $x(t)$  changes over a given interval  $\tau$  suggesting that there is a relationship, which indeed there is, between this time correlation function  $R(\tau)$  and the frequency content or spectral density  $W(f)$  of the noise.

Comparing Equations 3.133 and 3.128, since  $T \rightarrow \infty$  is implied in both cases, it is apparent that the autocorrelation function of  $x(t)$  for  $\tau = 0$  is also the mean square value, or

$$\overline{x^2} = R(0) \quad (3.134)$$

#### Relationship Between Power Spectral Density and Autocorrelation Function

Since  $R(\tau)$  is a function of the time delay variable  $\tau$ , it has a Fourier Transform given by

$$F_R(jf) = \int_{-T/2}^{+T/2} R(\tau) e^{-j 2\pi f \tau} d\tau \quad (3.135)$$

Substituting Equation 3.133 in 3.135 and then employing Equations 3.127 and 3.130, it can be shown that this Fourier Transform of the autocorrelation function is related to the Fourier Spectrum of the finite sample of  $x(t)$  by

$$\int_{-T/2}^{+T/2} R(\tau) e^{-j 2\pi f \tau} d\tau = \frac{1}{T} |F(jf)|^2 \quad (3.136)$$

From Equations 3.136 and 3.132, it is clear that when  $T$  is allowed to approach  $\infty$ , the power spectral density and the autocorrelation function can be related by

$$W(f) = 2 \int_{-\infty}^{+\infty} R(\tau) e^{-j 2\pi f \tau} d\tau \quad (3.137)$$

From Equation 3.126, this has the inverse transform

$$R(\tau) = \frac{1}{2} \int_{-\infty}^{+\infty} W(f) e^{j 2\pi f \tau} df \quad (3.138)$$

These are called the Weiner-Khinchin relations, and have been widely used in carrying out spectrum analysis of random data with digital computers. They can be further simplified, since both  $R(\tau)$  and  $W(f)$  are symmetrical about zero [i.e. -- even functions for which  $R(\tau) = R(-\tau)$  and  $W(f) = W(-f)$ ] so that they become

#### Weiner-Khinchin Relationships

$$W(f) = 4 \int_0^{\infty} R(\tau) \cos 2\pi f \tau d\tau \quad (3.139a)$$

$$R(\tau) = \int_0^{\infty} W(f) \cos 2\pi f \tau df \quad (3.139b)$$

#### Sinusoidal Response and Impulse Response of Single Degree-of-Freedom System

Consider a fixed-base single degree-of-freedom system (see Figure 3.3, page 3-3) with a resonance frequency  $f_o$ , damping constant  $\delta$  and spring constant  $k$ . If the mass  $m$  is driven by a sinusoidal force (expressed in complex form),  $P \exp(j 2\pi f_o t)$ , and the displacement of the mass is given by  $x(t)$ , then the steady state displacement response is the real part of

$$x(t) = \frac{P}{k} H(f) e^{j 2\pi f t} \quad (3.140)$$

where  $H(f)$  is defined as the Frequency Response Function.

#### Frequency Response Function

$$H(f) = 1 / \left[ 1 - (f/f_o)^2 + j 2 \delta f/f_o \right] \quad (3.141)$$

The absolute value of this has been identified earlier as the

#### Dynamic Magnification Factor

$$|H(f)| = 1 / \left[ \left( 1 - (f/f_o)^2 \right)^2 + (2 \delta f/f_o)^2 \right]^{1/2} \quad (3.142)$$

For any force input  $P(t)$ , the forced response of the system at time  $t$  can be given by the Duhamel or convolution integral which is

#### Duhamel Integral

$$x(t) = \int_{-\infty}^t h(t-\tau) P(\tau) d\tau \quad (3.143)$$

where  $h(t)$  is the unit impulse response given by

$$h(t) = \frac{1}{2\pi m f_o \sqrt{1-\delta^2}} e^{-2\pi \delta f_o t} \sin 2\pi f_o \sqrt{1-\delta^2} t \quad (3.144)$$

and  $\tau$  is a dummy time variable equal to or less than  $t$ . Letting  $\tau' = t - \tau$ , Equation 3.143 can be written as

$$x(t) = \int_0^{\infty} h(\tau') P(t-\tau') d\tau' \quad (3.145)$$

Again, if  $P(t)$  is a sinusoidal force  $P_0 \exp(j 2\pi f t)$ , then by using Equation 3.145, the forced displacement response is

$$x(t) = P_0 e^{j 2\pi f t} \int_0^{\infty} h(\tau') e^{-j 2\pi f \tau'} d\tau' \quad (3.146)$$

By comparing this to Equation 3.140, a relationship between the Frequency Response Function  $H(f)$  and the impulse response  $h(\tau')$  is obtained. Since  $\tau'$  is an arbitrary time variable, it can be replaced by  $t$  so that the relationship is

Fourier Transform of  
Impulse Response

$$H(f)/k = \int_0^{\infty} h(t) e^{-j 2\pi f t} dt \quad (3.147)$$

Thus, the Frequency Response Function  $H(f)$ , divided by the spring constant  $k$ , is the Fourier Transform of the unit impulse response  $h(t)$ . For other input and response variables, corresponding relationships can be obtained.

Autocorrelation and Power Spectral Density of Response

The above relationships can now all be combined to obtain the spectral density of the response. This is obtained by first writing the autocorrelation of the response  $R_x(\tau)$  from Equation 3.133 using the modified Duhamel integral in Equation 3.145. The result is

$$\begin{aligned} R_x(\tau) &= \frac{1}{T} \int_{-T/2}^{+T/2} x(t) \cdot x(t+\tau) dt \\ &= \frac{1}{T} \int_{-T/2}^{+T/2} \left[ \int_0^{\infty} h(\tau') P(t-\tau') d\tau' \right] \\ &\quad \times \left[ \int_0^{\infty} h(\tau'') P(t+\tau-\tau'') d\tau'' \right] dt \end{aligned} \quad (3.148)$$

where  $\tau'$  and  $\tau''$  are the respective dummy time variables for the Duhamel integrals while  $\tau$  is the fixed delay time associated with the autocorrelation. The time average of the  $P(t)$  terms with respect to time  $t$  can be simplified with

Equation 3.133. If the arbitrary time scale in these terms is shifted by  $+\tau'$ , then Equation 3.148 reduces to

$$R_x(\tau) = \int_0^{\infty} h(\tau') \int_0^{\infty} h(\tau'') R_p(\tau+\tau'-\tau'') d\tau' d\tau'' \quad (3.149)$$

where  $R_p(\tau+\tau'-\tau'')$  is the autocorrelation of the driving force for a delay time  $(\tau+\tau'-\tau'')$ . Now this result can be converted to the power spectral density of the response  $W_x(f)$  by using Equation 3.137. Thus, with a bit of algebra, the spectral density of the response can be written as

$$\begin{aligned} W_x(f) &= 2 \int_0^{\infty} h(\tau') e^{j 2\pi f \tau'} d\tau' \cdot \int_0^{\infty} h(\tau'') e^{-j 2\pi f \tau''} d\tau'' \\ &\quad \times \int_{-\infty}^{+\infty} R_p(\tau+\tau'-\tau'') e^{-j 2\pi f (\tau+\tau'-\tau'')} d(\tau+\tau'-\tau'') \end{aligned} \quad (3.150)$$

The first two integrals can be recognized as the Fourier Transform and its complex conjugate of the unit impulse response  $h(t)$ . However, these are equivalent to the frequency response function  $H(f)$  and its complex conjugate  $H^*(f)$  according to Equation 3.147. The third integral is the Fourier Transform of the autocorrelation function of the excitation which was shown in Equation 3.137 to be equal to the power spectral density of the excitation.

Applying Equation 3.147 to the first two integrals in Equation 3.150 and Equation 3.137 to the third, the result is

$$W_x(f) = 2 \frac{H^*(f)}{k} \cdot \frac{H(f)}{k} \cdot \frac{W_p(f)}{2}$$

or

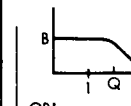
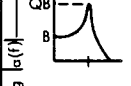
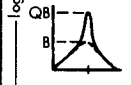

$$W_x(f) = W_p(f) \cdot |H(f)|^2 / k^2 \quad (3.151)$$

For the general case of response of a single degree-of-freedom system, the particular sinusoidal transfer function  $|H(f)/k|$  in Equation 3.151 is replaced by the general term  $|a(f)|$ . This general transfer function has been specified in Figure 3.8, page 3-8 for various input-output relationships for sinusoidal excitation of a single degree-of-freedom system. Thus, the same result given earlier in Equation 3.94 is formally derived.

The mean square response  $\overline{x^2}$  is obtained by integrating the response power spectral density according to Equation 3.131c. This provides the same result given earlier in Equation 3.95, or

$$\overline{x^2} = \int_0^{\infty} W_p(f) \cdot |a(f)|^2 df \quad (3.152)$$

Finally, this integration can be carried out for white noise excitation [ $W_p(f) = \text{constant}$ ] and particular forms of the sinusoidal transfer function  $|a(f)|$  for a single degree-of-freedom system (Reference 3.29). The resulting closed solutions specify the mean square response for the forms of  $|a(f)|$  indicated in the following chart.

Transfer Function $ a(f) $	Normalized Mean Square Response $\frac{\sigma_r^2}{x^2 W_p(f)} = \int_0^\infty  a(f) ^2 df$
 $B / [1 + (f/f_0 Q)^2]^{1/2}$	$\frac{\pi}{2} B^2 f_0 Q \quad (3.153)$
 $B  H(f) $	
 $B \frac{f}{f_0}  H(f) $	
 $B [1 + (f/f_0 Q)^2]^{1/2}  H(f) $ or $B  T(f) $	$\frac{\pi}{2} B^2 f_0 Q \left(1 + \frac{1}{Q^2}\right) \quad (3.154)$

The first form of  $|a(f)|$  does not exhibit the usual resonant response associated with a single degree-of-freedom system. It does represent, however, the frequency variation of the relative displacement of the spring and damper of a moving base mass-spring system for a constant driving force applied to the base (see Figure 3.6, page 3-7). In this case, the constant B is equal to  $1/k$ . This relative displacement is constant up to a cutoff frequency equal to  $Q f_0$  where  $f_0$  is the resonance frequency of the mass-spring system.

The second form of  $|a(f)|$  corresponds to the example considered earlier; namely, the frequency variation of the mass displacement for a fixed-base mass-spring system with a constant driving force.  $|H(f)|$  is the dynamic magnification factor given by Equation 3.142 and B is equal to  $1/k$ . The third form of  $|a(f)|$  corresponds to the frequency variation of velocity of the mass for this case and the constant B is equal to  $1/2\pi f_0 m = 1/Q c$  where m is the mass and c is the damping term.

For the last form of  $|a(f)|$ , the term  $|T(f)|$  is the transmissibility of a mass-spring system discussed in Section 3.2.1.5. The transmissibility is the ratio of amplitudes of a sinusoidal driving force to reaction force for a fixed base system. It is also the ratio of input to response motion for a moving base system. For this case,  $B = 1$  since the excitation and response variables are the same. Note that the closed solution for this case, given by Equation 3.154, is essentially the same as the general form in Equation 3.153. The additional term  $(1 + 1/Q^2)$  in the former is usually negligible for typical values of Q.

The integration required for Equation 3.152 to obtain these closed solutions must be carried out by a special method called contour integration which involves residue theory (References 3.29 and 3.12). The form shown here for the solution is considered the most meaningful for physical interpretation; however, a variety of other equivalent forms commonly appear in the literature.

For most other common forms of  $|a(f)|$ , involving an amplified response at resonance for a single degree-of-freedom system (see Figure 3.9, page 3-9), the integral in Equation 3.152 does not converge when  $W_p(f)$  is constant.

However, as indicated earlier in Section 3.2.3.6, if the integration limits are restricted to frequencies near the resonance frequency only, then, the mean square response within the effective resonant bandwidth of any linear single degree-of-freedom system, for white noise excitation, is approximately equal to the expression given by Equation 3.153.

Thus, the basic practical equations for response of a single degree of freedom system to random excitation have been formally derived. While a simpler approach can be used which treats a finite sample of random noise as a Fourier Series (Reference 3.2), the formal approach used here provides a more complete background on response to random loads. This is illustrated by the key relationships between power spectral density, the autocorrelation function, the Duhamel integral and the sinusoidal frequency response function of a single degree-of-freedom system. These relationships are obtained through application of the Fourier Transform. They will be employed with increasing frequency in the future as design problems related to random excitation and response become more prominent.

General Response Equation for Single Degree-of-Freedom System Under Random Excitation

To summarize, for any form of random excitation, with an input spectral density  $W_p(f)$  to a single degree-of-freedom system, the expression for the approximate rms response  $\sigma_r$  will have the form

$$\sigma_r \approx B \left[ \frac{\pi}{2} W_p(f) f_0 Q \right]^{1/2} \quad (3.155)$$

where B is the appropriate constant, relating the response units to the excitation. Except for any necessary conversion to g units when specifying an acceleration response, this constant is given by the constant part of the general sinusoidal transfer functions  $|a(f)|$  in Figure 3.9, page 3-9. However, it is only for those transfer functions which have a finite area that Equation 3.155 is an exact solution for a constant input spectrum.

3.2.3.11 Engineering Methods for Analyzing Random Response

The application of some of the principles discussed in Section 3.2.3 can be illustrated by the following examples. Simple graphical and computational aids are also provided



to assist in the solution of problems dealing with the response of single degree-of-freedom systems to random excitation.

Power Spectral Density

The power spectral density  $W(f)$  of a random variable is determined by first measuring the mean square value  $\overline{\Delta x^2}$  of the random quantity within a fixed narrow frequency band of width  $\Delta f_a$ . The power spectral density (or simply spectral density) is then given by

$$W(f) = \frac{\overline{\Delta x^2}}{\Delta f_a}$$

When the quantity measured is a motion variable such as acceleration, velocity, etc., the spectral density is usually identified as follows:

Variable	Power Spectral Density	Units
Acceleration	APSD	$g^2/\text{Hz}$
Velocity	VPSD	$(\text{in}/\text{sec})^2/\text{Hz}$
Displacement	DPSD	$\text{in}^2/\text{Hz}$

Throughout the rest of this section, the terms APSD, VPSD, etc., will be used to identify the corresponding power spectral density. Subscripts will be added to identify the spectral density with the absolute motion of the mass (x), the base (u), or the relative motion of the spring ( $\epsilon$ ), for a single degree-of-freedom system. The rms value of any random variable will be identified by the basic symbol  $\sigma$  with a corresponding subscript, such as x to indicate the rms value of the acceleration of the mass. The numerical value of acceleration is always given in terms of "g" units where g is the acceleration of gravity = 386 in/sec<sup>2</sup>.

At any given frequency f, if the original spectral density was measured with a sufficiently narrow filter (one with a bandwidth  $\Delta f_a$  much less than its center frequency f) these three quantities can be related by the following expressions for the units specified above.

$$\text{APSD} - g^2/\text{Hz} = 0.000265 f^2 \text{ (VPSD)} = 0.0105 f^4 \text{ (DPSD)}$$

$$\text{VPSD} - (\text{in}/\text{sec})^2/\text{Hz} = 3775 (\text{APSD})/f^2 = 39.5 f^2 \text{ (DPSD)}$$

$$\text{DPSD} - \text{in}^2/\text{Hz} = 95.6 (\text{APSD})/f^4 = 0.0253 (\text{VPSD})/f^2$$

Vibration is normally measured using accelerometer transducers to convert acceleration into an electrical voltage for data acquisition. Conversion from measured acceleration spectral density APSD to VPSD and DPSD can be made with the above expressions or by a conversion chart such as shown in Figure 3.42. A theoretical plot of the APSD for a single degree-of-system is also shown in this figure. This represents the acceleration that would be measured on a mass of a fixed-base mass-spring system driven by a random force with a constant force spectral

density. At resonance, the curve has a peak value approximately equal to  $Q^2$ , while above resonance, the acceleration spectral density approaches a constant value equal to the force spectral density divided by the square of the mass. Note that the same curve, plotted in terms of displacement spectral density DPSD would vary over a range of  $10^5$  while the APSD curve varies only over a range of  $10^2$ . While actual measured random vibration spectra on real structural systems will usually exhibit a much more complex pattern, the simplified graph in Figure 3.42 serves to illustrate basic trends in such data. Below the first structural resonance, the vibration tends to exhibit a constant displacement spectrum (stiffness controlled) while above resonance, a mean line through the data will frequently approximate a constant acceleration spectrum (mass controlled). Hence, it is usually more convenient to display random vibration in terms of its acceleration spectral density.

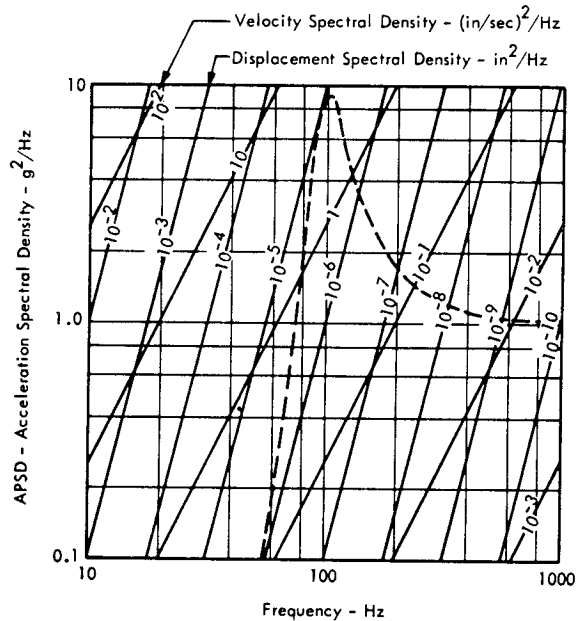


FIGURE 3.42 Conversion from Acceleration Power Spectral Density to Velocity and Displacement Power Spectral Densities Superimposed on Theoretical APSD<sub>x</sub> for Single Degree-of-Freedom System with  $f_o = 100$  Hz and  $Q = 3$  (See Figure 3.43)

Response of Fixed-Base System for Random Force Excitation of Mass

The methods for computing the response of a single degree of freedom system for random excitation have been outlined in Sections 3.2.3.6 and 3.2.3.10. To illustrate their application, consider the following example. Assume that the acceleration spectral density curve in Figure 3.42 is based on the following parameters.

Constant Force Spectral Density  $W_p(f) = 9560 \text{ lb}^2/\text{Hz}$   
 Spring Constant  $k = 10^5 \text{ lb/in}$   
 Weight  $W = 97.8 \text{ lb}$   
 Mass  $W/g = m = 0.253 \text{ lb sec}^2/\text{in}$   
 Natural Frequency (Undamped)  $f_o = \frac{1}{2\pi} \sqrt{k/m}$   
 $= 3.13 \sqrt{k/W}$   
 $= 100 \text{ Hz}$   
 Resonant Amplification Factor  $Q = 3$

Displacement Spectral Density

Below Resonance ( $f \ll f_o$ )

$$\text{DPSD}_x \rightarrow \frac{W_p(f)}{k^2} = 9.56 \times 10^{-7} \text{ in}^2/\text{Hz}$$

At Resonance ( $f = f_o$ )

$$\text{DPSD}_x(f_o) = \frac{W_p(f)}{k^2} Q^2 = 8.61 \times 10^{-6} \text{ in}^2/\text{Hz}$$

Acceleration Spectral Density

At Resonance ( $f = f_o$ )

$$\text{APSD}_x(f_o) = \frac{W_p(f)}{W^2} Q^2 = (4\pi^2 f_o^2/g)^2 \cdot \text{DPSD}_x = 9.0 \text{ g}^2/\text{Hz}$$

Above Resonance ( $f \gg f_o$ )

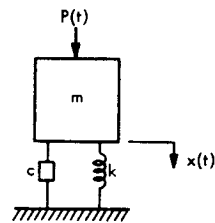
$$\text{APSD}_x \rightarrow \frac{W_p(f)}{W^2} = 1.0 \text{ g}^2/\text{Hz}$$

The following additional information for this case, illustrated in Figure 3.43a, can then be determined on the basis of the equations for the displacement and acceleration spectral densities which are

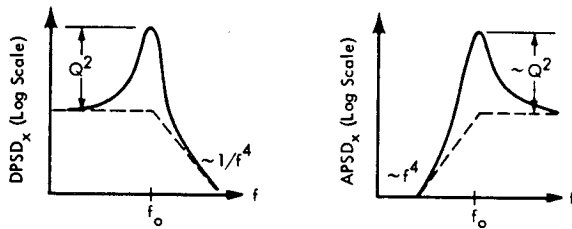
$$\text{DPSD}_x = \frac{W_p(f)}{k^2} |H(f)|^2 \quad - \text{in}^2/\text{Hz} \quad (3.156)$$

$$\text{APSD}_x = \frac{W_p(f)}{W^2} |H(f)|^2 \cdot (f/f_o)^4 \quad - \text{g}^2/\text{Hz} \quad (3.157)$$

where  $|H(f)|$  is the dynamic magnification factor given by Equation 3.142. The general shape of these spectral densities are compared in Figure 3.43b.



a) Single Degree of Freedom System Driven by a Random Force  $P(t)$  with a Constant Force Spectral Density



b) Displacement and Acceleration Spectral Densities for Example Shown in a)

FIGURE 3.43 Example of Random Force Excitation of Single Degree of Freedom System

rms Displacement

$$\overline{x^2} \text{ (Mean Square)} = \frac{\pi}{2} \frac{W_p(f)}{k^2} f_o Q = 4.51 \times 10^{-4} \text{ in}^2$$

$$\sigma_x \text{ - (rms)} = \sqrt{\overline{x^2}} = 0.0212 \text{ in}$$

rms Acceleration (Effective Value)

The effective rms acceleration of the mass can be calculated on the basis of the rms deflection or by an equivalent computation based on the acceleration spectral density plot. However, both methods must assume that the actual spectral density of the applied force decreases at frequencies above resonance. For a constant force spectral density at all frequencies, the mean square acceleration, represented by the area under the acceleration spectral density curve, would be infinite.

The computation based on the rms deflection assumes that practically all the energy in the random response is concentrated in the narrow bandwidth centered about the resonance frequency  $f_o$ . It will be recalled from the earlier discussions that a narrow band of random noise or vibration is very similar to sinusoidal motion with a randomly varying amplitude. Thus, the rms acceleration should be closely approximated by applying the relationships between acceleration  $\ddot{x}(t)$  and deflection  $x(t)$  for sinusoidal vibration. If a sinusoidal motion has a peak displacement  $X$  at a frequency  $f$ , the peak acceleration  $A$ , in  $g$ 's, is

$$A = \frac{(2\pi f)^2}{g} X = 0.1023 f^2 X - g \text{ (peak)}$$

Applying this equation, the rms acceleration for the random vibration would be approximately

$$\sigma_{\ddot{x}} \approx 0.1023 f_o^2 \sigma_x = 21.7 \text{ g (rms)} \quad (3.158)$$

All of the above computations are based on prior knowledge of the parameters of the single degree of freedom system and its excitation. More commonly, however, only measured acceleration spectral density response data are available. To determine the rms acceleration for only one resonant mode from such a spectral density measurement, which usually exhibits many resonant peaks, the following procedure can be employed.

As shown by the linear plot in Figure 3.44, the acceleration spectral density curve, in the vicinity of resonance of a single resonant mode, can be replaced by an equivalent narrow band with an effective bandwidth equal to

$$\Delta f_{\text{eff}} = \frac{\pi}{2} \frac{f_o}{Q} \quad (3.159)$$

and a constant acceleration spectral density equal to the maximum value at resonance,  $APSD_x(f_o)$ . The mean square acceleration within this equivalent band is then

$$\overline{\ddot{x}^2/g^2} = APSD_x(f_o) \cdot \frac{\pi}{2} \frac{f_o}{Q} - g^2 \quad (3.160)$$

Since  $APSD_x(f_o) = W_p(f) Q^2/W^2$ , the rms acceleration  $\sigma_{\ddot{x}}$  is

$$\sigma_{\ddot{x}} = \sqrt{\overline{\ddot{x}^2/g^2}} = \left[ \frac{\pi}{2} \frac{W_p(f) f_o Q}{W^2} \right]^{1/2} - g \quad (3.161)$$

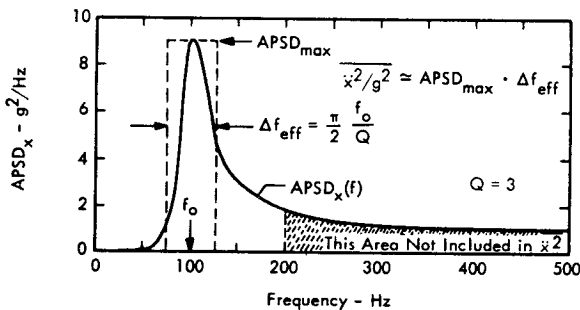


FIGURE 3.44 Example of Acceleration Spectral Density Curve for Response of Single Degree of Freedom System Replaced by an Equivalent Narrow Band with Constant Spectral Density

For the example above, the maximum acceleration response spectral density at  $f = f_o$  is  $APSD_x(f_o) \approx W_p(f)^2 Q^2/W^2 = 9.0 \text{ g}^2/\text{Hz}$ . (The true maximum, in this case, is actually higher by the factor  $[4 Q^2/(4 Q^2 - 1)]$  and occurs at a

frequency equal to  $f_o \sqrt{1/(1 - 1/2 Q^2)}$ , however, these differences are negligible for the usual values of  $Q$ .) Thus, using Equation 3.161, the effective rms acceleration is approximately equal to

$$\sigma_{\ddot{x}} = \left[ \frac{\pi}{2} \cdot 9 \cdot 100/3 \right]^{1/2} = 21.7 \text{ g (rms)} \quad (3.162)$$

which is the same result given by Equation 3.158.

If the actual acceleration spectral density curve in Figure 3.44 is integrated graphically, it is found that this rms acceleration corresponds approximately to the area under the curve up to a frequency of approximately  $2 f_o$ . Thus, the effective rms acceleration given by Equation 3.161 will be in error if there are any additional resonant peaks at frequencies less than  $2 f_o$ . This upper frequency limit will decrease for higher values of  $Q$ .

### Three Sigma Peak Displacement and Acceleration Response

Based on the Rayleigh distribution curve, three times the rms displacement or rms acceleration of this resonant response would not be exceeded, on the average, more than 1.1 percent of the time. This probable value is commonly used for defining a peak value of the response. For this example, this corresponds to a 3 sigma peak deflection of  $3 \times 0.0212 = 0.0636 \text{ in.}$  and a 3 sigma acceleration of  $65.1 \text{ g's.}$

### Acceleration Response of Base-Excited System for Random Acceleration of Base

For random excitation of the base of a mass-spring system (see Figure 3.6, page 3-7), the response acceleration spectral density  $APSD_x$  of the mass is given by

$$APSD_x = APSD_u \cdot |T(f)|^2 \quad (3.163)$$

where  $APSD_u$  is the acceleration spectral density of the input excitation and  $|T(f)|$  is the sinusoidal transmissibility for such a system (see Figure 3.7, page 3-8). The area under the transmissibility curve is finite so that for a constant input acceleration spectrum, the rms response of the mass can be given in closed form (see Equation 3.154). For the usual values of  $Q$ , this is very nearly equal to

$$\sigma_{\ddot{x}} \approx \left[ \frac{\pi}{2} APSD_u f_o Q \right]^{1/2} \quad (3.164)$$

Unlike the previous case for force excitation, this rms acceleration response includes the effect of response at all frequencies above and below resonance. For example, for a constant input acceleration spectral density of  $0.1 \text{ g}^2/\text{Hz}$ , a resonant frequency of 100 Hz, and a  $Q$  of 5, the mass would respond with an rms acceleration  $\sigma_{\ddot{x}}$  of  $8.86 \text{ g's}$  (rms). A 3 sigma peak response of  $26.6 \text{ g}$  would be exceeded about 1.1 percent of the time.

Absolute Displacement Response of Base-Excited Systems

The absolute displacement of the mass is a critical parameter for evaluation of clearance problems of base-excited mass-spring systems. The absolute rms deflection of the mass could be estimated by applying the same concept of equivalent sinusoidal motion used earlier for the force-excited fixed-base system. The effective rms deflection of the mass, in this case, would be

$$\sigma_x = \frac{g}{4\pi^2 f_o^2} \cdot \sigma_{\ddot{x}} = \frac{1}{0.102 f_o^2} \sigma_{\ddot{x}} = 0.0087 \text{ in.} \quad (3.165)$$

However, this displacement is based on the assumption that the actual input acceleration spectral density falls off sharply below the resonant frequency. As shown by the linear plot in Figure 3.45, the displacement spectral density of the mass would actually approach infinity at zero frequency for a constant acceleration spectral density input. The rms displacement of 0.0087 inch given by Equation 3.165 corresponds only to the area under this curve for frequencies above approximately  $0.8 f_o$ . Clearly, then, the true rms deflection of the mass, for a base excited system, will be highly dependent on the input acceleration spectrum below the resonant frequency. For example, if the input acceleration spectrum were constant from infinity down to  $1/4$  of the resonant frequency and zero below this frequency, the true rms deflection for the case considered here would be approximately double the value predicted by Equation 3.165.

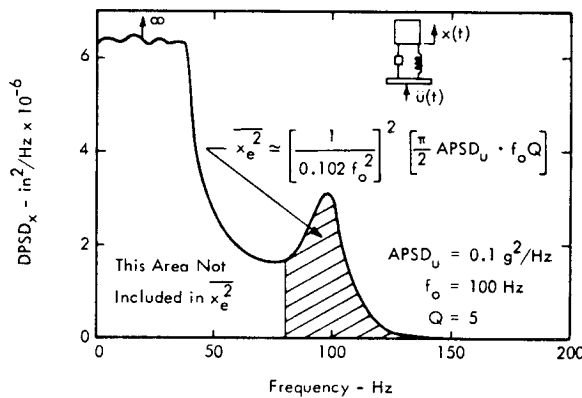


FIGURE 3.45 Linear Plot of Displacement Spectral Density of Mass for Random Excitation of Base of Mass-Spring System with a Constant Input Acceleration Spectral Density (APSD<sub>u</sub>)

When it is necessary to determine this deflection accurately, the acceleration signal from the accelerometer transducer should be integrated twice, before a spectrum analysis and rms value is obtained. This double integration is equivalent to dividing the acceleration signal by  $f^2$  thus converting it to a signal proportional to displacement. The rms value of this modified signal will then be directly proportional to the true rms deflection of the mass. This can be converted to a probable peak to peak deflection with a 1.1 percent probability of exceedance by multiplying the rms value by 6.

Relative Displacement Response of Base-Excited Systems

For a base-excited mass-spring system, the relative deflection  $\epsilon(t)$  of the spring defines the stress in this supporting member. If the input acceleration spectral density of the base excitation is  $APSD_u$ , the spectral density of the relative displacement of the spring is given by

$$DPSD_\epsilon = APSD_u \cdot \left[ \frac{g}{4\pi^2 f_o^2} \right]^2 |H(f)|^2 \quad (3.166)$$

where

$f_o$  = resonance frequency - Hz

$|H(f)|$  = dynamic magnification factor given by Equation 3.142.

Except for the type of excitation and the constant term  $[g/4\pi^2 f_o^2]^2$ , this equation has the same form as the expression for the displacement response spectrum  $DPSD_x$  for a fixed-based system. (See Equation 3.156 and Figure 3.43.) A closed expression is therefore available for the rms relative deflection for a constant input acceleration spectrum  $APSD_u$ . This is

$$\sigma_\epsilon = \sqrt{\epsilon^2} = \frac{g}{4\pi^2 f_o^2} \left[ \frac{\pi}{2} APSD_u \cdot f_o Q \right]^{1/2} \quad (3.167)$$

Comparing this solution with Equations 3.164 and 3.165, it is clear that the rms relative spring deflection is numerically equal to the approximate rms deflection of the mass for a random acceleration input to a moving base mass-spring system. However, the true deflection of the mass depends on the input spectrum below resonance while the relative spring deflection is practically independent of the spectrum outside the resonant bandwidth.

Graphical Aid for Predicting Peak Response of a Base-Excited System to Constant Input Acceleration Spectrum

If the random input to a moving base system has a constant acceleration spectral density, the acceleration response of the mass and relative deflection of the spring can be shown on a single graph of input spectral density  $APSD_u$  versus resonant frequency  $f_o$  for a given value of  $Q$ . Such a graph is shown in Figure 3.46 for a typical  $Q$  of 10. For convenient application to design problems, the acceleration response is specified by lines of constant 3 sigma peak acceleration. The relative deflection response is also given by lines of constant 3 sigma peak deflection. For example, if the resonant frequency  $f_o$  is 70 hertz and the input acceleration spectral density is  $1.0 g^2/Hz$ , the intersection of these two coordinates shows that the 3 sigma peak acceleration of the mass is 100 g and the 3 sigma peak relative deflection of the spring is 0.2 inch. This is also the approximate 3 sigma peak deflection of the mass due to vibration energy within the resonant bandwidth of the system. If a measured or predicted input acceleration spectral density plot is overlaid on Figure 3.46, the 3 sigma response can be read directly for any resonant frequency  $f_o$ .

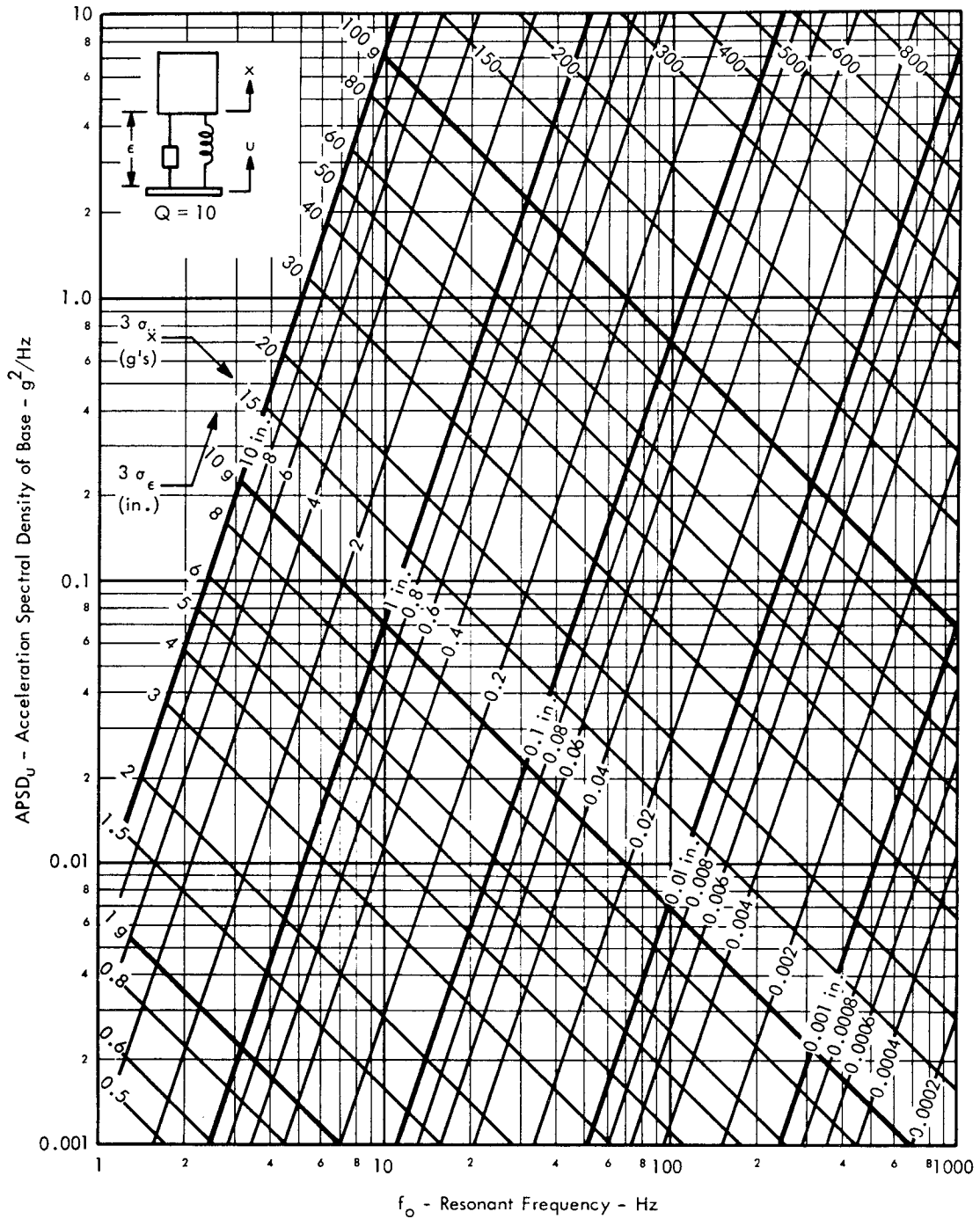


FIGURE 3.46 Design Chart for Predicting 3 Sigma Peak Acceleration Response ( $3\sigma_x$ ) and 3 Sigma Relative Deflection Response ( $3\sigma_\epsilon$ ) for Single Degree-of-Freedom with Constant Acceleration Spectral Density ( $APSD_0$ ) Input to Base

For other values of  $Q$ , the response values scale directly as  $\sqrt{Q/10}$ . The graph was constructed by using Equations 3.164 and 3.167 to predict the rms response.

Graphical Method for Evaluation of rms Value of a Wide Band Random Excitation

A common procedure for specifying a random vibration environment consists of constructing an envelope of the expected maximum acceleration spectrum. This envelope can be used for the definition of vibration tests or design of structure subjected to the random environment. It is frequently drawn, as shown in Figure 3.47, with connected straight line segments on a log-log plot of acceleration spectral density versus frequency. The rms acceleration for this acceleration spectrum envelope is useful for both test planning and random load design analysis. This rms value can be determined by first calculating the mean square

value or area of the spectrum under each part of the various straight line segments as illustrated in the insert in Figure 3.47. For each of these segments, the mean square value is given by the simple equations shown in the figure. The spectral density for each segment can be expressed in the form

$$APSD = W(f) = W_1 \cdot \left(\frac{f}{f_1}\right)^n \tag{3.168}$$

where  $W_1$  is the initial spectral density at frequency  $f_1$  and  $n$  is the exponent of  $f$  which defines the slope of the spectrum on the log-log plot. Thus, over the frequency limits  $f_1$  to  $f_2$ , the mean square value for any segment is the integral

$$\sigma^2 = \int_{f_1}^{f_2} W(f) \cdot df = W_1 \int_{f_1}^{f_2} \left(\frac{f}{f_1}\right)^n df \tag{3.169}$$

For  $n \neq -1$ , this is

$$\sigma^2 = \left[ W_1 \left(\frac{f_2}{f_1}\right)^n \cdot f_2 - W_1 f_1 \right] / (n + 1)$$

or

$$\sigma^2 = [W_2 f_2 - W_1 f_1] / (n + 1) \tag{3.170}$$

and for  $n = -1$ , it reduces to

$$\sigma^2 = 2.3 W_1 f_1 \log_{10} (f_2/f_1) \tag{3.171}$$

The overall rms value of the envelope is simply the square root of the sum of the mean square values for each segment.

For the typical case, illustrated in Figure 3.47, the rms acceleration for the spectrum envelope is 6.8 g (rms). The largest portion of this is represented by the third segment of the spectrum envelope with a slope of -1 extending from 200 to 800 Hertz.

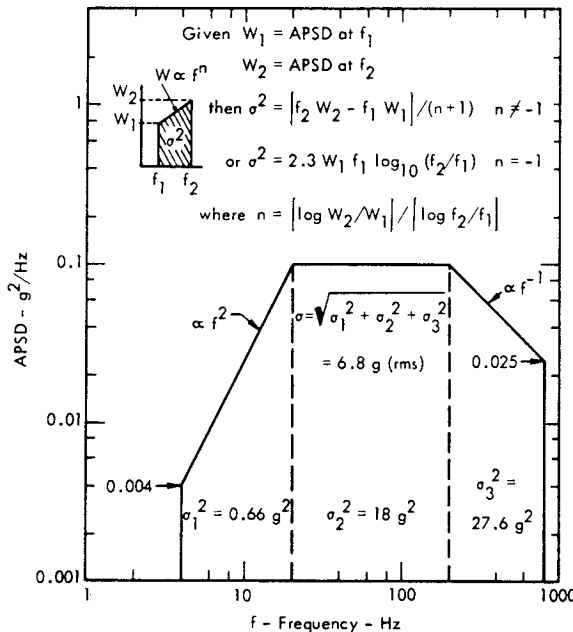


FIGURE 3.47 Example of Calculation of rms Acceleration for Vibration Test Envelope Plotted with Straight Line Segments on Log-Log Scale

### 3.3 VIBRATION RESPONSE OF COMPLEX STRUCTURE

The treatment of structural vibration in terms of the response of a single degree of freedom system must now be expanded to include the more complex behavior of real structure. As an illustration of such behavior, Figure 3.48 shows a hypothetical example of vibration response that might be measured at some point on a complex structure such as a rocket engine test stand. This represents the displacement response amplitude due to excitation by a single sinusoidal point force whose frequency slowly increases from 0 to a very high frequency. The pattern of vibration response observed may be broken down into three general regions.

- At the lowest frequencies, (Region I) the observed response has a characteristic behavior very similar to that of a single degree-of-freedom system. Below the first resonance frequency,  $f_0$ , the motion of the entire structure is controlled by the static stiffness of its load carrying members and its foundation. At the first resonance frequency, all or part of the mass of the structure acts as a rigid mass resting on this "static" spring thus exhibiting the general response of the simple mass-spring system discussed earlier in this chapter.
- At higher frequencies, the influence of several clearly identifiable resonant modes is observed (Region II). These individual resonant modes may consist of vibration of the basic mass-spring structure in several of its possible 6 modes (three translational directions and three rotational directions) or it may consist of the combined resonant response of the structure in only one direction but involving coupled vibration of various portions of the structure, each acting like a mass-spring system. In either case, the equivalent mass-spring elements involved can be identified by a dynamic and static analysis of the structure.
- At still higher frequencies, individual resonant modes are no longer discernible and the structural response becomes very complex and impractical to analyze exactly. In this frequency range, the modal density, or number of resonant modes within a given frequency interval, is more significant than the resonant frequency of any one resonant mode.

The analysis methods to be considered in the following will be primarily concerned with the first two regions illustrated in Figure 3.48. It is usually in this frequency range where the most significant loads on ground structure will occur as a result of sonic excitation. Further consideration of response in the higher frequency region III will be covered in Chapters 8 and 9.

In each of these frequency ranges, the response can be theoretically determined from the summation of the response of independent free vibration modes, called normal modes. Each mode can then be treated as a single degree-of-freedom system so that by summing the response of each mode,

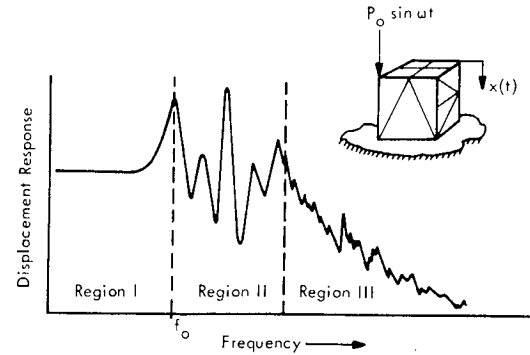


FIGURE 3.48 Illustration of Typical Vibration Response Characteristics of Complex Structure to Excitation by Sinusoidal Excitation with a Slowly Changing Frequency

the overall response can be determined. While it is often possible to define the most critical dynamic load on a structure in terms of the response of only the fundamental or lowest frequency mode, it is generally desirable or necessary to analyze the net response of several of these lowest modes. This is particularly important when conducting vibration tests or detailed dynamic analyses of large complex structural assemblies which are encountered in the design of rocket test facilities.

#### 3.3.1 METHODS OF VIBRATION ANALYSIS FOR COMPLEX STRUCTURE

There are two general approaches to the complex dynamic behavior of structural systems. The approach used most frequently assumes that the structure can be represented by a series of lumped or rigid masses connected to each other or to a fixed base by springs and dampers. Logically, this is identified as the lumped parameter approach. It is particularly useful for analyzing the vibration response of a structure which can be considered physically as just such an array of lumped elements. Such a discrete system has a finite number of normal modes determined by the number of mass elements employed and the number of directions each mass can move. The minimum number of coordinates required to uniquely define the motion of such a system is equal to the number of degrees of freedom.

For the second method, the structure is represented by one or more idealized distributed elements such as beams or plates which have a continuous distribution of mass and stiffness properties and an infinite number of vibration modes. However, it is possible to approximate the lower frequency modes of these distributed elements by lumped parameters. In this case, the continuous structural element is simulated by an array of lumped elements which exhibit the same general vibration characteristics as the continuous element. This lumped parameter approximation is not valid, however, for vibration modes with an order greater than the number of lumped elements used for the approximation. For example, a series of three masses, connected by appropriate springs, can represent, at best, only the first three vibration modes of a continuous beam. In fact, to obtain acceptable accuracy for the  $n$ th mode of a beam it is ordinarily necessary to employ at least  $n + 1$  lumped elements

to approximate the dynamic response characteristics of the  $n$ th mode (References 3.30 - 3.32). One exception involves the use of a single mass-spring element to simulate only the fundamental vibration mode of a distributed element such as a beam. In this case, the mass and spring element and its input force excitation can be adjusted, by conservation of energy principles, to be equivalent to the actual beam when the maximum deflection of the two systems are equal. A specific example of this approach is used in Chapter 8 for the analysis of building response to blast loads.

The principal methods, utilized in this manual, for analyzing the vibration response of either a lumped or distributed parameter system may be categorized as follows:

- Classical Normal Mode Method
- Mechanical Mobility Method
- Numerical Integration Method
- Empirical or Experimental Method

Examples of each of these methods appear in succeeding chapters of this manual; however, fundamentals of the first two only will be reviewed here (References 3.1 - 3.5, 3.33 - 3.35). Two examples of numerical integration methods are explained and utilized in Section 2 of Chapter 8 for analysis of blast loads on buildings. An extensive review of other numerical integration methods is given in Chapter 28 of Reference 3.1. The empirical or experimental method is self-explanatory and examples of its application will appear in Chapters 8, 9, 11 and the Appendix. This includes examples of full scale and model scale experimental techniques. The latter are particularly useful for detailed dynamic analysis of large structural systems.

Other methods exist for solving structural dynamics problems and the reader is referred to the literature for additional details. Notable among these other methods are:

- Passive and active electrical analog techniques, which can be usefully applied to analyze vibration of structure in the lower frequency range (Region I and II in Figure 3.48) (Reference 3.1 - Chapter 29).
- The transfer matrix method, which is particularly useful for modal analysis of linear chain configurations such as piping systems (Reference 3.36).
- Statistical energy method for analysis of vibration response at high frequencies where modal density is high (Region III) (References 3.37 - 3.39). Although this method is not yet fully developed as a practical design tool, it is a valuable addition to the field of structural vibration analysis.

### 3.3.1.1 Application of Digital Computer Techniques

There is an ever increasing trend towards the use of digital computers with their tremendous computational speed and potential for solving complex structural dynamics problems.

This provides the structural designer with a sophisticated analytical tool for carrying out detailed structural vibration analyses which were impractical a few years ago. Computations involving 20 to 30 degrees of freedom are handled as a matter of course, with the growing number of general and specialized computer programs designed specifically for structural vibration analysis. Computer programs, designed to handle over 200 degrees of freedom, are in current use by many structural dynamicists. Yet with all this overwhelming computerized analytical capability, it is still necessary to be able to solve less complex problems for simplified analyses and engineering studies of structural vibration. The material presented in the following is directed primarily at this level with the additional objective of providing a basic background for the more complex computerized methods.

### 3.3.1.2 Objectives of Dynamic Analysis

The methods selected for analysis of the vibration characteristics of a complex structure will be influenced by the end objectives. These objectives may require determination of:

- Peak dynamic deflections
- Maximum dynamic stresses
- Dynamic stability of structural system under cyclic loads (i.e. -- undesirable feedback of resonant structural vibration on a rocket engine test stand)
- Fatigue life under repeated loads
- Maximum acceleration loads on secondary structure and equipment
- Transmission of vibro-acoustic energy through structure.

The degree of sophistication and accuracy required to meet these objectives will vary over a wide range and an analysis method should be selected which is no more complex than necessary for the accuracy required for the problem. It is also desirable to select an analysis method which is consistent with any inherent inaccuracies in definition of the input excitation. A detailed structural analysis which predicts resonance frequencies within one percent is hardly practical for evaluating blast loads when the blast input itself may not be known better than  $\pm 50$  percent. On the other hand, a dynamic structural stability problem involving feedback between vibration of a test stand or fuel piping system and a rocket engine combustion chamber may require a very sophisticated analysis.

Therefore, a vibration analysis of the structure may range from a simple calculation of the dynamic deflection for a given load and estimated fundamental resonance frequency to carrying out a detailed analysis of the forced response of the structure to a complex dynamic load. The normal mode approach and the mechanical mobility approach, outlined in the following, provide two of the more useful vibration analysis techniques which have the flexibility to cover a wide range of such problems.



### 3.3.2 CLASSICAL NORMAL MODE ANALYSIS FOR LUMPED PARAMETER SYSTEMS

It will be convenient to define most of the basic concepts for analysis of multiple degree-of-freedom systems by illustrating their application to lumped parameter systems. It will be shown later that the same concepts also apply to distributed systems such as plates or beams. The application of normal mode analysis methods to lumped parameter systems can be illustrated by first analyzing a two degree of freedom system (Reference 3.2). An example of such a system is shown in Figure 3.49a. The system is defined by two masses,  $m_1$  and  $m_2$ , driven by forces  $P_1(t)$  and  $P_2(t)$ , which are coupled together by a parallel combination of a spring  $k$  and damper  $c$  and also connected to a fixed base by springs  $k_1$  and  $k_2$ , respectively. Motion of the system is restricted to the plane of the paper, and its position at any instant of time is defined by the mass coordinates  $x_1$  and  $x_2$ .

The two steps -- definition of the mechanical model and selection of the coordinate system, correspond to the key initial phase in any vibration analysis of a complex structure. The type of mechanical model chosen will generally establish the minimum possible error of the results while the type of analysis carried out on this model will usually establish the maximum error. The choice of a coordinate system is theoretically arbitrary. However, from a practical standpoint, an optimum choice can often be made which simplifies the mathematics. Without prior knowledge of the system, it is best to choose coordinates, as in Figure 3.49a, which correspond to absolute displacements and/or rotations at the center of mass of any element as measured from its equilibrium position. For motion excitation of simple spring-mass systems, the relative deflection of the springs may be a more convenient set of coordinates.

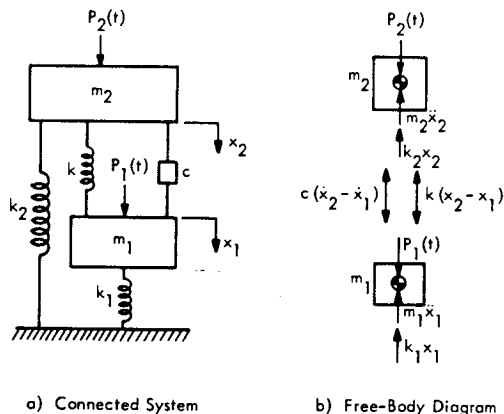


FIGURE 3.49 Two Degree-of-Freedom System

For some mass-spring systems, a detailed analysis may be unnecessary if only qualitative results are desired. A mechanical mobility model can be constructed, at this point, and the general vibration characteristics determined by inspection or by simple graphical analysis.

#### 3.3.2.1 Equations of Motion for Two Degree-of-Freedom System

Returning now to the system shown in Figure 3.49, the equation of motion for each mass can be written down by applying D'Alembert's principle for the equilibrium of dynamic forces acting on the center of mass. This is illustrated by the free body diagram in Figure 3.49b. [Note that this principle is equivalent to expressing Newton's second law of motion in the form of an equilibrium condition,  $\Sigma$  (Forces acting on center of mass) -  $m\ddot{x} = 0$ .] A consistent set of rules must be followed for such diagrams to insure proper values and signs for the forces and displacements.

- If displacements are taken from the position of static equilibrium, gravitational forces (weights) and corresponding static restraint forces cancel out and may be ignored.
- All externally applied forces and dynamic restraint forces acting on each mass must be added vectorially at its center of gravity.
- The net summation of these forces produces an acceleration  $\ddot{x}$  of the center of mass in the same direction as the net force which is opposed by the inertial force,  $-m\ddot{x}$ , acting in the opposite direction.
- The positive direction for force and displacement must be the same for each mass for a consistent sign convention.
- For rotational motion, a force is replaced by the moment about the center of gravity, mass is replaced by the mass moment of inertia about the same point, and displacements and accelerations become angles and angular accelerations about this point.

Following these rules, and choosing downward forces as positive, the equations of motion can be written for  $m_1$  as

$$P_1(t) + c(\dot{x}_2 - \dot{x}_1) + k(x_2 - x_1) - m_1 \ddot{x}_1 - k_1 x_1 = 0$$

or

$$m_1 \ddot{x}_1 + c(\dot{x}_1 - \dot{x}_2) + (k_1 + k)x_1 - kx_2 = P_1(t) \quad (3.172)$$

Similarly, for  $m_2$ ,

$$m_2 \ddot{x}_2 - c(\dot{x}_1 - \dot{x}_2) - kx_1 + (k_2 + k)x_2 = P_2(t) \quad (3.173)$$

Equations 3.172 and 3.173 represent a set of linear differential equations of second order. The variables  $x_1$  and  $x_2$  appear in both equations so that they are coupled through the damping parameter  $c$  and spring constant  $k$  and

must be solved simultaneously. It will be shown that the basic advantage of the normal mode method is that a complete simultaneous solution of this set of equations (one for each degree of freedom) can be avoided and a new set of independent equations of motion developed which can be readily solved individually.

### 3.3.2.2 Normal Mode Solution for Two Degree-of-Freedom System

The normal mode solution is based on the fact that the vibration response of the system in Figure 3.49 can be described in terms of its natural modes of vibration as a freely vibrating undamped system. In this case, when damping is eliminated ( $c = 0$ ) and the excitation removed, ( $P_1(t) = P_2(t) = 0$ ), the equations of motion for free undamped vibration become

$$\left. \begin{aligned} m_1 \ddot{x}_1 + (k_1 + k) x_1 - k x_2 &= 0 \\ m_2 \ddot{x}_2 - k x_1 + (k_2 + k) x_2 &= 0 \end{aligned} \right\} \quad (3.174)$$

Just as for the single degree-of-freedom system, the free vibration of each mass will be defined by the transient solution to these equations of motion and will have the form

$$\left. \begin{aligned} x_1(t) &= X_1 \sin(\omega t + \theta) \\ x_2(t) &= X_2 \sin(\omega t + \theta) \end{aligned} \right\} \quad (3.175)$$

Since there are two degrees of freedom, two values for the frequency of free vibration  $\omega$  can be expected. These are found by substituting the assumed solutions (Equation 3.175) into Equation 3.174. The time varying terms drop out leaving only the pair of algebraic expressions involving the system parameters and amplitudes of vibration.

$$(k_1 + k - \omega^2 m_1) X_1 - k X_2 = 0 \quad (3.176a)$$

$$-k X_1 + (k_2 + k - \omega^2 m_2) X_2 = 0 \quad (3.176b)$$

Unless  $X_1$  and  $X_2$  are zero (the trivial solution), this set of linear simultaneous equations is satisfied only when the determinant of the coefficients is zero or

$$\begin{vmatrix} k_1 + k - \omega^2 m_1 & -k \\ -k & k_2 + k - \omega^2 m_2 \end{vmatrix} = 0 \quad (3.177)$$

This is the characteristic equation of the system and when it is expanded into a polynomial in  $\omega$ , the frequency equation is obtained.

$$\omega^4 - \left( \frac{k_1 + k}{m_1} + \frac{k_2 + k}{m_2} \right) \omega^2 + \frac{k_1 k_2 + (k_1 + k_2) k}{m_1 m_2} = 0 \quad (3.178)$$

This equation has two real positive roots  $\omega_1$  and  $\omega_2$  which are the natural frequencies (or eigen values) for the normal modes of the system. For the two degree-of-freedom system in Figure 3.49, the roots are given by

$$\left. \begin{aligned} \omega_1 &= \left[ \frac{R}{2} + \frac{1}{2} \sqrt{R^2 - 4S} \right]^{1/2} \\ \omega_2 &= \left[ \frac{R}{2} - \frac{1}{2} \sqrt{R^2 - 4S} \right]^{1/2} \end{aligned} \right\} \quad (3.179)$$

where

$$R = \left[ \frac{k_1 + k}{m_1} + \frac{k_2 + k}{m_2} \right]$$

and

$$S = \left[ \frac{k_1 k_2 + (k_1 + k_2) k}{m_1 m_2} \right]$$

If each of these two natural frequencies are substituted back into Equation 3.176a or 3.176b, then two expressions are obtained for the ratios of the amplitudes  $X_1$  and  $X_2$ . These are identified as follows for each natural frequency.

For  $\omega_1$

$$\left. \frac{X_2}{X_1} \Big|_{\omega_1} = (k_1 + k - \omega_1^2 m_1) / k \right\}$$

and  $\omega_2$

$$\left. \frac{X_2}{X_1} \Big|_{\omega_2} = (k_1 + k - \omega_2^2 m_1) / k \right\} \quad (3.180)$$

These ratios represent the free vibration amplitude of mass  $m_2$  relative to the amplitude of  $m_1$  for each of the natural frequencies  $\omega_1$  and  $\omega_2$  of the system. The absolute values of these modal amplitudes are not defined at this point and it will be the convention in this manual to set the maximum relative amplitude for each mode equal to 1. These normalized values for the relative amplitudes of the mass elements are defined as the normal modes which define the (characteristic) mode shapes of the system. Other names such as natural modes or eigenvectors are also used. They will be identified by the term  $\phi_n(x_i)$  or simply  $\phi_{in}$  where subscript  $i$  refers to the  $i$ th mass element and  $n$  designates the  $n$ th natural frequency. In all cases,  $\phi_{in}$  will have a value between 1.0 and -1.0. A value of -1.0 for any mode would signify that the mass element involved was vibrating with a magnitude equal to but in the opposite direction from that of the reference mass which has the

maximum amplitude for that mode. This normalizing process will take on more significance when treating systems with many more modes or degrees of freedom. It is a basic part of the normal mode concept.

It is now clear that the free sinusoidal motion of each mass, vibrating in one of its normal modes, can be expressed as the product of a nondimensional normal mode shape  $\phi_{in}$  and a time varying amplitude which will be called the normal or principal coordinate  $q_n(t)$  for this mode. Thus, for mass  $m_1$ , the motion in the first mode will be described by

$$x_1(\omega_1, t) = \phi_{11} q_1(t) = \phi_{11} \bar{q}_1 \sin(\omega_1 t + \theta_1) \tag{3.181}$$

where

$\phi_{11}$  = the relative mode shape for mass  $m_1$  at the first natural frequency  $\omega_1$

$\bar{q}_1$  = the peak amplitude of this mode.

Similarly, for the second mass  $m_2$ , the motion at this same natural frequency will be given by

$$x_2(\omega_1, t) = \phi_{21} q_1(t) = \phi_{21} \bar{q}_1 \sin(\omega_1 t + \theta_1) \tag{3.182}$$

The time varying parts of these two equations will always be identical for a given mode so that, with no damping, both masses will vibrate exactly in phase (or exactly out of phase) with each other in each normal mode.

The choice of the name normal coordinate for the time varying quantity  $q_n(t)$  now seems appropriate, for  $q_n(t)$  represents a reference amplitude of the entire system in the  $n$ th mode. Each of these normal coordinates may be treated as the time varying amplitude of a single degree-of-freedom system, representing one normal mode, which is essentially independent of all the other modes of a multidegree of freedom system. Proof of this will be given in the following sections.

The general solution to the equations of motion for free vibration of the two degree-of-freedom system, given earlier by Equation 3.175, can now be expressed as the sum of the normal mode solutions in the form

$$x_1(t) = \phi_{11} \bar{q}_1 \sin(\omega_1 t + \theta_1) + \phi_{12} \bar{q}_2 \sin(\omega_2 t + \theta_2) \tag{3.183}$$

$$x_2(t) = \phi_{21} \bar{q}_1 \sin(\omega_1 t + \theta_1) + \phi_{22} \bar{q}_2 \sin(\omega_2 t + \theta_2)$$

Clearly, the general expression for the motion of the  $i$ th mass of a system with  $N$  degrees of freedom is the summation

$$x_i(t) = \sum_{n=1}^N \phi_{in} \bar{q}_n \sin(\omega_n t + \theta_n) \tag{3.184}$$

For free vibration, the constants  $\bar{q}_n$  and  $\theta_n$  will be determined by the initial conditions. There would be  $N$  such equations to describe the motion of the entire system containing  $N$  mass elements, each equation having  $N$  terms for the  $N$  natural frequencies. This array of  $N$  terms in  $N$  equations points to the application of matrix algebra as an obvious way to solve more complex systems. However, before considering the application of matrices to the general case, it will be convenient to develop most of the basic concepts of the normal mode method by treating specific examples of simple two degree-of-freedom systems.

### 3.3.2.3 Free Vibration Response of Symmetrical Two Degree-of-Freedom System

For one example, consider an undamped two degree of freedom system as shown in Figure 3.50a. This can also be represented in the form shown in Figure 3.50b which is an example of the form used for simulating the normal modes of a uniform beam where longitudinal motion of the springs is equivalent to lateral motion of the beam.

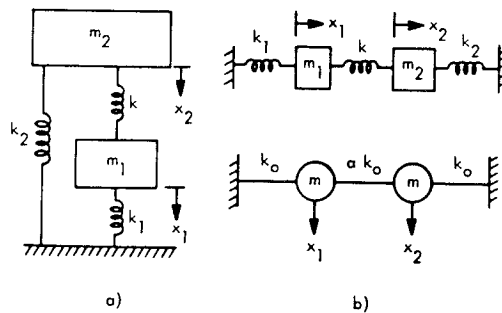


FIGURE 3.50 Undamped Two Degree-of-Freedom System  
a) Vertical Form, and b) Chain Form to Simulate Lumped Mass Model of a Beam  
where  $k_1 = k_2 = k_0$ ,  $k = a k_0$  and  $m_1 = m_2 = m$

For this case, let  $k_1 = k_2 = k_0$ ,  $m_1 = m_2 = m$  and  $k = a k_0$ . From Equation 3.178, the natural frequencies of this system will be the roots of the polynomial

$$\omega^4 - 2 [(1+a) k_0/m] \omega^2 + k_0^2 (1+2a)/m^2 = 0$$

The two positive roots or natural frequencies are

$$\left. \begin{aligned} \omega_1 &= \sqrt{k_0/m} \\ \omega_2 &= \sqrt{k_0 (1+2a)/m} \end{aligned} \right\} \tag{3.185}$$

The mode shapes are found by substituting these frequencies into Equation 3.180, after substituting the values for  $k_1$ ,  $k_2$ ,  $k$  and  $m_1$  given above. The resulting expressions are

$$\left. \frac{X_2}{X_1} \right|_{\omega_1} = 1$$

and

$$\left. \frac{x_2}{x_1} \right|_{\omega_2} = -1$$

so that for the first normal mode, the two masses have the same peak amplitude and are exactly in phase.

$$(\phi_{11} = \phi_{21} = 1)$$

For the second normal mode, the two masses have the same magnitude but opposite phases and

$$(\phi_{12} = 1 = -\phi_{22})$$

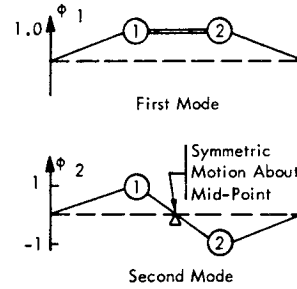
These mode shapes are illustrated in Figure 3.51a. Note that the first mode is a symmetric mode and there is no relative motion between the two masses, so that the coupling spring  $k$  can be replaced by a massless rigid link. The system then reduces to essentially one mass  $m_1 + m_2 = 2m$  resting on one spring with a spring constant equal to  $k_1 + k_2 = 2k_o$  and, as indicated by Equation 3.185, the natural frequency for this mode is simply  $\sqrt{k_o/m}$ .

The second mode is an antisymmetric mode for which the mid-point of the coupling spring is stationary. For the analogous lumped mass model of a beam, this would correspond to a point of zero lateral motion but with rotation about a pivot point. Such points of zero motion (in the direction which is characteristic for the mode) are called node points (or node lines in a two-dimensional vibrating system). The points (or lines) of maximum response are called antinodes.

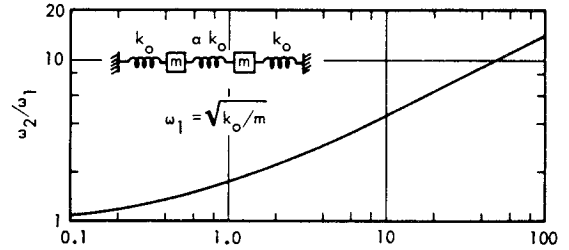
The natural frequency of the second mode was given in Equation 3.185. When it is normalized by the first mode frequency  $\omega_1 = \sqrt{k_o/m}$ , it can be defined in terms of the single parameter  $\alpha$  which is the stiffness of the coupling spring  $\alpha k_o$  relative to the stiffness  $k_o$  of the other two springs. This normalized second mode frequency is shown in Figure 3.51b.

The time history of free vibration of each mass of the two degree of freedom system can now be determined from the initial displacement  $x_i(t=0)$  and velocities  $\dot{x}_i(t=0)$  of each mass. The latter can be used with Equation 3.183 to find the unknown values of the normal coordinates  $q_n(t)$ . In this case, a set of four simultaneous equations (two for each mass) would have to be solved. However, a more direct method can be used based on the orthogonality of the normal modes which will be described in the following sections.

For the particular case of the symmetrical two degree-of-freedom system illustrated in Figure 3.50b, it can be shown that the amplitude  $\bar{q}_n$  and phase angle  $\theta_n$  of the normal coordinates are given by



a) Normal Mode Shape



b) Frequency  $\omega_2$  of Second Normal Mode Relative to Frequency  $\omega_1$  of First Mode

FIGURE 3.51 Mode Shapes and Natural Frequencies of Symmetrical Two Degree-of-Freedom System

$$\bar{q}_1 = \frac{1}{2} \sqrt{[x_1(0) + x_2(0)]^2 + [\dot{x}_1(0) + \dot{x}_2(0)]^2} / \omega_1^2$$

$$\theta_1 = \tan^{-1} \left\{ \omega_1 [x_1(0) + x_2(0)] / [\dot{x}_1(0) + \dot{x}_2(0)] \right\}$$

$$\bar{q}_2 = \frac{1}{2} \sqrt{[x_2(0) - x_1(0)]^2 + [\dot{x}_2(0) - \dot{x}_1(0)]^2} / \omega_2^2$$

$$\theta_2 = \tan^{-1} \left\{ \omega_2 [x_1(0) - x_2(0)] / [\dot{x}_1(0) - \dot{x}_2(0)] \right\}$$

where  $x_i(0)$  and  $\dot{x}_i(0)$  is the initial displacement and velocity of the  $i$ th mass. As an example, for the special case in Figure 3.51, consider only an initial velocity (e.g. - due to an impulse load) which is the same for each mass so that  $x_1(0) = x_2(0) = 0$  and  $\dot{x}_1(0) = \dot{x}_2(0) = \dot{x}_o$ . Then, from Equation 3.186,

$$\bar{q}_1 = X(0)/\omega_1, \quad \theta_1 = 0^\circ$$

and

$$\bar{q}_2 = 0$$

Thus, for a symmetrical initial condition for this symmetrical system, only the first normal mode is excited. If the initial velocity had been of equal magnitude but opposite phase for each mass, only the second normal mode would

be excited. Both modes would be excited equally if an initial velocity is imparted to only one of the masses. In this case, if the modal amplitudes are  $\bar{q}_1 = \bar{q}_2 = \bar{q}_0$ , the time history of the free vibration of the undamped system in Figure 3.51 would then be

$$x_1(t) = \bar{q}_0 [\sin \omega_1 t + \sin \omega_2 t]$$

$$x_2(t) = \bar{q}_0 [\sin \omega_1 t - \sin \omega_2 t]$$

which can also be expressed as

$$x_1(t) = 2 \bar{q}_0 \sin \left( \frac{\omega_1 + \omega_2}{2} t \right) \cos \left( \frac{\omega_2 - \omega_1}{2} t \right) \tag{3.187}$$

$$x_2(t) = 2 \bar{q}_0 \sin \left[ \frac{\omega_1 + \omega_2}{2} t + \frac{\pi}{2} \right] \cos \left[ \frac{\omega_2 - \omega_1}{2} t - \frac{\pi}{2} \right]$$

Thus, while each mode represents a perfectly in or out of phase motion of each mass, the combined motion of both modes is such that the envelope of the vibration of one mass is out of phase by 90 degrees with the other mass. This envelope has a repetition rate governed by the difference frequency  $(\omega_2 - \omega_1)$  which appears in the cosine term in Equation 3.187. This results in the well known pattern of vibration for such a system where the energy appears to shift back and forth from one mass to the other. This is illustrated in Figure 3.52 for the same system considered above where the coupling spring factor  $a$  is 0.4. This phenomena of beats is frequently observed for vibration of large structural systems with two closely adjacent modes. As shown in Figure 3.52, the peak displacement of each mass is the result of the combined peak responses in each of the two normal modes. When these are in-phase for one mass, they are out-of-phase for the other, resulting in a minimum response for the latter.

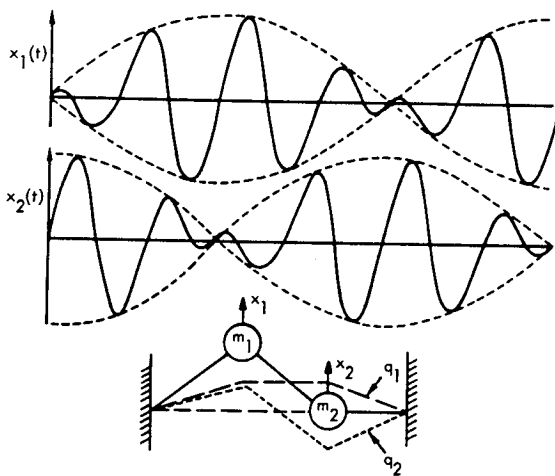


FIGURE 3.52 Vibration Time History of Two Degree-of-Freedom System Illustrating Oscillation of Energy from One Mass to the Other Due to Changing Phase Relationship Between the Two Modal Displacements  $q_1$  and  $q_2$

Thus, the total kinetic and potential energy of the system is momentarily concentrated in the motion of only one of the masses. The energy will then shift back and forth between the two masses as indicated in Figure 3.52. If there are no losses in the system, the total energy will remain constant at all times.

### 3.3.2.4 Energy, Generalized Mass and Stiffness of Two Degree-of-Freedom System

This consideration of the energy of the system can be extended to introduce the fundamental concept of orthogonality of normal modes. This is the most important property of a normal mode for it is the key to separating the equations of motion for the system into a set of independent single degree-of-freedom equations.

First, consider the maximum energy of the vibrating system. If damping is neglected, the instantaneous total energy will be the sum of the kinetic energy  $T$  of motion of the mass elements and the potential energy  $V$  stored in the displacement of the spring elements. For the two degree-of-freedom system in Figure 3.50a, the kinetic and potential energy for the system will be

$$\left. \begin{aligned} T &= \frac{1}{2} m_1 \dot{x}_1^2 + \frac{1}{2} m_2 \dot{x}_2^2 \\ V &= \frac{1}{2} k_1 x_1^2 + \frac{1}{2} k_2 x_2^2 + \frac{1}{2} k (x_2 - x_1)^2 \end{aligned} \right\} \tag{3.188}$$

However, the displacements  $x_1$  and  $x_2$  and their corresponding velocities can also be defined in terms of the normal mode solution.

Consider, therefore, the total energy for only one of the two normal modes for this system. Using Equations 3.181 and 3.182 in Equation 3.188, the kinetic and potential energy in the first normal mode at any instant will be

$$T(\omega_1) = \frac{1}{2} [m_1 \phi_{11}^2 + m_2 \phi_{21}^2] [\dot{q}_1(t)]^2$$

$$V(\omega_1) = \frac{1}{2} [(k_1+k) \phi_{11}^2 + (k_2+k) \phi_{21}^2 - 2k \phi_{11} \phi_{21}] [q_1(t)]^2$$

A similar expression can be developed for the instantaneous kinetic and potential energy in the second normal mode. It is logical, therefore, that a modal mass and stiffness would be defined so that, for the  $n$ th mode, the modal energies could be given by

$$\left. \begin{aligned} T(\omega_n) &= \frac{1}{2} M_n [\dot{q}_n(t)]^2 \\ V(\omega_n) &= \frac{1}{2} K_n [q_n(t)]^2 \end{aligned} \right\} \tag{3.189}$$

where

$$M_n = [m_1 \phi_{1n}^2 + m_2 \phi_{2n}^2] , \text{ and}$$

$$K_n = [(k_1+k) \phi_{1n}^2 + (k_2+k) \phi_{2n}^2 - 2k \phi_{1n} \phi_{2n}]$$

are the effective modal mass and stiffness, respectively, for the  $n$ th mode of the particular two degree of freedom system shown in Figure 3.50a. These modal parameters are called the GENERALIZED MASS,  $M_n$  and the GENERALIZED STIFFNESS,  $K_n$ . They represent a summation of the actual mass and stiffness of the system, weighted by the mode shape  $\phi_{in}$  in such a way that they can be used to define the modal energy for each mode in terms of its normal coordinates.

3.3.2.5 Generalized Mass and Stiffness for N Degree-of-Freedom System

Consider, now, the general case of  $N$  mass elements, each identified by the symbol  $m_i$ , which are connected together or to a fixed base by an array of springs as illustrated in Figure 3.53a. Since only one coordinate  $x_i$  is used to define the position of each mass, the kinetic energy of the entire system of  $N$  masses can be written down immediately as

$$T = \frac{1}{2} \sum_i^N m_i \dot{x}_i^2$$

where  $\dot{x}_i$  is the velocity of the  $i$ th mass.

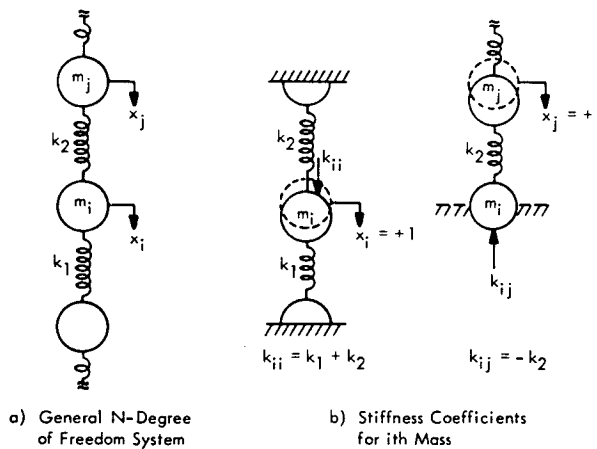


FIGURE 3.53 General Mode for N-Degree of Freedom System and Illustration of Procedure Used to Determine Stiffness Coefficients

For the more general system, the spring forces acting on each mass and the potential energy of the system are conveniently defined in terms of its stiffness coefficients. Referring to Figure 3.53b the stiffness coefficient  $k_{ij}$  for

the  $i$ th mass is conveniently defined as the restraint force that must be imposed on this mass if all except the  $j$ th mass are held fixed and the latter is slowly displaced in the positive direction by a unit distance. This concept is illustrated in Figure 3.53b for the two cases where  $i = j$  and  $i \neq j$ . It can be recognized from the figure that the "self" stiffness coefficient  $k_{ii}$  will simply be the summation of all the spring constants for the stiffness elements connected directly to the  $i$ th mass. Providing the system is constrained to a fixed base and therefore has no free rigid body modes at zero frequency, there will be  $N$   $k_{ij}$  terms for the  $N$  masses. These terms will always be positive if the sign convention is chosen that the direction of positive forces coincides with the direction of positive displacements.

Each "cross" stiffness or stiffness coupling coefficient  $k_{ij}$  ( $i \neq j$ ) will be numerically equal to the spring constant for the one stiffness element which connects the  $i$ th and  $j$ th mass elements. Providing all displacements are absolute displacements, or are all relative to a common base, then the stiffness coefficients are reciprocal so that the  $i$ th and  $j$ th masses may be interchanged and  $k_{ij} \equiv k_{ji}$ . Therefore, for  $N$  masses, there can be as many as  $(N^2 - N)/2$  independent cross-stiffness or stiffness coupling coefficients  $k_{ij}$  ( $i \neq j$ ). If the system consists of lumped masses and springs, then the number of independent cross-stiffness terms will be equal to the number of springs which connect the moving masses. However, if the stiffness elements consist of weightless continuous beams, then the number of independent cross-stiffness terms will tend to approach the maximum  $(N^2 - N)/2$ , depending on the configuration.

Now, if all masses are allowed to move, then the total spring force acting on the  $i$ th mass will be the summation of each of the spring force components  $k_{ij} x_j$  due to the displacement of the  $j$ th mass or

$$\Sigma(\text{Spring Forces on } i\text{th Mass}) = - \sum_j^N k_{ij} x_j$$

Thus, the equation of motion for free vibration of the  $i$ th mass becomes

$$m_i \ddot{x}_i + \sum_j^N k_{ij} x_j = 0$$

The potential energy for the  $N$  degree-of-freedom system can be expressed in a form similar to that for a single degree-of-freedom system where

$$V = \frac{1}{2} k x^2 = \frac{1}{2} (\text{Spring Force}) \cdot x$$

For the more complex system, the potential energy is the double summation

$$V = \sum_i^N \frac{1}{2} \left[ \sum_j^N k_{ij} x_j \right] x_i = \frac{1}{2} \sum_i^N \sum_j^N k_{ij} x_i x_j$$

Now the same process carried out earlier for the two degree-of-freedom system is repeated. The general coordinate  $x_i$  in the energy expressions for the  $N$  degree of freedom system is expanded into its normal coordinates  $\phi_{in} q_n$  and the kinetic and potential energies for the  $n$ th mode defined in the form given by Equation 3.189.

It is clear that the generalized mass and stiffness for the  $n$ th mode can now be expressed in a general form by

$$\text{Generalized Mass} \quad M_n = \sum_{i=1}^N m_i \phi_{in}^2 \quad (3.190)$$

$$\text{Generalized Stiffness} \quad K_n = \sum_{i=1}^N \sum_{j=1}^N k_{ij} \phi_{in} \phi_{jn} \quad (3.191)$$

where

- $N$  = number of degrees of freedom
- $m_i$  = the  $i$ th mass element
- $k_{ij}$  = the stiffness coefficient relating spring forces between the  $i$ th and  $j$ th mass
- $\phi_{in}, \phi_{jn}$  = mode shape for the  $i$ th and  $j$ th masses in the  $n$ th mode.

It will be shown in a later section how these last two equations can be expressed more conveniently, with matrix notation, in a form which is suitable for analyzing complex systems, particularly with digital computers.

### 3.3.2.6 Dynamically and Statically Coupled Systems

The single summation for the generalized mass in Equation 3.190 must be replaced by a double summation for systems where more than one coordinate is required to uniquely describe the motion of each mass element. This more general situation corresponds to systems which are called dynamically (or mass) coupled systems. These are encountered, for example, in the analysis of rigid body motion of constrained systems (Reference 3.2).

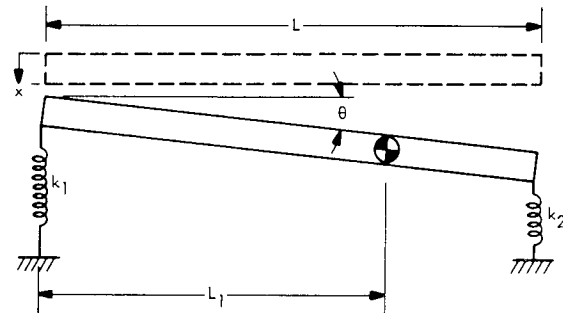
For instance, consider the combined translation and rotation of the unsymmetrical rigid beam mounted on springs which is illustrated in Figure 3.54a. For small displacements, its motion can be defined in terms of the vertical displacement  $x$  and rotation angle  $\theta$  about one end of the beam. The equation of motion in the  $x$  coordinate will be the sum of the translational forces acting on the mass or

$$m \ddot{x} + m L_1 \ddot{\theta} + (k_1 + k_2) x + k_2 L \theta = 0$$

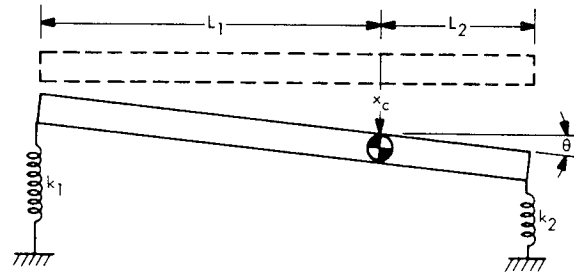
where  $L_1$  is the distance from the origin of  $x$  to the center of gravity of the beam and  $L$  is the total length of the beam. Similarly, the equation of motion in the  $\theta$  coordinate will be the summation of the rotational moments acting about the origin at the end of the beam, or

$$m L_1 \ddot{x} + (m L_1^2 + I_o) \ddot{\theta} + (k_2 x + k_2 L \theta) L = 0$$

where  $I_o$  is the mass moment of inertia of the beam about its center of gravity and  $(m L_1^2 + I_o)$  is the mass moment of inertia about the end.



a) Dynamically and Statically Coupled System



b) Statically Coupled Only (Dynamic Coupling Eliminated by Shifting Coordinates to Center of Mass)

FIGURE 3.54 Constrained Rigid Body System Which Exhibit Dynamic (Inertia) Coupling and Static (Stiffness) Coupling

The kinetic energy of the system can be given by the kinetic energy of translation of the center of mass and the kinetic energy of rotation about the center of mass. Using the coordinate system given in Figure 3.54a, this is

$$T = \frac{1}{2} m (\dot{x} + L_1 \dot{\theta})^2 + \frac{1}{2} I_o \dot{\theta}^2$$

or

$$T = \frac{1}{2} m \dot{x}^2 + m L_1 \dot{x} \dot{\theta} + \frac{1}{2} (m L_1^2 + I_o) \dot{\theta}^2$$

Whenever cross product terms appear in the kinetic energy equation, as is the case here, the system is said to be dynamically coupled. The inertia coupling also appears as a common factor  $m L_1$  in both equations of motion. The effect of this coupling is that inertial forces due to acceleration in the  $x$  coordinate also induce moments in the  $\theta$  coordinate and visa versa. This coupling effect is more readily visualized when the equations of motion are expressed in a matrix form.

$$\begin{matrix} & j \rightarrow \\ i \downarrow & \begin{bmatrix} m & mL_1 \\ mL_1 & mL_1^2 + I_o \end{bmatrix} \begin{bmatrix} \ddot{x} \\ \ddot{\theta} \end{bmatrix} + \begin{bmatrix} (k_1 + k_2) & k_2 L \\ k_2 L & k_2 L^2 \end{bmatrix} \begin{bmatrix} x \\ \theta \end{bmatrix} = 0 \\ & \text{Inertia Matrix} \qquad \qquad \text{Stiffness Matrix} \end{matrix}$$

The inertia coupling term  $m L_1$  appears as an off-diagonal term  $m_{ij} = m_{ji} = m L_1$  in the first square matrix which is called the inertia matrix  $[m_{ij}]$ .

The coupling effect of the off-diagonal "cross-stiffness" terms  $k_{ij} = k_{ji} = k_2 L$  is also apparent in the second square matrix called the stiffness matrix  $[k_{ij}]$ . This characterizes all the type of multi-degree of freedom systems considered earlier which are called statically coupled systems. As has been shown, these systems have stiffness coupling terms in their equations of motion and always exhibit cross-product terms in the expressions for potential energy.

Returning now to the example, there will be two normal modes for the system corresponding to the two degrees of freedom - translation and rotation. Thus, the coordinates  $x$  and  $\theta$  may be expressed in terms of the normal coordinates  $q_n$  by

$$x = \sum_n^2 \phi_{xn} q_n$$

$$\theta = \frac{1}{L} \sum_n^2 \phi_{\theta n} q_n$$

The expression for the kinetic energy of the system in the  $n$ th normal mode can then be written as

$$T(\omega_n) = \frac{1}{2} \left[ m \phi_{xn}^2 + 2mL_1 \phi_{xn} \frac{\phi_{\theta n}}{L} + (mL_1^2 + I_o) \frac{\phi_{\theta n}^2}{L^2} \right] \dot{q}_n^2$$

The generalized mass for this mode is given by the term in brackets in this equation. Thus, for dynamically coupled systems, the generalized mass for the  $n$ th mode is expressed in the general form by the double summation

$$M_n = \sum_i^N \sum_j^N m_{ij} \phi_{in} \phi_{jn} \tag{3.192}$$

where the inertia elements  $m_{ii}$  represent the actual masses or moments of inertia of the system and the elements  $m_{ij}$  ( $i \neq j$ ) represent the inertia coupling terms.

However, this complication can be avoided by choosing a coordinate system such that the displacement of each mass is specified by the motion of its center of gravity relative

to its equilibrium position. For problems involving rotation of rigid bodies, the same result is achieved if the coordinate system is selected to coincide with the principal axes of rotation. For systems which are not constrained to a fixed base, the equilibrium position is equivalent to the line (or surface) through the node points (or lines) of the rigid body (zero frequency) modes of vibration.

If this approach is used for the case of the rigid beam considered here, the origin for the coordinates  $x$  and  $\theta$  is shifted to the center of gravity as shown in Figure 3.54b. Summing the forces and moments about this point, the equations of motion for free vibration in the new coordinates  $x_c$  and  $\theta$  become, in matrix form

$$\begin{bmatrix} m & 0 \\ 0 & I_o \end{bmatrix} \begin{bmatrix} \ddot{x}_c \\ \ddot{\theta} \end{bmatrix} + \begin{bmatrix} (k_1 + k_2) & k_2 L_2 - k_1 L_1 \\ k_2 L_2 - k_1 L_1 & k_1 L_1^2 + k_2 L_2^2 \end{bmatrix} \begin{bmatrix} x_c \\ \theta \end{bmatrix} = 0$$

where  $L_2$  is the difference between  $L$  and  $L_1$ .

The off-diagonal terms on the inertia matrix have now been eliminated, so that the inertia matrix is diagonalized. Thus, the dynamic coupling is eliminated simply by choosing the coordinate system to coincide with the center of mass. Static coupling, due to the inherent geometry of the system, still remains as indicated by the off-diagonal terms in the stiffness matrix.

However, this two degree of freedom system can be statically decoupled if the supporting springs  $k_1$  and  $k_2$  are chosen such that

$$\frac{k_2}{k_1} = \frac{L_1}{L_2}$$

The off-diagonal static coupling terms will then drop out leaving two independent or uncoupled equations of motion in the coordinates  $x_c$  and  $\theta$ . Thus, if a vertical force is applied to the beam at the center of gravity, under this condition, the beam will undergo a pure translation motion without rotation. Similarly, if a moment is applied to the beam about its center of mass, only rotary motion without translation is induced. This illustrates the essential design objective for vibration isolation systems; namely, that the supporting springs be so located and sized as to eliminate both dynamic and static coupling of the vibration modes of the isolated rigid body. In this way, vibration of the body in one coordinate or mode does not excite any vibration in the other mode.

However, for flexible vibrating systems, generally only dynamic coupling can be eliminated by coordinate selection. Static or stiffness coupling remains as an inherent part of the geometry of the system. Thus, a method of coordinate decoupling is sought so that the actual motion of the structure may be described in terms of a set of mathematically decoupled equations of motion. This is the essential objective of the normal mode approach and is based on the concept of orthogonality of the normal modes.



### 3.3.2.7 Orthogonality of Normal Modes

To demonstrate the principle of orthogonality of normal modes, consider the total instantaneous energy of the system in Figure 3.50a as defined by the motion of both normal modes. The expressions for the latter (Equation 3.183) are inserted into the equations for the total kinetic and potential energy given by Equation 3.188. The resulting expression consists of terms involving squares of the mode shapes (i.e. --  $\phi_{11}^2$ ) and terms involving cross-products of mode shapes for two different modes (i.e. --  $\phi_{11} \cdot \phi_{12}$ ). That part of the total instantaneous energy involving the squared terms can be expressed in terms of the generalized mass and stiffness parameters as

$$T + V \Big|_{\text{squared terms}} = \frac{1}{2} \left[ M_1 \omega_1^2 \cos^2(\omega_1 t + \theta_1) + K_1 \sin^2(\omega_1 t + \theta_1) \right] \bar{q}_1^2 \\ + \frac{1}{2} \left[ M_2 \omega_2^2 \cos^2(\omega_2 t + \theta_1) + K_2 \sin^2(\omega_2 t + \theta_2) \right] \bar{q}_2^2$$

That part of the total instantaneous energy involving the cross product terms can be expressed in the general form for the two modes as

$$T + V \Big|_{\text{cross terms}} = \left[ \sum_{i=1}^2 m_i \phi_{i1} \phi_{i2} \right] \omega_1 \omega_2 \cos(\omega_1 t + \theta_1) \cos(\omega_2 t + \theta_2) \\ + \left[ \sum_{i=1}^2 \sum_{j=1}^2 k_{ij} \phi_{i1} \phi_{j2} \right] \sin(\omega_1 t + \theta_1) \sin(\omega_2 t + \theta_2)$$

Now the total energy of the freely vibrating undamped system must actually be constant at all times since no external forces act on it and there are no losses. This can only be true under the following conditions. (1) For the first energy equation, the sum of the squared cosine and sine terms will reduce to 1 for

$$M_1 \omega_1^2 = K_1$$

and

$$M_2 \omega_2^2 = K_2$$

(2) The bracketed terms in the second energy equation must be zero since there is no other way for it to be constant for all time. Extending these results to any two modes,  $n$  and  $m$ , of an  $N$  degree-of-freedom system, the basic orthogonality principle is obtained which can be stated as

$$\sum_{i=1}^N m_i \phi_{in} \phi_{im} = \begin{cases} 0 & n \neq m \\ M_n & n = m \end{cases} \quad (3.193)$$

and

$$\sum_{i=1}^N \sum_{j=1}^N k_{ij} \phi_{in} \phi_{jm} = \begin{cases} 0 & n \neq m \\ K_n & n = m \end{cases} \quad (3.194)$$

In addition, it is also evident that for any normal mode, the natural frequency  $\omega_n$  is related to the generalized mass  $M_n$  and generalized stiffness  $K_n$  by

$$\omega_n = \sqrt{K_n / M_n} \quad (3.195)$$

so that  $K_n$  can be more conveniently defined in terms of  $\omega_n$  and  $M_n$ .

The kinetic and potential energies of the system are defined by the sum of the energies in each mode or

$$T = \frac{1}{2} \sum_{n=1}^N M_n \omega_n^2 q_n^2(t) = \frac{1}{2} \sum_{n=1}^N M_n \dot{q}_n^2(t) \quad (3.196)$$

$$V = \frac{1}{2} \sum_{n=1}^N K_n q_n^2(t) = \frac{1}{2} \sum_{n=1}^N \omega_n^2 M_n q_n^2(t) \quad (3.197)$$

The fact that the cross product terms in the normal mode energy equation are zero may be interpreted physically as evidence that no work is done by one normal mode on another mode. This is not necessarily true when damping forces are considered. However, it will be shown later how practical results are obtained in vibration analysis by choosing a particular form of damping which eliminates this coupling effect.

As an example of the orthogonality principle, for the symmetrical two degree of freedom shown in Figure 3.51, where  $m_1 = m_2 = m$ , it was found that  $\phi_{11} = \phi_{12} = \phi_{21} = 1$ , and  $\phi_{22} = -1$ . Inserting these values in Equation 3.193, gives

$$\text{For } n = m = 1, \quad M_1 = m \cdot 1 \cdot 1 + m \cdot 1 \cdot 1 = 2m$$

$$\text{For } n = m = 2, \quad M_2 = m \cdot 1 \cdot 1 + m \cdot (-1)(-1) = 2m$$

$$\text{For } n = 1, m = 2, \quad M_{12} = m \cdot 1 \cdot 1 + m \cdot 1 \cdot (-1) = 0$$

The natural frequencies  $\omega_n$ , mode shapes  $\phi_{in}$ , and generalized mass  $M_n$  for each mode of a multi-degree of freedom system have been defined. All that remains to complete the normal mode solution is to solve for the time variation in the normal coordinate  $q_n(t)$ .

### 3.3.2.8 Application of Lagrange's Equation

The orthogonality property of the normal modes can now be used to separate the coupled equations of motion for an  $N$  degree-of-freedom system. However, the uncoupled equations of motion of the normal modes can be conveniently derived formally with the use of Lagrange's equation. This basic expression relates the energy of

a vibrating system to the dynamic forces acting in the system. For an undamped system without any externally applied forces, Lagrange's equation has the form

$$\frac{d}{dt} \left[ \frac{\partial T}{\partial \dot{q}_n} \right] - \frac{\partial T}{\partial q_n} + \frac{\partial V}{\partial q_n} = 0 \quad (3.198)$$

where

$T$  = total instantaneous kinetic energy of the system

$V$  = total instantaneous potential energy of the system

$q_n$  = normal coordinate for the  $n$ th normal mode.

This expression provides a simple and powerful method for developing the equations of motion of complex dynamic systems. Another method, called the Galerkin method, can also be used to achieve the same result (Reference 3.1, Chapter 48). One simplification can be made immediately. For most structural vibration problems, the kinetic energy is not a function of displacement so that the second term  $\partial T/\partial q_n$  is usually zero.

Inserting the expressions for the kinetic and potential energy, given by Equations 3.196 and 3.197, in Lagrange's equation, the result is

$$\frac{d}{dt} \left[ \frac{\partial}{\partial \dot{q}_n} \left( \frac{1}{2} \sum_n M_n \dot{q}_n^2(t) \right) \right] + \frac{\partial}{\partial q_n} \left( \frac{1}{2} \sum_n K_n q_n^2(t) \right) = 0$$

or

$$M_n \ddot{q}_n(t) + K_n q_n(t) = 0 \quad (3.199a)$$

where  $M_n, K_n$  = generalized mass and stiffness of  $n$ th mode.

Thus, a single independent equation of motion is obtained for the normal coordinate  $q_n(t)$  of each mode which corresponds to an expression for the free vibration of a single degree of freedom system. It is more conveniently expressed as

$$\ddot{q}_n(t) + \omega_n^2 q_n(t) = 0 \quad (3.199b)$$

where  $\omega_n = \sqrt{K_n/M_n}$ .

### 3.3.2.9 Free Vibration Response of N Degree-of-Freedom System

The free vibration of the  $i$ th mass of an undamped lumped parameter system can now be defined in terms of its normal modes by

$$x_i(t) = \sum_n \phi_{in} q_n(t) \quad (3.200)$$

where each  $q_n(t)$  is a solution to Equation 3.199b for each normal mode frequency  $\omega_n$  and will have the general form

$$q_n(t) = q_{no} \cos \omega_n t + \frac{\dot{q}_{no}}{\omega_n} \sin \omega_n t \quad (3.201)$$

The constants  $q_{no}$  and  $\dot{q}_{no}$  represent the initial conditions for each mode just as for the single degree-of-freedom system (see Equation 3.8, page 3.3). They will be determined by the initial displacement  $x_i(0)$  and velocity  $\dot{x}_i(0)$  for each mass of the system which can also be expressed in terms of the normal modes by

$$x_i(0) = \sum_n \phi_{in} q_n(t=0) = \sum_n \phi_{in} q_{no} \quad (3.202)$$

$$\dot{x}_i(0) = \sum_n \phi_{in} \dot{q}_n(t=0) = \sum_n \phi_{in} \dot{q}_{no} \quad (3.203)$$

If both sides of these expressions are multiplied by  $m_i \phi_{im}$  and summed over all the  $m_i$  masses, the orthogonality property can be invoked to solve for  $q_{no}$  and  $\dot{q}_{no}$ . The result, for Equation 3.202, is

$$\sum_i x_i(0) m_i \phi_{im} = \sum_n q_{no} \sum_i m_i \phi_{im} \phi_{in} = \begin{cases} q_{no} M_n, & m = n \\ 0, & m \neq n \end{cases}$$

where all the terms on the right side are zero except the one for  $n=m$ . A similar operation is carried out for Equation 3.203 so that the desired constants can be given by

$$\left. \begin{aligned} q_{no} &= \frac{1}{M_n} \sum_i x_i(0) m_i \phi_{in} \\ \dot{q}_{no} &= \frac{1}{M_n} \sum_i \dot{x}_i(0) m_i \phi_{in} \end{aligned} \right\} \quad (3.204)$$

Combining the above relationships, the free vibration response of the  $N$  degree-of-freedom system, due to an initial displacement  $x_i(0)$  and velocity  $\dot{x}_i(0)$  for each mass  $m_i$ , can be expressed in the form

$$x_i(t) = \sum_n \phi_{in} \bar{q}_n \sin(\omega_n t + \theta_n) \quad (3.205)$$

where

$$\left. \begin{aligned} \bar{q}_n &= \sqrt{q_{no}^2 + \dot{q}_{no}^2 / \omega_n^2} \\ \theta_n &= \tan^{-1} [q_{no} \omega_n / \dot{q}_{no}] \end{aligned} \right\} \quad (3.206)$$

Normal Mode Shapes (Equation 3.180)

$$\left. \frac{x_2}{x_1} \right|_{\omega_1} = \left[ 3k + k - (0.665)^2 \left( \frac{k}{m} \right) \cdot (5m) \right] / k = 1.79$$

$$\left. \frac{x_2}{x_1} \right|_{\omega_2} = \left[ 3k + k - (1.165)^2 \left( \frac{k}{m} \right) \cdot (5m) \right] / k = -2.79$$

Therefore, setting  $x_2(\omega_1) = x_2(\omega_2) = 1$ , the mode shapes are

$$\begin{aligned} \phi_{11} &= 0.559 & \phi_{12} &= -0.358 \\ \phi_{21} &= 1.0 & \phi_{22} &= 1.0 \end{aligned}$$

(Note that the choice of sign for  $\phi_{22}$  is arbitrary since the true value will depend on the initial conditions.)

Generalized Mass (Equation 3.190)

$$M_1 = (5m) (0.559)^2 + (m) (1) = 2.56 m$$

$$M_2 = (5m) (-0.358)^2 + (m) (1) = 1.64 m$$

Initial Conditions

If positive deflections of the system in Figure 3.55a are upward, then by a static analysis,

$$x_1(0) = P_s/k_1 = P_s/3k$$

$$x_2(0) = x_1(0) + P_s/k = 4 P_s/3k$$

and, from Equation 3.204, the constants  $q_{no}$  are

$$\begin{aligned} q_{10} &= \frac{1}{2.56 m} \left[ \left( \frac{1}{3} \right) (5m) (0.559) + \left( \frac{4}{3} \right) (m) (1) \right] \frac{P_s}{k} \\ &= 0.885 \frac{P_s}{k} \end{aligned}$$

$$\begin{aligned} q_{20} &= \frac{1}{1.64 m} \left[ \left( \frac{1}{3} \right) (5m) (-0.358) + \left( \frac{4}{3} \right) (m) (1) \right] \frac{P_s}{k} \\ &= 0.45 \frac{P_s}{k} \end{aligned}$$

Normal Coordinates (Equation 3.206)

Since

$$\dot{x}_i(0) = 0, \quad \dot{q}_{no} = 0,$$

and

$$\bar{q}_1 = q_{10}, \quad \bar{q}_2 = q_{20}$$

$$\theta_1 = \theta_2 = \tan^{-1} \infty = \pi/2$$

Modal Damping

Assume

$$\delta_1 = \delta_2 = 0.1$$

Therefore,

$$\sqrt{1 - \delta_n^2} \approx 1.0,$$

$$\theta_d \approx \tan^{-1} \delta = 5.7^\circ \cdot (\text{negligible})$$

Displacement Response (Equation 3.208)

If the response is normalized by the factor  $P_s/k$  for each mass, then, from Equation 3.208, with  $\sin(\omega_{dn}t + \theta_n) \approx \sin(\omega_n t + \pi/2) = \cos \omega_n t$ , the result for  $x_1(t)$  is

$$\begin{aligned} \frac{x_1(t)}{P_s/k} &= (0.559) (0.885) e^{-0.1 \omega_1 t} \cos \omega_1 t \\ &+ (-0.358) (0.45) e^{-0.1 \omega_2 t} \cos \omega_2 t \end{aligned}$$

Expressed in matrix form,  $x_1(t)$  and  $x_2(t)$  may be given by

$$\begin{aligned} \begin{Bmatrix} x_1(t) / \frac{P_s}{k} \\ x_2(t) / \frac{P_s}{k} \end{Bmatrix} &= \begin{Bmatrix} 0.495 \\ 0.885 \end{Bmatrix} e^{-0.1 \omega_1 t} \cos \omega_1 t \\ &+ \begin{Bmatrix} -0.16 \\ 0.45 \end{Bmatrix} e^{-0.1 \omega_2 t} \cos \omega_2 t \quad (3.209) \end{aligned}$$

Acceleration Response

Differentiating the displacement response twice, and inserting the values for  $\omega_1$  and  $\omega_2$ , the acceleration response, normalized by the factor  $P_s/m$ , is

$$\begin{aligned} \begin{Bmatrix} \ddot{x}_1(t) / \frac{P_s}{m} \\ \ddot{x}_2(t) / \frac{P_s}{m} \end{Bmatrix} &= - \begin{Bmatrix} 0.22 \\ 0.39 \end{Bmatrix} e^{-0.1 \omega_1 t} \cos \omega_1 t \\ &- \begin{Bmatrix} -0.22 \\ 0.61 \end{Bmatrix} e^{-0.1 \omega_2 t} \cos \omega_2 t \quad (3.210) \end{aligned}$$

Note that for any homogeneous system of mass elements ( $m_i = \text{constant}$ ), if the initial conditions are uniform over all mass elements (i.e.,  $x_i(0) = \text{constant}$ ), then the system will only vibrate in the symmetric normal modes since for antisymmetric modes, where the mode shape  $\phi_{in}$  is equally positive and negative, the summation  $\sum x_i(0) m_i \phi_{in}$  will be zero.

Addition of Damping Effects

Damping may be included, to a first approximation, by adding a viscous damping term to the equation of motion for each mode. Thus, Equation 3.199b becomes

$$\ddot{q}_n + 2 \delta_n \omega_n \dot{q}_n(t) + \omega_n^2 q_n(t) = 0 \quad (3.207)$$

where

$$\delta_n = \text{critical damping ratio for the } n\text{th mode}$$

$$= 1/Q_n \text{ where } Q_n = \text{amplification factor for the } n\text{th mode.}$$

The general solution for free vibration of the  $n$ th normal mode coordinate  $q_n(t)$  then becomes (compare with Equation 3.6, page 3-3)

$$q_n(t) = \frac{e^{-\delta_n \omega_n t}}{\sqrt{1-\delta_n^2}} \left[ q_{no} \cos(\omega_{dn}t - \theta_d) + \frac{\dot{q}_{no}}{\omega_n} \sin \omega_{dn}t \right]$$

where

$$\omega_{dn} = \omega_n \sqrt{1-\delta_n^2} = \text{damped normal mode frequency}$$

$$\theta_d = \tan^{-1} \delta_n / \sqrt{1-\delta_n^2}$$

The equations for the constants  $q_{no}$  and  $\dot{q}_{no}$  are not changed by damping. Since the phase shift  $\theta_d$  due to damping can generally be neglected, the damped transient displacement response of the  $i$ th mass of the multi-degree of freedom system can be expressed to a close approximation by

$$x_i(t) \approx \sum_n^N \phi_{in} \frac{e^{-\delta_n \omega_n t}}{\sqrt{1-\delta_n^2}} \bar{q}_n \sin(\omega_{dn}t + \theta_n) \quad (3.208)$$

where  $\bar{q}_n$  and  $\theta_n$  are given by Equations 3.206 and 3.204, and  $\delta_n$  is estimated for each natural mode. This result can be differentiated in the usual manner to obtain the velocity and acceleration response.

Example of Damped Transient Response of Two Degree-of-Freedom System

To illustrate the concepts developed to this point, consider the transient response of the simple two degree-of-freedom system shown in the insert in Figure 3.55a. It is assumed

that a static upward force  $P_s$  is applied up to the time  $t=0$  and is then suddenly removed. The resulting response will correspond to the transient motion for an initial displacement of each mass. For example, such a model could approximate the motion of a launch pad upon release of the hold down arms assuming initial transients due to thrust buildup had died out. Based on the parameters shown in the figure, the following results are obtained by using the equations derived earlier for the general two degree of freedom model in Figure 3.49.

Mass and Spring Parameters

$$m_1 = 5m \quad k_1 = 3k$$

$$m_2 = m \quad k_2 = 0$$

$$k = k$$

Undamped Natural Frequencies (Equation 3.179)

$$\omega_n = \left[ \frac{9}{10} \frac{k}{m} \pm \frac{1}{2} \sqrt{\left(\frac{9}{5} \frac{k}{m}\right)^2 - \frac{12}{5} \left(\frac{k}{m}\right)^2} \right]^{1/2}$$

or

$$\omega_1 = 0.665 \sqrt{k/m} \text{ radians/sec}$$

$$\omega_2 = 1.165 \sqrt{k/m} \text{ radians/sec}$$

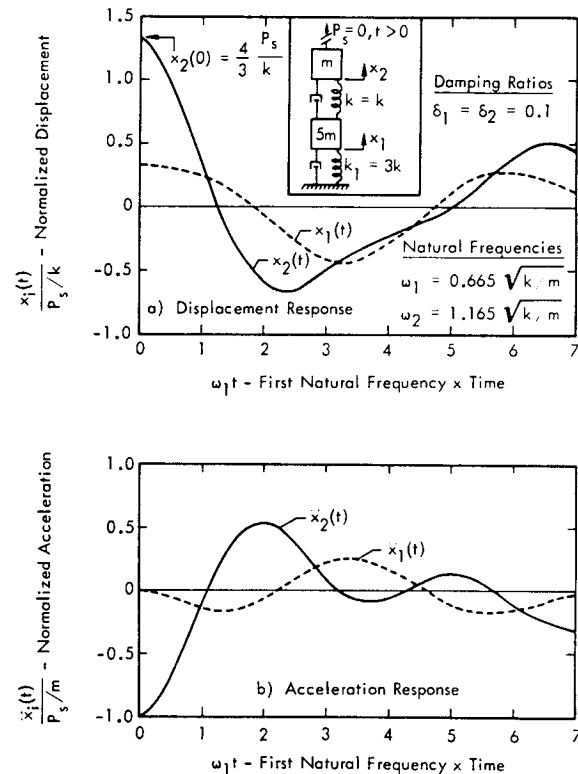


FIGURE 3.55 Example of Transient Response of Damped Two Degree-of-Freedom System with Initial Displacement Due to Static Force  $P_s$  Which is Suddenly Released at Time 0

These expressions for the displacement and acceleration response are plotted in Figure 3.55a and 3.55b, respectively, on a time scale normalized by the frequency  $\omega_1$  of the first normal mode. The plots illustrate one feature which is characteristic of the response of multi-degree-of-freedom systems: the displacement response is dominated by the response in the lowest natural mode frequency while the acceleration response is influenced equally or more strongly by the higher mode. However, for a transient response, the latter will usually decay more rapidly due to damping. If the phase shift due to damping had been included in these expressions, the arguments for each of the cosine terms would have been replaced by  $(\omega_{dn}t - \theta_d)$  for the displacement response and  $(\omega_{dn}t + \theta_d)$  for the acceleration response where  $\theta_d = \tan^{-1} \delta / \sqrt{1 - \delta^2}$ . This minor correction can usually be neglected.

This example illustrates how the normal mode approach can be used to determine the free vibration response of a multi-degree-of-freedom system by adding up the single degree of freedom response for each normal mode. The same principle will apply to the forced response of complex systems.

### 3.3.3 FORCED VIBRATION RESPONSE OF LUMPED PARAMETER SYSTEMS

Equations of motions for the forced response of lumped parameter multi-degree-of-freedom systems can be readily developed in terms of the normal coordinates by applying a more general form of Lagrange's equation. This can be expressed as

$$\frac{d}{dt} \left[ \frac{\partial T}{\partial \dot{q}_n} \right] - \frac{\partial T}{\partial q_n} + \frac{\partial V}{\partial q_n} + \mathcal{F}_{dn} = F_n \quad (3.211)$$

where

$T, V$  = total instantaneous kinetic and potential energy, respectively

$\mathcal{F}_{dn}$  = Generalized Damping Force for nth mode

$F_n$  = Generalized External Force for nth mode.

The two new terms  $\mathcal{F}_{dn}, F_n$  define the effective value of the damping forces and externally applied driving forces acting on the nth normal mode. They represent the non-conservative forces which add or subtract energy from the system. They can be determined by the amount of work done on the system by the external forces acting on a single normal mode and the amount of work done by the damping forces acting on a single mode.

#### 3.3.3.1 Generalized Force and Generalized Damping

If the total external force  $P_i$  acting on the ith mass element of a multi-degree-of-freedom system acts over an arbitrarily small displacement  $\Delta x_i$  in the direction of this force, the total work done is equal to

$$\Delta W_i = P_i \Delta x_i$$

Now  $\Delta x_i$  can also be expressed in terms of its normal modes by the summation over all modes as

$$\Delta x_i = \sum_n \phi_{in} \Delta q_n$$

where  $\phi_{in}$  is the relative deformation at this point in the nth mode and  $\Delta q_n$  is a small change in the normal coordinate of the nth mode. Then the total work done on the ith mass can also be expressed as

$$\Delta W_i = \sum_n P_i \phi_{in} \Delta q_n$$

The rate of change of this work with the change  $\Delta q_n$  in the nth normal coordinate is therefore the effective force on this point for the nth mode and is simply

$$\frac{\Delta W_i}{\Delta q_n} = P_i \phi_{in} \quad (3.212)$$

If this same process is repeated for each of the mass elements acted on by an external force, the total effective external force or generalized force  $F_n$  for the nth mode will be the summation

$$F_n = \sum_i P_i \phi_{in} \quad (3.213)$$

For dynamic loads, the actual loading  $P_i$  can vary with position over the structure as well as with time. The corresponding generalized force will also vary with time in the same fashion but with a different amplitude for each mode. For static loads, the actual loading can only vary with position and the corresponding generalized force varies only with mode number.

#### Generalized Damping

A slightly different approach is used to define the generalized damping force  $\mathcal{F}_{dn}$  (References 3.1, 3.34 and 3.36). If the damping force acting on the ith mass element is  $f_{di}$ , then, by analogy with Equation 3.213, the generalized damping force, which is a source of energy loss, will be

$$\mathcal{F}_{dn} = - \sum_i f_{di} \phi_{in} \quad (3.214)$$

If the viscous damping coefficient relating the damping force on the ith mass to the velocity of the jth mass is identified by the symbol  $c_{ij}$ , then the total viscous damping force  $f_{di}$  acting on this mass will be the summation

$$f_{di} = - c_{i1} \dot{x}_1 - c_{i2} \dot{x}_2 - \dots - c_{iw} \dot{x}_j = - \sum_j c_{ij} \dot{x}_j$$

In this case,  $\dot{x}_j$  is the velocity of the jth mass and  $c_{ij}$  is the force on the ith mass due to a unit velocity of the jth mass only, with all other masses held fixed.

In order to maintain the feature of orthogonality of the normal modes so that the equations of motion can be decoupled, it is necessary to restrict the value of the damping coefficient  $c_{ij}$  to one, or a linear summation, of the following three forms:

$$\begin{aligned} \text{UNIFORM VISCOUS DAMPING} \quad c_{ij} &= 2G k_{ij} \\ \text{UNIFORM STRUCTURAL DAMPING} \quad c_{ij} &= \frac{g}{\omega} k_{ij} \quad (3.215) \\ \text{UNIFORM MASS DAMPING} \quad c_{ij} &= B m_i \end{aligned}$$

where  $G$ ,  $g$ , and  $B$  are damping parameters which are constant for the entire system. In other words, the damping coefficient  $c_{ij}$  is restricted to being directly proportional to the corresponding stiffness coefficient  $k_{ij}$  or proportional to the mass  $m_i$  to which it is connected. Thus, for Uniform Viscous Damping, the damping force on the  $i$ th mass would be

$$f_{di} = -2G \sum_j^N k_{ij} \dot{x}_j$$

Now the velocity  $\dot{x}_j$  may be expressed as the sum of the velocities  $\phi_{jm} \dot{q}_m$  in all the normal modes, including the  $n$ th mode, by

$$\dot{x}_j = \sum_m^N \phi_{jm} \dot{q}_m$$

Combining these two expressions with Equation 3.214, the generalized damping force, for uniform viscous damping in the  $n$ th mode, becomes

$$\mathcal{F}_{dn} = 2G \sum_m^N \left[ \sum_i^N \sum_j^N k_{ij} \phi_{in} \phi_{jm} \right] \dot{q}_m$$

However, by orthogonality (see Equation 3.194), the term in brackets is equal to zero except for  $n = m$  when it is equal to the generalized stiffness  $K_n$  for the  $n$ th mode. Thus, only the  $n$ th term is left in the summation over  $m$  so that the generalized damping force is given by

$$\mathcal{F}_{dn} = 2G K_n \dot{q}_n = 2\omega_n^2 G M_n \dot{q}_n \quad (3.216)$$

Similar expressions can be developed for the other two forms of uniform damping in terms of  $K_n$  or  $M_n$ . However, there is yet another and more flexible choice for a generalized damping force for each normal mode. It may simply be specified as the product

$$\mathcal{F}_{dn} = C_n \dot{q}_n \quad (3.217)$$

where  $C_n$  is a generalized damping constant for the  $n$ th mode. This may also be given in the form

$$C_n = 2\delta_n \omega_n M_n = \frac{\omega_n M_n}{Q_n} \quad (3.218)$$

where  $\delta_n$  or  $Q_n$  may be estimated for each mode. This method of specifying damping is especially practical for analyzing the sonic response of large structural systems. In this case, damping is related, in a complex manner, to material properties and configuration details. Accurate calculation of the damping parameters for each mode becomes extremely difficult so that reliance is often placed on engineering data and experience to estimate an average  $Q_n$  for each of the damped modes.

For lumped parameter systems with discrete damping elements  $c_{ij}$  which are known and must be accounted for, an approximate generalized damping constant  $C_n$  for the  $n$ th mode may be computed (References 3.34 and 3.36). The damping energy lost by the system is defined by the Rayleigh dissipation function  $D$  which is 1/2 the rate of energy dissipation of the system. It is given by

$$D = \frac{1}{2} \sum_i^N \sum_j^N c_{ij} \dot{x}_i \dot{x}_j \quad (3.219)$$

where  $c_{ij}$  is the damping coefficient and  $\dot{x}_i$ ,  $\dot{x}_j$  are the velocities of the  $i$ th and  $j$ th masses.

The generalized damping force for the  $n$ th mode can then be defined in terms of this dissipation function as

$$\mathcal{F}_{dn} = \frac{\partial D}{\partial \dot{q}_n} \quad (3.220)$$

Now, the coordinates  $\dot{x}_i$  and  $\dot{x}_j$  are expanded in terms of normal coordinates which are computed assuming no damping. This assumes that damping does not materially change the normal mode shapes and natural frequencies. When these are inserted in Equation 3.219 and the result used in Equation 3.220, the resulting expression for the generalized damping force for the  $n$ th mode is

$$\mathcal{F}_{dn} = \sum_m^N \left[ \sum_i^N \sum_j^N c_{ij} \phi_{in} \phi_{jm} \right] \dot{q}_m$$

Since each of the normal coordinates  $\dot{q}_m$  is involved in the first summation over  $m$ , each equation of motion for the  $n$ th normal mode would be coupled to the equations for all other modes and the advantage of the normal mode approach would be lost. The common recourse, then, is to assume that the cross-mode coupling terms are negligible so that only the  $n$ th term in the summation over  $m$  is significant. This is equivalent to assuming that orthogonality also holds for the damping coefficients so that the damping force for the  $n$ th mode is given approximately by the equations

$$\mathcal{F}_{dn} \approx C_n \dot{q}_n$$

$$\text{Generalized Damping Constant} \quad C_n = \sum_i^N \sum_j^N c_{ij} \phi_{in} \phi_{jn} \quad (3.221)$$

Although accurate methods are available for computing the true normal modes, natural frequencies, and generalized parameters for damped multi-degree-of-freedom systems, they are very laborious and do not ordinarily provide

Case (3) Propagating Dynamic Loading  
 $P_j(t) = P_j \cdot f(t - \tau_j)$

This is the more general form of Case 2 where the time variation of load at the *i*th mass is delayed by a time  $\tau_i$ . This will cover the case of nonuniform structural loading by blast waves or random acoustic noise from a rocket engine. For the former, the quantity  $f(t - \tau_i)$  will be the deterministic time function which defines the pressure time history for the *i*th mass element. For propagating random acoustic noise,  $f(t - \tau_i)$  will be a random variable. In either case, the delay time  $\tau_i$  will be equal to a separation distance of the *i*th element, from a reference position, divided by an effective propagation velocity of the pressure wave. This type of loading is normally applied to distributed systems such as beams or plates.

Generalized Force and Joint Acceptance

The generalized force for the *n*th normal mode for any deterministic external loading of a lumped parameter system can be conveniently expressed as the product of three terms.

$$F_n(t) = P_o \cdot J_n \cdot f(t) \tag{3.223}$$

where

$$P_o = \sum_j^N P_j \text{ - the maximum amplitude of the load on all the elements of the systems.}$$

$$J_n = \frac{\sum_i P_i \phi_{in}}{P_o} \text{ JOINT ACCEPTANCE (also called mode participation factor) - the dimensionless ratio of the amplitude of the generalized force for the } n\text{th mode to the maximum amplitude of the total load}$$

$$\tag{3.224}$$

$\phi_{in}$  = mode shape at *i*th element for *n*th mode

$f(t)$  = dimensionless or relative time variation of load.

The term joint acceptance is adopted here in lieu of the term mode participation factor in order to maintain a consistent concept for this very useful parameter for any type of loading. The term was originally applied in the analysis of structural response to random acoustic loads (Reference 3.40). For random loads, it will be shown that joint acceptance squared is the ratio of the power spectral density of the generalized force to the power spectral density of the total load.

For each of the first two types of loading defined earlier (Case 1 and 2), the peak amplitude of the generalized force  $F_n = P_o J_n$  is independent of time and the joint acceptance  $J_n$  is only a function of mode number. With a propagating random load (Case 3), such as an acoustic wave of random noise, joint acceptance becomes very useful for relating the space-time variation of loads on the system. In this case, the joint acceptance will be shown to be a function of mode number and frequency of the

acoustic wave for a given effective wave velocity. For propagating deterministic loads, such as blast waves, whose time history can be defined exactly, joint acceptance is not a useful parameter and the generalized force is simply specified as a time-vary generalized load. These concepts will be illustrated later by examples.

Equivalent Loads for Foundation Motion

The normal mode approach can be usefully applied to the analysis of multiple degree of freedom systems which are attached to a moving foundation. The basic approach is to define the motion of the flexible system, relative to the motion of its foundation, in terms of the normal modes of the fixed base system and add the motion of the base to define the total absolute motion. Then the acceleration of the foundation becomes, in effect, an inertial load on each mass of the moving system. This may be illustrated by a simple example. Referring to Figure 3.56, the equations of motion of the three masses consisting of the foundation  $m_o$  and two lumped masses  $m_1$  and  $m_2$  may be determined from the free-body diagram in terms of the relative deflections  $\epsilon_1$  and  $\epsilon_2$  and the base acceleration  $\ddot{u}$ . The same procedure given in Section 3.3.2.6 is used to define the stiffness coefficients except that each mass is fixed relative to the foundation when computing the spring forces. The resulting equations are:

$$\left. \begin{aligned} -k_1 \epsilon_1 &= -m_o \ddot{u} + P_T(t) \\ m_1 \ddot{\epsilon}_1 + (k_1 + k_2) \epsilon_1 - k_2 \epsilon_2 &= -m_1 \ddot{u} \\ m_2 \ddot{\epsilon}_2 - k_2 \epsilon_1 + k_2 \epsilon_2 &= -m_2 \ddot{u} \end{aligned} \right\} \tag{3.225}$$

The first equation relates the driving force  $P(t)$  on the foundation to its acceleration  $\ddot{u}$  and the net spring force  $-k_1 \epsilon_1$ , acting on the foundation, due to relative deformation of the system. This equation is not required to define the relative motion of the system since an arbitrary foundation acceleration  $\ddot{u}$  or displacement  $u$  will be assumed. This in turn will define the relative motion  $\epsilon_1$ , which can then be used in the first equation to define the dependent driving force  $P_T(t)$ .

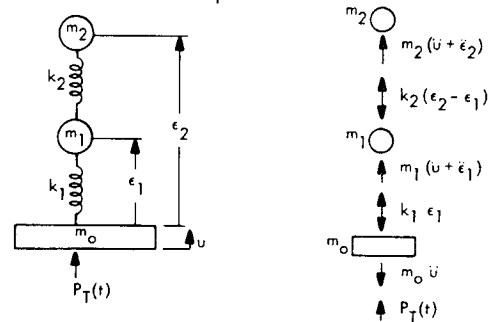


FIGURE 3.56 Dynamic Model and Free Body Diagram for Two Degree-of-Freedom System Attached to Moving Foundation with Finite Mass  $m_o$ . The deflections  $\epsilon_1$  and  $\epsilon_2$  correspond to the relative dynamic displacements of the masses  $m_1$  and  $m_2$  with respect to the moving foundation.

significant improvements in accuracy (Reference 3.1, Chapter 28; References 3.34 and 3.36).

The four forms for the generalized damping force outlined above are summarized in Table 3.3. The principal difference in these various models for the damping force is the variation in  $Q_n$  with frequency. Experience indicates that  $Q_n$  is roughly independent of frequency so that uniform structural damping is often selected as a suitable model. However, the same result is achieved by using the generalized model and specifying damping in terms of a constant  $Q_n$  instead of the generalized damping factor  $C_n$ . The latter approach will ordinarily be used in this manual. The method of calculating a generalized damping constant  $C_n$  will also be illustrated later in an example.

It is important to recognize that the various mathematical forms for damping outlined in Table 3.3 have been developed as convenient models for engineering analysis of damped complex structure. The analytical description of the various types of damping which actually occur in nature is more complex.

TABLE 3.3

SUMMARY OF VARIOUS FORMS OF UNIFORM DAMPING FOR MULTI-DEGREE-OF-FREEDOM SYSTEMS WHICH RETAIN THE ORTHOGONALITY PROPERTY FOR NORMAL MODES

Type of Uniform Damping	Damping Coefficient	Generalized Values		
		Damping Constant (2)	Damping Force - $c\dot{x}_n$	$Q_n = 1/2 \delta_n$
Generalized	$c_{ij}$	$C_n$	$C_n q_n$	$\omega_n M_n C_n$
Viscous	$2 G k_{ij}$	$2 G K_n$	$2 G K_n q_n$	$1/2 G \omega_n$
Structural	$\frac{g}{\omega} k_{ij}$	$\frac{g}{\omega} K_n$	$\frac{g}{\omega} K_n q_n$	$\frac{1}{g \omega_n}$
Mass	$B m_i$	$B M_n$	$B M_n q_n$	$\omega_n B$

- (1)  $G, g, B$  - Uniform damping constants for a given system.
- (2)  $M_n, K_n, C_n$  - Generalized mass, stiffness and damping constant for the  $n$ th normal mode.

Structural damping is also frequently identified as hysteretic damping and the damping and stiffness terms are combined into the complex quantity  $k_{ij} + j g k_{ij}$ . The generalized damping and stiffness forces in the equation of motion for each mode are then given by

$$K_n [1 + j g] q_n(t)$$

This method of specifying damping and stiffness is strictly applicable only when  $q_n(t)$  can be defined in terms of sinusoidal motion (Reference 3.36).

3.3.3.2 General Form of Solutions for Various Types of Excitation

The basic tools for defining the forced response of a damped multi-degree of freedom system in terms of its normal modes are now available. Starting with the equation for free

vibration of the undamped system (Equation 3.199a), and adding the terms for the generalized damping force  $C_n \dot{q}_n(t)$ , and the generalized driving force  $F_n(t)$ , the forced response of the damped system in its  $n$ th normal coordinate  $q_n(t)$  is

$$M_n \ddot{q}_n(t) + C_n \dot{q}_n(t) + K_n q_n(t) = F_n(t)$$

or, dividing through by  $M_n$ ,

$$\ddot{q}_n(t) + 2 \delta_n \omega_n \dot{q}_n(t) + \omega_n^2 q_n(t) = \frac{F_n(t)}{M_n} = \frac{\omega_n^2 F_n(t)}{K_n} \tag{3.222}$$

where

$$\delta_n = \text{critical damping ratio for } n\text{th normal mode} = 1/2 Q_n$$

$$\omega_n = \text{undamped natural frequency of } n\text{th normal mode}$$

$$M_n = \text{generalized mass given by Equation 3.193}$$

$$F_n(t) = \text{generalized force given by Equation 3.213}$$

This is identical, in form, to the equation of motion for forced excitation of a single degree of freedom given at the beginning of this chapter (see Equation 3.6, page 3-3).

The subscripts  $i$  and  $j$  have been used freely throughout the preceding sections with reference to any two mass elements of the lumped parameter system. It will be convenient from now on in dealing with forced response of the system to adopt the following convention on subscripts to identify response and excitation locations:

$i$  - refers to general location of any mass element of system, and specifically identifies a response point.

$j$  or  $k$  - refers to general location of one or more mass elements at which excitation is applied.

Definition of Loading for Multi-Degree-of-Freedom System

The forces  $P_i(t)$  applied to the  $i$ th mass (or inertia) elements of an  $N$  degree of freedom lumped parameter system may have several forms.

Case (1) Static Loading  $P_j(t) = P_{sj}$

The static load response can be determined by the normal mode approach to provide a convenient reference for the dynamic response magnification. For uniform static loading,  $P_{sj}$  is a constant at all points.

Case (2) In-Phase Dynamic Loading  $P_j(t) = P_j \cdot f(t)$

This is the most common type of loading considered where all loads vary in phase with the same time function  $f(t)$ . The amplitude of the load at each point  $P_i$  may be varied arbitrarily. For uniform dynamic loading, the amplitude  $P_i$  is a constant at all points.



Thus, considering only the last two equations, the effective excitation on each mass,  $-m_i \ddot{u}$ , is first set equal to zero. The system is then fixed with relative deflections  $\epsilon_i(t)$  becoming absolute deflections. The free vibration of the masses  $m_1$  and  $m_2$  can then be defined by their normal modes, or

$$\epsilon_i(t) = \sum_n^N \phi_{in} q_n(t)$$

where the mode shapes  $\phi_{in}$ , natural frequencies  $\omega_n$ , and generalized masses  $M_n$  for each mode will correspond to these values obtained for the fixed base system.

Now if the foundation is allowed to move, the generalized force for each mode will consist of the inertial force due to a uniform foundation acceleration  $\ddot{u}(t)$  in the same direction as the relative motions  $\epsilon_1(t)$  and  $\epsilon_2(t)$ . This may be expressed as for any other uniform dynamic load by

$$F_n(t) = -\ddot{u}(t) \sum_j m_j \phi_{jn} \quad (3.226)$$

or, in the convenient form given earlier,

$$F_n(t) = -P_o J_n f(t)$$

where

$$P_o = \ddot{U}_{\max} \sum_j m_j - \text{the maximum force necessary to accelerate the total mass of the flexible system without its base to the peak acceleration } \ddot{U}_{\max} \quad (3.227)$$

$$J_n = \frac{\sum_j m_j \phi_{jn}}{\sum_j m_j} - \text{the joint acceptance for the } n\text{th mode for uniform foundation motion} \quad (3.228)$$

$f(t)$  = the dimensionless time variation of the foundation acceleration.

Thus, the relative motion of the system can be determined by applying this generalized force to the equations of motion in normal coordinates  $q_n(t)$  for the fixed base system. In the example illustrated in Figure 3.56, the first spring  $k_1$ , and mass  $m_1$  may be considered as representing those spring and mass elements of a general system which are connected directly to the moving foundation mass  $m_o$ .

#### Concentrated Load and Superposition of Responses

When only one concentrated load  $P_j \cdot f(t)$  drives a multiple degree-of-freedom system at only one mass element, say the  $j$ th mass, then the generalized force for the  $n$ th mode is simply

$$F_n(t) = P_j \phi_{jn} \cdot f(t) \quad (3.229)$$

If several such concentrated loads are applied independently, the net response of the system is found by summing the response to each applied load independently. Since the dynamic system and its equations of motion are assumed to be linear, the principle of superposition applies in all cases. That is, the total response of the  $i$ th mass  $x_i(t)$  may be determined by analyzing the response of this mass to the load on the  $j$ th mass element and then summing the responses  $x_{ij}(t)$  for each such load over all the masses. This procedure is seldom necessary, however, since it will normally be possible to define one generalized force for each mode which accounts for all applied loads in the mode.

#### Summation of Responses in All Normal Modes

The response of the  $n$ th normal mode coordinate  $q_n(t)$  will be the solution to its equation of motion (Equation 3.222). For deterministic loads, the time history of the response of the  $i$ th mass will then be the summation over all modes given by

$$x_i(t) = \sum_n^N \phi_{in} q_n(t) \quad (3.230)$$

For random loads, the response at any point is specified by the summation of the power spectral density of the normal coordinate  $q_n(t)$  for each mode instead of the instantaneous values as specified by the preceding equation. Thus, the power spectral density  $W_x(i, f)$  of the response at  $x_i$  is the summation

$$W_x(i, f) = \sum_n^N \phi_{in}^2 \cdot W(q_n, f) \quad (3.231)$$

These last two equations define the basic method for summing up the normal mode responses at a given point in a lumped parameter system due to any type of loading. They are utilized frequently in the remainder of this chapter and in Chapters 8 and 9. The final step in solving for the response of the lumped parameter system is to obtain the solution for the normal coordinate  $q_n(t)$  or its power spectral density  $W(q_n, f)$ . The basic methods are summarized in the following sections.

#### 3.3.3.3 Response of Lumped Parameter Systems to Transient Loads

The forced response of  $q_n(t)$  for any deterministic load  $P(t)$  is given by the Duhamel integral.

$$q_n(t) = \frac{1}{\omega_{dn} M_n} \int_{t=0}^t F_n(\tau) e^{-\delta_n \omega_n(t-\tau)} \sin \omega_{dn}(t-\tau) d\tau \quad (3.232)$$

where

- $\omega_{dn}$  = damped natural frequency of nth normal mode
- $\omega_n$  = undamped natural frequency of nth normal mode
- $M_n$  = generalized mass for nth mode
- $F_n(\tau)$  = generalized force for nth mode at time  $t = \tau$
- $\delta_n$  = critical damping ratio for nth mode  
=  $1/2 Q_n$ .

For loads which vary uniformly in time at all points, this equation can be expressed in the following form which is more easily compared to the solutions for transient response of a single degree-of-freedom system.

$$\frac{q_n(t)}{q_{ns}} = \frac{\omega_n}{\sqrt{1-\delta_n^2}} \int_0^t f(\tau) e^{-\delta_n \omega_n(t-\tau)} \sin \omega_{dn}(t-\tau) d\tau \tag{3.233}$$

where

- $q_{ns} = \frac{P_o J_n}{\omega_n^2 M_n}$  = static response of nth normal mode coordinate to peak amplitude  $P_o J_n$  of generalized force for nth mode
- $P_o$  = peak amplitude of total applied force
- $J_n$  = joint acceptance for nth mode given by Equation 3.224
- $\omega_n^2 M_n = K_n$  = generalized stiffness of nth mode
- $f(\tau)$  = relative value of total applied force at time  $t = \tau$ .

The left side of this equation is identical in form to the solutions given in Section 3.2 for the transient displacement response of a fixed base single degree-of-freedom system relative to its maximum static response. Thus, the analytical and graphical solutions given in Section 3.2 may be used directly to solve for the response of the nth normal mode coordinate of a multi-degree-of-freedom system after making the obvious substitutions, including the following:

	Single Degree-of-Freedom Solution	Normal Coordinate Solution
Excitation	$P(t)$	$F_n(t)$
Response	$x(t)$	$q_n(t)$
Natural Frequency	$f_o = \omega_o/2\pi$	$f_n = \omega_n/2\pi$
Mass	$m$	$M_n$

Stiffness	$k$	$\rightarrow K_n = \omega_n^2 M_n$
Damping Ratio	$\delta$	$\rightarrow \delta_n$
Peak Excitation	$P$	$\rightarrow P_o J_n$
Static Response	$x_s = P/k$	$\rightarrow q_{ns} = P_o J_n / \omega_n^2 M_n$
Maximum Displacement	$x_{max}$	$\rightarrow q_{nmax}$

To illustrate the method outlined above for finding the transient response of a multiple degree-of-freedom system, consider the following example.

### 3.3.3.4 Response of Two Degree-of-Freedom System to Triangular Shock Load

Consider the response of the same fixed-base two degree of freedom system treated earlier to a triangular shock load as shown in Figure 3.57. The following parameters, required for the forced response solution, are obtained from the previous results for the free vibration response of this system (see Section 3.3.2.9).

Given

- Natural Frequencies  $\omega_1 = 0.665 \sqrt{k/m}$  radians/sec
- $\omega_2 = 1.165 \sqrt{k/m}$  radians/sec
- Generalized Mass  $M_1 = 2.56 m$
- $M_2 = 1.64 m$
- Mode Shapes  $\phi_{11} = 0.559$   $\phi_{12} = -0.358$
- $\phi_{21} = 1$   $\phi_{22} = 1$

Assume Triangular Shock Loads on Each Mass	$P_1(t) = 2P [1 - t/T]$
	$P_2(t) = P [1 - t/T]$
Let Duration	$T = \pi/\omega_1$

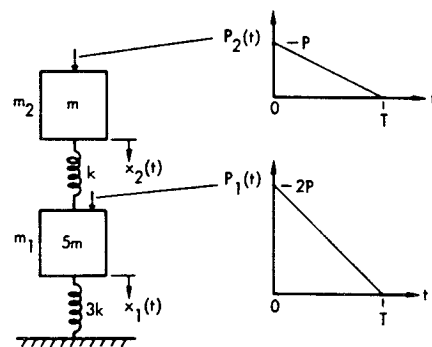


FIGURE 3.57 Triangular Shock Load on Two Degree-of-Freedom System

The transient response is found as follows, utilizing the analytical results presented earlier in Section 3.2 for a single degree-of-freedom system.

#### Total Load

$$P_o = \sum_j^N P_j = 3P$$

#### Joint Acceptance

$$J_1 = \sum_j^N \frac{P_j \phi_{i1}}{P_o} = \frac{1}{3P} [(.559) 2P + P] = 0.706$$

$$J_2 = \sum_j^N \frac{P_j \phi_{i2}}{P_o} = \frac{1}{3P} [(-.358) 2P + P] = 0.095$$

#### Static Response of nth Normal Coordinate

$$q_{ns} = \frac{P_o J_n}{\omega_n^2 M_n}$$

$$q_{1s} = \frac{(3P)(.706)}{(.665)^2 (k/m) (2.56 m)} = 1.875 \frac{P}{k}$$

$$q_{2s} = \frac{(3)(.095)}{(1.165)^2 (k/m) (1.64) m} = 0.127 \frac{P}{k}$$

#### Exact Solution for Peak Response to Triangular Pulse Load

An exact solution for the response may now be obtained by using these parameters in Equation 3.229 to solve for the response in each normal mode. The peak response is then found from an analysis of the summation of the instantaneous modal responses. If the lowest natural frequency of the system is greater than about 1/(3 times the duration of the triangular pulse load), the peak response of all modes will occur during the forced response period (i.e.  $t_{n \max} < T$ ). Thus, using the known solution for the forced response of a single degree-of-freedom system to a triangular pulse load, (see Equation 3.34, page 3-10), the net response of the  $i$ th mass for all the modes of the lumped system will be given by

$$x_i(t) = P_o \sum_n^N \frac{\phi_{in} J_n}{\omega_n^2 M_n} \times \left[ 1 - \frac{t}{T} + \sqrt{1 + \left(\frac{1}{\omega_n T}\right)^2} \sin(\omega_n t - \tan^{-1} \omega_n T) \right] \quad (3.234)$$

where

$$P_o = \text{Peak Value of Triangular Pulse Load} = \sum_j P_j$$

$$\phi_{in} = \text{Mode Shape of } i\text{th Mass for } n\text{th mode}$$

$$J_n = \text{Joint Acceptance for } n\text{th mode (see Equation 3.224)}$$

$$\omega_n = \text{Natural Frequency for } n\text{th mode}$$

$$M_n = \text{Generalized Mass for } n\text{th mode}$$

$$T = \text{Duration of Triangular Pulse.}$$

This solution assumes that the pulse occurs simultaneously on all loaded elements of the system.

This exact approach can only be effectively handled with a computer for a system with more than 3 or 4 normal modes. As an alternate procedure, an estimate of the peak response  $x_{i \max}$  of any element may be made by one of the following approximate methods.

#### Approximate Solution Using Shock Spectrum

The peak response in each normal mode is found by using the graphical solutions for the shock spectrum for a single degree of freedom system. This specifies the peak response relative to the static response for each normal mode. The following values are obtained for this example.

#### Maximum Response of Normal Coordinates to Triangular Shock

(Use Figure 3.10, page 3-11.)

$$\text{First mode, } T = \pi/\omega_1, \text{ and } f_1 T = 0.5, \text{ then } \frac{q_{1 \max}}{q_{1s}} = 1.20$$

$$\text{Second mode, } f_2 T = \frac{\omega_2}{\omega_1} f_1 T = 0.877, \text{ then } \frac{q_{2 \max}}{q_{2s}} = 1.49$$

#### Maximum Displacement of Each Mass in Each Mode

##### LOWER MASS

##### First Mode

$$x_{11 \max} = \phi_{11} q_{1 \max} = (.559)(1.2)(1.875) \frac{P}{k} = 1.26 \frac{P}{k}$$

##### Second Mode

$$x_{12 \max} = \phi_{12} q_{2 \max} = (-.358)(1.49)(.127) \frac{P}{k} = -0.07 \frac{P}{k}$$

UPPER MASS

First Mode

$$x_{21 \max} = 2.25 \frac{P}{k}$$

Second Mode

$$x_{22 \max} = 0.19 \frac{P}{k}$$

The net peak response for each mass is then found by summing up the peak responses in each mode,  $\phi_{in} q_{n \max}$ , according to one of the following rules (Reference 3.41).

Linear Summation Rule (An Absolute Upper Bound)

$$x_{i \max} \leq \sum_n^N |\phi_{in}| |q_{n \max}| \quad (3.235a)$$

Square Root Rule

$$x_{i \max} \approx \left[ \sum_n^N (\phi_{in} q_{n \max})^2 \right]^{1/2} \quad (3.235b)$$

The error in these approximations is not definable, in general, but is not expected to exceed +20 percent for the linear rule and  $\pm 20$  percent for the square root rule.

Approximate Graphical Solution Using Shock Spectrum and Time of Occurrence of Maximum in Each Mode

An improved estimate of the peak response can be obtained by utilizing the known time of occurrence  $t_{n \max}$  for the peak response of each mode, along with the peak response  $q_{n \max}$ , the static response  $q_{ns}$  and the natural frequency  $f_n = \omega_n / 2\pi$  in each mode.

Time of Occurrence of Maximum Displacement Peaks in Each Normal Mode

(Use Figure 3.11, page 3-12.)

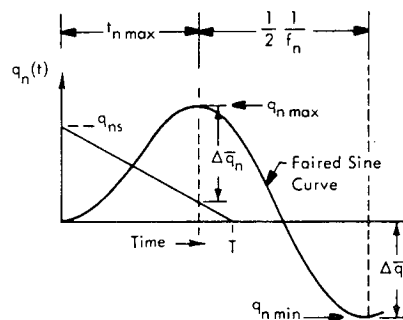
First Mode,  $f_1 T = 0.5, f_1 t_{1 \max} = 0.4, t_{1 \max} = 0.8 T$

Second Mode,  $f_2 T = 0.877, f_2 t_{2 \max} = 0.45, t_{2 \max} = 0.51 T$

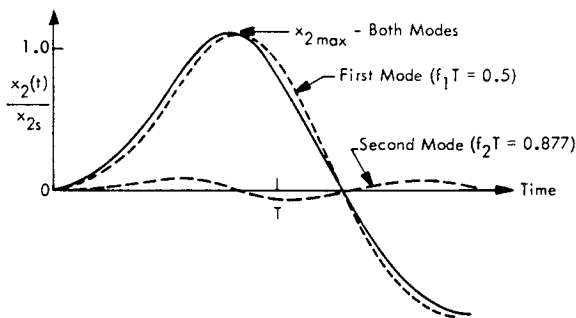
Given these parameters, an approximate graphical solution can be carried out using hand-drawn faired curves, as outlined in Figure 3.58a. This indicates the method for roughly estimating the time history for each normal mode coordinate  $q_n(t)$  given the maximum response and its time of occurrence. Such a procedure was used for this example to plot the net time history for the transient response of the upper mass to the triangular load pulse. The resulting plot is illustrated in Figure 3.58b. The hand-drawn faired curves are a close approximation to the true values. The predominant influence of the first mode on the displacement response is quite evident.

Comparison of Estimates of Peak Response to Triangular Pulse

The various methods for defining the peak response can be conveniently compared in terms of the peak dynamic response  $x_{i \max}$  of each mass relative to its static response  $x_{is}$  to the peak load. The latter is determined from the static response  $q_{ns}$  and mode shapes  $\phi_{in}$  for each mode.



a) Graphical Construction of Time History of Normal Coordinate  $q_n(t)$



b) Net Transient Response  $x_2(t)$  of Upper Mass Relative to Peak Static Response,  $x_{2s}$

FIGURE 3.58 Transient Response of Fixed Base Two Degree-of-Freedom System in Figure 3.57 to Triangular Shock Load (See Text for Details of Analysis Method)

Total Static Response of Each Mass to Peak Load

$$x_{1s} = \sum_n^2 \phi_{1n} q_{ns} = \left[ (.559)(1.875) \frac{P}{k} - (.358)(.127) \frac{P}{k} \right] = \frac{P}{k}$$

$$x_{2s} = \left[ (1)(1.875) \frac{P}{k} + (1)(.127) \frac{P}{k} \right] = 2 \frac{P}{k}$$

<u>Analysis Method</u>	$x_{1\max}/x_{1s}$	$x_{2\max}/x_{2s}$
Exact (Equation 3.234)	1.24	1.16
Linear Sum (Equation 3.235a)	1.33	1.22
Square Root Rule (Equation 3.235b)	1.26	1.13
Graphical Estimate (Figure 3.58b)	1.25	1.15

For this particular example, all three approximate methods provide reasonable results compared to the exact value.

Approximate Response Using Only First Few Normal Modes

As a general rule, for relatively uniform multiple degree of freedom systems driven by an approximately uniform transient load, the peak displacement response is closely approximated by the peak response in only the first 2 or 3 normal modes. This becomes readily apparent by examination of the frequency variation of the parameter  $J_n/\omega_n^2$  which appears in the general expression (Equation 3.233) for forced response to transient loads. The joint acceptance  $J_n$  is proportional to the sum  $\sum_j^N P_j \phi_{jn}$ . Above the first mode, the alternating signs of the mode shapes  $\phi_{jn}$  tend to cancel each other so that the summation tends to approach zero for a uniform load. Since  $1/\omega_n^2$  also decreases with increasing mode number, the trend is a rapidly decreasing displacement response with mode number for uniform loading.

This approximation becomes less accurate for the acceleration responses of lumped parameter systems where higher order modes become more important. It will be shown later that bending and shear stresses in distributed structure, such as beams, are also more sensitive to higher order normal modes.

3.3.3.5 Response of Lumped Parameter Systems to Sinusoidal Loads

For a single degree-of-freedom system under random excitation, it was shown earlier in Section 3.2.3 that the power spectral density of the response was related to the power spectral density of the excitation by the square of the absolute value of the steady state sinusoidal transfer function  $|a(f)|$ . This defines the amplitude of a general sinusoidal response variable (such as velocity of the mass) in terms of the amplitude of a general sinusoidal excitation P (such as force on the spring-supported mass).

For the multiple degree of freedom system under random excitation, a similar concept will still apply. However, the net response of the structure at any one point will now be the summation of the responses in each mode summed over all the inputs applied to the structure. In this case, the absolute value of  $a(f)$  is no longer adequate, therefore both amplitude and phase of this sinusoidal transfer function are required. Furthermore, it will now be used to define the sinusoidal response of each normal mode  $q_n(t)$

of a multi-modal system to a generalized sinusoidal force  $F_n \cos \omega t$  for this mode. Consider then, the form that  $a(f)$  will take in this case.

For a simple spring-mass system attached to a fixed base, the steady-state displacement response  $x(t)$  of the mass for a sinusoidal driving force with amplitude P and frequency  $\omega = 2\pi f$  was found to be (see page 3-6)

$$x(t) = \frac{P}{k} |H(f)| \cos(2\pi f t - \theta)$$

where

$$|H(f)| = 1 / \left[ \left( 1 - (f/f_0)^2 \right)^2 + (2\delta f/f_0)^2 \right]^{1/2} - \text{the dynamic magnification factor}$$

and

$$\theta = \tan^{-1} \frac{2\delta f/f_0}{1 - (f/f_0)^2} - \text{phase angle between response and excitation.}$$

The sinusoidal excitation could also be expressed as the Real  $[R]$  part of the complex expression

$$P \cos 2\pi f t = \mathcal{R} \left[ P e^{j 2\pi f t} \right] = \mathcal{R} \left[ P \cos 2\pi f t + j P \sin 2\pi f t \right]$$

Similarly, the sinusoidal response can be given as the real part of the complex form

$$x(t) = \frac{P}{k} H(f) e^{j 2\pi f t}$$

where

$$H(f) = \frac{1}{1 - (f/f_0)^2 + j 2\delta f/f_0} - \text{complex steady state frequency response function.}$$

The real form for  $x(t)$  is obtained by first transforming the complex frequency response function  $H(f)$  in the following manner.

$$\text{Let } H(f) = \frac{1}{a + j b}$$

$$\text{where } a = 1 - (f/f_0)^2, \quad b = (2\delta f/f_0)$$

Multiply  $a + j b$  by its absolute value  $\sqrt{a^2 + b^2}$  and divide by the same quantity to give

$$a + j b = \sqrt{a^2 + b^2} \left[ \frac{a}{\sqrt{a^2 + b^2}} + j \frac{b}{\sqrt{a^2 + b^2}} \right]$$

Since  $a$  and  $jb$  represent vectors at right angles to each other, of length  $a$  and  $b$  respectively, the resultant or absolute magnitude of these vectors has an angle  $\theta$  to the real part ( $a$ ) given by

$$\theta = \tan^{-1} \frac{b}{a}$$

Thus

$$\cos \theta = \frac{a}{\sqrt{a^2 + b^2}}, \quad \sin \theta = \frac{b}{\sqrt{a^2 + b^2}}$$

and  $a + jb$  may be written as

$$a + jb = |a + jb| [\cos \theta + j \sin \theta] = |a + jb| e^{j\theta}$$

When inverted, this becomes

$$\frac{1}{a + jb} = \left| \frac{1}{a + jb} \right| e^{-j\theta}$$

so that  $H(f)$  can be given by

$$H(f) = |H(f)| e^{-j\theta}$$

It will often be convenient to use the latter form for expressing the steady state sinusoidal transfer function  $\alpha(f)$ . In this case, it would be

$$\alpha(f) = \frac{x(t)}{P(t)} = \frac{|H(f)|}{k} e^{-j\theta} = |\alpha(f)| e^{-j\theta}$$

Thus, in this complex form,  $\alpha(f)$  or  $|\alpha(f)| e^{-j\theta}$  defines both the amplitude  $|H(f)|/k$  of the sinusoidal transfer function between displacement response and force input, and the corresponding phase angle. For any sinusoidal excitation, the single degree-of-freedom response may then be given in terms of  $\alpha(f)$  in the general form

$$\left[ \begin{array}{l} \text{Response as} \\ \text{Function of Time } t \end{array} \right] = \mathcal{R} \left\{ \left[ \begin{array}{l} \text{Excitation} \\ \text{Amplitude} \end{array} \right] |\alpha(f)| e^{-j\theta} \cdot e^{j2\pi f t} \right\} \quad (3.236)$$

For the previous example, this would take the form

$$x(t) = \mathcal{R} \left[ P |\alpha(f)| e^{-j\theta} e^{j2\pi f t} \right]$$

Expanding the complex vectors into sine and cosine terms and taking the real part, this becomes

$$x(t) = P |\alpha(f)| [\cos \theta \cos 2\pi f t + \sin \theta \sin 2\pi f t]$$

Applying the transformation

$$A \cos Z + B \sin Z = \sqrt{A^2 + B^2} \cos [Z - \tan^{-1} B/A]$$

the real part of  $x(t)$  becomes

$$x(t) = P |\alpha(f)| \cos (2\pi f t - \theta)$$

thus returning to the original form where  $|a(f)| = |H(f)|/k$ .

When applied to the sinusoidal response of multiple degree of freedom systems, the operation indicated in Equation 3.236 for the single degree-of-freedom system will define the sinusoidal response of the normal mode coordinate  $q_n(t)$  for each  $n$ th mode. The excitation will be the generalized force  $F_n \cos (2\pi f t) = \mathcal{R} \{ F_n \exp (j2\pi f t) \}$  for the same mode. Thus, the results given in Section 3.2.1 for the sinusoidal response of the single degree-of-freedom system can be applied directly to define the sinusoidal transfer function  $|\alpha_n(f)|$  for the  $n$ th normal mode of the multiple degree of freedom system. Applying this technique, the following general solutions are obtained for the sinusoidal response of a lumped parameter system for simultaneous or in-phase sinusoidal excitation. These solutions have the following general form, in terms of real variables.

$$x_i(t) = \sum_n^N \phi_{in} q_n(t)$$

where

$$q_n(t) = F_n |\alpha_n(f)| \cos (2\pi f t - \theta_n) - \text{normal mode response}$$

and

$$F_n = P_o J_n = \text{amplitude of generalized force for } n\text{th mode.}$$

#### IN-PHASE SINUSOIDAL FORCE ON EACH MASS

$$P_j(t) = P_j \cos (2\pi f t)$$

- Displacement of  $i$ th Mass

$$x_i(t) = P_o \left[ \sum_n^N J_n \phi_{in} |\alpha_n(f)| \cos (2\pi f t - \theta_n) \right] \quad (3.237)$$

where

$$P_o = \sum_j^N P_j - \text{amplitude of total sinusoidal force}$$

$$J_n = \left[ \sum_j^N P_j \phi_{jn} \right] / P_o - \text{joint acceptance for } n\text{th mode}$$

$$\phi_{in} = \text{mode shape at } i \text{ for } n\text{th mode}$$

$$|\alpha_n(f)| = \frac{|H(f)|}{4\pi^2 f^2 M_n} - \text{sinusoidal transfer function for } n\text{th mode}$$

$$|H(f)| = 1 / \left[ (1 - (f/f_n)^2)^2 + (2\delta_n f/f_n)^2 \right]^{1/2} - \text{dynamic magnification factor for } n\text{th mode}$$

$f_n$  = natural frequency of nth mode

$f$  = forcing frequency

$M_n$  = Generalized mass for nth mode

$$\theta_n = \tan^{-1} \frac{2 \delta_n f / f_n}{1 - (f / f_n)^2}$$

---

• Acceleration of ith Mass

$\ddot{x}_i(t)$  = (same as Equation 3.237 except)

$$|a(f)| = \left(\frac{f}{f_n}\right)^2 \frac{|H(f)|}{M_n}$$

and  $\theta_n$  is replaced with  $\theta_n - \pi$ .

---

• Reaction Force on Sth Fixed Support Point

If the Sth support point is connected directly to the ith mass by a spring element with a spring constant  $k_{si}$ , the reaction force at this point is  $k_{si} x_i(t)$  where  $x_i(t)$  is given by Equation 3.237.

ACCELERATION INPUT TO FOUNDATION

$$\ddot{u}(t) = \ddot{U} \cos(2\pi ft)$$

• Relative Displacement of ith Mass

$\ddot{\epsilon}_i(t) = \ddot{x}_i(t) - \ddot{u}(t)$  = (same as Equation 3.237 except:)

$$P_o = -\ddot{U} \sum_j^N m_j$$

$$J_n = \left[ \sum_j^N m_j \phi_{jn} \right] / \left[ \sum_j^N m_j \right]$$

---

• Relative Acceleration of ith Mass

$\ddot{\epsilon}_i(t) = \ddot{x}_i(t) - \ddot{u}(t)$  = (same as Equation 3.237 except:)

$P_o, J_n$  = as given above for the relative displacement

$$|a(f)| = \left(\frac{f}{f_n}\right)^2 \frac{|H(f)|}{M_n}$$

$\theta_n$  replaced with  $\theta_n - \pi$ .

---

• Driving Force for Rigid Foundation with Mass  $m_o$

$$P_T(t) = m_o \ddot{u}(t) - \sum_s^S k_{si} \epsilon_i(t) \quad (3.238)$$

where

$k_{si}$  = spring constant for each of S spring elements directly connected between sth point on moving foundation and ith mass

$\epsilon_i$  = corresponding relative deflection for this spring element.

In all cases, the phase angle  $\theta_n$  for each mode is the same as defined for Equation 3.237.

Phase Angle of Response in Each Mode

This phase angle  $\theta_n$  varies with the ratio of excitation frequency  $f$  to normal mode frequency  $f_n$  and with damping ratio  $\delta_n$  in the same manner as for a single degree-of-freedom system (see Figure 3.5b, page 3-6).

As an example, for the normal mode response described by Equation 3.237, for excitation frequencies well below the natural frequency of the mode, the modal displacement response will be nearly in-phase with the excitation. This characterizes the so-called stiffness controlled region for the mode. For excitation at the natural frequency ( $f = f_n$ ), the displacement response lags the excitation force by  $90^\circ$  but the velocity response leads the displacement by the same amount and is in-phase with the driving force. Thus, the driving force supplies power proportional to the product of force times response velocity which just balances the power dissipated by damping forces.

For excitation well above the natural frequency, the mode is mass- or inertia-controlled and the acceleration is nearly in-phase with the force. The displacement response lags the force excitation by  $180^\circ$  in this frequency range. This changing phase relationship can be visualized as shown in Figure 3.59 by considering the modal response as a vector which rotates at the circular frequency  $2\pi f$  and which lags behind the corresponding vector for the excitation by the phase angle  $\theta_n$ . The figure shows the locus of the response vector relative to the excitation force vector for a sinusoidal transfer function proportional to the frequency response function  $H(f)$  for a single degree-of-freedom system. Note the rapid change in phase angle, as the frequency  $f$  passes through the natural frequency  $f_n$ . This rate of change of  $\theta_n$  increases for lower values of damping.

3.3.3.6 Summation of Multiple Sinusoidal Responses

The preceding expressions for the response to in-phase sinusoidal excitation involve the summation of N sinusoidal terms to determine the total response over all modes at a given point on the system. A thorough understanding of this basic step is desirable for consideration of the response of complex structure to more complex sinusoidal and random excitation. The process is considered in some detail, therefore, in this section.

Although expressions can be developed for the overall instantaneous value of the summation of N sinusoidal components, a more useful parameter for design purposes is the mean square value of this summation, or its square root, the rms amplitude.

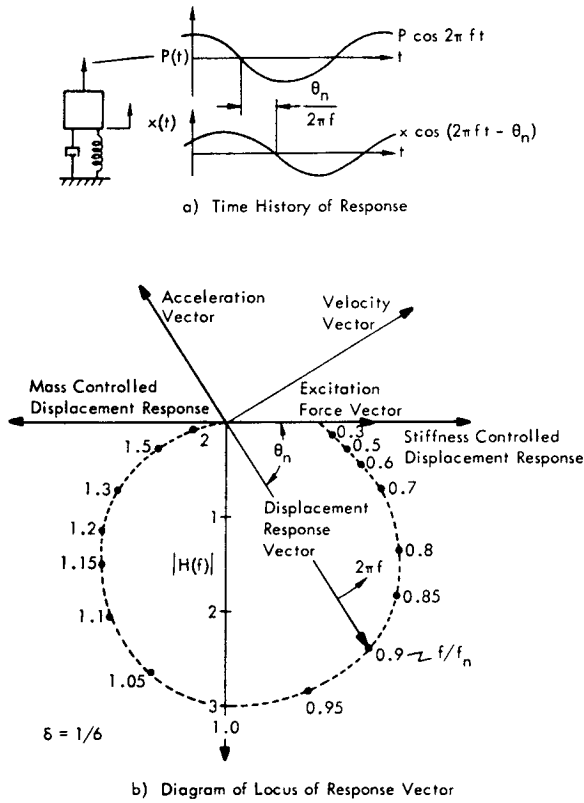


FIGURE 3.59 a) Time History and b) Vector Diagram for Displacement Response of Single Degree-of-Freedom System Corresponding to One Mode of a Multi-Modal System with Critical Damping Ratio = 1/6. For part b, radius of response vector given by  $|H(f)| = 1 / \sqrt{[1 - (f/f_n)^2]^2 + (2 \delta_n f/f_n)^2}$  and angle  $\theta_n$  by  $\tan^{-1} [2 \delta_n f/f_n / [1 - (f/f_n)^2]]$ . Position of vector shown for ratio of frequency of excitation to natural frequency of 0.9. Instantaneous value of response shown in part a is projection of response vector, rotating at angular frequency  $2\pi f$ , on horizontal axis.

The general equation for the mean square value of the sum of two time varying quantities is given by

$$\overline{x^2(t)} = \lim_{T \rightarrow \infty} \frac{1}{T} \int_{-T/2}^{+T/2} [x_1(t) + x_2(t)]^2 dt$$

Expanding the squared expression inside the integral and integrating each term, the mean square value becomes

$$\overline{x^2(t)} = \overline{x_1^2(t)} + \overline{x_2^2(t)} + 2 \overline{x_1(t) x_2(t)}$$

or, letting  $\overline{x^2(t)} = \overline{x^2}$ ,

$$\overline{x^2} = \overline{x_1^2(t)} + \overline{x_2^2(t)} + 2 \overline{x_1(t) x_2(t)}$$

where the bar designates the long time average or mean square value. This expression may be generalized to cover N components. Thus, if

$$x(t) = x_1(t) + x_2(t) + \dots + x_N(t) = \sum_n^N x_n(t)$$

the mean square value of  $x(t)$  is

$$\begin{aligned} \overline{x^2} &= \overline{x_1^2(t)} + \overline{x_2^2(t)} + \dots + \overline{x_N^2(t)} \\ &+ 2 \overline{x_1(t) x_2(t)} + \dots + 2 \overline{x_n(t) x_m(t)} \end{aligned}$$

The self-squared and cross product terms may be given by a single and double summation, respectively, or

$$\overline{x^2} = \sum_n^N \overline{x_n^2(t)} + \sum_{n \neq m}^N \sum_m^N \overline{x_n(t) x_m(t)} \tag{3.239}$$

Therefore, the mean square value of the sum of N time varying components has two parts: 1) the sum of the mean square value of each component, and 2) the sum of the time average value of all the cross products. Three special cases are of interest for sinusoidal components.

$$1) \quad \underline{x_n(t) = X_n \cos(2\pi f t - \gamma_n)}$$

In this case, each component has the same frequency  $f$  but a different amplitude  $X_n$  and phase  $\gamma_n$ . The mean square value of each component is known to be

$$\overline{x_n^2(t)} = \frac{1}{2} X_n^2$$

The time average value of the cross products may be determined as follows. If the  $n$ th and  $m$ th components are

$$x_n(t) = X_n \cos(2\pi f t - \gamma_n)$$

$$x_m(t) = X_m \cos(2\pi f t - \gamma_m)$$

Then, by using the trigonometric identity that

$$\cos A \cos B = \frac{1}{2} \cos(A + B) + \frac{1}{2} \cos(A - B)$$

the cross product may be expressed as

$$x_n(t) x_m(t) = \frac{1}{2} X_n X_m [\cos(4\pi f t - \gamma_m - \gamma_n) + \cos(\gamma_m - \gamma_n)]$$

Since the long time average of the first cosine term is zero, the long time average value of one cross product term is

$$\overline{x_n(t) x_m(t)} = \frac{1}{2} X_n X_m \cos(\gamma_m - \gamma_n) \tag{3.240}$$



Thus, the mean square value of the sum of two sinusoidal components, with amplitudes  $X_1$  and  $X_2$  respectively, is

$$\overline{x^2} = \frac{1}{2} X_1^2 + \frac{1}{2} X_2^2 + X_1 X_2 \cos(\gamma_2 - \gamma_1)$$

where  $\gamma_2 - \gamma_1$  is the relative phase difference between the two components. According to Equation 3.239, the mean square value of the sum of  $N$  such terms may be given by

$$\overline{x^2} = \frac{1}{2} \sum_n X_n^2 + \frac{1}{2} \sum_{n \neq m} X_n X_m \cos(\gamma_m - \gamma_n) \quad (3.241)$$

$$2) \quad \underline{x_n(t) = X_n \cos(2\pi f_n t - \gamma_n)}$$

In this case, each component has a different frequency  $f_n$ . The time average of the product of two sinusoids with different frequencies is always zero so that the cross product terms drop out and the mean square value of the sum of the individual components of different frequency is given by the first term in Equation 3.241.

$$3) \quad \underline{x_n(t) = X_n e^{-j\gamma_n} e^{j2\pi f t} = x_n(f) e^{j2\pi f t}}$$

This is identical to case 1) except that each component is given in complex form with a real amplitude  $X_n$  and phase angle  $\gamma_n$  or the equivalent complex amplitude  $x_n(f)$ . For just one such component, the mean square value is 1/2 the product of  $x_n(t)$  and its complex conjugate  $x_n^*(t)$ . This product cancels out the complex exponential terms as shown by the following.

$$\begin{aligned} \overline{x_n^2(t)} &= \frac{1}{2} x_n(t) x_n^*(t) = \frac{1}{2} [X_n e^{-j\gamma_n} e^{j2\pi f t}] [X_n e^{j\gamma_n} e^{-j2\pi f t}] \\ &= \frac{1}{2} X_n^2 e^{-j(\gamma_n - \gamma_n)} e^{j(2\pi f t - 2\pi f t)} \\ &= \frac{1}{2} X_n^2 = \frac{1}{2} |x_n(f)|^2 \end{aligned} \quad (3.242)$$

The same principle applies to a sum of complex terms. The mean square value of the sum is 1/2 the product of the sum and its complex conjugate. Thus, if the amplitude of the  $n$ th component is the complex quantity  $x_n(f) = |x_n(f)| e^{-j\gamma_n}$ , then the mean square value of the sum of just two such terms is

$$\begin{aligned} \overline{x^2} &= \frac{1}{2} [x_1(f) + x_2(f)] [x_1^*(f) + x_2^*(f)] \\ &= \frac{1}{2} [x_1(f)x_1^*(f) + x_2(f)x_2^*(f) + x_1(f)x_2^*(f) + x_1^*(f)x_2(f)] \end{aligned}$$

Each of the first two terms is equal to the mean square value of each component, as shown by Equation 3.242.

The sum of the complex conjugate cross-product terms is equal to

$$\begin{aligned} \frac{1}{2} x_1(f) x_2^*(f) + \frac{1}{2} x_1^*(f) x_2(f) &= \frac{1}{2} |x_1(f)| |x_2(f)| e^{j(\gamma_2 - \gamma_1)} \\ &+ \frac{1}{2} |x_1(f)| |x_2(f)| e^{-j(\gamma_2 - \gamma_1)} \end{aligned}$$

By expanding the complex exponentials into cosine and sine functions, it can be shown that the imaginary terms in the left side of this expression cancel out leaving the real quantity  $|x_1(f)| |x_2(f)| \cos(\gamma_2 - \gamma_1)$ . Thus, from Equation 3.240, an equivalent form for the time average value of both cross products of two sinusoidal components of the same frequency, but different phase, is

$$2 \overline{x_1(t) x_2(t)} = \frac{1}{2} x_1(f) x_2^*(f) + \frac{1}{2} x_1^*(f) x_2(f)$$

where  $x_1(f)$ ,  $x_2(f)$  are the complex amplitudes of  $x_1(t)$  and  $x_2(t)$ , respectively.

Therefore, 1/2 times the sum of complex conjugate cross-product pairs is equivalent to two times the time average value of their product. This, in turn, is equal to two times the product of their absolute values times the cosine of their relative phase angle.

Extending these results to the general case, the mean square value of the sum of  $N$  sinusoidal terms with a complex amplitude  $x_n(f)$  is

$$\overline{x^2} = \frac{1}{2} \sum_n |x_n(f)|^2 + \frac{1}{2} \sum_{n \neq m} x_n(f) x_m^*(f) \quad (3.243)$$

The double summation of the complex conjugate terms includes both pairs for  $n$  and  $m$  ( $m \neq n$ ). The imaginary parts therefore cancel out as shown for the case of two components. This expression is therefore equivalent to the result given in real form by Equation 3.241. The absolute magnitude  $|x_n(f)|$  of the complex form  $x_n(f)$  is the same as the real amplitude  $X_n$ .

The two equivalent expressions (Equations 3.241 and 3.243) for the mean square value of the sum of  $N$  sinusoidal terms provide the basic foundation for defining the response of multi-modal systems to excitation by one or more sinusoidal or random forces. With these expressions for the mean square value of  $N$  arbitrary sinusoidal components, it is possible to define the following specific cases for the response of multi-modal systems.

- Mean square value of response at one point over all normal modes
- Mean square generalized force in one mode due to multiple sinusoidal forces
- Mean square response in all  $N$  modes due to  $N$  sinusoidal forces.

Mean Square Response in All Modes

Consider, first, the case for only two modes. Assume that a two degree-of-freedom system is driven by a sinusoidal force and that the generalized force  $F_n(t)$  for each normal mode is given by

$$F_n(t) = F_n \cos(2\pi ft - \beta_n)$$

where

$F_n$  = amplitude of generalized force at frequency  $f$

$\beta_n$  = phase angle between generalized force and an arbitrary time reference.

The sinusoidal response of the  $i$ th mass in the  $n$ th mode is given by

$$x_{in}(t) = F_n |\alpha_n(f)| \phi_{in} \cos(2\pi ft - \beta_n - \theta_n)$$

where

$|\alpha_n(f)|$  = absolute value of sinusoidal transfer function for  $n$ th mode with phase angle  $\theta_n$

$\phi_{in}$  = mode shape at  $i$ th mass for  $n$ th mode.

This expression for the response in the  $n$ th mode is identical to the form given in case 1) in the preceding discussion. In this case, the amplitude  $x_n$  and phase angle  $\gamma_n$  of the  $n$ th sinusoidal component is

$$x_n = F_n |\alpha_n(f)| \phi_{in} \text{ - amplitude of response}$$

$$\gamma_n = \beta_n + \theta_n \text{ - phase angle}$$

Therefore, using Equation 3.241, the mean square value of the total response in two modes can be written down directly as

$$\begin{aligned} \overline{x_i^2} = & \frac{1}{2} \left[ F_1^2 |\alpha_1(f)|^2 \phi_{i1}^2 + F_2^2 |\alpha_2(f)|^2 \phi_{i2}^2 \right. \\ & \left. + 2 F_1 F_2 |\alpha_1(f)| |\alpha_2(f)| \phi_{i1} \phi_{i2} \cos \Delta_{mn} \right] \end{aligned} \quad (3.244)$$

where

$\Delta_{mn} = \beta_m - \beta_n + \theta_m - \theta_n$  = difference in phase between the  $m$ th and  $n$ th modal responses.

$\beta_m, \beta_n$  = relative phases of generalized forces for  $m$ th and  $n$ th modes, respectively

$\theta_m, \theta_n$  = phase angles of  $m$ th and  $n$ th sinusoidal transfer functions.

The mean square value of the net response in both modes is equal to the sum of two types of terms --  $1/2$  times the amplitude  $F_n |\alpha_{in}(f)|$  for each mode and a cross-product term equal to the product of the response amplitude  $F_n |\alpha_{in}(f)|$  in each mode times the cosine of the net difference in phase ( $\beta_m - \beta_n + \theta_m - \theta_n$ ) between the two modal responses.

For this equation and in the rest of this section, the response variable  $x_i(t)$  can be any desired quantity such as displacement or acceleration. Similarly, the generalized excitation "force" can also include foundation motion. The corresponding form for the sinusoidal transfer  $|\alpha_n(f)|$  is given by the definitions following Equation 3.237. It will also be understood that all input and response variables are sinusoids and the use of an argument ( $f$ ) to denote a sinusoidal variable at a frequency  $f$  is reserved for complex amplitudes or to denote complex sinusoidal transfer functions [i.e. -  $H(f)$  or  $a(f)$ ].

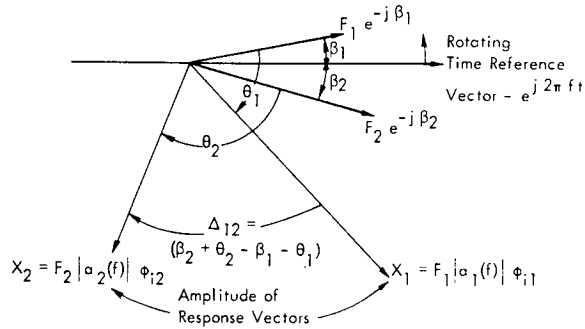
The amplitude  $X_i$  of the net response is simply the square root of the term in brackets in Equation 3.244. It is helpful to illustrate this summation of modal responses by treating each component as a vector. The summation process may then be visualized as shown by the diagram in Figure 3.60. Part (a) shows the two generalized force vectors with amplitudes  $F_1$  and  $F_2$  and phase angles  $\beta_1$  and  $\beta_2$  relative to an arbitrary reference line.

The response vectors  $X_1$  and  $X_2$  for each mode have the magnitudes  $F_1 |\alpha_1(f)| \phi_{i1}$  and  $F_2 |\alpha_2(f)| \phi_{i2}$  and phase angles  $\theta_1$  and  $\theta_2$ , relative to their excitation. The net phase angle between these response vectors is then  $\beta_2 - \beta_1 + \theta_2 - \theta_1$ . Part (b) shows how the total amplitude of the response vector is simply the vector summation of  $X_1$  and  $X_2$ . Thus, the amplitude of  $x_i(t)$  could be determined by simple trigonometric formulae for vector summation.

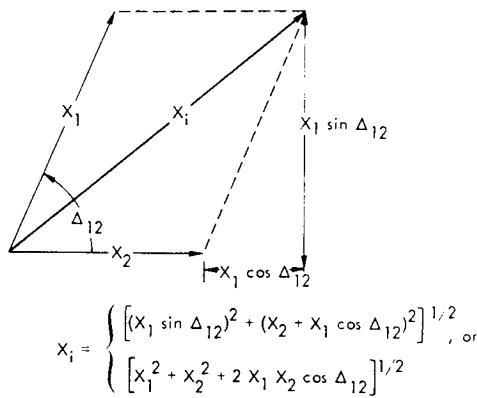
Extending this result to a system with  $N$  degrees of freedom, the mean square response for all modes will consist of the sum of all direct and cross-modal coupling terms. Thus the mean square sinusoidal response at the  $i$ th mass for  $N$  modes, each with a generalized sinusoidal force of amplitude  $F_n$ , sinusoidal transfer function  $|\alpha_n(f)| e^{-j\theta_n}$ , and mode shape  $\phi_{in}$  will be

$$\begin{aligned} \overline{x_i^2} = & \frac{1}{2} \sum_n^N F_n^2 |\alpha_n(f)|^2 \phi_{in}^2 \\ & + \frac{1}{2} \sum_{n \neq m}^N \sum_{m \neq n}^N F_n F_m |\alpha_n(f)| |\alpha_m(f)| \phi_{in} \phi_{im} \cos \Delta_{mn} \end{aligned} \quad (3.245)$$

(Note that the factor 2 in the cross term in Equation 3.244 is inherently accounted for by the double summation in Equation 3.245).



a) Vector Representation of Excitation and Response



b) Vector Summation of Modal Responses

FIGURE 3.60 Vector Representation of Combined Modal Response of Two Degree of Freedom System to Sinusoidal Excitation

If the generalized force  $F_n(t)$  for the  $n$ th mode were given in complex form as

$$F_n(t) = F_n e^{-j\beta_n} e^{j\omega t} = F_n(f) e^{j\omega t}$$

where

$F_n, \beta_n$  = amplitude and phase of generalized force for  $n$ th mode

$F_n(f)$  = corresponding complex amplitude,

then the mean square response at the  $i$ th mass for all modes may also be expressed in complex notation, using Equation 3.243, as

$$\begin{aligned} \overline{x_i^2} &= \frac{1}{2} \sum_n |F_n(f)|^2 |a_n(f)|^2 \phi_{in}^2 \\ &+ \frac{1}{2} \sum_{n \neq m}^N \sum_{m \neq n}^N F_n(f) F_m^*(f) a_n(f) a_m^*(f) \phi_{in} \phi_{im} \end{aligned} \quad (3.246)$$

Fortunately, it is usually possible to simplify either Equation 3.245 or Equation 3.246 which express the total response in all modes. The double summation, which defines the coupled response between each pair of different modes, is ordinarily neglected. It will be demonstrated later by a numerical example that this approximation is very good providing:

- the normal modes are well separated in natural frequency, and
- the primary concern is the determination of only the peak responses of a multi-modal system at excitation frequencies corresponding to its natural frequencies.

The potential error in this approximation may be further illustrated by examining the expression for the mean square response in  $N$  modes, given by Equation 3.245. Consider the error involved for the following three frequency regions:

- Excitation Frequency Below the Lowest Natural Frequency

In this frequency range, the relative phase shift between the transfer functions  $(\theta_m - \theta_n)$  will tend to be zero so that for in-phase excitation, where  $\beta_m = \beta_n$ , the modal cross-coupling terms will tend to be a maximum. However, at the most, they cannot exceed the sum of the mean square responses in each mode and will, in fact, always be less. Thus, omitting the modal coupling terms can underestimate the total mean square response by no more than a factor of two in this frequency range. A similar result is obtained for excitation above the highest natural frequency for a finite number of modes.

- Excitation Frequency Equal to the Natural Frequency for the  $n$ th Mode

In this case, the relative phase difference  $\theta_m - \theta_n$  between the transfer function  $a_n(f)$  for the  $n$ th mode and any other well separated mode will tend to approach  $\pm 90^\circ$  (see Figure 3.59). The term  $\cos \Delta_{mn}$  will then tend to approach

$$\cos(\beta_m - \beta_n + \pi/2) = \sin(\beta_m - \beta_n)$$

For in-phase loads, where  $\beta_m = \beta_n$ , the cross mode term will approach zero. In fact, the maximum mean square response is closely approximated by the response in just the one resonant mode.

- Excitation Frequency Between Two Normal Mode Frequencies

In this case, the relative phase difference  $\theta_m - \theta_n$  between the sinusoidal transfer functions will tend to approach  $\pm 180^\circ$  and the term  $\cos \Delta_{mn}$  will approach  $-\cos(\beta_m - \beta_n)$ . Thus, in this range, the omission of cross-mode terms will tend to overestimate the response. Again, however, the error is not ordinarily significant from a practical standpoint. Theoretically, if the generalized forces  $F_n, F_m$ , transfer functions  $|\alpha_n(f)|, |\alpha_m(f)|$  and mode shapes  $\phi_{in}, \phi_{im}$  were the same for any two modes at this frequency, the cross mode term could completely cancel the sum of the mean square responses for each mode, thus reducing the total response to zero. This rarely happens in real systems due to inherent nonuniformity of structure and loading.

Thus, for most practical cases, the maximum mean square response over all modes is approximately equal to the sum of the mean square responses in each mode. In this case, it is only necessary to define the mean square value of the generalized force for each mode.

Mean Square Generalized Force in One Mode for Multiple Sinusoidal Forces

Consider now the case illustrated in Figure 3.61 where multiple sinusoidal forces drive a multiple degree of freedom system. The instantaneous value of the generalized force  $F_n(t)$  in the  $n$ th mode has been defined as the summation

$$F_n(t) = \sum_j^N P_j(t) \phi_{jn}$$

where

$P_j(t)$  = instantaneous force at  $j$ th mass

$\phi_{jn}$  = mode shape at  $j$ th mass in the  $n$ th mode.

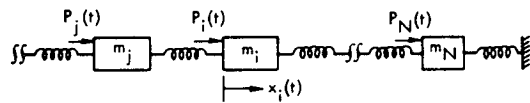


FIGURE 3.61 N Degree of Freedom Lumped Parameter System Acted on by N Independent Sinusoidal Forces.

When  $P_j(t)$  is a sinusoidal force with an amplitude  $P_j$  and phase  $\beta_j$  given by

$$P_j(t) = P_j \cos(2\pi ft - \beta_j)$$

then the mean square value of this generalized force, which is the weighted summation of  $N$  sinusoidal forces can be written down directly, using Equation 3.241, as

$$\overline{F_n^2(t)} = \frac{1}{2} F_n^2 = \frac{1}{2} \sum_j^N P_j^2 \phi_{jn}^2 + \frac{1}{2} \sum_{j \neq k}^N \sum_k^N P_j P_k \phi_{jn} \phi_{kn} \times \cos(\beta_k - \beta_j)$$

The summation of the mean square values of  $(1/2) P_j^2$  of each force and long time average values of their cross products

$$\frac{1}{2} P_j P_k \cos(\beta_k - \beta_j),$$

weighted by the corresponding mode shapes, is now taken over each of the  $j$ th points when a load is applied. The double summation requires that two general points, the  $j$ th and  $k$ th, be used in order that all possible cross-products are obtained. This expression can be further simplified by noting that the double summation also includes the summation of mean square forces  $(1/2) P_j^2 \phi_{jn}^2$  when  $j=k$ . Thus, the mean square generalized force in the  $n$ th mode for  $N$  external sinusoidal forces is

$$\frac{1}{2} F_n^2 = \frac{1}{2} \sum_j^N \sum_k^N P_j P_k \phi_{jn} \phi_{kn} \cos(\beta_k - \beta_j) \quad (3.247)$$

It will be convenient later, when considering response to random excitation, to express the mean square generalized force for sinusoidal excitation in an equivalent form as

$$\frac{1}{2} F_n^2 = \sum_j^N \sum_k^N \overline{P_j(t) P_k(t)} \phi_{jn} \phi_{kn} \quad (3.248)$$

where

$\overline{P_j(t) P_k(t)}$  = long time average value of the product of the sinusoidal forces  $P_j \cos(2\pi ft - \beta_j)$  and  $P_k \cos(2\pi ft - \beta_k)$ , or from Equation 3.240,

$$\overline{P_j(t) P_k(t)} = \frac{1}{2} P_j P_k \cos(\beta_k - \beta_j)$$

This long time average of the instantaneous value of two sinusoidal forces applied at locations  $j$  and  $k$  will be identified in general as the Narrow Band Space Correlation Function  $R_p(j, k, f, \tau = 0)$  or simply  $R_p(j, k, f)$ . The terms  $f$  and  $\tau = 0$  in the argument for this function imply that the product of the two forces  $P_j(t)$  and  $P_k(t)$  is computed for one sinusoidal frequency  $f$  (or an equivalent narrow band of random noise) and at the same instant of time without any time delay between the two quantities. The ( $\tau = 0$ ) term is dropped out for simplicity in notation.

Mean Square Response in N Modes for N Sinusoidal Forces

The expressions for the mean square response in all modes (Equation 3.245) and the mean square generalized force

(Equation 3.247) may now be combined. The resulting expression for the mean square response of the  $i$ th mass in  $N$  modes and for  $N$  sinusoidal driving forces may be conveniently given in the following form. This assumes that the cross coupling of modal responses, as given by the second term in Equation 3.245, can be neglected. The result is

$$\overline{x_i^2} = \frac{1}{2} P_o^2 \sum_n J_n^2 |\alpha_n(f)|^2 \phi_{in}^2 \quad (3.249)$$

where

$$P_o = \sum_j P_j = \text{amplitude of total force at frequency } f, \text{ neglecting any phase differences between forces}$$

$$\frac{1}{2} P_o^2 = \text{mean square value of this reference force}$$

$$J_n^2 = \begin{cases} \text{joint acceptance squared for } n\text{th mode -} \\ \text{ratio of mean squared generalized force} \\ \text{for } n\text{th mode to mean square reference} \\ \text{force} \\ \left( \frac{1}{P_o^2} \sum_j \sum_k P_j P_k \phi_{jn} \phi_{kn} \cos(\beta_k - \beta_j) \right) \end{cases} \quad (3.250)$$

$$|\alpha_n(f)| = \text{absolute value of sinusoidal transfer function in } n\text{th mode}$$

$$\phi_{in}, \phi_{jn}, \phi_{kn} = \text{mode shape in } n\text{th mode at } i\text{th response point and } j\text{th and } k\text{th load points, respectively.}$$

Note that the factor of  $1/2$  in Equation 3.249 cancels out when  $P_j$ ,  $P_k$  and  $P_o$  are specified in terms of rms values.

Although the choice of the reference force amplitude  $P_o$  is arbitrary, the definition used here is preferred since it defines the amplitude of the total dynamic force on the system assuming an in-phase load.

The basic expression for the joint acceptance squared, for multiple sinusoidal loads, given by Equation 3.250, will be applied later to the case of a propagating acoustic pressure load on structure where the phase shift between load points ( $\beta_k - \beta_j$ ) will be replaced by a propagation delay. The following special cases for the response to multiple sinusoidal loads may be defined by the value of the joint acceptance in each case.

#### N - In-Phase Sinusoidal Forces

In this case,  $\beta_k = \beta_j$  and the joint acceptance squared reduces to

$$J_n^2 = \frac{1}{P_o^2} \left[ \sum_j P_j \phi_{jn} \right]^2, \quad \beta_k = \beta_j \quad (3.251)$$

#### Uniform Dynamic Loading

For this case,  $\beta_k = \beta_j$ , and  $P_j = P_k$  so that the loading is not only in phase but uniform at all points. The joint acceptance squared is then

$$J_n^2 = \left[ \sum_j \phi_{jn} \right]^2, \quad \beta_k = \beta_j, \quad P_j = P_k \quad (3.252)$$

#### N - Uncorrelated Sinusoidal Forces

For  $N$  sinusoidal forces which are randomly phased, the time average value of the cross-products of forces  $P_j(t) P_k(t)$  is zero so that the cross-coupling terms in Equations 3.247, 3.248, and 3.250 are zero. The joint acceptance squared is the sum of the mean square value of each generalized force  $(1/2) P_j^2 \phi_{jn}^2$  normalized by the mean square reference force, or

$$J_n^2 = \frac{1}{P_o^2} \sum_j P_j^2 \phi_{jn}^2 \quad (3.253)$$

This is a suitable approximation to use for external acoustic loading of structure in certain cases where the sound pressure field may be considered as in-phase only over relatively small areas and randomly phased outside this area.

Since only one frequency of excitation has been considered, the amplitude  $X_i$  of the sinusoidal response defined by Equation 3.249 may also be determined from the mean square value  $\overline{x_i(t)^2}$ . This is given by

$$X_i = \sqrt{2} \left[ \overline{x_i(t)^2} \right]^{1/2} \quad (3.254)$$

Significant conclusions to be drawn from these last five expressions may be summarized as follows:

- The net mean square response at any point of a multi-modal system is closely approximated by the sum of the mean square responses in each mode.
- For the same total amplitude of load and modal transfer function, the relative mean square modal response is defined in terms of the joint acceptance squared - a relative measure of the mean square generalized force for each mode.
- The joint acceptance for any mode will tend to be a maximum for in-phase sinusoidal loads when the relative variation in force amplitude  $P_j$  with location  $j$  coincides with the variation in mode shape  $\phi_{jn}$  at the same location.
- The joint acceptance and hence the modal response will be zero for uniform loading of even modes where  $P_j$  is constant and  $\sum_j \phi_{jn} = 0$ .

- The relative mean square response in the nth mode for in-phase uniform loads to randomly phased equal loads is given by the ratio of the square of the sum of the mode shape at all points to the sum of the squares of the mode shapes at all points, or

$$\frac{\text{M.S. modal response - uniform loads}}{\text{M.S. modal response - equal but random loads}} = \frac{\left(\sum_j^N \phi_{jn}\right)^2}{\sum_j^N (\phi_{jn})^2}$$

Total Response for Multiple Forces, Including Cross-Mode Coupling Terms

The more general expression for the response in all modes, including modal cross-coupling terms, may be given in the following form. It is cited here for reference purposes only since it is seldom used for the modal analysis of complex structure. The general expression for this case was given by Equation 3.246. It can be given in a more convenient form by utilizing a new quantity called cross-joint acceptance  $J_{mn}^2$ . The resulting equation for the total mean square response at the ith mass over all modes, including modal coupling terms is

$$\overline{x_i^2} = \frac{1}{2} P_o^2 \left[ \sum_n^N J_n^2 |\alpha_n(f)|^2 \phi_{in}^2 + \sum_{n \neq m}^N \sum^N J_{mn}^2 \alpha_n(f) \alpha_m^*(f) \phi_{in} \phi_{im} \right] \quad (3.255)$$

The first summation is identical to Equation 3.249. Therefore, consider only the terms in the second summation.

- $\alpha_n(f), \alpha_m^*(f)$  = complex sinusoidal transfer for nth mode and complex conjugate for mth mode
- $\phi_{in}, \phi_{im}$  = corresponding mode shapes at ith mass
- $J_{mn}^2$  = cross joint acceptance between nth and mth mode.

Comparing this equation with Equation 3.246, it is apparent that the new term, cross-joint acceptance, is a complex quantity equal to

$$J_{mn}^2 = \frac{1}{P_o^2} F_n(f) F_m^*(f)$$

where

- $F_n(f)$  = complex magnitude of generalized force in nth mode
- $F_m^*(f)$  = complex conjugate of generalized force in mth mode.

(Note that  $1/2 \mathcal{R} [F_n(f) F_m^*(f)]$  is the mean square value of the generalized cross-mode coupling force.)

The complex magnitude of the generalized force in the nth mode is given by

$$F_n(f) = \sum_j^N P_j \phi_{jn} e^{-j \beta_j}$$

Similarly, the complex conjugate of the generalized force in the mth mode may be given by

$$F_m^*(f) = \sum_k^N P_k \phi_{km} e^{j \beta_k}$$

In this case, the summation is over k to allow for all possible cross-product terms between the forces  $P_j$  and  $P_k$ . Combining these expressions, the complex value for the cross-joint acceptance is given by

$$J_{mn}^2 = \frac{1}{P_o^2} \sum_j^N \sum_k^N P_j P_k \phi_{jn} \phi_{km} e^{j(\beta_k - \beta_j)} \quad (3.256)$$

where

$P_j, P_k$  = real amplitudes of forces at jth and kth mass with phase angles  $\beta_j$  and  $\beta_k$ , respectively

$\phi_j, \phi_{km}$  = mode shapes at corresponding points in nth and mth modes, respectively.

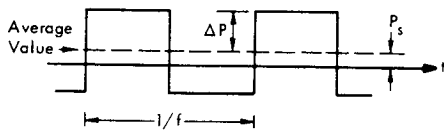
When this complex term is used in Equation 3.255, the complex conjugate cross products add up to a real quantity. For in-phase loads, where  $\beta_k - \beta_j = 0$ , a complex form is unnecessary for  $J_{mn}^2$  which, in this case, is simply the product  $J_m J_n$  of the joint acceptances in each mode. It should be pointed out that real expressions could always be developed in all of these preceding expressions. Complex notation, however, offers many advantages and short cuts in analysis in certain cases and has been introduced to illustrate its application.

Note that the expressions for joint acceptance (Equation 3.250) and cross joint acceptance (Equation 3.256) contain the quantity  $P_j P_k \cos(\beta_k - \beta_j)$  or  $P_j P_k \exp j(\beta_k - \beta_j)$ . The former has been shown to be equal to two times the long time average of the product of the instantaneous pressures,  $\overline{P_j(t) P_k(t)}$ . This is also equal to the real part of the complex form. This relationship will appear in a similar form when considering random loads. First, however, consider response to other forms of sinusoidal-like excitation.

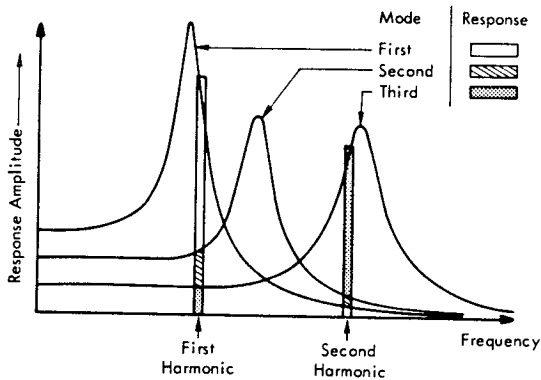
3.3.3.7 Response to Steady State and Transient Periodic Excitation

Steady State Complex Excitation

The methods developed in these last two sections may be used for analyzing the response of multi-degree of freedom in systems to steady state periodic excitation such as generated by reciprocating machinery or nonlinear hydraulic or pneumatic oscillating power sources. One extreme example of this type of excitation is illustrated in Figure 3.62a. Such a periodic nonsinusoidal force may be described by a Fourier series of sine and cosine functions as outlined in Section 3.2.2.5, page 3-15. For example, for the square wave illustrated in Figure 3.62a, the series would be



a) Periodic Force with Repetition Frequency  $f$



b) Selective Response for First Two Harmonics of Periodic Excitation by First and Third Normal Modes of Multi-Mode System

FIGURE 3.62 Response of Multi-Mode System to Periodic Excitation

$$P(t) = P_s + \frac{4 \Delta P}{\pi} \left[ \cos 2\pi f t + \frac{1}{3} \cos 6\pi f t + \frac{1}{5} \cos 10\pi f t + \dots \frac{\cos r (2\pi f t)}{r} \dots \right]_{r=1,3,5,\dots,\infty}$$

where

- $P_s$  = average or static value of force
- $\Delta P$  = peak amplitude of force in excess of  $P_s$
- $f$  = repetition frequency
- $r$  = odd integer.

In this case, the total force consists of a static component  $P_s$  plus an infinite series of sinusoidal components with different harmonic frequencies  $f, 3f, 5f$ , etc. The response of a multi-modal system to such an excitation is found by treating each harmonic force component separately. The methods outlined earlier for single or multiple sinusoidal forces, with one frequency, are applied to determine the instantaneous response over all modes for the  $r$ th harmonic component. The total instantaneous response is then found by superposition of the sum of these harmonic responses. Thus, at the  $i$ th mass, the total response  $x_i(t)$  would be

$$x_i(t) = \sum_r \sum_n x_{in}(rf, t) \tag{3.257}$$

where  $x_{in}(rf, t)$  is the instantaneous response of the  $i$ th mass in the  $n$ th mode to the  $r$ th harmonic component of the excitation.

Since there is no coupling between the response components for two frequencies, then neglecting modal coupling, the total mean square response  $x_i^2$  is a double summation of the mean square modal response  $x_{in}^2(rf, t)$  for each  $r$ th harmonic component and  $n$ th mode. The problem can often be simplified by considering only resonant responses of the  $n$ th normal modes of the structure which coincide approximately with the  $r$ th harmonic frequency components of the excitation. This situation is illustrated in Figure 3.62b where only the first and third normal modes of a system contribute significantly to the response from two harmonic components of a periodic excitation.

Transient Sinusoidal Excitation

Response of a multi-modal system to a sinusoidal load which changes amplitude and/or frequency with time is of interest in the dynamic response and testing of multi-modal structural systems.

The interest stems, in one case, from the need to minimize transient resonant responses when a changing sinusoidal excitation passes through the natural frequency of a critical normal mode. On the other hand, for vibration testing of structure, it is often necessary to maximize the resonant response from a sinusoidal input whose frequency is slowly changed. This type of transient sinusoidal signal is called a phase-coherent excitation (Reference 3.1, Chapter 22).

It is described by the general expression

$$P(t) = \bar{P}(t) \cos [2\pi f(t)t + \beta]$$

which indicates both the amplitude  $\bar{P}(t)$  and frequency  $f(t)$  changing with time. A general solution for this type of excitation to a multi-modal system could be made with the Duhamel integral according to the methods outlined by Section 3.3.3.3. The solutions are complex, however, and have been carried out only for a few special cases; the most common one being a sinusoidal input with a constant amplitude but linearly increasing frequency applied to a single degree of freedom system (References 3.34, 3.42, and 3.43).

The excitation has the form

$$P(t) = P \sin (\pi \dot{f} t^2 + \beta)$$

where

$P$  = Input Force amplitude

$\dot{f}$  = Linear Rate of Change of Frequency - Hz/sec

$\beta$  = initial phase angle.

The envelope of the peak response of a single degree of freedom system to this type of excitation is shown, in Reference 3.42, to be a function of the dimensionless parameter  $\dot{f} Q_n^2 / f_n^2$  where  $Q_n$  is the steady state dynamic magnification factor and  $f_n$  is the steady state resonance or natural frequency of the simple system. An effective dynamic magnification factor  $Q_{eff}$  may be defined as the ratio of peak response amplitude for the transient sinusoidal input to the static response (the deflection under a static load equal to the amplitude of the sine input). This is shown in Figure 3.63 as a function of the rate of change of frequency  $\dot{f}$  divided by the square of the steady state resonance frequency  $f_n$ . In this form, it is possible to include the case for no damping for which the steady state  $Q_n$  would be infinite (Reference 3.43). As indicated by the dashed line, the maximum relative response or effective  $Q$  is within 90% of the steady state value for  $\dot{f} Q_n^2 / f_n^2 < 1$ . For the case of zero damping, for which the steady state  $Q$  would be infinite, the effective  $Q$  is approximately equal to

$$Q_{eff} \approx 3.7 f_n / (\dot{f})^{1/2}, \quad (Q_n = \infty) \quad (3.258)$$

As shown by the insert in Figure 3.63, the actual resonant response, for an increasing frequency of excitation, occurs at a frequency above the steady state natural frequency  $f_n$ . This shift in apparent resonance frequency is less than 50 percent of the steady state resonant bandwidth  $f_n / Q_n$  for  $\dot{f} Q_n^2 / f_n^2$  less than 1. For very high sweep rates, the response also exhibits secondary peaks at even higher frequencies.

These results for the single degree-of-freedom system can be applied directly to a multi-modal system by again considering each normal mode as an independent single degree of freedom system. For example, if a resonant response of a particular normal mode of a structure should be limited to less than 4 times its response to a static load ( $Q_{eff} = 4$ ), then from Equation 3.250, the required sweep rate of a transient sinusoidal excitation may be conservatively estimated to be

$$\text{For } Q_{eff} \leq 4 \quad \dot{f} > \left( \frac{3.7 f_n}{4} \right)^2 \approx .86 f_n^2 \quad \text{Hz/sec .}$$

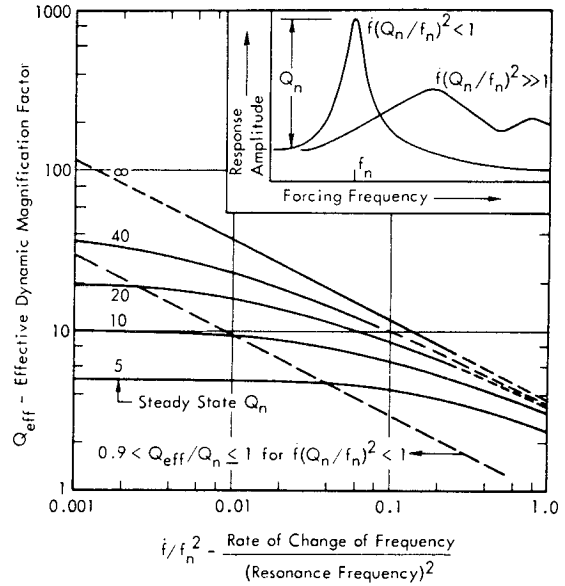


FIGURE 3.63 Effective Dynamic Magnification Factor for Single Degree of Freedom System Forced by Sinusoidal Excitation with a Frequency Increasing at a Linear Rate  $\dot{f}$ . Insert indicates decrease in maximum response and increase in apparent resonance frequency and bandwidth as parameter  $\dot{f} Q_n^2 / f_n^2$  becomes much greater than 1. (Adopted from References 3.42 and 3.43.)

With the usual amount of damping, the allowable sweep rate would decrease slightly. On the other hand, for a sinusoidal vibration test of such a structure, a resonant response amplitude within 90 percent of the steady state value would require a sinusoidal sweep rate less than

$$\text{For } Q_{eff} \approx .9 Q_n \quad \dot{f} < \left( \frac{f_n}{Q_n} \right)^2$$

In this case, the allowable sweep rate is critically dependent on damping.

### 3.3.3.8 Example of Response of Two Degree-of-Freedom System to Sinusoidal Excitation

The preceding discussion on sinusoidal response of multi-modal systems has been developed, in part, as background for defining the response of multiple degree-of-freedom systems to random excitation. A simple example will assist further in clarifying some of the concepts developed thus far. Matrix notation will also be used frequently in this example for the sake of further illustration of this useful technique. The formal methods for carrying out analysis of multi-modal system with matrix notation will be briefly reviewed in a later section. It should be emphasized that the forced response of the relatively simple system considered in this example can also be efficiently determined by other methods. However, the normal mode approach is used here for the sake of illustration of concepts applicable to more complex systems.



For the same two degree-of-freedom system described in Section 3.3.3.4, assume that a sinusoidal force  $P \cos 2\pi ft$  acts on the upper mass (see Figure 3.64). The normal mode parameters of the undamped system were determined in the previous example and can be given in the form of square matrices as:

Undamped System Parameters

$$\text{Natural Frequencies } [\omega_n] = \begin{bmatrix} n=1 & 2 \\ .665 \sqrt{k/m} & 0 \\ 0 & 1.165 \sqrt{k/m} \end{bmatrix}$$

$$\text{Generalized Mass } [M_n] = \begin{bmatrix} n=1 & 2 \\ 2.56 m & 0 \\ 0 & 1.64 m \end{bmatrix}$$

$$\text{Mode Shapes } [\phi_{in}] = \begin{bmatrix} n \rightarrow \\ \downarrow i \\ 0.559 & -0.358 \\ 1 & 1 \end{bmatrix}$$

Note that the symbol  $\begin{bmatrix} & \\ & \end{bmatrix}$  indicates a diagonal matrix where off-diagonal terms are zero. The following additional parameters are required to define the forced sinusoidal response of the damped system shown in Figure 3.64a.

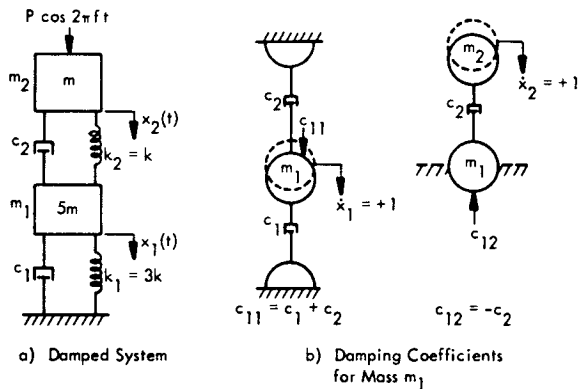


FIGURE 3.64 Damped Two Degree-of-Freedom System Driven by a Sinusoidal Force on Upper Mass Illustrating Method of Determining Damping Coefficients for Discrete Damping Elements

Amplitude of Total Load (Equation 3.237)

The scalar constant  $P_o$  equal to the amplitude of the total load. In this case, for a single applied force,

$$P_o = \sum_j^N P_j = P$$

Generalized Force

The column matrix specifying the generalized force for each mode. In this case,

$$\{F_n(t)\} = P_o \{J_n\} \cos(2\pi ft) = \begin{Bmatrix} P \\ P \end{Bmatrix} \cos(2\pi ft)$$

Joint Acceptance (Equation 3.237)

The column matrix, equal to the generalized force for each mode normalized by  $P_o$ . In this case,

$$\{J_n\} = \frac{\sum_j^N P_j \phi_{jn}}{P_o} = \begin{Bmatrix} 1 \\ 1 \end{Bmatrix} \begin{matrix} \text{- first mode} \\ \text{- second mode} \end{matrix}$$

Cross-Joint Acceptance (Equation 3.256)

The column matrix, in general complex, equal to the time average value of the generalized external force coupling two modes, normalized by the mean square value of the total load. In this case, a complex form is unnecessary since only one load is applied. Then, the joint acceptance is the product

$$J_{mn}^2 = J_m \cdot J_n = \begin{Bmatrix} 1 \\ 1 \end{Bmatrix} \begin{matrix} \text{- first mode} \\ \text{- second mode} \end{matrix}$$

Generalized Modal Damping

To illustrate the general approach for defining a generalized damping constant, assume the fixed damping elements as shown in Figure 3.64a. The damping coefficients  $c_{ij}$  are determined in the same way as the stiffness coefficients of the system are obtained (see Figure 3.64b). The resulting values may be given in the form of a damping coefficient matrix as

$$[c_{ij}] = \begin{bmatrix} i \rightarrow & j \rightarrow \\ \downarrow \\ c_1 + c_2 & -c_2 \\ -c_2 & +c_2 \end{bmatrix}$$

The generalized damping constants  $C_n$  for each mode are determined from the expression

$$C_n = \sum_i^N \sum_j^N c_{ij} \phi_{in} \phi_{jm} = \begin{cases} \sum (\text{damping coupling terms}) & n \neq m \\ \sum (\text{uncoupled damping terms}) & n = m \end{cases} \quad (3.259)$$

The damping coupling terms in this summation for  $n \neq m$  must be set equal to zero if the equations of motion for the normal modes are to be uncoupled. This can be illustrated by showing the results of this summation in the form of a square matrix having  $N^2$  terms.



where

$|a_n(f)|$  = absolute value of sinusoidal transfer function for nth mode

$\theta_n$  = phase angle of response in nth mode.

The total response at the  $i$ th mass is then the summation of the modal responses  $\phi_{in} a_n(t)$ . As discussed in the previous section, the amplitude of this total response may be expressed in a form which contains phase-coupling terms between the response in each mode. These are not to be confused with the absence of internal coupling forces between the equations of motion of the normal modes.

Displacement Response (Equations 3.237, 3.254 and 3.255)

The displacement amplitude response of the system is given in a general form, including cross-mode phase coupling terms, by using Equation 3.255 to give

$$X_i = P_o \left[ \sum_n \frac{J_n^2 \phi_{in}^2 |H_n(f)|^2}{\omega_n^4 M_n^2} + \sum_{n \neq m} \sum_m \frac{J_{mn}^2 \phi_{in} \phi_{im} H_n(f) H_m^*(f)}{\omega_n^2 \omega_m^2 M_n M_m} \right]^{1/2} \tag{3.260}$$

Since only one force is applied, the cross joint acceptance  $J_{mn}^2$  is real and the complex term  $H_n(f) H_m^*(f)$  may be replaced by its corresponding real value

$$|H_n(f)| |H_m(f)| \cos(\theta_m - \theta_n)$$

Substituting the parameters defined in the preceding paragraphs, the displacement response for the upper mass ( $i=2$ ) of this two degree-of-freedom system may be given in normalized form by

$$\frac{X_2}{P/k} = \left[ 0.784 |H_1(f)|^2 + 0.201 |H_2(f)|^2 + 0.792 |H_1(f)| |H_2(f)| \cos(\theta_2 - \theta_1) \right]^{1/2}$$

where

$$|H_n(f)|^2 = 1 / \left[ (1 - (f/f_n)^2)^2 + (2 \delta_n f/f_n)^2 \right]$$

$$f_1 = \omega_1 / 2\pi = (.665/2\pi) \sqrt{k/m}$$

$$f_2 = (1.165/2\pi) \sqrt{k/m}$$

$$\theta_n = \tan^{-1} \frac{2\delta f/f_n}{1 - (f/f_n)^2}$$

$$\delta_1, \delta_2 = 0.033, 0.058, \text{ respectively}$$

$P/k$  = arbitrary reference deflection equal to static deflection of upper mass, with lower mass fixed, for static load equal to amplitude  $P$  of applied sinusoidal force.

The first two terms in this expression constitute the direct modal response for each mode and the last term is the modal cross-coupling term. The resulting values are plotted in Figure 3.65 on a frequency scale normalized by the natural frequency of the first mode. This shows the total response and the response contributed by each mode. The plotted data points represent the total response amplitude without including modal cross-coupling terms. As expected, these values are very nearly equal to the envelope of the individual modal responses. Most important, however, is that the true total response at the two response peaks is essentially defined by the response of each mode. Thus, as indicated earlier, the modal cross-coupling terms are not significant near these points of maximum response.

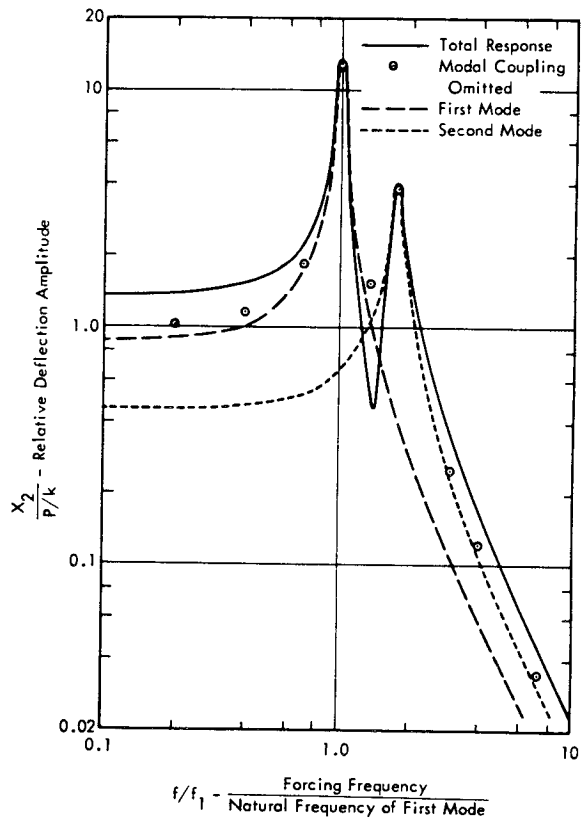


FIGURE 3.65 Displacement Amplitude Response of Upper Mass of Two Degree-of-Freedom System Shown in Figure 3.64 (Computed by Normal Mode Method)

Note that the apparent dynamic magnification factor or  $Q$  of the first resonance peak, defined as the ratio of peak dynamic deflection at resonance ( $X_2 = 13.3 P/k$ ) to the static response ( $X_2 = 1.33 P/k$ ) is only 10. This is less than the  $Q$  for the first normal mode ( $Q_1 = 15$ ) due to the contribution of the second mode to the static deflection. On the other hand, the  $Q$  based on the half-power bandwidth  $\Delta f_n$  of the resonant peak, where  $Q = f_n/\Delta f_n$ , is substantially the same for the total response as for the first mode only.

Acceleration Response

The amplitude of the acceleration response of the upper mass is given by

$$\ddot{X}_2 = -(2\pi f)^2 X_2$$

This may be expressed in a normalized form, using Equation 3.61, as

$$\ddot{X}_2 = -(2\pi f_1)^2 \left(\frac{f}{f_1}\right)^2 X_2 = -(0.665)^2 \left(\frac{f}{f_1}\right)^2 \frac{k}{m} X_2$$

or

$$\frac{|\ddot{X}_2|}{P/m} = -(0.665)^2 \left(\frac{f}{f_1}\right)^2 \left[\frac{X_2}{P/k}\right]$$

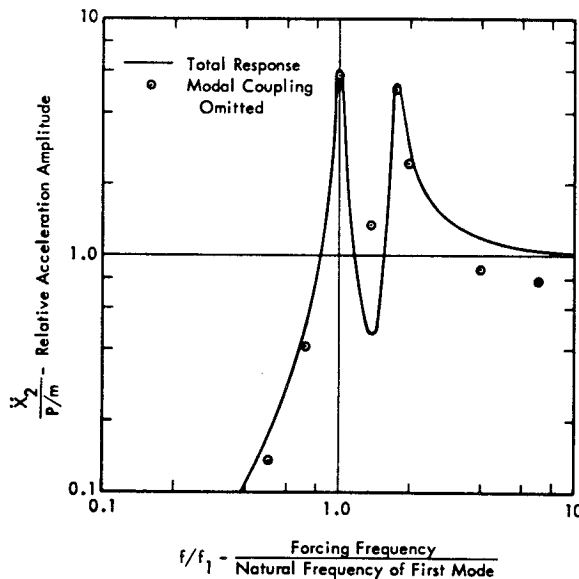


FIGURE 3.66 Acceleration Amplitude Response of Upper Mass of System Shown in Figure 3.64 (Computed by Normal Mode Method)

where

$P/m$  = arbitrary reference acceleration equal to "static" acceleration of upper mass for static force equal to amplitude  $P$  of applied sinusoidal force.

This expression is plotted in Figure 3.66. The computed response without the modal coupling term is also shown by the circled points. Again these are significantly different from the total response only at frequencies well removed from resonance.

The trend in the relative acceleration amplitude of the upper mass approaches unity at high frequencies. This is expected since this mass will tend to act like a free body at high frequencies with an acceleration equal to the excitation force  $P$  divided by the mass  $m$  or  $\ddot{X}_2 \rightarrow P/m$  for  $f \rightarrow \infty$ .

Forced Response - Two Sinusoidal Forces

To illustrate a more general case of sinusoidal excitation, consider the response of the upper mass of the same system shown in Figure 3.64 for two sinusoidal forces. Thus, let the driving force  $P_2(t)$  on the upper mass remain as

$$P_2(t) = P \cos 2\pi f t$$

Now apply a sinusoidal force to the lower mass at the same frequency but with a different phase and amplitude given by

$$P_1(t) = 2P \cos (2\pi f t - \beta_1)$$

The following parameters must be redefined for this case. Detailed calculations are omitted in order to emphasize the general form of the results.

Amplitude of Total Load

$$P_o = \sum_j^N P_j = 2P + P = 3P$$

Joint Acceptance

Due to the phase difference between the applied forces, the more general expression given by Equation 3.250 is used. This is

$$J_n^2 = \frac{1}{P_o^2} \sum_j^N \sum_k^N P_j P_k \phi_{jn} \phi_{kn} \cos (\beta_k - \beta_j)$$

Given the two loads specified and the mode shapes  $\phi_{in}$  defined earlier, the following values for  $J_n^2$  are obtained with this expression.

$$J_1^2 = 0.250 + 0.248 \cos \beta_1$$

$$J_2^2 = 0.168 - 0.159 \cos \beta_1$$

Cross-Joint Acceptance

The complex form for the cross-joint acceptance is required to conveniently include the effect of phase of the two forces. This is given by Equation 3.256 as

$$J_{mn}^2 = \frac{1}{P_o^2} \sum_j^N \sum_k^N P_j P_k \phi_{jn} \phi_{km} e^{j(\beta_k - \beta_j)}$$

where

$$P_j e^{-j\beta_j} = \text{complex magnitude of force at } j$$

$$P_k e^{j\beta_k} = \text{complex conjugate of magnitude of force at } k.$$

Setting  $P_j e^{-j\beta_j} = P$ , and

$$P_k e^{-j\beta_k} = 2P e^{-j\beta_1} = 2P (\cos \beta_1 - j \sin \beta_1),$$

the complex value of  $J_{mn}^2$ , in this case, can be shown to be

$$J_{mn}^2 = 0.022 + 0.0446 \cos \beta_1 - j 0.2038 \sin \beta_1$$

When these new values for the parameters  $P_o$ ,  $J_n^2$ , and  $J_{mn}^2$  are substituted in the general expression for the displacement response (Equation 3.260), along with the complex form for the frequency response functions  $H_n(f)$  for each mode, the total displacement or acceleration response to the two forces is readily determined. Except for the effect of phase between the forces, the results will be similar to those shown in Figures 3.63 and 3.64 for just one driving force. The effect of phase may be illustrated by considering the maximum amplitude of the acceleration response of the upper mass  $\ddot{x}_2$  at the two natural frequencies  $f_1$  and  $f_2$  of the system. In this case, the maximum acceleration response can be given in the same normalized form used previously by

$$\left. \frac{\ddot{x}_2}{P/m} \right|_{f=f_1} = 8.80 [1 + 0.990 \cos \beta_1 - 0.081 \sin \beta_1]^{1/2}$$

$$\left. \frac{\ddot{x}_2}{P/m} \right|_{f=f_2} = 6.51 [1 - 0.904 \cos \beta_1 - 0.261 \sin \beta_1]^{1/2}$$

These two expressions define the total resonant response amplitude including the direct response of both modes and the cross-mode response. (It is interesting to note that the primary contribution of the cross-mode response is contained in the sine terms in these expressions. The sine terms are, in turn, proportional to the imaginary part of the cross-joint acceptance  $J_{mn}^2$ .) The total acceleration response defined by these expressions is shown in Figure

3.67 by the solid and dashed lines. The response amplitude in each resonant normal mode is also plotted by data points. Again, this shows that the single mode approximation is generally very good at the natural frequencies of the system, particularly when the two sinusoidal forces are phased so as to maximize the particular natural mode considered.

As expected, the first mode response is maximized when the relative phase of the two applied forces is zero, corresponding to the in-phase motion of the two masses in this mode. Conversely, the second mode response is a maximum when the two forces are 180 degrees out of phase with each other, corresponding to the antisymmetric mode shape of this mode. This result is immediately apparent by examination of the joint acceptances  $J_1^2$  and  $J_2^2$  for each mode.

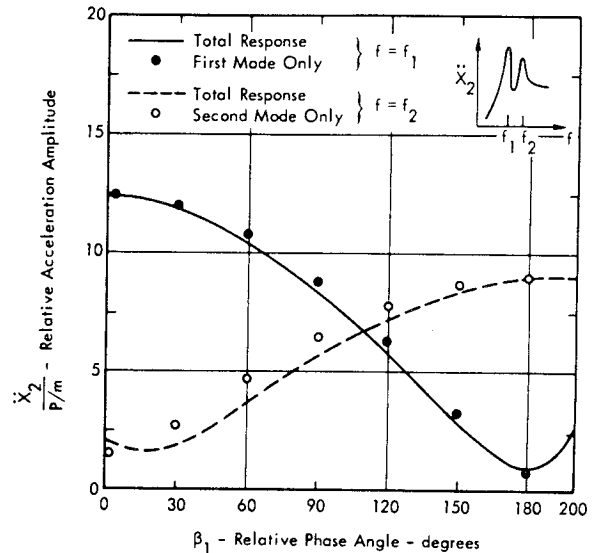


FIGURE 3.67 Change in Maximum Acceleration Response of Mass  $m_2$  in Two Degree-of-Freedom System Shown in Figure 3.64 Due to Relative Phase Between Two Sinusoidal Forces Driving Both Masses.  $P_1(t) = 2P \cos(2\pi f t - \beta_1)$ ,  $P_2(t) = P \cos(2\pi f t)$ . Data points represent computed response in only one mode at each excitation frequency,  $f_n$ .

3.3.3.9 Response of Lumped Parameter Systems to Random Excitation

The transition from sinusoidal to random excitation of lumped parameter systems may now be made in the following manner based on previously derived relationships.

- The mean square (M.S.) displacement response at the  $i$ th mass in the  $n$ th mode of a system, for a sinusoidal free excitation, was found to be (see Equation 3.249)

$$\overline{x_{in}^2} = \frac{1}{2} P_o^2 J_n^2 |a_n(f)|^2 \phi_{in}^2 \quad (3.261)$$

where

$\frac{1}{2} P_o^2$  = Mean Square Value of total sinusoidal force applied to system at frequency  $f$

$J_n^2$  = Joint Acceptance Squared or Relative Generalized Force at this frequency

$|\alpha_n(f)|$  =  $\begin{cases} \text{Absolute Value of Sinusoidal Transfer} \\ \text{Function which, in this case, is} \\ |H_n(f)|/4\pi^2 f_n^2 M_n \end{cases}$

$|H_n(f)|$  = Dynamic Magnification Factor for nth mode

$M_n$  = Generalized Mass for nth mode

$\phi_{in}$  = Mode shape at  $i$  for nth mode.

- Each normal mode can be treated as a single degree-of-freedom system with an effective transfer  $|\alpha_n(f)| \phi_{in}$  at the  $i$ th mass point.
- For random excitation of a single degree of freedom, it was shown in Section 3.2.3.10 that the power spectral density of the response was defined by the product of the power spectral density of the input excitation and the square of the absolute value of the sinusoidal transfer function. Therefore, for random excitation, the power spectral density of the displacement response  $W_x(i_n, f)$  at the  $i$ th mass in the  $n$ th mode is

$$W_x(i_n, f) = W_o(f) J_n^2(f) |\alpha_n(f)|^2 \phi_{in}^2 \quad (3.262)$$

when

$W_o(f)$  = Power Spectral Density (PSD) of reference force  $P_o$  at frequency  $f$

$J_n^2(f)$  = joint acceptance in  $n$ th mode at frequency  $f$  - the ratio of the PSD of the generalized force in  $n$ th mode to  $W_o(f)$ . (The convention is adopted of adding the argument  $(f)$  to the joint acceptance term to denote the ratio of PSD's.)

- Neglecting cross-mode coupling terms, the PSD of the total displacement response at the  $i$ th mass  $W_x(i, f)$  is the summation of the modal responses over all  $N$  modes. Substituting the value for  $|\alpha_n(f)|$  defined in Equation 3.261, this gives the general expression for the displacement response in all modes due to random excitation.

$$W_x(i, f) = W_o(f) \sum_n \frac{J_n^2(f) |H_n(f)|^2 \phi_{in}}{(4\pi^2 f_n^2 M_n)^2} \quad (3.263)$$

- Without further approximation, the total M.S. response over the entire frequency spectrum of the excitation will be the integral of this response PSD over frequency, or

$$\overline{x_i^2} = \sum_n \left[ \int_0^\infty W_o(f) \frac{J_n^2(f) |H_n(f)|^2 \phi_{in}^2}{(4\pi^2 f_n^2 M_n)^2} df \right] \quad (3.264)$$

Note that the order of the summation and integration can be interchanged since the response in each mode is treated independently when cross-mode coupling terms are neglected.

These last two expressions illustrate the general form for the response of structure to random excitation. The PSD and M.S. value of the acceleration response (in  $g^2/\text{Hz}$  or  $g^2$ ) is obtained by multiplying each term in the above summations by  $(4\pi^2 f^2)^2/g^2$  where  $g$  is the acceleration of gravity in units compatible with the units for the mass  $M_n$ . For multi-modal systems with a discrete number of well separated normal modes, the M.S. response over all modes can also be obtained, without requiring the integration above, by using the closed forms for the integral of  $|a(f)|^2$  over frequency given earlier in Section 3.2.3.10, page 3-39. For example, the M.S. acceleration in  $g$ 's at the  $i$ th mass over  $N$  discrete modes is approximately equal to (see Equation 3.161, page 3-42)

$$\overline{\ddot{x}_i^2}/g^2 \approx \sum_n \frac{\pi}{2} \frac{W_o(f_n) J_n^2(f_n) f_n Q_n \phi_{in}^2}{g^2 M_n^2} - g^2 \quad (3.265)$$

where

$W_o(f_n), J_n(f_n)$  = PSD of reference force and joint acceptance squared evaluated at the natural frequency  $f_n$  for each mode

$Q_n$  = Resonant Amplification Factor for  $n$ th mode.

The above expressions for response to random excitation differ from those for sinusoidal excitation in only two important aspects. 1) The response and excitation is specified in terms of a PSD centered about a frequency  $f$  instead of a M.S. value of a single frequency, and 2) the joint acceptance squared is now a ratio of the PSD's of generalized and reference forces.

The characteristics of the power spectral density of single random variables have been covered in detail in Section 3.2.3 and need not be considered further here. Referring to Equation 3.263, only two such variables need be considered for response of multi-modal systems to random excitation - the power spectral density  $W_o(f)$  of the reference

or total force  $\left[ P_o(t) = \sum_j^N P_j(t) \right]$  applied to the system, and

the power spectral density  $W_x(i, f)$  of the displacement response.

3.3.3.10 Joint Acceptance for Random Loads

The basic advantage of the joint acceptance parameter for defining the relative generalized force on structure under acoustic loading has not always been utilized due to a confusing number of definitions for this parameter. It is desirable, therefore, to briefly review these to establish a clear concept of joint acceptance in practical terms. To compute the response to random acoustic loads from rocket

noise, the joint acceptance squared  $J_n^2(f)$  for random excitation can always be defined by the equivalent value

$J_n^2$  for sinusoidal excitation. This stems from the fact that the ratio of the spectral densities of two random variables (i.e. - the generalized force and the reference force) evaluated about any given frequency is identical to the ratio of mean square values of two corresponding sinusoidal variables with the same frequency.

As shown earlier in Equations 3.247, 3.248 and 3.250, the joint acceptance squared  $J_n^2$  for sinusoidal excitation can be expressed in any of the following equivalent forms

$$J_n^2 = \frac{1}{P_o^2} \sum_j^N \sum_k^N P_j P_k \cos(\beta_k - \beta_j) \phi_{jn} \phi_{kn} \tag{3.266a}$$

$$J_n^2 = \frac{1}{\frac{1}{2} P_o^2} \sum_j^N \sum_k^N \overline{P_j(t) P_k(t)} \phi_{jn} \phi_{kn} \tag{3.266b}$$

or

$$J_n^2 = \frac{1}{\frac{1}{2} P_o^2} \sum_j^N \sum_k^N R_p(j, k, f) \phi_{jn} \phi_{kn} \tag{3.266c}$$

where

$R_p(j, k, f) = \overline{P_j(t) P_k(t)}$ , the narrow band space correlation function equal to the long time average of the instantaneous products of the sinusoidal forces  $P_j \cos(2\pi ft - \beta_j)$  and  $P_k \cos(2\pi ft - \beta_k)$

$$\frac{1}{2} P_o^2 = \text{Mean Square Value of Reference Force } P_o$$

$\phi_{jn}, \phi_{kn}$  = mode shapes at jth and kth load points in nth mode.

In most practical cases of acoustic loading on structure, it is possible to assume that the amplitudes of the sinusoidal forces at all points are constant (i.e. -  $P_j \equiv P_k \equiv P$ ). Thus, the reference force becomes simply

$$P_o = \sum_j^N P = NP$$

Dividing each term in Equation 3.266c by the mean square value  $\frac{1}{2} P^2$  of the constant sinusoidal force at each load point, a simpler form for the joint acceptance for sinusoidal excitation of lumped parameter systems is obtained.

$$J_n^2 = \frac{1}{N^2} \sum_j^N \sum_k^N \overline{R_p(j, k, f)} \phi_{jn} \phi_{kn} \tag{3.267}$$

where

$$\overline{R_p(j, k, f)} = \frac{\overline{P_j(t) P_k(t)}}{\frac{1}{2} P^2} - \text{the narrow band space correlation coefficient - a normalized value of the space correlation function which cannot exceed unity.}$$

The space correlation coefficient is also commonly used to define the relative correlation between any two spatially separated variables, not necessarily with equal amplitudes. In this case, the normalizing factor is the product of the rms amplitude of each variable. In the terminology of Equation 3.267, this would be

$$\overline{R_p(j, k, f)} = \frac{\overline{P_j(t) P_k(t)}}{\sqrt{\overline{P_j^2(t)}} \sqrt{\overline{P_k^2(t)}}} \tag{3.268}$$

Strictly speaking, this value of the space correlation coefficient cannot be used in Equation 3.267 to define joint acceptance unless the loading is uniform ( $P_j = P_k$ ) at all points. However, the error will tend to be small in most practical cases.

Joint Acceptance for Propagating Sinusoidal Acoustic Loads

For a structure under excitation by a propagating acoustic wave (see Chapter 4), the phase shift between the sinusoidal forces at any two locations on the structure (considered for now as lumped elements at say the jth and kth point) is given by

$$\beta_k - \beta_j = \frac{2\pi f \Delta_{jk}}{\bar{c}}$$

where

$\Delta_{jk}$  = the separation distance between the jth and kth points and

$\bar{c}$  = the propagation velocity of the acoustic load along the separation line  $\Delta_{jk}$  in the direction  $j \rightarrow k$ .

For the usual case where the amplitude of the acoustic wave at each point is constant, then, as shown in Figure 3.68, the sinusoidal force at the kth point  $P_k(t)$  is simply a delayed replica of the force at the jth point or

$$P_k(t) = P_j(t - \Delta_{jk}/\bar{c})$$

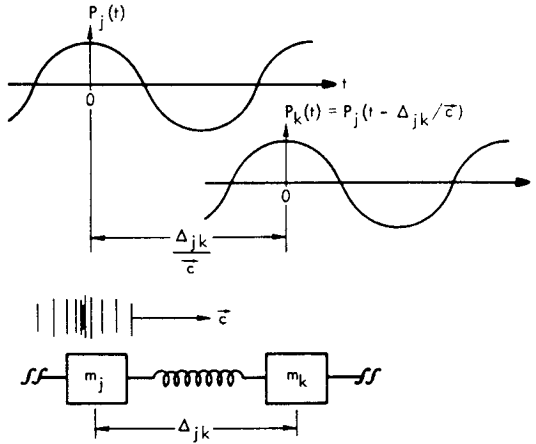


FIGURE 3.68 Sinusoidal Forces on Lumped Parameter System Due to Propagating Acoustic Wave Travelling With Velocity  $\bar{c}$  from j to k

The space correlation coefficient for these sinusoidal forces can then be expressed as

$$\overline{R_p(j, k, f)} = \frac{\overline{P_j(t) P_j(t - \Delta_{jk}/\bar{c})}}{\frac{1}{2} P_j^2} = \cos(2\pi f \Delta_{jk}/\bar{c}) \quad (3.269)$$

Thus, for this case of a single sinusoidal acoustic wave, the space correlation coefficient is simply a cosine function which has a maximum value of 1 whenever  $f \Delta_{jk}/\bar{c} = n$  where n is an integer.

This simple form for the space correlation function for a single sinusoidal acoustic wave can be used for most of the computations of structural response for acoustic loads on ground structure. One important exception occurs when it is necessary to account for the loading effect of more than one acoustic wave passing over the structure. As shown later in Chapters 4 and 8, the space correlation coefficient will be

$$\overline{R_p(j, k, f)} = \frac{\sin 2\pi f \Delta_{jk}/\bar{c}}{2\pi f \Delta_{jk}/\bar{c}} \quad (3.270)$$

for the limiting case of an infinite number of sinusoidal acoustic waves, passing over the structure, which arrive from all possible directions.

Joint Acceptance for Propagating Random Loads

The joint acceptance for acoustic loads may also be obtained from a measurement of the random acoustic levels on structure. In this case, a more general definition is required for joint acceptance. Since the true environment is, in fact, a random phenomena which contains energy at all frequencies, the measured random forces (or pressures) must be analyzed in a special manner to define their spectral content. This is necessary in order to compute the generalized forces acting on the structure as a function of frequency. The required analysis will define a space correlation function for a narrow band of random noise which corresponds to the space correlation for sinusoidal loads.

It was shown in Section 3.2.3.10 that the power spectral density  $W(f)$  of a single random variable  $x(t)$  is equal to two times the Fourier Transform of the autocorrelation function  $R(\tau)$  of  $x(t)$  (see Equations 3.133 and 139a, pages 3-37 and 3-38). Similarly, the power spectral density  $W_{F_n}(f)$  of a generalized random force for the nth mode  $F_n(t)$  is given by

$$W_{F_n}(f) = W_o(f) J_n^2(f) = 2 \int_{-\infty}^{\infty} R_{F_n}(\tau) e^{-j 2\pi f \tau} d\tau \quad (3.271)$$

where

$W_o(f)$  = Power Spectral Density of the reference force  $P_o$

$J_n^2(f)$  = Joint Acceptance Squared for the nth mode at frequency f

and

$$R_{F_n}(\tau) = \overline{F_n(t) F_n(t + \tau)} \quad (3.272)$$

The autocorrelation function  $R_{F_n}(\tau)$  is the long time average of the product of the instantaneous value of  $F_n(t)$  and its value  $F_n(t + \tau)$  at a later time  $\tau$ . This time averaged product is a function of the rapidity with which  $F_n(t)$  changes during the time  $\tau$  and hence contains information about the frequency content of  $F_n(t)$ . (Note that without any delay time, the time average of  $F_n(t) \cdot F_n(t)$  is simply the mean square value of  $F_n(t)$  which contains no information about frequency content.) The frequency spectrum of  $F_n(t)$  is obtained, therefore, by taking the Fourier Transform of its autocorrelation function  $R_{F_n}(\tau)$  as indicated by Equation 3.271.

If it is assumed that the random load is statistically "stationary" in time, then the autocorrelation function is independent of the absolute time t and only depends on the relative (positive or negative) time delay  $\tau$  so that

$$R_{F_n}(\tau) = \overline{F_n(t) F_n(t + \tau)} = R_{F_n}(-\tau) = \overline{F_n(t - \tau) F_n(t)}$$



Thus, as illustrated in Figure 3.69,  $R_{F_n}(\tau)$  is an even function which is symmetrical about  $\tau = 0$ . Then Equation 3.271 can be simplified to give the real value for the PSD of the generalized force as

$$W_{F_n}(f) = 4 \int_0^{\infty} R_{F_n}(\tau) \cos 2\pi f \tau \, d\tau \quad (3.273)$$

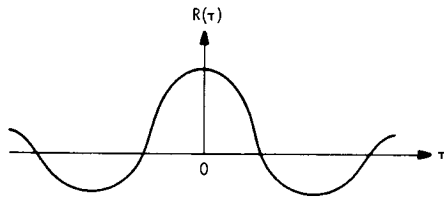


FIGURE 3.69 Typical Autocorrelation Function Illustrating the Symmetry of This Function About  $\tau = 0$

Since the instantaneous value of the generalized force  $F_n(t)$ , in general, is

$$F_n(t) = \sum_j^N P_j(t) \phi_{jn} = \sum_k^N P_k(t) \phi_{kn}$$

then the autocorrelation function of  $F_n(t)$  from Equation 3.272 is the double summation of the time averaged value of all cross products, or

$$R_{F_n}(\tau) = \sum_j^N \sum_k^N \overline{P_j(t) P_k(t + \tau)} \phi_{jn} \phi_{kn} \quad (3.274)$$

### 3.3.3.11 Cross-Correlation Functions and Cross-Power Spectral Density

Two new terms can now be defined:

#### Space-Time Cross-Correlation Function

$$R_p(j, k, \tau) = \overline{P_j(t) P_k(t + \tau)} \quad (3.275)$$

#### Cross-Power Spectral Density

$$\mathcal{H}_p(j, k, f) = 2 \int_{-\infty}^{+\infty} R_p(j, k, \tau) e^{-j 2\pi f \tau} \, d\tau \quad (3.276)$$

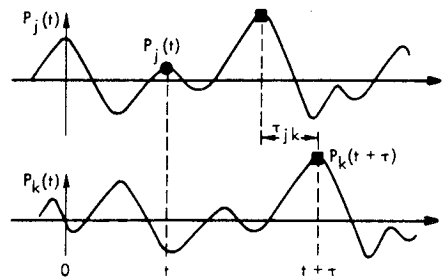
The space-time cross-correlation function (or simply cross correlation function) is the long time average of the random force  $P_j(t)$  at the  $j$ th point times the delayed value of the random force  $P_k(t + \tau)$  at the  $k$ th point. The cross-power spectral density (or cross PSD) is equal to two times the Fourier spectrum of this cross-correlation function. Thus, the cross PSD is the long time average of a narrow

band of frequency components, centered about a frequency  $f$ , in the cross-product  $P_j(t) P_k(t + \tau)$ . The cross correlation function and cross PSD can be obtained by suitable processing of measured random data by methods which will be described later. Consider now the form that these two quantities will have for a propagating wave of random noise.

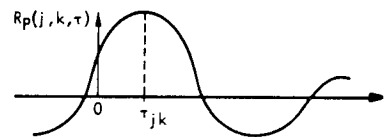
#### Cross-Correlation Function

As shown in Figure 3.70a, the time history of the random force  $P_k(t)$  at the  $k$ th point is delayed by the propagation time  $\tau_{jk}$  so that the cross-correlation function is

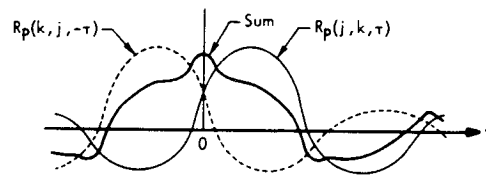
$$R_p(j, k, \tau) = \overline{P_j(t) P_k(t + \tau)} = \overline{P_j(t) P_j(t - \tau_{jk} + \tau)} \quad (3.277)$$



a) Cross Correlation of Random Noise at Two Points Separated by a Propagation Time of  $\tau_{jk}$



b) Cross Correlation Function Illustrating Symmetry About Propagation Time  $\tau_{jk}$



c) Mirror Symmetry of Cross-Correlation Pairs for "Stationary" Random Noise. The sum of these two functions is symmetrical about  $\tau = 0$ .

FIGURE 3.70 a) Time History of Propagating Random Noise at Two Points and b), c) Cross Correlation Functions Illustrating Unsymmetrical Form of Each Pair and Symmetrical Form of Sum

Thus, the cross-correlation function  $R(j, k, \tau)$  at two points, for a propagating wave of random noise, is equal to the autocorrelation function  $R(\tau')$  of the random noise at one

point for a time delay  $\tau' = \tau - \tau_{jk}$  where  $\tau_{jk}$  is the propagation time between the points. Again, if the propagating random noise is assumed to be statistically "stationary", then, as shown in Figure 3.70b, the cross-correlation function  $R_p(j, k, \tau)$  will be symmetrical about the propagation delay time  $\tau = \tau_{jk}$ , instead of  $\tau = 0$  as for the autocorrelation function.

A corresponding cross-correlation function  $R_p(k, j, -\tau)$  for the second cross product for each pair of forces can be defined as the time average of the force at  $k$  at time  $t$  multiplied by the force at  $j$  at an earlier time  $t - \tau$ . Thus, for "stationary" random noise, the cross-correlation function will have the important mirror image property, illustrated in Figure 3.70c, that

$$\overline{P_j(t) P_k(t + \tau)} = \overline{P_j(t - \tau) P_k(t)}$$

or

$$R_p(j, k, \tau) = R_p(k, j, -\tau)$$

Therefore, for any two points, there will be two terms in the summation indicated by Equation 3.274 for the autocorrelation of the generalized force. For the  $j$ th and  $k$ th points, these would be

$$\overline{P_j(t) P_k(t + \tau)} \phi_{jn} \phi_{kn} + \overline{P_j(t - \tau) P_k(t)} \phi_{jn} \phi_{kn}$$

or

$$[R_p(j, k, \tau) + R_p(k, j, -\tau)] \phi_{jn} \phi_{kn}$$

As shown in Figure 3.70c, the sum of the pair of cross-correlation functions, which are mirror images about  $\tau = 0$ , is an even function with exact symmetry about  $\tau = 0$ . This consideration of the symmetry properties of the cross-correlation function will help in understanding corresponding complex symmetry properties of the cross PSD.

#### Cross-Power Spectral Density

Due to the unsymmetrical nature of the cross correlation function  $R_p(j, k, \tau)$  about  $\tau = 0$ , the cross PSD  $\mathcal{W}_p(j, k, f)$  of this uneven function is complex. That is, it has both a real and imaginary term. However, by substituting each of the cross-correlation terms,  $R_p(j, k, \tau)$  and  $R_p(k, j, -\tau)$ , in Equation 3.276, it can be readily shown (Reference 3.3) that for "stationary" random noise, the corresponding cross PSD's will be complex conjugates of each other, or

$$\mathcal{W}_p(j, k, f) = \mathcal{W}_p^*(k, j, f)$$

Thus, the sum of this pair of cross-PSD or complex Fourier spectrum terms will be a real quantity; the imaginary terms cancel out. This is the expected result based on the previous observation that the sum of the pair of cross-correlation function terms is an even function and the Fourier spectrum of an even function is real.

Now with these new quantities, the PSD of the generalized force is obtained by first substituting Equation 3.274 into 3.271 to give

$$W_{F_n}(f) = W_o(f) J_n^2(f) \\ = 2 \int_{-\infty}^{\infty} \sum_j^N \sum_k^N \overline{P_j(t) P_k(t + \tau)} \phi_{jn} \phi_{kn} e^{-j 2\pi f t} dt$$

Carrying out the integration for each term in the double summation, using Equations 3.275 and 3.276, and solving for the joint acceptance  $J_n^2(f)$ , the later is given in terms of the cross PSD by

$$J_n^2(f) = \frac{\sum_j^N \sum_k^N \mathcal{W}_p(j, k, f) \phi_{jn} \phi_{kn}}{W_o(f)}$$

Further simplification is possible. Since, for each pair of terms in this double summation, the imaginary part of the cross PSD (called the quad spectrum) cancels out, only the real part of the cross-PSD, called the cospectrum is required. If this is identified as  $\mathcal{R}[\mathcal{W}_p(j, k, f)]$  or simply  $W_p(j, k, f)$ , then the joint acceptance becomes

$$J_n^2(f) = \frac{1}{W_o(f)} \sum_j^N \sum_k^N W_p(j, k, f) \phi_{jn} \phi_{kn} \quad (3.278a)$$

where

$$W_p(j, k, f) = 2 \int_{-\infty}^{\infty} R_p(j, k, \tau) \cos 2\pi f \tau d\tau \quad (3.278b)$$

the cospectrum equal to the real part of the cross PSD

and

$R_p(j, k, \tau)$  = cross-correlation function between  $j$ th and  $k$ th points.

Finally, for the special case where the PSD of the force at each point  $W_p(j, f)$  is a constant, then the PSD of the reference force is

$$W_o(f) = N W_p(j, f)$$

and the preceding expressions reduce to

$$J_n^2(f) = \frac{1}{N^2} \sum_j^N \sum_k^N \frac{W_p(j, k, f)}{W_p(j, f)} \phi_{jn} \phi_{kn} \quad (3.279)$$

Comparing this expression for the joint acceptance for random forces, with the corresponding equation for sinusoidal forces (Equation 3.267, page 3-88), it is clear that the ratio of the real part,  $W_p(j, k, f)$ , of the cross-PSD to

the PSD of the uniform propagating random force  $W_p(j, t)$  is identical to the space-correlation coefficient  $\bar{R}_p(j, k, f)$  for uniform propagating sinusoidal forces. The latter quantity is more suitable for analysis while the former may be obtained from measurements of random loads.

Measurement of Cross-Correlation Function and Cross-PSD

The more common methods for measuring the cross-correlation function and cross PSD are summarized in Figure 3.71. Part (a) illustrates the formal method for measuring the cross PSD with unfiltered random data. This process may be carried out on special analog correlation analyzers (Reference 3.44), or with the use of high speed digital computers specially programmed to carry out the same steps (Reference 3.45). (See also References 3.17, 3.22 and 3.45.)

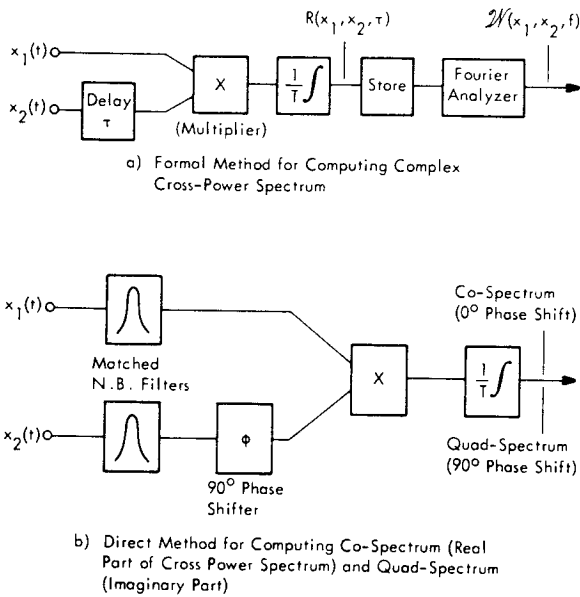


FIGURE 3.71 Methods for Measuring Cross-Power Spectral Density of Random Signals

Part (b) illustrates a simpler method for obtaining the real part of the cross PSD directly. This analysis procedure is equivalent to combining the operations indicated by Equations 3.275 and 3.276 and reversing the order of integration to determine the frequency spectrum first before carrying out the time averaging of the product. The real part of the cross PSD would then be

$$W_p(j, k, f) = \lim_{T \rightarrow \infty} \frac{2}{T} \int_{-T/2}^{+T/2} P_j(t) \left[ \int_{-\infty}^{+\infty} P_k(t+\tau) \cos 2\pi f \tau d\tau \right] dt$$

Note that the term within the brackets is equivalent to the frequency spectrum of  $P_k(t)$ . The analog form of this mathematical operation is shown in Part b of Figure 3.71. It eliminates the need for a time delay device and a Fourier spectrum computer but requires a set of matched narrow

band filters with a variable band-center frequency. Providing the filter bands are sufficiently narrow, the time average product of the filtered signals for  $0^\circ$  relative phase between channels, is approximately equal to the real part of the cross PSD and hence is equivalent to the narrow band space correlation function  $R_p(j, k, f)$ . In either system, the final result may be normalized by the product of the rms values of each narrow band signal to obtain a narrow band space correlation coefficient  $\bar{R}_p(j, k, f)$ . This may then be used directly in Equation 3.267 to compute the joint acceptance.

Cross-Correlation for Frozen and Decaying Propagating Random Loads

For the types of "frozen" propagating waves considered so far in this discussion, there is no change in the instantaneous amplitude of the propagating random force as measured in a time frame which moves with the same propagation velocity. In this case, the maximum of the cross-correlation function at the delayed time of symmetry ( $\tau = \tau_{jk}$ ), is theoretically the same as the maximum value of the auto-correlation function of  $\tau = 0$  which is equal to the mean square value  $P_j^2(t)$  of the random force. Practical measurements of the cross correlation for this type of "frozen" propagating wave may exhibit a substantial decrease in the maximum value of the cross correlation at increasing separation distances due to the finite size of measuring systems and small perturbations in the propagating wave. This is illustrated in Figure 3.72a.

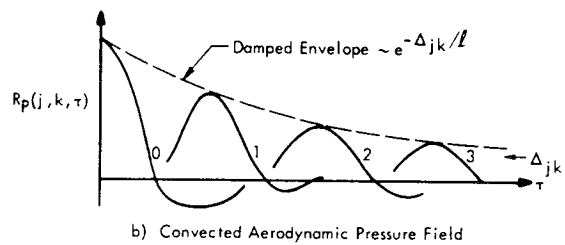
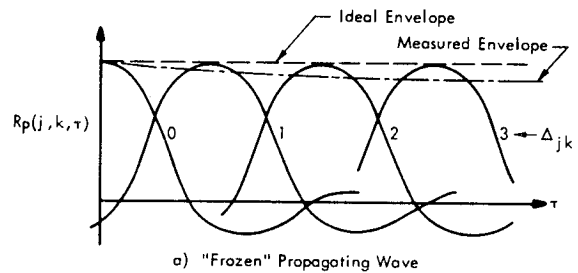


FIGURE 3.72 Cross Correlation Functions for a) Ideal "Frozen" Wave, and b) Convected Aerodynamic Flow with Decaying Coherence. Measured Envelope shown in part a) represents decay due to finite transducer size and small deviations in the "frozen" character of the propagating wave.

Another type of random loading is encountered for structure subjected to a convected flow of turbulent gases such as exists in a rocket engine exhaust. This type of loading is called aerodynamic or hydrodynamic noise. The idealized model of a "frozen" pattern of propagating random forces must now be replaced by a changing pattern of random forces which no longer remain coherent as measured in a moving time frame. The net effect of this changing coherence of the convected fluctuating pressure field is that the maximum value of the cross-correlation function decreases as the separation distance between measurement points increases. This decrease in coherence is frequently defined by expressing the cross-correlation function  $R_p(j, k, f)$  in the form of an exponentially damped auto-correlation function by

$$R_p(j, k, \tau) = e^{-\Delta_{jk}/\ell} R_p(j, \tau - \Delta_{jk}/\bar{c})$$

where

$\Delta_{jk}$  = separation distance between j and k

$\ell$  = characteristic length for the turbulent flow

$\bar{c}$  = convection velocity of flow

$R_p(\tau - \Delta_{jk}/\bar{c})$  = autocorrelation function of force at j for an effective delay time  $(\tau - \Delta_{jk}/\bar{c})$  where  $\tau$  is the actual delay time for the cross-correlation function.

Such a damped correlation function has the typical appearance shown in Figure 3.72b. Each curve represents the variation in the cross-correlation function as a function of  $\tau$  for a given separation distance  $\Delta_{jk}$ . The envelope of these curves, which peak at a value of  $\tau = \Delta_{jk}/\bar{c}$ , corresponds to the damping term in the preceding expression. The damping constant or characteristic length  $\ell$  is usually proportional to the ratio of a characteristic (convection) velocity  $\bar{c}$  to frequency  $f$ . In this case, it is necessary to filter the correlated signals representing  $P_j(t)$  and  $P_k(t)$  to obtain a narrow-band cross-correlation function. When normalized by the product of the rms values of  $P_j(t)$  and  $P_k(t)$ , this will be the narrow band cross-correlation coefficient given by

$$\bar{R}_p(j, k, \tau, f) = e^{-a \Delta_{jk} f / \bar{c}} \cos 2\pi f [\tau - \Delta_{jk}/\bar{c}]$$

where  $a$  = empirical constant.

The exponential damping term is then determined by setting the time delay  $\tau = \Delta_{jk}/\bar{c}$ . Once this damping term is evaluated, the narrow band space correlation coefficient  $\bar{R}_p(j, k, f)$  is obtained by setting  $\tau = 0$  in the above expression.

### 3.3.3.12 Summary of Terminology for Random Loads

The terminology utilized in this section is summarized below.

- Narrow Band Space Correlation Function (Required to Compute Joint Acceptance)

$R_p(j, k, f) = \overline{P_j(t) P_k(t)}$  where the  $\overline{\quad}$  denotes the long time average of  $P_j(t)$  times  $P_k(t)$ . These are sinusoids or equivalent narrow band random variables with frequency  $f$ .

- Autocorrelation Function

$R_p(j, \tau) = \overline{P_j(t) P_j(t + \tau)}$  - no restrictions on frequency content.

- Cross-Correlation Function

$R_p(j, k, \tau) = \overline{P_j(t) P_k(t + \tau)}$  - no restrictions on frequency content.

- Narrow-Band Cross-Correlation Function

$R_p(j, k, f, \tau) = \overline{P_j(t) P_k(t + \tau)}$  and  $P_j(t)$ ,  $P_k(t)$  are sinusoids or equivalent narrow band random variables with frequency  $f$ .

When normalized by the product of the rms values of the product terms, these "functions" become "coefficients" with a maximum possible value of +1 and a minimum possible value of -1. They may be used to determine the following spectral density functions.

- Power Spectral Density (PSD)

$W_p(j, f) = 2$  times Fourier Transform of autocorrelation function.

- Cross-Power Spectral Density (Cross-PSD)

$\mathcal{W}_p(j, k, f) = 2$  times Fourier Transform of cross correlation function

- Co-Spectrum (Equation 3.278a)

$W_p(j, k, f) = \text{Real Part of cross-PSD}$ . (When normalized by  $W_p(j, f)$  for uniform loading, this is the same as the narrow band space correlation coefficient.)

- Quad-Spectrum

$Q_p(j, k, f) = \text{imaginary part of Cross-PSD}$

Typical values for some of these quantities are summarized by the following expressions and in Figure 3.73.

Plane Sinusoidal Acoustic Wave with Frequency  $f$

- Narrow Band Space Correlation Coefficient Between  $j$  and  $k$

$\bar{R}_p(j, k, f) = \cos(2\pi f \Delta_{jk}/\bar{c})$ , where  $\Delta_{jk}$  = propagation distance between  $j$  and  $k$ , and  $\bar{c}$  = propagation velocity between  $j$  and  $k$ .

Plane Acoustic Wave of Low Pass Band of White Noise [ $W_p(f) = \text{Constant}$ ] with Upper Frequency Limit of  $f_b$

- Autocorrelation Coefficient at Point  $j$

$$\bar{R}_p(j, \tau) = \frac{\sin(2\pi f_b \tau)}{2\pi f_b \tau} \quad (\text{See Figure 3.73a})$$

- Cross-Correlation Coefficient Between  $j$  and  $k$

$$\bar{R}_p(j, k, \tau) = \frac{\sin[2\pi f_b (\tau - \Delta_{jk}/\bar{c})]}{2\pi f_b (\tau - \Delta_{jk}/\bar{c})}$$

- Cross-PSD Between  $j$  and  $k$

$$\mathcal{Y}_p(j, k, f) = W_p(f) [\cos(2\pi f \Delta_{jk}/\bar{c}) - j \sin(2\pi f \Delta_{jk}/\bar{c})]$$

- Co-Spectrum

$$W_p(j, k, f) = W_p(f) \cos(2\pi f \Delta_{jk}/\bar{c})$$

- Quad-Spectrum

$$Q_p(j, k, f) = -W_p(f) \sin(2\pi f \Delta_{jk}/\bar{c})$$

Band of "White" Random Noise with Frequency Limits  $f_a \rightarrow f_b$  ( $W_p(f) = \text{Constant}$  Between  $f_a$  and  $f_b$ )

- Autocorrelation Coefficient

$$\bar{R}_p(j, \tau) = \frac{\sin[2\pi (f_b - f_a) \tau]}{2\pi (f_b - f_a) \tau} \cos\left[2\pi \left(\frac{f_a + f_b}{2}\right) \tau\right]$$

(See Figure 3.73b)

Random Noise with Constant PSD from 0 to Frequency  $f_b$  and Sloping Off at Rate  $\propto 1/f^2$  Above  $f_b$

- Autocorrelation Coefficient

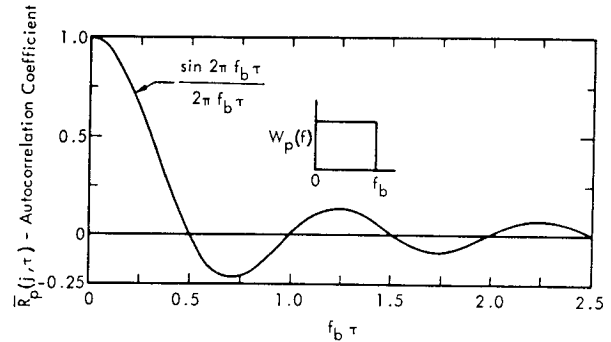
$$R_p(j, \tau) = \frac{1}{2} \left[ \frac{\sin v}{v} + \cos v - \frac{\pi}{2} v + v S_i(v) \right]$$

(See Figure 3.73c)

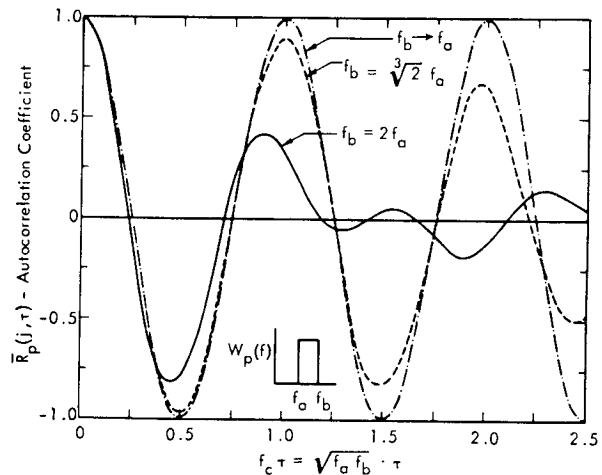
where

$$v = 2\pi f_b \tau$$

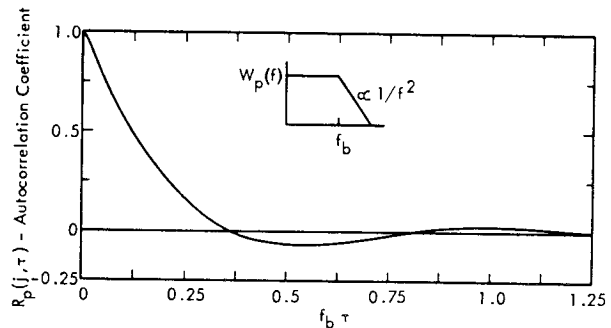
$$S_i(v) = \int_0^v \frac{\sin v}{v} dv - \text{the } S_i \text{ function (tabulated in Reference 3.48).}$$



a) Ideal Low-Pass Band of White Noise



b) Ideal Band of White Noise



c) Low-Pass Band of White Noise with Decrease  $\propto 1/f^2$  Above Cutoff

FIGURE 3.73 Autocorrelation Coefficients of Bands of Random Noise with a Constant Spectral Density in the Pass Band

General Expression for Response of Lumped Parameter Systems to Random Excitation

Although seldom required for practical analysis, the most general expression for the PSD,  $W_x(i, f)$  of the random response at the  $i$ th point of a lumped parameter system to random excitation may be expressed in the following compact form. This includes the response in all modes, including cross coupling terms, and is not restricted to uniform loading.

$$W_x(i, f) = W_o(f) \sum_n \sum_m \phi_{in} \phi_{im} \alpha_n(f) \alpha_m^*(f) J_{mn}^2$$

where

$$W_o(f) = \sum_j W_p(j, f) \text{ - PSD of total load}$$

$\phi_{in}, \phi_{im}$  = mode shapes at  $i$  in  $n$ th and  $m$ th mode

$\alpha_n(f)$  = complex sinusoidal transfer function for  $n$ th mode

$\alpha_m^*(f)$  = complex conjugate of transfer function for  $m$ th mode

$J_{mn}^2$  = complex cross joint acceptance

$$= \sum_j \sum_k \frac{\mathcal{H}_p(j, k, f) \phi_{jn} \phi_{km}}{W_o(f)}$$

$\mathcal{H}_p(j, k, f)$  = cross PSD between random load at  $j$  and  $k$

$\phi_{jn}, \phi_{km}$  = mode shapes at  $j$  and  $k$  in  $n$ th and  $m$ th modes, respectively.

As pointed out earlier, the complex conjugate pairs  $\alpha_n(f) \alpha_m^*(f)$  and  $J_{mn}^2, J_{nm}^2$  will combine to cancel out all imaginary terms in the final summation over modes  $n$  and  $m$ .

3.3.4 MATRIX METHODS FOR NORMAL MODE ANALYSIS OF LUMPED PARAMETER SYSTEMS

The potential application of matrix methods has been illustrated in preceding sections of this chapter for the analysis of the normal mode response of lumped parameter systems. This section briefly reviews some of the basic matrix operations utilized for this analysis. The intent is to provide only a minimum background to familiarize the reader with key steps which are employed in the matrix analysis of dynamic response of lumped parameter systems. For a more thorough discussion of matrix methods, the reader is referred to standard texts on mathematical analysis methods, such as Reference 3.49 or to References 3.36 and 3.1, Chapter 28, for a detailed discussion of the application of matrices to vibration analysis. For all except the simplest systems, the matrix computations described are normally carried out with digital computers. However, matrix notation itself is frequently used for convenience to express dynamic equations of motion of complex systems in a very compact form.

3.3.4.1 Matrix Definitions

A matrix is a rectangular array of elements arranged in  $n$  columns each containing  $m$  terms making up an  $m$  row by  $n$  column array of the order  $m \times n$ . As an example, the following is a matrix of stiffness coefficients (see Section 3.3.2.5 for definition of stiffness coefficients).

Square Matrix  $[k_{ij}] = \begin{matrix} & \begin{matrix} j \rightarrow \\ k_{11} & k_{12} & k_{13} \\ k_{21} & k_{22} & k_{23} \\ k_{31} & k_{32} & k_{33} \end{matrix} \\ \begin{matrix} \downarrow \\ i \\ m \end{matrix} & \end{matrix}$

This illustrates a  $3 \times 3$  SQUARE MATRIX where  $n = m = 3$

and the term  $k_{ij}$  is the matrix element in the  $i$ th row and  $j$ th column. For a COLUMN MATRIX,  $n = 1$  and for a ROW MATRIX,  $m = 1$ , such as illustrated by the following modal matrices.

Column Matrix  $\{\phi_i\} = \begin{Bmatrix} \phi_1 \\ \phi_2 \\ \vdots \\ \phi_n \end{Bmatrix}$

Row Matrix  $[\phi_i] = [\phi_1 \ \phi_2 \ \dots \ \phi_m]$

Other special matrices are:

Diagonal Matrix - A square matrix with zero elements everywhere except on the main diagonal. This is usually indicated by tick marks in the upper left and lower right-hand corner of the matrix bracket. For example,

$$[a_{ii}] = \begin{bmatrix} a_1 & 0 & 0 \\ 0 & a_2 & 0 \\ 0 & 0 & a_3 \end{bmatrix}$$

Unity (or Identity) Matrix - A diagonal matrix, indicated by the symbol  $[I]$ , whose nonzero elements are equal to unity. This is equivalent to the algebraic number 1. For example, for  $n = m = 3$ ,

$$[I] = \begin{bmatrix} 1 & 0 & 0 \\ 0 & 1 & 0 \\ 0 & 0 & 1 \end{bmatrix}$$

Zero (or Null) Matrix - A matrix with all elements equal to zero.

Transpose of a Matrix - A matrix for which the rows and columns are interchanged. Thus, the  $i$ th row is replaced by the  $j$ th column and visa versa. The transpose of the preceding stiffness matrix is identified by the superscript T and is

$$[k_{ij}]^T = [k_{ji}] = \begin{bmatrix} k_{11} & k_{21} & k_{31} \\ k_{12} & k_{22} & k_{32} \\ k_{13} & k_{23} & k_{33} \end{bmatrix}$$

The transpose of a column matrix is a row matrix or

$$\{\phi_i\}^T = [\phi_i]$$

Symmetric Matrix - A square matrix whose off-diagonal elements are symmetrical about the main diagonal. The preceding stiffness matrix is symmetric when  $k_{ij} = k_{ji}$ . By the above definitions, a symmetric matrix and its transpose are equal.

Equality of Matrices - Two matrices of the same order,  $[A] = [a_{ij}]$  and  $[B] = [b_{ij}]$  are equal if every element of  $[A]$  is equal to the corresponding element of  $[B]$  or  $a_{ij} = b_{ij}$ .

#### Determinant of a Square Matrix

A square matrix can represent the  $n \times n$  coefficients  $[a_{ij}]$  in a set of  $n$  linear equations of  $n$  variables. The determinant  $|a_{ij}|$  of this  $n \times n$  coefficient matrix is a scalar quantity where the elements  $a_{ij}$  in the determinant are identical to the corresponding elements in the square matrix. Some of the more useful rules for evaluation of determinants are listed for reference purposes.

If a  $3 \times 3$  square matrix is given by

$$[a_{ij}] = \begin{bmatrix} a_{11} & a_{12} & a_{13} \\ a_{21} & a_{22} & a_{23} \\ a_{31} & a_{32} & a_{33} \end{bmatrix}$$

its determinant can be written as

$$\begin{aligned} |a_{ij}| &= a_{11}(a_{22}a_{33} - a_{32}a_{23}) \\ &\quad - a_{12}(a_{21}a_{33} - a_{23}a_{31}) \\ &\quad + a_{13}(a_{21}a_{32} - a_{22}a_{31}) \end{aligned}$$

The determinant of a matrix  $[A]$  is

- Equal to zero if one row (or column) is a linear combination of one or more other rows or columns. For example, if  $a_{2j} = \text{constant} \times a_{3j}$  or if  $a_{2j} = a_{3j} + a_{4j}$ , then  $|a_{ij}| = 0$ .
- Unchanged if the rows and columns are interchanged.
- Unchanged if all elements in one row (or column) are multiplied by a constant and added to corresponding elements in another row (or column).
- Changed in sign if two rows (or columns) are interchanged.
- Multiplied by a constant  $c$  if each element in one row (or column) is multiplied by  $c$ .

Singular Matrix - A matrix whose determinant is zero.

#### 3.3.4.2 Matrix Operations

Matrix Addition and Subtraction - Two matrices of the same order (i.e., same number of rows and columns for both matrices) can be added or subtracted by adding or subtracting the corresponding elements in each matrix to form a new matrix of the same order.

$$[a_{ij}] + [b_{ij}] = [a_{ij} + b_{ij}]$$

Multiplication or Division of a Matrix by a Constant - The product of a matrix  $[a_{ij}]$  and a constant  $c$  is equivalent to multiplying every element in the matrix by a constant. Thus,

$$c [a_{ij}] = [c a_{ij}]$$

The inverse operation may be used, for example, to divide each element in a modal matrix by a normalizing constant.

Matrix Multiplication - The matrix analysis of the equations of motion of structural systems involves various forms of matrix multiplication. The governing rules for this operation are summarized as follows:

- Conformable Matrices - A product of two matrices is possible only when they are conformable; that is, when the number of columns ( $n$ ) in  $[a_{ij}]$  is equal to the number of rows ( $m$ ) in  $[b_{jk}]$ .
- Order of Multiplication - The order of multiplication of the matrices cannot, in general, be reversed without changing its value. That is, representing each matrix by the symbols A and B.

$$A \times B \neq B \times A$$

The product of a matrix  $\begin{bmatrix} a_{ij} \end{bmatrix}$  of order  $m, n$  times a matrix  $\begin{bmatrix} b_{jk} \end{bmatrix}$  of order  $n, p$  is a new matrix  $\begin{bmatrix} c_{ik} \end{bmatrix}$  of order  $m, p$ . That is,

$$\begin{matrix} m & n & p \\ \downarrow & \rightarrow & \rightarrow \\ \begin{bmatrix} a_{ij} \end{bmatrix} & \times & \begin{bmatrix} b_{jk} \end{bmatrix} = \begin{bmatrix} c_{ik} \end{bmatrix} \\ \downarrow & & \downarrow \end{matrix}$$

Each element  $c_{ik}$  in the product matrix is equal the sum of products of the  $j$ th element in the  $i$ th row of  $\begin{bmatrix} a_{ij} \end{bmatrix}$  times the corresponding  $j$ th element in the  $k$ th column of  $\begin{bmatrix} b_{jk} \end{bmatrix}$  or

$$c_{ik} = \sum_{j=1}^n a_{ij} b_{jk}$$

This operation can be represented by the diagram

$$i \begin{bmatrix} \vdots \\ a_{ij} \\ \vdots \end{bmatrix} \times \begin{bmatrix} \vdots \\ b_{jk} \\ \vdots \end{bmatrix} = i \begin{bmatrix} \dots \sum_j a_{ij} b_{jk} \end{bmatrix}$$

As an example,

$$\begin{bmatrix} a_{11} & a_{12} \\ a_{21} & a_{22} \end{bmatrix} \times \begin{bmatrix} b_{11} & b_{12} \\ b_{21} & b_{22} \end{bmatrix}$$

$$= \begin{bmatrix} (a_{11} b_{11} + a_{12} b_{21}) & (a_{11} b_{12} + a_{12} b_{22}) \\ (a_{21} b_{11} + a_{22} b_{21}) & (a_{21} b_{12} + a_{22} b_{22}) \end{bmatrix}$$

The general rules for matrix multiplication are:

square matrix x square matrix	= square matrix
column matrix x row matrix	= square matrix
square matrix x column matrix	= column matrix
row matrix x square matrix	= row matrix
row matrix x column matrix	= scalar constant
symmetrical matrix x symmetrical matrix	≠ symmetrical matrix
matrix x transpose of matrix	= symmetrical matrix
transpose of (A x B)	= B <sup>T</sup> x A <sup>T</sup>
unit matrix I x A	= A x I = A
Associative law (A x B) x C	= A x (B x C)
Premultiplication of A by B	= B x A
Postmultiplication of A by B	= A x B

Matrix Inversion

A basic step in matrix analysis involves inversion of square matrices. If it exists, the inverse (A<sup>-1</sup>) of a square matrix (A) has the property

$$A^{-1} \times A = A \times A^{-1} = I \text{ (unity matrix)}$$

The inverse can be found only for square matrices which have a nonzero determinant. For example, the inverse of a stiffness matrix  $\begin{bmatrix} k_{ij} \end{bmatrix}$  for a structure is called the flexibility matrix  $\begin{bmatrix} \delta_{ij} \end{bmatrix} = \begin{bmatrix} k_{ij} \end{bmatrix}^{-1}$ . It defines the deflection of the structure at one point for a unit load at another point. This flexibility matrix does not exist if the structure is unrestrained so that rigid body motions can occur for any applied force. In this case, the stiffness matrix usually contains a zero term along its main diagonal and its determinant is zero. Such a matrix is singular and has no inverse.

Special computer methods are available for finding the inverse of large matrices (e.g., Reference 3.1, Chapter 28). For relatively simple systems, the formal method for finding the inverse of a matrix A can be employed for hand calculations (Reference 3.49). This general method is illustrated by the following example

- Given  $A = \begin{bmatrix} a_{11} & a_{12} \\ a_{21} & a_{22} \end{bmatrix}$

- Form the Minor  $M_{ij}$  of each  $a_{ij}$  element of the determinant of A by deleting the  $i$ th row and the  $j$ th column. Multiply the remaining determinant by the sign  $(-1)^{i+j}$  to form the cofactor of  $a_{ij}$ . That is,

Cofactor of  $a_{11} = (-1)^{1+1} M_{11}$

$$= +1 \cdot \begin{vmatrix} \overset{\cdot}{a}_{11} & \overset{\cdot}{-} a_{12} \\ a_{21} & a_{22} \end{vmatrix} = + a_{22}$$

Cofactor of  $a_{12} = (-1)^{1+2} M_{12}$

$$= -1 \times \begin{vmatrix} \overset{\cdot}{a}_{11} & \overset{\cdot}{-} a_{12} \\ a_{21} & a_{22} \end{vmatrix} = - a_{21}, \text{ etc.}$$

- Form the transpose of the matrix of cofactors of A. This is called the adjoint matrix of A and is equal to

$$\text{Adjoint Matrix of } A = \left[ (-1)^{i+j} M_{ij} \right]^T = \begin{bmatrix} a_{22} & -a_{21} \\ -a_{12} & a_{11} \end{bmatrix}^T$$



- The inverse of A is the adjoint matrix divided by the determinant of A or

$$A^{-1} = \frac{\left[ (-1)^{i+j} M_{ij} \right]^T}{|A|} = \frac{\begin{bmatrix} a_{22} & -a_{12} \\ -a_{21} & a_{11} \end{bmatrix}}{a_{11} \times a_{22} - a_{12} \times a_{21}}$$

- This can be checked to show that  $A^{-1} A = I$ . Other techniques for matrix inversion, such as the elimination method (Reference 3.1, Chapter 28) are more efficient for hand calculation of larger order matrices.

### 3.3.4.3 Matrix Solution of Equations of Motion

The general form for the equation of motion of the  $i$ th mass of an  $N$  degree of freedom lumped parameter system without dynamic coupling can be given by (see Sections 3.3.2.6 and 3.3.3.1)

$$m_i \ddot{x}_i(t) + \sum_j c_{ij} \dot{x}_j(t) + \sum_j k_{ij} x_j(t) = P_i(t)$$

The two summation terms define the total damping and spring forces acting on the  $i$ th mass in terms of the damping and stiffness coefficient  $c_{ij}$  and  $k_{ij}$ . The sum of  $N$  such equation required to describe the motion of all  $N$  masses is

$$\sum_i m_i \ddot{x}_i(t) + \sum_i \sum_j c_{ij} \dot{x}_j(t) + \sum_i \sum_j k_{ij} x_j(t) = \sum_i P_i(t) \tag{3.280}$$

Applying the rules of matrix multiplication, this set of  $N$  equations can be expressed in matrix form as

$$\begin{bmatrix} m_1 & 0 & \dots & 0 \\ 0 & m_2 & & 0 \\ \vdots & & \ddots & \\ 0 & 0 & \dots & m_N \end{bmatrix} \begin{Bmatrix} \ddot{x}_1 \\ \ddot{x}_2 \\ \vdots \\ \ddot{x}_N \end{Bmatrix} + \begin{bmatrix} c_{11} & c_{12} & \dots & c_{1N} \\ c_{21} & c_{22} & & c_{2N} \\ \vdots & & \ddots & \\ c_{N1} & c_{N2} & \dots & c_{NN} \end{bmatrix} \begin{Bmatrix} \dot{x}_1 \\ \dot{x}_2 \\ \vdots \\ \dot{x}_N \end{Bmatrix}$$

$$+ \begin{bmatrix} k_{11} & k_{12} & \dots & k_{1N} \\ k_{21} & k_{22} & & k_{2N} \\ \vdots & & \ddots & \\ k_{N1} & k_{N2} & \dots & k_{NN} \end{bmatrix} \begin{Bmatrix} x_1 \\ x_2 \\ \vdots \\ x_N \end{Bmatrix} = \begin{Bmatrix} P_1 \\ P_2 \\ \vdots \\ P_N \end{Bmatrix}$$

or simply

$$\left[ m_i \right] \left\{ \ddot{x}_i \right\} + \left[ c_{ij} \right] \left\{ \dot{x}_i \right\} + \left[ k_{ij} \right] \left\{ x_i \right\} = \left\{ P_i \right\} \tag{3.281}$$

where

$$\begin{aligned} \left[ m_i \right] &= \text{diagonal mass matrix} & \left\{ x_i \right\} &= \text{column deflection matrix} \\ \left[ c_{ij} \right] &= \text{square damping matrix} & \left\{ P_i \right\} &= \text{column force matrix} \\ \left[ k_{ij} \right] &= \text{square stiffness matrix} \end{aligned}$$

### Generalized Coordinates and Matrix Symmetry

Providing the position of the center of gravity of each lumped mass  $m_i$  is uniquely described by only one independent variable  $x_i$ , the mass matrix  $\left[ m_i \right]$  will always be diagonal and the damping and stiffness matrices  $\left[ c_{ij} \right]$  and  $\left[ k_{ij} \right]$  will always be symmetric about the diagonal. These independent variables are called GENERALIZED COORDINATES and, for structural systems fixed to a rigid foundation, define the absolute deflections  $x_i$  of the center of gravity of each mass. As shown earlier in Section 3.3.3.2, for systems attached to a moving foundation, the generalized coordinates are the displacements relative to this moving foundation, or more precisely, relative to a line through the nodes of the free body nodes.

### Frequency Equation and Normal Modes

The normal mode solution of the equations of motion (3.281) is obtained by first setting the damping and external forces to zero. This will then define an equation of motion for free undamped vibration which can have a harmonic solution of the form

$$x_i(t) = X_i e^{j\omega t}$$

Substituting this solution into Equation 3.281 with  $\left[ c_{ij} \right]$  and  $\left\{ P_i \right\} = 0$ , gives

$$\left[ m_i \right] \left\{ -\omega^2 X_i \right\} + \left[ k_{ij} \right] \left\{ X_i \right\} = 0 \tag{3.282}$$

where  $X_i$  = displacement amplitude of the  $i$ th mass.

Applying the rules of matrix addition, this can be expressed as

$$\left[ (k_{ij} - \omega^2 m_i) \right] \left\{ X_i \right\} = 0$$

This represents a set of  $N$  homogeneous equations for the vibration of the  $N$  masses in their normal modes. The non-trivial solution to this set of equations (one for which  $\left\{ x_i \right\} \neq 0$ ) is obtained by setting the determinant of the first matrix equal to zero or

$$\left| (k_{ij} - \omega^2 m_i) \right| = 0 \quad (3.283)$$

This is the characteristic equation for the system and its roots are the values of  $\omega$  which cause the determinant to go to zero. These are the natural frequencies of the normal modes. For  $N$  masses, there will be  $N$  real roots or natural frequencies which satisfy this equation.

- For fixed-base systems which do not exhibit rigid body motion, the roots are always positive. (Such a system is called positive-definite.)
- For unconstrained systems, one or more of the roots or "natural frequencies" will be zero, corresponding to the rigid body modes of the structure. For this case, the stiffness matrix  $[k_{ij}]$  will be singular, and will contain one or more zeroes along its main diagonal.

Several methods may be used to find the roots or natural frequencies from Equation 3.282 or 3.283. Some of the more common methods may be summarized as follows.

#### Trial and Error Solution of Frequency Equation

The determinant or frequency equation given by Equation 3.283 is expanded into its polynomial by the usual methods for determinant expansion. Beyond a three degree-of-freedom system, however, a closed solution becomes very difficult. A trial and error solution can be carried out on computers to evaluate the polynomial expansion of the frequency equation as  $\omega$  is increased in fixed increments from zero. The natural frequencies are those values of  $\omega$  which cause the polynomial to approach zero. Successive trials for values of  $\omega$  can reduce the error to any desired practical value. A principal advantage of the method is that one or more natural frequencies can be quickly determined over any preselected frequency range of interest. However, errors can occur when resolving two modes which have nearly the same natural frequency.

The method is also relatively inefficient when all modes of a complex system must be computed. It is also limited to finding only the natural frequencies  $\omega_n$ . The normal mode shapes  $\phi_{in}$  are determined separately by substituting the natural frequencies back into Equation 3.282. The deflection amplitudes  $X_i$  are determined by solving  $N-1$  of the resulting simultaneous equations with any one of the amplitudes arbitrarily set to unity. The resulting values of  $X_{in}$  (one for each mass and modal frequency  $\omega_n$ ) are then normalized to unit value for the maximum deflection in each mode to obtain the mode shapes  $\phi_{in}$ .

The following two methods are alternate forms of the Stodola method. They have the advantage of providing the simultaneous solution for both the natural frequency  $\omega_n$  and normal mode shapes  $\phi_{in}$  in one basic iteration process.

They represent one form of the methods more commonly employed in computer analysis of multi-degree of freedom systems (References 3.33, and 3.1, Chapter 28).

#### Matrix Iteration Using the Stiffness Matrix

This method is most useful when it is desired to compute the highest natural frequency first since this is the first mode determined in the iteration process. Equation 3.282 is premultiplied through by the inverse of the inertia matrix  $[m_i]^{-1}$  and by  $1/\omega^2$  to give

$$\{X_i\} = \frac{1}{\omega^2} [m_i]^{-1} [k_{ij}] \{X_i\}$$

Note that since  $[m_i]^{-1}$  is diagonal and never singular, its inverse can be shown to be the matrix of the reciprocals of each element or

$$[m_i]^{-1} = \begin{bmatrix} 1 \\ m_i \end{bmatrix}$$

Let the matrix product  $[m_i]^{-1} [k_{ij}]$  be designated as the square matrix  $[B]$ .

The basic frequency equation to be evaluated then becomes

$$\{X_i\} = \frac{1}{\omega^2} [B] \{X_i\} \quad (3.284)$$

The iteration process, carried out with this expression, converges on the HIGHEST or  $N$ th natural frequency of the system in the following steps:

- A trial value of the column matrix of amplitudes  $\{X_i\}$  is assumed. If this trial value is arbitrarily chosen so that its largest element is unity, it may be considered to be a first order approximation for the mode shape  $\{\phi_{iN}\}_{r=1}$  for the  $N$ th normal mode.
- The assumed value  $\{\phi_{iN}\}_r$  is inserted in the right side of Equation 3.284 and the product  $[B] \{\phi_{iN}\}_r$  is evaluated. Let the element with the largest absolute value in this product be identified as the quantity  $\beta_{r+1}$ . If this normalizing factor is now divided out of the product  $[B] \{\phi_{iN}\}_r$ , then the first iteration step provides a 2nd approximation  $\{\phi_{iN}\}_{r+1}$  for the mode shape given by

$$\{\phi_{iN}\}_{r+1} = \frac{\beta_{r+1}}{\omega^2} \overline{[B] \{\phi_{iN}\}_{r=1}} \quad (3.285)$$

where the bar signifies a normalized value for the product matrix using the normalizing factor  $\beta_{r+1}$ .

- If  $\{\phi_{iN}\}_{r+1} = \{\phi_{iN}\}_r$ , within the desired accuracy, then

Nth Natural Frequency

$$\omega_N = \sqrt{\beta_{r+1}} \text{ - the highest or Nth natural frequency}$$

Nth Mode Shape

$$\{\phi_{iN}\} = \{\phi_{iN}\}_{r+1} \text{ - the column vector expressing the mode shape of the highest or Nth mode.}$$

- If the desired accuracy is not achieved in the first iteration, the new estimated mode shape column matrix  $\{\phi_{iN}\}_{r+1}$  is inserted back into Equation 3.285 and the iteration process continued (i.e.,  $r = 1, 2$ , etc.) until Equation 3.285 is satisfied to the desired accuracy.
- The process tends to be self-correcting; however, errors in the operation extend the number of iterations required to achieve the desired accuracy (Reference 3.33).
- For most problems, only a few iterations are required to achieve very good accuracy unless  $\omega_N$  is very close to the next lower natural frequency  $\omega_{N-1}$ .

Iteration for Lower Modes

For the next lower natural frequency  $\omega_{N-1}$ , additional steps are required. The next lower mode is modified, based on the concept of orthogonality of the normal modes, to remove all influence of the previously computed modes. This is carried out in the following manner (Reference 3.2).

The displacement  $x_i$  of each mass can be given by the summation of its normal modes as

$$x_i(t) = \sum_n^N q_n(t) \phi_{in}$$

Multiplying both sides by  $\phi_{im} m_i$ , summing over all the masses, and applying the orthogonality principle, a non-zero result is obtained only when  $n = m$ , which gives

$$\sum_i^N x_i(t) \phi_{in} m_i = q_n(t) \sum_i^N m_i \phi_{in}^2$$

To eliminate the influence of the highest mode on the displacements  $x_i(t)$ ,  $q_N$  is set equal to zero in the previous expression. Dividing out the time varying part for  $x(t)$  and  $q_n(t)$ , an algebraic equation is obtained involving all the displacement amplitudes  $X_i$ . For any value of  $n$ , it has the form

$$X_1 \phi_{1n} m_1 + X_2 \phi_{2n} m_2 + X_3 \phi_{3n} m_3 + \dots + X_N \phi_{Nn} m_n = 0 \tag{3.286}$$

If the Nth mode is to be "swept out" of the iteration process,  $n$  is set equal to  $N$ . It is convenient to solve this equation for the variable with the largest amplitude in terms of the remaining variables. Assuming this is  $X_N$ , the displacements can then be given by

$$\begin{aligned} X_1 &= X_1 \\ X_2 &= X_2 \\ &\vdots \\ X_{N-1} &= X_{N-1} \\ X_N &= -a_1 X_1 - a_2 X_2 \dots - a_{N-1} X_{N-1} \end{aligned}$$

$$\text{where } a_1 = \frac{\phi_{1N} m_2}{\phi_{NN} m_N}, a_2 = \frac{\phi_{2N} m_3}{\phi_{NN} m_N} \dots$$

This can be expressed in matrix form as

$$\begin{Bmatrix} X_1 \\ X_2 \\ \vdots \\ X_{N-1} \\ X_N \end{Bmatrix} = \begin{bmatrix} 1 & 0 & 0 & \dots & 0 \\ 0 & 1 & 0 & \dots & 0 \\ \vdots & \vdots & \ddots & \ddots & \vdots \\ 0 & 0 & & 1 & 0 \\ -a_1 & -a_2 & & & -a_{N-1} & 0 \end{bmatrix} \begin{Bmatrix} X_1 \\ X_2 \\ \vdots \\ X_{N-1} \\ X_N \end{Bmatrix} \tag{3.287}$$

The square matrix on the right side is called the Sweeping Matrix  $[S_N]$  for the Nth mode. It has the form of an identity matrix with the Nth row replaced by the coefficients for  $X_N$  in terms of the remaining variables. The result is that the Nth column has only zeroes. This sweeping matrix is then used to define a new frequency equation for the next lower (N-1) mode as

$$\{X_i\}_{N-1} = \frac{1}{\omega^2} [B] [S_N] \{X_i\}_{N-1}$$

The same iteration process carried out for the Nth mode is now repeated except that the iteration equation (3.285) is modified by the sweeping matrix to become

$$\{\phi_{i,N-1}\}_{r+1} = \frac{\beta_{r+1}}{\omega^2} \overline{[B] [S_N] \{\phi_{i,N-1}\}_r} \tag{3.288}$$

In this case, the normalizing factor  $\beta_{r+1}$  is the quantity necessary to normalize to unity the largest element in the product  $[B] [S_N] \{\phi_{i,N-1}\}_r$ . Again, the bar designates a normalized value for this product.

For the next lower mode ( $\omega_{N-2}$ ), two equations of the form given by Equation 3.286 can be written, one for  $n=N$  and one for  $n=N-1$  using the mode shapes  $\phi_{iN}$  and  $\phi_{iN-1}$  already determined. These two equations can now be solved for  $X_N$  and  $X_{N-1}$  in terms of the remaining variables  $X_1 \rightarrow X_{N-2}$ . A second sweeping matrix  $[S_2]$  can then be determined which will contain two rows of coefficients and two columns of zeroes thus reducing the order of the matrix equation by one more step. The same iteration process defined by Equation 3.287 is then repeated using  $[S_{N-1}]$  in place of  $[S_N]$  to find the value of  $\omega_{N-2}$  and  $\{\phi_{i,N-2}\}$ . Care must be taken to insure that round-off errors are not accumulated in the sweeping matrices to maintain accuracy as the number of iteration cycles increases.

This iteration process, which is based on systems defined by stiffness coefficients, has the advantage of relative simplicity for determination of the highest modes of a system. A simple example will serve to illustrate application of the basic iteration process. First, however, consider the last approach which has the advantage of converging first on the lowest or fundamental mode of a system.

Matrix Iteration for Systems Described by Flexibility Coefficients

The static analysis of structure is normally carried out most conveniently with the use of flexibility or influence coefficients. Consider the uniform-section cantilevered beam shown in Figure 3.74a. An estimate of the first three bending vibrating modes of this beam may be obtained by treating the beam as shown in Figure 3.74b as three lumped masses, each corresponding to one-third the beam mass. The deflection of the  $i$ th mass can be expressed in terms of flexibility coefficients, identified here by  $\delta_{ij}$ , by the equation

$$X_i = \delta_{i1} P_1 + \delta_{i2} P_2 + \delta_{i3} P_3$$

where  $P_1, P_2, P_3$  represent the forces applied to the masses, and  $\delta_{ij}$  is a flexibility influence coefficient equal to the positive displacement of the  $i$ th mass for a unit force applied to the  $j$ th mass, in the positive direction; all other forces being zero. In general, there is no simple relationship between flexibility coefficients  $\delta_{ij}$  and stiffness coefficients  $k_{ij}$ . For the former, the structure is loaded by a unit force at only one point and otherwise free. For the latter, all points except the point of unit deflection (see Figure 3.53) are constrained by a pinned support.

An extensive tabulation of formulae for influence coefficients for simple uniform beam and plate structures is given in Reference 3.51. For special cases, well-known methods such as the application of the moment-area theorem and matrix-force methods may be applied to determine the structural deflection to unit loads (References 3.36 and 3.51).

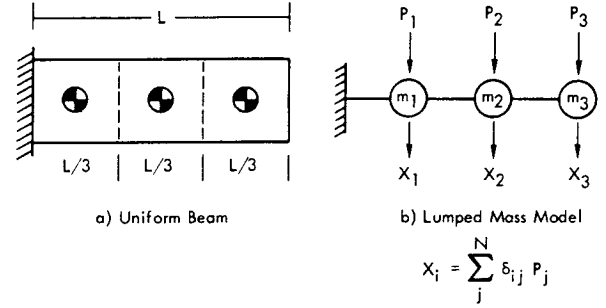


FIGURE 3.74 Lumped Mass Model of a Uniform Cantilevered Beam of Area  $A$ , Density  $\rho$ , Bending Stiffness  $EI$ . The influence coefficient  $\delta_{ij}$  represents the deflection at  $i$  for a unit force at  $j$  with all other forces equal to zero.

The preceding equation can be conveniently given in matrix form as

$$\{X_i\} = [\delta_{ij}] \{P_i\}$$

where  $[\delta_{ij}]$  = flexibility matrix - matrix of flexibility coefficients  $\delta_{ij}$

$\{P_i\}$  = column matrix of the applied loads.

For the case illustrated in Figure 3.74, the flexibility matrix is

$$[\delta_{ij}] = \frac{L^3}{648 EI} \begin{bmatrix} 1 & 4 & 7 \\ 4 & 27 & 54 \\ 7 & 54 & 125 \end{bmatrix}$$

where  $EI$  = Bending Stiffness of Beam.

For example, a unit downward force at the middle of the beam ( $j = 2$ ), will produce a downward deflection of  $4L^3/648 EI$  at the first mass ( $i = 1$ ). As with the stiffness matrix, the flexibility matrix is symmetric or

$$[\delta_{ij}] = [\delta_{ji}]$$

For vibratory motion of the lumped mass model of the beam in Figure 3.74b, the "applied forces"  $P_i$  become the inertia forces  $-m_i \ddot{x}_i(t)$  which oppose the motion. For free harmonic vibration of the beam at a frequency  $\omega$ , where  $-m_i \ddot{x}_i(t) = \omega^2 m_i x_i(t)$ , the equation of motion of the  $i$ th mass is

$$x_i(t) = \omega^2 [\delta_{i1} m_1 x_1(t) + \delta_{i2} m_2 x_2(t) + \delta_{i3} m_3 x_3(t)]$$

The equations of motion for all three lumped masses are given in matrix form by

$$\{x_i(t)\} = \omega^2 [\delta_{ij}] [m_i] \{x_i(t)\}$$

The product of the flexibility matrix  $[\delta_{ij}]$  and the inertia matrix  $[m_i]$  is called the dynamic matrix  $[D]$ . Thus, dividing out the time varying part of  $x_i(t)$ , the basic frequency equation to be evaluated by iteration is the matrix equation in terms of amplitudes  $X_i$

$$\{X_i\} = \omega^2 [D] \{X_i\} \tag{3.288}$$

Note that matrix inversion is not required in this case. In some cases, however, it is desirable to compute the normal modes with this expression but starting with the stiffness matrix. The latter is then inverted to give the dynamic matrix as

$$[D] = [k_{ij}]^{-1} [m_i]$$

since  $[k_{ij}]^{-1} = [\delta_{ij}]$

Comparing Equation 3.288 with the equivalent expression (Equation 3.284) based on equations of motion in terms of stiffness coefficients, it is clear that one is the inverse of the other but that the same iteration process can be used. The result of this iteration, however, converges on the value of the first or fundamental normal mode  $\omega_1$ . The basic iteration process for Equation 3.288 may be expressed as

$$\{\phi_{i1}\}_{r+1} = \omega^2 \beta_{r+1} \overline{[D]} \{\phi_{i1}\}_r \tag{3.289}$$

When iteration has satisfied Equation 3.289 - i.e.,

$$\{\phi_{i1}\}_{r+1} \approx \{\phi_{i1}\}_r$$

then the fundamental frequency  $\omega_1$  is

$$\omega_1 \approx \sqrt{1/\beta_{r+1}}$$

where

$\beta_{r+1}$  = magnitude of largest element in the product  $[D] \{\phi_i\}_r$  which is designated in normalized form by the bar.

The same steps, outlined previously, are carried out but starting with an initial trial value  $\{\phi_{i1}\}_r$  for the mode shape of the first mode. This initial value is conveniently taken as unity for the point of estimated maximum deflection and zero elsewhere. The remaining steps in the procedure are essentially the same as discussed for the previous method and are best illustrated by working out the example shown in Figure 3.74.

### 3.3.4.4 Example of Matrix Iteration Methods

Based on the flexibility matrix for the beam illustrated in Figure 3.74 and the even distribution of the lumped mass elements, the dynamic matrix is given by

$$[D] = [\delta_{ij}] [m_i] = \frac{(\rho AL/3) L^3}{648 EI} \begin{bmatrix} 1 & 4 & 7 \\ 4 & 27 & 54 \\ 7 & 54 & 125 \end{bmatrix} \begin{bmatrix} 1 & 0 & 0 \\ 0 & 1 & 0 \\ 0 & 0 & 1 \end{bmatrix}$$

where the mass of each "lump"  $\rho AL/3$  has been divided out of the inertia matrix.

### FIRST MODE

Assume, for the first trial, that the mode shape of the first mode is

First Trial  $\{\phi_{i1}\}_1 = \begin{Bmatrix} 0 \\ 0 \\ 1 \end{Bmatrix}$

Combining these two quantities in Equation 3.289, carrying out the required matrix multiplication, and dividing out the magnitude  $\beta_{r+1}$  of the largest element gives the first iterated value of  $\{\phi_{i1}\}_{r+1}$  as

### Second Trial

$$\{\phi_{i1}\}_2 = \omega^2 \frac{\rho AL^4}{1944 EI} \begin{bmatrix} 1 & 4 & 7 \\ 4 & 27 & 54 \\ 7 & 54 & 125 \end{bmatrix} \begin{bmatrix} 1 & 0 & 0 \\ 0 & 1 & 0 \\ 0 & 0 & 1 \end{bmatrix} \begin{Bmatrix} 0 \\ 0 \\ 1 \end{Bmatrix}$$

or

$$\{\phi_{i1}\}_2 = \omega^2 \frac{\rho AL^4}{1944 EI} (125) \begin{Bmatrix} 7/125 \\ 54/125 \\ 1 \end{Bmatrix} = \omega^2 \beta_2 \begin{Bmatrix} 0.056 \\ 0.431 \\ 1 \end{Bmatrix}$$

Using the new estimate for  $\{\phi_i\}$  each time, two more iterations give

Third Trial  $\{\phi_{i1}\}_3 = \omega^2 \frac{\rho AL^4}{1944 EI} (148.7) \begin{Bmatrix} 0.059 \\ 0.442 \\ 1 \end{Bmatrix}$

Fourth Trial  $\{\phi_{i1}\}_4 = \omega^2 \frac{\rho AL^4}{1944 EI} (149.2) \begin{Bmatrix} 0.059 \\ 0.444 \\ 1 \end{Bmatrix}$

Clearly, only three trials would be adequate for good accuracy. From the last trial, the fundamental frequency and mode shape are

$$\omega_1 \approx \sqrt{\frac{1944 EI}{(149.2) \rho AL^4}} = \frac{3.61}{L^2} \sqrt{\frac{EI}{\rho A}}$$

$$\{\phi_{i1}\} = \begin{Bmatrix} 0.059 \\ 0.444 \\ 1 \end{Bmatrix}$$

### SECOND MODE

The contribution of the first mode is set to zero ( $q_1 = 0$ ). From Equation 3.286, for  $N = 3$  and  $n = 1$ , the equation relating the displacement amplitudes of all the masses in the first mode is

$$X_1 \phi_{11} m_1 + X_2 \phi_{21} m_2 + X_3 \phi_{31} m_3 = 0$$

Solving this for  $X_3$  (the term with unit modal amplitude) in terms of  $X_1$  and  $X_2$ , the sweeping matrix  $[S_1]$  for the first mode can be developed in the same manner as in Equation

3.287. The result in this case, where  $\phi_{31} = 1$  and  $m_1 = m_2 = m_3$ , is

$$[S_1] = \begin{bmatrix} 1 & 0 & 0 \\ 0 & 1 & 0 \\ -0.059 & -0.444 & 0 \end{bmatrix}$$

The modified iteration equation for the second mode then becomes

$$\{\phi_{i2}\}_{r+1} = \omega^2 \beta_{r+1} \overline{[D][S_1]} \{\phi_{i2}\}_r$$

For a first trial, select

First Trial  $\{\phi_{i2}\}_1 = \begin{Bmatrix} 0 \\ 1 \\ 0 \end{Bmatrix}$

Using the sweeping matrix in the above expression, the second trial value for the second mode becomes

Second Trial  $\{\phi_{i2}\}_2 = \frac{\omega^2 \rho A L^4}{1944 EI} (3.05) \begin{Bmatrix} .295 \\ 1 \\ -.46 \end{Bmatrix}$

After two more iterations, the result is

Fourth Trial  $\{\phi_{i2}\}_4 = \frac{\omega^2 \rho A L^4}{1944 EI} (3.316) \begin{Bmatrix} 0.330 \\ 1 \\ -.462 \end{Bmatrix}$

Thus, the second mode is defined by

$$\omega_2 = \sqrt{\frac{1944 EI}{(3.316)\rho A L^4}} = \frac{24.2}{L^2} \sqrt{\frac{EI}{\rho A}}$$

$$\{\phi_{i2}\} = \begin{Bmatrix} 0.330 \\ 1 \\ -.462 \end{Bmatrix}$$

Third Mode

Proceeding in the same manner as before, the first and second modal contributions are set equal to zero giving the two algebraic expressions (see Equation 3.286)

$$\begin{aligned} n = 1, & \quad 0.059 X_1 + 0.44 X_2 + X_3 = 0 \\ n = 2, & \quad 0.33 X_1 + X_2 - 0.462 X_3 = 0 \end{aligned}$$

Solving these simultaneously for  $X_2$  and  $X_3$  in terms of  $X_1$ , the second sweeping matrix becomes

$$[S_2] = \begin{bmatrix} 1 & 0 & 0 \\ -0.296 & 0 & 0 \\ 0.710 & 0 & 0 \end{bmatrix}$$

Using this new sweeping matrix, the third mode would be

$$\{\phi_{i3}\}_{r+1} = \frac{\omega^2 \rho A L^4}{1944 EI} \begin{bmatrix} 1 & 4 & 7 \\ 4 & 27 & 54 \\ 7 & 54 & 125 \end{bmatrix} \begin{bmatrix} 1 & 0 & 0 \\ -0.296 & 0 & 0 \\ 0.710 & 0 & 0 \end{bmatrix} \{\phi_{i3}\}_r$$

No iteration is required for this last mode since the second sweeping matrix has reduced the product of  $[D]$  and  $[S_2]$  to a column matrix. Carrying out this product and normalizing, the third mode is obtained directly as

$$\{\phi_{i3}\} = \frac{\omega^2 \rho A L^4}{1944 EI} (0.314) \begin{Bmatrix} 1 \\ -0.525 \\ -0.414 \end{Bmatrix}$$

and

$$\omega_3 = \sqrt{\frac{1944 EI}{(0.314)\rho A L^4}} = \frac{78.6}{L^2} \sqrt{\frac{EI}{\rho A}}$$

The natural frequencies computed by this iteration process for the lumped mass model of the beam are compared in the following with the exact values based on the theory for vibrations of beams.

Comparison of Nondimensional Values of First Three Natural Frequencies of a Uniform Cantilevered Beam

$$\alpha = \omega_n L^2 \sqrt{\frac{\rho A}{EI}}$$

	Exact	Lumped Model	Error
First Mode	3.52	3.61	+2.6%
Second Mode	22.4	24.2	+8.0%
Third Mode	61.7	78.6	+27.4%

Clearly, the lumped mass model with three masses has poor accuracy beyond the  $n = 2$  mode.

The same iteration process could also be carried out with the frequency equation expressed in terms of the stiffness matrix. The latter is ordinarily computed directly rather than invert the flexibility matrix since this process is subject to an accumulation of round-off errors. This stems from the "nearly singular" nature of the typical flexibility matrix where one element on the main diagonal is small relative to the largest element as is the case in this example. Although this approach would converge initially on the third mode of the lumped mass model, the same error in the natural frequency is present due to the inaccuracy of the lumped mass model at the higher modes.

This simple example has served to illustrate several aspects of matrix iteration for the analysis of lumped parameter systems. Two points need to be emphasized.

- The iteration process is relatively simple for systems which can be analyzed by hand calculation. It defines both the modal frequencies and mode shapes in one basic process.
- Lumped models of continuous structure are conveniently analyzed by expressing the equations of motion of the structure in terms of the flexibility matrix.

There are a number of other commonly used forms of the basic frequency equation in matrix format which are cited in the literature. For example, one form is

$$\frac{1}{\omega^2} [I] \{X_i\} + [D] \{X_i\} = 0$$

where  $[I]$  is the identity matrix and  $[D]$  is the dynamic matrix. The symbol  $\lambda$  (or  $\lambda^2$ ) is often used in place of  $1/\omega^2$ . The above form emphasizes more clearly the formal matrix operation carried out in the iteration process - the matching of each element in the column matrix  $\{X_i\}$  on each side of the equation by an appropriate choice for  $\omega$  and  $\{X_i\}$ . The final results are equivalent, however, to that illustrated by the preceding example. For computer analysis, the frequency equation is conveniently expressed as the determinant (Reference 3.53)

$$\left| -\frac{1}{\omega^2} [I] + [L] [\delta_{ij}] [L]^T \right| = 0$$

where  $[L]^T [L] =$  the inertia matrix  $[m_{ij}]$ . For  $[m_{ij}] = [m_i]$ , a diagonal inertia matrix, then  $[L]$  is a diagonal matrix whose elements are equal to the square roots of the corresponding mass elements. The advantage of this form is that both  $[I]$  and the matrix product on the right side are symmetric, considerably simplifying machine computation of the roots  $\omega_n^2$  of the determinant (Reference 3.1, Chapter 28).

It must be emphasized that the methods employed for digital computer analysis of normal mode frequencies and mode shapes are frequently much more sophisticated than the simple method outlined above, in order to maintain high accuracy for very complex systems. Calculation with matrices of the order of 100 x 100 elements is not uncommon in the current state of the art. Some of these special computer techniques are discussed in detail in Chapter 28 of Reference 3.1.

### 3.3.4.5 Upper and Lower Bounds for Natural Frequencies

The natural frequencies for an N degree-of-freedom system must satisfy certain mathematical conditions. These constraints provide a simple method for estimating the upper and lower bound of the lowest and highest natural frequencies without carrying out detailed calculations. They also provide a means of checking the final results (References 3.36 and 3.1, Chapter 28).

#### BOUNDS ON LOWEST NATURAL FREQUENCY

When the equations of motion are expressed in terms of the flexibility matrix, the frequency equation can be expressed as

$$\{X_i\} = \omega^2 [D] \{X_i\}$$

Then it can be shown that the first natural frequency  $\omega_1$ , which satisfies this equation must lie within the limits

$$\omega_{1 \min}^2 < \omega_1^2 < N \omega_{1 \min}^2 \quad (3.290a)$$

where

N = Number of Degrees of Freedom represented (i.e., number of mass elements considered).

$$\omega_{1 \min}^2 = 1/t_r [D], \text{ and} \quad (3.290b)$$

$$t_r [D] = \text{Trace of the Dynamic Matrix} \\ [D] = [k_{ij}]^{-1} [m_i]$$

The trace of a matrix is the sum of the main diagonal elements. Thus, if

$$[D] = \frac{m}{k} \begin{bmatrix} 4 & 8 & 5 \\ 3 & 2 & 2 \\ 7 & 4 & 1 \end{bmatrix}$$

then

$$t_r [D] = (4 + 2 + 1) \frac{m}{k} = 7 \frac{m}{k}$$

and the first natural frequency for this three degree-of-freedom system would lie between

$$\frac{1}{7} \frac{k}{m} < \omega_1^2 < \frac{3}{7} \frac{k}{m}$$

For the example worked out in the previous section, this criteria would become

$$\frac{1944 EI}{153 \rho A L^4} = 12.7 \frac{EI}{\rho A L^4} < \omega_1^2 < 38.1 \frac{EI}{\rho A L^4}$$

The actual value of  $\omega_1^2$  computed was  $13 EI/\rho A L^4$  - close to the lower bound.

#### BOUNDS ON HIGHEST NATURAL FREQUENCY

When the equations of motion are expressed in terms of the stiffness matrix, the frequency equation can be expressed as

$$\{X_i\} = \frac{1}{\omega^2} [B] \{X_i\}$$

The highest natural frequency  $\omega_N$  computed with this expression (the first frequency determined by the iteration process in this case) is limited to

$$\frac{1}{N} \omega_{N \max}^2 < \omega_N^2 < \omega_{N \max}^2 \quad (3.291a)$$

where

$$\omega_{N \max}^2 = t_r [B] \tag{3.291b}$$

and  $[B] = [m_i]^{-1} [k_{ij}]$

For example, if

$$[B] = \frac{k}{m} \begin{bmatrix} 5 & 2 & 1 \\ 3 & 2 & 8 \\ 7 & 4 & 7 \end{bmatrix}$$

then  $t_r [B] = [5 + 2 + 7] \frac{k}{m} = 14 \frac{k}{m}$

and  $\omega_N^2$  would lie between

$$\frac{14}{3} \frac{k}{m} < \omega_N^2 < 14 \frac{k}{m}$$

CHECK CONDITIONS FOR THE NATURAL FREQUENCIES

The above criteria are primarily based on the following equalities for the sum of the natural frequencies:

$$\sum_n \frac{1}{\omega_n^2} = t_r [D] = t_r ([k_{ij}]^{-1} [m_i]) \tag{3.292a}$$

and

$$\sum_n \omega_n^2 = t_r [B] = t_r ([m_i]^{-1} [k_{ij}]) \tag{3.292b}$$

An additional useful check on calculations is provided by the criteria for the product of all the natural frequencies signified by the expressions

$$\prod_n \frac{1}{\omega_n^2} = |D| = \text{Determinant of dynamic matrix} \tag{3.292a}$$

and

$$\prod_n \omega_n^2 = |B| = \text{Determinant of } [B] \text{ matrix} \tag{3.292b}$$

3.3.4.6 Normal Mode Response in Matrix Form

Once the mode shapes  $\phi_{in}$  and natural frequencies  $\omega_n$  of the normal modes of a dynamic system have been defined, the following basic matrices can be used to transform the coupled set of equations of motion for all the masses to an uncoupled set of equations of motion for the normal coordinates  $q_n(t)$ .

$$\text{MODAL MATRIX} - [\phi_i] = \begin{matrix} & n \rightarrow & & N \\ \begin{matrix} i \downarrow \\ \vdots \\ N \end{matrix} & \begin{bmatrix} \phi_{11} & \phi_{12} & \cdots & \phi_{1N} \\ \phi_{21} & \phi_{22} & & \vdots \\ \vdots & \vdots & & \vdots \\ \phi_{N1} & \phi_{N2} & \cdots & \phi_{NN} \end{bmatrix} & & \end{matrix} \tag{3.293}$$

This is the square  $N \times N$  matrix consisting of all the column mode shape matrices  $\{\phi_{in}\}$  for each  $n$ th mode.

$$\text{SPECTRAL MATRIX} - [\omega_n^2] = \begin{bmatrix} \omega_1^2 & 0 & & 0 \\ 0 & \omega_2^2 & & 0 \\ \vdots & & \ddots & \\ 0 & & & \omega_N^2 \end{bmatrix}$$

This is a diagonal matrix containing the square of the  $N$  natural frequencies.

GENERALIZED MASS MATRIX -  $[M_n]$

The general definition for the Generalized Mass  $M_n$  of a lumped parameter system was given in Section 3.3.2.5 by the summation (assuming dynamically uncoupled systems)

$$\sum_i m_i \phi_{in} \phi_{jm} = \begin{cases} 0, & n \neq m \\ M_n, & n = m \end{cases} \tag{3.294}$$

The zero value for this summation stems from the orthogonality of the normal modes as shown in Section 3.3.2.7. This same relationship may be expressed in compact matrix form in the following manner.

$$[\phi]^T [m_i] [\phi] = [M_n] \tag{3.295}$$

where

$[M_n]$  = diagonal matrix containing the generalized masses for the  $N$  modes, and

$[m_i]$  = diagonal inertia matrix.

This basic operation is widely used in matrix analysis; it can be illustrated for the simple case of a two degree-of-freedom system. Thus, if

$$[m_i] = \begin{bmatrix} m_1 & 0 \\ 0 & m_2 \end{bmatrix}, \text{ and}$$

$$[\phi] = \begin{bmatrix} \phi_{11} & \phi_{12} \\ \phi_{21} & \phi_{22} \end{bmatrix},$$

the operation indicated by Equation 3.295 is



$$\begin{bmatrix} \phi_{11} & \phi_{21} \\ \phi_{12} & \phi_{22} \end{bmatrix} \begin{bmatrix} m_1 & 0 \\ 0 & m_2 \end{bmatrix} \begin{bmatrix} \phi_{11} & \phi_{12} \\ \phi_{21} & \phi_{22} \end{bmatrix} = \begin{bmatrix} M_1 & 0 \\ 0 & M_2 \end{bmatrix}$$

which can be expanded to

$$\begin{bmatrix} m_1 \phi_{11}^2 + m_2 \phi_{21}^2 & m_1 \phi_{11} \phi_{12} + m_2 \phi_{21} \phi_{22} \\ m_1 \phi_{11} \phi_{12} + m_2 \phi_{21} \phi_{22} & m_1 \phi_{12}^2 + m_2 \phi_{22}^2 \end{bmatrix} = \begin{bmatrix} M_1 & 0 \\ 0 & M_2 \end{bmatrix}$$

According to Equation 3.295, the off-diagonal elements in the left-hand matrix are zero and the diagonal terms are equal to the generalized masses  $M_1$  and  $M_2$ , respectively, thus demonstrating the validity of Equation 3.295. For just one mode, say the  $n$ th, this equation can be reduced to

$$\{\phi_{in}\}^T [m_{ij}] \{\phi_{in}\} = M_n \quad (3.296)$$

#### GENERALIZED STIFFNESS MATRIX - $[K_n]$

Applying the same principle of orthogonality and the type of operation indicated by Equation 3.296, the diagonalized generalized stiffness matrix is given by

$$[\phi]^T [k_{ij}] [\phi] = [K_n] \quad (3.297)$$

and for the  $n$ th mode, the generalized stiffness  $K_n$  is

$$\{\phi_{in}\}^T [k_{ij}] \{\phi_{in}\} = K_n = \omega_n^2 M_n \quad (3.298)$$

where

$$[k_{ij}] = \text{stiffness matrix}$$

#### GENERALIZED DAMPING MATRIX - $[C_n]$

If one of the forms of generalized damping, discussed in Section 3.3.3.1, is assumed, or if off-diagonal damping terms in the generalized damping matrix are neglected, then the latter is also diagonal. For just one mode, the generalized damping constant  $C_n$  is given by

$$\{\phi_{in}\}^T [c_{ij}] \{\phi_{in}\} = C_n = \frac{\omega_n M_n}{Q_n} \quad (3.299)$$

where

$Q_n$  = Resonant Amplification Factor for  $n$ th mode, and

$[c_{ij}]$  = damping matrix.

#### GENERALIZED FORCE MATRIX - $\{F_n(t)\}$

The generalized force for the  $n$ th mode has been defined as the summation

$$F_n(t) = \sum_j^N P_j(t) \phi_{jn}$$

According to the rules of matrix multiplication, this quantity can be expressed as the matrix product of a row matrix of the mode shape times a column matrix of the applied forces  $P_j(t)$ . Thus,

$$F_n(t) = \{\phi_{jn}\}^T \{P_j(t)\} \quad (3.300)$$

The column matrix specifying the generalized forces  $\{F_n(t)\}$  in all modes is then formed by including all the other transposed mode shape matrices to give

$$\{F_n(t)\} = [\phi]^T \{P_j(t)\} \quad (3.301)$$

If both sides of this expression were divided by the total force  $P_0$  applied to the system, the result would be a definition of the column matrix of Joint Acceptances (or mode participation factors) equal to the relative generalized forces for all modes (see Section 3.3.3.1).

#### DEFLECTION MATRIX IN NORMAL MODES

The displacement  $x_i(t)$  of each mass element in the lumped parameter system can be expressed as the sum of its normal mode responses, in the usual form

$$x_i(t) = \sum_n^N \phi_{in} q_n(t) \quad (3.302)$$

or, in matrix form, by the product of the row matrix  $[\phi_{in}]$  of the mode shapes at  $i$  in all  $N$  modes times a column matrix  $\{q_n(t)\}$  of the normal coordinates, or

$$x_i(t) = [\phi_{in}] \{q_n(t)\} \quad (3.303a)$$

Thus, a column matrix of the deflections  $\{x_i(t)\}$  for all masses is given by the product

$$\{x_i(t)\} = [\phi_i] \{q_n(t)\} \quad (3.303b)$$

where  $[\phi_i]$  = modal matrix defined by Equation 3.293.

In expanded form, this matrix formulation would be

$$\begin{Bmatrix} x_1(t) \\ x_2(t) \\ \vdots \\ x_N(t) \end{Bmatrix} = \begin{matrix} \overset{n \rightarrow}{\downarrow} \\ \begin{bmatrix} \phi_{11} & \phi_{12} & \cdots & \phi_{1N} \\ \phi_{21} & \phi_{22} & \cdots & \\ \vdots & & & \\ \phi_{N1} & \phi_{N2} & \cdots & \phi_{NN} \end{bmatrix} \end{matrix} \begin{Bmatrix} q_1(t) \\ q_2(t) \\ \vdots \\ q_N(t) \end{Bmatrix}$$

The product of the  $i$ th row of the modal matrix and the column matrix  $\{q_n(t)\}$  is equivalent to the summation in Equation 3.302 for the  $i$ th displacement.

UNCOUPLED EQUATIONS OF MOTION IN NORMAL MODES

Let the coupled equations of motion for the forced response of the lumped parameter system be given in matrix form as

$$[m_i] \{\ddot{x}_i(t)\} + [c_{ij}] \{\dot{x}_i(t)\} + [k_{ij}] \{x_i(t)\} = \{P_i(t)\}$$

Two steps will suffice to show the decoupled form for these equations in normal modes.

- Substitute  $[\phi] \{q_n(t)\}$  for  $\{x_i(t)\}$
- Premultiply both sides of the equation by the transpose of the modal matrix  $[\phi]^T$

Considering each term obtained by this procedure,

$$[\phi]^T [m_i] [\phi] \{\ddot{q}_n(t)\} = [M_n] \{\ddot{q}_n(t)\} \quad (\text{see Equation 3.295})$$

$$[\phi]^T [c_{ij}] [\phi] \{\dot{q}_n(t)\} = [C_n] \{\dot{q}_n(t)\} \quad (\text{assuming damping decoupling})$$

$$[\phi]^T [k_{ij}] [\phi] \{q_n(t)\} = [K_n] \{q_n(t)\} \quad (\text{see Equation 3.297})$$

$$[\phi]^T \{P_j(t)\} = \{F_n(t)\} \quad (\text{see Equation 3.301})$$

The expressions on the right side now constitute a set of uncoupled terms which make up the uncoupled equations of motion in normal modes. A typical equation for the nth mode is

$$M_n \ddot{q}_n(t) + C_n \dot{q}_n(t) + K_n q_n(t) = F_n(t)$$

or, in the more convenient form

$$\ddot{q}_n(t) + \frac{\omega_n}{Q_n} \dot{q}_n(t) + \omega_n^2 q_n(t) = \frac{F_n(t)}{M_n} \quad (3.304)$$

Thus, the familiar single degree of freedom equation is again obtained, this time through the use of matrix analysis. The matrix approach provides, therefore, a powerful method for transforming the basic equations of motion to uncoupled equations for each normal mode. The methods for determining the forced response of each normal coordinate  $q_n(t)$  have been discussed earlier in Sections 3.3.2 and 3.3.3. It is generally convenient at this point, having applied matrix analysis to define the equation of motion for each normal coordinate, to return to the general expressions given in Sections 3.3.3.3-9 for the response of lumped parameter systems to various types of loads. Two key parameters used for these latter expressions can be specified in matrix form.

$$\text{Generalized Mass for nth Mode} \quad M_n = \{\phi_{in}\}^T [m_i] \{\phi_{in}\}$$

$$\text{Joint Acceptance for nth Mode} \quad J_n = \frac{1}{P_o} \{\phi_{jn}\}^T \{P_j\}$$

where  $P_j$  = Amplitude of load at the jth point

$$P_o = \sum_j^N P_j \text{ - total applied load}$$

$\{\phi_{in}\}^T, \{\phi_{jn}\}^T$  = row matrix or transpose of column matrix expressing the mode shape in all N modes at the ith and jth points, respectively.

Although the discussion up to this point has been limited to lumped parameter systems, the concepts developed, methods of solution and terminology will still be applicable to the analysis of distributed or continuous structure which is considered in the next section.

### 3.3.5 RESPONSE OF STRUCTURE WITH DISTRIBUTED MASS AND STIFFNESS

The types of structure utilized for ground facilities at rocket launch and test sites and for adjacent residential areas covers a broad spectrum ranging from relatively simple metal or wood panel structure to complex reinforced steel and concrete structure. Practical methods for predicting the response of such structure to sonic loads are generally restricted to an analysis of the response of individual beam and wall (or equivalent plate) elements. However, this limitation is not necessarily a serious one. The response of these structural elements will determine to a large extent, the critical sonic loads and sound transmission characteristics of complex structure. This will become more apparent in the development of design methods in Chapters 5, 8 and 9. Therefore, this section on continuous structure with distributed mass and stiffness is primarily

limited to the vibration response of individual beam and plate elements. The normal mode approach is still applicable for vibration analysis of this type of structure by effectively modifying the expressions developed earlier for lumped parameter systems in the following manner:

- Replace discrete lumped masses by differentially small length or area segments for beams and plates, respectively.
- Replace summations of forces, deflections, etc., over lumped mass elements by single or double integrals over the differential length or area segments for beams and plates.
- Replace finite stiffness elements with differential stiffness functions which define local stiffness characteristics of distributed structure.

This transition is illustrated conceptually in Figure 3.75.

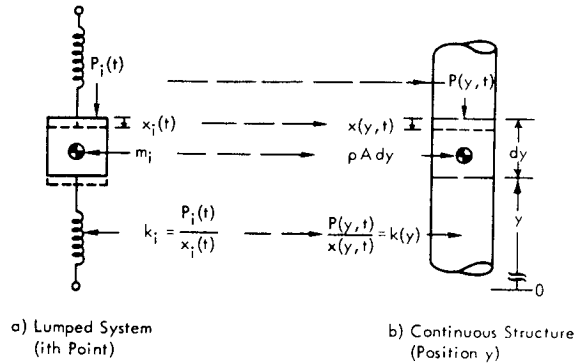


FIGURE 3.75 Transition from Lumped Parameter System to Continuous Structure Represented by Longitudinal Vibration of a Bar with Density  $\rho$  and Cross Section  $A$

Notation for Continuous Structure

To maintain consistency in notation for this chapter,  $X$  will be retained as the variable for linear displacement. However, the following changes in terminology will be required:

Variable	Lumped System	Continuous System
Mass Location	$i, j$	$\{y, y' - \text{Positions on a Beam}$ $\{y, z; y', z' - \text{Positions on a Plate}$
Driving Force	$P_j(t)$	$\begin{cases} P(y, t) - \text{Longitudinal Load on Beam} \\ bp(y, t) dy - \text{Lateral Load on Beam} \\ p(y, z, t) dy dz - \text{Lateral Load on Plate} \end{cases}$
Number of Normal Modes	$N$	$\begin{cases} L/dy \rightarrow \infty - \text{Beam} \\ A/(dy \cdot dz) \rightarrow \infty^2 - \text{Plate} \end{cases}$

As indicated, the lateral driving force for a beam (of width  $b$ ) or a plate is specified by the force per unit length  $bp(y, t)$  or force per unit area  $p(y, z, t)$ . Note that the last item is equivalent to saying that there are an infinite number of discrete mass elements along the beam and a doubly infinite number in the two directions on a plate.

3.3.5.1 Free and Forced Undamped Vibration of Continuous Structure

The equation of motion for a freely vibrating simple structural element may be given in a general form, comparable to the equations for lumped systems, by

$$(M) \ddot{X} + (K) X = 0 \tag{3.305}$$

where  $X$  represents a general displacement variable for a one- or two-dimensional element. The inertia parameter  $M$  and differential stiffness operator  $K$  for various types of linear elastic structural elements are summarized in Table 3.4. The expressions for bars are given in general form

where the inertia or stiffness properties can change as a function of position along the element. The inertia parameter,  $M$  multiplied by the acceleration  $\ddot{X}$ , represents the local inertia force on a differential element of mass while the differential stiffness term,  $K$  operating on  $X$ , defines the local internal elastic restoring force on this element. For example, according to Table 3.4, the equation of motion for free longitudinal vibration of a uniform beam has the following form, where  $\ddot{X} = \partial^2 x(y, t) / \partial t^2$  and  $X = x(y, t)$ .

$$\rho A \frac{\partial^2 x(y, t)}{\partial t^2} - EA \frac{\partial^2 x(y, t)}{\partial y^2} = 0 \tag{3.306}$$

In this case,  $x(y, t)$  represents the longitudinal deformation of the beam at position  $y$  and time  $t$  such as illustrated in Figure 3.75b. (A positive value of  $x$  corresponds to a positive dilatation in the bar.) This expression can be derived from physical principles by recognizing that the total longitudinal compressive force  $P_y$  acting at any position along the beam is equal to the compressive stress ( $E \cdot \text{Strain} = -E \partial x / \partial y$ ) times the cross-sectional area  $A$ . The change in this force across any differential section  $dy$  is

$$\frac{\partial P(y)}{\partial y} dy = -(EA \partial^2 x / \partial y^2) dy$$

This increment of internal force must then be balanced by the inertial force  $(\rho A dy) \partial^2 x / \partial t^2$  acting on this element. Cancelling out the  $dy$  terms, the expression given by Equation 3.306 is obtained. A similar method is used to obtain the other mass and stiffness terms listed in Table 3.4 (see, for example, References 3.2 and 3.5).

Elastic Wave Motion in Continuous Structure

Equation 3.306 represents one form of the "wave equation" and will be encountered again in Chapter 4 for acoustic waves. One solution to this type of equation will consist of functions of the form

$$x(y, t) = X^+ \sin \left[ \frac{\omega}{c_L} (y - c_L t) \right] + X^- \sin \left[ \frac{\omega}{c_L} (y + c_L t) \right] \tag{3.307}$$

where







$$X^+ \sin \left[ \frac{\omega}{c_L} (y - c_L t) \right]$$

defines the instantaneous amplitude of an sinusoidal elastic wave disturbance with a frequency  $\omega = 2\pi f$  which is traveling in the direction of positive  $y$  with a velocity  $c_L$  and

$$X^- \sin \left[ \frac{\omega}{c_L} (y + c_L t) \right]$$

represents the same type of wave traveling in the negative  $y$  direction with the same velocity. This is illustrated conceptually in Figure 3.76. Clearly, the instantaneous amplitude of the first wave is constant for any constant value of the quantity  $(y - c_L t)$ . Thus, the same amplitude occurs at increasing values of  $y$  at a time  $t = y/c_L$ . If either term

TABLE 3.4  
 INERTIA AND STIFFNESS TERMS AND ELASTIC WAVE VELOCITY  
 FOR VIBRATION OF SIMPLE ELASTIC STRUCTURAL ELEMENTS<sup>(1)</sup>

	Element	Motion	Inertia Parameter - M	Stiffness Operator - K	Wave Velocity <sup>(2)</sup>
String		Lateral	$\rho A(y)$	$-T \frac{\partial^2}{\partial y^2}$	$c_T = \sqrt{T/\rho A}$
Bar		Longitudinal (Compression)	$\rho A(y)$	$-\frac{\partial}{\partial y} \left( EA \frac{\partial}{\partial y} \right)$	$c_L = \sqrt{E/\rho}$
Bar		Torsional (Shear)	$\rho J(y)$	$-\frac{\partial}{\partial y} \left( K_r G \frac{\partial}{\partial y} \right)$	$c_s = \sqrt{\frac{G K_r}{\rho J}}$
Beam		Lateral (Bending)	$\rho A(y)$	$\frac{\partial^2}{\partial y^2} \left( EI \frac{\partial^2}{\partial y^2} \right)$	$c_B = \sqrt{\omega} \left[ \frac{E I}{\rho A} \right]^{1/4}$
Plate			$\rho h(y, z)$	$D \nabla^4$	$c_B' = \sqrt{\omega} \left[ \frac{D}{\rho h} \right]^{1/4}$
Membrane		Lateral	$\rho h(y, z)$	$-S \nabla^2$	$c_\eta = \sqrt{S/\rho h}$

Symbols

$\rho$  = Mass Density

$A$  = Cross-Sectional Area

$J$  = Polar Area Moment of Inertia

$h$  = Thickness

$T$  = Tension

$S$  = Tension per Unit Length

$E$  = Modulus of Elasticity (Young's Modulus)

$$\nabla^4 = \frac{\partial^4}{\partial y^4} + 2 \frac{\partial^4}{\partial y^2 \partial z^2}$$

$$\nabla^2 = \frac{\partial^2}{\partial y^2} + \frac{\partial^2}{\partial z^2} \text{ - Laplacian Operator}$$

$K_r$  = Torsional Constant  
 (=  $J$  for Circular Sections)

( $\approx A^4/4\pi^2 J$  for Solid Sections)

$G$  = Modulus of Rigidity (Shear Modulus)

$I$  = Area Moment of Inertia

$$D = Eh^3/12(1 - \nu^2)$$

$\nu$  = Poisson's Ratio

$\omega$  = Frequency - radians/sec

(1) References 3.2, 3.5, 3.6 and 3.53.

(2) Wave velocity for uniform structural elements indicated by the symbol  $c$  with appropriate subscript.

in Equation 3.307 is inserted in Equation 3.306, an equation is obtained for the wave velocity  $c_L$ , in this case a longitudinal compression wave, given by

$$c_L^2 = E/\rho$$

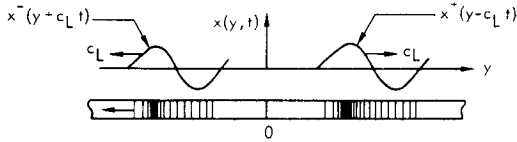


FIGURE 3.76 Longitudinal Compression Waves Traveling with a Velocity  $c_L$  in an Infinite Bar

This compression wave velocity  $c_L$  is also called the bar velocity or longitudinal speed of sound. It is this elastic wave motion which basically distinguishes the vibration response of structure with distributed mass and stiffness from the vibration response of lumped mass systems. The expressions which define the velocity of various types of elastic waves for simple structural elements are given in the last column of Table 3.4. Note that for longitudinal compression waves in bars, the wave velocity is dependent only on material properties while for torsional vibration, the shear wave velocity depends on material properties and on the geometry of the bar. One example of the practical significance of this type of traveling elastic wave is the critical influence of longitudinal elastic wave velocities in hydraulic pipes on the severity of dynamic loads due to water-hammer effects. Values for the longitudinal velocity  $c_L$  and torsional or shear velocity  $c_s$  for a number of common materials are listed in Table 3.39 at the end of this chapter.

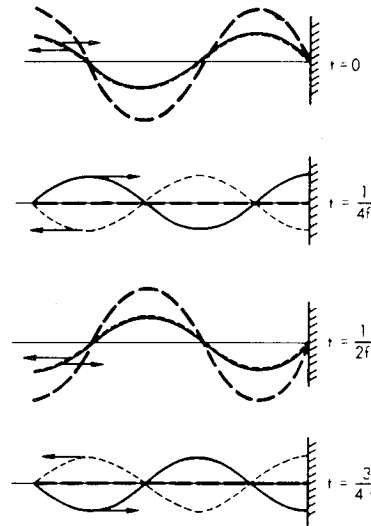
For lateral bending waves in beams and plates, the wave velocities indicated by the expressions in Table 3.4 are dependent not only on material and section properties but on the frequency  $\omega$  of vibration. Such waves are called dispersive waves, in contrast to nominally nondispersive longitudinal and torsional waves in bars. In this case, different frequency components of a complex elastic bending wave travel at different velocities through the structure - the waves with a lower frequency traveling with a lower velocity. As an example, traveling bending or flexural waves in beams and plates constitute one of the principal mechanisms for transmission of vibration in buildings and frame structure.

This brief discussion of traveling elastic waves in structure has been limited to only a few of the principal features of this complex phenomenon in order to provide a better physical understanding of the vibration of continuous structural elements. The topic of wave motion will appear again in this manual for, to a large extent, it represents a major distinguishing feature of sonic loading on buildings as distinguished from the stationary nature of static loads. The subject of acoustic waves will be covered in Chapters 4 and 9. Propagation of damped elastic waves in structure is considered later in this chapter. Propagation of damped acoustic and seismic waves is covered in Chapter 7.

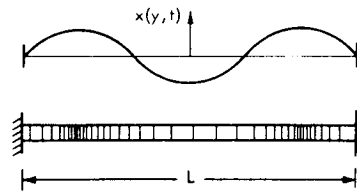
Standing Waves and Normal Modes

The complex features of traveling elastic waves are simplified when structural elements of a finite length are considered. When a traveling compression wave in a bar strikes a rigid boundary, a reflected wave is generated, as shown in Figure 3.77a, which travels in the opposite direction and has an amplitude and phase such that the condition of zero deflection at the rigid boundary is satisfied by the sum of the incident and reflected waves. This results in a so-called Standing Wave of longitudinal vibration in the bar as illustrated in Figure 3.77a by the heavy dashed line. The summation of the incident and reflected waves add up to a time-varying motion which does not propagate along the bar. If the rigid boundary depicted in Figure 3.77a is located at the position  $y = 0$ , then, using Equation 3.307 to define the incident and reflected waves, it can be shown that their amplitudes  $X^+$  and  $X^-$  are equal. The combined deflection of the two waves may be expressed as separable space and time functions by

$$x(y, t) = 2X \sin \frac{\omega y}{c_L} \cos \omega t$$



a) Reflected (----) and Standing (— —) Waves Generated by an Incident (—) Longitudinal Compression Wave in a Bar Striking a Rigid Boundary. Shown at four different times separated by 1/4 of the period ( $1/f$ ) of the incident wave.



b) Fixed-Fixed Bar Vibrating Longitudinally in Its Third Normal Mode. Standing wave vibration for  $f_3 = 3(c_L/2L)$ .

FIGURE 3.77 Standing Waves and Normal Modes for Longitudinal Vibration of a Bar

If another rigid boundary is placed on the bar at a distance  $y = L$  from the first boundary, then standing longitudinal compression waves can exist in such a bar only for those frequencies for which boundary conditions of zero deflection are satisfied at both ends - that is, for  $\omega L/c_L = n\pi$  or  $f_n = n(c_L/2L)$ . A convenient physical interpretation of this simple expression for the natural frequency is obtained by considering  $2L/n$  as the wavelength  $\lambda_n = c_L/f_n$  for the  $n$ th longitudinal mode of vibration for the bar fixed at both ends. That is, for  $n = 1$ , a wave, starting at one end of the bar which travels to the other end and upon reflection, returns to the starting point, must travel one wavelength, or  $2L$ , for the proper conditions of zero displacement to be met at each end. Thus, it is convenient to define a quantity  $K$  called a wave number where  $K = 2\pi/\lambda = 2\pi f/c_L$ . For the  $n$ th normal mode of the fixed bar, where  $f_n = n c_L/2L$ , the dimensionless quantity  $K_n L = 2\pi(n c_L/2L)(L/c_L) = n\pi$  can also be used to define the  $n$ th natural frequency. The case for  $n = 3$  is illustrated in Figure 3.77b. Frequencies which satisfy this criteria are the natural frequencies  $\omega_n$  or the normal modes of longitudinal vibration for a fixed-fixed bar.

The same concept of standing waves applies to the lateral bending vibration of beams and plates in their normal modes. For example, as shown in Figure 3.78, the normal modes of a simply supported beam and plate have corresponding natural frequencies, indicated in the figure, which can be defined in terms of the ratio of the corresponding wave velocity  $c_B$  or  $c'_B$  to a characteristic length. The wave number parameter  $K$  for bending waves in beams is defined by  $K = 2\pi/\lambda = 2\pi f/c_B$  where  $\lambda$  is now a bending wavelength and  $c_B$  is the bending wave velocity in the beam. However, a different form is normally used to express the natural frequency for this type of vibration for, as noted earlier, the wave velocity for bending vibration of beams and plates is, itself, dependent on frequency. Nevertheless, the relationship between normal modes and standing waves still applies.

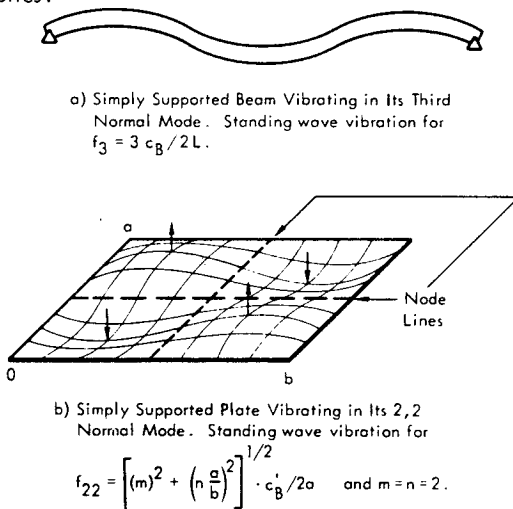


FIGURE 3.78. Typical Normal Modes for Free Flexural Vibration of Structural Elements

In general, therefore, the vibration of a finite continuous structural element can be defined in terms of its normal modes by a summation of terms of the form  $\phi_n(y) q_n(t)$  where  $\phi_n(y)$  represents the shape of the  $n$ th normal mode and  $q_n(t)$  represents the time variation for this mode. For a two-dimensional structure, the  $m$ th mode shape  $\phi_{mn}(y, z)$  is usually specified by a product  $\phi_m(y) \phi_n(z)$  of two one-dimensional mode shapes in the  $m$ th and  $n$ th mode, respectively. Assuming harmonic motion for the normal mode of a one-dimensional structure, then  $x(y, t)$  can be given in the form  $\bar{q} \phi(y) e^{j\omega t}$ . Substituting this into the basic equation of motion (Equation 3.305), the time varying part drops out leaving the Frequency Equation for the normal modes which is

$$\left[ -\omega^2 M + K \right] \phi(y) = 0 \tag{3.308}$$

where  $M$  and  $K$  are the inertia and stiffness terms identified in Table 3.4. The mode shape functions  $\phi(y)$  which satisfy this equation must also be able to satisfy the boundary conditions imposed at the ends of the element. The boundary conditions applicable for ideal end conditions and for partial fixity and other nonideal end conditions for longitudinal, torsional and lateral vibration of bars and beams are summarized in Table 3.5, page 3-113.

General Form for Normal Mode Shapes

For lateral vibration of strings and longitudinal or torsional vibration of bars, the general normal mode shape which can satisfy Equation 3.308 and the appropriate boundary conditions in Table 3.5 is a summation of circular or sine and cosine functions given by

$$\phi(y) = A \cos Ky + B \sin Ky \tag{3.309}$$

For lateral bending of a beam, or for lateral bending along one dimension of a plate, the general mode shape which can satisfy Equation 3.308 and the boundary conditions in Table 3.5 is a summation of circular and hyperbolic functions and is conveniently expressed as

$$\phi(y) = A (\cosh Ky + \cos Ky) + B (\cosh Ky - \cos Ky) + C (\sinh Ky + \sin Ky) + D (\sinh Ky - \sin Ky) \tag{3.310}$$

where

$$K = \omega / (\text{wave velocity}) - \text{see Table 3.4}$$

$$\omega = \text{Frequency in radians/sec}$$

$A, B, C, D$  = Coefficients to be determined from boundary conditions. (For ideal boundary conditions, two of these coefficients will always be zero.)

The unknown coefficients, the natural frequency for each mode, and the mode shape for free vibration in the normal modes are determined by the following steps:

- 1) Apply the known boundary conditions from Table 3.5 to Equations 3.309 or 3.310 or their appropriate derivatives (two conditions are required for Equation 3.309 and four for Equation 3.310).
- 2) Solve the resulting set of linear algebraic equations for all but one of the unknown coefficients and for the roots or natural frequencies  $\omega_n$ , using a standard variable elimination method or determinant solution methods. (The natural frequency  $\omega_n$  is determined in a nondimensional form as  $\omega_n L/c = K_n L$  where  $L$  is the length of the element and  $c$  is the appropriate wave velocity.)
- 3) Determine the mode shapes by substituting  $\omega_n L/c = K_n L$  back into the corresponding equation for the mode shape.
- 4) Normalize the maximum value of the mode shape to unity. (Alternate methods make this step unnecessary but it is used here for consistency with the convention adopted for lumped parameter systems.)

Solutions for the normal vibration modes of a wide variety of idealized structural elements, using the procedures outlined above, are well known and are thoroughly documented in the literature. Representative cases of practical interest will be illustrated in subsequent sections.

Resonance frequencies and, in some cases, mode shapes for most of the known solutions to Equation 3.308 for a wide variety of simple structural elements with ideal boundary conditions are included in the charts and tables at the end of this chapter. Additional aspects covering longitudinal and torsional vibration of bars and lateral vibration of beams and plates are covered in the next sections.

#### Forced Response Without the Use of Normal Modes

For forced excitation of a distributed structural element at its boundaries (i.e. - foundation force or displacement input), it is often convenient to obtain a solution without resorting to the normal mode approach. It is important to distinguish this direct approach from the normal mode method when applying boundary conditions for distributed systems. When boundary conditions which specify an excitation such as a driving force or input motion are used, the resulting equations of forced motion are nonhomogeneous. That is, at least one of the set of equations obtained by inserting the boundary conditions, has a nonzero forcing term on the right side. In this case, the usual frequency equation based on free vibration is not obtained. The forced response is determined directly without computing the normal modes by solving the set of nonhomogeneous equations for all of the unknown coefficients (A, B, etc.) in Equation 3.309 or 3.310 without solving for natural frequencies. Evidence of the predominant effect of the normal mode response becomes apparent, however, since the forced response becomes maximum at the natural frequencies of the normal modes.

Variations of this method, such as the Transfer Matrix method (References 3.34 and 3.36) are very useful for computing the vibration response of complex distributed structure such as structural frames or piping arrays. For all but relatively simple systems, however, the methods require extensive computations which generally involve the use of computers. For single structural elements, the normal mode approach offers considerable simplification as will be clear from subsequent examples.

#### Generalized Mass for Distributed Structural Elements

Just as for lumped parameter systems, normal modes for distributed structural elements are orthogonal with respect to the distributed mass. This condition is defined by the following equations for one- and two-dimensional structure (References 3.2 and 3.5).

##### For Bars and Beams of Length L

$$\int_0^L \rho A(y) \phi_n(y) \phi_m(y) dy = \begin{cases} M_n & m = n \\ 0 & m \neq n \end{cases} \quad (3.311)$$

##### For Plates with Sides a, b

$$\int_0^a \int_0^b \rho h(y, z) \phi_{mn}(y, z) \phi_{rs}(y, z) dy dz = \begin{cases} M_{mn} & m = r \\ & n = s \\ 0 & m \neq r \\ & n \neq s \end{cases} \quad (3.312)$$

where

$M_n, M_{mn}$  = Generalized Mass for  $n$ th mode of one-dimensional structure and  $m$ th mode of two-dimensional structure, respectively

$\rho A(y)$  = mass per unit length =  $\rho A$  for uniform beam

$\rho h(y, z)$  = mass per unit area =  $\rho h$  for uniform plate.

#### Generalized Forces for Distributed Structural Elements

The generalized force  $F_n(t)$  for the  $n$ th mode of a beam loaded by a distributed dynamic force  $b p(y, t)$  per unit length, where  $b$  is the beam width and  $p(y, t)$  is the pressure at  $y$ , is (see Section 3.3.3.1)

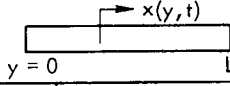
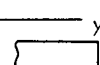
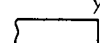
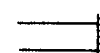

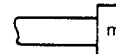
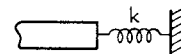
$$F_n(t) = b \int_0^L p(y, t) \phi_n(y) dy \quad (3.313a)$$

For a plate loaded by a distributed pressure  $p(y, z, t)$ , the generalized force for the  $m$ th mode is

$$F_{mn}(t) = \int_0^a \int_0^b p(y, z, t) \phi_{mn}(y, z) dy dz \quad (3.313b)$$

TABLE 3.5

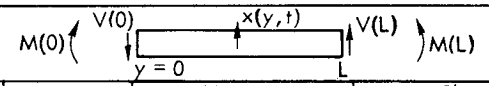
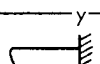
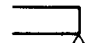
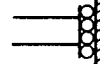
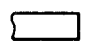
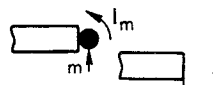
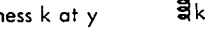

BOUNDARY CONDITIONS FOR LONGITUDINAL, TORSIONAL AND LATERAL VIBRATION OF UNIFORM BARS AND BEAMS

LONGITUDINAL VIBRATION OF BARS				
Boundary Condition		Deflection at $y^{(1)}$ $x(y,t)$	Compressive Force at $y$ $EA \partial x(y,t)/\partial y$	
			$y = 0$	$y = L$
Free at $y$		-	0	0
Fixed at $y$		0	-	-
Compressive Load $P$ at $y$		-	$-P$	$-P$
Inertial Load $m$ at $y$		-	$+ m_o \frac{\partial^2 x(0,t)}{\partial t^2}$	$- m_L \frac{\partial^2 x(L,t)}{\partial t^2}$
Stiffness Load $k$ at $y$		-	$+ k_o x(0,t)$	$- k_L x(L,t)$

TORSIONAL VIBRATION OF BARS

Same as for Longitudinal Vibration of Bar Except:

- Replace Force  $P$  by Moment  $M$
- Replace Mass  $m$  by Mass Moment of Inertia  $I$
- Replace Stiffness  $k$  by Torsional Stiffness  $k_r$

LATERAL VIBRATION OF BEAMS					
Boundary Condition		Deflection $x(y)$	Slope $\partial x(y,t)/\partial y$	Moment $M = EI \partial^2 x(y,t)/\partial y^2$	Shear $V = -EI \partial^3 x(y,t)/\partial y^3$
Pinned at $y$		0	-	0	-
Guided at $y$		-	0	-	0
Free at $y$		-	-	0	0
Inertial Load $m, I_m$ at $y$		-	-	$- I_m \frac{\partial^3 x(y,t)}{\partial y \partial t^2}$	$- m \frac{\partial^2 x(y,t)}{\partial t^2}$
Pure Translational Stiffness $k$ at $y$		-	0	-	$k x(y,t)$
Pure Torsional Stiffness $k_r$ at $y$		0	-	$k_r \frac{\partial x(y,t)}{\partial y}$	-

(1) Positive  $x$  implies dilatation - i.e., expansion of bar.



These expressions for the generalized force on distributed structure can be used to define the forced response of such structure to arbitrary loads using the methods developed earlier for lumped parameter systems (see Sections 3.3.2.9 and 3.3.3.1-3.3.3.9). The generalized force may also be expressed in normalized form in terms of the Joint Acceptance (or mode participation factor). For example, for a beam of length  $L$  subjected to a distributed sinusoidal acoustic load, the mean square generalized force for the  $n$ th mode can be written down from Equation 3.267 (page 3-88) using the rules cited at the beginning of this section for transition from lumped to continuous systems. The result is

$$\overline{F_n^2(t)} = \frac{1}{2} p_o^2 J_n^2 \tag{3.314}$$

where

$$J_n^2 = \frac{1}{L^2} \int_0^L \int_0^L \overline{R_p(y, y', t)} \phi_n(y) \phi_n(y') dy dy' -$$

the joint acceptance squared for a dynamic pressure with a constant amplitude but varying phase sinusoid

$$\overline{R_p(y, y', t)} = \frac{\overline{p(y, t) p(y', t)}}{p^2(t)} - \text{the (narrow band) space-correlation coefficient between the instantaneous pressure } p(y, t) \text{ at point } y \text{ and the pressure } p(y', t) \text{ at another point } y'$$

$$\overline{p^2(t)} = \text{mean square value of the constant amplitude pressure at any point}$$

$$\frac{1}{2} p_o^2 = (bL)^2 \overline{p^2(t)} - \text{mean square value of the total force on beam of span } b \text{ and length } L.$$

The above expression for joint acceptance squared for sinusoidal acoustic loads on beams will be evaluated in detail in Chapter 8 when analyzing the response of building structure to acoustic loads.

### 3.3.5.2 Longitudinal Vibration of Bars

The normal mode characteristics for longitudinal vibration of uniform bars, obtained by applying the concepts outlined in the previous section, are summarized below. (See Tables 3.26 and 3.39 at the end of this chapter.)

Equation of Motion for Free Vibration  $\ddot{x}(y, t) - c_L^2 x''(y, t) = 0$  (3.315)

where, for convenience in notation,

$$\ddot{x}(y, t) = \frac{\partial^2 x(y, t)}{\partial t^2}, \text{ and } x''(y, t) = \frac{\partial^2 x(y, t)}{\partial y^2}$$

Longitudinal Wave Velocity  $c_L = \sqrt{E/\rho}$

## MODAL CHARACTERISTICS

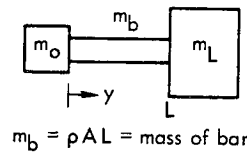
Boundary Condition	Mode Shape <sup>(1)</sup> $\phi_n(y)$	Natural Frequency <sup>(2)</sup> $f_n$
	Fixed-Free $\sin(2n-1) \frac{\pi}{2} \frac{y}{L}$	$(2n-1) c_L / 4L$ $n = 1, 2, 3$
	Fixed-Fixed $\sin n\pi \frac{y}{L}$	$n c_L / 2L$ $n = 0, 1, 2$
	Free-Free $\cos n\pi \frac{y}{L}$	$n c_L / 2L$ $n = 0, 1, 2$

(1) Generalized Mass  $M_n = \frac{1}{2} \rho AL = \frac{1}{2}$  (Mass of Bar)

(2)  $n = 0$  modes refer to rigid body translation modes.

### Special Cases

- Unequal Mass Loading at End of Free-Free Bar



Mode Shape (Not Normalized to Unity)

$$\phi_n \left( \frac{y}{L} \right) = \cos K_n L \left( \frac{y}{L} \right) - \frac{m_o}{m_b} K_n L \sin K_n L \left( \frac{y}{L} \right) \tag{3.316}$$

where  $K_n L = \frac{\omega_n L}{c_L} = \text{nondimensional natural frequency}$

### Frequency Equation

$$\tan K_n L = \frac{K_n L \left[ \frac{m_L}{m_b} + \frac{m_o}{m_b} \right]}{\left[ \frac{m_L m_o}{m_b^2} (K_n L)^2 - 1 \right]} \tag{3.317}$$

The natural frequencies or values of  $\omega_n L / c_L$  which satisfy this transcendental equation can be determined by graphical methods. A plot of the first three natural frequencies, excluding rigid body modes, is shown in nondimensional form in Figure 3.79 as a function of the mass ratios  $m_o / m_b$  and  $m_L / m_b$ . Note that for  $m_o / m_b = \infty$ , and  $m_L / m_b = 0$ , the frequency corresponds to that for the clamped-free beam. This special case and the one following are useful for analyzing longitudinal vibration modes of critical elements of piping systems or other structural systems subjected to longitudinal vibration.

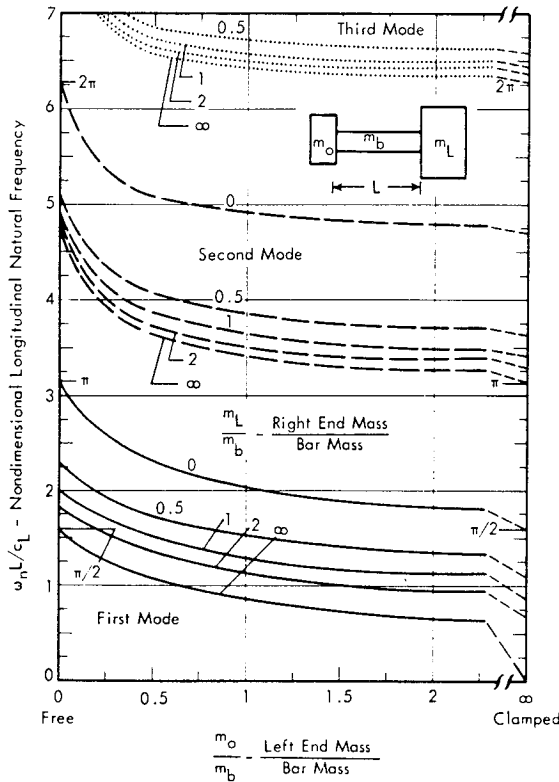
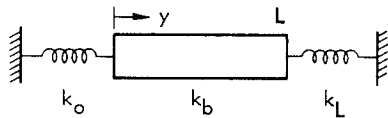


FIGURE 3.79 First Three Natural Frequencies for Longitudinal Vibration of Uniform Bar with Unequal Masses on Each End (Rigid Body Modes Excluded)

• Unequal Spring Loading at Ends of Free-Free Bar



$$k_b = \frac{EA}{L} = \text{static stiffness of bar}$$

Mode Shape (Not Normalized to Unity)

$$\phi_n \left( \frac{y}{L} \right) = \cos K_n L \left( \frac{y}{L} \right) + \frac{k_o}{k_b} \frac{1}{K_n L} \sin K_n L \left( \frac{y}{L} \right) \tag{3.318}$$

Frequency Equation

$$\tan K_n L = \frac{K_n L \left( \frac{k_b}{k_L} + \frac{k_b}{k_o} \right)}{\left[ \frac{k_b^2}{k_o k_L} (K_n L)^2 - 1 \right]} \tag{3.319}$$

where  $K_n L = \omega_n L / c_L =$  nondimensional natural frequency.

This transcendental equation has the identical form as Equation 3.317 if  $k_b/k_L$  is substituted for  $m_L/m_b$  and  $k_b/k_o$  substituted for  $m_o/m_b$ . The natural frequencies

may therefore be determined from Figure 3.79 by making this transformation. For example, for  $k_o/k_b = \infty$  and  $k_L/k_b = 0$ , the corresponding values for  $m_o/m_b$  and  $m_L/m_b$  are 0 and  $\infty$ , respectively. Both cases correspond to a clamped-free bar and, as indicated in Figure 3.79, the natural frequency for the first mode is  $\omega_1 L / c_L = \pi/2$  or  $f_1 = c_L / 4L$  which agrees with the frequency specified for this case.

The boundary conditions for these special cases are defined by treating the force acting on the bar as positive for a compression load which corresponds to a negative strain  $\partial x(y) / \partial y$  (Reference 3.6). The boundary conditions, cited earlier in Table 3.5, are:

Mass Load      Spring Load

At  $y=0$ , Force =  $EA x'(0,t) = +m_o \ddot{x}(0,t)$  or  $+k_o x(0,t)$

At  $y=L$ , Force =  $EA x'(L,t) = -m_L \ddot{x}(L,t)$  or  $-k_L x(L,t)$

Note that the internal force on the beam changes sign from one end to the other. The mode shapes and frequency equation are determined for each case by substituting the general solution for the equation of motion

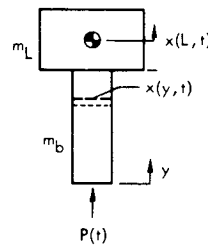
$$x(y,t) = [C \cos Ky + D \sin Ky] e^{j\omega t} \tag{3.320}$$

into the above boundary condition expressions at  $y = 0$  and solving for the ratio of the coefficient D to C. This result is then used with the second boundary condition at  $y=L$  to find the frequency equation (e.g., Equations 3.316-3.319).

Forced Longitudinal Vibration Response of Mass Loaded Bar

As indicated in the previous section, a direct solution for forced response is frequently desirable without resorting to the normal mode approach. Such a case is illustrated in

Figure 3.80 for a mass-loaded bar driven by axial force  $P(t) = P \cos \omega t$ . Since the driving force is applied only at the end, the general solution (Equation 3.320) for free vibration can still be used but with different boundary conditions. These are



At  $y = 0$ , Driving Force,  $EA x'(0,t) = P(t)$

At  $y = L$ , Inertial Force Due to Mass Load,  $EA x'(L,t) = -m_L \ddot{x}(L,t)$

FIGURE 3.80 Mass Loaded Bar Driven Longitudinally at End by Force  $P(t)$

Note that the externally applied force is assumed positive in the direction of compression and results in a negative strain. Applying these boundary conditions to Equation 3.320, a solution is obtained for both of the coefficients C and D in terms of the applied force amplitude P.

Applying the boundary condition at  $y = 0$  to Equation 3.320, the coefficient  $D$  is determined to be

$$D = \frac{P}{EAK}$$

Applying the boundary condition at  $y=L$  to Equation 3.320 and using the above value for  $D$ ,  $C$  becomes

$$C = -\frac{P}{EAK} \left[ \frac{\cos KL - \frac{\omega^2 m_L}{EAK} \sin KL}{\frac{\omega^2 m_L}{EAK} \cos KL + \sin KL} \right]$$

where

$$K = \omega/c_L = 2\pi f/c_L$$

$$E = \text{Modulus of Elasticity Bar}$$

$$m_L = \text{End Mass}$$

Express  $\omega^2 m_L/EAK$  as  $K^2 c_L^2 m_L/EAK = KLE m_L/\rho EAL = KL m_L/m_b$  where  $m_b = \rho AL$  - the mass of the bar. Combining the above to define the axial displacement and taking the second derivative with respect to time to determine acceleration and setting  $y=L$ , the axial acceleration at the mass  $m$ , can be expressed as

$$\ddot{x}(L, t) = \frac{P}{m_L} \left[ \frac{1}{\cos KL + \frac{m_b}{m_L} \frac{\sin KL}{KL}} \right] \cos \omega t \quad (3.321)$$

This equation defines the frequency response function relating the acceleration of the mass to the driving force as a function of frequency  $\omega$ . The frequency is contained in the parameter  $KL = \omega L/c_L$ . Although a normal mode solution is not utilized, the natural frequencies of the system are the frequencies for which the denominator of the term in brackets goes to zero, or

$$\omega_n L/c_L = K_n L \text{ for } \tan K_n L = -\frac{m_L}{m_b} K_n L \quad (3.322)$$

This agrees with the result given by Equation 3.317 for the more general case when the mass  $m_o$  in the latter expression is set to zero.

Note that as frequency approaches zero in Equation 3.321, the right side becomes simply  $P/[m_L + m_b]$  which is the "static" acceleration of the bar and mass load for a steady applied force. However, for illustration of trends in the response function, it is convenient to plot the quantity  $|\ddot{x}(L)|/(P/m_L)$ . This is the ratio of the absolute amplitude of the acceleration at the mass  $m_L$  to the static acceleration  $P/m_L$  which would exist if the force were applied directly to this mass. This is the form plotted in Figure 3.81 as a function of the dimensionless frequency parameter  $KL/2\pi = fL/c_L$  for two different values of the mass ratio  $m_b/m_L$ . Without damping in the system, the response becomes infinite at the natural frequencies given by the values of  $KL$  which satisfy Equation 3.322.

### Maximum Response at Resonance

An estimate of the maximum acceleration response, including material damping effects of the bar, can be made in the following manner.

- Replace  $KL$  by  $KL [1 - j(\eta/2)]$  - this provides an approximation for the effect of material damping in longitudinal vibration where  $\eta$  is the extensional loss factor of the material. The quantity  $j\eta$ , ( $j = \sqrt{-1}$ ) is the ratio of the imaginary (or loss) part of the elastic modulus, to the real (or elastic) part. This will be explained more fully in Section 3.3.7.

- Expand the sine and cosine terms with complex arguments using the approximation that

$$\cos KL \approx \cos KL + jKL \frac{\eta}{2} \sin KL, \text{ and}$$

$$\sin KL \approx \sin KL - jKL \frac{\eta}{2} \cos KL.$$

(This is valid for the lower modes of a typical bar-type structure with loss factors of the order of 0.05 or less where  $KL \eta/2 < 0.5$ .)

- Assume, as usual, that the undamped and damped natural frequencies are essentially the same so that the relationship given by Equation 3.321 for  $KL$  at resonance can be used.

Making these substitutions in Equation 3.321, a close approximation for the absolute value of the maximum response amplitude at resonance becomes

$$\left| \frac{\ddot{x}(L)}{P/m_L} \right|_{\max} \approx \left[ \frac{(2/\eta) K_n L}{(K_n L)^2 + \left(\frac{m_b}{m_L}\right)^2 + \frac{m_b}{m_L}} \right] \frac{1}{\sin K_n L} \quad (3.323)$$

where

$K_n L = \omega_n L/c_L$  - the value of  $KL$  at resonance. (These may be determined, for the first two natural frequencies, by the ordinate values in Figure 3.79 for  $m_o/m_b = 0$ .)

Since  $K_n L = \omega_n L/c_L \approx (2n-1)\pi/2$  for  $m_L > m_b$ , which is the usual case for practical situations of interest, then  $\sin K_n L \approx \pm 1$ . The absolute value of the maximum response at resonance is, then, approximately equal to the term in brackets. This expression indicates two aspects of the forced longitudinal response when damping is caused by losses in the bar material.

- The apparent damping will tend to increase at higher mode numbers as  $K_n L$  increases. This can be interpreted as a measure of the loss in vibration energy transmitted from one end of the bar to the other.
- Damping decreases for low values of  $m_b/m_L$ . This is logical since the bar is the only source of damping included in the system.

The maximum response amplitude predicted by Equation 3.323 is shown by data points in Figure 3.81 for the case  $\eta = 0.02$  - a typical value for a material loss factor, corresponding to a Q of 50. For practical situations, involving longitudinal vibration of "bars," such as a pipe system terminated in a large valve, joint damping and friction damping would be present so that Equation 3.323 may be considered as an upper bound for the maximum response.

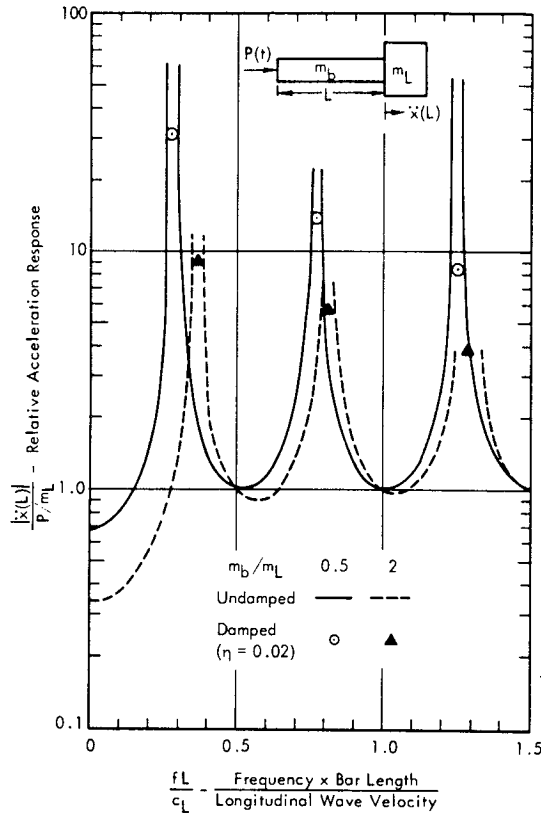


FIGURE 3.81 Acceleration Response at End of Mass-Loaded Bar Driven by Sinusoidal Axial Force  $P(t)$  Expressed as Ratio of Acceleration Amplitude at End of Beam to "Static" Acceleration  $P/m_L$  for Two Values of Bar to Load Mass Ratio. Data points indicate maximum response at resonance for beam with material damping defined by the loss factor  $\eta \approx 1/Q$ .

Minimum Response at Anti-Resonance

Between the resonance frequencies, the acceleration response function tends to reach a minimum near  $KL \approx n\pi$  for  $n = 1, 2, \text{ etc.}$  The acceleration response function given by Equation 3.321 then reduces to

$$\left| \frac{\ddot{x}(L)}{P/m_L} \right|_{\min} \approx 1 \tag{3.324}$$

This is apparent in Figure 3.81 indicating that an approximate lower bound for the acceleration transmitted to the mass load is simply the "static" acceleration for the load driven directly by the applied force.

Although restricted to a relatively simple case, the two expressions given by Equations 3.323 and 3.324 provide a reasonable basis for estimating the upper and lower bounds for response of a mass-loaded bar driven by an axial force.

Transmissibility Response for a Mass-Loaded Bar

For a longitudinal acceleration input, it is only necessary to change the input boundary condition to

$$x(0, t) = -\ddot{x}_0(t)/\omega^2$$

where  $\ddot{x}_0(t)$  is an input sinusoidal acceleration at  $y = 0$ .

The ratio of acceleration amplitude at the mass-loaded end  $x(L, t)$  to this input acceleration amplitude (i.e., the transmissibility) can then be shown to be

$$\frac{\ddot{x}(L)}{\ddot{x}_0} = \frac{1}{\cos KL - \frac{m_L}{m_b} KL \sin KL} \tag{3.325}$$

where  $KL = 2\pi fL/c_L$ .

In this case, the resonance frequencies occur when  $\cos KL = (m_L/m_b) KL \sin KL$  so that maximum transmissibility for a motion input to a mass-loaded bar occurs for  $\omega_n L/c_L = K_n L$  where

$$\cot K_n L = \frac{m_L}{m_b} K_n L$$

This has been evaluated in Figure 3.82 for the case of  $m_L/m_b = 2$ . The equivalent transmissibility obtained for a lumped mass-spring system is also shown. The frequency scale is normalized by the resonance frequency  $f_0$  of the

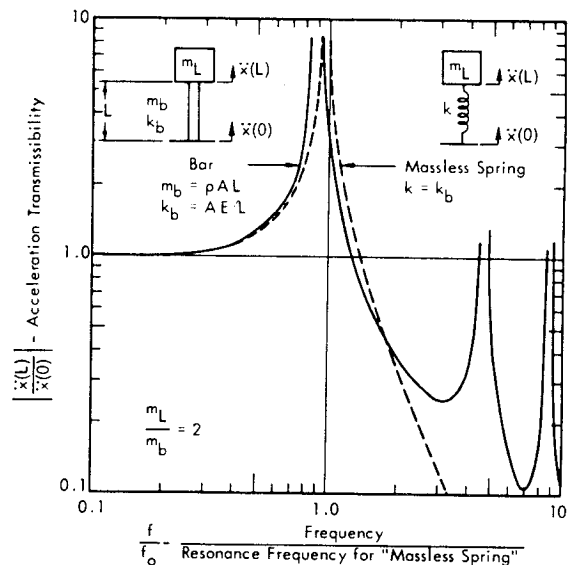


FIGURE 3.82 Acceleration Transmissibility for Mass-Loaded Bar Driven by Sinusoidal Axial Acceleration  $\ddot{x}(0, t)$  Compared to Transmissibility for Massless Spring with Same Stiffness

mass load  $m_L$  on a weightless spring which has the same static stiffness  $k = EA/L$  as the bar. This figure illustrates the effect of longitudinal wave motion in a spring which tends to limit the isolation provided by standard vibration mounts (Reference 3.1, Chapter 30). Further practical details of this effect are considered in Chapters 9 and 11.

The approximate upper bound for the transmissibility at the longitudinal resonances can be determined in the same manner as before by including material damping. The result is

$$\left| \frac{\ddot{X}(L)}{\ddot{X}_o} \right|_{\max} \approx \frac{(2/\eta) m_b/m_L}{[(K_n L)^2 + (m_b/m_L)^2 + 1]} \frac{1}{\cos K_n L} \quad (3.326)$$

where  $K_n L$  is the value of  $\omega_n L/c_L$  at the longitudinal resonance and  $\eta$  is the extensional loss factor of the bar material.

The lower bound for the transmissibility occurs at the anti-resonance frequencies  $\omega_{an}$  and is approximately equal to

$$\left| \frac{\ddot{X}(L)}{\ddot{X}_o} \right|_{\min} \approx \frac{m_b}{m_L} \frac{c_L}{\omega_n L} \quad \text{for } m_L > m_b \quad (3.327)$$

where

$$\frac{\omega_{an} L}{c_L} \approx \frac{2n-1}{2} \pi \quad \text{at the anti-resonance frequencies for } m_L > m_b.$$

(It is worth noting that these minimum values of response given by Equations 3.324 and 3.327 would be more difficult to determine had a normal mode analysis method been used. It would have been necessary to include cross mode coupling terms in the latter to obtain accurate results at these points of minimum anti-resonant response.)

#### Summary of Response Characteristics for Sinusoidal Longitudinal Vibration of Mass and Stiffness Loaded Bars

The same methods applied to analyze the forced response and transmissibility for an axially-driven mass-loaded bar can also be applied to stiffness loaded bars. A unified summary of these characteristics for both cases is given in Table 3.6. The various response functions are given in terms of a load parameter  $\alpha = m_b/m_L$  or  $k_L/k_b$ . The general trend in these response characteristics for force or motion excitation has been illustrated in Figures 3.81 and 3.82. Note that the response characteristics for force input to a mass-loaded bar are identical to those for motion input to spring-loaded bar.

#### Example

Consider the case of a 3-inch diameter, 10-foot steel bar driven by a 50-pound peak sinusoidal force at the free end and loaded at the other end by a 500-pound weight. Find the first two natural frequencies and peak acceleration of the mass for excitation of the bar at these frequencies. Assume the loss factor for the bar material is taken as 0.01:

#### Longitudinal Wave Velocity (From Table 3.39)

$$c_L = 16,820 \text{ ft/sec} \approx 2 \times 10^5 \text{ in/sec}$$

#### Bar Weight

$$m_b g = \rho_w A L = (.3) \frac{(3.14) (3)^2}{4} (120) = 254 \text{ lb}$$

#### Mass Ratio

$$m_L g / m_b g = 500/254 \approx 2$$

Resonance Frequency - From Figure 3.79 for  $m_o = 0$  and  $m_L/m_o = 2$

$$\omega_1 L/c_L = 1.82 \quad \therefore f_1 = (1.82) (2 \times 10^5) / (6.28) (120) = 484 \text{ Hz}$$

$$\omega_2 L/c_L = 4.8 \quad \therefore f_2 = 1270 \text{ Hz}$$

Maximum Acceleration at Resonance (From Equation 3.323)

$$\left| \frac{\ddot{X}(L) m_L}{P} \right|_{\max} = \frac{(2/\eta) K_1 L}{(K_1 L)^2 + (m_b/m_L)^2 + (m_b/m_L)} \frac{1}{\sin K_1 L}$$

For

$$\eta = 0.01$$

$$K_1 L = \omega_1 L/c_L = 1.82, \quad \sin K_1 L = 0.969$$

$$m_b/m_L = 0.5 \quad P = 50 \text{ lb}$$

$$m_L g = 500 \text{ lb}$$

$$\text{At } f_1, \left| \frac{\ddot{X}(L)}{g} \right|_{\max} = 9.2 \text{ g peak at } 484 \text{ Hz}$$

Similarly, for  $f_2$ ,  $K_2 L = \omega_2 L/c_L = 4.8$

$$\text{At } f_2, \left| \frac{\ddot{X}(L)}{g} \right|_{\max} = 4.1 \text{ g peak at } 1270 \text{ Hz}$$

#### Shock Response of Uniform Bars for Transient Axial Loads

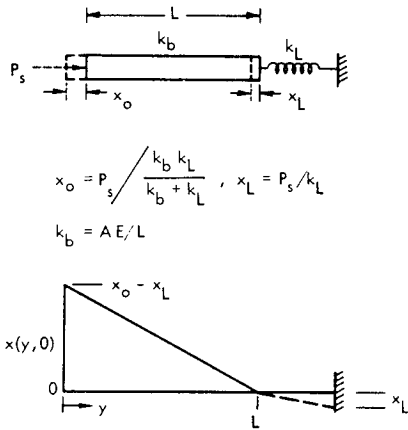
Transient axial loads are commonly encountered in rocket test facilities on such items as hold-down arms, hydraulic systems, etc. Two common forms for such situations are

- Transient response due to the sudden release of a static preload, and
- Transient response due to the sudden application of a load.

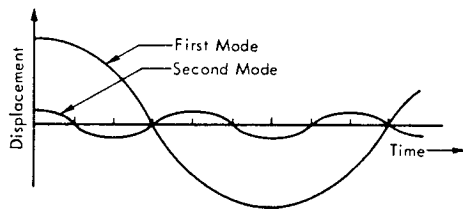
For the first type of transient load, a normal mode approach now becomes convenient (Reference 3.5). Methods for analyzing the free transient vibration of a lumped-parameter multi-degree of freedom system with finite initial conditions may be applied to continuous structure (see Section 3.3.2.9, page 3-59).

**Example**

As an example, consider the case illustrated in Figure 3.83 of a uniform bar with stiffness  $k_b = EA/L$  attached to a rigid foundation by a lumped spring  $k_L$ . The transient displacement of the free end of the undamped bar, upon sudden release of a preload  $P_s$ , can be determined by the following procedure.



a) Initial Displacement of Bar Attached to a Rigid Foundation by Lumped Spring and Under Static Axial Load



b) Typical Time History of Free-Free Vibration at End of Bar After Release of Preload

FIGURE 3.83 Free Transient Vibration of Bar for Initial Axial Displacement

- Use Equation 3.205, page 3-59 to define the transient vibration of a multi-modal system. For zero initial velocity, the motion of the bar may be given by the summation over the normal modes as

$$x(y, t) = \sum_n^N \phi_n(y) \bar{q}_n \cos(\omega_n t)$$

where  $\phi_n(y)$  = mode shape for free vibration of bar  
 $= \cos K_n L (y/L)$

where  $K_n L = \omega_n L / c_L$  = nondimensional natural frequency for free transient vibration of bar with one end free and other end attached to lumped spring.

$\bar{q}_n$  = amplitude of normal coordinate of nth mode.

- Determine  $\omega_n L / c_L$  as roots of  $\cot K_n L = (k_L / k_b) K_n L$ . (These can be obtained from Figure 3.79 by replacing  $K_n L / k_b$  by  $m_b / m_L$  and reading the values of  $\omega_n L / c_L$  from the right hand side of the graph where  $m_o / m_b = \infty$ . As a first approximation, for  $k_L / k_b \gg 1$ , use  $K_n L = \omega_n L / c_L = (2n-1) \pi / 2$ ,  $n = 1, 2$ , etc.
- Determine  $\bar{q}_n$  from Equations 3.206 and 3.204, page 3-59, modified for continuous structure. For zero initial velocity, this gives

$$\bar{q}_n = q_{no} = \frac{\rho A}{M_n} \int_0^L x(y, 0) \cos K_n L \left( \frac{y}{L} \right) dy$$

where

$\rho A$  = mass per unit length of bar

$M_n$  = generalized mass of bar

$x(y, 0)$  = initial static deflection of bar as a function of  $y$  (see Figure 3.83a).

For the case of  $k_L = \infty$  (rigid support at end of bar, this integral will give, for an initial static deflection equal to  $x(y, 0) = X_o (1 - y/L)$ ,

$$\bar{q}_n = \frac{\rho A L}{M_n} \cdot \left[ \frac{2}{2n-1} \cdot \frac{1}{\pi} \right]^2 X_o$$

The first term  $\rho A L / M_n$  is the ratio of the bar mass to the generalized mass and is equal to 2 for a rigid foundation, so that

$$\bar{q}_n = \frac{8}{\pi^2} X_o, \quad \frac{8}{9\pi^2} X_o, \quad \frac{8}{25\pi^2} X_o$$

for  $n = 1, 2, 3$ , etc.

For the first natural mode, the displacement at the free end ( $y = 0$ ) will then be

$$x(0, t) = \frac{8}{\pi^2} X_o \cos \frac{\pi}{2} \frac{c_L}{L} t$$

where  $X_o$  = initial deformation (for  $k_L = \infty$ )

$c_L$  = longitudinal wave velocity ( $\approx 2 \times 10^5$  in./sec for most metals)

A typical time history of the displacement for the first two modes is illustrated in Figure 3.83b.

- Add any significant rigid body motion for vibration of a rigid bar with mass  $\rho A L$  on a finite foundation spring.

This illustrates the typical situation for free vibration of a multi-degree of freedom system due to an initial displacement - the principal transient displacement is in the first mode. However, the acceleration will increase as the square of the mode number, so that at the end of the bar, the amplitude of the acceleration in each mode would be, for  $\omega_n L / c_L = (2n - 1) \pi / 2$ ,

$$\dot{q}_n = \omega_n^2 a_n = 2 \left(\frac{c_L}{L}\right)^2 X_o - \alpha \text{ constant independent of mode number.}$$

This illustrates the typical result observed for transient longitudinal vibration in bars; high accelerations are developed at high frequencies.

For transient applied forces, the longitudinal vibration response of continuous structural elements can be carried out by either of the following methods.

- Apply Fourier or Laplace Transform techniques using the sinusoidal frequency response functions defined in Table 3.6. (See Sections 3.2.2.4-3.2.2.7.)
- Use the normal mode and graphical analysis techniques, discussed in Section 3.3.3.3, for analyzing the forced transient response of lumped parameter systems. As before, summations over lumped masses are replaced by integrals over the element.

The normal mode shapes and relative generalized masses which would be applicable for this latter approach are summarized as follows:

Normal Mode Shapes for Axial Excitation of Bars Loaded by a Mass or Stiffness at End Opposite to Input Excitation

Force Excitation or Free Vibration with Finite Initial Conditions

$$\phi_n(y) = \cos K_n L \left(\frac{y}{L}\right)$$

Motion Excitation

$$\phi_n(y) = \sin K_n L \left(\frac{y}{L}\right)$$

Natural Frequencies - (See third row in Table 3.6)

Generalized Mass

$$M_n = m_b \int_0^L \phi_n^2(y) dy$$

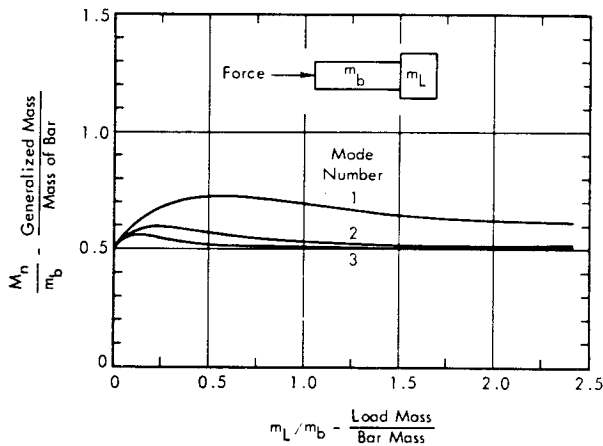


FIGURE 3.84 Generalized Mass for Normal Modes of Mass Loaded Bar Excited by Axial Force

For mass-loaded bars, the generalized mass of the combined system will be significantly different from 1/2 the bar mass for only the lower modes of vibration as indicated in Figure 3.84. For motion excitation, the generalized mass ratio for the first mode is somewhat greater than indicated in Figure 3.84. In this case, the normal modes excited correspond to those of a clamped-free bar while for force excitation and free vibration, the modes excited correspond to free-free modes.

3.3.5.3 Torsional Vibration of Bars

As shown by Equation 3.305 and Table 3.4, pages 3-108 and 109, the equation of motion for free torsional vibration of uniform bars can be written as

$$\rho J \ddot{\theta}(y, t) = K_r G \theta''(y, t)$$

or as

$$\ddot{\theta}(y, t) = c_s^2 \theta''(y, t) \tag{3.328}$$

where

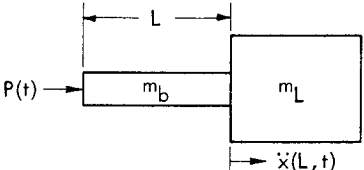
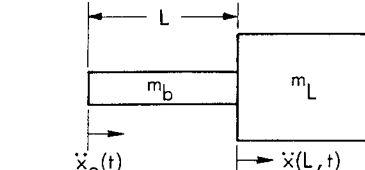
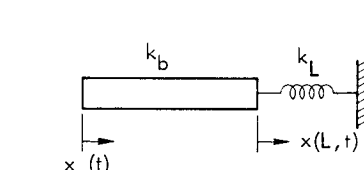
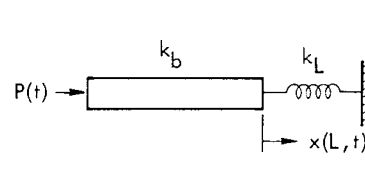
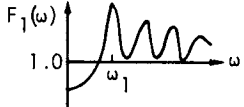
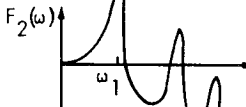
- $\theta$  = angular displacement
- $\rho$  = mass density
- $J$  = polar moment of inertia of cross section
- $G$  = shear modulus
- $c_s$  = shear wave velocity
- $K_r$  =  $\begin{cases} = \text{torsional constant (or torsion factor)} \\ = J \text{ for circular sections.} \end{cases}$

This equation is identical in form to the plane wave equation for longitudinal vibration in bars (Equation 3.315). Thus, all of the concepts for free and forced vibration developed for the latter are fully applicable to torsional vibration of bars if the following substitutions are made:

	<u>Longitudinal Vibration</u>	<u>Torsional Vibration</u>
Displacement	$x(y, t)$	$\rightarrow \theta(y, t)$
Inertia/Length	$\rho A$	$\rightarrow \rho J$
Stiffness/Length	$EA$	$\rightarrow K_r G$
Wave Velocity	$c_L = \sqrt{E/\rho}$	$\rightarrow c_s = \sqrt{K_r G/J\rho}$ (Shear)
Spring Constant	$k = AE/L$	$\rightarrow k_r \begin{cases} = K_r G/L - \text{Any Section} \\ = JG/L - \text{Circular Bars or Pipes} \\ \approx A^4 G/4\pi^2 JL - \text{Any Solid Section Without Reentrant Angles} \end{cases}$
Axial Load	$P(t)$	$\rightarrow M(t)$ Moment
Inertial Load	$m$	$\rightarrow I_m$ - Mass Moment of Inertia
Spring Load	$k$	$\rightarrow k_r$ - Torsional Spring Constant

TABLE 3.6

SUMMARY OF FORCED RESPONSE AND TRANSMISSIBILITIES FOR MASS AND SPRING LOADED UNIFORM BARS DRIVEN LONGITUDINALLY BY SINUSOIDAL FORCE OR MOTION EXCITATION

<p>Load Parameter</p> $\alpha = m_b/m_L$ $m_b = \rho AL$		
$\alpha = k_L/k_b$ $= k_b = EA/L$		
<p>Equation for Resonance Frequency</p> $K_n L = \omega_n L / c_L$ $c_L = \sqrt{E/\rho}$	$\tan K_n L = -\frac{K_n L}{\alpha}$ $\omega_n L \left. \begin{array}{l} \approx \frac{2n-1}{2} \pi, \alpha \ll 1 \\ \approx n\pi, \alpha \gg 1 \end{array} \right\}$	$\cot K_n L = +\frac{K_n L}{\alpha}$ $\omega_n L \left. \begin{array}{l} \approx n\pi, \alpha \ll 1 \\ \approx \frac{2n-1}{2} \pi, \alpha \gg 1 \end{array} \right\}$
<p>Forced Response</p> <p>Mass Load</p> <p>Spring Load</p>	$\left. \begin{array}{l} \frac{\dot{x}(L, t)}{P(t)/m_L} \\ \frac{x(L, t)}{x_o(t)} \end{array} \right\} = F_1(KL, \alpha)$	$\left. \begin{array}{l} \frac{\dot{x}(L, t)}{\dot{x}_o(t)} \\ \frac{x(L, t)}{P(t)/k_b} \end{array} \right\} = F_2(KL, \alpha)$
<p>Frequency Response Equation (Zero Damping)</p>	$F_1(KL, \alpha) = \frac{1}{\left[ \cos KL + \alpha \frac{\sin KL}{KL} \right]}$	$F_2(KL, \alpha) = \left[ \frac{1}{\cos KL - \frac{KL}{\alpha} \sin KL} \right]$
<p>Maximum Damped Response at Resonance</p> <p>(<math>\eta = \text{Loss Factor} \ll 1</math>)</p>	$F_1 _{\max} \approx \frac{(2/\eta) K_n L}{[(K_n L)^2 + \alpha^2 + \alpha]} \frac{1}{\sin K_n L}$	$F_2 _{\max} \approx \frac{(2/\eta) \alpha}{[(K_n L)^2 + \alpha^2 + 1]} \cos K_n L$
<p>Minimum Response at Anti-Resonance Frequencies</p> <p><math>\omega_{an}</math></p>	$F_1 _{\min} \approx 1, \omega > \omega_1$ $\text{at } \omega_{an} L / c_L \approx \begin{cases} n\pi, \alpha \ll 1, n = 1, 2 \\ (2n-1)\pi/2, \alpha \gg 1 \end{cases}$	$F_2 _{\min} \approx \alpha c_L / \omega_{an} L$ $\text{at } \omega_{an} L / c_L \approx \begin{cases} (2n-1)\pi/2, \alpha \ll 1 \\ n\pi, \alpha \gg 1 \end{cases}$
<p>Typical Response Curve</p>	 <p>See Figure 3.81</p>	 <p>See Figure 3.82</p>



A table of torsional spring constants  $k_r$  and polar moments of inertia  $J$  is given in Table 3.24 at the end of this chapter. Values for the torsional constant  $K_r$  may be determined from this table by computing  $K_r = k_r L/G$ . The torsional constant  $K_r$  for most standard structural cross sections is also listed in standard handbooks. (It is frequently identified by the symbol  $J$  and should not be confused with the usage in this manual where  $J$  is polar moment of inertia for any section.) The polar moment of inertia  $J$  is the sum of the two orthogonal moments of inertia  $I_x$  and  $I_y$  about axes in the plane of the section. These values are also readily available in standard structural design handbooks.

The natural frequencies for torsional vibration of circular section bars will be equal to the ratio  $\sqrt{G/E}$  times the corresponding longitudinal natural frequencies for a given bar. For common metals,  $\sqrt{G/E} = \sqrt{1/2(1+\nu)} \approx 0.62$ . For open section beams or angle section, the ratio of torsional to longitudinal frequencies for the same boundary conditions will generally be much less than this factor due to the reduced torsional stiffness of such sections relative to their axial stiffness.

### 3.3.5.4 Lateral Vibration of Beams

Based on Equation 3.305 and the definition of the mass and stiffness terms for free lateral vibration of uniform beams, given in Table 3.4, the equation of motion for such vibration is conveniently given in the following form, using (') and (·) to signify partial differentiation with respect to  $y$  and  $t$ , respectively.

$$EI x''''(y,t) + \rho A \ddot{x}(y,t) = 0 \quad (3.329)$$

where  $EI$  = Bending Stiffness per unit length

$\rho A$  = Mass per unit length.

This equation is derived from the Bernoulli-Euler theory for flexure of beams which assumes that plane sections of the beam remain plane in bending and the radius of curvature of the deflected beam is large compared to the beam depth (References 3.5 and 3.34). This amounts to neglecting effects of shear deformation rotary inertia forces. For most engineering problems dealing with beam vibration, these assumptions are acceptable. The general solution to this equation defines the natural modes of vibration as the infinite series of normal mode solutions, or

$$x(y,t) = \sum_n^N q_n(t) \phi_n(y)$$

where

$q_n(t)$  = Normal coordinate defining time varying amplitude of  $n$ th mode, and

$\phi_n(y)$  = Mode shape for  $n$ th mode given in general form by Equation 3.310, page 3-111.

By carrying out the steps outlined in Section 3.3.5.1, expressions for the mode shape  $\phi_n(y)$ , frequency equation, natural frequencies  $\omega_n$  and generalized mass can be determined for any boundary condition. Detailed derivations are given in most texts on structural vibration and acoustics (see, for example, References 3.2, 3.5, 3.6 and 3.34).

As an example, consider the case of a clamped-clamped beam. Let the free harmonic vibration in the  $n$ th normal mode be expressed as

$$x_n(y,t) = \bar{q}_n \phi_n(y) e^{j\omega_n t}$$

where

$$\phi_n(y) = A [\cosh K_n y + \cos K_n y] + B [\cosh K_n y - \cos K_n y] \\ + C [\sinh K_n y + \sin K_n y] + D [\sinh K_n y - \sin K_n y]$$

$\bar{q}_n$  = modal amplitude

$\omega_n$  = natural frequency of  $n$ th normal mode

$K_n = \omega_n / c_B$  = wave number for  $n$ th mode.

Substituting  $x_n(y,t)$  into Equation 3.329 gives

$$[EI \phi_n''''(y) - \omega_n^2 \rho A \phi_n(y)] \bar{q}_n e^{j\omega_n t} = 0$$

where the quantity in brackets is an ordinary differential equation in  $y$  only which is satisfied by the general expression for the mode shape  $\phi_n(y)$  given above.

Now apply the four boundary conditions for this case, as defined in Table 3.5, page 3-113.

- 1) Displacement = 0 at  $y = 0$  or  $\phi_n(0) = 0$
- 2) Slope = 0 at  $y = 0$  or  $\phi_n'(0) = 0$
- 3) Displacement = 0 at  $y = L$  or  $\phi_n(L) = 0$
- 4) Slope = 0 at  $y = L$  or  $\phi_n'(L) = 0$

Substituting  $\phi_n(y)$  into these boundary conditions gives

- 1)  $A(1+1) + B(1-1) + C(0+0) + D(0-0) = 0$   
or  $A = 0$
- 2)  $K_n B [0+0] + K_n C [1+1] + K_n D [1-1] = 0$   
or  $C = 0$
- 3)  $B [\cosh K_n L - \cos K_n L] + D [\sinh K_n L - \sin K_n L] = 0$
- 4)  $K_n B [\sinh K_n L + \sin K_n L] + K_n D [\cosh K_n L - \cos K_n L] = 0$

Solving these last two equations simultaneously, the ratio  $D/B$  and the frequency equation for  $K_n L$  are obtained as

$$\frac{D}{B} = - \frac{\cosh K_n L - \cos K_n L}{\sinh K_n L - \sin K_n L}, \text{ and}$$

Frequency Equation  $\cos K_n L \cosh K_n L = 1$

The infinite number of discrete values of  $K_n L$  which satisfy the last equation define the natural frequencies of the clamped-clamped beam. From these values, the ratio  $D/B$  can be determined for each mode and the un-normalized mode shape determined. Dividing through by the maximum value  $A_n$  for each mode, the normalized mode shape is specified as

$$\phi_n(y) = A_n [\cosh K_n L \bar{y} - \cos K_n L \bar{y} - \sigma_n (\sinh K_n L \bar{y} - \sin K_n L \bar{y})]$$

where

$\bar{y} = y/L$  - relative position on beam

$\sigma_n = D/B A_n$  - normalized ratio of  $D/B$ .

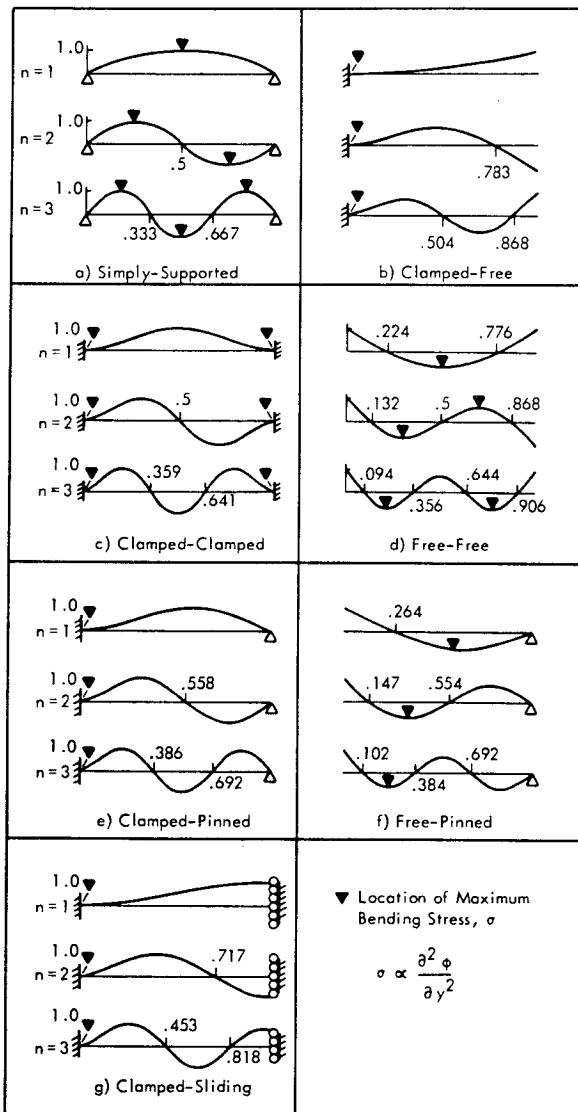


FIGURE 3.85 Mode Shapes, Location of Node Points and Locations of Maximum Stress for First Three Modes for Lateral Vibration of Uniform Beams

The generalized Mass  $M_n$  for the nth mode is then found using this expression in Equation 3.311, page 3.112, with the corresponding value of  $K_n L$ .

Following the same procedure, the well known solutions obtained for uniform beams with common ideal boundary conditions are summarized below. Mode shapes are normalized to a maximum value of unity in all cases by multiplying the mode shape expression, as necessary, by the normalizing constant  $A_n$ . Mode shapes for the cases considered are plotted in Figure 3.85 along with the location of node points and location of the maximum bending stress. The following parameters are defined for all cases.

- Mode Shape in terms of  $K_n L \bar{y}$

where  $K_n L = \omega_n L / c_B = 2\pi L / \lambda_{Bn}$

= dimensionless frequency parameter

$c_B =$  Bending Wave Velocity at  $\omega_n$   
 $= \sqrt{\omega_n [EI/\rho A]}^{1/4}$

$\lambda_{Bn} =$  Bending Wavelength

$\bar{y} = y/L$  - relative position on beam.

- Frequency Equation in terms of  $K_n L$
- Natural Frequencies - roots of frequency equations in terms of  $K_n L$ , or

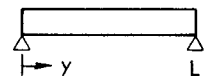
$$f_n L^2 \sqrt{\frac{EI}{\rho A}} = (K_n L)^2 / 2\pi, \text{ or } L/\lambda_{Bn} = K_n L / 2\pi$$

- Generalized Mass

$$M_n = m_b \int_0^L \phi_n^2 \bar{y} d\bar{y}$$

where  $m_b = \rho A L$  - mass of uniform beam.

SIMPLY-SUPPORTED (PINNED) BEAM



- Mode Shape (See Figure 3.85a)

$$\phi_n(y) = \sin K_n L \bar{y}$$

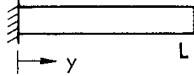
- Frequency Equation -  $\sin K_n L = 0$
- Natural Frequencies

n	$K_n L$	$f_n L^2 \sqrt{EI/\rho A}$	$L/\lambda_{Bn}$
1	$\pi$	$\pi/2$	1/2
Any n	$n\pi$	$n^2 \pi/2$	$n/2$

- Generalized Mass

$$M_n = \frac{1}{2} m_b$$

**CLAMPED-FREE (CANTILEVERED) BEAM**



- Mode Shape - Normalized to Unit Maximum Value (See Figure 3.85b)

$$\phi_n(y) = \frac{1}{2} [\cosh K_n L \bar{y} - \cos K_n L \bar{y} - \sigma_n (\sinh K_n L \bar{y} - \sin K_n L \bar{y})]$$

$$\sigma_1 = 0.734, \quad \sigma_2 = 1.018, \quad \sigma_3 = 0.999, \quad \sigma_n (n > 3) = 1$$

- Frequency Equation

$$\cos K_n L \cosh K_n L = -1$$

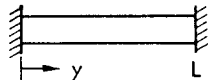
- Natural Frequencies

n	$K_n L$	$f_n L^2 / \sqrt{EI/\rho A}$	$L/\lambda_{Bn}$
1	1.875	0.560	0.299
2	4.694	3.507	0.747
3	7.855	9.819	1.250
$n > 3$	$(n - \frac{1}{2})\pi$	$(n - \frac{1}{2})^2 \pi/2$	$(n - \frac{1}{2})/2$

- Generalized Mass

$$M_n = \frac{1}{4} m_b$$

**CLAMPED-CLAMPED (BUILT-IN) BEAM**



- Mode Shape (See Figure 3.85c)

$$\phi_n(\bar{y}) = A_n [\cosh K_n L \bar{y} - \cos K_n L \bar{y} - \sigma_n (\sinh K_n L \bar{y} - \sin K_n L \bar{y})]$$

n	$A_n$	$\sigma_n$
1	0.630	0.982
2	0.663	1.001
3	0.661	1.000-
$n > 3$	0.661	1.000

- Frequency Equation

$$\cos K_n L \cosh K_n L = 1$$

- Natural Frequencies

n	$K_n L$	$f_n L^2 / \sqrt{EI/\rho A}$	$L/\lambda_{Bn}$
1	4.730	3.561	0.753
2	7.853	9.815	1.250+
3	10.996	19.242	1.750
$n > 3$	$\sim (n + \frac{1}{2})\pi$	$\sim (n + \frac{1}{2})^2 \pi/2$	$\sim (n + \frac{1}{2})/2$

- Generalized Mass

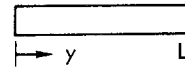
$$M_1 = 0.396 m_b$$

$$M_2 = 0.439 m_b$$

$$M_3 = 0.437 m_b$$

$$M_n = 0.437 m_b, \quad n > 3$$

**FREE-FREE BEAM**



- Mode Shape (See Figure 3.85d)

$$\phi_n(\bar{y}) = \frac{1}{2} [\cosh K_n L \bar{y} + \cos K_n L \bar{y} - \sigma_n (\sinh K_n L \bar{y} + \sin K_n L \bar{y})]$$

- $\sigma_n$

- Frequency Equation

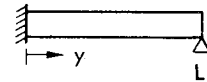
- Natural Frequencies

Same as for Clamped-Clamped Beam

- Generalized Mass

$$M_n = \frac{1}{4} m_b$$

**CLAMPED-PINNED BEAM**



- Mode Shape (See Figure 3.85e)

$$\phi_n(\bar{y}) = A_n [\cosh K_n L \bar{y} - \cos K_n L \bar{y} - \sigma_n (\sinh K_n L \bar{y} - \sin K_n L \bar{y})]$$

n	$A_n$	$\sigma_n$
1	0.663	1.001
2	0.661	1.000+
$n > 2$	0.661	$\sim 1.0$

- Frequency Equation

$$\tan K_n L = -\tanh K_n L$$

- Natural Frequencies

n	$K_n L$	$f_n L^2 / \sqrt{EI/\rho A}$	$L/\lambda_{Bn}$
1	3.927	2.454	0.625
2	7.069	7.952	1.125
$n > 2$	$(n + \frac{1}{4})\pi$	$(n + \frac{1}{4})^2 \pi/2$	$(n + \frac{1}{4})/2$

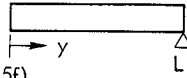
- Generalized Mass

$$M_1 = 0.439 m_b$$

$$M_2 = 0.437 m_b$$

$$M_n = 0.437 m_b, \quad n > 2$$

**FREE-PINNED BEAM**



- Mode Shape (See Figure 3.85f)

$$\phi_n(\bar{y}) = \frac{1}{2} \left[ \cosh K_n L \bar{y} + \cos K_n L \bar{y} - \sigma_n (\sinh K_n L \bar{y} + \sin K_n L \bar{y}) \right]$$

- $\sigma_n$
  - Frequency Equation
  - Natural Frequencies
  - Generalized Mass
- } Same as for Clamped-Pinned Beam; plus a rigid body mode at zero frequency

$$M_n = \frac{1}{4} m_b$$

- Frequency Equation

$$\cos K_n L = 0$$

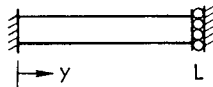
- Natural Frequencies

n	$K_n L$	$f_n L^2 / \sqrt{EI/\rho A}$	$L/\lambda_{Bn}$
1	$\pi/2$	$\pi/8$	1/4
Any n	$(n - \frac{1}{2})\pi$	$(n - \frac{1}{2})^2 \pi/2$	$(n - \frac{1}{2})/2$

- Generalized Mass

$$M_n = \frac{1}{2} m_b$$

**CLAMPED-GUIDED BEAM**



- Mode Shape (See Figure 3.85g)

$$\phi_n(\bar{y}) = A_n \left[ \cosh K_n L \bar{y} - \cos K_n L \bar{y} - \sigma_n (\sinh K_n L \bar{y} - \sin K_n L \bar{y}) \right]$$

n	$A_n$	$\sigma_n$
1	0.630	0.982
2	0.661	1.000-
$n > 2$	$\sim 0.661$	$\sim 1.000$

- Frequency Equation

$$\tan K_n L = -\tanh K_n L$$

- Natural Frequencies

n	$K_n L$	$f_n L^2 / \sqrt{EI/\rho A}$	$L/\lambda_{Bn}$
1	2.365	0.890	0.376
2	5.498	4.809	0.875-
$n > 2$	$\sim (n - \frac{1}{4})\pi$	$(n - \frac{1}{4})^2 \pi/2$	$(n - \frac{1}{4})/2$

- Generalized Mass

$$M_1 = 0.396 m_b$$

$$M_2 = 0.437 m_b$$

$$M_n = 0.437 m_b, \quad n > 2$$

A more detailed listing of natural frequencies for lateral vibration of single and multiple uniform beams is given in Tables 3.27 and 3.28 at the end of this chapter. The frequency is specified in a simpler form using the following transformation

$$f_n = \frac{(K_n L)^2}{2\pi L^2} \sqrt{\frac{E}{\rho} \frac{I}{A}} = \frac{(K_n L)^2}{2\pi} \frac{r}{L^2} c_L$$

where

$$r = \sqrt{I/A} = \text{radius gyration of cross section}$$

$$c_L = \sqrt{E/\rho} = \text{longitudinal wave velocity (or speed of sound in bar)}$$

$$K_n L = \text{nth root of frequency equation.}$$

By using a typical value for  $c_L$  of  $2.02 \times 10^5$  in/sec for steel, this can be given as

$$f_n = C_n \frac{r}{L^2} \times 10^4 \times K_m$$

where

$$C_n = \frac{(K_n L)^2}{2\pi} c_{L \text{ steel}} \times 10^{-4} - \text{a frequency constant for steel beams}$$

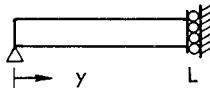
$$K_m = \frac{c_{L \text{ material}}}{c_{L \text{ steel}}} - \text{a material constant equal to ratio of longitudinal wave velocities in given material and steel.}$$

Values of the material constant  $K_m$  are listed in Table 3.39.

**Effect of Rotary Inertia and Shear Forces**

For a beam whose length is small compared to its radius of gyration, a refined theory is required to account for finite rotary inertia effects of each plane section of the beam about its centroidal bending axis. In addition, finite shearing forces exist which tend to distort the cross section

**PINNED-GUIDED BEAM**



- Mode Shape (Equivalent to 1/2 of Pinned-Pinned Beam Vibrating in Odd Modes)

$$\phi_n(\bar{y}) = \sin K_n L \bar{y}$$

of the beam in bending. The Timoshenko beam theory accounts for these effects in a more exact equation of motion for lateral vibration of beams (Reference 3.5). The resulting equation is

$$EI x''''(y, t) + \rho A \ddot{x}(y, t) - \rho I \left[ \ddot{x}''(y, t) + \frac{E}{\kappa G} \ddot{x}''''(y, t) - \frac{\rho}{\kappa G} \ddot{\ddot{x}}(y, t) \right] = 0 \tag{3.330}$$

The third term in this expression,  $-\rho I \partial^4 x(y, t) / \partial y^2 \partial t^2$ , represents the effect of rotary inertia forces while the last two terms define the effect of shear deformation. The factor  $\kappa$  is a constant dependent on the geometry of the cross section and can be taken to be 5/6 and 9/10 for rectangular and circular cross sections, respectively (References 3.5 and 3.1, Chapter 7). The solution to this equation which satisfies the boundary conditions for a simply supported beam, assuming harmonic motion, is an infinite series of terms of the form

$$x(y, t) = \bar{q}_n \sin(n\pi y/L) \cos(\omega_n t)$$

Substituting this into Equation 3.330, a frequency equation is obtained which can be conveniently expressed in the form

$$\left(\frac{\pi n r}{L}\right)^4 \frac{E}{\kappa G} \left(\frac{\omega_n}{\omega_{no}}\right)^4 - \left[1 + \left(1 + \frac{E}{\kappa G}\right) \left(\frac{\pi n r}{L}\right)^2\right] \left(\frac{\omega_n}{\omega_{no}}\right)^2 + 1 = 0 \tag{3.331a}$$

where

$$\omega_{no} = \left(\frac{n\pi}{L}\right)^2 \sqrt{\frac{EI}{\rho A}} \text{ - the natural frequency for a simply supported beam without rotary inertia and shear effects, and}$$

$$r = \sqrt{I/A} \text{ - radius of gyration.}$$

This expression has been used to determine the relative decrease in natural frequency  $\omega_n/\omega_{no}$  for a simply supported beam when effects of rotary inertia and shear are included. The results are shown in Figure 3.86 as a function of the ratio of the radius of gyration  $r$  to beam length  $L$  for several values of the mode number  $n$  and for a typical value of  $E/\kappa G$  of 3.2 for metal beams. The effect of rotary inertia only can be isolated by letting the shear modulus  $G$  approach infinity in Equation 3.331a. The resulting equation reduces to

$$\omega_n/\omega_{no} = 1 / \left[1 + \left(\frac{\pi n r}{L}\right)^2\right]^{1/2} \tag{3.331b}$$

This correction for rotary inertia effects is also shown in Figure 3.86 for the first mode only. For values of  $nr/L$  less than 0.1, the decrease in natural frequency is primarily due to the effect of shear forces while rotary inertia effects become predominant for  $nr/L > 0.3$ . In either case, for typical beams where  $r/L$  is of the order of 0.02 or less, this correction will not be significant for the lower modes of vibration. Figure 3.87 illustrates comparable results reported in Reference 3.54 for a cantilevered beam.

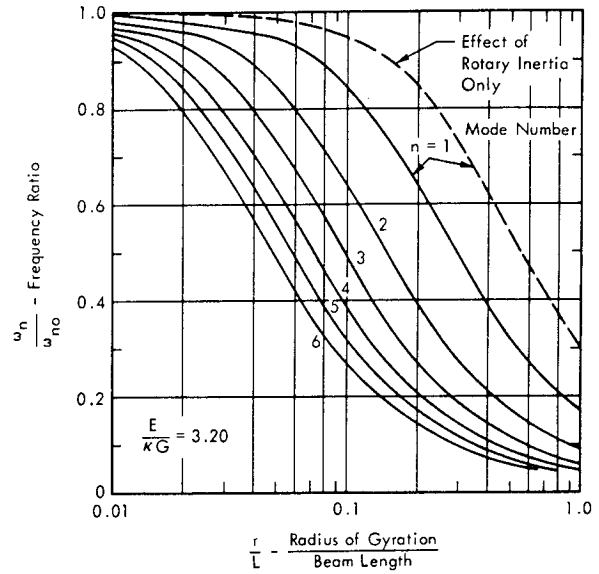


FIGURE 3.86 Relative Decrease in Natural Frequency of a Simply Supported Beam when Rotary Inertia Effects (Dashed Line) and Both Rotary Inertia and Shear Effects are Accounted For.  $\omega_{no}$  = Natural Frequency without Rotary Inertia and Shear Effects (Reference 3.5)

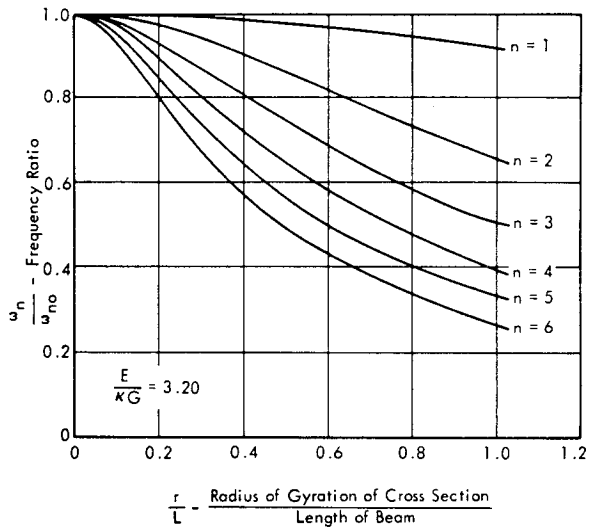


FIGURE 3.87 Relative Decrease in Natural Frequency of a Uniform Cantilevered Beam when Rotary Inertia and Shear Effects are Included.  $\omega_{no}$  = Natural Frequency Without Rotary Inertia and Shear (From C. M. Harris and C. F. Crede, "Shock and Vibration Handbook," Chapter 7, Copyright 1961, McGraw-Hill Book Co. Inc.)

Effect of Axial Loads on Lateral Vibrations of Beams

An axial tensile load imposed on a beam tends to increase its natural frequencies of lateral vibration. Conversely, a compressive load decreases the natural frequencies. An approximate expression for this change in frequency of a pinned-pinned beam under an axial compressive load (-P) or tensile load (+P) is given by (Reference 3.1, Chapter 7)

$$f_n = f_{no} \left[1 \pm \frac{P/P_1}{n^2}\right]^{1/2} \tag{3.332}$$

where

$$P_1^i = \text{critical buckling load} = \pi^2 EI/L^2 \text{ for simply supported beams}$$

$n$  = mode number

$f_{no}$  = natural frequency in  $n$ th mode without axial load.

For a first approximation, this expression may also be applied to a beam with arbitrary end conditions by choosing the appropriate value for the buckling load  $P_1^i$ . For end conditions other than pinned-pinned, the critical buckling load is

Clamped-Free	$P_1^i = \pi^2 EI/4L^2$
Clamped-Pinned	$P_1^i = 2\pi^2 EI/L^2$
Clamped-Clamped	$P_1^i = 4\pi^2 EI/L^2$

For a more exact analysis, the following approach can be used. The equation of motion for free vibration of a uniform beam-column loaded axially with a static force  $P$  is (References 3.55 and 3.56)

$$EI x''''(y, t) + P x''(y, t) + \rho A \ddot{x}(y, t) = 0 \quad (3.333a)$$

The second term  $P x''(y, t) = P \partial^2 x(y, t)/\partial y^2$  represents the rate of change with  $y$  of the effective shear force  $P \partial x(y, t)/\partial y$  on the beam due to an axial load. The general solution to this modified equation of motion (compare with Equation 3.329) is given by an infinite series of normal mode terms where the  $n$ th term can be conveniently expressed as

$$x_n(y, t) = \left[ A \cosh \alpha_n \bar{y} + B \sinh \alpha_n \bar{y} + C \cos \beta_n \bar{y} + D \sin \beta_n \bar{y} \right] e^{j\omega_n t} \quad (3.333b)$$

and

$$\alpha_n = \left[ \sqrt{(PL^2/2EI)^2 + (K_n L)^4} - PL^2/2EI \right]^{1/2}$$

$$\beta_n = \left[ \sqrt{(PL^2/2EI)^2 + (K_n L)^4} + PL^2/2EI \right]^{1/2}$$

$EI$  = bending stiffness per unit length

$\rho A$  = mass per unit length

$L$  = length of beam column

$$(K_n L)^2 = \omega_n L^2 \sqrt{\frac{EI}{\rho A}} = \text{dimensionless natural frequency.}$$

For the case of a fixed-free beam column, the applicable boundary conditions at the fixed end ( $y = 0$ ) are specified in Table 3.5, page 3-113. At the free end, where the static load is applied ( $y = L$ ), the boundary conditions are

$$\text{Bending Moment} = EI x''(L, t) = 0$$

$$\text{Total Shear} = -EI x'''(L, t) - P x'(L, t) = 0$$

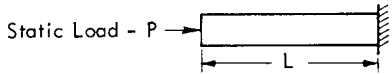
Applying these boundary conditions to the general solution, and solving for three of the unknown coefficients (i.e.,  $B$ ,  $C$  and  $D$  in terms of  $A$ ), a frequency equation is obtained which defines the natural frequencies  $\omega_n$  as the roots of

$$1 + \left[ 2 \frac{(PL^2/2EI)^2}{(K_n L)^4} + 1 \right] \cosh \alpha_n \cos \beta_n - \frac{PL^2/2EI}{(K_n L)^2} \sinh \alpha_n \cos \beta_n = 0 \quad (3.334)$$

The first three roots or values of  $K_n L$  which satisfy this equation have been reported in Reference 3.55 for several values of the axial load parameter  $PL^2/2EI$ . These are tabulated below as a dimensionless natural frequency  $f_n L^2/\sqrt{EI/\rho A}$ .

TABLE 3.7

FIRST THREE NATURAL FREQUENCIES FOR CLAMPED-FREE BEAM COLUMN UNDER AXIAL LOAD

$$f_n L^2/\sqrt{EI/\rho A}$$


$n$	$\frac{PL^2}{2EI}$	0	0.25	0.5	0.75	1.0	1.2	$\frac{\pi^2}{8}$
1		0.560	0.503	0.438	0.359	0.252	0.096	0
2		3.506	3.447	3.887	3.326	3.263	3.212	-
3		9.820	9.769	9.720	9.669	9.618	9.576	-

For zero axial load,  $PL^2/2EI = 0$  and the dimensionless frequencies are identical to the values specified earlier for a clamped-free beam. For an axial load equal to the critical buckling load for a clamped-free beam ( $P = \pi^2 EI/4L^2$ ), the parameter  $PL^2/2EI$  is equal to  $\pi^2/8$  and the fundamental frequency goes to zero. As predicted by the simpler expression in Equation 3.332, the influence of an axial load on the second and higher modes is reduced.

The variation in the fundamental natural frequency for axially loaded beams with other boundary conditions has been evaluated in Reference 3.56 using this exact method, and the results are summarized in Table 3.29 at the end of the chapter. For normal static loads, the effect of axial loads can generally be ignored. However, for blast loads on buildings, the dynamic response of the fundamental modes of the building framework may be significantly influenced by the combined effect of axial and lateral loads.

A related effect on the natural bending frequency of a beam constrained by immovable supports, occurs when the amplitude of vibration is significantly greater than the radius of gyration of the beam. This represents the non-linear effect of large displacement amplitudes. In this case, tensile forces are developed in the beam when its

support points are not permitted to move axially. The relative increase in the fundamental natural frequency  $f_1$  of a beam with rigidly-held pinned supports is given in Table 3.8 as a function of the peak displacement amplitude  $X_{\max}$  divided by the radius of gyration  $\sqrt{I/A}$  of the beam (Reference 3.1, Chapter 7). The natural frequency for small displacements is  $f_{10}$ .

TABLE 3.8

RELATIVE CHANGE IN FUNDAMENTAL NATURAL FREQUENCY OF A PINNED-PINNED BEAM DUE TO TENSILE FORCES GENERATED BY LARGE DISPLACEMENT AMPLITUDES

$X_{\max}/\sqrt{I/A}$	0	0.5	1.0	1.5	2.0	3.0	4.0
$f_1/f_{10}$	1.0	1.026	1.089	1.190	1.316	1.626	1.976

Effect of Partial Fixity on Lateral Vibration of Uniform Beams

True boundary conditions for a typical structural beam will normally lie between simply-supported and clamped. The variation in vibration characteristics of uniform beams with other than ideal boundary conditions has been examined in detail in References 3.57 and 3.58. Numerical results reported for the case of a uniform beam with varying degrees of rotational end fixity but infinitely stiff translational fixity are briefly reviewed here. This represents a suitable analytical model of practical mounting conditions in real structure. The theoretical approach may be briefly summarized as follows.

The equation of motion for a uniform beam (neglecting rotary inertia and shear effects) is utilized in the form given by Equation 3.329. The general solution to this equation is the infinite series of normal mode solutions where the mode shape is conveniently expressed in the form

$$\phi_n(y) = A \cosh K_n L \bar{y} + B \sinh K_n L \bar{y} + C \cos K_n L \bar{y} + D \sin K_n L \bar{y}$$

where

$$K_n L = \omega_n L / c_B = \text{the dimensional frequency parameter, and}$$

$$\bar{y} = y/L.$$

The boundary conditions applicable for this case are illustrated in Figure 3.88a. Note that the sign convention shown for positive internal and support moments at the ends of the bar is dictated by the dynamic equilibrium of the system. The required four boundary equations are (see Table 3.5)

$$\phi_n(0) = \phi_n(L) = 0 \text{ (no translation at ends)}$$

$$\frac{EI}{L^2} \phi_n''(\bar{y}) \Big|_{y=0} = \frac{k_r}{L} \phi_n'(\bar{y}) \Big|_{y=0}$$

$$\frac{EI}{L^2} \phi_n''(\bar{y}) \Big|_{y=L} = -\frac{k_{rL}}{L} \phi_n'(\bar{y}) \Big|_{y=L}$$

where

$$\frac{1}{L} \phi_n'(y) = \frac{1}{L} \frac{\partial \phi(\bar{y})}{\partial (y/L)} = \frac{\partial \phi(\bar{y})}{\partial \bar{y}}$$

Substituting the mode shape into these equations, the resulting frequency equation is

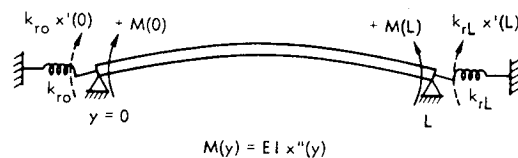
$$\frac{k_{r0} k_{rL} L^2}{(EI)^2 (K_n L)^2} (\cos K_n L \cosh K_n L - 1) + \left( \frac{k_{r0} L + k_{rL} L}{EI \cdot K_n L} \right) (\cos K_n L \sinh K_n L - \sin K_n L \cosh K_n L) - 2 K_n L \sin K_n L \sinh K_n L = 0 \tag{3.335}$$

The natural frequencies  $f_n = \omega_n / 2\pi$  are determined, from the roots of this expression, for given values of the end fixity parameters

$$L k_{r0} / EI \text{ and } L k_{rL} / EI, \text{ where } f_n \text{ is given}$$

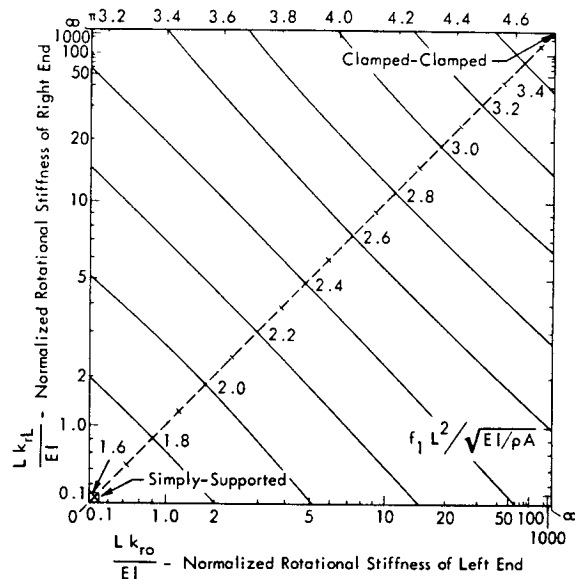
$$f_n = \frac{(K_n L)^2}{2\pi L^2} \sqrt{\frac{EI}{\rho A}}$$

Results are shown in Figures 3.88b, c, and d in the form of contours of constant values of the quantity  $f_n L^2 / \sqrt{EI/\rho A}$  for the first three modes as a function of the end fixity parameters at each end of a beam. The ordinate and abscissa scales are nonlinear due to a transformation of the



a) Boundary Conditions for Beam with Partial Rotational Fixity at Ends

$K_n L$  - Roots of Frequency Equation (3.335) for Symmetrical End Fixity ( $k_{r0} = k_{rL}$ )



b) First Mode

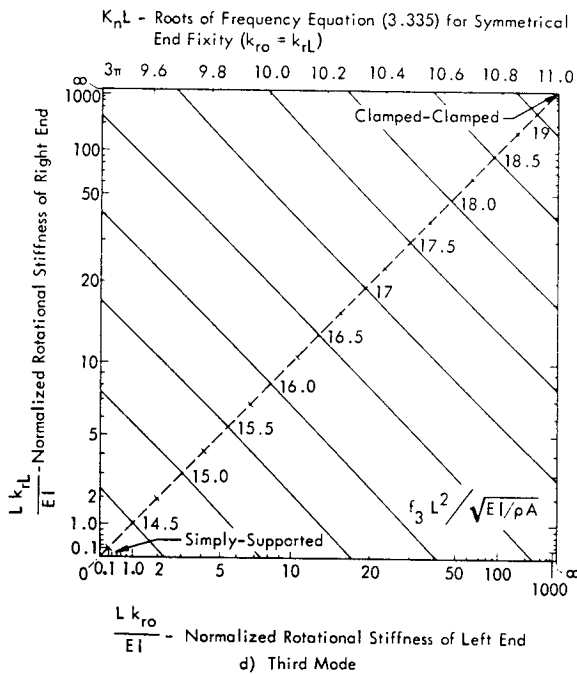
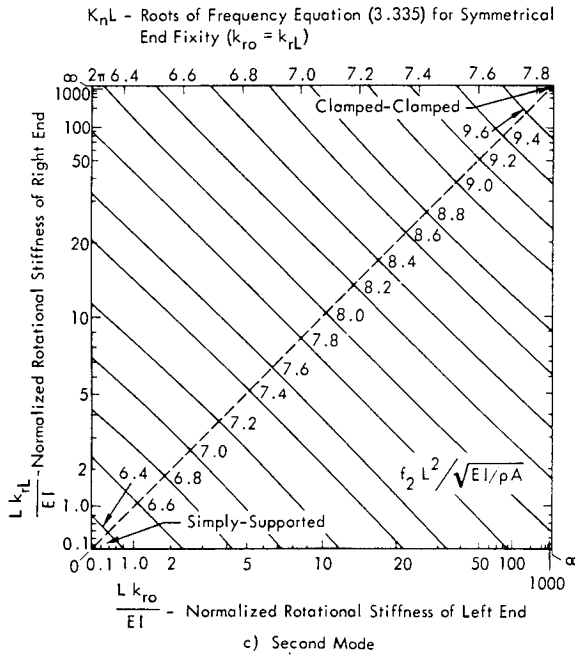


FIGURE 3.88 Contours of Normalized Frequency  $f_n L^2 / \sqrt{EI/\rho A}$  for First Three Modes of Uniform Beam on Pinned Support and Varying Rotational Restraint (From References 3.57 and 3.58)

original results made for convenience in illustration. In the lower left-hand corner in each graph,  $k_{r0}$  and  $k_{rL}$  are equal to zero, and the frequency is equal to that for a simply supported beam. In the opposite corner,  $k_{r0}$  and  $k_{rL}$  approach infinity, which is equivalent to the end fixity for a clamped-clamped beam. Therefore, all values for the first three natural frequencies between these two extremes are represented. Significant deviations from the

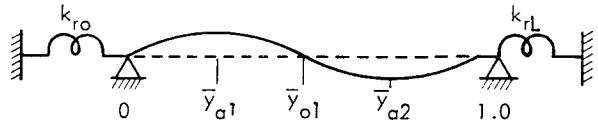
two ideal conditions occur when either of the fixity parameters  $L k_r / EI$  lie between about 1 and 100. For a symmetrical end fixity, the natural frequency can be read from values on a 45° line between the two opposite corners. The resulting values are also shown at the top of each graph in terms of  $K_n L$  where

$$K_n L = \left[ 2\pi f_n L^2 \sqrt{EI/\rho A} \right]^{1/2}$$

The change in edge fixity will, of course, also change the mode shape of the beam. This is also covered in Reference 3.57 and the results are briefly summarized in Table 3.9

TABLE 3.9

LOCATION OF ANTI-NODES ( $\bar{y}_a$ ), NODES ( $\bar{y}_o$ ), FOR FIRST THREE NORMAL MODES OF UNIFORM BEAM WITH VARYING ROTATIONAL EDGE FIXITY AND INFINITE TRANSLATIONAL FIXITY



Edge Fixity $L k_r / EI$	Mode n	Symmetric, $k_{r0} = k_{rL}$			
		Anti-Nodes $\bar{y}_a$		Nodes $\bar{y}_o$	
0(1)	1	0.5	--	--	--
	2	0.25	0.75	--	0.50
	3	0.167	0.50	0.833	0.333
2.5	1	0.5	--	--	--
	2	0.258	0.742	--	0.50
	3	0.173	0.50	0.827	0.328
10	1	0.50	--	--	--
	2	0.270	0.730	--	0.50
	3	0.183	0.50	0.817	0.325
40	1	0.5	--	--	--
	2	0.282	0.718	--	--
	3	0.196	0.50	0.804	0.314
$\infty(2)$	1	0.5	--	--	--
	2	0.290	0.710	--	0.50
	3	0.207	0.50	0.793	0.307
Anti-Symmetric, $k_{r0} = 0$					
0(1)	1	0.476	--	--	--
	2	0.25	0.75	--	0.50
	3	0.167	0.50	0.833	0.333
2.5	1	0.499	--	--	--
	2	0.245	0.735	--	0.487
	3	0.164	0.493	0.824	0.329
10	1	0.476	--	--	--
	2	0.237	0.713	--	0.468
	3	0.162	0.482	0.810	0.322
40	1	0.447	--	--	--
	2	0.228	0.692	--	0.452
	3	0.157	0.471	0.791	0.314
$\infty(2)$	1	0.428	--	--	--
	2	0.222	0.678	--	0.441
	3	0.153	0.462	0.776	0.307

(1) Simply-Supported  
(2) Clamped-Clamped ( $k_{r0} = k_{rL}$ ), Pinned-Clamped ( $k_{r0} = 0$ )



by listing the location of the points of maximum deflection (anti-nodes) and zero deflection (nodes) as a function of the edge fixity parameters  $L k_r/EI$  for the first three normal modes of a uniform beam. Values are specified for symmetrical edge fixity where  $k_{rO} = k_{rL}$  and for the extreme unsymmetrical case where  $k_{rO} \equiv 0$  and only  $k_{rL}$  changes.

3.3.5.5 Effect of Mass and Stiffness Loads on Lateral Vibration of Beams

It is frequently necessary to determine the effect of localized or distributed mass loads on the vibration response of beams, particularly when analyzing the vibration environment of equipment. The various analytical methods utilized for this problem can be grouped into three categories according to whether the mass load is 1) greater than, 2) comparable to, or 3) less than the beam mass.

1) Mass Load Much Greater than Beam Mass

For this category, the influence of the distributed mass of the beam is small relative to the load mass and the principal vibration characteristics of the system are defined by the stiffness properties of the beam and the mass load. If this load is itself uniformly distributed but does not add to the stiffness of the configuration, only the effective mass per unit length ( $\rho A$ ) of the beam is increased and the natural frequencies  $f_n$  are decreased by the factor

$$\frac{f_n \text{ (with uniform "limp" mass load)}}{f_n \text{ (without mass load)}} = \sqrt{\frac{\text{beam mass}}{\text{beam} + \text{load mass}}}$$

For large concentrated mass loads, a lumped parameter approach can be used. The lumped springs of the mass-loaded system are defined by the stiffness or flexibility influence coefficients of the beam. An example of this method, using matrix iteration techniques, has been presented earlier in Section 3.3.4.4.

2) Mass Load Comparable to Beam Mass

A lumped parameter approach is still suitable for this category providing enough "lumps" are used to adequately define the mass characteristics of the beam itself (see Section 3.3.4.4).

An alternate and more accurate approach for this case is possible using transfer matrix techniques. This method properly accounts for both the distributed mass and stiffness of the beam elements and lumped-mass loads. Equations of motion are developed which satisfy the boundary conditions, such as defined in Table 3.5, for deflection, slope, moment and shear at each end of the beam elements connecting the various masses. A suitable introduction to this powerful technique is contained in Reference 3.2 while a thorough treatment is presented in Reference 3.36. As pointed out earlier, this method can be used to obtain the forced response of a system directly without the application of normal mode concepts.

In this section, a similar approach is used to determine the natural frequencies for the special case of only one lumped mass load in the center of a simply supported beam. It is also possible to use the normal modes for the unloaded bar to define the new frequencies with a load. However, the method is generally awkward for all but the simplest cases. It involves solving a new set of  $N$  simultaneous equations to define the new natural frequencies and mode shapes for the system defined by its  $N$  natural modes (Reference 3.2).

3) Mass Load Much Less Than Beam Mass

For this case, it can be assumed that the mode shape for lower modes of vibration are not significantly influenced by an added mass load. The normal mode approach then provides a particularly useful technique for analyzing the influence of such loads on the fundamental natural frequency of beams. It can be extended to include distributed or localized mass or stiffness loads, regardless of the relative beam to load mass or stiffness ratios if only the fundamental frequency is to be estimated. The accuracy obtainable with this method is generally adequate for engineering design purposes.

Natural Frequencies of Mass and Stiffness Loaded Beam with Pinned Ends

Consider the case, illustrated in Figure 3.89a, of a simply supported beam supporting a point mass  $m$  at the center. If rotary inertia of the mass load is neglected, only the odd modes of vibration of the beam will be influenced by this mass load since the center is a node point for even modes. By symmetry, the odd modes of the pinned-pinned beam of lengths  $L$  can be represented by the modes of a pinned-guided beam of length  $L/2$  with  $1/2$  the mass load at its guided end (see Figure 3.89b). The boundary conditions for this case are

$$\begin{aligned} \text{At } y = 0, \quad & x(0, t) = 0 \quad - \text{ (zero displacement)} \\ & x''(0, t) = 0 \quad - \text{ (zero moment)} \\ \text{At } y = L, \quad & x'(L/2, t) = 0 \quad - \text{ (zero slope)} \\ & -EI x'''(L/2, t) = -\frac{m}{2} \ddot{x}(L/2, t), \quad \text{(shear = inertia force)} \end{aligned}$$

Applying these to the general expression for the mode shape (Equation 3.310), all the unknown coefficients  $A, B, C, D$  are eliminated leaving the frequency equation

$$2 \frac{m_b}{m} = \frac{K_n L}{2} \left[ \tan \frac{K_n L}{2} - \tanh \frac{K_n L}{2} \right] \quad (3.336)$$

where

$$m_b = \rho A L \text{ - the mass of the beam}$$

$$m = \text{load mass at center.}$$

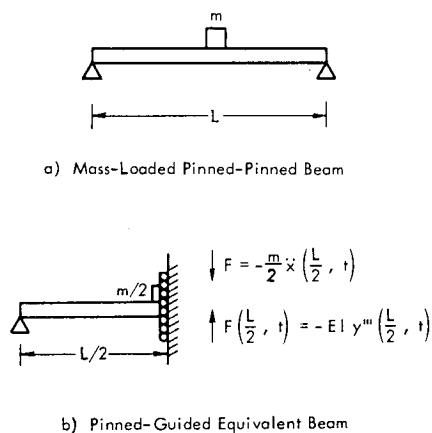


FIGURE 3.89 Equivalent Model of Pinned-Pinned Beam Supporting a Mass  $m$  at Center. Odd modes of pinned-pinned beam, which are influenced by presence of center mass, are represented by mode of pinned-guided beam of  $1/2$  the length.

By solving for the roots  $K_n L$  of this expression, the natural frequencies  $\omega_n = (K_n L)^2 \sqrt{EI/\rho A/L^2}$  are determined. The results for the first four odd modes are shown in Figure 3.90 as the ratio  $\omega_n/\omega_{n0}$  where  $\omega_{n0} = (n\pi)^2 \sqrt{EI/\rho A/L^2}$  are the natural frequencies for the unloaded simply supported beam. The principal effect of the mass loading is to sharply reduce the fundamental frequency as load increases. The reduction is less significant for the higher modes. No changes are indicated, of course, for even order modes of this idealized model. A similar approach can be used for mass loading of a clamped-clamped beam. The equivalent model is treated as a clamped-guided beam and the results are shown in Figure 3.91.

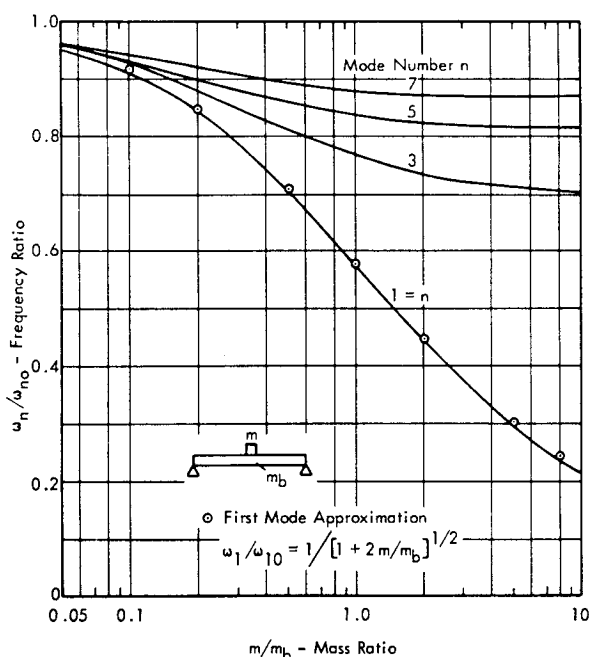


FIGURE 3.90 Relative Change in Natural Frequencies of Odd Modes of Pinned-Pinned Beam of Mass  $m_b$  Supporting a Point Mass  $m$  at the Center.  $\omega_{n0}$  =  $n$ th natural frequency without mass.

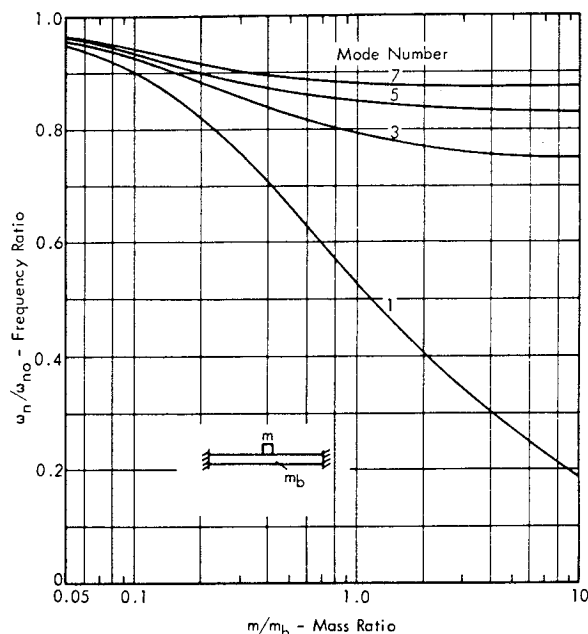


FIGURE 3.91 Relative Change in Natural Frequencies of Odd Modes of Clamped-Clamped Beam of Mass  $m_b$  Supporting a Point Mass  $m$  at the Center.  $\omega_{n0}$  =  $n$ th natural frequency without mass.

Single Mode Approximation for the Effect of Mass and Spring Loads

The influence of mass and spring loads on the fundamental natural frequency of a beam can be closely approximated by treating the loads as generalized forces acting on the fundamental mode. The equation of motion for free vibration in this mode is then modified to become

$$\ddot{q}_1(t) + \omega_{10}^2 q_1(t) = \frac{F_1(t)}{M_1} \tag{3.337}$$

where

$q_1(t)$  = Normal Coordinate in Fundamental Mode

$F_1(t)$  = Generalized Restraint Force Developed by added load

$M_1$  = Generalized Mass of the Unloaded Beam

$\omega_{10}$  = Natural Frequency of First Mode of Unloaded Beam.

Consider the case, illustrated in Figure 3.92, of a pinned-pinned beam restrained by a lumped spring  $k_1$  located at  $y_1$  and carrying a lumped mass  $m_2$  at a point  $y_2$ . The generalized force  $F_1(t)$  is the product of the spring and inertia "restraint" forces multiplied by the mode shapes  $\phi_1(y)$  at their corresponding locations. The forces are negative since they tend to oppose the motion of the beam, or

$$F_1(t) = -k_1 x(y_1, t) \phi_1(y_1) - m_2 \ddot{x}(y_2, t) \phi_1(y_2)$$

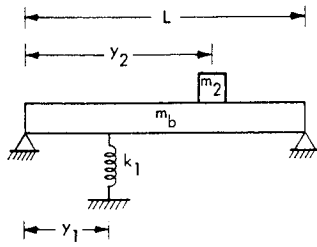


FIGURE 3.92 Pinned-Pinned Beam Restrained by a Spring  $k_1$  and Supporting a Mass  $m_2$  at Points  $y_1$  and  $y_2$ , Respectively

Expressing  $x(y, t)$  in terms of its first modal component  $q_1(t) \phi_1(y)$ , and assuming harmonic vibration, so that  $q_1(t) = \bar{q}_1 e^{j\omega t}$ , Equation 3.337 becomes

$$[-\omega^2 + \omega_{10}^2] \bar{q}_1 e^{j\omega t} = \frac{1}{M_1} [-k_1 \phi_1^2(y_1) + \omega^2 m_2 \phi_1^2(y_2)] \bar{q}_1 e^{j\omega t}$$

This can be solved for the new natural frequency of the loaded system to give

$$\omega = \omega_{10} \left[ \frac{1 + (k_1 / \omega_{10}^2 M_1) \phi_1^2(y_1)}{1 + (m_2 / M_1) \phi_1^2(y_2)} \right]^{1/2} \quad (3.338)$$

This is a general result applicable to a beam with any boundary conditions where  $\omega_{10}$  is the unloaded fundamental natural frequency,  $M_1$  is the generalized mass of the beam and  $\phi_1(y)$  is its fundamental mode shape. For the more general case of  $S$  lumped spring restraints, each with a stiffness  $k_i$  located at  $y_i$  and  $R$  lumped masses  $m_j$  located at  $y_j$ , the modified fundamental natural frequency of the loaded beam becomes

$$\omega = \omega_{10} \left[ \frac{1 + \left( \sum_i^S k_i \phi_1^2(y_i) \right) / \omega_{10}^2 M_1}{1 + \left( \sum_j^R m_j \phi_1^2(y_j) \right) / M_1} \right]^{1/2} \quad (3.339)$$

For the case of just a mass load  $m$  at the center of pinned-pinned beam where  $M_1 = (1/2)$  the mass of the beam  $m_b$  and  $\phi_1(L/2) = 1$ , the fundamental frequency becomes

$$\omega = \omega_{10} \left[ \frac{1}{1 + 2m/m_b} \right]^{1/2} \quad (3.340)$$

The relative change in fundamental natural frequency  $\omega/\omega_{10}$ , predicted by this expression, is shown by data points on Figure 3.90 for comparison with the exact solution given earlier for this case. The single mode approximation clearly agrees very well with the exact value for any mass ratio  $m/m_b$ .

The above general expression (Equation 3.339) for correcting fundamental natural frequencies of beams, due to loading, can be readily applied to a wide variety of equipment or structural vibration problems using the tables at the end of this chapter to determine the fundamental frequency  $\omega_{10}$  of the unloaded beam.

#### The Rayleigh Energy Method

The fundamental natural frequency of any vibrating system can also be estimated by the well-known Rayleigh energy method. If the fundamental mode of vibration is treated as an equivalent single degree-of-freedom system, then the total energy of the system is equal to its maximum kinetic energy  $T_{\max}$  as it passes through an equilibrium position, or to its maximum potential (or strain) energy  $V_{\max}$  as it reaches the point of maximum displacement. Assuming harmonic motion for the displacement  $x(y, t) = x(y) \cos \omega_1 t$ , then the fundamental frequency  $\omega_1$  can be determined by equating the maximum kinetic and potential energy to give

$$\frac{1}{2} \overline{M \dot{x}^2(y)} = \omega_1^2 \left[ \frac{1}{2} \overline{M x^2(y)} \right] = \frac{1}{2} \overline{K x^2(y)}$$

or

$$\omega_1^2 = \frac{\overline{K x^2(y)}}{\overline{M x^2(y)}}$$

where  $M$  and  $K$  represent general inertia and stiffness properties of the system and the bar signifies summation over all elements. The specific steps for this simple method are summarized as follows:

- A mode shape is estimated for the fundamental mode. This may be based on the deflection for a uniform static load or on a simple approximation for the dynamic mode shape. Typical expressions, normalized to a maximum value of unity, are listed below.

#### Pinned-Pinned Beam

$$\text{Static Shape} \quad - x(y) = \frac{16}{5} \left[ (y/L)^4 - 2(y/L)^3 + y/L \right]$$

$$\text{Dynamic Shape} \quad - x(y) = \sin(\pi y/L)$$

#### Clamped-Clamped Beam

$$\text{Static Shape} \quad - x(y) = 16 \left[ 2(y/L)^3 - (y/L)^2 - (y/L)^4 \right]$$

$$\text{Dynamic Shape} \quad - x(y) = \frac{1}{2} [1 - \cos(2\pi y/L)]$$

#### Clamped-Free Beam

$$\text{Static Shape} \quad - x(y) = \frac{1}{3} \left[ (y/L)^4 - 4(y/L)^3 + 6(y/L)^2 \right]$$

$$\text{Dynamic Shape} \quad - x(y) = 1 - \cos\left(\frac{\pi}{2} \frac{y}{L}\right)$$

The approximate shape selected must satisfy minimum conditions of zero deflection at a support point and zero slope at a built-in or clamped support. Increased accuracy in the estimated fundamental frequency is obtained for mode shapes which also satisfy boundary conditions for moment and shear.

- Given the assumed mode shape, the fundamental frequency is estimated using one of the following expressions. Terminology is the same as that used in Table 3.4, page 3.109.

Longitudinal Vibration of Arbitrary Bar

$$\omega_1^2 \approx \frac{\int_0^L EA \left[ \frac{dx(y)}{dy} \right]^2 dy}{\int_0^L \rho A [x(y)]^2 dy} \tag{3.341}$$

(The general case of a bar with varying stiffness EA and mass ρA per unit length is considered by including these parameters within the integral.)

Torsional Vibration of Arbitrary Bar

$$\omega_1^2 \approx \frac{\int_0^L K_r G \left[ \frac{d\theta(y)}{dy} \right]^2 dy}{\int_0^L \rho J [\theta(y)]^2 dy} \tag{3.342}$$

Lateral Vibration of Beams

$$\omega_1^2 \approx \frac{\int_0^L EI \left[ \frac{\partial^2 x(y)}{\partial y^2} \right]^2 dy}{\int_0^L \rho A [x(y)]^2 dy} \tag{3.343}$$

Lateral Vibration of Plates

$$\omega_1^2 \approx \frac{\iint_{00}^{ab} D \left\{ \left[ \frac{\partial^2 x(y,z)}{\partial y^2} \right]^2 + \left[ \frac{\partial^2 x(y,z)}{\partial z^2} \right]^2 \right\} dy dz}{\iint_{00}^{ab} \rho h [x(y,z)]^2 dy dz}$$

$$+ \frac{\iint_{00}^{ab} D \left\{ 2\nu \left[ \frac{\partial^4 x(y,z)}{\partial y^2 \partial z^2} \right] + 2(1-\nu) \left[ \frac{\partial^2 x(y,z)}{\partial y \partial z} \right]^2 \right\} dy dz}{\iint_{00}^{ab} \rho h [x(y,z)]^2 dy dz} \tag{3.344}$$

Natural frequencies estimated with these expressions will always be slightly higher than the true value unless the exact mode shape is used. However, with any reasonable estimate for a mode shape, fundamental frequencies can be estimated within a few percent. Expressions for static deflection shapes of a wide variety of beam and plate configurations are available in Reference 3.50 for application to this method.

Addition of Mass and Spring Loads

The influence of added mass or spring loads on fundamental frequencies can also be readily evaluated with the Rayleigh method. For example, to evaluate the effect of adding S lumped springs of stiffness k<sub>i</sub> at positions y<sub>i</sub> and R lumped masses m<sub>j</sub> at positions y<sub>j</sub> to a uniform beam, Equation 3.343 is modified to become

$$\omega_1^2 \approx \frac{EI \int_0^L \left[ \frac{dx(y)}{dy} \right]^2 dy + \sum_i^S k_i x^2(y_i)}{\rho A \int_0^L [x(y)]^2 dy + \sum_j^R m_j x^2(y_j)} \tag{3.345}$$

If the assumed mode shape x(y) is normalized to a maximum value of unity, then the numerator and denominator of this equation are equivalent to the total generalized stiffness and mass, respectively, of the loaded beam. The resulting expression is essentially equivalent to that given earlier (Equation 3.339) based on the single mode approximation.

Example of Application of Rayleigh Method

To illustrate an application of the Rayleigh energy method, consider the change in fundamental frequency of a pinned-pinned uniform beam caused by moving the support points symmetrically toward the center of the beam. The result can be used to estimate resonant frequencies for practical configurations of simply-supported beams or to predict any desired increase in resonance frequency of a beam-like mounting structure for equipment.

Assume the mode shape illustrated in Figure 3.93a is sinusoidal and given by

$$x(y) = X_0 \sin\left(\pi \frac{y}{L}\right) - \sin\left(\pi \frac{d}{L}\right)$$

where  $X_0$  = arbitrary reference amplitude.

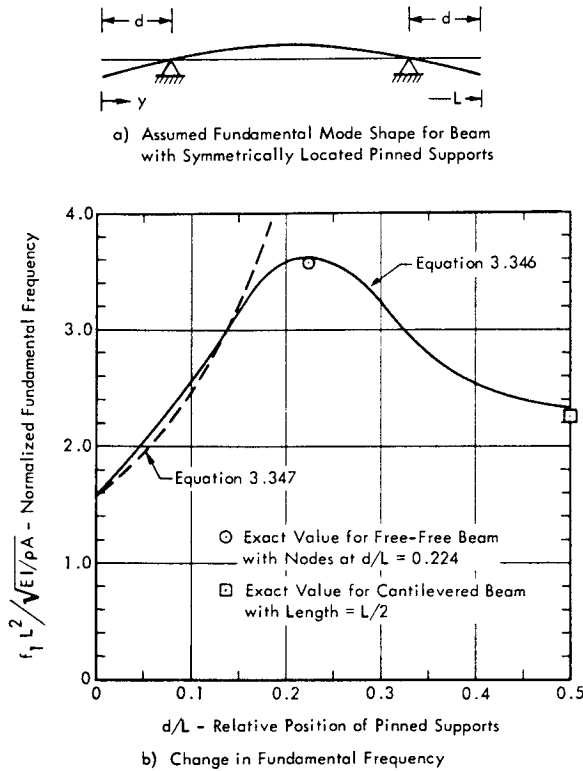


FIGURE 3.93 Effect of Change in Position of Pinned Supports on Fundamental Frequency of Uniform Beam

This expression satisfies the condition for zero deflection at  $y = d$  and thus meets the minimum criteria for an approximate mode shape. The condition of zero moment at the ends ( $x''(y) = 0$  at  $y = 0, L$ ) is also satisfied thus improving the accuracy expected from the estimate. Inserting this mode shape in Equation 3.343 and carrying out the required integration, the resulting expression for the fundamental frequency is

$$f_1 = \frac{\omega_1}{2\pi} = \frac{\pi}{2} \frac{1}{L^2} \sqrt{\frac{EI}{\rho A}} \left[ \frac{1}{1 - \frac{8}{\pi} \sin^2 \frac{\pi d}{L} + 2 \sin^2 \frac{\pi d}{L}} \right]^{1/2} \quad (3.346)$$

For  $d = 0$ , this reduces to the fundamental frequency for a pinned-pinned beam

$$f_{10} = \frac{\pi}{2} \sqrt{EI/\rho A} / L^2$$

Two additional checks can be made.

- For  $d/L = 0.224$ , the value for  $f_1$  should correspond approximately to that of a free-free beam which has nodes at these points in its fundamental mode (see Figure 3.85e).
- For  $d/L = 1/2$ , the frequency of the beam supported at the middle should correspond approximately to that of a cantilevered beam of length  $L/2$ .

The following compares these approximate values to the corresponding exact values.

	Equation 3.346	Exact
Free-Free Beam ( $d/L = 0.224$ )	$f_1 = \frac{3.608}{L^2} \sqrt{\frac{EI}{\rho A}}$	$f_1 = \frac{3.561}{L^2} \sqrt{\frac{EI}{\rho A}}$
Cantilevered Beam ( $d/L = 0.5$ )	$f_1 = \frac{0.583}{(L/2)^2} \sqrt{\frac{EI}{\rho A}}$	$f_1 = \frac{0.560}{(L/2)^2} \sqrt{\frac{EI}{\rho A}}$

It is noteworthy that for  $d/L < 0.15$ , the fundamental frequency of the beam is approximately equal to the value predicted for a pinned-pinned beam with a length  $L' = L - 2d$  equal to the distance between the supports, or

$$f_1 \approx \frac{\pi}{2} \frac{1}{L'} \sqrt{\frac{EI}{\rho A}} \left[ \frac{1}{1 - 2d/L} \right]^2, \quad d/L < 0.15 \quad (3.347)$$

These results are summarized in Figure 3.93b.

### 3.3.5.6 Lateral Vibration of Plates

Based on Equation 3.305 and the definitions of inertia and stiffness terms in Table 3.5, the equation of motion for free undamped vibration of a uniform plate, with a surface density  $\rho h$  and no in-plane membrane forces, is given by

$$D \nabla^4 x(y, z, t) + \rho h x(y, z, t) = 0 \quad (3.348)$$

where

$$\nabla^4 x(y, z, t) = \frac{\partial^4 x(y, z, t)}{\partial y^4} + \frac{2 \partial^4 x(y, z, t)}{\partial y^2 \partial z^2} + \frac{\partial^4 x(y, z, t)}{\partial z^4}$$

$$D = Eh^3/12(1 - \nu^2) = \text{Plate Stiffness}$$

$$\nu = \text{Poisson's ratio.}$$

A general solution for this equation can be given in the form of a doubly infinite series of normal modes as

$$x(y, z, t) = \sum_m \sum_n \bar{q}_{mn} \phi_{mn}(y, z) e^{j \omega_{mn} t} \quad (3.349)$$

where

$$\bar{q}_{mn} = \text{amplitude of normal coordinate in } m\text{th mode}$$

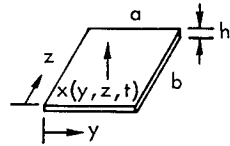
$$\phi_{mn}(y, z) = \text{mode shape for } m\text{th mode.}$$

$$\omega_{mn} = \text{natural frequency of } m\text{th mode.}$$

Simply Supported (Pinned) Plate

For the simply supported panel, the boundary conditions on all four edges are equivalent to those specified in Table 3.5 for a pinned ended beam. The natural frequencies and generalized mass are determined by essentially the same procedure as for beams.

• Boundary Conditions



$$\left. \begin{matrix} \text{Deflection} \\ \text{Moment} \end{matrix} \right\} = 0, \quad \begin{matrix} y = 0, a \\ z = 0, b \end{matrix}$$

• Mode Shape

$$\phi_{mn}(y, z) = \phi_m(y) \cdot \phi_n(z) = \sin \frac{m\pi y}{a} \sin \frac{n\pi z}{b} \quad (3.350a)$$

m = number of half waves along side a  
n = number of half waves along side b

• Natural Frequencies

$$\omega_{mn} = \pi^2 \sqrt{\frac{D}{\rho h}} \left[ \left(\frac{m}{a}\right)^2 + \left(\frac{n}{b}\right)^2 \right] \quad (3.350b)$$

$$\text{or } \omega_{mn} = (K_{mn} a)^2 \sqrt{D/\rho h a^4}$$

where  $K_{mn} a = \pi \sqrt{m^2 + (n a/b)^2}$  - dimensionless frequency parameter analogous to  $K_{nL}$  for beams

• Generalized Mass

$$M_{mn} = \frac{1}{4} \rho a b h = \frac{1}{4} (\text{Mass of Panel}) \quad (3.350c)$$

• Bending Wave Velocity for mnth Mode

$$c_B^i = \sqrt{\omega_{mn}} \left[ \frac{D}{\rho h} \right]^{1/4} = K_{mn} \sqrt{D/\rho h} \quad (3.350d)$$

$K_{mn} = 2\pi/\lambda_{B_{mn}}^i$ , where  $\lambda_{B_{mn}}^i$  = Bending Wavelength

• Ratio of Side a to Bending Wavelength  $\lambda_{B_{mn}}^i$

$$a/\lambda_{B_{mn}}^i = \frac{f_{mn} a}{c_B^i} = \frac{1}{2} \left[ m^2 + (n a/b)^2 \right]^{1/2} \quad (3.350e)$$

For this case, the mode shape is separable into the product of two functions  $\phi_m(y)$  and  $\phi_n(z)$  for the two directions on the plate. These mode shapes are identical to those for pinned-pinned beams parallel to sides a and b, respectively. Hence, the generalized mass fraction of 1/4 for the simply supported plate is the product of the generalized mass fraction of 1/2 for two simply supported beams.

Convenient alternate forms for specifying the natural frequency of simply supported plates are given by

$$1) \quad 2\pi f_{mn} = \omega_{mn} = \left[ \left(\frac{m\pi}{a}\right)^2 \sqrt{\frac{E I'}{\rho A'}} + \left(\frac{n\pi}{b}\right)^2 \sqrt{\frac{E I'}{\rho A'}} \right] \frac{1}{\sqrt{1-\nu^2}}$$

where  $I' = h^3/12$  - the moment of inertia for a segment of the plate equal to a beam of unit width and thickness h parallel to a side, and

$\sqrt{I'/A'}$  = radius of gyration for this unit width beam with a cross-sectional area  $A' = 1 \cdot h$ .

$$2) \quad f_{mn} = C_n \frac{h}{a^2} \times 10^4 K_m \quad (3.351)$$

where

$$C_n = \frac{(K_{mn} a)^2}{2\pi \sqrt{12(1-\nu^2)}} c_{L\text{steel}} \times 10^{-4} - \text{frequency constant for steel plates}$$

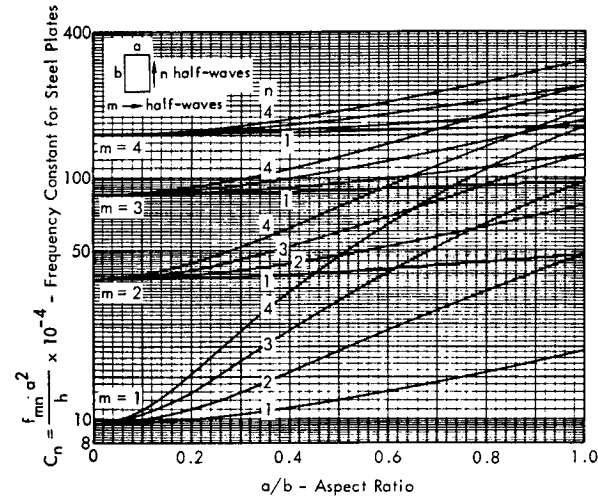
$$c_{L\text{steel}} = \sqrt{E/\rho} \text{ for steel} = 2.02 \times 10^5 \text{ in/sec}$$

$$K_m = \frac{c_L}{c_{L\text{steel}}} = \text{relative longitudinal wave velocities in plate material and in steel}$$

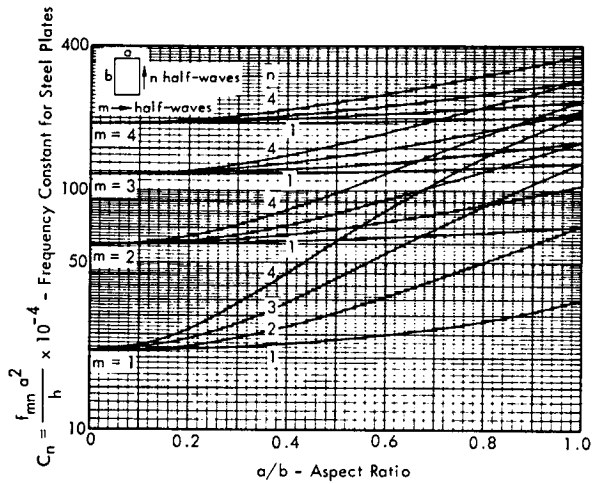
h, a = thickness and side a in inches.

The first alternate form emphasizes that the mnth natural frequency of a simply supported plate is approximately equal to the sum of the mth and nth natural frequencies of simply supported beams with a thickness h and lengths a and b, respectively. The approximation would be exact except for the factor  $1/\sqrt{1-\nu^2} \approx 0.954$  for  $\nu = 0.3$ .

The second version illustrates the form used in the tables at the end of this chapter where values for the natural frequency of plates with a variety of boundary conditions and shapes are specified by the appropriate values for the frequency constant  $C_n$ . Values for this constant for several modes of simply supported steel plates are plotted in Figure 3.94a for convenient reference at this point.



a) Pinned Edges

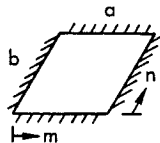


b) Clamped Edges

FIGURE 3.94 Frequency Constant  $C_n$  for Natural Frequencies of Simply-Supported and Clamped-Clamped Steel Plates. Constant to be used in Equation 3.351 ( $c_L = 2.02 \times 10^5$  in/sec,  $\nu = 0.3$ ).

Clamped-Clamped Plates

- Boundary Conditions



$$\left. \begin{matrix} \text{Deflection} \\ \text{Slope} \end{matrix} \right\} = 0, \quad \begin{matrix} y = 0, a \\ z = 0, b \end{matrix}$$

- Mode Shape (Approximate)

$$\Phi_{mn}(y, z) = \Phi_m(y) \cdot \Phi_n(z)$$

$\Phi_m(y), \Phi_n(z)$  = Mode Shapes for Clamped-Clamped Beams (see Section 3.3.5.4)

- Natural Frequencies (Approximate)

$$f_{mn} = C_n \frac{h}{a^2} \times 10^4 \text{ - Hz}$$

$h$  = thickness - in.

$a$  = length of shortest side - in.

$$C_n = A_o \left[ A_m + A_n \left(\frac{a}{b}\right)^4 + 2 \left(\frac{a}{b}\right)^2 B_m B_n \right]^{1/2}$$

$m, n$	$A_m, A_n$	$B_m, B_n$
1	5.139	1.246
2	39.05	4.666
3	150.06	10.021

$$A_o = \frac{\pi}{2} \frac{c_L \times 10^{-4}}{\sqrt{12(1-\nu^2)}} = 9.60 \text{ for steel}$$

- Generalized Mass (Approximate)

		$M_{mn}/\rho abh$		
$n$	$m \rightarrow$	1	2	3
1		0.157	0.174	0.173
2		0.174	0.193	0.192
3		0.173	0.192	0.191

In this case, the approximation used implies that all node lines are parallel to the sides of the panel. As shown in Table 3.31, this is not true for the fourth and fifth modes of a square clamped-clamped plate (Reference 3.5). However, the error is very small in the computed frequencies for other modes. The frequency constant  $C_n$  for clamped-clamped steel plates, computed by this approximation, is plotted in Figure 3.94b.

Other Boundary Conditions

The Ritz method, which is a refined version of the Rayleigh energy approach, is frequently used for a more exact analysis of the mode shapes and natural frequencies of the clamped-clamped plate and for most other rectangular plate configurations other than the simply-supported case (Reference 3.5). The mode shape is defined in a series form and the amplitudes of each term in the series are adjusted by an iterative process until the frequency determined from the basic Rayleigh energy equation (i.e., Equation 3.344) is a minimum.

Most of the natural frequencies for rectangular plates with the various boundary conditions and geometrical shapes shown in Table 3.31 have been determined by this method. These solutions are summarized from the literature in References 3.1, 3.53 and 3.59 - 3.62.

The following trends are observed in all cases of lateral vibrations of plates.

- Natural frequency is directly proportional to thickness for uniform plates, and inversely proportional to the square of the length of the sides for a constant thickness.
- The minimum natural frequency for the fundamental mode is controlled by the length of the shortest side.
- Natural frequency is directly proportional to the speed of longitudinal waves  $c_L$ . For most construction materials,  $c_L$  lies within a range of  $0.5$  to  $2 \times 10^5$  in/sec, with most metals having a value near  $2 \times 10^5$  in/sec (see Table 3.39).

Bending Wavelengths in Plates

The expressions given above for natural frequencies of plates tend to obscure the basic standing wave aspect of normal mode vibration. It is convenient to consider vibrations of plates from this viewpoint since it provides a very simple method for estimating lateral bending frequencies (Reference 3.63). The bending wavelength  $\lambda_B'$  for free flexural waves in a plate with a stiffness  $D = Eh^3/12(1-\nu^2)$  and surface density  $\rho h$  can be defined in a general form by

$$\lambda_B' = c_B'/f$$

where

$$c_B' = \sqrt{2\pi f} [D/\rho h]^{1/4} \text{ - bending wave velocity.} \tag{3.352}$$

For uniform plates with a typical Poisson's ratio  $\nu = 0.3$ , this reduces to

$$\lambda_B' \approx \sqrt{1.90 c_L h/f}$$

and

$$c_B' \approx \sqrt{1.90 c_L h f} \tag{3.353}$$

where

$c_L$  = velocity of longitudinal waves in bars

$f$  = frequency

$h$  = plate thickness.

The expression for bending wavelength is plotted in Figure 3.95a-d for typical thicknesses of common construction ma-

terials. The figures may also be used for uniform beams with a thickness  $h$  since the only change is a minor decrease in the constant 1.90 to 1.81 for  $\nu = 0.3$ . Application of this figure may be illustrated as follows.

For a plate which is pinned on two opposite edges and free on the others, the fundamental vibration mode occurs at the frequency for which the bending wavelength  $\lambda_B'$  is equal to twice the span between the simple supports. This is the lowest frequency for which a standing wave can occur for this type of boundary condition. For simple supports on all four sides, the lowest natural frequency is approximately equal to the sum of the "standing wave" frequencies for each span. As an example, for an 8-inch thick concrete wall 10 feet high by 40 feet long, considered as simply supported, the frequencies corresponding to bending wavelengths of  $2 \times 10$  feet and  $2 \times 40$  feet are found to be 37 Hertz and 2.3 Hertz, respectively, from Figure 3.95b. Thus, the estimated fundamental frequency is  $37 + 2.3 \approx 39$  Hertz.

The relationship between bending wavelength  $\lambda_B'$  and span length for other types of boundary conditions may be determined from the values for  $L/\lambda_{Bn}$  specified in Section 3.3.5.4 for lateral vibrations of beams.

Upper Limit for Bending Wavelengths

The plot in Figure 3.95b shows a line indicating an upper limit of validity. This represents the approximate high frequency bound for validity of Equation 3.35 which occurs when the bending wavelength  $\lambda_B'$  is equal to less than 6 times the plate thickness. For shorter wavelengths, the bending wave velocity in the plate  $c_B'$  is no longer predicted accurately by Equation 3.352. The latter would indicate that this wave velocity would increase without limit as frequency increases. In fact, when the bending wavelength becomes much less than 6 times the plate thickness,  $c_B'$  approaches the velocity  $c_r$  of Rayleigh waves in the plate (Reference 3.64). This wave velocity  $c_r$  is related to the longitudinal  $c_L$  and shear  $c_s$  wave velocities as indicated in Table 3.10.

TABLE 3.10

RATIO OF RAYLEIGH WAVE VELOCITY  $c_r$  IN PLATES TO LONGITUDINAL BAR VELOCITY  $c_L$  AND SHEAR WAVE VELOCITY  $c_s$  AS A FUNCTION OF POISSON'S RATIO

Poisson's Ratio	$c_r/c_L$	$c_r/c_s$
0	0.617	0.874
0.1	0.600	0.891
0.2	0.587	0.910
0.3	0.575	0.927
0.4	0.562	0.942
0.5	0.551	0.955



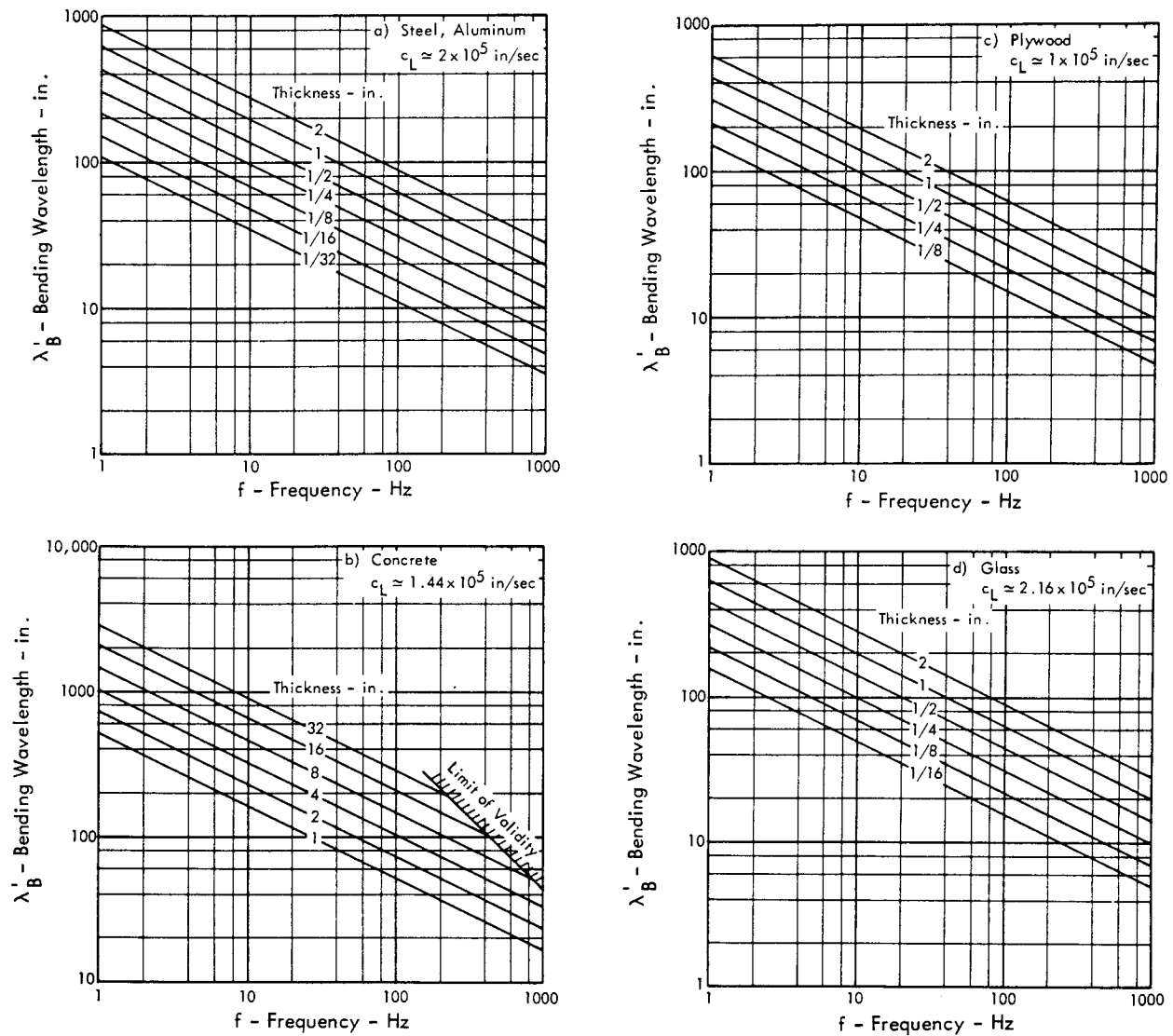


FIGURE 3.95 Bending Wavelengths in Uniform Plates for Various Materials and Thicknesses (Adopted, in Part, from Reference 3.63)

Figure 3.96 shows the variation in the velocity  $c'_B$  of free flexural bending waves in a plate, as a function of the plate thickness to bending wavelength ratio (Reference 3.64). The bending wave velocity is normalized by the shear wave velocity  $c_s$  and for short wavelengths, approaches the asymptotic value of about  $0.93 c_s$ , corresponding to the Rayleigh wave speed. For long wavelengths,  $c'_B/c_s$  is proportional to  $h/\lambda'_B = fh/c'_B$  or

$$c'_B \propto \sqrt{c_s f h} \propto \sqrt{c_L f h}$$

since  $c_s$  and  $c_L$  are directly proportional. This is the long wavelength limit indicated by the dashed line passing through the origin.

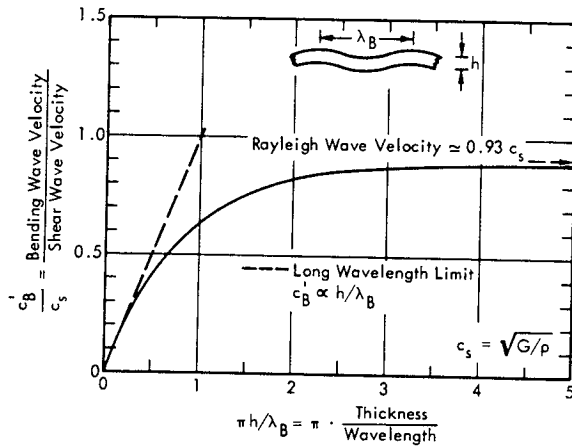


FIGURE 3.96 Change in Velocity of Lateral Bending Waves in a Semi-Infinite Slab as a Function of the Thickness to Wavelength Ratio (from Reference 3.64)

Rayleigh waves are a form of transverse shear waves which travel on the surface of the plate. They represent only one part of the more complex process of elastic wave motion which occurs at high frequencies where the structural dimensions become large relative to the flexural wavelengths. This more complex form of flexural vibration of plates is the result of the finite effects of rotary inertia and shear forces. As noted earlier for beams, these effects tend to decrease the natural frequency below that predicted by the simpler "long wavelength" theory (e.g., Bernoulli-Euler beam theory). This is simply another way of showing that the bending wave velocity begins to reach a limiting value.

Further consideration of this process is not desirable here since it introduces another order of magnitude in the complexity of structural vibrations, comparable to or greater than the difference between statics and conventional structural dynamics. The phenomenon is mentioned primarily to illustrate the "high frequency" limitations in the usual theory. Further treatment of the subject is available in the literature, including a compact summary in Reference 3.64.

### 3.3.5.7 Natural Frequencies for Plates with Non-Ideal Boundary Conditions

Edge conditions of real structures, such as the walls or roof of a building, or of equipment mounting plates, will range between free and fully clamped, depending on the type of construction. The typical variation in the fundamental natural frequency for such varying edge conditions is shown in the following table, where the fundamental frequency of a panel with simple supports on four sides is assigned a value of 1.

TABLE 3.11

RELATIVE FUNDAMENTAL FREQUENCIES OF PANELS WITH SIDES a AND b AND VARYING IDEAL BOUNDARY CONDITIONS (F = Free, P = Pinned, C = Clamped)

Side a b	a/b = 1			a/b = 1/2		
	F	P	C	F	P	C
F	0.71	0.50	1.12	0.47	0.20	0.44
P	0.50	1	1.47	0.80	1	1.11
C	1.12	1.47	1.82	1.79	1.94	2.00

For panels whose supports on all four sides range from fully pinned to fully clamped with aspect ratios varying from 1:1 to 2:1, a variation in fundamental frequency of 2:1 is indicated in Table 3.11. Engineering judgement would often be sufficient to estimate the fundamental frequency between these two extremes.

When improved accuracy is required, the effect of variable edge fixity of a panel could be estimated using the results for beams given in Figures 3.88b to 3.88d, page 3-128. These figures specified the first three natural frequencies of a uniform beam with rigid pinned supports having rotational fixity varying from 0 (pinned edge) to  $\infty$  (clamped edge). For application to a plate, the variable edge fixity parameter for the beam,  $k_r L/EI$  would become  $k'_r a/D$  where  $k'_r$  is a rotational stiffness per unit length along side (a), and  $D = Eh^3/12(1 - \nu^2)$  is the bending stiffness of the plate. An interpolation method could then be used to estimate the fundamental plate frequency. Essentially, this would consist of determining the change in natural frequency of an equivalent beam with partial fixity, relative to the total change between a pinned and clamped condition. The average correction factors for each pair of panel edges could then be used to estimate the relative change in the natural frequency of the plate between pinned and fully clamped conditions. Although only approximate, the method would provide refined estimates suitable for engineering design.

Natural Frequencies of Uniform Square Plates Bounded by Flexible Beams

A common panel support configuration encountered in practice consists of a uniform plate supported by beams, such as illustrated in Figure 3.97a. Reference 3.65 analyzes the case of a square uniform plate resting on four equal beams which are pinned at the ends. In order to determine the fundamental frequency, the plate and beam were divided into finite elements and a numerical computation was made of the modified equation of motion for the system. Rotary inertia effects in the beam and plate were neglected. The results are shown in Figure 3.97b in terms of the frequency constant  $C_n$  as a function of the relative beam-to-plate stiffness and mass ratios. The applicable parameters are defined in Figure 3.97a. As indicated, the supporting beams have no significant stiffening influence on the plate until the stiffness ratio  $2 E_b I_b / a D$  exceeds 0.2. As this parameter approaches  $\infty$ , the frequency of the plate-beam combination approaches that of a pinned-pinned plate. In the absence of supporting beams, the problem reduces to a plate pinned at the four corners. The natural frequencies for several variations of this case are shown in Table 3.32 at the end of this chapter.

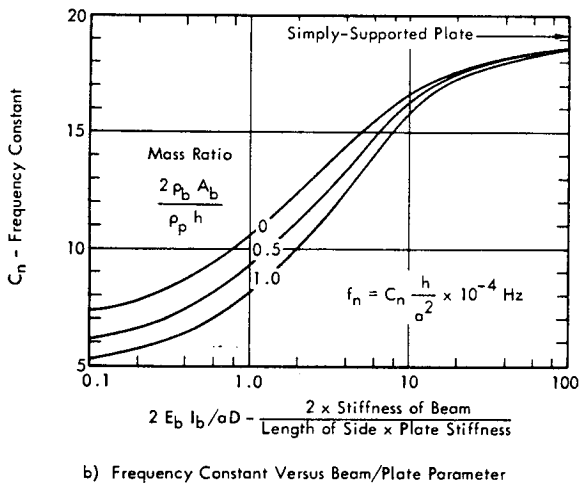
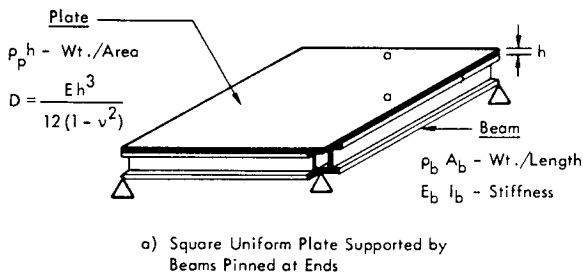


FIGURE 3.97 Fundamental Natural Frequency of a Uniform Square Steel Plate on Beam Supports of Varying Stiffness and Mass (Adopted from Reference 3.65)

3.3.5.8 Natural Frequencies of Non-Homogeneous Plates

Practical methods for defining plate vibration must include techniques applicable to such configurations as:

- Corrugated or Rib-Stiffened Panels
- Honeycomb Panels
- Concrete Block Walls

Nonhomogeneous walls which have a different stiffness  $D$  in each direction are generally classified as anisotropic plates. Several of the more commonly encountered configurations in the first category have been analyzed in detail in Reference 3.66. The basic analytical approach includes consideration of rotary inertia effects of the stiffeners since any flexure of the stiffened panel will involve significant rotary motion of the center of mass of the stiffener cross section. When this effect is included with the different stiffness in each direction of a simply supported stiffened panel, a general frequency equation is

$$f_{mn} = \frac{1}{2\pi} \left[ \frac{D_a \left(\frac{m\pi}{a}\right)^4 + 2H \left(\frac{m\pi}{a}\right)^2 \left(\frac{n\pi}{b}\right)^2 + D_b \left(\frac{n\pi}{b}\right)^4}{\rho h + I_a \left(\frac{m\pi}{a}\right)^2 + I_b \left(\frac{n\pi}{b}\right)^2} \right]^{1/2} \quad (3.354)$$

where

$D_a, D_b$  = plate stiffness in the direction of side  $a$  and  $b$ , respectively,

$H$  = a cross stiffness parameter involving stiffness in each direction of the plate, and

$I_a, I_b$  = mass moments of inertia of a unit area of the panel and stiffeners about the centroidal axes in the  $a$  and  $b$  direction, respectively.

Table 3.37 at the end of the chapter gives specific expressions for these mass and stiffness parameters for ribstiffened, corrugated, and uniform but anisotropic plates.

Honeycomb Panels

The vibration characteristics of honeycomb panels, such as illustrated in Figure 3.98, can be expressed in terms of the properties for an equivalent solid panel with the same total thickness modified by a correction factor to account for the different mass and stiffness properties.

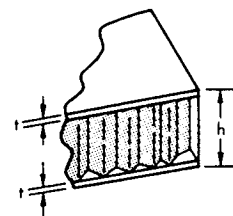


FIGURE 3.98 Typical Honeycomb Panel

The bending stiffness  $D$  of a honeycomb panel can be assumed to be equal in each direction and equal to  $E I' / (1 - \nu^2)$  where  $I'$  is the area moment of inertia about the centroidal axis of a unit width strip of the panel. For a typical honeycomb panel, the moment of inertia of the core material is negligible so that  $I'$  becomes

$$I' = 2 \int_{h/2-t}^{h/2} r^2 dA = 2 \int_{h/2-t}^{h/2} r^2 (1 \cdot dr) \quad (3.355)$$

where  $r$  is the distance of an elemental strip of thickness  $dr$  from the centroidal bending axis. For  $t \ll h$ , this is very nearly equal to

$$I' \approx \frac{h^2 t}{2}$$

so that the bending stiffness is

$$D \approx \frac{E h^2 t}{2(1-\nu^2)} \approx D_s \left( \frac{6t}{h} \right) \quad (3.356a)$$

where

$D_s = E h^3 / 12 (1 - \nu^2)$  - the bending stiffness of a solid panel with the same total thickness  $h$ .

Let the total mass per unit area, including the core, be defined as  $m_p$ , and let the mass per unit area of the skin be  $m_s = 2 \rho t$  where  $\rho$  is the mass density of the skin material. The natural frequencies  $f_{mn}$  and bending wavelength  $\lambda_B$  will then be given by

$$f_{mn} \approx f_{mn_s} \sqrt{\frac{6t}{h} \cdot \frac{\rho h}{m_p}} = \sqrt{\frac{3 m_s}{m_p}} \quad (3.356b)$$

$$\lambda'_B \approx \lambda'_{B_s} \left[ \frac{3 m_s}{m_p} \right]^{1/4} \quad (3.356c)$$

where

$f_{mn_s}, \lambda'_{B_s}$  = natural frequencies and bending wavelengths of a solid panel with the same total thickness  $h$ .

For typical metal honeycomb panels,  $m_s/m_p$  is about 2/3 so that the natural frequencies and bending wavelengths are about  $\sqrt{2}$  and  $2^{1/4}$  greater, respectively, than a solid panel of the same skin material and same total thickness  $h$ .

Concrete Block Walls

Concrete masonry walls are subject to considerable variation in their dynamic properties due to variations in materials, construction methods and condition of the wall. Whenever possible, experimental data should be used as a check against theoretical calculations. The bending stiffness  $D$  of a concrete block can be estimated by

$$D \approx \alpha E h^3 / 12 \quad (3.357a)$$

where  $\alpha$  is a constant equal to 0.8 for hollow block walls and 1.0 for solid block walls. The true thickness  $h$  is about 3/8" less than the nominal wall thickness (Reference 3.9). For preliminary calculations, an average value of  $E$  of  $2.0 \times 10^6$  psi is recommended for dense concrete blocks and  $1 \times 10^6$  for cinder or pumice type blocks. Theoretical and experimental values for the bending stiffness are compared in the following table of design data for concrete block walls. The agreement between computed and measured values is generally very good.

TABLE 3.12

DESIGN PARAMETERS FOR VIBRATION CHARACTERISTICS OF CONCRETE BLOCK WALLS

Type of Wall	Nominal Thickness (in.)	Actual Thickness (in.)	Surface Weight <sup>(1)</sup> lb/ft <sup>2</sup>	D - Bending (Equation 3.356) 10 <sup>6</sup> lb-in.	Stiffness Exptl. Data <sup>(1)</sup> 10 <sup>6</sup> lb-in.	c <sub>L</sub> 10 <sup>5</sup> in/sec	C <sub>n</sub> Frequency Constant 10 <sup>4</sup> in <sup>2</sup> /sec
Solid Dense Concrete Block	4	3-5/8	37	6.5	6.05	1.1	15.5
Solid Dense Concrete Block	6	5-5/8	57.5	30	--	1.1	26.5
Hollow Dense Concrete Block	6	5-5/8	35	24	28.3	1.1	30.5
Hollow Dense Concrete Block	8	7-5/8	47.5	60	--	1.1	41.5
Hollow Cinder Block	6	5-5/8	25	12	10.2	1.1	25.5
Hollow Cinder Block	8	7-5/8	34	30	--	1.1	35

(1) Computed from experimental data in Reference 3.9.

The last column in Table 3.12 defines a modified frequency constant  $C'_n$  to be used in a simplified equation for the natural frequencies of the wall, assuming simply-supported edges.

$$f_{mn} = C'_n \left[ \left(\frac{m}{a}\right)^2 + \left(\frac{n}{b}\right)^2 \right] \quad (3.357b)$$

where  $a, b$  = dimensions of wall - inches

$m, n$  = respective mode numbers.

3.3.5.9 Normal Modes of Mass and Stiffness Loaded Plates

The effect of added lumped masses or spring restraints on the natural frequencies of a plate can be conveniently estimated by applying the single mode approximation method or the equivalent Rayleigh energy method discussed in Section 3.3.5.5. For example, a general expression for the approximate fundamental natural frequency of a plate loaded by  $R$  masses  $m_i$  at points  $y_i, z_i$  on the panel would be

$$f_1 = f_{10} \left[ 1 + \left( \sum_i^R m_i \phi_1^2(y_i) \phi_1^2(z_i) \right) / M_{11} \right] \quad (3.358a)$$

where

$f_{10}$  = the fundamental frequency without mass loads

$\phi_1(y_i)$  = mode shape in the fundamental mode at  $y_i$  (along the  $y$  direction)

$\phi_1(z_i)$  = mode shape in the fundamental mode at  $z_i$

$M_{11}$  = generalized mass of the unloaded panel.

The summation term within the brackets can be recognized as the generalized mass of the added point masses. For the case of a single mass  $m$  located at the center of a simply-supported panel with a mass  $m_p$ , Equation 3.358a reduces to

$$f_1 = f_{10} \sqrt{1 + 4m/m_p} \quad (3.358b)$$

Thus, a center mass has four times the effective value of the panel mass at this point. For other panel boundary conditions, a comparable expression is obtained where the factor 4 is replaced by  $1/(\text{Generalized Mass Fraction of Base Panel})$ ; for clamped plates, the factor would be 6.37.

As shown earlier for simply-supported and fully-clamped beams, the effect of a center mass on the higher natural frequencies is much less than the effect on the fundamental frequency. However, there is one very important effect of mass loading on panels which is not shown by the above expressions. This is the change in mode shape at high frequencies. As illustrated in Figure 3.99, a point mass load

at the center of a panel will tend to act like a pinned support point for higher order modes of the panel. Thus, as the frequency of vibration increases, the motion of the mass is reduced, relative to the peak modal amplitude of the panel. At very high frequencies, the mass tends to remain essentially stationary. This attenuation in response amplitude of the mass becomes significant for frequencies above a limiting value defined by (Reference 3.44)

$$f_l \geq \frac{0.37 c_L \rho h^2}{m} \quad (3.359)$$

where

$m$  = point mass load

$c_L$  = longitudinal wave velocity (see Table 3.39)

$\rho$  = panel mass density

$h$  = panel thickness.

This attenuation effect can be usefully employed as a means of vibration isolation for plate mounted equipment. However, for lightweight panels, vibration response measurements are subject to errors caused by this mass loading effect -- which is due to the finite mass of the accelerometers. Above the limiting frequency  $f_l$  defined by Equation 3.359, the measured acceleration response will decrease, inversely with the square of frequency, below the response that would be measured with a massless accelerometer.

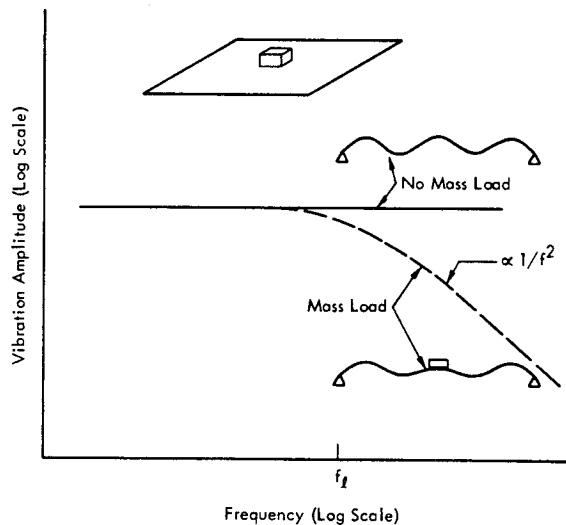


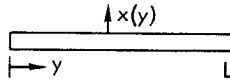
FIGURE 3.99 Change in Mode Shape and Response Amplitude of a Panel Loaded by a Point Mass.  $f_l$  is limiting frequency for change in response as defined by Equation 3.359.

3.3.6 FORCED RESPONSE OF BEAMS AND PLATES TO LATERAL LOADS

The basic concepts for defining the forced vibration response of beams and plates in terms of their normal modes has already been developed in detail for lumped parameter systems in Section 3.3.3. By applying the transformations in terminology between lumped and continuous systems outlined on page 3-108, the expressions for forced response of continuous structure are readily developed. Several specific cases will be considered which are pertinent for analysis of acoustic and blast loads on structure.

3.3.6.1 Normal Mode Solution for a Uniform Static Load

STATIC LOAD ON BEAMS



For a uniform load on a simply-supported beam, the deflection  $x(y, t)$  may be defined by the infinite series of normal modes as

$$x(y, t) = \sum_n q_n(t) \phi_n(y)$$

where

$$\phi_n(y) = \sin n\pi \bar{y} \text{ for a simply-supported beam}$$

$$\bar{y} = y/L$$

$$q_n(t) = \text{nth normal coordinate.}$$

The equation of motion for  $q_n(t)$  is the single degree-of-freedom equation

$$\ddot{q}_n(t) + \omega_n^2 q_n(t) = \frac{F_n(t)}{M_n}$$

where

$$\omega_n = \text{natural frequency of nth mode}$$

$$F_n(t) = b \int_0^L p(y, t) \phi_n(y) dy - \text{the generalized force for the nth mode with a pressure } p(y, t) \text{ at } y \text{ which is constant for all points on the beam.}$$

$$b = \text{width of beam}$$

$$M_n = \text{generalized mass for nth mode.}$$

For a uniform static load,  $q_n(t) = 0$  and  $b p(y, t) = P_s$ , which is the uniform static force per unit length. The generalized force for the nth mode then becomes

$$F_n = P_s \int_0^L \sin n\pi \frac{y}{L} dy = \begin{cases} 2 P_s L / n\pi, & n = \text{odd} \\ 0 & n = \text{even} \end{cases}$$

In this case, the joint acceptance  $J_n$ , or ratio of generalized force to total load would be

$$J_n = \frac{F_n}{P_s L} = \frac{2}{n\pi}$$

The modal amplitude  $\bar{q}_n$  is

$$\bar{q}_n = \frac{F_n}{\omega_n^2 M_n} = \frac{2 P_s L}{n\pi \omega_n^2 M_n}$$

For a simply supported beam with a stiffness  $EI$  and mass  $\rho A$  per unit length, the generalized mass  $M_n$  is  $1/2 \rho A L$  and the natural frequency is

$$\omega_n = \left(\frac{n\pi}{L}\right)^2 \sqrt{\frac{EI}{\rho A}}$$

Thus, the peak static deflection  $X_{s \max}$  at the center of the beam, where  $\bar{y} = 1/2$  and  $\sin n\pi \bar{y} = \sin n\pi/2$ , is obtained by combining the above expressions to give

$$X_{s \max} = \frac{P_s L^4}{EI} \sum_n \frac{4 \sin n\pi/2}{(n\pi)^5} \tag{3.360}$$

The even terms in this series are zero, since  $\sin n\pi/2 = 0$  for  $n = \text{even}$ , while the odd terms are alternately positive and negative for  $n = 1, 3, 5, 7, \text{etc.}$  The magnitude of each of the first five terms in this series is shown in Table 3.13.

TABLE 3.13

CONTRIBUTION OF NORMAL MODES TO PEAK DEFLECTION OF SIMPLY-SUPPORTED BEAM UNDER A UNIFORM STATIC LOAD

Mode (n)	1	3	5	7	9
$\frac{\sin n\pi/2}{n^5}$	1	-0.00411	+0.00032	-0.00006	+0.00002
$\sum_n \frac{\sin n\pi/2}{n^5}$	1	0.99589	0.99621	0.99615	0.99617
Relative Contribution of Each Mode	+100.3%	-0.41%	+0.032%	-0.006%	+0.002

Only the first term or fundamental mode contributes significantly to the total deflection. The peak deflection, including the first five terms, is given by

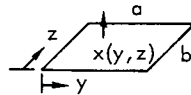
$$X_{s \max} = 0.9962 \frac{4}{\pi^5} \frac{P_s L^4}{EI} = 0.01302 \frac{P_s L^4}{EI} \tag{3.361}$$

This compares with the usual value for the peak deflection at the center of a simply-supported beam under a uniform static load given by (Reference 3.50)

$$X_{s \max} = \frac{5}{384} \frac{P_s L^4}{EI} = 0.01302 \frac{P_s L^4}{EI}$$

The significance of this result is to clearly demonstrate that the deflection of a simply-supported beam vibrating in its first vibration mode has essentially the same shape as the deflection under a static load. Thus, when the beam can be designed on the basis of a static load or static deflection, a peak dynamic deflection in the fundamental mode for a dynamic load can be related to an equivalent static load which would produce the same peak deflection.

STATIC LOAD ON PLATES



The same procedure may be applied to the static load on a panel. For a simply-supported panel with sides (a) and (b) the essential results may be briefly summarized as follows:

Mode Shape  
(in mnth mode)  $\phi_{mn}(y, z) = \sin m\pi \bar{y} \sin n\pi \bar{z}$

Total Deflection  
(in all modes)  $x(y, z) = \sum_m \sum_n \bar{q}_{mn} \sin m\pi \bar{y} \sin n\pi \bar{z}$

where  $\bar{y}, \bar{z} = y/a$  and  $z/b$ , respectively, and

$\bar{q}_{mn}$  = peak deflection in mnth mode.

Natural Frequencies  $\omega_{mn} = \pi^2 \sqrt{\frac{D}{\rho h}} \left[ \left(\frac{m}{a}\right)^2 + \left(\frac{n}{b}\right)^2 \right]$

Applied Pressure  $p(y, z) = p_s$  - uniform static pressure

Generalized Force

$$F_{mn} = \begin{cases} p_s ab \int_0^a \int_0^b \sin m\pi \bar{y} \sin n\pi \bar{z} d\bar{y} d\bar{z} \\ 4ab p_s / mn \pi^2, & m, n - \text{odd} \\ 0 & m \text{ or } n - \text{even} \end{cases}$$

Joint Acceptance  
(for uniform static load)  $J_{mn} = F_{mn} / p_s ab$

Generalized Mass  $M_{mn} = \frac{1}{4} \rho abh$  for a panel thickness h.

Normal Coordinate  $\bar{q}_{mn} = \frac{F_{mn}}{\omega_{mn}^2 M_{mn}}$

where  $\omega_{mn}^2 M_{mn}$  is the generalized stiffness for the mnth mode.

Maximum Deflection  
(at center of panel)

$$X_{s \max} = \sum_m \sum_n \bar{q}_{mn}, \quad m, n = \text{odd only}$$

or  $X_{s \max} = \alpha \frac{P_s a^4}{D}$

where

$$\alpha = \frac{16}{\pi^6} \sum_m \sum_n \left[ \frac{\sin m\pi/2 \sin n\pi/2}{mn [m^2 + (na/b)^2]^2} \right]_{m, n - \text{odd}}$$

(3.362)

The final result specifies the peak static deflection in terms of a rapidly converging double summation of terms derived from the normal mode expansion of the deflection. The percent contribution of the first few terms in this series are listed in Table 3.14 for a square plate with simply-supported edges. For this case, the value of  $\alpha$ , including all terms, is 0.004448.

TABLE 3.14

PERCENT CONTRIBUTION OF FIRST FEW ODD ORDER TERMS IN NORMAL MODE EXPANSION OF DEFLECTION OF A SIMPLY-SUPPORTED SQUARE PLATE FOR A UNIFORM STATIC LOAD

n → \ m ↓	1	3	5
1	+100.4%	-1.36%	+0.121%
3	-1.36	+0.140	-0.0236
5	+0.121	-0.0236	+0.0065
7	-0.0234	+0.0058	-0.0021

Clearly, the first mode term ( $m = n = 1$ ) is again the principal component for the static deflection. This term is simply

$$\alpha_1 = \frac{16}{\pi^6} \frac{1}{\left[1 + \left(\frac{a}{b}\right)^2\right]^2} \quad (3.363)$$

Values for  $\alpha$  are listed in Table 3.15 for several aspect ratios using Equation 3.362 for the exact value and Equation 3.363 for the first mode only.

TABLE 3.15

VALUE OF  $100 \alpha = 100 X_{s \max} D/p_s a^4$  FOR MAXIMUM DEFLECTION  $X_{s \max}$  TO SIMPLY-SUPPORTED PLATE WITH SHORT SIDE (a), AND BENDING STIFFNESS D UNDER UNIFORM STATIC PRESSURE  $p_s$

a/b →	1.0	0.5	0.2	0
First Mode (Equation 3.363)	0.416	1.064	1.535	1.67
Exact Value (Equation 3.362)	0.405	1.012	1.298	1.302

The exact values shown in the last row correspond with values from Reference 3.66.

Apparently, the first mode approximation for the total deflection of a simply-supported plate under a static load is less accurate as the panel aspect ratio becomes less than 1. However, the deflection for the first mode is always on the conservative side. Thus, a peak dynamic deflection of a simply-supported panel in its first mode can be related to an equivalent static load which would give approximately the same peak deflection.

Panel Stress Defined in Terms of Normal Modes

It is also desirable to examine the modal summation which defines the stress in the panel for a uniform static load. The bending stress  $\sigma(y)$  in a panel in the y direction can be given by (Reference 3.5)

$$\sigma(y) = -\frac{6D}{h^2} \left[ \frac{\partial^2 x(y,z)}{\partial y^2} + \nu \frac{\partial^2 x(y,z)}{\partial z^2} \right] \quad (3.364a)$$

where  $\nu$  = Poisson's ratio.

For the z direction, the corresponding expression is

$$\sigma(z) = -\frac{6D}{h^2} \left[ \frac{\partial^2 x(y,z)}{\partial z^2} + \nu \frac{\partial^2 x(y,z)}{\partial y^2} \right] \quad (3.364b)$$

Applying these expressions, it is found that the peak static stress occurs at the center of the panel in a direction parallel to the shortest side. It is given by

$$\sigma_{s \max} = \gamma p_s \left(\frac{a}{h}\right)^2 \quad (3.365)$$

where

$$\gamma = \frac{96}{\pi^4} \sum_{m, n \text{ odd}} \sum_{n} \left[ \frac{(m^2 + \nu(na/b)^2) \sin m(\pi/2) \sin(n\pi/2)}{mn [m^2 + (na/b)^2]^2} \right]$$

The series still converges but not as rapidly as for the series which defines the deflection. This is due to the influence of curvature (i.e.,  $\partial^2 x(y,z)/\partial y^2$ ) of the higher order modes. These become more significant in the modal expansion for stress. For example, for a simply-supported square plate, with  $\nu = 0.3$ , the percent contribution of the largest five terms in this series relative to the total summation is given by

$$\begin{aligned} m = n = 1 & \quad \gamma_{1,1}/\gamma = +111.7 \\ m = 3, n = 1 & \quad \gamma_{3,1}/\gamma = -10.7 \\ m = 1, n = 3 & \quad \gamma_{1,3}/\gamma = -4.2 \\ m = 5, n = 1 & \quad \gamma_{5,1}/\gamma = +2.6 \\ m = 3, n = 3 & \quad \gamma_{3,3}/\gamma = +1.4 \end{aligned}$$

The value of  $\gamma$  for the first mode only, and the exact value including all modes, is listed in Table 3.16 for several aspect ratios of a simply-supported plate, for  $\nu = 0.3$ .

TABLE 3.16

VALUE OF  $\gamma = (\sigma_{s \max}/p_s) (h/a)^2$  FOR MAXIMUM STRESS  $\sigma_{s \max}$  FROM A UNIFORM STATIC PRESSURE  $p_s$  ON A SIMPLY-SUPPORTED PLATE WITH SHORT SIDE (a) AND THICKNESS (h)

a/b →	1.0	0.5	0.2	0
First Mode Only	0.320	0.679	0.920	0.985
Exact Value (Equation 3.365)	0.287	0.610	0.746	0.750
% Error in First Mode Approximation	+11.5%	+11.3%	+23.3%	+31.3%

The increased significance of the higher modes is clearly evident. However, the single mode approximation is conservative by 11 to 31%. That is, for a given effective dynamic pressure  $p(f)$  acting on the first mode ( $f_{1,1}$ ) of a simply-supported panel, an equivalent static pressure  $p_s$  which would produce the same peak stress would be 11 to 31% less than  $p(f)$ .

To complete this modal analysis of static loads on plates, it is convenient to express the maximum static stress  $\sigma_{s \max}$  in terms of the maximum static deflection  $X_{s \max}$ . This is obtained by combining Equation 3.362 for the deflection-to-load ratio with Equation 3.365 for the maximum stress-to-load ratio to give

$$\sigma_{s \max} = \beta E \left(\frac{h}{a}\right) \frac{X_{s \max}}{a} \quad (3.366)$$

$$\beta = \gamma / 12 a (1 - \nu^2)$$

and  $\gamma$ ,  $a$  are given by Equations 3.365 and 3.362, respectively. This quantity is tabulated below for several aspect ratios and for  $\nu = 0.3$ .



TABLE 3.17

VALUE OF  $\beta = \sigma_{s \max} a^2 / Eh X_{s \max}$  FOR MAXIMUM STRESS  $\sigma_{s \max}$  IN SIMPLY-SUPPORTED PLATE WITH A UNIFORM STATIC LOAD AND MAXIMUM CENTER DEFLECTION OF  $X_{s \max}$

$a/b \rightarrow$	1.0	0.5	0.2	0
First Mode Only	7.05	5.83	5.49	5.40
Exact (Equation 3.367)	6.49	5.51	5.26	5.26
% Error in First Mode Approximation	+8.7%	+5.7%	+4.1%	+2.7%

The first mode approximation for the static stress, based on peak deflection, is close to the exact value for all aspect ratios. Thus, a peak dynamic deflection in the first mode can be related to an equivalent static stress in a panel having the same total static deflection.

The same analysis was carried out for a clamped-clamped plate to show how the first mode approximation for the parameters  $\alpha$ ,  $\gamma$  and  $\beta$  compare with the exact values. For the first mode approximation, the mode shape was taken to be the product of the mode shapes for clamped-clamped beams. The exact values were computed from values specified in Reference 3.50 for a static load on a clamped-clamped plate. The results are summarized in Table 3.18.

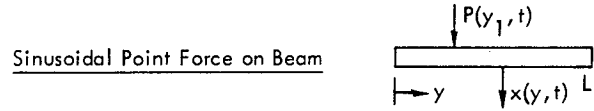
TABLE 3.18

VALUES OF  $\alpha$ ,  $\gamma$ , AND  $\beta$  FOR FIRST MODE AND ALL MODES (EXACT) OF A CLAMPED-CLAMPED PLATE WITH UNIFORM STATIC PRESSURE  $p_s$  WHERE  $\alpha = X_{s \max} D / p_s a^4$ ,  $\gamma = \sigma_{s \max} h^2 / p_s a^2$ , AND  $\beta = \sigma_{s \max} a^2 / Eh X_{s \max}$  FOR MAXIMUM DEFLECTION  $X_{s \max}$  AND MAXIMUM STRESS  $\sigma_{s \max}$

$a/b \rightarrow$	1.0	0.5	0.2	0.0
$\alpha$				
First Mode	0.00139	0.00298	0.00352	0.0036
Exact	0.00138	0.00277		0.00285
$\gamma$				
First Mode	0.309	0.453	0.493	0.497
Exact	0.308	0.497		0.50
$\beta$				
First Mode	2.04	1.39	1.28	1.26
Exact	2.04	1.64		1.60

3.3.6.2 Response of Beams and Plates for Sinusoidal Loads

The general expression for the response of a damped lumped parameter system to sinusoidal excitation was given in Section 3.3.3.5 (e.g., Equation 3.237, page 3-71). When this is applied to sinusoidal loads on beams, the general form for the instantaneous deflection  $x(y, t)$ , at a point  $y$  to a sinusoidal force with a frequency  $f$ , can be summarized as follows:



- Driving Force

$$P(y_1, t) = P \cos 2\pi f t \quad \text{at } y = y_1$$

- Displacement

$$x(y, t) = \sum_n^{\infty} q_n(t) \phi_n(y) \quad (3.367)$$

- Normal Coordinate

$$q_n(t) = \frac{P_o J_n |H_n(f)|}{(2\pi f_n)^2 M_n} \cos(2\pi f t - \theta_n) \quad (3.368a)$$

$\phi_n(y)$  = mode shape at  $y$  in  $n$ th mode

$P_o = P$ , amplitude of total force

$J_n = \phi_n(y_1)$  - joint acceptance or relative generalized force for point force at  $y_1$

$H_n(f) = 1 / \sqrt{[1 - (f/f_n)^2]^2 + (2\delta_n f/f_n)^2}^{1/2}$  - the dynamic magnification factor for  $n$ th mode

$\delta_n$  = critical damping ratio for  $n$ th mode

$\theta_n = \tan^{-1} \frac{2\delta_n f/f_n}{1 - (f/f_n)^2}$  - phase angle for response of  $n$ th mode

$f_n$  -  $n$ th natural frequency

$M_n$  - generalized mass for  $n$ th mode.

For the velocity response  $\dot{x}(y, t)$  at any point  $y$ , replace  $x(y, t)$  by  $\dot{x}(y, t)$  and  $q_n(t)$  by  $\dot{q}_n(t)$  in Equation 3.367 where  $\dot{q}_n(t)$  is given by

- Modal Velocity

$$\dot{q}_n(y, t) = \frac{P_o (f/f_n) J_n |H_n(f)|}{2\pi f_n M_n} \cos\left(2\pi f t - \theta_n + \frac{\pi}{2}\right) \quad (3.368b)$$

For the acceleration response  $\ddot{x}(y,t)$  at any point  $y$ , replace  $x(y,t)$  by  $\ddot{x}(y,t)$  and  $\ddot{q}_n(t)$  in Equation 3.367 where  $\ddot{q}_n(t)$  is given by

• Modal Acceleration

$$\ddot{q}_n(y,t) = - \frac{P_0 (f/f_n)^2 J_n |H_n(f)|}{M_n} \cos(2\pi f t - \theta_n) \tag{3.368c}$$

These three expressions are, in fact, completely general covering any form of steady state sinusoidal loading on a beam or a plate. It will only be necessary to define the expressions for  $P_0$ ,  $J_n$ ,  $\phi_n(y)$ ,  $M_n$  and  $f_n$ , for the particular type of load and configuration to be considered.

Damping has been ignored in the discussion of free vibration of beams and plates. This is consistent with the fact that only the lower order modes and frequencies of vibration are significant. These are not significantly influenced by the usual amounts of damping in structure. However, damping must be introduced again in order to limit the forced sinusoidal response amplitude at the resonant or natural frequencies of the structural element. For the time being, damping will be defined in terms of the critical damping factor  $\delta_n$  for each normal mode which is treated as an equivalent single degree of freedom system. Depending on the configuration, the value of  $\delta_n$  may range from as high as 0.2 ( $Q_n = 2.5$ ) to as low as 0.001 ( $Q_n = 500$ ). Typical values for built-up structural elements are of the order of 0.02.

The total response at any arbitrary point  $y$  on a beam to a sinusoidal point force is the summation of normal modes as defined by Equation 3.367. The summation of modal responses for a sinusoidal excitation was covered in detail in Section 3.3.3.6 and need not be repeated here. A few specific examples will illustrate the unique character of this modal response for a continuous structural element such as a beam.

Response of Simply-Supported Beam to Point Sinusoidal Force with Amplitude P Applied at Center

For this case, the following parameters apply (see Section 3.3.5.4)

- Mode Shape  $\phi_n(y) = \sin n\pi y/L$
- Natural Frequency  $f_n = \frac{\pi}{2} \left(\frac{n}{L}\right)^2 \sqrt{EI/\rho A}$
- Generalized Mass  $M_n = \frac{1}{2} \rho A L$
- Joint Acceptance  $J_n = \sin n\pi/2 = \begin{cases} \pm 1, n = \text{odd} \\ 0, n = \text{even} \end{cases}$

• Displacement Response at Center

At the center, the product of the joint acceptance  $J_n$  and response mode shape  $\phi_n(y)$  will be  $J_n \phi_n(y) = \phi_n^2(L/2) = (\sin n\pi/2)^2 = 1$  for  $n = \text{odd}$  or 0 for  $n = \text{even}$ . Thus, applying Equation 3.368a the displacement response is

$$x(L/2,t) = \frac{2PL^3}{\pi^4 EI} \sum_{n, \text{ odd}} \frac{|H_n(f)| \cos(2\pi f t - \theta_n)}{n^4} \tag{3.369}$$

where  $EI$  = bending stiffness of beam.

The amplitude of this displacement response, illustrated in Figure 3.100, is closely approximated by the first mode ( $n=1$ ) since the modal amplitude decreases as  $1/f^2$ . Since the generalized force for even modes is zero, excitation at frequencies corresponding to the natural frequencies for these modes does not result in a resonant response. However, a sharp null in the response will occur at a slightly higher frequency where the modal responses tend to add up to zero. At very low frequencies, the magnification factor  $|H_n(f)|$  approaches unity, and the peak displacement will be approximately equal to  $2 PL^3/\pi^4 EI$  or  $0.0206 PL^3/EI$ . This compares with the usual value of  $(1/48) PL^3/EI$  based on static considerations (Reference 3.50).

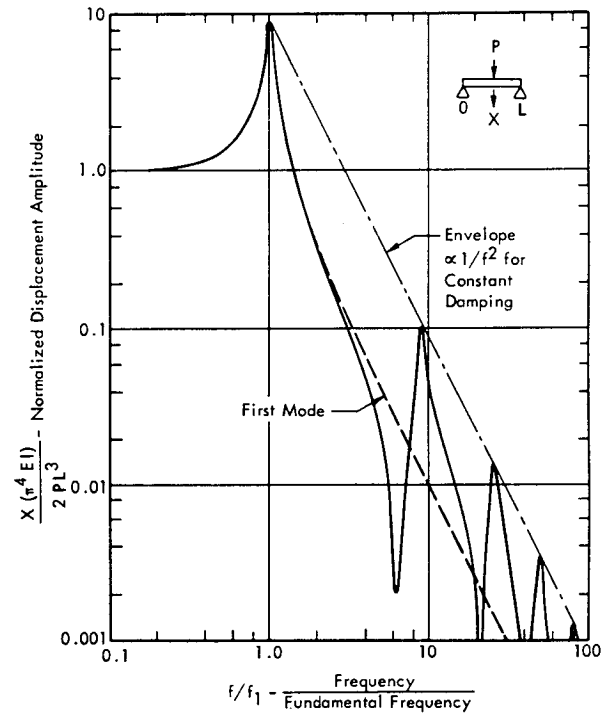


FIGURE 3.100 Normalized Displacement Response at Mid-Span of Simply-Supported Beam Driven by Sinusoidal Force at Same Point.  $Q$  for each mode  $\approx 9$ .

• Acceleration Response at Center

Applying Equation 3.368c, the acceleration response at this point is given, in g's, by

$$\frac{\ddot{x}(L/2,t)}{g} = \frac{-P}{W_b} \sum_{n, \text{ odd}} 2 (f/f_n)^2 |H_n(f)| \cos(2\pi f t - \theta_n) \tag{3.370}$$

where  $W_b = \rho A L g$  - the weight of the beam.

Note that all terms of this series are equally important - a single mode approximation is only usable near the natural frequency for any one normal mode.

• Acceleration Response at One-Quarter Span

For a response at  $y = L/4$ , with a point force excitation at the center, the product of the joint acceptance and response mode shape is

$$J_n \phi_n(y) = \phi_n(L/2) \phi_n(L/4) = \sin(n\pi/2) \sin(n\pi/4)$$

This represents a series which varies with  $n$  as  $+1/\sqrt{2}$ ,  $0$ ,  $-1/\sqrt{2}$ ,  $0$ ,  $-1/\sqrt{2}$ ,  $0$ ,  $+1/\sqrt{2}$ ,  $0$ ,  $+1/\sqrt{2}$ , etc. The acceleration amplitude for this case will be given by the same basic modal summation as in Equation 3.370 but with the weighting factor,  $\sin(n\pi/2) \sin(n\pi/4)$ , applied to each term.

The acceleration responses for these last two cases are shown in Figure 3.101. For a constant amplitude driving force, the amplitude of each mode is constant as defined by the ratio of force to mass. The primary difference between the response at the center and at the quarter span point is the absence of any sharp nulls for the latter. This is the net result of the more complex phase or sign of each of the odd modes for this case.

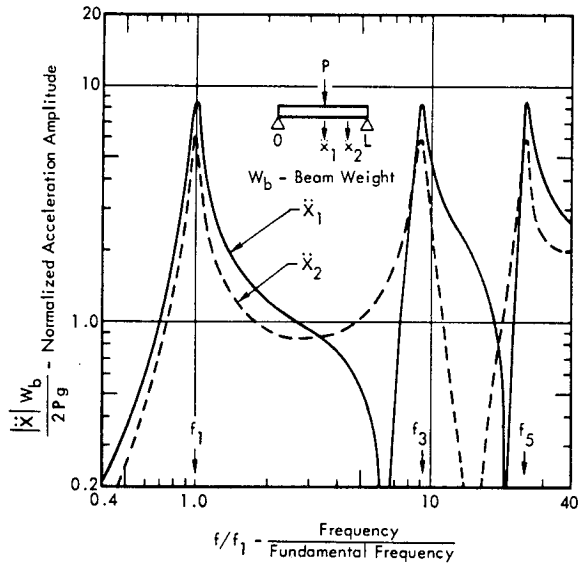


FIGURE 3.101 Normalized Acceleration Response at Mid-Span ( $\ddot{X}_1$ ) and 1/4 Span ( $\ddot{X}_2$ ) of Simply-Supported Beam Driven by Sinusoidal Force at Center.  $Q$  for each mode  $\approx 9$ .

Graphical Construction of Multi-Mode Response Function

The curves in Figures 3.100 and 3.101 can be constructed by a graphical method employing a simple template for the basic shape of the term  $|H_n(f)|$  which is plotted on a log-log scale. By accounting for the change in amplitude,

natural frequency  $f_n$  and the change in phase below and above the natural frequency of each term, a simple algebraic summation can be made graphically and an approximate response function determined. The accuracy is limited only the finite number of modes plotted.

This graphical method, illustrated in Figure 3.102, may be explained more readily by considering the form of Equation 3.370 for zero damping. In this case,  $\theta_n$  is zero and the acceleration amplitude can be represented by the series

$$\frac{\ddot{X}(L/2)}{g} = \frac{2P}{W_b} \sum_n \frac{(f/f_n)^2}{1 - (f/f_n)^2} \tag{3.371}$$

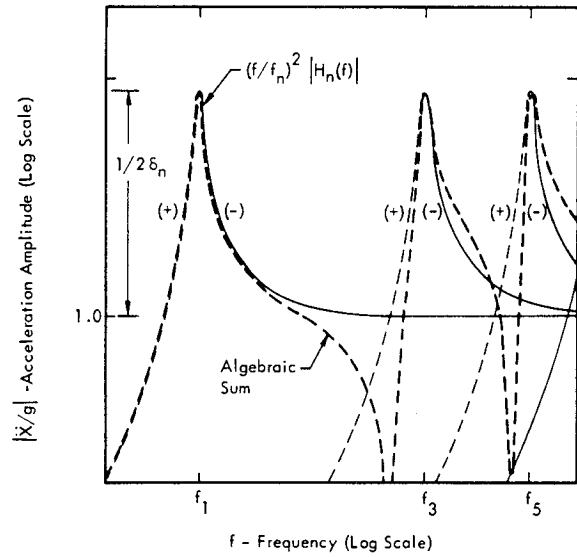


FIGURE 3.102 Graphical Construction of Overall Response by Algebraic Summation of Modal Responses. Case illustrated is acceleration response at center of beam due to point force at center (see Figure 3.101).

The phase of each term has only two values;  $+1$  or  $0$  degrees for  $f < f_n$ , and  $-1$  or  $180$  degrees for  $f > f_n$ . Thus, by algebraically adding up the response curves for each mode, utilizing the change in sign for each curve above and below resonance, a plot of the overall response can be readily constructed. As shown in Figure 3.102, this summation process also identifies the anti-resonance frequencies for which the response approaches a minimum. Note that this graphical procedure inherently includes the cross-modal response discussed in Section 3.3.3.6.

Space-Average of Mean Square Response

It is convenient to specify a characteristic response over the entire beam as the space-average of the mean square value. Let the displacement response at any point on the beam be given by the summation of normal modes as

$$x(y, t) = \sum_n a_n(t) \phi_n(y) \tag{3.372}$$

where

$q_n(t) = \bar{q}_n \cos(2\pi ft - \theta_n)$  - the modal displacement with amplitude  $\bar{q}_n$  and phase angle  $\theta_n$

$\phi_n(y)$  = mode shape at  $y$  in  $n$ th mode.

Applying the concepts developed in Section 3.3.3.6 for lumped parameter systems, the mean square value of this response at one point on the beam can be given as

$$\overline{x^2(y)} = \frac{1}{2} \sum_n \bar{q}_n^2 \phi_n^2(y) + \frac{1}{2} \sum_{n \neq m} \bar{q}_n \bar{q}_m \phi_n(y) \phi_m(y) \cos(\theta_m - \theta_n) \quad (3.373)$$

The first term defines the sum of the mean square responses in each mode while the second double summation defines the cross mode responses corresponding to all the cross products obtained when Equation 3.372 is squared. The space average of this mean square response will be denoted by a double bar and is given by

$$\overline{\overline{x^2}} = \frac{1}{L} \int_0^L \overline{x^2(y)} dy$$

Consider for now the value of only the cross-mode coupling terms in this integral. Since only the mode shapes  $\phi_n(y)$  vary with  $y$ , the integration can be expressed as

$$\overline{\overline{x^2}}_{\text{cross-terms}} = \frac{1}{2L} \bar{q}_n \bar{q}_m \cos(\theta_m - \theta_n) \int_0^L \phi_n(y) \phi_m(y) dy$$

If the integral itself is multiplied and divided by the mass per unit length along the beam  $\rho A$ , then by invoking the orthogonality property of the normal modes, (see Equation 3.311, page 3-112)

$$\frac{1}{\rho AL} \int_0^L \rho A \phi_n(y) \phi_m(y) dy = \begin{cases} 0 & n \neq m \\ \frac{M_n}{\rho AL} & n = m \end{cases}$$

However, by definition, the cross-mode terms involve only pairs of modal responses for which  $n \neq m$ . Thus, the space average of the mean square response over the structure cancels out the cross-mode coupling terms. The net result is that the space average mean square response over the beam reduces to

$$\overline{\overline{x^2}} = \left( \sum_n \frac{1}{2} \bar{q}_n^2 \right) \frac{1}{L} \int_0^L \phi_n^2(y) dy \quad (3.374a)$$

This is a general form for the space average mean square response for any one-dimensional structure. For a two-dimensional structure, such as a plate with sides (a) and (b), the comparable expression is

$$\overline{\overline{x^2}} = \sum_n \sum_m \frac{1}{2} \bar{q}_{mn}^2 \cdot \frac{1}{ab} \int_0^a \int_0^b \phi_{mn}^2(y, z) dy dz \quad (3.374b)$$

where  $\frac{1}{2} \bar{q}_{mn}^2$  is the mean square amplitude of the  $m$ th normal mode response equal to  $1/2$  the square of the modal amplitude  $q_{mn}$ .

The integrals in these last two equations define, in effect, a mean square mode shape  $\overline{\phi_n^2}$  or  $\overline{\phi_{mn}^2}$ . The following values are obtained for common boundary conditions.

• Simply-Supported Beam

$$\overline{\phi_{mn}^2} = \frac{1}{L} \int_0^L \sin^2(n\pi y/L) dy = \frac{1}{2}$$

• Simply-Supported Plate

$$\overline{\phi_{mn}^2} = \left(\frac{1}{2}\right)^2$$

• Clamped-Clamped Beam

$$\begin{aligned} n = 1, \quad \overline{\phi_1^2} &= 0.396 \\ n = 2, \quad \overline{\phi_2^2} &= 0.439 \\ n \geq 3, \quad \overline{\phi_3^2} &= 0.437 \end{aligned}$$

• Clamped-Clamped Plate

$$m, n = 1, \quad \overline{\phi_{11}^2} = (0.396)^2$$

For example, the space average mean square acceleration response in  $g^2$  of a simply-supported beam to a point force at the center is obtained by combining Equations 3.370 and 3.374a with the above relationships to give

$$\left. \begin{aligned} \overline{\overline{\ddot{x}^2}} &= \left(\frac{P}{W_b}\right)^2 \sum_n \left[ \left(\frac{f}{f_n}\right)^2 |H_n(f)| \right]^2_{n = \text{odd}} \\ &= 0, \quad n = \text{even} \end{aligned} \right\} \quad (3.375)$$

where  $W_b = \rho ALg$  - the weight of the beam.

For any single mode, this space average mean square acceleration will be approximately equal to  $(P/W_b)^2 (f/f_n)^2$  for  $f \gg f_n$ . The latter value is equivalent to the static acceleration that would be obtained by applying a steady acceleration with a magnitude  $P$  equal to the amplitude of the point driving force.

- Joint Acceptance

$$J_{mn} = \frac{1}{P_0} \int_0^a \int_0^b p \phi_{mn}(y, z) dy dz$$

$$= \begin{cases} 4/mn \pi^2, & m \text{ and } n \text{ odd} \\ 0, & m \text{ or } n - \text{even} \end{cases}$$

- Generalized Mass

$$M_n = \frac{1}{4} \rho a b h = \frac{1}{4} \frac{w a b}{g}$$

where  $h$  = plate thickness

$$w/g = \rho h = \text{surface mass density}$$

- Natural Frequency

$$f_n = \frac{\pi}{2} \sqrt{D/\rho h} \left[ \left( \frac{m}{a} \right)^2 + \left( \frac{n}{b} \right)^2 \right]$$

Typical response functions for a simply-supported plate with a uniform (in-phase) sinusoidal load may be summarized as follows.

- Maximum Displacement Response at Center of Panel

$$x \left( \frac{a}{2}, \frac{b}{2}, t \right) = \frac{\rho a^4}{D} \sum_m \sum_n a_{mn}(t)$$

where (3.377a)

$$a_{mn} = \frac{16}{\pi^6} \frac{\sin(m\pi/2)\sin(n\pi/2) |H_{mn}(f)| \cos(2\pi f t - \theta_n)}{mn [m^2 + (na/b)^2]^2}$$

- Space Average Mean Square Displacement

$$\overline{x^2} = \frac{1}{2} p^2 \sum_m \sum_n \left[ \frac{8 |H_{mn}(f)|}{mn \pi^2 (2\pi f_{mn})^2 \rho h} \right]^2 \quad (3.377b)$$

- Space Average Mean Square Velocity

$$\overline{\dot{x}^2} = \frac{1}{2} p^2 \sum_m \sum_n \left[ \frac{8 (f/f_{mn}) |H_{mn}(f)|}{mn \pi^2 (2\pi f_{mn} \rho h)} \right]^2 \quad (3.377c)$$

- Space Average Mean Square Acceleration

$$\overline{\ddot{x}^2} = \frac{1}{2} \left( \frac{p}{\rho h} \right)^2 \sum_m \sum_n \left[ \frac{8 (f/f_m)^2 |H_m(f)|}{mn \pi^2} \right]^2 \quad (3.377d)$$

Similar expressions for beams or plates with other boundary conditions are determined by using the basic relationships specified in Sections 3.3.5.4 and 3.3.5.6, respectively.

### 3.3.6.3 Response of a Beam to a Traveling Step Load

The load on a structure subjected to a traveling overpressure wave from a blast may be approximated by a propagating sudden change in pressure with a constant amplitude  $p_{so}$  traveling with a velocity  $v$  across the structure. Consider the case illustrated in Figure 3.104 where a simply-supported beam with a length  $L$  and width  $b$  is subjected to such a traveling load. The generalized force acting on the beam in the  $n$ th mode is defined for two separate time periods which are: a) the time of passage of the pressure front across the beam, and b) the time following this transit time  $t = L/v$ . ( $t = 0$  coincides with the time of arrival of the pressure step at the left end of the beam.) The response of the beam during these two periods can be determined as follows.

- $0 < t < L/v$  - Pressure Step Passing Over Beam

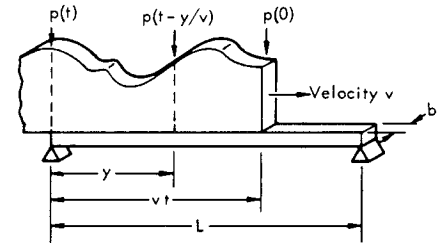


FIGURE 3.104 General Problem of a Step Change in Pressure Traveling Over a Simply-Supported Beam

For any time  $t < L/v$ , the pressure at any point  $y$  which lies within the propagation distance  $vt$ , is the constant pressure  $p_{so}$ . The generalized force  $F_n(t)$  over the entire beam can be determined, therefore, by integrating only over the distance  $y = 0$  to  $y = vt$ , or

$$F_n(t) = b \int_0^{vt} p(t-y/v) \phi_n(y) dy = p_{so} b \int_0^{vt} \sin \frac{n\pi y}{L} dy$$

$$= \frac{p_{so} b L}{\pi n} \left[ 1 - \cos \frac{\pi n v t}{L} \right]_{t < L/v} \quad (3.378)$$

The time varying generalized force is equivalent to a suddenly applied static load  $p_{so} b L / \pi n$  minus a suddenly applied cosine load  $- p_{so} b L [\cos \pi n v t / L] / \pi n$ . The displacement of the beam may be defined by the superposition principle as

$$x(y, t) = \sum_n [q_{n1}(t) + q_{n2}(t)] \phi_n(y) \quad (3.379)$$

where

$q_{n1}(t)$  = response of  $n$ th normal coordinate to a step input, and

$q_{n2}(t)$  = response of  $n$ th normal coordinate to a cosine input.

Response of Simply-Supported Beam to a Uniform Sinusoidal Pressure

The preceding results for the response of a beam to a point force can be extended to distributed uniform sinusoidal pressure  $p(y, t) = p \cos(2\pi ft)$  which acts in-phase at all points on the beam. It is only necessary to redefine the following terms.

- Amplitude of Total Force

$$P_o = pbL$$

where  $bL$  = surface area of beam of length  $L$  and width  $b$

- Joint Acceptance

$$J_n = \frac{b}{P_o} \int_0^L P \sin(n\pi y/L) \cdot dy$$

$$= \begin{cases} 2/n\pi, & n = \text{odd} \\ 0, & n = \text{even} \end{cases}$$

(Note that the total force and joint acceptance for a uniform dynamic pressure on the beam are identical to those specified in Section 3.3.6.1 for a uniform static load.) Utilizing these new values for the total force  $P_o$  and the joint acceptance  $J_n$  in Equation 3.368 or 3.374a, the following typical response functions can be defined for a uniform sinusoidal pressure on a simply-supported beam.

- Displacement Response at Point  $y$

$$x(y, t) = \frac{pbL^4}{EI} \sum_{n, \text{odd}} \frac{4 |H_n(f)| (\sin n\pi y/L) \cos(2\pi ft - \theta_n)}{(\pi n)^5} \quad (3.376a)$$

where  $pb$  = the driving force per unit length.

Except for the frequency and time varying terms,  $|H_n(f)|$  and  $\cos(2\pi ft - \theta_n)$ , this is identical to Equation 3.360 for a static load.

- Acceleration Response at Center ( $y = L/2$ )

$$\ddot{x}(L/2, t) = \frac{pbL}{W_b} \sum_{n, \text{odd}} \frac{4 \sin(n\pi/2)}{n\pi} (f/f_n)^2 |H_n(f)| \cos(2\pi ft - \theta_n) \quad (3.376b)$$

where  $W_b = \rho AL$  g - weight of beam.

Unlike the acceleration response to a point force, the amplitude of the modal acceleration response for a uniform load decreases as  $1/n$  above the fundamental mode. This is equivalent to a decrease as  $\sqrt{1/f_n}$  since  $f_n \propto n^2$ . The sign of every other odd mode changes from +1 to -1 in contrast to the constant sign for a point for point force excitation.

- Space Average Mean Square Acceleration

$$\overline{\ddot{x}^2} = \left(\frac{pbL}{W_b}\right)^2 \sum_n \left[\frac{2}{n\pi} (f/f_n)^2 |H_n(f)|\right]^2 \quad (3.376c)$$

The essential difference between the mean square response for the distributed versus point force is defined by the difference in the joint acceptance ( $2/n\pi$  versus  $\pm 1$ ) for the two forms of excitation for a simply-supported beam. This concept is illustrated in Figure 3.103.

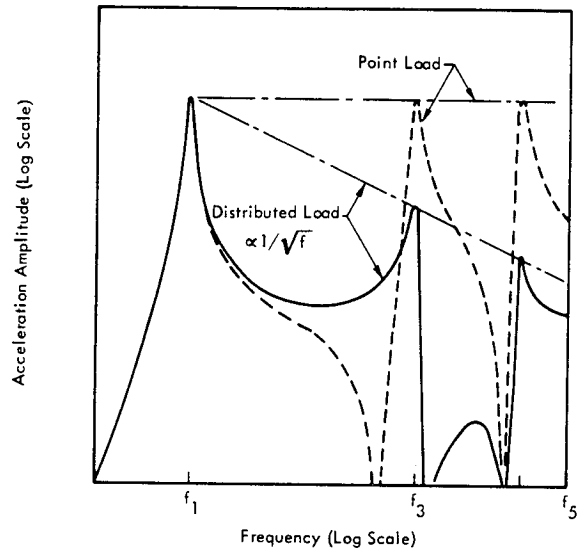


FIGURE 3.103 General Trend in Maximum Acceleration Response at Center of Simply-Supported Beam Loaded by Uniform Distributed Sinusoidal Pressure or Point Force at Center. Only odd modes excited in each case.  $Q$  assumed to be constant for each mode.

Response of Simply-Supported Plate to a Uniform Sinusoidal Pressure

The response of a simply-supported plate with a stiffness  $D$ , sides (a) and (b) and thickness (h) to a uniform pressure  $p(y, z, t) = p \cos(2\pi ft)$  can be determined by substituting the following parameters in the general response equations (3.368 or 3.374b).

- Amplitude of Total Force

$$P_o = pab$$

where  $ab$  = area of plate

- Mode Shape

$$\phi_{mn}(y, z) = \sin(m\pi y/a) \sin(n\pi z/b)$$

The complete solutions for the response of a single degree of freedom system (i.e.,  $n$ th normal mode) to these transient inputs were given in Table 3.1, page 3-5. Applying these solutions to this case, assuming no damping and letting the load per unit length  $p_{so} b$  be given by  $P_{so}$ , then  $q_1(t) + q_2(t)$  become

$$q_1(t) + q_2(t) = \frac{P_{so} L}{\pi n \omega_n^2 M_n} \left[ 1 - \cos \omega_n t - H_n(f) \left( \cos \frac{\pi n v t}{L} - \cos \omega_n t \right) \right]$$

where

$\omega_n^2 M_n$  = generalized stiffness of beam for  $n$ th mode with a natural frequency  $\omega_n$  and generalized mass  $M_n$

$H_n(f) = 1 / \left[ 1 - \left( \frac{\pi n v}{\omega_n L} \right)^2 \right]$  - the dynamic magnification factor.

The complete solution for the displacement of any point during this period is the summation over all modes given by

$$x(y, t) = \frac{P_{so} L^4}{EI} \sum_n \frac{2 \sin(\pi n y/L)}{(\pi n)^5} \left[ 1 + \frac{v^2 \cos \omega_n t - \cos v \omega_n t}{1 - v^2} \right] \quad (3.380)$$

where  $v = \pi n v / \omega_n L = n v / 2 f_n L$

For an infinite propagation velocity, ( $v \rightarrow \infty$ ) this expression reduces to the usual form for the displacement under a static load equal to  $1/2 P_{so}$  (see Equation 3.360). The factor of  $1/2$  represents the average relative static pressure during the passage of the shock front over the beam.

There is a critical velocity of propagation of the pressure change for which the response of the undamped beam would appear to become infinite. This occurs when

$$1 - (n v / 2 f_n L)^2 = 0$$

or

$$v = 2 f_n L / n \quad (3.381a)$$

As shown in Section 3.3.5.4, the velocity of bending or flexural waves  $c_B$  in the beam at the  $n$ th natural frequency is

$$c_B = f_n \lambda_n = f_n (2L/n) \quad (3.381b)$$

where  $\lambda_n$  is the bending wavelength. Thus, this critical propagation velocity  $v$  for the  $n$ th mode is identical to the bending wave velocity  $c_B$  in the beam for the same mode.

This coincidence of the propagation velocity of a traveling load and the propagation velocity of resultant bending waves is a very important phenomena which will appear later in Chapters 8 and 9 in the discussion of response of walls to propagating acoustic pressure waves.

For the case of a propagating "static" pressure wave, a finite response is actually obtained when  $v \rightarrow 2 f_n L / n$ . Letting  $v \rightarrow 1$  in Equation 3.380, the bracketed quantity becomes  $[1 - \cos \omega_n t]$  which is the relative response of a single degree of freedom system to an instantaneous change in force. Thus, at "coincidence," when  $v = c_B$ , the beam responds to the traveling pressure wave as if it were applied instantly over the entire beam but with an amplitude of  $1/2$  its peak value.

The maximum response of the beam during this transit period occurs at the end when  $t = L/v$ . This leads to a consideration of the response after the pressure front has passed over the beam.

#### • $t > L/v$ - Pressure Step Past the Beam

During this period, the beam response will consist of the residual transient vibration generated during the first period plus the pure static deflection under the load. Let  $t' = t - L/v$  be the time variable for this period. The general solution for the  $n$ th normal coordinate is

$$q_{nr}(t') = A \cos \omega_n t' + B \sin \omega_n t' + \bar{q}_{ns} \quad (3.382)$$

where

$$\bar{q}_{ns} = \frac{2 P_{so} L}{\pi n \omega_n^2 M_n} = \frac{4 P_{so} L^4}{(\pi n)^5 EI} - \text{the static deflection for the uniform static load during this final period.}$$

The constants  $A$  and  $B$  must satisfy the initial conditions of displacement  $q_n(t' = 0)$  and velocity  $\dot{q}_n(t' = 0)$ . These, in turn, are determined by the response at the end of the first period at the time  $t = L/v$ . The displacement and velocity at this time are found from Equation 3.380 to be

$$x(y, t = L/v) = \frac{P_{so} L^4}{EI} \sum_n \frac{2 \sin(\pi n y/L)}{(\pi n)^5} \times \left[ 1 + \frac{v^2 \cos \pi n / v - \cos \pi n}{1 - v^2} \right]_{t = L/v} \quad (3.383a)$$

$$\dot{x}(y, t = L/v) = \frac{P_{so} L^4}{EI} \sum_n \frac{2 \sin(\pi n y/L)}{(\pi n)^5} \omega_n \times \left[ \frac{v^2 \sin \pi n / v}{1 - v^2} \right]_{t = L/v} \quad (3.383b)$$

where  $v = \pi n v / \omega_n L$ .

Solving Equation 3.382 for the initial displacement and velocity, utilizing the above expressions to determine the constants  $A$  and  $B$ , the displacement of the beam during this period is given by the modal summation

$$x(y,t) = \frac{P_{so} L^4}{EI} \sum_n \frac{4 \sin(\pi n y/L)}{(\pi n)^5} \times \left[ \left( \frac{v^2 \cos(\pi n/v) - \cos \pi n}{2(1-v^2)} - \frac{1}{2} \right) \cos \omega_n t' + \frac{v^2 \sin(\pi n/v)}{2(1-v^2)} \sin(\omega_n t') + 1 \right]_{t > L/v} \quad (3.383c)$$

The bracketed quantity in this expression defines the total displacement (following the passage of the pressure front) relative to the displacement for a stationary static load. This relative dynamic response is shown in Figure 3.105 as a function of  $v$  (or  $nv/2f_n L$ ) for the first mode of the beam. The maximum response occurs when  $v \rightarrow \infty$  and approaches a value of 2 which is the expected dynamic response factor for a suddenly applied load (i.e., infinite propagation velocity).

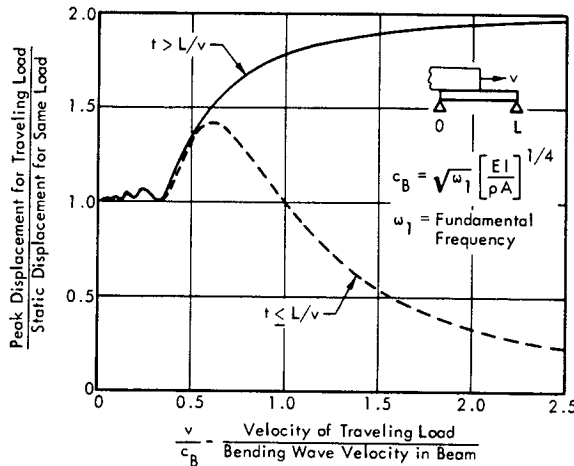


FIGURE 3.105 Relative Dynamic Displacement in First Normal Mode of a Simply-Supported Beam Subjected to a Traveling Step Load. Solid line for peak displacement after step load has passed over beam. Dashed line for peak displacement during transit time of load over beam.

Only during the passage of the pressure front across the beam is there any evidence of a coincidence effect on the dynamic response of the beam. This is shown by the dashed line, in Figure 3.105, which represents the maximum relative displacement at the end of the transit time ( $t = L/v$ ) as defined by Equation 3.383a. In contrast to the important influence of coincidence for traveling dynamic loads which will be shown later in Chapters 8 and 9, the "coincidence effect" is relatively insignificant for the type of traveling "static load" considered here.

### 3.3.6.4 Response of a Beam to Motion of Its Supports

In addition to the types of excitation considered so far, excitation due to motion of the support points is commonly encountered. As an example, consider the case illustrated

in Figure 3.106a on the following page of a simply-supported beam driven by a sinusoidal motion  $U \cos(2\pi f t)$  at its pinned ends. The equation of motion of a beam with moving supports can be expressed in terms of the absolute motion,  $x(y,t)$  of the beam or in terms of the sum of the support motion  $u(t)$  and the relative deflection,  $\epsilon(y,t)$  of the beam. Thus, if the bending stiffness is  $EI$ , the mass per unit length is  $\rho A$ , and  $x(y,t) = u(t) + \epsilon(y,t)$ , the equation of motion can be written as

$$EI \frac{\partial^4 x(y,t)}{\partial y^4} + \rho A \frac{\partial^2 x(y,t)}{\partial t^2} = 0 \quad (3.384a)$$

or as

$$EI \frac{\partial^4 \epsilon(y,t)}{\partial y^4} + \rho A \frac{\partial^2 \epsilon(y,t)}{\partial t^2} = -\rho A \frac{\partial^2 u(t)}{\partial t^2} \quad (3.384b)$$

since

$$\frac{\partial^4 x}{\partial y^4} = \frac{\partial^4 \epsilon}{\partial y^4} \quad \text{for} \quad \frac{\partial^4 u}{\partial y^4} = 0$$

A direct solution for the forced response is obtained with Equation 3.384a by specifying the motion of the end supports as boundary conditions. As discussed earlier in Section 3.3.5.1, this results in a set of nonhomogeneous equations which are solved simultaneously without resorting to normal modes. A normal mode solution is obtained with Equation 3.385b by treating the inertia load  $\rho A \partial^2 u(t)/\partial t^2$ , generated by the support motion, as a distributed external load on the beam. This concept was discussed in some detail for lumped parameter systems in Section 3.3.3.2.

### Direct Solution Method

For the direct solution method, the boundary conditions are

$$x(0,t) = x(L,t) = u(t)$$

$$x''(0,t) = x''(L,t) = 0 \quad (\text{zero moment at pinned ends})$$

Applying these conditions to the general solution for lateral vibration of beams (see Equation 3.310, page 3-111), the closed form solution for the amplitude of the absolute motion of an undamped simply-supported beam of length  $L$ , for symmetrical motion of its supports is (References 3.67 and 3.1, Chapter 7)

$$X(y) = \frac{U}{2} \left[ \cosh Ky - \tanh \frac{KL}{2} \sinh Ky + \cos Ky + \tan \frac{KL}{2} \sin Ky \right] \quad (3.385)$$

where

$$K = \omega/c_B = \sqrt{\omega} \left[ \rho A/EI \right]^{1/4}$$

$$\omega = 2\pi f = \text{frequency of excitation}$$

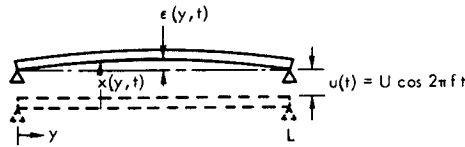
$$c_B = \text{bending wave velocity}$$

$$U = \text{amplitude of excitation } u(t) = U \cos \omega t$$

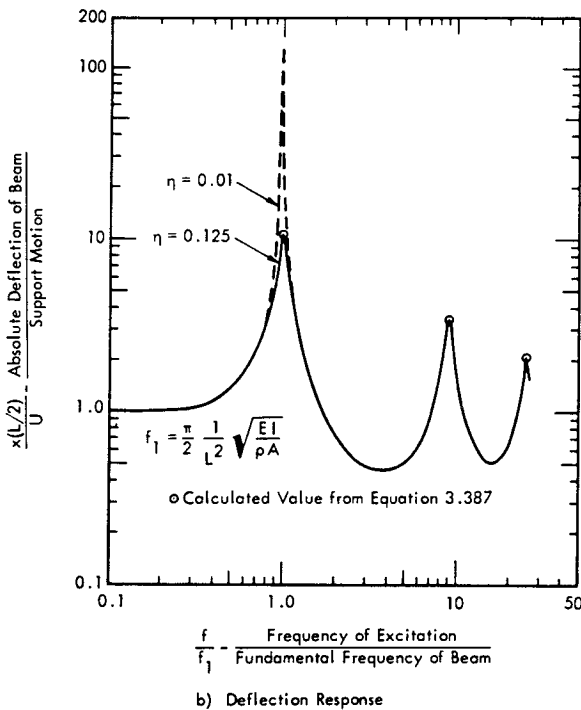


For  $KL = n\pi$ , with  $n = \text{odd}$ , the last term ( $\tan KL/2$ ) goes to infinity since this corresponds to the value of  $KL$  for the  $n$ th natural frequency of a simply-supported beam.

A finite response for excitation of these natural frequencies is obtained by including material damping in the system. Considering only the motion at the center of the beam ( $y = L/2$ ) at excitation frequencies near resonance, Equation 3.385 indicates that only the last term is significant for low values of damping.



a) Foundation Motion of a Simply-Supported Beam



b) Deflection Response

FIGURE 3.106 Absolute Deflection at Mid Span of a Simply-Supported Damped Beam with Moving Supports and Loss Factor  $\eta$

Damping Effects

To incorporate damping, replace  $K$  by its approximate value  $K(1 - j\eta/4)$  for damped flexural vibrations of a structural element. The loss factor  $\eta$  defines the relative magnitude of the imaginary or "lossy" part of the complex modulus of elasticity  $E(1 + j\eta)$ . As discussed later in Section 3.3.7.1, a complex modulus is used to define hysteresis damping for structural materials. Incorporating these changes, it can be shown that at resonance Equation 3.385 is closely approximated by

$$X\left(\frac{L}{2}\right)_{\max} \approx U \left[ \frac{\sinh \eta KL/4 \sin KL/2}{\cos KL + \cosh \eta KL/4} \right] e^{-j\pi/2}$$

As indicated by the complex quantity  $\exp(-j\pi/2)$ , the displacement response lags behind the input motion by 90 degrees at resonance. For low damping and for  $KL = \pi, 3\pi, 5\pi$ , etc. at the natural frequencies of the beam, the displacement amplitude can be simplified further to

$$X\left(\frac{L}{2}\right)_{\max} \approx \frac{4}{n\pi} \frac{U}{\eta} e^{-j\pi/2}, \quad n = 1, 3, 5, \text{ etc.} \quad (3.386)$$

The approximation for the maximum response given by this expression is shown in Figure 3.106b along with the exact response, without damping, given by Equation 3.385. Note that these response functions also define the absolute acceleration response for a given acceleration input.

While it is generally possible to determine a simplified form for such complex response functions at the resonance frequencies of the structure, the direct solution method is generally awkward unless the expressions are to be evaluated by digital computers.

Normal Mode Solution

A normal mode solution for the relative displacement  $\epsilon(y, t)$  is readily obtained, using Equation 3.384b. Define the generalized force for the  $n$ th mode as

$$F_n(t) = \rho A \ddot{u}(t) \int_0^L \phi_n(y) dy$$

where

$$\phi_n(y) = \sin n\pi y/L \text{ for a simply-supported beam, and}$$

$$\ddot{u}(t) = -(2\pi f)^2 U \cos(2\pi f t) \text{ - the acceleration of the supports.}$$

Thus, the generalized force can be expressed as

$$F_n(t) = P_o J_n \cos(2\pi f t)$$

where

$$P_o = -\rho A L (2\pi f)^2 U \text{ - amplitude of the total inertial force due to motion of the supports}$$

$$J_n = \frac{1}{L} \int_0^L \sin(n\pi y/L) dy \text{ - joint acceptance}$$

$$= \begin{cases} 2/n\pi, & n = \text{odd} \\ 0 & n = \text{even} \end{cases}$$

Apply this to the equation of motion for the  $n$ th normal coordinate  $q_n(t)$ , including damping. As shown in Section 3.3.3.5, the solution for steady state sinusoidal excitation is

$$q_n(t) = \frac{P_o J_n |H_n(f)| \cos(2\pi f_n t - \theta_n)}{(2\pi f_n)^2 M_n}$$

where

$$|H_n(f)| = \text{dynamic magnification factor (see p. 3-146).}$$

For excitation at the  $n$ th natural frequency  $f = f_n$  and  $|H_n(f)|$  reduces to  $1/2 \delta_n \approx 1/\eta$  where  $\delta_n = \text{critical damping ratio}$ . Therefore, combining the above relationships, The maximum amplitude of the relative deflection  $\epsilon(y)$  in the  $n$ th mode has an absolute value at the center of the beam equal to

$$|\epsilon(L/2)_n|_{\max} = \frac{4}{\pi n} \frac{U}{\eta}, \quad n = 1, 3, 5, \text{ etc.} \quad (3.387)$$

Since low damping is assumed, the maximum amplitude of the absolute deflection  $X(L/2)$  is very nearly equal to the relative deflection  $\epsilon(L/2)$  so that Equations 3.387 and 3.386 provide essentially equivalent results. It should be pointed out that, at resonance, the relative deflection  $\epsilon(t)$  is in-phase with the support motion and hence leads the absolute deflection  $x(t)$  by 90 degrees.

The basic concepts outlined for this simple case can be readily extended to other types of structural elements to evaluate their response to foundation motion. The normal mode approach provides a particularly simple method for evaluating the peak response at a resonant condition.

3.3.6.5 Reaction Forces at Boundaries of Beams and Plates

For the analysis of vibration transmission through structures, it is desirable to define the forces developed at support points of vibrating beams and plates due to external loads or local vibratory forces located on the member.

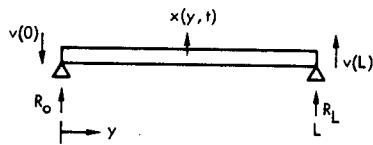


FIGURE 3.107 Reaction Forces Developed at Support Points of Vibrating Beam

The basic method for defining the reaction forces at support points may be demonstrated by considering the case illustrated in Figure 3.107. As shown in Table 3.5, the vertical shear  $V(y, t)$  at any section of the beam of stiffness  $EI$  and deflection  $x(y, t)$  is

$$V(y, t) = -EI x'''(y, t)$$

This is the shear force as viewed, for example, from the left end of the beam so that the reaction forces which oppose this shear at each end are

$$\text{Left Reaction Force } R_o(t) = +EI x'''(0, t)$$

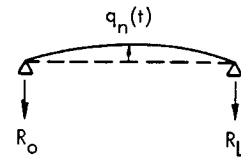
$$\text{Right Reaction Force } R_L(t) = -EI x'''(L, t)$$

Using a normal mode expansion for the deflection, the reaction force at the left end can be given by

$$R_o(t) = +EI \sum_n^{\infty} q_n(t) \phi_n'''(0) \quad (3.389)$$

where  $\phi_n'''(0)$  is the third derivative of the mode shape with respect to  $y$  at  $y = 0$ . This general form for the reaction force at  $y = 0$  can be applied to any beam whose motion is described in terms of normal modes. Based on the expressions developed in Section 3.3.6.2 for the forced response of simply-supported beams, the following expressions for the reaction load at the ends of a simply-supported beam can be derived. In all cases, the mode shape  $\phi_n(y)$  is assumed to be  $\sin(n\pi y/L)$ . Sinusoidal loads or motions are specified in a general form i.e.,  $P(t)$ , omitting the usual  $\cos(2\pi ft)$  term. The resulting expressions relate the reaction loads to the excitation force or an equivalent inertial force.

• General Vibratory Motion of Beam



$$R_o(t) = -W_b \sum_n^{\infty} \left(\frac{1}{\pi n}\right) \frac{1}{g} \ddot{q}_n(t) \quad (3.390a)$$

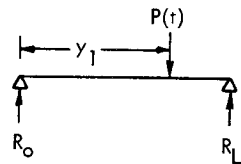
$$R_L(t) = R_o(t) [-(-1)^n], \quad n = 1, 2, 3, \text{ etc.}$$

where  $W_b = \text{weight of beam}$

$q_n(t) = \text{modal acceleration in } n\text{th mode}$

$g = \text{acceleration of gravity}$

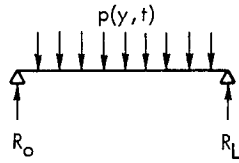
• Point Sinusoidal Force at  $y_1$



$$R_o(t) = +P(t) \sum_n^{\infty} \left(\frac{2}{\pi n}\right) \sin(n\pi y_1/L) |H_n(f)| \quad (3.390b)$$

$$R_L(t) = R_o(t) [-(-1)^n], \quad n = 1, 2, 3, (y_1 \neq L/2)$$

• Uniform Sinusoidal Force per Unit Length



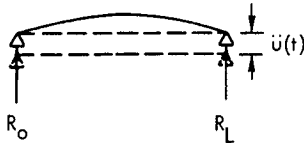
$$R_O(t) = p(y, t) L \sum_n \left(\frac{2}{\pi n}\right)^2 |H_n(f)|_{n = \text{odd}} \quad (3.390c)$$

$$R_L(t) = R_O(t)$$

where

$$|H_n(f)| = 1 / \left[ \left(1 - (f/f_n)^2\right)^2 + \left(2 \delta_n f/f_n\right)^2 \right]^{1/2}$$

• Uniform Vertical Acceleration of Pinned-Supports



$$R_O(t) = W_b \frac{\ddot{u}(t)}{g} \left[ \sum_n \left(\frac{2}{\pi n}\right)^2 |H_n(f)| - 1 \right]_{n = \text{odd}} \quad (3.390d)$$

$$R_L(t) = R_O(t)$$

For the first two cases illustrated above, both odd and even modes are possible. For even modes, the two reaction forces are 180 degrees out of phase. For the last two cases, the assumed symmetrical loadings suppresses any even modes.

Reaction Forces at the Boundaries of Vibrating Plates

A similar concept can be used to determine reaction forces at the boundaries of plates. The total reaction forces are defined by more complex expressions which account for the vertical forces due to vertical shear and twisting moments along the edges of the plate (Reference 3.66).

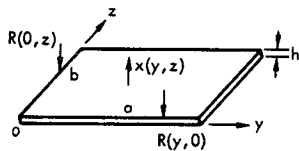


FIGURE 3.108 Vertical Reaction Forces (per Unit Length) Along Edges of Vibrating Plates

Based on the coordinate system illustrated in Figure 3.108, the vertical reaction force per unit length  $R(y, 0)$  along side (a), for a lateral deflection  $x = x(y, z)$ , can be expressed as

$$R(y, 0) = + D \left[ \frac{\partial}{\partial z} \left( \frac{\partial^2 x}{\partial y^2} + \frac{\partial^2 x}{\partial z^2} \right) + (1 - \nu) \frac{\partial^3 x}{\partial z \partial y^2} \right] \quad (3.391a)$$

where  $D, \nu =$  plate stiffness and Poisson's ratio, respectively.

Along side (b), the reaction force  $R(0, z)$  is

$$R(0, z) = + \left[ \frac{\partial}{\partial y} \left( \frac{\partial^2 x}{\partial y^2} + \frac{\partial^2 x}{\partial z^2} \right) + (1 - \nu) \frac{\partial^3 x}{\partial y \partial z^2} \right] \quad (3.391b)$$

(Note that the internal force acting on the edge of the plate has the opposite sign.)

A general evaluation of reaction loads for plates is not practical here. For example, the reaction forces at the corners of a rectangular plate are not considered (Reference 3.66). It is sufficient to illustrate the general trend by considering the reaction forces at the edge of a simply-supported plate with a stiffness  $D$ , thickness  $h$ , mass density  $\rho$ , which is vibrating in the  $m$ th normal mode with a deflection given by

$$x_{mn}(y, z, t) = a_{mn}(t) \left[ \sin\left(m \frac{\pi y}{a}\right) \sin\left(n \frac{\pi z}{b}\right) \right]$$

The frequency for this mode is given by

$$2\pi f_{mn} = \omega_{mn} = \pi^2 \sqrt{\frac{D}{\rho h}} \left[ \left(\frac{m}{a}\right)^2 + \left(\frac{n}{b}\right)^2 \right]$$

Using these expressions in Equation 3.391a, it can be shown that the amplitude of the reaction force per unit length along side (a) is

$$R(y, 0) = - \frac{W_p}{a} \sum_m \sum_n \frac{1}{\pi n} \frac{\bar{q}_{mn}}{g} \frac{\left[ 1 + (2 - \nu) \left(\frac{m/a}{n/b}\right)^2 \right]}{\left[ 1 + \left(\frac{m/a}{n/b}\right)^2 \right]^2} \sin\left(m\pi \frac{y}{a}\right) \quad (3.392)$$

where

$W_p/a =$  weight of plate per length of side (a)

$\bar{q}_{mn} =$  peak amplitude of  $m$ th mode at center of plate.

The similarity is clear when this equation is compared with Equation 3.390a for the beam. For example, for a square plate vibrating in its 1,1 mode, setting  $\nu = 0.3$ , the reaction force along side (a) per unit length would be

$$R(y, 0) = - \frac{W_p}{a} \frac{1}{\pi} \frac{\bar{q}_n}{g} \frac{[2.7]}{[4]} \sin\left(\pi \frac{y}{a}\right)$$

Replacing  $\sin \pi y/a$  by  $2/\pi$ , the average reaction force per unit length will be  $(2.7) (\pi/2)/4$ . This is 0.43 times as great as an equivalent beam with the same weight per unit width  $W_p/a$  and the same peak acceleration in g's at the center.

3.3.6.6 Dynamic Stress at Resonance of Vibrating Structure

In lieu of carrying out detailed dynamic stress calculations on complex structure exposed to high intensity dynamic loads, such as rocket noise or blast overpressure, simplified alternate methods can be used in certain cases. One such method is based on the relationship between peak vibratory stress in a simple structure at resonance and its peak velocity (Reference 3.68). The method is particularly well suited for approximate stress analysis, using the method of normal modes to define structural response to a dynamic load.

The concept may be illustrated simply by analyzing the peak dynamic stress in a bar vibrating longitudinally in one of its normal modes.

For the clamped-free bar illustrated in Figure 3.109, the displacement amplitude of any element of the bar from its neutral unstressed position will be equal to (see Section 3.3.5.2)

$$x(y) = \bar{q}_n \sin\left(\frac{3}{2} \pi \frac{y}{L}\right)$$

where  $\bar{q}_n$  = amplitude of maximum deflection at the anti-node points at  $y = L/3$  and  $L$ .

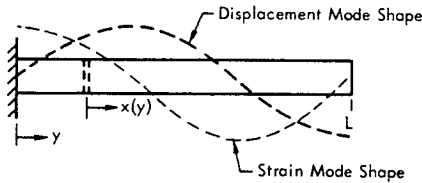


FIGURE 3.109 Deflection and Strain in a Clamped-Free Bar Vibrating in Its Second Natural Frequency  $f_2 = \frac{3}{4} c_L/L$ , where  $c_L$  = longitudinal wave velocity in bar.

The natural frequencies for this configuration are given, in general, by

$$f_n L/c_L = (2n-1)/4$$

or, for this case, where  $n = 2$ ,

$$f_n = \frac{3}{4} \frac{c_L}{L}$$

where  $c_L$  = longitudinal wave velocity in the bar.

Since the vibration in this normal mode can be assumed to be sinusoidal, the maximum velocity at the displacement node points will have an amplitude equal to

$$\bar{q}_n = 2\pi f_n \bar{q}_n = \frac{3\pi}{2L} c_L \cdot \bar{q}_n$$

The strain  $\xi = \partial x(y,t)/\partial y$  in the bar is a maximum at the antinodes, in this case at  $y = 0$  and  $2/3 L$ . Since, for this case, the mode shape is also sinusoidal the maximum strain at either strain node point is the same (neglecting damping) and is equal to

$$\xi_{n \max} = \left. \frac{\partial x(y,t)}{\partial y} \right|_{\max} = \frac{3\pi}{2L} \bar{q}_n$$

Comparing these two expressions, it is clear that the maximum strain and maximum velocity are related by

$$\xi_{n \max} = \frac{\bar{q}_n}{c_L} \tag{3.393}$$

This simple relationship turns out to be very general for all longitudinal vibration of bars in their normal modes. In fact, with the addition of an appropriate shape factor  $K_s$ , it will be shown that a similar relationship holds for all simple structural elements vibrating harmonically in a normal mode. The maximum dynamic stress  $\sigma_{n \max}$  in the  $n$ th normal mode is simply  $E \cdot \xi_{n \max}$ . Thus,

$$\xi_{n \max} = K_s \frac{\bar{q}_n}{c_L} \tag{3.394a}$$

and

$$\sigma_{n \max} = K_s E \frac{\bar{q}_n}{c_L} \tag{3.394b}$$

The factor  $K_s$  has the following values for common types of uniform structural elements (Reference 3.68).

- Longitudinal Vibration of Uniform Bars,  $K_s = 1$
- Torsional Vibration of Uniform Bar,  $K_s = 1$  (Replace  $c_L$  by  $c_s$ )
- Lateral Vibration of Uniform Beams,  $K_s = \bar{c}/\sqrt{I/A}$   
 $\bar{c}$  = distance from neutral plane to outermost fiber  
 $\sqrt{I/A}$  = radius of gyration
- Lateral Vibration of Rectangular Solid Bars,  $K_s = \sqrt{3}$
- Lateral Vibration of Circular Solid Bars,  $K_s = 2$
- Lateral Vibration of Plates,  $K_s = 1.2 - 2.0$  ( $K_s$  varies with mode, Poisson's ratio and bending wavelength)

The usefulness of this simple proportionality between maximum velocity at a displacement node and the maximum stress at a strain node should be emphasized.

- The proportionality constant,  $K_s$  varies over a rather limited range for the simple elements considered.
- The only other quantity involved, the longitudinal velocity of compressional or sound waves in the material  $c_L$ , is nearly the same for all metals (see Table 3.39 at the end of this chapter).
- The relationship is independent of the size of the structure. In practice, the maximum velocity of the structure in any mode will vary with the type of loading, the stiffness of the structure and its natural frequency.

A more general derivation of Equation 3.394 for beams and plates may be given as follows.

Velocity-Stress Relationship for Beams

The bending stress in a beam is

$$\sigma = M \bar{c} / I$$

where

M = bending moment

$\bar{c}$  = distance from centroid to outermost fiber

I = area moment of inertia.

The bending moment M for lateral vibration of a beam has an amplitude given by

$$M = EI \frac{\partial^2 x(y)}{\partial y^2}$$

where EI = stiffness of beam.

Assume a sinusoidal mode shape for the nth normal mode so that the modal deflection is

$$x_n(y) = \bar{q}_n \phi_n(y) = A \sin \omega_n y / c_B + B \cos \omega_n y / c_B$$

where

$\bar{q}_n$  = amplitude of nth mode, and

$$c_B = \sqrt{\omega_n} [EI/\rho A]^{1/4} \text{ - bending wave velocity.}$$

Using this expression to find the bending moment M and inserting the result in the first equation for the stress

$$\sigma_n = - E \bar{c} \bar{q}_n \left( \frac{\omega_n}{c_B} \right)^2 \phi_n(y)$$

Substituting in the expression for  $c_B$  and choosing the maximum value for the mode shape  $\phi_n(y) = 1$ , the maximum stress in this mode can be shown to be:

$$\sigma_{n \max} = \frac{E \bar{c}}{\sqrt{I/A}} \cdot \frac{\omega_n \cdot \bar{q}_n}{\sqrt{E/\rho}}$$

or

$$\sigma_{n \max} = K_s \cdot E \frac{\bar{q}_n}{c_L} \tag{3.395}$$

where  $K_s = \bar{c} / \sqrt{I/A}$

This is the same value for  $K_s$  for beams defined earlier.

Velocity-Stress Relationship for Plates

In a similar manner, it can be shown that for plates with sides (a) and (b) whose mode shapes can be approximated by sinusoids, the value of the shape factor  $K_s$  is given by (Reference 3.68)

$$K_s = \sqrt{\frac{3}{1 - \nu^2}} \left[ \frac{1 + \nu \left( \frac{a/m}{b/n} \right)^2}{1 + \left( \frac{a/m}{b/n} \right)^2} \right]_{a < b} \tag{3.396}$$

where

$\nu$  = Poisson's ratio

$a/m$  = 1/2 "sinusoidal" wavelength along short side a

$b/n$  = 1/2 "sinusoidal" wavelength along side b.

This shape factor is plotted in Figure 3.110 for plates with sinusoidal-like mode shapes and  $\nu = 0.3$ . The direction of the maximum stress, in this case, is parallel to side (a) and falls at a displacement node point which is also a point of maximum curvature.

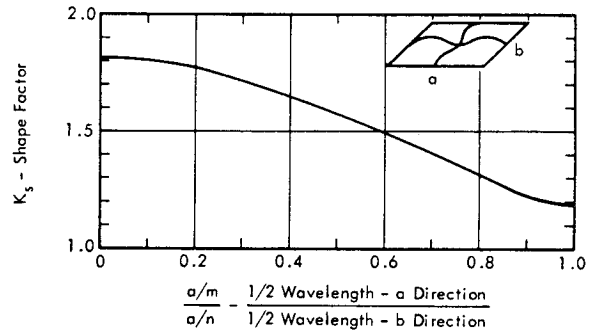


FIGURE 3.110 Shape Factor  $K_s$  in Equation 3.395 Relating Maximum Stress in Simply-Supported Panel to Maximum Velocity at Node Point

3.3.7 DAMPING OF CONTINUOUS STRUCTURE

Analytical methods for including damping in the vibration analysis of structure have been considered in preceding sections, particularly Section 3.3.3.1. Some aspects of the type of damping encountered in the analysis of vibration, and propagating of vibration through damped structure are briefly considered in this section.

3.3.7.1 Types of Damping

The various ideal forms of damping, discussed in Section 3.3.3.1 are often selected for their convenience in analysis rather than accurate models of the damping process itself. This is a realistic approach; however, there are many forms of damping which may be experienced by vibrating structure. No one mathematical model can accurately describe all these various forms so that it is common practice to assume a simplified model which exhibits the same general effect of damping that is observed in practice. The various forms of mechanical damping may be categorized as follows (References 3.69, and 3.1, Chapter 36).

INTERNAL OR MATERIAL HYSTERESIS DAMPING

- DYNAMIC HYSTERESIS DAMPING (Stress-strain laws are dependent on strain-rate or velocity)

- ▲ Viscoelastic Damping (Nonmetals)
- ▲ Anelastic Damping (Metals - significant only at very low stress levels)

- STATIC HYSTERESIS DAMPING (Stress-strain laws are dependent on strain or displacement and independent of strain rate)

- ▲ Plastic Strain Damping
- ▲ Magnetoelastic Damping

INTERFACE DAMPING

- SURFACES WITHOUT BONDING MEDIA

- ▲ Coulomb Friction (Dry slip damping)
- ▲ Viscous Damping (Lubricated joint)
- ▲ Separation Damping (Contact surface chatter)

- SURFACES WITH BONDING MEDIA

- ▲ Viscoelastic Shear Damping

EXTERNAL DAMPING

- ACOUSTIC RADIATION DAMPING

- AERODYNAMIC DAMPING

- ▲ Viscous Drag
- ▲ Aerodynamic Pressure Drag

Analytical Models for Damping

Refined analytical models for the damping force generated by these various forms of damping have the common feature that the damping force is opposite to the direction of velocity. This directionality is inherent in the definition of the damping force  $f_d$  for linear viscous damping which is commonly assumed for vibration analysis. General forms for the damping force for the other types of damping can be defined by the following. For viscous and dynamic hysteresis damping,  $c$  represents a proportionality constant between damping force  $f_d$  and velocity. For static hysteresis damping, let  $h$  represent the proportionality constant between damping force and displacement. For coulomb damping, let  $f_c$  represent a constant friction force. The general forms for damping can then be given as

$$\begin{aligned} \text{Linear Viscous Damping} & \quad f_d = -c \dot{x} \\ \text{Nonlinear Viscous Damping} & \quad f_d = -c \dot{x} |\dot{x}|^{n-1} \quad n \geq 1 \end{aligned}$$

$$\text{Linear Hysteresis Damping} \quad f_d = -h |x| \frac{\dot{x}}{|\dot{x}|}$$

$$\text{Nonlinear Hysteresis Damping} \quad f_d = -h |x|^n \frac{\dot{x}}{|\dot{x}|}$$

$$\text{Coulomb Friction Damping} \quad f_d = -f_c \frac{\dot{x}}{|\dot{x}|}$$

The awkward form required for other than linear viscous damping is apparent.

Static Hysteresis Damping

Static hysteresis damping is the most significant form of internal energy loss for most structural materials. Fortunately, a convenient mathematical form for linear static hysteresis damping can be employed, providing the vibration is restricted to sinusoidal motion (Reference 3.70). It will be assumed that this form of damping is implied from here on when describing hysteresis damping in general. Hysteresis damping forces are dependent on displacement rather than velocity, but act in the direction opposite to velocity. If the sinusoidal displacement  $x(t)$  and velocity  $\dot{x}(t)$  can be defined with complex notation by

$$x(t) = X e^{j\omega t}$$

$$\dot{x}(t) = j\omega X e^{j\omega t} = j\omega x(t)$$

then the hysteretic damping force can be expressed as

$$f_d(t) = -j h x(t) = -\frac{h}{\omega} \dot{x}(t) \quad (3.397)$$

where  $\omega$  is the sinusoidal frequency.

By this approach, a hysteretic damping force can be described mathematically so that it is proportional to the absolute value of displacement  $|x| = |\dot{x}|/\omega$  but acting 180 degrees out of phase with velocity. That is,

$$f_d = -h |x(t)| \frac{\dot{x}(t)}{|\dot{x}(t)|} = -\frac{h}{\omega} \dot{x}(t)$$

when  $x(t)$  is sinusoidal.

The equivalent forms for a hysteretic damping force given by Equation 3.397 makes it possible to specify the damping force in real or complex form.

Hysteretic Damping for Lumped Systems

When the damping is attributed to hysteresis losses in lumped-spring elements with a stiffness  $k$ , then the damping force can be given as

$$\begin{aligned} & \left. \begin{aligned} f_d(t) &= -2k G \dot{x}(t) \\ \text{or as } f_d(t) &= -j k g x(t) \end{aligned} \right\} \quad (3.398) \end{aligned}$$

where  $g = 2 G \omega =$  the structural damping constant.

For analysis purposes, either form of Equation 3.398 can be used, the choice depending on the expected trend in damping as a function of frequency (see Table 3.3, page 3-64).

Hysteretic Damping for Continuous Structure

Stiffness properties of continuous structural elements with distributed mass are specified in terms of their modulus of elasticity  $E$  or shear modulus  $G$ . Hysteretic damping is accounted for, in this case, by defining the modulus of elasticity in a complex form as

$$E^* = E (1 + j \eta) \tag{3.399a}$$

where

$E$  = the real or pure elastic modulus

$j E \eta$  = imaginary or lossy part of the modulus corresponding to the quantity  $j k g$  for the lumped spring, and

$\eta$  = material loss factor (extensional).

Similarly, the complex shear modulus can be given as

$$G^* = G (1 + j \beta) \tag{3.399b}$$

where

$G$  = pure elastic shear modulus, and

$\beta$  = material loss factor in shear.

Damping Energy

The damping energy  $D_o$  dissipated by a damping element during one cycle of vibration is represented by the net work done by the damping force  $f_d$  over one cycle. If a linear viscous damper ( $c$ ) is connected in parallel with a spring ( $k$ ) and the combination driven by a sinusoidal force  $P(t) = P \cos \omega t$ , it can be shown that the driving force varies with displacement of the spring-damper along an elliptical path, as illustrated in Figure 3.111a. The area within this elliptical loop represents the damping energy  $D_o$  lost per cycle and is given by (Reference 3.69)

$$D_o = \oint f_d(x) dx = \pi c \omega X \tag{3.400a}$$

where  $X$  = amplitude of the displacement.

For a structural member such as a bar with linear hysteretic damping, the variation in the dynamic stress-strain curve for a sinusoidal driving force varies along a hysteretic-type loop such as illustrated in Figure 3.111b. The area within this loop is the damping energy  $D_o$  for a continuous structural element. It is given by (Reference 3.69)

$$D_o = \frac{\pi \sigma_{max}^2 \eta V_o}{E} \tag{3.400b}$$

where

$\sigma_{max}$  = maximum stress in bar

$\eta$  = material loss factor

$V_o$  = volume of bar =  $AL$

$E$  = modulus of elasticity.

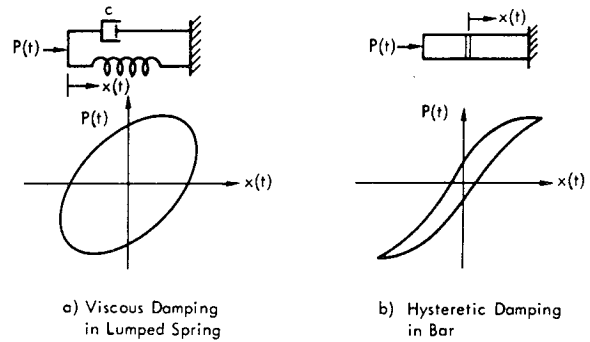


FIGURE 3.111 Variation in Driving Force  $P(t)$  with Displacement  $x(t)$  for Spring Elements with Viscous (a) or Hysteretic (b) Damping. Driving force is sinusoidal. Area within loop represents damping energy lost per cycle of vibration.

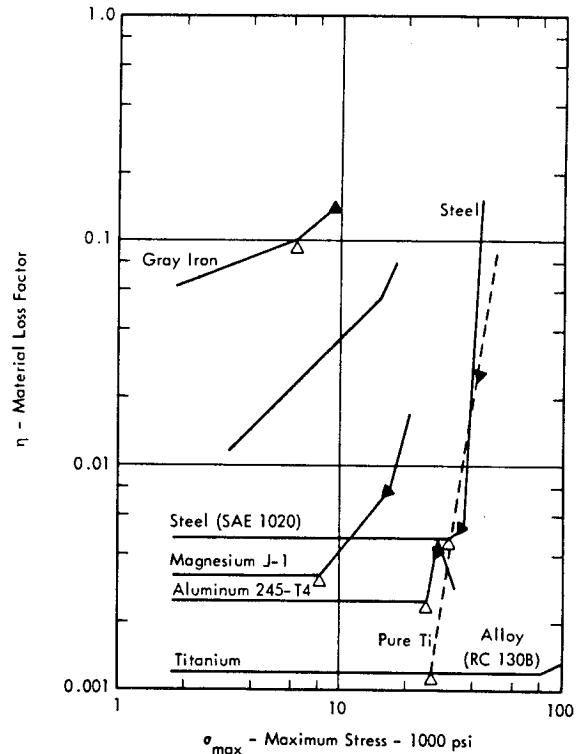


FIGURE 3.112 Material Loss Factor  $\eta$  Versus Maximum Stress  $\sigma_{max}$  for Several Metals. Critical stress sensitivity limit  $\sigma_L$  indicated by ( $\Delta$ ). Endurance limit for  $2 \times 10^7$  fatigue cycles indicated by ( $\blacktriangledown$ ). (Data from Reference 3.1, Chapter 36)

In contrast to viscous damping, the damping energy for linear (static) hysteresis damping is independent of frequency, providing  $\eta$  is not frequency dependent. For many engineering materials, this is approximately true so that hysteresis damping is generally a better approximation for damping effects in structure when interface and external damping mechanisms are not present. On the other hand, materials used for damping and vibration isolation of structure tend to exhibit more nearly viscous damping characteristics.

Most structural materials exhibit a nonlinear damping behavior as evidenced by a deviation in the proportionality between damping energy  $D_o$  and the square of the maximum stress  $\sigma_{max}$  indicated in Equation 3.400b. This deviation becomes particularly marked at the so-called critical stress sensitivity limit  $\sigma_L$ .

The critical stress sensitivity limit  $\sigma_L$  is of the order of 50 - 100 percent of the endurance stress  $\sigma_e$  for most materials. Above this limiting stress, the effective loss factor  $\eta$  for the material tends to increase rapidly. This trend is illustrated in Figure 3.112 for several common materials. Other damping characteristics of materials exhibiting either dynamic or static hysteresis damping are shown in Table 3.19.

3.3.7.2 Propagation of Damped Longitudinal and Flexural Waves in Structure

The velocity of longitudinal waves in bars  $c_L$  and the velocity of flexural bending waves in uniform beams  $c_B$  and uniform plates  $c_B'$  can be defined in the form

$$c_L = \sqrt{E/\rho} \tag{3.401a}$$

$$c_B = \sqrt{\omega c_L r} \tag{3.401b}$$

$$c_B' = \sqrt{\omega c_L h} [1/12 (1 - \nu^2)]^{1/4} \tag{3.401c}$$

where

$E$  = modulus of elasticity

$\omega$  = frequency - radians/sec

$r$  = radius of gyration  $\sqrt{I/A}$  for beams

$h$  = plate thickness, and

$\nu$  = Poisson's ratio.

TABLE 3.19

CHARACTERISTICS OF MATERIAL HYSTERESIS DAMPING<sup>(1)</sup>

Type	DYNAMIC HYSTERESIS		STATIC HYSTERESIS	
	Viscoelastic	Anelastic (Internal Friction)	Plastic Strain	Magnetoelastic
Mechanism	Internal Structural Changes, Thermal and Eddy Currents		Plastic Flow	Magnetoelasticity
Stress-Strain Laws	Linear Plus Strain-Rate Effects		Nonlinear No Rate Effects	No Rate Effects
Damping Energy - D	$D \propto \sigma^2$ $\eta = 0.01 - 1.5$	$D \propto \sigma^2$ $\eta = 0.001 - 0.01$	$D \propto \sigma^n$ $\eta = 0.001 - 0.5 (\sigma < \sigma_L)^{(2)}$ $0.001 - > 0.1 (\sigma > \sigma_L)$	$D \propto \sigma^3$ $\eta = 0.01 - 0.08$
$\eta$ Affected By: Stress	No	No	Small Effect ( $\sigma < \sigma_L$ ) Large Effect ( $\sigma > \sigma_L$ )	$\eta \propto \sigma$
Frequency	Critical	Critical	No	No
Temperature	Critical	Critical	Mixed Effect	Yes
Stress Cycles	No	No	No ( $\sigma < \sigma_L$ ) Yes ( $\sigma > \sigma_L$ )	No
Static Load			Little Effect or Increases $\eta$	Yes - Reduces $\eta$
Stress Range of Importance	All Stresses	Low Stress	Medium to High	Low - Medium

(1) From Reference 3.1, Chapter 36.

(2)  $\sigma_L$  = critical stress sensitivity limit.



To include the effect of material hysteresis damping, the modulus of elasticity is expressed in complex form as shown in Equation 3.399a. When this complex form is used in Equation 3.401a, b or c, it may be shown that the ratio of damped velocities to the corresponding undamped velocities to the corresponding undamped velocities is given by

- For longitudinal waves,

$$c_{L_d}/c_L = \sqrt{\frac{2(1+\eta^2)}{\sqrt{1+\eta^2}+1}} \quad (3.402a)$$

- For bending waves,

$$\left. \begin{matrix} c_{B_d}/c_B \\ \text{or} \\ c'_{B_d}/c'_B \end{matrix} \right\} = \frac{[1+\eta^2]^{1/4}}{\left[ \frac{1}{2}(1+\eta^2)^{1/4} + \sqrt{\frac{1}{2}\sqrt{1+\eta^2}+1} \right]^{1/2}} \quad (3.402b)$$

The subscript d signifies the damped velocity. As shown in Figure 3.113, this change in velocity of longitudinal and bending waves is not significant for loss factors in the usual range of less than 0.2.

A much more important influence of the damping is the attenuation of these waves as they travel through the structure. This attenuation can be defined in terms of the frac-

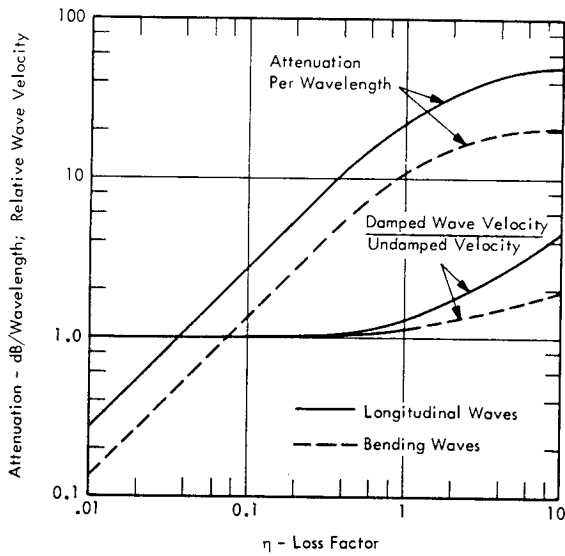


FIGURE 3.113 Propagation Loss and Wave Velocity for Longitudinal (or Torsional) Waves and Bending Waves in Medium with Complex Elastic Modulus  $E^* = E(1 + j\eta)$

tional loss in amplitude per unit wavelength by an exponential loss term  $e^{-\alpha y}$  which defines the decrease in amplitude of a longitudinal or bending wave as it travels the distance  $y$  in the bar (or beam). The attenuation can be expressed in a convenient form by the attenuation constant  $\mu$  in decibels (dB) per wavelength  $\lambda$  where  $\lambda$  is the longitudinal or bending wavelength (see Chapter 4 for explanation of decibel attenuation). The constant  $\mu$  is defined by the following expressions.

Attenuation Constant for Longitudinal Waves

$$\mu_L = 2\pi (8.68) \left[ \frac{(\sqrt{1+\eta^2}-1)}{\sqrt{1+\eta^2}+1} \right]^{1/2} \text{ dB/wavelength} \quad (3.403a)$$

Attenuation Constant for Bending Waves

$$\mu_B = 2\pi (8.68) \left[ \frac{(1+\eta^2)^{1/4} - \sqrt{\frac{1}{2}(\sqrt{1+\eta^2}+1)}}{(1+\eta^2)^{1/4} + \sqrt{\frac{1}{2}(\sqrt{1+\eta^2}+1)}} \right]^{1/2} \text{ dB/wavelength.} \quad (3.403b)$$

The corresponding values for  $\mu_L$  and  $\mu_B$  are shown in Figure 3.113 as a function of the loss factor  $\eta$ .

For loss factors less than about 0.4, these two equations reduce to:

Longitudinal Waves

$$\mu_L = 8.68 \pi \eta - \text{dB/wavelength}$$

Bending Waves

$$\mu_B = 4.34 \pi \eta - \text{dB/wavelength}$$

General observations which can be made relative to the attenuation of damped structural waves are:

- 1) For longitudinal waves, the wave velocity is essentially constant and the attenuation rate increases linearly with frequency. The attenuation per wavelength is independent of frequency and directly proportional to the material loss factor  $\eta$ .
- 2) For lateral bending waves in beams, the wave velocity and the attenuation rate both increase with the square root of frequency. The attenuation per wavelength, then, is still independent of frequency but is 1/2 as much per wavelength as for longitudinal waves.

### 3.4 VIBRATION DESIGN TABLES

Tables 3.20 through 3.39, presented in this section, provide a convenient summary of vibration design formulas and tabulations of natural frequencies for structural elements. These tables provide an extension of the analytical treatment of structural vibration discussed in previous sec-

tions of this chapter. The tables were compiled from a thorough review of previously published design charts and recent results from the literature. Additional details have been provided, as necessary, to maintain clarity and accuracy of presentation for the benefit of the user.

The content of the tables is summarized in the following list of titles.

TABLE	TITLE	PAGE
3.20	EQUATIONS FOR STRENGTH OF MATERIALS . . . . .	3-164
3.21	SPRING STIFFNESS OF BEAMS . . . . .	3-164
3.22	STIFFNESS OF VARIOUS BASIC ELEMENTS . . . . .	3-165
3.23	STIFFNESS OF VARIOUS PLATE ELEMENTS . . . . .	3-166
3.24	TORSIONAL STIFFNESS AND POLAR MOMENT OF INERTIA OF STRAIGHT UNIFORM BEAM WITH COMMON SECTION . . . . .	3-167
3.25	NATURAL FREQUENCIES OF SIMPLE TRANSLATIONAL SYSTEMS . . . . .	3-168
3.26	NATURAL FREQUENCIES OF UNIFORM BEAMS FOR LONGITUDINAL AND TORSIONAL VIBRATIONS AND IN UNIFORM PIPES FOR LONGITUDINAL ACOUSTICAL RESONANCE . . . . .	3-169
3.27	NATURAL FREQUENCIES OF BEAMS IN FLEXURE . . . . .	3-170
3.28	NATURAL FREQUENCIES OF BEAMS ON MULTIPLE EQUALLY SPACED SUPPORTS . . . . .	3-171
3.29	FUNDAMENTAL FREQUENCIES OF COLUMNS IN LATERAL VIBRATION . . . . .	3-173
3.30	NATURAL FREQUENCIES OF AXIALLY LOADED BEAM CARRYING DISTRIBUTED MASSES AND DISTRIBUTED FOUNDATION SUPPORTS . . . . .	3-174
3.31	NATURAL FREQUENCIES AND MODE SHAPES OF UNIFORM PLATES IN FLEXURE . . . . .	3-176
3.32	NATURAL FREQUENCIES OF PLATE IN FLEXURE . . . . .	3-181
3.33	NATURAL FREQUENCY OF CIRCULAR PLATES OF UNIFORM THICKNESS . . . . .	3-182
3.34	NATURAL FREQUENCIES OF CIRCULAR MEMBRANES . . . . .	3-183
3.35	NATURAL FREQUENCY OF UNIFORM RING VIBRATING IN ITS OWN PLANE . . . . .	3-184
3.36	NATURAL FREQUENCIES OF UNIFORM RING IN FLEXURAL (NORMAL TO ITS OWN PLANE) AND TORSIONAL VIBRATIONS . . . . .	3-184
3.37	NATURAL FREQUENCIES OF AN ANISOTROPIC (ORTHOTROPIC) PLATE IN FLEXURE . . . . .	3-185
3.38	NATURAL FREQUENCIES OF PLATE IN FLEXURE, WITH CLOSED CAVITY BEHIND . . . . .	3-187
3.39	POISSON'S RATIO, YOUNG'S MODULUS, MODULUS OF RIGIDITY, SOUND VELOCITY, AND MATERIAL CORRECTION FACTOR FOR SOME ENGINEERING MATERIALS . . . . .	3-188

TABLE 3.20  
EQUATIONS FOR STRENGTH OF MATERIALS

Tensile, Compressive or Shear Stress	$\sigma = \frac{F}{A} = E\epsilon$	Vertical Shear Stress	$\sigma_s = \frac{VQ}{Ib'}$
Elongation	$e = \frac{FL}{AE} = L\epsilon$	Strain Energy per Unit Volume	$U = \frac{1}{2} \frac{\sigma^2}{E}$
Strain Due to a Load	$\epsilon = \frac{\sigma}{E}$	Stress Due to Simultaneous Axial and Transverse Loading of Beam	$\sigma_{max} = \frac{F}{A} \pm \frac{Mc}{I}$
Modulus of Elasticity	$E = \frac{\sigma}{\epsilon}$		
Bending Stress	$\sigma_b = \frac{Mc}{I}$ Where Bending Moment, $M = EI \frac{d^2y}{dx^2}$	Stress Due to Combined Bending and Torsion of Circular Bar With Radius r	$\sigma_{b\ max} = \frac{M'r}{I}$ $\sigma_{s\ max} = \frac{T'r}{J}$ Where $M' = \frac{1}{2} (M + \sqrt{M^2 + T^2})$ $T' = \sqrt{M^2 + T^2}$
Torsional Shear Stress	$\sigma_s = \frac{Tc}{K_r}$		
Twist of Rotational Displacement	$\theta = \frac{TL}{KG}$		

TABLE 3.21  
SPRING STIFFNESS OF BEAMS

Beam System	Translational (Due to Force F)	Rotational (Due to Moment M)	Beam System	Translational (Due to Force F)	Rotational (Due to Moment M)
	$k = \frac{3EI}{L^3}$	$k_r = \frac{EI}{L}$		$k = \frac{3EI L^3}{(ab)^3}$	$k_r = \frac{EI L^3}{ab(L^2 - 3ab)}$
	$k = \frac{3EIL}{(ab)^2}$	$k_r = \frac{3EIL}{L^2 - 3ab}$			$k_r = \frac{3EI}{L}$
	$k = \frac{96EI}{b(5b^2 - 3L^2)}$	$k_r = \frac{4EIL^3}{b[4L^3 - 3b(L+a)(L+b)]}$			$k_r = \frac{4EI}{L}$

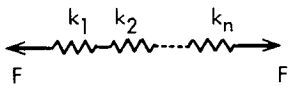
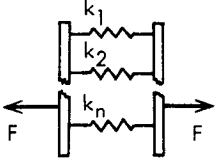




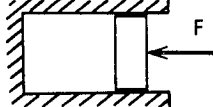
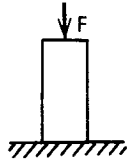
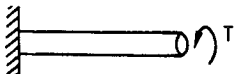
Symbols for Tables 3.20 and 3.21:

- A = Cross-Sectional Area
- c = Distance from the Neutral Axis to Extreme Stressed Fiber
- E = Modulus of Elasticity
- F = Concentrated Load
- G = Modulus of Rigidity
- I = Area Moment of Inertia

- M = Bending Moment
- k = Translational Spring Constant
- k<sub>r</sub> = Rotational Spring Constant
- V = Total Vertical Shear
- b' = Distance Across a Beam (Normal to Direction of Load) Measured Through the Point in Question

- Q = A'  $\bar{y}$ , where A' is Portion of Area of Cross Section Lying Above (or Below) b', and  $\bar{y}$ , is Distance from Neutral Axis to Centroid of A'
- T = Torque
- J = Polar Movement of Inertia
- K<sub>r</sub> = Torsional Constant (= k L/G, and = J for Circular Section)

TABLE 3.22  
STIFFNESS OF VARIOUS BASIC ELEMENTS

Springs in Series		$1/k_{total} = \sum_1^n 1/k_n$
Springs in Parallel		$k_{total} = \sum_1^n k_n$
Helical Spring in Axial Loading		$\frac{F}{\delta} = k = \frac{Gd^4}{8nD^3}$
Helical Spring in Torsion		$\frac{T}{\phi} = k_r = \frac{Ed^4}{64nD}$
Helical Spring in Bending		$\frac{M}{\theta} = k = \frac{Ed^4}{32nd} \cdot \frac{1}{1 + E/2G}$
Spiral Spring Under Torsion		$k_r = T/\phi = EI/L$
Pneumatic or Hydraulic Stiffness of Closed Chamber		$k = \frac{A^2 \rho c^2}{V}$
Column Under Vertical Load		$k = \frac{AE}{L}$
Uniform Shaft Under Torsion		$k_r = GJ/L$ See Table 3.24

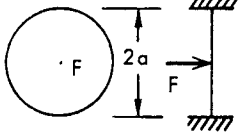
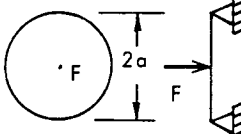
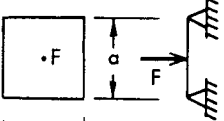
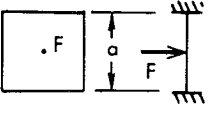
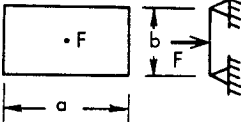
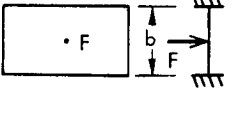
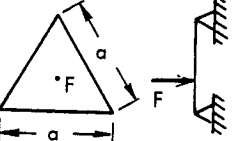
Symbols:

E = Modulus of Elasticity  
L = Length, or Total Spring Length  
I = Area Moment of Inertia  
G = Shear Modulus  
J = Polar Moment of Inertia  
T = Torsion  
 $\phi$  = Torsional Angle

F = Axial Force  
M = Bending Moment  
 $\theta$  = Flexural Angle  
 $\delta$  = Axial Deflection  
d = Wire Diameter  
D = Mean Coil Diameter  
n = Number of Coils

k = Spring Constant  
 $k_r$  = Torsional Spring Constant (Torsional Stiffness)  
A = Area of Piston or Column  
 $\rho$  = Mass Density of Media in Chamber  
c = Speed of Sound for Media in Chamber  
V = Chamber Volume

TABLE 3.23  
 STIFFNESS OF VARIOUS PLATE ELEMENTS  
 (Reference 3.53)

Circular Plate: All Edges Clamped		$k = \frac{16\pi D}{a^2}$								
All Edges Simply Supported		$k = \frac{16\pi D}{a^2} \left( \frac{1 + \nu}{3 + \nu} \right)$								
Square Plate: All Edges Simply Supported		$k = 86.1 D/a^2$								
All Edges Clamped		$k = 192.2 D/a^2$								
Rectangular Plates: All Edges Simply Supported		$k = 59.2 (1 + 0.462 r^4) D/b^2$ $r = b/a < 1$								
All Edges Clamped		$k = D\gamma/b^2$ <table border="1" data-bbox="865 1339 1159 1423"> <tr> <td>a/b</td> <td>4</td> <td>2</td> <td>1</td> </tr> <tr> <td><math>\gamma</math></td> <td>167</td> <td>147</td> <td>192</td> </tr> </table>	a/b	4	2	1	$\gamma$	167	147	192
a/b	4	2	1							
$\gamma$	167	147	192							
Equilateral Triangular Plate, All Edges Simply Supported		$k = 175 D/a^2$								

Symbols:

$k$  = Force/Deflection, Spring Constant

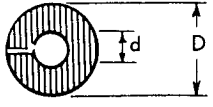
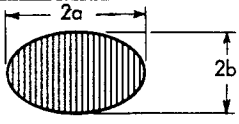

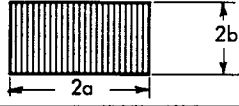


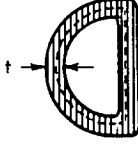
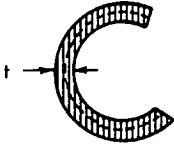
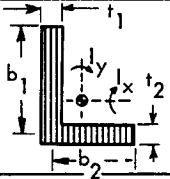
$$D = \frac{Eh^3}{12(1 - \nu^2)}$$

$E$  = Modulus of Elasticity

$\nu$  = Poisson's Ratio

$h$  = Plate Thickness

TABLE 3.24  
 TORSIONAL STIFFNESS,  $k_r$ , AND POLAR MOMENT OF INERTIA,  $J$ , OF  
 STRAIGHT UNIFORM BEAM WITH COMMON SECTION  
 (Reference 3.5J)

Circle: Closed or Split		Closed: $k_r = \frac{\pi}{32} (D^4 - d^4) \frac{G}{L}$ $J = \frac{\pi}{32} (D^4 - d^4)$	Split: $k_r = \frac{\pi}{24} d (D-d)^3 \frac{G}{L}$										
Ellipse		$k_r = \frac{\pi a^3 b^3}{a^2 + b^2} \frac{G}{L}$	$J = \frac{\pi}{4} ab (a^2 + b^2)$										
Square Hexagon		Square: $k_r = 0.1406 a^4 \frac{G}{L}$ $J = a^4/6$	Hexagon: $k_r = 2.69 a^4 \frac{G}{L}$ $J = A(12r^2 + a^2)/24$										
Rectangle		$k_r = ab^3 \left[ \frac{16}{3} - 3.36 \frac{b}{a} \left( 1 - \frac{b^4}{12a^4} \right) \right] \frac{G}{L}, J = \frac{4}{3} ab (a^2 + b^2)$											
Equilateral Triangle		$k_r = \frac{\sqrt{3} a^4}{80} \frac{G}{L}$	$J = \frac{3\sqrt{3}}{32} a^4$										
Any Solid Compact Section Without Reentrant Angles		$k_r = q \frac{GJ}{L}$ , where $qGJ$ = Torsional Rigidity $J = \int r^2 dA$ $q = \frac{A^4}{40J^2}$ (= 1, for Circular Section)											
Any Thin Closed Tube of Uniform Thickness $t$		$k_r \approx \frac{4A^2 t}{S} \frac{G}{L}$											
Any Thin Open Tube of Uniform Thickness $t$		$k_r \approx \frac{St^3}{3} \frac{G}{L}$											
Any Open-Section Beam		$k_r \approx \left[ \sum \beta_i b_i t_i^3 / 3 \right] G/L$ $J = I_x + I_y$ <table border="1" style="display: inline-table; vertical-align: middle;"> <tr> <td><math>b_i/t_i</math></td> <td>1</td> <td>2</td> <td>4</td> <td><math>\infty</math></td> </tr> <tr> <td><math>\beta_i</math></td> <td>.423</td> <td>.689</td> <td>.844</td> <td>1</td> </tr> </table> (Reference 3.73)		$b_i/t_i$	1	2	4	$\infty$	$\beta_i$	.423	.689	.844	1
$b_i/t_i$	1	2	4	$\infty$									
$\beta_i$	.423	.689	.844	1									

A = Cross-Sectional Area

S = Mean Circumferential Length  
(Length of Dotted Lines Shown)

L = Length of Beam, or bar

J = Polar Moment of Inertia of Area About Polar Axis  
Through Centroid (⊙)

I = Area Moment of Inertia About In-Plane Axes Through  
Centroid

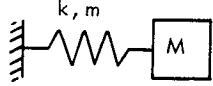
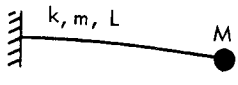

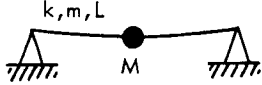
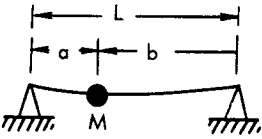
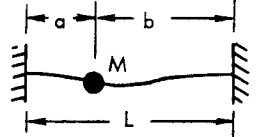
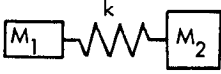
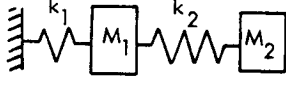

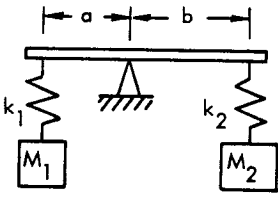
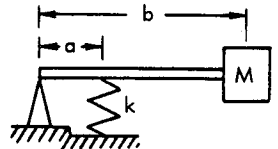
G = Modulus of Rigidity (Shear Modulus)

$k_r$  = Torsional Stiffness = Moment/Angular Deflection  
(Also known as Torsional Rigidity per unit length)

$K_r$  = Torsional Constant =  $k_r L/G$

TABLE 3.25

NATURAL FREQUENCIES OF SIMPLE TRANSLATIONAL SYSTEMS

	SYSTEM	NATURAL FREQUENCY, $f_n$ , Hz.
Massive-Spring Mass System		$\frac{1}{2\pi} \sqrt{k/(M + 0.33m)}$
Point Mass on Cantilever Beam		$\frac{1}{2\pi} \sqrt{3 EI / [L^3 (M + 0.23m)]}$
Point Mass at Center of Clamped Beam		$\frac{1}{2\pi} \sqrt{192 EI / [L^3 (M + 0.375m)]}$
Point Mass at Center of Simply Supported Beam		$\frac{1}{2\pi} \sqrt{48 EI / [L^3 (M + 0.5m)]}$
Simply Supported Massless Beam With Off-Center Point Mass		$\frac{1}{2\pi} \sqrt{3 EI L / a^2 b^2 M}$
Clamped-Clamped Massless Beam With Off-Center Point Mass		$\frac{1}{2\pi} \sqrt{3 EI L^3 / a^3 b^3 M}$
Mass-Spring Mass System		$\frac{1}{2\pi} \sqrt{k (M_1 + M_2) / M_1 M_2}$
Multi-Mass Spring Systems		$\frac{\sqrt{2}/4\pi}{} \{ k_1/M_1 + k_2/M_1 + k_2/M_2 \pm [(k_1/M_1 + k_2/M_1 + k_2/M_2)^2 - 4k_1k_2/M_1M_2]^{1/2} \}^{1/2}$
		$\frac{\sqrt{2}/4\pi}{} \{ (k_1 + k_2)/M_1 + (k_2 + k_3)/M_2 \pm [((k_1 + k_2)/M_1 + (k_2 + k_3)/M_2)^2 - 4(k_1k_2 + k_2k_3 + k_3k_1)/M_1M_2]^{1/2} \}^{1/2}$
Mass Spring and Lever Systems (Inertia of Lever Negligible)		$\frac{1}{2\pi} \sqrt{\left( \frac{1}{M_1} + \frac{a^2}{b^2 M_2} \right) / \left( \frac{1}{k_1} + \frac{a^2}{b^2 k_2} \right)}$
		$\frac{1}{2\pi} \frac{a}{b} \sqrt{k/M}$

Symbols:

M = Point Mass

m = Total Mass of Spring Element

k = Spring Constant

a, b = Distances

E = Young's Modulus

I = Area Moment of Inertia of Beam

L = Beam Length

(References 3.1 and 3.53)

TABLE 3.26

NATURAL FREQUENCIES OF UNIFORM BEAMS FOR LONGITUDINAL AND TORSIONAL VIBRATIONS AND IN UNIFORM PIPES FOR LONGITUDINAL ACOUSTICAL RESONANCE

	SYSTEM-MODE SHAPE	NATURAL FREQUENCY, Hz.
Longitudinal or Torsional Vibration of Uniform Clamped-Free Beam		$f_n = \frac{2n-1}{4} \frac{c'}{L}$ $c' = \text{speed of sound in beam}$ $= \sqrt{E/\rho} \text{ in longitudinal vibration}$ $= \sqrt{G/\rho} \text{ in torsional vibration}$
Longitudinal or Torsional Vibration of Uniform Clamped-Clamped Beam		$f_n = \frac{n}{2} \frac{c'}{L}$ $c' = \text{speed of sound in beam. (See above)}$
Longitudinal Acoustical Resonance of Uniform Pipe System (with Pressure Mode Shape shown); Closed-Closed Pipe		$f_n = \frac{n}{2} \frac{c}{L}$ $c = \text{speed of sound in gas}$
Open-Open Pipe with and without Baffle		$f_n = \frac{n}{2} \frac{c}{L'}$ $L' \approx L + 1.2a - \text{No Baffles}$ $\approx L + 1.45a - \text{Baffle at one end}$ $\approx L + 1.7a - \text{Baffle at both ends}$
Piston-Driven Closed Pipe		$f_n = \frac{2n-1}{4} \frac{c}{L}$
Piston-Driven Open Pipe with and without Baffle at end		$f_n \approx \frac{n}{2} \frac{c}{L'}$ $(f_n < c/4\pi a)$ $L' \approx L + 0.85a \text{ (with Baffle)}$ $L' \approx L + 0.6a \text{ (without Baffle)}$
Helmholtz Resonator with and without Piston Driver		<p>Fundamental Mode</p> $f_1 \approx \frac{c}{2\pi L'} \sqrt{\frac{V_t}{V}} \quad (f_1 < c/2\pi a \text{ and } f_1 < c/4\pi L)$ $L' \approx L + 0.85a \text{ (with piston)}$ $L' \approx L + 1.45a \text{ (without piston)}$ $V_t = \pi a^2 L' \quad V = \text{cavity volume.}$



TABLE 3.27

NATURAL FREQUENCIES OF BEAMS IN FLEXURE

$$f_n = C_n \frac{r}{L^2} \times 10^4 \times K_m$$

where  $f_n$  =  $n^{\text{th}}$  Natural Frequency, Hz.

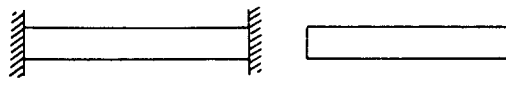
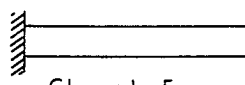
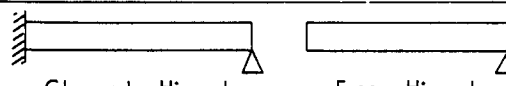
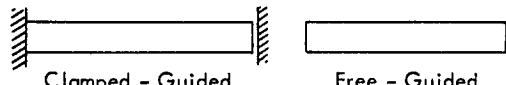
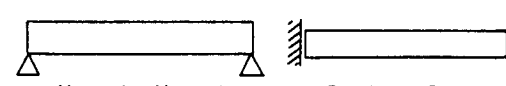
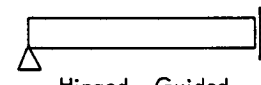
$C_n$  = Frequency Constant of  $n^{\text{th}}$  Mode, Listed in Table Below

$r$  = Radius of Gyration of Cross-Section of Beam,  $\sqrt{I/A}$ , Inches

$L$  = Length of Beam, Inches

$K_m$  = Material Constant, See Table 3.39

$C_n$

UNIFORM BEAMS	MODE NUMBER, $n$				
	1	2	3	4	5
 <p>Clamped - Clamped      Free - Free</p>	71.95	198.29	388.73	642.60	959.94
 <p>Clamped - Free</p>	11.30	70.85	198.30	388.73	642.60
 <p>Clamped - Hinged      Free - Hinged</p>	49.57	160.65	335.17	573.20	874.65
 <p>Clamped - Guided      Free - Guided</p>	17.98	97.18	239.98	446.25	715.98
 <p>Hinged - Hinged      Guided - Guided</p>	31.73	126.93	285.60	507.73	793.33
 <p>Hinged - Guided</p>	7.93	71.40	198.33	388.73	642.60

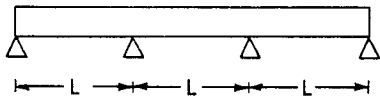
(Reference 3.59)

TABLE 3.28

NATURAL FREQUENCIES OF BEAMS ON MULTIPLE EQUALLY SPACED SUPPORTS

$$f_n = C_n \frac{r}{L^2} \times 10^4 \times K_m$$

- where  $f_n$  =  $n^{\text{th}}$  Natural Frequency, Hz.  
 $C_n$  = Frequency Constant of  $n^{\text{th}}$  Mode, Listed in Table Below  
 $r$  = Radius of Gyration of Cross-Section of Beam,  $\sqrt{I/A}$ , Inches  
 $L$  = Span Length, Inches  
 $K_m$  = Material Constant, See Table 3.39

BEAM SYSTEM	NUMBER OF SPANS	MODE NUMBER, n				
		1	2	3	4	5
 <p>Uniform Beam, Extreme Ends Simply Supported; Equal Spans</p>	1	31.73	126.94	285.61	507.76	793.37
	2	31.73	49.59	126.94	160.66	285.61
	3	31.73	40.52	59.56	126.94	143.98
	4	31.73	37.02	49.59	63.99	126.94
	5	31.73	34.99	44.19	55.29	66.72
	6	31.73	34.32	40.52	49.59	59.56
	7	31.73	33.67	38.40	45.70	53.63
	8	31.73	33.02	37.02	42.70	49.59
	9	31.73	33.02	35.66	40.52	46.46
	10	31.73	33.02	34.99	39.10	44.19
	11	31.73	32.37	34.32	37.70	41.97
	12	31.73	32.37	34.32	37.02	40.52

(Reference 3.59)

TABLE 3.28 (CONTINUED)

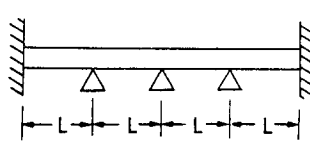
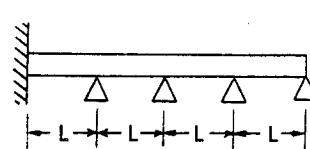
BEAM SYSTEM	NUMBER OF SPANS	$C_n$				
		MODE NUMBER, $n$				
		1	2	3	4	5
Uniform Beam, Extreme Ends Clamped; Equal Spans  	1	72.36	198.34	388.75	642.63	959.98
	2	49.59	72.36	160.66	198.34	335.20
	3	40.52	59.56	72.36	143.98	178.25
	4	37.02	49.59	63.99	72.36	137.30
	5	34.99	44.19	55.29	66.72	72.36
	6	34.32	40.52	49.59	59.56	67.65
	7	33.67	38.40	45.70	53.63	62.20
	8	33.02	37.02	42.70	49.59	56.98
	9	33.02	35.66	40.52	46.46	52.81
	10	33.02	34.99	39.10	44.19	49.59
	11	32.37	34.32	37.70	41.97	47.23
	12	32.37	34.32	37.02	40.52	44.94
Uniform Beam, Extreme Ends Clamped - Simply Supported; Equal Spans  	1	49.59	160.66	335.2	573.21	874.69
	2	37.02	63.99	137.30	185.85	301.05
	3	34.32	49.59	67.65	132.07	160.66
	4	33.02	42.70	56.98	69.51	129.49
	5	33.02	39.10	49.59	61.31	70.45
	6	32.37	37.02	44.94	54.46	63.99
	7	32.37	35.66	41.97	49.59	57.84
	8	32.37	34.99	39.81	45.70	53.63
	9	31.73	34.32	38.40	43.44	49.59
	10	31.73	33.67	37.02	41.24	46.46
	11	31.73	33.67	36.33	39.61	44.19

TABLE 3.29  
 FUNDAMENTAL FREQUENCIES OF COLUMNS IN LATERAL VIBRATION  
 (Reference 3.56)

$$f_1 = C_1 \frac{r}{L^2} \times 10^4 \times K_m$$

- where  $f_1$  = Fundamental Frequency, Hz.  
 $C_1$  = Frequency Constant, Listed in Table Below  
 $r$  = Radius of Gyration,  $\sqrt{I/A}$ , Inches  
 $L$  = Length of Column, Inches  
 $K_m$  = Material Constant, See Table 3.39

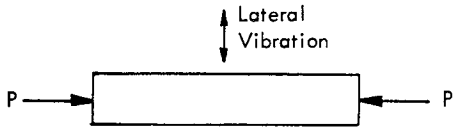
COLUMN	$C_1$				
	Boundary Condition				
<p>Symbols:</p> <p><math>P</math> = column axial load</p> <p><math>P_1'</math> = critical buckling load  <math>= \xi (\pi/L)^2 EI</math></p> <p><math>E</math> = modulus of elasticity</p> <p><math>I</math> = minimum area moment of inertia of column</p> <p><math>\xi</math> = 1/4 for C-F column                      = 1 for S-S column                      = 2 for C-S column                      = 4 for C-C column</p> <p>Boundary Conditions:</p> <p>C = clamped</p> <p>F = free</p> <p>S = simply supported</p>	$\frac{P}{P_1'}$	C-F	S-S	C-S	C-C
	0	11.30	31.73	49.57	71.95
	.1	10.71	29.96	46.92	68.02
	.2	10.14	28.25	44.35	64.23
	.3	9.52	26.43	41.62	60.19
	.4	8.85	24.46	38.69	55.82
	.5	8.11	22.33	35.49	51.05
	.6	7.29	19.97	31.96	45.74
	.7	6.34	17.30	27.97	39.69
	.8	5.20	14.13	23.27	32.47
	.9	3.73	9.99	17.31	23.01
	1.0	0			

TABLE 3.30

NATURAL FREQUENCIES OF AXIALLY LOADED BEAM CARRYING DISTRIBUTED MASSES AND DISTRIBUTED FOUNDATION SUPPORTS (Reference 3.71)

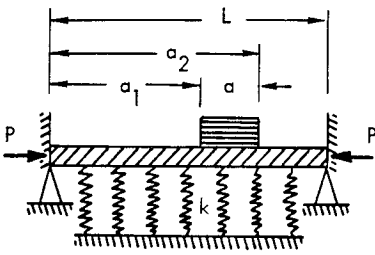
SYSTEM	NATURAL FREQUENCY, $f_n$ , Hz.
<p>Axially Loaded Beams Carrying Distributed Masses and Distributed Foundation Supports.</p>  <p>Symbols:</p> <p><math>r</math> = radius of gyration of beam, <math>\sqrt{I/A}</math>, inches</p> <p><math>L</math> = length of beam, inches</p> <p><math>C_n</math> = frequency constant of an unloaded beam (simply supported or clamped), as listed in Table 3.27</p> <p><math>K_m</math> = material constant. See Table 3.39</p> <p><math>a, a_1, a_2</math> = distances, see figure above</p> <p><math>W</math> = total weight of applied load, lb</p> <p><math>W_b</math> = weight of beam, lb</p> <p><math>n</math> = mode number = 1, 2</p> <p><math>k</math> = foundation modulus in lb/in<sup>2</sup></p> <p><math>P'_n</math> = critical buckling load, lb</p> <p><math>E</math> = modulus of elasticity, lb/in<sup>2</sup></p> <p><math>I</math> = moment of inertia of beam cross section</p> <p><math>P</math> = axial load, lb</p> <p><math>\mathcal{L}</math> = coefficient representing mass distribution for simply supported beams</p> <p><math>N</math> = coefficient representing mass distribution for clamped beams.</p> <p><math>\xi_n</math> = buckling load constant</p>	<p>Simply supported at both ends:</p> $f_n = C_n \frac{r}{L^2} \times 10^4 \times K_m \times A_n$ <p>for <math>n = 1, 2</math></p> <p>Clamped-clamped at both ends:</p> $f_n = C_n \frac{r}{L^2} \times 10^4 \times K_m \times B_n$ <p>for <math>n = 1, 2</math></p> <p>where:</p> $A_n = \left[ \frac{1 - \frac{P}{P'_n} + \left(\frac{L}{n\pi}\right)^4 \frac{k}{EI}}{1 + \frac{W}{W_b} \frac{\mathcal{L}_n}{a}} \right]^{1/2}$ $B_1 = \left[ \frac{1 - \frac{P}{P'_1} + \frac{3}{16} \left(\frac{L}{\pi}\right)^4 \frac{k}{EI}}{1 + \frac{W}{W_b} \frac{N_1}{a}} \right]^{1/2}$ $B_2 = \left[ \frac{1 - \frac{.996P}{P'_2} + \frac{1}{41} \left(\frac{L}{\pi}\right)^4 \frac{k}{EI}}{1 + \frac{W}{W_b} \frac{N_2}{a}} \right]^{1/2}$ $P'_n = \xi_n \pi^2 EI / L^2$ <p>where:</p> $\mathcal{L}_n = a - \frac{L}{2n\pi} \left( \sin \frac{2n\pi a_2}{L} + \sin \frac{2n\pi a_1}{L} \right)$ $N_1 = a - \frac{2L}{3\pi} \left( \sin \frac{2\pi a_2}{L} - \sin \frac{2\pi a_1}{L} \right)$ $+ \frac{L}{12\pi} \left( \sin \frac{4\pi a_2}{L} - \sin \frac{4\pi a_1}{L} \right)$

TABLE 3.30 (CONTINUED)

SYSTEM	NATURAL FREQUENCY, $f_n$ , Hz.																																																																								
<p><math>\xi_n</math> = Buckling Load Constant</p> <p>Values of <math>\xi_n</math>:</p> <table border="1" style="margin-left: auto; margin-right: auto; border-collapse: collapse;"> <thead> <tr> <th style="text-align: center;">Mode No. <math>n</math></th> <th style="text-align: center;">1</th> <th style="text-align: center;">2</th> </tr> </thead> <tbody> <tr> <td style="text-align: center;">Clamped Ends</td> <td style="text-align: center;">4</td> <td style="text-align: center;">8.17</td> </tr> <tr> <td style="text-align: center;">Simply Supported Ends</td> <td style="text-align: center;">1</td> <td style="text-align: center;">4</td> </tr> </tbody> </table>	Mode No. $n$	1	2	Clamped Ends	4	8.17	Simply Supported Ends	1	4	$N_2 = a - \frac{L}{4\pi} \left( \sin \frac{2\pi a_2}{L} + \sin \frac{4\pi a_2}{L} - \sin \frac{2\pi a_1}{L} - \sin \frac{4\pi a_1}{L} \right) + \frac{L}{12\pi} \left( \sin \frac{6\pi a_2}{L} - \sin \frac{6\pi a_1}{L} \right)$ <p>For the symmetrical case where</p> $a_1 = (L - a_2):$ <table border="1" style="margin-left: auto; margin-right: auto; border-collapse: collapse;"> <thead> <tr> <th style="text-align: center;"><math>a/L</math></th> <th style="text-align: center;">1st Mode <math>L_1/a</math></th> <th style="text-align: center;">2nd Mode <math>L_2/a</math></th> <th style="text-align: center;">1st Mode <math>N_1/a</math></th> <th style="text-align: center;">2nd Mode <math>N_2/a</math></th> </tr> </thead> <tbody> <tr><td style="text-align: center;">0</td><td style="text-align: center;">2.000</td><td style="text-align: center;">0</td><td style="text-align: center;">2.667</td><td style="text-align: center;">0</td></tr> <tr><td style="text-align: center;">.1</td><td style="text-align: center;">1.984</td><td style="text-align: center;">0.065</td><td style="text-align: center;">2.623</td><td style="text-align: center;">0.127</td></tr> <tr><td style="text-align: center;">.2</td><td style="text-align: center;">1.936</td><td style="text-align: center;">0.243</td><td style="text-align: center;">2.500</td><td style="text-align: center;">0.459</td></tr> <tr><td style="text-align: center;">.3</td><td style="text-align: center;">1.859</td><td style="text-align: center;">0.495</td><td style="text-align: center;">2.313</td><td style="text-align: center;">0.870</td></tr> <tr><td style="text-align: center;">.4</td><td style="text-align: center;">1.756</td><td style="text-align: center;">0.766</td><td style="text-align: center;">2.087</td><td style="text-align: center;">1.223</td></tr> <tr><td style="text-align: center;">.5</td><td style="text-align: center;">1.637</td><td style="text-align: center;">1.000</td><td style="text-align: center;">1.849</td><td style="text-align: center;">1.424</td></tr> <tr><td style="text-align: center;">.6</td><td style="text-align: center;">1.504</td><td style="text-align: center;">1.156</td><td style="text-align: center;">1.621</td><td style="text-align: center;">1.460</td></tr> <tr><td style="text-align: center;">.7</td><td style="text-align: center;">1.368</td><td style="text-align: center;">1.216</td><td style="text-align: center;">1.418</td><td style="text-align: center;">1.377</td></tr> <tr><td style="text-align: center;">.8</td><td style="text-align: center;">1.234</td><td style="text-align: center;">1.189</td><td style="text-align: center;">1.249</td><td style="text-align: center;">1.243</td></tr> <tr><td style="text-align: center;">.9</td><td style="text-align: center;">1.109</td><td style="text-align: center;">1.104</td><td style="text-align: center;">1.111</td><td style="text-align: center;">1.111</td></tr> <tr><td style="text-align: center;">1.0</td><td style="text-align: center;">1.000</td><td style="text-align: center;">1.000</td><td style="text-align: center;">1.000</td><td style="text-align: center;">1.000</td></tr> </tbody> </table>				$a/L$	1st Mode $L_1/a$	2nd Mode $L_2/a$	1st Mode $N_1/a$	2nd Mode $N_2/a$	0	2.000	0	2.667	0	.1	1.984	0.065	2.623	0.127	.2	1.936	0.243	2.500	0.459	.3	1.859	0.495	2.313	0.870	.4	1.756	0.766	2.087	1.223	.5	1.637	1.000	1.849	1.424	.6	1.504	1.156	1.621	1.460	.7	1.368	1.216	1.418	1.377	.8	1.234	1.189	1.249	1.243	.9	1.109	1.104	1.111	1.111	1.0	1.000	1.000	1.000	1.000
Mode No. $n$	1	2																																																																							
Clamped Ends	4	8.17																																																																							
Simply Supported Ends	1	4																																																																							
$a/L$	1st Mode $L_1/a$	2nd Mode $L_2/a$	1st Mode $N_1/a$	2nd Mode $N_2/a$																																																																					
0	2.000	0	2.667	0																																																																					
.1	1.984	0.065	2.623	0.127																																																																					
.2	1.936	0.243	2.500	0.459																																																																					
.3	1.859	0.495	2.313	0.870																																																																					
.4	1.756	0.766	2.087	1.223																																																																					
.5	1.637	1.000	1.849	1.424																																																																					
.6	1.504	1.156	1.621	1.460																																																																					
.7	1.368	1.216	1.418	1.377																																																																					
.8	1.234	1.189	1.249	1.243																																																																					
.9	1.109	1.104	1.111	1.111																																																																					
1.0	1.000	1.000	1.000	1.000																																																																					

TABLE 3.31  
NATURAL FREQUENCIES AND MODE SHAPES OF UNIFORM PLATES IN FLEXURE

$$f_n = C_n \frac{h}{a^2} \times 10^4 \times K_m$$

where  $f_n$  =  $n^{\text{th}}$  Natural Frequency, Hz.

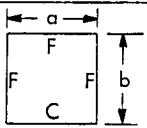



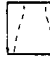
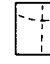
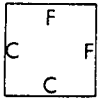
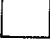
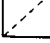


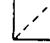
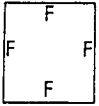


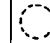


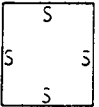


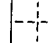

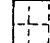
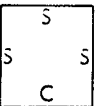

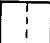



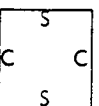

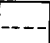

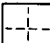
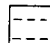
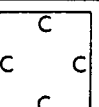


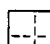
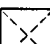

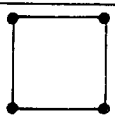

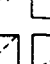
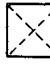


$C_n$  = Frequency Constant of  $n^{\text{th}}$  Mode, Listed in Tables Below

$h$  = Thickness of Plate, Inches

$a$  = Side of Plate, Inches

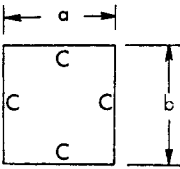
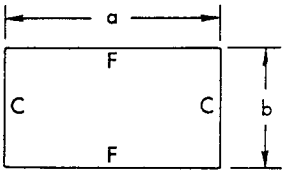
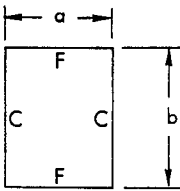
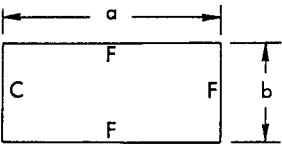
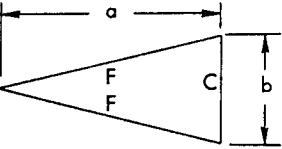
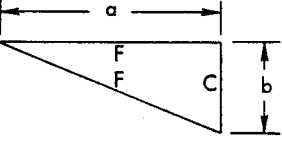
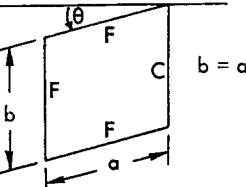
$K_m$  = Material Constant, See Table 3.39

$C_n$

SQUARE PLATES $b = a$	MODE NUMBER, $n$					
	1	2	3	4	5	6
	3.40 	8.32 	20.86 	26.71 	30.32 	
	6.77 	23.43 	26.07 	46.75 	61.44 	
	13.72 	19.99 	23.26 	34.98 	59.93 	63.47
	19.20 	48.00 	76.82 	96.01 	124.82 	163.25
	23.01 	50.28 	57.06 	83.79 	97.58 	110.13
	28.16 	53.26 	67.44 	92.02 	99.43 	125.60
	35.01 	71.42 	105.36 	128.03 	128.71 	160.72
	6.91 	15.29 	18.60 	37.35 	42.28 	

F = Free, C = Clamped, S = Simply Supported (=Pinned) (References 3.59 and 3.62)

TABLE 3.31 (CONTINUED)

UNIFORM PLATES	a/b	C <sub>n</sub>			
		MODE NUMBER, n   MODE SHAPE (p, q) IN BRACKET			
		1	2	3	4
	1.0	35.0 (1,1)	71.4 (1,2) (2,1)	105.3 (2,2)	128.0 (1,3) (3,1)
	0.8	29.1 (1,1)	51.1 (1,2)	66.6 (2,1)	86.7 (1,3)
	0.6	25.1 (1,1)	36.2 (1,2)	55.4 (1,3)	63.5 (2,1)
	0.4	23.0 (1,1)	27.1 (1,2)	33.5 (1,3)	45.4 (1,4)
	0.2	22.0 (1,1)	22.7 (1,2)	24.2 (1,3)	26.3 (1,4)
 	1.0	21.5 (1,1)	25.6 (1,2)	42.3 (1,3)	59.4 (2,1)
	1/8	21.4 (1,1)	27.6 (1,2)	54.2 (1,3)	59.2 (2,1)
	1/6	21.3 (1,1)	31.5 (1,2)	59.0 (2,1)	74.2 (1,3)
	1/4	21.2 (1,1)	40.4 (1,2)	58.6 (2,1)	89.3 (2,2)
	1/2	21.0 (1,1)	57.0 (2,1)	70.0 (1,2)	115.0 (3,1)
	1.0	21.5 (1,1)	25.6 (1,2)	42.3 (1,3)	59.4 (2,1)
	0.8	21.5 (1,1)	24.2 (1,2)	34.8 (1,3)	56.5 (1,4)
	0.6	21.5 (1,1)	23.1 (1,2)	28.9 (1,3)	40.6 (1,4)
	0.4	21.6 (1,1)	22.3 (1,2)	24.8 (1,3)	29.7 (1,4)
	0.2	21.6 (1,1)	21.8 (1,2)	22.4 (1,3)	23.5 (1,4)
	0.5	3.41 (1,1)	5.23 (1,2)	9.98 (1,3)	21.4 (2,1)
	1.0	3.40 (1,1)	8.32 (1,2)	20.9 (2,1)	26.7 (1,3)
	2.0	3.38 (1,1)	14.5 (1,2)	21.0 (2,1)	49.9 (2,2)
	5.0	3.36 (1,1)	20.9 (2,1)	33.8 (1,2)	103.0 (2,2)
	2	6.7 (1,1)	28.6 (2,1)	56.6	137
	4	6.6 (1,1)	28.5 (2,1)	83.5	240
	8	6.6 (1,1)	28.4 (2,1)	146.1	457
	14	6.6 (1,1)	28.4 (2,1)	246	790
	2	5.5 (1,1)	23.6 (2,1)		
	4	6.2 (1,1)	26.7 (2,1)		
	7	6.4 (1,1)	28.1 (2,1)		
	θ =				
	15°	3.50 (1,1)	8.63 (1,2)		
	30°	3.85 (1,1)	9.91 (1,2)		
	45°	4.69 (1,1)	13.38 (1,2)		

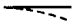
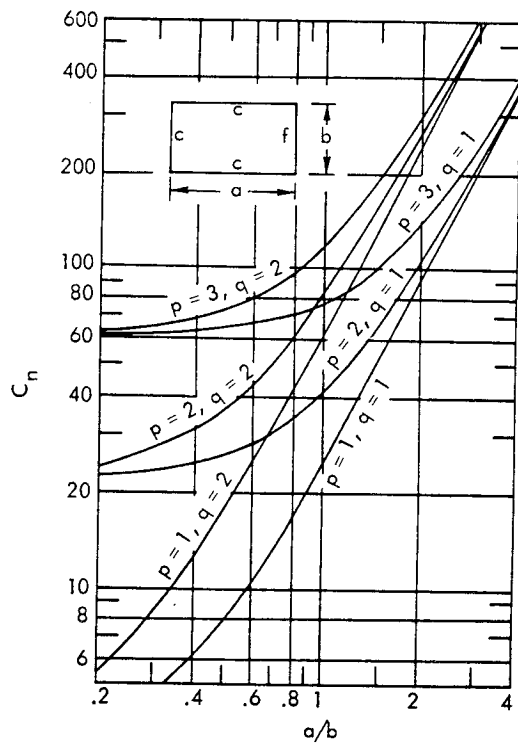
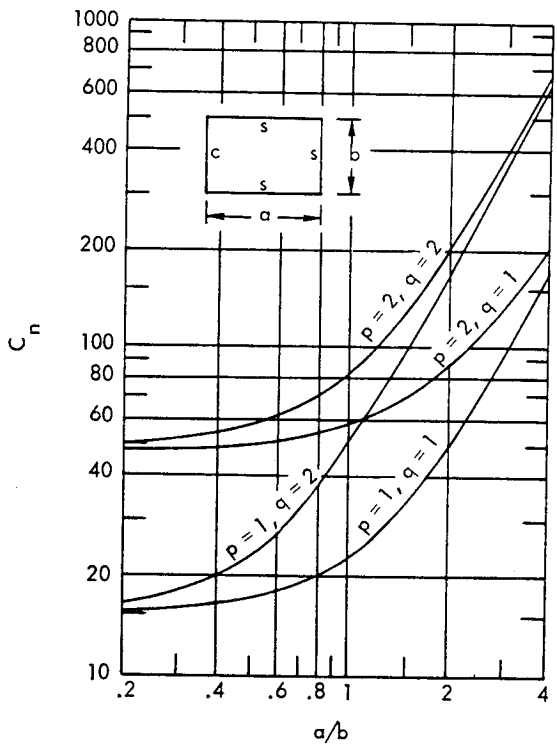
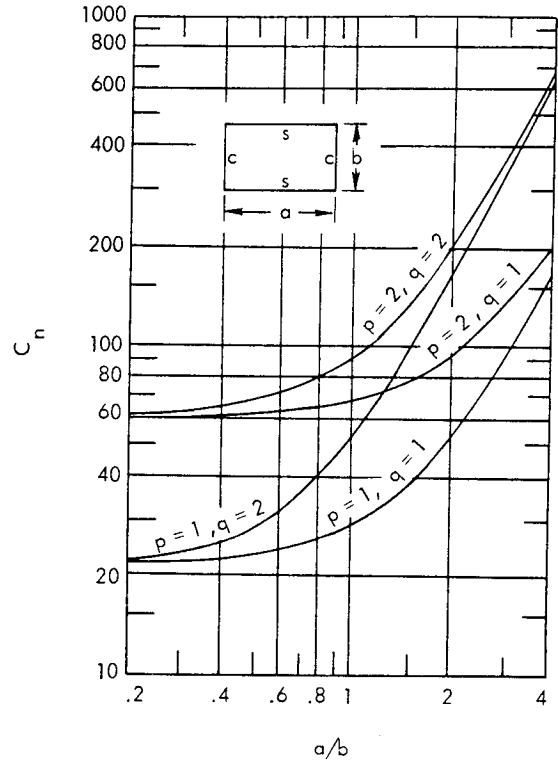
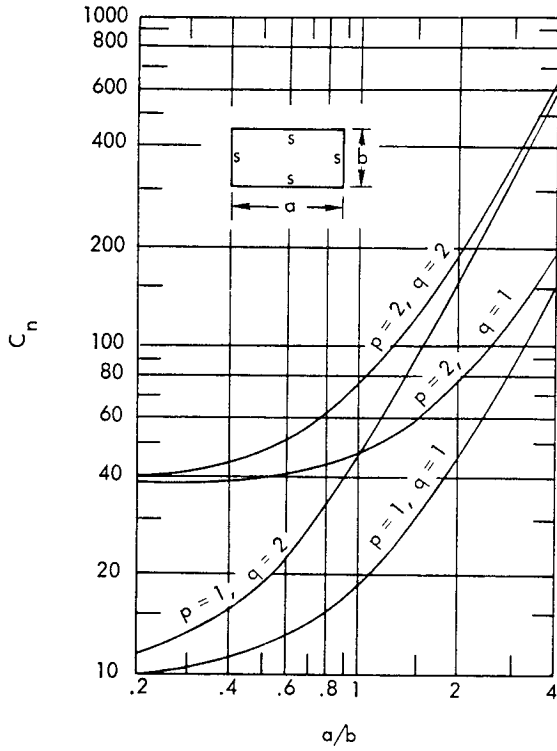
F = Free, C = Clamped; p\* = Number of Half Waves Along Side a, q = Number of Half Waves Along Side b  
 \* For the last four cases, cantilever mode  exists when p = 1.

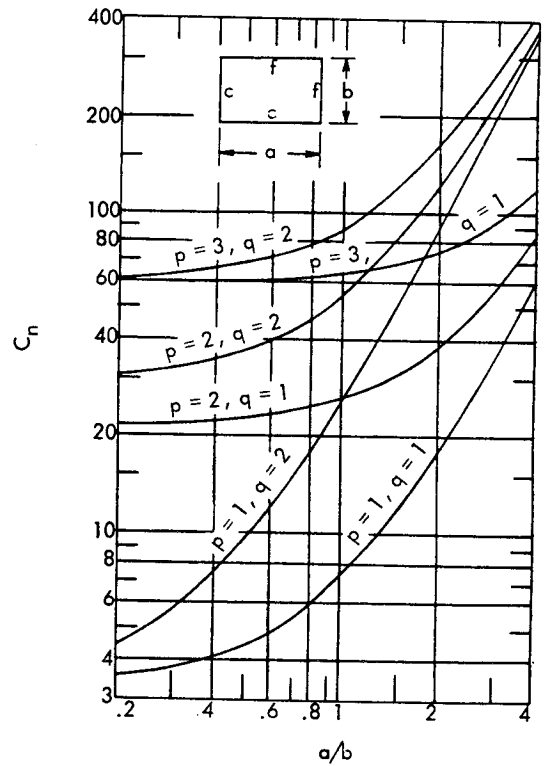
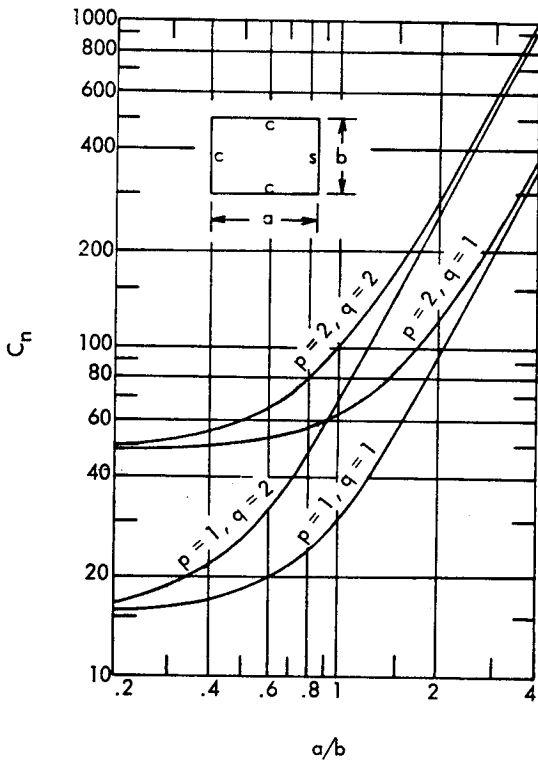
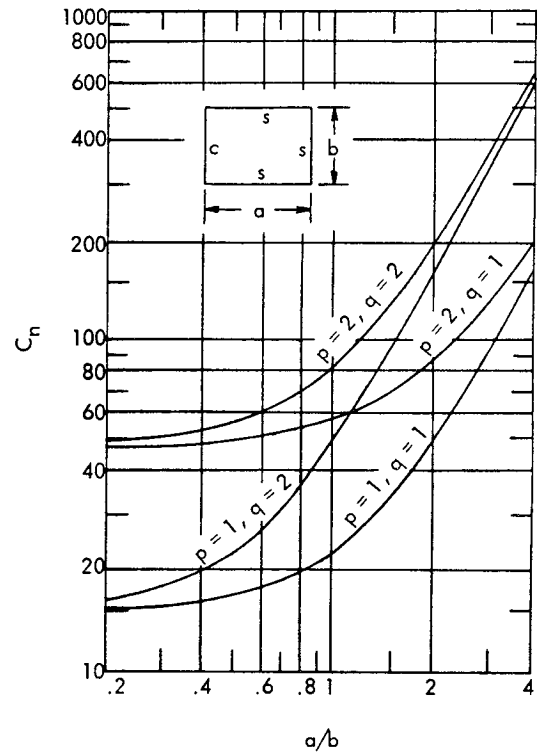
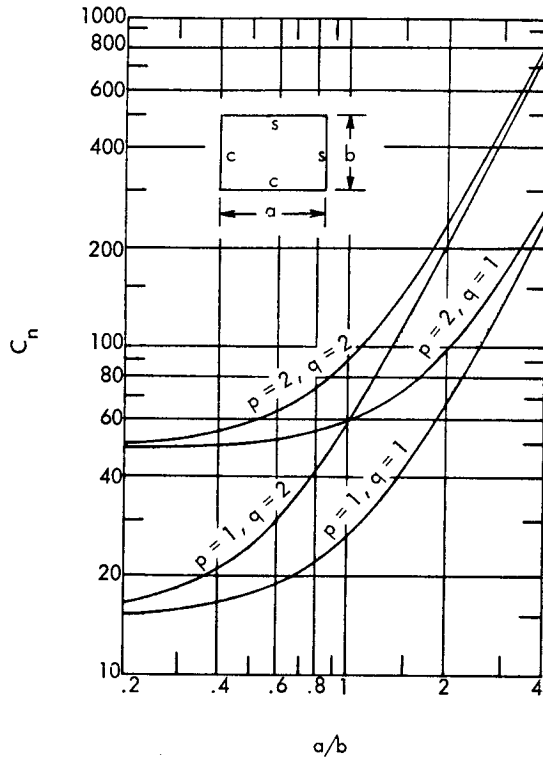


TABLE 3.31 (CONTINUED)



$p$  = Number of Half Waves Along Side  $a$ ,  $q$  = Number of Half Waves Along Side  $b$ . (References 3.61 and 3.76)

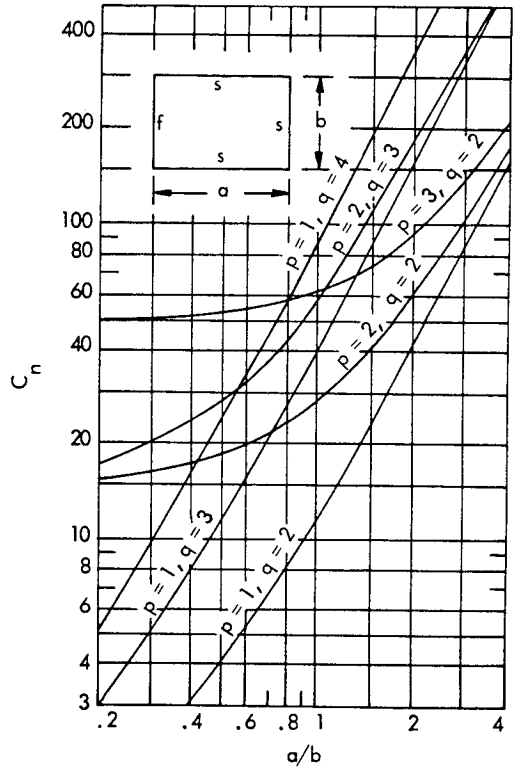
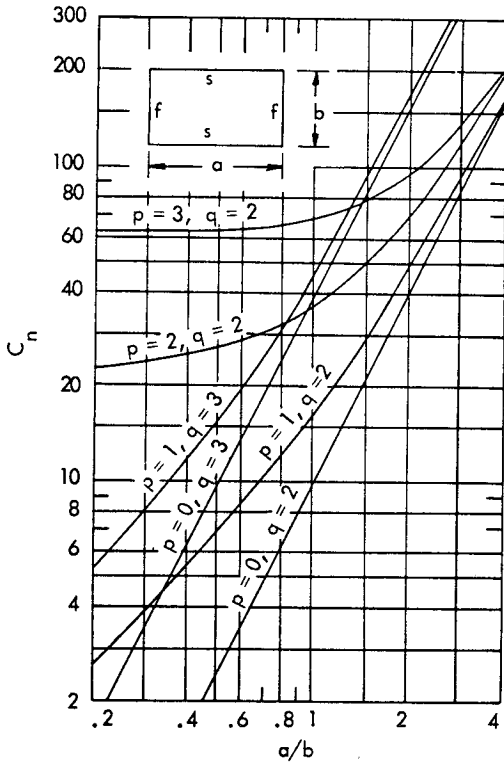
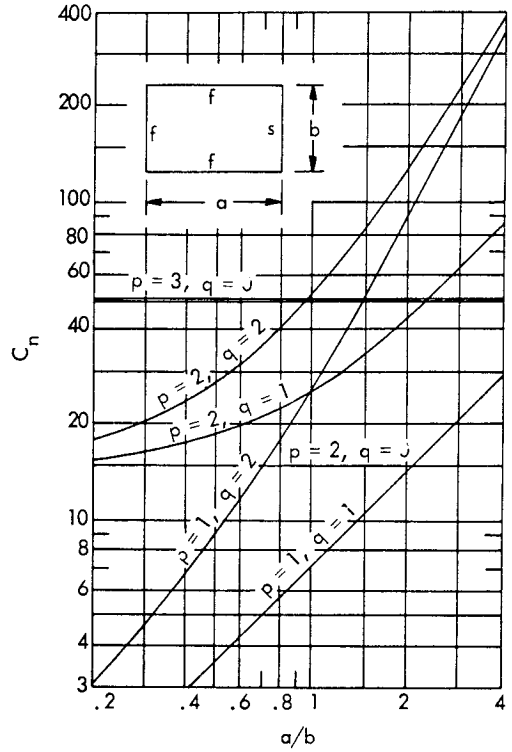
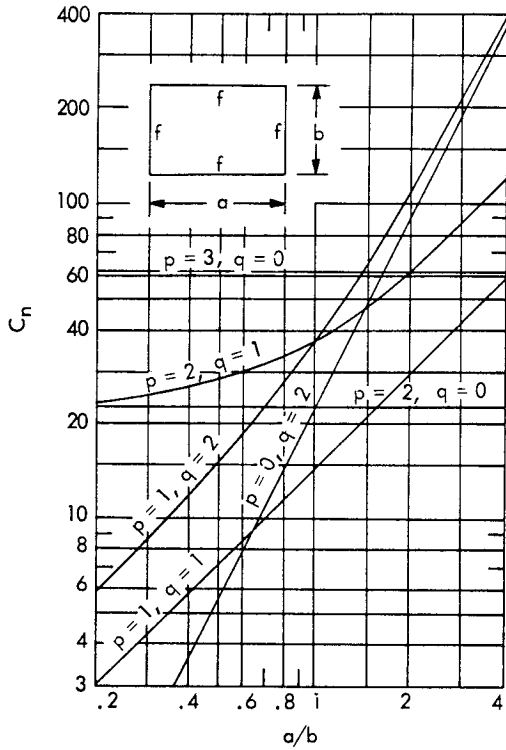
TABLE 3.31 (CONTINUED)



$p$  = Number of Half Waves Along Side  $a$ ,  $q$  = Number of Half Waves Along Side  $b$ .  
 In the last case, cantilever mode exists when  $p$  or  $q$  is 1.

(References 3.61 and 3.76)

TABLE 3.31 (CONTINUED)



$p, q$  = number of node lines perpendicular to side  $a$ , or  $b$ , respectively. (References 3.61 and 3.76)

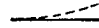
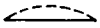
NOTE:  $p$  and  $q$  are defined differently on this page. Both  and  would be defined as first vibration mode, but notice that the first one has one node line and the second has two. This new definition of  $p$  and  $q$  is necessary due to the presence of free edge(s).

TABLE 3.32  
 NATURAL FREQUENCIES OF PLATE IN FLEXURE (Reference 3.72)

$$f_n = C_n \frac{h}{a^2} \times 10^4 \times K_m$$

where  $f_n$  =  $n^{\text{th}}$  Natural Frequency, Hz.

$C_n$  = Frequency Constant of  $n^{\text{th}}$  Mode, Listed in Tables Below

$h$  = Thickness of Plate, Inches

$a$  = Side of Plate, Inches

$K_m$  = Material Constant, See Table 3.39

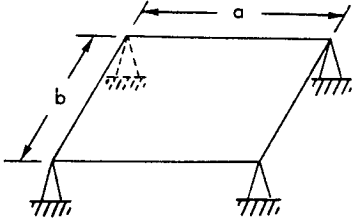
SYSTEM	$C_n$ NATURAL FREQUENCY, $f_n$ , Hz					
Uniform Plate Simply Supported at Four Corners  	$a/b$	1.0	1.5	2.0	2.5	3.0
	$C_1$	6.91	8.67	9.02	9.09	9.16
	$a/b$	4.0	6.0	8.0	10.0	$\infty$
	$C_1$	9.28	9.39	9.46	9.54	9.58
	For $a/b = 1$					
	$n$	1	2	3	4	5
	$C_n$	6.91	15.29	18.60	37.35	42.28

TABLE 3.33

NATURAL FREQUENCY OF CIRCULAR PLATES OF UNIFORM THICKNESS

$$f_{m,n} = C_{m,n} \frac{h}{R^2} \times 10^4 \times K_m$$

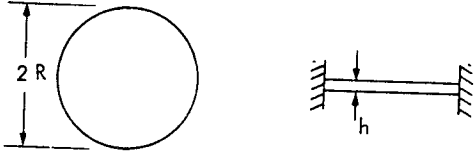
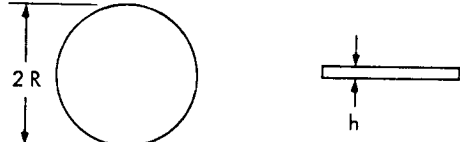
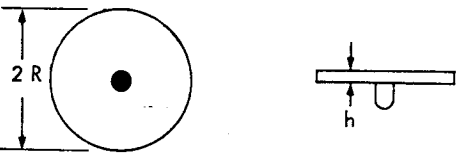
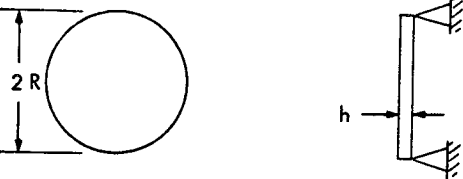
where  $f_{m,n}$  =  $m$ - $n$ <sup>th</sup> Natural Frequency, Hz.

$C_{m,n}$  = Frequency Constant of  $m$ - $n$ <sup>th</sup> Mode, Listed in Table Below

$h$  = Thickness of Plate, Inches

$R$  = Radius of Plate, Inches

$K_m$  = Material Constant, See Table 3.39

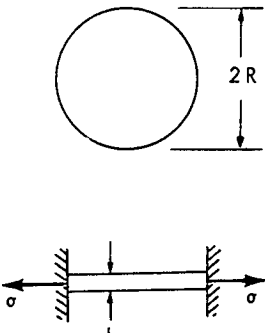
CIRCULAR PLATES	NUMBER OF NODAL CIRCLES, $m$	$C_{m,n}$ NUMBER OF NODAL DIAMETERS, $n$			
		0	1	2	3
Clamped at Circumference 	0	9.936	20.651	33.906	
	1	38.713			
	2	86.516			
Free Circumference 	0			5.110	11.902
	1	8.832	19.970	34.295	51.491
	2	37.487	58.255		
Clamped at Center 	0	3.649			
	1	20.349			
	2	59.053			
	3	116.490			
Simply Supported at Circumference 	0	0			
	1	5.0			

(Reference 3.53)

TABLE 3.34  
NATURAL FREQUENCIES OF CIRCULAR MEMBRANES

$$f_{m,n} = C_{m,n} \frac{1}{R} \sqrt{\frac{\sigma}{h}} \times K_m$$

- where  $f_{m,n}$  = Natural Frequency, Hz.  
 $C_{m,n}$  = Frequency Constant of m-n<sup>th</sup> Mode, Listed in Table Below  
 $R$  = Membrane Radius, Inches  
 $h$  = Membrane Thickness, Inches  
 $\sigma$  = Tension at Circumference, lb/in.  
 $K_m$  = Material Constant, See Table 3.39

CIRCULAR MEMBRANE	NUMBER OF NODAL CIRCLES, m	NUMBER OF NODAL DIAMETERS, n					
		0	1	2	3	4	5
	1	14.09	22.49	30.12	37.46	44.56	51.55
	2	32.41	41.22	49.44	57.30	64.94	72.22
	3	50.79	59.71	64.94	76.45	84.55	92.18
	4	69.28	78.09	86.90	95.12	103.34	111.56
	5	87.48	96.88	105.68	113.91	122.13	130.35
	6	106.27	115.08	123.89	132.69	140.91	149.13
	7	124.47	133.87	142.68	150.90	159.70	167.92
	8	143.26	152.07	160.88	169.68	178.49	186.71

(Reference 3.53)

TABLE 3.35  
NATURAL FREQUENCY OF UNIFORM RING VIBRATING IN ITS OWN PLANE

$$f_n = C_n \frac{r}{R^2} \times 10^4 \times K_m$$

where  $f_n = n^{\text{th}}$  Natural Frequency, Hz.


$C_n =$  Frequency Constant of  $n^{\text{th}}$  Mode, Listed in Table Below

$r =$  Radius of Gyration,  $\sqrt{I/A}$ , for Bending in its Own Plane, Inches

$R =$  Ring Mean Radius ( $\gg$  Thickness of Ring), Inches

$K_m =$  Material Constant, See Table 3.39

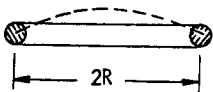
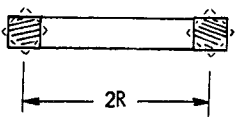
$C_n$

CIRCULAR RING	PURE RADIAL MODE	MODE NUMBER, n				
		2	3	4	5	6
Circular or Rectangular Cross Section 	$f_1 = \frac{c_L}{2\pi R}$	8.62	24.4	46.7	75.6	111.0

$c_L =$  Velocity of Longitudinal (Sound) Waves in Material. (Reference 3.1)

TABLE 3.36

NATURAL FREQUENCIES OF UNIFORM RING IN FLEXURAL (NORMAL TO ITS OWN PLANE) AND TORSIONAL VIBRATIONS

VIBRATION	CIRCULAR RING	NATURAL FREQUENCY, $f_n$ , Hz.
Flexural		$f_n = \frac{r}{2\pi} \frac{c_L}{R^2} \sqrt{\frac{n^2(n^2-1)^2}{n^2+1+\nu}}$ for $n > 1$ Rectangular or Circular Cross Section
Torsional		$f_n = \frac{1}{\pi} \frac{c_s}{R} \sqrt{(n-1)^2 + (1+\nu)}$ for $n \geq 1$ Circular Cross Section  $f_1 = \frac{1}{2\pi} \frac{c_L}{R} \sqrt{I_x/J}$ Rectangular Cross Section

Symbols:

$c_L =$  Velocity of Longitudinal (Sound) Waves in Material =  $\sqrt{E/\rho}$ , in/sec (See Table 3.39)

$c_s =$  Velocity of Shear Waves in Material =  $\sqrt{G/\rho}$ , in/sec

$\nu =$  Poisson's Ratio

$r =$  Radius of Gyration, Inches

$R =$  Ring Mean Radius ( $\gg$  Thickness of Ring), Inches

$J =$  Polar Moment of Inertia, in<sup>4</sup>

$I_x =$  Moment of Inertia With Respect to Radial Line, in<sup>4</sup>

$n =$  Mode Number, Integer

(Reference 3.1)

TABLE 3.37  
 NATURAL FREQUENCIES OF AN ANISOTROPIC (ORTHOTROPIC) PLATE IN FLEXURE  
 (Reference 3.66)

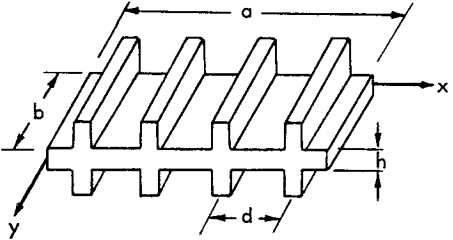
SYSTEM	NATURAL FREQUENCY, $f_{m,n}$
<p>Anisotropic Plates                      All Edges Simply Supported</p> <p>Case 1:</p>  <p>Case 2:</p> <p>Same as Case 1 except an additional set of rib stiffeners running parallel to x axis, e distance apart.</p>	$f_{m,n} = \frac{1}{2\pi} \left\{ \left[ D_x \left( \frac{m\pi}{a} \right)^4 + 2H \left( \frac{m\pi}{a} \right)^2 \left( \frac{n\pi}{b} \right)^2 + D_y \left( \frac{n\pi}{b} \right)^4 \right] \div \left[ \rho h + I_x \left( \frac{m\pi}{a} \right)^2 + I_y \left( \frac{n\pi}{b} \right)^2 \right] \right\}^{1/2} - \text{Hz}$ <p>where <math>\rho h</math> = mass density of the plate per unit area  <math>I_i</math> = mass moment of inertia of the plate per unit area about i axis; <math>i = x, y</math>.  <math>m</math> = Number of Half Waves along Side a  <math>n</math> = Number of Half Waves along Side b</p> <p><math>D_x, D_y</math> and <math>H</math> are defined below for a few typical special cases:</p> <p>Case 1:</p> $D_x = H = E h^3 / 12(1 - \nu^2)$ $D_y = D_x + (E_y^i I_x^i / d)$ <p>For symbols <math>E_x^i, E_y^i, I_x^i, I_y^i</math>, see Case 5.</p> <p>Case 2:</p> $D_x = \left[ E h^3 / 12(1 - \nu^2) \right] + \left[ E_x^i I_y^i / e \right]$ $D_y = \left[ E h^3 / 12(1 - \nu^2) \right] + \left[ E_y^i I_x^i / d \right]$ $H = E h^3 / 12(1 - \nu^2)$



TABLE 3.37 (CONTINUED)

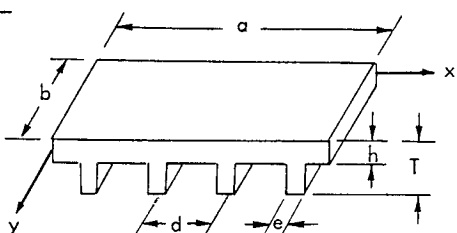
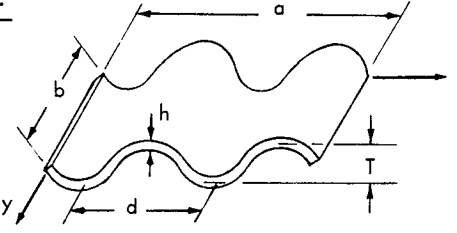
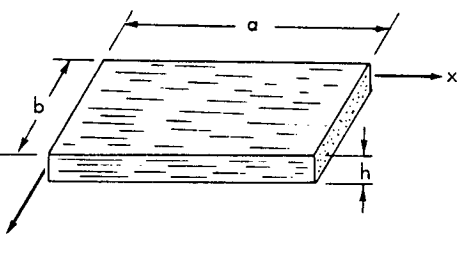
<p>Case 3:</p> 	<p>Case 3:</p> $D_x = Edh^3/12(d - e + eh^3/T^3)$ $D_y = EI_x/d = Ee(T - 0.5h)^3/3d$ $H = (Gh^3/6) + (k_r b/2d)$ <p><math>k_r</math> = torsional stiffness of one rib</p> <p>See Table 3.24</p>
<p>Case 4:</p> 	<p>Case 4:</p> $D_x = Edh^3/12(1 - \nu^2)S$ $D_y = EI_x = ET^2h \left( 0.19 + 0.156 \frac{T^2}{d^2} \right) / \left( 8 + 1.25 \frac{T^2}{d^2} \right)$ $H = SEh^3/12(1 + \nu)d$ $S = d \left[ 1 + (\pi T/4d)^2 \right]$
<p>Case 5:</p> <p>Uniform Plate of Anisotropic Material!</p> <p><math>E_x \neq E_y</math></p> 	<p>Case 5:</p> $D_x = E_x'' h^3/12$ $D_y = E_y'' h^3/12$ $H = \frac{E'' h^3}{12} + \frac{G h^3}{6}$ <p>and</p> $E_x'' = \left[ \frac{E}{(1 - \nu^2)} \right] \text{ along } x \text{ direction}$ $E_y'' = \left[ \frac{E}{(1 - \nu^2)} \right] \text{ along } y \text{ direction}$ $E'' = \left[ \frac{\nu E}{(1 - \nu^2)} \right] \text{ along either } x \text{ or } y \text{ direction}$ <p>where:</p> <p><math>E</math> = modulus of elasticity of base plate</p> <p><math>E_x', E_y'</math> = modulus of elasticity of rib stiffener, or modulus of elasticity of an anisotropic plate in x or y direction</p> <p><math>I_x', I_y'</math> = moment of inertia of a stiffener, taken with respect to the middle axis (x or y) of the cross section of base plate</p> <p><math>\nu</math> = Poisson's ratio of plate</p> <p><math>G</math> = modulus of rigidity of plate without rib stiffener.</p>

TABLE 3.38

NATURAL FREQUENCIES OF PLATE IN FLEXURE, WITH CLOSED CAVITY BEHIND

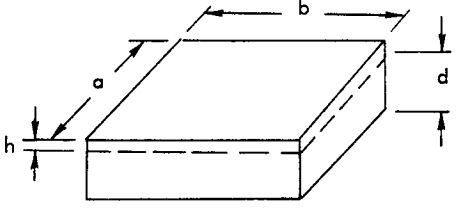
SYSTEM	NATURAL FREQUENCY, $f_n$ , Hz.
<p>Simply Supported or Clamped Rectangular Plate with Closed Cavity Behind.</p>  <p>Symbols:</p> <ul style="list-style-type: none"> <li><math>a, b</math> = Length of Plate, in.</li> <li><math>d</math> = Cavity Depth, in.</li> <li><math>A</math> = Area = <math>a \times b</math>, in<sup>2</sup></li> <li><math>V</math> = Volume = <math>a \times b \times d</math>, in<sup>3</sup></li> <li><math>\lambda</math> = Wave Length of Natural Frequency, in.</li> <li><math>h</math> = Thickness of Plate, in.</li> <li><math>\rho</math> = Mass Density of gas, lb-sec<sup>2</sup>/in</li> <li><math>c</math> = Velocity of Sound of Gas in Cavity, in./sec</li> </ul>	$f_n = f'_n \times K_c \text{ Hz.}$ <p>where <math>f'_n = n^{\text{th}}</math> Natural Frequency of the System, Hz.</p> $f'_n = n^{\text{th}}$ Natural Frequency of Plate Without Closed Cavity. $= C_n \frac{h}{a^2} \times 10^4 \times K_m, \text{ Hz. See Table 3.31}$ <p><math>K_c</math> = Cavity Correction Factor</p> $= \sqrt{1 + \frac{k_c}{k_p}}$ <p><math>k_c</math> = Cavity Stiffness</p> $= \frac{A^2 \rho c^2}{V}, \text{ lb/in}$ <p><math>k_p</math> = Plate Stiffness</p> $= (2\pi f'_n)^2 M, \text{ lb/in}$ <p><math>M</math> = Total Mass of Plate, lb-sec<sup>2</sup>/in</p> <p><b>LIMITATION:</b></p> <p>For the closed cavity to become effective on plate natural frequency, cavity depth, <math>d</math> must be less than <math>\lambda/16</math> for the simply supported plate and less than <math>\lambda/48</math> for the clamped plate</p>

TABLE 3.39

POISSON'S RATIO, YOUNG'S MODULUS, MODULUS OF RIGIDITY,  
SOUND VELOCITY, AND MATERIAL CORRECTION FACTOR FOR SOME  
ENGINEERING MATERIALS (References 3.1, 3.6, 3.7, 3.9, 3.33, 3.53, 3.74 and 3.75)

Material (at Temperature* in Bracket)	Poisson's Ratio $\nu$	Modulus of Elasticity, E (Young's Mod.) $\times 10^{-6}$ psi	Modulus of Rigidity, G $\times 10^{-6}$ psi	Longitudinal Sound Velocity in Bars $c_L = \sqrt{E/\rho}$ , Hz	Material Correction Factor $K_m = \sqrt{\frac{E}{\rho} \frac{\rho_s}{E_s}}$
Average Steel	0.30	30.0	12.0	16,820	1.000
Aluminum	0.33	10.3	3.8	16,600	0.985
Brass, Bronze	0.33-0.37	15.2	5.0	11,480	0.680
Cast Steel	0.28-0.31	29.0-30.5	11.5-12.5	16,500-17,000	0.98-1.01
Cast Steel (200)				15,710	0.933
Concrete	0.07-0.10	0.8-3.4	0.07-0.15	8,000-15,000	0.46-0.67
Copper	0.33-0.37	17.0	6.5	11,670	0.682
Copper (100-200)				9,690-10,080	0.575-0.598
Cork	$\approx 0$			1,640	0.0974
Glass	0.16-0.24	9.0-12.5	3.5-4.0	16,400-19,700	0.97-1.17
Granite		7.0		19,680	1.169
Iron, Cast	0.17-0.25	15.0-22.0	6.0-11.0	12,500-15,000	0.74-0.86
Iron, Wrought	0.28-0.30	25.0-30.0	11.0-12.5	16,000-17,600	0.95-1.02
Lead	0.40-0.45	2.4	6.8	4,000	0.238
Magnesium	0.35	6.2	2.3	16,200	0.961
Marble		7.2		12,500	0.743
Monel Metal	0.33	25.5	9.5	14,700	0.872
Nickel	0.31	30.5	11.5	16,000	0.955
Plywood	0.30-0.40	1.5-1.8		7,000-10,000	$\approx 0.42$
Silver	0.38	11.0	4.0	8,800	0.522
Silver (100)				8,660	0.515
Tin, Rolled	0.33	8.0	3.0	9,000	0.535
Titanite	0.32	16.0-17.0	6.0-6.4	16,300-16,700	0.97-0.99
Titanium (90-200)				15,300-16,300	0.91-0.97
Titanium (325-540)				13,100-14,600	0.78-0.87
Woods:					
Along Fibers	0.23-0.45	1.2-2.0		11,000-16,000	0.65-0.95
Across Fibers		0.1		4,000-4,500	0.24-0.27
Zinc, Rolled	0.25	15.2	6.1	12,600	0.749

\* Room Temperature is Implied Where No Entry Appears; Temperature in °C

Symbols: E = Young's Modulus for Material, lb/in<sup>2</sup>

$\rho$  = Mass Density for Material, lb-sec<sup>2</sup>/in.<sup>4</sup>

$E_s$  = Young's Modulus for Steel =  $30 \times 10^6$  lb/in<sup>2</sup>

$\rho_s$  = Mass Density for Steel =  $735 \times 10^{-6}$  lb-sec<sup>2</sup>/in.<sup>4</sup>

## REFERENCES

- 3.1 Harris, C. M. and Crede, C. F., "Shock and Vibration Handbook," McGraw-Hill Book Co., N. Y., 1961.
- 3.2 Thomson, W. T., "Vibration Theory and Applications," Prentice-Hall, N. J., 1965.
- 3.3 Robson, J. D., "An Introduction to Random Vibration," Elsevier Publishing Company, N. Y., 1964.
- 3.4 Den Hartog, J. P., "Mechanical Vibrations," McGraw-Hill Book Co., N. Y., 1956.
- 3.5 Timoshenko, S. and Young, D. H., "Vibration Problems in Engineering," D. Van Nostrand Co., Princeton, N. J., 1961.
- 3.6 Kinsler, L. E. and Frey, A. R., "Fundamentals of Acoustics," John Wiley and Sons, N. Y., 1962.
- 3.7 Beranek, L. L., "Acoustics," McGraw-Hill Book Co., N. Y., 1954.
- 3.8 Lindsay, R. B., "Mechanical Radiation," McGraw-Hill Book Co., N. Y., 1960.
- 3.9 Beranek, L. L., ed., "Noise Reduction," McGraw-Hill Book Co., N. Y., 1960.
- 3.10 Sokolnikoff, I. S. and Redheffer, R. M., "Mathematics of Physics and Modern Engineering," McGraw-Hill Book Co., N. Y., 1958.
- 3.11 Bracewell, R., "The Fourier Transform and Its Applications," McGraw-Hill Book Co., N. Y., 1965.
- 3.12 Gardner, M. F. and Barnes, J. L., "Transients in Linear Systems," Volume I, John Wiley and Sons, Inc., N. Y., 1942.
- 3.13 Thompson, W. T., "Laplace Transformation," Prentice-Hall, Inc., Englewood Cliffs, N. J., 1950.
- 3.14 Bateman Manuscript Project, "Tables of Integral Transforms," Volume I, McGraw-Hill Book Co., N. Y., 1954.
- 3.15 Sutherland, L. C., "The Fourier Spectra of Transient Excitations and Maximum Residual Responses of an Undamped Single Degree of Freedom System - A Generalized Approach," Wyle Laboratories Tech. Memorandum, TM 67-4, 1967.
- 3.16 Davenport, W. B. and Root, W. L., "An Introduction to the Theory of Random Signals and Noise," McGraw-Hill Book Co., N. Y., 1958.
- 3.17 Bendat, J. S., "Principles and Applications of Random Noise Theory," John Wiley and Sons, Inc., N. Y., 1958.
- 3.18 S. O. Rice, "Mathematical Analysis of Random Noise," Dover Publications, Inc., N. Y., 1954.
- 3.19 Eldred, K., Roberts, W. and White, R., "Structural Vibration in Space Vehicles," WADD Tech. Report 61-62, Dec. 1961.
- 3.20 Crandall, S. H., ed., "Random Vibration," The Technology Press of M.I.T., Cambridge, Mass., 1958.
- 3.21 Clarkson, B. L., "The Design of Structures to Resist Jet Noise Fatigue," J. Roy. Aero. Soc. 66, 1962 pp. 603-613.
- 3.22 Bozich, D. J., "Digital Analysis of Saturn Environment Test Response Data," The Shock and Vibration Bulletin, Feb. 1967.
- 3.23 Blackman, R. B. and Tukey, J. W., "The Measurement of Power Spectra," Bell System Tech. Journ., Vol. 37, 1958, pp. 185-282, 485-569.
- 3.24 Slepian, D., "Fluctuations in Random Noise Power," Bell System Tech. Journ., Vol. 37, 1958, pp. 163-184.
- 3.25 Burington, R. S. and May, C. M., "Handbook of Probability and Statistics with Tables," Handbook Publishers, Inc., Sandusky, Ohio.
- 3.26 Miller, K. S., "Engineering Mathematics," Holt, Winston and Rhinehart, Inc., N. Y., 1957.
- 3.27 Lyon, R. H., "On the Vibration Statistics of a Randomly Excited Hard-Spring Oscillator, II," J. Acoust. Soc. Am. 33, 1961, pp. 1395-1403.
- 3.28 Sutherland, L. C., "Cumulative Peak Distributions of Non-Stationary Random Vibration Environments," Paper Before Acoust. Soc. Am., Seattle, Washington, 1962.
- 3.29 Crandall, S. H. and Mark, W. D., "Random Vibration in Mechanical Systems," Academic Press, N. Y., 1963.
- 3.30 Archer, J. S., "Consistent Mass Matrix for Distributed Mass Systems," J. Structural Division, ASCE, Aug. 1963, pp. 161-178.
- 3.31 Livesley, R. K., "The Equivalence of Continuous and Discrete Mass Distributions in Certain Vibration Problems," Quart. J. Mech. Appl. Math. 8, 1955.
- 3.32 Leckie, F. A. and Lindberg, G. M., "The Effect of Lumped Parameters on Beam Frequencies," The Aero. Quart., Aug. 1963.
- 3.33 Norris, C. H., et al., "Structural Design for Dynamic Loads," McGraw-Hill Book Co., N. Y., 1959.

- 3.34 Bishop, R. E. D. and Johnson, D. C., "The Mechanics of Vibration," Cambridge University Press, N. Y., 1960.
- 3.35 Barton, M. V., ed., "Shock and Structural Response," Colloquium of Papers, Am. Soc. Mech. Engr., 1960.
- 3.36 Pestel, E. C. and Leckie, F. A., "Matrix Methods in Elastomechanics," McGraw-Hill Book Co., N. Y., 1963.
- 3.37 Ungar, E., "Fundamentals of Statistical Energy Analysis of Vibrating Systems," Air Force Flight Dynamics Laboratory Report TR-66-52, May 1966.
- 3.38 Smith, P. W., Jr. and Lyon, R. H., "Sound and Structural Vibration," NASA CR-160, Mar. 1965.
- 3.39 Skudrzyk, E. J., "Vibrations of a System with a Finite or an Infinite Number of Resonances," J. Acoust. Soc. Am. 30, Dec. 1958, pp. 1140-1152.
- 3.40 Powell, A., "On the Fatigue Failure of Structures Due to Vibrations Excited by Random Pressure Fields," J. Acoust. Soc. Am. 30, Dec. 1958, pp. 1130-1135.
- 3.41 Veletsos, A. S. and Newmark, N. M., "Design Procedures for Shock Isolation Systems of Underground Protective Structures. Vol. 3 - Response Spectra of Single-Degree-of-Freedom Elastic and Inelastic Systems," Air Force Weapons Laboratory RTD-TDR-63-3096, Vol. III, Jun. 1964.
- 3.42 Beranek, L. L., "Acoustic Measurements," John Wiley and Sons, Inc., N. Y., 1949, pp. 538-540.
- 3.43 Lewis, F. M., "Vibration During Acceleration Through a Critical Speed," Trans. ASME, 54, 1932, pp. APM-253.
- 3.44 Keast, D. M., "Measurements in Mechanical Dynamics," McGraw-Hill Book Co., N. Y., 1957.
- 3.45 White, R. W., "Predicted Vibration Responses of Apollo Structure and Effects of Pressure Correlation Lengths on Response," Wyle Laboratories Research Staff Report WR 67-4, Mar. 1967.
- 3.46 Cooley, J. W. and Tukey, J. W., "An Algorithm for the Machine Calculation of Complex Fourier Series," Math. of Comp., 19, 1965, p. 90.
- 3.47 Bendat, J. S. and Piersol, A. G., "Measurement and Analysis of Random Data," John Wiley and Sons, N. Y., 1966.
- 3.48 Abramowitz, M. and Stegun, I., ed., "Handbook of Mathematical Functions with Formulas, Graphs, and Mathematical Tables," National Bureau of Standards, Applied Mathematics Series 55, Jun. 1964.
- 3.49 Pipes, L. A., "Applied Mathematics for Engineers and Physicists," McGraw-Hill Book Co., N. Y., 1958.
- 3.50 Roark, R. J., "Formulas for Stress and Strain," McGraw-Hill Book Co., N. Y., 1954.
- 3.51 Timoshenko, S. and MacCullough, G. H., "Elements of Strength of Materials," D. Van Nostrand, Inc., N. Y., 1940.
- 3.52 Neubert, V. H. and Ezell, W. H., "Dynamic Behavior of a Foundation-Like Structure," from Plunkett, R., ed., "Mechanical Impedance Methods for Mechanical Vibrations," ASME Colloquium, N. Y., 1958.
- 3.53 Ungar, E. E., "Mechanical Vibrations," Chap. 6, from Rothbart, H. A., ed., "Mechanical Design and Systems Handbook," McGraw-Hill Book Co., 1964.
- 3.54 Sutherland, J. G. and Goodman, L. E., "Vibrations of Prismatic Bars Including Rotary Inertia and Shear Corrections," Dept. of Civil Engineering, University of Illinois, Apr. 15, 1951 (Also in Chapter 7, Reference 3.1).
- 3.55 Shinozuka, M., "Random Vibration of a Beam Column," Dept. of Civil Engin. and Engin. Mech., Columbia University, Tech. Report No. 10, Oct. 1964.
- 3.56 Amba-Rao, C., "Effect of End Conditions on the Lateral Frequencies of Uniform Straight Columns," J. Acoust. Soc. Am. 42, Oct. 1967, pp. 900-901.
- 3.57 White, R. W., "Vibration Characteristics of Beams and Plates Mounted on Elastic and Inertial Supports," Wyle Laboratories Research Staff Report WR 64-2, Aug. 1964.
- 3.58 Carmichael, T. E., "The Vibration of a Rectangular Plate with Edges Elastically Restrained Against Rotation," Quart. J. Mech. Appl. Math., Vol. XII, 1959, pp. 29-42.
- 3.59 Macduff, J. N. and Felgar, R. P., "Vibration Design Charts," Trans. ASME 79, 1957, pp. 1459-1475.
- 3.60 Macduff, J. N. and Felgar, R. P., "Vibration Design Charts," Machine Design, Feb. 1957.
- 3.61 Vet, M., "Natural Frequencies of Thin Rectangular Plates," Machine Design, Jun. 1965; "Thin-Plate Natural Frequencies," Machine Design, Jun. 1966.
- 3.62 Young, D., "Vibration of Rectangular Plates by the Ritz Method," J. Appl. Mech. 17, 1950, pp. 448-453.

- 3.63 Cremer, L., "Insulation of Air-Borne Sound by Rigid Partitions," Ch. 11.2, WADC Tech. Report 52-204, Vol. 1, Suppl. 1, 1955.
- 3.64 Zajac, E. E., "Propagation of Elastic Waves," Chap. 64, from Flugge, W., ed., "Handbook of Engineering Mechanics," McGraw-Hill Book Co., N. Y., 1962.
- 3.65 Cox, H. L. and Benfield, W. A., "Vibration of Uniform Square Plates Bounded by Flexible Beams," J. Acoust. Soc. Am. 31, Jul. 1959, pp. 963-966.
- 3.66 Timoshenko, S. P. and Woinowsky-Krieger, S., "Theory of Plates and Shells," McGraw-Hill Book Co., N. Y., 1959.
- 3.67 Wyle Laboratories Research Staff, "Vibration of a Beam on Moving Supports," Progress Report, under Contract NAS8-11217, Feb. 1965.
- 3.68 Hunt, F. V., "Velocity-Strain Ratio for Vibrating Elastic Bodies," J. Acoust. Soc. Am. 32, Sept. 1960, pp. 1123-1128.
- 3.69 Ruzicka, J. E., ed., "Structural Damping," Collection of Papers Before ASME Symposium, Dec. 1959.
- 3.70 Soroka, W., "Note on Relation of Structural and Viscous Damping," J. Aeron. Sci. 16, 1959, p. 409.
- 3.71 Cox, H. L., "Vibration of Axially Loaded Beams Carrying Distributed Masses," J. Acoust. Soc. Am. 30, 1958, pp. 568-571.
- 3.72 Cox, H. L. and Boxer, J., "Vibration of Rectangular Plate Points Supported at the Corners," Aeron. Quart., Feb. 1960, pp. 41-50.
- 3.73 Perry, D. J., "Aircraft Structures," McGraw-Hill Book Co., N. Y., 1950.
- 3.74 Koelle, H. H., ed., "Handbook of Astronautical Engineering," McGraw-Hill Book Co., N. Y., 1961.
- 3.75 Gray, D. E., ed., "American Institute of Physics Handbook," McGraw-Hill Book Co., N. Y., 1963, 2nd ed.
- 3.76 Warburton, G. B., "The Vibration of Rectangular Plates," Proc. Inst. Mech. Engrs. (London) 168, 1954, pp. 371-384.

4.2.3 ACOUSTICAL QUANTITIES

4.2.3.1 Sound Pressure

The sound pressure measured at a point is expressed as a sound pressure level (SPL) in decibels through

$$SPL = 20 \log_{10} (p/p_{ref}) \quad (4.1)$$

where

- $p_{ref}$  = reference pressure, dyne/cm<sup>2</sup>
- $p$  = measured effective pressure of the sound wave, dyne/cm<sup>2</sup>

The effective sound pressure  $p$  is the root-mean-square value of the instantaneous sound pressure, averaged over an integrating time long enough to make its value insensitive to small changes in the length of the averaging time. Time averaging of random signals is discussed in Chapter 3. The reference value  $p_{ref} = 0.0002$  dynes/cm<sup>2</sup> (microbars) is customary and is used throughout this manual. However, other reference values are sometimes used and the reference value should always be stated. Typical values of sound pressure level for various environments and for stated distances from single sources in a free field are given in Figure 4.5, from Reference 4.3. Chart 12.3 (Chapter 12) provides a graphical conversion between sound pressure and SPL.

4.2.3.2 Sound Intensity

The sound intensity is the acoustic power flow per unit area. It is an intermediate quantity that may be obtained from sound pressure measurements wherever the pressure and particle velocity are in phase (i.e., for a plane wave) and integrated over incremental areas surrounding a source to obtain the sound power. For a plane wave, the time averaged value of  $I = \overline{p\dot{u}}$  becomes

$$I = \frac{p^2}{\rho_a c}$$

Intensity is expressed as an intensity level through

$$IL = 10 \log_{10} \left( \frac{I}{I_{ref}} \right) \quad (4.2)$$

where

- IL = Intensity level, dB
- $I$  = Intensity, watts/m<sup>2</sup>
- $I_{ref}$  = Reference intensity, watts/m<sup>2</sup>

The reference value of  $I = 10^{-12}$  watts/m<sup>2</sup> is standard; Chart 12.2 provides a graphical conversion from intensity to IL.

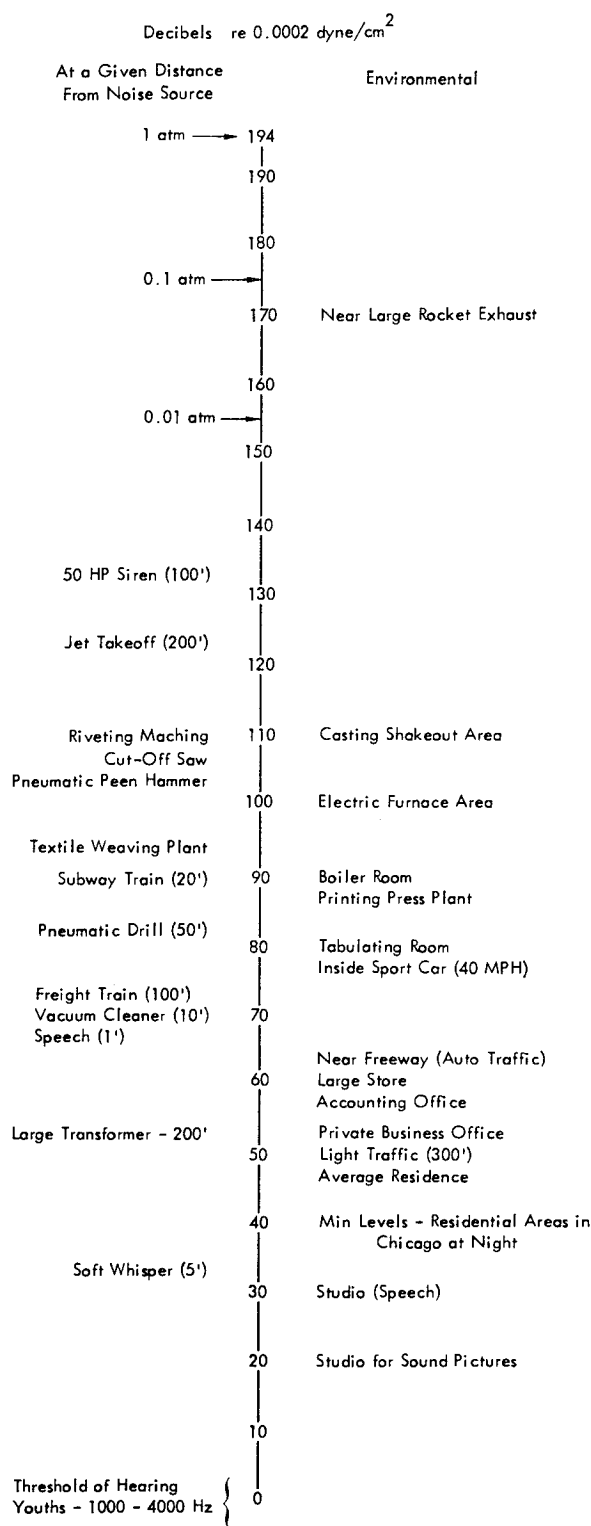


FIGURE 4.5 Typical Sound Pressure Levels (from Reference 4.3)

4.2.3.3 Sound Power

The sound power, or total sound energy radiated by a source per unit time, can be obtained from sound pressure level measurements over an imaginary surface surrounding the source as it radiates into a free field, provided the measurements are taken in the far field (where the acoustic wave front is essentially plane). The sound power can also be obtained from sound pressure measurements in the diffuse field of a source operating in a reverberant room. The sound power level in decibels is obtained from

$$PWL = 10 \log_{10} \left( \frac{W}{W_{ref}} \right) \quad (4.3)$$

where

PWL = Sound power level, dB

W = Acoustic power, watts

W<sub>ref</sub> = Reference power, 10<sup>-13</sup> watts

The reference value of 10<sup>-13</sup> watts is used throughout this manual, but a value of 10<sup>-12</sup> watts is sometimes found in the literature; the value being used should always be stated. Figure 4.6 (from Reference 4.3) shows typical power and power levels for acoustic sources. It can be seen, for example, that the Saturn rocket engine generates the same sound power as about 40 million large chipping hammers. Chart 12.1 (Chapter 12) provides a graphical conversion between sound power ratios and corresponding decibels.

4.2.3.4 Directional Characteristics

For a simple source in free space (which radiates sound omnidirectionally, see Section 4.4), the sound power level and the sound pressure level at a point in decibels, with reference values for power and pressure as given above, are related by:

$$SPL = PWL - 20 \log_{10} r + 10.6$$

where r is the distance from source to measurement point in feet. This relation accounts only for spherical spreading and not for any atmospheric effects. A 6 dB decrease in SPL for every doubling of distance results from the second term. Most sources are directional; that is, lines of equal sound pressure level in any plane are not concentric circles about the source, e.g., Figure 4.7. Data for the sound fields about directional sources are often given in terms of directivity factor, Q, or directivity index, DI, variation with angle. The directivity factor is the ratio of the intensity (at a designated angular location) at a stated distance r to the intensity that would occur at the same point for a simple source radiating (omnidirectionally) at the same total acoustic power. The directivity index is

$$DI = 10 \log_{10} Q$$

Then the sound pressure level at a point is related to the sound power level of a directional source by:

$$SPL = PWL + DI - 10 \log_{10} r + 10.6$$

with units the same as those given above. Other correction factors, as for nonstandard atmospheric conditions and attenuation by the atmosphere, are given in Chapter 7.

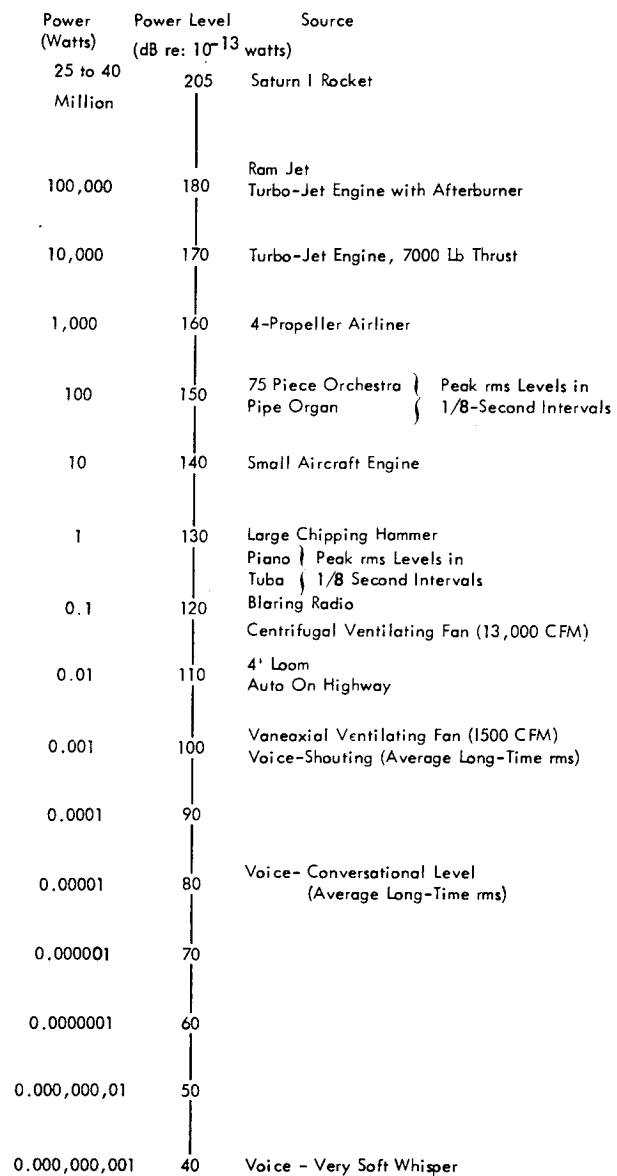


FIGURE 4.6 Typical Acoustic Power and Power Level Magnitudes (from Reference 4.3)



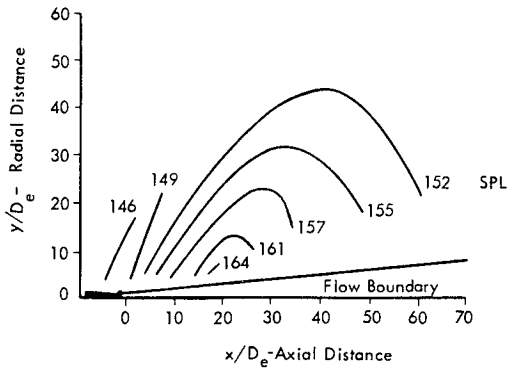


FIGURE 4.7 Typical Contours of Equal Overall SPL in dB re .0002 Microbar for a Rocket with Distance Expressed in Terms of Nozzle Exit Diameter ( $D_e$ )

4.2.3.5 Spectral Characteristics

The analysis of a signal into its distribution across the frequency spectrum can be performed in very fine or broad frequency bands, according to the characteristics of the source and the use to which the data will be put. The overall level (for power or pressure) is a single figure which provides no information on the spectral content. The first level of information on spectral content is obtained from analyzing the signal in octave bands. Octave bands have constant percentage bandwidths with the upper frequency limit of each band twice the value of its lower frequency limit. The audible range of frequencies is covered in ten octaves.

The next level of detail is based on one-third octave bands, where one-third octave is the interval between two frequencies with the ratio cube root of two. The current standard for the spectrum allocation into octave and third-octave bands is the preferred series given in Reference 4.4; the table of center frequencies is given in Table 12.12, page 12-12. A series of octave bands widely used in the past ranged 75 - 150 Hz, 150 - 300 Hz, etc., and much published data still exists in this form. A method for converting octave-band levels given in this older series to levels in the preferred series is given in Appendix A of Reference 4.5.

The most detailed spectral distribution information is the spectrum level. Pressure spectrum level is the effective sound pressure level of the sound energy contained in a bandwidth of 1 Hz centered at a specified frequency; power spectrum level is the power level in a band 1 Hz wide centered at a specified frequency. Chart 12.4, page 12-10, gives a graphic conversion from octave or third-octave band levels to spectrum levels. Rarely is such detail as from 1 Hz bandwidth analysis required. Between the two extremes of octave band levels and spectrum levels are numerous nonstandardized analysis bands, of two types: (1) constant percentage bandwidths and (2) constant bandwidths of equal frequency increments. A 6 Hz bandwidth filter usually gives more than adequate definition unless the data extends to unusually low frequencies (< 50 Hz).

The choice of level of detail for analysis of a signal into frequency bands must be based on the characteristics of the source. The two extremes of source spectral characteristics are white noise (equal energy per unit frequency bandwidth over a specified total frequency band), Figure 4.8(a), and pure tones (single-frequency sine waves), Figure 4.8 (b). In interpreting acoustical data, it is necessary to bear in mind that, depending on the source, the various degrees of resolution can yield very different results for the same signal input. As an example, Figure 4.9 compares a real spectrum (for a continuous random signal with a superposed sinusoidal signal at 400 Hz) with the apparent spectra obtained for various degrees of resolution.

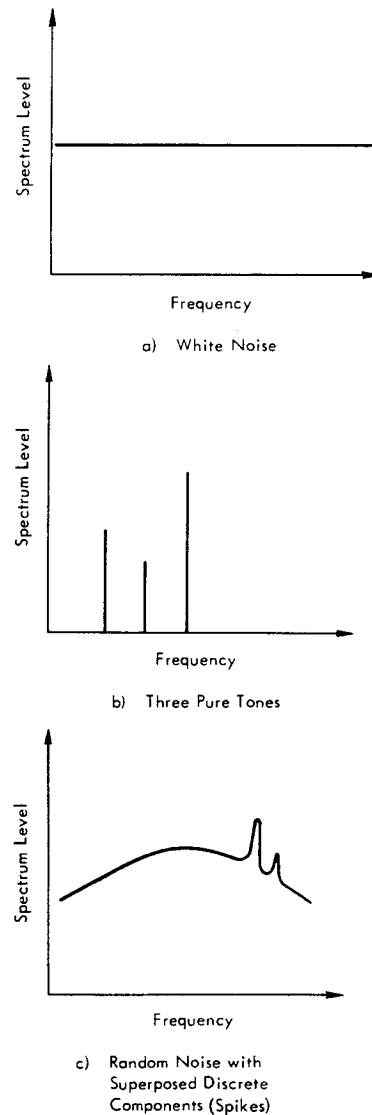


FIGURE 4.8 Spectral Content of Several Signals

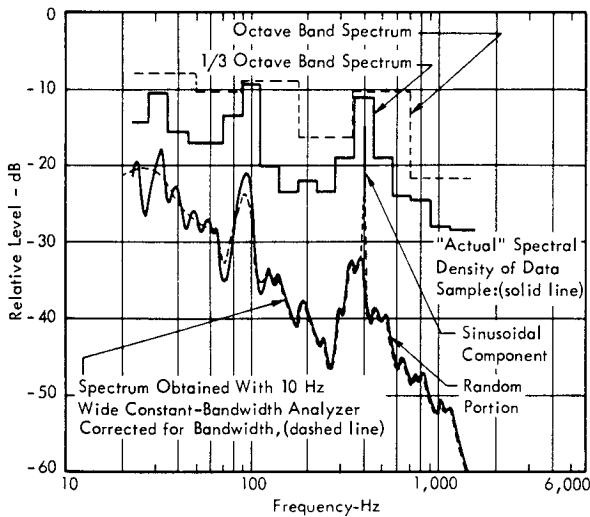


FIGURE 4.9 Comparison of the Outputs of Several Levels of Spectral Analysis for the Same Input Signal (From Reference 4.6)

### 4.3 THE ACOUSTIC WAVE EQUATION

The following section, by presenting the assumptions and simplifications underlying the acoustic wave equation, provides a foundation for the subsequent sections on source radiation and transmission.

A one-dimensional derivation of the wave equation for acoustic waves in a gas is developed here to show the basic assumptions and approximations involved in conventional linear acoustics theory. Some convenient properties of the wave equation and useful physical concepts are also presented.

#### 4.3.1 DERIVATION

First, viewing the propagation of an acoustic wave through a gas on the molecular scale, imagine that at some instant the molecules of a gas are distributed as shown in Figure 4.10(a). The lines, a b c d, form a conceptual "control volume" containing a particular number of molecules. The undisturbed gas has no mean velocity, as the random molecular motion has no preferred direction. Introduce a disturbance propagating into the control volume from the left propagating at a velocity  $\bar{c}$  and traversing the box in a time  $\delta t$ . The gas is more dense ahead of the transitional layer and, as the wave propagates, the box must become smaller if it is to contain the same number of molecules, the side cd moving to c'd' as the wave passes to the other side of the box. Since no movement of molecules is allowed across side c'd', this side must move with the mean velocity  $u$  while the volume has decreased in the ratio  $(\bar{c} - u)/\bar{c}$ , and the density has increased inversely.

Viewing the motion on a larger scale, consider a one-dimensional case of fluid flowing through a control volume, Figure 4.11, defined by two fixed planes of unit area normal to the single coordinate direction  $x$ , located at positions  $x_a$  and  $x_b$ . The fluid has density  $\rho$  and velocity  $u$ , both functions of position  $x$  and time  $t$ . The mass flow across the control volume must be conserved; that is:

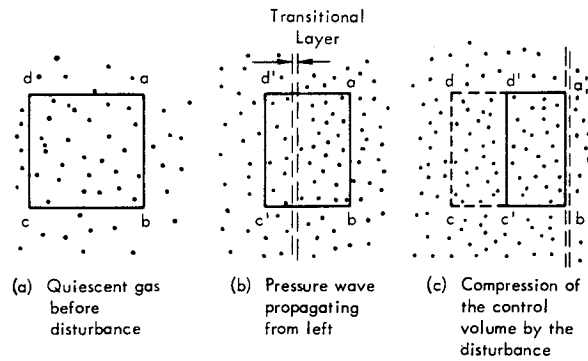


FIGURE 4.10 Typical Instantaneous Position of Gas Molecules

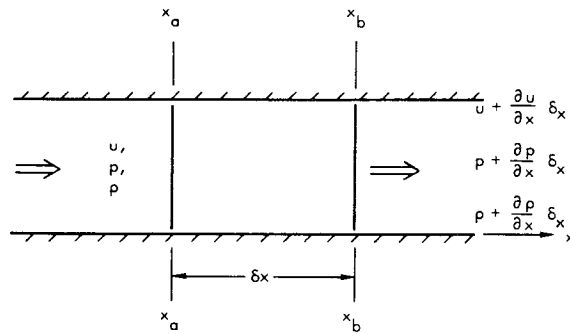


FIGURE 4.11 One-Dimensional Control Volume For Wave Equation Derivation

$$(\text{mass influx}) - (\text{mass efflux}) + \overset{0}{\text{internal sources}} = \text{net internal change of mass}$$

A small enough element has been taken so that the rates of change with distance can be considered linear and the statement of mass conservation becomes

$$\rho u - \left( \rho + \frac{\partial \rho}{\partial x} \delta x \right) \left( u + \frac{\partial u}{\partial x} \delta x \right) = \frac{\partial}{\partial t} (\bar{\rho} \delta x)$$

where  $\bar{\rho}$  is the mean value of  $\rho$  in the element. Let  $\delta x \rightarrow 0$  and take  $\bar{\rho} \cong \rho$ :

$$\rho u - \left( \rho + \frac{\partial \rho}{\partial x} dx \right) \left( u + \frac{\partial u}{\partial x} dx \right) = \frac{\partial}{\partial t} (\rho dx)$$

Expanding, dividing through by  $dx$ , and neglecting second order terms leaves:

$$u \frac{\partial \rho}{\partial x} + \rho \frac{\partial u}{\partial x} + \frac{\partial \rho}{\partial t} = 0$$

$$\frac{\partial \rho}{\partial t} + \frac{\partial(\rho u)}{\partial x} = 0 ; \text{ Continuity Equation} \quad (4.4)$$

Momentum is also conserved across the fluid element; that is, the net force or differential pressure acting in the  $+x$  direction must equal the rate of change of momentum of the intervening fluid. Therefore,

$$p - \left( p + \frac{\partial p}{\partial x} \delta x \right) = \rho u \left( u + \frac{\partial u}{\partial x} \delta x - u \right) + \frac{\partial}{\partial t} (\rho u \delta x)$$

letting  $\delta x \rightarrow 0$ , dividing by  $\delta x$ , and collecting terms gives

$$\frac{\partial(\rho u)}{\partial t} + \frac{\partial(\rho u^2)}{\partial x} = - \frac{\partial p}{\partial x} \quad ; \quad \text{Momentum Equation (4.5)}$$

The condensation  $\tilde{\rho}$ , or fractional change in density is defined in terms of the instantaneous density  $\rho$  and the ambient mean density  $\rho_a$ :

$$\tilde{\rho} = (\rho - \rho_a) / \rho_a$$

Make the acoustical approximations:

- (1) The fluctuations are of small amplitude,  $\tilde{\rho} \ll 1$ .
- (2) The mean velocity of the medium is zero (more specifically, that

$$u \frac{\partial u}{\partial x} \ll \frac{\partial u}{\partial t}$$

Then introduction into the continuity and momentum equations of (a)  $\rho = \rho_a(1 + \tilde{\rho})$  and (b) the acoustical approximations will give for the continuity equation

$$\frac{\partial \tilde{\rho}}{\partial t} + \frac{\partial u}{\partial x} = 0 \quad (4.6)$$

and for the momentum equation

$$\frac{\partial u}{\partial t} + u \frac{\partial u}{\partial x} = - \frac{1}{\rho_a(1 + \tilde{\rho})} \frac{\partial p}{\partial x}$$

Because of the smallness of  $\tilde{\rho}$ , the binomial theorem can be applied to give

$$\frac{1}{1 + \tilde{\rho}} \cong 1 - \tilde{\rho}$$

Again neglecting second order terms and taking  $\rho \cong \rho_a$ , the momentum equation becomes:

$$\frac{\partial u}{\partial t} + \frac{1}{\rho} \frac{\partial p}{\partial x} = 0 \quad (4.7)$$

Equations 4.6 and 4.7 are linear differential equations in three variables ( $p$ ,  $u$ ,  $\rho$ ); a third relation is needed for solution.

Take the pressure as a function of only one of the two other state variables (density and temperature), say  $p = p(\rho)$ . Since acoustic wave propagation is an isentropic process, the specific relation is

$$p \propto \rho^\gamma$$

Thus  $\frac{\partial p}{\partial \rho} \rightarrow \frac{dp}{d\rho}$ . Evaluated at ambient conditions, this gives the speed of sound in the medium:

$$\left. \frac{dp}{d\rho} \right|_a = c^2 \quad (4.8)$$

Then the momentum equation becomes

$$\frac{\partial u}{\partial t} + c^2 \frac{\partial \tilde{\rho}}{\partial x} = 0 \quad (4.9)$$

By cross differentiating the linearized continuity and momentum equations (4.6 and 4.9) and adding the two resulting equations, one obtains the wave equation which can be expressed in terms of acoustic pressure as

$$\frac{\partial^2 p}{\partial x^2} - \frac{1}{c^2} \frac{\partial^2 p}{\partial t^2} = 0 \quad ; \quad \text{Wave Equation (4.10)}$$

The wave equation can also be expressed in terms of the velocity perturbation, the compression, and the particle displacement, as well as in terms of the pressure.

#### 4.3.2 SOLUTIONS

The solution for the wave equation is, in terms of a general variable  $\phi$ :

$$\phi(t, x) = \Phi_+(t - x/c) + \Phi_-(t + x/c) \quad (4.11)$$

The functions  $\Phi_+$  and  $\Phi_-$  are quite arbitrary; that is, any functions of the variables  $(t - x/c)$  and  $(t + x/c)$  will satisfy the wave equation as long as they do not violate the assumptions on which it is based. The first term  $\Phi_+$  represents a wave (of arbitrary shape) propagating in the  $+x$  direction at velocity  $c$  and the  $\Phi_-$  term represents a wave motion traveling in the  $-x$  direction.

The wave equation is linear, so solutions can be constructed by superposition, and Fourier synthesis can be applied to construct any desired wave shape from harmonic components: sines and cosines or exponentials. For this reason, and because of the occurrence of harmonic functions in acoustics, the harmonic forms of wave equation solution are of the most practical interest. As an example, take the particle displacement  $d$ :

$$d = f_1(t - x/c) + f_2(t + x/c)$$

In a harmonic wave, the frequency  $f$  (or inverse of the period  $T$ ) is related to the angular frequency  $\omega$  by  $\omega = 2\pi f$  and to the wavelength  $\lambda$  by  $\lambda = c/f$ . The propagation parameters are conveniently taken as  $\omega(t - x/c)$  and  $\omega(t + x/c)$ . Then the solution in complex form is

$$\underline{d} = \underline{A} e^{j\omega(t - x/c)} + \underline{B} e^{j\omega(t + x/c)} \quad (4.12)$$

where  $\underline{A}$  is the complex displacement amplitude of a plane wave of frequency  $\omega$  traveling in the  $+x$  direction at velocity  $c$ , and the  $\underline{B}$  is the complex amplitude of a similar wave traveling in the  $-x$  direction. In complex form the other important acoustic variables are:

$$\underline{p} = -\rho_a c^2 \frac{\partial \underline{d}}{\partial x} = j \rho_a c \omega (\underline{d}_+ - \underline{d}_-) \quad (4.13)$$

$$\underline{p} = -\frac{\partial \underline{d}}{\partial x} = j \frac{\omega}{c} (\underline{d}_+ - \underline{d}_-) \quad (4.14)$$

$$\underline{u} = \frac{\partial \underline{d}}{\partial t} = j \omega (\underline{d}_+ + \underline{d}_-) \quad (4.15)$$

where  $d_+$  is the first term in 4.12 and  $d_-$  is the second. The instantaneous values for these acoustic variables are given by the real parts of Equations 4.12 through 4.15, obtained through applying the relationship

$$e^{j\theta} = \cos \theta + j \sin \theta$$

For example, in the special case where  $A$  and  $B$  are real constants  $A$  and  $B$ , the instantaneous values are

$$\begin{aligned} d &= A \cos \left( \omega t - \frac{\omega}{c} x \right) + B \cos \left( \omega t + \frac{\omega}{c} x \right) \\ p &= -\rho_a c \omega \left[ A \sin \left( \omega t - \frac{\omega}{c} x \right) - B \sin \left( \omega t + \frac{\omega}{c} x \right) \right] \\ \tilde{p} &= -\frac{\omega}{c} \left[ A \sin \left( \omega t - \frac{\omega}{c} x \right) - B \sin \left( \omega t + \frac{\omega}{c} x \right) \right] \\ u &= -\omega \left[ A \sin \left( \omega t - \frac{\omega}{c} x \right) + B \sin \left( \omega t + \frac{\omega}{c} x \right) \right] \end{aligned}$$

Some useful interrelations among the acoustic variables should be noted:

$$\begin{aligned} p &= \rho_a c^2 \tilde{p} \\ p &= \rho_a c u \end{aligned} \quad (4.16)$$

for waves running in the  $+x$  direction; and

$$p = -\rho_a c u$$

for waves running in the  $-x$  direction. The relations between pressure and velocity are applicable to plane waves only.

### 4.3.3 SOME PHYSICAL CONCEPTS

The energy flow crossing unit area normal to the propagation direction can be found by considering the work done by the fluid. The work is done at a rate  $(pu)$  on a surface of unit area normal to the propagation direction. The energy of waves propagating in the  $+x$  direction crosses unit area at a time-averaged rate given by

$$I = \overline{pu} \quad (4.17)$$

where  $I$  is the acoustic intensity, introduced in Section 4.2. For a plane wave signifying a time averaged mean square value by a  $\overline{\quad}$ , this is equivalent to

$$I = \frac{\overline{p^2}}{\rho_a c} = \rho_a c \overline{u^2} \quad (4.18)$$

For waves propagating in the  $-x$  direction, a negative sign occurs, showing that acoustic power is always propagated with the wave, whether the wave is compressive or expansive. The total acoustic power of a source can be determined by integrating, over a closed surface about the source, the values of intensity obtained from pressure microphone measurements in the far field.

For a wave propagating in one direction, in time  $t$  the energy passing unit area will be  $It$ , occupying a distance  $ct$ . On the average, within each unit volume of the fluid medium there is an amount of acoustic energy given by

$$\epsilon = I/c = \frac{\overline{p^2}}{\rho_a c^2} = \rho_a \overline{u^2} \quad (4.19)$$

and this quantity is called the energy density of the sound wave. This concept is used, for example, to define a diffuse sound field; a diffuse field exists when the energy density is uniform in the entire region considered and when all directions of energy flux (in all parts of the region) are equally probable.

The product  $\rho_a c$  appears repeatedly in the above relations; it is called the characteristic impedance of the medium. For a plane wave it is equal to the specific acoustic impedance, which is defined as the ratio of driving pressure  $p$  to resulting particle velocity  $u$ , analogous to voltage and current in an electrical circuit. For plane waves, the specific acoustic impedance is purely resistive, since the particle velocity vector is always along the propagation direction. For air at standard temperature and pressure the value of  $\rho_a c$  is 415 mks rayls ( $\text{kg}/\text{m}^2 \text{ sec}$ ). For other than plane waves, the specific acoustic impedance includes a reactive part (as the particle motion can be elliptic or circular) and becomes a property of the source as well as the medium. This subject is expanded in the following sections on sources and on analogies.

## 4.4 ELEMENTARY SOUND SOURCES

An acoustic source is a region of space, in contact with a compressible fluid medium such as air, where new acoustic energy is being generated. Any vibrating object will radiate sound into the air, the amount being dependent on the vibration amplitude of each part of the vibrating object, the area of each part and the time pattern of the vibrations. The acoustic field of any vibrating object can be synthesized from an array of simple sources (with the proper amplitudes, relative time patterns and spatial distribution) to represent the vibrating object. Therefore, it is useful to review first the acoustic field of a simple source and methods of constructing more complex sources from combinations of the simple source (References 4.7 through 4.10). This is followed by a discussion of the sound radiated by cylindrical and piston sources.

### 4.4.1 THE SIMPLE SOURCE OR MONOPOLE

Consider a sphere that vibrates uniformly over its entire surface, producing particle motions aligned with its radial direction, of equal phase and amplitude over the entire spherical surface at any given time. This source can be visualized as a round balloon with air being periodically pumped in and out so that the surface contracts and expands uniformly. To be treated as a simple source (or monopole) it must have a radius that is small compared to the shortest wavelength of interest.

With a three-dimensional control volume and a procedure similar to that in Section 4.3, one can derive a wave equation in three dimensions:

$$\nabla^2 \phi - \frac{1}{c^2} \frac{\partial^2 \phi}{\partial t^2} = 0 \quad (4.20)$$

where  $\nabla^2$  is the Laplacian operator and  $\phi$  is any physical quantity which satisfies the wave equation; e.g., the particle displacement  $d$ , particle velocity  $u$ , acoustic pressure  $p$ , compression  $\tilde{p}$  and velocity potential  $\phi$ . The velocity potential is defined by

$$u_i = - \frac{\partial \phi}{\partial x_i}$$

(where  $i$  is a direction index) and is related to the acoustic pressure by

$$p = \rho_a \frac{\partial \phi}{\partial t}$$

The Laplacian of the pressure  $\nabla^2 p$  at a point is proportional to the difference between the average pressure near the point and the pressure just at the point. The wave equation states that, for a concentration of pressure at a point, the pressure will tend to decrease. In spherical coordinates  $(r, \theta, \psi)$  the Laplacian operator is (explicitly):

$$\nabla^2 = \frac{1}{r^2} \frac{\partial}{\partial r} \left( r^2 \frac{\partial}{\partial r} \right) + \frac{1}{r^2 \sin \theta} \frac{\partial}{\partial \theta} \left( \sin \theta \frac{\partial}{\partial \theta} \right) + \frac{1}{r^2 \sin^2 \theta} \frac{\partial}{\partial \psi^2}$$

The monopole represents the spherically symmetric case (i.e., the acoustic parameters such as  $p(r,t)$  are independent of the angular coordinates  $\theta, \psi$ ) and the wave equation, expressed in terms of the compression  $\tilde{p}$ , reduces to:

$$\frac{\partial^2 (r \tilde{p})}{\partial r^2} - \frac{1}{c^2} \frac{\partial^2 (r \tilde{p})}{\partial t^2} = 0 \quad (4.21)$$

Since the one-dimensional wave equation had a solution of the form

$$\tilde{p} = f_1(t - x/c) + f_2(t + x/c)$$

then solutions of the wave equation for spherical symmetry will have the form

$$(r \tilde{p}) = f_1(t - r/c) + f_2(t + r/c) \quad (4.22)$$

The first term represents a spherical wave diverging from the origin at velocity  $c$ ; and the second, a wave converging on the origin. Converging waves have little physical significance; and the solution becomes invalid very near the origin, as the large amplitude buildup violates the small amplitude assumption in the derivation of the acoustic wave equation. Only the first term is retained.

Considering diverging waves only, a harmonic solution of the wave equation, in terms of the velocity potential  $\phi$ , for example, is

$$\phi = \frac{S}{4\pi r} e^{j(\omega t - \frac{\omega}{c} r)} \quad (4.23)$$

where  $S$  is a constant representing the monopole strength, or amplitude of the volume source in the expanding and contracting balloon representation of the monopole source.

#### 4.4.1.1 The Field of a Monopole

The field properties of a monopole radiating into free space are next reviewed. The field properties are all functions of radial distance only, and not of angle; that is, the radiation is nondirectional, and surfaces of equal phase and amplitude are spheres centered on the source.

The radial component of the particle velocity is obtained from the definition of the velocity potential and Equation 4.23

$$u_r = - \frac{\partial \phi}{\partial r} = \frac{S}{4\pi r^2} \cdot e^{j(\omega t - \frac{\omega}{c} r)} \left( 1 + j \frac{\omega}{c} r \right) \quad (4.24)$$

The pressure fluctuation is

$$p = \rho_a \frac{\partial \phi}{\partial t} = \frac{S}{4\pi r} \cdot j\omega \rho_a e^{j(\omega t - \frac{\omega}{c} r)} \quad (4.25)$$

The specific acoustic impedance (ratio of the pressure fluctuation to the particle velocity component in the direction of radiation) is

$$z = \frac{p}{u_r} = \rho_a c \left( \frac{j \frac{\omega}{c} r}{1 + j \frac{\omega}{c} r} \right) \quad (4.26)$$

In the case of a plane wave, the specific acoustic impedance was simply  $z = \rho_a c$ , a property of the medium. For a spherical wave, it depends also on the source frequency  $\omega$  and the distance  $r$  from the source; these two can be combined into a radial distance in terms of wavelengths, for any given medium.

The field can be examined in two parts; in order of increasing distance from the source, they are

- The near field
- The far field

The hydrodynamic region is that part of the near field nearest the source where only a small portion of the fluctuations which exist are radiated away. Very near the source, e.g., where  $\frac{\omega}{c} r \ll 1$ , the radial component of particle velocity reduces to:

$$u_r \rightarrow \frac{S}{4\pi r^2} e^{j\omega t}$$

For the acoustic pressure, for  $\frac{\omega}{c} r \ll 1$ :

$$p \rightarrow \frac{S}{4\pi r} j\omega \rho_a e^{j\omega t}$$

and for the specific acoustic impedance:

$$z \rightarrow j\omega \rho_a r$$

In the hydrodynamic region, therefore, the acoustic pressure decreases inversely with distance from the source, and the particle velocity inversely with the square of the distance. The flow is just like that of a source in incompressible flow, and the impedance is reduced to its purely reactive part. Physically, this means that the shell of fluid surrounding the source exhibits inertia as it expands or contracts, but does not dissipate the kinetic energy associated with the motion. Analogous to the case of a purely inductive electrical circuit, the energy is alternately supplied and absorbed by the source.

To obtain the far field limit, let  $\frac{\omega}{c} r \gg 1$ ; then the acoustic parameters approach the values:

$$u_r \rightarrow \frac{S}{4\pi r} \cdot j \frac{\omega}{c} \cdot e^{j(\omega t - \frac{\omega}{c} r)}$$

$$p \rightarrow \frac{S}{4\pi r} \cdot j\omega \rho_a e^{j(\omega t - \frac{\omega}{c} r)}$$

$$z \rightarrow \rho_a c$$

Both the particle velocity and the pressure fall off inversely with the radius; and they are in phase, so that the impedance is purely resistive. The impedance is a function of the medium only, and is the same as for plane waves. In the far field, the spherical waves have diverged to such a large radius of curvature that they are effectively plane waves.

In the intermediate region of the near field, the quantity  $(\frac{\omega}{c} r)$  is neither very large nor very small, all the terms in Equations 4.24 through 4.26 must be retained, and the impedance contains both reactive and resistive parts. Therefore, the pressure and the radial particle velocity are not in phase, and a pressure microphone cannot give a measure of the intensity. Analogous to alternating current, a knowledge of the power flow requires the phase angle between voltage ( $p$ ) and current ( $u$ ). Figure 4.12 shows the behavior of a spherical wave with distance from the source; the abscissa  $(\frac{\omega}{c} r)$  is equivalent to  $2\pi$  times the distance in wavelengths. In practice, the far field begins where a 6 dB drop in sound pressure level occurs for each doubling of distance from the source.

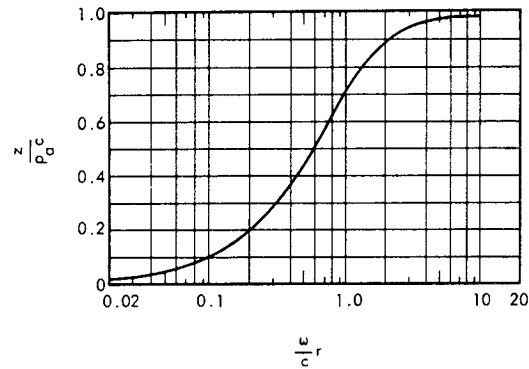
#### 4.4.1.2 Source Power

The sound intensity  $I$ , or time-average rate of energy propagation per unit area, can be integrated over an imaginary surface enclosing the source, to give the total acoustic power of the source. Taking a spherical surface in the

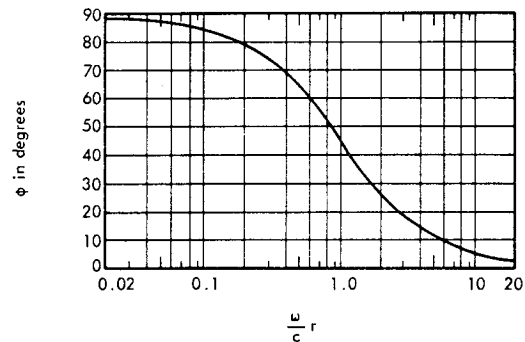
far field, so that the pressure and particle velocity are in phase, the total acoustic power of a monopole is given by:

$$W_s = 4\pi r^2 I = \frac{\rho_a \omega^2}{4\pi c} |S|^2 \quad (4.27)$$

where  $|$  means absolute magnitude, and where  $\rho_a S$  can be interpreted as the instantaneous mass flow rate  $\dot{m}$  or from the source. The sound power of a monopole, therefore, is proportional to the density of the medium, inversely proportional to the wave propagation speed and proportional to the square of frequency.



(a) Ratio of the Specific Acoustic Impedance of a Spherical Wave to that of a Plane Wave



(b) Phase Angle Between Pressure and Particle Velocity in a Spherical Wave

FIGURE 4.12 Behavior of a Spherical Wave with Distance from the Source (from Reference 4.7)

#### 4.4.1.3 Examples of Monopole Sources

A physical source need not be spherical to act as a monopole source; if its dimensions are small compared to a wavelength, the waves spread out around the source and nearly uniform spherical wave fronts result. For example, loudspeakers radiate as simple sources when mounted in one side of a closed box and operating at low frequencies. The same is true of an exhaust pipe from a reciprocating engine,

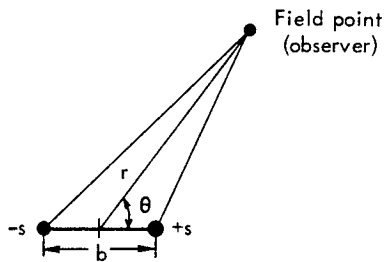
low frequency noise from unstable burning in a rocket engine, the human voice, and other devices that employ intermittent airflows (e.g., the pulse jet and some whistles and sirens). Generally, monopole radiation can be expected whenever there is a fluctuating mass in a fluid flow and the typical dimension is much smaller than a wavelength. Given a physical source in steady operation in a free field with most of its energy in the audible frequency range, a judgement on whether or not to treat the source as a monopole can be made by walking around it at a constant (far field) radius; no perceptible changes in level or frequency content should occur for a simple source.

#### 4.4.2 SOURCES CONSTRUCTED FROM MONOPOLES

Combinations of monopoles can be used to represent higher order sound sources. The properties of the next two higher order of source (dipoles and quadrupoles) are next introduced.

##### 4.4.2.1 The Dipole Source

To produce monopole radiation requires a periodic volume fluctuation in a small region of space, the source point. The dipole source can be constructed from two monopoles of equal magnitude but opposite sign, located a short distance  $b$  apart, as illustrated in the sketch below. There is no net change of volume, but a change of momentum (as the flow direction between the two monopoles alternates), and so the dipole is associated with a fluctuating force rather than a fluctuating volume. The lateral oscillation of a small solid object, such as a sphere, exerts a fluctuating force on the adjacent fluid and radiates a dipole field. Very near the source, the fluid motion is the same as that of a hydrodynamic source-sink pair.



Provided the vector distance between the two monopoles is small compared to a wavelength and compared to the radial distance to the observer, they can be treated as a single point source. Use of the point source concept requires that the observation point be a sufficient distance from the source that the field behavior is independent of the size of the source. The sound waves from a large source vary with absolute distance differently from waves produced by a small source, but at a distance of several (3 to 4) times the largest dimension of the radiating source, spherical spreading is approached, and the point source concept can be applied. In the mathematical derivation of the dipole, this is implied by a limiting process in which the distance  $b \rightarrow 0$  as  $s \rightarrow \infty$ , such that the product  $sb$  (the dipole strength) remains constant.

The following acoustic pressure and particle velocity components (radial and tangential) occur at the field point  $r, \theta$  when the dipole strength  $D = Sb$ :

$$p = \left(\frac{\omega}{c}\right)^2 D \frac{\rho_a c}{4\pi r} \cos \theta \left(1 - \frac{j}{\frac{\omega}{c} r}\right) e^{j(\omega t - \frac{\omega}{c} r)} \quad (4.28)$$

$$u_r = -\frac{\left(\frac{\omega}{c}\right)^2 D}{4\pi r} \cos \theta \left(1 - \frac{2j}{\frac{\omega}{c} r} - \frac{2}{\left(\frac{\omega}{c} r\right)^2}\right) e^{j(\omega t - \frac{\omega}{c} r)} \quad (4.29)$$

$$u_\theta = -\frac{j \frac{\omega}{c} D}{4\pi r^2} \sin \theta \left(1 - \frac{j}{\frac{\omega}{c} r}\right) e^{j(\omega t - \frac{\omega}{c} r)} \quad (4.30)$$

and the total sound power of the dipole source is

$$W_d = \frac{\rho_a \omega^4}{12\pi c^3} |D|^2 \quad (4.31)$$

The directionality of the dipole field is evident from the dependence on  $\theta$ , which exists even in the far field. For  $\left(\frac{\omega}{c} r\right) \gg 1$ :

$$p \rightarrow -\left(\frac{\omega}{c}\right)^2 D \frac{\rho_a c}{4\pi r} \cos \theta e^{j(\omega t - \frac{\omega}{c} r)} \quad (4.32)$$

$$u_r \rightarrow \frac{p}{\rho_a c}, \quad u_\theta \rightarrow 0$$

The pressure amplitude varies inversely with  $r$ , but has a maximum along the dipole axis and drops to zero at  $\theta = \pi/2$ . Figure 4.13 qualitatively compares the directivity of a dipole with that of a monopole in terms of surfaces of equal intensity. The nonspherical directivity pattern of the dipole occurs because of the time delay between the signal received from one source (monopole component of the dipole) and that from the other source.

Examples of dipole sources encountered in practice are a rotating propeller, the aeolian tones produced by wind blowing across cylinders (wires), and the combination of a turbulent flow and a solid boundary, all of which involve a fluctuating force.

##### 4.4.2.2 The Quadrupole Source

The next higher order point source is the quadrupole, constructed of two dipoles of opposite sign. It has two defining axes, one from the direction of the dipole strength and one from the vector joining the two dipoles. The general case is the oblique quadrupole, where the two axes cross at some oblique angle; but it can always be resolved into a set of longitudinal quadrupoles (with axes parallel)

and lateral quadrupoles (with axes perpendicular). The quadrupole strength is

$$Q = abS$$

where  $a$  and  $b$  are the two typical dimensions of the quadrupole and  $S$  is the strength of the four simple sources of which it is composed. The acoustic power from a lateral quadrupole is

$$W_Q = \frac{\rho_a \omega^6}{60\pi c^5} |Q|^2 \quad (4.33)$$

and that for a longitudinal quadrupole is larger by a factor of three. The most important example of quadrupole radiation is the noise generated by free turbulent flows as from a jet engine exhaust; jet noise characteristics are satisfied by a set of convected lateral quadrupoles.

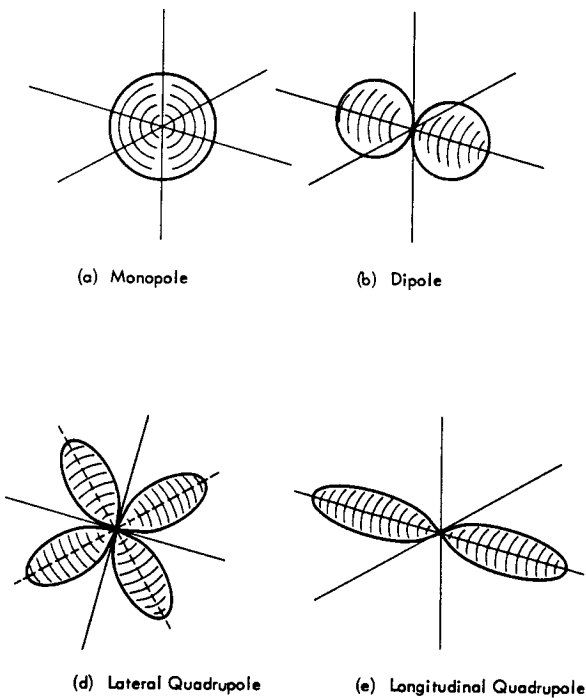


Figure 4.13 Directivity Comparison of Point Sources, Qualitative Three-Dimensional View Showing Surfaces of Equal Intensity

The three basic point sources, when compared on the basis of sound power show

$$W_S \sim \omega^2/c$$

$$W_D \sim \omega^4/c^3$$

$$W_Q \sim \omega^6/c^5$$

Therefore, in a flow containing more than one type of source, the simple source may be dominant at low frequencies, and the higher order sources dominant at higher frequencies. A qualitative comparison of source directivities is given in Figure 4.13.

#### 4.4.3 SOUND FIELD OF A MOVING SOURCE

When a sound source is moving at some translational velocity with respect to the observer, several important changes in its sound field occur, in addition to the well-known shift in apparent frequency as a source approaches or leaves an observer in its path. The motion of a source increases the intensity in the direction of motion, and at the same time decreases to a lesser degree the intensity in the opposite direction. The net result is that a moving source radiates more acoustic power than the same source when stationary, with the power output strongly dependent on the Mach number of the motion. Figure 4.14 shows, for example, the increase in power output and the change in directional patterns for a moving lateral quadrupole.

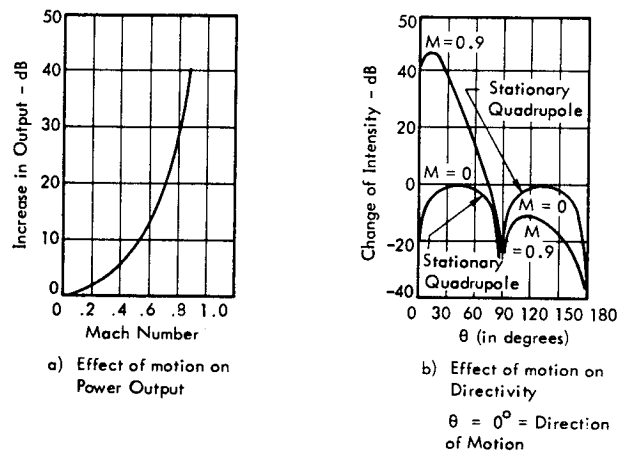
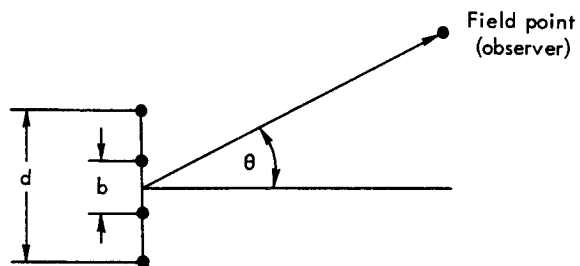


Figure 4.14 Effect of Motion on the Power and Directional Patterns of a Lateral Quadrupole (from Reference 4.8)

#### 4.4.4 LINE, CYLINDER AND PISTON SOURCES

##### 4.4.4.1 Line Source

A line source can be constructed from a linear array of  $n$  simple sources (vibrating in phase) on a line length  $d$  spaced a distance  $b$  apart.





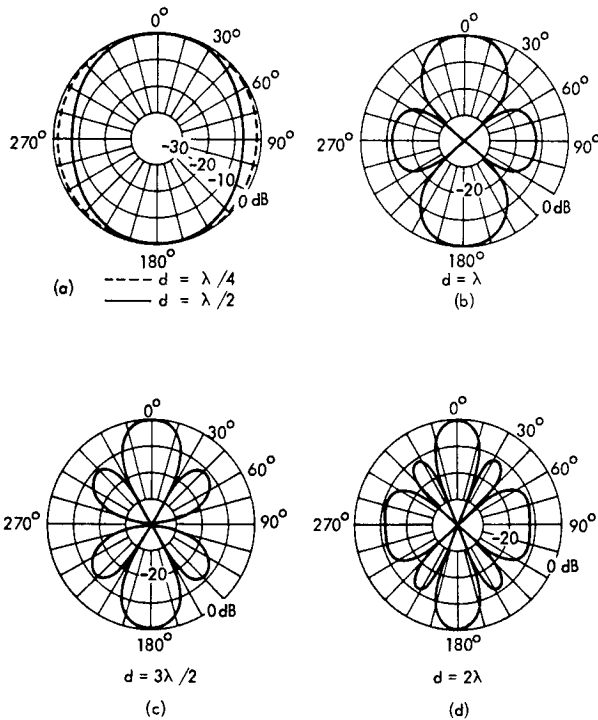


FIGURE 4.15 Directivity Patterns for a Linear Array of Four Simple In-Phase Sources at Even Spacing (Adapted from Reference 4.9)

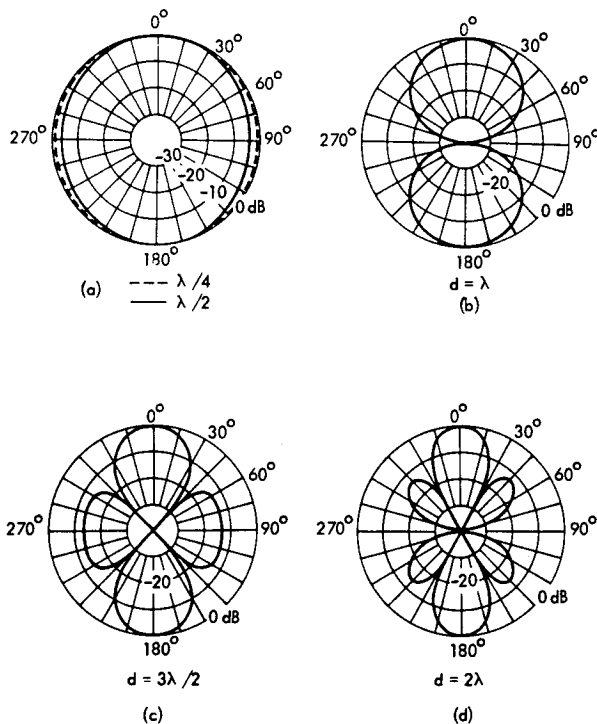


FIGURE 4.16 Directivity Patterns for a Line Source Radiating Uniformly Along Its Length (Adapted from Reference 4.9)

Figure 4.15 shows the directivity patterns for an array of four simple sources in a line at even spacing. The directivity patterns are lines of constant (far field) intensity in a plane passing through the source. As the extent of the radiator increases (in terms of wavelengths), the sharper the principal lobe (along  $\theta = 0$ ) becomes, and the larger the number of side lobes. Alternately, for a radiator of given length, this trend corresponds to increasing frequencies (decreasing wavelength). The line source result is obtained as the number of simple sources  $n \rightarrow \infty$  and the spacing distance  $b \rightarrow 0$ ; the directivity patterns for this case are given in Figure 4.16. A line source of infinite extent corresponds to the limiting case (zero radius) of an infinite cylindrical source, next discussed.

4.4.4.2 Cylinder Source

The general solution of the wave equation in cylindrical coordinates for the case of uniform radiation from a cylinder is given, for example, in Reference 4.10. For large distances from an infinite pulsating cylinder,  $r \rightarrow \infty$ , the expression for the acoustic pressure reduces to:

$$p \rightarrow A \sqrt{\frac{2}{\pi \left(\frac{\omega}{c} r\right)}} e^{j \left(\omega t - \frac{\omega}{c} r\right) + j \pi / 4}$$

The far field pressure, for a cylinder source, decreases as  $1/\sqrt{r}$  with distance from the source, corresponding to a 3 decibel decrease in sound pressure level for doubling of distance. At small distances from the cylinder,  $r \rightarrow 0$ :

$$p \rightarrow -j \left(\frac{2A}{\pi}\right) \ln(r) e^{j \omega t}$$

The value of the constant A is determined from the fact that the velocity of the air normal to the surface must equal the surface velocity. For a cylinder of radius small compared to a wavelength, the pressure and particle velocity at large distances (in wavelengths) from the cylinder are

$$p \rightarrow \pi \rho_0 a U_0 \sqrt{\frac{\omega c}{2 \pi r}} e^{j \left(\omega t - \frac{\omega}{c} r\right) + j(\pi / 4)} \tag{4.34}$$

$$u_r \rightarrow \pi a U_0 \sqrt{\frac{\omega}{2 \pi r c}} e^{j \left(\omega t - \frac{\omega}{c} r\right) + j(\pi / 4)} \tag{4.35}$$

where  $U_0$  is the cylinder surface velocity amplitude and  $a$  is the cylinder radius. Again the product of the real parts of the pressure and the particle velocity gives the energy flow per unit area; and the radiated power per unit length of cylinder is:

$$W = 1/2 \pi^2 a^2 \rho_0 \omega U_0^2 \tag{4.36}$$

4.4.4.3 Piston Source

The field of many radiating sources (such as vibrating plates and high frequency radiation from an open pipe) can be predicted from the model using an oscillating rigid circular piston. The piston's rigidity means that all parts of its surface vibrate in phase and that its motion is independent of the acoustic loading on its surface.

Unbaffled Piston

For the case of an unbaffled rigid circular piston radiating into free space, the field is given (to a first approximation) by a dipole source, Figure 4.17, since each axial movement compresses the air on one end and simultaneously rarefies it on the other. The dipole approximation is most valid for low frequency radiation ( $\frac{\omega}{c} a < 1$ ).

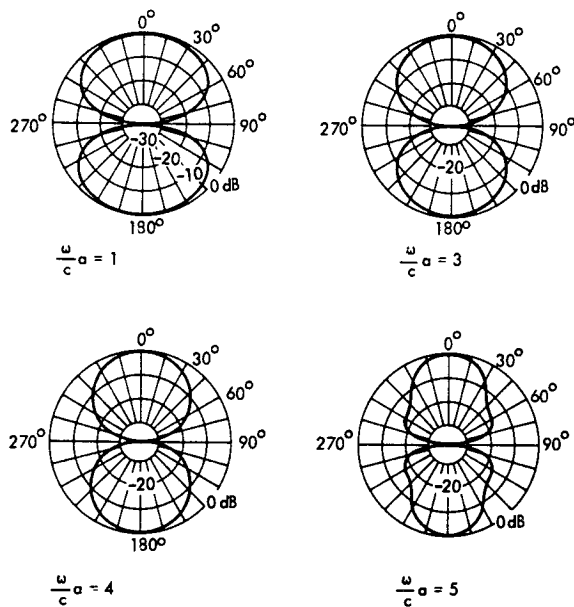


FIGURE 4.17 Directivity Patterns for an Unbaffled Rigid Circular Piston of Radius  $a$  (Adapted from Reference 4.9)

Piston in an Infinite Baffle

When the rigid circular piston is placed in a rigid infinite wall (baffle), Figure 4.18, the piston radiates only into half-space, and the acoustic pressure at a field point (obtained from the sum of contributions from all the elemental surface areas of the piston) is

$$p = \frac{1}{2} \frac{j\omega}{r} \rho_a U_o a^2 \left[ \frac{2 J_1(\frac{\omega}{c} a \sin \theta)}{\frac{\omega}{c} a \sin \theta} \right] e^{j(\omega t - \frac{\omega}{c} r)} \quad (4.37)$$

where

$U_o$  = piston velocity amplitude

$J_1$  = Bessel function of first kind.

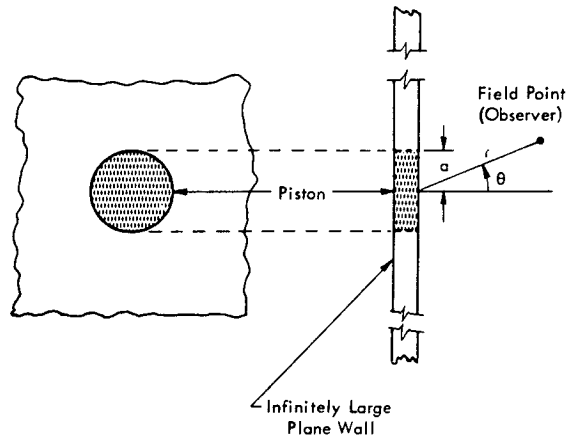


FIGURE 4.18 Rigid Circular Piston in an Infinite Baffle

The resulting directivity patterns, Figure 4.19, approximate that of a monopole at low frequencies, becoming increasingly directional and adding side lobes as the frequency increases. These patterns are very similar to those of a direct-radiator loudspeaker or the low frequency radiation from a plate vibrating in its first mode. As for all the foregoing directivity patterns, the result is only applicable to the far field; i.e., for a field point at a distance  $r$  large compared to the typical source dimension  $a$ .

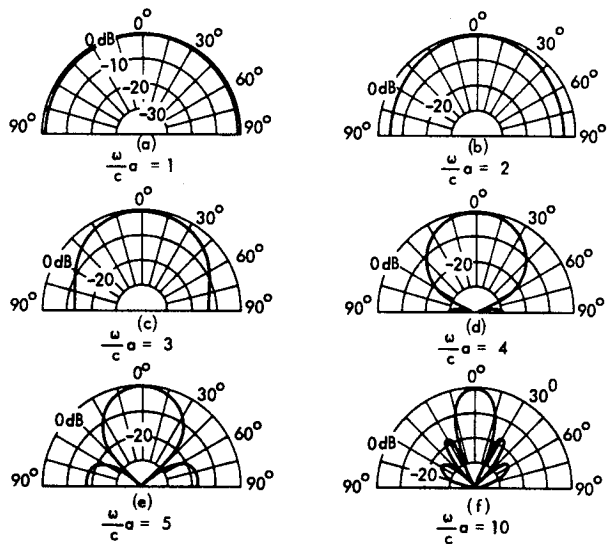


FIGURE 4.19 Directivity Patterns for a Rigid Circular Piston in an Infinite Baffle (Adapted from Reference 4.9)

Piston in the End of a Tube

A rigid piston in the end of a long circular tube, Figure 4.20, can radiate in all directions, and the analysis for the field includes the effect of diffraction around the edge of the tube. The directivity patterns are given in Figure 4.21, again approximating a monopole directivity at low frequencies, but gradually changing to a more complex pattern with a major and a minor lobe as the frequency increases.

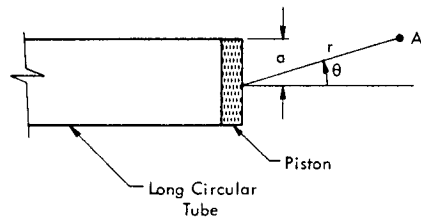


FIGURE 4.20 Rigid Circular Piston in the End of a Circular Tube

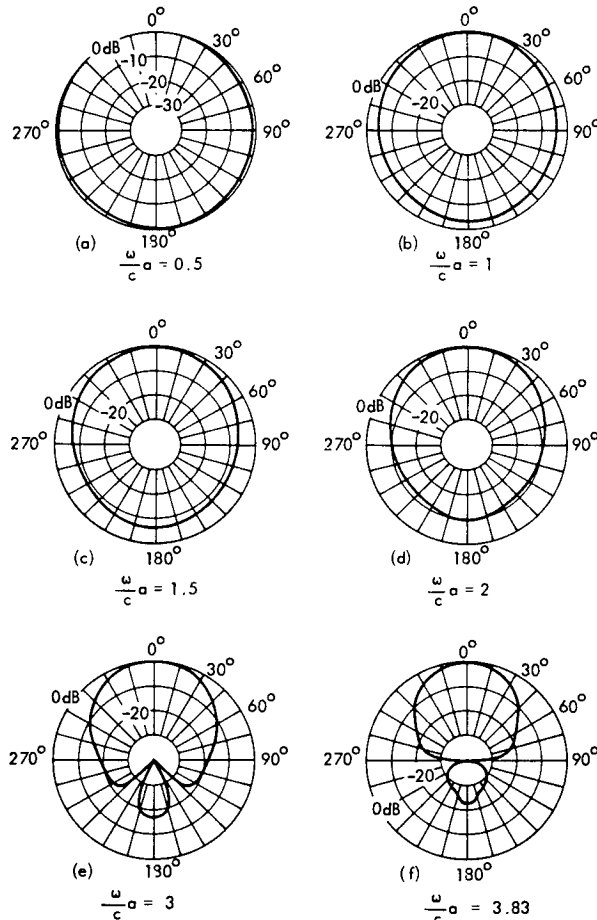


FIGURE 4.21 Directivity Patterns for a Rigid Piston in the End of a Long Tube (Adapted from Reference 4.9)

An important general conclusion can be drawn from all the foregoing directionality patterns. In each case, at sufficiently low frequencies, the source radiates equally in all directions, whereas at high frequencies, the radiation is substantially forward. The changeover point occurs roughly when the wavelength of sound is less than twice the maximum dimension of the radiator. This conclusion applies generally to all types of stationary acoustic source distributions. Thus, for sufficiently high frequencies (long wavelength) the sound radiation is highly directional, and several approximate methods of analysis become valid, as discussed in the next section.

#### 4.5 EFFECTS OF BOUNDARIES

The foregoing properties of sources and their fields were for sources operating in a free field; that is, in an infinite medium free of surfaces. A detailed treatment of transmission, reflection and absorption of architectural elements is given in Chapter 9, supplemented by design data on transmission loss data for walls and absorption of materials in Chapter 12. Chapter 8 includes design charts for diffraction of acoustic waves by rectangular obstacles, and Chapter 7 covers the shielding of one obstacle by another against blast waves. The purpose of this section is to introduce the physical concepts involved when sound waves encounter an obstacle or a surface, as well as some practical results in familiar cases.

When a wave encounters an obstacle, some of the wave is deflected, and the resulting pattern depends on the relative size of the obstacle and the wavelength. The difference between the actual wave and the undisturbed (free field) wave is termed the scattered wave; it spreads out from the obstacle, interfering with the original (free field) wave pattern. For obstacles which are large in relation to the wavelength of the incident plane wave, half of the scattered wave (the reflected wave) spreads out uniformly from the obstacle while the other half (the interfering wave) cancels the plane wave behind the obstacle to form a sharply defined shadow zone. This case warrants the use of geometrical optics or ray acoustics and applies to large surfaces or walls. For an obstacle small in terms of wavelengths, the scattered wave propagates in all directions and there is no sharp shadow. The following section treats the cases where the wavelength is longer than or of the same order as the obstacle, which occurs frequently for sound waves.

##### 4.5.1 EFFECTS OF OBSTACLES

Cylindrical and spherical obstacles will be used to illustrate scattering effects: the angular distribution of the scattered wave on the pressure variation over the obstacle and hence the force on the obstacle.

##### 4.5.1.1 Scattering of Plane Waves by a Cylinder

To find the scattering by a cylinder of radius  $a$ , consider a plane wave traveling along a path normal to the cylinder axis. It will be convenient to work in cylindrical coordinates  $(r, \phi)$ , following Morse, (Reference 4.10) and to use subscripts  $i$  for the incident wave and  $r$  for the scattered (or reflected) wave. For an oncoming plane wave of intensity  $I_0$  propagating along the  $+x$  axis, the acoustic pressure is

$$p_i = p_o e^{j(\omega t - \frac{\omega}{c} x)} = p_o e^{j(\omega t - \frac{\omega}{c} r \cos \phi)} \quad (4.38)$$

where the pressure amplitude for plane waves is related to the intensity by

$$p_o^2 = 2 \rho_a c I_0$$

Expressing the plane wave in cylindrical coordinates requires a series of Bessel functions, representing a series of cylindrical waves:

$$P_i = P_o \left[ J_0 \left( \frac{\omega}{c} r \right) + 2 \sum_{m=1}^{\infty} (-j)^m \cos(m\phi) J_m \left( \frac{\omega}{c} r \right) \right] e^{j\omega t} \tag{4.39}$$

The corresponding radial particle velocity is

$$u_r = \frac{P_o}{\rho c} \left\{ -j J_1 \left( \frac{\omega}{c} r \right) + \sum_{m=1}^{\infty} (-j)^{m+1} \left[ J_{m+1} \left( \frac{\omega}{c} r \right) - J_{m-1} \left( \frac{\omega}{c} r \right) \right] \cos(m\phi) \right\} e^{j\omega t} \tag{4.40}$$

Now inserting the cylinder into this field of plane waves with its axis at  $r = 0$ , the field is distorted by the addition of a scattered (outgoing) wave to suit the boundary condition that the radial particle velocity be zero at the cylinder surface,  $r = a$ . The expressions for the scattered wave pressure and radial particle velocity are also series of Bessel functions and contain a series of coefficients  $A_m$  to be determined by setting the radial particle velocities  $u_i$  and  $u_r$  equal at  $r = a$ . These coefficients include a phase angle  $\gamma_m$  that entirely determines the behavior of the scattered wave, defined as

$$\gamma_m = - \frac{\pi m}{(m!)^2} \left( \frac{\omega}{c} a \right)^{2m}$$

For the far field, at a distance  $r$ , large compared to the cylinder radius and the wavelength of the plane wave  $\left( \frac{\omega}{c} a \gg 1 \right)$ , the pressure and radial velocity of the scattered wave simplify to:

$$P_r \rightarrow - \left( \frac{4 \rho_a c I_o a}{\pi r} \right)^{1/2} \psi_r(\phi) e^{j(\omega t - \frac{\omega}{c} r)} \tag{4.41}$$

$$u_r \rightarrow \frac{\bar{P}_r}{\rho_a c} \tag{4.42}$$

and the scattered intensity at a point  $(r, \phi)$  is

$$I_r = \frac{2 I_o a}{\pi r} |\psi_r(\phi)|^2 \tag{4.43}$$

where

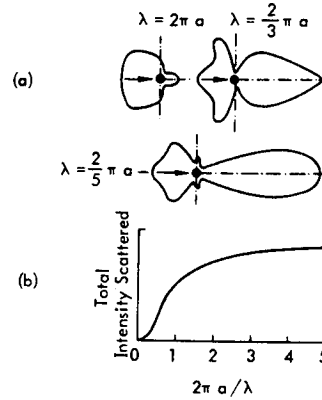
$$\psi_r(\phi) = \frac{1}{\sqrt{\frac{\omega}{c} a}} \sum_{m=0}^{\infty} \epsilon_m \sin(\gamma_m) e^{j\gamma_m} \cos(m\phi)$$

$$|\psi_r|^2 = \frac{1}{\frac{\omega}{c} a} \sum_{m,n=0}^{\infty} \epsilon_m \epsilon_n \sin \gamma_m \sin \gamma_n \cos(\gamma_m - \gamma_n) \times \cos(m\phi) \cos(n\phi)$$

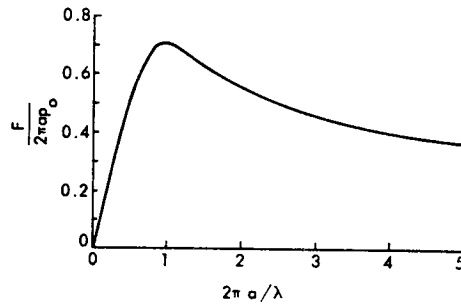
and

$$\epsilon_0 = 1, \epsilon_m = 2 \quad (m > 0).$$

The intensity pattern is shown qualitatively in polar plots, (Figure 4.22), for several values of wavelength  $\lambda$  and cylinder radius  $a$ . For long wavelengths, the scattering is small and is almost uniform in the backward directions. For higher frequencies, diffraction peaks appear and move forward. The total scattered intensity rises rapidly with decreasing wavelength up to  $2\pi a/\lambda \cong 1$  and then levels off.



(a) Variation of Directionality of the Scattered Wave with Wavelength  $\lambda$  and Cylinder Radius  $a$ ; and  
(b) Variation of Total Scattered Intensity with Wavelength  $\lambda$  and Cylinder Radius  $a$



(c) Amplitude of the Side Force  $F$  on the Cylinder, for Scattering of a Plane Wave of Pressure Amplitude  $p_o$  and Wavelength  $\lambda$

FIGURE 4.22 Scattering of a Plane Wave by a Cylinder (from Reference 4.10)

The ratio of the total scattered power to the power of the incident plane wave approaches the following limiting values at very long and at very short wavelengths respectively:

$$\frac{W_r}{W_i} \rightarrow \begin{cases} 6\pi^5 a^4 / \lambda^3 & \text{for } \lambda \gg 2\pi a \\ 4a & \text{for } \lambda \ll 2\pi a \end{cases}$$

Thus, the limiting value for total scattered power at very short wavelengths is the power contained in a beam of incident plane waves twice as wide as the cylinder diameter. A curve showing numerical values of the power ratio is given in Chapter 8 for all wavelengths.

The acoustic pressure distribution over the cylinder surface gives a side force on the cylinder, obtained from integrating the sum of the plane wave and the scattered wave around the cylinder. For wavelengths large with respect to the cylinder ( $\lambda \gg a$ ), the net force per unit cylinder length is

$$F = 4a p_o \left( \frac{1}{\frac{\omega}{c} a C_1} \right) e^{j\omega t + j\gamma_1 - j\frac{\pi}{2}} \quad (4.44)$$

where

$$C_1 = \sqrt{\frac{2}{\pi \frac{\omega}{c} a}}$$

The portion of the exponent ( $+\gamma_1 - \pi/2$ ) represents the phase angle by which the force lags the pressure of the undisturbed plane wave at  $r=0$ .

At low frequencies,  $\omega \ll (c/a)$ , the force approaches the value

$$F \rightarrow -j\omega \left( \frac{4\pi^2 a^2}{c} \right) p_o e^{j\omega t} \quad (4.45)$$

and for high frequencies,  $\lambda \ll 2\pi a$ ,

$$F \rightarrow \sqrt{4a\lambda} p_o e^{j\left(\omega t - \frac{\omega}{c} a\right) - j\pi/4} \quad (4.46)$$

The side force per unit cylinder length is shown in Figure 4.22 as a function of  $2\pi a/\lambda$ . For low frequencies, the force is proportional to frequency, peaks at a wavelength equal to one cylinder circumference, and then decreases with increasing frequency. For very long waves (at the low frequency extreme) the distortion of the plane wave due to the presence of the cylinder contributes a factor of two to the net force on the cylinder.

#### 4.5.1.2 Scattering of Plane Waves by a Sphere

The procedure for a sphere is very similar to that for a cylinder. Following Morse, (Reference 4.10), conversion of the incident plane wave to polar coordinates, for a right-running wave on the polar axis, gives

$$\begin{aligned} p_i &= p_o e^{j\left(\omega t - \frac{\omega}{c} r \cos \theta\right)} \\ &= p_o \sum_{m=0}^{\infty} (2m+1) (-j)^m P_m(\cos \theta) \mathcal{L}_m\left(\frac{\omega}{c} r\right) e^{j\omega t} \end{aligned} \quad (4.47)$$

where  $P_m$  is the Legendre function of order  $m$ , and  $\mathcal{L}_m$  is the spherical Bessel function. The acoustic pressure of the scattered wave (for a sphere of radius  $a$  centered at the origin) is

$$\begin{aligned} p_r &= -p_o \sum_{m=0}^{\infty} (2m+1) (-j)^{m+1} e^{j\delta_m} \sin \delta_m P_m(\cos \theta) \\ &\quad \times \left[ \mathcal{L}_m\left(\frac{\omega}{c} r\right) - j n_m\left(\frac{\omega}{c} r\right) \right] e^{j\omega t} \end{aligned} \quad (4.48)$$

where  $n_m$  is the Neumann function, and the phase angles  $\delta_m$  are functions of  $m$  and of wavelength through  $\left(\frac{\omega}{c} a\right)$

The intensity of the scattered wave at a far field point  $r \gg a$  is

$$\begin{aligned} I_s &= \left(\frac{a}{r}\right)^2 I_o \left(\frac{1}{\frac{\omega}{c} a}\right)^2 \sum_{m,n=0}^{\infty} (2m+1)(2n+1) \times \\ &\quad \sin \delta_m \sin \delta_n \cos(\delta_m - \delta_n) P_m(\cos \theta) P_n(\cos \theta) \end{aligned}$$

which for low frequencies ( $\frac{\omega}{c} a \ll 1$ ) approaches the value

$$I_s \rightarrow \frac{1}{9} \left(\frac{\omega}{c}\right)^4 \frac{a^6}{r} I_o (1 - 3 \cos \theta)^2 \quad (4.49)$$

and for high frequencies ( $\frac{\omega}{c} a \gg 1$ ) approaches

$$I_s \rightarrow \frac{a^2}{4r^2} \left[ 1 + \cot^2(\theta/2) J_1^2\left(\frac{\omega}{c} a \sin \theta\right) \right] \quad (4.50)$$

Figure 4.23 shows the angular distribution of scattered intensity for a plane wave encountering a sphere, and the forward directionality increases with frequency similar to the case of a cylinder. The net pressure amplitude at the point of the sphere nearest the oncoming wave is also given in Figure 4.23.

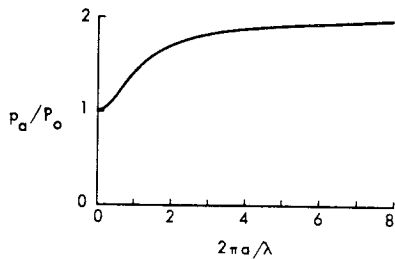
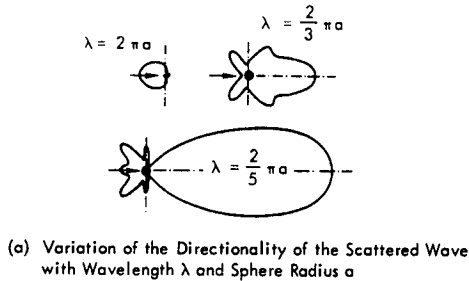


FIGURE 4.23 Scattering of a Plane Wave by a Sphere (From Reference 4.10)

4.5.1.3 Practical Consequences

In the audible frequency range 20 - 20,000 Hz, the primary effects of scattering by solid objects arise in acoustical measurements and in hearing. For sound waves in air the following approximate frequency-wavelength relation holds:

$\lambda$ (feet)	$f$ (Hz)
100	11
10	110
1	1,100
0.1	11,000

Wavelengths in the audible range, then, range roughly from 10 feet to 0.1 foot. Given a spherical microphone, the measured amplitude will be larger than the actual amplitude of the plane wave being measured for wavelengths shorter than its circumference approaching a 100 percent error at high frequencies, (Figure 4.23), and significant microphone corrections will be required for frequencies much above 10 kHz, depending on microphone size. The presence of an obstacle in the sound field behind the microphone (that is, on an extension of the line connecting source and microphone) also requires corrections to the measured sound pressure levels, (Table 4.2). In the 1 kHz region, just where loudness curves indicate human hearing is the most sensitive, a significant distortion is caused by an obstacle the size of the human head, which probably accounts for our sound direction-sensing ability. At the lowest end of the frequency scale (10 < f < 100 Hz) solid obstacles the size of buildings (10 < λ < 100 feet) can have significant scattering effects. Scattering by atmospheric turbulence also corresponds to the low end of the frequency scale; this is discussed further in Chapter 7.

TABLE 4.2

THE EFFECT OF AN OBSTACLE ON SOUND PRESSURE LEVELS MEASURED BY A MICROPHONE LOCATED ON A LINE BETWEEN THE SOUND SOURCE AND OBSTACLE (FROM REFERENCE 4.11)

Obstacle	r/a	Size of Obstacle in Wavelengths, a/λ		
		ΔdB < 0.5	ΔdB < 1.0	Max Δ dB
Sphere	1	< 0.038	< 0.064	6.0 a/λ > 1.0
	4	< 0.093	< 0.145	1.3 a/λ > 0.25
	10	--	--	0.5 a/λ > 0.25
Cylinder	1	< 0.038	< 0.047	~ 6.0 a/λ > .4
	4	< 0.025	< 0.038	~ 4.0
	50	< 0.058	--	~ 1.0
	200	--	--	~ 0.5

} a/λ > .12

a = radius of obstacle; r = distance from center of obstacle to observation point;  
 ΔdB = change in sound level due to obstacle; λ = wavelength of incident plane wave field.

4.5.2 REFLECTION OF SOUND AT AN INTERFACE

For obstacles that are large compared with the wavelength of the incident sound, the obstacle may be approximated by a plane surface and the interaction treated in terms of the reflection, absorption and transmission properties of the obstacle. This topic is primarily of interest in architectural acoustics and is covered in Chapter 9, including oblique incidence (incident waves striking the surface at angles other than 90 degrees), diffuse incidence (incident waves arriving from all angles) and effects of absorption at the surface. An introduction to reflection at a surface is given below for the simpler one-dimensional case of normal incidence, using sound propagation in tubes as an example. Neglecting the viscosity of the medium, the model excludes the edge effect of the tube walls on propagation of the wave, and the results represent the one-dimensional propagation of a plane wave in an infinite medium. To obtain plane wave fronts in a tube requires a small enough tube diameter that the ratio of the sound wavelength to the tube radius,  $\lambda/a > 3$ .

Consider a rigid cylindrical tube, closed by a rigid, perfectly reflecting wall at one end, and a flat piston oscillating sinusoidally to generate the sound wave at the other end (Figure 4.24). The piston oscillates with an angular frequency  $\omega$ , and peak velocity amplitude  $U_0$  occurring at  $x = 0$ . The piston velocity is the real part of

$$u = U_0 e^{j\omega t}$$

Since reflections are to be included, both right-running and left-running waves must be considered; a convenient form for the particle velocity is

$$u(x, t) = u_+ e^{j(\omega t - \frac{\omega}{c} x)} + u_- e^{j(\omega t + \frac{\omega}{c} x)} \quad (4.51)$$

and the corresponding acoustic pressure is

$$p(x, t) = p_+ e^{j(\omega t - \frac{\omega}{c} x)} + p_- e^{j(\omega t + \frac{\omega}{c} x)} \quad (4.52)$$

with  $p_+$ ,  $p_-$ ,  $u_+$  and  $u_-$  complex quantities to be evaluated from the boundary conditions. The boundary conditions to be met are (a) zero particle velocity at the end (for a non-absorbing termination) and (b) at the piston face, a particle velocity equal to that of the piston.

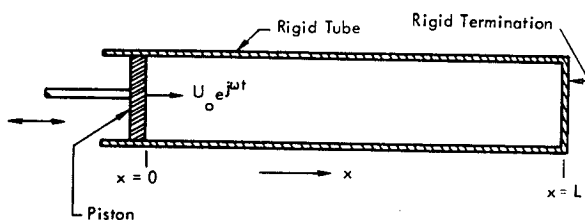


FIGURE 4.24 Oscillating Piston in the End of a Tube

At  $x = 0$ ,

$$u_+ + u_- = u_0$$

At  $x = L$

$$u_+ e^{-j\frac{\omega}{c} L} + u_- e^{j\frac{\omega}{c} L} = 0$$

Using the relation between sine and exponential functions, then

$$u_- = \frac{u_0 e^{-j\frac{\omega}{c} L}}{-2j \sin(\frac{\omega}{c} L)}$$

$$u_+ = \frac{u_0 e^{j\frac{\omega}{c} L}}{2j \sin(\frac{\omega}{c} L)}$$

and the solution for the particle velocity is

$$u(x, t) = u_0 \frac{\sin(\frac{\omega}{c} L - \frac{\omega}{c} x)}{\sin(\frac{\omega}{c} L)} e^{j\omega t} \quad (4.53)$$

For a given tube length L and wave frequency  $\omega$ , the particle velocity varies from zero at  $x = L$  to a maximum at the quarter-wavelength point  $(L - x) = \lambda/4$ . The direct wave and the reflected wave alternately cancel and reinforce each other, to produce a standing wave. The wave pattern produced by the sum does not propagate along the tube, but exhibits nodes (planes of zero velocity) and antinodes (planes of maximum particle velocity) that are stationary in space, (Figure 4.25). The nodes are

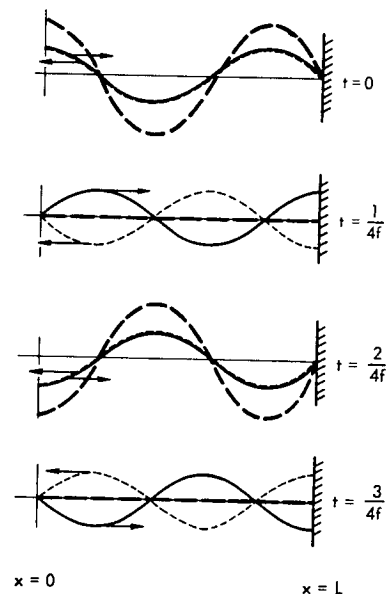


FIGURE 4.25 Standing Waves (—) Generated by Incident (—) and Reflected (----) Waves in a Tube with Rigid Termination

located at  $x = \frac{n\lambda}{2} - L$ , and the antinodes a quarter wavelength away. The root-mean-square particle velocity  $u$  evidently can become very large at the antinodes (for certain combinations of frequency and tube length) and is only prevented from becoming infinite (which would violate the acoustic approximation on which the wave equation derivation was based) by the presence of some dissipation in the tube. This is termed the resonance condition and occurs at  $(\frac{\omega}{c}L) = \pi/2$ ; the first resonant frequency corresponds to a wavelength four times the pipe length.

The acoustic pressure (complex rms time average) is

$$p = -j\rho_a c u_o \frac{\cos(\frac{\omega}{c}L - \frac{\omega}{c}x)}{\sin(\frac{\omega}{c}L)} \quad (4.54)$$

which reaches a maximum where the particle velocity is zero, and is zero where the particle velocity is maximum.

The specific acoustic impedance is  $p/u$ :

$$z = -j\rho_a c \cot(\frac{\omega}{c}L - \frac{\omega}{c}x) \quad (4.55)$$

At all frequencies the impedance either leads or follows the pressure by 90 degrees, depending on whether  $(-z/j)$  is negative or positive.

The input impedance of the tube is obtained from the specific acoustic impedance at  $x = 0$  and is a constant. When the value of  $\frac{\omega}{c}(L - x)$  is small (that is, for short tubes or low frequencies) the impedance may be approximated by a constant. Consider the first two terms of the cotangent series:

$$\cot\left[\frac{\omega}{c}(L - x)\right] \cong \frac{1}{\frac{\omega}{c}(L - x)} - \frac{1}{3}\frac{\omega}{c}(L - x)$$

For small values of  $\frac{\omega}{c}(L - x)$  the second term may be neglected. For example, replacing the value of  $\cot\left[\frac{\omega}{c}(L - x)\right]$  by the first term of the series within an accuracy of 3 percent requires that the tube length be less than 1/20 wavelength. When this occurs, the tube can be treated as a single lumped element over which the acoustic parameters effectively do not vary with position. A short length of tube can be represented as a capacitor, where the value of the capacitance  $C_s$  is given by the relation

$$z = \frac{1}{\frac{j\omega}{\rho_a c^2}(L - x)} \cong \frac{1}{j\omega C_s}$$

Another form is based on the acoustic impedance  $Z_A$  of the element, which differs from the specific acoustic impedance  $z$  by an area factor, thus relating to a tube of specific dimensions.

$$Z_A = \frac{1}{S} z = \frac{1}{j\omega(V/\rho_a c^2)} \cong \frac{1}{j\omega C_A}$$

This is an example of an acoustical element which is amenable to analog methods involving lumped parameter circuits.

## 4.6 ANALOG METHODS

### 4.6.1 BASIS OF ANALOGIES

When the differential equation for the dynamics of one system is of the same form as that for another, solutions are applicable to both systems through the use of analog relationships between system elements. Because of the similarities among mechanical, electrical and acoustical systems, electrical networks can be used to represent both acoustical and mechanical systems. Two major advantages result: (1) The dynamics of complete systems containing all three elements can be analyzed, and (2) The expeditious techniques of electrical circuit theory can be applied in estimating frequency response characteristics.

In some frequency ranges, acoustical elements must be treated as distributed elements, with their values a function of two independent variables (corresponding to partial differential equations), analogous to electrical transmission lines or large-amplitude mechanical vibrations. Analog methods in acoustics are most advantageous; however, in the frequency ranges where acoustical elements can be treated as functions of a single variable (corresponding to ordinary differential equations), analogous to lumped parameter electrical circuits. The input impedance of a tube, for example, (Section 4.5), is effectively a constant at low frequencies, allowing the tube to be treated as a capacitance element. It is the intent of this section to introduce the basic concepts involved in lumped parameter analog treatment of acoustical elements, and to provide a limited reference table of circuit elements and equations.

Mathematically, the elements in an electrical network (e.g., resistance, inductance, capacitance) are the coefficients in the set of differential equations describing the network. Identification of the analogous elements in another (linear) physical system consists of setting up the differential equations for that system; the coefficients then bear a one-to-one correspondence. The number of differential equations required to describe the dynamics of a system corresponds to the number of degrees of freedom of the system. In the analogous electrical circuit, the number of degrees of freedom corresponds to the number of nodes (as the set of equations can be derived by continuity of current flow into each node), or to the number of loops (as the set of equations can be derived by summing voltage drops around each loop).



4.6.2 THE IMPEDANCE AND MOBILITY ANALOGIES

The two basic analog systems are the impedance analogy (in which a mechanical force corresponds to an electrical voltage and velocity to current) and the mobility analogy (in which velocity corresponds to voltage and force to current). Briefly, the primary property (impedance or inverse mobility) connected with an element is the ratio of the potential drop across the element to the current through the element. Thus the impedance  $Z$  and mobility  $\mathcal{M}$  are defined by:

$$\text{Impedance, } Z - \begin{cases} \text{Electrical: } \frac{e}{i}, \text{ voltage} \\ \text{Mechanical: } \frac{f}{\dot{x}}, \text{ force} \\ \text{Acoustical: } \frac{p}{U}, \text{ pressure} \end{cases} \begin{matrix} \text{current} \\ \text{velocity} \\ \text{volume} \\ \text{velocity} \end{matrix}$$

$$\text{Mobility, } \mathcal{M} - \begin{cases} \text{Mechanical: } \frac{\dot{x}}{f}, \text{ velocity} \\ \text{Acoustical: } \frac{U}{p}, \text{ volume} \\ \text{Electrical: } \frac{i}{e}, \text{ current} \end{cases} \begin{matrix} \text{force} \\ \text{force} \\ \text{force} \end{matrix}$$

The relations among circuit elements in the electrical, mechanical and acoustical systems are:

Electrical	Mechanical		Acoustical
	$Z$	$\mathcal{M}$	
Voltage	Force	Velocity	Pressure
Current	Velocity	Force	Volume velocity
Inductance	Mass	Compliance	Acoustical reactance
Capacitance	Compliance	1/Mass	Acoustical compliance
Resistance	Mechanical resistance	1/Mechanical resistance	Acoustical resistance

The mobility analog is most practical in application to mechanical systems, or to systems with electromechanical or electroacoustic coupling involved; the impedance analogy is widely practical in acoustical applications and will be used exclusively here to represent acoustical elements. An extensive reference table of elements is given in Reference 4.12, covering all three physical systems (electrical, mechanical and acoustical) and both analog methods (mobility and impedance), and the reader is also referred to References 4.9 and 4.13. Table 4.3 (from Olsen, Reference 4.13) summarizes the useful analogous quantities (according to the impedance analogy) together with their symbols, basic dimensions, and units.

The simplest example is the single-degree-of-freedom system involving all three types of circuit elements. In the mechanical system, this is the simple mass-spring-damper system, Figure 4.26. In the impedance analogy, this

corresponds to the simple R-L-C electrical circuit and to the acoustical Helmholtz resonator. In the mechanical system, the mass provides an inertial force, the spring provides a restoring force proportional to the displacement, the dashpot provides a force proportional to velocity and against the direction of motion, and the system receives a sinusoidal force input analogous to sinusoidal voltage source in the electrical circuit.

The Helmholtz resonator consists of a chamber of air connected to the atmosphere by a narrow neck. The mass of air in the neck provides the inertia, the enclosed air in the chamber provides the stiffness (spring); and the frictional drag in the neck, the resistance.

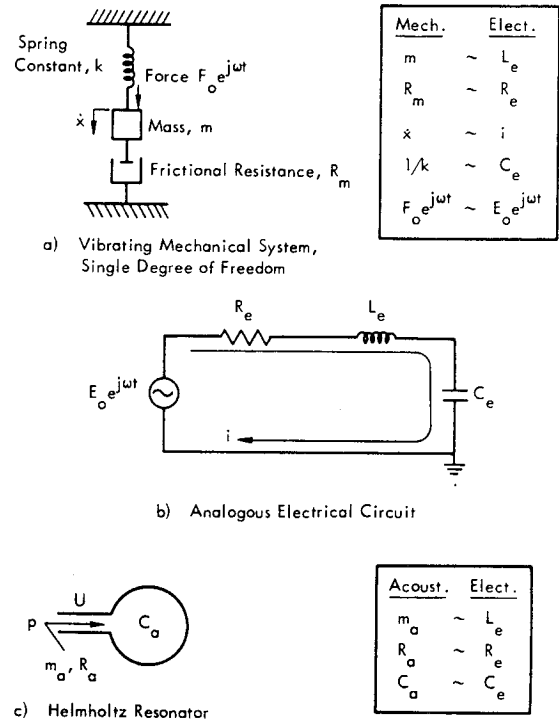


FIGURE 4.26 Example of Analogous One-Degree-of-Freedom System: Mechanical, Electrical and Acoustical

4.6.3 IMPEDANCE VALUES FOR ACOUSTICAL ELEMENTS

The concepts of specific acoustic impedance of sound sources and characteristic impedance of the medium are familiar from Sections 4.3 and 4.4. The acoustic impedance differs from the specific acoustic impedance only by an area factor, for that area involved in the volume flow.

$$z = \frac{p}{u}, \quad Z_A = \frac{p}{U}$$

where  $p$  is the acoustic pressure,  $u$  the particle velocity, and  $U$  the volume velocity for the flow area of the element in question. The mechanical impedance of an acoustical element represents the air load upon its moving surface,

Electrical				Mechanical Rectilinear				Mechanical Rotational				Acoustical			
Quantity	Unit	Sym- bol	Dimensions	Quantity	Unit	Sym- bol	Dimension	Quantity	Unit	Sym- bol	Dimension	Quantity	Unit	Sym- bol	Dimension
Electromotive Force	Volts $\times 10^8$	e	$M^{1/2}L^{3/2}T^{-2}$	Force	Dynes, Pounds	$f_m$	$MLT^{-2}$	Torque	Dyne - cm, in. - lb	$F_r$	$ML^2T^{-2}$	Pressure	Dynes per Square Centimeter	p	$ML^{-1}T^{-2}$
Charge or Quantity	Coulombs $\times 10^{-1}$	q	$M^{1/2}L^{1/2}$	Linear Dis- placement	Centimeters, Inches	x	L	Angular Displace- ment	Radians	$\phi$	1	Volume Dis- placement	Cubic Cen- timeters	X	$L^3$
Current	Amperes $\times 10^{-1}$	i	$M^{1/2}L^{1/2}T^{-1}$	Linear Velocity	cm/sec in./sec	$\dot{x}$ or v	$LT^{-1}$	Angular Velocity	Radians per Second	$\dot{\phi}$ or $\theta$	$T^{-1}$	Volume Current	Cubic Cen- timeter/sec	$\dot{X}$ or U	$L^3T^{-1}$
Electrical Impedance	Ohms $\times 10^9$	$Z_e$	$LT^{-1}$	Mechanical Impedance	Mechanical Ohms	$Z_m$	$MT^{-1}$	Rotational Impedance	Rotational Ohms	$Z_r$	$ML^2T^{-1}$	Acoustical Impedance	Acoustical Ohms	$Z_a$	$ML^{-4}T^{-1}$
Electrical Resistance	Ohms $\times 10^9$	$R_e$	$LT^{-1}$	Mechanical Resistance	Mechanical Ohms	$R_m$	$MT^{-1}$	Rotational Resistance	Rotational Ohms	$R_r$	$ML^2T^{-1}$	Acoustical Resistance	Acoustical Ohms	$R_a$	$ML^{-4}T^{-1}$
Electrical Reactance	Ohms $\times 10^9$	$X_e$	$LT^{-1}$	Mechanical Reactance	Mechanical Ohms	$X_m$	$MT^{-1}$	Rotational Reactance	Rotational Ohms	$X_r$	$ML^2T^{-1}$	Acoustical Reactance	Acoustical Ohms	$X_a$	$ML^{-4}T^{-1}$
Inductance	Henries $\times 10^9$	L	L	Mass	Grams, Slugs	m	M	Moment of Inertia	Grams - cm <sup>2</sup> lb-sec <sup>2</sup> - in.	I	$ML^2$	Inertance	Grams per (Centimeter) <sup>4</sup>	M	$ML^{-4}$
Electrical Capacitance	Farads $\times 10^{-9}$	$C_e$	$L^{-1}T^2$	Compliance	Cm/dyne In/lb	$c_m$	$M^{-1}T^2$	Rotational Compliance	Radians/Dyne-cm Radians/in. - lb	$C_r$	$M^{-1}L^{-2}T^2$	Acoustical Capacitance	(Centimeter) <sup>5</sup> per Dyne	$C_a$	$M^{-1}L^4T^2$
Power	Ergs per Second	$P_e$	$ML^2T^{-3}$	Power	Ergs/sec In-lb/sec	$P_m$	$ML^2T^{-3}$	Power	Ergs/sec in.-lb/sec	$P_r$	$ML^2T^{-3}$	Power	Ergs per Second	$P_a$	$ML^2T^{-3}$

TABLE 4.3

SUMMARY OF ANALOGOUS QUANTITIES IN THE IMPEDANCE ANALOGY  
(From H. F. Olson, "Acoustical Engineering," Chapter 4, Copyright 1957,  
D. Van Nostrand Company, Inc.)

as defined by the ratio of driving force to the velocity of the surface. Table 4.4 lists working equations for calculating the acoustic impedance and mechanical impedance values of several acoustical elements, beginning with the

sources introduced in Section 4.4. Values of the resistive and reactive parts of the specific acoustic impedance are given in the accompanying charts, from Olsen, where impedance values for numerous other acoustical elements can also be found.

TABLE 4.4  
IMPEDANCE EVALUATION EQUATIONS FOR ACOUSTICAL ELEMENTS

Element	Impedance Equations	Definitions
Pulsating Sphere (monopole)	$\frac{Z_a}{\rho c} = \frac{1}{4\pi a^2} \left[ \frac{(\frac{\omega}{c} a)^2 + j \frac{\omega}{c} a}{1 + j (\frac{\omega}{c} a)^2} \right]$ $\frac{Z_m}{\rho c} = (4\pi a^2)^2 \frac{Z_a}{\rho c}$	$Z_m$ = mechanical impedance, mechanical ohms $\rho$ = density, gm/cm <sup>3</sup> $c$ = velocity of sound, cm/sec $\omega$ = frequency, radians/sec $a$ = radius of vibrating body, cm
Oscillating Sphere (dipole)	$\frac{Z_a}{\rho c} = \frac{1}{12\pi a^2} \left\{ \frac{(\frac{\omega}{c} a)^4 + j \left[ 2 \frac{\omega}{c} a + (\frac{\omega}{c} a)^3 \right]}{4 + (\frac{\omega}{c} a)^4} \right\}$ $\frac{Z_m}{\rho c} = (4\pi a^2)^2 \frac{Z_a}{\rho c}$	$Z_a$ = acoustical impedance, acoustical ohms
Pulsating Cylinder	$\frac{Z_a}{\rho c} = \frac{1}{2\pi a} \left[ \frac{(2 \frac{\omega}{c} a)^2 + j 2 \frac{\omega}{c} a}{1 + (2 \frac{\omega}{c} a)^2} \right] \text{ (See Figure 4.28)}$ $\frac{Z_m}{\rho c} = (2\pi a)^2 \frac{Z_a}{\rho c}$	
Piston in Free Space	$\frac{Z_a}{\rho c} = \frac{1}{\pi a^2 \rho c} (r_1 + j x_1) \text{ (see Figure 4.28)}$ $\frac{Z_m}{\rho c} = (\pi a^2)^2 \frac{Z_a}{\rho c}$ <p style="text-align: center;">for all piston cases.</p>	$r_1$ = acoustical resistance per unit area, ohms $x_1$ = acoustical reactance per unit area, ohms

TABLE 4.4 (CONTINUED)

Element	Impedance Equation	Definitions
Piston in Infinite Baffle	$\frac{Z_a}{\rho c} = \frac{1}{\pi a^2} \left[ 1 - \frac{J_1 \left( 2 \frac{\omega}{c} a \right)}{\frac{\omega}{c} a} \right] + j \frac{\omega K_1 \left( 2 \frac{\omega}{c} a \right)}{2\pi a^4 c \left( \frac{\omega}{c} \right)^3}$ <p style="text-align: center;">(see Figure 4.27)</p>	$J_1, K_1$ = Bessel functions of first and second kinds
Piston in End of Semi-Infinite Tube	$\frac{Z_a}{\rho c} = \frac{1}{\pi a^2 \rho c} (r_1 + j x_1) \text{ (see Figure 4.27)}$	
Tube, Small Diameter and Short Length, $L \ll \lambda$	$\frac{Z_a}{\rho c} = \frac{L}{\pi a^2 \rho c} \left( \frac{8\mu}{a^2} + \frac{4}{3} j \omega \rho \right)$	$\mu$ = viscosity coefficient, $1.86 \times 10^{-4}$ for air
Narrow Slit, $d \ll L \ll \lambda$	$\frac{Z_a}{\rho c} = \frac{1}{\rho c} \left( \frac{12 \mu w}{d^3 L} + j \frac{6 \rho w \omega}{5 L d} \right)$	$L$ = tube length, cm $d$ = width of slit normal to flow direction, cm $w$ = length of slit in direction of flow, cm
Circular Orifice in Thin Wall	Multiply by 2 the values for piston in infinite baffle.	
Horn, Infinite Cylindrical	$\frac{Z_{A1}}{\rho c S} = 1$	$Z_{A1}$ = input impedance (at throat), ohms
Horn, Finite Cylindrical	$\frac{Z_{A1}}{\rho c} = \frac{1}{S_1} \left[ \frac{S_1 Z_{A2} \cos \left( \frac{\omega}{c} L \right) + j \rho c \sin \left( \frac{\omega}{c} L \right)}{j S_1 Z_{A2} \sin \left( \frac{\omega}{c} L \right) + \rho c \cos \left( \frac{\omega}{c} L \right)} \right]$	$S$ = Cross-sectional area, $\text{cm}^2$ $Z_{A2}$ = output impedance (at mouth), ohms $S_1$ = throat cross-sectional area, $\text{cm}^2$ $L$ = horn axial length, cm $S_2$ = mouth cross-sectional area $\text{cm}^2$

TABLE 4.4 (CONTINUED)

Element	Impedance Equation	Definitions
Horn, Infinite Conical	$\frac{Z_A}{\rho c} = \frac{1}{S_1} \left[ \frac{\left(\frac{\omega}{c} x_1\right)^2}{1 + \left(\frac{\omega}{c} x_1\right)^2} + j \frac{\frac{\omega}{c} x_1}{1 + \left(\frac{\omega}{c} x_1\right)^2} \right]$	$x_1$ = distance of throat from $x = 0$ , cm $x_2$ = distance of mouth from $x = 0$ , cm
Horn, Finite Conical	$\frac{Z_{A1}}{\rho c} = \frac{1}{S_1} \left[ \frac{j Z_{A2} \sin \frac{\omega}{c} (L - \theta_2) + \frac{\rho c}{S_2} \sin \frac{\omega}{c} L}{Z_{A2} \frac{\sin \frac{\omega}{c} (L + \theta_1 - \theta_2)}{\sin \frac{\omega}{c} \theta_1 \sin \frac{\omega}{c} \theta_2} - j \frac{\rho c}{S_2} \frac{\sin \frac{\omega}{c} (L + \theta_1)}{\sin \frac{\omega}{c} \theta_1} \right]$	$\left(\frac{\omega}{c} \theta_1\right) = \tan^{-1} \left(\frac{\omega}{c} x_1\right)$ $\left(\frac{\omega}{c} \theta_2\right) = \tan^{-1} \left(\frac{\omega}{c} x_2\right)$ $m$ = flare constant of an exponential horn, defined by the cross-sectional area variation $S = S_1 e^{mx}$ $\omega_o$ = cutoff frequency, radians/sec
Horn, Infinite Exponential	Above Cutoff frequency, $\frac{\omega}{c} > \frac{m}{2}$ :  $\frac{Z_A}{\rho c} = \frac{1}{S_1} \left[ \sqrt{1 - \left(\frac{m}{2\frac{\omega}{c}}\right)^2} + j \frac{m}{2\frac{\omega}{c}} \right]$ or  $= \frac{1}{S_1} \left[ \sqrt{1 - \left(\frac{\omega_o}{\omega}\right)^2} + \frac{\omega_o}{\omega} \right]$	

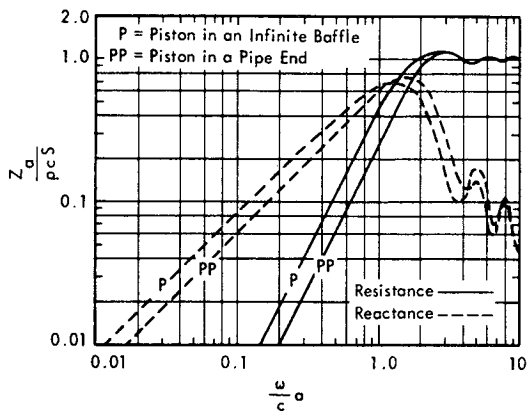


FIGURE 4.27 Acoustical Resistance and Reactance per Unit Radiating Area, Normalized to the Characteristic Impedance of the Medium: Piston in an Infinite Baffle; Piston in an Infinite Tube (Data from Reference 4.14)

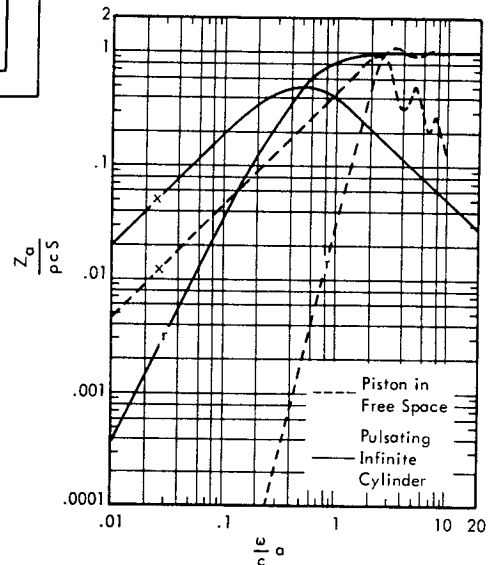


FIGURE 4.28 Acoustical Resistance  $r$  and Reactance  $x$  per Unit Radiating Area, Normalized to the Characteristic Impedance of the Medium: Pulsating Infinite Cylinder; Piston in Free Space (From H. F. Olsen, "Acoustical Engineering," Chapter 5, Copyright 1957, D. Van Nostrand Company, Inc.)

4.7 INTERPRETATION OF ACOUSTICAL DATA

Facility designers of rocket launch installations will base much of their design on data from acoustical measurements (e.g., characteristics of a noise source or transmission loss of a wall). The interpretation of acoustical data requires some knowledge of sources of error in acoustical measurements. The following sections introduce the elements of sound measuring systems, some precautions necessary in their use, and a chart for combining levels in decibels.

4.7.1 ELEMENTS OF SOUND MEASURING SYSTEM

The basic elements of any sound measuring system (such as two typical systems illustrated in Figure 4.29) are a pressure-sensitive transducer to convert the fluctuating pressure to a fluctuating voltage, the electronic circuitry for operating upon the voltage signal as desired (which may include filters for frequency analysis or weighting circuits for emphasizing some frequencies more than others), and a readout (such as a meter dial or a strip recorder) or data storage for later analysis. For cases where the sound varies rapidly with time (such as rocket launches or engine starting transients), or where a finer frequency analysis is required, the signal may be tape recorded for later analysis by (1) spectrum analyzer and level recorder or (2) analog-to-digital conversion and analysis by digital computer.

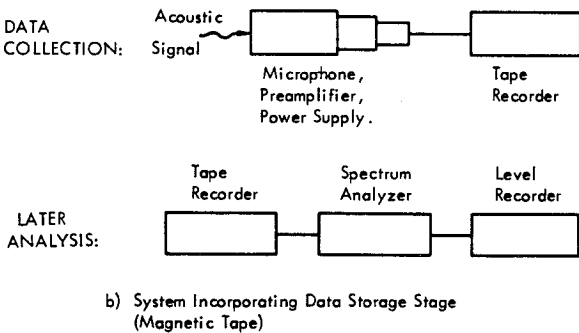
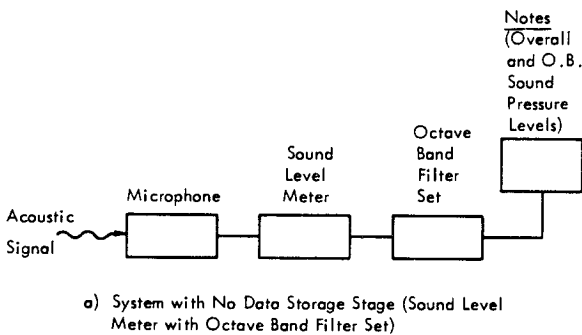


FIGURE 4.29 Two Instrumentation Systems for Acoustic Data Collection and Analysis

4.7.2 SOUND LEVEL METERS

Minimum equipment for the measurement of sound pressure levels and sound levels, according to the applicable American Standard (Reference 4.15), consists of (1) a sound level meter as specified in Reference 4.16, and (2) an octave band filter set as specified in Reference 4.5. Such sound level meters can be used to advantage when the sound source is steady over a sufficient time to allow sequential switching through the octave bands or when only the overall levels are desired and are not fluctuating rapidly.

If the noise to be measured is characterized by a momentary, very high peak pressure and rapid decay rate (i.e., impulsive noise, such as from a drop hammer), a standard sound level meter cannot follow the rapid transient, and would give values as much as 30 dB too low, even on the fast scale. An accessory peak reading instrument (impulse noise analyzer) can be used to obtain the peak SPL and the average SPL over various short averaging times.

The standard terminology for measured levels is

- Sound pressure level: A level (overall or by octave bands) to which no frequency-dependent weighting has been applied.
- Sound level: An overall value obtained from applying a frequency-dependent weighting network.

The three weighting networks available on standard sound level meters are represented by their frequency response specification curves, Figure 4.30, and tolerance limits from Reference 4.16. The A network is most frequently used for ranking noises according to their annoyance to people, as it is the single-number value which correlates best with annoyance judgment experimental results. Simpler instrumentation than called for in the American Standard exists in the form of sound survey meters, which give only the three weighted overall sound level readings, but overall levels are generally insufficient for facility design purposes.

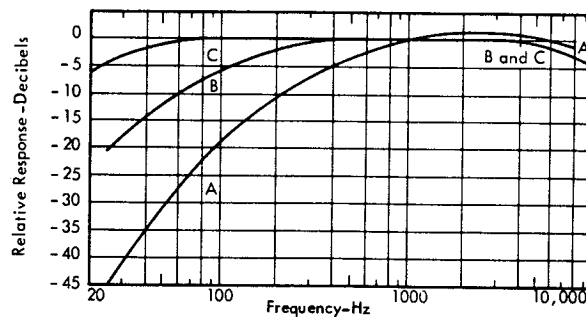


FIGURE 4.30 Frequency Response Specification For Weighting Networks of Standard Sound Level Meters, For Sound Arriving at Random Incidence (From Reference 4.16)

### 4.7.3 PRECAUTIONS

Sound field measurements must take into account such properties of the atmosphere and surroundings as will affect the signal received by the microphone and hence the interpretation of the source acoustic properties. These include weather conditions, terrain, reflecting and absorbing surfaces such as the ground plane and buildings; techniques for taking these into account are given in Chapter 7. Beyond this, a number of precautions apply to use of the instrumentation, which should be borne in mind by users of the resulting data. Errors arising from insufficient resolution in the spectral analysis of a signal were mentioned in Section 4.2. The following list gives the most frequent sources of error in acoustical data.

- Field distortion by nearby obstacles
- Ambient acoustical noise
- Wind Noise
- Electrical noise in the instrumentation system
- Frequency response limitations of instrumentation system components (e.g., microphone, Figure 4.31, or tape recorder)
- Effects of temperature extremes on instrumentation or power supply

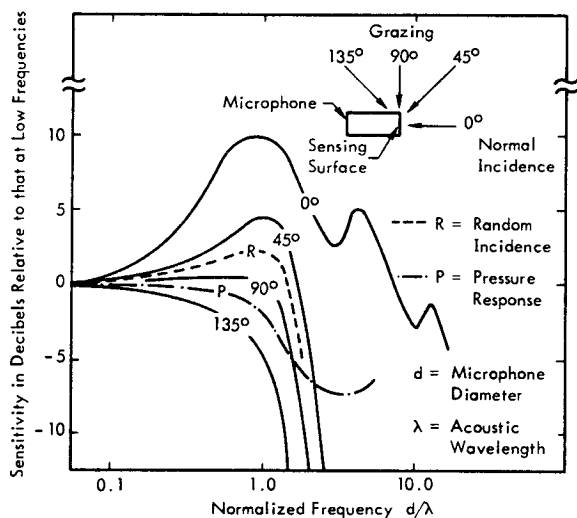


FIGURE 4.31 Typical Microphone Frequency Response Variation with Incidence, Frequency, and Microphone Size. (From Reference 4.6)

For purposes of resolving conflicting data trends, the reader should consult References 4.3, 4.6, and 4.7 as well as the cited standard documents and instruction manuals published by manufacturers of the instrumentation involved in the collection and analysis of the data in question.

### 4.7.4 ADDITION OF LEVELS IN DECIBELS

The combining of several noise levels stated in decibels is often required; for example, to obtain a combined level from several levels in different frequency bands or to obtain the cumulative effect of transmission loss through several layers. Since decibels are a logarithmic quantity and cannot be added directly, one must convert back to the original physical quantity, perform the addition, and convert the answer to decibels. To facilitate this procedure, charts or tables, such as Figure 4.32 (taken from Reference 4.3), are useful. Greater accuracy is seldom warranted, due to accuracy limitations in the data; but when it is desired, Table 12.11, Chapter 12, is useful.

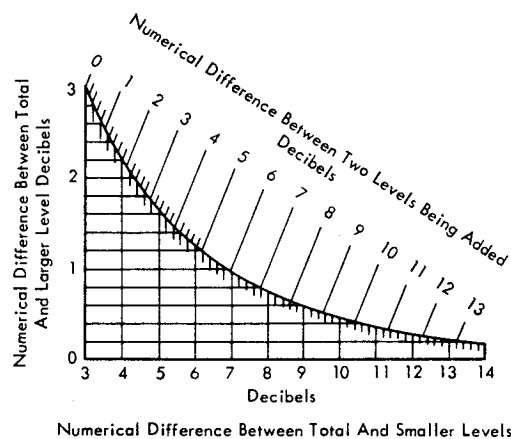


FIGURE 4.32 Chart For Combining Levels of Uncorrelated Noise Signals (From Reference 4.3)

**To Add Levels:**

Enter the chart with the "Numerical Difference Between Two Levels Being Added." Follow the line corresponding to this value to its intersection with the curved line, then left to read the "Numerical Difference Between Total and Larger Level." Add this value to the larger level to determine the total.

Example: Combine 75 dB and 80 dB. The difference is 5 dB. The 5-dB line intersects the curved line at 1.2 dB on the vertical scale. Thus the total value is 80 + 1.2 or 81.2 dB.

**To Subtract Levels:**

Enter the chart with the "Numerical Difference Between Total and Larger Levels" if this value is less than 3 dB. Enter the chart with the "Numerical Difference Between Total and Smaller Levels" if this value is between 3 and 14 dB. Follow the line corresponding to this value to its intersection with the curved line, then either left or down to read the "Numerical Difference Between Total and Larger (Smaller) Levels." Subtract this value from the total level to determine the unknown level.

Example: Subtract 81 dB from 90 dB. The difference is 9 dB. The 9-dB vertical line intersects the curved line at 0.6 dB on the vertical scale. Thus the unknown level is 90 - 0.6 or 89.4 dB.

## REFERENCES

- 4.1 Kinsler, L.E., and Frey, A.R., "Fundamentals of Acoustics" John Wiley and Sons, New York, 1950.
- 4.2 "Acoustical Terminology (Including Mechanical Shock and Vibration)," Standard S1.1-1960, USA Standards Institute, New York, 1960.
- 4.3 Peterson, A.P.G., and Gross, E.E. Jr., "Handbook of Noise Measurement," 6th ed., General Radio Co., West Concord, Mass., 1967.
- 4.4 "Preferred Frequencies and Band Numbers for Acoustical Measurement," Standard S1.6-1967, USA Standards Institute, New York, 1967.
- 4.5 "Octave, Half-Octave, and Third-Octave Band Filter Sets," Standard S1.11-1966, USA Standards Institute, New York, 1967.
- 4.6 Keast, D.N., "Measurements in Mechanical Dynamics," McGraw-Hill, New York, 1967.
- 4.7 Beranek, L.L., "Acoustic Measurements," John Wiley and Sons, New York, 1949.
- 4.8 Stephens, R.W.B., and Bate, A.E., "Acoustics and Vibrational Physics," St. Martin's Press, New York, 1966.
- 4.9 Beranek, L.L., "Acoustics," McGraw-Hill, New York, 1954.
- 4.10 Morse, P.M., "Vibration and Sound," McGraw-Hill, New York, 1948.
- 4.11 Morgan, W.V., Sutherland, L.C., and Young, K.J., "The Use of Acoustic Scale Models for Investigating Near Field Noise of Jet and Rocket Engines," WADD TR 61-178, April, 1961.
- 4.12 Firestone, F.A., "Twixt Earth and Sky with Rod and Tube; the Mobility and Classical Impedance Analogies," Jour. Acoust. Soc. Amer. 28, 6, 1117 - 1153, 1956.
- 4.13 Olsen, H.F., "Acoustical Engineering," Van Nostrand, New York, 1957.
- 4.14 Allen, C.H., "Noise Control," Chap. 7, Mechanical Design and Systems Handbook, Rothbart, H.A. (ed), McGraw-Hill, New York, 1964.
- 4.15 "Physical Measurement of Sound," Standard S1.2-1962, USA Standards Institute, New York, 1962 (Corrected 1965).
- 4.16 "Specification for General Purpose Sound Level Meters," Standard S1.4-1961, USA Standards Institute, New York, 1961.



**CHAPTER 4**  
**FUNDAMENTALS OF ACOUSTICS**

TABLE OF CONTENTS

SECTION		PAGE
4.1	<u>INTRODUCTION</u> . . . . .	4-1
4.1.1	THE NATURE OF ACOUSTIC WAVES . . . . .	4-1
4.1.2	PROPAGATION VELOCITY OF ACOUSTIC WAVES . . . . .	4-2
4.1.3	THE STRUCTURE OF NOISE CONTROL PROBLEMS . . . . .	4-3
4.1.3.1	Source Properties . . . . .	4-3
4.1.3.2	Receivers . . . . .	4-3
4.1.3.3	Transmission Path . . . . .	4-3
4.2	<u>QUANTITATIVE DESCRIPTION OF SOUND</u> . . . . .	4-3
4.2.1	DECIBEL SCALE . . . . .	4-4
4.2.2	UNITS . . . . .	4-4
4.2.3	ACOUSTICAL QUANTITIES : . . . . .	4-5
4.2.3.1	Sound Pressure . . . . .	4-5
4.2.3.2	Sound Intensity . . . . .	4-5
4.2.3.3	Sound Power . . . . .	4-6
4.2.3.4	Directional Characteristics . . . . .	4-6
4.2.3.5	Spectral Characteristics . . . . .	4-7
4.3	<u>THE ACOUSTIC WAVE EQUATION</u> . . . . .	4-8
4.3.1	DERIVATION . . . . .	4-8
4.3.2	SOLUTIONS . . . . .	4-9
4.3.3	SOME PHYSICAL CONCEPTS . . . . .	4-10
4.4	<u>ELEMENTARY SOUND SOURCES</u> . . . . .	4-10
4.4.1	THE SIMPLE SOURCE OR MONOPOLE . . . . .	4-10
4.4.1.1	The Field of a Monopole . . . . .	4-11
4.4.1.2	Source Power . . . . .	4-12
4.4.1.3	Examples of Monopole Sources . . . . .	4-12
4.4.2	SOURCES CONSTRUCTED FROM MONOPOLES . . . . .	4-13
4.4.2.1	The Dipole Source . . . . .	4-13
4.4.2.2	The Quadrupole Source . . . . .	4-13
4.4.3	SOUND FIELD OF A MOVING SOURCE . . . . .	4-14
4.4.4	LINE, CYLINDER AND PISTON SOURCES . . . . .	4-14
4.4.4.1	Line Source . . . . .	4-14
4.4.4.2	Cylinder Source . . . . .	4-15
4.4.4.3	Piston Source . . . . .	4-16
4.5	<u>EFFECTS OF BOUNDARIES</u> . . . . .	4-17
4.5.1	EFFECTS OF OBSTACLES . . . . .	4-17
4.5.1.1	Scattering of Plane Waves by a Cylinder . . . . .	4-17
4.5.1.2	Scattering of Plane Waves by a Sphere . . . . .	4-19
4.5.1.3	Practical Consequences . . . . .	4-20
4.5.2	REFLECTION OF SOUND AT AN INTERFACE . . . . .	4-21
4.6	<u>ANALOG METHODS</u> . . . . .	4-22
4.6.1	BASIS OF ANALOGIES . . . . .	4-22
4.6.2	THE IMPEDANCE AND MOBILITY ANALOGIES . . . . .	4-23
4.6.3	IMPEDANCE VALUES FOR ACOUSTICAL ELEMENTS . . . . .	4-23
4.7	<u>INTERPRETATION OF ACOUSTICAL DATA</u> . . . . .	4-28
4.7.1	ELEMENTS OF SOUND MEASURING SYSTEM . . . . .	4-28
4.7.2	SOUND LEVEL METERS . . . . .	4-28
4.7.3	PRECAUTIONS . . . . .	4-29
4.7.4	ADDITION OF LEVELS IN DECIBELS . . . . .	4-29
	REFERENCES . . . . .	4-30

## CHAPTER 4

### FUNDAMENTALS OF ACOUSTICS

#### 4.1 INTRODUCTION

Acoustics treats the generation, transmission and reception of acoustic waves, both audible and inaudible. The purpose of this chapter is to introduce some fundamental concepts on acoustics so that the methods given in later chapters can be more easily understood and applied. The topics covered here include the physical nature of sound propagation through the air, properties of simple sources radiating into an infinite medium, effects of discontinuities and obstacles in the medium, the use of equivalent analog or network methods to solve acoustical problems, and sources of error in data from acoustical measurements.

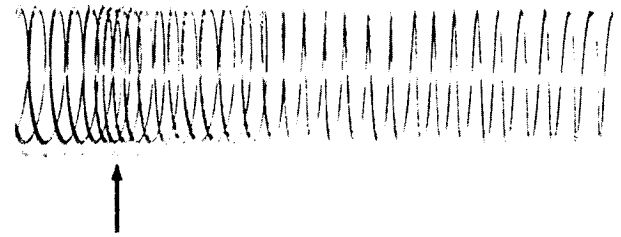
##### 4.1.1 THE NATURE OF ACOUSTIC WAVES

Examples of wave motion are very common. All small-amplitude wave motion has in common two properties:

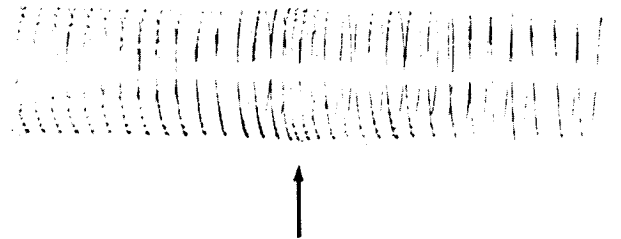
- Energy is propagated to distant points,
- The disturbance travels through the medium without giving the medium as a whole any permanent displacement.

Both of these properties are easily observed in the motion of waves across an initially smooth water surface where a pebble is dropped into the water. The ripples spread outward carrying energy with them, until they meet a solid boundary or the energy is dissipated. Any small float on the water surface is only disturbed as the wave passes, and is not swept bodily along with the wave. Another visible example occurs when one end of a rope lying on the ground is shaken up and down: A wave runs along the rope, the up and down motion being communicated from the end as the wave goes up, just enough to pass the disturbance onward, yet the rope's final position is not changed from its original position. In all these cases the local velocity imparted to the medium as the disturbance passes (particle velocity) is very much less than the velocity at which the disturbance is propagated through the medium.

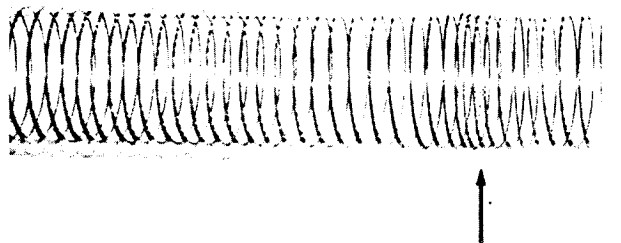
Acoustic waves differ from those in the above two examples in that 1) generally they are waves in three dimensions, and so can be more complicated than those in one or two dimensions, and 2) they are longitudinal waves. In the rope and water wave examples, the waves were transverse; each part of the rope, for example, moved in a direction perpendicular to the propagation direction of the wave as it passed. In the case of acoustic waves in air, the (statistical) average disturbance experienced by the molecules of air is in the direction of the wave propagation. There are no alternating crests and troughs, as with the transverse waves on a water surface, but alternate compressions and rarefactions. This kind of motion can be seen in the longitudinal vibrations of a spiral spring, Figure 4.1. Fluids, such as air or water, have mass density and volume elasticity. The elasticity causes the fluid to resist compression (providing the restoring force that keeps the wave going), and the inertia of the mass density causes the motion to "overshoot" into a rarefaction.



a) Time  $t_1$



b) Time  $t_2 > t_1$

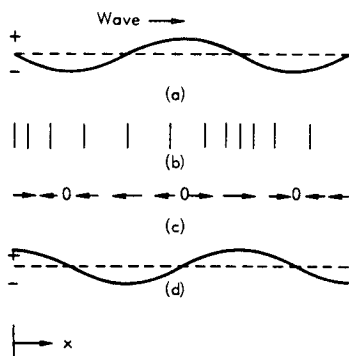


c) Time  $t_3 > t_2$

FIGURE 4.1 Longitudinal Wave in a Spiral Spring

As an introduction to the physical characteristics of acoustic waves, consider the propagation of a sinusoidal plane wave. Plane waves are those whose wave fronts (points of equal phase) lie on a plane surface normal to the direction of propagation. For example, the sound propagated in tubes or at large distances from a source have approximately plane wave fronts. An acoustic disturbance at any point can be defined in terms of the instantaneous displacement of a particle of the medium, the particle velocity, pressure fluctuation, or density fluctuation. The acoustic pressure is the difference between instantaneous and ambient mean pressure. The compression is the fractional change in density (referenced to the ambient mean density). In most cases of practical interest, the acoustic pressure is sufficient to specify a sound field; units in use for acoustical pressure are lb/in<sup>2</sup> and dynes/cm<sup>2</sup>.

A pictorial representation of the phase relationships among the acoustic variables is given in Figure 4.2. For a wave traveling in the +x direction, the acoustic pressure  $p$ , compression  $\tilde{\rho}$ , and particle velocity  $u$  are in phase with each other and lead the particle displacement  $d$  by a quarter cycle. For waves traveling in the -x direction, the particle velocity leads the displacement by a quarter cycle, and compression and pressure lag by a quarter cycle. This difference in phase relations for waves moving in opposite directions occurs because pressure and compression are scalars while velocity and displacement are vectors. Regardless of the propagation direction, a maximum in pressure and compression is associated with a maximum of particle velocity in the propagation direction, and all three lead the maximum displacement by a quarter cycle.



- (a) Particle Displacement  $d$ .
- (b) Particle Spacing when Displaced as Shown in (a)
- (c) Particle Velocity  $u$ .
- (d) Acoustic Pressure  $p$ , and Compression  $\tilde{\rho}$ .

FIGURE 4.2 Phase Relations For a Plane Wave Traveling in the + x Direction, as Functions of Position (From Reference 4.1)

#### 4.1.2 PROPAGATION VELOCITY OF ACOUSTIC WAVES

An acoustic wave is, by definition, of sufficiently small amplitude that it does not alter the temperature of the medium. Its propagation velocity is, therefore, a function only of the medium and not of any property of the wave. In an ideal gas (such as air) the absolute pressure  $p$ , absolute temperature  $T$ , and density  $\rho$  are connected through the equation of state

$$p = \rho RT$$

where  $R$  is the gas constant. The two properties of the gas which influence the wave propagation are its isothermal compressibility  $K$ , and coefficient of thermal expansion  $\beta$ . The isothermal compressibility is the fractional rate of exchange of volume (or density) with pressure, at constant temperature; and coefficient of thermal expansion is the fractional change in volume (or density) with temperature at constant pressure. For a perfect gas, they are simply related to the pressure and temperature, respectively, such that the wave propagation velocity can be shown to be

$$c = \sqrt{\gamma RT}$$

where  $\gamma$  is the ratio of specific heats,  $c_p/c_v = 1.4$  for air at standard conditions (1 atmosphere pressure and 20°C); and the acoustic velocity is 1127 feet per second.

The propagation velocity of acoustic waves in a gas can also be simply derived from kinetic theory. Consider the molecules as they collide with each other and any solid boundaries. The pressure in the gas is caused by its molecular motion and in an ideal gas is given by

$$p = (1/3) \rho \overline{v^2}$$

where  $\overline{v^2}$  is the meansquare molecular velocity and  $\rho$  is the density (composed of the number of molecules present per unit volume). Then the propagation velocity is

$$c = \sqrt{\overline{v^2}/3}$$

In liquids and solids, where intermolecular forces are large, the speed of sound is much larger than this root-mean-square speed of vibration of a molecule about its mean position. In solids,  $c$  is roughly equal to the mean speed a molecule would have if its amplitude of vibration were equal to the mean distance between molecules. However, wave propagation in solids becomes complex, as both longitudinal and transverse waves can occur; see Chapter 3.

### 4.1.3 THE STRUCTURE OF NOISE CONTROL PROBLEMS

All noise control problems involve three basic elements: the sound source, the receiver, and the transmission path between source and receiver. A knowledge of the characteristics of and means of modifying all three is required for an economically efficient solution to any noise control problem. In the simple example of Figure 4.3, the source is the engine noise from a rocket launch, and the receiver may be either the building structure or the occupants of the building. The transmission path includes the effects of the atmosphere and of intervening terrain and obstacles, and of the building structure. The problem may be alleviated by suppression at the source, by modifying the transmission path, by local protection of the receiver, or by the best combination of all three.

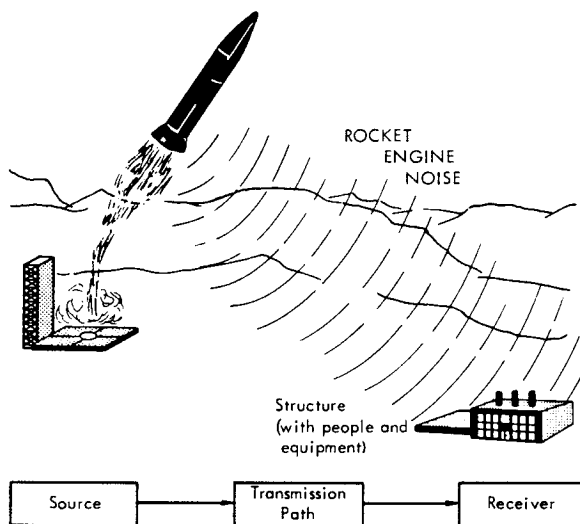


FIGURE 4.3 Elements of a Noise Control Problem

#### 4.1.3.1 Source Properties

The properties of a sound source for which numerical values must be known are its

- Total sound power produced
- Directivity, or angular distribution of the power
- Frequency characteristics of the sound, which can be included by giving directivity as a function of frequency.
- Decay with radial distance from the source, in a free field.

The required properties of acoustic sources relevant to this manual are given in Chapter 6. In the present section, emphasis is placed on some physical concepts helpful in understanding the behavior of these sources.

#### 4.1.3.2 Receivers

In the present application, the possible receivers include structures, people, and sensitive equipment. In each case the criteria for limiting the acoustic exposure, and means of modifying the receiver or protecting it locally in order to raise the acoustic environment limits, must be known by the designer. The subject of receivers is covered in Chapters 8, 10 and 11.

#### 4.1.3.3 Transmission Path

The transmission between source and receiver is affected by propagation (effects of the medium, such as the dissipation or diversion of acoustic energy before it reaches the receiver), by obstacles in the transmission path, and by transmission properties of structures surrounding the receiver. Propagation through the medium is thoroughly covered in Chapter 7, along with shielding effects of buildings, barriers and ground covers. Coverage of sound transmission loss through structures and absorption at surfaces is given in Chapter 9, but an introduction to the reflection and absorption of sound is provided in this chapter.

## 4.2 QUANTITATIVE DESCRIPTION OF SOUND

The fundamental physical quantities, units and reference levels used to describe and measure acoustic waves in air are next introduced. The most fundamental quantity is the acoustic pressure; from measurements of pressure, such secondary quantities (Figure 4.4) as intensity over a given plane, energy density in a given volume, and acoustic power of a source can be calculated under certain field conditions. Since the propagation, transmission and reception characteristics of sound vary with frequency, it is usually necessary to make predictions or analyze data in a form that shows the distribution of pressure or power over the frequency spectrum. Typical precautions and operations required in the use of data from acoustic measurements are briefly discussed at the end of this chapter.

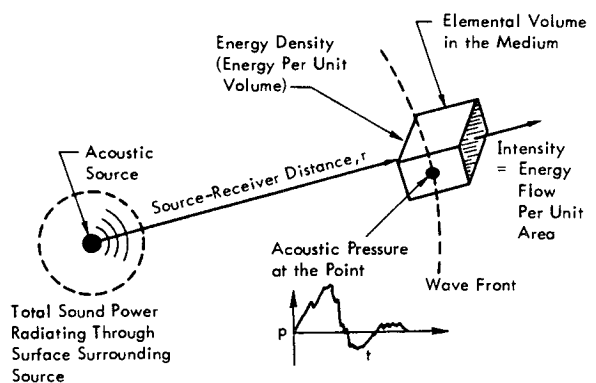


FIGURE 4.4 Conceptual Diagram for Physical Acoustical Quantities

## 4.2.1 DECIBEL SCALE

Because magnitudes of pressure and power encountered in practice range over more than 12 orders of magnitude, it is convenient to use a logarithmic scale and express the resulting levels in decibels. Levels in decibels (dB) are formed from the logarithm of a ratio of the measured quantity to a reference value, and since several reference values are in use, the reference being used should always be stated. Strictly speaking, a level in decibels denotes a ratio of two quantities that are proportional to power. However, common practice has extended the decibel scale to sound pressure levels, for which the proportionality is exact only for plane waves. The decibel scale is often

used to express relative levels; here one of the two quantities being compared is used as the reference level.

## 4.2.2 UNITS

Acoustical quantities are normally expressed in either metric cgs units or mks units. Tables are given in Chapter 12 for conversion among cgs, mks and English units. The most frequently encountered quantities used in acoustics, aside from those used in analog methods (given in Section 4.6) are listed in Table 4.1 in cgs and mks units. A complete list of standard definitions and units (for shock and vibration as well as acoustics) is available in Reference 4.2.

TABLE 4.1  
BASIC ACOUSTICAL UNITS

Quantity	Dimension	cgs Unit	mks Unit	Conversion Factor*
Sound pressure	$ML^{-1}T^{-2}$	dyne/cm <sup>2</sup> (microbar)	newton/m <sup>2</sup>	$10^{-1}$
Velocity	$LT^{-1}$	cm/sec	m/sec	$10^{-2}$
Frequency	$T^{-1}$	hertz (or sec <sup>-1</sup> )	hertz	-
Density	$ML^{-3}$	gm/cm <sup>3</sup>	kg/m <sup>3</sup>	$10^3$
Volume velocity	$L^3T^{-1}$	cm <sup>3</sup> /sec	m <sup>3</sup> /sec	$10^{-6}$
Sound energy	$ML^2T^{-2}$	erg	joule	$10^{-7}$
Sound energy density	$ML^{-1}T^{-2}$	erg/cm <sup>3</sup>	joule/m <sup>3</sup>	$10^{-1}$
Sound intensity	$MT^{-3}$	erg/sec cm <sup>2</sup>	watt/m <sup>2</sup>	$10^{-3}$
Sound power	$ML^2T^{-3}$	erg/sec	watt	$10^{-7}$
Acoustic impedance (resistance, reactance)	$ML^{-4}T^{-1}$	acoustical ohm	mks acoustical ohm	$10^5$
Specific acoustic impedance	$ML^{-2}T^{-1}$	rayl	mks rayl	10

\* Multiply values in cgs system by conversion factor to obtain value in mks system.

**CHAPTER 5**  
**SONIC AND VIBRATION**  
**CONTROL PLANNING**

TABLE OF CONTENTS

<u>SECTION</u>	<u>PAGE</u>
5.1	5-1
5.2	5-1
5.2.1	5-1
5.2.2	5-3
5.2.3	5-5
5.2.4	5-5
5.2.4.1	5-6
5.2.4.2	5-6
5.2.4.3	5-7
5.2.5	5-8
5.2.6	5-8
5.2.6.1	5-8
5.2.6.2	5-9
5.3	5-10
5.3.1	5-10
5.3.1.1	5-10
5.3.1.2	5-12
5.3.2	5-13
5.3.2.1	5-14
5.3.2.2	5-18
5.3.3	5-20
5.3.4	5-21
5.4	5-21
5.4.1	5-21
5.4.1.1	5-21
5.4.1.2	5-21
5.4.1.3	5-21
5.4.2	5-23
5.4.3	5-24
5.4.4	5-24
5.5	5-25
5.5.1	5-25
5.5.2	5-26
5.5.2.1	5-26
5.5.2.2	5-26
REFERENCES	5-26



## CHAPTER 5

### SONIC AND VIBRATION CONTROL PLANNING

#### 5.1 INTRODUCTION

The development of new or enlarged ground facilities for the testing or launching of rocket vehicles requires a concerted planning effort well in advance of starting construction. Decisions reached during this planning stage may involve major commitments of resources in manpower, finances, and materials. These decisions must be made on the basis of a systematic evaluation of a series of alternative choices which may involve such elements as

- Site location
- Land acquisition
- On-site facility lay-out
- General concepts for protective design

As this decision process gains momentum, more detailed problems become significant, often requiring supporting trade-off studies to provide a reasonable basis for making a choice between one or more design concepts. Ultimately, a detailed development plan evolves, which must be implemented by a technical staff employing a broad spectrum of skills including experience in:

- Land utilization
- Architectural design
- Facility operational requirements
- Civil and mechanical engineering design
- Electronic and electromechanical equipment design
- Human factors design
- Medical safety

Thus, the purpose of this chapter is to: 1) provide a general guide for carrying out this planning effort in the area of sonic and vibration environments, 2) briefly review the principal design criteria involved for the protection of structures, personnel and equipment in these environments, and 3) review the general concepts for environmental control which can be employed to meet these criteria. The chapter forms a logical introduction to the specific technical material contained in the succeeding chapters which consider the various technical facets of sonic and vibration environments for ground facilities in more detail.

#### 5.2 THE SYSTEM APPROACH

A logical starting point for this planning guide is to consider the system approach for defining the basic control concepts to be evaluated in detail.

The scope of problems discussed ranges from the decision that a new rocket ground test or launch facility is required to the beginning of detail design for a single facility unit. Therefore, it will be of interest (1) to the project leader/planner who will be making the early, large-scale decisions and (2) as introductory material to the engineer/designer who will be responsible for the design of each facility unit and will be utilizing the design chapters of this manual. For convenience, the term vibro-acoustic, employed in this next section, will be understood to imply all of the acoustic, blast and vibration environments to be considered.

##### 5.2.1 ELEMENTS OF THE GENERAL VIBRO-ACOUSTIC DESIGN PROBLEM FOR A ROCKET FACILITY

Every vibro-acoustic design problem can be condensed, in its simplest form, into a source-transmission path-receiver relationship. The design problem is to control the vibro-acoustic environment at the receiver so that it does not exceed some maximum allowable level established by the receiver, by selecting that combination of design solutions which corresponds to minimum system cost. That is,

$$\text{(Source Characteristic)} + \left[ \sum \text{(Control Elements)} \right]_{\text{min. cost}} \\ = \text{Receiver Criterion Level}$$

The technical elements of the vibro-acoustic protection design problem (listing specific categories of sources, path elements and receivers applicable to rocket facility planning) are given in Figure 5.1. The figure also refers to chapters of the manual containing specific design information in each of the categories.

##### Sources

The sources are listed in order of their importance in setting the design strength for facility components. This is followed by a listing of the support equipment necessary to any rocket testing complex. The blast and engine noise sources are subdivided into

- Ground test facilities
- Launch facilities.

This division is necessary because there are more methods available for reducing the source magnitude for captive rocket firings than for rocket launches. In ground test facilities, the engine noise can be suppressed by selected or modified terrain, and the amount of propellant available

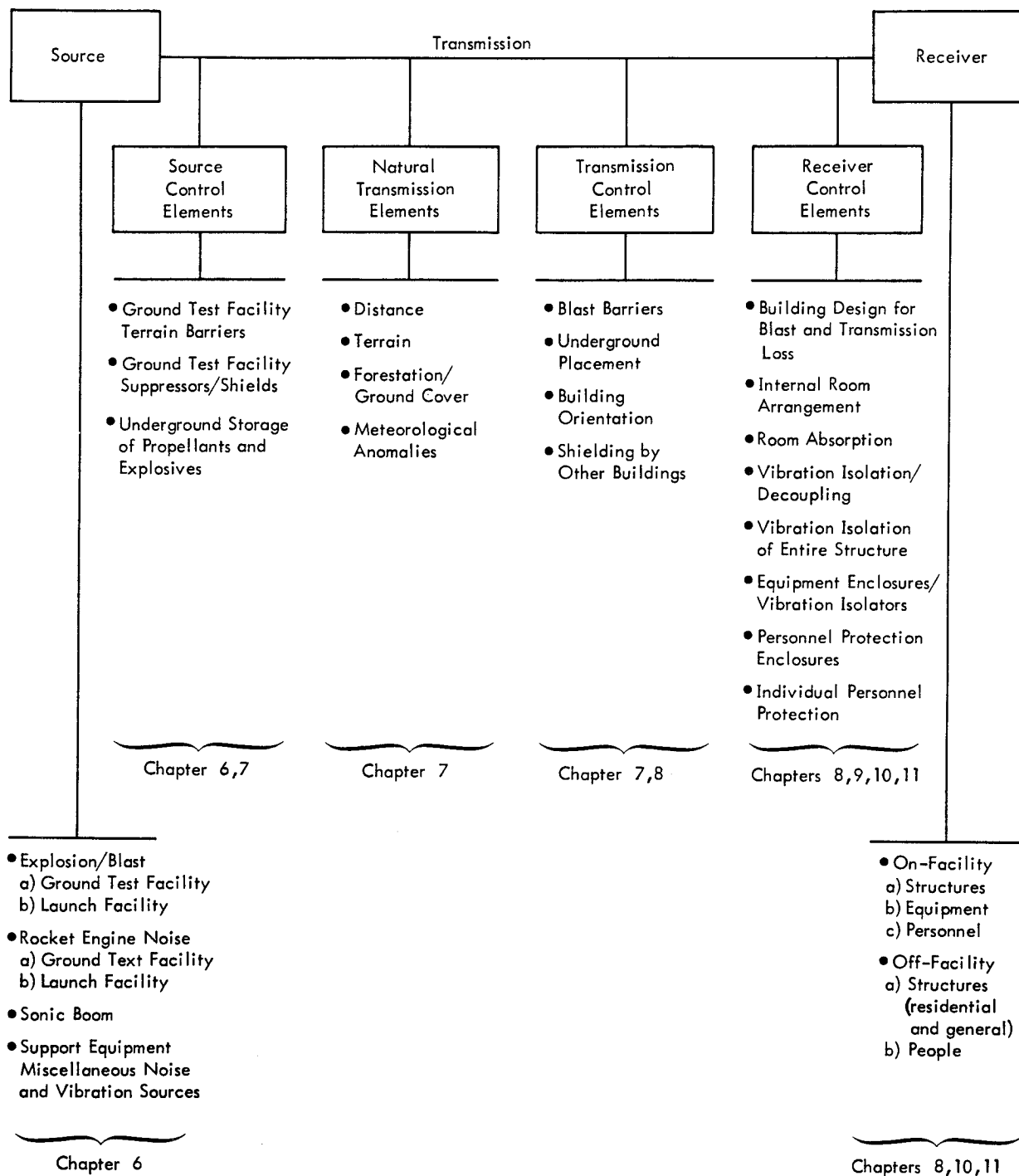


FIGURE 5.1 Technical Elements of Protective Design for Sonic Loads and Vibro-Acoustic Environments

for an explosion can be limited by underground storage and automatic shutoff mechanisms. Figure 5.2 compares the sources of lateral building loads with the two natural loadings (wind and earthquake), for which design criteria in building design are customary.

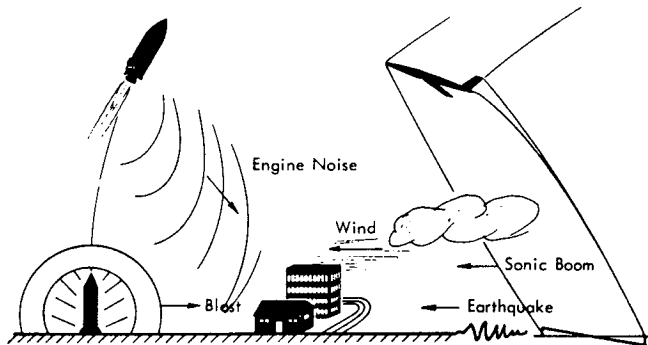


FIGURE 5.2 Sources of Lateral Building Loads at Rocket Test Sites

#### Receivers

The receivers are listed in Figure 5.1 in groups according to the degree of control that can be utilized in their protection:

- On-facility receivers
- Off-facility receivers.

The facility designer can control the location and design of all structures and equipment, and can control the exposure of personnel by establishing "restricted areas" within the base perimeter. However, once the rocket site location is selected and sufficient land purchased to provide a buffer zone for any surrounding (present or future) communities, there is usually no further means available for the facility manager to protect the structures or people in those communities short of curtailing the test operations. Thus, the initial site selection and required land acquisition is a critical initial problem to be resolved.

#### Transmission Path

The transmission path between any source-receiver pair must include all control elements (relevant to that specific pair) necessary to bring the environment down to the limits implied by the receiver. The transmission path, Figure 5.1, is subdivided into source control elements, (implying localized treatment of the source), receiver control elements (with magnitudes subject to influence by careful site selection and placement of sources and facility units), and those elements of transmission path control requiring engineering design and construction. The lists of sources and receivers are complete; while the transmission path elements are typical, to illustrate the general nature of the protection design problem. Each of the decrements in the transmission path implies an element of cost which will feed into the final system selection process.

### 5.2.2 PROBLEM SCOPE

The problems to be solved in a facility design project begin with the initial decision that a facility is required and involves consideration of the range of engine size/thrust levels and propellant types, plus a time span of operational years for the facility. The scope of the problems to be considered decreases (while the level of detail required for solution increases) as the facility design project proceeds along a time scale such as illustrated in Figure 5.3. The facility design process may be broken down into three major phases:

- Site selection
- Site Layout planning
- Design of facility units.

#### Site Selection

Site selection involves choosing a geographical location which will satisfy all the requirements relevant to a rocket facility, including, for example, supporting logistic and transportation facilities, power and communications; for a launch facility, the effect of geographic location on orbits which can be attained is an important factor. Clear space for protection of surrounding communities will be required in case of nuclear rocket or toxic fuels accidents.

The vibro-acoustic portion of the site selection phase includes the establishment of an outer facility perimeter and an inner limit boundary for adjacent communities, with an intermediate buffer zone cleared of residents and maintained clear in the future by land purchase (see Figure 5.3a). The expense of relocating whole communities and the variation of land prices in different regions may have a large influence on the location of the rocket facility. The extent of the buffer zone will usually be determined by the blast environment from explosions for launch bases, but may be determined by community noise from rocket engine firings, particularly for rocket ground test facilities where the blast source size and location are sufficiently controlled. Establishment of the land area for the facility and its perimeter will require tradeoff considerations of distance versus design in order to protect facility units, as well as surrounding communities, from blast and noise. In fact, it is in the site selection phase that the major step toward protection of the surrounding communities can be achieved.

#### Site Layout

The site layout planning phase consists of the placement of the facility units within the facility perimeter (Figure 5.3b). Environmental protection (e.g., hilly terrain, dense forest, distance) may be utilized to obtain maximum separation of blast or noise sources from sensitive receivers. Figure 5.4 illustrates the importance of distance between source and receiver in determining the design loads on the receiver.

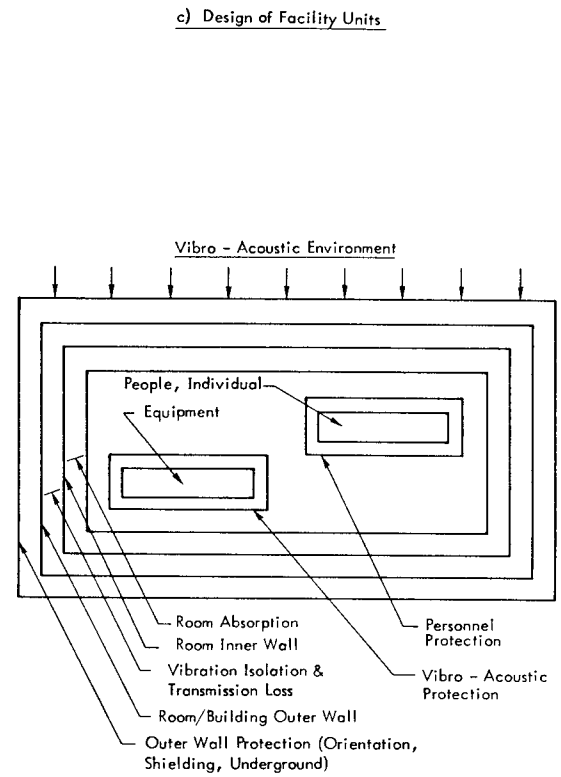
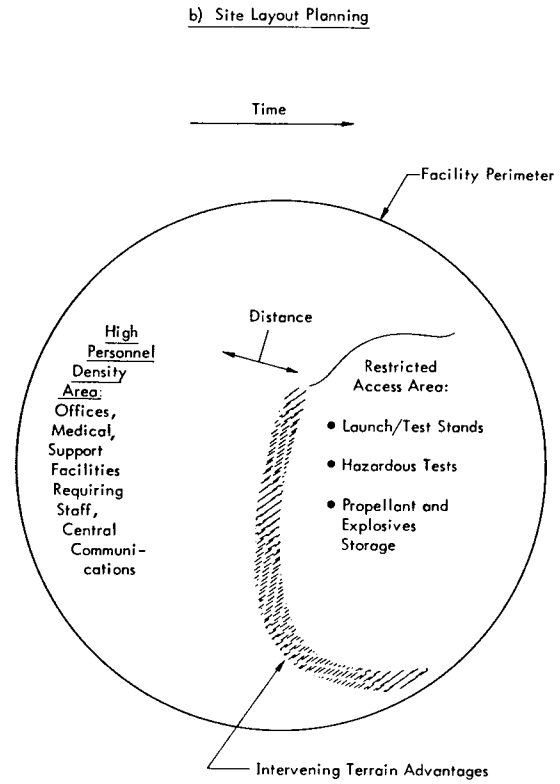
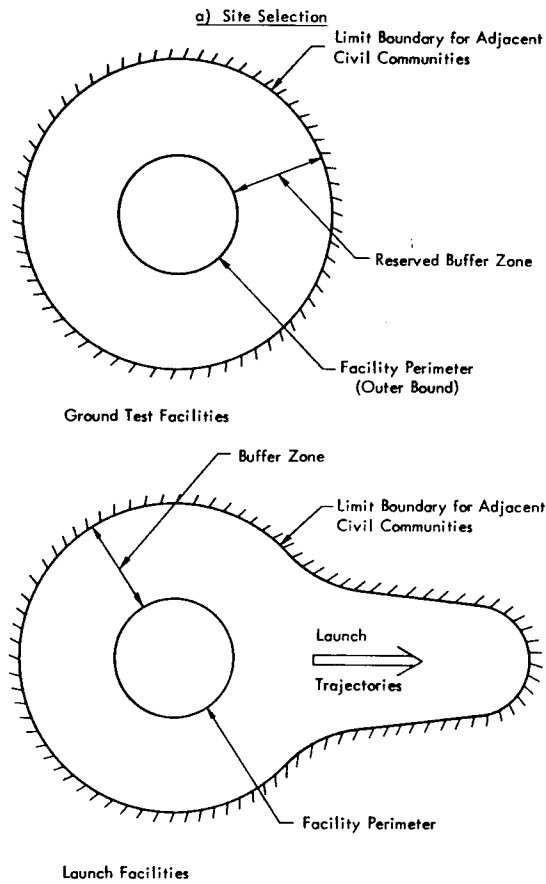


FIGURE 5.3 Problem Scope in Order of Decreasing Scale

For planning purposes, various functional elements of the facility are classified by criteria levels, and receivers are grouped within each function. Judicious placement of functions on the facility map will greatly influence the total cost of noise and blast protection.

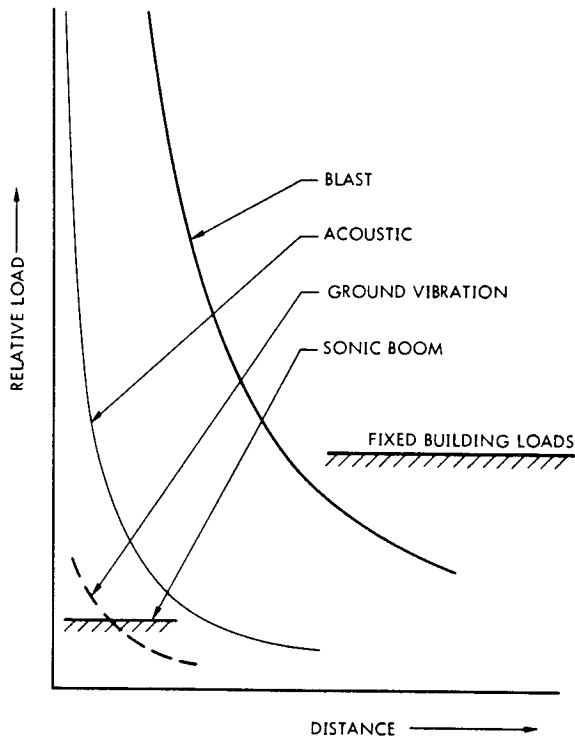


FIGURE 5.4 The Importance of Distance as a Protective Measure

Once the function and location of each facility unit has been established in the layout phase, the next step is the design of each unit (Figure 5.3c). A facility unit may be defined as any structure or building on the site. The required amount of total transmission path control is established by the environment at that location and the criteria for the receiver. In designing a unit which will contain personnel and equipment, each of the three sets of receiver criteria must be considered, and the dominant or design-critical source determined for each. In general, the most cost-effective set of design solutions for a facility unit involving several receiver types will be that combination which meets all criteria, but does not exceed any. This implies that no segment of the transmission path has been overdesigned. For example, in a building designed to withstand blast, and only occupied by personnel during firings, the personnel hearing loss criterion would not be allowed to cause major overdesign of the building

### 5.2.3 SYSTEM COST MINIMIZATION

Aside from the necessary protection of life and health and the requirement that all the facility units fulfill their operating function, the single theme running through the entire design process is cost. Every design solution implies a cost figure, and cost tradeoff studies will be required at different levels as the facility design progresses. The minimization of total system cost is the criterion by which alternate solutions can be compared. Preliminary cost studies, while inaccurate compared to later detailed cost estimates, should be used to identify parameters having a large influence on total system cost, and to guide the large, early decisions of site selection and layout. A simple illustration of a cost trade-off evaluation is given in Figure 5.5, using site selection for a ground test facility as an example. The tradeoff is between (a) the cost of control at the source (e.g., constructed barriers or suppressors for rocket engine noise at the test stands, and undergrounding and blast-proof flow cutoff mechanisms for propellants and (b) the cost of land acquisition to increase the distance to inhabited areas. In an actual case, there would be a family of source control cost curves, corresponding to degrees of control. While the minimum cost point is controlling in the example shown, the minimum acceptable distance for protection of life and health in adjacent communities may control in others, if it falls to the right of the minimum cost point.

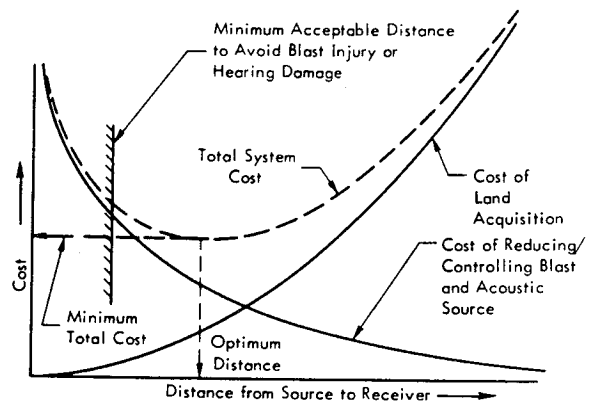


FIGURE 5.5 Cost Minimization Example: The Site Selection Problem for a Ground Test Facility

### 5.2.4 TYPICAL ENVIRONMENT TRENDS APPLICABLE TO SITE PLANNING

Site selection and facility layout planning considerations require two basic types of information about each major source:

- Magnitude variation with distance
- Time-dependent characteristics

For the sake of illustration, Figures 5.6 through 5.11 show qualitative trends of these two factors for the two major types of source inherent in a rocket facility. Ground vibration, while not necessarily a major design environment, is also illustrated:

- The acoustic environment from rocket engine firings
- The ground vibration from rocket engine firings
- The blast environment from propellant explosions

The natural forces (wind and earthquake) may set design requirements for some facility units, but they are not influenced by facility unit location on the site, and so are not included in these figures. These various environments are covered in detail in the next two chapters.

#### 5.2.4.1 The Acoustic Environment From Rocket Engine Firings

The acoustic environment (airborne noise) from rocket engine firings can be grossly described in terms of the overall sound pressure level variation with distance (Figure 5.6) and the frequency distribution of acoustic energy (Figure 5.7). The overall acoustic power level (and hence the sound pressure level at a given distance) can be estimated for a rocket of any size from its thrust and exit velocity. Approximately 0.4 percent of the jet mechanical energy is typically converted into acoustic energy; the conservative extreme is 1 percent. Ideally, every doubling of distance between the source and receiver decreases the overall sound pressure level at the receiver by 6 decibels. Additional atmospheric attenuation can provide a further significant reduction in overall noise levels for distances beyond 4 miles. Conversely, extreme conditions of atmospheric focusing can result in levels appreciably higher than expected for the normal attenuation. As discussed in Chapter 7, an upper bound for focusing conditions is approximated by decreasing the sound levels at a rate of only 3 dB per doubling of distance.

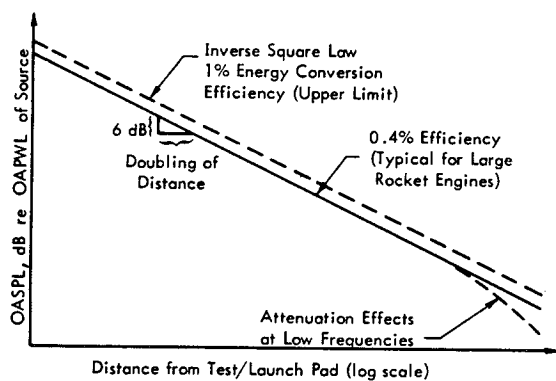


FIGURE 5.6 Magnitude Trend with Distance, Acoustic Environment from a Rocket Engine Source

#### Rocket Noise Frequency Spectrum

Besides generating more total acoustic power, larger rockets produce relatively more of their acoustic power at low frequencies, Figure 5.7. When the distribution of sound pressure across the frequency spectrum (relative to overall sound pressure level) is plotted against a dimensionless frequency, all rockets fall into a single line. As a result, given the measurement point and the rocket exit diameter and exit velocity, (1) the rocket noise spectrum can be predicted and (2) larger exit diameters result in a shift to lower frequencies. Peaks in the vicinity of 20-50 Hz for Saturn class vehicles shift to 8-10 Hz for 10-20 million pound thrust rockets. Since the shift is accompanied by an increased level for the entire curve (Figure 5.7), increases on the order of 10 dB can occur at frequencies below 20 Hz.

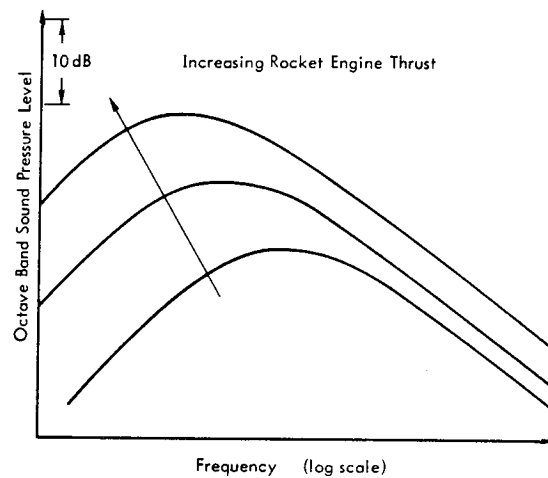


FIGURE 5.7 Trend of Acoustic Energy Distribution Over the Frequency Range with Increasing Rocket Size

#### 5.2.4.2 The Ground Vibration Environment From Rocket Engine Firings

In acoustic fields of the magnitudes generated by large rocket firings, the airborne waves can induce appreciable ground vibrations. However, these ground vibrations are a result of local pressure fluctuations in the acoustic wave traveling out from the source.

In this case, the ground tends to act like just another acoustic medium and the frequency spectrum of the ground vibration is very similar to that of the acoustic spectrum; Figure 5.8. However, potentially damaging levels of air-coupled ground vibration are unlikely except in the immediate vicinity of a rocket stand. In this region, direct coupled vibration induced by fluctuating engine thrust forces and the turbulent exhaust blast on the ground may predominate. This direct coupled or seismic vibration attenuates much more rapidly with distance than the air coupled ground vibration; See Figure 5.9. Thus, beyond the immediate vicinity of a test stand or launch pad area, ground vibration is not expected to be a significant design load.

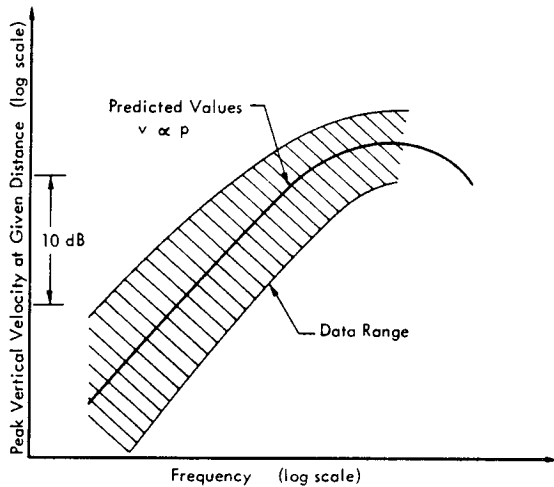


FIGURE 5.8 Trend in Spectrum of Ground Vibration Velocity from Rocket Firings

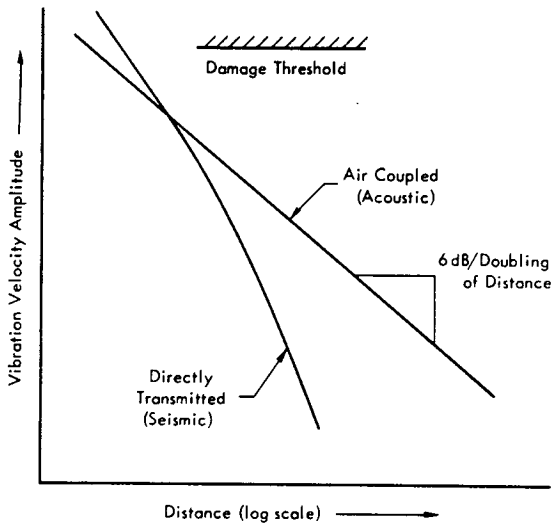


FIGURE 5.9 Illustration of Trend in Attenuation with Distance of Air-Coupled and Direct Coupled Ground Vibration Near Rocket Test Stand

It should be noted that for above-ground buildings, the vibration protection design requirements in a rocket noise field are established by the acoustic field itself and not the induced ground vibrations. Underground buildings located close to a test stand (i.e., less than 1000 ft) may require some vibration isolation from the ground vibration in this region.

5.2.4.3 Blast Environment

The blast environment from possible propellant explosions is often the dominant source in site selection and function placement, and the controlling design factor for many facility units (e.g., for distances on the order of 3 - 5 miles). This is particularly true for launch facilities (as opposed to ground test facilities) where the entire propellant supply of the launch vehicle is potentially available for an explosion. Therefore, consideration of the

blast overpressure magnitude and duration trends with distance, Figure 5.10, will play a crucial part in the facility design. Specific values for these parameters will be given later in this chapter in terms of the equivalent weight of TNT of the propellants.

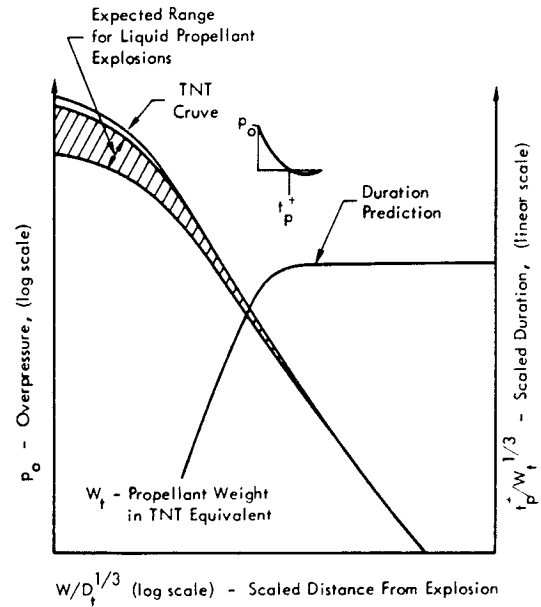


FIGURE 5.10 Magnitude and Duration Trends, Air Blast Environment from Propellant Explosions

Assessing the methods and costs of designing a building against failure from blast involves a consideration of the duration of the blast relative to the natural period (i.e.,  $1/(\text{natural frequency})$ ) of the structural walls exposed to the blast. This dynamic response effect can be translated into an effective static pressure on the building, Figure 5.11, which would produce the same peak deflection of the walls.

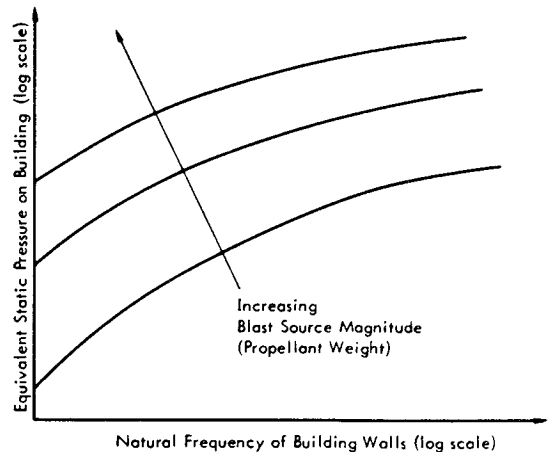


FIGURE 5.11 Trend in Equivalent Static Pressure with Natural Frequency of Building Walls for Given Source Distance and Several Blast Source Sizes

5.2.5 DETERMINATION OF THE DESIGN-CRITICAL CASE

Any receiver on a rocket facility will be exposed to an environment from several major sources, and a determination must be made as to which source produces the controlling environment for the design.

For the case where the receiver is a building, Figure 5.12 illustrates the trends (with distance from the source) for all the dynamic loads in addition to normal static design loads. All the dynamic loads have been reduced to equivalent static loads, to provide a single-number-scale comparison, from which the design-critical source can be selected. The design level for wind and earthquake loads depend on the meteorological and geological records of the area (and in many cases, standard building requirements for structural design.) Although sonic boom overpressure is shown as a dynamic input load, it will not be significant as a design load on primary building structures due to necessary operational restrictions placed on super-sonic aircraft flights.

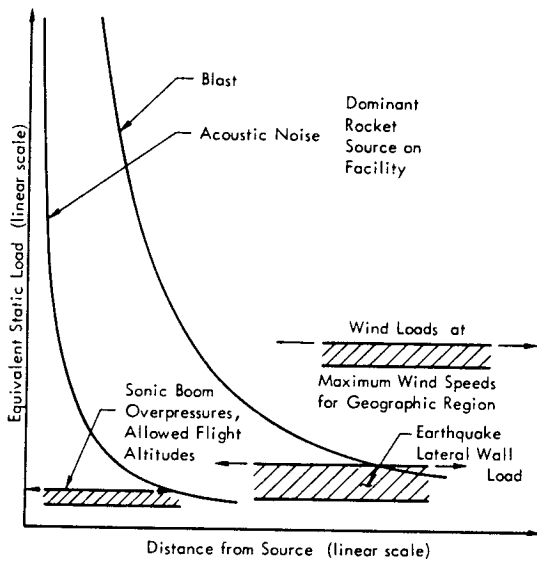


FIGURE 5.12 Screening to Select the Design-Critical Source by Comparison in Terms of Equivalent Static Loads

If the building represented in Figure 5.12 is designed to survive a blast environment, it will generally be more expensive than one designed only against acoustic noise, for regions near the source. For large rockets, the region in which blast is the controlling source has a radius of 3 to 5 miles.

For structures and equipment not involving personnel safety, the decision on the degree of blast protection to be provided is an economic one, made by comparing the cost of a given level of protection against the cost of replacement or repair of failed units, Figure 5.13. This

comparison requires a prediction of the probable number of failure-critical blasts during the facility lifetime. The crossover point may be markedly different in the case of a launch facility (where a launch vehicle explosion is a major disaster and is guarded against by many precautionary measures and preflight checks) as compared with a ground test facility for development work (where explosions are more frequent and inevitable).

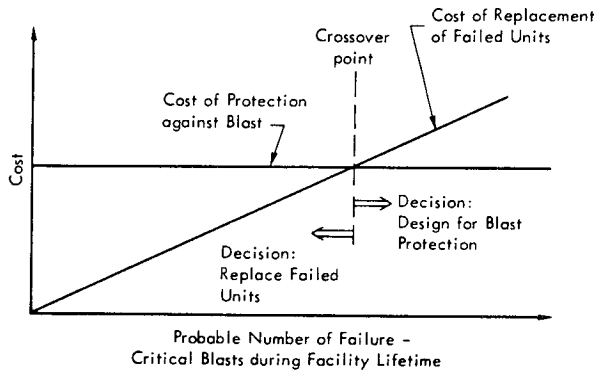


FIGURE 5.13 Cost-Based Decision on Necessity for Vibro-Acoustic Protection of Structures and Equipment Units not Involving Personnel Safety

5.2.6 THE DESIGN PROCESS FOR A FACILITY UNIT

Given a facility unit of defined function and location for which internal and external environmental criteria are defined, the designer must then develop a concept which meets all the technical requirements (the usual functional requirements as well as the vibro-acoustic criteria) at near-minimum cost or within budget.

5.2.6.1 The General Design Process With Vibro-Acoustic and Cost Considerations

The flow of the design process, for any general facility unit design problem with vibro-acoustic inputs, is diagrammed in Figure 5.14. The designer is given a description of the building functional requirements, of which the vibro-acoustic portion are the criteria for an acceptable environment and the actual local environment expected from the various vibro-acoustic sources. From this initial point, the process proceeds through the preliminary design phase, including layout of the functional spaces within the building (with vibro-acoustic inputs such as orientation with respect to the source and shielding of one room by others). The initial preliminary design phase culminates in a technically feasible design meeting the criteria, with its cost estimated. An iterative process of modifying design solutions (and sometimes compromising on the criteria) follows, until a suitably cost-effective preliminary design has been achieved. This forms the basis for the detailed design, specifications and cost estimate for the facility unit.



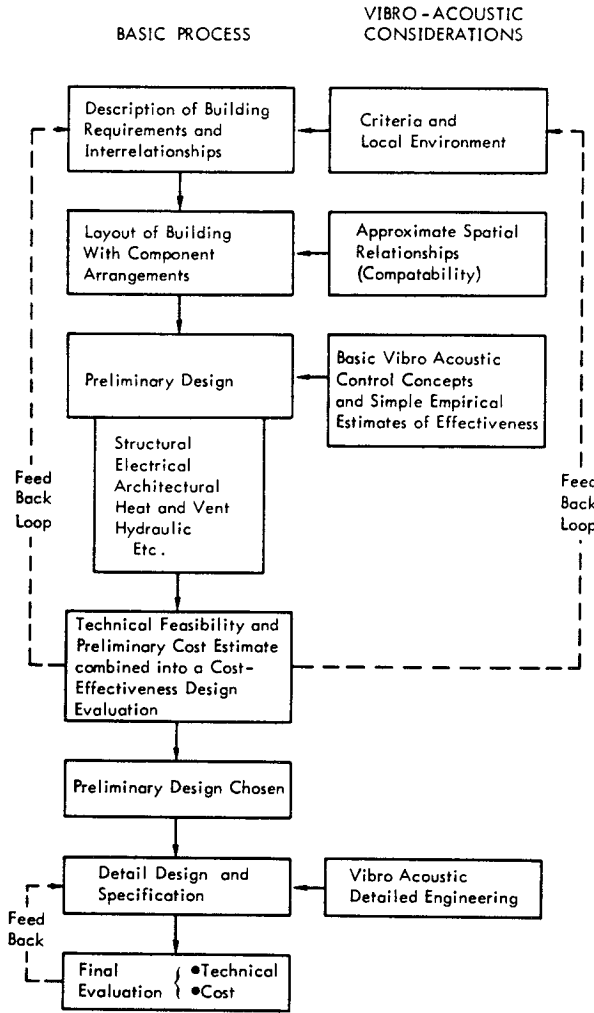


FIGURE 5.14 A Typical Design Process with Addition of Vibro-Acoustic and Cost Considerations

5.2.6.2 Design Check Lists

As a rough guideline to the technical content of the protective design process, design check lists are given below for the three classes of receivers:

- Structures
- Personnel
- Equipment

These check lists relate only to the vibro-acoustic considerations in the design process and must be supplemented by coverage of the other (standard) design requirements.

Protection of Structures Against Blast, Acoustic and Vibration Environments

- During site selection, use adjacent structures and terrain for shielding against blast and acoustic pressure waves; orient heaviest wall towards probable source and/or construct additional shielding walls; alternatively, plan for partial or total underground placement.

- Employ wall and roof venting to equalize pressure loading when protected interior is not essential; or include blow-out panels in walls.
- Where architecturally feasible, use curved external walls for extra stiffness and resistance to blast pressure waves.
- Minimize lengths of unsupported flat roof and wall spans to provide for added stiffness and reduced deflection and stress levels; and stagger supports in order to localize vibrations; also, consider double wall construction when economically feasible, and use air gap as decoupling mechanism.
- Design for added bracing of joints between walls, floors and roof to limit joint deformation and possibility of joint separation and failure; or construct joints with large inertial discontinuities to provide vibration reflection boundaries and limit vibration transmission through structure; or construct open joints with minimum of structural load transmitting capabilities to minimize vibration transmission.
- Limit use of large glass windows, and provide soft rubber mounting at edges at all necessary windows; use special glass having high transmission loss; and externally shield windows from source.
- Avoid use of internal masonry when this could possibly crack and collapse, and lead to personnel injuries.
- Minimize use of large unsupported panels near regions of high intensity noise. Add damping by insulation or surface coating to reduce sonic vibration. Anticipate fatigue failure sensitivity around any joint, particularly when stress gradients are very high.
- For blast designed structure, allow plastic deformation whenever feasible to minimize conservative design problems.
- Optimize balance of design requirements for blast resistance of walls and doors to achieve maximum economy in construction.
- Whenever possible, increase separation of structure and blast or noise sources so as to prevent dynamic loads becoming the critical design load.

Personnel Protection

- Composite noise rating in nearest adjacent communities due to rocket firings below acceptable level for all anticipated engine sizes.
- Distance to nearest adjacent community sufficient to insure against glass breakage from blast, for largest propellant charge anticipated.
- Facility restricted areas with limited personnel access (a) during hazardous propellant transfer operations, and (b) during rocket firings.
- Blast-proof buildings for all personnel participating in hazardous/rocket firing operations.

- Inhabited structures designed to isolate personnel from the low vibration frequencies critical to human performance.
- Hearing protection devices provided and required where set by rocket-firing noise levels.
- Support and office personnel protected from blast and broken glass injury (e.g., by distance/building orientation/glass shield screening).
- Support/office/communications personnel provided with adequate speech communication environment (e.g., by distance, building design).

#### Equipment Protection Design Against Vibration Due to External Sources

- Minimum use of cantilevered mounting for parts.
- Use of chassis-clamps for wire lead-connected components larger than about 0.4 in. in diameter.
- Wire lead connections made to minimize fatigue failure (e.g., short leads with some slack plus insulation covering to provide damping).
- Internal and external wiring laced into a cable and secured to chassis at frequent intervals to prevent conductor vibration fatigue.
- Use of close-fitting alignment pins or guides to bear shock and vibration loads between chassis, assemblies and enclosures.
- Heavier parts located as close as possible to load bearing structure.
- Maximum rigidity of mounting chassis without excessive weight.
- Adequate reinforcement at corners of mounting structure and at other stress concentration points.
- Proper bend radii of sheet metal parts.
- Minimum unsupported spans of circuit cards.
- Static balance of rotating or pivoting parts.
- Minimum use of large unsupported cabinet walls for component mounting.
- Proper choice and application of shock mounts to achieve desired isolation with minimum cross-coupling between modes of vibration.
- Adequate clearances to avoid collision.

### 5.3 DESIGN CRITERIA FOR SONIC LOADS ON STRUCTURE

The preceding section has developed, in general form, the system approach utilized for evaluating sonic loads on ground facilities and the essential steps in the design process. The basic initial input to this process for sonic or vibro-acoustic loads is the specification of environmental criteria - in other words, the definition of environmental levels to which the facility element must be designed (or protected) to be able to perform its function.

#### 5.3.1 CONVENTIONAL LATERAL DESIGN LOADS ON BUILDINGS

In order to put these criteria in perspective, conventional static lateral design loads on building walls due to wind and earthquake forces are considered first.

##### 5.3.1.1 Wind Loads

Maximum wind loads on a building depend on (Reference 5.1):

- Wind Speed -  $V$
- Height above ground -  $H$
- Gust Factor -  $C_{GH}$
- Shape Factor -  $C_R$
- Geographical location
- Storm Frequency

The last two factors must be determined individually for each location based on local measurements. Standard procedures for determining the wind load on terms of the first four factors are summarized as follows using the procedures specified in Reference 5.1.

#### WIND SPEED

Design wind speeds are given in terms of the fastest-single-mile wind speed equal to the wind speed in miles per hour based on the shortest recorded time interval the wind traveled horizontally a distance of 1 mile and measured at a distance of 30 feet above the ground. Standard values for this wind speed, based on a 50 year recurrence interval, range from 60 to 120 MPH in the United States. (Reference 5.2). For sea level conditions, the steady "dynamic" pressure due to this wind is

$$q_o = \frac{1}{2} \rho V^2$$

$$= 0.00256 V^2 \text{ lb/ft}^2$$

where  $V$  = velocity in MPH

Height above Ground

At distances other than 30 ft, the wind velocity  $V_H$  at height H is computed by the "1/7"th power law as

$$V_h = V_{30} \left( \frac{H}{30} \right)^{1/7}$$

Gust Factor

A standard gust factor  $C_{GH} = 1.3$  is normally used to increase the fastest-single-mile wind speed so that the fastest gust velocity  $V_{i30}$ , at 30 ft is

$$V_{i30} = C_{GH} V_{30}$$

Shape Factor

The resultant wind pressure on a rectangular building is equal to the incident wind dynamic pressure multiplied by a shape factor  $C_R = [0.8 - (-0.5)] = 1.3$  where (0.8) represents the relative pressure on the windward face and (-0.5) represents the relative suction pressure on the leeward side.

Wind Load

From the above relationships, the resultant design wind pressure on a rectangular building at any height H is

$$P_{iH} = C_D 0.00256 (V_{iH})^2$$

$$= 0.00333 (C_{GH} V_{30})^2 (H/30)^{2/7} \quad (5.1)$$

For H = 30 ft, and  $C_{GH} = 1.3$ , this reduces to a resultant design wind pressure at 30 ft of

$$P_{i30} = 0.00562 V_{30}^2 \text{ lb/ft}^2 \quad (5.2)$$

Values for this resultant wind pressure on rectangular buildings are shown in Figure 5.15. Similar design wind loads are specified in standard building code manuals.

The wind load on the windward wall of the building (at a height of 30 ft) will be equal to (0.8/1.3) or 0.615 times the values given by equation 5.2. For hurricane winds, such as at Cape Kennedy, the maximum wind velocity, including gusts, is used in place of  $C_{GH} V_{30}$  in equation 5.1.

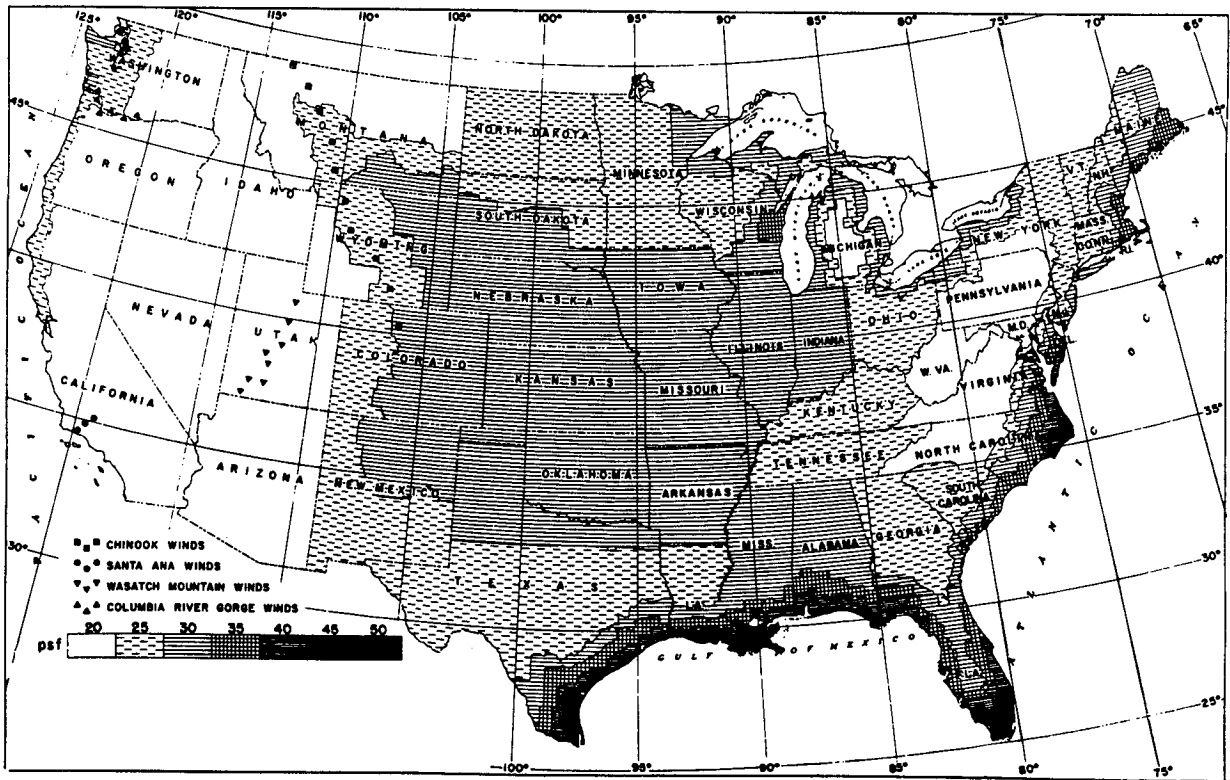


FIGURE 5.15 Minimum Allowable Resultant Wind Pressure at 30 Feet (Reference 5.1)

Spectrum of Wind Load

These wind pressures are considered equivalent to static loads even though they are based, in part, on maximum loads during momentary gusts. The actual frequency spectrum of storm turbulence near the ground has been reported in Reference 5.3 and, as shown in Figure 5.16, the peak frequency of the mean square fluctuating velocity is well below natural frequencies of building components. Thus, the dynamic portion of design wind loads is generally negligible.

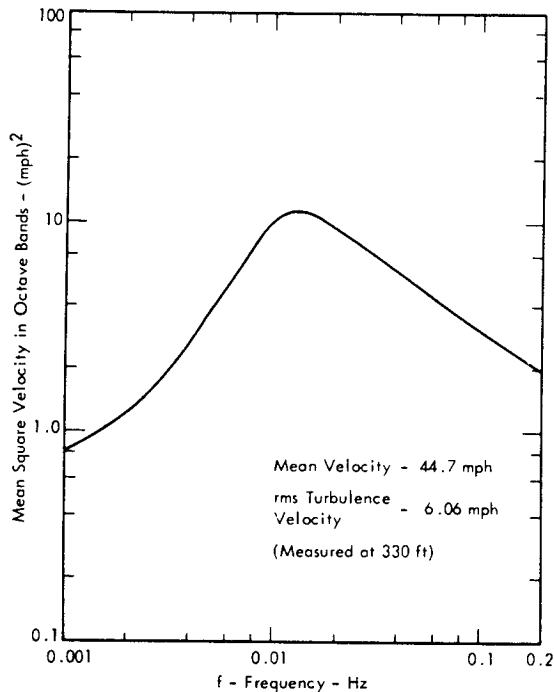


FIGURE 5.16 Spectrum of Fluctuating Velocity Components in a Strong Wind. Expressed as the mean square velocity in (mph)<sup>2</sup> over octave band intervals (data from Reference 5.3).

5.3.1.2 Earthquake Loads

Lateral loads are imposed on buildings during excitation by earthquakes. Conventional building code methods for specifying the magnitude of these lateral loads normally reduce to the following simple procedures.

Net Horizontal Loads on Entire Building

$$\text{Total Lateral Force} = C \cdot W \tag{5.3}$$

where  $W$  = Weight of Building  
 $C$  = load factor in g's that varies with frequency

A typical value for the load factor  $C$  is shown in Figure 5.17 for buildings in the seismic zone 3 for the United States. This is the zone of most damaging earthquakes as illustrated in Figure 5.18.

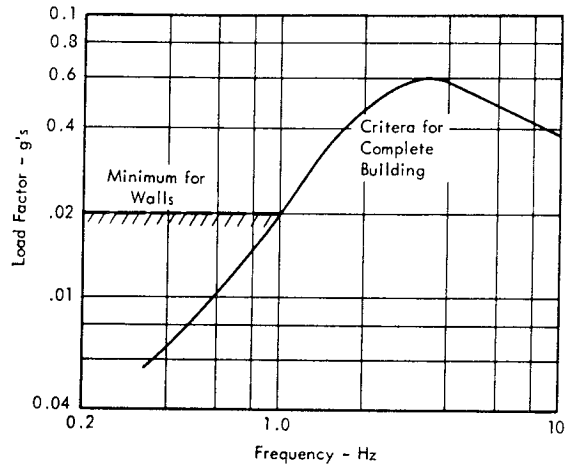


FIGURE 5.17 Typical Spectra for Earthquake Load Factor - Seismic Zone 3

Lateral Load on Building Walls

$$\text{Pressure} = C_p \cdot W \tag{5.4}$$

where  $C_p$  = constant load factor = 0.2 g's  
 $W$  = surface weight of wall - lb/ft<sup>2</sup>

This is a highly simplified method for specifying the dynamic loads imposed by earthquakes in terms of an equivalent static inertial load. The next level of sophistication in determining the load is often based on the use of a shock response spectrum such as illustrated in Figure 5.19.

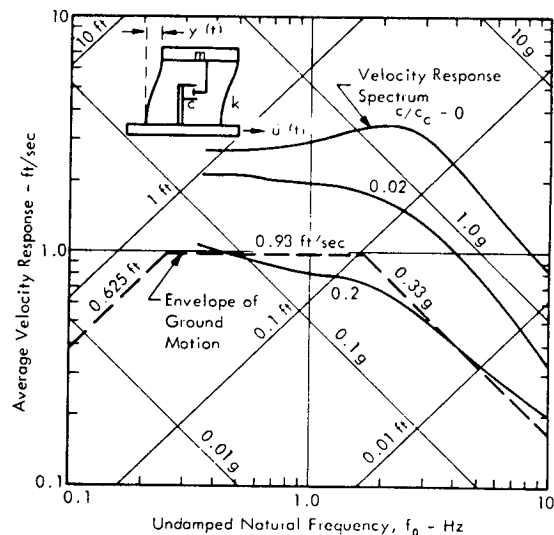


FIGURE 5.19 Average Velocity Displacement and Acceleration Response Spectrum Equivalent to the El Centro, 1949 Earthquake (Solid Lines) Compared to the Maximum Envelope of the Observed Ground Motion for this Earthquake (Dashed Line) (Data from Reference 5.4)

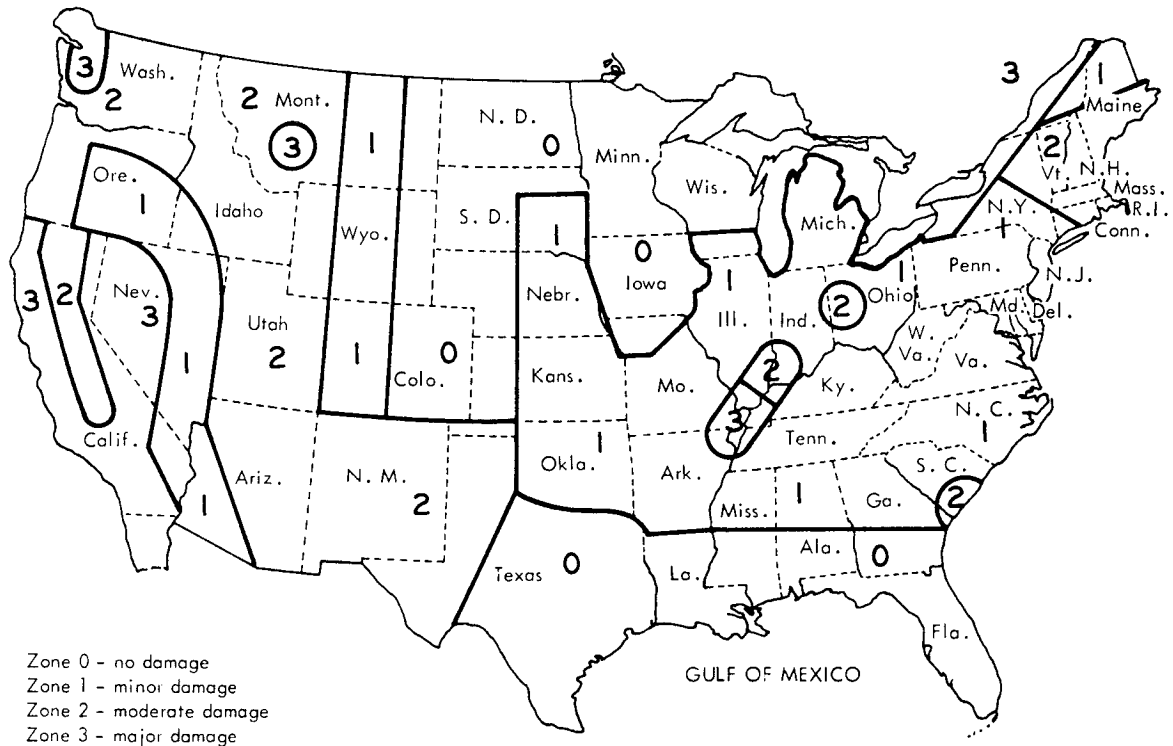


FIGURE 5.18 Seismicity Zones of the United States Based on Structural Damage by Earthquakes (Reference 5.4)

This shows the envelope of the maximum displacement, velocity, and acceleration response of the simple mass-spring system illustrated in the figure with varying degrees of damping (specified by the critical damping ratio  $c/c_c$ ) for a lateral base motion equal to the actual ground motion recorded for a typical "design" earthquake. The envelope of the ground motion recorded for the El Centro, California 1940 earthquake is also shown in the figure. Buildings exposed to this severe input motion would experience a lateral motion at about 0.33 g at frequencies above 2 Hz and about 0.9 ft/sec at frequencies between 0.3 and 2 Hz. This is a severe lateral load on buildings which generally have lateral bending resonance frequencies in this frequency range.

Regardless of the method used to specify earthquake loads, the important point is that earthquake loads are indeed dynamic loads with maximum energy in the same general frequency range as primary resonances of buildings. Buildings designed to withstand these loads will therefore exhibit different, and generally more resistant, dynamic response to sonic or blast loads near rocket test facilities.

### 5.3.2 BLAST DAMAGE CRITERIA FOR STRUCTURE

Damage to structure due to an explosion is caused by two major phenomena which accompany any blast.

- The rise of an excess of pressure over normal atmosphere, called overpressure, and the dynamic pressure due to the wind originated by the explosion.
- The fragmented missiles which are generated by the explosion.

Design criteria for these effects are presented in this section.

The formation of the shock wave from propellant explosions and the relationships of its parameters are discussed in detail in Chapter 6 where design charts are presented for predicting these last parameters. For convenience in the presentation of blast damage criteria to buildings, the blast parameter curves in Chapter 6 are plotted in the modified form illustrated in Figure 5.20.

The peak overpressure and peak dynamic pressure are plotted versus the equivalent positive phase duration with distance and TNT weight as parameters. These modified figures are very useful for determining the environmental conditions created by any propellant explosion with known equivalent TNT yield. As shown by Figure 5.20, lines of constant positive phase impulse become straight lines with a slope of -1 on this plot. This provides a simple form for identifying the equivalent triangular pulse load on the structure for a given distance  $R$  and equivalent TNT weight ( $W_T$ ). Detailed plots for the overpressure  $p_{s0}$  and

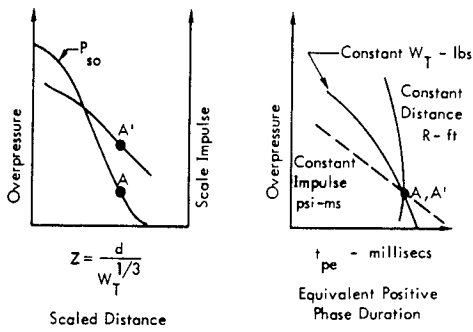


FIGURE 5.20 Development of Design Criteria Curves for Blast Environments by Cross-Plotting Curves of Overpressure and Impulse vs Scaled Distance to Obtain Contours of Constant Distance [R], TNT Weight [ $W_T$ ] and Positive Phase Impulse [ $I^+$ ] in a Plot of Overpressure [ $P_{so}$ ] vs Equivalent Duration [ $t_{pe}$ ]

dynamic pressure  $q_{so}$  for propellant explosions are shown in this form in Figures 5.21 and 5.22.

5.3.2.1 Blast Damage Due to Overpressure and Dynamic Pressure

To predict the exact degree of damage occurring to any specific structure due to propellant explosions, detailed calculations are required, as shown in Section 8.2, Chapter 8, and exact generalizations cannot be specified. However, by combining the information collected from blast damage tests on structures with trends indicated by analytical investigations, simplified design criteria for blast damage to structures can be developed. These are presented here as a design tool for predicting the degree of blast damage expected for common types of structures located near rocket launch and test facilities.

The following data are derived primarily from Reference 5.5 and are based principally on surveys made at Nagasaki and Hiroshima and on the results of blast tests carried out at the Nevada test site in 1953 and 1955. The types of buildings considered are:

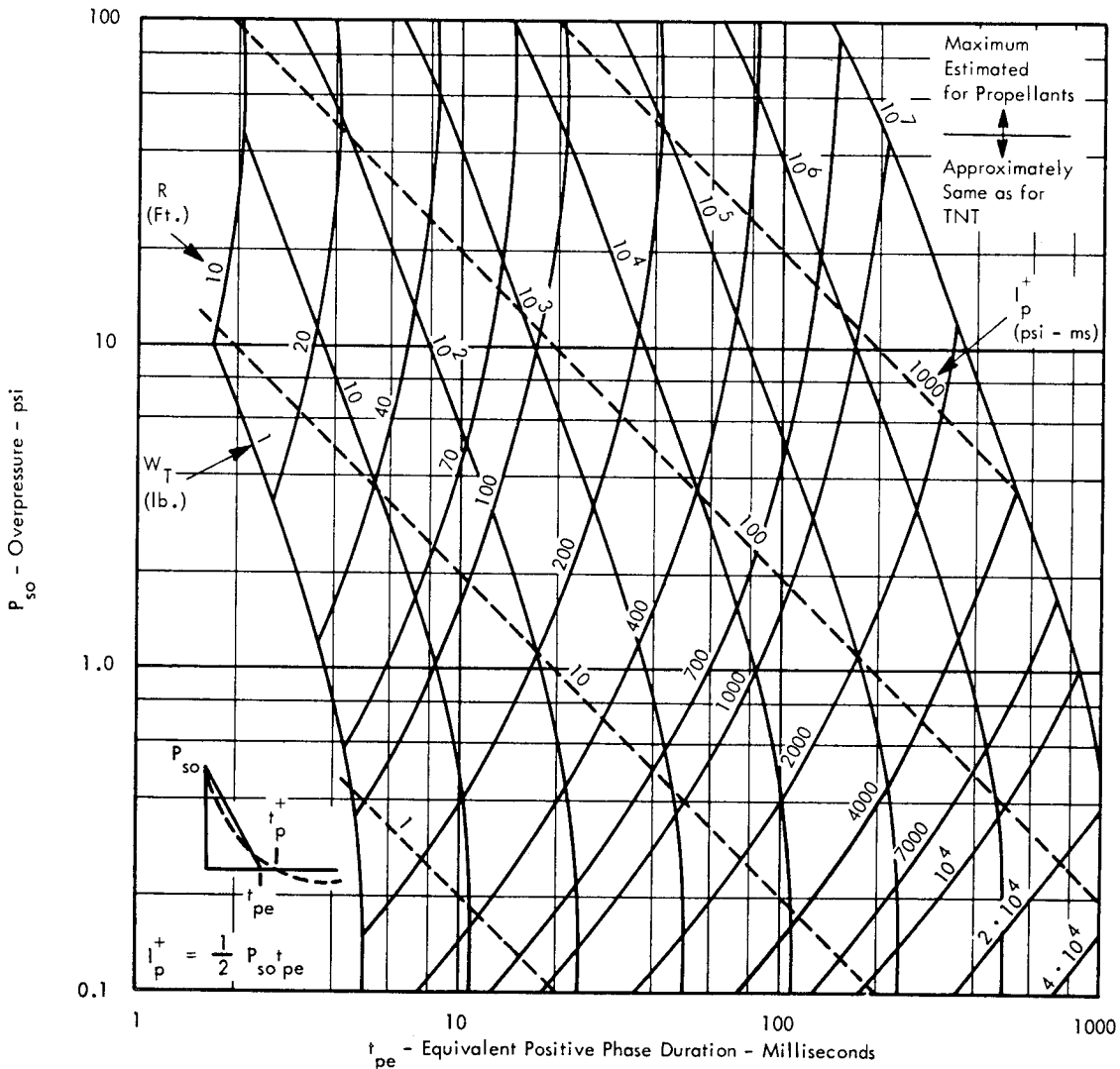


FIGURE 5.21 Estimated Maximum Overpressure ( $p_{so}$ ) and Equivalent Duration ( $t_{pe}$ ) for Propellant Explosions - Related to Distance (R) and Equivalent TNT Weight ( $W_T$ )

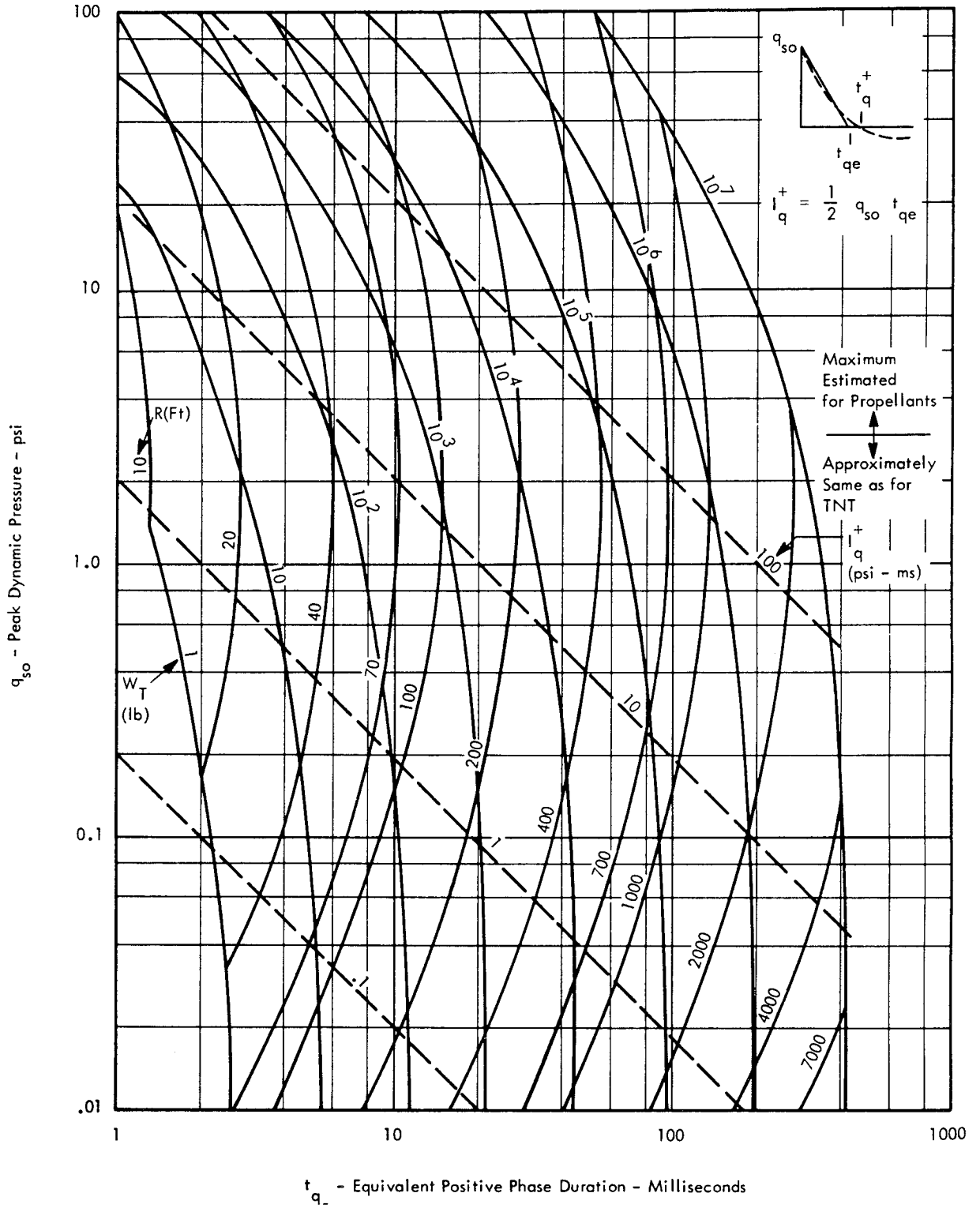


FIGURE 5.22 Estimated Peak Dynamic Pressure ( $q_{so}$ ) and Equivalent Duration ( $t_{qe}$ ) for Propellant Explosions - Related to Distance ( $R$ ) and Equivalent TNT Weight ( $W_T$ )

1. Wood-Frame building
2. Masonry, load-bearing wall, apartment house type buildings
3. Blast resistant, reinforced concrete buildings
4. Earthquake resistant, reinforced concrete frame office type buildings
5. Reinforced concrete frame, office type buildings
6. Earthquake resistant, steel frame, office type buildings
7. Steel frame, office type buildings
8. Steel frame, industrial buildings.

The buildings in categories 1 through 3 are most sensitive to blast overpressure, while the remaining types are sensitive to dynamic pressure and are usually called drag-type buildings. Three degrees of damage are considered.

- **Slight Damage** - A degree of damage to buildings resulting in broken windows, slight damage to roofing and siding and blowing down of light interior partitions.
- **Moderate Damage** - The principal members are damaged so that the effective use of the structure is precluded unless major repairs are made.
- **Severe Damage** - A degree of damage that precludes further use of the structure without essentially complete reconstruction.

Ranges of peak blast overpressure values which may cause slight damage are presented in Table 5.1. For wood frame and masonry buildings, the expected damage depends primarily on the peak blast overpressure because of the short periods of vibration and small plastic deformation at failure for this type of structure. Criteria for moderate and severe damage for this type of structure are listed in Table 5.2.

TABLE 5.1

BLAST DAMAGE CRITERIA FOR FAILURE OF PEAK OVERPRESSURE - SENSITIVE ELEMENTS  
(Data from Reference 5.8)

Structural Element	Failure	Approximate Incident Blast Overpressure (psi)
Glass windows, large and small.	Shattering usually, occasional frame failure.	0.5-1.0
Corrugated asbestos siding.	Shattering.	1.0-2.0
Corrugated steel or aluminum paneling.	Connection failure followed by buckling.	1.0-2.0
Wood siding panels, standard house construction.	Usually failure occurs at the main connections allowing a whole panel to be blown in.	1.0-2.0

TABLE 5.2

LIMITING VALUES OF BLAST PEAK OVERPRESSURE FOR WHICH DAMAGE IS INCURRED BY THE TYPE OF STRUCTURE INDICATED<sup>(1)</sup>

Type of Building	Moderate Damage	Severe Damage
	psi	psi
Wood-Frame	2.0	3.3
Masonry, Load Bearing Wall, Apartment House Type	4.0	4.7

(1) Data from References 5.5 and 5.8.

Figures 5.23 through 5.28 show the zones of moderate and severe damage for each type of building from 3 to 8 as described above. These curves have been plotted over simplified versions of Figures 5.21 and 5.22 so that it is possible to predict the damage in terms of the TNT-equivalent weight and distance or in terms of other shock parameters (such as, peak overpressure ( $p_{so}$ ) or peak dynamic pressure ( $q_{so}$ ), equivalent positive phase duration and positive impulse).

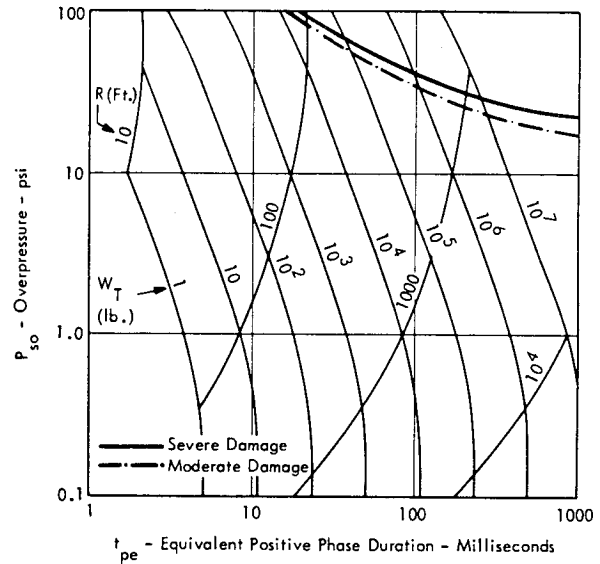


FIGURE 5.23 Blast Damage Criteria for Reinforced Concrete Buildings  
(Criteria Adapted from Reference 5.6)

Figures 5.24 through 5.28 show that the limiting curves for the moderate and severe damage are approximated by the isoimpulse lines. However, the damage criteria lines approach lower values of impulse in the high pressure region. This divergence can be explained by the fact that the equivalent TNT weight for propellant explosions is based on the calculated terminal yield at a large distance from the explosion. In the close field, the apparent yield is smaller than the actual yield (as shown in Figure 6.30 of Chapter 6). Therefore, if the actual value of impulse yield



is used to determine the equivalent TNT weight, the limiting curves would approach values of constant impulse. Criteria for limiting values of impulse for types 3 through 8 are listed in Table 5.3. Figures 5.23 through 5.28 show that the damage criteria curves tend to become horizontal lines in the low pressure region, approaching minimum values of peak overpressure or peak dynamic pressure under which no damage occurs. These limit values are listed in Table 5.4.

The minimum values of both peak overpressure and peak dynamic pressure are presented in this table. Blast resistant reinforced concrete buildings are most sensitive to overpressure while for the others the limiting value is dynamic pressure.

The blast design criteria presented in this section must be employed with discretion since they are based on

- Limited experimental data, and
- A necessarily rough grouping of structure into a limited number of types without any differentiation for different resistance characteristics of buildings within each type.

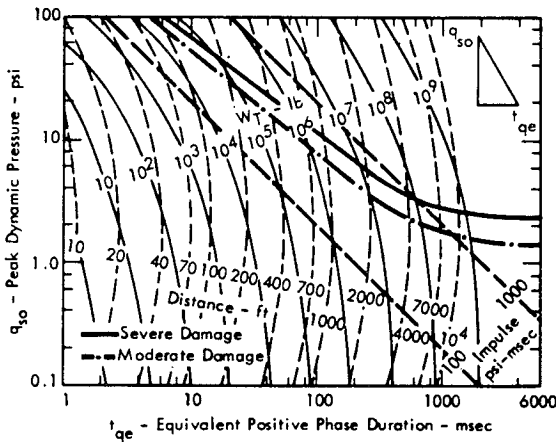


FIGURE 5.24 Blast Damage Criteria for Earthquake-Resistant Office-Type Building (Criteria Adapted from Reference 5.6)

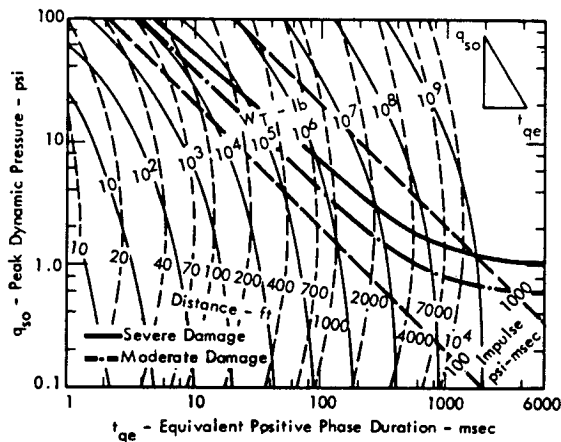


FIGURE 5.25 Blast Damage Criteria for Reinforced Concrete Frame Office-Type Building (Criteria Adapted from Reference 5.6)

However, the blast criteria presented in this section provide a comprehensive summary useful to the designer for initial evaluation of blast hazards when siting and laying out rocket test facilities.

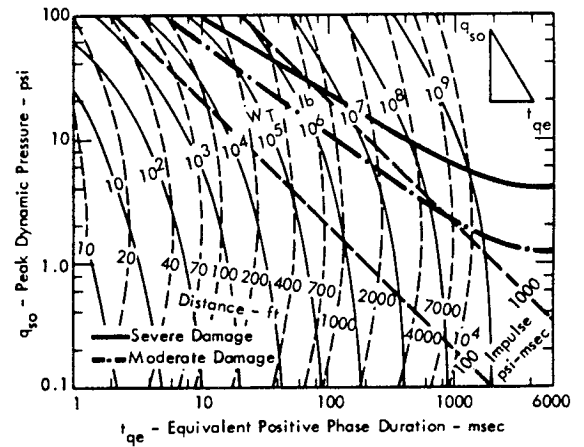


FIGURE 5.26 Blast Damage Criteria for Steel Frame Earthquake-Resistant Office-Type Building (Criteria Adapted from Reference 5.6)

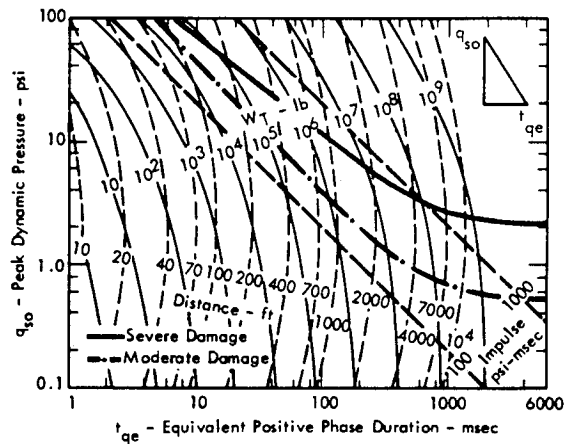


FIGURE 5.27 Blast Damage Criteria for Steel Frame Office-Type Building (Criteria Adapted from Reference 5.6)

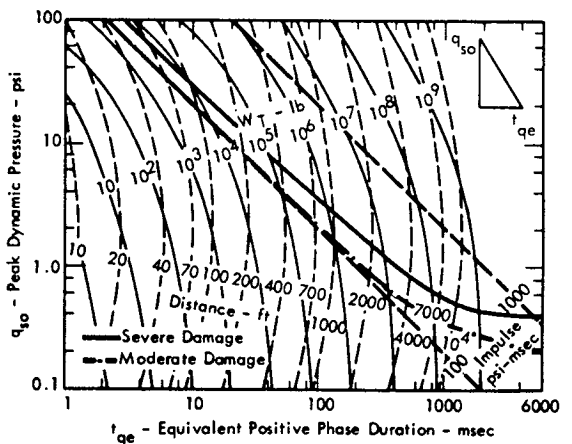


FIGURE 5.28 Blast Damage Criteria for Steel Frame Industrial Building (Criteria Adapted from Reference 5.6)

TABLE 5.3

LIMITING VALUES OF BLAST POSITIVE PHASE IMPULSE FOR WHICH DAMAGE IS INCURRED BY THE TYPE OF STRUCTURES INDICATED

Type of Building	Moderate Damage	Severe Damage
	psi x msec	psi x msec
Earthquake Resistant Reinforced Concrete Frame, Office Type	400	750
Reinforced Concrete Frame, Office Type	200	400
Earthquake Resistant Steel Frame, Office Type	600	1000
Steel Frame Office Type	200	650
Steel Frame Industrial Type	100	200

TABLE 5.4

MINIMUM VALUES OF PEAK OVERPRESSURE AND PEAK DYNAMIC PRESSURE UNDER WHICH NO SEVERE OR MODERATE DAMAGE OCCURS

Type of Building	Moderate Damage		Severe Damage	
	Peak Overpressure (psi)	Peak Dynamic Pressure (psi)	Peak Overpressure (psi)	Peak Dynamic Pressure (psi)
Blast Resistant Reinforced Concrete	18.0	6.5	21.0	8.8
Earthquake Resistant Reinforced Concrete Frame, Office Type	7.8	1.3	10.0	2.2
Reinforced Concrete Frame, Office Type	5.2	0.6	7.0	1.1
Earthquake Resistant Steel Frame, Office Type	7.8	1.3	14.0	4.0
Steel Frame, Office Type	5.0	0.55	10.0	2.2
Steel Frame Industrial Type	2.8	0.18	4.2	0.4

5.3.2.2 Blast Damage Due to Fragmentation

A significant amount of blast damage to structure can be due to the fragmented materials which are thrown out at high velocity by the explosion. These fragments originate both from the rocket and from the adjacent structure and ground surface.

The following important parameters can be predicted for the fragments coming from the rocket body (Reference 5.6).

- The striking velocity of a fragment that impacts a target at some distance from an exploding rocket.
- The depth of penetration into mild steel.
- Maximum fragment distance.

Striking Velocity - The velocity,  $V_s$ , with which a fragment strikes a target at a distance  $R$ , away from an exploding rocket is a function of the initial velocity, mass, and average presented area of the fragment. The striking velocity is found from the following equation.

$$V_s = V_o e^{-kR} \tag{5.5}$$

where

$$k = C_D \frac{A}{m} \rho_a$$

$V_s$  = striking velocity (ft/sec)

$V_o$  = initial velocity (ft/sec) [ $\approx 6400$  ft/sec for rocket explosions according to Gurney Law (Reference 5.6)]

$R$  = distance traveled (ft)

$C_D$  = drag coefficient (see Table 8.2.1, Chapter 8)

$\frac{A}{m}$  = average presented area per unit mass ( $\text{ft}^3/\text{lb-sec}^2$ ) (Table 5.5)

$\rho_o$  = air density  
0.00238 lb-sec<sup>2</sup>/ft<sup>4</sup> (59°F at sea level)

TABLE 5.5

STEEL FRAGMENTS PRESENTED AREA/MASS ( $A/m$ ) (Data from Reference 5.6)

Mass (oz.)	Sphere ft <sup>2</sup> /lb	Cube ft <sup>2</sup> /lb
1/8	0.098	0.122
1/4	0.078	0.097
1/2	0.062	0.077
1	0.049	0.061

Depth of Penetration - The depth of penetration of irregular fragments into mild steel can be computed by the following Demarre's empirical equation (Reference 5.6)

$$d = 0.112 m^{1/3} \left( \frac{V_s}{1000} \right)^{4/3} \tag{5.6}$$

where

$d$  = depth of penetration (inches)

$m$  = mass (ounces)

$V_s$  = striking velocity (ft/sec)

The graph of Figure 5.29 is a plot of the depth of penetration versus striking velocity for fragments of 1/8, 1/4, 1/2 and 1 ounce.

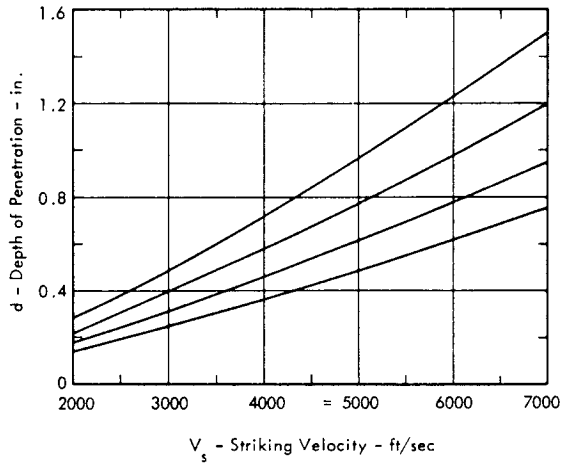


FIGURE 5.29 Depth of Fragment Penetration into Mild Steel vs Striking Velocity (Reference 5.6)

**Maximum Fragment Distance** - Figure 5.30 illustrates the observed maximum range reached by all types of fragments as a function of the equivalent explosive weight. The upper bound of this curve is recommended as a design criteria for maximum range of blast-generated missiles when calculations outlined above cannot be made.

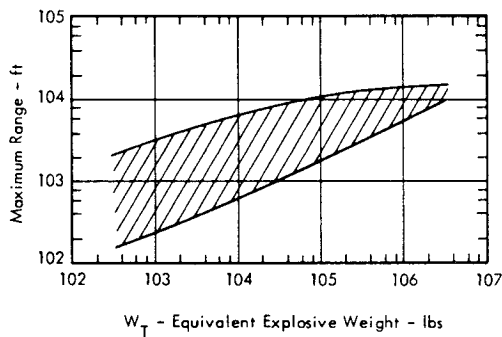


FIGURE 5.30 Equivalent TNT Weight vs Maximum Range of Primary Fragments Generated by the Explosion (From Reference 5.6)

Information for the fragmentation from the ground is relatively scarce. However, some data are available concerning the missile density distribution as a function of fragment size, equivalent explosive weight, ground material and distance from the explosion.

Figures 5.31 and 5.32 present empirically derived curves of density of ejecta from the ground versus distance from the explosion for 5-, 100-, and 500-ton explosions over clay and basalt soils.

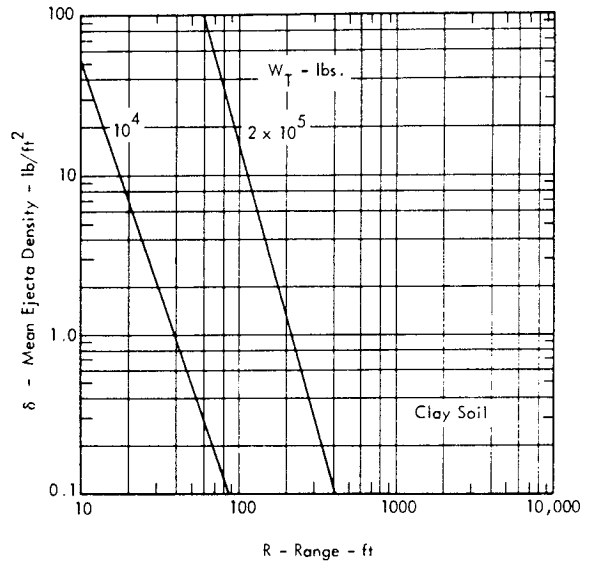


FIGURE 5.31 Earth Ejecta Density Distribution vs Range for 5 and 100 Ton ( $W_T = 10^4$  or  $2 \times 10^5$  lbs) Surface Explosions (From Reference 5.6)

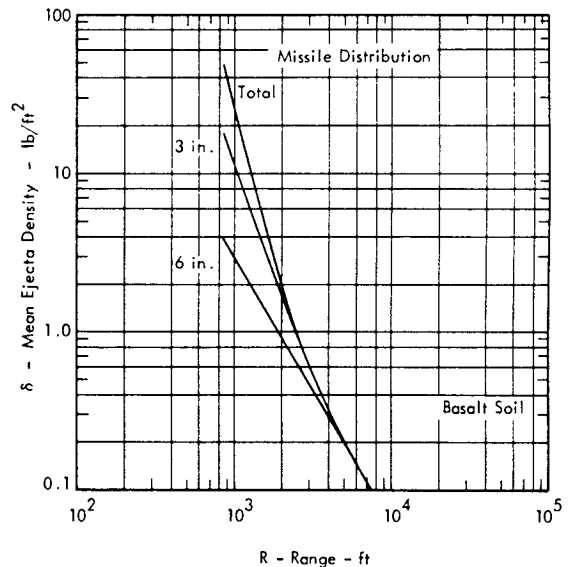


FIGURE 5.32 Earth Ejecta Density Distribution vs Range for a 500 Ton ( $W_T = 10^6$  lbs) Surface Explosion (From Reference 5.6)

For other ground materials and charge weights, the following relationship can be used to determine ejecta density (Reference 5.6)

$$\delta = \kappa R^{-n} W^{n-1} \quad (5.7)$$

where

$\delta$  = ejecta density (lb/sq ft)

$R$  = distance from the explosion (ft)

$W$  = equivalent explosive weight (tons)

$n = \begin{cases} 2.93 & \text{for } W \leq 50 \text{ tons} \\ 3.65 & \text{for } W > 50 \text{ tons} \end{cases}$

$\kappa$  = constant tabulated in Table 5.6 for different earth media.

TABLE 5.6

CONSTANT  $\kappa$  TO BE USED IN EJECTA DENSITY PREDICTIONS (Reference 5.6)

Earth Material	$\kappa$	
	Up to 50 Tons	50 Tons and Up
Desert Alluvium	$8.64 \times 10^3$	$9.24 \times 10^4$
Basalt	$1.77 \times 10^3$	$1.89 \times 10^4$
Residual Clay	$2.43 \times 10^4$	$2.59 \times 10^5$
Clay (Unsaturated)	$6.66 \times 10^3$	$7.10 \times 10^4$
Clay (Saturated)	$1.34 \times 10^4$	$1.43 \times 10^5$
Limestone	$2.60 \times 10^3$	$2.77 \times 10^4$

5.3.3 CRITERIA FOR ACOUSTIC LOADS ON BUILDINGS

A criteria for acoustic loads on wall structure can be expressed in the form of a critical 1/3 octave band sound level at the fundamental frequency of a wall which is the approximate threshold for acoustically induced fatigue failure. The analytical methods by which this criteria is developed are covered in detail in section 8.1.5, Chapter 8. From this analysis, it can be shown that the critical 1/3 octave band sound pressure (rms-psi) can be given by

$$p(f)_c \approx \frac{3}{2} \frac{\pi}{g} \left[ \frac{\sqrt{2}}{\pi} \right]^{1/2} \frac{c_L \sigma_c}{K_s F F_p E} \cdot \frac{f_{mn} w}{\sqrt{Q_{mn}}} \quad (5.8)$$

- where
- $c_L$  = longitudinal wave velocity in bars of wall material - in/sec
  - $\sigma_c$  = critical stress in wall - lb/in<sup>2</sup>
  - $K_s$  = shape factor  $\approx 1.57$  for a simply supported plate with an aspect ratio of 2:1
  - $F_c$  = stress concentration factor

$F_p$  = effective peak to rms ratio for random response

$J_{mn}$  = joint acceptance (a relative effective driving force) for  $mn^{\text{th}}$  mode of panel

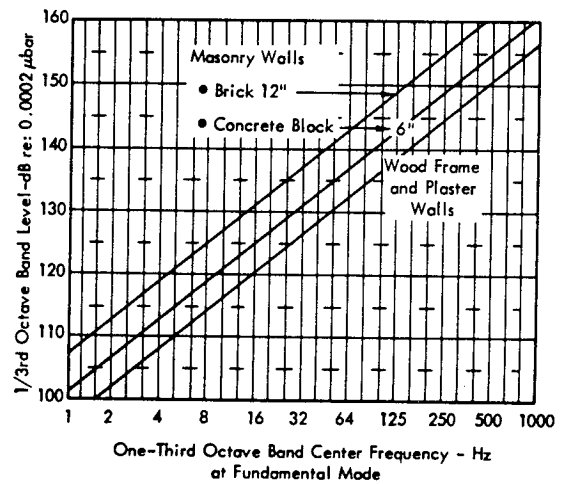
$E$  = modulus of elasticity - lb/in<sup>2</sup>

$Q_{mn}$  = resonant amplification factor for  $mn^{\text{th}}$  mode

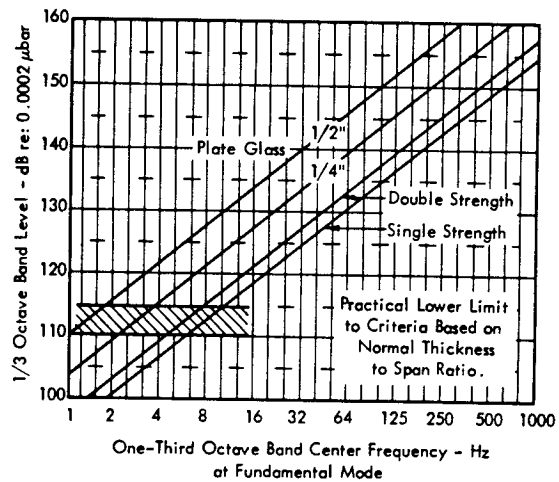
$w$  = surface weight of wall - lb/in<sup>2</sup>

$f_{mn}$  = natural frequency of  $mn^{\text{th}}$  mode - Hz.

Applying this expression for a number of common wall materials, the acoustic criteria curves shown in Figure 5.33 are developed. These are based on a typical simply supported wall with an aspect ratio of 2:1, a stress concentration factor of 1.5 and appropriate values for the remaining constants as defined in Chapter 3,8, and 12.



a) Wall Structure



b) Windows

FIGURE 5.33 Acoustic Environment Criteria for Damage to Walls and Windows. Based on Critical 1/3rd Octave Band Sound Level at Fundamental Frequency of Panel.

It must be emphasized that these curves define the critical 1/3 octave band level at the fundamental natural frequency of the wall. By superimposing a predicted environment on these curves, the possibility of acoustically induced failure is readily determined.

#### 5.3.4 CRITERIA FOR SONIC BOOM LOADS

The structural elements which are most sensitive to sonic boom loads are light wood-frame walls and ceilings and windows. It is shown in Section 8.3 that the maximum stress in wood-frame members for houses exposed to sonic boom loads is given approximately by

$$\sigma_{\max} \approx 28 p_o - \text{psi} \quad (5.9)$$

where  $p_o$  = sonic boom overpressure in lb/ft<sup>2</sup>

For controlled sonic booms in populated areas, the overpressures will be generally less than 5 lbs/sq. ft and will not generate significant stresses in wooden building frame members.

Stresses developed in plaster and gypsum board walls may be as much as twice the value predicted by equation 5.9. Stresses imposed by normal sonic booms on such structure, will not be expected to cause failure, providing the material is in good repair.

#### Window Damage Criteria for Sonic Boom Loads

A similar criteria is developed in Section 8.3, Chapter 8, for sonic boom damage to windows. It is shown that no sonic boom damage to windows is expected for

$$p_o \left(\frac{a}{h}\right)^2 \leq 0.8 \times 10^6 \text{ lb/sq. ft} \quad (5.10)$$

where  $a/h$  = ratio of average side dimension to thickness.

Standard building codes for windows restrict the maximum value of  $a/h$  to approximately (Reference 5.9)

$$\frac{a}{h} \leq 330 \sqrt{a/b}$$

where  $a/b$  = window aspect ratio

For controlled levels of sonic boom overpressure, and for windows in good repair, these two criteria combine to indicate that sonic boom damage to windows is unlikely.

### 5.4 DESIGN CRITERIA FOR PERSONNEL ENVIRONMENT

Detailed working values and techniques for establishing personnel protection design criteria are given in Chapter 10. Summarized values are presented here to provide a general indication of the types and magnitudes of criteria to be expected for personnel protection.

#### 5.4.1 ACOUSTIC ENVIRONMENT CRITERIA

The primary criteria elements for on-facility personnel in a noise environment deal with protecting against hearing loss and providing a suitable environment for necessary voice communications. For people in adjacent communities, the acoustic environment criteria are set by levels found acceptable to the public.

##### 5.4.1.1 Hearing Damage Risk Criteria

Figure 5.34 gives the hearing damage risk contours for limiting daily exposure to noise for daily durations from less than a minute to 8 hours. For frequencies below 1000 Hz, where most of the acoustic energy of large rockets is produced, 135 dB is the maximum allowable exposure level without ear protection, regardless of the time duration. Therefore, hearing protection is a more restrictive criterion than the threshold of pain, Figure 5.34, which is approximately 140 dB. Air Force Regulation 160-3, which gives slightly more conservative damage risk contours, specifies a maximum exposure level at 150 dB under any condition (with ear protection). No effect on working efficiency occurs at sound pressure levels less than 90 dB, a less restrictive criterion than the 8-hour hearing loss contour.

At frequencies below the range of hearing damage risk contours (below 100 Hz), limit criteria for noise are set by the unpleasant effects of induced body vibrations, Figure 5.35, providing ear protection is used. The most sensitive range of frequencies is 30-50 Hz, where levels above 100-120 dB become unpleasant. There is no evidence of permanent damage for sound pressure levels up to 153 dB.

##### 5.4.1.2 Criteria for Voice Communication in Noise

A widely used parameter for estimating the speech interference qualities of a noise environment is the Speech Interference Level (SIL), which is the arithmetic average of sound pressure levels in three octave bands in the speech range (Chapter 10). Table 5.7 summarizes the values of SIL which barely permit reliable speech intelligibility at various talker-listener distances and voice levels.

##### 5.4.1.3 Community Annoyance Criteria

A currently preferred method of predicting community response (likelihood of complaints or group action) to noise, is based on the relation between data on complaints and the corresponding values of the noise on the Composite Noise Rating (CNR) scale shown in Figure 5.36. The CNR scale shown is based on statistical results for individual subjective response (or "noisiness" judgments) on the PNdB scale, modified by weighting factors to account for

- Time histories of noise stimulus exposure.
- Background noise.
- Temporal factors; time of day, time of year.
- Frequency of firings.
- Previous exposure
- Population distribution

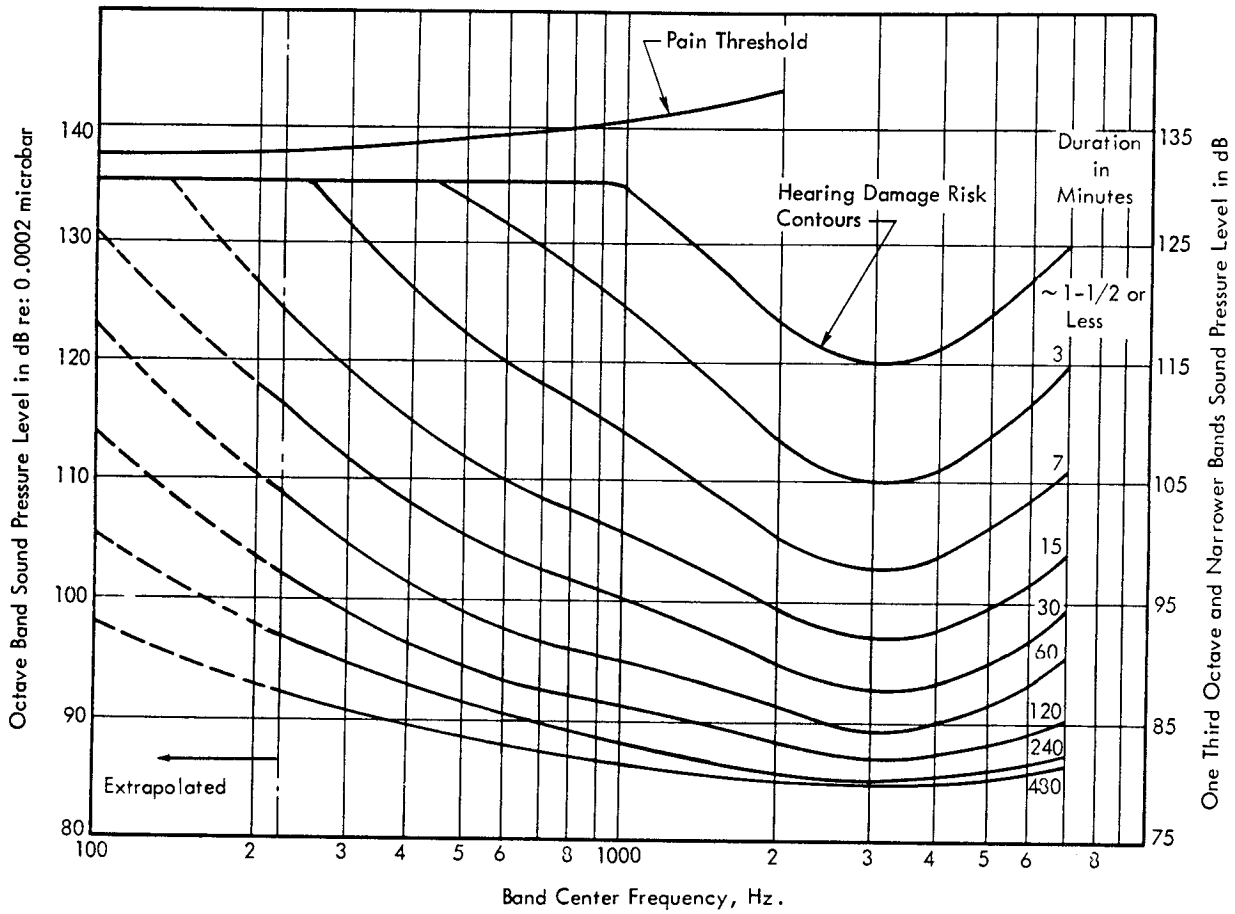


FIGURE 5.34 Hearing Damage Risk and Pain Threshold Limit Criteria

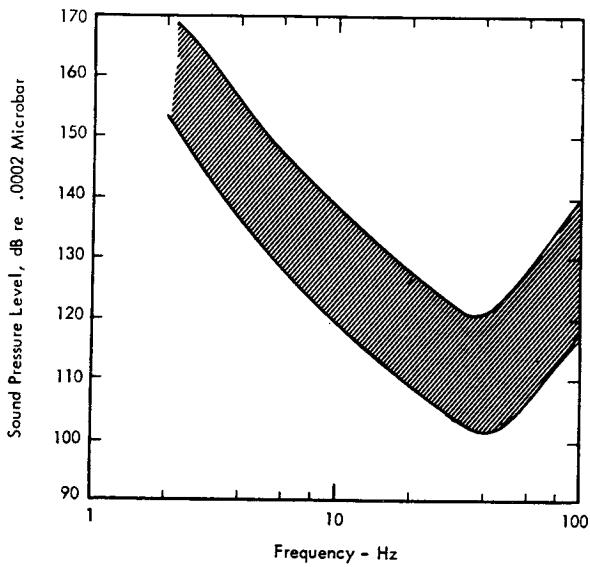


FIGURE 5.35 Discrete Frequency Sound Pressure Level Corresponding to Chest Accelerations Judged "Unpleasant"

TABLE 5.7

SPEECH INTERFERENCE LEVELS\* THAT BARELY PERMIT RELIABLE SPEECH COMMUNICATION

Distance (ft)	Voice Level (Average Male)			
	Normal	Raised	Very Loud	Shouting
0.5	71	77	83	89
1	65	71	77	83
2	59	65	71	77
3	55	61	67	73
4	53	59	65	71
5	51	57	63	69
6	49	55	61	67
12	43	49	55	61

\* Average octave band sound level. In decibels re: 0.0002 microbar in the frequency range from 600 to 4800 Hz.

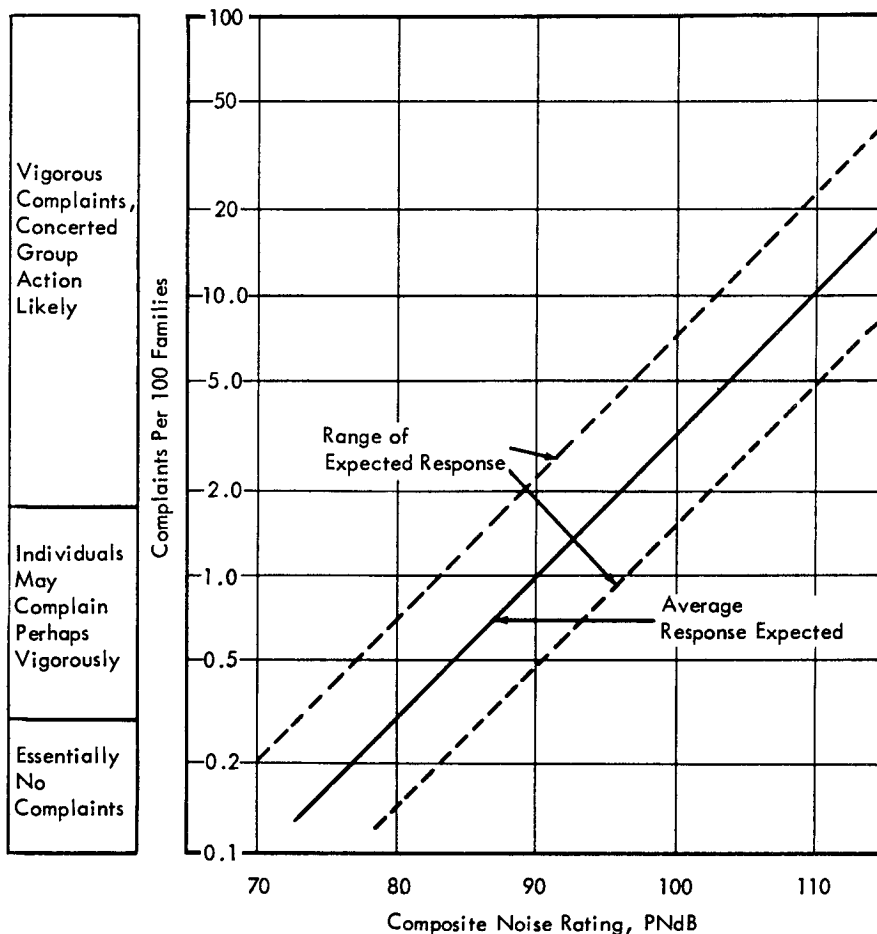


FIGURE 5.36 Relationship between Expected Community Reaction and Composite Noise Rating (See Chapter 10)

Significant community complaint levels can be expected if CNR values of 95 dB are exceeded, and a 6 PNdB increase in CNR corresponds to a doubling of complaint response.

allowable free field blast overpressure of about 0.2 psi to avoid window breakage, making hearing protection criteria even less relevant.

5.4.2 BLAST CRITERIA

Personnel in exposed places at the time of an explosion accident would be subject to direct blast effects such as eardrum rupture or lung damage as well as such secondary effects as injury by blast-generated missiles.

Table 5.8 gives threshold blast overpressures which would produce the direct effects, for fast rise-time long-duration blasts typical of propellant explosions, both for personnel in open areas and for personnel in front of reflecting walls (which increase the effective overpressure). During rocket firing operations, the minimum safety requirements (distance) imposed by blast damage criteria (2 psi overpressures) will tend to predominate over hearing risk criteria.

When safety considerations include injury by blast-generated missiles or glass splinters from a broken window, minimum personnel distance from the blast source is increased by a factor of about 5.7, based on a maximum

TABLE 5.8

THRESHOLD BLAST PRESSURE FOR PRIMARY EFFECTS OF FAST RISE TIME - LONG DURATION BLAST PULSE

Effect	INCIDENT PRESSURE	
	No Reflection (psi)	With Reflection (psi)
Ear Drum Rupture	5	2.3
Lung Damage Threshold	10-12	4.4-5.1
Lethality 1% Fatalities	30-42	11-15
( $t_p^+ > 0.1$ sec) 50% Fatalities	42-57	15-18
99% Fatalities	57-80	19-24

( $t_p^+$  is the duration of the positive phase of the blast.)

5.4.3 SONIC BOOM CRITERIA

No acoustic protection is considered necessary for facility personnel exposed to sonic booms, since no damage either to the eardrum or of any other kind has been experienced even for the highest boom overpressures which can be generated by low-flying aircraft. However, injury by glass splinters from shattered windows is possible for such extreme cases.

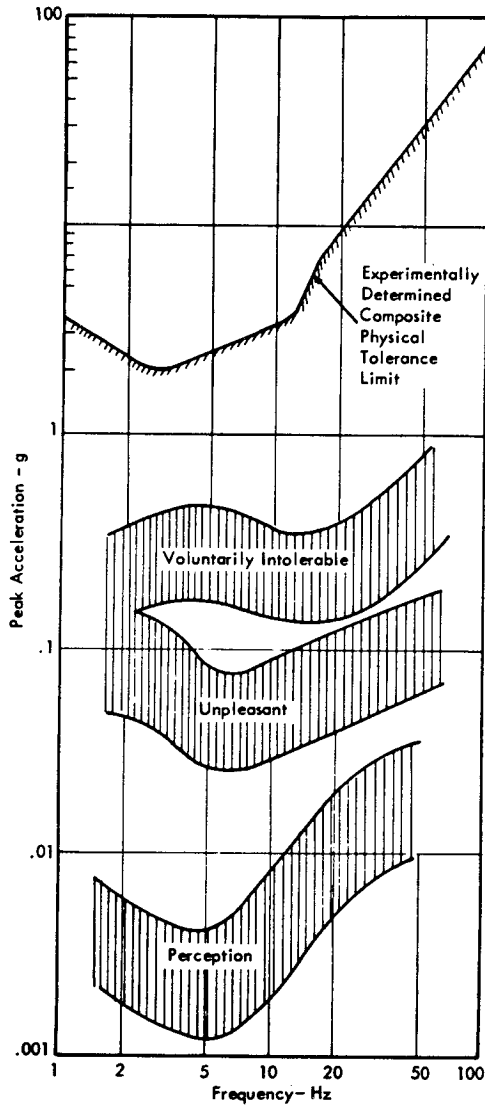


FIGURE 5.37 Tolerance Criteria for Sinusoidal Vibrations (See Chapter 10)

5.4.4 VIBRATION-ENVIRONMENT CRITERIA

Two primary elements enter into vibration control criteria for personnel: the degree of human tolerance to vibration, and the effects of vibration upon task performance. Figure 5.37 summarizes the peak accelerations (for sinusoidal vibrations) corresponding to varying degrees of unpleasantness. An absolute tolerance limit is also shown. For the absolute limit, the most critical frequency region is 2-10 Hz (corresponding to 2-3 g), with the tolerable level increasing rapidly for frequencies above 10 Hz. Figure 5.38 shows the criteria regions based on task performance; again the minimum occurs at 2-10 Hz. The region of "very difficult" task performance corresponds roughly to the extreme of the "unpleasant region" in the tolerance criteria (about 0.1 g); and the lower limit of the region of "impossible" task performance corresponds roughly to the voluntary tolerance limit below 10 Hz (0.2-0.5 g).

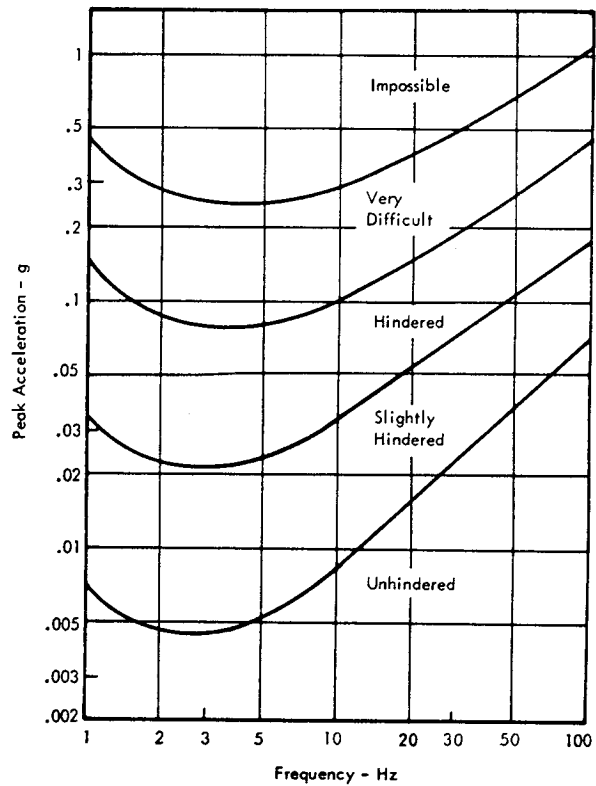


FIGURE 5.38 Criteria for Vibration Effects on Task Performance



### 5.5 DESIGN CRITERIA FOR EQUIPMENT ENVIRONMENT

Detailed environmental design and control requirements for equipment are given in Chapter 11. Summarized values are presented here for protection of equipment in acoustic noise fields, and against blast and sonic boom.

#### 5.5.1 ACOUSTIC ENVIRONMENT CRITERIA

It is desirable to establish environmental criteria for equipment on the basis of

- Reliability requirements

- Equipment type
- Mounting or installation configuration.

Values of recommended acoustic environment limits for the major generic classes of sensitive ground support equipment are given in Table 5.9. These limits have been determined from data on failure rates of generic equipment types in a laboratory environment, multiplied by factors (against failure rate) to account for operational conditions. Effects (on failure rates) of exceeding these limit values can be estimated from data in Chapter 11.

TABLE 5.9  
RECOMMENDED ACOUSTIC DESIGN ENVIRONMENT FOR GROUND  
SUPPORT EQUIPMENT

(Maximum Octave Band Sound Levels in the 200 - 2000 Hz  
frequency range or at the frequency of internal  
equipment resonances - dB re: 0.0002 Microbar)

TYPE OF EQUIPMENT	MOUNTING	
	Cabinet or Shock Mtd.	Rigid Mtg. or Blast Proof Enclosure
<u>Electronic Equipment</u>		
Accelerometers		
Isolated Bending Type	—	140
Compression Type		145
Isolated Compression Type		155
Heavy Duty Relays, Switches	130	140
Sensitive Relays } Potentiometers } Commutators }	120	130
Solid State Components Resistors Capacitors	145	155
Vacuum Tubes Signal < 10 mv Signal > 10 mv	100 120	110 130
Laboratory Electronic Equipment not Covered Above	100	110
Ruggedized Electronic Equipment not Covered Above	120	130
<u>Pneumatic, Hydraulic Equipment</u>		
Low Pressure Components (< 10 psi)	130	140
High Pressure Components (> 10 psi)	140-150	150-160
<u>Pyrotechnic Components</u>	—	150-160

## 5.5.2 BLAST AND SONIC BOOM CRITERIA

### 5.5.2.1 External or Unprotected Equipment

Exposed ground equipment near rocket launch and test stands is subject to damage by blast from propellant explosions, and the decision must always be made whether to protect the equipment or consider it expendable. For some equipment (such as meteorological instruments or radar scanners) it may be technically infeasible to provide a protective housing without interfering with the function of the equipment. For equipment that forms part of a launch tower complex, the blast environment from an explosion on that pad may be so severe that the equipment must be considered expendable and designed only to withstand explosions on other pads.

Peak overpressures from blast and sonic boom can range from 2 psf for normal sonic boom overpressures, through 120 psf for very low-flying aircraft, to more than 100 psi near propellant explosions. For any but the most remote

locations or expendable equipment, the design criteria will therefore be set by the blast environment. For equipment which must continue to function during an explosion or for which internal damage must be prevented, Table 5.10 gives blast overpressure limitations and the related acoustic equivalents on which they are based.

### 5.5.2.2 Internal or Protected Equipment

For equipment housed in blast-resistant buildings, the criteria for additional equipment protection requirements must take into account the entire vibration-excitation path between the blast and the equipment. This requires a blast load analysis for the particular building structure as given in Chapter 8, and specific blast or sonic boom overpressure criteria cannot be expressed without reference to the building characteristics. Once the transfer effects of the building are known, equipment protection criteria in terms of acoustic noise (for airborne inputs) and vibration (for structure-borne inputs) can be applied.

TABLE 5.10  
ESTIMATED BLAST OVERPRESSURE CRITERIA FOR EQUIPMENT

	Octave Band Level at Equipment Resonance dB re: 0.0002 microbar	Equivalent Incident Blast Overpressure psi	
		Q = 5	Q = 25
MALFUNCTION (Sensitive Equipment)	130	.01	.023
DAMAGE (Sensitive Equipment) / MALFUNCTION (Rugged Equipment)	150	.11	.23
DAMAGE (Rugged Equipment)	170	1.0	2.2
	190	8.0	15.0

Q = Dynamic Magnification Factor

## REFERENCES

- 5.1 Brekke, B. N., "Wind Pressures in Various Areas of the United States," U. S. Dept. Commerce, Building Materials and Structures Report 152, Apr. 1959.
- 5.2 Thom, H. C. S., "Distribution of Extreme Winds in the United States," J. Struct. Div., ASCE, Apr. 1960.
- 5.3 Van der Hoven, I., "Power Spectrum of Horizontal Wind Speed in the Frequency Range of 0.0007 to 900 Cycles per Hour," J. Meteorol. 14, 1957, pp. 160-164.
- 5.4 Housner, G. W., "Vibration of Structure Induced by Seismic Waves, Part I, Earthquakes," Chapter 50, "Shock and Vibration Handbook," Harris, C. M. and Crede, C. E., ed., McGraw-Hill Book Co., N. Y., 1961.
- 5.5 Glasstone, S., "The Effects of Nuclear Weapons," U. S. Atomic Energy Commission, Apr. 1962.
- 5.6 Anderson, T. O., et al., "Blast, Fragmentation and Damage," U. S. Naval Ordnance Laboratory, Silver Spring, Maryland, Nov. 1966.
- 5.7 Willoughby, A. B., et al., "Study of Liquid Propellant Blast Hazards," Project PYRO Progress Report for Period Ending 30 Jun. 1965, URS Corp.
- 5.8 Monk, C. B., Jr., "Resistance of Structural Clay Masonry to Dynamic Forces," Structural Clay Products Research Foundation, Research Report No. 7, Nov. 1958.
- 5.9 Uniform Building Code, International Conference of Building Officials, Pasadena, California.

**CHAPTER 6**  
**SOURCE CHARACTERISTICS**

## CHAPTER 6

### SOURCE CHARACTERISTICS

The basic character of the sources of sonic loading; rocket noise, blast overpressure, and sonic boom, are covered in detail in this chapter. A thorough understanding of the source is the essential first step in any detailed analysis of sonic loading on facilities adjacent to rocket engine launch and test sites. For this reason, emphasis is placed on the first two sources.

#### 6.1 ROCKET ENGINE NOISE

##### 6.1.1 INTRODUCTION

The prediction of noise from rocket engines is primarily dependent on analysis and correlation of measured data. While the general mechanism for rocket noise generation is broadly understood, a useful theoretical analysis of the radiated sound field is not practical within the present state of the art. Even for subsonic jets, the basic aerodynamic noise generated by mixing of the flow with the ambient air, while more completely understood theoretically, (Reference 6.1), can not be completely defined without resorting to experimental data.

For a supersonic rocket exhaust, two basic mechanisms are responsible for the noise produced. First there is the turbulence shear flow noise, as for a subsonic jet, and which is associated mainly with the subsonic downstream exhaust flow. Secondly, there are the sources due to the supersonic aspects of the flow; the Mach wave radiation of supersonically convected turbulence, the nozzle boundary layer lip-shock interaction, and the turbulence shock wave interactions downstream in the flow of a nonideally expanded flow.

It is believed that the first source is the major mechanism of the radiated sound, while the other sources have only a small modifying effect on the total acoustic field.

Additional noise generation will occur from a deflected rocket exhaust due to interaction of the jet with the standing shock wave of the deflector. The details of all these mechanisms are still under examination, (Reference 6.2) and the exact proportion of the noise field generated by each process has not yet been determined. Thus, prediction methods will rely on measured data and can use theoretical considerations only in helping to explain the effects of various flow conditions, vehicle velocity, deflected flow, and clustered rocket engine configurations.

The general characteristics of rocket noise can be summarized in the following manner. The noise power generated for a supersonic ( $M > 3$ ) rocket exhaust scales proportionally to the third power of the jet velocity. The sound field emitted is highly directional, and the sound pressure levels measured in different directions can vary as much as 20 dB for the same distance. Most of the sound is radiated at an acute angle to the jet flow direction, with the angle of maximum level increasing with jet velocity. The low frequency noise is generated by the downstream flow, and its maximum makes a smaller angle to the jet flow than the high frequency noise, which is radiated from the flow near the nozzle. The shock wave interaction and Mach wave noise are formed in the initial part of the flow. It is estimated that up to 25 percent of the noise could be generated here, although there is some controversy over the relative importance of this type of noise, (References 6.3 and 6.4).

An empirical prediction method for rocket engine noise will be given in the following sections. Some examples of the noise field of some large boosters will also be presented, and the way the sound varies with altitude and velocity is indicated. Certain empirical curves are also presented to allow the sound pressure levels to be predicted at the launch pad area, the umbilical tower, and other regions in the immediate near field. The effects of water cooling on noise suppression are also mentioned. Finally, a method for estimating the temperature and velocity of the exhaust blast is given.

TABLE OF CONTENTS

<u>SECTION</u>		<u>PAGE</u>
6.1	<u>ROCKET ENGINE NOISE</u> .....	6-1
6.1.1	INTRODUCTION .....	6-1
6.1.2	DESCRIPTION OF ROCKET NOISE .....	6-2
6.1.2.1	The Acoustic Efficiency of Rocket Noise Generation .....	6-2
6.1.2.2	The Spectrum of Overall Noise Power .....	6-2
6.1.2.3	Inverse Square Radiation .....	6-3
6.1.2.4	Directivity of Sound Radiation .....	6-3
6.1.2.5	Atmospheric Attenuation .....	6-4
6.1.3	VEHICLE VELOCITY EFFECT ON THE SOUND GENERATED .....	6-4
6.1.4	FAR FIELD PREDICTION OF ROCKET ENGINE NOISE .....	6-5
6.1.5	COMPARISON OF MEASURED AND PREDICTED VALUES .....	6-6
6.1.6	NOISE FIELD PRODUCED BY LARGE BOOSTERS .....	6-8
6.1.7	STATIC TEST FIRINGS .....	6-11
6.1.8	WATER COOLING AT TEST STANDS .....	6-11
6.1.9	LAUNCH PAD NOISE .....	6-12
6.1.9.1	A Point Near the Exhaust Flow .....	6-12
6.1.9.2	Umbilical Tower .....	6-13
6.1.9.3	Deflected Exhaust Flow .....	6-13
6.1.9.4	General Launch Pad Sound Pressure Levels .....	6-14
6.1.9.5	Shielding by Buildings .....	6-15
6.1.10	EXHAUST BLAST VELOCITY AND TEMPERATURE ENVIRONMENTS .....	6-16
6.1.11	CONCLUDING REMARKS .....	6-17
6.2	<u>PROPELLANT EXPLOSIONS</u> .....	6-19
6.2.1	INTRODUCTION .....	6-19
6.2.2	EXPLOSION ENERGY OF ROCKET PROPELLANTS .....	6-19
6.2.2.1	Explosion Energies for Possible Future Vehicle Configurations .....	6-22
6.2.3	THE SHOCK WAVE FORMATION .....	6-25
6.2.3.1	The Origin of the Air Shock .....	6-25
6.2.3.2	Air-Shock Ground Interactions .....	6-25
6.2.3.3	Elements Determining the Air Shock Parameters .....	6-26
6.2.3.4	The Close-and Far-Field .....	6-26
6.2.4	BLAST SCALING LAWS .....	6-26
6.2.5	DESIGN CHARTS .....	6-28
6.2.5.1	Peak Overpressure Charts .....	6-28
6.2.5.2	Peak Dynamic Pressure .....	6-30
6.2.5.3	Duration of Positive Phase .....	6-33
6.2.5.4	Positive Impulses for Overpressure and Dynamic Pressure .....	6-34
6.2.5.5	Time Variations of Overpressure and Dynamic Pressure .....	6-34
6.2.6	USE OF DESIGN CHARTS AND NUMERICAL EXAMPLES .....	6-35
6.2.6.1	Numerical Examples .....	6-35
6.2.7	CONCLUDING REMARKS .....	6-38
6.3	<u>SONIC BOOM</u> .....	6-39
6.3.1	INTRODUCTION .....	6-39
6.3.2	SONIC BOOM CHARACTERISTICS .....	6-39
6.3.2.1	Energy Spectral Density .....	6-41
6.3.3	ATMOSPHERIC VARIATION EFFECTS .....	6-42
6.3.4	CONCLUDING REMARKS .....	6-43
	REFERENCES .....	6-43

6.1.2 DESCRIPTION OF ROCKET NOISE

The octave band sound pressure observed at a point distant from a rocket exhaust is given by the following expression:

$$\begin{aligned} \text{OBSPL} &= \text{OAPWL} + \phi(f D_e/V_e) \\ &\quad - 10 \log_{10} (r+h) r + D I \\ &\quad - a r/1000 + C - 10.5 \end{aligned}$$

where

OAPWL = the total acoustic power generated by the rocket and equals  $10 \log_{10} \eta 0.678 T V_e + 130$  where T is the thrust in pounds and  $V_e$  is the jet exit velocity in fps.

$\phi(f D_e/V_e)$  = a function which describes that part of the acoustic power occurring in an octave band centered at the frequency f, relative to the total acoustic power.  $D_e$  is the nozzle exit diameter of the engine.

r = the distance from the rocket exhaust to the observer.

h = the height of the vehicle above the ground.

DI = a term that accounts for the directionality of the sound field radiated.

$a r/1000$  = a term to account for the atmospheric absorption of the propagating sound, and

c = a factor to allow for the effect of the vehicle, which affects the total sound produced, the directivity pattern and the frequency of the sound heard by the observer.

Each of these terms will be discussed in the following sections.

6.1.2.1 The Acoustic Efficiency of Rocket Noise Generation

Acoustic efficiency relates the acoustic power generated to the mechanical power of a rocket. Measurements have shown that the acoustic efficiency increases as the jet velocity increases, asymptotically approaching a value of about 0.6 percent for a 10,000 fps exhaust flow. Further, it is suggested in Reference 6.5, that an increase in overall thrust is accompanied by an increase in acoustic efficiency.

Figure 6.1 shows a series of measured acoustic efficiencies for a wide range of chemical rockets. On the basis of these results, it is recommended that an acoustic efficiency of 1 percent be used in all predictions. This will give a slightly conservative value.

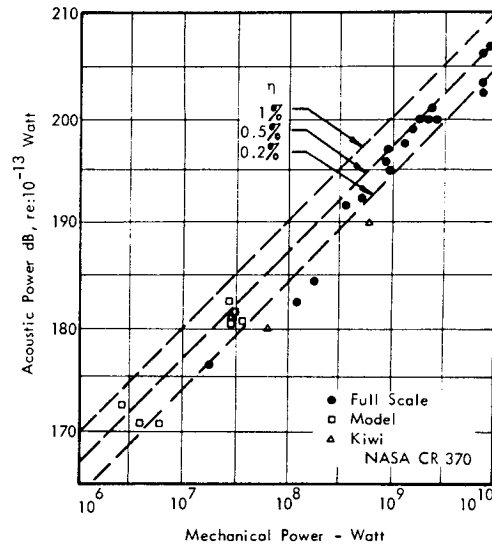


FIGURE 6.1 Acoustic Efficiency of Rocket Noise Generation

6.1.2.2 The Spectrum of Overall Noise Power

Figure 6.2 shows the normalized octave band spectrum of the sound power generated by a rocket, where the values are obtained by integrating the far field measurements to obtain the total noise generated. The values are for a free undeflected flow, and are given relative to the overall sound power produced by the rocket. This result is for a rocket exhaust flow only, where the basic flow properties of velocity and density are reasonably consistent for all modern chemical rockets. Various other normalizing factors have been suggested in order to extend these results to include all flows (References 6.4 and 6.6), but the curve given here has proved to be most satisfactory for rocket exhaust flow noise.

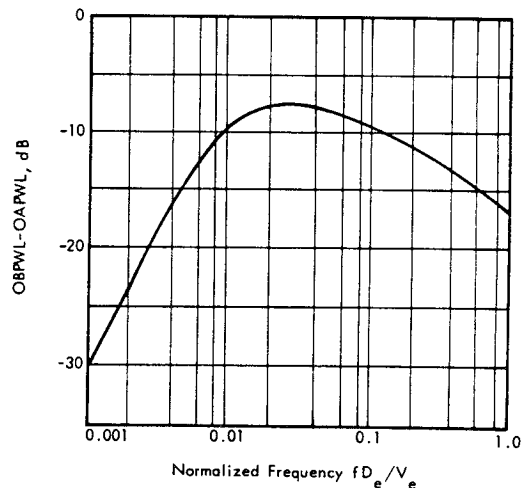


FIGURE 6.2 Normalized Octave Band Spectra of Acoustic Power

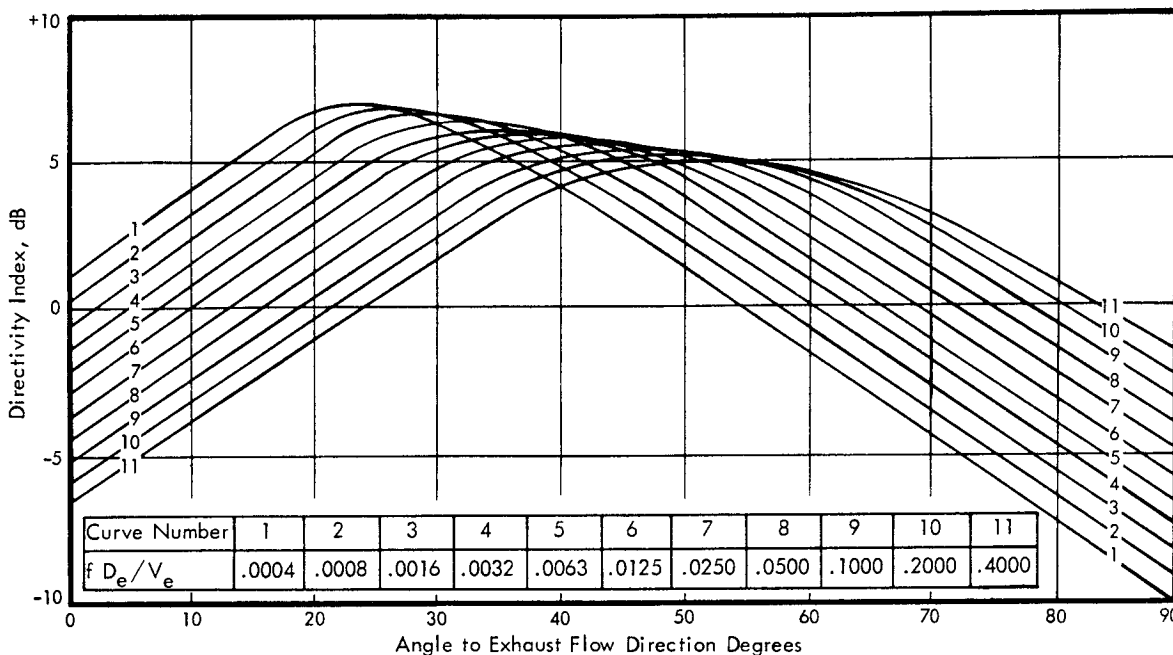


FIGURE 6.3 Directivity Curves

For clustered nozzles, the diameter used is selected as the equivalent diameter of a single circular nozzle, whose exit area equals the sum of all the nozzles. This approach is only directly applicable for closely spaced nozzles. When the nozzles are widely spaced, then a complicated flow pattern occurs, and it will be necessary to solve this flow to accurately predict the noise generated. The sound generated by the different flow regions must be determined. Because of the relatively slow rate of exhaust flow width growth, compared to subsonic jets, the individual nozzle flows do not mix and combine immediately. Therefore, the sound generated by widely spaced nozzles can have similar characteristics to that of a single nozzle. For most clustered flows the two techniques, of either considering the nozzles as having individual mixing flows or taking a sufficiently large area to geometrically include all the nozzles at the exit plane, prove equally inaccurate. The former gives a spectrum that peaks at too high a frequency; the latter gives a spectrum that peaks at too low a frequency. The use of an equivalent single nozzle exit area gives a good representation, and is recommended as a simple alternative to the flow solution technique of Reference 6.4.

6.1.2.3 Inverse Square Radiation

The sound pressure level reduces with distance from the source, as the acoustic power spreads over an increasingly larger area. A convenient measure of the average sound level in the far field of a source is the Space Average Sound Pressure Level (SPL). This is defined as the sound pressure level that would be observed if the sound was radiated equally in all directions.

At normal atmospheric conditions,

$$\overline{SPL} = OAPWL - 10 \log_{10} A + 0.5 \quad (6.1)$$

where  $A$  is the area in square ft, and  $OAPWL$  is the overall sound power generated in dB re:  $10^{-13}$  watts.

For spherical radiation the value of  $A$  is  $4\pi r^2$ , where  $r$  is the distance to the observation point in feet. For hemispherical radiation, when the rocket booster is on the ground, the area becomes equal to  $2\pi r^2$ . As the rocket climbs through the atmosphere, for an observer on the ground some distance from the launch point, the area is a sphere with a segment removed. The area  $A$  is then given by,

$$A = 2\pi(r + h)r \quad (6.2)$$

where  $r$  is the distance from the rocket to the observer and  $h$  is the height of the rocket above the ground.

6.1.2.4 Directivity of Sound Radiation

The sound field radiated by rockets is highly directional. Figure 6.3 shows the recommended directivity curves for calculating the sound field. The values are based on a series of experimental measurements (References 6.4, 6.7, 6.8 and 6.9) and are given for Strouhal numbers based on the exit flow conditions. These curves can easily be extended, by following the basic shift of a standard curve, for frequencies outside the range presented. The curves indicate the characteristics of rocket engine noise,

with a highly directional sound field and the angle of maximum radiation increasing with increasing frequency. These curves are plotted to a normalized value such that each curve, when integrated over a spherical surface, will give a zero value. In use, the Directivity Index is added to the Space Average Sound Pressure Level to give the required directional properties of the rocket engine sound field.

6.1.2.5 Atmospheric Attenuation

The sound radiated will also be attenuated by the effect of atmospheric absorption. This phenomena is discussed in detail in Chapter 7, and Figure 6.4 shows the curve used for calculation purposes in this chapter. The curve defines empirically the observed increased attenuation for increasing frequencies. This suggested value is a conservative estimate, based on measurements for rocket noise propagation and is preferred for the calculations. The data used for this curve were limited to frequencies below 1000 Hz, and the recommended value is given by the following empirical expression.

$$a = 0.02 f^{0.566} \text{ dB/1000 ft} \quad (6.3)$$

This expression should not be used for frequencies above 1000 Hz.

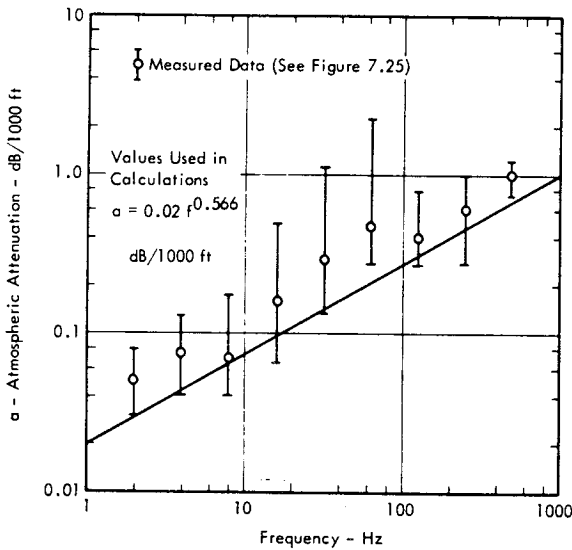


FIGURE 6.4 Atmospheric Attenuation

6.1.3 VEHICLE VELOCITY EFFECT ON THE SOUND GENERATED

The motion of the vehicle through the atmosphere will cause three effects on the sound generated.

- a) The overall noise generated will be reduced because the relative velocity of the jet to the atmosphere will be reduced.
- b) The directivity pattern of the sound radiated will change.
- c) The frequency of sound radiated will change due to the Doppler effect.

Examination of the results of Reference 6.10 indicates how the directivity change can be simply allowed for by shifting the angle of radiation to a new value. Figure 6.5 shows the angle of maximum sound radiation in several frequency bands as a function of vehicle velocity, as obtained from the directivity curves of Reference 6.10. These values were obtained by a reverse prediction calculation using measured acoustic results from the Saturn 1 vehicle. These results show a strong trend for the maximum angle of radiation to decrease with increasing vehicle velocity. The slope of the mean line through the data is

$$\frac{\Delta(\theta_{\max})}{\Delta V_v} = -0.021 \text{ deg/fps} \quad (6.4)$$

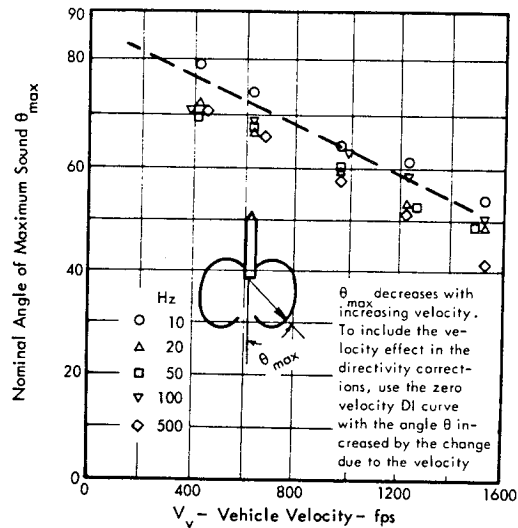


FIGURE 6.5 Velocity Effect on Directivity

The effect of velocity can be included by shifting the directivity curves towards the zero angle axis by the value given by expression (6.4). In practice the value of the angle between the rocket exhaust flow direction and the radius to the observer is increased by  $0.021 V_v$  in reading the Directivity Index from Figure 6.3. This has the additional effect of reducing the total noise generated, since now the Directivity Index curve integrates over a sphere to give an increasingly negative value as the velocity increases. A series of check calculations has indicated that this inherent correction is too great and so a further correction C is added to the level calculated. This is equal to the vehicle velocity times a constant given by,



$$C/V_v = 0.00135 \text{ dB/fps} \quad (6.5)$$

In combination with the shift in the directivity curve, this produces the required reduction in the level to account for forward velocity effects on sound level.

To apply the Doppler frequency effect, the octave band sound level is calculated for a given octave band frequency and then the frequency is corrected according to the equation,

$$f_p = f_o \left[ \frac{c}{c + V_v \cos \theta} \right] \quad (6.6)$$

where  $f_o$  = octave band frequency at zero velocity

$c$  = speed of sound in air

$V_v$  = vehicle velocity

$\theta$  = the angle between the exhaust flow direction and the line from the vehicle to the observer.

Obviously, these corrections cannot be applied indefinitely for an ever increasing velocity, since this would produce a noise peak at less than zero degrees. A restriction is therefore placed on the application of these corrections. They are not to be applied to velocities over 1200 fps. At higher velocities, the 1200 fps corrections are used. This is a fair restriction, since the sound field radiated backwards from the rocket rising vertically at the speed of sound will be generally well below the maximum levels during launch.

#### 6.1.4 FAR FIELD PREDICTION OF ROCKET ENGINE NOISE

A technique for predicting the far field noise of a rocket rising through the atmosphere will now be given, based on the discussion of the previous two sections.

The information required is,

Rocket Thrust	T	pounds
Exit Gas Velocity -	$V_e$	fps
Nozzle Exit Diameter -	$D_e$	ft
No. of Nozzles -	$n$	
Trajectory Height -	$h$	ft
Vehicle velocity -	$V_v$	fps
Distance to observer from point immediately under the Rocket	$d$	ft

The actual trajectory of the vehicle can be used to determine the angle of the vehicle to the line joining the rocket and observer, and to calculate the distance to the observer. For a vertical trajectory the distance to the observer is

simply  $r = (h^2 + d^2)^{1/2}$ , and the angle of sound radiation

is given by  $\theta = \tan^{-1} d/h$

#### Steps in the Prediction Method

- a) Calculate total noise power generated

$$\text{OAPWL} = 10 \log_{10} 0.00678 T V_e + 130 \quad (6.7)$$

dB, re:  $10^{-13}$  watts.

- b) Calculate spectrum of overall power generated. For each octave band center frequency  $f_o$ , calculate  $f_o D_e^2/V_e$

For multi-nozzle rockets use equivalent diameter

$$D_e' = D_e \sqrt{n} \quad \text{and calculate}$$

$$f_o D_e'^2/V_e$$

Then the Octave Band Power Level (OBPWL) is determined from Figure 6.2.

- c) Calculate the Space Average Sound Pressure Level for the octave band,

$$\overline{\text{OBSPL}} = \text{OBPWL} - 10 \log_{10} (r + h)r - 10.5 \quad (6.8)$$

- d) Calculate the angle from observer to rocket

$$\theta = \tan^{-1} (d/h)$$

for vertical trajectory.

- e) Calculate corrections for vehicle velocity

$$\theta' = \theta + 0.021 V_v \quad (6.9)$$

( $\theta$  and  $\theta'$  in degrees)

$$C = 0.00135 V_v \text{ dB} \quad (6.10)$$

- f) Obtain Directivity Index, DI, for octave band from Figure 6.3, using the value of  $\theta'$ .

- g) Correct the octave band center frequency to account for the Doppler frequency change.

$$f_p = f_o \left[ \frac{c}{c + V_v \cos \theta} \right] \quad (6.11)$$

where  $c$  is the speed of sound in the atmosphere and may be taken to be 1100 ft/sec. for practical purposes.

- h) Determine Atmospheric Absorption rate ( $a$ ) from Figure 6.4, at the Doppler frequency  $f_p$ , and the Total Atmospheric Absorption as

$$a r / 1000 \quad \text{dB}$$

- i) Calculate the predicted Octave Band Sound Pressure Level

$$\text{OBSPL} = \overline{\text{OBSPL}} + \text{DI} - a r / 1000 + C \quad (6.12)$$

dB, re. 0.0002 microbars.

- j) Repeat steps b) to i) for other required octave bands. The resultant values are Octave Band Sound Pressure Levels for octave bands centered

at the Doppler frequencies  $f_p$ .

- k) Plot spectrum to determine levels in required octave bands centered on standard frequencies (2, 4, 8, 16, 32, 64, 125, 250, 500 etc. Hz.).

6.1.5 COMPARISON OF MEASURED AND PREDICTED VALUES

Reference 6.11 gives the measured far field sound pressure levels during the launch of the SA-6 vehicle.

The relevant parameters are approximately,

Thrust	=	$1.3 \times 10^6$ pounds
Nozzle Exit Dia.	=	3.8 ft
No. of Nozzles	=	8
Exit Gas Velocity	=	$8 \times 10^3$ fps.

The trajectory for this vehicle was determined, and the sound history at three observation points calculated using the prediction methods of Section 6.1.4. The process was computerized and the empirical prediction curves fitted by polynomial expressions where applicable. Some of the calculated results are compared with the measured levels in Figures 6.6 to 6.8. The measured one-third octave band results have been converted into octave band levels for this comparison. The distances chosen for the calculations are not exactly equal the distances to the measuring stations, which were set at various positions in different directions to the launch point. However, a comparison with similar distances is sufficient to show the agreement, without the need for correcting for the different distances.

The scatter inherent in the measurements, due to atmospheric focussing and attenuation effects, means that several observation points in different directions have to be considered to validate the prediction method.

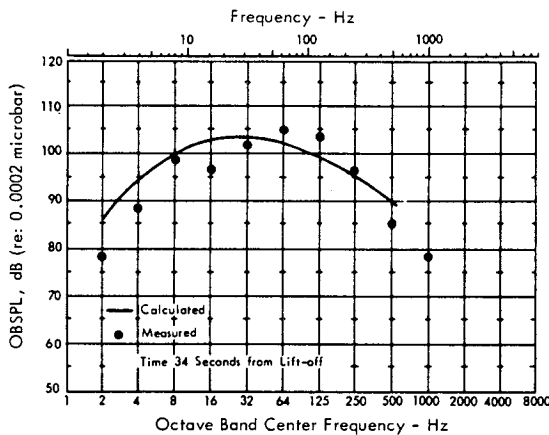


FIGURE 6.6 Octave Band Sound Pressure Level at 17100 ft, Saturn SA-6

In Figure 6.6, the sound pressure level at a point 17,100 ft. from the launch pad was calculated and is compared with the measured value at an observation point (Hangar D), 16,890 feet distant from the launch pad. The observed values are for the time 34 seconds after lift off, and the time necessary for the sound to propagate to the observation point is included in the calculations. The agreement is fair. The measured results show considerable scatter, and a peaked spectrum. Obviously, a prediction technique based on a smoothed curve through many measured data points will not account for minor variations in the spectrum shape observed for any one measurement. Such random variations can be accounted for by adding an appropriate design margin when predicting sonic loads on buildings.

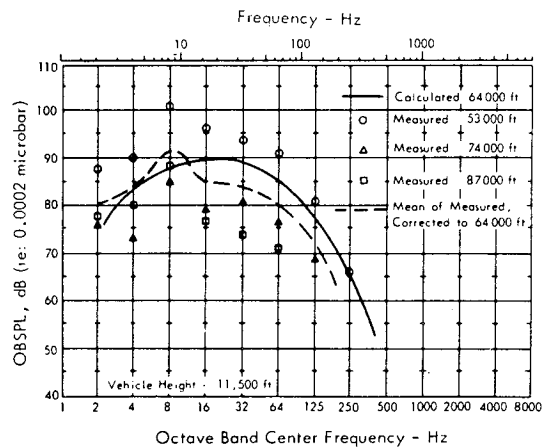
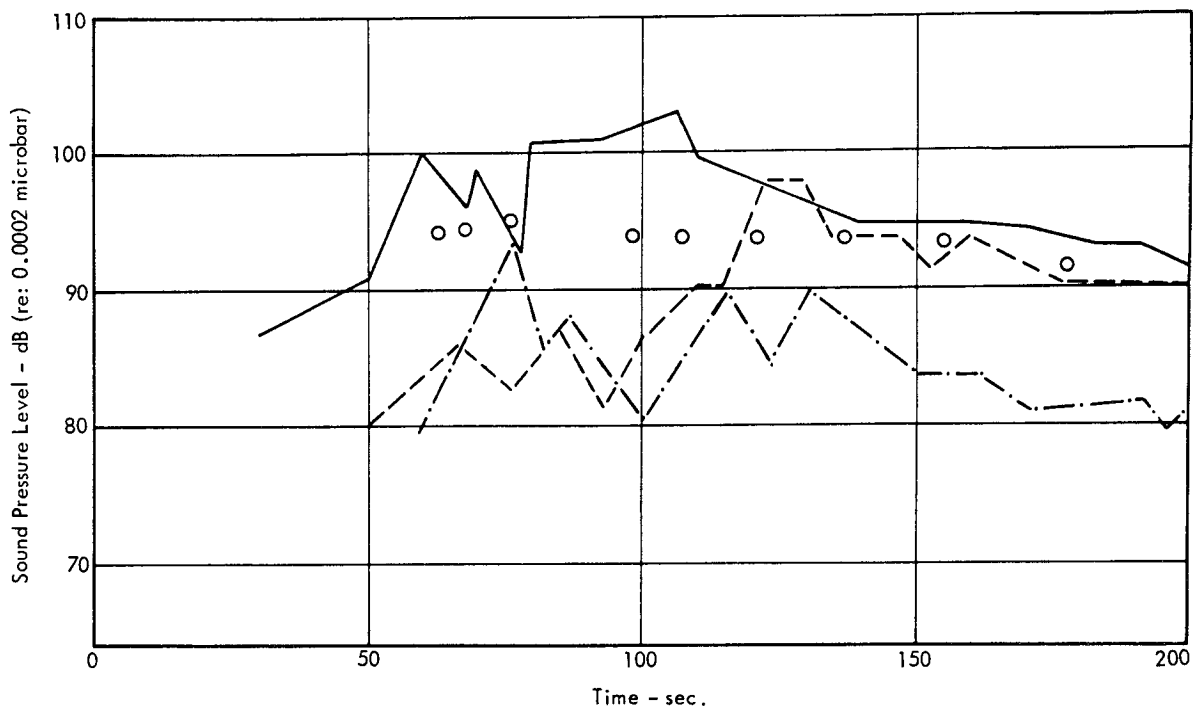


FIGURE 6.7 Saturn SA-6, Sound Pressure Level at 64,000 ft, 100 Sec. After Lift-Off

Figure 6.7 shows the measured and far field results for a distant ground point for a time 100 sec. after lift off. The calculated results are for a ground point 64,000 ft. distant from the launch pad. The measured results are for three points, 53,000, 74,000 and 87,000 ft. from the launch pad. They are all in different directions and should be within  $\pm 2$  dB of each other based only on the different inverse square law loss. However, the degree of scatter that is actually observed in the measured levels is considerable and is indicative of unpredictable propagation anomalies discussed in Chapter 7. The measured data were also corrected for spreading and attenuation losses (based on Figure 6.4) to a distance of 64,000 ft. and then averaged. As shown in Figure 6.7 this average measured level illustrates more clearly the validity of the prediction method which is based on nominal propagation conditions.



- Calculated Values  
64 000 ft.
- A Avon-by-Sea  
—————
- B First Federal Building,  
Cocoa Beach  
- - - - -
- C Titusville - Cocoa  
Airport  
- · - · - ·

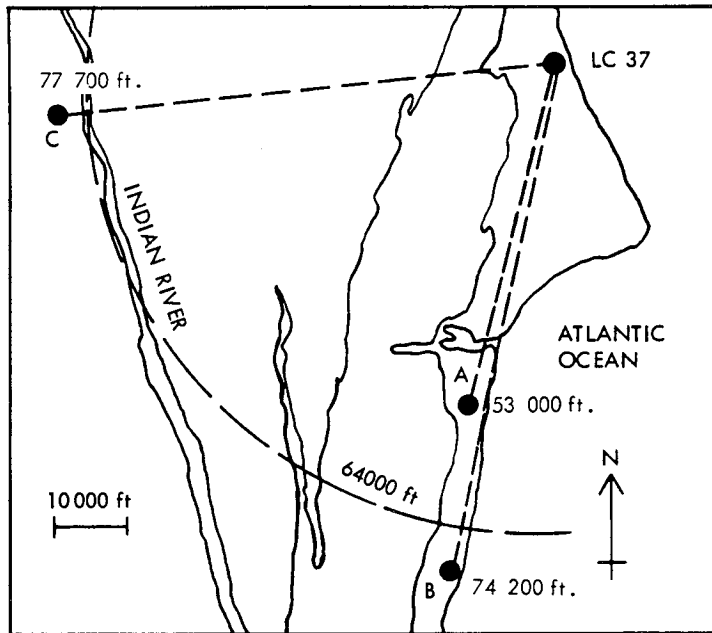


FIGURE 6.8 Calculated and Measured Time Histories of Noise - SA-6 Launch

Figure 6.8 shows the time histories of the overall levels at three distant points, and the calculated results for 64,000 ft. from the launch pad. The calculated results, indicated by the open circles, provide a reasonable estimate of an average of the measured data. However, the latter exhibit considerable scatter. During the early part of the flight, points B and C, at approximately the same distance, have comparable sound levels, but are 10 to 15 dB below point A which is about 24,000 ft. closer. On the other hand, during the latter part of the flight, points A and B, in the same direction from the pad, show similar sound levels but exceed the levels at point C by about 10 dB.

These results indicate two points. First, there is the reasonably good agreement between the predicted and average measured results. Second, a wide range of scatter is shown for the measured levels for points at a similar distance, but different directions from the rocket. These differences are due to; wind effects, atmospheric focussing, and effects of the trajectory. Therefore, the reader is cautioned that the calculated results represent a nominal prediction for an average day. Thus, the calculated values can be used to give the expected "mean" levels. An estimate of any possible increase due to propagation anomalies can be obtained from Chapter 7 to determine possible maximum levels.

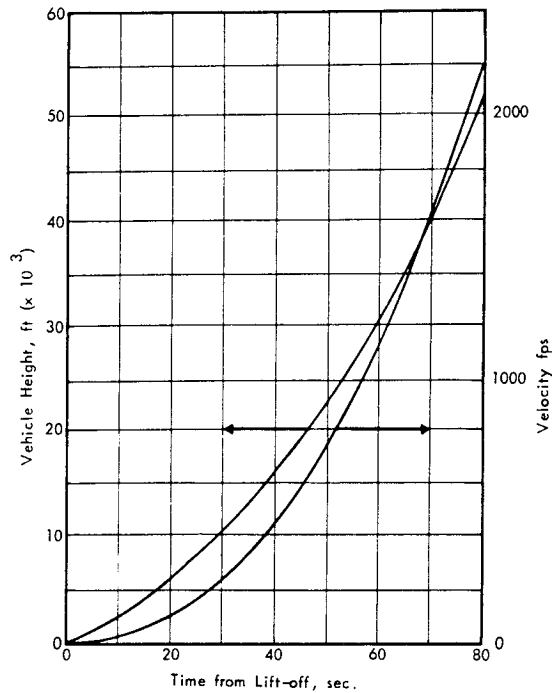


FIGURE 6.9 Large Booster - Typical Trajectory

Other vehicles were considered, but those listed are typical of existing and proposed large boosters. Figure 6.10 shows the octave band spectra of the predicted noise power for the listed boosters. The largest booster sound power is characterized by very low frequency content, and, in fact, most of the sound power will be in the sub-audible region. However, because of the increased amounts of sound generated, the levels of the high frequencies will still be significantly higher than for the Saturn 1 vehicle (Rocket 1).

6.1.6 NOISE FIELD PRODUCED BY LARGE BOOSTERS

The calculated results of the last section were obtained using a computerized version of the prediction technique given in Section 6.1.4. This program was then applied to a series of large boosters, both existing and proposed, described in References 6.15 and 6.16, to indicate the expected far field sound levels that would occur during the flight of such vehicles. The details of the boosters considered are listed in Table 6.1, which also gives the calculated overall sound power generated. They were all considered as following the trajectory given in Figure 6.9, which is typical of those for the Saturn vehicles. The levels were calculated for the following three observation points, on the assumption that the booster was climbing vertically.

- Point a) 1000 ft. typical of the distance to the edge of the launch pad.
- b) 17,100 ft. typical of the distance to the nearest inhabited building during a launch at the Kennedy Space Center.
- c) 64,000 ft. typical of the distance to the nearest civilian inhabited areas.

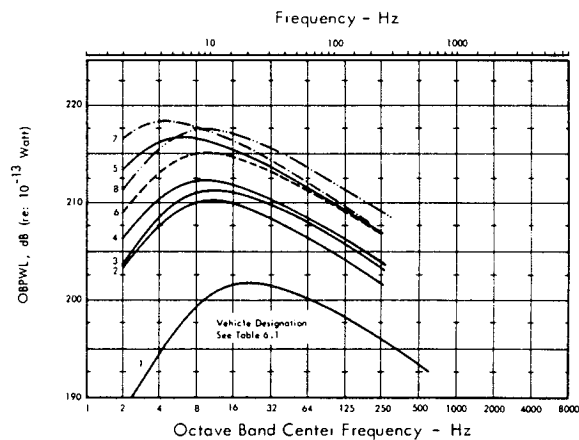


FIGURE 6.10 Octave Band Sound Power Level for Large Boosters

TABLE 6.1  
BOOSTERS CONSIDERED FOR THE CALCULATIONS

Designation	1	2	3	4	5	6	7	8
	Sat 1B	Sat V	Ad.Sat V	Sat V + Solid	1C (2) (3) Class I	24-G (2) (3) Class II	33 (2)	T 65 C (2)
Thrust pounds x 10 <sup>6</sup>	1.6	7.5	9.0	$\frac{7.5}{3.4}$	32.4	18	30.2	55
Engines	8 x HI	5 x FI	5 x FIA	$\frac{5 \times \text{FIA}}{4 \times 120''}$	18 x FIA	18 x HPI	24 x HPI	6 x 260''
Nozzle Nominal Exit Dia. ft.	3.81	11.2	11.75	$\frac{11.75}{11.2}$	11.75	8.42	8.42	23.5
OAPWL (1) dB, re:10 <sup>-13</sup> watt	209	216.5	218	218.5	223.5	222	224	225
Type	← LOX - RP →			$\frac{\text{LOX-RP}}{\text{Solid}}$	LOX-RP	LOX - H <sub>2</sub>		Solid

- (1) Based on 1 percent Acoustic Efficiency
- (2) From Reference 6.15
- (3) From Reference 6.16

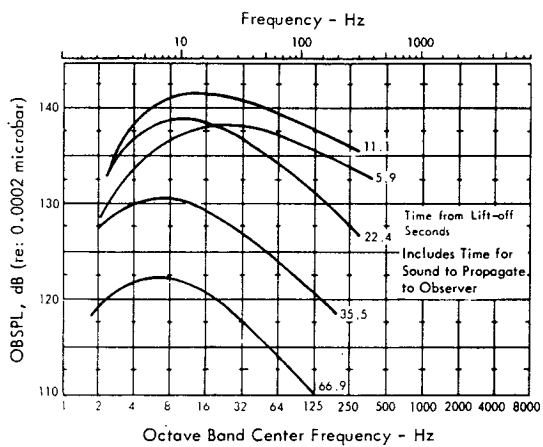
For two of the eight boosters, a complete time history of sound pressure level at the three observation points was calculated, and the results are summarized in Figures 6.11 and 6.12. Figure 6.11a shows the octave band spectrum of sound pressure level at various times for Rocket No. 3, an advanced Saturn V vehicle. The results show a shift in the sound heard to lower frequencies as the vehicle rises. This is the result of the combined effect of the Doppler frequency shift and the higher atmospheric absorption for the higher frequency sound. At 17,100 ft. (Figure 6.11 b) the low frequency noise remains high and only starts to fall after some considerable time from lift-off. The high frequency levels fall away very rapidly. For the 64,000 ft. observation point (Figure 6.11 c), this effect is magnified, and the low frequency sound remains high to the final point of the calculations. The overall level is decreasing, but this decrease is almost all due to the reduction in high frequency noise.

The time histories of the overall sound level for Rocket No. 3 shown in Figure 6.11 d, show a leveling off of the sound after the initial peak. Further, this initial peak is only significant for the nearest observation point. The leveling off of the sound occurs because the decrease in sound level due to the greater distance between the rocket and the observer is off-set by the directionality effect of the sound field. The Directivity Index curve gives higher values as the rocket rises and the angle of radiation decreases. Once past the peak angle of sound radiation,

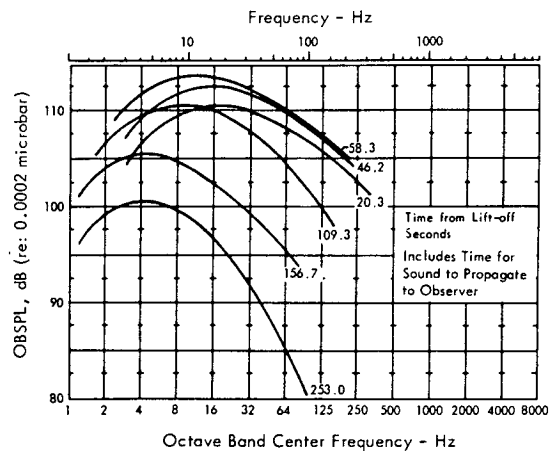
the noise falls off rapidly. For the far observation point, the sound field remains constant within 5 dB over the whole of the initial flight. Therefore, the structures and personnel exposed to this level receive a continuous loading for some 300 seconds.

It must be pointed out that these calculations assume a vertical trajectory. As shown earlier in Figure 6.8, the measured results for an actual trajectory, which would include a horizontal down-range component, show significant scatter. The discrepancies caused by the different distances of the real trajectory are compounded by the variations in sound pressure level caused by the atmospheric effects. It can therefore be concluded that these calculated levels are representative of those levels that actually would occur.

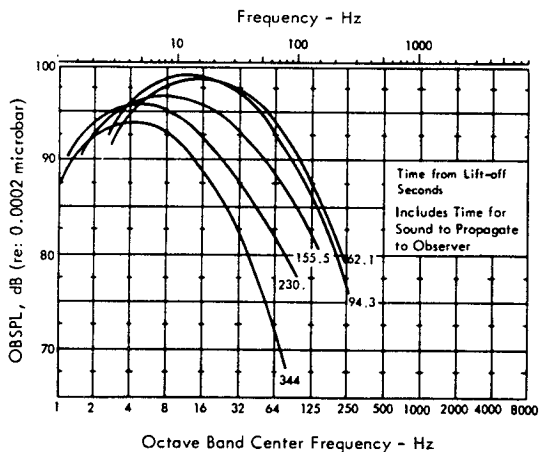
Figure 6.12 shows the calculated results for Rocket Number 8, which was the largest booster considered. Here the octave band spectra of sound at the 17,100 feet observation point are plotted, and they show the very low frequency content of the sound generated. However, because of the large size of the booster, the levels at 64 Hz. still remain very high. Also for this booster, the sound level is not attenuated so rapidly, because the atmospheric attenuation effects are not so significant at these lower frequencies. The overall level for the 64,000 ft. point shows a consistent sound pressure level near 110 dB through the whole initial flight phase. This is similar to the levels experienced directly beneath jet aircraft at takeoff.



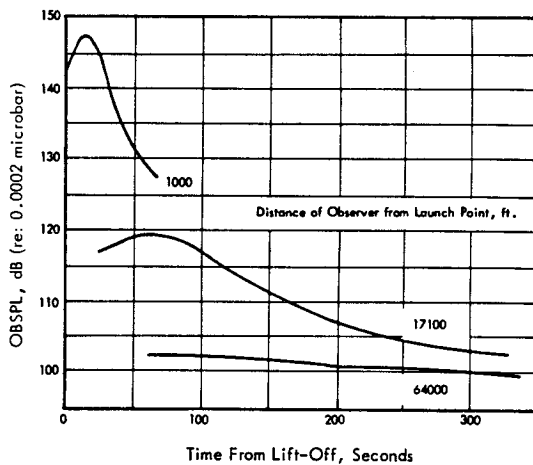
a) Spectra of Sound Pressure Level, Observer at 1000 ft



b) Spectra of Sound Pressure Level, Observer at 17,100 ft

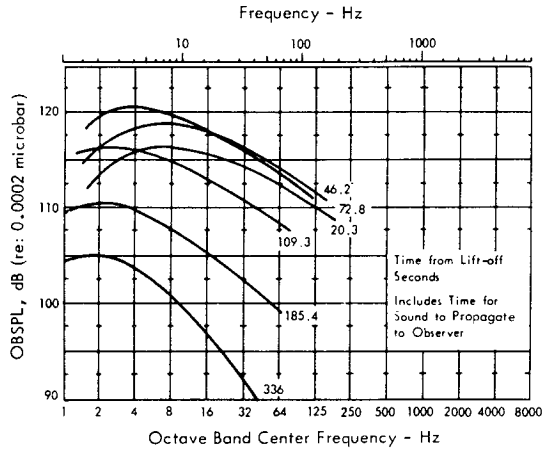


c) Spectra of Sound Pressure Level, Observer at 64,000 ft

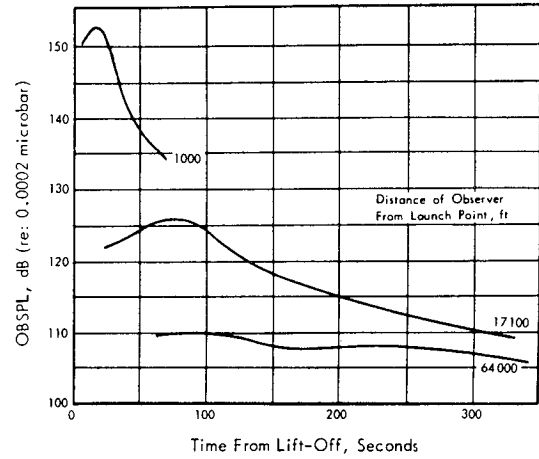


d) Overall Sound Time History

FIGURE 6.11 Calculated Noise Field for Rocket Number 3, ( $9 \times 10^6$  lbs Thrust)



a) Spectra of Sound Pressure Level, Observer at 17,100 ft



b) Overall Sound Time History

FIGURE 6.12 Calculated Noise Field for Rocket Number 8, ( $55 \times 10^6$  lbs Thrust)

6.1.7 STATIC TEST FIRINGS

For captive test firings, the sound can be calculated in a similar manner as for the flight cases. The exhaust flow will normally be deflected to just above the horizontal direction. By assuming that the total flow is in this direction, the sound pressure levels can be calculated as before, except that the total sound is now radiated into a hemisphere. Therefore, the area for the calculation of the Space Average Sound Pressure Level is now

$$A = 2\pi r^2 \tag{6.13}$$

where  $r$  is the distance to the observer.

The directivity curves can be applied as before, the angle being measured between the deflected flow and the line to the observer.

It should be noted that additional ground attenuation can occur which will generally reduce the level for an observer on the ground. However, the possibility of sound reinforcement by focussing can occur as discussed in Chapter 7, and this may increase the level. This means that a wide range of scatter from the calculated value can occur, and should be recognized in planning for facilities and equipment located near the test stands.

6.1.8 WATER COOLING AT TEST STANDS

The addition of large quantities of water into the exhaust stream is an accepted method of cooling the deflector during static test firings, and has the added advantage of causing a reduction in the noise generated. The mass of the water causes the mixing process of the exhaust flow to proceed more quickly with a resulting smaller volume of flow for noise generation. However, it is necessary to add large quantities of water to obtain significant silencing.

The curve of Figure 6.13 shows the expected decrease in overall level of the acoustic power generated for various ratios of cooling water mass flow. These results were obtained from the values given in Reference 6.12 for model and full scale rockets.

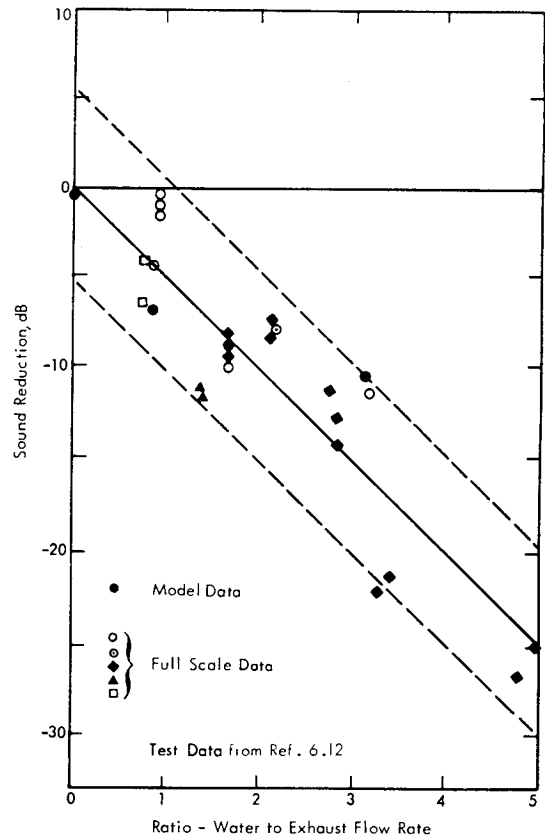


FIGURE 6.13 Water Cooling, Overall Sound Reduction

The noise reduction will be greatest for the low frequency sound; the high frequency noise originating from those regions of the exhaust flow before the water is added. The estimated reduction of Figure 6.13 should therefore not be applied directly across the spectrum. Figure 6.14 shows the recommended reduction in the peak octave band sound power level, as given in Reference 6.12. The reduction in the other octave bands will vary with configuration and the reduction will be greater for lower frequencies and less for higher frequencies as indicated in Figure 6.14. However, these results should be used with caution when the distance of the nozzle from the deflector is greater than about five nozzle diameters.

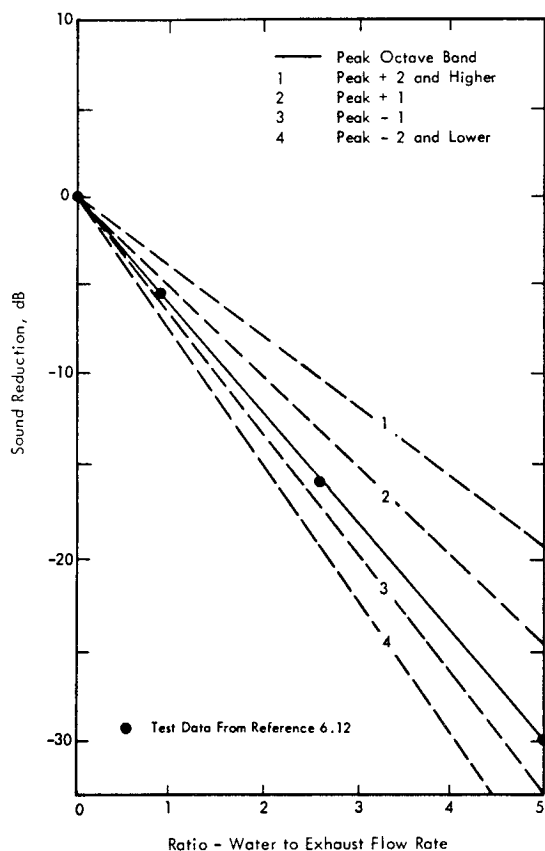


FIGURE 6.14 Water Cooling, Octave Band Sound Reduction

### 6.1.9 LAUNCH PAD NOISE

The structures in the immediate launch pad area will receive an intense acoustic loading during the launch phase and, similarly, equipment and buildings associated with test stands will have to be carefully designed to eliminate acoustic response effects. The electronic equipment and systems in the umbilical tower and rooms in the tower and base will have to be protected. The following notes indicate how to estimate the external sound pressure levels in these areas. The problem of prediction is that the rocket exhaust noise cannot be considered as radiating from a single point. The sound will be generated over a region that will be large compared with the dimensions to the observer. A position near the exhaust flow will receive sound from a series of directions. Also, if the observer is sufficiently close to the flow, near field effects (hydrodynamic effects) will occur, and the sound levels increased from those simply calculated on the basis of the far field measurements. The following empirical techniques are presented to help determine the noise field in this immediate pad region.

#### 6.1.9.1 A Point Near the Exhaust Flow

Near the flow, the sound field will be characterized by a complex distribution of multiple sources. As the observer moves farther from the flow, then the sources can be approximated to a point. However, for the large boosters listed in Table 6.1, this approximation will not be valid within 1000 ft. of the exhaust flow. The recommended technique is therefore to utilize the source distribution given in Figure 6.15. This type of representation is not strictly correct, since the exhaust flow will contain a spectrum of sources at each point, and not just a single frequency. However, the method does allow empirical results to be quickly calculated. The distance down the jet to each source is given in terms of the core length,  $x_t$ . This core length is defined by

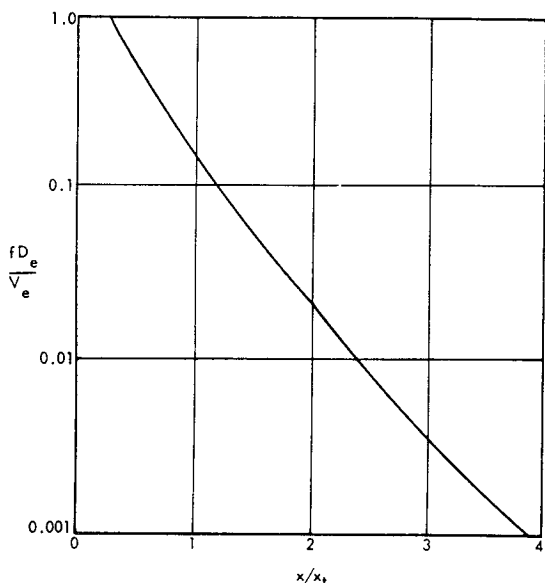
$$x_t = 3.45 D_e (1 + 0.38M)^2 \quad (6.14)$$

where  $M$  is the exit Mach number of the flow and  $D_e$  is the exit diameter of the nozzle. For multiple nozzles, the equivalent diameter is used, as before,

$$D'_e = \sqrt{n} D_e$$

Then, once the total acoustic power and octave band spectrum have been calculated, the source location for each octave band is calculated, and the distance to the observer measured. The directivity functions of Figure 6.3 are then used, with the calculated Space Average Sound Pressure Level, to obtain the Octave Band Sound Pressure Level. For regions very close to the rocket exhaust, the sound level can be estimated from near field measurements for rocket engines which have been reduced to equal sound level contours, such as shown in Figure 6.16.





$x$  is Distance Downstream  
 $x_t$  is Distance to Coretip given by Eq. (6.14)  
 $x_t \approx 15 D_e$  if  $M$  Unknown

FIGURE 6.15 Source Distribution in Exhaust Stream (Reference 6.4)

### 6.1.9.2 Umbilical Tower

For the umbilical tower, a different situation exists. The maximum level in each octave band will occur at different times. The exhaust stream will pass by the observation point on the tower as the vehicle rises, and so the level on the tower will vary as different parts of the flow are presented. For testing purposes, and calculating transmission losses into the rooms, the maximum level in each octave band will be required. These maxima will not be added to give a maximum overall level because they do not occur simultaneously. For this case, to calculate the maximum sound pressure level in each octave band, the Space Average Sound Pressure Level is calculated from the power spectrum using the distance directly from the center of the exhaust flow to the observation point. This value is corrected by subtracting a factor for the spread of the sources at the frequency under consideration.

$$\text{OBSPL} = \overline{\text{OBL}} - 5 \quad (6.15)$$

dB, re: 0.0002 microbar

The factor 5 dB is calculated by taking -10 dB for the jet spreading, based on the calculated source distribution given in Reference 6.4, and adding 5 dB for the directivity effect. As an example, the maximum sound pressure level measured in the 16 Hz. octave band for the umbilical tower of the Saturn V rocket is calculated as follows. Assuming the vehicle center line to be 30 ft. from the observation point, and noting the 16 Hz. octave band power level is 209.6 dB, the Space Average Sound Pressure Level for this octave band is

$$\begin{aligned} \overline{\text{OBL}}_{16} &= 209.6 - 10 \log_{10} 4\pi(30)^2 \\ &= 169 \text{ dB, re: 0.0002 microbar} \end{aligned}$$

Then the maximum sound pressure level at the umbilical tower in this octave band is,

$$\begin{aligned} \text{OBSPL}_{16} &= 169 - 5 \\ &= 164 \text{ dB, re: 0.0002 microbar} \end{aligned}$$

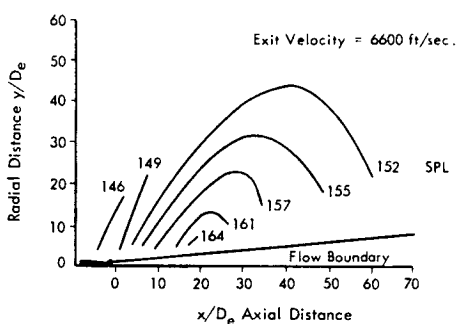


FIGURE 6.16 Typical Contours of Equal Overall SPL in dB re .0002 Microbar for a Rocket with Distance Expressed in Terms of Nozzle Exit Diameter ( $D_e$ )

### 6.1.9.3 Deflected Exhaust Flow

When the rocket rises from the pad, part of the exhaust flow will be vertical from the nozzle to the deflector, and this length will increase as the vehicle rises. Then, in calculating near field levels, the two component parts of the flow must be considered. This is normally done by utilizing the source location technique of Figure 6.15.

A further effect is caused by the deflector altering the properties of the jet exhaust significantly from the undeflected case. This can cause the characteristics of the radiated soundfield to change. An unconstrained deflector plate will cause the exhaust flow to spread and produce an

elliptical sound field around the jet axis direction. This will generally be advantageous for points on the ground, since less sound will be radiated horizontally compared to the upwards direction. The ellipticity of the sound field will depend on the spreading of the exhaust flow and will also change with frequency. The higher frequency sound, coming from the region nearer the deflector will show a greater variation because of the higher aspect ratio of the exhaust flow cross-sectional area. As the flow continues downstream, it will tend to form back to a circular cross-section. Figure 6.17 shows the ellipticity of the sound field formed by a flat plate deflector, and is obtained from the results of References 6.14 and 6.4. The peak octave band and overall level give the same effect, which is more pronounced for the high frequency sound and less pronounced for the low frequency sound. The corrections for an observation point on the ground, when the deflected rocket is fired down onto a flat plate ( $\phi = 90$  degrees) and turned horizontal are given in Table 6.2.

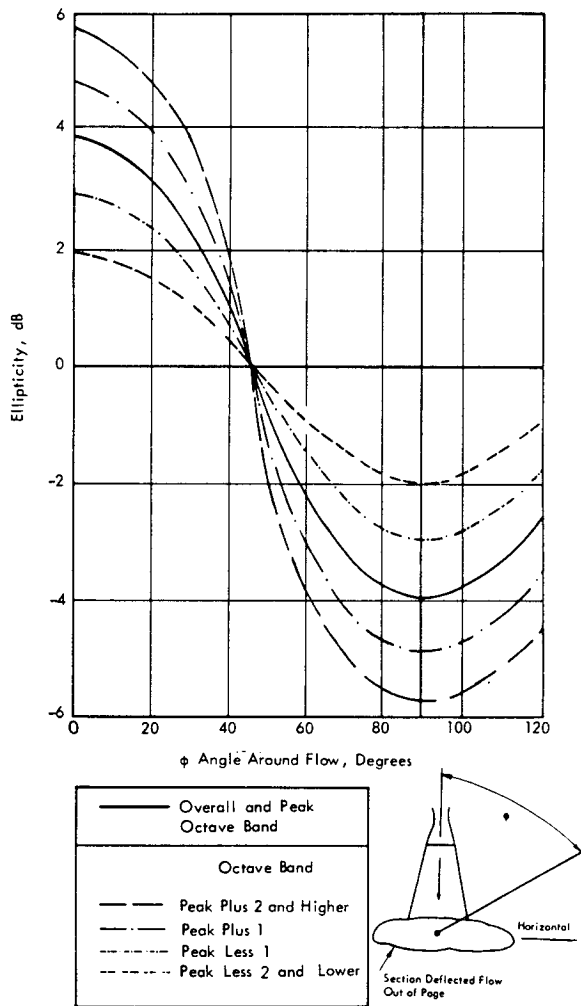


FIGURE 6.17 Ellipticity of Deflected Flow Sound Field

However, it should be noted that most deflectors have sides, and that the exhaust flow will be contained so it issues as a flow with an even cross-section. In this case, no ellipticity advantages can be obtained for the sound levels on the ground.

TABLE 6.2

ELLIPTICITY CORRECTIONS FOR FLAT PLATE EXHAUST DEFLECTOR AND GROUND OBSERVER

Octave Band	Correction dB
Peak and Overall Level	-4
Peak Plus 1	-5
Peak Plus 2 and above	-6
Peak less 1	-3
Peak less 2 and lower	-2

6.1.9.4 General Launch Pad Sound Pressure Levels

Because the problem of launch pad acoustic environment prediction is complicated, it is often best simply dealt with by prediction from other measured results. Figures 6.18 and 6.19 show the estimated sound level contours for a rocket of overall acoustic power 216 dB, re:  $10^{-13}$  watts. The overall levels are given for the exhaust flow deflected in one direction in Figure 6.18, and in two directions in Figure 6.19. The overall sound levels can be scaled for other rockets on the basis of exit velocity and diameter as follows.

For two different rocket engines with exit velocities  $V_1$  and  $V_2$ , and exit diameters,  $D_1$  and  $D_2$ , for the same acoustic efficiency, the mean square pressures  $P_1^2$  and  $P_2^2$ , at similar positions,  $r_1$  and  $r_2$ , at the same angle relative to the exhaust will be approximately related by;

$$\frac{P_1^2}{P_2^2} = \left(\frac{D_1}{D_2}\right)^2 \left(\frac{r_2}{r_1}\right)^2 \left(\frac{V_1}{V_2}\right)^3 \tag{6.16}$$

Thus, the sound pressure levels for one may be estimated from known data for the other by the expression,

$$SPL_1 = SPL_2 - 20 \log r_1/D_1 + 20 \log r_2/D_2 + 30 \log V_1/V_2 \tag{6.17}$$

Thus, at the same number of nozzle diameters  $r/D_e$  and for the same nominal jet exit velocity, acoustic efficiency and directivity factor, the overall sound pressure levels will be the same at the two similar positions. The exit diameter should be based on an equivalent or characteristic diameter of the flow.

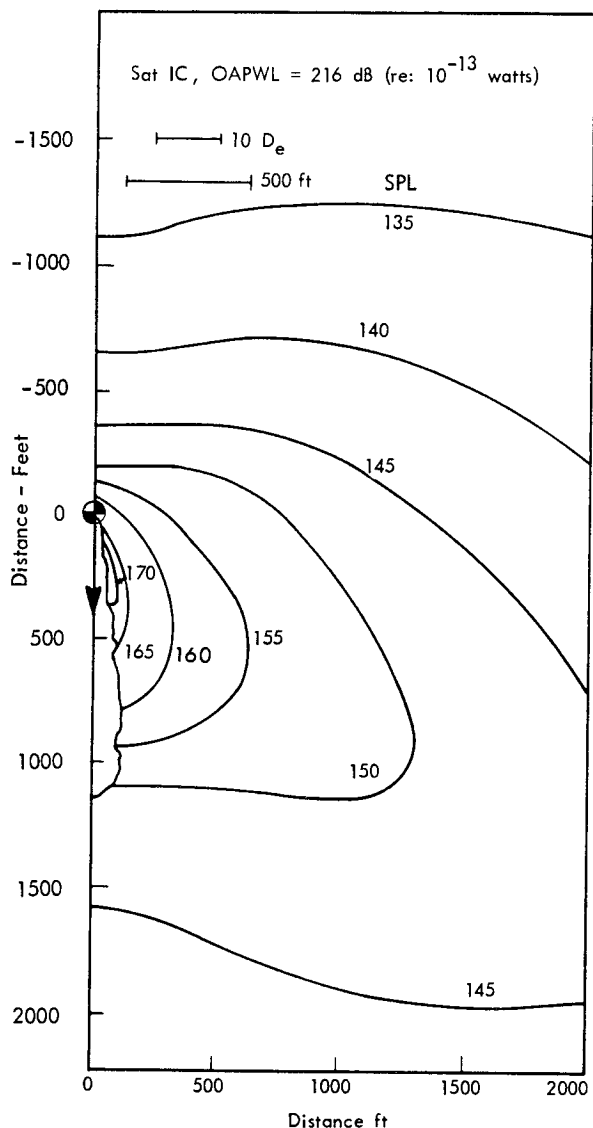


FIGURE 6.18 Near Field Noise Contours, Static Firing, Exhaust Deflected in One Direction

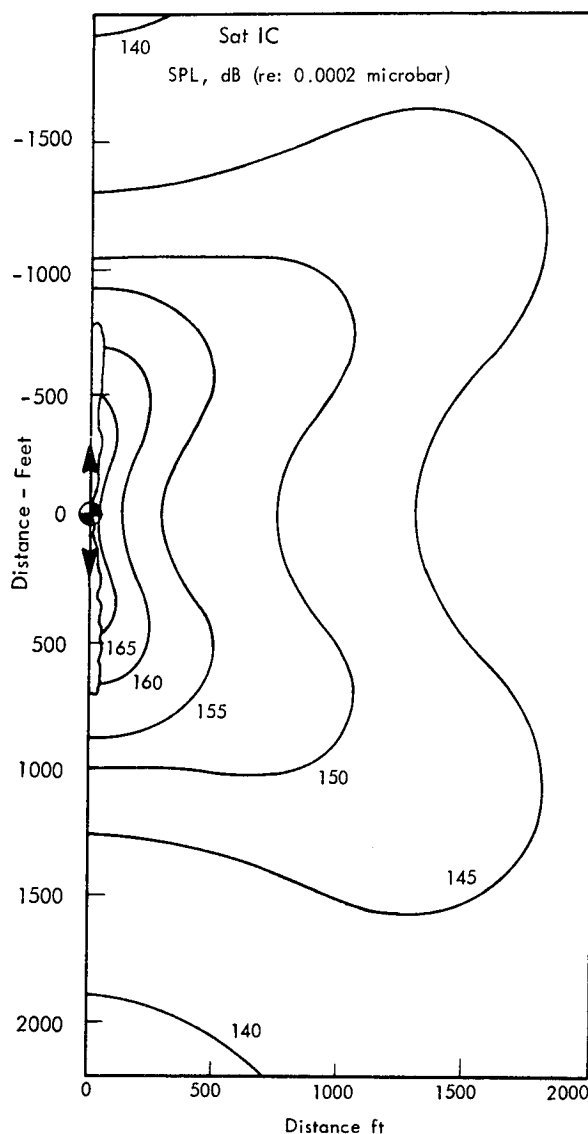


FIGURE 6.19 Near Field Noise Contours, Static Firing, Exhaust Deflected Equally in Two Opposite Directions

6.1.9.5 Shielding by Buildings

For buildings in the immediate vicinity of the launch pad area, there will be a shielding effect for those walls facing away from the rocket. Doors or other openings into launch pad buildings will normally be located on such walls. Thus, it will be important to know the external sound levels on shielded walls containing low sound transmission loss paths. The shielding effect of the building is a function of frequency and may be estimated on the basis of Fresnel diffraction theory by using the following parameter.

$$v = h \left( \frac{2}{\lambda} \right)^{1/2} \tag{5.18}$$

where  $h$  is the distance down from the top of the building to the observer, and  $\lambda$  is the wave length of sound. Figure 6.20 illustrates the arrangement. In this case the building is assumed to be at least four times as wide as the distance  $h$ . Then the reduction in each octave band, from the level that would exist without a building is

$$\Delta = 7 \log_{10} v - 7.1 \text{ dB} \tag{6.19}$$

for  $0.1 \leq v \leq 2.0$

and

$$\Delta = 20 \log_{10} v - 7.1 \text{ dB} \tag{6.20}$$

for  $v > 2.0$ .

Once the vehicle lifts from the pad, this shielding effect will be reduced and finally lost when the vehicle is effectively overhead. This should be borne into consideration for buildings at the launch pad. Further details on diffraction of sound around buildings are covered in Chapter 8.

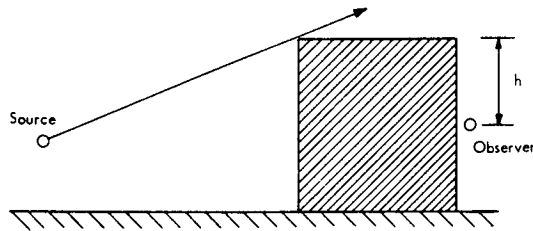
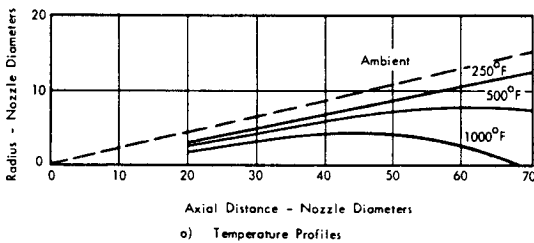


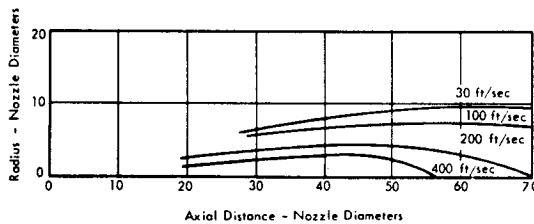
FIGURE 6.20 Building Shielding

6.1.10 EXHAUST BLAST VELOCITY AND TEMPERATURE ENVIRONMENTS

As the vehicle lifts from the launch pad, the exhaust flow will spill over the deflector opening and the launch area will be subjected to blast velocity and high temperature loads. In addition, the effect of ground wind will cause the vehicle to drift from a vertical trajectory, and the exhaust gas impingement will spread even further. Also if the drift is towards the umbilical tower, then the exhaust flow can envelop the tower. These loadings can be estimated by scaling the normalized results of Figure 6.21.



a) Temperature Profiles



b) Velocity Profiles

FIGURE 6.21 Rocket Exhaust Velocity and Temperature Profile

In Figure 6.21, the temperature and velocity profiles for a typical rocket engine exhaust are given in terms of the nozzle exit diameter. These results are for a typical rocket with gas exit velocity of 8500 fps, exit Mach number of 3.2, and gas exit temperature of 3600 °R. The results can be scaled to other rocket engines of different exit conditions by use of a core length  $x_c$ . This will be  $15 D_e$

for the example of Figure 6.21. For a different flow velocity, the new core length is calculated using Equation (6.14), the axial scale adjusted, and the given velocities scaled according to the exit velocities. These profiles can then be overlayed on a drawing of the launch pad and umbilical tower to give the predicted loadings. The results are positioned on the vehicle trajectory to determine the maximum loading during launch.

For clustered nozzles, the contours for a single nozzle are calculated and applied in turn to each of the outer nozzles, and the results smoothed to provide the final contours.

The fluctuating velocities in the exhaust stream can be estimated as having an rms intensity of 0.1 times the mean velocity. Thus, at the 100 fps contour, the fluctuating velocity rms intensity will be 10 fps. If  $V$  is the mean velocity, then the static pressure is

$$P \approx 1/2 \rho V^2 \tag{6.21}$$

where  $\rho$  is the density, and assumed 0.0015 slug/ft<sup>3</sup> if unknown,

and  $P$  is then the pressure in psf.

The fluctuating velocity component will result in a fluctuating pressure. Setting the intensity of the fluctuating velocity component equal to 0.1 times the mean velocity, the fluctuating pressure intensity is

$$p' = 20 \log_{10} P \text{ (psf)} + 113.5 \tag{6.22}$$

in dB, re: 0.0002 microbar.

The spectrum of the fluctuating pressures can be estimated from the turbulence spectrum and the results of Figure 6.22 may be used with the calculated overall level. Here  $x$  is the distance from the nozzle to the point under consideration, and  $x_c$  is the length of the laminar core as given by Equation 6.14.

The drift in the vertical trajectory due to the wind loading is quickly calculated from the basic parameters. The total wind drag loading can be obtained by assuming a drag coefficient of 1, and then the sideways acceleration calculated from the vehicle mass.

$$\ddot{y} = F/M \tag{6.23}$$

where  $\ddot{y}$  is the sideways acceleration in fps

$M$  is the vehicle on-pad mass in slugs

and  $F$  is the applied wind force in pounds.

The initial vehicle acceleration,  $\ddot{z}$ , is obtained from the trajectory details, or estimated as typically 0.3 g (9.6 ft/sec<sup>2</sup>). Then the drift angle is given by,

$$\tan^{-1} \theta = \ddot{y}/\ddot{z} \tag{6.24}$$

where  $\theta$  is the angle of the trajectory to the vertical.

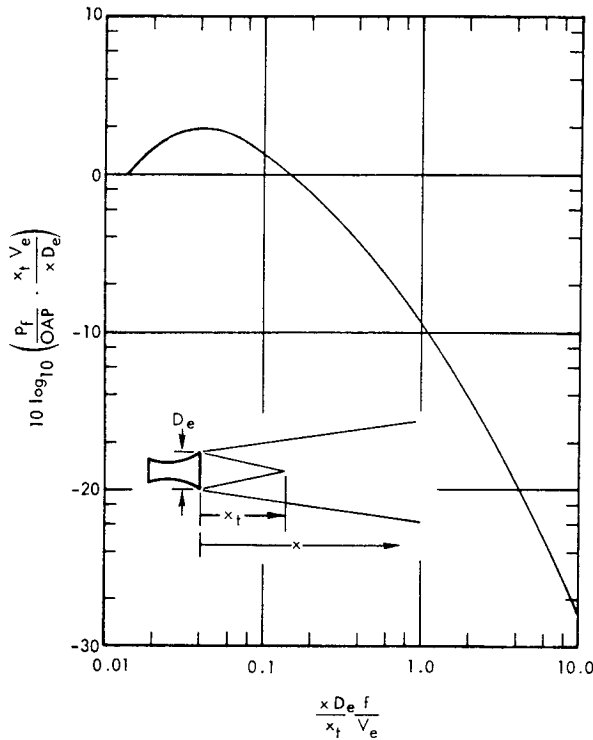


FIGURE 6.22 Normalized Spectra for Fluctuating Pressures Due to Exhaust Impingement

The effect of wind drift will be to increase the loadings for a point over which the vehicle moves. The temperature loading can show a significant increase due to this effect in the first few seconds of flight.

As an example, the contours of the exhaust blast velocity and temperature for the Saturn V, both with a vertical trajectory and the maximum allowable wind drift, were

calculated. The maximum loadings that would then occur were plotted on a plan of the launch area in Figure 6.23. The results show that drift causes the contours to be shifted by almost 50 ft at the pad level, and that the roof of the Pad Terminal Connection Room could then fall into the area of influence. The contours of Figure 6.23 show that the temperatures over the Instrument Bay Rooms could reach 240°F, which would require special roofing. The blast velocity will not be too significant at these points, 150 ft from the initial center line of the vehicle, although a mean pressure of over 1 psf will be felt. The fluctuating loading will be small, and generally insignificant compared to the acoustic loading.

The launcher umbilical tower will receive considerable loading if the maximum allowable drift occurs directly towards the tower. The vehicle will just clear the top of the tower, and the top landings and associated systems will be placed directly into the exhaust flow.

### 6.1.11 CONCLUDING REMARKS

The techniques recommended here for rocket noise prediction are empirical. They do not involve the detailed studies of source spectrum location or the detailed mechanisms of noise generation. However, they will produce consistent results, in good agreement with measured values. Recent studies have indicated the complicated nature of rocket jet noise generation, and techniques to determine the relative importance of the different noise generation processes have been proposed, (Reference 6.2). There is still some degree of controversy over the source allocation in the exhaust flow, and the methods of dealing completely with deflected and clustered flows remain uncertain. Therefore, it is recommended that the empirical methods presented here are the most suitable for quick estimation of the rocket exhaust noise environment. If more detailed answers are preferred, then it is recommended that the source spectrum location technique of Reference 6.4 be utilized. Finally, it should be noted that the empirical results are limited to the present and next generation of chemical rocket exhaust flows.

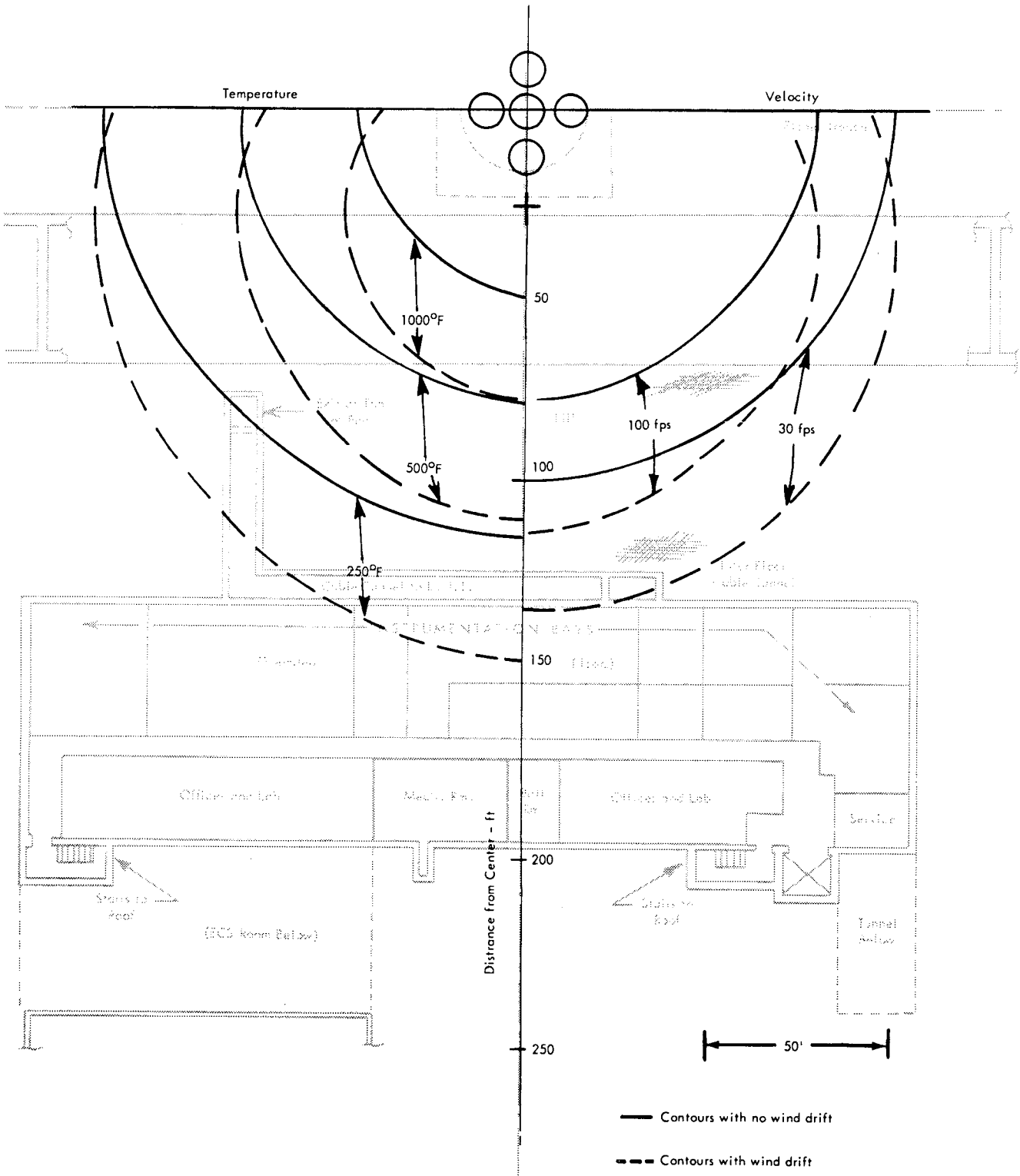


FIGURE 6.23 Exhaust Blast Velocity and Temperature Profiles, Complex 39, Roof of Pad Terminal Connection Room, Kennedy Space Center

## 6.2 PROPELLANT EXPLOSIONS

### 6.2.1 INTRODUCTION

The uncontrolled release of energy stored within rocket propellants will result in an uncontrolled chemical reaction which may take the form of a deflagration or detonation. When the chemical reaction process occurs at a low rate of energy release, it is called a (slow) burning or deflagration. If the reaction process occurs at a high rate of energy release, the reaction is called a detonation and it is characterized by a reaction front moving at a supersonic speed, burned gas flowing after the front, and a pressure increase through the front (now called a shock front). A detonation wave in the propellants generates the shock wave in air that characterizes the blast of rocket explosions. Thus, the capability of some propellants to react at a high rate of energy release makes them possible "explosives".

The propellant explosions covered in this manual include both liquid and solid propellants, however, the emphasis is placed on liquid oxygen ( $LO_2$ ) for the oxidizer and either the hydrocarbon (RP-1) or liquid hydrogen ( $LH_2$ ) for the fuel. These are stressed since they represent the most common types of propellants proposed for future rocket booster vehicles. (Ref. 6.15, 6.16)

The predicted blast parameters are based partly on data from "equivalent" TNT explosions, with additional details from theoretical analyses of nuclear explosions, (Ref. 6.17 - 6.21). However, the essential differences between explosions from solid explosives and liquid propellants are recognized and have been analyzed in detail (Ref. 6.22 - 6.24). Available experimental data are used, where appropriate, to support the estimated blast parameters proposed for regions close to rocket propellant explosions. (Ref. 6.25) The latter data will not be presented in detail, however, since they represent only preliminary results from part of an extensive and continuing program (Project Pyro) directed towards a detailed experimental evaluation of propellant blast phenomena.

### 6.2.2 EXPLOSION ENERGY OF ROCKET PROPELLANTS

For an explosion to occur, reacting propellants must first, of all, mix. This can occur accidentally, for instance, because of leaks or rupture of the tanks or propellant feed systems, or intentionally due to initiation of a vehicle destruct signal. The fuel to oxidizer mixture ratio must fall within a certain range before the reaction can start. This reaction can then start spontaneously because of the strong affinity of the propellants (hypergolic propellants) or be started by external energy sources such as: heat, an electrical spark, shock, friction, et cetera. Once the reaction is started, the heat released by the initial reaction will be sufficient to trigger further reaction in the remaining propellants. The speed of this chain reaction defines the rate of energy release for given propellants. The rate of energy release is not a constant but varies with the mixture ratio, the temperature of the propellants, the degree of turbulence, and the amount of propellant.

The total energy released will be a function of the amount of mixed propellant which will, in turn, depend on the geometry of the propellant tankage, the geometry of the surrounding launch or test stand, the position and velocity of the vehicle, the mode of the failure, the rate of vaporization of the released gases, the rate of liquid mixing, the physical characteristics of the propellants and, finally, the delay in the ignition process. Thus, the energy which is expected to be released,  $E_o$ , might be expressed in the form

$$E_o = \eta_e \cdot E \cdot \left[ \eta_m \cdot W_p \right] \quad (6.25)$$

where

$\eta_e$  = Chemical efficiency of the explosion for a given quantity of reacting propellant

$E$  = Energy released per unit propellant weight for 100 percent efficiency

$\eta_m$  = Fraction of the total propellant weight,  $W_p$ , that is mixed.

No successful attempts to predict values of  $\eta_e$  and  $\eta_m$  have been found in the literature.

The expression for the theoretical energy  $E$  released by an explosion of reacting propellants can be stated in the following form (Reference 6.30 and 6.24):

$$E = \int p dV = -H + Q \quad (6.26)$$

where

$\int p dV$  = Mechanical work done by explosion products on surrounding atmosphere

$H$  = Heat of explosion (change in chemical energy)

$Q$  = Internal energy (change in temperature and entropy).

To define  $H$  and  $Q$ , it would be necessary to know the products of the explosion. These cannot be readily determined for most propellant explosion reactants. However, for perfect or stoichiometric burning of the fuel in a balanced or oxidizer rich mixture, the heat of the explosion can be assumed equal to the heat of combustion. The heat of the explosion is inherently negative, as viewed from the point of view of a decrease of chemical energy, and its net contribution to the energy of an explosion is therefore positive. Since it is generally the larger source of explosive energy and can be defined in terms of the known heat of combustion, it is listed in the fourth column of Table 6.3. The value indicated is actually the ideal heat of combustion for one pound of fuel divided by one plus the mixture ratio to convert it to an energy per pound of propellant. The mixture ratios used, shown in the third column of Table 6.3 are typical values, not stoichiometric values, so that the maximum heat of explosion indicated is only a rough estimate of the explosive energy for comparison of various fuel combinations.

TABLE 6.3  
ENERGIES OF PROPELLANT COMBINATIONS

PROPELLANT COMBINATION OXIDIZER FUEL	(1) MIXTURE RATIO	H MAXIMUM HEAT OF EXPLOSION BTU/lb.	Y P TNT (2) EQUIVALENT YIELD %	E <sub>0</sub> TNT EQUIV. EXPLOSION ENERGY BTU/lb.
TNT (Explosive)	-	1170	100	2000
Oxygen Hydrogen	5:1	8590	60	1200
Oxygen RP-1	2.25:1	5700	10	200
Oxygen Ammonia	1.3:1	3470	10	200
Oxygen Ethyl Alcohol	1.5:1	5120	10	200
RFNA Aniline	3:1	8250	10	200
RFNA UDMH	2.6:1	3940	10	200
RFNA JP-4	4.1:1	3630	10	200
Nitrogen Tetroxide Hydrazine	1.1:1	3950	5	100
Nitrogen Tetroxide 50% UDMH 50% Hydrazine	2:1	3750	5	100
Tetranitromethane Hydrazine	1.4:1	3460	100	2000
Bromine Pentafluoride Ammonia	6:1	1140	10	200
Chlorine Trifluoride Ammonia	3:1	2000	10	200
Chlorine Trifluoride Hydrazine	2.5:1	2380	5	100

1) Nominal weight ratios (Reference 6.28 , and 6.29)

2) Static test standonly - see Table 6.4



Thus, as indicated by the preceding discussion, theoretical prediction of the total energy in a rocket propellant explosion must rely on data which are either not readily available or have not been calculated. It is necessary, therefore, to use experimental or empirical results.

Since results were not yet available from Project Pyro on explosive yields of various propellant combinations, it was considered advisable, for this manual, to use the TNT equivalents as recommended by the Department of Defense in Reference 6.26. These are listed in Table 6.4 for static test stands and launch pads. They represent the weight of an equivalent charge of TNT, expressed as a percentage of the total propellant weight which releases the same total energy,  $E_o$ .

Therefore,  $E_o$  may be estimated by the following relation-

$$E_o = Y_p W_p E_{TNT}$$

where

$Y_p$  = Fractional TNT equivalent yield

$W_p$  = Weight of propellant

$E_{TNT}$  = Energy released per unit weight of TNT (2000 BTU/lb).

Values of  $E_o$ , calculated by the above expression are presented in the last column of Table 6.3. A comparison of the maximum heat of explosion and TNT equivalent energy  $E_o$  shows that the latter varies from 2.3 to 5.8 percent of the former.

TABLE 6.4  
ROCKET PROPELLANT (TNT) EQUIVALENCIES

Propellant Combination	Static Test Stands	Range Launch Pads
LO <sub>2</sub> - LH <sub>2</sub>	60%	60%
LO <sub>2</sub> - LH <sub>2</sub> + RP - 1	Sum of { (60% for LO <sub>2</sub> - LH <sub>2</sub> (10% for LO <sub>2</sub> - RP-1	Sum of { (60% for LO <sub>2</sub> - LH <sub>2</sub> (20% for LO <sub>2</sub> - RP-1
LO <sub>2</sub> - RP-1 or LO <sub>2</sub> - NH <sub>3</sub>	10%	20% up to 500,000 pounds plus 10% over 500,000 pounds
RFNA - Aniline*	10%	10%
RFNA - UDMH*	10%	10%
RFNA - UDMH + JP-4*	10%	10%
N <sub>2</sub> O <sub>4</sub> - UDMH + N <sub>2</sub> H <sub>4</sub> *	5%	10%
N <sub>2</sub> O <sub>4</sub> - UDMH + N <sub>2</sub> H <sub>4</sub> - Solid*	5% plus the explosive equivalent of the solid propellant	10% plus the explosive equivalent of the solid propellant
Tetranitromethane (alone or in combination)	100%	100%
Nitromethane (alone or in combination)	100%	100%
Solid	20%	20%

\* These are hypergolic combinations.

Basis: Recommendations of ASESB Work Group on Explosive Equivalents for Liquid Propellants. Tetranitromethane and nitromethane are known to be detonable.

- NOTES:
1. The percentage factors to be used to determine the explosive equivalencies of propellant mixtures at launch pads and static test stands when such propellants are located above ground and are unconfined except for their tankage. Any configurations other than stated above should be considered on an individual basis to determine the equivalencies.
  2. The equivalencies of any non-nuclear explosives will be added to the above equivalencies.
  3. The above values were obtained from Reference 6.26.

### 6.2.2.1 Explosion Energies for Possible Future Vehicle Configurations

It is useful to list briefly the configurations which may be characteristic of future rockets in order to determine the energy which might be released in an accidental explosion. For this purpose, data on 8 rocket configurations have been grouped in Table 6.5. From the current Saturn IB ( $1.5 \times 10^6$  lb of thrust) to the advanced LH<sub>2</sub> - LO<sub>2</sub> configurations ( $30.2 \times 10^6$  lb of thrust), the explosive energy is seen to increase from  $.37 \times 10^{12}$  ft. lb. ( $.24 \times 10^6$  lb. TNT-equivalent) to  $19.9 \times 10^{12}$  ft. lb. ( $12.8 \times 10^6$  lb. TNT-equivalent) which means that the peak overpressure might, in the future, be 60 times what is presently expected from a Saturn IB explosion. However, the TNT-equivalencies of Table 6.5 were calculated using the propellant percentages suggested by Reference 6.26 (Table 6.4) and it is felt that these percentages are conservative for large rockets since, for the latter, a lower mixing efficiency is anticipated. However, actual experience with a current vehicle in the 300,000 pound thrust class has indicated that a 10 percent equivalent TNT yield for LOX/RP-1 is realistic. It is believed that a  $5 \times 10^6$  lb. TNT-equivalency can be considered reasonable for the largest of the above future

vehicles. On the other hand, the reader is cautioned to use the D.O.D. specifications in Reference 6.26 until they have been officially superseded. A  $5 \times 10^6$  lb TNT equivalent explosion is then chosen to carry out sample calculations which can be repeated for any other TNT equivalency. Table 6.5 also includes the estimated maximum chemical energy and mechanical energy available. The maximum chemical energies exceed both the mechanical and explosive energies. The chemical energies are based on heats of combustion of 51,500 BTU/lb for H<sub>2</sub> and 18,500 BTU/lb for RP-1. It would have been more accurate to choose about 40,000 and 16,000 BTU/lb, respectively, to take into account the fact that the mixture ratios actually used are not stoichiometric. The mechanical energy is the total kinetic energy of the exhaust gases estimated by  $Wp (V_e^2/2g)$  where  $Wp$  is the propellant weight,  $V_e$  the exit velocity, and  $g$  is the acceleration of gravity. The estimated TNT equivalent explosion energy is about 10 to 40 percent of the mechanical energy.

TABLE 6.5

FUTURE VEHICLE CONFIGURATIONS

Number Designation <sup>(5)</sup>	1 Saturn IB	2 Saturn V	3 Advanced Saturn	4 Saturn V Plus Solid	5 IC Class I	6 24-6 Class II	7 33	8 T65C
Number of Stages	2	3	3	3	3	3	2	3
Lift-off Thrust (lb x 10 <sup>6</sup> )	1.5	7.5	9.0	7.5 3.4 <sup>(6)</sup>	32.4	18.0	30.2	54.9
Lift-off Weight (lb x 10 <sup>6</sup> )	1.37	6.8	8.0	9.5	25.2	14.4	24.2	38.1
Total Length (ft.)	225	361	410	336	454	386	377	535
Maximum Diameter (ft.)	22	33	33	55	69	70.5	80	70
FIRST STAGES Propellants and Weight (lb x 10 <sup>6</sup> )	{ LOX 0.69 <sup>(1)</sup> RP-1 0.31 <sup>(1)</sup>	{ LOX 3.2 <sup>(1)</sup> RP-1 1.42 <sup>(1)</sup>	{ LOX 3.74 <sup>(1)</sup> RP-1 1.66 <sup>(1)</sup>	{ LOX 3.05 <sup>(1)</sup> RP-1 1.35 <sup>(1)</sup> + Solid	{ LOX 12.91 RP-1 5.74	{ LOX 9.08 LH <sub>2</sub> 1.3	{ LOX 18.6 LH <sub>2</sub> 2.7	Solid
Mixture Ratio <sup>(3)</sup>	2.25:1 <sup>(1)</sup>	2.25:1 <sup>(1)</sup>	2.25:1 <sup>(1)</sup>	2.25:1 <sup>(1)</sup>	2.25:1	7:1	7:1	-

TABLE 6.5 (CONTINUED)

Number Designation <sup>(5)</sup>	1 Saturn 1B	2 Saturn V	3 Advanced Saturn	4 Saturn V Plus Solid	5 IC Class I	6 24-6 Class II	7 33	8 T65C
Total Propellant Weight (lb x 10 <sup>6</sup> )	1.0	4.62	5.40	4.40 1.68 <sup>(6)</sup>	18.65	10.38	21.3	25.0
Engines Number and Type	8 H-1	5 F-1	5 F-1A	5 F-1A 4-120 in	18 F-1A	18HP-1	24HP-1	6-260 in
Exit Velocity <sup>(1)</sup> (ft/sec)	8,100	9,300	10,200	10,200 7,800 <sup>(6)</sup>	10,200	12,300	12,300	8,500
Maximum Chemical Energy (lb. ft x 10 <sup>12</sup> ) <sup>(2)</sup>	4.45	20.4	23.9	19.4 3.5 <sup>(6)</sup>	82.5	52.0	108.0	50.5
Total Mechanical Energy (lb. ft x 10 <sup>12</sup> )	1.02	6.2	8.72	7.1 1.6 <sup>(6)</sup>	30.2	24.4	50.1	28.1
TNT Equivalent (lb x 10 <sup>6</sup> )	0.10	0.462	0.54	0.78	1.86	6.22	12.8	5.0
SECOND STAGES								
Propellants and Weight (lb x 10 <sup>6</sup> )	LOX 0.198 <sup>(1)</sup> LH <sub>2</sub> 0.039 <sup>(1)</sup>	LOX 0.7825 <sup>(1)</sup> LH <sub>2</sub> 0.1565 <sup>(1)</sup>	LOX 1.0 <sup>(1)</sup> LH <sub>2</sub> 0.2 <sup>(1)</sup>	LOX 1.0 <sup>(1)</sup> LH <sub>2</sub> 0.2 <sup>(1)</sup>	LOX 2.398 LH <sub>2</sub> 0.587	LOX 1.4 LH <sub>2</sub> 0.206	LOX 0.05 LH <sub>2</sub> 0.01	LOX 6.85 LH <sub>2</sub> 1.37
Mixture Ratio <sup>(3)</sup>	5:1 <sup>(1)</sup>	5:1 <sup>(1)</sup>	5:1 <sup>(1)</sup>	5:1 <sup>(1)</sup>	5:1	7:1	5:1	5:1
Total Propellant Weight (lb x 10 <sup>6</sup> )	0.237	0.939	1.2	1.2	3.53	1.6	0.06	8.22
Engines Number and Type	1J-2	5J-2	5 RL-20	5J-2	3M-1B	2HP-1	6LR-115	3M-1
Exit Velocity <sup>(1)</sup> (ft/sec)	12500	12500	12500	12500	12500	12500	12500	12500
Maximum Chemical Energy (lb. ft x 10 <sup>12</sup> ) <sup>(2)</sup>	1.57	6.25	8.0	8.0	23.5	8.24	0.4	54.8
Total Mechanical Energy (lb. ft x 10 <sup>12</sup> )	0.576	2.28	2.92	2.92	8.57	3.88	0.146	20.0
TNT Equivalent (lb x 10 <sup>6</sup> )	0.142	0.563	0.72	0.72	2.12	0.96	0.036	4.92

TABLE 6.5 (CONTINUED)

Number Designation <sup>(5)</sup>	1 Saturn 1B	2 Saturn V	3 Advanced Saturn	4 Saturn V Plus Solid	5 IC Class I	6 24-6 Class II	7 33	8 T65C
THIRD STAGES								
Propellants and Weights (lb x 10 <sup>6</sup> )	-	LOX 0.198 <sub>(1)</sub> LH <sub>2</sub> 0.0394 <sub>(1)</sub>	LOX 0.292 <sub>(1)</sub> LH <sub>2</sub> 0.058 <sub>(1)</sub>	LOX 0.292 <sub>(1)</sub> LH <sub>2</sub> 0.058 <sub>(1)</sub>	LOX 0.05 LH <sub>2</sub> 0.01	LOX 0.05 LH <sub>2</sub> 0.01	-	N <sub>2</sub> O <sub>4</sub> 0.0485 Aerozine 0.027
Mixture Ratio <sup>(3)</sup>	-	5:1 <sub>(1)</sub>	5:1 <sub>(1)</sub>	5:1 <sub>(1)</sub>	5:1	5:1	-	1.8:1
Total Propellant Weight (lb x 10 <sup>6</sup> )	-	0.237	0.350	0.350	0.06	0.06	-	0.0576
Engines Number and Type	-	1 J-2	1 RL-20P3	1 RL-20P3	6LR-115	6LR-115	-	2T-20K
Exit Velocity <sup>(1)</sup> (ft/sec)	-	12500	12500	12500	12500	12500	-	Not Available
Maximum Chemical Energy (lb.ft x 10 <sup>12</sup> )	-	1.575	2.32	2.32	0.4	0.4	-	Not Available
Total Mechanical Energy (lb.ft x 10 <sup>12</sup> )	-	0.576	0.850	0.850	0.146	0.146	-	Not Available
TNT Equivalent (lb x 10 <sup>6</sup> )	-	0.142	0.21	0.21	0.036	0.036	-	Not Available
TOTALS								
Maximum Chemical Energy (lb.ft x 10 <sup>12</sup> )	6.02	28.22	34.22	33.22	106.4	60.64	108.4	106
Mechanical Energy (lb.ft x 10 <sup>12</sup> )	1.59	9.06	12.49	12.47	38.9	28.43	50.25	48.1
TNT EQUIVALENT <sup>(4)</sup> (lb.ft x 10 <sup>12</sup> )	0.375	1.81	2.28	2.65	6.24	11.2	19.9	15.4
TNT EQUIVALENT <sup>(4)</sup> (lb x 10 <sup>6</sup> )	0.242	1.17	1.47	1.71	4.02	7.22	12.84	9.92
<p>(1) Theoretical Value, the effective value being unknown</p> <p>(2) Based on 18,500 BTU/lb for RP-1; 51,500 BTU/lb for H<sub>2</sub>; 2600 BTU/lb for solids</p> <p>(3) The mixture ratio is not necessarily equal to the ratio of the propellant weights</p> <p>(4) TNT Equivalencies in lb.ft are equal to TNT equivalencies in lb. TNT times 1.55 x 10<sup>6</sup></p> <p>(5) Data of configurations 1 through 4 from personal communication with R. Jewell, Chief of Advanced Methods and Research Section, P and VE, MSFC, Huntsville, Alabama - Data of configurations 5 through 8 from Reference 6.15</p> <p>(6) Solid strap-on</p>								

6.2.3 THE SHOCK WAVE FORMATION

6.2.3.1 The Origin of the Air Shock

If the energy stored in a rocket propellant is under an uncontrolled situation, a deflagration or a detonation occurs. A deflagration creates a pressure wave in air which is far less important, from a structural design viewpoint, than the shock wave produced by a detonation. Consider a mixture of liquid propellants resulting from a tank rupture and assume that a detonation starts at a point in the mixture. Then the detonation propagates through the mixture at high speed until the interface between the propellant mixture and air is reached. At this point a volume of high energy gases is present, where the propellant mixture existed previously. The gases, surrounded by an atmosphere at lower pressure, expand outward, thus generating a shock wave in the atmosphere itself. This wave is called a shock wave, because the air properties change suddenly at its front. On the shock front, the pressure, density, and temperature of the air rise almost instantaneously. Behind the shock, a strong blast wind is initiated which moves in the direction of the shock wave. Eventually, the pressure and density will decay to values lower than their original ambient values and the wind will reverse its direction. Finally, the pressure and temperature will return to ambient levels and the blast wind will cease. The variations of pressure, density, temperature, and particle velocity with time and distance are illustrated qualitatively in Figure 6.24.

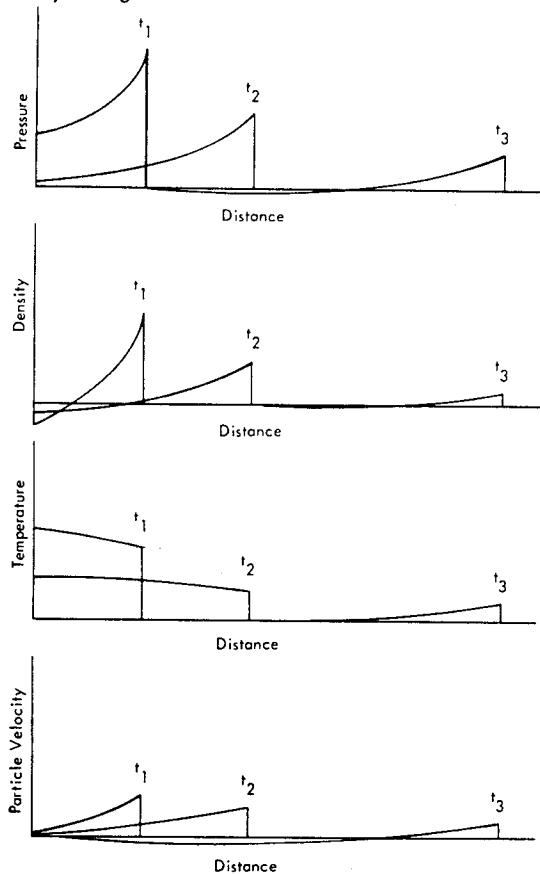


FIGURE 6.24 Qualitative Variations of Air Blast Parameters with Distance and Time

6.2.3.2 Air-Shock Ground Interactions

So far an explosion in an unbounded space has been described. This is the case of a rocket exploding at a high altitude. If the explosion occurs on the ground surface, the air blast parameters will correspond approximately to an unbounded explosion releasing twice as much energy.

When the explosion occurs during the initial part of the flight near the ground, the shock pattern is slightly more complicated. In this case the shock is reflected when it reaches the ground and the incident and reflected shocks originate a third shock called the "Mach Stem" which is normal to the ground at the ground level. The blast parameters as experienced by an observer standing on the ground, may now be different from those previously described. Sketch A of Figure 6.25 illustrates the reflection process. Sketch B illustrates a particular aspect of the reflection process; the generation of the "Mach Stem". It was stated above that a strong wind follows the shock front. A similar wind also follows the reflected shock, and has to be parallel to the ground. Since this is not always compatible with a two shock system, a single shock is created near the ground. This third shock is the "Mach Stem", and is stronger than both the incident and reflected shocks. Before the formation of the "Mach Stem", in what is called the "Regular Reflected Region", an observer, somewhat above the ground level, would actually experience two shocks. After the formation of the "Mach Stem" an observer would experience one or two shocks according to whether he is located below or above the triple point surface (Sketch C, Figure 6.25).

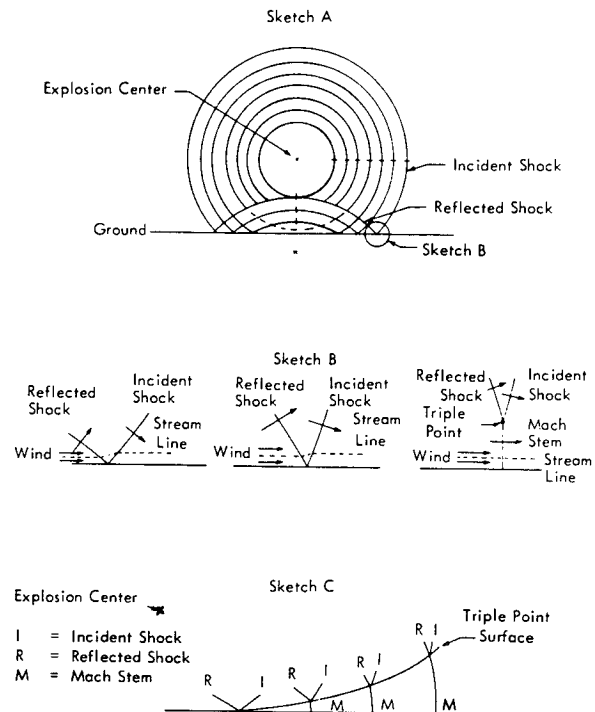


FIGURE 6.25 Ground Reflection of a Spherical Blast Wave and Mach Stem Foundation

### 6.2.3.3 Elements Determining the Air Shock Parameters

At large distances from an explosion, the explosion energy is the major element in defining the air shock parameters. Unfortunately, as indicated earlier, no useful theoretical methods are available for predicting the amount of energy that is released in a rocket explosion. Thus, the empirical methods for defining the total energy released, in terms of TNT equivalent, must be used. It will be shown, in fact, that only the TNT equivalent and the distance from the blast center are necessary to define the nominal air shock parameters at large distances from a propellant explosion. For an explosion of a large rocket, such distances extend beyond about 1000 ft. with peak overpressures less than about 1 atmosphere.

For very large distances, weather effects become as important as the total energy. Communities located at a distance of 20 miles would suffer no damage from a rocket explosion of  $5 \times 10^6$  lb TNT energy equivalent for a uniform atmosphere. The peak overpressure would be .04 psi and window breakage would normally not be expected. But under extreme atmospheric focusing conditions, the local peak overpressure can be multiplied by a factor of 5, thus, reaching an overpressure which would normally be expected by an explosion with about 4 times the energy of the actual explosion, and window breakage would very likely occur. Propagation anomalies associated with blast are covered in more detail in Chapter 7. Nominal weather conditions without focusing are assumed throughout the remainder of this chapter.

For regions close to a blast, the rate at which the energy is released, and the initial air shock velocity also influence the air parameters. This region generally encompasses only the immediate vicinity of a launch pad or rocket test site.

### 6.2.3.4 The Close- and Far-Field

The close-field is the region within which the air blast parameters are functions of explosive mass to energy ratio, rate of energy release, initial air shock velocity, and chemical properties of the explosive, in addition to the total energy released.

The far-field is the region within which the air blast parameters are functions only of the total energy released.

If it were possible to theoretically calculate all the shock parameters for a propellant explosion, there would be no need to distinguish between the close-field and far-field. Such a theoretical calculation has, in fact, been successfully made for TNT explosions by Brode. (Reference 6.18). In the far field of a propellant explosion, where only energy released is significant, it does not matter where the energy comes from, and air shock parameters computed (or observed) for a TNT explosion, are applicable to propellant explosions.

In the close-field however, results for TNT are not directly applicable to propellant explosions due to the influence of the additional effects such as rate of energy release. Thus, a deviation from the TNT blast parameters is expected in this region. This will be illustrated subsequently.

For explosions from a large rocket, it is convenient to use the following ranges of overpressure to distinguish the two fields.

Far-Field:	Peak overpressure	$\leq$	14.7 psi
Close-Field:	Peak overpressure	$\geq$	14.7 psi

### 6.2.4 BLAST SCALING LAWS

The charts which are given in Section 6.2.5 for the calculations of the blast parameters are entered with TNT equivalencies using scaling laws. It is therefore necessary to define these blast scaling laws, and their ranges of applications. These relationships are simply defined in the present section. Detailed explanations are given in Reference 6.27.

The energy of any explosion is commonly measured in terms of the weight of a given explosive whose explosion energy is known. TNT, which releases 252.28 K cal/mole or  $1.55 \times 10^6$  ft. lb/lb<sub>TNT</sub>, is currently used as the equivalent energy unit for explosions. The "yield" of all propellant explosions is the equivalent TNT weight expressed as a percentage of the propellant weight.

Brode has shown theoretically that the overpressure  $P_{so}$  from a free air blast can be defined in dimensionless form as follows. (Reference 6.18.)

$$\frac{P_{so}}{P_o} = F_1(\lambda) = F_1\left(\frac{d}{(E/P_o)^{1/3}}\right)$$

where:

$P_{so}$	=	Peak overpressure due to TNT explosion
$P_o$	=	Atmosphere pressure = 2116 lb/ft <sup>2</sup> (Standard atmosphere)
$\lambda$	=	Reduced distance
$d$	=	Actual distance in ft.
$E$	=	Energy of blast in lb · ft
$F_1(\lambda)$	=	Function of the parameter $\lambda$

Since for standard atmospheric conditions,

$$\frac{E}{P_o} = \frac{W_T \times 1.55 \times 10^6}{2116} = 733 W_T$$

where  $W_T$  = Weight of TNT in Lb,  $P_{so}$  may be expressed by the following function

$$P_{so} = F_2(Z)$$

where  $Z = d/W_T^{1/3} = 9.02 \lambda$  — free air burst.

This means that for equal values of  $Z$ ,  $P_{so}$  is the same, or in other words, for a given overpressure, the distances scale with the cube root of TNT equivalency. For a surface burst, the blast parameters are equivalent to that of a free air burst with twice the energy of the surface burst. Thus, the theoretical blast parameters for a free air burst can be used for a surface burst. In this case

$$Z = \sqrt[3]{2} \cdot 9.02 \lambda = 11.37 \lambda \text{ - surface burst.}$$

The same scaling can be applied to the altitude of an above the ground explosion. Thus, the following relationships can be written:

$$\frac{d}{d_r} = \frac{h}{h_r} = \frac{W_T^{1/3}}{W_{Tr}^{1/3}} \quad (6.27)$$

These scaling laws state that: For a given overpressure, the distance from the explosion ( $d$ ), and explosion altitude ( $h$ ) are proportional to the cube root of the explosion energy ( $W_T$ ). Cube root scaling can also be applied to arrival time, phase durations, and impulse provided that the distances are first scaled according to the cube root law.

This comes from the following theoretical dimensionless relationships (Reference 6.18) for duration and impulse of the positive overpressure pulse.

$$D_p^+ = \frac{t_p^+ c_o}{[E/p_o]^{1/3}} = \Phi \left( \frac{d}{[E/p_o]^{1/3}} \right) \quad (6.28)$$

$$i_p^+ = \int_{\tau_s}^{\tau_s + D_p^+} \frac{P_{so}}{p_o} d\tau = \Psi \left( \frac{d}{[E/p_o]^{1/3}} \right) \quad (6.29)$$

where:

$D_p^+$  = Reduced duration of positive phase (dimensionless)

$t_p^+$  = True duration of positive phase

$c_o$  = Speed of sound

$i_p^+$  = Characteristic positive phase impulse (dimensionless)

$\tau_s$  = Reduced time of arrival  $\frac{t_s c_o}{[E/p_o]^{1/3}}$

$t_s$  = Time of arrival

From Equations 6.28 and 6.29 for standard atmospheric conditions it follows that:

$$\frac{t_p^+}{W_T^{1/3}} = \Phi_2 \left( \frac{d}{W_T^{1/3}} \right) \quad (6.30)$$

$$i_p^+ = \int_{\tau_s}^{\tau_s + D_p^+} \frac{P_{so}}{p_o} d\tau = \frac{c_o}{p_o (E/p_o)^{1/3}} \int_{t_s}^{t_s + t_p^+} P_{so} dt$$

$$= K_2 \frac{i_p^+}{W_T^{1/3}} = \Psi_1 \left( \frac{d}{W_T^{1/3}} \right)$$

$$\therefore \frac{i_p^+}{W_T^{1/3}} = \Psi_2 \left( \frac{d}{W_T^{1/3}} \right) \quad (6.31)$$

where  $i_p^+$  is the true positive phase impulse. Now, according to relationships 6.30 and 6.31 it is possible to write:

$$\left\{ \begin{array}{l} \frac{d}{d_r} = \frac{W_T^{1/3}}{W_{Tr}^{1/3}} \quad \text{a)} \\ \frac{t_p^+}{t_{pr}^+} = \frac{W_T^{1/3}}{W_{Tr}^{1/3}} \quad \text{c)} \end{array} \right\} \text{ and } \left\{ \begin{array}{l} \frac{d}{d_r} = \frac{W_T^{1/3}}{W_{Tr}^{1/3}} \quad \text{b)} \\ \frac{i_p^+}{i_{pr}^+} = \frac{W_T^{1/3}}{W_{Tr}^{1/3}} \quad \text{d)} \end{array} \right. \quad (6.32)$$

Therefore, for a given reference explosion energy ( $W_{Tr}$ ), if distances ( $d_r$ ), explosion altitudes ( $h_r$ ), impulses ( $i_{pr}^+$ ) and time and durations ( $t_{pr}^+$ ) are known as functions of peak overpressures, the corresponding values for a different explosion energy can be readily computed. The numerical examples of Section 6.2.6 will help in understanding the use of the above expressions.

In using the blast design charts of this manual, attention must be paid to the fact that the charts can be used for blast prediction of loaded rockets on the launching pad or in flight as well as for static test vehicles, partially or fully loaded which are fired at remote locations not connected with propellant storage areas. For tests of engine chambers only, further elements must be considered. During an engine test the propellants are generally fed from storage areas through pipes while the test is in process. In this case the propellant in the pipes should be considered as well as the possible delay between an initial explosion and the actual shut-down of the feeding system. Experience shows that this time is relevant. Extension of a possible explosion in the testing area to the storage areas and vice versa must also be considered. For these and other storage problems, the specifications given in Reference 6.26 are recommended. These are briefly summarized in Chapter 4.

6.2.5 DESIGN CHARTS

It has been shown (Section 6.2.3.4) that to predict blast parameters from rocket explosions, different criteria and approximations have to be used for different peak overpressure ranges.

In the present section, charts based on TNT data are given for the far-field region. Although, these can be used for the close-field as well, the results would be conservative. Estimated values for propellants are therefore provided as an alternate.

The number of significant figures used in the examples in the following section are not always consistent with the approximations inherent in the design charts in this section. Nevertheless, they are retained to help the reader follow the problems and to avoid large errors at the end of the chain-calculations. It is left to the reader to round off the numbers.

6.2.5.1 Peak Overpressure Charts

To determine the peak overpressure, due to the explosion of a known weight of propellant at a given distance, Figure 6.26 can be used. Here, peak overpressure,  $p_{50}$ , is plotted versus scaled distance,  $Z$ , which equals the ground zero distance,  $d$ , divided by the cube root of the TNT equivalent weight,  $W_T$  of propellant.

The TNT curve of Figure 6.26 has been plotted according to experimental data obtained from tests run by Ballistic Research Laboratories for pressures up to 1000 psi. The very low pressure results were obtained by Wyle Laboratories. The results for pressures in the range 1000 to 8000 psi were obtained according to the Brode theory (Reference 6.18). A comparison also has been made in Figure 6.27 between this theoretical value and experimental data, and very little difference is observed.

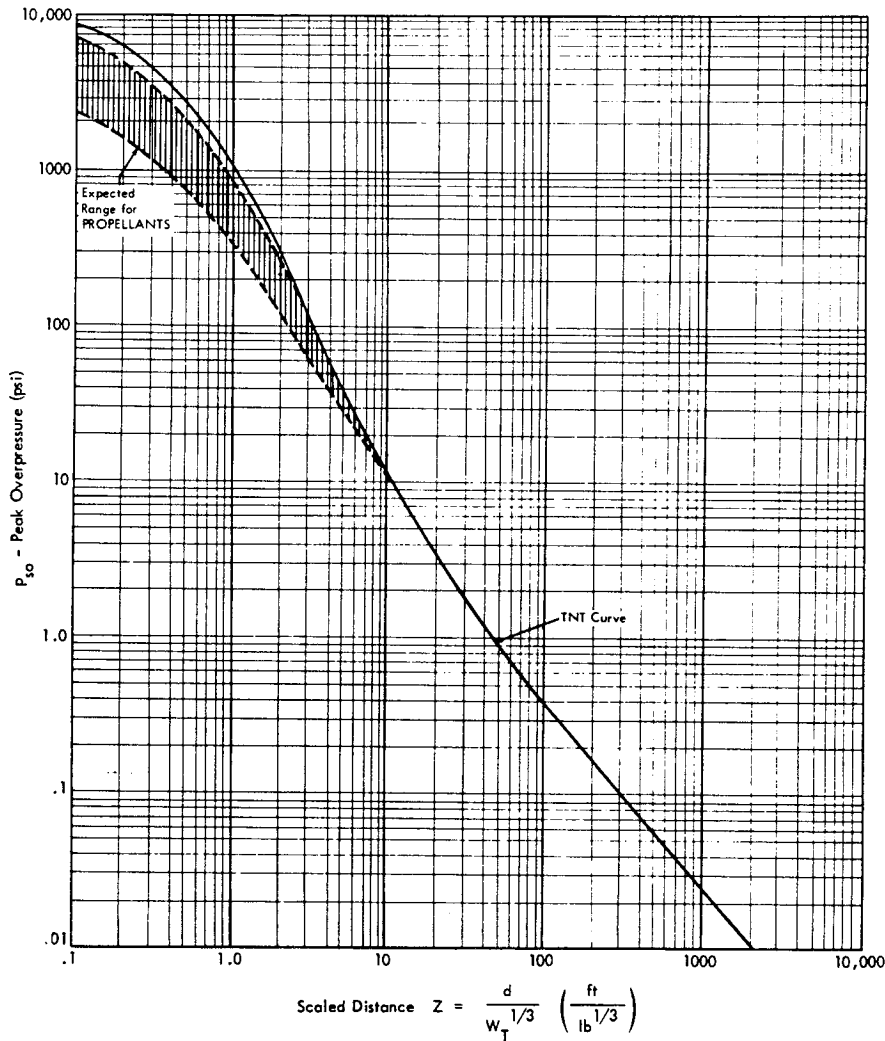


FIGURE 6.26 Peak Overpressure versus Scaled Distance for TNT Surface Explosion



In Figure 6.26, the expected range for propellant explosions has been estimated according to theory, outlined in Reference 6.24, supported by experimental data obtained from Project Pyro tests performed at the Air Force Rocket Propulsion Laboratory, Edwards, California, for NASA, Marshall Space Flight Center. (Reference 6.25).

The Project Pyro tests have included several variables which can be summarized as follows:

Propellant Type

Initial Conditions

- Weight
- Length-To-Diameter Ratio of Tank
- Propellant Orientation
- Horizontal Velocity
- Vertical Velocity

Boundary Conditions

- Confinement Within the Missile
- Confinement by the Ground Surface and Vertical Cylindrical Walls

Ignition Conditions

- Time
- Type

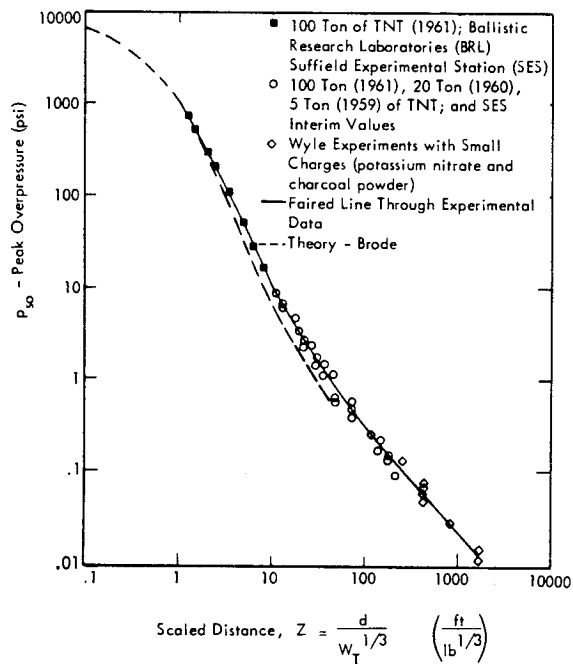


FIGURE 6.27 Peak Overpressure versus Scaled Distance for Very Large and Very Small Charges (References 6.17 and 6.18)

Experimental results obtained from a few of these tests have been plotted in Figure 6.28 (for 200 lb and 1000 lb LO<sub>2</sub>/RP-1 explosion tests) and in Figure 6.29 (for 200 lb LO<sub>2</sub>/LH<sub>2</sub> explosion tests) on the basis of the observed terminal yield. These data are representative only, and do not illustrate the important results obtained from Project Pyro on variation in yield of propellants.

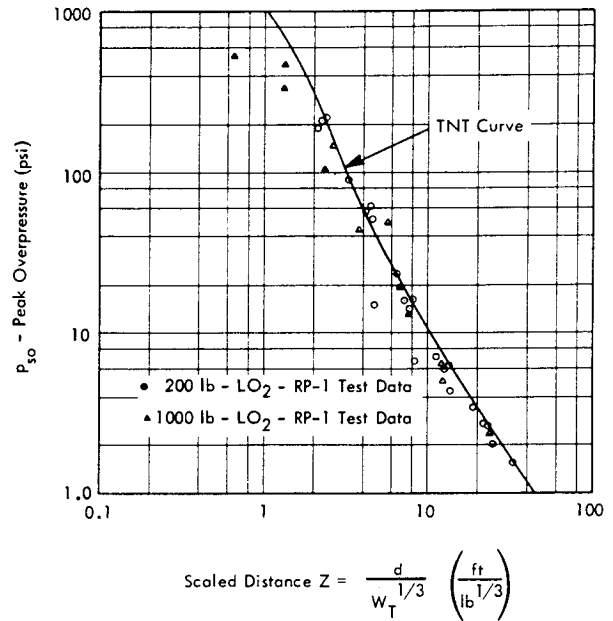


FIGURE 6.28 Peak Overpressure versus Scaled Distance for 200 lb and 1000 lb LO<sub>2</sub> - RP-1 Tests (Data from Reference 6.25)

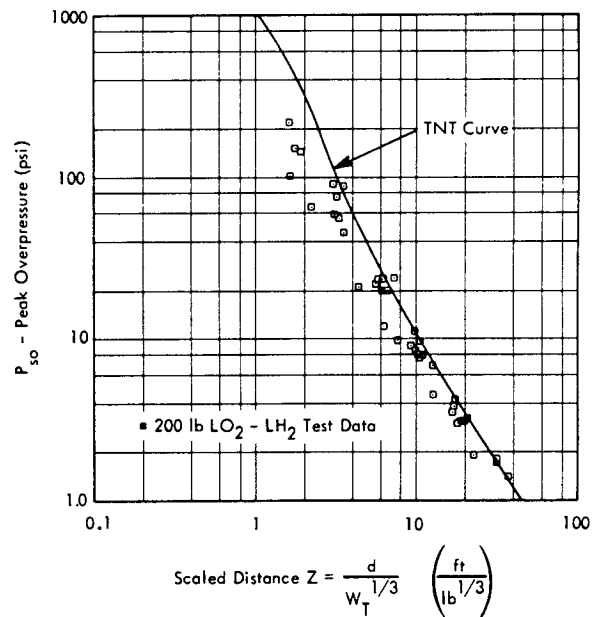


FIGURE 6.29 Peak Overpressure versus Scaled Distance for 200 lb LO<sub>2</sub>/LH<sub>2</sub> Tests (Data from Reference 6.25)

The explosive behavior of the propellant mixture in many cases is different from that of TNT so that explosive yield generally is a function of distance and of the shock wave parameters used in the computation. This behavior appears to take two general forms (Reference 6.25). For very low yields, about 1 percent and less, both pressure and impulse yields increase with increasing distance from the explosion, with the yields tending toward a constant value (The Terminal Yield) at large distances. The impulse yield is usually higher than the pressure yield and changes more slowly with distance.

For higher yields, about 10 percent and greater, the pressure yield behaves in the same fashion, but the impulse yield at close distances is much greater than the pressure yield and tends to decrease with increasing distance and ultimately approaches the pressure yield value. These trends are illustrated in Figure 6.30. Figures 6.28 and 6.29 confirm what has been previously stated, that is, in the close-field, many parameters, besides the energy released, influence the blast overpressure; for this reason in Figure 6.26, an expected range of  $P_{s0}$  values is presented instead of just one curve.

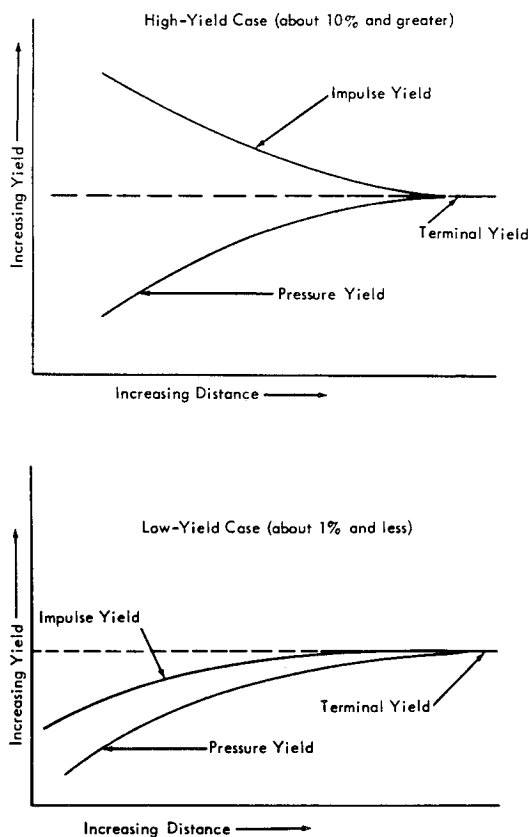


FIGURE 6.30 General Behavior of Yield - Distance Relations

Within the far-field region (which means for peak overpressure less than 14.7 psi for TNT equivalencies of the order of  $5 \times 10^6$  lb, as mentioned in Section 6.2.3) the physical differences between air blast from rocket explosion and TNT are not going to be any larger than those possibly produced by secondary effects and can be considered falling within the reliability limit of the TNT curves themselves. Hence, within this far-field region, the use of TNT air blast charts to predict rocket explosion air blast parameters can be considered useful and sufficiently accurate for engineering design in most cases.

Additional charts are presented in this section (Figure 6.31, 6.32, 6.33, and 6.34), giving the values of peak overpressure as function of ground zero distance and of burst altitude for a charge of  $10^6$  lb of TNT. In these figures, good surface conditions refer to ground conditions approaching the ideal reflecting ones, namely, ice, water or concrete surface. (Reference 6.20).

Average surface conditions refer to all other possible surface conditions. These curves (from Reference 6.21) are based upon experimental data (solid lines) established as a result of full scale nuclear explosions and upon theory and high explosive experiments (dashed lines). The validity for extrapolation to propellant explosions must await results of experimental programs on propellant blast such as Project Pyro. Assuming the blast energy is well defined, peak overpressures and distances from Figure 6.26 are reliable to  $\pm 10$  percent. Peak overpressures from Figures 6.31 to 6.34 are reliable to  $\pm 20$  percent; distances to  $\pm 17$  percent.

#### 6.2.5.2 Peak Dynamic Pressure

To predict the peak dynamic pressure of the wind following the blast wave, Figure 6.35 can be used for a surface burst or an air burst for peak dynamic pressures less than 1.5 psi. For air bursts with peak dynamic pressures greater than 1.5 psi, use Figure 6.36. As far as the reliability is concerned, peak dynamic pressures from Figures 6.35 and 6.36 are reliable to  $\pm 25$  percent, for peak dynamic pressure  $\leq 14.7$  psi. (Reference 6.20, 6.21)

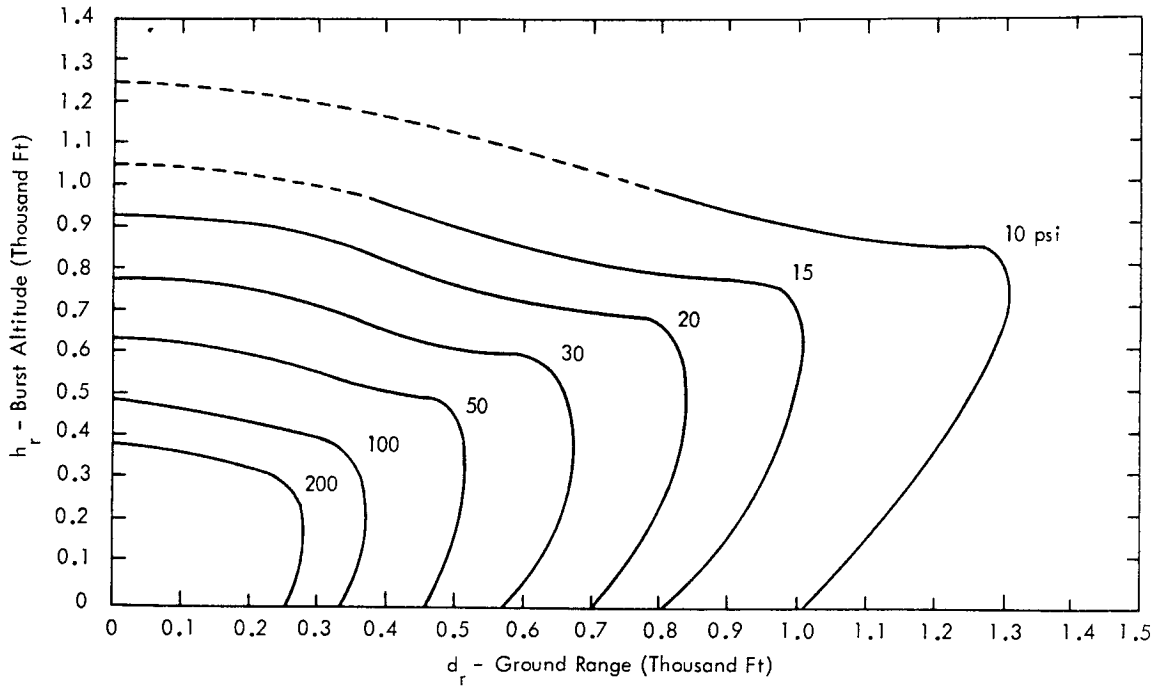


FIGURE 6.31 Peak Overpressure on the Surface as a Function of Burst Altitude and Ground Zero Distance; 10<sup>6</sup> lbs of TNT at Sea Level for Good Surface Conditions

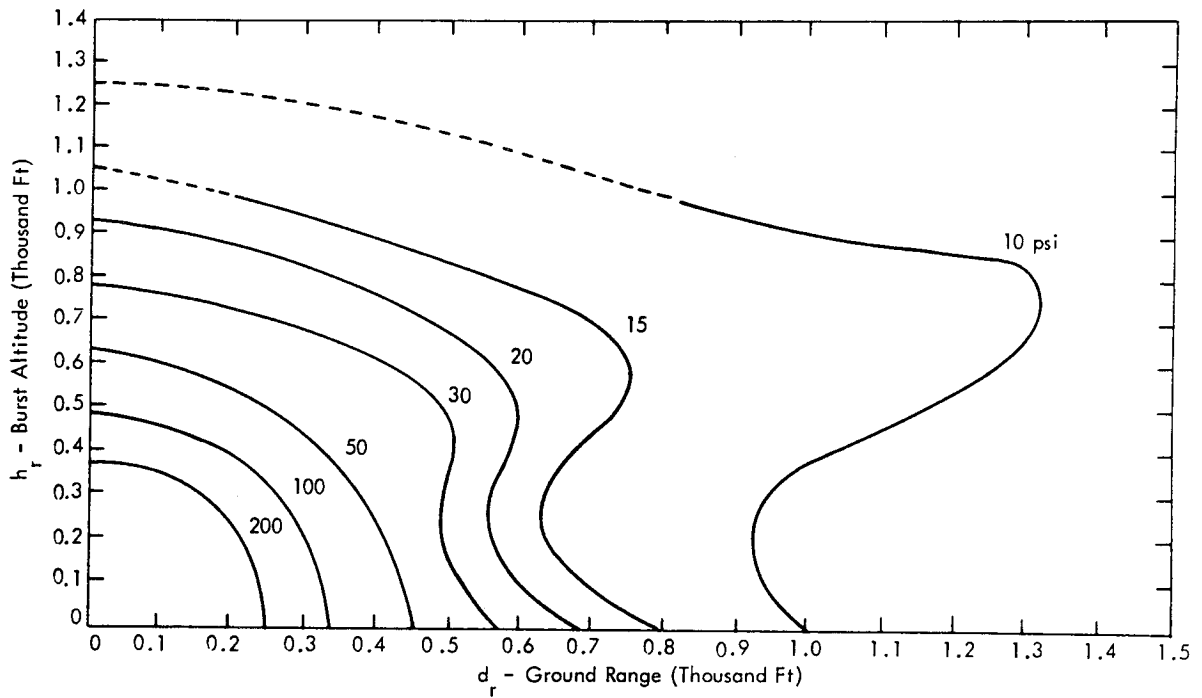


FIGURE 6.32 Peak Overpressure on the Surface as a Function of Burst Altitude and Ground Zero Distance; 10<sup>6</sup> lbs of TNT at Sea Level for Average Surface Conditions

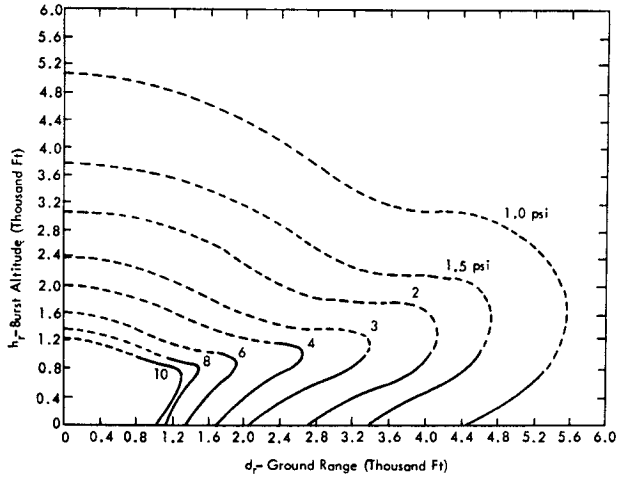


FIGURE 6.33 Peak Overpressure on the Surface as a Function of Burst Altitude and Ground Zero Distance;  $10^6$  lbs of TNT at Sea Level for Good Surface Conditions

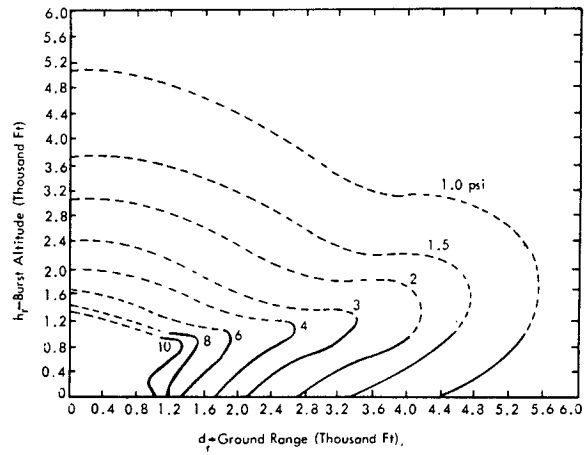


FIGURE 6.34 Peak Overpressure on the Surface as a Function of Burst Altitude and Ground Zero Distance;  $10^6$  lbs of TNT at Sea Level for Average Surface Conditions

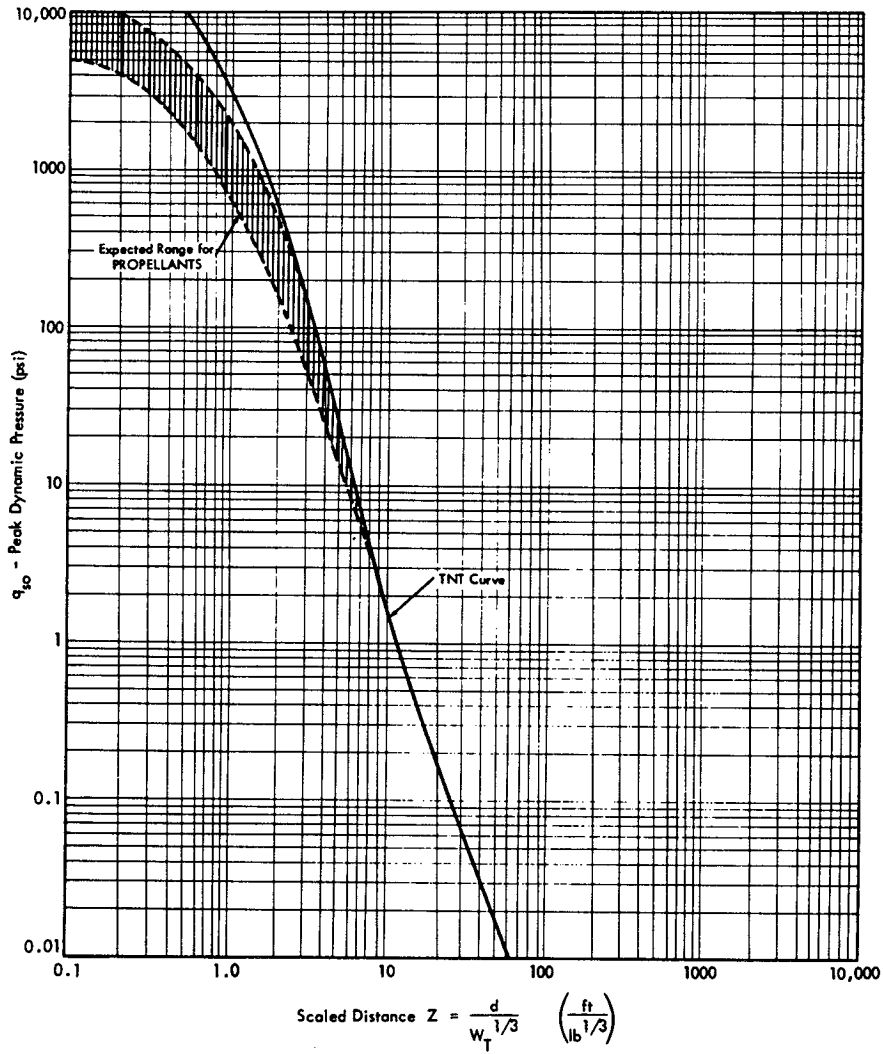


FIGURE 6.35 Peak Dynamic Pressure versus Scaled Distance for TNT Surface Explosion

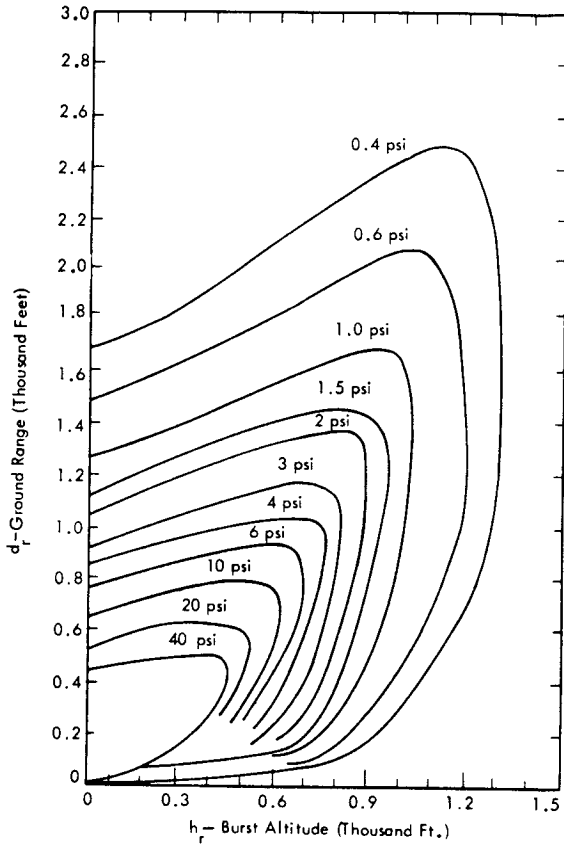


FIGURE 6.36 Peak Dynamic Pressure on the Surface (Horizontal Component) as a Function of Burst Altitude and Ground Zero Distance;  $10^6$  lb of TNT at Sea Level for Good Surface Conditions

6.2.5.3 Duration of Positive Phase

To predict the time duration of the positive phase of overpressure,  $t_p^+$ , and dynamic pressure,  $t_q^+$ , Figure 6.37 and 6.38 can be used. The former applies to a surface burst. Figure 6.37 has been plotted according to Brode's theory (Reference 6.18) for TNT explosions. Measured durations of particle velocity (Reference 6.31) from a 100 ton TNT surface blast and experimental data of overpressure positive phase durations from a spill test of 200 pounds of  $LO_2-LH_2$  have been plotted in the same figure, assuming a TNT equivalency of 60 percent for the  $LO_2-LH_2$  combination. These data show a good correlation between the actual values and the theoretical curves which can be considered reliable to  $\pm 10$  percent.

Figure 6.38, applicable to an air burst, has been derived from Reference 6.21 and is based on experimental data from nuclear explosions.

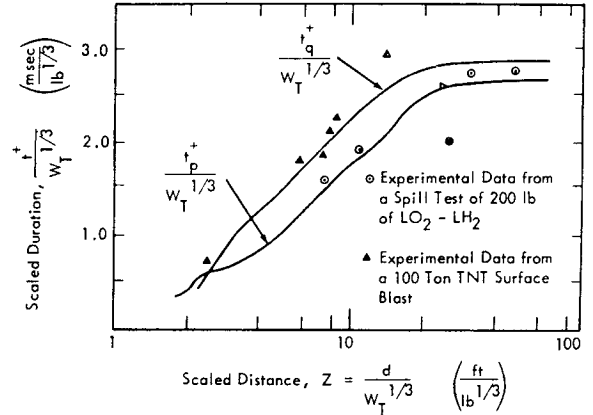


FIGURE 6.37 Scaled Duration of Positive Phases of Overpressure,  $\frac{t_p^+}{W_T^{1/3}}$ , and Velocity,  $\frac{t_q^+}{W_T^{1/3}}$ , versus Scaled Distance

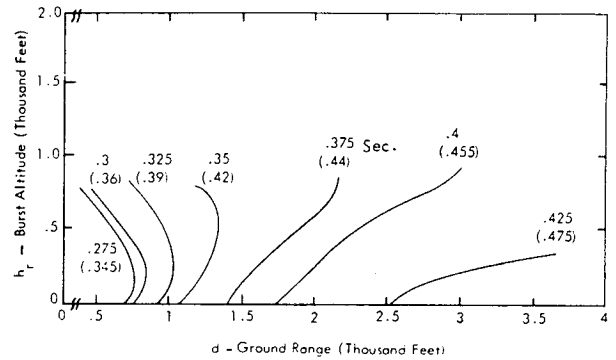


FIGURE 6.38 Durations of Positive Phases of Overpressure and Dynamic Pressure (in parentheses) versus Burst Altitude and Ground Zero Distance for a  $10^6$  lb TNT Equivalent Rocket Explosion

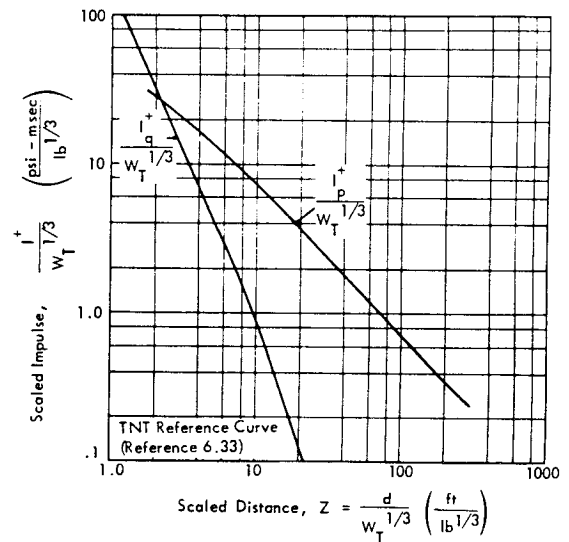


FIGURE 6.39 Scaled Positive Impulses for Overpressure,  $\frac{I_p^+}{W_T^{1/3}}$ , and Dynamic Pressure,  $\frac{I_q^+}{W_T^{1/3}}$ , versus Scaled Distance

6.2.5.4 Positive Impulses for Overpressure and Dynamic Pressure

The positive impulse for overpressure,  $I_p^+$ , and the positive impulse for dynamic pressure,  $I_q^+$ , due to rocket explosions can be predicted from Figure 6.39.

In this figure, the curve  $I_p^+/W_T^{1/3}$  versus scaled distance, called "TNT Reference Curve", is based on records from 20-ton and 100-ton TNT shots from Reference 6.33. The curve  $I_q^+/W_T^{1/3}$  is derived from Brode's Theory (Reference 6.18) for TNT explosions. The reliability of Figure 6.39 can be considered to be  $\pm 20$  percent.

In Figure 6.40 and 6.41, a comparison is made between the TNT Reference Curve, the curve plotted according to Brode's theory, and experimental data from LO<sub>2</sub>-RP-1 and LO<sub>2</sub>-LH<sub>2</sub> tests for Project Pyro (Reference 6.25); the values are based on the observed terminal yield. These figures show a reasonable agreement between the experimental data and the TNT Reference Curve.

For application to blast loading problems, it is often more convenient to use the effective value of the overpressure or dynamic pressure duration. This is defined as the duration of a triangular pulse with the same initial peak value and the same positive phase impulse as the actual blast pulse. Values for the effective value of  $t_p^+$  and  $t_q^+$  are given in Section 2 of Chapter 8.

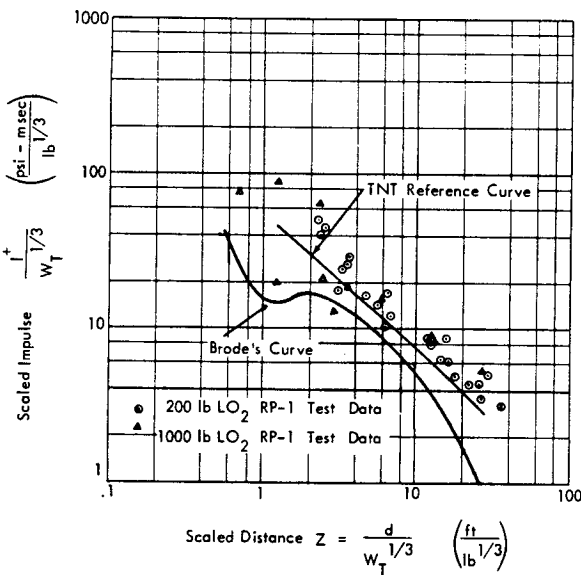


FIGURE 6.40 Experimental and Theoretical Values of Scaled Impulse versus Scaled Distance - LO<sub>2</sub>/RP-1 (Data from Reference 6.25)

6.2.5.5 Time Variations of Overpressure and Dynamic Pressure

Figures 6.42 and 6.43, (from Reference 6.18) may be used to define the range of time variations of overpressure and dynamic pressure by using the calculated peak overpressure, dynamic pressure, and overpressure and dynamic pressure durations with their respective reliability limits. All the curves within such ranges have to be considered possible; hence, the worst of them, from a structural design viewpoint, should be considered. The average curve is the most probable one.

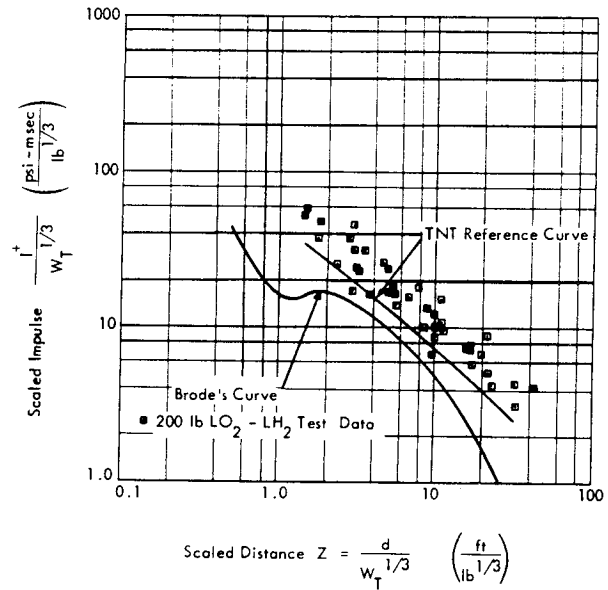


FIGURE 6.41 Experimental and Theoretical Values of Scaled Impulse versus Scaled Distance - LO<sub>2</sub>/LH<sub>2</sub> (Data from Reference 6.25)

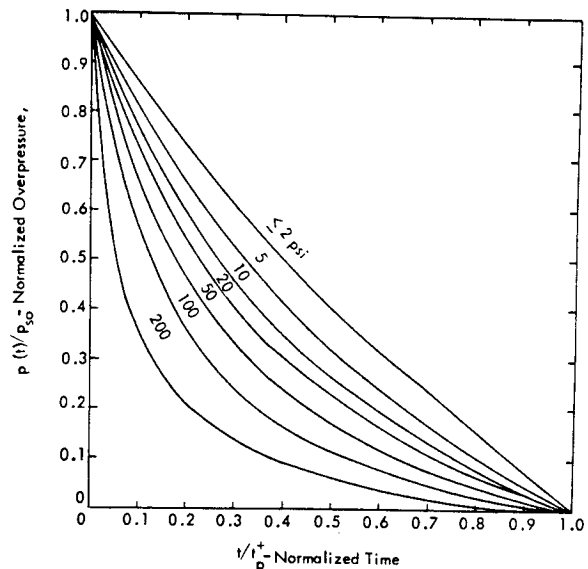


FIGURE 6.42 Rate of Decay of Pressure with Time for Various Values of the Peak Overpressure

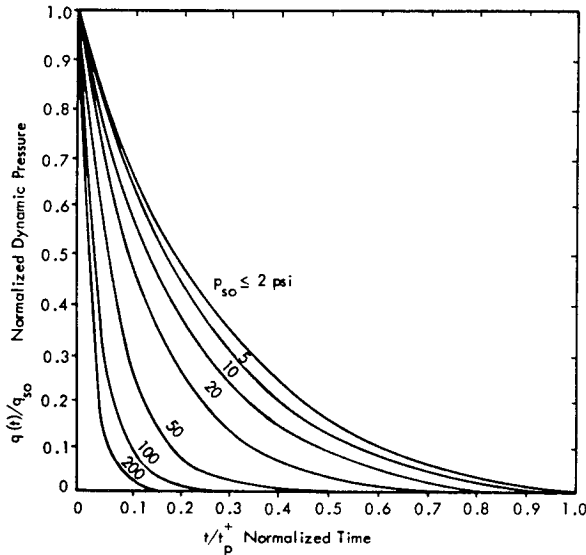


FIGURE 6.43 Rate of Decay of Dynamic Pressure with Time for Various Values of the Peak Overpressure

6.2.6 USE OF DESIGN CHARTS AND NUMERICAL EXAMPLES

Examples are given in this Section to clarify the use of the scaling laws and charts presented in the previous Section. They will cover some of the most frequent problems met by designers.

6.2.6.1 Numerical Examples

- (a) Given - A TNT-equivalency of  $5 \times 10^6$  lb ( $W_T$ ) and assuming a ground explosion.

Find - The distance at which the peak overpressures would be  $\leq 14.7$  psi.

Solution - From Figure 6.26, the scaled distance,  $Z$ , can be found knowing the peak overpressure,  $p_{so}$ ; thus,

$$Z = \frac{d}{W_T^{1/3}} = 8.0 \text{ ft/lb}^{1/3}$$

$$\therefore d = 8 \times (5 \times 10^6)^{1/3} = 1.37 \times 10^3 \text{ ft.}$$

Considering the reliability of Figure 6.26 ( $\pm 10$  percent):

$$d = (1.37 + 0.137) 10^3 = 1.507 \times 10^3 \text{ ft.}$$

- (b) Given - A TNT-equivalency of  $5 \times 10^6$  lb ( $W_T$ ) and assuming a ground explosion.

Find - The peak overpressure at a distance of 5,810 ft.

Solution - From Figure 6.26,  $p_{so}$  can be found knowing  $Z$ .

$$Z = \frac{5810}{(5 \times 10^6)^{1/3}} = 34 \text{ ft/lb}^{1/3}$$

and from Figure 6.26

$$p_{so} = 1.4 \text{ psi}$$

Considering the reliability of Figure 6.26 ( $\pm 10$  percent):

$$p_{so} = 1.4 \pm 0.14 \text{ psi}$$

- (c) Given - A TNT-equivalency of  $5 \times 10^6$  lb ( $W_T$ )

Find - The distance from ground zero for which the peak overpressure would be  $< 14.7$  psi considering possible inflight explosions.

Solution - Define surface conditions: To be conservative, assume good ground conditions. From Figure 6.31, interpolating between 10 and 15 psi, it is seen that the 14.7 psi line has a vertical tangent at about 1,020 ft. from ground zero and 500 to 800 ft. burst altitude. This means that a  $10^6$  lb TNT explosion at an altitude of 500 to 800 ft. can give a peak overpressure of 14.7 psi or higher up to a maximum distance of 1,020 ft. Applying the scaling laws, (Section 6.2.4)

$$h = h_r(W_T/W_{Tr})^{1/3} = (0.85 \text{ to } 1.37) 10^3 \text{ ft.}$$

$$d = d_r(W_T/W_{Tr})^{1/3} = 1.74 \times 10^3 \text{ ft.}$$

Considering the reliability of Figure 6.31 (17 percent), the desired distance is

$$d = (1.74 + 0.296) 10^3 = 2.04 \times 10^3 \text{ ft.}$$

for a blast altitude of 710 to 1,600 ft.

- (d) Given - A TNT-equivalency of  $5 \times 10^6$  lb ( $W_T$ ) and assuming a ground explosion.

Find - the peak dynamic pressure ( $q_{so}$ ) at a distance of 1,370 ft. (where  $p_{so} = 14.7 \pm 1.47$  psi).

Solution - Define the surface conditions: To be conservative, assume good ground conditions. From Figure 6.35,  $q_{so}$  can be found knowing the scaled distance,  $Z$ .

$$Z = \frac{1370}{(5 \times 10^6)^{1/3}} = 8.0 \text{ ft/lb}^{1/3}$$

and from Figure 6.35  $q_{50} = 4.0$  psi.

Considering the reliability of Figure 6.35, ( $\pm 25$  percent)

$$q_{50} = (4.0 \pm 1.0) \text{ psi}$$

- (e) Given - A TNT-equivalency of  $5 \times 10^6$  lb ( $W_T$ )

Find - The peak dynamic pressure ( $q_{50}$ ) at a distance of 1,740 ft. from ground zero, assuming the explosion to occur at an altitude of about 1,000 ft. (the peak overpressure at the point would be 14.7 psi).

Solution - Define the surface conditions: Assume good ground conditions. From Figure 6.36,  $q_{50}$  can be found knowing the reference distance and the reference altitude for the explosion under consideration.

Applying the scaling laws (Section 6.2.4)

$$d_r = d(W_{Tr}/W_T)^{1/3} = 1.02 \times 10^3 \text{ ft.}$$

$$h_r = h(W_{Tr}/W_T)^{1/3} = 0.585 \times 10^3 \text{ ft.}$$

and from Figure 6.36,  $q_{50} = 0.75$  psi.

Considering the reliability of Figure 6.36, ( $\pm 25$  percent)

$$q_{50} = (0.75 \pm 0.19) \text{ psi.}$$

- (f) Given - A TNT-equivalency of  $5 \times 10^6$  lb ( $W_T$ ) and assuming ground explosion.

Find - The duration of positive overpressure phase ( $t_p^+$ ) and of positive dynamic pressure phase ( $t_q^+$ ) at a distance of 1,370 ft. (where the peak overpressure would be  $14.7 \pm 1.47$  psi).

Solution - From Figure 6.37, the two durations ( $t_p^+$  and  $t_q^+$ ) can be estimated knowing the scaled distance for the explosion under consideration.

$$Z = \frac{1370}{(5 \times 10^6)^{1/3}} = 8.0 \text{ ft/lb}^{1/3}$$

and from Figure 6.37

$$\frac{t_p^+}{W_T^{1/3}} = 1.45 \text{ msec/lb}^{1/3}$$

and

$$\frac{t_q^+}{W_T^{1/3}} = 2.0 \text{ msec/lb}^{1/3}$$

Then

$$t_p^+ = 1.45 (5 \cdot 10^6)^{1/3} = 0.248 \text{ sec.}$$

$$t_q^+ = 2.0 (5 \cdot 10^6)^{1/3} = 0.342 \text{ sec.}$$

Considering the reliability of Figure 6.37 ( $\pm 10$  percent)

$$t_p^+ = (0.248 \pm 0.025) \text{ sec.}$$

$$t_q^+ = (0.342 \pm 0.034) \text{ sec.}$$

- (g) Given - A TNT-equivalency of  $5 \times 10^6$  lb ( $W_T$ ).

Find - The durations of positive overpressure phase ( $t_p^+$ ) and of positive dynamic pressure phase ( $t_q^+$ ) at a distance of 1,740 ft. from ground zero assuming the explosion to occur at an altitude of about 1,000 ft. (the overpressure at the same point would be  $14.7 \pm 2.9$  psi).

Solution - From Figure 6.38, the two durations ( $t_p^+$  and  $t_q^+$ ) can be estimated knowing the reference altitude and reference distance for the explosion under consideration.

Applying the scaling laws, (Section 6.2.4)

$$d_r = d(W_{Tr}/W_T)^{1/3} = 1.020 \times 10^3 \text{ ft.}$$

$$h_r = h(W_{Tr}/W_T)^{1/3} = 0.585 \times 10^3 \text{ ft.}$$

and from Figure 6.38, ( $t_p^+$ )<sub>r</sub> = 0.33 sec.

and ( $t_q^+$ )<sub>r</sub> = 0.40 sec.

Applying again the scaling laws:

$$t_p^+ = (t_p^+)_r (W_T/W_{Tr})^{1/3} = 0.56 \text{ sec.}$$

$$t_q^+ = (t_q^+)_r (W_T/W_{Tr})^{1/3} = 0.68 \text{ sec.}$$

Considering the reliability of Figure 6.38 ( $\pm 50$  percent)

$$t_p^+ = (0.56 \pm 0.28) \text{ sec.}$$

and  $t_q^+ = (0.68 \pm 0.34) \text{ sec.}$



(h) Given - A TNT-equivalency of  $5 \times 10^6$  lb ( $W_T$ ) and assuming a ground explosion.

Find - The overpressure positive impulse,  $i_p^+$ , and dynamic pressure impulse,  $i_q^+$ , at a distance of 3420 ft.

Solution - From Figure 6.39, the two impulses can be estimated knowing the scaled distance,  $Z$ , for the explosion under consideration.

$$Z = \frac{3420}{(5 \times 10^6)^{1/3}} = 20.0 \text{ ft/lb}^{1/3}$$

and from Figure 6.39

$$i_p^+ / W_T^{1/3} = 4.0 \text{ psi - msec/lb}^{1/3}$$

$$i_q^+ / W_T^{1/3} = 0.3 \text{ psi - msec/lb}^{1/3}$$

Then

$$i_p^+ = 0.68 \text{ psi-sec}$$

$$i_q^+ = 0.051 \text{ psi-sec}$$

and considering the reliability of Figure 6.39

$$i_p^+ = 0.68 \pm 0.14 \text{ psi-sec}$$

$$i_q^+ = 0.051 \pm 0.01 \text{ psi-sec}$$

(i) Given - A TNT-equivalency of  $5 \times 10^6$  lb ( $W_T$ ) and assuming a ground explosion.

Find - The time variation of overpressure and dynamic pressure at a distance of 5,810 ft., (where  $p_s = 1.47 \pm 0.15$  psi).

Solution - It is necessary to have already determined the peak dynamic pressure and overpressure and the dynamic pressure positive phase duration with their relative reliability limits. The following values are assumed to be the results of calculations:

Peak overpressure:  $p_{so} = 1.47 \pm 0.15$  psi

Peak dynamic pressure:  $q_{so} = 0.052 \pm 0.010$  psi

Overpressure positive phase duration:  $t_p^+ = 0.786 \pm 0.079$  sec.

Dynamic pressure positive phase duration:  $t_q^+ = 0.839 \pm 0.084$  sec.

Now Figures 6.42 and 6.43 can be used to calculate the following tables.

TABLE 6.6 CALCULATED RANGE OF TIME HISTORY OF OVERPRESSURE PULSE (POSITIVE PHASE ONLY) AT 5810 FT FROM  $5 \times 10^6$  LB TNT-EQUIVALENT EXPLOSION

Read From Figure 6.42		Calculated from First Two Columns by Setting: (Upper Limit)		Calculated from First Two Columns by Setting: (Lower Limit)	
		$p_{so} = 1.62$ psi	$t_p^+ = 0.865$ sec.	$p_{so} = 1.32$ psi	$t_p^+ = 0.707$ sec.
$p(t)/p_{so}$	$t/t_p^+$	$p(t)$ psi	$t$ sec	$p(t)$ psi	$t$ sec
1.0	0.0	1.62	0.0	1.32	0.0
0.9	0.07	1.45	0.060	1.19	0.049
0.8	0.15	1.29	0.130	1.06	0.106
0.7	0.23	1.13	0.199	0.93	0.162
0.6	0.31	0.97	0.268	0.79	0.219
0.5	0.40	0.81	0.346	0.66	0.283
0.4	0.50	0.65	0.432	0.53	0.354
0.3	0.62	0.48	0.536	0.40	0.439
0.2	0.75	0.32	0.650	0.26	0.530
0.1	0.87	0.16	0.753	0.13	0.615
0.0	1.0	0.0	0.865	0.0	0.707

TABLE 6.7 CALCULATED RANGE OF TIME HISTORY OF DYNAMIC PRESSURE PULSE (POSITIVE PHASE ONLY) AT 5810 FT FROM  $5 \times 10^6$  LB TNT-EQUIVALENT EXPLOSION

Read From Figure 6.43		Calculated from First Two Columns by Setting: (Upper Limit)		Calculated from First Two Columns by Setting: (Lower Limit)	
		$q_{so} = 0.062 \text{ psi}$	$t_q^+ = 0.923 \text{ sec.}$	$q_{so} = .042 \text{ psi}$	$t_q^+ = .755 \text{ sec.}$
$q(t)/q_{so}$	$t/t_q^+$	$q(t)$ psi	$t$ sec	$q(t)$ psi	$t$ sec
1.0	0.0	0.062	0.0	0.042	0.0
0.9	0.03	0.056	0.028	0.038	0.022
0.8	0.07	0.050	0.065	0.033	0.053
0.7	0.10	0.043	0.092	0.029	0.075
0.6	0.14	0.037	0.129	0.025	0.108
0.5	0.20	0.031	0.184	0.021	0.151
0.4	0.26	0.025	0.240	0.016	0.196
0.3	0.34	0.019	0.314	0.012	0.256
0.2	0.44	0.012	0.406	0.008	0.332
0.1	0.59	0.006	0.545	0.004	0.445
0.0	1.0	0.0	0.923	0.0	0.755

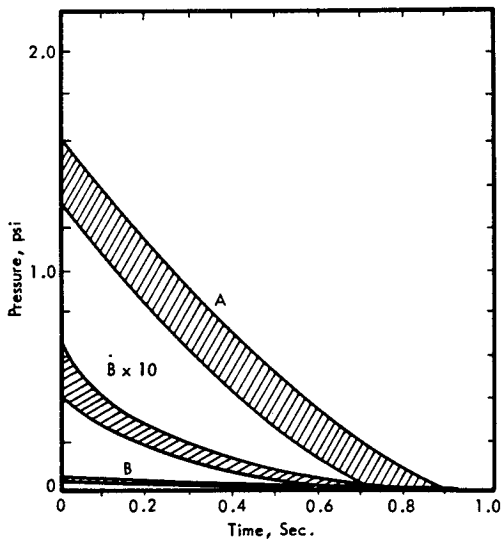


FIGURE 6.44 A Time Variation of Overpressure at a Distance of 5,810 feet from a  $5 \times 10^6$  lb TNT Equivalent Rocket Explosion  
 B Time Variation of Dynamic Pressure at a Distance of 5,810 feet from a  $5 \times 10^6$  lb TNT Equivalent Rocket Explosion

The results of these two tables are plotted in Figure 6.44.

Any curve within the calculated range is acceptable, the average curve being the more likely one.

6.2.7 CONCLUDING REMARKS

The design charts presented in this section for the calculations of rocket explosion air blast parameters are based on the use of the equivalent TNT explosion concept. For the far-field region, the blast parameters associated with the equivalent TNT weight give sufficient accuracy for blast load design, but for the close-field, they overestimate the blast loads significantly. This is due to the major differences between rate of energy release and explosive mass to energy ratio between propellants and TNT. However, in the far-field region, the blast parameters are a function, almost exclusively, of the total energy released during the explosion.

The design curves given are based on experimental results for TNT with limited support by experimental data on propellant explosions. However, more experimental information is desired to improve the design curves presented. Of particular value will be statistical data on actual yield obtained under a variety of conditions for a given quantity of propellants.

6.3 SONIC BOOM

6.3.1 INTRODUCTION

The flight of an aircraft at supersonic speeds through the atmosphere results in a series of shock waves emanating from the vehicle, originating from points of area change. These waves propagate along a conical front extending aft and outward from the aircraft. Near the aircraft, these waves interact with each other and with expansion waves, gradually converging into a single bow wave and a single tail wave for the vehicle, Figure 6.45. An observer in the near field of the vehicle will experience a complex pattern of sudden pressure changes dependent on the airplane's area distribution. In the far field, an observer will experience an N-shaped pressure-time variation as the bow and tail waves pass by at the aircraft velocity. For typical supersonic operating altitudes, structures on the ground will be in the far field, so that the characteristics of the N-wave are of most interest.

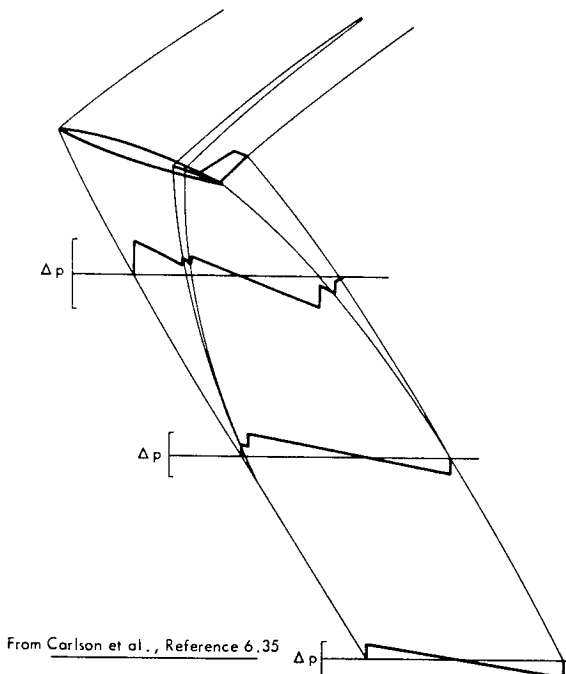


FIGURE 6.45 Typical Shock Wave Patterns

Figure 6.46 shows the variety of loading events experienced by a building as the N-wave sweeps over it toward the left. First the building is forced laterally due to the initial positive loading on its front surface. Then it would be forced inward from all directions, next forced outward, and finally displaced laterally again because of the negative pressure acting on the back surface. The duration of the N-wave at a point and its corresponding length at an instant of time depend primarily on the aircraft speed and length respectively. For supersonic transport aircraft, the overpressure signature may be 1,000 feet in length and 0.4 second in duration.

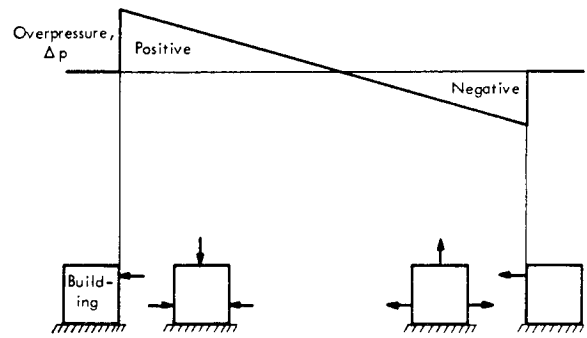


FIGURE 6.46 Sequence of Applied Loading From Hubbard, Reference 6.36

In addition to this airborne pressure pattern, buildings can experience earthborne acceleration transients as the shock front passing over the ground excites the surface layers of the earth. These surface waves may propagate faster than the trace of the airborne wave front along the surface, thus arriving before the airborne N-wave. However, these earthborne accelerations are expected to have magnitudes much lower than those associated with earthquake damage.

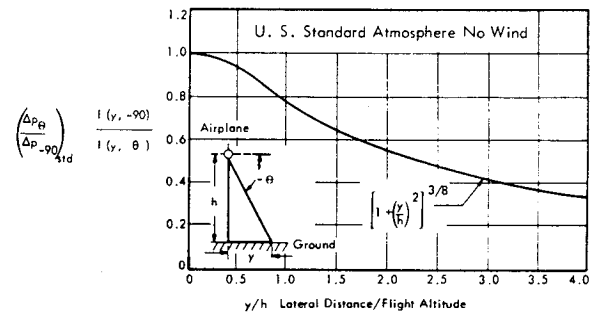


FIGURE 6.47 Lateral Distribution of Shock Wave Strength

6.3.2 SONIC BOOM CHARACTERISTICS

As the conical shock front propagates away from the vehicle in directions always normal to the shocks, variations of temperature in the atmosphere cause a refraction of the ray paths. For the normal temperature gradient in a standard atmosphere, the ray paths are bent concave upward, so that the overpressure signature on the ground is limited to a finite width corridor and is of decreasing strength away from the flight path locus within this corridor. Figure 6.47 shows the lateral distribution of shock wave strength based on data for flight Mach numbers from 1.2 to 3.0 and flight altitudes of 42,000 to 74,000 feet. The quantity  $I(y, \theta)$ , which is a property of airplane geometry only, has been brought into the ordinate to give a single curve for all airplane geometries. The lateral extent of the overpressure corridor on each side of the ground track is given in Figure 6.48 for a 1962 U. S. Standard Atmosphere and for a surface elevation at

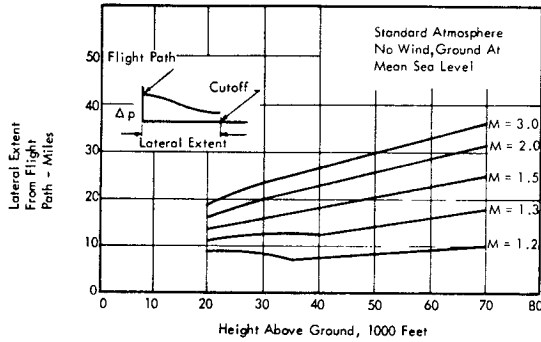


FIGURE 6.48 Lateral Extent of Pressure Signature at Ground From Kane, Reference 6.37

sea level. Total corridor widths of about 60 miles are expected for aircraft cruising at about Mach 3, for example. This corridor is bounded fore and aft by the moving parabola formed by the intersection of the conical shock front with the earth surface.

The N-wave produced in the far field of supersonic aircraft can be described by the magnitude of the initial pressure rise, ( $\Delta p$ ), The duration between the initial and final waves, ( $\Delta t$ ), and the spectral content. The magnitude of the peak overpressure at the ground is controlled primarily by the aircraft volume and weight and by its operating altitude. Of secondary importance are the operating Mach number and the details of the vehicle area and lift distribution, and such atmospheric conditions as temperature and wind gradients and turbulence patterns. Typical peak overpressure magnitudes for several aircraft types are shown in Figure 6.49 as a function of flight altitude. The lower three regions represent exposures currently experienced or anticipated in steady flight. The region labeled "training maneuvers" represents accelerating flight for current aircraft, where overpressures as high as 6 psf can occur.

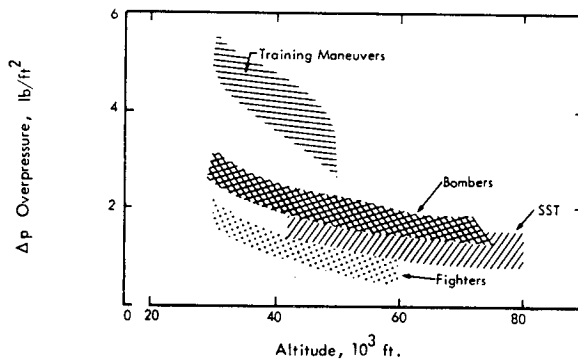


FIGURE 6.49 Typical Sonic Boom Overpressures From Hubbard, Reference 6.36

Effects of vehicle weight and flight altitude on peak overpressure at a point in the far field of a typical vehicle (of length 230 feet and flying at a Mach number of 1.4) are given in Figure 6.50. The decrease of peak overpressure with altitude is due to the attenuation of the shock waves as they are propagated over longer distances in the atmosphere. The curve for zero weight shows the portion of the overpressure for non-zero vehicle weights

are due to the additional wave generation implied by lift requirements.

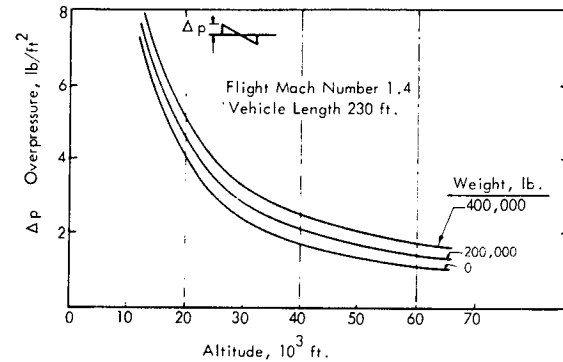


FIGURE 6.50 Effect of Weight and Altitude on Far Field Overpressure, From McLean et al., Reference 6.38

A quantity of importance to structural designers is the impulse, or time integral of the positive portion of the pressure pulse. The total duration of the N-wave is influenced primarily by the vehicle length. Typical duration values are 0.04 second for present-day fighter aircraft, 0.2 second for the longest present-day supersonic aircraft, and 0.4 second for the proposed supersonic transport. Since vehicle weight has a second order effect on the magnitude of the overpressure, the positive pressure impulse is affected in two ways even for vehicles of equal length. The effects of weight and altitude on impulse (for the same vehicle and flight Mach numbers as those in Figure 6.50) are shown in Figure 6.51. Increase in operating altitude above about 40,000 feet does not decrease the impulse for large transport-type aircraft.

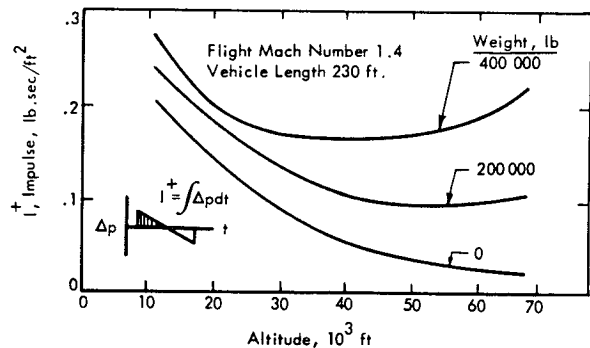


FIGURE 6.51 Effects of Vehicle Weight and Altitude on Impulse at Ground, From McLean et al., Reference 6.38

The standard measurement height for overpressure signature is at ground level, and this has been implied in all the foregoing discussions of wave characteristics at the earth surface. However, portions of a building structure at different heights above the ground will experience both the direct waves and those reflected from the ground. For typical building heights and overpressure signature

lengths, the entire building will be within the region of superposed direct and reflected waves, Figure 6.52. The resulting wave pattern (even excluding reflections from the building itself) is not the simple N-wave but such composite patterns as those in Figure 6.52.

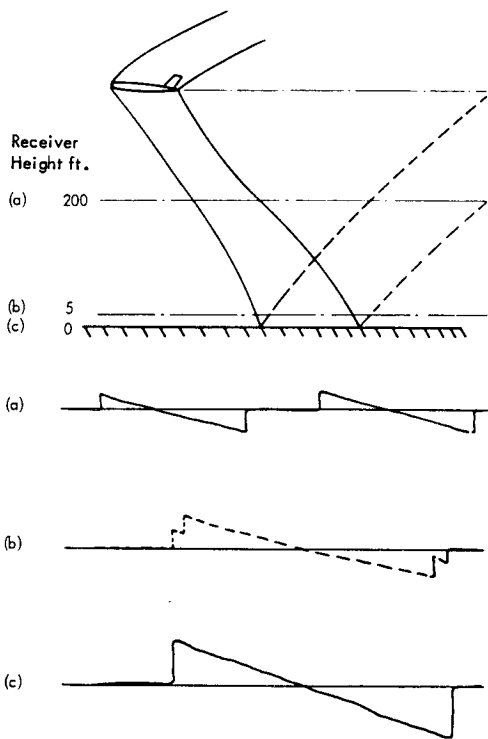


FIGURE 6.52 Effect of Elevation on Received Sonic Boom Signatures From Hilton et al., Reference 6.39

The idealized time history of a sonic boom can be represented by the expression

$$p(t) = \Delta p - \frac{2 \Delta p}{\tau} \cdot t \text{ for } 0 \leq t \leq \tau$$

and

$$p(t) = 0 \text{ for } t > \tau, t < 0.$$

It can be shown (Reference 6.40) that at high frequencies the energy spectral density (ESD) is

$$\left| p(\omega) \right|_{\max}^2 = \frac{4 \Delta p^2}{\omega^2}$$

and at low frequencies

$$\left| p(\omega) \right|_{\max}^2 = \frac{\Delta p \omega^2 \tau^4}{36}$$

Thus, the ESD rises and falls at 6 dB per octave and the low frequency content is highly dependent upon the duration, increasing by 12 dB per duration doubling. It is also found (Reference 6.40) that the frequency of the spectral peak is given approximately by the solution to the equation

$$\sin \omega \tau = \frac{8}{\omega \tau}$$

To illustrate the importance of the duration effect, Figure 6.53, taken from Reference 6.40, shows the effect of aircraft size on the boom spectrum for aircraft from a small fighter through a hypothetical transport. The same value of peak overpressure is assumed in each case. It is clear from this figure that although the audible part of the spectrum is practically unaffected, the infrasonic energy increases rapidly with aircraft size and it is to be expected that the dynamic response of large buildings due to a sonic boom will be much greater for the larger aircraft.

### 6.3.2.1 Energy Spectral Density

For purposes of estimating dynamic response to the transient N wave, the spectral distribution of the input energy is desired. The energy spectral density of a time-varying pressure is

$$\left| P(\omega) \right|^2 = \left| \int_{-\infty}^{\infty} p(t) e^{-i\omega t} dt \right|^2$$

where:

- $\left| P(\omega) \right|^2$  = energy spectral density
- $p(t)$  = instantaneous pressure at time  $t$
- $\omega$  = frequency in radians

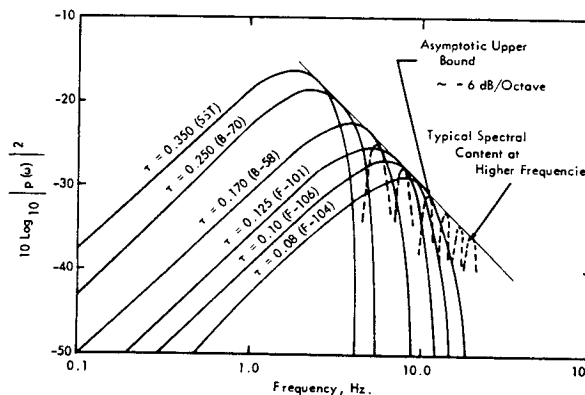


FIGURE 6.53 Energy Spectra of Sonic Booms for Various Aircraft and a Hypothetical SST (From Reference 6.40).

6.3.3 ATMOSPHERIC VARIATION EFFECTS

All the foregoing description has dealt with steady flight in a standard atmosphere. Variations of temperature and pressure with altitude and the presence of winds in the atmosphere will affect the wave propagation and, therefore, the strength, distribution and extent of the shock waves at the ground. Although the effect of variable properties in stratified nonhomogeneous atmospheres has been calculated for nominal variations in the atmosphere (Figure 6.54), actual observations of the variations of the overpressure about the calculated value for a typical atmosphere show a much greater range of values than indicated by theory. Extensive records of sonic boom were recorded during the recent series of test over Oklahoma City and the statistical variation in the observations are shown in Table 6.8.

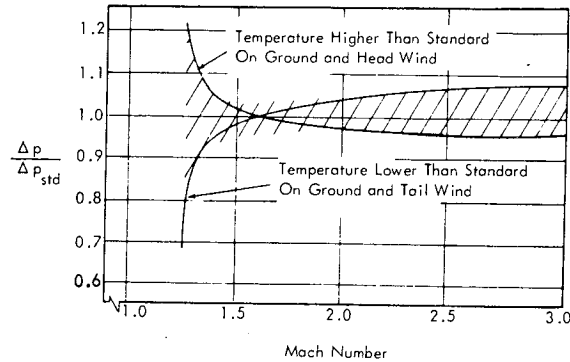


FIGURE 6.54 Range of Calculated Overpressure Variations in Non-standard Atmospheres, From Kane, Reference 6.37

TABLE 6.8

STATISTICAL DEVIATION IN MEASURED SONIC BOOM PARAMETER FROM CALCULATED VALUES (FROM REFERENCE 6.41)

Aircraft	- Two Airplanes - 21,000 - 41,000 feet, Mach 1.2 - 2.0					
Observation Point	- Three Locations - 0, 5, and 10 miles perpendicular to track					
	$\frac{\Delta p_{meas}}{\Delta p_{calc}}$			$\frac{l^+_{meas}}{l^+_{calc}}$		
	$\Delta p_{calc}$ from volume and lift theory, from methods of NASA TR-198			$l^+_{calc}$ from theory of Whitham (Reference 6.42) assuming far field, neglecting lift effects, and $t^+ = t^-$ .		
Range - Miles	0	5	10	0	5	10
Percentage of Results*						
99 Percent	0.465	0.56	0.47	0.55	0.66	0.57
50 Percent	0.885	1.13	1.16	0.88	1.01	1.063
1 Percent	1.68	2.27	2.98	1.42	1.55	1.98

\*Percentage of Results Greater Than Tabulated Ratio of Measured vs Calculated Value, Based on Log-Normal Distribution.

Departures from a quiescent atmosphere, especially the turbulence arising from thermal instability in the first few hundred feet of the atmosphere, can significantly affect the shape of the sonic boom signature and thus its spectral energy distribution. The clean N-waves which occur when the lower atmosphere is quiescent can be rounded off

to a nearly sinusoidal shape by a highly turbulent lower atmosphere. Again, observed results have shown the wide variation in N-wave signature that is possible. The typical type of N-waves observed from tests reported in Reference 6.41 are shown in Figure 6.55, along with their relative frequency of occurrence.

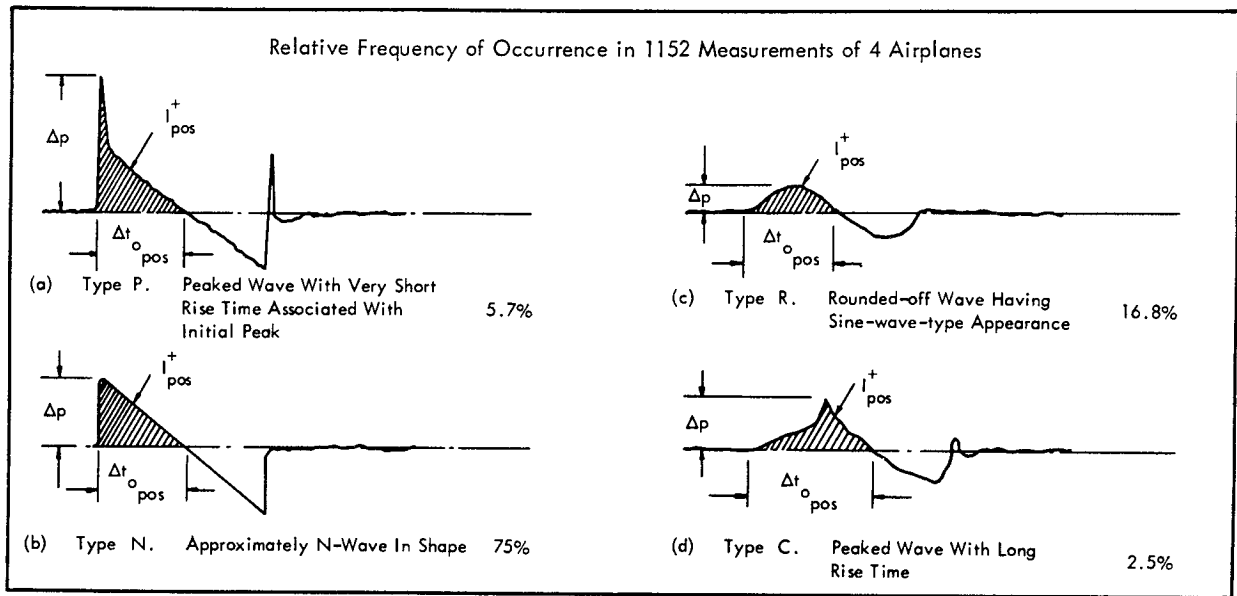


FIGURE 6.55 Schematic Diagrams Showing Some Categories of Waveforms Measured at Ground Level During Sonic Boom Tests, (From Reference 6.41)

Aircraft maneuvers involving longitudinal, lateral or normal accelerations can result in pressure buildups on the ground called "superbooms", due to the convergence or focusing of shock waves into a small region. Although the aircraft and shock waves are moving, the superboom areas are fixed and do not move with the aircraft. Theoretical methods are available for predicting ground overpressures during accelerated flight including effects of atmospheric temperature variation and wind gradients. Limited experimental measurements for aircraft in level linear acceleration have shown overpressure magnitudes about 2.5 times as large as for the corresponding conditions in steady flight. However, these superbooms are limited in their spatial extent. (Reference 6.43).

#### 6.3.4 CONCLUDING REMARKS

In summary, facilities and residential areas in the vicinity of rocket launch and test sites may be exposed to reoccurring sonic booms of the order of 5 psf (2.5 X 2 psf nominal value) for overflight of future supersonic transports. The N-waves will have a time duration of about 0.4 second and a positive phase impulse of 0.5 lb sec/ft<sup>2</sup>. For rocket test sites near experimental flight test facilities such as Edwards Air Force Base, peak overpressures up to 10 psf may be experienced from smaller aircraft. Maximum expected impulses would still be of the order of 0.5 lb sec/ft<sup>2</sup>. However, the time histories may no longer be ideal N-waves in such cases and may cause more severe structural responses.

#### REFERENCES

- 6.1 Lighthill, M.J., "On Sound Generated Aerodynamically", Part 1, Proc. Roy. Soc. A. 211, (1952). Part 2, Proc. Roy. Soc. A. 222, (1954).
- 6.2 Ollerhead, J.B., "On the Prediction of the Near Field Noise of Supersonic Jets," Wyle Research Staff Report WR 66-45, (1966).
- 6.3 Ffowcs-Williams, J.E., "The Noise from Turbulence Convected at High Speed," Phil. Trans. Roy. Soc. A. 255, (1963).
- 6.4 Potter, R.C. and Crocker, M.J., "Acoustic Prediction Methods for Rocket Engines," NASA CR-566, (1966).
- 6.5 Guest, S.H., "Acoustic Efficiency Trends for High Thrust Boosters," NASA TN D-1999, (1964).
- 6.6 Eldred, K. McK., Roberts, W. and White, R., "Structural Vibrations in Space Vehicles," WADD Tech. Rep. 61-62, (1961).
- 6.7 Cole, J.N. et al., "Noise Radiation from Fourteen Types of Rockets in the 1000 to 130,000 Pound Thrust Range," WADC Tech. Rep. 57-354, (1957).
- 6.8 Mayes, W.H. et al., "Near Field and Far Field Noise Surveys of Solid-Fuel Rocket Engines for a Range of Nozzle Exit Pressures," NASA TN D-21, (1959).

- 6.9 Morgan, W.V. and Young, K.J., "Studies of Rocket Noise Simulation with Substitute Gas Jets, and the Effects of Vehicle Motion on Jet Noise," ASD-TDR-62-787, (1962).
- 6.10 Wilhold, G.A. et al., "A Technique for Predicting Far Field Acoustic Environments Due to a Moving Rocket Sound Source," NASA TN D-1832, (1963).
- 6.11 J. F. K. Space Flight Center, "Final Results of Sound Pressure Level Measurements During SA-6 Launch," TR-78-1, (1964).
- 6.12 Shulman, A. L., "Attenuation of Rocket Engine Noise by Water Injection into the Flame Bucket," Paper H6, 65th Meeting ASA, New York, N.Y. May (1963).
- 6.13 Mayes, W.H., Lanfor, W.E., Hubbard, H.H., "Near Field and Far Field Noise Surveys of Solid Fuel Rocket Engines for a Range of Nozzle Exit Pressure," NASA TN D-21, August 1959.
- 6.14 Cole, J.N. et al., "Effects of Various Exhaust Blast Deflectors on the Acoustic Noise Characteristics of 1000 Pound Thrust Rockets," WADD TR 60-6, (1960).
- 6.15 Young, J. and Heindrichs, J., "Structural Dynamics Conceptual Design" - Part I NOVA TN-19, The Martin Co., (1963).
- 6.16 Huber, W.G., "Post-Saturn Launch Vehicle Study" (Part II), Condensed Summary Report, NASA TMX-53010, (1964).
- 6.17 Kingery, C.N., Keefer, J. H. and Day, J.D., "Surface Air Blast Measurements from a 100-Ton TNT Detonation," B. R. L. Memorandum Report, Number 1410, (1962).
- 6.18 Brode, H. L., "Numerical Solution of Spherical Blast Waves," J. Appl. Physics, Vol. 26, (786), (1955).  
"Point Source Explosions in Air," The Rand Corp., Research Memo RM-1824-AEC, (1956).  
"The Blast Wave in Air Resulting from a High Temperature High Pressure Sphere of Air," The Rand Corp., Research Memo RM-1825-AEC, (1956).  
"A Calculation of the Blast Wave from a Spherical Charge of TNT," AD 144302, (1957).  
"Blast Wave from a Spherical Charge," The Physics of Fluids, Vol. 2, No. 2, (1959).  
"A Review of Nuclear Explosion Phenomena Pertinent to Protective Construction," R-425-PR, (1964).
- 6.19 Bethe, H.A., Fuchs, K., Hirschfelder, J.G., Magee, J.L., Peierls, R.E. and Von Neuman, J., "Blast Wave," Los Alamos Report 2000, (1947).
- 6.20 Glasstone, S., (ed), "The Effects of Nuclear Weapons," U.S. Atomic Energy Comm., (1962).
- 6.21 Holmes and Narver, Inc. Ed., "Design Manual AEC Test Structures," TID-16347, (1961).
- 6.22 Bracco, F.V., "A Method for Predicting the Air Blast Parameters from Liquid Propellant Rocket Explosions," Wyle Laboratories Report WR-64-11, (1964).
- 6.23 Bracco, F.V., "Air Blast Parameters Close to a Liquid Propellant Explosion," Paper Before 2nd Working Group on Hazards, Interagency Chemical Rocket Propulsion Group, (1965).
- 6.24 Bracco, F.V., "Chemical and Dynamic Aspects of Propellant Explosions," Wyle Laboratories Report WR 66-42 (1966).
- 6.25 Willoughby, A.B. et al., Study of Liquid Propellant Hazards Project Pyro, "Misc. Progress Reports, (1965-1966).
- 6.26 D.O.D. Document 4145-21, "Quantity-Distance Storage Criteria for Liquid Propellant," (1964).
- 6.27 Bracco, F.V., "Air Shock Parameters and Design Criteria for Rocket Explosions," Wyle Laboratories Report, WR 65-21, (1965).
- 6.28 Zucrow, M.J., "Rocket Jet Propulsion," Ch. 10, Aircraft and Missile Propulsion, Vol. II, pp. 467-8, Wiley and Sons, (1958).
- 6.29 Besserer, C.W., "Missile Engineering Handbook," pp. 301-306, D. Van Nostrand, (1958).
- 6.30 Kinney, G.F., "Explosive Shocks in Air," MacMillan, G., N.Y., (1962).
- 6.31 Smith, H.D., Clark, R.W. and Mayor, R.P., "Evaluation of Model Techniques for the Investigation of Structural Response to Blast Loads," MIT, Report Number R63 16, (1963).
- 6.32 Kingery, C.N. and Panill, B.F., "Peak Over-Pressure versus Scaled Distance for TNT Surface Burst," B.R.L. Memorandum Report, Number 1518, (1964).
- 6.33 "Operation SNOW BALL Project Descriptions," Vol. I, Data Center Special Report, 24-1, DASA 1516-1, AD 441 974.
- 6.34 Taylor, G., "The Formation of a Blast Wave by a Very Intense Explosion," Proc. Roy. Soc. London, A 201 (159-186), (1950).
- 6.35 Carlson, H.W., Mack, R.J. and Morris, O.A., "Sonic Boom Pressure-Field Estimation Techniques," Jour. Acoust. Soc. Amer. 39, 5, Part 2, 60-18, (1966).



- 6.36 Hubbard, H.H., "Nature of the Sonic Boom Problem," *Jour. Acoust. Soc. Amer.* 39, 5, Part 2, 1-9, (1966).
- 6.37 Kane, E.J., "Some Effects of the Nonuniform Atmosphere on the Propagation of Sonic Booms," *Jour. Acoust. Soc. Amer.* 39, 5, Part 2, 26-30, (1966).
- 6.38 Mclean, F.E. and Shrout, B.L., "Design Methods for Minimization of Sonic Boom Pressure Field Disturbances," *Jour. Acoust. Soc. Amer.* 39, 5, Part 2, 19-25, (1966).
- 6.39 Hilton, D.A., and Newman, Jr., J.W., "Instrumentation Techniques for Measurement of Sonic Boom Signatures," *Jour. Acoust. Soc. Amer.* 39, 5, Part 2, 31-35, (1966).
- 6.40 Kryter, U.D., et al., "Definition of the Effects of Booms from the SST on Structures, People, and Animals", Stanford Research Institute Report for the National Sonic Boom Evaluation Office, Dept. of the Air Force, Under Contract AF 49 (638)-1690, June 1966.
- 6.41 Hilton, D.A., et al, "Sonic Boom Exposures During FAA Community Response Studies over a Six-Month Period in the Oklahoma City Area," NASA TN D-2539, (1964).
- 6.42 Whitham, G.B., "The Behavior of Supersonic Flow Past a Body of Revolution, Far from the Axis." *Proc. Roy. Soc.* A201, (1950).
- 6.43 Lansing, D.L. and Magleri, D.J., "Comparison of Measured and Calculated Sonic-Boom Ground Patterns Due to Several Different Aircraft Manuevers," NASA TN D-2730, (1965).

**CHAPTER 7**

**PROPAGATION OF  
SONIC PRESSURE WAVES  
AND GROUND VIBRATION**

TABLE OF CONTENTS

<u>SECTION</u>	<u>PAGE</u>
7.1	<u>INTRODUCTION</u> . . . . . 7-1
7.2	<u>PROPAGATION EFFECTS OF ACOUSTIC WAVES</u> . . . . . 7-1
7.2.1	AMBIENT ATMOSPHERIC CONDITIONS . . . . . 7-1
7.2.2	SPREADING LOSSES . . . . . 7-2
7.2.2.1	Sound Field Near a Finite Size Sound Source . . . . . 7-2
7.2.2.2	Influence of Ground Reflecting Plane . . . . . 7-3
7.2.3	CLASSICAL ABSORPTION LOSSES . . . . . 7-3
7.2.4	MOLECULAR ABSORPTION . . . . . 7-5
7.2.4.1	Review of Theory . . . . . 7-5
7.2.4.2	Rotational Mode of Molecular Absorption . . . . . 7-6
7.2.4.3	Vibrational Absorption Mode . . . . . 7-6
7.2.5	HEAT RADIATION LOSSES . . . . . 7-9
7.2.6	DESIGN VALUES FOR AIR ABSORPTION . . . . . 7-9
7.2.6.1	Summary of Theoretical Values . . . . . 7-9
7.2.6.2	Comparison of Theory with Measured Data . . . . . 7-10
7.2.6.3	Summary of Design Values . . . . . 7-13
7.2.7	ATTENUATION OF BARRIERS AND GROUND COVER . . . . . 7-14
7.2.7.1	Attenuation of Barriers . . . . . 7-14
7.2.7.2	Attenuation by Ground Cover . . . . . 7-15
7.2.8	PROPAGATION ANOMALIES . . . . . 7-16
7.2.8.1	Attenuation Due to Ground Winds and Turbulence . . . . . 7-16
7.2.8.2	Reinforcement of Sound Due to Focusing . . . . . 7-22
7.2.8.3	Statistical Variations in Propagation Losses . . . . . 7-25
7.2.9	DESIGN VALUES FOR ACOUSTIC PROPAGATION LOSSES . . . . . 7-25
7.2.9.1	Determine Overall Acoustic Power and Spectrum of Source . . . . . 7-26
7.2.9.2	Determine Source and Receiver Position and Terrain Between Them . . . . . 7-26
7.2.9.3	Calculate the Inverse Square Law Losses . . . . . 7-26
7.2.9.4	Determine the Atmospheric Absorption Losses . . . . . 7-26
7.2.9.5	Estimate the Additional Losses Which Increase the Absorption . . . . . 7-27
7.2.9.6	Estimate the Effect of Sound Focusing . . . . . 7-27
7.2.9.7	Review of the Calculations . . . . . 7-28
7.3	<u>PROPAGATION LOSSES OF BLAST WAVES</u> . . . . . 7-28
7.3.1	FOCUSING ANOMALIES . . . . . 7-28
7.3.1.1	Magnification of Blast Pressures by Focusing . . . . . 7-28
7.3.1.2	Cylindrical Spreading Model for Blast Focusing . . . . . 7-29
7.3.2	SHIELDING EFFECTS ON THE BLAST LOADING OF STRUCTURES . . . . . 7-29
7.3.3	SUPPRESSION OF BLAST WAVES BY BURIED EXPLOSIVES . . . . . 7-30
7.3.3.1	Suppression of Overpressure Pulse . . . . . 7-31
7.3.3.2	Suppression of Positive Phase Impulse . . . . . 7-31
7.4	<u>PROPAGATION CHARACTERISTICS OF SEISMIC GROUND WAVES</u> . . . . . 7-31
7.4.1	SONICALLY COUPLED GROUND MOTION . . . . . 7-31
7.4.1.1	Experimental Measurement of Sonically-Coupled Ground Motion . . . . . 7-32
7.4.2	DIRECTLY COUPLED GROUND MOTION . . . . . 7-34
7.4.2.1	General Propagation Characteristics of Seismic Waves Transmitted Through the Ground . . . . . 7-35
7.4.2.2	Velocity of Seismic Waves . . . . . 7-35
7.4.2.3	Spreading Loss for Seismic Waves . . . . . 7-36
7.4.2.4	Absorption Losses for Seismic Waves . . . . . 7-36
7.4.2.5	Overall Propagation Losses for Mechanical Sources . . . . . 7-37
7.4.2.6	Overall Propagation Losses for Aerodynamic Sources . . . . . 7-38
7.4.2.7	Overall Propagation Losses for Buried Explosive Sources . . . . . 7-38
	REFERENCES . . . . . 7-39

## CHAPTER 7

# PROPAGATION OF SONIC PRESSURE WAVES AND GROUND VIBRATION

### 7.1 INTRODUCTION

Determining propagation losses is a basic step in the analysis of any source-transmission-receiver problem involving sonic energy. The following chapter treats this subject in three parts - propagation of acoustic waves, blast waves, and ground waves. More is known about propagation of acoustic waves, so this topic is considered first. This also allows propagation effects common to all three sources to be more effectively covered.

### 7.2 PROPAGATION EFFECTS OF ACOUSTIC WAVES

Propagation effects between an acoustic source and receiver may be classified by the following phenomena (References 7.1 and 7.2).

- Divergence Losses (Losses Due to Spreading)
- Absorption Losses (Losses Due to Energy Dissipation or Conversion in Homogeneous Medium)
- Refraction Effects (Gain or Loss Due to Bending of Sound Rays in Nonuniform Medium)
- Scattering Losses (Scattering Due to Inhomogeneities of Media or Obstacles on Ground)

For application to design problems, it is convenient to regroup the various types of propagation effects into three broad categories as follows:

#### Nominal or Predictable Effects

- Effect of Static Properties of the Atmosphere on Sound Power Generated by a Source
- Losses Due to Spreading or Divergence of the Wave Front
- Losses Due to Classical Absorption, Molecular Absorption, and Heat Radiation
- Losses by Barriers or Ground Cover

#### Slowly Varying Propagation Anomalies

- Spreading Anomalies Due to Quasi-Static Non-uniformity of the Atmosphere
- Attenuation Anomalies Due to Scattering of Energy in the Atmosphere

#### Rapidly Varying Propagation Anomalies

- Varying Propagation Due to Fluctuating Conditions of the Atmosphere

The latter category of rapidly varying propagation anomalies, which cause the average received level to vary over a period of minutes or less, will not be covered since it is

not generally a significant factor for design. It should be pointed out that the physical phenomena involved in these propagation anomalies is known but theoretical design methods cannot always be developed to account for them. The slowly varying anomalies represent the combined effects of loss mechanisms which are sufficiently variable or unknown as to make theoretical predictions of limited value for design. In this case, semiempirical or statistical estimates are desired. These estimates, coupled with the prediction nominal losses, form the basis for conservative design estimates of propagation effects.

A thorough review of sound propagation in air, published by Nyborg and Mintzer (Reference 7.1), in 1955, provides limited information applicable to propagation effects of low frequency rocket noise. Emphasis will be placed, in this section, on sound propagation at frequencies below 1,000 Hz. Available data on sound propagation in air down to about 2 Hz is included here, along with recently reported measurements of sound absorption in the audible frequency range. These data have been utilized to develop new methods for predicting the minimum and maximum propagation loss in the low frequency range. A combined theoretical and empirical correlation of the absorption loss data, for example, provides for the first time a unique means of predicting the minimum absorption loss at frequencies well below the range of published data.

### 7.2.1 AMBIENT ATMOSPHERIC CONDITIONS

If a point source of sound is placed in a uniform, stationary, infinite medium, the mean square sound pressure at a distance  $r$  from the source may be expressed by

$$p^2 = \frac{W}{4\pi r^2} \cdot \rho c \cdot e^{-2\alpha r} \quad (7.1)$$

where

$$p^2 = \text{mean square pressure - Newtons/m}^2$$

$$W = \text{acoustic power output - Watts}$$

$$r = \text{distance from source - meters (m)}$$

$$\rho = \text{mass density of medium - kg/m}^3$$

$$c = \text{velocity of sound in medium - m/sec}$$

$$\alpha = \text{pressure attenuation constant - Nepers/m}$$

For a constant power output, the mean square pressure varies directly as the characteristic impedance of the medium  $\rho c$ , inversely as the square of the radius  $r$ , and decays exponentially with radius according to the attenuation constant  $\alpha$ . The latter defines the fractional decrease in sound pressure per unit distance, in a sound wave, due to dissipation of acoustic energy by various loss mechanisms. For noise from rocket exhaust, the sound power is also a function of  $\rho c$ . In fact, it can be shown that the mean square pressure in the far field of a rocket noise source is expected to vary as  $p^2/c^4$  (Reference 7.3). This is equivalent to the mean square sound pressure varying with  $P_o^2/T^4$  where  $P_o$  is the ambient pressure and  $T$  is the absolute ambient temperature. Based on this relationship, the change,

in decibels, in rocket noise due to different ambient conditions can be specified as shown in Table 7.1. Reference conditions of 760 mm of Hg (14.7 psi) and 15°C (59°F) were used. As an example, if a rocket noise measurement is made when the atmospheric pressure is 800 mm Hg (15.5 psi) and the ambient temperature is -20°C (-4°F), the correction factor  $C_A$ , given in the last column of Table 7.1 shows that the measured sound level will be 2.7 dB above the level expected for nominal reference conditions. For normal sea level conditions, the variations in sound level of about  $\pm 2$  dB would usually be within the accuracy of the predicted sound levels for a given rocket engine.

TABLE 7.1

## EFFECT OF AMBIENT CONDITIONS ON ROCKET NOISE SOUND PRESSURE LEVELS

$$C_A = 10 \log (P_o/760)^2 (288/T^{\circ}\text{K}) - \text{dB}$$

Altitude ft	$P_o$ Pressure mm Hg	Temperature		$C_A$ ① dB
		°C	°F	
Sea Level	800	-20	-4	+2.7
		15	59	+0.4
		40	104	-1.0
	760	-20	-4	+2.3
		15	59	0.0
		40	104	-1.5
	720	-20	-4	+1.8
		15	50	-0.5
		40	104	-1.9
5,000	632	5.1	41.1	-1.0
10,000	523	-4.8	23.4	-2.0
20,000	350	-24.6	-12.2	-4.2
30,000	226	-44.6	-48.4	-6.5

① Change in sound level at large distances from a rocket noise source due to difference between pressure and temperature specified and reference conditions ( $P_o = 760$  mm Hg,  $T = 288^{\circ}\text{K}$  or  $59^{\circ}\text{F}$ )

## 7.2.2 SPREADING LOSSES

The mean square sound pressure level in the field of a point source of sound radiating into free space varies inversely as the square of the radius from the source, due to spherical spreading of the wave front.

This spherical spreading loss is shown in Figure 7.1, assuming a reference distance of 1 foot. While the inverse square law is useful for estimating sound levels at large distances from a rocket noise source, the finite size of this source and the effect of a reflecting ground plane will cause significant deviations from this inverse square law in regions close to a rocket exhaust flow or near the ground.

The sound level along a given radial line from the nozzle exit will then approach a finite upper limit not predicted by Equation 7.1.

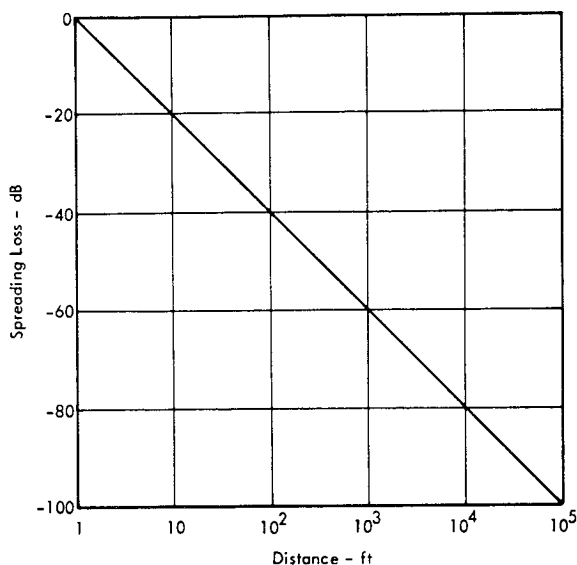


FIGURE 7.1 Inverse Square Law Spreading Loss for Point Source Radiating Into Free Space, Relative to Sound Level at 1 ft from Source

## 7.2.2.1 Sound Field Near a Finite Size Sound Source

The source of rocket exhaust noise can be represented conceptually by a distribution of sources which extend out to 50 nozzle diameters from the nozzle exit. Figure 7.2 shows the relative sound level along radial lines at 90 degrees and 45 degrees to the axis of an array of 10 equally spaced uncorrelated point sources and with an origin at one end of the array. Since the sources are assumed to be uncorrelated, the mean square sound pressure at any point is simply the sum of the mean square pressures contributed by each source acting independently. These results indicate that the spreading loss begins to deviate significantly from the inverse square law at distances of the order of 1 source length (i.e., about 50 nozzle diameters) from one end of the extended source. A similar deviation from inverse square also occurs close to a single finite size acoustic source such as a plate vibrating in its fundamental mode. In this case, the deviation is negligible for distances greater than  $2L^2/\lambda$  where  $L$  is a characteristic source dimension and  $\lambda$  is the radiated wavelength.

The region near a sound source where the sound level deviates from the inverse square law due to these finite size effects of the source is called the near field. The region beyond this near field is called the far field of an acoustic source and may be considered as the region where the sound field corresponds to that of a point source.

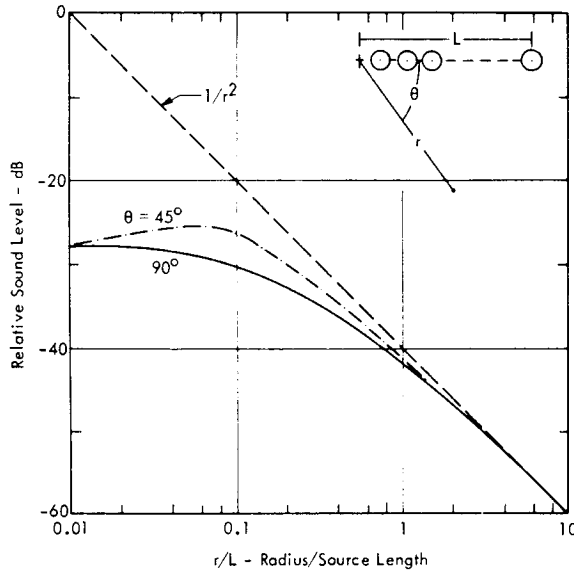


FIGURE 7.2 Deviation from Inverse Square Law in Near Field of Finite Size Source Consisting of a Linear Array of 10 Equally Spaced Uncorrelated Point Sources

7.2.2.2 Influence of Ground Reflecting Plane

The presence of a ground reflecting plane near a noise source can have two effects on the radiated sound field. First, the sound power output of the source will be increased if the ground plane is rigid and located closer than approximately 1/6 to 1/2 of the radiated wavelength, depending on the type of source (Reference 7.4). The maximum increase is 3 dB if the source-to-ground plane separation approaches zero and the volume velocity of the source remains constant. This increase in sound power output is due to an increase in the acoustic radiation efficiency of the source.

The second effect of a ground plane involves the interference between the direct and reflected sound (References 7.5 and 7.6). The deviations from an inverse square law depend on the height  $h$  of the source above the ground, the radius  $r$  from the source, and  $\lambda$ , the wavelength of the sound. The variation in the sound level radiated by a point source of an ideal octave band of noise as a function of a normalized radius  $r\lambda/h^2$  is shown in Figure 7.3 for various values of the ratio  $r/h$  of distance to height of source and receiver. The wavelength for the normalized distance is for the geometric mean frequency of the octave band. The choice of these normalizing parameters provides a reasonable collapse for the curves for  $r/h > 2.0$ . For practical cases, where the source is a deflected rocket exhaust 50 feet off the ground, the mean of the curves for  $r/h > 20$  in Figure 7.3 would be suitable for estimating the ground effect for distances greater than 100 feet. As an example of this ground reflection effect, assume the source is located approximately 50 feet off the ground and the receiver or sound level measurement is located at this same height at 2000 feet from the source ( $r/h = 40$ ).

If the wavelength  $\lambda$  is converted to the corresponding frequency,  $f = 1120/\lambda$ , then for frequencies below 90 Hz, ( $r\lambda/h^2 > 10$ ), the measured octave band level will be about 4-6 dB higher than would be observed without a ground plane present. At an octave band center frequency of about 200 Hz ( $r\lambda/h^2 \approx 4.5$ ), the sound level will tend to show a marked decrease in level below the free field value (without a ground plane) due to the destructive interference of the direct and reflected sound rays from the source. At frequencies above 450 Hz, ( $r\lambda/h^2 < 2$ ), the reflecting ground plane increases the level about 2-3 dB. These effects have been verified experimentally (Reference 7.6) although the decrease in level for  $r\lambda/h^2 \sim 4$  is not as sharp as indicated by the ideal curves in Figure 7.3.

In summary, the effects of ground reflection and a finite size source should be considered when predicting the sound field of rocket noise, particularly in the near field region.

7.2.3 CLASSICAL ABSORPTION LOSSES

All sonic disturbances lose energy in propagating through air due to the irreversible conversion of acoustical energy into heat energy. This energy transfer process may be broken down into three types: classical absorption losses which are inherent in all gases due to basic gas transport phenomena, molecular absorption losses which are associated with resonance phenomena within polyatomic gases, and losses due to radiation of heat energy (Reference 7.7). Classical absorption losses are briefly reviewed in this section and, for each type, a simplified expression for the attenuation constant is given in terms of the decibel attenuation per 1,000 feet at normal atmospheric pressure and 59°F. The exact expression is also given in terms of nepers per unit distance (References 7.1 and 7.7). The attenuation in decibels is equal to 8.68 times the attenuation in nepers (see Table 12.10, Chapter 12).

Viscous Loss

Cause -- Due to viscous drag forces opposing "particle" motion of sound wave

Attenuation Constant

Approximate  $\alpha_v = 2.58 \times 10^{-8} f^2 \text{ dB}/1,000 \text{ ft}$   
 Exact  $\alpha_v = \frac{2\pi^2 f^2}{\gamma P_o c} \left[ \eta_B + \frac{4\eta}{3} \right] \text{ Np}/\text{unit distance}$  (7.2)

Heat Conduction Loss

Cause -- Due to heat transfer between adjacent condensation and rarefaction regions within the gas

Attenuation Constant

Approximate  $\alpha_n = 1.08 \times 10^{-8} f^2 \text{ dB}/1,000 \text{ ft}$   
 Exact  $\alpha_n = \frac{2\pi^2 f^2}{\gamma P_o c} \left[ \frac{(\gamma-1)k}{C_p} \right] \text{ Np}/\text{unit distance}$  (7.3)

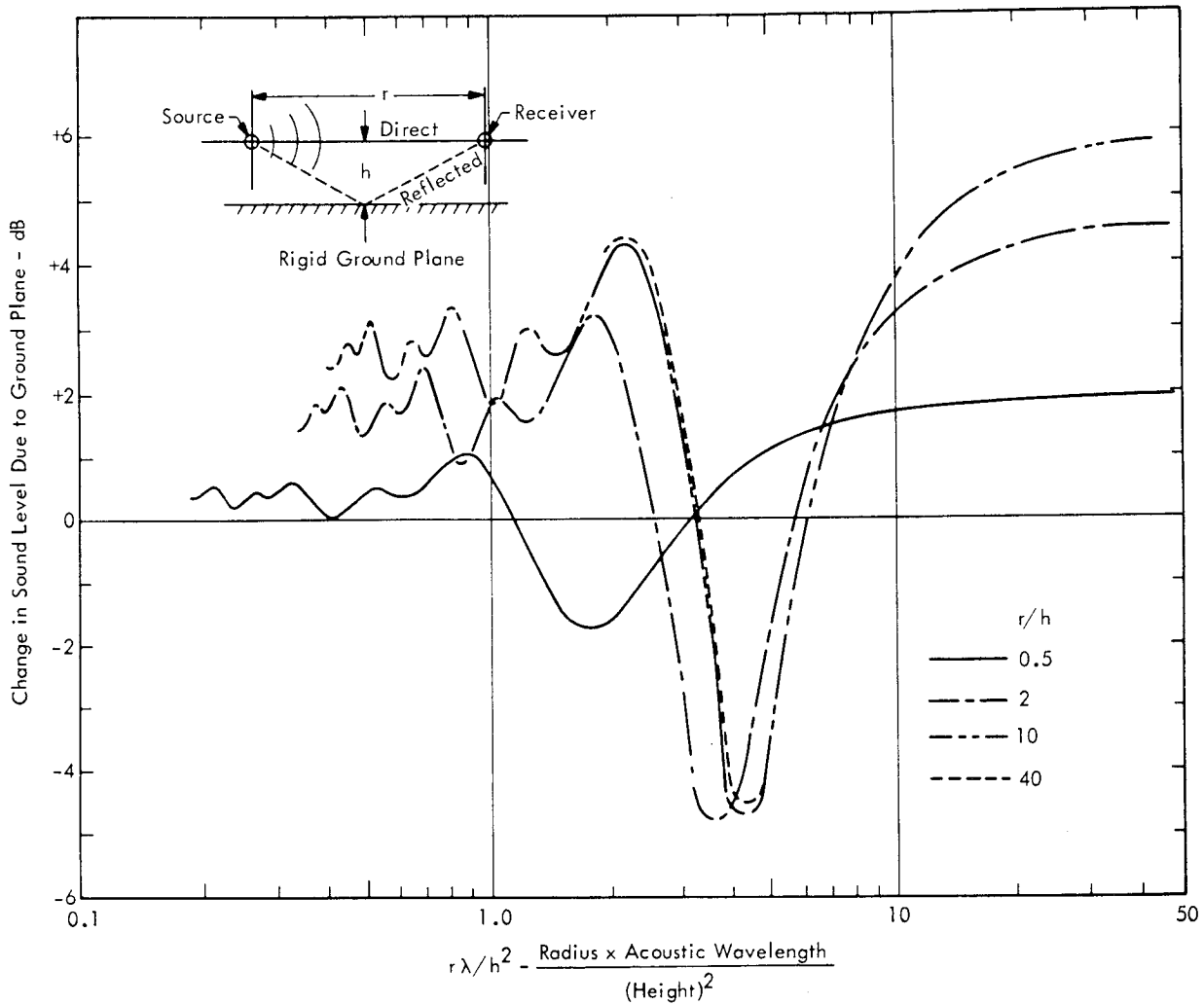


FIGURE 7.3 Change in Octave Band Sound Level Due to Presence of Rigid Ground Plane Below a Horizontal Source-Receiver Path. Source is an ideal octave band of white noise with an acoustic wavelength  $\lambda$  at the geometric center frequency of the band.

Diffusion Loss

Cause -- Mutual diffusion between oxygen and nitrogen molecules in air

Attenuation Constant

Approximate  $\alpha_d = 0.38 \times 10^{-8} f^2 \text{ dB}/1,000 \text{ ft}$

Exact  $\alpha_d = \frac{2\pi^2 f^2}{\gamma P_o c} \left[ \frac{(\gamma-1)AD_{o-n}}{\gamma} \right] =$   
 $N_p/\text{unit distance} \quad (7.4)$

The terminology used in the above expressions is identified as follows. The physical values for the constants are for a temperature of 59°F and an atmospheric pressure of 14.7 psi.

- $f$  = frequency - Hz
- $\gamma$  = specific heat ratio - (1.403)
- $P_o$  = atmospheric pressure - (2,117 lb/ft<sup>2</sup>)
- $c$  = speed of sound - (1,117 ft/sec)
- $\eta_B$  = bulk viscosity coefficient - (Stokes theory assumes  $\eta_B = 0$ )
- $\eta$  = shear viscosity coefficient - (3.745 x 10<sup>-7</sup> lb-sec/ft<sup>2</sup>)
- $k$  = thermal conductivity - (4.02 x 10<sup>-6</sup> BTU/sec °R ft)
- $C_p$  = specific heat at constant pressure - (7.71 BTU ft/lb °R sec<sup>2</sup>)
- $A$  = molecular constant - (0.51 for air)
- $D_{o-n}$  = oxygen-nitrogen diffusion coefficient (0.214 x 10<sup>-3</sup> ft<sup>2</sup>/sec).

Based on these constants and Equations 7.2 - 7.4, the total classical absorption at 59°F and normal atmospheric pressure is

$$\alpha_{cl} = 4.04 \times 10^{-8} f^2 - \text{dB}/1,000 \text{ ft} \quad (7.5)$$

As shown in the next section, one form of molecular absorption loss adds an additional 20 percent to this classical loss which varies with the square of frequency.

### 7.2.4 MOLECULAR ABSORPTION

Molecular absorption accounts for energy losses due to a relaxation phenomenon of the molecules of the air which are excited into resonance by the passage of a sound wave. The principal effect involves an interaction of water vapor molecules with the resonance of oxygen molecules so that molecular absorption is highly dependent on the humidity content of the air. Other gases in air also exhibit molecular absorption losses but to a negligible degree in the low frequency range. Molecular absorption is reviewed in detail since it is the basis for the minimum attenuation loss at very low frequencies characteristic of rocket noise.

#### 7.2.4.1 Review of Theory

A theoretical explanation for molecular absorption was first given by Kneser in 1933 (Reference 7.8) concurrently with experimental studies by Knudsen (Reference 7.9). A detailed series of measurements of absorption in air were recently conducted under well-controlled conditions by Harris, and Harris and Tempest (References 7.10, 7.11, 7.12 and 7.13). These results, corrected for classical absorption, demonstrate the well known fact that the theory accurately predicts the maximum attenuation, but fails to predict attenuation at all ranges of humidity. An explanation for this discrepancy is still lacking; however, a clear definition of the basic characteristics of molecular absorption is desired to ensure consistent design estimates of attenuation of low frequency rocket noise. The following simplified explanation for the theory of molecular absorption is adapted from thorough reviews of the subject by Dean (Reference 7.7), Knudsen (Reference 7.14), and Henderson (Reference 7.15).

For diatomic gases (those having two atoms per molecule), internal energy states of the gas molecules include two rotational modes of the atoms about two mutually perpendicular axes, and one vibrational mode of the atoms along the line of centers as well as three translational modes. Excitation of the rotational and vibrational modes is attributed to transfer of energy from the translational modes by collision of the molecules. The translational energy is, in turn, determined by the temperature of the gas.

Now, under adiabatic compression by a sound wave, air is momentarily heated during each compression cycle. This also increases the translational energy of the gas molecules, thus increasing its ability to transfer energy to another molecule by collision. However, if the period of the sound wave is much less than the finite time, known as the relaxation time, which is required for this process, the energy transfer will not have time to take place. The gas

then exists, statistically, in an unexcited state (i.e., the rotational or vibrational modes are not excited). On the other hand, if the period of the sound wave is much greater than the relaxation time, sufficient time is available in each cycle of the sound wave for the energy transfer to occur. On the average, the gas will now have a higher internal energy due to the additional energy of the internal rotational and/or vibrational modes.

For intermediate periods of the sound compression cycle, energy will be extracted from the sound field by absorption into this internal energy mode of the gas molecules. The amount of energy extracted will be proportional to the energy of the rotational or vibrational modes which are excited and will exhibit a resonance phenomenon between the excitation frequency  $f$ , and relaxation frequency  $f_m \sim 1/\text{relaxation time}$ . Thus, maximum energy loss occurs when these two frequencies are equal. This loss of energy is the mechanism for molecular absorption in polyatomic gases.

The resonance effect for molecular absorption losses is evident in the equation for the absorption loss per unit wavelength,  $\mu$ , which is given by (References 7.7 and 7.15)

$$\mu = \mu_{\max} \frac{2f/f_m}{1 + (f/f_m)^2} \quad (7.6)$$

where

- $\mu_{\max}$  = maximum attenuation in terms of the fractional reduction of sound pressure per unit wavelength  $\lambda$  -- a quantity which is independent of frequency
- $f$  = frequency of sound wave
- $f_m$  = relaxation frequency at which maximum absorption occurs.

For practical purposes, molecular absorption is more conveniently expressed as an absorption loss per unit distance. It can again be defined as the product of a term which is independent of frequency and a frequency-dependent term by

$$\alpha = \frac{\mu}{\lambda} = \left[ \alpha_{\max} \cdot \frac{f_m}{f} \right] \left[ \frac{2(f/f_m)^2}{1 + (f/f_m)^2} \right] \quad (7.7)$$

where

$$\lambda = c/f = \text{wavelength of sound of frequency } f \text{ and sound velocity } c$$

so that

$$\alpha_{\max} \frac{f_m}{f} = \frac{\mu_{\max} f_m}{c} = \text{absorption loss per unit distance at relaxation frequency}$$



and

$$\frac{2(f/f_m)^2}{1 + (f/f_m)^2} = \text{relative absorption loss, proportional to } f^2 \text{ for } f \ll f_m \text{ and equal to 2 for } f \gg f_m.$$

Equations 7.6 and 7.7 for the molecular absorption are plotted in normalized form in Figure 7.4. The values of  $\mu$  and  $\alpha$  have been divided by their respective frequency-independent terms  $\mu_{\max}$  and  $\alpha_{\max} f_m/f$  and plotted as a function of the frequency ratio  $f/f_m$ . The normalized plot for  $\mu/\mu_{\max}$  clearly illustrates the "resonance" effect at  $f/f_m = 1$ .

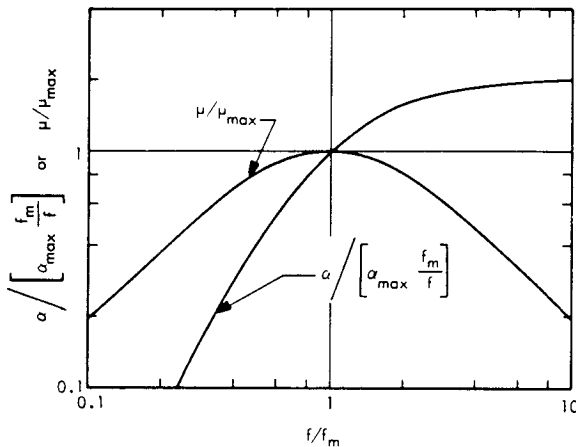


FIGURE 7.4 Variation in Normalized Molecular Absorption Coefficients with Frequency.  $\mu$  = absorption loss per wavelength and  $\alpha$  = absorption loss per unit distance.

According to Equations 7.6 and 7.7, two parameters  $\mu_{\max}$  and  $f_m$  are necessary and sufficient to define molecular absorption loss. However, since this process involves two modes of vibration, rotational and vibrational, there are two values of each parameter to be defined. It will be shown that only the relaxation frequency  $f_m$  for the vibrational mode is not accurately predicted by theory. For the sake of brevity, only the essential final equations of the theory are summarized without detailed deviations.

#### 7.2.4.2 Rotational Mode of Molecular Absorption

The value of the maximum absorption loss per wavelength  $\mu_{\max}$  for the rotational mode can be given by the constant (References 7.7 and 7.8)

$$\mu_{\max}(\text{rot}) = 2\pi/5 \sqrt{21} \quad (7.8)$$

This mode of absorption loss is not dependent on humidity and the relaxation frequency, or frequency of maximum absorption, is of the order of one billion hertz and is given by (Reference 7.7)

$$f_{\max}(\text{rot}) = \frac{3\phi P_o}{4\pi\eta} \sqrt{\frac{7}{3}} \quad (7.9)$$

where

$\phi$  = probability of energy excitation per collision = 0.26 for oxygen in air

$P_o$  = ambient pressure

$\eta$  = shear viscosity coefficient.

When these last two expressions are used in Equation 7.7 and the values for the constants inserted for a temperature of 59°F and sea-level pressure (see Section 7.2.3), the absorption loss for the rotational mode, given in dB per 1000 ft, for the audio frequency range is

$$a_{(\text{rot})} = 0.80 \times 10^{-8} f^2 - \text{dB}/1,000 \text{ ft} \quad (7.10)$$

Thus, the rotational mode portion of molecular absorption loss varies with the square of frequency in the same manner as the classical absorption loss and adds an additional 20 percent to this loss.

#### Experimental Verification of Total Absorption Loss for Dry Air

The total predicted absorption loss for dry air at a temperature of 59°F is given by the sum of the classical loss and the rotational absorption mode, which equals  $4.84 \times 10^{-8} f^2 - \text{dB}/1000 \text{ ft}$ . The loss increases with temperature by about 0.05% per °F from 0° to 100°F.

The total absorption observed in the laboratory for dry air at a temperature of 20°C is about  $2.00 \times 10^{-11} f^2 \text{ Np}/\text{m}$  (Reference 7.16). When corrected to 59°F and expressed in practical units, this is  $5.3 \times 10^{-8} f^2 \text{ dB}/1000 \text{ ft}$  which is within 10 percent of the predicted value. In general, this loss is negligible in the normal frequency range of interest for rocket noise.

#### 7.2.4.3 Vibrational Absorption Mode

The vibrational mode of molecular absorption is the predominant known mechanism for absorption loss in the low frequency range. It is due to energy absorption by oxygen ( $\text{O}_2$ ) molecules vibrating in their lowest excited state. The vibrational mode is one of axial vibration of the two  $\text{O}_2$  atoms along their line of centers. Excitation of this mode involves the collision of oxygen and nitrogen molecules with water molecules, hence this loss mechanism is very sensitive to moisture content of the air. However, its maximum values is not dependent on humidity.

In a normal mixture of air, with 21 percent oxygen, the maximum absorption per wavelength in air for this mode is 0.21 times the value for pure oxygen and can be shown to be (References 7.7 and 7.8)

$$\mu_{\max} (\text{vib}) = (0.21) \frac{2\pi}{35} (E/RT)^2 e^{-E/RT} \quad (7.11)$$

where

E = the vibrational energy associated with this mode - BTU/mole

R = the universal gas constant - BTU/mole, °R

T = absolute temperature - °R.

This vibrational energy E divided by the universal gas constant R is equivalent to a characteristic temperature. For the lowest vibrational mode of oxygen, this is

$$\frac{E}{R} \approx 2239^\circ\text{K} \text{ or } 4030^\circ\text{R} \quad (\text{Reference 7.20})$$

Thus, for an ambient temperature of 59°F (T = 519°R) the maximum molecular absorption due to the vibrational mode, when expressed in dB/1000 ft, is

$$\begin{aligned} \alpha_{\max} &= 8680 \cdot \mu_{\max} f/c \\ &= 0.0078 f - \text{dB}/1000 \text{ ft at } 59^\circ\text{F} \end{aligned} \quad (7.12)$$

At temperatures other than 59°F, the maximum absorption is given by

$$\alpha_{\max} = 0.0078 f \left( \frac{519}{T^\circ\text{R}} \right)^{2.5} e^{7.77(1-519/T^\circ\text{R})} - \text{dB}/1000 \text{ ft} \quad (7.13)$$

Experimental Verification of Maximum Absorption for Vibrational Mode

According to Equation 7.12, the maximum absorption coefficient will vary directly with frequency. This linear relationship has been clearly established by numerous experimenters. The proportionality constant or slope of maximum attenuation versus frequency will also vary with temperature according to Equation 7.13. Recent experimentally measured values of this constant (Harris and Tempest, Reference 7.11) are compared in Figure 7.5 with the value predicted by Equation 7.13 and show very nearly the same variation with temperature. Similar agreement has been obtained by several other investigations. Thus, at a temperature of 35°F, reading from Figure 7.5, the maximum molecular absorption in the vibrational mode would be given by  $\alpha_{\max} = 0.006 f - \text{dB}/1000 \text{ ft}$ .

Relaxation Frequency - Theory

The second parameter required for defining molecular absorption by this vibrational mode, the relaxation frequency  $f_m$ , cannot be predicted theoretically. It is necessary to resort to experimental results. However, some theoretical concepts are available to guide interpretation of the data. Since the absorption process is dependent on collisions of oxygen molecules, it can be shown that the influence of humidity content of the air on the relaxation frequency,

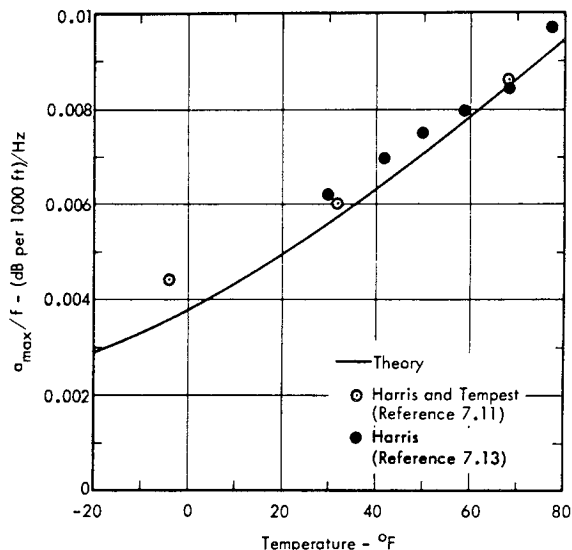


FIGURE 7.5 Slope of Maximum Molecular Absorption Coefficient Versus Frequency as a Function of Ambient Temperature - Theory and Experimental Data. (Each  $\odot$  data point is a mean slope through measurements plotted in Figure 7 of Reference 7.11.)

which, in turn, depends on the rate of these collisions, would have the following simplified form (Reference 7.20)

$$f_m = \frac{P_o}{(T)^{0.8}} [a h^2 + b h + c] \quad (7.14)$$

where

- a, b, c = constants to be determined experimentally
- h = percent of water molecules in air (percent mole ratio)
- T = absolute temperature
- $P_o$  = atmospheric pressure.

The three constants a, b, and c in Equation 7.14 can be interpreted as follows. The constant c is the lowest relaxation frequency due to energy absorption by collisions of O<sub>2</sub> and N<sub>2</sub> molecules in dry air. The constant (b) depends on the number and rate of energy exchange between O<sub>2</sub> - H<sub>2</sub>O and N<sub>2</sub> - H<sub>2</sub>O collisions. The constant (c) depends primarily on the number and rate of energy exchange between double H<sub>2</sub>O - H<sub>2</sub>O collisions (References 7.7, 7.17 and 7.20). The temperature variation for  $f_m$ , indicated in Equation 7.14, is a preliminary estimate based on the theoretical review by Dean (Reference 7.7).

Relaxation Frequency - Experimental Data

By analysis of experimental measurements of the variation of  $f_m$  with humidity, it is possible to obtain a reasonable estimate of these constants. Such an analysis was carried out, utilizing the data from Harris (Reference 7.10), Harris

and Tempest (Reference 7.12), Evans and Bazley (Reference 7.18 and Knotzel (Reference 7.19), which is summarized in References 7.10 and 7.11. A "best fit" line was constructed for the data based on Equation 7.14, and is shown in Figure 7.6. Included in this figure are data from Reference 7.11, covering temperature conditions down to -20°C (-4°F) and 200 mm Hg (3.9 psi).

This theoretical curve with empirically derived constants is defined by the equation

$$f_m = \frac{P'}{(T')^{0.8}} \left[ 10 + 6.5 \times 10^3 h + 4.36 \times 10^4 h^2 \right] - \text{Hz} \tag{7.15}$$

where P' and T' are the ambient pressure and temperature relative to a reference condition for the experimental data of 20°C and 760 mm of Hg. The first or zero order term in this equation was estimated from data reported in Reference 7.20 for the relaxation frequency for pure dry oxygen.

The suggested theoretical value for f<sub>m</sub> first proposed by Kneser (Reference 7.8) is also shown in Figure 7.6. It differs appreciably from the experimental data and is defined by only one squared term in h given by

$$f_m = 5.8 \times 10^4 h^2 - \text{Hz} \tag{7.16}$$

For practical applications, it is desirable to establish a more accurate but equally simple expression for the relaxation frequency in terms of humidity content expressed in more conventional units.

Humidity content is expressed in these two equations in terms of percent of water molecules in air to be consistent with theory. However, humidity content of air is more commonly expressed in terms of the percent of relative humidity or absolute humidity h' in gm/m<sup>3</sup>. A conversion chart is given in Figure 7.7 which relates these three quantities (Reference 7.1). (Note that the percent mole ratio on the lower scale of Figure 7.7 has been multiplied by 10.)

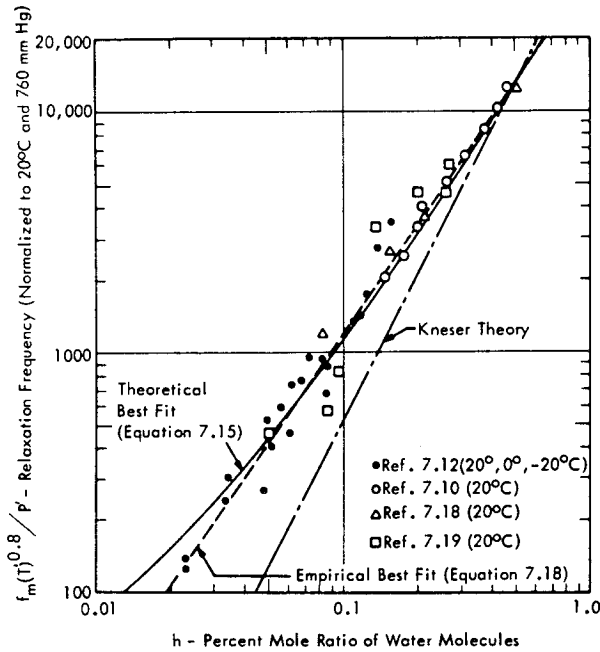


FIGURE 7.6 Comparison of Data on Relaxation Frequency for Vibrational Mode of Molecular Absorption with Kneser Theory and Revised Theoretical and Empirical Best Fit to Data

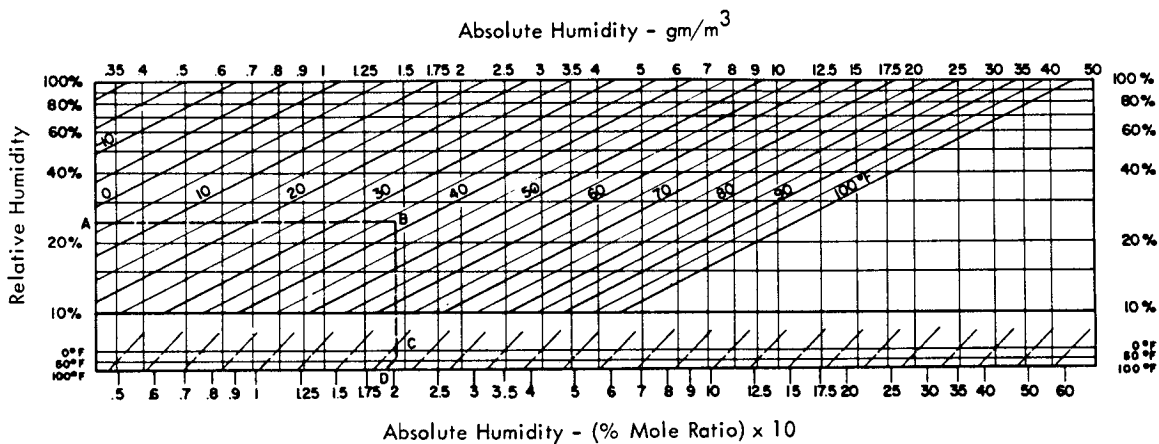


FIGURE 7.7 Chart for Converting Units of Humidity (from Reference 7.1). To convert from Relative Humidity A at Temperature B, drop vertically to point C at intersection with lower temperature scale, then along slanted line to point D which is 10 times percent mole ratio. Absolute humidity in gm/m<sup>3</sup> lies directly above point B on top scale.

The conversion from absolute humidity  $h$ , expressed as percent mole ratio of water molecules, to absolute humidity  $h'$  in terms of  $\text{gm}/\text{m}^3$  is given by

$$h' = 7.57 h P^*/T^* - \text{gm}/\text{m}^3 \quad (7.17)$$

where

$P^*$  = ambient pressure relative to the reference value of 14.7 psi

$T^*$  = ambient temperature relative to the reference value of 519°R (59°F).

For the audio frequency range and for the normal range of humidity, a simple empirical fit to the data in Figure 7.6 was made, as shown by the straight line. The equation for this line, expressed in terms of  $h'$ , is given by

$$f_m = \frac{(T^*)^{0.7}}{(P^*)^{0.5}} 1800 (h')^{1.5} - \text{Hz} \quad (7.18)$$

where  $h'$  is the absolute humidity in  $\text{gm}/\text{m}^3$  at the reference temperature and pressure. The terms  $T^*$  and  $P^*$ , defined earlier for Equation 7.17, account for the temperature and pressure variation in  $f_m$  indicated by Equations 7.14 and 7.15. Although Equation 7.18 fits the data in Figure 7.6, the predicted variation of  $f_m$  with temperature is opposite to a trend indicated by new data in Reference 7.13. However, the temperature correction is small in most practical cases.

The theoretical molecular absorption due to the vibrational mode can now be calculated for any frequency and humidity by combining Equations 7.7 and 7.12. The resulting equation, based on the reference conditions where  $T^*$  and  $P^*$  = 1, is

$$a_{\text{mol}} = \frac{0.0156 f^2/f_m}{\left[1 + \left(\frac{f}{f_m}\right)^2\right]} \text{ dB}/1000 \text{ ft} \quad (7.19)$$

where  $f_m$  is given by Equation 7.18 or, more accurately, by Equation 7.15.

### 7.2.5 HEAT RADIATION LOSSES

The derivation of the maximum value of radiation absorption is given by Dean in Reference 7.7 following Smith, (Reference 7.21). Sound waves radiate heat generated by compression of the air and so transfer energy out of the propagating sound wave. Smith's approach to the problem was based on recognizing the phenomenon as one of heat radiation from a gas rather than radiation from a solid body (Stefan-Boltzmann Law) which had been the preferred approach. As a result, an expression was obtained for the radiation constant which was directly proportional to the frequency of the sound wave. Dean evaluated these results and defined an upper bound to the radiation absorption loss as a function of temperature, pressure, and frequency. The following theoretical expression was obtained for the upper

bound for the heat radiation loss normalized to 59°F and sea level pressure. (This includes a tenfold increase in Dean's result to correct a typographical error in Equation 7.6 of Reference 7.7.)

$$a_{\text{rad}} = \frac{0.116 T^{*3} \times 10^{-3}}{P^*} f - \text{dB}/1000 \text{ ft} \quad (7.20)$$

where

$T^*$  = absolute temperature relative to 519°R

$P^*$  = pressure relative to 14.7 psi, and

$f$  = frequency in Hz.

For a given temperature and pressure, the heat radiation absorption loss is directly proportional to frequency, and for normal temperature and pressures ( $T^* = P^* = 1$ ), the loss is small. The equation for this radiation loss is an estimate of the maximum possible loss, as discussed by Dean, and the relationship to the first power of the frequency is exactly the same as for the maximum molecular absorption loss. No experimental data is available to verify this absorption loss due to radiation.

### 7.2.6 DESIGN VALUES FOR AIR ABSORPTION

#### 7.2.6.1 Summary of Theoretical Values

The various theoretical components for air absorption, discussed in the previous sections, are summarized in Figure 7.8 for air at 59°F and sea level pressure. These theoretical values are shown for reference purposes only. Final design values for air absorption will be based on experimental data.

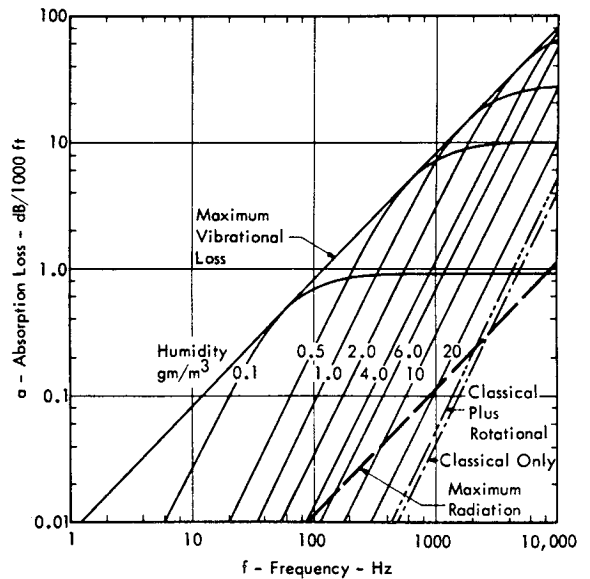


FIGURE 7.8 Summary of Components of Theoretical Sound Absorption in Air at Sea Level Atmosphere Pressure and 59°F

### 7.2.6.2 Comparison of Theory with Measured Data

Measured values of air absorption are compared in this section with the theoretical values in Figure 7.8. The comparison shows that the well known discrepancy with theory can be described empirically in a consistent manner, and the results form the basis of the design charts for air absorption presented later.

#### Experimental Data

The first set of experimental results to be considered are the laboratory measurements of Harris, and Harris and Tempest (References 7.10 and 7.11). These laboratory measurements were considered to be more consistent and complete than any previous results, including those in References 7.9 and 7.18. The data were obtained by measurement of the acoustic decay in a sphere containing air at various values of relative humidity at 0°C and 20°C. Figure 7.9 shows the results for normal atmospheric pressure and the two temperatures. The measured values plotted are the smoothed results as published and have been corrected, where necessary, for classical absorption losses. For comparison with the theory, the data were normalized by the relaxation frequency,  $f_m$ , and the corresponding maximum absorption  $a_{\max} f_m/f$  which is equivalent to  $a_{\max}$  for  $f = f_m$ . The relaxation frequency was calculated from the empirically derived expression, Equation 7.15, which was the best fit to the experimental results in Figure 7.6.

The value for the maximum absorption at the relaxation frequency was calculated from the theoretical value given by Equation 7.13 which was also confirmed by experimental data (see Figure 7.5). The expression for the molecular absorption from the Kneser theory is also plotted in Figure 7.9. The experimental data agree quite well with the theory for both temperatures over a wide range of relative humidity but clearly show the well known discrepancy with theory at frequencies below about 0.1 of the relaxation frequency  $f_m$ . An empirically derived curve was therefore developed which fits the experimental data over the entire range of frequencies. Before considering this empirical expression, results from field tests of air to ground propagation are presented.

Figure 7.10 shows the experimental data for air to ground measurements of rocket and jet noise normalized in the same manner as in Figure 7.9. Only those results were included which showed consistency of measurements, and for which atmospheric and experimental conditions were well defined. Also shown are values computed from previously published design charts which are also based on field data. It should be noted that the results shown from References 7.23 and 7.24 represent the average of a large number of air to ground propagation measurements and thus have high statistical significance. Ground to ground measurements, such as reported in References 7.26 and 7.27, were not included because of the additional effects of ground cover, and temperature and wind gradients, discussed in later sections of this Chapter.

The results shown in Figure 7.10 cover a wider frequency range below the relaxation frequency than the laboratory results, and once again show a good collapse and the same consistent deviation from the Kneser theory.

#### Derivation of Empirical Curve

The current theory of sound absorption does not provide any explanation for this observed anomaly. The empirical curve in Figures 7.9 and 7.10, which describes the data quite well, was therefore developed in the following manner.

An initial attempt to explain the anomaly by adding another relaxation process, using Kneser theory, was not successful. Therefore, a second approach was based on the assumption that another process is occurring at the molecular level and proportional to the frequency alone, and the expression for the molecular absorption would be modified to become

$$a'_{\text{mol}} = a_1 f + \frac{a_{\max} 2 (f/f_m)^2}{1 + (f/f_m)^2}$$

where the second term is that due to the Kneser theory, the first term allows for the additional effect and  $a_1$  is a constant to be determined. However, it was found that this expression did not provide a satisfactory fit over the whole range of normalized frequency for the experimental results.

Finally, it was hypothesized that the additional loss was indeed due to a molecular energy loss process, but would occur randomly according to the motion of the molecules. Therefore, it was assumed that the total loss would be given by the square root of the mean square values for each loss or

$$a'_{\text{mol}} = \left\{ (a_1 f)^2 + \left[ \frac{2 a_{\max} (f/f_m)^2}{1 + (f/f_m)^2} \right]^2 \right\}^{1/2} \quad (7.21)$$

For comparison with the experimental data, this can be normalized to the form

$$\frac{a'_{\text{mol}}}{a_{\max}} = \left\{ \left[ \frac{a_1}{a_2} \cdot \frac{f}{f_m} \right]^2 + \left[ \frac{2 (f/f_m)^2}{1 + (f/f_m)^2} \right]^2 \right\}^{1/2} \quad (7.22)$$

where  $a_2 = a_{\max}/f_m$  which would be a function of temperature and pressure only for  $f = f_m$ .

This result was fitted to the experimental results to give the empirical curve of Figures 7.9 and 7.10 with the value of  $a_1/a_2 = 0.18$ . This curve gives a good fit over the whole range of laboratory and field data and provides a

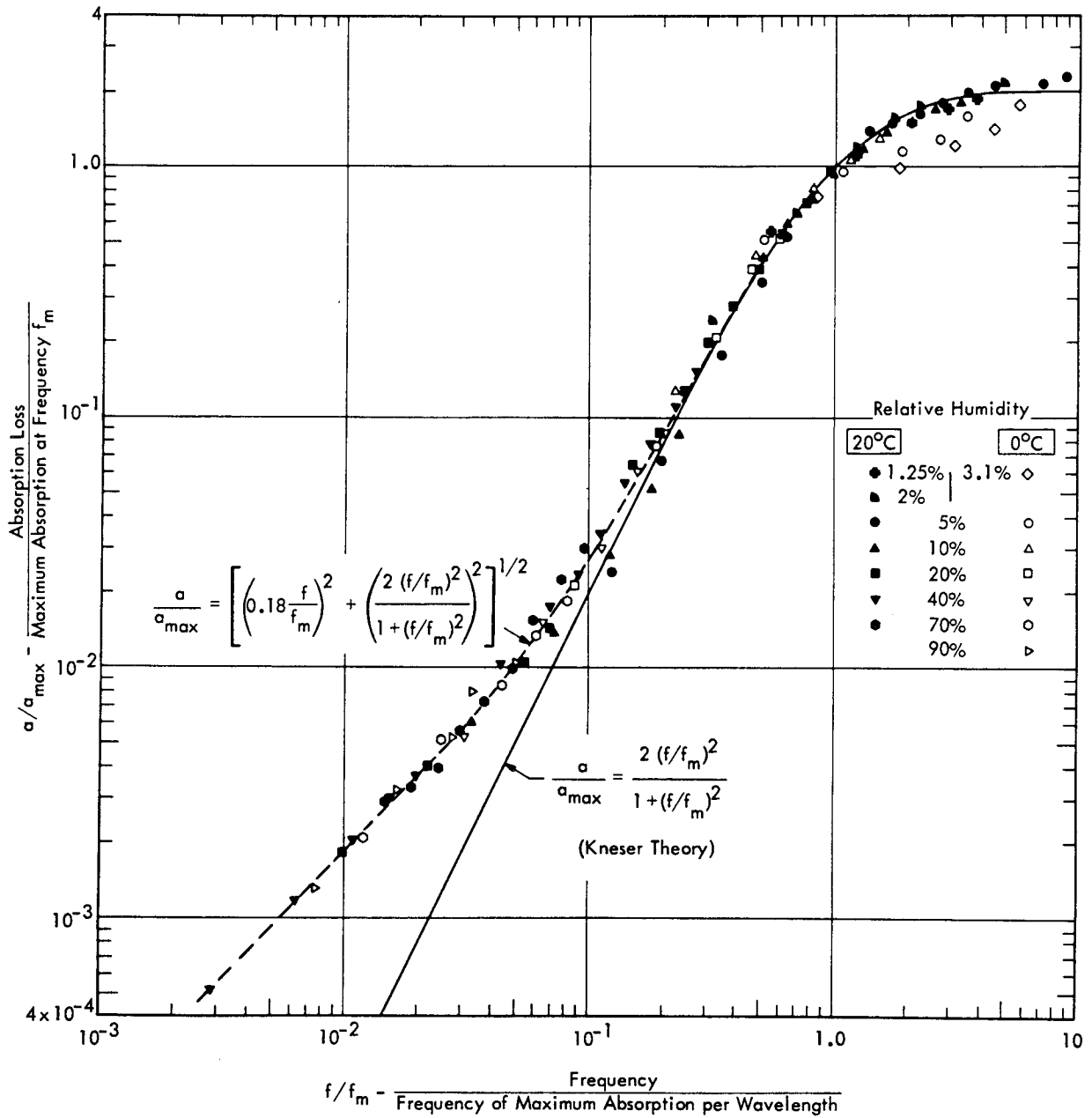


FIGURE 7.9 Comparison of Laboratory Measurements of Molecular Absorption Loss with Kneser Theory and Empirically Modified Theory. (Measurements represent smoothed data from Harris, Reference 7.10, and Harris and Tempest, Reference 7.11, corrected for classical absorption loss)

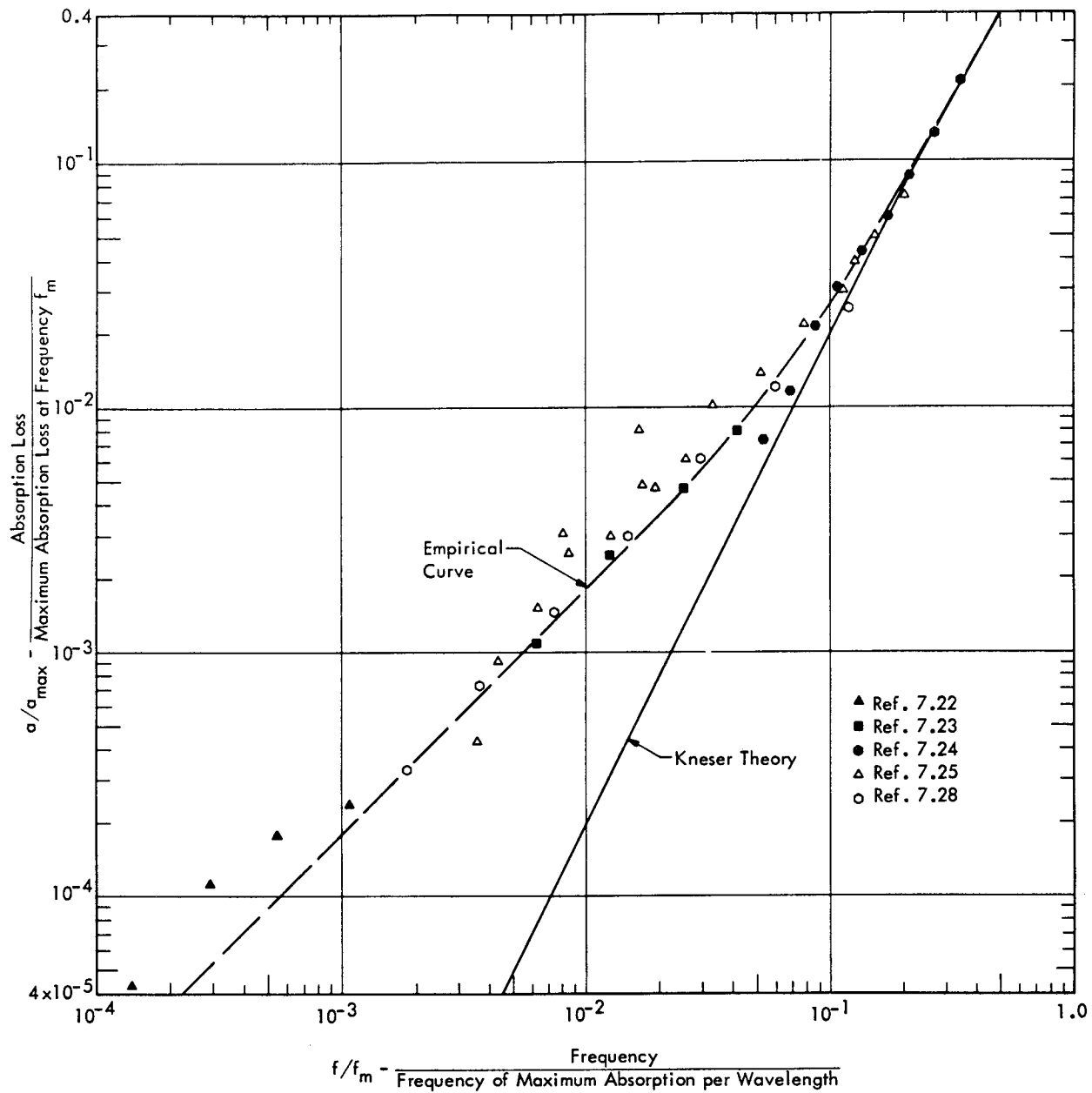


FIGURE 7.10 Comparison of Observed Air to Ground Absorption Loss (Corrected for Classical Absorption) with Empirically Revised Curve for Molecular Loss. (Data from References 7.23 and 7.24 represent average of large number of Field Measurements, and data from References 7.25 and 7.28 represent previously published design values.)

consistent basis for defining the discrepancy with the theoretical values of molecular absorption loss. It must be emphasized that Equation 7.22 has not been verified for extreme values of temperature and pressure outside the range normally encountered in the field. There was some indication in the data that the constant  $a_1/a_2$  should change slightly with temperature over the range of 0° to 20°C. However, the evidence was insufficient to warrant this modification. Therefore, in order to provide a simple expression for computing design curves for atmospheric absorption which are consistent with experimental data in Figures 7.9 and 7.10, Equation 7.22 will be used with the value of the constant  $a_1/a_2 = 0.18$ .

7.2.6.3 Summary of Design Values

The recommended expressions for calculating the various components of air absorption are:

Classical Losses at 59°F

$$a_{cl} = 5.3 \times 10^{-8} f^2 - \text{dB}/1000 \text{ ft} \quad (7.23)$$

where the constant is based on observed results.

Heat Radiation Losses

As shown by Equation 7.20, the maximum value for this loss is proportional to frequency. Since the empirical correction to the molecular loss data is also proportional to frequency, but with a much higher value, any heat radiation loss was assumed to be accounted for by the correction and was therefore not included in the calculation of final design values.

Molecular Losses Plus Empirically Derived Correction

$$a'_{mol} = a_{max} \left\{ \left[ 0.18 \frac{f}{f_m} \right]^2 + \left[ \frac{2 (f/f_m)^2}{1 + (f/f_m)^2} \right]^2 \right\}^{1/2} - \text{dB}/1000 \text{ ft} \quad (7.24)$$

where

$$a_{max} = 0.0078 f_m (T^*)^{-2.5} e^{7.77 (1 - 1/T^*)}$$

$$f_m = (10 + 6600 h + 44,400 h^2) P^*/(T^*)^{0.8} - \text{Hz}$$

$$h = \frac{h'}{7.57} \frac{T^*}{P^*} \quad \text{Percent Mole Ratio}$$

$$h' = \text{humidity gm}/\text{m}^3$$

and  $P^*$  and  $T^*$  are the pressure and temperature normalized to the reference values of 14.7 psi and 519°R (59°F). These expressions are plotted in Figure 7.11 for three different temperatures and sea level pressure. Figure 7.11a is for the reference temperature of 59°F and Figures 7.11b and c

are for temperatures of 20°F and 100°F, respectively. The results are plotted for a range of humidities and show that at low frequencies the values for the corrected molecular absorption  $a'_{mol}$  are the same at all humidities. This is expected since the additional term introduced into the

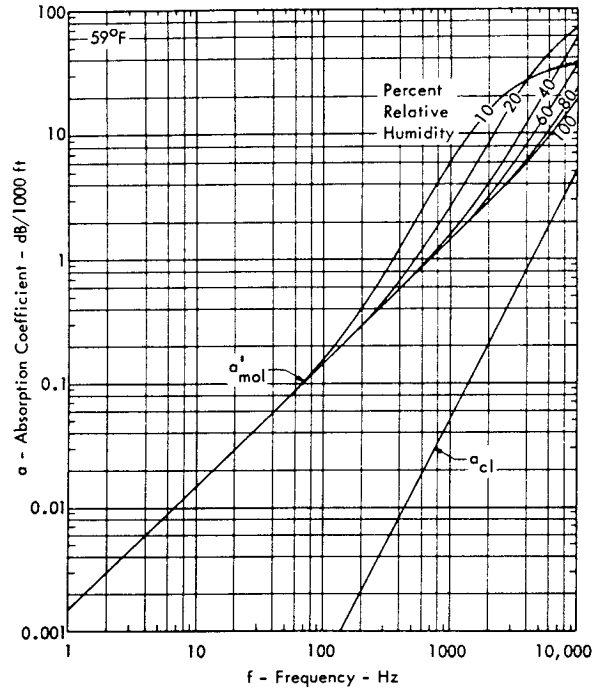


FIGURE 7.11a Design Values for Air Absorption Losses at 59°F

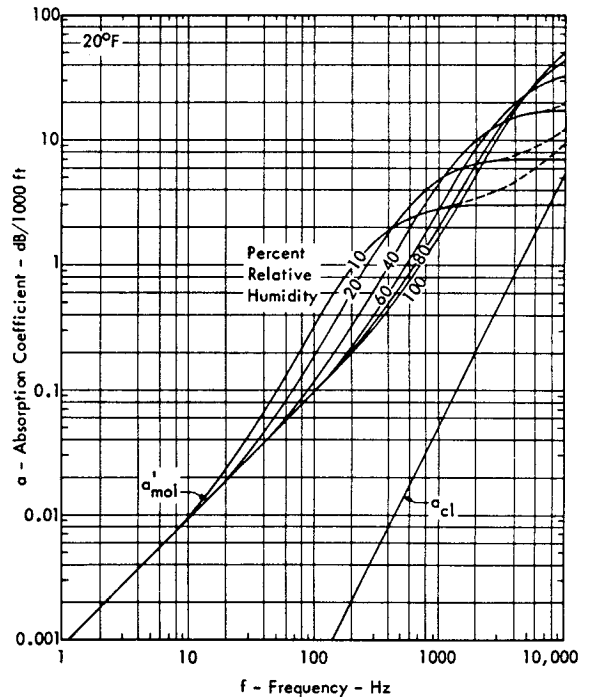


FIGURE 7.11b Design Values for Air Absorption Losses at 20°F



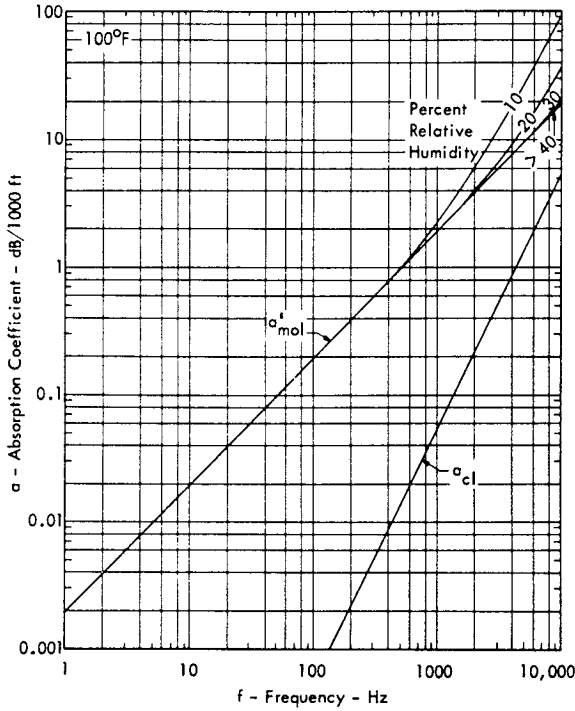


FIGURE 7.11c Design Values for Air Absorption Losses at 100°F

theory is independent of humidity and will control the results at low frequencies. In addition, the empirical expression will also differ from the Kneser theory at frequencies much greater than  $f_m$ , when once again the new term will dominate, and the absorption coefficient will exceed twice the value of  $\alpha_{max}$ . This extrapolation of the empirical term is indicated by dashed lines at the very high frequencies in Figure 7.11b. However, within the range of frequencies of interest for rocket noise, the effect is small. The molecular loss at different temperatures can be interpolated from Figures 7.11a, b and c or can be calculated directly from Equation 7.24. This equation provides a unique and simple expression for molecular loss which is consistent with observed values and which can be readily extrapolated to low frequencies. The classical absorption loss  $\alpha_{cl}$  is also shown in Figure 7.11 and should be added to  $\alpha_{mol}$  at high frequencies.

7.2.7 ATTENUATION OF BARRIERS AND GROUND COVER

7.2.7.1 Attenuation of Barriers

A building or structure directly between the source and the observer will increase the attenuation of the transmission path. The exact attenuation depends on the location of the source and observer, the dimensions of the barrier, relative to the wavelength of the sound, and the atmospheric conditions. The sound field is diffracted by the barrier such that sound is heard in the shadow zone behind the barrier. The acoustic shielding will be most effective for high frequency sound when the acoustic wavelength is much less than the barrier height.

The acoustic shielding loss will be reduced for low frequencies, and particularly as the wavelength of sound approaches the typical barrier dimension. Variations in the speed of sound and wind in the air can cause the shadow zone to be effectively displaced, and in some cases eliminated. In addition, the presence of a ground plane can cause further effects.

The theoretical approach using Fresnel diffraction theory becomes impractical for any thing other than a rigid barrier and a uniform homogeneous atmosphere. Because of these limitations, semiempirical methods are normally used for calculating engineering values of barrier attenuation.

Figure 7.12, from Reference 7.1, shows the loss due to the shielding of a single thin barrier, in terms of the normalized frequency parameter  $v$ , defined by the dimensions shown on the figure. This result is applicable for free space when the source and receiver are some distance from a thin rigid barrier. Figure 7.13 shows calculated results for an example given in Reference 7.1. Here a hanger was directly positioned between the source, an airplane engine, and the receiver. The calculated values were obtained from Figure 7.12 for each octave band by assuming a rigid barrier at the hanger center line, and positioning a mirror image source directly below the ground to account for the ground reflection effects. The measured and calculated results show quite reasonable agreement. The peak in the measured noise reduction at 135 Hz is believed to be due to interference effects. The agreement is not as good at higher frequencies where the measured loss is less than that predicted by the theory. This is a real effect caused by turbulent scattering of sound around, and transmission through the barrier, and is a definite limitation of the theory. Therefore, maximum barrier attenuations are limited to 25 dB at high frequencies.

Finally, Figure 7.14 is included, based on the results given by Beranek (Reference 7.28), and can be used for preliminary engineering estimates of barrier attenuation.

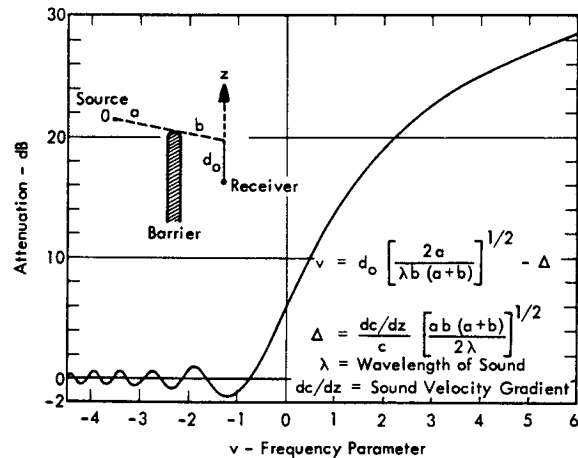


FIGURE 7.12 Attenuation in Sound Level Caused by a Wall, Including Effect of Diffraction by Vertical Sound Velocity Gradient  $dc/dz$ .  $\Delta = 0$  for homogeneous medium (from Reference 7.1).

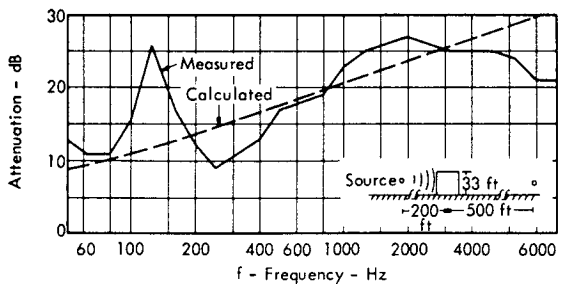


FIGURE 7.13 Measured Attenuation Due to a Barrier (from Reference 7.1)

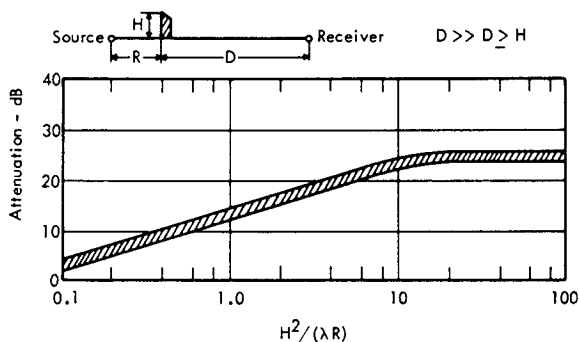


FIGURE 7.14 Chart for Estimating Excess Attenuation Due to Rigid Barrier (From Reference 7.28)

7.2.7.2 Attenuation by Ground Cover

When the receiver and source are close to the ground, additional attenuation provided by natural ground cover can become important. The extra attenuation will depend

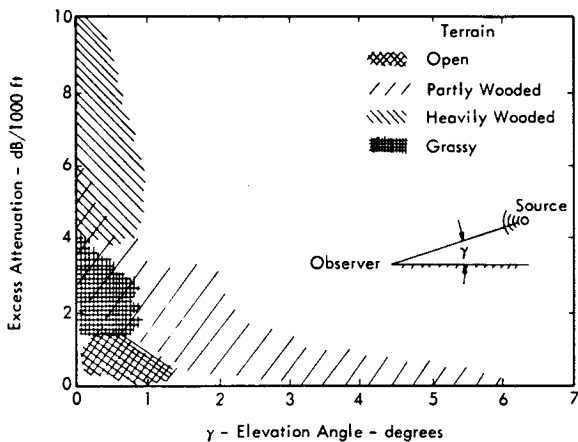


FIGURE 7.15 Effect of Terrain and Elevation Angle on Propagation Loss Coefficient in 150-300 Hz Band (Adapted From Reference 7.30)

on the type of foliage, the frequency, and the angle between the source-receiver path and the ground. Figure 7.15, taken from Reference 7.30, shows some typical values for the attenuation rate for various angles of elevation of the source and types of ground cover. For example, propagation of noise from a static firing through dense woods can be expected to show an additional loss of 5-10 dB/1000 ft in the 150-300 Hz octave band. During a launch, however, attenuation by ground cover will be essentially eliminated when the source to receiver elevation angle exceeds about 5 degrees.

The additional absorption provided by ground cover may also exhibit a "resonance" effect with a maximum absorption in the mid-frequency range (References 7.26, 7.27 and 7.29). This is illustrated in Figure 7.16 for horizontal propagation over a grassy terrain. Similar results were obtained by Franken and Bishop (Reference 7.31) in a recent series of measurements of aircraft noise propagation at and near airports. For some of these measurements, buildings and homes were directly between the source and receiver, giving an interrupted line of sight. However, these results again indicate a pronounced low frequency excess attenuation, with a maximum effect in the range of 125-250 Hz.

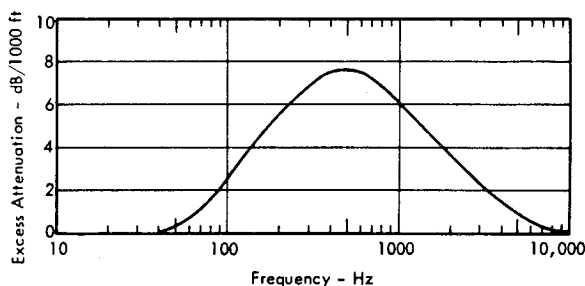


FIGURE 7.16 Ground Absorption Over High Grass, Source and Receiver 6 ft Above Ground

Most rocket facilities will be set in reasonably clear areas, but the sources could be high off the ground, so that the ground effect is minimum at relatively short ranges. The S-1C vehicle test stand at Marshall Space Flight Center, for example, has a deflector located some distance above the ground plane with the exhaust flow deflected up at about 30 degrees to the horizontal, so that the predominant exhaust flow noise sources are well above the ground.

In summary, the effect of extra ground attenuation should be considered near static test stands when both source and receiver are close to the ground. Although ground absorption losses can occur for propagation over very long ranges, available data indicate the loss can be neglected. In this case, maximum levels will be generally governed by focusing effects which are not influenced significantly by the ground. For shorter ranges, say within the bounds of a test facility, the values given in Figure 7.16 will be sufficient for estimating the extra ground absorption.

### 7.2.8 PROPAGATION ANOMALIES

In this section other propagation effects, influenced by weather conditions, will be presented. They are treated separately because they represent effects that are generally difficult to predict and in some cases to substantiate. These deviations from the calculated inverse square loss, atmospheric absorption, barrier effect, and ground effects are generally the direct result of a nonuniform atmosphere and scattering. They represent transient effects which can change the propagation loss by as much as 20 to 30 dB within a matter of hours. Nevertheless, these variable losses may be considered in special cases for a fixed ground installation. Other transient attenuation effects due to fog, rain or snow will not be considered in this manual since they are unlikely to be considered for design purposes.

#### 7.2.8.1 Attenuation Due to Ground Winds and Turbulence

Two effects are considered which increase sound attenuation, first, the additional attenuation of sound propagating up-wind, and secondly, that due to scattering effects by turbulence.

##### Ground Wind Effects

The wind itself causes some absorption due to sound propagation against the wind direction, but this effect will be generally negligible. The principal reduction of sound upwind of a source is due to the creation of a shadow zone caused by wind velocity and temperature gradients directing the sound up and away from the ground. These gradients are dependent on the ground conditions since the actual boundary layer temperature and ground wind profiles are directly determined by the ground cover.

An acoustic shadow zone will form when the effective sonic velocity decreases with altitude, either as a result of temperature changes or velocity changes in the boundary layer of surface winds. Figure 7.17 illustrates the formation of such a shadow zone, with the sound velocity gradient causing the acoustic rays to be bent away from the earth's surface. If the velocity gradient is steep, the shadow zone may be bounded by a single ray. Figure 7.18 shows a typical shadow zone formed by a wind gradient. This figure shows how sound is apparently cut off for a large region upwind and to the side of the source. For a negative temperature gradient, the boundary of the shadow zone will be a circle centered at the source. However, this type of shadow zone due to temperature gradients is not considered here and the reader is referred to Reference 7.37 for further details.

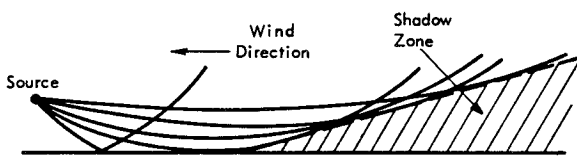


FIGURE 7.17 Formation of Shadow Zone Caused By Increase in Wind Velocity with Altitude

In practice, some sound penetrates the boundary of wind-generated acoustic shadows and a finite attenuation occurs upwind compared to that which would be observed with no wind effect. This attenuation will vary with the frequency of the source, the wind gradient, and the direction to the receiver, given by the angle  $\phi$  in Figure 7.18. A calculation and tabulation of this attenuation has been presented in Reference 7.32 in the form of charts suitable for the calculation of aircraft noise, with the aircraft and receiver at the ground. Lacking any comparable data for rocket noise, these results are presented here as a suitable method for predicting ground wind attenuation of noise from rocket test stands. The method is considered reliable for those cases where the rocket is fired nearly horizontally close to the ground and for attenuation over distances less than 1-2 miles.

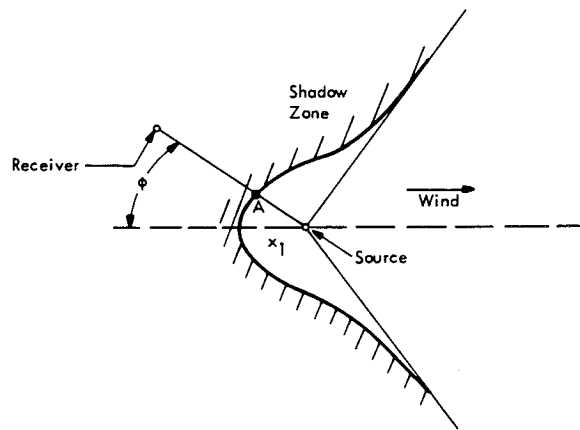


FIGURE 7.18 Upwind Shadow Zone (From Reference 7.1)

The distance from a source to the upwind boundary of the shadow zone (Point A, shown in Figure 7.18), is typically 200 ft for a 10 mph wind and source and receiver at 6 ft altitude. The exact distance depends on wind gradient, velocity, and the height of the source and receiver. For rockets at test and launch stands, the height of the acoustic source could be considerably higher than for aircraft and this distance will increase. For aircraft noise, the typical attenuation upwind, in excess of inverse square law and absorption losses, reaches a maximum value of 30 dB in the 600-1200 Hz frequency band and at a distance of about 1000 ft from the source (Reference 7.32). The observed attenuation decreases with an increase in the angle  $\phi$  of the receiver to the upwind direction, as shown in Figure 7.18 and 7.20.

The recommended procedure for allowing for wind shadow effects, following Reference 7.32, is to first estimate the location and distance to the shadow zone. The distance  $x_1$  upwind to the edge of the shadow zone decreases as the wind velocity increases, and can be taken as approximately proportional to the square root of the velocity. The distance  $x_1$  also increases in direct proportion to the height  $h$  of source and receiver.

For illustration, consider the following example. Referring to Figure 7.19, and assuming  $x_1 = 200$  ft for a source and receiver height of 6 ft and a mean wind speed  $V$  of 10 mph (14.6 fps), then for other wind speeds or heights, the distance  $x_1$  will be

$$x_1 = 200 \left( \frac{V}{14.6} \right)^{1/2} \frac{h}{6} = 8.73 V^{1/2} h \quad (7.25)$$

where

$h$  = the height of the source and receiver (or mean height if both are at different heights) - ft

$V$  = wind velocity (fps), and

$x_1$  = distance to the start of the shadow zone - ft.

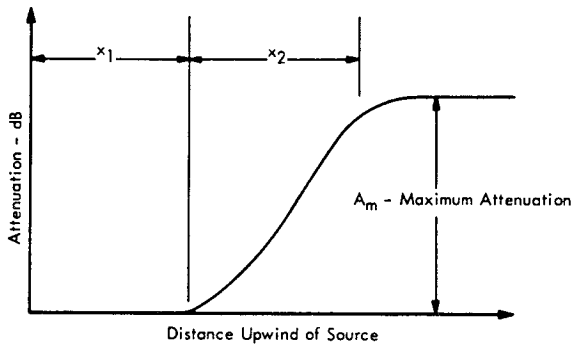


FIGURE 7.19 Attenuation Upwind of Source Due to Wind for a Source and Receiver at an Average Height  $h$  Above Ground

The maximum attenuation  $A_m$  is given in Figure 7.20 as a function of frequency and the angle  $\phi$ . This maximum occurs at a distance  $x_2$  from the edge of the shadow zone given by

$$x_2 = 34.9 V^{1/2} h \quad (7.26)$$

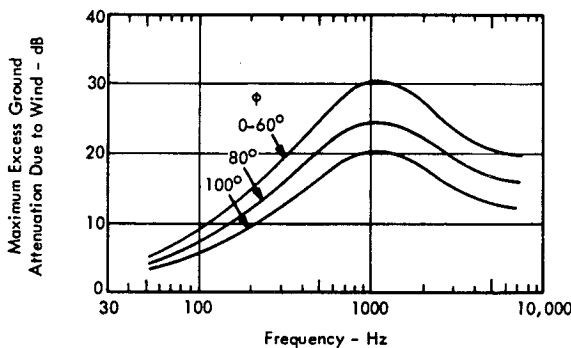


FIGURE 7.20 Maximum Excess Ground Attenuation Due to Wind Shadow Effect (from Reference 7.32)

Strictly, this distance is a function of the frequency and angle  $\phi$  also, but the above expression is a good approximation. Once these two distances are determined, then a curve such as Figure 7.19 can be constructed using the maximum attenuation given by Figure 7.20 for the required direction, and the shadow effect determined. When the angle  $\phi$  becomes greater than 120 degrees, the shadow effect is best disregarded. A final point concerns the effect of ground wind on low frequency sound of large rocket boosters. The typical acoustic spectrum for these boosters, such as the first stage of the Saturn V rocket, peaks at a frequency near 10-30 Hz, and the shadow zone attenuation predicted by Figure 7.20 would be less than 5 dB. The relatively small shadow zone attenuation would be representative over short distances from a rocket fired close to the ground. However, it will be shown later that at large distances from a rocket test stand (e.g., > 2 miles), much higher attenuations can occur at these low frequencies due to wind and temperature gradients at high altitudes. Thus, the frequency variation of shadow zone attenuation, indicated in Figure 7.20, should be considered a minimum value for frequencies below 100 Hz and applicable for relatively short distances from a test stand.

It must be emphasized that the procedures outlined above are basically empirical, due to the lack of a practical theoretical approach. A complete description of the process is given in References 7.1 and 7.32 and should be referred to if a more detailed examination of a particular problem is required.

### Scattering by Turbulence

Additional attenuation of low frequency rocket noise can be caused by turbulence scattering. The same mechanism may apply equally well to reduce the propagation loss in a different direction. The primary emphasis herein will be concerned with attenuation effect due to scattering and hence it is treated in this section. Basically, the scattering of an irregular sound field, such as produced by a rocket, will tend to cause an equalization of the acoustic intensity propagating in all directions at large distances from the source. This process of intensity leveling is a direct result of scattering of the sound field by patches of nonuniform sound velocity in the atmosphere. Thus, a highly directional sound profile for a rocket can be gradually rounded out by scattering to a more nearly nondirectional pattern at greater and greater distances from the source. This effect, which is illustrated in Figure 7.21, is a very significant one to be considered when positioning a rocket test site so as to minimize community noise levels in a given direction.

A simplified analytical model for this scattering effect was developed utilizing the concept of Rayleigh scattering (References 7.33 and 7.36). The model is applicable in a frequency range where the acoustic wavelength is of the order of or less than the size of the scattering patch and thus assumes that the scattered sound is not highly directional. A unique set of experimental data on the effect of scattering, reported in Reference 7.34, was used to estimate the scattering parameters.

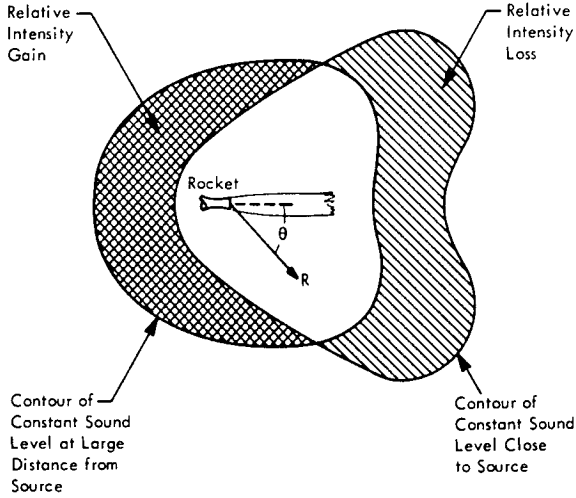


FIGURE 7.21 Conceptual Illustration of Redistribution of Sound Intensity Due to Scattering by Turbulence Resulting in Additional Loss in Intensity in Direction of Maximum Noise and Gain in Intensity in Direction of Minimum Noise

The essential features of the analytical model may be explained as follows. The direct sound intensity  $I_r$  from a source of rocket noise, without scattering or absorption loss, and assuming hemispherical radiation, is given by

$$I_r = \frac{W_o}{2\pi r^2} G(\beta) \quad (7.27)$$

where

$W_o$  = sound power of the source

$r$  = distance from source to scattering patch

$G(\beta)$  = directivity index of the source

$\beta$  = angle relative to the jet axis.

When this direct radiation is incident on a scattering patch of nonuniform atmosphere with a scattering cross section  $a_s$  and a characteristic volume  $v_s$ , then within an incremental volume  $dV$  in the sound field, an increment of scattered sound power  $dW_s$  is generated which is equal to the incident intensity  $I_r$  times the scattering cross section  $a_s$  times the number of scattering patches  $dV/v_s$  in the volume element  $dV$  or

$$dW_s = I_r a_s dV/v_s$$

The ratio  $a_s/v_s$  may be considered as a scattering loss coefficient  $m_s$  in units of 1/distance. In other words, if the radial thickness of the volume element is  $dr$ , the direct sound suffers a fractional loss  $(a_s/v_s) dr = m_s dr$  in passing through this volume. Thus, if the incident intensity of the direct sound at this volume is  $I_r$ , the loss in intensity is

$$dI_r = -I_r m_s dr$$

or

$$\frac{dI_r}{I_r} = -m_s dr$$

Upon integration, this gives the exponential loss in the direct sound intensity at any radius  $r$  due to scattering only. The spreading loss can also be included to give a new estimate for the direct intensity as

$$I_r = \frac{W_o}{2\pi r^2} G(\beta) e^{-m_s r} \quad (7.28)$$

To a first approximation, the increment of intensity  $dI_s$  of the scattered sound generated in this volume element, as observed at some point on the ground a distance  $r_s$  from the scattering patch, will be

$$dI_s = \frac{dW_s}{2\pi r_s^2} S(\gamma)$$

The quantity  $S(\gamma)$  is the directivity of the scattered sound field where  $\gamma$  is the angle between the incident sound ray and the vector  $r_s$  to the observation point on the ground.

Combining the above relationships it can be shown that the total intensity of the scattered sound at a fixed observation point on the ground a distance  $R$  from the source and an angle  $\theta$  from the axis of symmetry (e.g. - jet exhaust axis) can be expressed in the general form

$$I_s = \int_V dI_s = \frac{m_s W_o}{2\pi R} \int_V \frac{G(\beta) S(\gamma) dV/R^3}{2\pi (r_s/R)^2} \quad (7.29)$$

where

$r_s$  = distance from scattering element  $dV$  to observer, a function of  $R$ ,  $r$ ,  $\beta$  and  $\theta$

$\gamma$  = the scattering angle, a function of  $R$ ,  $r$ ,  $\beta$  and  $\theta$

$R$  = radius from source to observer

$\beta$  = angle relative to jet axis

$\theta$  = the fixed value of  $\beta$  for the observation point (measured in a horizontal plane).

This volume integral would be carried out over a semi-infinite space bounded by the ground.

Although the integral can be readily solved for special cases, such as for nondirectional scattering  $S(\gamma) = 1$ , and for observation points on the axis of symmetry,  $\theta = 0, \pi$ , the uncertainties in the actual directional characteristics of the scattered sound dictate that an empirical expression be used for now. Thus, the dimensionless integral in Equation 7.29 is replaced by an empirical constant  $K_s(\theta)$  which

should be a function of  $\theta$  only so that the scattered intensity can be expressed in the form

$$I_s \approx \frac{K_s(\theta) m_s W_o}{2\pi R} \quad (7.30)$$

The constant  $K_s(\theta)$  may be considered a measure of the relative effectiveness of the scattered field in returning scattered power back to the ground. It will be a constant for a particular directionality of the scattered field  $S(\gamma)$  and direct field  $G(\beta)$ , and may vary with the observation angle  $\theta$ .

The important point to note is that, for this simple model, the scattered sound field is equivalent to a cylindrical source at the same location as the primary source but with a sound power equal to  $K_s(\theta) \cdot m_s$  times the primary source power. The cylindrical spreading loss for this "scattering source" is understandable when it is recognized that the scattered power is proportional to the volume ( $\propto r^3$ ) of the sound field, times the direct intensity ( $\propto 1/r^2$ ), divided by a characteristic distance squared ( $\propto r^2$ ), thus giving an intensity proportional to  $1/r$  instead of  $1/r^2$ . When the direct and scattered intensities are combined at a point on the ground, the total intensity can be expressed as

$$I_t = \left[ \frac{W_o G(\theta)}{2\pi R^2} \right] \left[ e^{-m_s R} + \frac{K_s(\theta)}{G(\theta)} m_s R \right] \quad (7.31)$$

The first term in brackets is the usual expression for the direct sound intensity at a distance  $R$  from a point source of power  $W_o$  and directivity  $G(\theta)$ .

The second term in brackets is the approximate correction for scattering and includes an exponential loss term for the decrease in direct intensity and a first approximation to the additive term due to the scattered field. Second order effects for the latter including additional scattering losses and absorption losses are ignored. Thus, scattering loss,  $L_s$ , expressed in decibel form, with distance  $R$  in units of 1000 ft and  $m_s$  in units of  $1/1000$  ft, is given, to a first approximation, by

$$L_s = 10 \log \left[ e^{-m_s R} + \frac{K_s(\theta)}{G(\theta)} m_s R \right] - \text{dB} \quad (7.32)$$

The test data employed to evaluate the constants  $m_s$  and  $K_s(\theta)$  in the above expression consisted of overall sound levels measured along one radial line from two large rocket engine noise sources fired diametrically opposed in rapid sequence (Reference 7.34). The first was the S-1 booster with the exhaust from its eight engines, developing  $1.5 \times 10^6$  pounds thrust, deflected at 7 degrees to the direction of the microphones. The second was a single F-1 engine, again with  $1.5 \times 10^6$  pounds thrust, but with the exhaust flow deflected at 187 degrees away from the line of microphones. The two sources were on opposite sides of the same stand and were fired within a total time of 6 minutes so that the atmospheric conditions were considered essentially identical for both tests. The sound levels measured for the

F-1 engine were lower because of the inherent directivity of the noise field in the direction opposite to the deflected exhaust flow. However, the two sources were found to have essentially the same overall acoustic power level and power spectra at a distance of 1000 ft from the test stand. The results are plotted in Figure 7.22 and clearly show that the difference in measured sound levels, caused by the directivity, decreases with increasing distance from the two sources. This difference falls from 18.4 dB, at 1000 ft (0.305 km) to 8 dB at 52,000 ft (15.8 km) from the test stand.

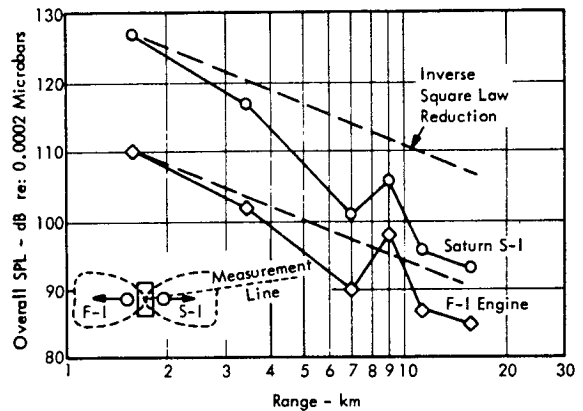


FIGURE 7.22 Overall Sound Pressure Levels for Two Sources of Rocket Engine Noise Measured Along One Line Under the Same Atmospheric Conditions to Illustrate the Redistribution of Energy Due to Scattering. (Increased level at 9 km is due to focusing.) (Data from Reference 7.34)

This change is believed to be due to a smoothing of the directivity pattern with distance as a result of scattering. Thus, the sound level of the S-1 decreased more rapidly as acoustic energy scattered toward the direction of lower sound intensity radiation. In addition to the scattering effect, the atmospheric attenuation of the sound from the F-1 engine would be expected to be greater because of its greater high frequency content in the direction of measurement. However, this effect would cause the measured sound levels for the two tests to diverge rather than converge, as observed. Undoubtedly this latter effect occurs, but it is apparently not sufficient to overcome the progressive smoothing of the angular distribution of intensity due to scattering.

This scattering attenuation can be interpreted with Equation 7.32 by assuming that at the same observation point for the two sources ( $R = \text{constant}$ ,  $\theta = 7$  or  $187$  degrees), the scattering loss coefficient  $m_s$  is approximately the same. The measured directivity indices at 1000 ft for the two sources, given in Reference 7.34, are

For the S-1 engine,  $G(7^\circ) \approx 2.3$  (+3.6 dB)

For the F-1 engine,  $G(187^\circ) \approx 0.033$  (-14.8 dB)

Therefore, the difference in sound levels observed at various distances for the two tests should be described approximately by the difference in directivity close to the source (18.4 dB at 1000 ft) plus the difference in scattering loss. The latter can be determined from Equation 7.32 so that the observed relative sound level  $\Delta L$  should be given by

$$\Delta L = 18.4 + 10 \log \left[ \frac{e^{-m_s R} + K_s(\theta) m_s R / 2.3}{e^{-m_s R} + K_s(\theta) m_s R / 0.33} \right] \quad (7.33)$$

As shown in Figure 7.23, this expression shows reasonable agreement with the experimental data for empirically derived values of the scattering loss coefficient  $m_s = 0.05/1000$  ft and directionality coefficient  $K_s(\theta) = 0.03$ . The particular values of  $m_s$  and  $K_s(\theta)$  given here were chosen partly on the basis of the limited data in Figures 7.22 and 7.23 but were also constrained to be consistent with more extensive data on excess attenuation at low frequencies to be discussed shortly. With the limited data available, these scattering parameters must be considered as rough estimates useful for making a preliminary evaluation of scattering effects of rocket noise.

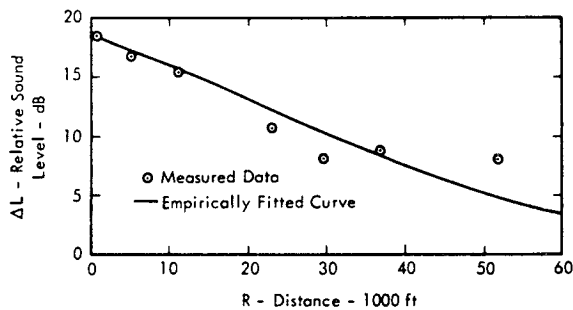


FIGURE 7.23 Comparison of Relative Difference in Sound Level of Data in Figure 7.22 with Empirically Fitted Curve Based on Analytical Model of Scattering (see Equation 7.33 in Text)

Based on these values, a preliminary estimate of the scattering loss of overall noise levels for rockets in the 1.5 million pound thrust class is given by

$$L_s \approx 10 \log \left[ e^{-0.05 R} + 0.0015 R / G(\theta) \right] - \text{dB} \quad (7.34)$$

where

$G(\theta)$  = directivity factor for the rocket noise field,  
and

$R$  = distance from test pad in units of 1000 ft.

This expression is plotted in Figure 7.24 as a function of range for several values of the directivity index  $DI = 10 \log G(\theta)$ . In the direction of maximum radiation of the direct sound, where  $DI \approx 0$  to  $+5$  dB, the net effect of scattering, indicated in Figure 7.24, is to show a linear propagation loss with distance which is approximately equal to 0.2 dB/1000 ft out to about 40,000 ft. This average scattering loss rate is consistent with other data on propagation losses of low frequency rocket noise in a nonstratified but turbulent atmosphere (see Section 7.2.8.2). Along a radial line for which the direct radiation is low ( $DI \approx -15$  dB), the effect of scattering shows a slight propagation gain which would approach a value equivalent to a cylindrical instead of spherical spreading loss for the sound field at about 20,000 ft. This concept of transition from a spherical to a cylindrical spreading loss will also appear later on in the discussion of focusing anomalies but for entirely different reasons and with a much more significant effect.

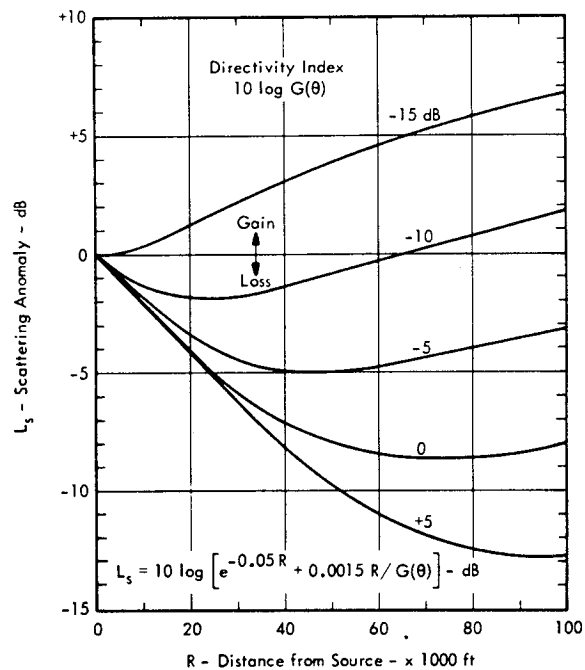


FIGURE 7.24 Estimated Typical Effect of Atmospheric Scattering on Propagation of Overall Noise Level for Static Firing Tests of Large Rockets in the 1.5 Million lb Thrust Class. All other spreading, refraction and absorption losses are excluded. Applicable in a frequency range of 20-30 Hz.

It is important to recognize that the scattering attenuation discussed in this section is an additional loss (or gain) which does not include air absorption losses or gross changes in propagation caused by large scale changes in the sound velocity profile of the atmosphere. It represents only the nominal propagation effect due to scattering by patches of nonuniform sound velocity in the atmosphere. Since this patchiness is due to a fluctuation in air temperature or air

turbulence, scattering losses will vary considerably with weather conditions. Of more practical importance, however, is the variation of the scattering loss rate with frequency since the estimated scattering losses in Figure 7.24 are only applicable over a limited frequency range of about 20-30 Hz. Peak frequencies of noise from rocket engines with thrusts appreciably different from 1.5 million pounds will fall outside this range of frequencies.

Frequency Variation of Scattering Losses

To provide some means of predicting scattering loss at other frequencies, low frequency sound propagation data from a number of Saturn static firings have been analyzed. The tests were conducted by NASA at the Marshall Space Flight Center prior to 1965 (Reference 7.35). The data were carefully screened to exclude propagation anomalies due to long range focusing effects (see next section) or shadow zones close to the source due to surface winds. The attenuation rate was determined by the slope of a best-fit straight line drawn through a linear plot of the excess attenuation versus range and covered distances out to 70,000 feet. The resulting average and extreme values of excess attenuation are shown in Figure 7.25.

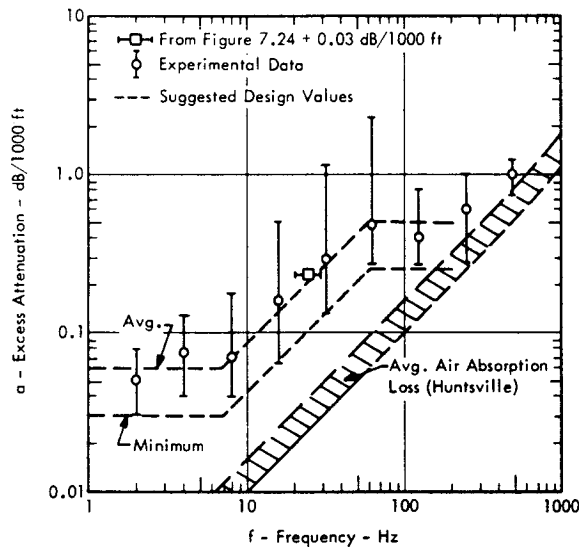


FIGURE 7.25 Excess Attenuation Computed from Observed Octave Band Sound Levels for Saturn S-I and F-I Static Firings at Huntsville, Alabama. Data selected to eliminate refraction effects of strong wind and temperature gradients in order to illustrate scattering losses, in direction of maximum radiation, in excess of air absorption losses. (Data From Reference 7.35)

To identify the amount of attenuation attributable to scattering, the approximation range of air absorption losses in the Huntsville area have been determined based on the methods discussed in Section 7.2. This range is also plotted in Figure 7.25 and clearly shows that an additional excess attenuation is observed at frequencies below 200 Hz. The average attenuation rate for scattering loss in the direction

of maximum radiation of rocket noise, discussed in the preceding paragraphs, is also shown in this figure and includes a correction for average air absorption loss. Although the data in Figure 7.25 vary in extreme values, in some cases by roughly an order of magnitude, the average and minimum values indicate a predictable trend useful for preliminary engineering estimates.

Design Values for Low Frequency Excess Attenuation

For long range propagation of low frequency rocket noise in the direction of maximum radiation, the following expressions are suggested for predicting the combined excess attenuation due to scattering and air absorption.

Average Values

$$\begin{aligned} \bar{\alpha}_o &= 0.06 - \text{dB}/1000 \text{ ft} && 0-7 \text{ Hz} \\ \bar{\alpha}_o &= 0.0085 f_{\text{Hz}} - \text{dB}/1000 \text{ ft} && 7-60 \text{ Hz} \\ \bar{\alpha}_o &= 0.5 - \text{dB}/1000 \text{ ft} && 60-200 \text{ Hz} \end{aligned}$$

Minimum Values

$$\begin{aligned} \alpha_{o \text{ min}} &= 0.03 - \text{dB}/1000 \text{ ft} && 0-7 \text{ Hz} \\ \alpha_{o \text{ min}} &= 0.0042 f - \text{dB}/1000 \text{ ft} && 7-60 \text{ Hz} \\ \alpha_{o \text{ min}} &= 0.25 - \text{dB}/1000 \text{ ft} && 60-200 \text{ Hz} \end{aligned}$$

These suggested values are not extended above 200 Hz since air absorption is dominant above this frequency and methods for predicting this loss have already been covered in Section 7.2.

These values are subject to several limitations.

- They are based entirely on data taken in one geographical area (Huntsville, Alabama) and should be applied with caution to any other location, particularly where average weather conditions are very different.
- They should not be used when the sound velocity profile is very nonuniform resulting in major refraction effects.
- They are applicable for horizontal propagation of rocket noise in the direction of maximum radiation over distances between 5000 and 100,000 ft. For other directions, the results in Figure 7.24 may be used as a preliminary guide. At shorter ranges, the indicated loss would be insignificant. The values have not been validated at ranges beyond 70,000-100,000 ft and are not reliable at greater distances.
- For vertical propagation of launch noise, the minimum values indicated above are recommended for engineering estimates of attenuation losses due to scattering and air absorption at frequencies below 200 Hz.



7.2.8.2 Reinforcement of Sound Due to Focusing

This section specifically covers focusing effects which decrease the nominal attenuation losses. This sound reinforcement is caused by an atmospheric focusing mechanism and occurs when sound radiated into the atmosphere is refracted downward by local variations in the speed of sound. This causes a bending of sound rays which then reach the surface at some distance from the source. The mechanism is similar to that described for the upwind shadow effect but is the result of variations in the acoustic propagation speed at much higher altitudes, and further, that these variations in the effective sound velocity are the result of temperature gradients in the atmosphere as well as wind velocity gradients. The increase in sound level associated with this focusing effect can be 10 to 20 dB and must be considered carefully when evaluating community noise problems associated with rocket test sites.

For design purposes in locating rocket test sites, it will be sufficient to establish an upper bound for the increased level due to focusing in a given region and estimate the occurrence of this maximum level. Each of these aspects is considered here. First, however, consider the specific characteristics of the focusing effect.

Figure 7.26 illustrates this phenomenon by showing how an acoustic ray can be turned back to the earth's surface by a positive acoustic velocity gradient. Part (a) of Figure 7.26 illustrates a uniformly increasing speed of sound  $c$  with altitude  $z$ , and part (b) shows the resultant path of an acoustic ray starting out at an initial angle  $\theta$  to the horizontal.

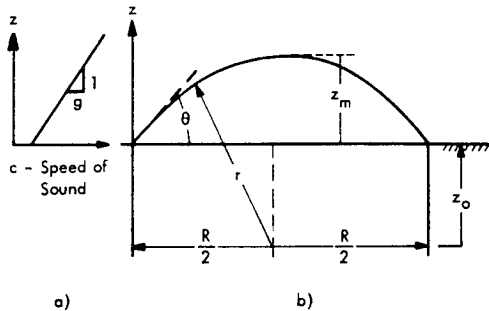


FIGURE 7.26 Sound Ray Trace in a Constant Positive Sound Velocity Gradient

By well known theory, discussed in References 7.2 and 7.37, it can be shown that the path of a sound ray in a medium with a constant sound velocity gradient,  $g = dc/dz$ , is described by a circular arc whose radius  $r$  is given by

$$r = \frac{c_0}{g \cos \theta} \tag{7.35}$$

where  $c_0$  is the initial effective speed of sound at the origin of the ray which leaves the source with an initial angle  $\theta$  to the horizontal. For a combined wind and temperature gradient, an effective speed of sound  $c$  is given by

the acoustic velocity plus the component of wind velocity  $u \cos \theta$  in the direction  $\theta$  of the ray. The maximum height reached by this ray is given by

$$z_m = r - r \cos \theta = \frac{c_0}{g} \left[ \frac{1 - \cos \theta}{\cos \theta} \right] \tag{7.36}$$

In Figure 7.26, the sound velocity gradient is positive so the center of the ray tracing radius is located a distance  $z_0$  below the ground, given by

$$z_0 = -r \cos \theta = -c_0/g \tag{7.37}$$

and to the side of the source a distance equal to one-half the range  $R$  of the ray, which is

$$R = 2r \sin \theta = 2c_0 \tan \theta/g \approx 2c_0 \theta/g \text{ when } \theta \ll 1 \tag{7.38}$$

The ray then returns to the horizontal ground plane at this distance  $R$ . For a constant positive gradient of the effective speed of sound, all rays emanating from the source over an angular range of  $\theta = 0$  to 90 degrees will return to the ground. Each sound ray can be considered to be the axis of a tube containing a portion of the energy radiated by the source. Sound focusing, and corresponding increases in sound pressure level, will then occur when a large number of these ray tubes return to earth over a small area on the earth's surface.

This type of acoustic refraction or focusing occurs for a wide variety of complex velocity profiles. Figure 7.27, from Reference 7.38, shows several ray patterns formed by different acoustic velocity profiles in the atmosphere. Figure 7.27a illustrates the case for a zero velocity gradient where no focusing effects occur. Figure 7.27b is for a negative velocity gradient, and again no focusing occurs since all the sound is refracted upward into the air. This is similar to the shadow zone formation created by a wind boundary layer. Figure 7.27c shows the effect of a constant positive velocity gradient, where all rays are refracted or bent back to the ground but no single focusing area is evident. Finally, in Figure 7.27d, the strong focusing effect that is created by a two-stage, first negative and then positive, velocity gradient. The pattern of the exact ray paths and the location of the focusing point for the more complex sound velocity profiles can be calculated by the methods of Reference 7.2. Digital and analog computer techniques are also frequently used to trace out ray paths for an arbitrary velocity profile (References 7.38 and 7.39). However, the determination of the increased sound pressure level at a focusing region is difficult and is more readily accomplished for a particular case by the use of empirical prediction methods. This approach is utilized here to estimate an upper bound for the maximum sound level and its probability of occurrence.

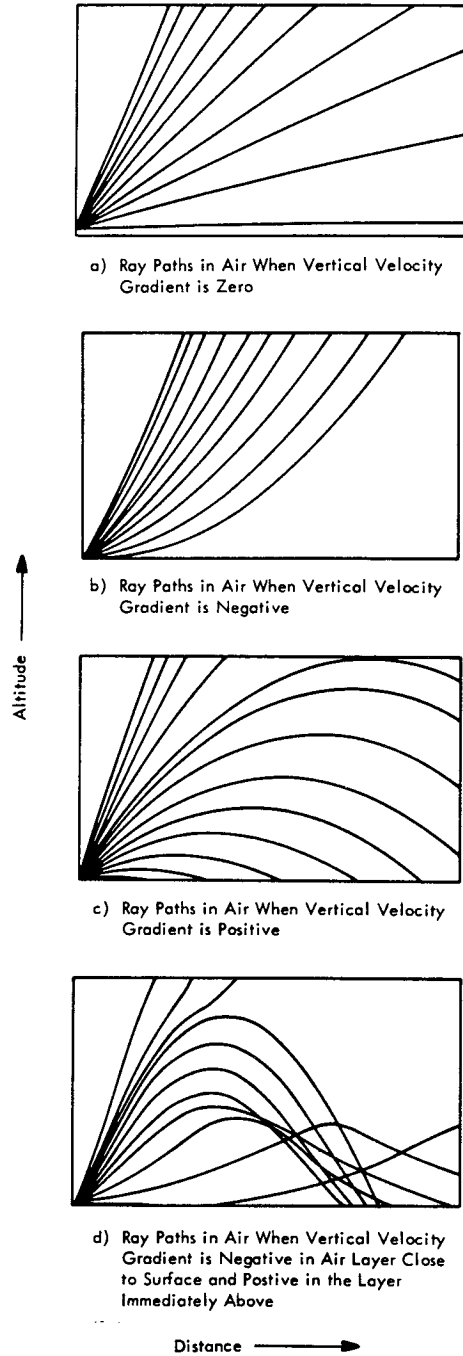


FIGURE 7.27 Various Ray Patterns for Different Sonic Velocity Profiles (From Reference 7.38)

Upper Bound for Focusing Magnitude

Data illustrating the actual change in sound level due to focusing effects are given in Figure 7.28. These data were obtained during static firings of the Saturn S-IC Stage conducted by NASA at the Marshall Space Flight Center and

have been summarized in Reference 7.40. The propagation losses in overall sound level, measured along one line in a direction of maximum radiation, were classified into groups according to six different idealized types of velocity profiles shown in Figure 7.28a. The "0" category corresponds to the case for a zero temperature and wind gradient and may be considered a close simulation of an ideal uniform atmosphere where focusing or shadow zones are absent. As shown in Figure 7.28b, the average attenuation in excess of inverse square law, for this category, is about 0.22 dB/1000 ft. This minimum loss is considered to be the net effect of the atmospheric absorption loss (see Figure 7.11) for the typical low frequency noise spectrum of the S-IC engine, and attenuation due to scattering losses for propagation in the direction of maximum radiation (see Figure 7.25). The decrease in absorption loss at 45-50,000 ft, shown in Figure 7.28b, is caused by the effect on sound propagation of a hill located in this region.

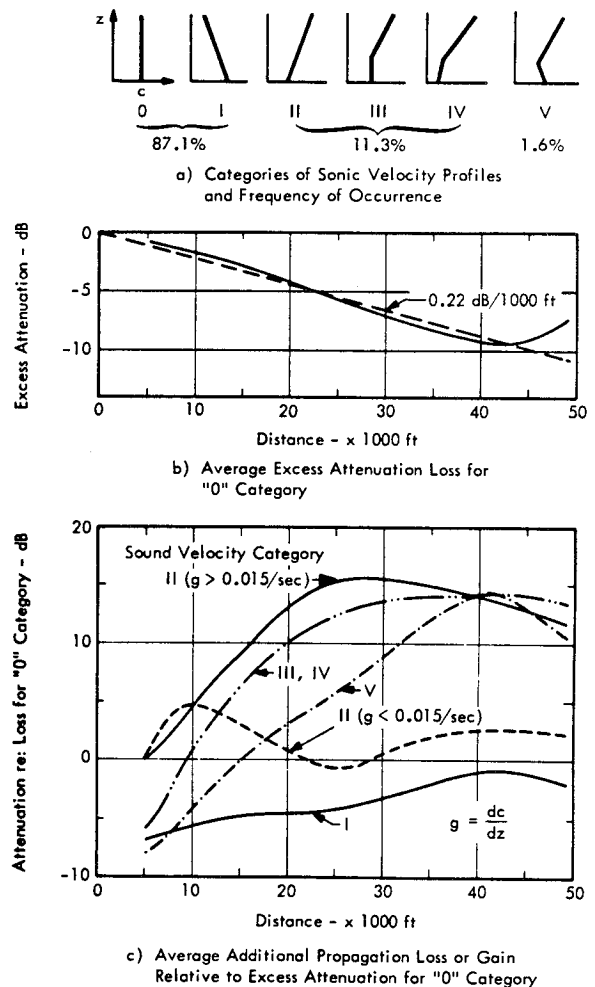


FIGURE 7.28 Average Sound Propagation for Static Tests of Saturn S-IC Illustrating Focusing Gain for Nonuniform Atmosphere (Standard Deviation of the Data, Obtained From Reference 7.40, is About  $\pm 5$  dB)

The second velocity profile category (Type I) has a negative velocity gradient similar to that for upwind propagation and hence there is an additional loss in propagation beyond inverse square law and air absorption loss. The average value of this additional loss is shown for this category in Figure 7.28c. Note that the loss is greatest near the source and decreases to less than 2-3 dB at distances greater than about 30,000 ft. The average frequency of occurrence for the 0 and 1 categories, in total, is 87.1 percent.

For each of the remaining velocity profile categories (II-V), focusing occurs due to the positive velocity gradient. When this gradient,  $g = dc/dz$ , is constant and less than 0.015/sec (the effective speed of sound  $c$  and altitude  $z$  are measured in compatible units), then the focusing is relatively weak, and reaches a maximum at a distance of about 10,000 ft. For higher positive gradients and for all the other more complex profiles shown, the average value of the maximum focusing effect is about 15 dB. In general, this maximum is reached at increasing distances from the source as the initial velocity gradient decreases.

To illustrate application of the data in Figure 7.28, consider the following example. Assume a Type V sound velocity profile has been measured just prior to a static firing of the Saturn S-1C. At a distance of 40,000 ft, the sound level may be predicted as follows. Once the nominal level is known, based on inverse square law, a loss of  $(40)(0.22) \approx 9$  dB, due to air absorption and scattering, is subtracted and a 14 dB gain, due to focusing, is added to give a net propagation gain of +5 dB above inverse square law. The expected variation about this average level would have a standard deviation of about  $\pm 5$  dB.

The frequency of occurrence of the sound velocity profiles, which caused focusing in the single direction of measurement, was 12.9 percent. The profile which caused focusing at the greatest distance (Type V) occurred about 1.6 percent of the time.

An approximate upper bound to the maximum effect of focusing is illustrated in Figure 7.29. This shows the envelope of the excess attenuation, measured for a large number of Saturn static firing tests, including the data from Figure 7.28, and illustrates that, in the limit, the maximum focusing effect at any location can be estimated by assuming that the sound field has a cylindrical rather than a spherical spreading loss. In other words, the intensity is proportional to  $1/R$  rather than  $1/R^2$ . As indicated in the figure, the maximum observed excess attenuation or propagation gain (relative to the inverse square law), corrected by an average absorption and scattering loss of 0.22 dB/ft, is approximately equivalent to a cylindrical spreading loss. For the latter, the absolute sound level decreases 10 dB for every tenfold increase in distance from the source, instead of 20 dB, as for spherical spreading.

It must be emphasized that the cylindrical spreading model defines only an approximate upper bound or envelope for the focusing effect at all locations and weather conditions. For any one particular weather condition, a finite focusing

zone will usually occur with a definite boundary such as illustrated by a typical measurement in Figure 7.30. A well defined focal zone boundary is apparent at a distance of about 13,000 ft where the far field sound level suddenly increases by 11 dB.

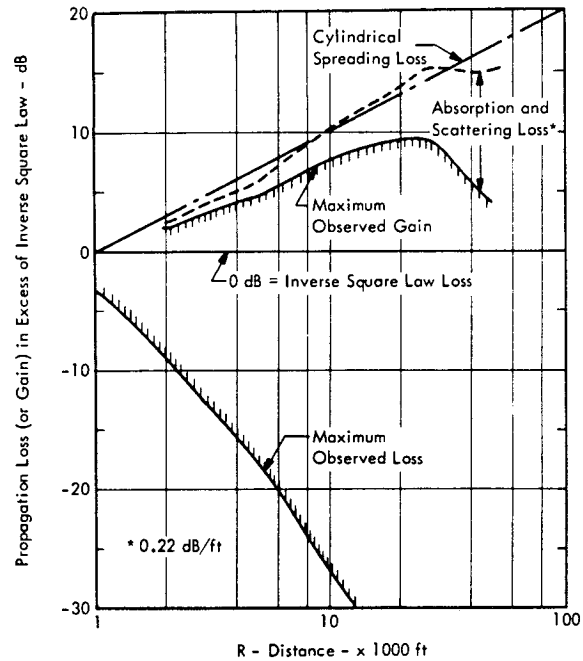


FIGURE 7.29 Envelope of Propagation Loss (or Gain) for Overall Sound Levels Measured for a Large Number of Static Firings of Saturn I. Upper bound approximated by cylindrical spreading loss minus average air absorption loss. (Data from References 7.35, 7.39 and 7.40)

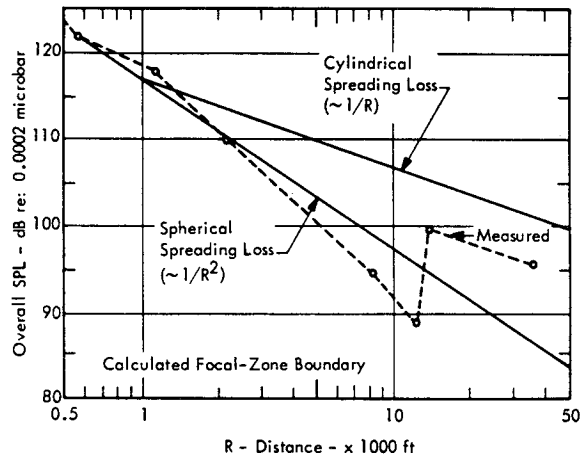


FIGURE 7.30 Variation of Overall Sound Levels Upon Entry Into Focal Zone, Saturn Static Test Firing, Huntsville, Alabama, 10 December 1960 (From Reference 7.39)

### Statistical Probability of Focusing Conditions

As indicated earlier in Figure 7.28, focusing conditions were observed for 12.9 percent of the measurements recorded along a particular azimuth for a large number of Saturn I static test firings. A more complete study of the variation in focusing conditions with azimuth and season of the year has been reported in Reference 7.41. The results, given in Figure 7.31 show how examination of the prevailing wind and temperature profiles can be used to give an immediate assessment of the probability of focusing at a particular location. As indicated in the figure, if the initial choice of a rocket test site in this area were such as to have a 260-degree azimuth to the nearest population center, then there would be little chance of sound focusing and resulting community annoyance. On the other hand, if the azimuth between the test site and the nearby community were 100 degrees, then focusing of the sound radiated would occur on a significant number of occasions during the year, particularly during the winter.

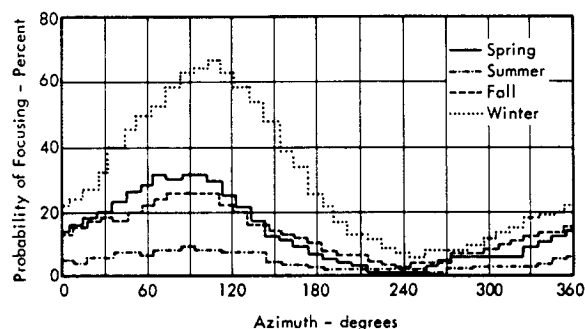


FIGURE 7.31 Probabilities of Sound Focusing by Azimuth, Nashville, Tennessee, 17:00 Hours, Local Time (Data From Reference 7.41)

Similar studies of focusing conditions have been made for other locations (References 7.41 and 7.42). A typical example is illustrated in Figure 7.32 which shows the average percent of time maximum focusing, partial focusing, and "no focusing" conditions would exist during each month of the year between the Saturn V launch site at Cape Kennedy and the city of Titusville, Florida. The predicted occurrences are based on an analysis, reported in Reference 7.42, of rawinsonde data from November 1956 to November 1958. It is important to note, however, that noise generated by a rocket vehicle during the launch phase is not as subject to focusing effects as is noise from ground firings. Thus, Figure 7.29 is included primarily to illustrate that the statistical variation in focusing can vary with general geographical location as well as with azimuth angle and time of year. These examples illustrate how a careful review of atmospheric conditions at a proposed test site can indicate whether sound focusing will be a serious problem or not for nearby communities.

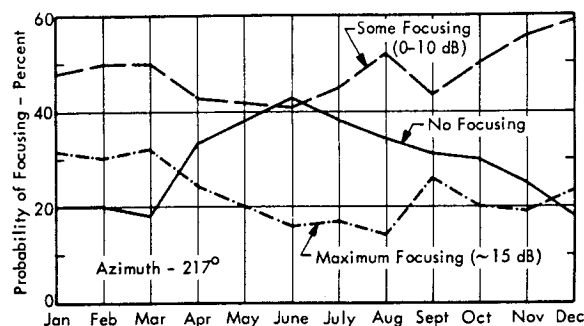


FIGURE 7.32 Average Monthly Variation in Focusing Conditions Over a Two-Year Period Between Saturn V Launch Site and Titusville, Florida (Data From Reference 7.42)

### 7.2.8.3 Statistical Variations in Propagation Losses

It is clear, by now, that there are a large number of variable factors which can influence propagation over a fixed path. Some statistical measure of the overall variation in this propagation loss is desirable. Two independent sets of data were available for analysis of this variation. The first set provides data on maximum overall levels for several Saturn S-I launches, observed at 75,000 ft from the launch pad at Cape Kennedy (Reference 7.42). The propagation, in this case, was more nearly vertical and hence not subject to strong focusing or wind effects. The second involved over 580 measurements during a 35-day period at a single frequency (250 Hz) and over a fixed horizontal line-of-sight range, subject to focusing and wind effects, of 23,400 ft over a large lake (Reference 7.43). Analysis of these data provides an indication of the statistical variation in propagation losses that can be expected for a wide range of conditions.

A cumulative distribution of the deviation in sound level from the expected value based on an inverse square law spreading loss is shown for these two sets of data in Figure 7.33. This figure shows the statistical variation in the excess attenuation in dB/1000 ft at 25 and 250 Hz. While the data are insufficient to develop a general mathematical model for the statistical variation in propagation loss, two points are clear. The distribution of the excess attenuation tends to follow a normal distribution, and the standard deviation is higher, as expected, for the horizontal propagation case at the higher frequency.

### 7.2.9 DESIGN VALUES FOR ACOUSTIC PROPAGATION LOSSES

The following procedure is recommended for estimating propagation losses for design purposes. Unless specific values for a given set of atmospheric conditions are required, it is recommended that the range of losses be calculated. This range will depend on the direction of propagation and the variation in climatic conditions. For horizontal or ground to ground propagation, the variation in profiles of speed of sound will be particularly important. For air to ground or ground to ground propagation, the

variation in temperature and humidity should also be considered. The results will then give a maximum and minimum propagation loss and should indicate the probability of occurrence for each extreme value.

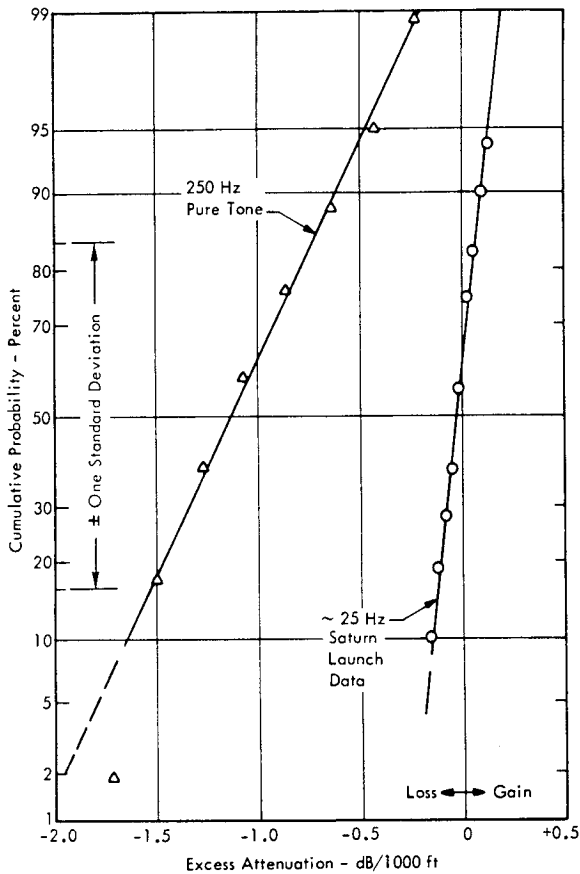


FIGURE 7.33 Typical Illustration of Cumulative Probability Distribution for Excess Attenuation Losses. Data for 250 Hz over 23,400 ft horizontal range from Reference 7.43. Data for Saturn launch levels over 75,000 ft slant range from Reference 7.42.

7.2.9.1 Determine Overall Acoustic Power and Spectrum of Source

Using the methods given in Chapter 6, the overall power and power spectrum can be determined in octave or 1/3 octave band levels, except where large discrete frequency sources are known to occur. In this case, the discrete frequency sources should be considered separately and the resultant value added to those for the broad band noise.

7.2.9.2 Determine Source and Receiver Position and Terrain Between Them

The height of both source and receiver off the ground should be noted, and the nature of the terrain between them described. For example, is there a direct line of sight between receiver and source; are there buildings that will cause acoustic shielding; what is the ground cover?

7.2.9.3 Calculate the Inverse Square Law Losses

The nominal Sound Pressure Level, based on inverse square law, can be obtained from the Acoustic Power Level (PWL) in dB re:  $10^{-13}$  watts both for the overall signal and the octave band values by the expression

$$SPL = PWL - 10 \log_{10} (4\pi R^2) + 0.5 - dB \quad (7.39)$$

where R = distance from source in ft.

7.2.9.4 Determine the Atmospheric Absorption Losses

For simplicity, the results of molecular absorption only need be considered, unless the air is very dry. The results of Figure 7.11 can be used to obtain the value. The range of temperature and humidity expected should be used to estimate the range of losses that can occur. Typical variations in the average seasonal profiles of temperature and humidity at several locations are shown in Figures 7.34 and 7.35.

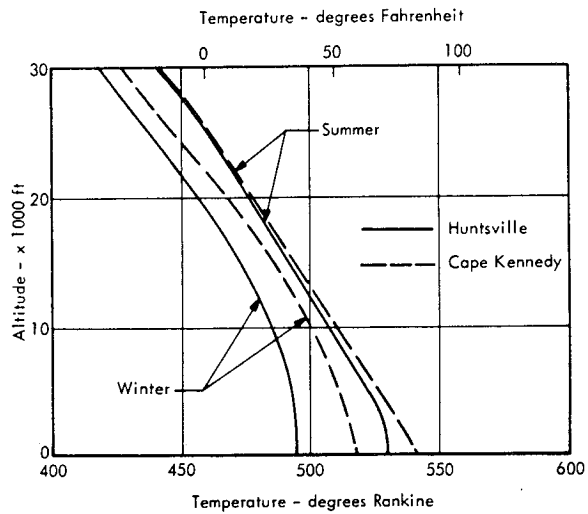


FIGURE 7.34 Average Seasonal Temperature Profiles at Huntsville, Alabama and Cape Kennedy, Florida (Data From Reference 7.44)

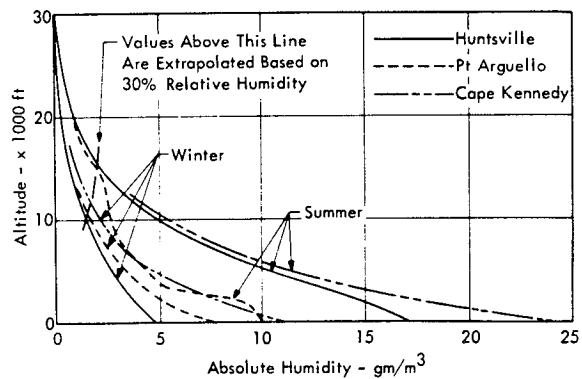


FIGURE 7.35 Average Seasonal Absolute Humidity Profiles at Huntsville, Alabama, Pt Arguello, California and Cape Kennedy, Florida (Data From Reference 7.44)

7.2.9.5 Estimate the Additional Losses Which Increase the Absorption

For short distances, less than 5000 to 10,000 ft, these losses involve shielding, ground absorption, and wind attenuation. Apply the methods of Section 7.2.7 and Figure 7.14 for barriers, Figures 7.15 and 7.16 for ground effects and Figures 7.17 to 7.20 for wind effects, to estimate the maximum effect of these additional losses. These are ordinarily ignored for propagation beyond 2 miles.

For distances greater than 5000 ft, scattering losses will become significant below 200 Hz and may be estimated by the data in Figure 7.25. For conservative design values for either horizontal or vertical propagation, the following expressions are recommended for the combined atmospheric absorption and scattering losses below 200 Hz.

Frequency Range	Excess Attenuation
0-7 Hz	0.03 - dB/1000 ft
7-60 Hz	0.0042 f (Hz) - dB/1000 ft
60-200 Hz	0.25 - dB/1000 ft

7.2.9.6 Estimate the Effect of Sound Focusing

This propagation effect is described in Section 7.2.8.2 and represents an additional correction to the preceding calculations to account for sound focusing effects. After a careful examination of the prevailing weather conditions at the test site, the possibility of sound focusing can be estimated. For horizontal ground to ground propagation, the maximum probable effect of focusing can be estimated by assuming that cylindrical spreading loss rather than spherical spreading loss occurs. The resulting propagation loss can be obtained by following the methods of the previous sections, but using a spreading loss, in dB, equal to 1/2 the usual value based on the inverse square loss. The probability of this maximum focusing effect occurring should be noted. When such extreme focusing effects can interfere with operating schedules of test firings due to limitations in allowable community noise levels, the probability of focusing should be further broken down by time of day and direction. For vertical propagation of noise from a launch firing, focusing effects would be significant only during the on-pad phase of the launch. This can generally be neglected since maximum noise levels in a community will occur after lift-off of the rocket.

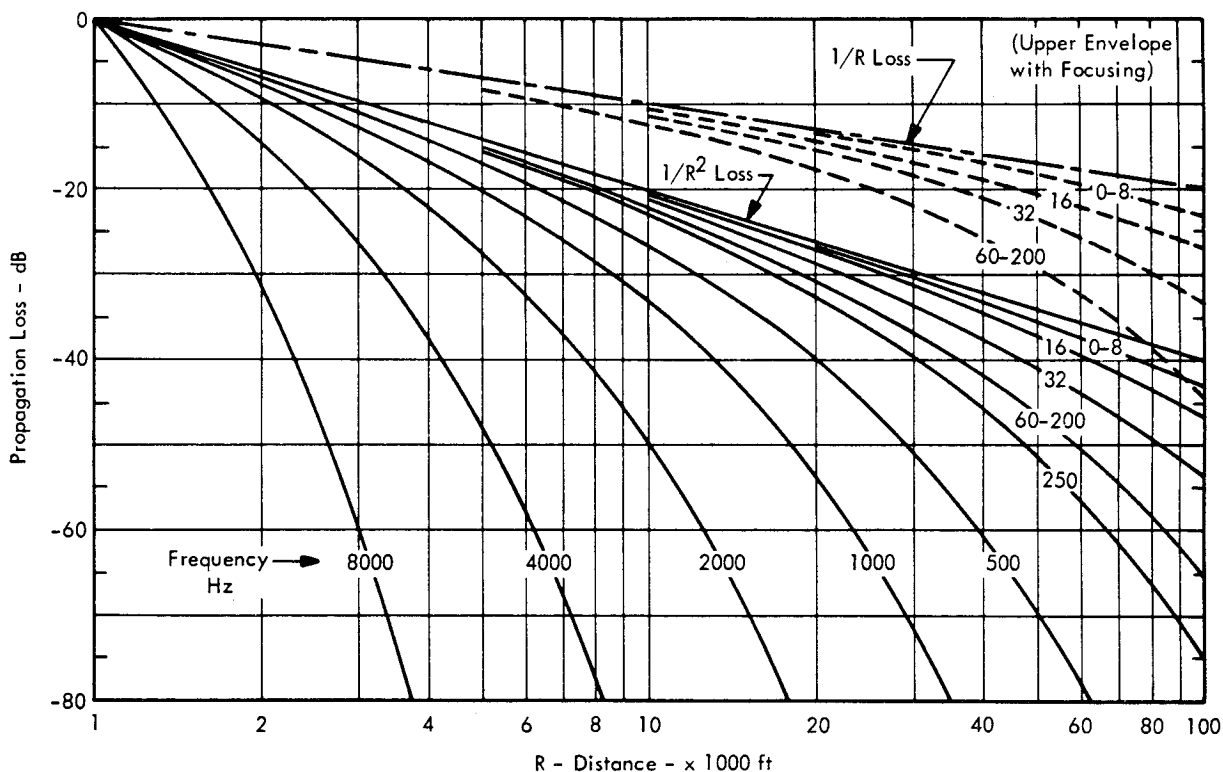


FIGURE 7.36 Design Curves for Long Range Propagation Loss of Rocket Noise. Spherical (1/R<sup>2</sup>) spreading loss applicable for nominal conditions for air to ground or ground to ground propagation. Cylindrical (1/R) spreading loss applicable for maximum focusing conditions with ground to ground propagation. Excess absorption loss based on minimum scattering and air absorption loss below 200 Hz (see Figure 7.25), and air absorption at 59°F and 60 percent relative humidity above 200 Hz.

7.2.9.7 Review of the Calculations

The procedures outlined above will provide reasonable estimates of the maximum sound levels that can occur for rocket firings. A complete analysis of the propagation loss should give the values of maximum and minimum attenuation for the overall level, octave band levels, and any discrete frequency sounds. The probability of the extreme values occurring should be carefully noted for any fixed test sites near populated areas. For preliminary estimates, the combined effects of spreading, absorption, and scattering losses are given in Figure 7.36 for several frequencies as a function of distance. These are based on the minimum values of absorption and scattering loss, suggested earlier, for frequencies below 200Hz and on the calculated values of air absorption loss for higher frequencies, using a standard temperature of 59°F and 60 percent relative humidity. For convenience, a reference level of 0 dB is assumed for all frequencies at a distance of 1000 ft.

The propagation losses shown in Figure 7.36 illustrate the typical range of attenuation that may be expected as a function of frequency and distance. However, the full effect of atmospheric and terrain conditions should be calculated to obtain a more accurate result.

7.3 PROPAGATION LOSSES OF BLAST WAVES

The overpressures generated by an explosion attenuate more rapidly with distance than a sound wave due to the inherently nonlinear processes involved in propagation of blast waves. The nominal attenuation of blast waves with distance has therefore been treated in Chapter 6 as part of the basic description of the overpressures associated with rocket propellant explosions. However, three special problems related to blast wave propagation are treated in this chapter.

- Focusing Anomalies of Blast Waves
- Shielding Effects of Structures
- Suppression of Blast Waves by Burial of the Source

7.3.1 FOCUSING ANOMALIES

The effects of atmospheric focusing can be particularly significant for the high blast overpressures due to explosions. The differential between potentially damaging and safe blast overpressures for structural damage or injury to humans is small. Thus, any increase in the nominal overpressure expected from a potential explosive source can significantly increase the area of potential damage zones. For this reason, care must always be taken in reviewing predicted blast overpressures to ensure that any probable focusing effects are included. The potential increase in blast hazards due to focusing effects may be analyzed in terms of

- Direction and probability of occurrence of a blast focusing zone
- Radius from the explosive source to the focusing zone

- Increase in overpressure within a focus zone.

The method for predicting the occurrence of blast focusing is the same as described earlier in Section 7.7.8 and involves tracing of sonic ray paths in the atmosphere for a known sound velocity profile. The direction and probability of occurrence of blast focusing may be estimated from analysis of prevailing atmospheric conditions in the vicinity of a potential blast site.

To determine the range of a blast focusing zone, a ray tracing analysis must be carried out for a specific set of sound velocity profiles. A very helpful guide to this problem is given in Reference 7.38. This handbook on blast focusing contains a large number of examples and design charts relating range of blast focus zones to sound velocity profile parameters.

7.3.1.1 Magnification of Blast Pressures by Focusing

The increase in blast overpressure within a focus zone is not as well documented nor as readily predicted as location of the zone. In the absence of definitive data, two alternate approaches are presented. The first is based on the magnification factors for blast overpressure which are recommended in Reference 7.38. These are shown in Figure 7.37 as a function of the general type of sound velocity profile. The magnification factors range from 0, for a negative velocity gradient, to 100 for a negative gradient near the surface followed by a strong positive gradient above. The higher factors are very likely conservative and should be applied with discretion.

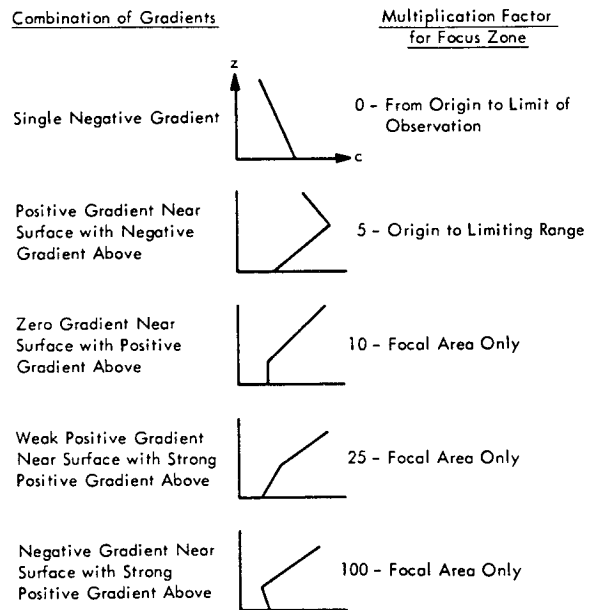


FIGURE 7.37 Increase in Blast Overpressure at a Focal Zone as a Function of Type of Sound Velocity Profile (From Reference 7.38)

7.3.1.2 Cylindrical Spreading Model for Blast Focusing

As an alternate approach for predicting the increase in blast overpressure due to focusing, the concept of cylindrical spreading loss, applied earlier to acoustic focusing, may also be used to define an upper bound to focusing magnification, regardless of location. However, since normal blast overpressure decays more rapidly than dictated by a spherical spreading loss, it is necessary to utilize blast scaling laws in order to define the effect of cylindrical spreading. As discussed in Section 2 of Chapter 6, free air blast overpressures scale as a function of the quantity

$$R/W_T^{1/3}$$

where

R = distance from blast

$W_T$  = weight of equivalent TNT explosive - proportional to the explosive energy.

This ratio may be considered to be proportional to the inverse of the cube root of explosive energy density within a sphere of radius R, or

$$R/W_T^{1/3} \propto 1 / \left[ W_T / \left( \frac{4}{3} \pi R^3 \right) \right]^{1/3}$$

The same principle can be applied to a cylindrical blast field. Since the energy density within a cylinder of radius R and a characteristic altitude H would be

$$W_T / \pi R^2 H = W_T / \pi R^3 \left( \frac{H}{R} \right)$$

a modified scaling parameter for a cylindrical blast field would be

$$(3H/4R)^{1/3} \cdot R/W_T^{1/3}$$

Thus, if the usual scaling parameter  $R/W_T^{1/3}$  is multiplied by the factor  $(3H/4R)^{1/3}$ , a modified blast overpressure can be determined from the same graphs relating overpressure to  $R/W_T^{1/3}$  for a free surface blast (see Figure 6.26, Chapter 6). This modified overpressure may be considered a first approximation to the maximum value that can occur at a focal zone. Based on the experimental data on acoustic focusing presented earlier in Section 7.2.8, a characteristic height H for which a cylindrical spreading model can be applied is about 1000 ft. This would correspond to the effective altitude of a strong temperature inversion layer. With this value of H, the following values for the magnification factor for blast overpressures were computed for a range of TNT equivalent weights ( $W_T$ ) from  $10^4$  to  $10^6$  pounds.

TABLE 7.2

ESTIMATED MAGNIFICATION FACTOR FOR BLAST FOCUSING BASED ON CYLINDRICAL SPREADING MODEL ( $W_T = 10^4 - 10^6$  lb)

R - Distance from Blast (H = 1000 ft)	Magnification Factor
1,250 ft	1.2
2,500	1.7
5,000	2.4
10,000	3.0
20,000	3.9
40,000	5.2
80,000	6.7

These magnification factors are appreciably lower than the values suggested in Figure 7.37 and are considered more realistic for design purposes. It might be added that they are of the same order of magnitude as observed in sonic boom measurements where atmospheric focusing and aircraft maneuvers cause so-called superbooms of the order of 3 to 4 times the nominal values. The increase of the magnification factor with range is also consistent with a physical interpretation of the focusing effect.

As an example of the effect of focusing on modifying a safe radius from a blast, consider the case for a TNT equivalent weight of  $10^6$  lb and a safe unreflected overpressure of 0.2 psi. This would correspond approximately to a criteria for window damage from a maximum credible explosion of a Saturn V booster (see Chapter 6). Without blast focusing, the safe radius would be about 16,000 ft. With blast focusing, assuming a magnification factor based on the cylindrical spreading model, the "safe radius" would increase to about 75,000 ft. The radius based on the magnification factors in Figure 7.37 could be much greater or less, depending on the actual location of the focal zone.

To summarize, blast focusing can significantly increase hazardous overpressures from an explosion. Reasonable magnification factors are predicted by a cylindrical spreading model for the blast field. However, this model only indicates a possible upper bound to focused blast overpressures without regard to location of the focal zone. For critical structures located in areas where focal zones have a high probability of occurrence, possible effects of blast focusing should receive careful consideration.

7.3.2 SHIELDING EFFECTS ON THE BLAST LOADING OF STRUCTURES

Substantial reduction in blast loads on buildings can be achieved by mutual shielding effects. Only experimental results on the amount of reduction are presented since very little theoretical information is available on this subject.



Results from tests reported by the Sandia Corporation (Reference 7.45), on shielding from blast waves by parallel structures, are shown in Figures 7.38, 7.39 and 7.40. These figures show the average net overpressure time histories measured on full scale structures. The average net overpressure is the mean difference in pressure between the front and back walls of the building. Due to the restricted number of tests, no attempt to generalize the results would be justified. However, some approximate concepts about blast shielding effects of structures can be obtained. Based on an analysis of these results, the parameters which influence the blast load on a shielding rectangular building, are summarized in the following paragraphs.

The Ratio Between the Height of the Shielded Structure and Its Separation from the Shield

The net peak overpressure will not be reduced if the building is separated from its blast shield by a distance greater than four times the shield height. If the separation distance is one to two times the shield height, the reduction in peak overpressure is approximately 50 percent.

The Depth of the Shield

A reduction of the shield depth from a value equal to the height of the shielded structure to one quarter of this value causes a rise of 30 percent in the net peak overpressure.

The Length of the Shield

The length of the shield has almost the same influence as the depth of the shield.

The Height of the Shield

The influence of the height of the shield on the net peak overpressure is comparable with the influence of the depth and the length of the shield.

Positive Phase Impulse

Due to the interactions between the shield and the shielded building, the variations of the positive phase impulse are usually small for a shield height equal to the separation distance. In some cases, such as illustrated in Figure 7.39, the positive phase impulse for the shielded building is even larger than that for the same building without shielding.

The limited data indicate that for rectangular buildings, shielding can provide a reduction of 30 to 40 percent in peak net overpressure for a shield height, length and depth comparable to corresponding dimensions for the shielded building and separated less than twice the building height. Changes in positive phase impulse due to shielding are not particularly significant.

**7.3.3 SUPPRESSION OF BLAST WAVES BY BURIED EXPLOSIVES**

When an explosive charge is buried, the blast overpressure is sharply reduced as burial depth is increased. This technique offers the most effective method for decreasing the size of a blast hazard area for storage of potentially explosive rocket fuels or pyrotechnic materials.

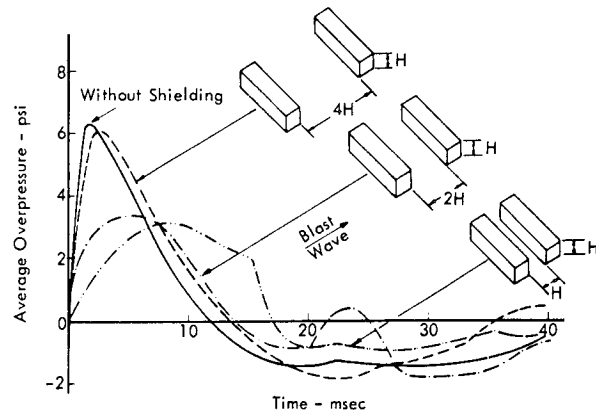


FIGURE 7.38 Experimental Average Net Overpressure Time History for Shielded Buildings Separated from the Shield by Various Distances (Reference 7.45)

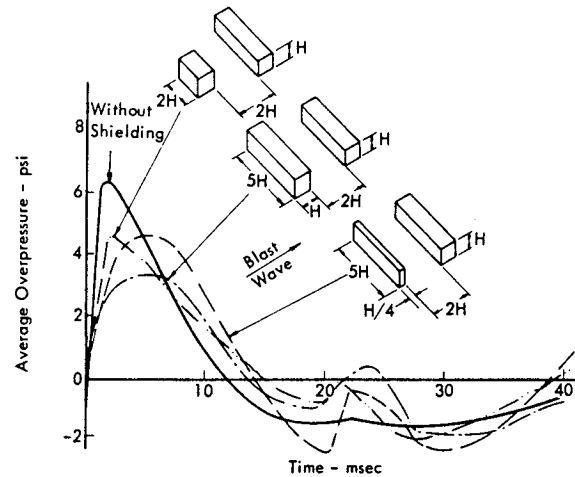


FIGURE 7.39 Experimental Average Net Overpressure Time History for Buildings Shielded by Structures Having Various Lengths and Depths (Reference 7.45)

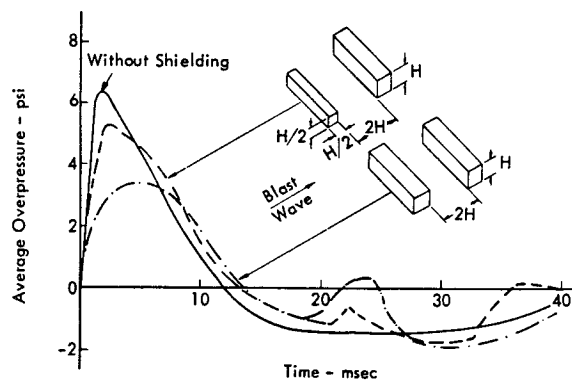


FIGURE 7.40 Experimental Average Net Overpressure Time History for Buildings Shielded by Structures Having Various Heights and Depths (Reference 7.45)

### 7.3.3.1 Suppression of Overpressure Pulse

Design values for the attenuation in the air-coupled blast overpressure, due to the venting gases from a buried charge, may be estimated from the experimental data summarized in Figure 7.41. The curves shown represent smoothed data from tests conducted with 40,000 lb charges of high energy explosive buried in alluvium and basalt (Reference 7.47). Results are also shown, from Reference 7.47, for a test with 1,000,000 lb of high energy explosive in alluvium and from Reference 7.48 for tests with 256 lb of H.E. in sandy gravel. The attenuation versus scaled range for these additional data, covering a wide range of charge weights, are comparable to the values observed for the 40,000 lb charges buried at the same scaled depth.

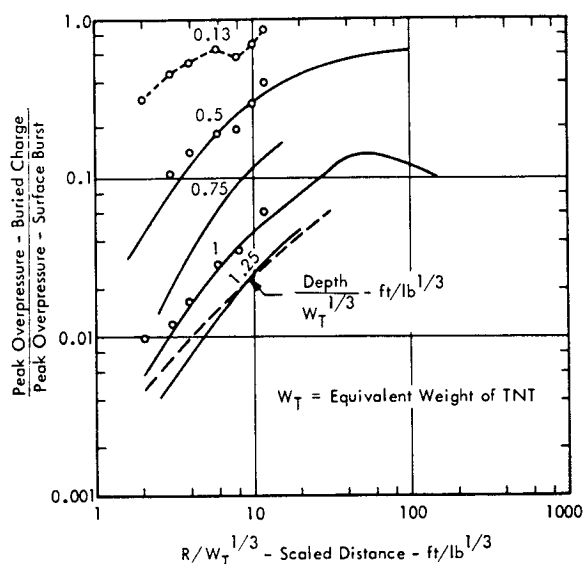


FIGURE 7.41 Observed Attenuation of Peak Overpressure from Air Shock for High Explosives Buried in Ground. Solid lines for 40,000 lb of H.E. in alluvium soil ( $\text{Depth}/W_T^{1/3} = 0.5$  and  $1$ ) and in basalt ( $\text{Depth}/W_T^{1/3} = 0.75, 1.25$ ); dashed line for 1,000,000 lb of H.E. at scaled depth of 1.25 in alluvium (Data from Reference 7.47). Data points (o) for 256 lb of H.E. in sand-gravel mix at 0.13, 0.5 and 1.0 scaled depth (Data from Reference 7.48).

The reduction in overpressure for a buried charge is greatest close to the blast center. For example, a surface mounted fuel storage tank with an explosive potential equivalent to 100,000 lb of TNT could produce a peak overpressure of 10 psi at a distance of 464 ft. At the same distance, ( $R/W_T^{1/3} = 10$ ) burial of the tank by an effective depth of 46 feet ( $\text{Depth}/W_T^{1/3} = 1.0$ ) would be expected to produce peak overpressures less than 0.5 psi according to Figure 7.41.

Explosion of a buried charge induces a mechanical ground shock which also generates an overpressure pulse at the surface. However, this ground-coupled air shock is lower than the overpressure blast wave from the venting gases

and is attenuated more rapidly by burial at increasing depth (Reference 7.47). The attenuation of the ground motion itself associated with both buried and surface blasts is treated in the following section.

### 7.3.3.2 Suppression of Positive Phase Impulse

The effect of burial on the positive phase pressure impulse  $I_p^+$  is roughly independent of scaled distance from the blast, according to the data given in References 7.47 and 7.48. The reduction in impulse may be roughly estimated by the expression

$$I_{p(\text{buried})}^+ \approx I_{p(\text{surface})}^+ \cdot 10^{-0.87 (\text{Depth}/W_T^{1/3})} \quad (7.40)$$

## 7.4 PROPAGATION CHARACTERISTICS OF SEISMIC GROUND WAVES

Ground vibration or seismic waves are generated by varying sonic or mechanical pressures on the earth's surface. Some of the principal characteristics of these waves will be discussed in the remainder of this chapter with the primary emphasis being placed on the propagation characteristics of ground vibration. During an engine firing or an accidental explosion, the ground vibration generated locally at the surface by the traveling pressure wave can be expected to be predominant over any mechanically excited ground vibration except in the immediate vicinity of the source. Once the local coupling between this sonic pressure and the ground motion is defined, the spreading and attenuation losses of the sonic pressure field itself (i.e., engine noise or blast wave), as discussed earlier in this chapter, will define the "propagation losses" of this locally generated ground motion. Thus, the first part of this section will consider the coupling factor for sonically induced ground motion. Seismic ground vibration, transmitted mechanically from one fixed source, such as a vibrating thrust stand, can also be significant for certain situations around rocket test facilities. In this case, the wave velocity, spreading and attenuation losses of this mechanically transmitted seismic motion are of interest and will be considered at the end of this section.

### 7.4.1 SONICALLY COUPLED GROUND MOTION

Experimental measurements of ground motion from high energy explosions have demonstrated that the strongest component of motion coincides approximately with the arrival of the blast overpressure wave (References 7.49 and 7.50). A typical example of such a measurement is illustrated in Figure 7.42. This shows the arrival time for the air shock and ground wave versus range as measured for a 40,000 lb TNT surface explosion at the Suffield Experiment Station (Reference 7.49). The time and range scales have been normalized by the cube root of the charge weight to allow extrapolation of the data to other TNT equivalents. The arrival of the ground wave lags slightly behind the air shock for blast overpressures greater than 10 psi. At lower overpressures, the two arrival times are essentially identical and the slope of the data rapidly approaches that of the ambient acoustic velocity line.

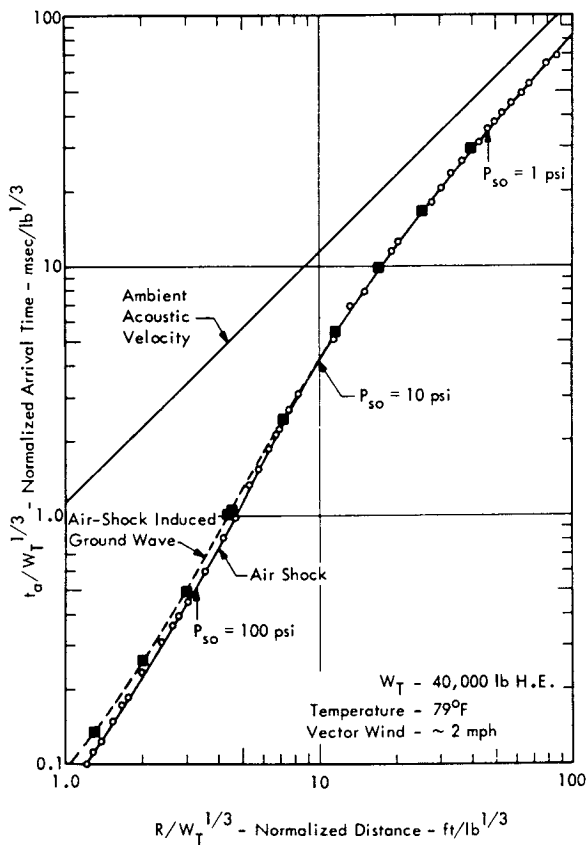


FIGURE 7.42 Arrival Time of Air Shock Wave and Maximum Ground Wave Observed for Surface Explosion of 40,000 lb of High Explosive. Normalized by Cube Root Scaling Law (Data from Reference 7.49).

Similar observations have been made for the strongest ground motion associated with rocket noise from launch and static firings of the Saturn S-1 booster (References 7.54 - 7.57). In this case, the observed arrival times for the strongest ground motion and peak sound pressure corresponds to the velocity of the sonic pressure wave.

These results have led to the choice of a simple one-dimensional theoretical model to explain, to a first approximation, the observed ground motion. In other words, the local motion of the ground surface, subjected to a travelling pressure wave is assumed to be that of a semi-infinite elastic medium subjected to a stationary but time-varying pressure load (References 7.51 and 7.52). While this simple model represents a gross simplification of the true situation, its application is consistent with the scatter in experimental data and lack of detailed knowledge of the seismic properties of the ground in a given location. The essential result predicted by this analytical model is that the peak vertical ground velocity  $V_p$  at the surface is given by the equation for the particle velocity of a plane "acoustic" wave as

$$V_p = \frac{P_p}{\rho c_d}$$

where

$P_p$  = peak sonic pressure (peak side-on overpressure for blast wave or peak sound pressure for acoustic wave)

$\rho$  = mass density of soil

$c_d$  = effective seismic velocity for dilatational or compression waves in ground.

It can be anticipated that this expression will underestimate the true ground velocity. Since the propagation velocity of the travelling pressure wave will be of the same order of magnitude as the velocity of seismic waves near the surface, a dynamic amplification effect may be expected. Although useful theoretical models have been developed which include this effect (e.g. - References 7.51 and 7.60), lack of detailed knowledge of seismic characteristics of local soil structure make it difficult to apply such theories at this time.

Fortunately, sufficient experimental data are available so that an empirical expression can be defined which relates peak surface velocity to peak sonic pressure. This is given by

$$V_p = K \cdot P_p \quad (7.41)$$

where  $K$  is an experimentally determined constant.

This simple method is based on a remarkable consistency for the available experimental data, References 7.50 and 7.53 - 7.59, which indicates that the average value of  $K$  falls in the range of 0.8 to 1.2 in/sec/psi and has a maximum value of about 1.5 - 2 in/sec/psi.

#### 7.4.1.1 Experimental Measurement of Sonically-Coupled Ground Motion

##### Air-Shock-Induced Ground Motion

The typical downward velocity of the surface of the ground during passage of a blast wave is illustrated in idealized form in Figure 7.43. Extensive measurements of ground motion during nuclear and high explosive tests at the Nevada Test Station have established the correlation between peak vertical velocity  $V_p$  and peak overpressure  $P_{so}$  illustrated in Figure 7.44 (Reference 7.50). The solid line through the data represents an average correlation and gives a value for  $K$ , in Equation 7.41, of 0.8 for  $V_p$  in in/sec and  $P_{so}$  in psi. An upper bound to the data is described by  $K = 1.5$  in/sec/psi. A theoretically predicted value is also shown based on the expected values for  $\rho$  and  $c_d$  in this location as given in Reference 7.50. As anticipated, this theoretical line is below the average line and forms an approximate lower bound to the data.

A limited amount of data relating ground velocity to blast overpressure is also reported in Reference 7.53 and was obtained during an explosively destructive test of a solid propellant motor conducted at the Naval Ordnance Test

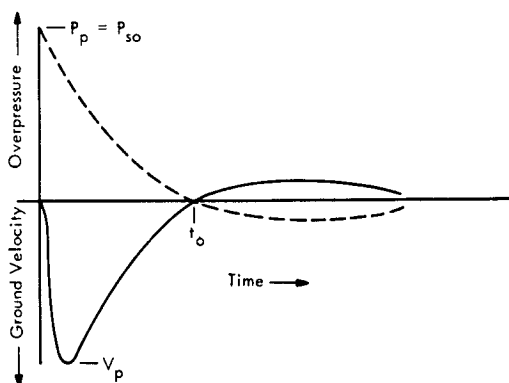


FIGURE 7.43 Idealized Form of Typical Downward Velocity of the Ground Surface During Passage of a Blast Wave

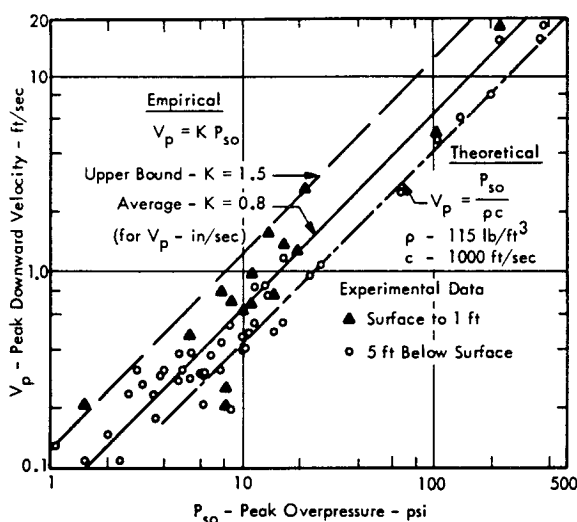


FIGURE 7.44 Correlation of Peak Downward Velocity of Ground Near or at Surface with Blast Overpressure. Velocity computed from accelerograms prior to arrival of directly transmitted ground wave (Data from Reference 7.50).

Station, China Lake, California. From extrapolation of the measured overpressures to those locations for which ground velocities were measured, the observed value of  $K$  was  $0.92 \pm 0.30$  in/sec/psi. In this case, seismic properties of the soil had also been measured and are tabulated below (from Reference 7.53).

SEISMIC VELOCITIES				
DEPTH ft	Compressional fps	Shear fps	Density lb/cu-ft	Poisson's Ratio
0-160	1509	607	125	0.4
160-490	5709	2510	131	0.38
490-1475	7005	3379	131	0.35

Using the values for density and compressional wave velocity in the first 160 ft layer, a predicted ratio of  $V_p$  to  $P_{so}$  would be 0.29 in/sec/psi which is well below the average observed value of 0.92.

Acoustic-Pressure-Induced Ground Motion

An extensive series of measurements on ground motion during launch of the first four Saturn I vehicles are reported in References 7.54-7.56. The data were obtained on several types of instruments which measured velocity directly, or displacement, from which velocity could be computed. Unlike the ground motion for a blast wave, motion during a rocket vehicle firing has a complex time history characteristic of relatively narrow band random vibration which corresponds to the random nature of the acoustic excitation. Direct correlation between instantaneous ground velocity and sound pressure was not possible for this data. It was possible, however, to establish a correlation between the envelope of the peak velocity, during launch, to the corresponding envelope of the peak sound pressures. This was determined in the following manner.

For each launch and measurement location, several values of the instantaneous peak velocity had been obtained from the seismograph records and tabulated in References 7.54-7.56. These tabulated values, observed at various radii ( $R = 200 - 5500$  ft) from the launch pad, were normalized to a common distance of 1000 ft by multiplying each velocity by the factor  $R/1000$ . This assumed that spreading loss of the ground velocity would correspond to the  $1/R$  spreading loss for the sound pressure (e.g. - inverse square law spreading loss for sound intensity).

The normalized peak velocities that occurred throughout the launch were then grouped into octave band frequency intervals according to the observed frequency or period of vibration for each peak. An average and upper and lower bound of velocity was computed for each octave interval.

Similarly, a peak sound pressure for each octave was computed using the methods given in Chapter 6 to establish an upper envelope for the launch sound pressures at 1000 ft from the pad. The peak octave band pressure was taken to be 3 times the maximum rms octave band pressure during launch.

Finally, it was assumed that the peak velocity within each octave band,  $V_p(f)$  could be predicted from the peak acoustic pressure in the same octave  $P_p(f)$  by the expression

$$V_p(f) = K P_p(f) - \text{in/sec} \tag{7.42}$$

where  $P_p(f) = 3$  times rms octave band pressure - psi.

As shown in Figure 7.45, the peak velocity predicted by this expression agrees very well with the average of the measured peak velocities when  $K$  is taken to be 1.0 in/sec/psi. Although the data exhibit appreciable scatter, the correlation between measured and empirically predicted values is encouraging and indicates that the parameter  $K$  does not vary appreciably with frequency. An

approximate upper bound to the data would be predicted by  $K = 2.0$  in/sec/psi. (Valid data at 2 Hz and above 32 Hz are not available due to limitations in the measuring systems - References 7.57 and 7.58.)

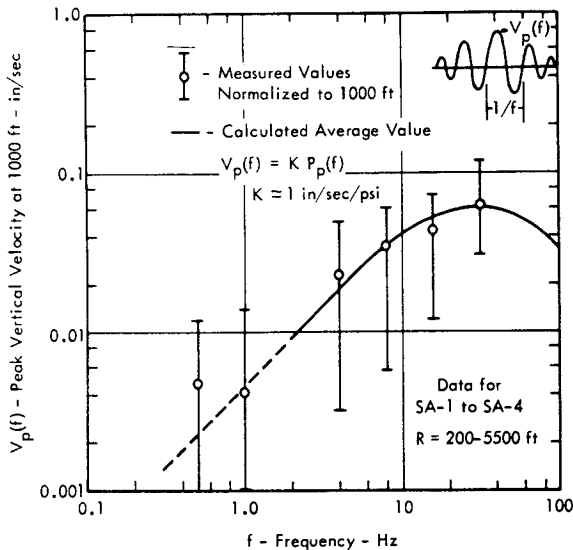


FIGURE 7.45 Correlation of Measured and Calculated Peak Vertical Ground Velocity  $V_p(f)$ , Normalized to Distance  $R = 1000$  ft by Factor  $R/1000$ , for Saturn Launch Firings. Calculated values based on 3-sigma peak octave band pressure  $P_p(f)$  at same radius and frequency (Data from References 7.54 - 7.56).

It is important to recognize that the peak velocities shown in Figure 7.45 represent an average of a large number of single peaks read from oscillograms at different times during the launch of four different Saturn S-1 vehicles. They represent, therefore, an envelope of the maximum velocity versus frequency at any time during launch. The same statement can be made for the peak acoustic pressures so that Figure 7.45 represents a correlation of the maximum envelopes of ground velocities and acoustic pressures during launch. The actual variation of ground velocity with time and frequency would then be expected to follow the variation in peak acoustic pressure with time and frequency, according to Equation 7.42.

One field measurement of seismic velocity on the ground surface, near the location where the above data were obtained, is reported in Reference 7.58. A velocity of 650 ft/sec was measured. Assuming this corresponds to the effective seismic velocity for compressional waves, and using a density of 115 lb/cu ft for the soil, a theoretical prediction of the ratio of peak velocity to peak pressure would give a value of  $K = 1/\rho c_d = 0.745$  which is significantly less than the average values based on the measured data.

The last set of data were obtained from measurements of ground vibration during each of five static firings of the

Saturn I at Huntsville, Alabama. The limited data, summarized in Reference 7.59, show that the average ratio  $K$  of peak vertical velocity to peak acoustic pressure was about 1.2 in/sec/psi with an upper bound equivalent to  $K = 2.2$ . A theoretically predicted value for  $K = 1/\rho c_d$  ranged from 0.48 to 0.84 in/sec/psi for a density of 115 lb/cu ft and a seismic velocity estimated to fall between 600 and 1000 ft/sec.

For both sets of acoustic data, the maximum horizontal motions were approximately the same as the vertical motion.

In summary, the experimental data covering both blast- and acoustic-induced ground motion shows an average ratio of peak vertical velocity to peak pressure ranging from 0.80 to 0.92 in/sec/psi for air shock induced motion to 1.0 to 1.2 in/sec/psi for acoustic pressure induced motion. An upper bound to the measured peak velocity is about twice the average value. The data bear out the theoretical expectation that velocity should be directly proportional to pressure. The theoretical proportionality constant  $1/\rho c_d$  based on a simple one-dimensional model predicts a peak velocity 25 to 300 percent lower than the average measured values.

Finally, it must be emphasized that the simplified treatment of ground motion presented here has omitted the details of the very complex pattern of seismic waves, both air-coupled and directly transmitted, which are present for sonic excitation of the ground. The objective has been to provide a simple means of estimating only the maximum surface motion.

#### 7.4.2 DIRECTLY COUPLED GROUND MOTION

The transmission of vibration energy directly through the ground can be of interest for rocket test sites in at least three situations.

- Ground vibration transmitted into a building near the firing pad when the building and its foundation are isolated from ground motion induced by the acoustic noise.
- Ground vibration of sensitive equipment by unbalanced forces from nearby machinery anchored to the ground.
- Ground motion resulting from accidental explosion of semiburied or buried explosive materials such as rocket propellant storage tanks.

Pertinent information on propagation losses associated with this type of directly transmitted ground vibration is presented in this final section. For engineering design purposes, only simple theoretical approaches to this complex vibration transmission process are practical. Just as for the air-coupled ground motion, the theory for the directly transmitted motion must be backed up, or in many cases, replaced by empirical results in order to obtain useful results. For a more thorough discussion of this complex subject, the reader is referred to References 7.51, 7.61 and 7.62.

7.4.2.1 General Propagation Characteristics of Seismic Waves Transmitted Through the Ground

For a localized source of vibratory motion on the surface of the ground, the propagation of energy away from the source will take the form of elastic body waves (i.e. - compressional and shear waves) which radiate energy into the ground in all directions and surface waves which radiate energy away along the surface of the ground. At some distant point from the source, the ground motion will be the summation of all of these waves which travel at different velocities, have different particle motions relative to the direction of propagation of the wave, and experience different amounts of energy loss or absorption loss per unit distance. Added to this complexity is the fact that the medium itself changes its elastic properties with depth causing refraction effects. Thus, as illustrated in Figure 7.46, the propagation of directly transmitted ground vibration becomes very complex.

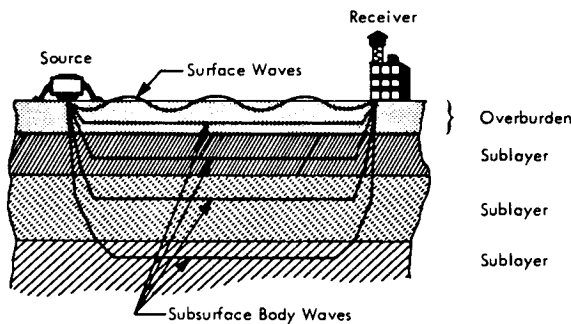


FIGURE 7.46 Propagation of Ground Vibration Illustrating Different Types of Seismic Waves and Varying Propagation Paths Between Vibration Source and Receiver

For any one of these types of seismic waves, an idealized analytical model for the propagation loss could take the form

$$A(f) = A_0(f) \left( \frac{R_0}{R} \right)^n e^{-\alpha(f) R} \quad (7.43)$$

where

$A(f)$  = amplitude (i.e. - displacement, velocity, etc.) of wave at distance  $R$  and frequency  $f$

$A_0(f)$  = initial amplitude at a reference distance  $R_0$

$n$  = 1/2 for cylindrical waves and 1 for spherical waves, and

$\alpha(f)$  = absorption loss coefficient which is a function of the frequency and type of wave motion.

The velocity of the wave can be specified in terms of the elastic constants of the medium. For compressional or dilatational waves, involving particle motion in the same direction as the wave propagation, this velocity  $c_d$  is given by

$$c_d = c_L \left[ \frac{1 - \nu}{(1 + \nu)(1 - 2\nu)} \right]^{1/2} \quad (7.44)$$

where

$c_L = \sqrt{E/\rho}$  = velocity of one-dimensional compression waves

$E$  = modulus of elasticity

$\rho$  = mass density

$\nu$  = Poisson's ratio  $\approx 0.4 \pm 0.1$  for soils.

For shear waves, involving particle motion perpendicular to the direction of propagation, the velocity  $c_s$  is

$$c_s = \sqrt{\frac{G}{\rho}} = c_L \left[ \frac{1}{2(1 + \nu)} \right]^{1/2} \quad (7.45)$$

where  $G$  = shear modulus.

The Rayleigh wave generally is the most prominent form of the surface wave and has a particle motion in an elliptical path in a vertical plane which is parallel to the direction of propagation. Its propagation velocity is slightly less than the shear wave velocity in the upper layer of the ground.

Specific data are given in the following which can assist in defining the velocity of compressional and shear waves,  $c_d$  and  $c_s$ , the spreading loss exponent  $n$ , the absorption loss factor  $\alpha(f)$  and the initial amplitude  $A_0$ .

7.4.2.2 Velocity of Seismic Waves

The elastic modulus of typical surface soils increases with depth due to the increased confining pressure of the overlying soil. A typical example of this increase in one-dimensional compression wave velocity with confining pressure is shown in Figure 7.47 for two types of sandy soils at two different densities. The increase in shear wave velocity with pressure for two types of saturated clay soil is shown in Figure 7.48 (Reference 7.62). Due to the cohesive nature of soil, the confining pressure will be less than the pressure that would exist due solely to the weight of the overlying soil (Reference 7.51).

The effect of pressure on seismic velocity is very important in the propagation of blast shock waves through soil. In this case, the dynamic overpressures in the soil are sufficiently high to affect the wave velocity, hence causing a distortion of the shape of the wave front. However, for normal dynamic soil pressures encountered for mechanical or acoustic sources, this nonlinear effect can be neglected.

The soil near the surface may be highly structured with specific layers of varying density and elastic modulus. The corresponding velocities for compressional waves can range widely from about 600-3300 ft/sec for loose and dry soils

near the surface to 3000-8500 ft/sec for coarse and compact soils on up to 14,000 ft/sec for sandstone and compacted soils. However, the typical range of seismic velocities illustrated in Figures 7.47 and 7.48 are more representative of the propagation velocities of the most significant ground vibration waves near the surface.

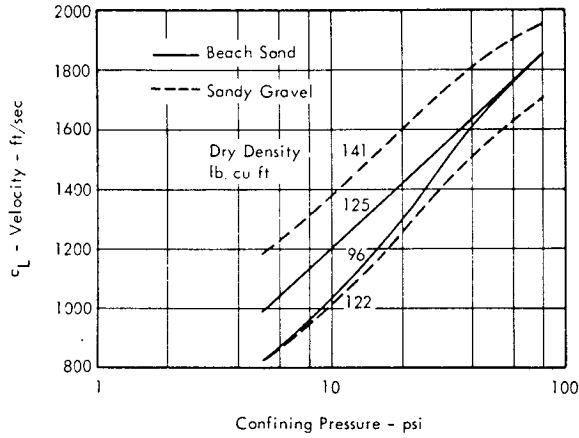


FIGURE 7.47 Velocity of Longitudinal or One-Dimensional Compression Waves in Sandy Soils as a Function of Confining Pressure (Data from Reference 7.62)

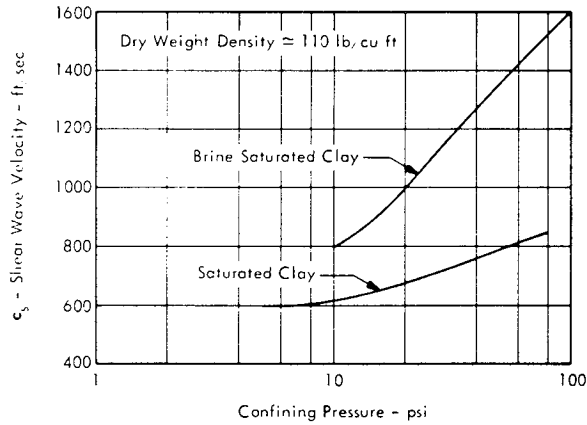


FIGURE 7.48 Velocity of Shear Waves in Saturated Clay Soils as a Function of Confining Pressure (Data from Reference 7.62)

7.4.2.3 Spreading Loss for Seismic Waves

Within a given layer of uniform mixture of soil, the increasing velocity of compressional and shear waves with depth will tend to refract the ray paths of the wave front causing them to bend back towards the surface of the earth. The effect is identical to that discussed earlier in Section 7.2.8.2 for focusing of acoustic waves. It would be expected, therefore, that the minimum spreading losses

for ground vibration would tend to be cylindrical ( $n = 0.5$ ) instead of spherical ( $n = 1$ ). (Note that  $n = 1$  for amplitude spreading loss corresponds to  $n = 2$  or inverse square law for intensity spreading loss.) However, no data are available which substantiate such a trend. In fact, it will be shown that for blast-induced directly transmitted ground motion, the spreading loss exponent is about 1.5 for peak displacement, 2.5 for peak velocity and 3.5 for acceleration (References 7.51 and 7.63). These values for the spreading loss exponent exceed the expected maximum value of 1 for spherical spreading. The higher values for the spreading loss exponent can be attributed to additional energy loss by viscous effects and transmission of energy into lower layers of the soil.

7.4.2.4 Absorption Losses for Seismic Waves

Viscous effects in the transmission of elastic waves through soil act to remove energy just as for acoustic waves. However, the loss coefficient  $\alpha(f)$  varies approximately linearly with frequency. For longitudinal waves (one-dimensional compression waves), the attenuation coefficient, expressed in units of dB/ft, is given by (Reference 7.61)

$$\alpha = 8.68 \alpha(f) = \frac{8.68 \pi \eta f}{c_L} \text{ - dB/ft} \quad (7.46)$$

where

$\alpha(f)$  = exponential loss factor in Equation 7.43

$\eta$  = damping loss factor of the soil - the ratio of the imaginary to real part of the elastic modulus, and

$c_L = \sqrt{E/\rho}$ , the speed of longitudinal waves in the soil.

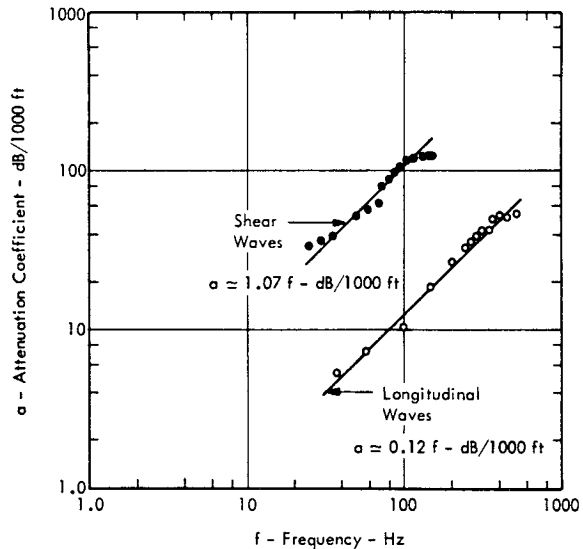


FIGURE 7.49 Attenuation Coefficient Versus Frequency for Longitudinal and Shear Waves in Shale (Reference 7.61)

Measured values for the attenuation coefficient  $a$  for a typical sedimentary rock (Pierre Shale) are shown in Figure 7.49 for both longitudinal and shear waves (Reference 7.61). An approximate linear dependence on frequency is evident. For other earth materials, values of  $a$  have been obtained from measured data (Reference 7.63), or have been computed from published values for  $\eta$  and  $c_L$  by Equation 7.46 (References 7.61 and 7.62). These are listed in Table 7.3. For soils, the attenuation coefficient varies from 0.32  $f$  to 3.44  $f$  - dB/1000 ft with a typical value of 1.5  $f$  - dB/1000 ft. Thus, for a frequency of 20 Hz, an attenuation loss of approximately 3 dB, in excess of the spreading loss, would occur in a distance of 100 ft.

TABLE 7.3

ATTENUATION COEFFICIENTS FOR SOIL AND ROCK MATERIALS FOR LONGITUDINAL WAVES

Material	Frequency Range Hz	$c_L$ ft/sec	$a$ - Attenuation Coefficient dB/1000 ft
(2) Beach Sand	--	800-1800	0.76 $f$ - 1.7 $f$ (1)
(2) Dry Sand	--	~1100	0.37 $f$
(2) Saturated Sand	--	2040	0.82 $f$
(2) Sandy Gravel	--	1200-2000	0.68 $f$ - 1.13 $f$
(2) Saturated Clay	--	1000-1470	1.8 $f$ - 3.44 $f$
(3) Sandstone	10-40 40-120	7200	0.042 $f$ 0.182 $f$
(3) Limestone (Shelly)	10-40 40-120	13,000 13,000	0.0063 $f$ 0.0335 $f$
(3) Granite (Quincy)	40-120	13,800	0.0335 $f$
(3) Rock	40-5000		0.053 $f$ - 0.82 $f$
(4) Earth Crust	~1	9850	0.019 $f$

(1)  $f$  - frequency in Hz.

(2) Reference 7.62 - calculated values from measured damping loss factor.

(3) Reference 7.61.

(4) Reference 7.63.

In general, the data indicate negligible losses for vibration frequencies below 20 Hz transmitted through soils over distances less than 100 ft. However, the attenuation coefficients in soil are roughly 2 orders of magnitude higher than in air thus clearly showing the negligible significance of ground vibration directly transmitted over long distances compared to air-coupled ground vibration.

#### 7.4.2.5 Overall Propagation Losses for Mechanical Sources

In the absence of experimental data, the following procedure is recommended to estimate the directly transmitted vibration from steady-state mechanical sources resting on the ground surface such as rocket test stands or large machinery.

- (1) Define the size of the source relative to the transmitted wavelength  $\lambda$  in the ground by

$$R_o/\lambda = R_o f/c_s \quad (7.47)$$

where

$R_o$  = equivalent radius at the base of the mechanical source - ft

$f$  = frequency of vibration - Hz

$c_s$  = shear wave velocity in top 5 feet - ft/sec.

- (2) For  $R_o/\lambda \gg 1$ , the ground may be assumed to be resistive and the peak velocity of the ground at the source  $V_o(f)$  can be estimated by

$$V_o(f) \approx 2 P_o(f) - \text{in/sec} \quad (7.48)$$

where

$P_o(f)$  = Peak dynamic pressure in psi on the ground generated by the mechanical source at the frequency  $f$ .

Assume the spreading loss is given by an exponent  $n = 1/2$  and the absorption loss by

$$A = 1.5 f (R/1000) \text{ dB}$$

Thus, the ground velocity at a distance  $R$  may be roughly estimated by an expression in decibel form

$$10 \log V(f) = 10 \log [2 P_o(f)] - 10 \log (R/R_o) - 1.5 f R/1000, \text{ dB re: 1 in/sec} \quad (7.49)$$

where  $V(f)$ ,  $P_o(f)$  and  $R$  are in in/sec, psi and ft, respectively. Ground displacements or accelerations may be estimated by the usual expressions for simple harmonic motion.

- (3) For  $R_o/\lambda \ll 1$ , the ground may be assumed to be stiffness controlled and the peak displacement at the source  $X_o(f)$  may be estimated by (Reference 7.64)

$$X_o(f) \approx \frac{(1-\nu)F(f)}{4 G R_o} - \text{in.} \quad (7.50)$$

where

$\nu$  = Poisson's ratio for soil ~0.4

$F(f)$  = peak dynamic force in lb driving soil at the frequency  $f$

$G$  = shear modulus of soil - psi  
 $= E/2(1+\nu)$   
 (For typical surface soils,  $G \sim 6000$ - $10,000$  psi)

Apply the same spreading and attenuation loss as in the previous case.



- (4) For  $R_0/\lambda \sim 1$ , use both of the previous methods and fair the results together.

#### 7.4.2.6 Overall Propagation Losses for Aerodynamic Sources

For ground vibration generated by aerodynamic pressures from the exhaust of a rocket engine impinging directly on the ground, proceed as in step (2) of 7.4.2.5 using the methods given in Section 6.1.10 of Chapter 6 to estimate the peak pressures on the ground.

#### 7.4.2.7 Overall Propagation Losses for Buried Explosive Sources

Considerable experimental data on directly transmitted ground motion are available from tests with buried high explosives. The data have been correlated into empirical expressions for the directly transmitted ground motion (Reference 7.51). A typical wave form of this ground motion from a blast is shown in Figure 7.50.

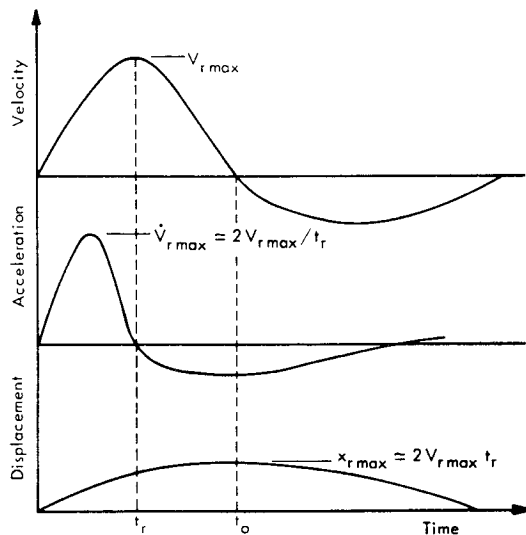


FIGURE 7.50 Idealized Pulse Shapes of Directly Transmitted Ground Motion from Buried Explosive Charges (Reference 7.51)

The rise time  $t_r$  of the acceleration pulse has been found to be approximately equal to (Reference 7.51)

$$t_r \approx \frac{1}{6} \frac{R}{c_d} \quad (7.51)$$

where

$R$  = slant range from center of blast

$c_d$  = velocity of compressional waves.

Based on this observation and the idealized models, for the velocity and displacement pulse shapes shown in Figure 7.50, the following expressions have been derived from

the data in Reference 7.51. They are based on a one-dimensional model for the wave propagation, thus allowing extrapolation of measured ground acceleration to estimates of ground velocity and displacement. The maximum velocity,  $V_{r \max}$ , in a radial direction from the source, can be estimated by

#### VELOCITY

$$V_{r \max} \approx 2000 \left( R/W_T^{1/3} \right)^{-2.5} - \text{in/sec} \quad (7.52)$$

where

$R$  = radius in ft

$W_T$  = equivalent TNT weight - lb.

The constant of 2000 represents an average proportionality factor from experimental data in Reference 7.51 for explosions in dry clay, dry sand, and sandstone.

The maximum tangential velocity was estimated in Reference 7.51 to be

$$V_{t \max} \approx \frac{2}{3} V_{r \max} - \text{in/sec}$$

From Equations 7.51 and 7.52, and the relationship between peak velocity, acceleration and displacement shown in Figure 7.50, the expressions for the maximum radial and tangential acceleration  $a_{r \max}$  and  $a_{t \max}$  and corresponding displacements  $x_{r \max}$  and  $x_{t \max}$  are

#### ACCELERATION

$$a_{r \max} \cdot W_T^{1/3} \approx \frac{2000 c_d}{32.2} \left[ R/W_T^{1/3} \right]^{-3.5} - g's \cdot \text{lb}^{1/3} \quad (7.53)$$

$$a_{t \max} \approx a_{r \max} - g's$$

The compressional wave velocity  $c_d$ , in ft/sec, may be estimated from Equation 7.44 and Figure 7.47 for typical sandy soils.

#### DISPLACEMENT

$$\frac{x_{\max}}{W_T^{1/3}} \approx \frac{2000}{3 c_d} \left[ R/W_T^{1/3} \right]^{-1.5} - \text{in/lb}^{1/3} \quad (7.54)$$

$$x_{t \max} \approx \frac{1}{3} x_{r \max} - \text{in.}$$

The use of the cube root of the charge weight  $W_T$  in the equations above is consistent with the normal method for scaling blast phenomena. Since these expressions were developed from data with high explosives, they should give conservative results when applied to explosions of buried liquid propellants.

## REFERENCES

- 7.1 Nyborg, W. L., and Mintzer, D., "Review of Sound Propagation in the Lower Atmosphere", WADC Technical Report 54-602, May 1955.
- 7.2 Horton, J. W., "Fundamentals of Sonar", U. S. Naval Institute, Annapolis, Maryland, 1957.
- 7.3 Schultz, T., "Effect of Altitude on Output of Sound Sources", Noise Control 5, May 1959, pp. 17-21.
- 7.4 Ingard, K. U., and Lamb, G. L., "The Effect of a Reflecting Plane on the Power Output of Sound Sources", J. Acoust. Soc. Am. 29, Jun. 1957, pp. 743-744.
- 7.5 Howes, W. L., "Ground Reflection of Jet Noise", NASA TR R-35, 1959.
- 7.6 Morgan, W. V., Sutherland, L. C. and Young, K. J., "The Use of Acoustic Scale Models for Investigating Near Field Noise of Jet and Rocket Engines", WADD TR 61-178, Apr. 1961.
- 7.7 Dean, E. A., "Absorption of Low Frequency Sound in a Homogeneous Atmosphere", Schellenger Research Laboratory, Report 1237, Aug. 1959.
- 7.8 Kneser, H., "The Interpretation of the Anomalous Sound-Absorption in Air and Oxygen in Terms of Molecular Collisions", J. Acoust. Soc. Am. 5, 1933, pp. 122-126.
- 7.9 Knudsen, V. O., "The Absorption of Sound in Air, in Oxygen, and in Nitrogen, Effects of Humidity and Temperature", J. Acoust. Soc. Am. 5, 1933, pp. 11-17.
- 7.10 Harris, C. M., "Absorption of Sound in the Audio Range", J. Acoust. Soc. Am. 35, 1963, pp. 11-17.
- 7.11 Harris, C. M. and Tempest, W., "Absorption of Sound Below 1000 cps", J. Acoust. Soc. Am. 36, 1964, pp. 2390-2394.
- 7.12 Harris, C. M., and Tempest, W., "Absorption of Sound in Air Below 1000 cps", NASA CR-237, 1965.
- 7.13 Harris, C. M., "Absorption of Sound in Air Versus Humidity and Temperature", NASA CR-647, 1967.
- 7.14 Knudsen, V. O., "The Absorption of Sound in Gases", J. Acoust. Soc. Am. 6, 1935, p. 199.
- 7.15 Henderson, M. C., "Sound in Air: Absorption and Dispersion", Sound 2, 1963, pp. 28-36.
- 7.16 Sivian, L. J., "High Frequency Absorption in Air and Other Gases", J. Acoust. Soc. Am. 19, 1947, pp. 914-918.
- 7.17 Clark, A., and Henderson, M. C., "Vibrational Relaxation in Dry and Moist Oxygen", J. Acoust. Soc. Am. 35, 1963, p. 1909(A).
- 7.18 Evans, E. J., and Bazley, E. N., Acoustica 6, 1956, p. 238.
- 7.19 Knotzel, H., "Absorption of Audible Sound in Air and Its Dependence on Humidity and Temperature", Akust. 2, Vol. 5, 1940, p. 246.
- 7.20 Henderson, M. C., and Herzfeld, K. F., "Effect of Water Vapor on the Napier Frequency of Oxygen and Air", J. Acoust. Soc. Am. 37, 1965, pp. 986-988.
- 7.21 Smith, P. W., Jr., "Effect of Heat Radiation on Sound Propagation in Gases", J. Acoust. Soc. Am. 29, 1957, pp. 693-698.
- 7.22 Jewell, R., NASA, Personal Communication.
- 7.23 Sabine, H. J., "Sound Propagation Near the Earth's Surface as Influenced by Weather Conditions", Four Parts, TR 57-353, 1957-61.
- 7.24 Parkin, P. H., and Scholes, W. E., "Air to Ground Attenuation", J. Acoust. Soc. Am. 26, 1954, p. 1021.
- 7.25 "Standard Values of Atmospheric Absorption as a Function of Temperature and Humidity for Use in Evaluating Aircraft Flyover Noise", SAE ARP-866, 1964.
- 7.26 Parkin, P. H., and Scholes, W. E., "The Horizontal Propagation of Sound from a Jet Engine Close to the Ground, at Radlett", J. Sound Vib. 1, No. 1, 1964, pp. 1-13.
- 7.27 Parkin, P. H., and Scholes, W. E., "The Horizontal Propagation of Sound from a Jet Engine Close to the Ground, at Hatfield", J. Sound Vib. 2, No. 4, 1964, pp. 353-374.
- 7.28 Beranek, L., "Noise Reduction", McGraw-Hill Book Co., N. Y., 1960, p. 193.
- 7.29 Wiener, F. M., and Keast, D. N., "Experimental Study of the Propagation of Sound Over Ground", J. Acoust. Soc. Am. 31, No. 6, 1959, pp. 724-733.
- 7.30 Hubbard, H. H., and Maglieri, O. J., "An Investigation of Sound Phenomena Relating to Aural Detection of Airplanes", NACA TN 4337, 1958.
- 7.31 Franken, P. A., and Bishop, D. E., "The Propagation of Sound from Airport Ground Operations", NASA CR-767, 1967.
- 7.32 "Method of Calculating the Attenuation of Aircraft Ground to Ground Noise Propagation During Take-off and Landing", SAE AIR 923, 1966.

- 7.33 Lord Rayleigh, "The Theory of Sound", Vol. 2, Dover Publications, N. Y., 1945, p. 149.
- 7.34 Tedrick, R. N., "Acoustical Measurements of Static Tests of Clustered and Single-Nozzle Rocket Engines", J. Acoust. Soc. Am. 36, 1964, pp. 2027-2032.
- 7.35 Jewell, R., NASA, MSFC, Huntsville, Alabama, Personal Communication.
- 7.36 Liebermann, L., "The Effect of Temperature Inhomogeneities in the Ocean on the Propagation of Sound", J. Acoust. Soc. Am. 23, Sept. 1951, pp. 563-570.
- 7.37 Rudnick, I., "Handbook of Noise Control", Chapter 3, Harris, C. M., ed., McGraw-Hill Book Co., N. Y., 1957.
- 7.38 Perkins, B., Jr., and Jackson, W. F., "Handbook for Prediction of Air Blast Focusing", Ballistic Research Laboratories, Aberdeen Maryland, Rept. No. 1240, 1964.
- 7.39 Tedrick, R. N., "Meteorological Focusing of Acoustic Energy", Sound, Vol. 2, No. 6, 1963.
- 7.40 Tedrick, R. N., and Polly, R. C., "A Preliminary Investigation of the Measured Atmospheric Propagation Effects Upon Sound Propagation", NASA MTP - Test 63-6, May 1963.
- 7.41 Essenwanger, O., "Profile Types of Sound Speed in the Lower Atmosphere and their Relationships to Acoustic Focusing", U. S. Army Missile Command, Redstone Arsenal, Alabama, Report RR-TR-66-6, 1966.
- 7.42 Peverly, R. W., "Determination of Rocket Engine Noise Damage to Community Dwellings Near Launch Sites", Martin Co., Report CR-64-65, Vol. 1, Dec. 1964.
- 7.43 Young, K. J., The Boeing Co., Aero-Space Div., Personal Communication.
- 7.44 Bolt, Beranek, and Newman, Inc., "Acoustical Considerations in the Planning and Operation of Launching and Static Test Facilities for Large Space Vehicles - Phase I", Report No. 884, Dec. 1961.
- 7.45 Merritt, M. L., "Shielding from Blast Waves by Parallel Structures", Sandia Corp., Albuquerque, N. M., Report No. AFSWP-224, Oct. 1952.
- 7.46 Coulter, G. A., "The Shielding Effect of Walls", Ballistic Research Laboratories, Aberdeen, Maryland, Technical Note 585, 1952.
- 7.47 Vortman, L. J., "Air Blast Suppression as a Function of Explosive-Charge Burial Depth", J. Acoust. Soc. Am. 40, Jul. 1966, pp. 229-239.
- 7.48 Anderson, T. O., et al., "Blast, Fragmentation and Damage", Preliminary Report by Explosions Research Dept., U. S. Naval Ordnance Laboratory, Nov. 21, 1966.
- 7.49 Jones, G. H. S., "Strong Motion Seismic Effects of the Suffield Explosions", Suffield Report No. 208; Defense Research Board of Canada, Report No. D89-16-01-05, 1963.
- 7.50 Merritt, J. L., and Newmark, N. M., "Nuclear Geoplosics - Part V - Effects on Underground Structures", DASA Report 1285(V), May 1964.
- 7.51 Newmark, N. M., and Haltiwanger, J. D., "Air Force Design Manual - Principles and Practices for Design of Hardened Structures", Air Force Special Weapons Center, Report AFSWC-TDR-62-138, Dec. 1962.
- 7.52 Cook, R. K., and Young, J. M., "Strange Sounds in the Atmosphere, Part II", Sound, Vol. 1, May-Jun. 1962.
- 7.53 Mickey, W. V., and Shugart, T. R., "Seismic Disturbances Generated by Titan III 624A Solid Motor Sled Test", U. S. Dept. of Commerce, Coast and Geodetic Survey, Oct. 1964.
- 7.54 Mickey, W. V., et al., "Ground Motions Induced by Saturn SA-1 Launch at Cape Canaveral, Florida", U. S. Dept. of Commerce, Coast and Geodetic Survey, Jun. 1962.
- 7.55 Mickey, W. V., "Seismic Effects of Saturn SA-2 and Moon Probe Launches", U. S. Dept. of Commerce, Coast and Geodetic Survey, Jun. 1962.
- 7.56 Mickey, W. V., and Shugart, T. R., "Near Range Seismic Effects of Saturn SA-3 and SA-4 Missile Launches", U. S. Dept. of Commerce, Coast and Geodetic Survey, Sept. 1963.
- 7.57 Wyle Laboratories Unpublished Test Data.
- 7.58 Mickey, W. V., "Seismic Investigations of Missile Launchings", U. S. Dept. of Commerce, Coast and Geodetic Survey, Jan. 1962.
- 7.59 Sutherland, L. C., and Eldred, K. McK., "Estimating the Acoustic Loading on Building Structures Near Launch Sites", Wyle Laboratories, Paper Before Acoust. Soc. Am., Washington, D. C., Jun. 1965.
- 7.60 Wenzel, A., "Ground Motion Response to Acoustic Pressure Waves", Wyle Laboratories, Research Report WR 66-26, 1966.
- 7.61 White, J. E., "Seismic Waves", McGraw-Hill Book Co., N. Y., 1965.

- 7.62 Whitman, R. V., and Clark, G. B., "Nuclear Geoplosics - Part II - Mechanical Properties of Earth Materials", DASA Report 1285 (II), May 1964.
- 7.63 Willis, D. E., and Wilson, J. T., "Maximum Vertical Ground Displacement of Seismic Waves Generated by Explosive Blasts", Bull. Seismol. Soc. Am. 50, Jul. 1960, pp. 455-459.
- 7.64 Sutherland, L. C., "A Brief Review of the Impedance of Soil Presented to a Reaction Mass", Wyle Laboratories, Research Staff, Report WR 65-39, Dec. 1965.

**CHAPTER 8**  
**ACOUSTIC AND BLAST**  
**LOADS ON BUILDINGS**

TABLE OF CONTENTS

<u>SECTION</u>		<u>PAGE</u>
8.1	<u>ACOUSTIC EXCITATION AND RESPONSE OF BUILDING STRUCTURE</u> . . . . .	8-1
8.1.1	NET ACOUSTIC PRESSURE ON EXTERNAL WALLS . . . . .	8-1
8.1.1.1	Effective Sound Pressure on an Infinite Flexible Wall . . . . .	8-2
8.1.1.2	Effective Sound Pressure on Finite Size Rectangular Walls . . . . .	8-3
8.1.1.3	Net Acoustic Force on Rigid Unbaffled Obstacles . . . . .	8-7
8.1.1.4	Summary of Corrections for Reflection and Diffraction . . . . .	8-9
8.1.2	STRUCTURAL ACOUSTIC COUPLING . . . . .	8-9
8.1.2.1	Modal Response of Structure to Acoustic Excitation . . . . .	8-9
8.1.2.2	Joint Acceptance for Beams Under Acoustic Excitation by Plane Progressive Waves . . . . .	8-11
8.1.2.3	Joint Acceptance for Beams in a Reverberant Sound Field . . . . .	8-17
8.1.2.4	Joint Acceptance for Plates for Plane Progressive Waves . . . . .	8-19
8.1.2.5	Joint Acceptance for Plates in a Diffuse Sound Field . . . . .	8-22
8.1.2.6	Joint Acceptance for Cylindrical Structure . . . . .	8-22
8.1.3	VIBRO-ACOUSTIC RESPONSE OF BUILDING WALLS . . . . .	8-23
8.1.3.1	Specification of Excitation and Response Variables . . . . .	8-23
8.1.3.2	Response of a Simply-Supported Wall to a Plane Progressive Wave . . . . .	8-24
8.1.3.3	Maximum Fundamental Mode Response of a Panel for Grazing Incidence . . . . .	8-25
8.1.3.4	Maximum Fundamental Mode Response of a Panel for Normal Incidence . . . . .	8-26
8.1.3.5	Response of Higher Modes to Plane Progressive Waves and Diffuse Sound Fields . . . . .	8-28
8.1.3.6	Damping of Wall Vibration Response . . . . .	8-31
8.1.4	EMPIRICAL METHOD FOR PREDICTING VIBRO-ACOUSTIC RESPONSE . . . . .	8-32
8.1.4.1	Vibro-Acoustic Response of Full-Scale Structure . . . . .	8-33
8.1.4.2	Vibro-Acoustic Response of a Model Scale Building . . . . .	8-36
8.1.4.3	Empirical Prediction Procedures . . . . .	8-37
8.1.4.4	Acoustic Excitation of Bending Vibrations of Buildings . . . . .	8-40
8.1.5	EVALUATION OF ACOUSTIC FATIGUE OF BUILDING STRUCTURE . . . . .	8-40
8.1.5.1	Dynamic Stresses in Structure Subjected to Acoustic Loads . . . . .	8-41
8.1.5.2	Classical Method for Dynamic Stress Analysis . . . . .	8-41
8.1.5.3	The Modal Velocity Method for Predicting Dynamic Stresses . . . . .	8-42
8.1.5.4	Fatigue Damage for Acoustic Loads on Ground Structure . . . . .	8-43
8.2	<u>EXTERNAL BLAST LOADS ON BUILDINGS</u> . . . . .	8-46
8.2.1	DETERMINATION OF BLAST LOADS . . . . .	8-46
8.2.1.1	Loading on Rectangular Structures Without Openings . . . . .	8-46
8.2.1.2	Loading on Rectangular Structures with Openings More than 5 Percent and Less than 50 Percent of the Area of the Walls . . . . .	8-51
8.2.1.3	Loading on Rectangular Structures with Openings More than 50 Percent of the Area of the Walls . . . . .	8-56
8.2.1.4	Loading on Structures with Gabled Roofs . . . . .	8-57
8.2.1.5	Loading on Cylindrical Structures . . . . .	8-59
8.2.1.6	Loading on Domes . . . . .	8-62
8.2.1.7	Loading on Buried Structures . . . . .	8-63
8.2.2	COMPUTATION OF DYNAMIC STRUCTURAL RESPONSE . . . . .	8-67
8.2.2.1	Substitution of the Actual Building with a Spring-Mass System . . . . .	8-67
8.2.2.2	Idealization of the Load Acting on Structures . . . . .	8-73
8.2.2.3	Methods of Analyzing Dynamic System Response to Blast Loads . . . . .	8-73
8.2.3	NUMERICAL EXAMPLE . . . . .	8-80
8.3	<u>RESPONSE OF GROUND STRUCTURE TO SONIC BOOM LOADS</u> . . . . .	8-86
8.3.1	TYPE OF BUILDING DAMAGE CAUSED BY SONIC BOOMS . . . . .	8-86
8.3.1.1	Primary Structure for Industrial Buildings . . . . .	8-86
8.3.1.2	Residential Structure . . . . .	8-87

TABLE OF CONTENTS (CONTINUED)

<u>SECTION</u>		<u>PAGE</u>
8.3.2	CORRELATION OF MEASURED AND PREDICTED DYNAMIC STRESSES IN RESIDENTIAL STRUCTURE .....	8-87
8.3.2.1	Correlation of Measured Strain with Theoretical Shock Spectrum .....	8-88
8.3.2.2	Correlation of Measured Strain and Pseudo-Velocity .....	8-89
8.3.2.3	Correlation of Predicted and Observed Damage in Residential Structure for Sonic Boom Loads .....	8-89
8.3.3	WINDOW DAMAGE BY SONIC BOOMS .....	8-91
8.3.3.1	Static Failure Strength of Glass Windows .....	8-91
8.3.3.2	Failure Strength of Windows for Sonic Boom Loads .....	8-91
8.3.4	VALID DAMAGE CLAIMS FOR SONIC BOOM DAMAGE .....	8-93
	REFERENCES .....	8-93

## CHAPTER 8

### ACOUSTIC AND BLAST LOADS ON BUILDINGS

Three types of sonic loads on buildings are considered in this manual: acoustic noise from rocket engines, blast loads from propellant explosions, and overpressures from sonic booms. Therefore, this chapter is divided into three sections which treat the loading and primary structural response characteristics for each of these forms of sonic excitation. Chapter 3 discusses, in detail, the common analytical methods which are utilized for the various types of dynamic loads considered in this chapter. However, the practical design approaches are distinctly different for each form of dynamic loading. To emphasize these differences, a convenient separate numbering sequence is employed for figures, equations, and references throughout this chapter. Thus, Section 8.1 refers to acoustic loads, 8.2 refers to blast loads, 8.3 to sonic boom loads. The figures, equations and references are numbered accordingly in each subsection.

#### 8.1 ACOUSTIC EXCITATION AND RESPONSE OF BUILDING STRUCTURES

The basic concepts involved in the analysis of acoustic loads on building structures may be illustrated as shown in Figure 8.1.1.

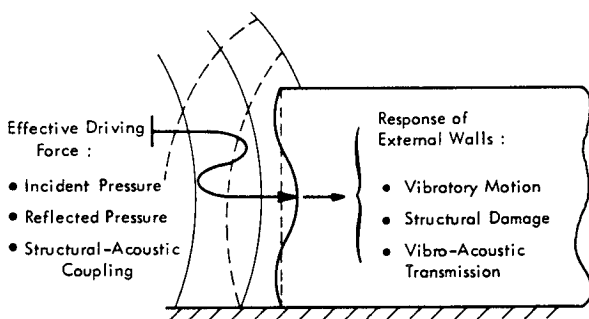


FIGURE 8.1.1 General Aspects of Acoustic Loads on External Walls of Buildings.

The problem breaks down into the essential elements illustrated, namely: (1) the determination of the effective acoustic driving force on the walls of the building, and (2) an evaluation of the resultant vibratory response and potential structural damage. A further breakdown of the primary variables involved in this problem may be outlined as follows:

#### • Effective Acoustic Force

##### ▲ Incident Sound Field

Varies with source and transmission path, including effect of nearby reflecting surfaces such as a ground plane (see Chapters 6 and 7).

##### ▲ Reflected Sound Field

Varies primarily with the ratio of acoustic wavelength  $\lambda$  to characteristic dimension  $L_c$  of the structure and secondarily with the incidence angle of the impinging sound wave.

##### ▲ Structural-Acoustic Coupling

Depends on the coupling between bending waves in the wall and the effective acoustic wavelength of the sound field. This coupling is defined by the joint acceptance or ratio of effective (generalized) force to the incident force on a rigid wall.

#### • Response of External Walls

##### ▲ Vibratory Motion

Proportional to the effective acoustic force and inversely proportional to the structural "impedance" (i.e., mass, damping or stiffness) of the wall.

##### ▲ Structural Damage

Varies with the peak structural displacement, velocity or acceleration, depending on the type of potential damage involved.

##### ▲ Vibro-Acoustic Transmission

Proportional to the vibratory motion of the wall, and dependent on the internal acoustic and vibration transmission paths inside the building (see Chapter 9).

It is assumed that methods such as those covered in Chapters 6 and 7 have been applied to define the incident sound field. It is also assumed that this pressure field is characterized by the type of wide-band random acoustic noise generated by a rocket engine exhaust. However, the design methods presented in this section can be applied to any form of acoustic excitation of ground structure.

#### 8.1.1 NET ACOUSTIC PRESSURE ON EXTERNAL WALLS

The first step in defining the effective acoustic force is to determine the net acoustic pressure on the external wall. This net pressure is the resultant of the incident pressure field and the reflected pressure field. If the wall is assumed to be perfectly rigid and to extend to infinity in both directions, the reflected pressure is just twice the incident pressure regardless of the angle of incidence of the sound wave. This is accounted for by adding 6 decibels (dB) to the estimated incident sound pressure level. (See Section 4.2.1 of Chapter 4 for definitions of sound pressure level and the decibel scale.) This simple rule is often adequate for preliminary design purposes. However, the resulting net acoustic pressure may be overly conservative. For problems requiring a more careful analysis, the reflected pressure field on a wall of finite flexibility and size needs to be considered. Examine first the net acoustic pressure on a wall of infinite extent but finite flexibility.



### 8.1.1.1 Effective Sound Pressure on an Infinite Flexible Wall

Consider the case illustrated in Figure 8.1.2 of a plane wave sound field impinging at normal incidence on a thin flexible wall extending to infinity in both directions. The following simple analysis shows that the acoustically induced motion of any surface is determined by defining the net excitation pressure as that which would exist if the surface were rigid.

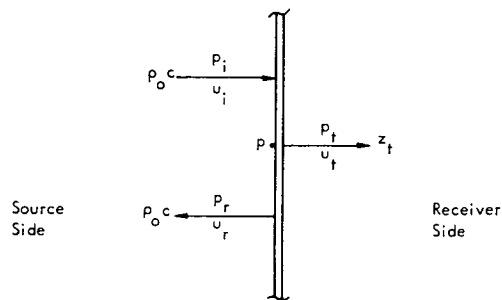


FIGURE 8.1.2 Plane Wave Sound Field Impinging on an Infinite Flexible Wall.

This principle can be demonstrated by analyzing the velocity of an infinite wall in terms of the incident acoustic pressure. The analysis utilizes some of the basic principles of acoustics which are developed in Chapters 4 and 9. If the wall is impervious, then the following boundary conditions can be defined.

- The arithmetic sum of the incident pressure ( $p_i$ ) and the reflected pressure ( $p_r$ ) equals the total pressure ( $p$ ) on the source side of the wall, or

$$p = p_i + p_r \quad (8.1.1)$$

- The vector sum of the particle velocities of the incident wave ( $u_i$ ) and the reflected wave ( $u_r$ ) must equal the velocity of the wall. This is also the initial particle velocity  $u_t$  of the transmitted sound wave with a pressure  $p_t$  on the opposite side of the wall, or

$$u_t = u_i + u_r \quad (8.1.2)$$

The following additional parameters can be defined:

- Specific acoustic impedance ( $\rho_0 c$ ) of the incident plane wave is the ratio of the pressure to particle velocity, or

$$\frac{p_i}{u_i} = \rho_0 c \quad (8.1.3)$$

- Specific acoustic impedance ( $-\rho_0 c$ ) of the reflected plane wave

$$\frac{p_r}{u_r} = -\rho_0 c \quad (8.1.4)$$

(The minus sign stems from the fact that the particle velocity of the reflected plane wave is opposite to the direction of the incident wave.)

- Specific acoustic impedance ( $z_t$ ) of the transmitted sound wave

$$\frac{p_t}{u_t} = z_t \quad (8.1.5)$$

- Specific transmission impedance ( $z_w$ ) of the flexible wall (the ratio of the net pressure differential across the wall to the wall velocity)

$$\frac{p - p_t}{u_t} = z_w \quad (8.1.6)$$

By combining Equations 8.1.2 - 8.1.4 to solve for the velocity  $u_t$  of the wall, and applying Equations 8.1.1 and 8.1.6 to eliminate  $p_r$  and  $p$ ,  $u_t$  can be expressed as

$$u_t = \frac{2 p_i - p_t - z_w u_t}{\rho_0 c}$$

Finally, using Equation 8.1.5 to eliminate  $p_t$  and solving for the wall velocity  $u_t$  in terms of the incident pressure gives

$$u_t = \frac{2 p_i}{z_w + z_t + \rho_0 c} \quad (8.1.7)$$

The result obtained verifies the statement made earlier that the motion of the infinite flexible wall can be defined in terms of the net pressure  $2 p_i$  that would be measured at the surface of a rigid infinite wall. The influence of the pressure radiated by the moving wall is accounted for by two impedance terms in the denominator of Equation 8.1.7 --  $\rho_0 c$ , which accounts for the reradiation by the moving wall on the source side; and  $z_t$ , which accounts for the radiation by the wall on the receiver side. Stated differently, the pressure on the surface of any flexible obstacle in a sound field is the sum of three components:

- The incident pressure,
- The pressure reflected by the obstacle when it is rigid, and
- The pressure radiated by the motion of the obstacle.

The effective pressure used to define this motion is the sum of the first two components. The last component is accounted for, as necessary, by adding radiation impedance terms to the structural impedance of the wall.

The effect of acoustic radiation loading on the acoustic response of a wall will be considered in detail later.

Measured Sound Pressures Near a Large Flexible Wall

The influence of wall motion on sound pressures measured near an acoustically driven flexible wall should be considered briefly since such measurements are frequently utilized for environmental prediction or testing. The ratio of the actual pressure (p) at the wall to the net pressure (2 p<sub>i</sub>) that would be observed for a perfectly rigid wall can be determined from the preceding equations. This ratio is:

$$\frac{p}{2 p_i} = \left[ \frac{z_w + z_t}{z_w + z_t + \rho_o c} \right] \quad (8.1.8)$$

Assume that the specific acoustic impedance on the receiver side (z<sub>t</sub>) is equal to ρ<sub>o</sub> c. Furthermore, let the specific transmission impedance of the wall be given by the complex form for a single degree of freedom system.

$$z_w = r + j \left( \omega m - \frac{k}{\omega} \right)$$

$$= \frac{\omega_n m}{Q_n} + j \omega m \left[ 1 - \left( \frac{\omega_n}{\omega} \right)^2 \right]$$

where

$\omega_n = \sqrt{k/m}$  - the natural frequency for the nth normal mode of the wall

$Q_n = \omega_o m/r$  - the resonance amplification factor for this natural mode

$m \approx$  effective surface mass density of the wall

$k = \omega_n^2 m$  - effective stiffness of the wall per unit area

$j = \sqrt{-1}$

$r =$  resistance of wall.

Equation 8.1.8 can then be expressed as

$$\frac{p}{2 p_i} = \frac{1 + \frac{\omega_n m}{\rho_o c Q} + \frac{j \omega m}{\rho_o c} \left[ 1 - \left( \frac{\omega_n}{\omega} \right)^2 \right]}{2 + \frac{\omega_n m}{\rho_o c Q} + \frac{j \omega m}{\rho_o c} \left[ 1 - \left( \frac{\omega_n}{\omega} \right)^2 \right]}$$

At resonance,  $\omega = \omega_n$ , and the reactive terms drop out. If  $\omega_n m/Q$  is much greater than 1 (i.e., heavy well-damped wall), then the ratio of the observed to rigid-wall pressure will be nearly equal to 1. On the other hand, for light-weight walls with low damping, for the lower order resonant modes,  $\omega_n m/Q$  may be much less than ρ<sub>o</sub> c. In the limit, the observed pressure at the wall could be 1/2 or 6 dB less than the effective value for a rigid wall.

Example

As an example, consider the change in observed sound pressure from the rigid wall value that would be measured at the surface of a 1/4" simply-supported steel plate with a fundamental resonance frequency of 20 Hz. The effective surface mass m can be assumed to be approximately 1/4 the actual surface mass density. The factor of 1/4 represents the generalized mass fraction for a simply-supported plate (see Chapter 3, Section 3.3.5.6). For a Q<sub>n</sub> of 25, and weight density for steel of 0.3 lb/in<sup>3</sup>, the quantity  $\omega_n m/Q_n$  would be  $(2\pi)(20)(1/4)(.3)(1/4)/(386) = 0.000244 \text{ lb-sec/in}^3$ . The specific acoustic impedance of air (ρ<sub>o</sub> c) is normally 0.00153 lb-sec/in<sup>3</sup> at 59°F. At resonance, the ratio of the observed pressure to the rigid wall value would be

$$\frac{p}{2 p_i} = \frac{1 + .000244/.00153}{2 + .000244/.00153} = 0.536$$

This corresponds to a decrease of 5.4 dB below the rigid wall value of 1.0. For excitation frequencies of resonance, the ratio p/2 p<sub>i</sub> will be very nearly equal to 1.

Thus, sound levels measured very near a large acoustically driven flexible wall will deviate from the rigid wall values by 0 to 6 dB in the manner illustrated in Figure 8.1.3. Therefore, an improved estimate of the effective driving pressure on a surface, obtained from measured sound levels in a wide-band random noise field, would correspond to an upper envelope of the observed frequency spectrum. Sharp "valleys" in the spectrum at the resonance frequencies of the wall would be ignored.

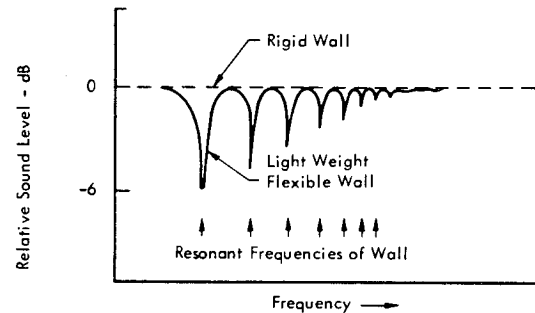


FIGURE 8.1.3 Illustration of Deviation of Sound Pressure Level Measured at Surface of Infinite Flexible Wall from Rigid-Wall Values. Maximum deviation is 6dB for Lower Resonance Frequencies of Light Weight Walls with Low Damping.

8.1.1.2 Effective Sound Pressure on Finite Size Rectangular Walls

So far, the wall has been assumed to be infinite in extent. Consider now, the effective pressure on a rigid wall of finite size located on one side of a building and immersed in a plane wave sound field. Due to diffraction effects, the total incident plus reflected pressure would no longer be just twice the incident pressure. Instead, the total pressure would exhibit the following general trend as a function of the ratio of a characteristic wall dimension L<sub>c</sub> to the acoustic wavelength λ.

- For  $L_c/\lambda < 0.2$

Total pressure  $\rightarrow$  incident pressure on all sides.

- For  $0.2 < L_c/\lambda < 1.0$

Total pressure varies from 0.25 to 3 times incident pressure on all sides. This corresponds to a variation of -14 to +9.5 dB.

- For  $1.0 < L_c/\lambda < 4.0$

Average total pressure  $\sim 2 \rightarrow 2.5$  times incident pressure on wall facing sound field (+6 to +8 dB).

Average total pressure  $\sim 0.25 \rightarrow 1.0$  times incident pressure on opposite wall (-14 to 0 dB).

Average total pressure  $\sim 0.5 \rightarrow 1.5$  times incident pressure on walls and roof at grazing incidence to sound field (-6 to +3.5 dB).

These approximate trends are based on detailed experimental results reported in Reference 8.1.1. They clearly indicate the wide range of variation that can occur on the surfaces of a three-dimensional obstacle due to the effects of diffraction. Therefore, a more detailed examination of these data is desirable.

#### Diffraction for Rectangular Obstacles

As reported in Reference 8.1.1, measurements were made of the sound pressure level relative to free field levels on the face of a 25 cm (0.82 ft) rigid cube and a rectangular parallelepiped resting on a ground plane. The rectangular parallelepiped consisted of two 25 cm cubes stacked vertically. The sound levels measured on the surface of these rigid obstacles were then compared to the pressure in the incident plane sound wave to define the total incident plus reflected pressure on a typical three-dimensional rectangular obstacle. Similar data from earlier theoretical and experimental studies on diffraction of cubes did not adequately define the diffracted sound field over exposed faces of rectangular obstacles on the ground (References 8.1.2 and 8.1.3). Results from a recent theoretical study of the diffraction for a free cube, reported in Reference 8.1.4, provided more detailed theoretical support for experimental data in Reference 8.1.1 on the variation in sound pressure over the surface of a cubical obstacle. The theoretical approach to the problem is the classical one which establishes the sound field reflected from an obstacle by requiring that the sum of the particle velocities for the incident and reflected fields be zero at the rigid surface of the obstacle (Reference 8.1.2).

The more significant results from these studies are summarized in Figures 8.1.4 - 8.1.6. The relative change in sound pressure level due to diffraction is shown as a function of the ratio of the height ( $a$ ) of the cube to the acoustic wavelength  $\lambda$ . This is equivalent to a normalized frequency  $f a/c$  where  $c$  is the velocity of sound.

Figure 8.1.4 shows this diffraction correction at three typical locations on the front face of a cubical obstacle for normal incidence of a plane incident sound wave. Both

experimental results from Reference 8.1.1 and theoretical results from Reference 8.1.4 are illustrated.

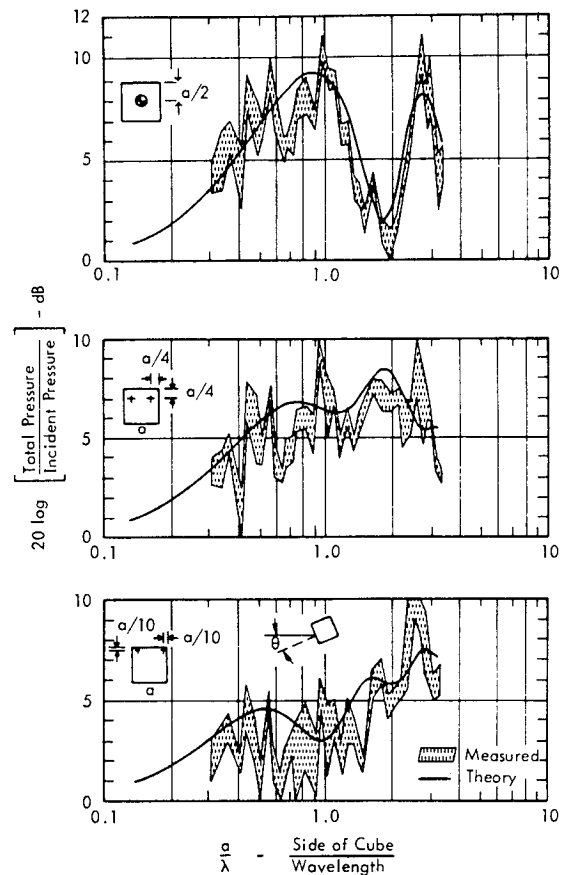


FIGURE 8.1.4 Experimental and Theoretical Diffraction Effect on Front Face of Cubical Obstacle (Measured with Cube on Ground, Theory for Cube in Free Space,  $\theta = 0^\circ$ , Data from Reference 8.1.1 and 8.1.9).

The experimental results show a general trend in agreement with the theory. However, there are significant differences due to reflection from the ground plane and from the other faces of the cube. This was neglected in the theoretical calculations. Note that diffraction causes the observed pressure to be as much as 10 dB above the incident pressure at the center. Contours of constant values of the measured diffraction correction are shown in Figure 8.1.5 for the front, side and back of the cube for an incidence angle  $\phi$  of  $0^\circ$  in the front face (i.e., normal incidence). Similar diffraction correction contours for the stacked cubes are shown in Figure 8.1.6. Note that for the cubical obstacle, the sound pressure on the rear face, for  $a/\lambda = 0.5$ , reaches a maximum of 6 dB above the incident sound level. This is analogous to the optical "bright spot" on the back of a disk, illuminated by a light beam (Reference 8.1.2).

Reference 8.1.1 reports additional diffraction measurements for incidence angles other than normal (i.e.,  $\phi \neq 0^\circ$ ) on the front wall. The general trend of this data is similar to that shown in Figures 8.1.4 - 8.1.6.

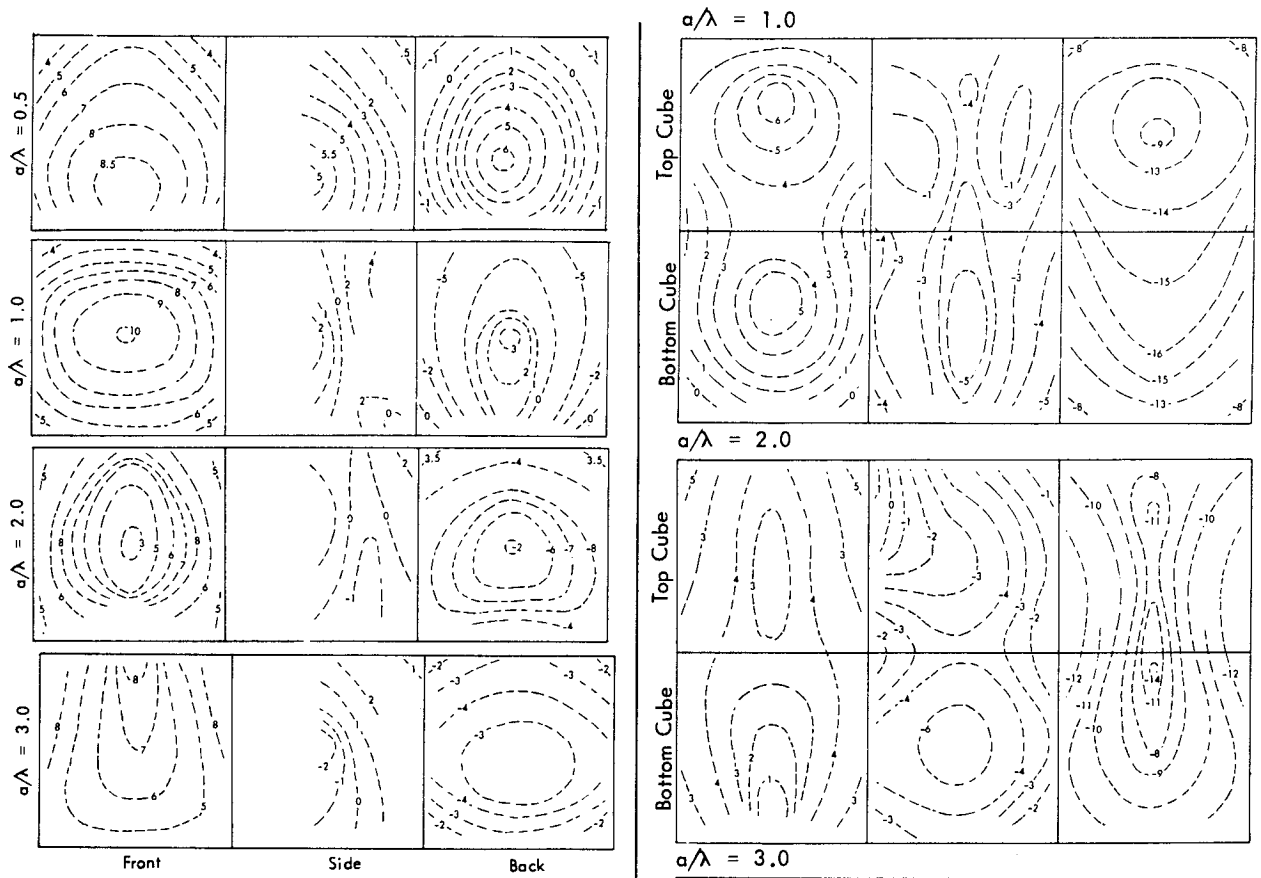


FIGURE 8.1.5 Contours of Equal Sound Pressure Levels Relative to the Incident Pressure at the Center of Cube - Single Cube Obstacle on Ground, Normal Incident on Front Face.

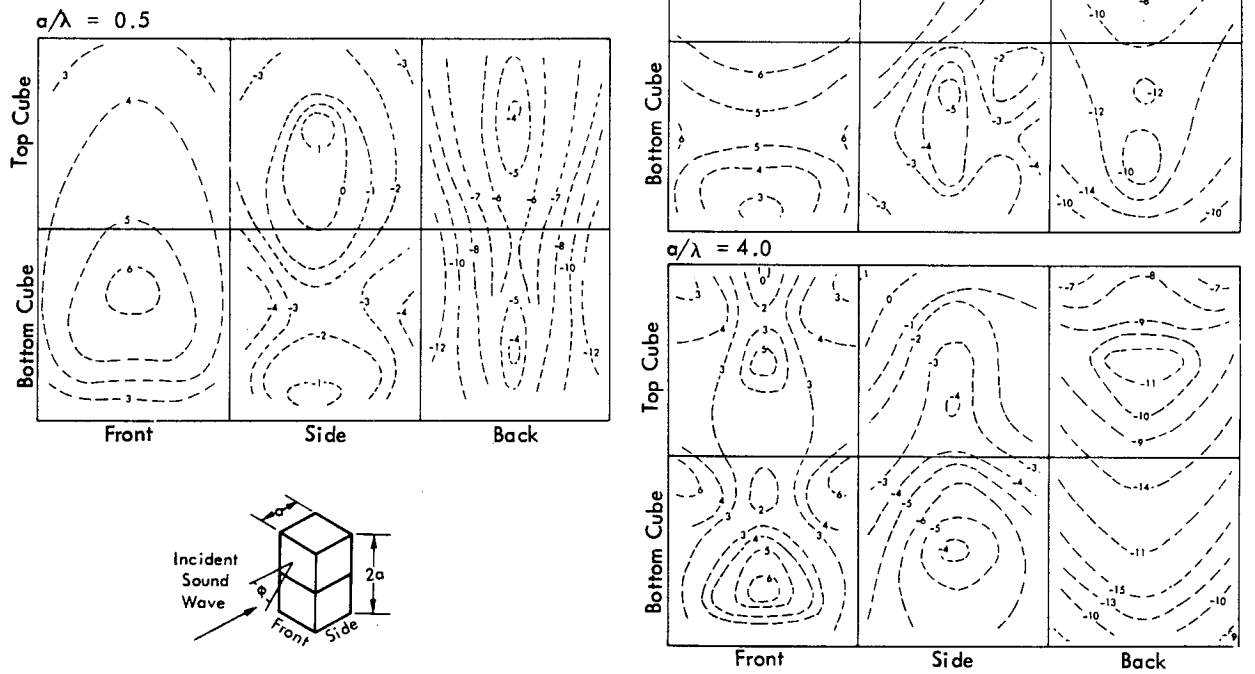
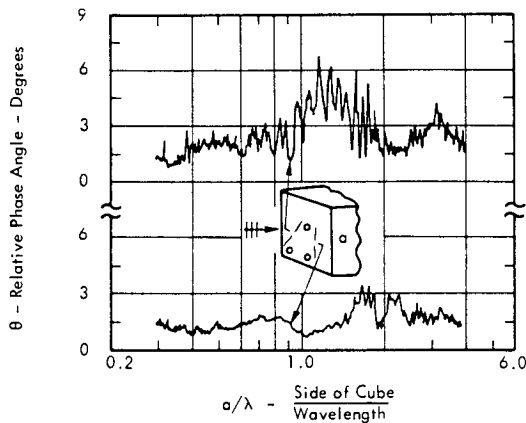


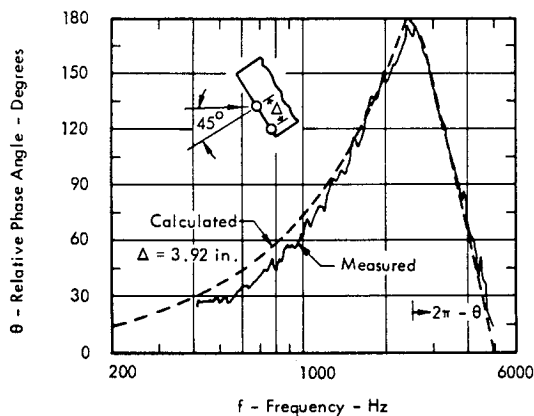
FIGURE 8.1.6 Contours of Equal Sound Pressure Level Relative to Incident Pressure at the Center of the Lower Cube - Double Cube Obstacle on Ground

Phase Variation of Total Pressure on Obstacle

The phase angle between the sound pressures at various points on the front, side, and rear face of the cubical obstacle were also reported in Reference 8.1.1. For normal incidence on the front face, the phase angle varied significantly above the normal  $0^\circ$  phase shift that would be observed in an ideal incident plane wave front. This variation, illustrated in Figure 8.1.7a for two typical pairs of points, is attributed to the combined effects of ground reflection and diffraction. However, at an incidence angle of  $45^\circ$  in the front face, the observed phase angle,  $\theta$ , between various points agreed closely with the expected value  $\theta = 2\pi \Delta/c$  due to the propagation delay over a path length  $\Delta$  in the direction of the incident wave which travels with the velocity  $c$ . A typical result for this case is illustrated in Figure 8.1.7b.



a) Phase Shift on Front Face for Normal Incidence



b) Phase Shift on Front Face per  $45^\circ$  Incidence

FIGURE 8.1.7 Phase Shift Between Total Pressure at Pairs of Points on Front Face of Cubical Obstacle on Ground in Plane Wave Sound Field (Data from Reference 8.1.1)

For incidence angles of  $90^\circ$  or greater, the phase shift in the total pressure across the surface of an obstacle varied widely due to the marked effects of diffraction and ground reflection. Generalizations are not practical in this case.

The effect of a varying phase across any one wall of the obstacle will tend to reduce the effective acoustic driving force for the lowest vibration motion of this wall. The effect on higher modes will be complex. For some modes, the change in phase could increase the effective driving force, and for others decrease it. This suggests that in defining the effective or generalized acoustic force at the higher modes of a building wall, it would be reasonable to assume that the phase varies randomly over the surface. The implications of this concept will be considered in a later section.

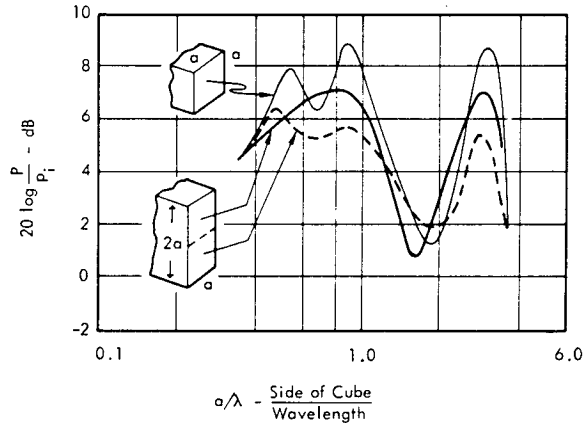


FIGURE 8.1.8 Diffraction Effect Observed at Center of One Face of Single Cube and Center of Upper and Lower Half of Double Stacked Cubes for Normally Incident Plane Waves. (From Reference 8.1.1)

Characteristic Diffraction Length

Figure 8.1.8 shows the average diffraction effect observed at the center of one face of a single cube and at the center of the upper and lower halves of the stacked cubes. The strong similarity in all three curves indicates that, to a first approximation, the characteristic diffraction length  $L_c$  for any rectangular wall can be taken as the minimum dimension (width or height) of the wall. It will be shown later in Section 8.2 that this same rule applies to the diffraction of blast waves striking a wall face-on. In this case, the so-called "clearing time" required for a reflected overpressure wave to reduce to the incident blast wave is also determined by the minimum dimension of the wall.

The results illustrated in Figures 8.1.4 - 8.1.6 and 8.1.8, may be used to estimate the net pressure on closed rectangular surface. In particular, for the worst case of a wall facing the incident sound wave, an average diffraction correction may be estimated based on the preceding conclusion about a characteristic length and the diffraction effect for rectangular structure. A recommended design value for the average diffraction effect on rectangular obstacles is shown in Figure 8.1.9. Ignoring phase, deviations from this average correction at particular locations on the wall will generally be less than  $\pm 3$  dB.

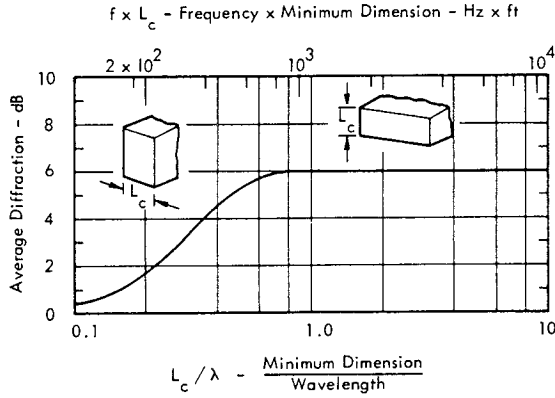


FIGURE 8.1.9 Average Diffraction Correction to be Added to Incident Sound Pressure Level on Front Face of Enclosed Rectangular Walls to Determine Effective Sound Pressure Level for Normally Incident Plane Waves.

8.1.1.3 Net Acoustic Force on Rigid Unbaffled Obstacles

The configuration treated in the last section assumed that the wall was baffled so that no sound waves reached its back side. It is also necessary to consider the net acoustic force acting on open-type structures or obstacles which are not baffled. One example of such a configuration would be the type of open frame structure employed for service towers, or arming towers, near launch sites. Such primary structures are not ordinarily subject to sonic fatigue damage. However, acoustically induced vibration can be significant for environmental design of frame-mounted equipment.

An approximate analytical approach to the problem is possible by treating the unbaffled shapes as infinite cylinders or spheres. The theory for the net acoustic force acting on these rigid obstacles in a plane wave sound field is well documented in the literature (References 8.1.5 - 8.1.7). The essential details of this theory are reviewed in Chapter 4. The analysis is carried out in essentially the same classical manner as for the rigid plate, the essential difference being the coordinate system used to define the sound pressure reflected from a cylindrical or spherical surface. For either case, the total instantaneous pressure at any point  $y$  on the surface is the sum of the instantaneous incident pressure  $p_i(y, t)$  and the reflected pressure  $p_r(y, t)$ . The net force  $P(t)$  is the integral over the obstacle surface of the product  $[p_i(y, t) + p_r(y, t)] \times$  [local area normal to the direction of incident wave]. This may be represented by the integral

$$P(t) = \oint_A [p_i(y, t) + p_r(y, t)] \cdot d\vec{A}_n \quad (8.1.10)$$

where

$d\vec{A}_n$  = normal component of differential element of surface area at point  $y$ .

Total Force on Cylinder in a Plane Wave Sound Field

The ratio of the amplitude  $P$  of the total net force per unit length to the amplitude of the "incident force" per unit length ( $d p_i$ ) is shown in Figure 8.1.10 for a cylinder of diameter  $d$  in a plane wave sound field. This net force varies as a function of the dimensionless frequency parameter  $f d/c = d/\lambda$  where  $f$  is the frequency,  $d$  is the cylinder diameter,  $c$  is the speed of sound in air, and  $\lambda$  is the acoustic wavelength. The ratio  $P/d p_i$  reaches a value of 2.15 for  $f d/c = 1/\pi$  or  $\pi d/\lambda = 1$  (Reference 8.1.5). Thus, when the wavelength is equal to the circumference of the cylinder, the net force is slightly greater than twice the product of the incident pressure times the normal area per unit length ( $d$ ).

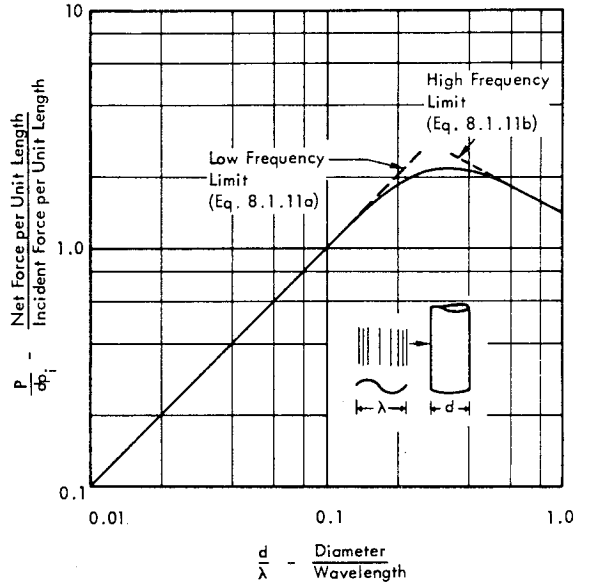


FIGURE 8.1.10 Net Acoustic Force Per Unit Length on Rigid Cylinder Relative to Incident Force of Plane Wave at Normal Incidence. (From Reference 8.1.5).

• Low Frequency Limit

At low frequencies, where  $\pi f d/c \ll 1$ , the net force is approximately equal to

$$P \approx \pi^2 \left[ \frac{f d}{c} \right] \cdot [d p_i] \quad \pi f d/c \ll 1 \quad (8.1.11a)$$

where  $f d/c = d/\lambda$

• High Frequency Limit

At high frequencies, where  $\pi f d/c \gg 1$ , the net force is approximately equal to

$$P \approx \sqrt{\frac{2c}{f d}} [d p_i] \quad \pi f d/c \gg 1 \quad (8.1.11b)$$

Each of these limiting approximations is shown in Figure 8.1.10.

A simple approximation for the low frequency limit of this net force can also be developed for application to any two-dimensional obstacle. Let the pressure of an incident sinusoidal sound wave at the point on the cylinder nearest to the source be given by

$$p_i(0, t) = p_i \cos \omega t$$

The circumferential distance between this point and the opposite side of the cylinder is  $\pi d/2$ . If this is considered to be an effective difference in path length between the incident pressures at these points, then the pressure at the back side will be

$$p_i \left( \frac{\pi d}{2}, t \right) = p_i \cos (\omega t - \pi \omega d/2c)$$

where  $c$  = speed of sound in air.

Assume the net force per unit length  $P(t)$  on the cylinder is equal to the difference between these two pressures times the normal area per unit length which is

$$P(t) = d p_i [\cos (\omega t - \pi \omega d/2c) - \cos \omega t]$$

$$P(t) = 2 d p_i \sin \left( \frac{\pi \omega d}{4c} \right) \cos \left( \omega t - \frac{\pi \omega d}{4c} \right)$$

For low frequencies where  $\omega d/2c = \pi f d/c \ll 1$ , then  $\sin (\pi \omega d/4c) \approx \pi \omega d/4c$  so that the amplitude of this force is approximately equal to

$$P \approx \pi^2 [f d/c] [d p_i] \pi f d/c \ll 1 \tag{8.1.12}$$

This is the same net force found for the low-frequency limit by the exact solution (Equation 8.1.11a). Thus, a simple estimate for the amplitude of the net acoustic force per unit length on any two-dimensional un baffled obstacle in a plane wave sound field could be given by

$$P \approx \pi \left[ \frac{f S}{c} \right] [A_n p_i] f S/c \ll 1 \tag{8.1.13a}$$

where

$S$  = circumference of obstacle

$A_n$  = frontal area per unit length.

Cast in a different form, the ratio of the net pressure  $P/A_n$  to the incident pressure is

$$\frac{P/A_n}{p_i} \approx \left[ \frac{\pi f S}{c} \right] = \left[ \frac{\pi S}{\lambda} \right] \pi f S/c \ll 1 \tag{8.1.13b}$$

The quantity in brackets shows that the net force on un baffled obstacles in a normally incident sound field varies directly with frequency when the acoustic wavelength exceeds the circumference of the obstacle. Based on a detailed analysis in Reference 8.1.8 of the diffraction of

sound for infinite cylinders, the effect of an incidence angle other than  $90^\circ$  to the cylinder axis may be accounted for by multiplying the circumferential path length  $S$  by  $(\cos \beta)$ .  $\beta$  is the angle between the normal to the cylinder axis and the direction of an incident plane wave.

Total Force on Sphere in a Plane Wave Sound Field

Three-dimensional obstacles can be simulated by a rigid sphere. The absolute amplitude of the net force per unit area on a sphere, relative to the incident pressure  $p_i$  in a plane wave sound field, can be given in closed form by the expression

$$\frac{P}{p_i (\pi d^2/4)} = \frac{2\pi f d/c}{\sqrt{1 + 4 (\pi f d/2c)^4}} \tag{8.1.14}$$

where

$P$  = total acoustic force on sphere

$d$  = diameter of sphere

$f$  = frequency

$c$  = speed of sound.

This is simplified but exact form of the more complex expression normally given in the literature for the acoustic force in rigid spheres (see Section 4.5.1.2 in Chapter 4). This expression is compared in Figure 8.1.11 on a decibel scale with the result given earlier for the cylinder. The basic similarity of the diffraction effect for the two obstacles is clear. For the sphere, the low and high frequency limits are readily determined from Equation 8.1.14.

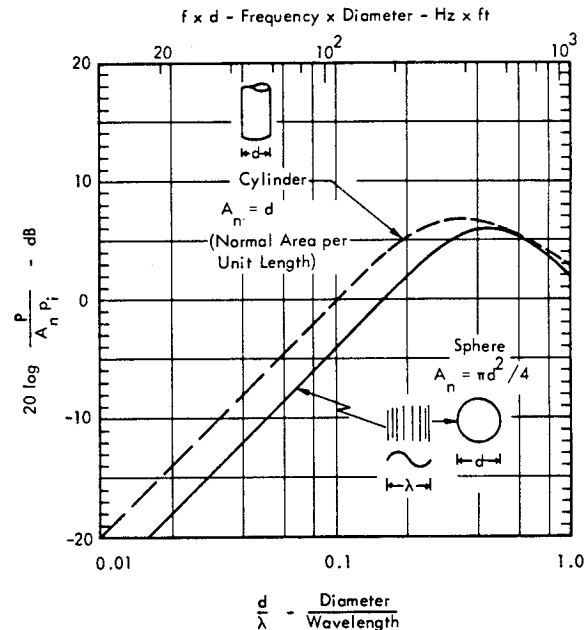


FIGURE 8.1.11 Net Acoustic Force  $P$  in Rigid Sphere, Relative to Incident Pressure  $p_i$  times Area  $A_n$  Normal to Plane Wave Compared to Same Ratio for Cylinder. (From Figure 8.1.10).

- Low Frequency Limit, for  $\pi d/\lambda \ll 1$ ,

$$\frac{P}{p_i (\pi d^2/4)} \approx 2\pi [fd/c]$$

- High Frequency Limit, for  $\pi d/\lambda \gg 1$ ,

$$\frac{P}{p_i (\pi d^2/4)} \approx \frac{4}{\pi} [fd/c]$$

#### 8.1.1.4 Summary of Corrections for Reflection and Diffraction

The following simplified rules summarize the average corrections to be applied to incident sound pressure levels on structures to account for reflection and diffraction effects. The corrections are defined according to the product of the frequency  $f$  in Hz and a characteristic length in feet.

- Enclosed building walls with shortest dimension,  $L_c$  in ft

▲ For  $f \cdot L_c < 700$ , add correction specified by Figure 8.1.9 to incident sound pressure level.

▲ For  $f \cdot L_c > 700$ , add 6 dB to incident sound pressure level.

▲ See Figures 8.1.4 – 8.1.6 for detailed estimates of variations in sound pressure levels over walls.

- Unbaffled two-dimensional structural members with circumference  $S$ , in feet, in plane wave sound field at normal incidence.

▲ For  $f \cdot S < 700$ , multiply incident pressure by  $fS/350$  to define effective acoustic pressure, or add

$$[20 \log_{10} (f \cdot S) - 51 \text{ dB}]$$

to incident sound pressure level (SPL).

▲ For  $700 < f \cdot S < 1750$ , multiply incident pressure by 2.0 to define acoustic pressure, or add 6 dB to incident SPL.

▲ For  $f \cdot S > 1750$ , multiply incident pressure by  $85/\sqrt{fS}$  to define effective acoustic pressure, or add

$$[38.5 - 10 \log (f \cdot S)] \text{ dB}$$

to incident SPL.

- Unbaffled three-dimensional obstacles with average circumference  $S$ , in feet, in plane wave sound field.

▲ For  $f \cdot S < 1100$ , multiply incident pressure by  $fS/550$  to define effective acoustic pressure, or add

$$[20 \log (f \cdot S) - 56 \text{ dB}]$$

to incident SPL.

▲ For  $1100 < f \cdot S < 2250$ , multiply incident pressure by 2 to define effective pressure, or add 6 dB to incident SPL.

▲ For  $f \cdot S > 2250$ , multiply incident pressure by  $4500/fS$

to define effective pressure, or add

$$[73 - 20 \log (f \cdot S)] \text{ dB}$$

to incident SPL.

It is important to recognize that the simplified treatment of diffraction discussed in this section has taken little or no account of the phase of the total pressure acting on the structure. Only the changes in amplitude of the incident pressure due to reflection or diffraction have been considered. One example of the validity of this simplified approach is given in Figure 11.9, page 11-12 of Chapter 11. This shows how the change in the measured acoustic vibration response of a simple structural panel, with and without a baffle, is predicted on the basis of diffraction theory for a rigid cylinder. Without a baffle, the panel response decreases due to the decrease in net pressure or force per unit area when the panel span ( $d$ ) is much less than the acoustic wavelength (see Figure 8.1.10). Additional experimental data will be considered later in this chapter to illustrate the diffraction correction applicable for a finite panel in a rectangular building. The effect of phase or correlation of the net pressure on a panel surface must now be considered in more detail in order to define the acoustic vibration response of flexible structure.

## 8.1.2 STRUCTURAL ACOUSTIC COUPLING

A simple analysis of the response of an infinite flexible wall to a normally incident plane wave, derived in Section 8.1.1.1, defined the effective driving pressure on an infinite flexible wall. However, a more general approach is now required to determine the vibro-acoustic response of finite walls. Specifically, it is necessary to employ the concepts developed in detail in Chapter 3, Section 3.3, on the normal mode response of complex structures to distributed sinusoidal and random loads.

### 8.1.2.1 Modal Response of Structure to Acoustic Excitation

To illustrate the application of these concepts to acoustic excitation, consider the case shown in Figure 8.1.12 of a beam of length  $L$  loaded by a uniformly distributed acoustic pressure  $p(y, t) = p \cos(2\pi ft)$ . The beam is mounted in an infinite baffle so that no diffraction effects are present. (It will be assumed throughout the remainder of this section that the amplitude  $p$  of the pressure acting on the structure is actually 2 times the amplitude  $p_i$  of the incident pressure.) The displacement response  $x(y, t)$  at any point  $y$  along the beam can be described by the summation of the displacements in its infinite number of normal modes by

$$x(y, t) = \sum_n q_n(t) \phi_n(y) \quad (8.1.16)$$

where

$q_n(t)$  = instantaneous displacement of the normal coordinate for the  $n$ th normal mode

$\phi_n(y)$  = relative mode shape for  $n$ th mode at point  $y$ . (Throughout this manual, mode shapes are normalized to a maximum value of unity.)



The equation of motion for the forced response of the nth normal mode is specified by (see Equation 3.222, page 3-64)

$$\ddot{q}_n(t) + 2 \delta_n \omega_n \dot{q}_n(t) + \omega_n^2 q_n(t) = \frac{F_n(t)}{M_n} \quad (8.1.17)$$

where

$\delta_n = 1/2 Q_n$ , critical damping ratio for nth mode

$\omega_n = 2\pi f_n$  = natural frequency of nth mode

$F_n(t) = b \int_0^L p(y,t) \phi_n(y) dy$  - the generalized force for the nth mode

$b p(y,t) dy$  = differential force on the beam over the length  $dy$  where  $p(y,t)$  is the pressure and  $b$  is the beam width

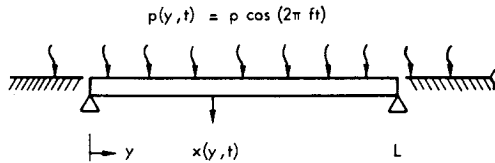


FIGURE 8.1.12 Uniformly Distributed Acoustic Pressure Acting on Beam Mounted in an Infinite Baffle.

**Sinusoidal Excitation**

For a steady state sinusoidal excitation, the solution to this equation of motion for one mode was shown to be (Section 3.3.3.5)

$$q_n(t) = \frac{P_o J_n(f) |H_n(f)| \cos \cdot (2\pi f_n t - \theta_n)}{\omega_n^2 M_n} \quad (8.1.18)$$

where

$P_o = b \int_0^L p(y) dy$  = amplitude of total sinusoidal force on beam (without regard to phase of pressures along beam)

$J_n(f) = \frac{b}{P_o} \int_0^L p(y) \phi_n(y) dy$  - joint acceptance or amplitude of the generalized force  $F_n$  to the total force  $P_o$

$|H_n(f)| = 1 / \sqrt{[1 - (f/f_n)^2]^2 + (2\delta_n f/f_n)^2}^{1/2}$   
 = the dynamic magnification factor for the nth mode

$\theta_n = \tan^{-1} \frac{2\delta_n f/f_n}{1 - (f/f_n)^2}$  - the phase angle for the response in the nth mode.

For the case of a simply supported beam, illustrated in Figure 8.1.12, the mode shape  $\phi_n(y) = \sin(\pi n y/L)$  where  $n=1,2,3$ , etc. If the pressure acts uniformly and in phase at all points on the beam, then  $P_o = pbL$  and the joint acceptance is

$$J_n(f) = \frac{1}{L} \int_0^L \sin\left(\pi n \frac{y}{L}\right) dy$$

$$= -\frac{1}{\pi n} [\cos \pi n - 1] = \begin{cases} \frac{2}{\pi n}, & n = \text{odd} \\ 0, & n = \text{even} \end{cases}$$

Note that the convention is adopted in this chapter of using the frequency argument ( $f$ ) for the joint acceptance parameter  $J_n(f)$ . In Chapter 3, this notation was reserved for joint acceptance with random excitation. However, it has been pointed out in Section 3.3.3.10 of Chapter 3 that, for analysis purposes, the joint acceptance parameter is the same for either sinusoidal or stationary random excitation.

The total instantaneous displacement at  $y$  is obtained by inserting Equation 8.1.18 back into Equation 8.1.16 and carrying out the summation over all modes. However, a more convenient measure of the total response is given by the mean square value which is

$$\overline{x^2(y,t)} = \lim_{T \rightarrow \infty} \frac{1}{T} \int_{-T/2}^{+T/2} x^2(y,t) dt \quad (8.1.19)$$

This mean square sinusoidal response at the excitation frequency  $f$  is made up of two parts; the sum of the mean square response in each mode, and the sum of the cross-mode responses. It has been shown that cross mode response terms are generally negligible for excitation at the natural frequencies of a multi-mode system (see Section 3.3.3.6, Chapter 3). Thus, for practical purposes, the mean square displacement at point  $y$  on the beam is given, to a close approximation, by just the summation of the mean square responses in each mode (see Equation 3.249, page 3-78)

$$\overline{x^2(y,t)} = \frac{1}{2} \overline{x^2(y)} \approx \frac{1}{2} P_o^2 \sum_n \frac{J_n^2(f) |H_n(f)|^2 \phi_n^2(y)}{\omega_n^4 M_n^2} \quad (8.1.20a)$$

where

$X(y)$  = amplitude of total sinusoidal displacement at  $y$ .

The corresponding mean square acceleration at this point is

$$\overline{\ddot{x}^2(y,t)} = \frac{1}{2} \overline{\ddot{x}^2(y)} \approx \frac{1}{2} P_o^2 \sum_n \frac{J_n^2(f) (f/f_n)^4 |H_n(f)|^2 \phi_n^2(y)}{M_n^2} \quad (8.1.20b)$$

The joint acceptance squared  $J_n^2(f)$  is now equal to the mean square generalized force  $\overline{F_n^2(t)}$  to the mean square total sinusoidal force  $\frac{1}{2} p_o^2$ .

According to the definition given with Equation 8.1.17, the generalized force  $F_n(t)$  may be considered as the summation of all the elemental generalized forces

$$b p(y, t) \phi_n(y) \Delta y$$

acting on each beam segment having an area  $b \Delta y$ . The mean square value of this summation will then consist of the time-averaged product of two such summations and may be expressed as

$$\overline{F_n^2(t)} = b^2 \left[ \overline{p(y_1, t) \phi_n(y_1) + p(y_2, t) \phi_n(y_2) + \dots} \right] \\ \times \left[ \overline{p(y_1, t) \phi_n(y_1) + p(y_2, t) \phi_n(y_2) + \dots} \right] \Delta y^2$$

As noted earlier, the bar signifies a long time average. The product of these force "summations" (which become integrals in the limit as  $\Delta y \rightarrow 0$ ) must include all possible cross product terms for different points on the beam, such as

$$p(y, t) \phi_n(y) \cdot p(y', t) \phi_n(y') \quad \text{where } y \neq y'$$

Thus, when expressed in integral form, the mean square value of this generalized force, normalized by the mean square value of the total value  $\frac{1}{2} p_o^2$  becomes the joint acceptance squared  $J_n^2(f)$  given by

$$J_n^2(f) = \frac{b^2}{\frac{1}{2} p_o^2} \int_0^L \int_0^L \overline{p(y, t) p(y', t)} \phi_n(y) \phi_n(y') dy dy'$$

where

$$\overline{p(y, t) p(y', t)} = \text{long time average of the product of the pressures at two general positions } y \text{ and } y' \text{ along the beam.}$$

For all cases to be considered, the amplitude of the pressure  $p(y)$  at each point will be assumed to be a constant ( $p$ ). Thus, the mean square value of the total force  $\frac{1}{2} p_o^2$  on the beam is  $\frac{1}{2} p^2 (bL)^2$  and the joint acceptance squared can be expressed in the simpler form

$$J_n^2(f) = \frac{1}{L^2} \int_0^L \int_0^L \overline{R_p}(y, y', f) \phi_n(y) \phi_n(y') dy dy' \quad (8.1.21)$$

The term  $\overline{R_p}(y, y', f)$  is the (narrow band) space correlation coefficient for the points  $y$  and  $y'$  of a frequency  $f$ . For a sinusoidal acoustic wave with a constant pressure amplitude  $p$  traveling over the beam, this is defined by

$$\overline{R_p}(y, y', f) = \frac{\overline{p(y, t) p(y', t)}}{\frac{1}{2} p^2} \quad (8.1.22)$$

#### Random Excitation

When the acoustic excitation consists of random noise, the mean square response for sinusoidal excitation at a single frequency is replaced by its equivalent for random loads, the power spectral density  $W_x(y, f)$ . This defines, in effect, the mean square value of the response at point  $y$  with a 1 Hz bandwidth centered about the frequency  $f$ .

The total mean square sinusoidal force  $\frac{1}{2} p_o^2$  is also replaced by the corresponding power spectral density of the random force  $W_o(f) = W_p(f) \cdot (bL)^2$ . In this case,  $W_p(f)$  is the constant power spectral density of the pressure on the beam at the frequency  $f$ . When these changes are incorporated into Equation 8.1.20a or 8.2.20b, the response to random excitation is readily defined. For example, the power spectral density of the acceleration response at  $y$  for a distributed random load (neglecting cross-mode coupling terms) is:

$$W_{\ddot{x}}(y, f) = W_o(f) \sum_n \frac{J_n^2(f) (f/f_n)^4 |H_n(f)|^2 \phi_n^2(y)}{M_n^2} \quad (8.1.23)$$

Note that the expression for joint acceptance squared for sinusoidal excitation (Equation 8.1.21) can still be used to predict the response to random excitation. An alternate and more general method for defining joint acceptance for random excitation is discussed in detail in Section 3.3.3.11 of Chapter 3. This method is applied when the spatial correlation of the pressure field is determined by measuring its cross-power spectral density. This method is not utilized in this chapter.

In this brief review of the basic modal response equations the principal objective has been to focus attention on the joint acceptance parameter. This is the key factor which defines the structural acoustic coupling characteristics between acoustic excitation and the structural response (Reference 8.1.9). The following section gives a detailed analysis of joint acceptance for a variety of structural elements under acoustic loading. For convenience, the term joint acceptance squared will be abbreviated as simply joint acceptance from here on.

#### 8.1.2.2 Joint Acceptance for Beams Under Acoustic Excitation by Plane Progressive Waves

The instantaneous pressure  $p(y, t)$  in a plane progressive wave traveling in the  $y$  positive direction over a beam lying along the same axis may be described by

$$p(y, t) = p \cos [2\pi f t - 2\pi y/\lambda] \quad (8.1.24)$$

where

- $p$  = amplitude of the pressure wave
- $f$  = frequency - Hz
- $\lambda = c/f$  - the acoustic wavelength
- $c$  = speed of sound.

For a more general situation, consider the case illustrated in Figure 8.1.13 where a plane wave impinges on the beam at an angle  $\psi$  from the vertical. It is assumed that the latter is mounted in an infinite baffle. As indicated by the figure, the effective or trace wavelength  $\lambda_t$  along the beam is now stretched out and is defined by

$$\lambda_t = \lambda / \sin \psi$$

Thus, replacing  $\lambda$  in Equation 8.1.23 by  $\lambda_t$ , the pressure along the beam is simply

$$p(y,t) = p \cos [2\pi f t - 2\pi y / \lambda_t] \quad (8.1.25)$$

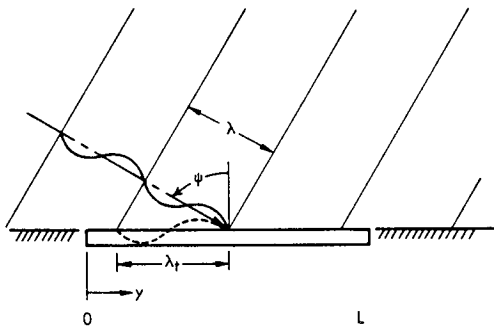


FIGURE 8.1.13 Acoustic Excitation of a Beam by a Plane Progressive Wave with a Wavelength  $\lambda = c/f$  Traveling at an Angle  $\psi$  to the Vertical.

Applying Equation 8.1.22, the space correlation coefficient for this constant amplitude traveling wave is the time averaged product of  $p(y,t)$  and  $p(y',t)$  normalized by the product of their rms values. This can be expressed as

$$\bar{R}_p(y,y',t) = \cos [2\pi (y - y') / \lambda_t] \quad (8.1.26)$$

where

$$\lambda_t = \lambda / \sin \psi = c / f \sin \psi, \text{ and}$$

$$c / \sin \psi = \bar{c}, \text{ trace or propagation velocity of wave across beam.}$$

The joint acceptance can now be determined for any beam configuration by substituting this expression for the space correlation coefficient back into Equation 8.1.21.

Rigid Beam

For a rigid beam which moves vertically up and down like a piston, the mode shape corresponds to a rigid body or zero-frequency mode and is equal to 1. Thus, the joint acceptance for the rigid beam is

$$J_o^2(f) = \frac{1}{L^2} \int_0^L \int_0^L \cos \frac{2\pi (y - y')}{\lambda_t} dy dy' \quad (8.1.27)$$

$$= \left[ \frac{\sin \pi L / \lambda_t}{\pi L / \lambda_t} \right]^2$$

This is plotted in Figure 8.1.14 as a function of the ratio of beam length to trace wavelength  $L / \lambda_t = (fL \sin \psi) / c$ . The ordinate scale is given numerically as  $J_n^2$  or in decibel form as  $10 \log J_n^2$ . The upper envelope of this curve is defined by

$$L / \lambda_t \ll 1 / \pi, \quad J_n^2(f) \approx 1.0$$

$$L / \lambda_t \gg 1 / \pi, \quad J_n^2(f) \approx \left[ \frac{\pi L}{\lambda_t} \right]^2 = \left[ \frac{\pi f L \sin \psi}{c} \right]^2$$

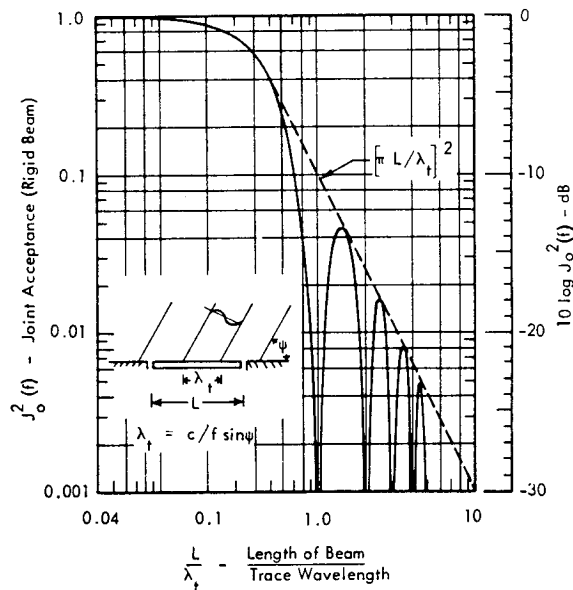


FIGURE 8.1.14 Joint Acceptance Squared for Plane Progressive Wave Traveling Over Rigid Beam with Trace Wavelength  $\lambda_t$ .

Whenever the number of trace wavelengths on the beam is equal to an integer  $n$  or  $L / \lambda_t = 1, 2, 3, \text{ etc.}$ , the average pressure over the beam is zero so that the joint acceptance or relative generalized force is zero.

Simply-Supported Beam

The mode shape for the simply-supported beam can be expressed in the form

$$\phi_n(y) = \sin n\pi y/L$$

or as

$$\phi_n(y) = \sin 2\pi y/\lambda_{Bn}$$

where

$\lambda_{Bn} = 2L/n = c_B/f_n$  - the bending wavelength in the  $n$ th mode of a simply-supported beam (see Section 3.3.5.4 of Chapter 3), and

$c_B$  = bending wave velocity in beam.

Substituting the first form into Equation 8.1.21 and using Equation 8.1.26 for the space correlation coefficient, it can be shown that the joint acceptance for simply-supported beams is given by (Reference 8.1.9)

$$J_n^2(f) = \frac{2}{(n\pi)^2} \left[ \frac{1}{1 - \left(\frac{2L/n}{\lambda_t}\right)^2} \right]^2 \left[ 1 - \cos n\pi \cos(2\pi L/\lambda_t) \right] \tag{8.1.28}$$

This expression is plotted in Figure 8.1.15 as a function of the beam length to trace wavelength ratio  $L/\lambda_t$  with mode numbers  $n = 1$  to 10 as a parameter. In this figure, part a shows the joint acceptance for the odd modes of the simply supported beam and part b shows the even modes. Full curves are shown for modes 1, 2, 9 and 10; while only prominent peaks are indicated for the other 6 modes. Envelopes for the upper bounds of these complex curves may be approximated as follows:

Odd Modes

- $L/\lambda_t = \frac{fL \sin \psi}{c} < 0.2$ ,  $J_n^2(f)_{\max} \approx \left(\frac{2}{n\pi}\right)^2$
- $L/\lambda_t = \frac{n}{2}$ ,  $J_n^2(f)_{\max} \approx \frac{1}{4}$
- $L/\lambda_t \gg \frac{n}{2}$ ,  $J_n^2(f)_{\max} \approx \left(\frac{n}{2\pi}\right)^2 / \left(\frac{L}{\lambda_t}\right)^4$

Even Modes

- $L/\lambda_t < 0.2$ ,  $J_n^2(f) \rightarrow \left(\frac{2L}{n\lambda_t}\right)^2$
- $L/\lambda_t = \frac{n}{2}$ ,  $J_n^2(f)_{\max} \approx \frac{1}{4}$
- $L/\lambda_t \gg \frac{n}{2}$ ,  $J_n^2(f)_{\max} \approx \left(\frac{n}{2\pi}\right)^2 / \left(\frac{L}{\lambda_t}\right)^4$

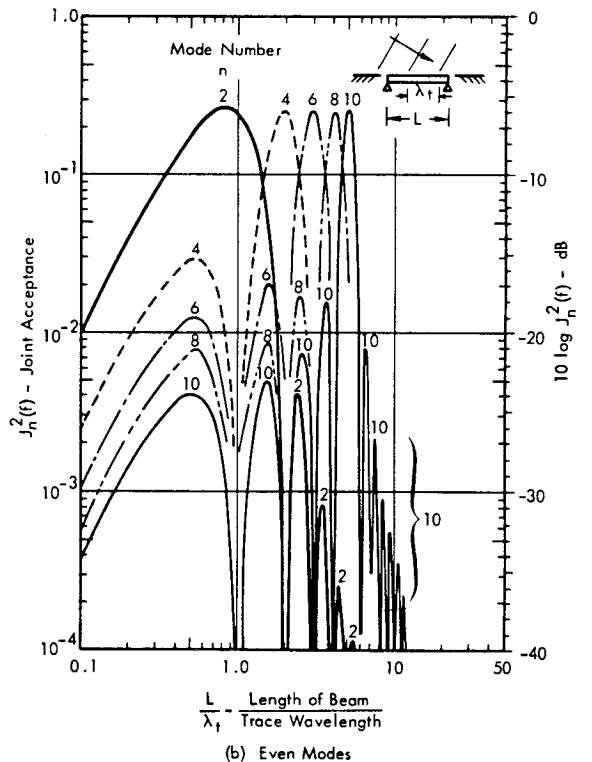
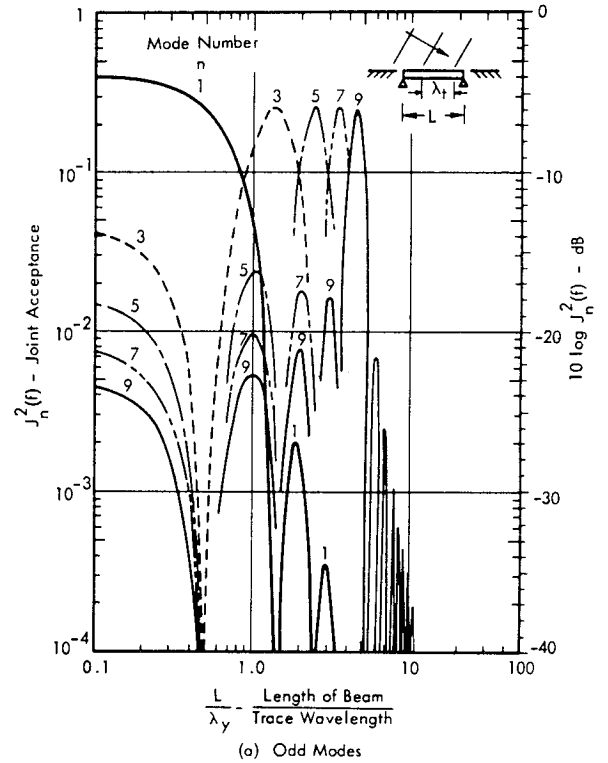


FIGURE 8.1.15 Joint Acceptance for Simply Supported Beam in a Plane Progressive Wave Field

When the incidence angle  $\psi$  approaches  $0^\circ$  (i.e., normal incidence) the trace wavelength  $\lambda_t$  approaches infinity and pressure over the panel is uniformly in-phase at all points. The joint acceptance then approaches the expected value for this type of normal loading (see Section 3.3.6.2). In this case, for  $L/\lambda_t \rightarrow 0$ , even modes are not excited so that  $J_n^2(f) = 0$  for  $n = \text{even}$ , while  $J_n^2(f) = (2/n\pi)^2$ .

Coincidence Effect for Simply Supported Beams

For all modes except the fundamental mode, the joint acceptance approaches a maximum value at coincidence. For a given angle of incidence  $\psi$ , coincidence occurs when the trace wavelength  $\lambda_t = c/f \sin \psi$  of the acoustic excitation is just equal to the bending wavelength  $\lambda_B$  in the beam. For the  $n$ th mode of a simply-supported beam, the bending wavelength,  $\lambda_{Bn}$  is equal to  $2L/n$  so that, at coincidence for this boundary condition,

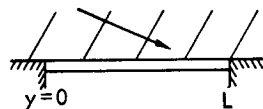
$$\frac{L}{\lambda_t} = \frac{n}{2} \tag{8.1.29}$$

An examination of Figure 8.1.15 will show that the maximum joint acceptance for all modes above the fundamental occurs very near this value of  $L/\lambda_t$ . (Both the denominator and numerator of Equation 8.1.18 for the joint acceptance approach zero for  $L/\lambda_t = n/2$ . However, in the limit, a finite value of 1/4 is obtained. The true maximum value of  $J_n^2(f)$  for  $n \geq 2$  is slightly greater than 1/4 and occurs for  $L/\lambda_t$  slightly less than  $n/2$ .)

To develop a better understanding of the physical concepts involved in acoustic excitation of structure, it is useful to view the joint acceptance curves in Figure 8.1.15a as representing weighting functions for wavelength filters. The effective (or generalized) acoustic force acting on each normal of the beam is attenuated by this "filtering effect" at frequencies for which the acoustic and structural bending wavelengths do not coincide. This effect is emphasized by replotting some of the joint acceptance curves of Figure 8.1.15 as a function of the ratio of structural bending wavelength  $\lambda_{Bn} = 2L/n$  to acoustic trace wavelength  $\lambda_t$ . This form, shown in Figure 8.1.16, illustrates more dramatically the major influence of the coincidence or wave matching effect on the relative acoustic force acting on each mode.

Practical aspects of the effect of coincidence on the response of structure to noise will be considered later in this chapter and in Chapter 9. Consider, now, joint acceptance values for other types of structural elements.

Clamped-Clamped Beams



The mode shape for the clamped-clamped beam can be specified in a general form by

$$\phi_n(\bar{y}) = A_n [\phi(K_n L)]$$

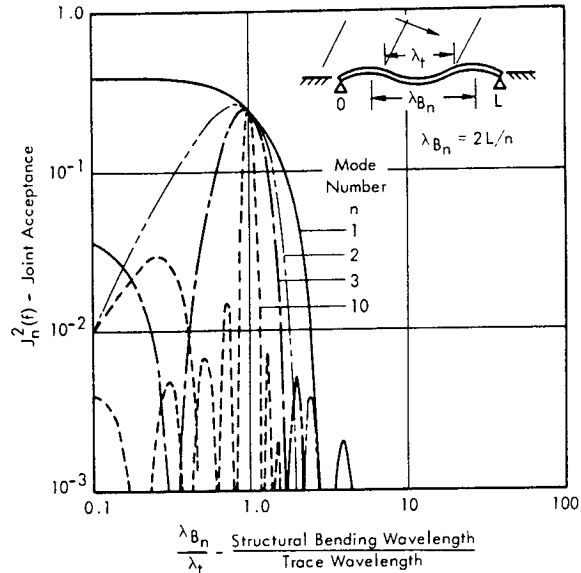


FIGURE 8.1.16 Joint Acceptance for Simply Supported Beam in Progressive Wave Field. (Plotted in terms of structural/acoustic wavelength ratio to emphasize wave filtering effect.)

where

$\phi$  = A general mode shape function of the frequency parameter which is defined in Section 3.3.5.4 of Chapter 3.

$\omega_n$  = natural frequency for  $n$ th mode of beam

$c_B, \lambda_{Bn}$  = velocity of bending waves and bending wavelength, respectively, for  $n$ th mode of the beam

$A_n$  = normalizing constant which reduces the general mode shape function to unit value at the point of maximum deflection, defined in Section 3.3.5.4 of Chapter 3.

The joint acceptance for this case has been evaluated analytically and numerically in Reference 8.1.10. The solution is carried out in the same manner as for the simply supported beam using Equation 8.1.21.

Due to the complexity of the final result for this case, only the approximate envelope for frequencies near or below coincidence is considered. Values for this envelope are specified below in terms of the ratio of beam length  $L$  to trace wavelength and the normalizing constant  $A_n$  for the mode shape of clamped-clamped beams.

Odd Modes

•  $L/\lambda_t = \frac{fL \sin \psi}{c} \rightarrow 0$

- ▲ First Mode  $J_1^2(f)_{\max} = 0.275$
- ▲ Higher Modes<sup>(1)</sup>  $J_n^2(f)_{\max} \approx \left[ \frac{64 A_n^2}{[(2n+1)\pi]^2} \right]_{n=3,5,7..}$

- $L/\lambda_t \approx \frac{n}{2} + \frac{1}{4}, n > 1$   $J_n^2(f)_{\max} \approx 0.21$   
(Coincidence)

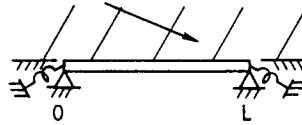
Even Modes

- $L/\lambda_t \rightarrow 0(1)$   $J_n^2(f)_{\max} \approx \frac{32 A_n^2}{[2n+1]^2} \left(\frac{L}{\lambda_t}\right)^2$   $n=2, 4, 6, \dots$

- $L/\lambda_t \approx \frac{n}{2} + \frac{1}{4}$   $J_n^2(f)_{\max} \approx 0.21$   
(Coincidence)

(1) For  $n \geq 2$ , normalizing constant  $A_n \approx 0.661$

Partially Clamped Beams



A general evaluation of the natural frequencies of beams resting on rigidly mounted pinned supports but with varying rotational and fixity was covered in Section 3.3.5. of Chapter 3. These results were taken for a study reported in Reference 8.1.11 which also included a numerical evaluation of the joint acceptance for such beams. The rotational end fixity ranged from zero restraint at both ends through fully clamped at one end only to fully clamped at both ends. The envelope of the resulting joint acceptances are given in Figure 8.1.17a, b and c.

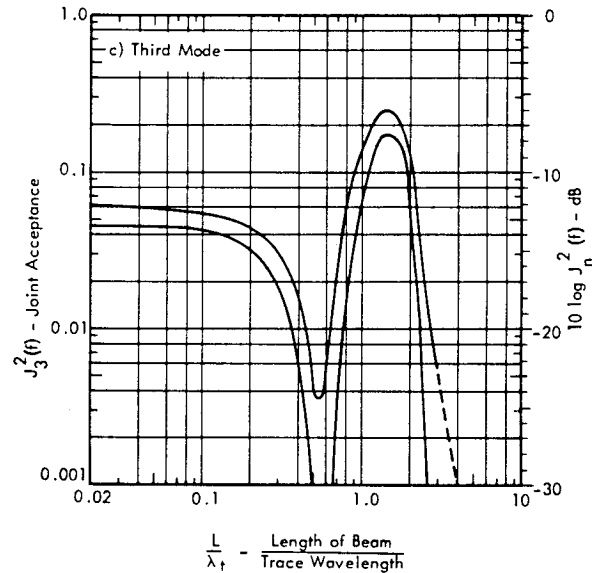
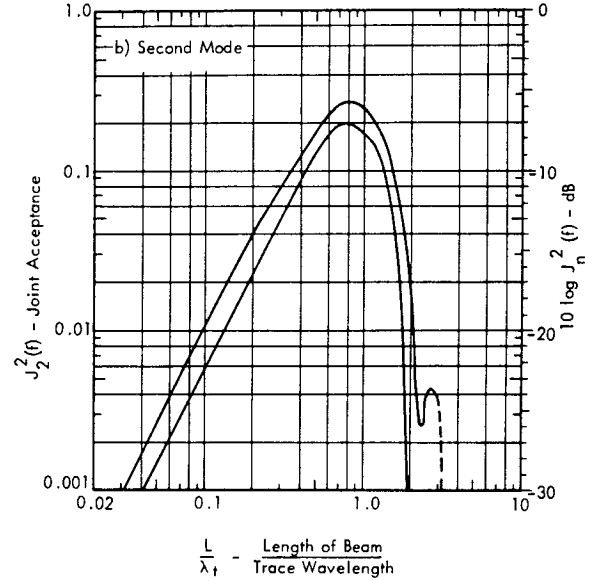
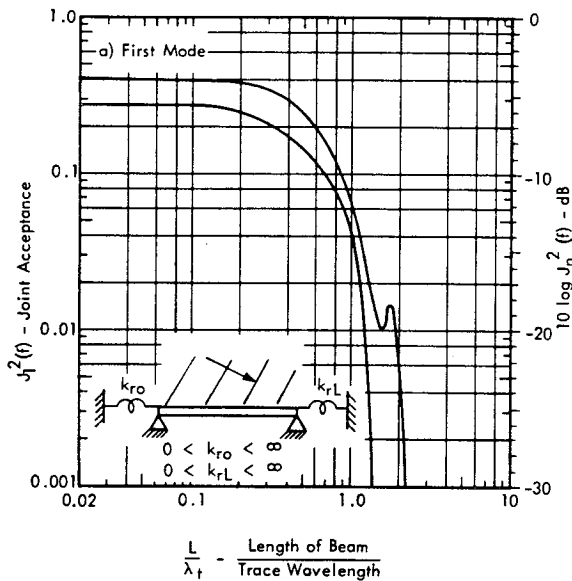
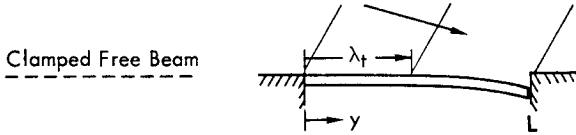


FIGURE 8.1.17 Envelope of Joint Acceptance for First Three Modes of a Beam on Simple Supports but with Rotational End Fixity Ranging from Free at Both Ends to Fully Clamped at Both Ends. (Data from Reference 8.1.11)

Comparing the values shown in these figures with those for the simply supported beam (Figure 8.1.15), it is apparent that the latter form an approximate upper bound for these envelopes which include the case for the fully clamped beam. The maximum values for joint acceptance in Figure 8.1.15 are therefore recommended for frequencies at or below coincidence for any beam element with partial fixity at either end. It will be shown later that above coincidence, a higher value of joint acceptance than shown in Figures 8.1.15 - 8.1.17 should be used. However, for most of the practical problems of interest for this manual, the frequency range of interest is generally below coincidence.

Beams with One End Free or Guided

The joint acceptance for the special case of a beam with one free or guided end provides an estimate of the structural acoustic coupling to the fundamental mode of a building. The following expressions for joint acceptance are shown graphically in Figure 8.1.18. The results will be applied in a later section in this chapter.



The fundamental mode shape was approximated by

$$\phi_1(y) \approx 1 - \cos\left(\frac{\pi y}{2L}\right)$$

Using this expression for the mode shape in Equation 8.1.21, and applying Equation 8.1.26 for the space correlation for a plane wave, the joint acceptance can be shown to be

$$J_1^2(f) = \frac{(2/\pi)^2}{1 - 16\alpha^2} \left[ \frac{1 - 8\alpha^2}{8\alpha^2} + \frac{2}{1 - 16\alpha^2} - \frac{\cos 2\pi\alpha}{8\alpha^2} - \frac{\sin 2\pi\alpha}{2\alpha(1 - 16\alpha^2)} \right] \quad (8.1.30)$$

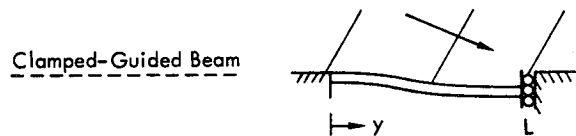
where  $\alpha = L/\lambda_t = fL \sin \psi / c$ , the ratio of beam length to trace wavelength.

The limiting values for this expression are

•  $L/\lambda_t = \frac{fL \sin \psi}{c} \rightarrow 0, \quad J_1^2(f) \rightarrow \left[1 - \frac{2}{\pi}\right]^2 = 0.132$

•  $L/\lambda_t \gg 1 \quad J_1^2(f) \rightarrow \frac{1}{4\pi^2} \left/ \left(\frac{L}{\lambda_t}\right)^2\right.$

Following the same method, the following additional cases can be defined.



• Approximate Shape of Fundamental Mode

$$\phi_1(y) \approx \frac{1}{2} [1 - \cos \pi y/L]$$

• Joint Acceptance

$$J_1^2(f) = \left(\frac{2}{\pi}\right)^2 \left[ \frac{1 - \cos 2\pi\alpha}{32\alpha^2} + \frac{\alpha^2(1 + \cos 2\pi\alpha)}{4(1 - 4\alpha^2)^2} \right] \quad (8.1.31)$$

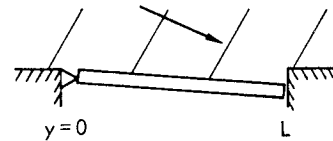
where  $\alpha = L/\lambda_t$

• Limiting Values

▲  $L/\lambda_t \rightarrow 0, \quad J_1^2(f) \rightarrow \frac{1}{4}$

▲  $L/\lambda_t \rightarrow \infty, \quad J_1^2(f) \rightarrow \frac{1}{2\pi^2} \left/ \left(\frac{L}{\lambda_t}\right)^2\right.$

Pinned-Free Beam



• Mode Shape

$$\phi_1(y) = y/L \quad (\text{Rigid Body Mode})$$

• Joint Acceptance

$$J_1^2(f) = \left(\frac{2}{\pi}\right)^2 \left( \frac{1}{16\pi^2\alpha^4} \right) \left[ \frac{1 - \cos 2\pi\alpha}{2} + \pi\alpha(\pi\alpha - \sin 2\pi\alpha) \right] \quad (8.1.32)$$

where  $\alpha = L/\lambda_t$

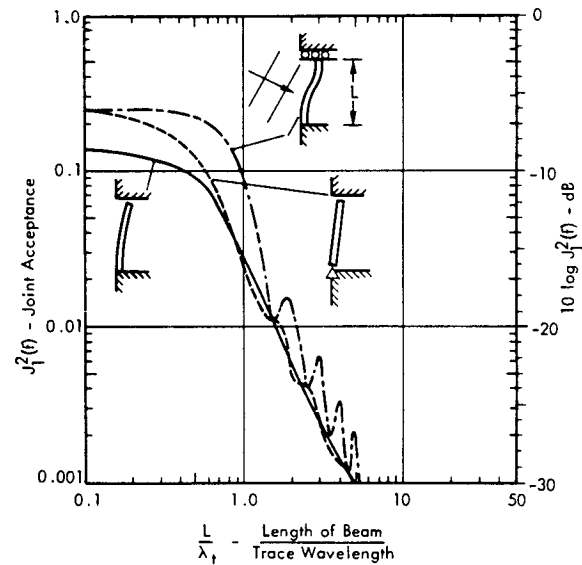


FIGURE 8.1.18 Joint Acceptance for The Fundamental Mode of Beams with One End Free or Guided - An Approximation for the First Bending Mode of Tall Buildings Subjected to Acoustic Excitation.

• Limiting Values

$$\begin{aligned} \triangle L/\lambda_t \rightarrow 0, & \quad J_1^2(f) \rightarrow \frac{1}{4} \\ \triangle L/\lambda_t \rightarrow \infty, & \quad J_1^2(f) \rightarrow \frac{1}{4\pi^2} \left/ \left( \frac{L}{\lambda_t} \right)^2 \right. \end{aligned}$$

The limiting values for long trace wavelengths (approaching normal incidence) are somewhat less than for the fundamental mode of a pinned-pinned beam for which  $J_1^2(f) \approx 0.4$ . For short trace wavelengths (or high frequencies), the joint acceptance for these beam configurations decreases inversely as the square of the ratio  $L/\lambda_t$  instead of the fourth power as for the simply-supported beam.

8.1.2.3 Joint Acceptance for Beams in a Reverberant Sound Field

Structure exposed to a reverberant sound field is subjected to a very large number of pressure waves arriving at random from many directions, such as illustrated conceptually in Figure 8.1.19. If each wave has a constant amplitude, or more precisely, if the energy incident on the structure from each direction is constant and the correlation between the waves arriving from any two directions is zero, then the space correlation of the pressure acting on the structure can be defined analytically. This makes it possible to compute the joint acceptance for a structure exposed to such a sound field. This ideal type of reverberant sound field is called a diffuse field and serves as a reasonable approximation for many practical cases of sound fields inside enclosures with low sound absorption (see Chapter 9). As suggested earlier in Section 8.1.1.2, it may also be considered as a conservative approximation for external sound field on a building at high frequencies where the building dimensions are much greater than the acoustic wavelength. At these frequencies, diffraction and ground reflection effects tend to cause a random vibration in the phase of the total incident plus reflected pressure on the external walls of the buildings.

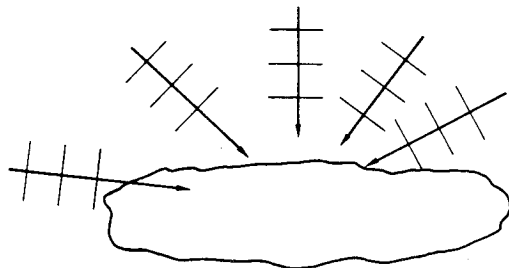


FIGURE 8.1.19 Reverberant Sound Field Consisting of an Infinite Number of Plane Waves Arriving at All Possible Angles.

Narrow Band Space Correlation for a Random Diffuse Field

Consider the case illustrated in Figure 8.1.20 for just one out of all possible waves in a diffuse sound field. The wave is assumed to be sinusoidal with a frequency  $f$  and to arrive at a given point  $y$  on a surface with an angle of in-

cidence  $\gamma$  relative to the line  $y - y'$ . If the incident plus reflected pressures at  $y$  for any two of these sinusoidal waves are identified as  $p_1(y, t)$  and  $p_2(y, t)$ , the total instantaneous pressure at  $y$  for these two waves is the sum  $p_1(y, t) + p_2(y, t)$ . The space correlation function  $R_p(y, y', f)$  along the line  $y - y'$  will be the time-averaged product

$$R_p(y, y', f) = \overline{[p_1(y, t) + p_2(y, t)] [p_1(y', t) + p_2(y', t)]}$$

If the phase coherence or correlation between these two waves is a random variable, then on the average, the cross-product terms in this correlation function will be zero. The space correlation function for the randomly phased waves will simply be the sum of the space correlation functions for each wave or

$$R_p(y, y', f) = \overline{p_1(y, t) p_1(y', t)} + \overline{p_2(y, t) p_2(y', t)}$$

Since the amplitude of each wave in a diffuse sound field is constant, then the space correlation coefficient for one wave arriving at an angle  $\gamma$  will be (See Equation 8.1.26)

$$\overline{R}_p(y, y', f) = \cos [2\pi f (y - y') (\cos \gamma)/c]$$

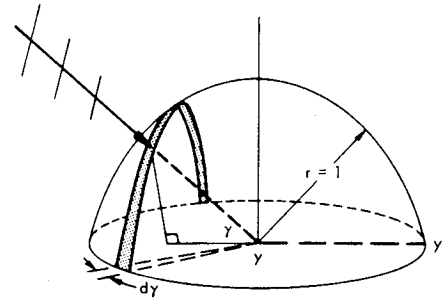


FIGURE 8.1.20 Illustration of One Out of an Infinite Number of Plane Waves in a Diffuse Sound Field Arriving at an Angle  $\gamma$  Relative to a Line  $y - y'$ . Space correlation coefficient along  $y - y'$  for this wave is  $\cos [2\pi f (y - y') (\cos \gamma)/c]$

The space correlation for all the waves can then be determined as follows. All waves which pass through point  $y$  must also pass through an imaginary unit hemisphere centered on  $y$  which has an area  $A = 2\pi(1)^2$ . The total number of waves through  $y$  which arrive at an incidence angle  $\gamma$ , must be proportional to the area of the surface element  $dA = \pi \sin \gamma d\gamma$  which is intersected by these waves. (See Figure 8.1.10). Therefore, the space correlation coefficient for the waves at an angle  $\gamma$  is weighted by the ratio  $\frac{dA}{A} = \frac{1}{2} \sin \gamma d\gamma$ . Thus, summing up overall values of  $\gamma$  from 0 to  $\pi$  the overall space correlation is given by the integral

$$\overline{R}_p(y, y', f) = \frac{1}{2} \int_0^\pi \cos [2\pi f (y - y') (\cos \gamma)/c] \sin \gamma d\gamma$$



Carrying out this integration provides the following simple form for the space correlation coefficient for a diffuse field.

$$\overline{R}_p(y, y', f) = \frac{\sin [2\pi \Delta y / \lambda]}{2\pi \Delta y / \lambda} \quad (8.1.33)$$

where  $\Delta y = (y - y')$  - the separation distance between  $y$  and  $y'$   
 $\lambda =$  the acoustic wavelength.

An equivalent form of this expression has been illustrated in Figure 3.73a page 3-94.

Joint Acceptance for Simply-Supported Beams in a Diffuse Sound Field

The joint acceptance for simply-supported beams in a diffuse sound field has been evaluated in detail in Reference 8.1.12. The closed expression for  $J_n^2(f)$  was derived from Equation 8.1.21 using the above expression for the space correlation coefficient. Details of the derivation, which employed a special coordinate transformation are omitted here. The final expression, for a simply supported beam of length  $L$ , is

$$J_n^2(f) = \frac{1}{(2\pi m)^2 L/\lambda} \left[ C_{in} \left\{ \pi \left( m + \frac{2L}{\lambda} \right) \right\} - C_{in} \left\{ \pi \left( m - \frac{2L}{\lambda} \right) \right\} \right] + \frac{1}{4\pi L/\lambda} \left[ S_i \left\{ \pi \left( m + \frac{2L}{\lambda} \right) \right\} - S_i \left\{ \pi \left( m - \frac{2L}{\lambda} \right) \right\} \right] + \frac{1}{(m\pi)^2} \left[ \frac{1 - (-1)^m \cos(2\pi L/\lambda)}{1 - (2L/m\lambda)^2} \right] \quad (8.1.34)$$

where  $C_{in}(v) = \int_0^v \frac{1 - \cos z}{z} dz$  (cosine integral)

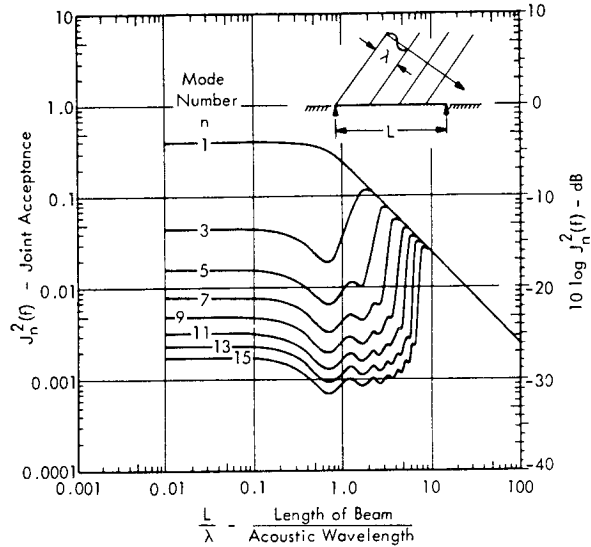
$S_i(v) = \int_0^v \frac{\sin z}{z} dz$  (sine integral)

$\lambda = c/f$  - acoustic wavelength

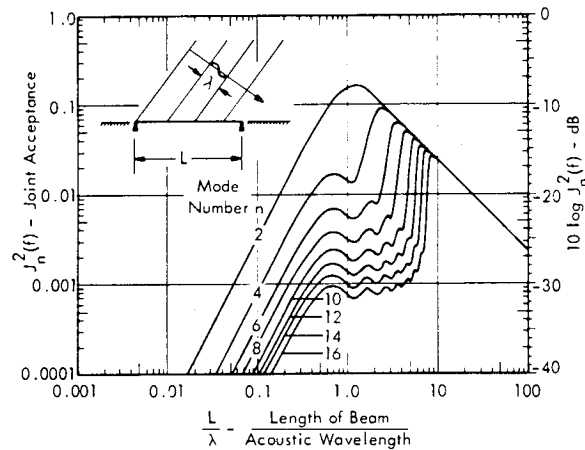
Values of the cosine and sine integral functions,  $C_{in}(y)$  and  $S_i(v)$ , are tabulated in Reference 8.1.13. The resulting values for joint acceptance for the odd and even modes are shown in Figure 8.1.21a and b, respectively.

Comparison of Joint Acceptance for a Progressive Wave and Diffuse Field

For purposes of comparison, the joint acceptance for the first three modes of a simply-supported beam for both a progressive wave and a diffuse field are shown in Figure 8.1.22.



a) Odd Numbers of Elastic Half-Waves  $n$



b) Even Numbers of Elastic Half-Waves  $n$

FIGURE 8.1.21 Joint-Acceptance for a Simply-Supported Beam Subjected to a Reverberant Acoustic Field.

It is important to recognize that joint acceptance for the case of a plane progressive wave is specified in terms of the ratio of beam length to trace wavelength  $L/\lambda_t = \frac{L \sin \psi}{\lambda}$  while the ratio of beam length to acoustic wavelength is used for a diffuse field. Note that a coincidence peak shows up in the joint acceptance curves for a diffuse field for all modes above the fundamental. This peak occurs at a value of  $L/\lambda \approx (n + 1)/2$ . This corresponds to a coincidence peak that would occur for a plane progressive wave at an incidence angle  $\psi$  of about  $48^\circ$ . Thus, an effective angle of incidence for a diffuse field, as far as coincidence is concerned, would be  $48^\circ$ .

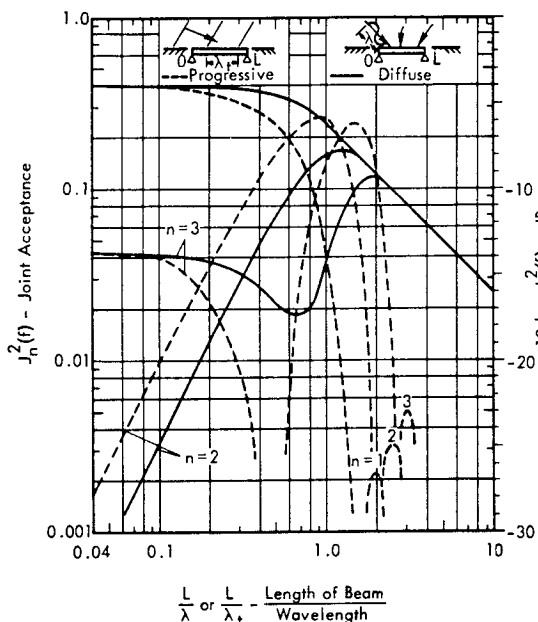


FIGURE 8.1.22 Comparison of Joint Acceptance for First Three Modes of Simply Supported Beam for Progressive Wave and Diffuse Field.

The limiting values of  $J_n^2(f)$  for a simply-supported beam for the two types of sound fields are compared in Table 8.1.1. Based on these expressions for the limiting envelopes for the two types of fields, the following general conclusions can be drawn:

- Below Coincidence (Low Frequencies)
  - ▲ Odd Modes
 

$J_n^2(f)$  is the same for normal incidence for progressive waves and for low frequencies for diffuse fields.
  - ▲ Even Modes
 

For the same acoustic wavelength (same frequency of excitation)  $J_n^2(f)$  for progressive waves can range from 0 to 3 times (+4.7dB) the  $J_n^2(f)$  for diffuse fields, depending on the angle of incidence.
- At coincidence; Approx. Maximum Value for  $J_n^2(f)$ 
  - ▲ Odd and Even Modes
 

For  $n > 1$ ,  $J_{n, \max}^2(f)$  for diffuse field is  $2/(n + 1)$  less than the maximum for progressive waves.
- Above Coincidence (High Frequencies)
  - ▲ Odd and Even Modes
 

Maximum value for  $J_n^2(f)$  for diffuse fields decreases smoothly as  $(L/\lambda)^{-1}$  in contrast to the upper envelope for plane progressive waves which decreases as  $(L/\lambda)^{-4}$  in the limit.

TABLE 8.1.1

COMPARISON OF LIMITING VALUES OF JOINT ACCEPTANCE FOR A SIMPLY-SUPPORTED BEAM FOR A PROGRESSIVE WAVE AND A DIFFUSE SOUND FIELD

$L/\lambda^{(1)}$	$J_n^2(f)$	
	Progressive Waves	Diffuse Field
<b>Odd Modes</b>		
$L/\lambda \rightarrow 0$	$(2/n\pi)^2$	$(2/n\pi)^2$
$L/\lambda = n/2$	1/4	--
$L/\lambda = (n+1)/2$	--	$1/2(n+1)$
$L/\lambda \gg n/2$	$(\frac{n}{2\pi})^2 / (\frac{L}{\lambda_t})^4$	$\frac{1}{4} / (\frac{L}{\lambda})$
<b>Even Modes</b>		
$L/\lambda \rightarrow 0$	$(2L/n\lambda_t)^2$	$\frac{1}{3}(2L/n\lambda)^2$
$L/\lambda = n/2$	1/4	--
$L/\lambda = (n+1)/2$	--	$1/2(n+1)$
$L/\lambda \gg n/2$	$(\frac{n}{2\pi})^2 / (\frac{L}{\lambda_t})^4$	$\frac{1}{4} / (\frac{L}{\lambda})$

(1)  $\lambda = \lambda_t$ , Trace Wavelength for a Progressive Wave

Perhaps the single most important feature of this comparison, as far as structural loads on buildings are concerned, is that the joint acceptance for the fundamental mode, well below coincidence, is the same for either progressive or diffuse sound fields. This simplifies design calculations for the dynamic response, in the first mode, of a typical structure exposed to a wide variety of sound fields. Examples of such calculations will be given later. First, however, it is necessary to define the joint acceptance for plates.

8.1.2.4 Joint Acceptance for Plates for Plane Progressive Waves

The mode shape for bending vibrations of plates is normally specified as the product of beam mode shapes with boundary conditions corresponding to those for the plate in each direction. As pointed out in Section 3.3.5.6, Chapter 3, this is an exact method for a simply-supported plate and provides a very close approximation to the mode shape for plates with other boundary conditions.

Simply-Supported Plates

Figure 8.1.23 illustrates a simply-supported plate under acoustic excitation by a plane progressive sinusoidal acoustic wave impinging at an angle  $\psi$  to a normal through the plate and at an angle  $\beta$  (in the plane of the plate) relative to the  $y$  axis. The acoustic pressure  $p(y, z, t)$  at any point  $y, z$  on the plate can be defined in terms of the trace wavelengths  $\lambda_y$  and  $\lambda_z$  along the  $y$  and  $z$  of the plate. The sinusoidal pressure along a reference wave front through the origin ( $y, z = 0$ ) can be conveniently specified as  $p(0, 0, t) = p \cos 2\pi f t$ . At any point  $y, z$  on the plate, the instantaneous pressure is then given by

$$p(y, z, t) = p \cos [2\pi (f t - \Delta / \lambda_t)]$$

where  $\Delta = y (\cos \beta) - z (\sin \beta)$ , the path length (along the trace of the incident wave on the plate) between the reference wave front and the point  $y, z$ .

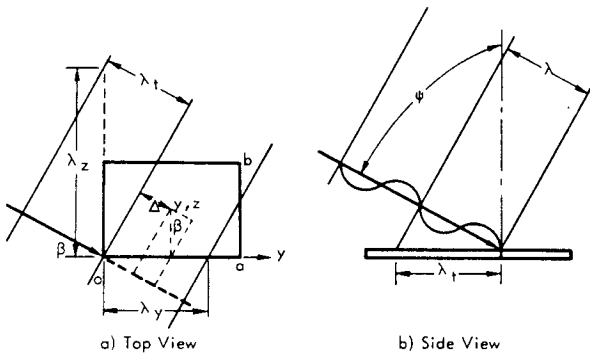


FIGURE 8.1.23 Plane Progressive Wave Impinging on Plate at an Angle  $\psi$  to a Normal and at an Angle  $\beta$  to the  $y$  Axis.

The space correlation coefficient  $\bar{R}_p(y, y', z, z', f)$  for this general case for a plate can be written down directly by comparison with the equation for the space correlation for a plane wave on a beam (Equations 8.1.25 and 8.1.26). The result is

$$\bar{R}_p(y, y', z, z', f) = \cos [2\pi (\Delta - \Delta') / \lambda_t] \tag{8.1.35}$$

where

$$(\Delta - \Delta') = (y - y') \cos \beta - (z - z') \sin \beta, \text{ and}$$

$$\lambda_t = \lambda / \sin \psi .$$

Since this space correlation coefficient for the plate is still just a cosine function, it can never exceed the corresponding value for a beam (i.e.,  $\cos [2\pi(y - y') / \lambda_t]$ ). The only difference will be a more complex variation in the correlation (and hence the resulting joint acceptance) as the compound incidence angles  $\psi$  and  $\beta$  vary from  $-\pi/2$  to  $+\pi/2$  and 0 to  $2\pi$ , respectively.

The joint acceptance for this general case of a plane progressive wave in a simply-supported plate may be expressed as

$$J_{mn}^2(f) = \frac{1}{(ab)^2} \int_0^a \int_0^a \int_0^b \int_0^b \bar{R}_p(y, y', z, z', f) \phi_{mn}(y, z) \times \phi_{mn}(y', z') dy dy' dz dz' \tag{8.1.36}$$

where  $\phi_{mn}(y, z) = \phi_m(y) \times \phi_n(z)$ , the product of the mode shapes at  $y, z$  for two simply-supported beams

$$\phi_m(y) = \sin (m\pi y/a)$$

$$\phi_n(z) = \sin (n\pi z/b), \text{ and}$$

$\bar{R}_p(y, y', z, z')$  = the space correlation coefficient given by Equation 8.1.35.

This has been evaluated in Reference 8.1.14 to show the variation in  $J_{mn}^2(f)$  for a simply-supported plate as a function of the incidence angles  $\psi$  and  $\beta$ . Typical results are shown in Figure 8.1.24 in the form of contours of  $10 \log J_{mn}^2(f)$  relative to its maximum value for a given  $mn$  mode.

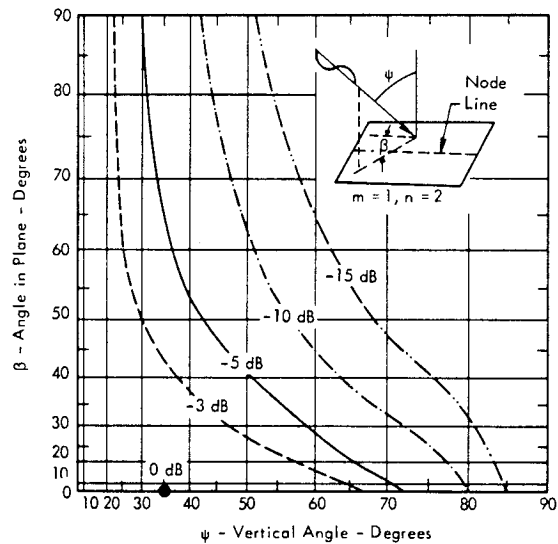


FIGURE 8.1.24 Contours of  $10 \log J_{mn}^2(f)$  in dB, Relative to Maximum Value, as a Function of Angles of Incidence  $\psi$  and  $\beta$  for Plane Wave Excitation of a Rectangular Panel Vibrating in its 1,2 mode (Data From Reference 8.1.14)

For convenience in analysis, it is customary to assume that the incident wave is traveling in a direction parallel to one edge, say the  $y$  axis, so that  $\beta = 0$ . Applying this condition to Equation 8.1.35, the space correlation coefficient at any point on the panel becomes

$$\bar{R}_p(y, y', z, z', f) = \cos [2\pi (y - y') / \lambda_t] \tag{8.1.37}$$

This is the same value obtained for a beam along the y axis. In other words, the instantaneous pressure along the wave front is in-phase at all points along a line parallel to the z axis so that the space correlation is unity in the z direction. Inserting this expression for the space correlation coefficient in Equation 8.1.36, the joint acceptance for the simply-supported plate in a plane progressive wave field traveling parallel to one edge reduces to the product of the joint acceptances for beams along the y and z axis, or

$$J_{mn}^2(f) = J_m^2(f) \cdot J_n^2(f) \tag{8.1.38}$$

where

$$J_m^2(f) = \frac{2}{(m\pi)^2} \left[ \frac{1}{1 - \left(\frac{2a/m}{\lambda_t}\right)^2} \right]^2 [1 - \cos m\pi \cos (2\pi a/\lambda_t)]$$

is the joint acceptance along the y axis (side a) (8.1.39a)

$$J_n^2(f) = \left(\frac{2}{n\pi}\right)^2 \text{ is the joint acceptance along the z axis (side b), and} \tag{8.1.39b}$$

$\lambda_t =$  trace wavelength.

Except for the change in notation for a two-dimensional structure, the first term  $J_m^2(f)$  is identical to the joint acceptance for a plane progressive wave driving the mth mode of a simply-supported beam of length a (see Equation 8.1.28). The second term is the joint acceptance for a uniform acoustic pressure (i.e., normally incident wave) driving the nth mode of a simply-supported beam of length b.

Specific values of joint acceptance for the mnth mode of a simply-supported plate, for  $\beta = 0$ , can be obtained by multiplying the values shown in Figure 8.1.15 for the mth mode along side a by the factor  $(2/n\pi)^2$  for the nth mode along side b. The maximum value for the joint acceptance  $J_{mn}^2(f)$  for the first mode ( $m, n = 1$ ) of a simply-supported plate occurs for the case of a uniform load or normally incident wave. This maximum value is

$$J_{1,1}^2(f)_{\max} = \left(\frac{2}{\pi}\right)^4 = 0.164$$

This is also the value for the maximum joint acceptance for a simply-supported plate for any angle of incidence providing the ratio of the longest side b to the acoustic wavelength is less than 0.2. This can be reduced to the following simple rule for the fundamental mode of a simply-supported plate. For (Frequency) x (Long Side in ft) < 220 Hz - ft,

$$J_{1,1}^2 = (2/\pi)^4$$

A more detailed consideration of specific values for the joint acceptance of simply-supported plates is not practical at this point. This is best considered later by examples which include response characteristics of the plate.

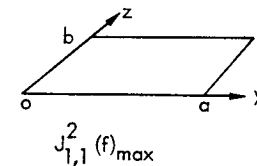
Other Boundary Conditions

The same approach used for the simply-supported plate can be applied for any boundary conditions, where the plane wave travels parallel to side a. The joint acceptance for the mnth mode is given by the product form in Equation 8.1.38. The joint acceptance  $J_m^2(f)$  for side a is defined by the corresponding value for a plane wave traveling over a beam with the appropriate boundary conditions at  $y = 0, a$ .  $J_n^2(f)$  for the other direction is the joint acceptance for a uniform pressure on a beam with the appropriate boundary conditions at  $z = 0, b$ . Thus, the previous expressions developed for beams in a plane wave field can be applied directly to plates.

The maximum value of the joint acceptance for the fundamental mode of plates with a variety of boundary conditions is summarized in Table 8.1.2. These values are applicable for a uniform load (normal incidence) or for excitation by a progressive wave with a wavelength which is large relative to a typical panel dimension. As indicated by the table, the range of  $J_{1,1}^2(f)$  for the extreme range of boundary conditions is about 23:1 (13.7 dB range). However, it will be shown later that the range in maximum acceleration response for the various boundary conditions noted in Table 8.1.2 will be much less.

TABLE 8.1.2

MAXIMUM VALUE OF MAXIMUM JOINT ACCEPTANCE SQUARED FOR FUNDAMENTAL MODE OF UNIFORM PLATES WITH VARIOUS BOUNDARY CONDITIONS<sup>(1)</sup> UNDER UNIFORM ACOUSTIC LOADS



Boundary Condition at y = 0, a	Boundary Condition at z = 0, b			
	SS	SC	CC	CF
FF	0.405	0.325	0.2755	0.132
SS	0.164	0.132	0.111	0.0535
SC		0.106	0.0895	0.0429
CC			0.0760	0.0364
CF				0.0174

- (1) F = Free
- S = Simple or Pinned Edge
- C = Clamped or Fixed Edge

In all cases, mounting in an infinite baffle is assumed.

8.1.2.5 Joint Acceptance for Plates in a Diffuse Sound Field

The space correlation coefficient  $R_p(y, y', z, z', f)$  for a diffuse sound field was defined earlier by Equation 8.1.33 for application to the joint acceptance for a beam. Theoretically, the same basic expression could be used to determine the joint acceptance for a plate in a diffuse sound field. The space correlation coefficient will become

$$\bar{R}_p(y, y', z, z', f) = \frac{\sin 2\pi \Delta/\lambda}{2\pi \Delta/\lambda}$$

where

$$\Delta = \sqrt{(y - y')^2 + (z - z')^2}$$

$$\lambda = c/f - \text{acoustic wavelength.}$$

The coefficient is equal to zero for  $\Delta = \lambda/2$  or when

$$(y - y')^2 + (z - z')^2 = \left(\frac{\lambda}{2}\right)^2$$

This is the equation for a circle with a center at  $y = y', z = z'$  and a radius =  $\lambda/2$ . Thus, as illustrated by the three-dimensional plot in Figure 8.1.25a, this true value for the space correlation of a diffuse field has circular symmetry about the origin. Unfortunately, the joint acceptance for a plate based on this exact expression for the space correlation has not been evaluated so that it is necessary to assume a simplified separable form given by

$$\bar{R}_p(y, y', z, z', f) = \frac{\sin 2\pi (y - y')/\lambda}{2\pi (y - y')/\lambda} \cdot \frac{\sin 2\pi (z - z')/\lambda}{2\pi (z - z')/\lambda} \tag{8.1.40}$$

In this form, the space correlation coefficient has square symmetry, as illustrated in Figure 8.1.25b, with its first zero value along the lines

$$y - y' = \pm \lambda/2 \quad \text{and} \quad z - z' = \pm \lambda/2$$

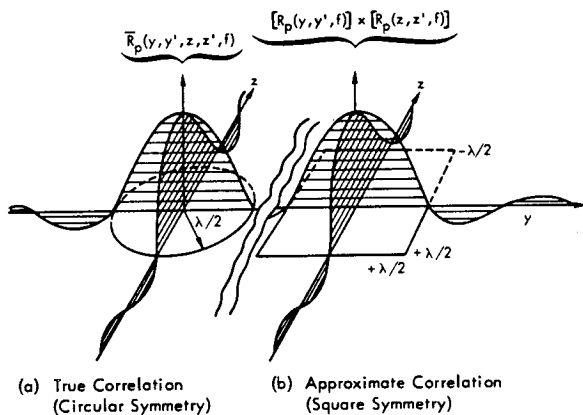


FIGURE 8.1.25 True (a) and Approximate (b) Forms for the Space Correlation Coefficient for Diffuse Sound Fields. The latter is used for analysis purposes.

Applying this approximate form for the space correlation coefficient for a plate in a diffuse field, the joint acceptance can again be given in the product form of Equation 8.1.38 where each term corresponds to the joint acceptance for a beam.

Thus, to a first approximation, the joint acceptance (squared) for the  $m$ th mode of a simply-supported plate in a diffuse field will be the product of the values shown in Figure 8.1.21 for the corresponding  $m$ th and  $n$ th modes of beams. The resulting approximate joint acceptances for the  $m = 1$  and  $n = 1, 2, 3$  modes of a simply-supported square plate in a diffuse field are shown in Figure 8.1.26 as a function of the length ( $a$ ) of one side to the true acoustic wavelength  $\lambda = c/f$ . Due to the approximation in the space correlation coefficient, the joint acceptances shown will be slightly higher than the true values. For  $a/\lambda$  less than 0.5, the error will be approximately equal to the square of the ratio of the two volumes depicted in Figure 8.1.25. This will amount to an overestimate of  $J_{mn}^2(f)$  of the order of  $(4/\pi)^2$  or +2 dB.

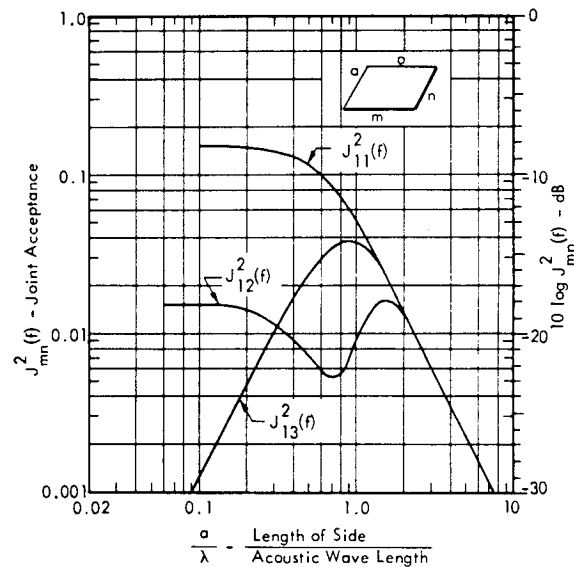


FIGURE 8.1.26 The Joint Acceptance of Three Vibration Modes (1-1, 1-2, and 1-3) of a Simply-Supported Square Panel in a Diffuse Sound Field

8.1.2.6 Joint Acceptance for Cylindrical Structure

A number of studies on the response of cylindrical structure to acoustic excitation have been reported in the literature including References 8.1.8, 8.1.12, 8.1.15 and 8.1.16. These studies were concerned primarily with the vibro-acoustic response of aerospace flight vehicles and are, therefore, not considered in this manual. However, the methods of analysis are essentially the same as those applied for ground structure. For example, the joint acceptance for any cylindrical-type ground structure to plane progressive waves or a diffuse field could utilize the extensive results reported in Reference 8.1.12. Space correlation of the pressure on infinite cylinders in a diffuse field, including the effects of diffraction, is treated in Reference 8.1.8.

Another approach for predicting the vibro-acoustic response of all types of structure, particularly including cylindrical structure, has been under development for the last eight years. This method, reviewed most recently in Reference 8.1.16, applies concepts of energy flow through statistically defined structure. However, this potentially powerful technique for predicting environmental vibration in structure is not suitable at this time for analyzing sonic loads on ground structure. In this case, practical analysis methods must necessarily emphasize the lower modes of vibration which are not conveniently described statistically.

8.1.3 VIBRO-ACOUSTIC RESPONSE OF BUILDING WALLS

The basic elements of the normal mode method for predicting the response of beams to sinusoidal and random acoustic excitation was briefly reviewed in Section 8.1.2.1. The following sections utilize these concepts, along with the preceding results for joint acceptance for plates, to predict the vibration response of building walls to acoustic excitation. Other general concepts of vibration and acoustics reviewed in Chapters 3 and 4 are also utilized.

These analytical methods for predicting vibro-acoustic response will necessarily include certain simplifying assumptions. It is essential, therefore, to back them up by experimental verification. This is covered in subsequent sections and will include the development of a semi-empirical prediction method based on the correlation of theory with measured vibro-acoustic response data.

8.1.3.1 Specification of Excitation and Response Variables

The time-varying quantities used for analyzing the vibro-acoustic response of walls may be summarized as follows:

VARIABLE	USED TO DEFINE:
Acoustic Pressure	Excitation
Deflection	Dynamic Stress in Wall
Velocity	Sound Transmission or Dynamic Stress (see Section 3.3.6.6)
Acceleration	Inertial Loads and Environmental Vibration
Stress	Fatigue Damage Analysis
Reaction Loads	Structural Loads and Vibration Input to Building

Excitation Variable

Assuming the excitation consists of random acoustic noise, the acoustic pressure may be specified, in units of psi, in one of the following forms.

- Pressure Spectral Density,  $W_p(f)$  - the mean square pressure in  $(\text{psi})^2/\text{Hz}$  within a unit bandwidth centered about the frequency  $f$ .

- One-Third Octave Band Pressure,  $p(f)$  - the rms pressure in (psi) in a constant percentage frequency band  $\Delta f = 0.232 f$  where  $f$  is the center frequency of the band. For a smoothly varying pressure spectrum,

$$p(f) = [0.232 f W_p(f)]^{1/2} \tag{8.1.41}$$

- Octave Band Pressure - the rms pressure in (psi) in a constant percentage frequency band  $\Delta f = f/\sqrt{2}$  where  $f$  is the center frequency of the band.

Each of these three methods for specifying the acoustic pressure can be expressed in decibel form as the pressure spectrum (or pressure spectral density) level, one-third octave band level and octave band level, respectively. (See Charts 12.3 and 12.4, Chapter 12 for conversion between pressure units to level in decibels and Chapter 4 for discussion of decibel scale.) A typical acoustic spectrum for rocket noise is shown in Figure 8.1.27 to illustrate these various forms for specifying the excitation.

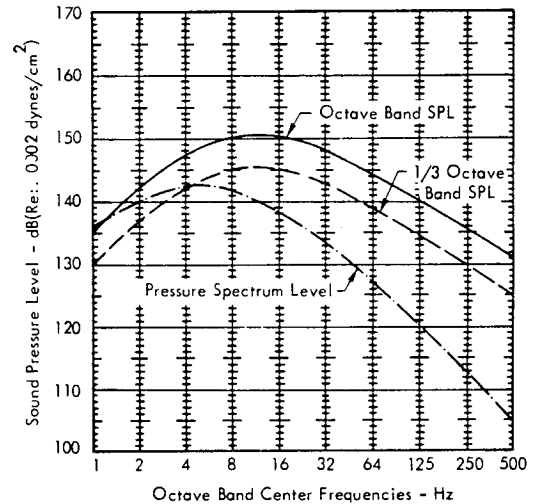


FIGURE 8.1.27 Typical Acoustic Spectra for Rocket Noise Shown in Three Different Forms

It is assumed for now that the effective pressure on the wall has been defined, including any effects of diffraction discussed earlier in this chapter.

Response Variables

It will be convenient to analyze the basic response of a wall to random acoustic excitation in terms of the acceleration power spectral density at an arbitrary point  $y, z$  on this wall. The quantity will be specified in the commonly used units of  $g^2/\text{Hz}$  as defined by the symbol  $W_a(y, z, f)$  where the subscript (a) denotes acceleration in g's in place of the absolute units previously denoted by  $\ddot{x}$ . The relationship between this quantity and the other response variables indicated earlier will be illustrated later.

For practical design purposes, the wall response may also be specified in such forms as

- Overall Mean Square Deflection

$$\overline{x^2(y, z, t)} - (\text{inches})^2$$

- Root Mean Square (rms) Deflection

$$\tilde{X}(y, z) = \sqrt{\overline{x^2(y, z, t)}} - \text{inches}$$

- Peak Deflection

$$X(y, z)_{\text{max}} - \text{inches}$$

- rms Velocity at the Frequency f

$$\tilde{\dot{X}}(y, z, f) - \text{in/sec}$$

- Peak Velocity

$$\dot{X}(y, z)_{\text{max}} - \text{in/sec}$$

- Space Average Acceleration PSD

$$\overline{W_a}(f) - g^2/\text{Hz}$$

- Space Average rms Velocity at a Frequency f

$$\overline{\tilde{X}}(f) - \text{in}^2/\text{Hz}$$

The application of these various forms for the response will also be illustrated by subsequent examples.

8.1.3.2 Response of a Simply-Supported Wall to a Plane Progressive Wave

An expression was given in Section 8.1.2.1 for the response of a beam to a random acoustic load (Equation 8.1.23). For the simply-supported wall illustrated in Figure 8.1.28 under excitation by a plane progressive wave traveling parallel to side a, the comparable expression for the acceleration spectral density at a point y, z, in g<sup>2</sup>/Hz, is

$$W_a(y, z, f) = W_o(f) \sum_m \sum_n \frac{J_{mn}^2(f/f_{mn})^4 |H_{mn}(f)|^2 \Phi_{mn}^2(y, z)}{g^2 M_{mn}^2} \tag{8.1.42}$$

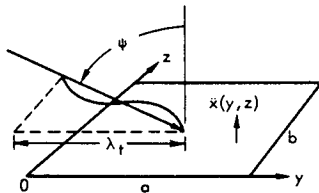


FIGURE 8.1.28 Simply Supported Panel Under Excitation by a Plane Progressive Wave with a Trace Wavelength  $\lambda_t$  Traveling Parallel to Side a

where

$$W_o(f) = W_p(f) \cdot (ab)^2, \text{ PSD of total acoustic force on plate}$$

$$W_p(f) = \text{PSD in (psi)}^2/\text{Hz for acoustic pressure on the panel at a frequency f. (This is assumed to be constant over the panel.)}$$

$$J_{mn}^2(f) = [J_m^2(f)] [J_n^2(f)] = \text{product of joint acceptances for simply-supported beams parallel to sides a and b, respectively}$$

$$g^2 M_{mn}^2 = \left[ \frac{1}{4} \rho a b h g \right]^2 = \left[ \frac{1}{4} \cdot \text{Weight of Plate} \right]^2 - \text{lb}^2$$

$$|H_{mn}(f)| = 1 / \left[ \left( 1 - (f/f_{mn})^2 \right)^2 + \left( 2 \delta_{mn} f/f_{mn} \right)^2 \right]^{1/2}$$

- the dynamic magnification factor for the mnth mode

$$f_{mn} = \frac{\pi}{2} \sqrt{\frac{D}{\rho h}} \left[ \left( \frac{m}{a} \right)^2 + \left( \frac{n}{b} \right)^2 \right] - \text{mnth natural frequency}$$

$$\Phi_{mn}(y, z) = \sin(m\pi y/a) \cdot \sin(n\pi z/b) - \text{mode shape for simply-supported plate at y, z}$$

$$\rho h = \text{surface mass density of plate}$$

$$D = \text{plate stiffness} - \text{in-lb.}$$

The trace wavelength along side (a), in Figure 8.1.28, is given by  $\lambda_t = c/f \sin \psi$  where  $\psi$  is the incidence angle and c is the speed of sound. Thus,  $J_m^2(f)$  in this expression is given by Figure 8.1.16 or Equation 8.1.28 where side a replaces the beam length L. For side b, the trace wavelength is infinite and  $J_n^2(f) = (2/n\pi)^2$  at all frequencies.

It will be useful to consider the ratio of an acceleration response in g's to an acoustic pressure in psi, all multiplied by the structural surface weight density w in psi, as an acoustic mobility. The nondimensional ratio

$$W_a(f) \cdot w^2 / W_p(f)$$

will then be referred to as the square of the acoustic mobility. This convenient dimensionless quantity is essentially an expression of the familiar  $F = ma$  cast in an appropriate form for acoustic excitation of structure.

It is also convenient to consider only the space average of the acceleration response. Thus, a simplified form for the preceding expression is obtained by dividing both sides by the PSD of the acoustic field  $W_p(f)$  and multiplying both sides by the square of the surface weight w. This gives the dimensionless ratio

$$\frac{\overline{W_a}(f) \cdot w^2}{W_p(f)} = \sum_m \sum_n \frac{\Phi_{mn}^2}{\epsilon_{mn}^2} J_m^2(f) J_n^2(f) (f/f_{mn})^4 |H_{mn}(f)|^2 \tag{8.1.43}$$

where

$\overline{W}_a(f)$  = space average of the acceleration PSD

$W_p(f)$  = PSD of the uniform random pressure field propagating over the wall

$w = \rho a b h g / ab = \rho h g$  - the surface weight density for the wall - psi

$\overline{\phi}_{mn}^2$  = mean square mode shape [=  $(1/2)^2$  for a simply-supported plate]

$\epsilon_{mn}$  = generalized mass fraction or ratio of generalized mass to actual mass [= 1/4 for simply-supported plate]

This expression provides a simply nondimensional form for the space-average acceleration spectral density response on a uniform plate with any boundary condition. It will only be necessary to change the parameters  $\epsilon_{mn}$ ,  $J_m^2(f)$ ,  $J_n^2(f)$ ,  $f_{mn}$ , and  $\overline{\phi}_{mn}^2$  for the particular boundary conditions involved. As shown in Section 3.3.6.2 of Chapter 3, the space average response for a uniform structure cancels out the cross mode coupling terms so that Equation 8.1.43 is exact. To determine the approximate response of a particular point (y, z), neglecting cross-mode terms, the equation is divided by the mean square mode shape  $\overline{\phi}_{mn}^2$  and multiplied by the actual mode shape squared  $\phi_{mn}^2(y, z)$  at this point.

For this case of a wave traveling parallel to one side of the wall, only two terms in Equation 8.1.43 vary with frequency,  $J_m^2(f)$  and  $(f/f_{mn})^4 |H_{mn}(f)|$ . The joint acceptance term depends on mode number m but is independent of the natural frequency  $f_{mn}$ . The dynamic magnification factor (for acceleration)  $(f/f_{mn})^4 |H_{mn}(f)|$  depends on the natural frequency  $f_{mn}$  but has the same relative form for all modes.

Clearly, the maximum acceleration response will occur for any mode when these two functions are a maximum. This interaction between the joint acceptance and the dynamic magnification factor is best visualized by considering a few of the lower modes of a wall, one mode at a time.

8.1.3.3 Maximum Fundamental Mode Response of a Panel for Grazing Incidence

The variation in the two frequency varying terms in Equation 8.1.43 is shown conceptually in Figure 8.1.29a for grazing incidence excitation of a panel. When these two terms are combined, the acoustic mobility for this case will vary with frequency as shown in Figure 8.1.29b. This illustrates the decrease in the acceleration response for a grazing incidence sound wave as a function of the parameter  $f_{1,1} a/c$  where (a) is the side parallel to the direction of the incident wave and c is the speed of sound. Although this parameter could be generalized for other angles of incidence by replacing c by the trace velocity  $c/\sin \psi$ , the most conservative case for an influence of joint acceptance on panel response occurs for a grazing incidence sound wave.

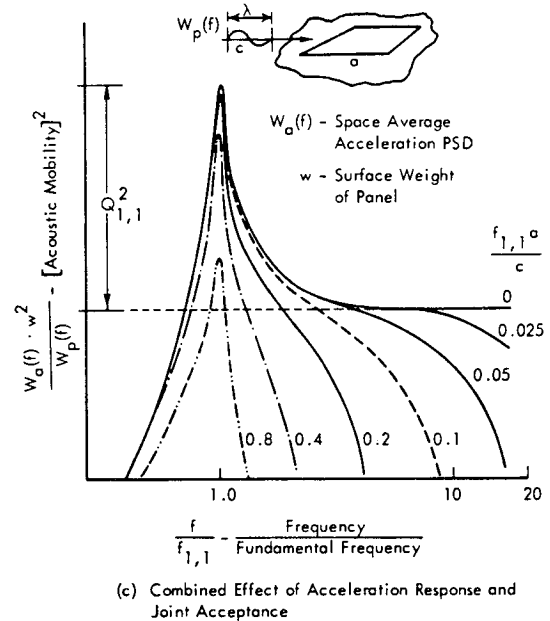
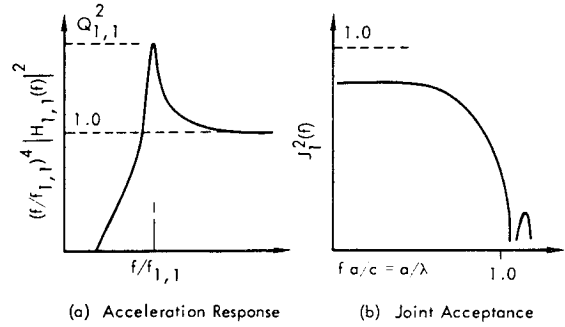


FIGURE 8.1.29  $[Acoustic\ Mobility]^2$  for the Fundamental Mode of a Panel Subjected to a Grazing Incidence Plane Wave of Random Noise. The parameter  $f_{1,1} a/c$  represents the ratio of the length of side a to the acoustic wavelength  $c/f_{1,1}$  of the fundamental natural frequency of the panel.

Therefore, the following criteria can be established for a limiting value for the parameter  $f_{1,1} a/c$  where a is in inches and  $c = 13,400$  in/sec.

- For  $f_{1,1} a < 1340$  in/sec, the maximum response at resonance, for a wall subjected to a grazing incidence sound wave, is not significantly changed by the decrease in joint acceptance for short wavelengths.

This criteria can be related to the panel dimensions through the expression for the fundamental frequency  $f_{1,1}$  of the panel. The result is a criteria for the maximum ratio of wall thickness h to side (a), above which, the decrease in joint acceptance for short wavelengths must be accounted for when computing the maximum fundamental mode response for a grazing incidence sound wave. Values for this



critical ratio of  $h/a$  are specified in Table 8.1.3 for a few common building materials and for simply-supported and clamped-clamped square plates. As shown by the following example, this simple criteria for the ratio of thickness to a side dimension can be related to general building code requirements.

TABLE 8.1.3

CRITICAL RATIO OF PANEL THICKNESS TO LENGTH OF SIDE (a) FOR SQUARE PANEL SUBJECTED TO GRAZING INCIDENCE SOUND WAVES

(For  $h/a$  greater than this value, the maximum response of the panel in its fundamental mode will be less due to a decrease in joint acceptance.)

Panel Material	h/a	
	Simply-Supported	Clamped-Clamped
Steel, Aluminum	1/140	1/260
Concrete	1/75	1/135
Plywood	1/93	1/150

Example

A common building requirement for masonry walls requires a standard thickness of 8 inches and a maximum area between supporting tie columns of 256 sq ft (Reference 8.1.17). For a 16-ft height, a 16-ft width would be allowable. The thickness-to-wall-width ratio would be  $8/(16)(12) = 1/24$ . This is greater than the critical ratio of 1/75 for concrete. In general, therefore, the fundamental mode of such walls to a grazing incidence sound wave along the width will be significantly less than for normal incidence due to the decrease in joint acceptance at the fundamental frequency of the wall.

A general expression for this critical value of  $h/a$  for the fundamental mode of any uniform panel is given by

$$\frac{h}{a} \leq \frac{2\pi c \sqrt{12(1-\nu^2)}}{(K_{1,1}a)^2 c_L} \left[ \frac{fa}{c} \right]_{cr} \quad (8.1.44)$$

where

$c$  = speed of sound in air

$c_L$  = speed of longitudinal waves in panel material ( $= \sqrt{E/\rho}$ )

$\nu$  = Poisson's ratio

$(K_{1,1}a)^2$  = dimensionless frequency constant in the general expression for the fundamental frequency of the panel (See Section 3.3.5.6, Chapter 3)

$$= \begin{cases} 19.74 & \text{for a square simply-supported plate} \\ 35.98 & \text{for a square clamped-clamped plate} \end{cases}$$

The critical value for  $h/a$  increases rapidly as the incidence angle decreases until finally, for normal incidence, the joint acceptance becomes constant for all values of the incident wavelength and is independent of the value of  $h/a$ .

8.1.3.4 Maximum Fundamental Mode Response of a Panel for Normal Incidence

For excitation by a normally incident plane wave of random noise, the maximum value for the acoustic mobility in the fundamental mode can be defined from Equation 8.1.43 setting  $m, n = 1$ . The joint acceptances  $J_m^2(f)$  and  $J_n^2(f)$  for this case have been defined earlier in Table 8.1.2. The maximum value for the acceleration response function  $(f/f_{mn})^4 |H_{mn}(f)|$  for  $f = f_{mn}$  is simply  $Q_{1,1}$  which is the resonant amplification factor for the fundamental mode. The other parameters  $\phi_{1,1}^2$  and  $\epsilon_{1,1}$  are defined in Section 3.3.5 of Chapter 3. The resulting maximum values for the space average acoustic mobility and maximum acoustic mobility of the point of maximum panel deflection are specified in Table 8.1.4 for several panel boundary conditions. The maximum mobility is obtained from Equation 8.1.43 (for  $m, n = 1$ ) by replacing the mean square mode shape  $\phi_{mn}^2$  by unity. For convenience, the actual table entries correspond to the linear value of acoustic mobility for a unit value for  $Q_{1,1}$  as defined by

$$\begin{aligned} \left. \frac{\text{(acoustic mobility)}}{Q_{1,1}} \right|_{f=f_{1,1}} &= \frac{[\text{accel.} - g\text{'s}] \times [\text{surface wt.}]}{[\text{acoustic pressure}] \times Q_n} \Bigg|_{f=f_{1,1}} \\ &= \left[ \frac{\bar{W}_a(f) \cdot w^2}{W_p(f) \cdot Q_{1,1}^2} \right]^{1/2} \quad \text{- space average} \\ \text{or} &= \left[ \frac{W_a(f) \cdot w^2}{W_p(f) \cdot Q_{1,1}^2} \right]_{\max}^{1/2} \quad \text{- maximum deflection} \end{aligned}$$

The entries in Table 8.1.4 represent the acceleration in g's for a single frequency or a narrow band of random noise centered at the panel fundamental frequency  $f_{1,1}$  for a unit value of surface weight in psi, a unit value of acoustic pressure in psi at the same frequency (measured or computed for the same bandwidth) and for a unit value of the resonant amplification factor  $Q_{1,1}$ .

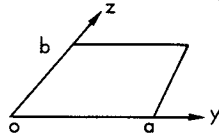
Perhaps the most significant result to be obtained from Table 8.1.4 is that the range for the maximum acoustic mobility (or relative acceleration response) of the fundamental mode does not vary by more than a factor of 1.7 for a variety of boundary conditions. This corresponds to a variation in mean square response levels of  $(1.7)^2 = 2.9$  or 4.7 dB which is comparable to the accuracy of a predicted

acoustic environment. It is reasonable, therefore, to assume simply-supported edges when making initial estimates of the acceleration response in the fundamental mode response of any panel to a normal incidence acoustic wave. Deviations in the predictions for other boundary conditions will be small. A much greater variation will occur in the panel displacement response due to large differences in natural frequencies for various boundary conditions.

TALBE 8.1.4

MAXIMUM VALUE OF THE ACOUSTIC MOBILITY IN THE FUNDAMENTAL MODE FOR UNIFORM PANELS WITH VARIOUS BOUNDARY CONDITIONS SUBJECTED TO A NORMALLY INCIDENT PLANE WAVE

[First entry for each boundary condition is space average acoustic mobility. Second entry is acoustic mobility at point of maximum deflection. See text for definition of acoustic mobility (c).]



$$\textcircled{1}, \left[ \frac{\overline{W}_a(f) \cdot w^2}{W_p(f) \cdot Q_{1,1}^2} \right]^{1/2} \quad \text{or} \quad \textcircled{2}, \left[ \frac{W_a(f) \cdot w^2}{W_p(f) \cdot Q_{1,1}^2} \right]^{1/2}_{\text{max}}$$

Boundary Condition at y = 0, a	Boundary Condition at z = 0, b			
	SS	SC	CC	CF
FF $\textcircled{1}$	0.90	0.86	0.83	0.72
FF $\textcircled{2}$	1.27	1.30	1.33	1.45
SS	0.81(a) 1.62(b)	0.77 1.65	0.75 1.69	0.65 1.85
SC		0.74 1.68	0.71 1.72	0.62 1.89
CC			0.69 1.75	0.60 1.92
CF				0.53 2.11

F = Free Edge; S = Simple or Pinned Edge; C = Clamped or Fixed Edge

(a)  $8/\pi^2$

(b)  $16/\pi^2$

(c) All values are for single frequency or narrow band of noise at fundamental frequency of panel. They also apply to the fundamental mode response for a diffuse field when the quantity  $f_{1,1} a/c$  is less than 0.5.

Application of this table and methods for computing other response parameters for the fundamental mode of a panel are illustrated in the following example.

Example

Assume the following conditions:

• Panel

- Square steel panel -  $a = 87.5$  in.,  $h = 1$  in.
- Simple supports on four sides
- Surface weight,  $w = 0.3$  psi
- Fundamental frequency,  $f_{1,1} = 25$  Hz
- Resonant amplification factor,  $Q_{1,1} = 20$

• Acoustic Excitation

- Normal Incidence Acoustic Field
- One-third octave band level at 25 Hz = 159 dB
- From Chart 12.3, Chapter 12, rms pressure = 0.261 psi
- Filter bandwidth  $\Delta f = 0.233 f = 5.83$  Hz

$$\text{Pressure spectral density } W_p(f) = \frac{(0.261)^2}{5.83} = 0.011 \text{ (psi)}^2/\text{Hz}$$

• Space Average Acoustic Mobility - (From Table 8.1.4)

$$\left[ \frac{\overline{W}_a(f) \cdot w^2}{W_p(f) \cdot Q_{1,1}^2} \right]^{1/2} = 0.81$$

• Find: Space Average Acceleration Spectral Density,  $\overline{W}_a(f)$

$$\begin{aligned} \overline{W}_a(f) &= (0.81)^2 \cdot \frac{W_p(f) \cdot Q_{1,1}^2}{w^2} \\ &= \frac{(0.81)^2 (0.011) (20)^2}{(0.3)^2} = 32.0 \text{ g}^2/\text{Hz} \end{aligned}$$

• Find: Power Spectral Density of Maximum Displacement at Center of Panel -  $W_x(a/2, b/2, f)$

First, find the maximum acceleration APSD. From Table 8.1.4, the maximum acoustic mobility at the point of maximum deflection is

$$\left. \frac{W_a(f) \cdot w^2}{W_p(f)} \right|_{\text{max}} = (1.62)^2 \cdot Q_{1,1}^2$$

and

$$\begin{aligned} W_a(f)_{\text{max}} &= W_a(a/2, b/2, f) = \frac{(1.62)^2 (0.011) (20)^2}{(0.3)^2} \\ &= 128 \text{ g}^2/\text{Hz} \end{aligned}$$

From Section 3.2.3.11, page 3-42,

$$\begin{aligned} W_x(f)_{\text{max}} &= 95.6 W_a(f)_{\text{max}} / f_{1,1}^4 \\ &= (95.6)(128)/(25)^4 = \underline{\underline{0.0315 \text{ in}^2/\text{Hz}}} \end{aligned}$$

- Find: Maximum rms Displacement in Fundamental Mode -  $X_{\max}$

From Section 3.2.3.11, page 3-42,

$$\tilde{X}_{\max} = \left[ \frac{\pi}{2} W_{x(f)\max} \cdot \frac{f_{1,1}}{Q_{1,1}} \right]^{1/2}$$

$$= [(1.57)(0.0315)(25)/20]^{1/2} \approx \underline{0.25 \text{ in.}}, \text{ rms}$$

- Find: Peak Displacement in Fundamental Mode -  $X_{\max}$

From Section 3.2.3.11, page 3.42,

$$X_{\max} \approx 3 \cdot \tilde{X}_{\max} = \underline{0.75 \text{ in.}}$$

- Find: Peak Stress in Fundamental Mode -  $\sigma_{\max}$   
(Based on Peak Deflection)

From Section 3.3.6.1, page 3-145, stress in fundamental mode for a peak deflection in this mode of 0.75 in. is

$$\sigma_{\max} = \beta \cdot E \frac{h}{a} \frac{X_{\max}}{a}$$

where

- $\beta = 7.05$  for square plate with Poisson's ratio = 0.3
- $E = 3 \times 10^7$  psi for steel
- $a = 87.5$  in.
- $h = 1.0$  in.
- $X_{\max} = 0.75$  in.

$$\therefore \sigma_{\max} = \frac{(7.05)(3 \times 10^7)(1)(0.75)}{(87.5)^2} = \underline{20,700 \text{ psi}}$$

- Find: Peak Stress in Fundamental Mode -  $\sigma_{\max}$   
(Based on Peak Velocity)

From Section 3.3.6.6, page 3-156, peak dynamic stress for structure vibrating in a sinusoidal mode is

$$\sigma_{\max} = K_s \cdot E \cdot \frac{\dot{X}_{\max}}{c_L}$$

where

- $K_s =$  dynamic stress constant  
 $= 1.18$  for square plate with Poisson's ratio = 0.3
- $c_L = 2 \times 10^5$  in/sec - longitudinal (bar) velocity of sound in steel
- $\dot{X}_{\max} =$  peak velocity of panel in a fundamental mode.

Since mode is harmonic,

$$\dot{X}_{\max} = 2\pi f X_{\max}$$

$$= (6.28)(25)(0.75) = 117.5 \text{ in/sec}$$

$$\therefore \sigma_{\max} = \frac{(1.18)(3 \times 10^7)(117.5)}{(2 \times 10^5)} = \underline{20,800 \text{ psi}}$$

Correction for Other Angles of Incidence

The previous section pointed out the decrease in maximum response of a panel for a grazing incidence wave due to the decrease in the joint acceptance. This effect may be accounted for by first carrying out the type of analysis indicated above and then applying the correction indicated in Figure 8.1.30. This is simply the joint acceptance (squared) for a "beam" of length (a) relative to its maximum value for normal incidence. The beam, in this case, corresponds to the side of the panel in the direction of travel of the incident wave. The correction to be applied to the fundamental mode response is plotted as a function of the ratio  $a/\lambda_{to}$  where

$$\lambda_{to} = \frac{f_{1,1} \sin \psi}{c} - \text{the trace wavelength at the fundamental frequency of the panel for an incidence angle } \psi.$$

The correction to be applied to the fundamental mode response for a diffuse field can be obtained from Figure 8.1.26.

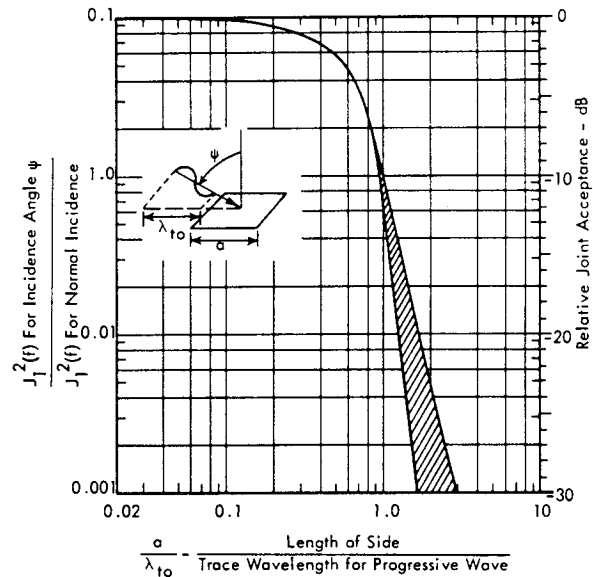


FIGURE 8.1.30 Relative Joint Acceptance for Fundamental Mode of a Simply Supported Panel Under Excitation by a Plane Wave Traveling Parallel to Side a.

8.1.3.5 Response of Higher Modes to Plane Progressive Waves and Diffuse Sound Fields

Simple theoretical generalizations for the vibro-acoustic response of higher order modes are difficult. This is due to the wide range of possible conditions for the effective trace wavelength and the complex variation of the joint acceptance for the higher modes whose frequencies can vary appreciably from one structure to the next. This complexity is indicated in Figure 8.1.31 by the variation in the peak modal response of a simply-supported panel subjected to grazing and normal incidence acoustic waves. Only the peak responses at each natural frequency are indicated by this bar chart. Although similar trends exist in the overall envelope for all modes, variations in the individual modes is appreciable.

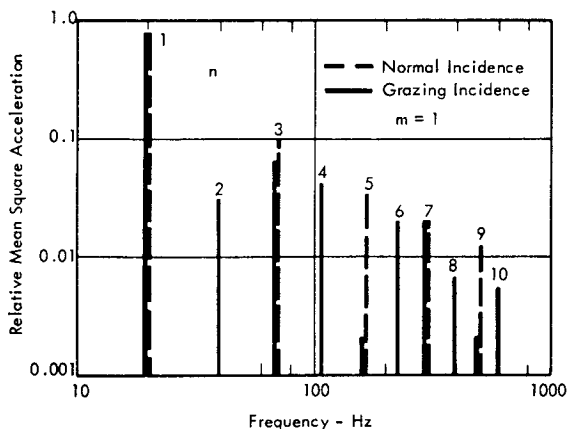


FIGURE 8.1.31 Relative Mean Square Acceleration Response in the First 10 Modes ( $m = 1, n = 1 \rightarrow 10$ ) of a Simply Supported Panel for Excitation by Grazing and Normal Incidence Plane Waves

Although handcalculations can be made for higher modes, using plots for the joint acceptance such as given earlier in Figures 8.1.15 to 8.1.17, the process is tedious and subject to considerable error. However, calculations can be readily carried out by a digital computer to define the overall response of a structure to higher order modes. One example of such a computation is shown in Figure 8.1.32 for the case of an 8 ft by 10 ft concrete block wall exposed to a diffuse sound field. The space average acceleration spectral densities are computed values for a constant pressure spectral density for the acoustic excitation. The calculations are carried out digitally using Equation 8.1.43.

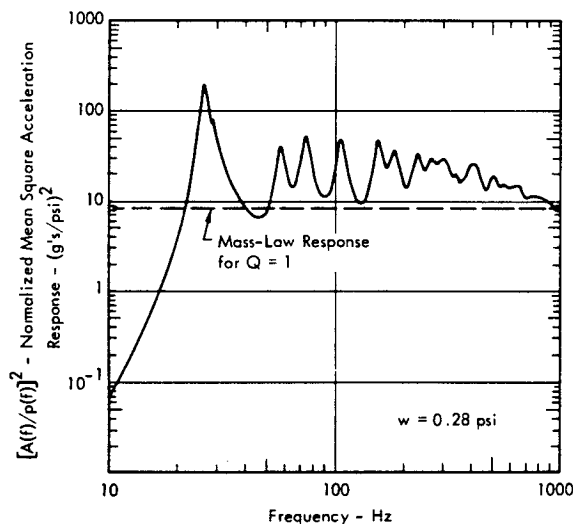


FIGURE 8.1.32 Normalized Space Average Acceleration Spectral Density Response Computed for an 8' x 10' x 8" Concrete Block Wall Exposed to a Diffuse Sound Field with Constant Pressure Spectral Density

Region of High Modal Density

For excitation of a panel by wide band random noise, a very large number of normal modes will be excited. At frequencies well above the lowest discrete structural modes,

the frequency interval between modes will eventually become comparable to the resonant bandwidth of each individual resonant mode. The modal density for plates or number of resonant modes per unit bandwidth,  $N_p$ , can be shown to be

$$N_p = \sqrt{3(1 - \nu^2)} A / c_L h$$

where

$A$  = area of panel

$c_L$  = longitudinal "bar" velocity in panel material =  $\sqrt{E/\rho}$

$h$  = panel thickness.

From this relationship, it can be shown that for simply-supported plates, the frequency  $f_n$  at which interval between adjacent modes is equal to the resonant bandwidth  $f_n/Q$ , is

$$f_n = \frac{2Q}{\pi} \left[ \frac{2 a/b}{1 + (a/b)^2} \right] \cdot f_{1,1}$$

where

$a/b$  = the panel aspect ratio

$f_{1,1}$  = the fundamental panel frequency

$Q$  = average resonant amplification factor for each mode.

In general, it is found that for panels with some fixity on all four edges and an aspect ratio of 0.5 to 1, this threshold frequency for the high modal density region varies from about 0.22  $Q$  to 0.63  $Q$  times the fundamental frequency,  $f_{1,1}$ . At frequencies above this threshold value, the contribution of any one mode to the mean square response within a finite band is small. The influence of damping of any one mode is decreased and the effective resonant amplification factor  $Q_{eff}$  at the frequency  $f$  approaches a value given by

$$Q_{eff} = \left[ \frac{\pi}{2} f Q N_p \right]^{1/2}$$

where

$Q$  = average resonant amplification factor for each mode

$N_p$  = modal density for plates defined above.

Thus, in this frequency range, an upper bound for the space average acoustic mobility for a simply-supported plate approaches a value given by

$$\left[ \frac{\overline{W}_a(f) \cdot w^2}{W_p(f)} \right]^{1/2} \approx \frac{8}{\pi^2} \left[ \frac{\pi}{2} f Q \cdot N_p j^2(f) \right]^{1/2} \tag{8.1.45a}$$

where

$j^2(f)$  = the RELATIVE value of the envelope of  $J_n^2(f)$  at the frequency  $f$  for the higher order modes with respect to its value  $(4/\pi^2)^2$  for the fundamental mode at normal incidence.

This relative value of the envelope of joint acceptance  $j^2(f)$  can be estimated for a plate in a diffuse field according to the values specified in Table 8.1.1 for a beam in a diffuse field. The approximate value for square simply-supported plates with side (a) would be

$$j^2(f) \approx \begin{cases} 1 & , \frac{fa}{c} < 1/2 \\ \frac{1}{4} / \left(\frac{fa}{c}\right)^2 & , \frac{fa}{c} \gg 1/2 \end{cases} \quad (8.1.45b)$$

While absolute values for the acoustic mobility might be predicted from these two preceding expressions, they are developed only to suggest trends in the acceleration response of structure in the region of high modal density. In essence, then, the trend indicated for excitation by a diffuse field is

$$\frac{(\text{accel.} - g\text{'s})(\text{surface wt.} \cdot \text{psi})}{(\text{acoustic pressure} - \text{psi})} \propto \begin{cases} [f \cdot Q \cdot N_p]^{1/2} & , \frac{fa}{c} < \frac{1}{2} \\ \left[\frac{Q N_p}{f}\right]^{1/2} & , \frac{fa}{c} \gg \frac{1}{2} \end{cases}$$

Thus, when there are a large number of modes within the resonant bandwidth  $f_{mn}/Q$  of any one mode, or when  $N_p f/Q \gg 1$ , the acceleration amplitude response in a diffuse field would be proportional to the square root of  $Q$  instead of the first power. The variation with frequency would range from being proportional to the square root of frequency, to being inversely proportional to the square root of frequency, depending on the ratio of the length of the panel (a) to the acoustic wavelength  $\lambda = c/f$ .

A different trend in acoustic mobility can be expected for progressive waves at high frequencies where the upper envelope of the joint acceptance varies in a more complex fashion with mode number.

Infinite Plate Region

At still higher frequencies, normal modes will be so severely damped by the losses in the plate that they will not be evident and the plate will tend to behave (except near the edges) as if there were no boundaries. The average impedance of the plate no longer acts like a pure mass at these frequencies and, instead, tends to act like a pure resistance. This is indicated by the resistive impedance  $R$  presented to a point force applied to an infinite plate which is

$$R = 8 \sqrt{D \rho h}$$

where

$R$  = ratio of applied force to panel velocity at this point

$D$  = panel stiffness

$$= E h^3 / 12 (1 - \nu^2) \text{ for uniform plates}$$

$\rho h$  = surface mass density of plate of thickness  $h$ .

Applying this same trend for a distributed pressure load, the ratio of acceleration response to acoustic pressure would tend to vary as

$$\frac{\text{acceleration}}{\text{pressure}} \propto \frac{\text{frequency} \times \text{velocity}}{\text{pressure}} \propto f/R$$

This would indicate an increasing trend in acoustic mobility directly proportional to frequency. The frequency where this region begins can be roughly estimated by considering the attenuation rate of bending waves in the plate. Since it is the reflection of these waves which generate the standing waves of the normal modes of vibration, when these bending waves are attenuated sufficiently in traveling one span of the plate, standing waves and hence normal modes of vibration will become insignificant.

The attenuation rate of lateral bending waves in plates per unit wavelength is given by (see Section 3.3.7, Chapter 3)

$$\mu = 4.34 \pi \eta \text{ dB/wavelength}$$

where

$\eta$  = the material loss factor  $\approx 1/Q$ .

The bending wavelength,  $\lambda_B'$ , of plates of thickness  $h$  is given by

$$\lambda_B' = \sqrt{1.9 c_L h / f}$$

Thus, in traveling a distance  $a$  equal to an average span of the plate, the attenuation in the amplitude of free bending waves would be

$$A = \frac{\mu a}{\lambda_B'} = \frac{4.34 \pi a}{Q} \sqrt{\frac{f}{1.9 c_L h}} - \text{dB}$$

Choosing a dB loss (or decrease in amplitude by 50 percent) as a minimum criteria for the lower frequency of this "infinite plate" region, the response characteristics of the panel would tend to behave like a resistance for

$$f > 0.36 \frac{c_L h Q^2}{a^2}$$

By superimposing the loss due to attenuation of these bending waves on top of the trend for a linear increase in acceleration response due to the resistive behavior of the panel, the acceleration response will tend to be more nearly constant.

Coincidence Frequency

The coincidence effect, discussed earlier in Section 8.1.2.2, is one significant feature of the vibro-acoustic response of structure at higher frequencies which can be predicted more accurately than the trends indicated above. While the effect is generally not significant from the standpoint of structural loads, it has an effect at excitation frequencies which are important for equipment vibration problems and for sound transmission. The latter aspect is discussed in more detail in Chapter 9.

The following conditions exist at coincidence for acoustic excitation of any structure.

- Acoustic trace wavelength = structural bending wavelength

$$\lambda_t = \lambda_B$$

or

$$\frac{c}{f \sin \psi} = \frac{c_B}{f}$$

- Acoustic trace velocity = bending wave velocity

$$\frac{c}{\sin \psi} = c_B$$

where  $c_B$  is the bending wave velocity in the structure.

The lowest frequency for which this coincidence effect can occur is called the critical frequency  $f_c$  and is defined by

$$f_c \approx \frac{c^2}{1.9 c_L h} \quad \text{Hz} \quad (8.1.45)$$

where

$c$  = speed of sound in air

$c_L$  = longitudinal wave velocity in a bar of the same material as the wall (see Table 3.39, Chapter 3)

$h$  = wall thickness.

For concrete walls, where  $c_L \approx 1.1 \times 10^5$  in-sec, the critical frequency is approximately equal to

$$f_c \approx 860/h$$

where  $h$  = wall thickness in inches.

Typical thicknesses of concrete walls used near rocket test facilities may range from 8 to 24 inches so that the critical frequency for such walls ranges from about 35 to 110 Hz. The maximum response of the structure will occur when the

minimum coincidence frequency also coincides with a natural frequency of the structure. For this condition, the response is limited only by the internal or external damping of the structure.

8.1.3.6 Damping of Wall Vibration Response

A basic limitation in any analytical approach for predicting the vibration response of structure to noise is the uncertainty about the damping of the structure. The various significant forms for this damping are shown in Figure 8.1.33.

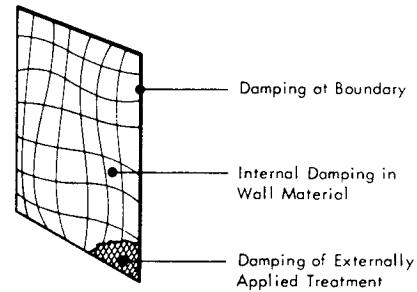


FIGURE 8.1.33 Various Significant Forms of Damping of Wall Vibration

Internal damping of structure has been discussed more fully in Section 3.3.7 of Chapter 3. Practical details of externally applied damping treatment and damping of laminated panel structure is discussed in Chapter 9.

Damping at joints of structural walls is frequently responsible for a major part of the energy loss in the structure. While improved methods are being developed to enhance the damping characteristics of joints, there is relatively little application of this technique for ground structure (Reference 8.1.18).

Some of the more significant aspects of acoustic radiation damping are briefly considered here.

Acoustic Radiation Damping of Walls

For the lower vibration modes of walls, energy is radiated away in the form of acoustic waves. If all other sources of damping are ignored, the approximate value for the resonant amplification factor of a square wall vibrating in its fundamental frequency  $f_{1,1}$  can be determined by the acoustic radiation resistance on both sides of a square plate (Reference 8.1.19). The resulting value for  $Q$  is

$$Q_{1,1} \approx \frac{2\pi f_{1,1} \cdot w/g}{r_A} \quad (8.1.46)$$

where

$w$  = surface weight of the wall with side ( $a$ )

$r_A$  = mechanical resistance per unit area for acoustic radiation from both sides of a square plate. (See Chapter 4 for exact expression for circular piston.)

$$\approx \begin{cases} \pi^2 \rho_o c \left(\frac{f_a}{c}\right)^2, & \frac{f_a}{c} < 1/2\pi \\ \rho_o c, & \frac{f_a}{c} > 1/2\pi \end{cases}$$

$\rho_o c$  = characteristic impedance of air  
= 0.00153 lb-sec/in<sup>3</sup> at 59°F

$c$  = speed of sound in air = 13,400 in/sec.

For the case of the square steel panel considered in the previous example, the required parameters are

$$f_{1,1} = 25 \text{ Hz}$$

$$w = 0.3 \text{ lb/in}^2$$

$$g = 386 \text{ in/sec}^2$$

$$a = 85 \text{ in.}$$

$$\frac{f_{1,1} a}{c} = \frac{(25)(85)}{13,400} \approx 0.1 < 1/2\pi$$

$$r_A \approx 0.00015 \text{ lb-sec/in}^3$$

Thus, the  $Q$  due to acoustic damping alone would be

$$Q_{1,1} = \frac{(6.28)(25)(.3)}{(386)(.00015)} = 810$$

This is a much higher value for the resonant amplification factor than normally observed for actual structure and simply represents an example of the general result that acoustic radiation damping of walls radiating into free space is negligible. A general form for the overall  $Q$  for a square plate vibrating at its fundamental frequency  $f_{1,1}$ , relative to the resonant amplification factor  $Q_m$  due to mechanical losses only, can be shown to be, for  $(2\pi f_{1,1} a/c) < 1$ ,

$$\frac{Q}{Q_m} = \frac{1}{1 + \frac{\pi^2}{2} \frac{\rho_o}{\rho} \frac{c_L}{c} \frac{1}{\sqrt{12(1-v^2)}}}$$

where

$\rho_o, \rho$  = mass densities of air and plate material

$c_L$  = velocity of longitudinal waves in the plate material

$v$  = Poisson's ratio.

This is a constant for a given material and has the value 1/1.0032 for steel and 1/1.0096 for aluminum. Clearly, the affect of acoustic radiation damping can normally be neglected. Quite the opposite result is obtained, however, for wall panels which radiate into a closed duct. In this case, the radiation damping can drastically reduce the maximum response of the fundamental mode of the wall. This can be a significant factor, for example, in sonic fatigue tests of panels conducted in a plane wave test facility when the panel area is of the same order as the cross section of the plane wave test section (Reference 8.1.20).

#### 8.1.4 EMPIRICAL METHOD FOR PREDICTING VIBRO-ACOUSTIC RESPONSE

From the preceding discussion on theoretical approaches for predicting vibro-acoustic response of structure, it may be concluded that

- Response of the fundamental mode response should be predictable providing the modal damping can be defined.
- Effects of diffraction for finite size walls in buildings can be accounted for approximately for the lowest mode of the panel.
- Trends in the response of higher modes can be roughly estimated by simple expressions usable for design purposes. However, significant variations in these trends may be expected for different types of acoustic fields and for different panel configurations.
- It is convenient to define the vibro-acoustic response of structure in terms of a nondimensional "acoustic mobility" parameter equal to the product of the acceleration in  $g$ 's times the surface weight density in psi divided by the acoustic pressure in psi.

In order to verify these theoretical predictions and provide necessary additional details of the response which are not readily predictable, experimental data are required. This section summarizes the available experimental results on acoustic vibration response of ground structure. The data are taken primarily from results reported in Reference 8.1.1 and are presented in the form of acoustic mobility curves as a function of frequency relative to the fundamental frequency of the structure.

The data are then applied, along with the theory in the previous section, to define a simplified semi-empirical method for predicting vibro-acoustic response of ground structure.

The analyzer bandwidth for all of the vibro-acoustic response data reported in Reference 8.1.1 was 16 Hz for part of the tests and one-third octave bands for the remainder. The results obtained with the fixed 16 Hz bandwidth filter have been adjusted to correspond to those measured with the one-third octave band filters. Thus, empirical values of acoustical mobility defined in this

section are equal to the ratio of the rms acceleration  $[A(f)]$  in g's to rms pressure  $[p(f)]$  in psi in one-third octave bands, all multiplied by the surface weight  $[w]$  in psi. This modified form for acoustic mobility is chosen for practical convenience to be consistent with simple methods for experimental analysis and design calculations. The symbol  $M_A$  will be used to identify this dimensionless ratio  $A(f) \cdot w/p(f)$ . The acoustic mobility defined in this form differs from the ideal narrow band value specified in the previous section. The two are related as follows:

For the Fundamental Frequency  $f_{1,1}$

$$M_A^2 = \left[ \frac{A(f) \cdot w}{p(f)} \right]^2 = \frac{\frac{\pi}{2} W_a(f) (f/Q) \cdot w^2}{(0.232 f) W_p(f)} \Bigg|_{f=f_{1,1}}$$

or

$$M_A^2 = \left[ \frac{\pi/2}{0.232 Q} \right] \cdot \left[ \frac{W_a(f) \cdot w^2}{W_p(f)} \right]_{f=f_{1,1}} \quad (8.1.47)$$

(The constant 0.232 represents the relative bandwidth of a one-third octave band filter.)

For the High Modal Density Region

At frequencies where there are many resonant modes within the resonant bandwidth of any one mode, the narrow band acceleration spectrum will vary relatively slowly so that the ideal acoustic mobility will be similar to that measured with a one-third octave band filter (see Equation 8.1.45a).

These subtle differences between practical values for acoustic mobility, based on measured data and the theoretical "narrow-band" value, must be clearly recognized when comparing various empirical vibro-acoustic prediction methods.

#### 8.1.4.1 Vibro-Acoustic Response of Full-Scale Structure

Experimental results from acoustic tests of various types of full scale structural specimens are summarized in this section. The test results were obtained from the detailed measurements reported in Reference 8.1.1.

##### Corrugated Steel Industrial Walls

Four 20 ft by 18 ft industrial walls employing 26-gauge corrugated wall panels were evaluated for vibro-acoustic response in a wide-band noise field. The four wall specimens differed in detail in terms of the following parameters:

- Design Wind Load, 10-25 lb/ft<sup>2</sup>
- Average Surface Weight, 1.59-1.80 lb/ft<sup>2</sup> (including supporting steel girts)
- Fasteners - Ranging from No. 14A Self-Tapping Screws to Blind Lock Rivets
- Insulation - Three walls without insulations; one wall lined with 1-1/2 inch vinyl-backed fiberglass bats.

A photograph of two of the walls in-place, viewed from inside the 100,000 cu ft acoustically reverberant test chamber, is shown in Figure 8.1.34. The acoustic excitation consisted of wide-band random noise covering the frequency range from 20 to 3000 Hz. Overall acoustic test levels ranged from 130 to 156 dB. The normalized acceleration response measurements made on these walls are summarized in Figure 8.1.35 by values for the acoustic mobility plotted on a decibel scale.

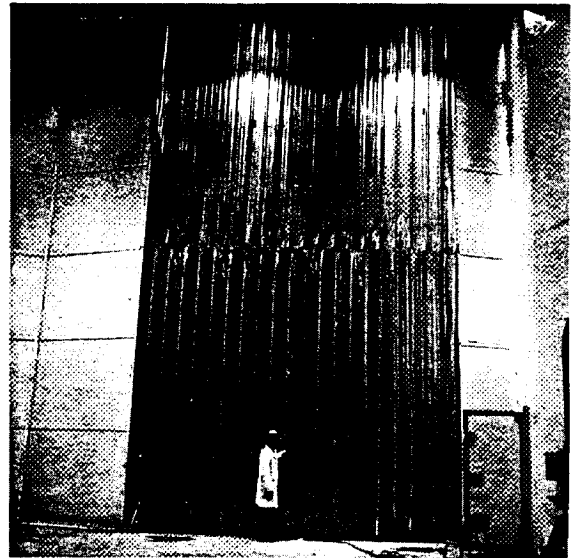
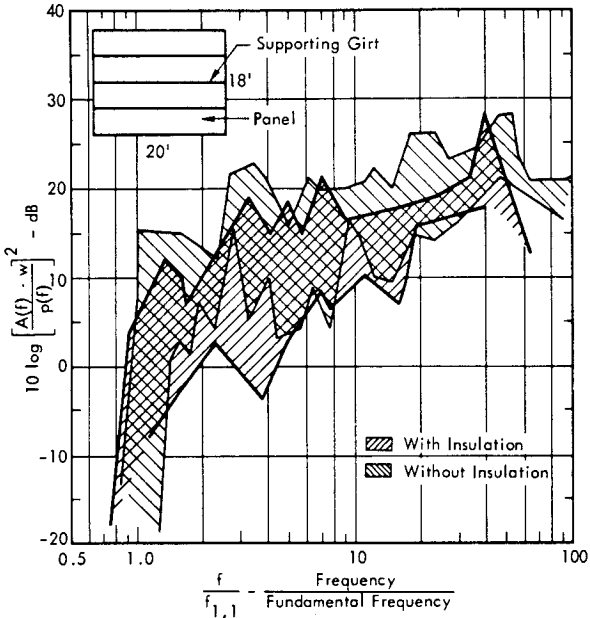


FIGURE 8.1.34 Exterior Side of Industrial Building Wall A (Upper Half), Industrial Steel Building Wall B (Lower Half) Viewed from Within 100,000 Cubic Foot Reverberation Facility

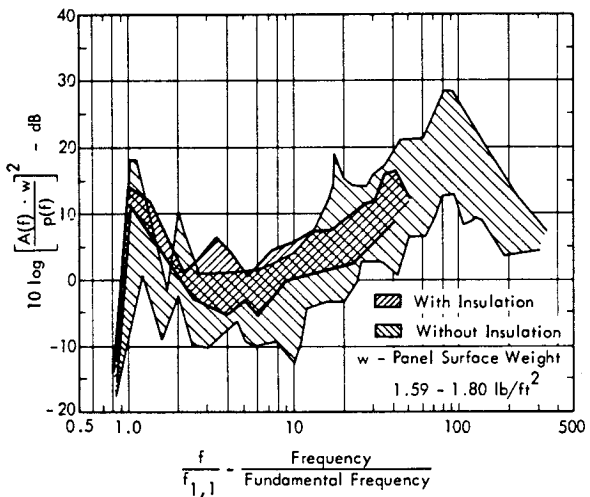
Due to the large size of the test chamber, radiation damping effects on the wall were absent so that the results shown are representative of the vibro-acoustic response in free space for excitation by a randomly incident sound field.



Figure 8.1.35a shows the normalized acceleration response as measured at locations between the lateral stiffeners (or girts) which were used to support the panel sections. Figure 8.1.35b shows similar data obtained directly on the stiffeners. Data reported for the wall lined with insulation indicated a damping effect which resulted in slightly lower response levels.



(a) Acceleration Measured on Panel Between Girts



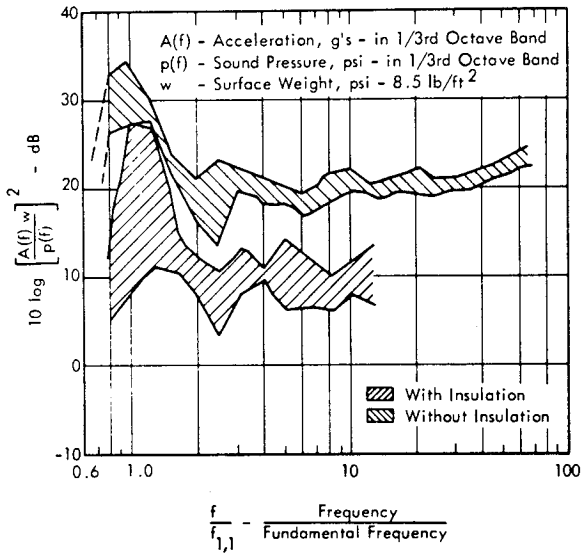
(b) Acceleration Measured on Panel Support Girts

FIGURE 8.1.35 Measured Acoustic Mobility For 20 ft by 18 ft, 26-Gauge Corrugated Steel Walls

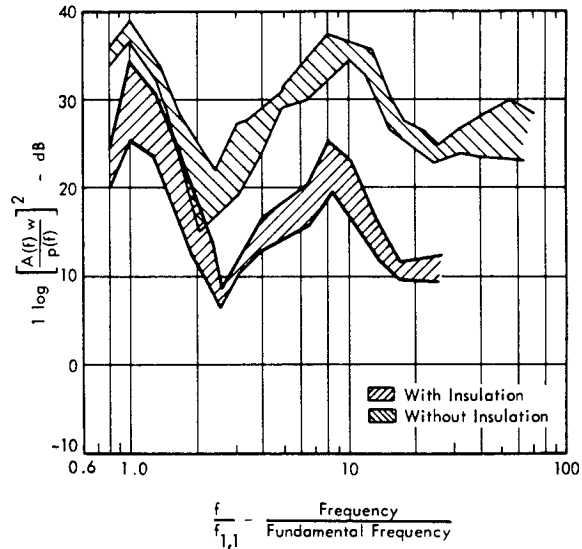
Residential Structure

Results from acoustic tests of several different types of residential structure, defined in detail in Reference 8.1.1, are summarized in the following figures. The data have been normalized to the acoustic mobility for the types of residential structure listed below.

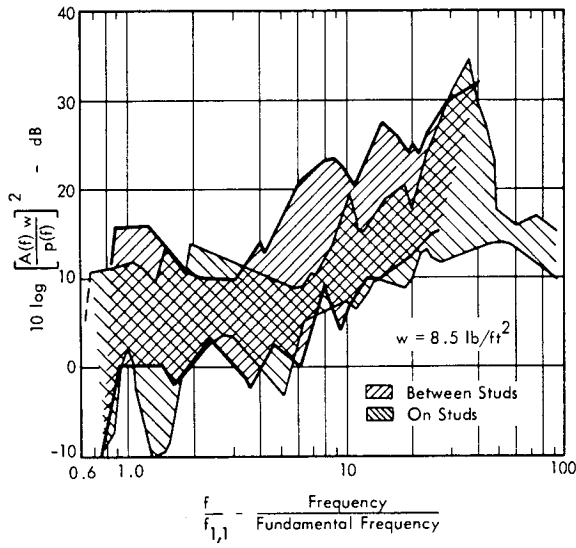
- 8 ft by 10 ft section of a standard wood frame wall with and without insulation (see Figures 8.1.36a,b)
- 8 ft by 10 ft section of insulated wood frame walls with wood or aluminum windows (see Figure 8.1.36c)
- 8 ft by 10 ft section of a standard 8 in. hollow concrete block wall (see Figure 8.1.36d)
- 14 ft by 10 ft section of a wood frame roof with and without a finished ceiling (see Figure 8.1.36e)



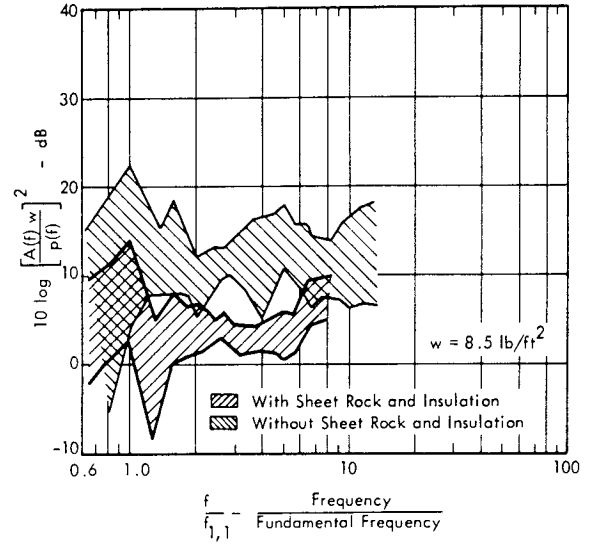
a) Wood-Frame Wall, Acceleration Measured on Studs



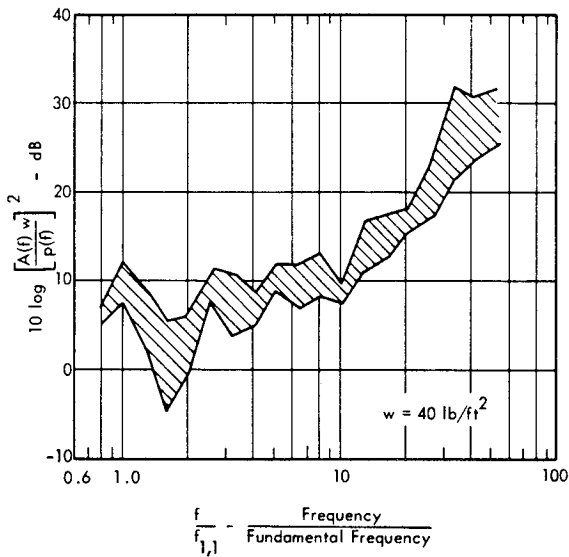
b) Wood-Frame Wall, Acceleration Measured between Studs



c) Wood-Frame Wall with Window



e) Wood-Frame Roof Section



d) 8 inch Concrete Block Wall

FIGURE 8.1.36. Envelope of Measured Acoustic Mobility for Residential Walls. (Reference 8.1.1)

These envelopes of acoustic mobility exhibited the general trends indicated below.

- The acceleration response was usually reduced very significantly by the addition of insulating materials such as fiberglass blankets.
- Response measurements made at locations between the the wood studs generally exhibited a marked increase in the frequency range from 60 to 200 Hz relative to the response of the wood frame.
- The presence of a window tended to reduce the maximum response in the fundamental mode.

Results from these two sets of full scale test data will be incorporated into design charts in Section 8.1.4.3.

### 8.1.4.2 Vibro-Acoustic Response of a Model Scale Building

The results analyzed above provide a basis for defining the acoustic mobility of isolated wall specimens mounted in a rigid "infinite" baffle, that is, effects of diffraction and sound transmission through adjacent wall areas were not represented. A comprehensive model test is also reported in Reference 8.1.1, which provides basic data on the vibro-acoustic response of a three-story, four-bay building structure. Results from this test provide basic data on these additional effects on the acoustic response of ground structure. As discussed in detail in Reference 8.1.1, the model was constructed on a 1:16 scale to closely simulate the bending stiffnesses and weight distributions of a typical steel frame curtain-wall structure. Some of the details of this model are illustrated in Figure 8.1.37 and 8.1.38. Additional scaling details not shown included:

- Simulation of moment- and shear-carrying connections between beams and girders as used in typical building construction.
- Simulation of different bending stiffnesses in each direction for the scale model wall and roof panels to correspond, dynamically, to similar characteristics of full scale corrugated steel and concrete structure.

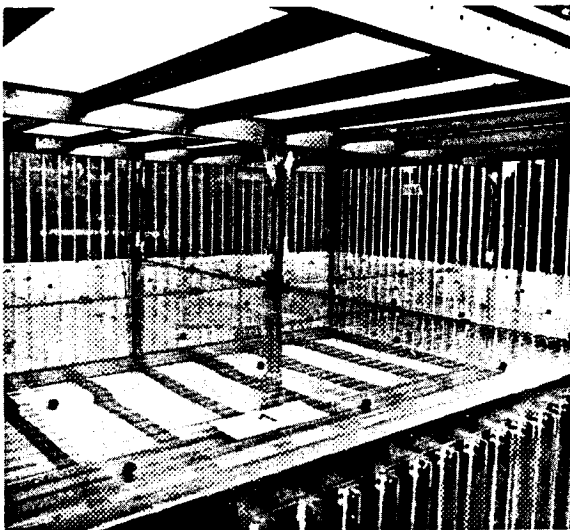


FIGURE 8.1.37 Model Building Wall and Floor Installation Details

The scale model was excited acoustically by a single source of wide band random noise located at an equivalent full scale distance of 640 feet from the building. Acceleration measurements made at various wall, floor and roof locations on the building are summarized in the form of acoustic mobility curves in Figure 8.1.39a. Part (a) shows the lateral (normal to surface) responses measured on side walls and on the second floor and roof. The data are segregated into two groups - one referring to measurements at the center of the wall or ceiling panel in a given bay; the other group representing responses near a column. The

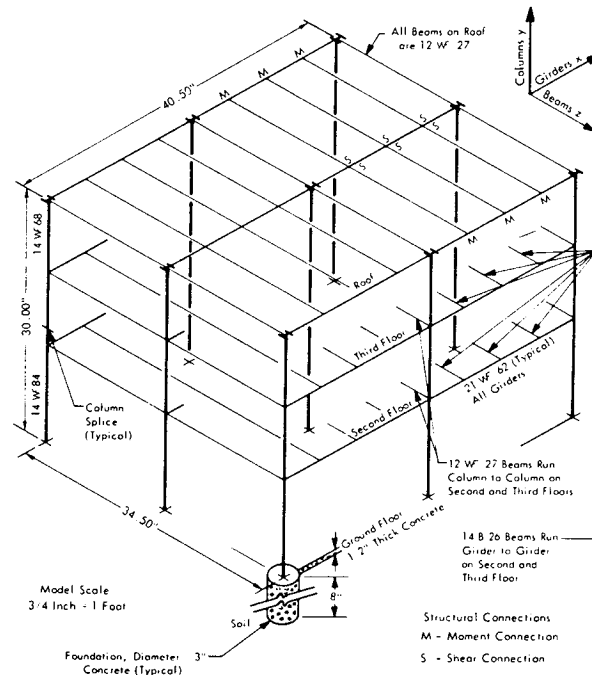


FIGURE 8.1.38 Model Building Structural Frame

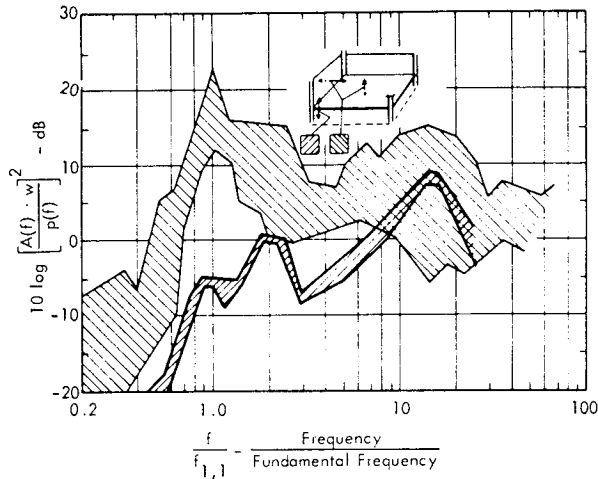
narrow range of the latter data is due to the smaller number of measurements available for these locations. Near the fundamental panel frequency, the acoustic mobility observed at the center of the wall and roof panels is, of course, much greater than the values near column supports.

Part (b) of Figure 8.1.39 summarizes the maximum envelope of "acoustic mobility" for the in-plane responses measured at 22 locations on the model. The values are well below those for lateral motion near the fundamental panel frequency but increase rapidly at higher modes to become comparable to the latter motion mobilities. This can be considered to be the frequency range corresponding to a reverberant vibration field.

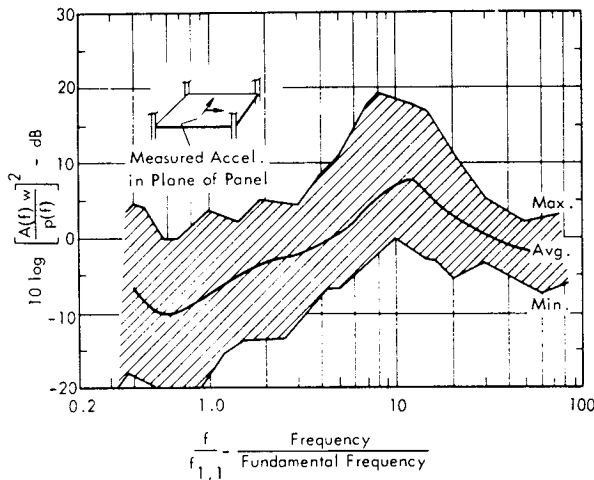
#### Diffraction Effects on Model

The shortest dimension at the front face of the model was 30 inches. According to Figure 8.1.9 in Section 8.1.1.2, the effective sound pressure on the model building would gradually increase to twice the incident sound pressure over a frequency range from 67 to 370 Hz. The natural frequencies of the wall and roof panels for the model building varied from 125 to 315 Hz. Thus, the effective total pressure acting on the walls near the fundamental mode would be from 0 to 3 dB below the ideal value for an infinite baffle, and mobilities observed near these modes would be slightly less than expected from the previously described panel tests.

Additional details on vibration transmission measurements on this model building are discussed in Chapter 9.



(a) Lateral Acoustic Mobility of Model Walls and Floors (Based on Nine Measurement Locations)



(b) In-Plane Acoustic Mobility of Model Walls (Based on Twenty-One Measurement Locations)

FIGURE 8.1.39 Acoustic Mobility for Model Scale Building Structure (Data from Reference 3.1.1)

8.1.4.3 Empirical Prediction Procedures

The experimental data reviewed in the previous section can be used to develop an empirical method for predicting vibro-acoustic response of structure. First, consider the results obtained near the fundamental mode of the panels or walls.

Estimated Acoustic Mobility for Fundamental Mode

The estimated average value and standard deviation for the acoustic mobility of industrial and residential structure in the fundamental mode are listed in Table 8.1.5. These may be compared with predicted values based on the theory developed in Section 8.1.3. From Table 8.1.4, the space average acoustic mobility  $\bar{A}(f) \cdot w/p(f)$  for a simply-

supported panel under excitation by a normal incidence wave would be, according to Equation 8.1.47

$$\begin{aligned} \left[ \frac{\bar{A}(f) \cdot w}{p(f)} \right]_{f=f_{1,1}} &= \left[ \frac{\pi/2}{0.232 Q} \right]^{1/2} \left[ \frac{8}{\pi^2} Q \right] \\ &= 2.12 \sqrt{Q} \end{aligned}$$

TABLE 8.1.5

TYPICAL MEAN VALUES AND STANDARD DEVIATION FOR MEASURED ACOUSTIC MOBILITY FOR THE FUNDAMENTAL MODE OF VARIOUS STRUCTURES

Mean value specified as the dimensionless quantity  $\bar{M}_A = \bar{A}(f) \cdot w/p(f)$  where  $\bar{A}(f)$  = space average acceleration in g's at the fundamental frequency,  $p(f)$  is the pressure in psi at this pressure and  $w$  is the surface weight in psi. Mean and standard deviation also given in decibel form as  $10 \log (\bar{M}_A)^2$ .

Type of Structure	Acoustic Mobility		
	$\bar{M}_A$ (Mean)	$10 \log [\bar{M}_A]^2$ (Mean)	(Std. Dev.)
Corrugated Steel Walls (1)	5.6	15.0	4.5
Wood Residential Walls (1)	8.0	18.0	4.0
Scale Model Building (1)	4.5	13.0	4.2
Average for Ground Structure	6.0	15.5	4.2
Average for Rocket Vehicle Structure (2)	8.0	18.0	6.0

(1) Data from Reference 8.1.1

(2) Data from Reference 8.1.21

Lacking any statistically reliable data on the resonant amplification factor  $Q$  for ground structure, values from evaluation of space vehicle vibration data are used to provide a theoretical prediction for the acoustic mobility. The distribution for measured values of  $Q$  for flight vehicle structure, from Reference 8.1.20, is shown in Figure 8.1.40, in the form of a probability density plot for the damping factor  $\eta = 1/Q$ . Based on these data, the approximate mean value for  $Q$  is 18.5 which gives a predicted mean value for the ideal space average acoustic mobility of  $2.12 \sqrt{18.5} = 9.1$  for a single panel. As expected, this is similar to the average values shown in Table 8.1.5 of 6.0 for ground structure and 8.0 for rocket vehicle structure.

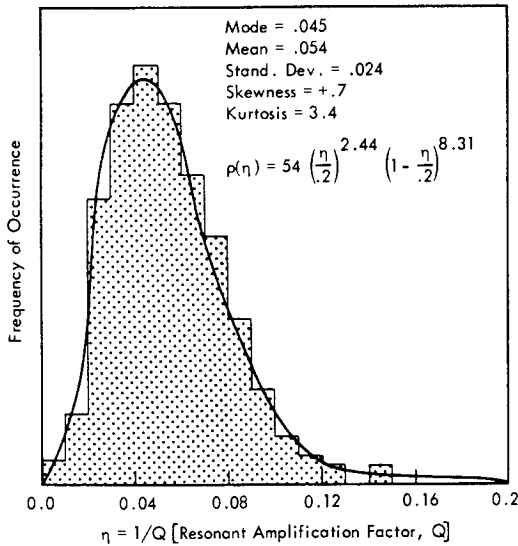


FIGURE 8.1.40 Statistical Distribution of Resonant Amplification Factor, Q, Observed for Flight Vehicle Vibration (Data from Reference 8.1.20)

Empirically Derived Design Values for Acoustic Mobility for Ground Structure

Estimated values for the average and standard deviation for acoustic mobility at the fundamental frequency are specified in Table 8.1.5. These can be used as a foundation for empirically derived values for the acoustic mobility for typical ground structure at all frequencies. These are shown in Figures 8.1.41 and 8.1.42 for industrial-type walls and residential walls, respectively. These figures are developed in the following manner.

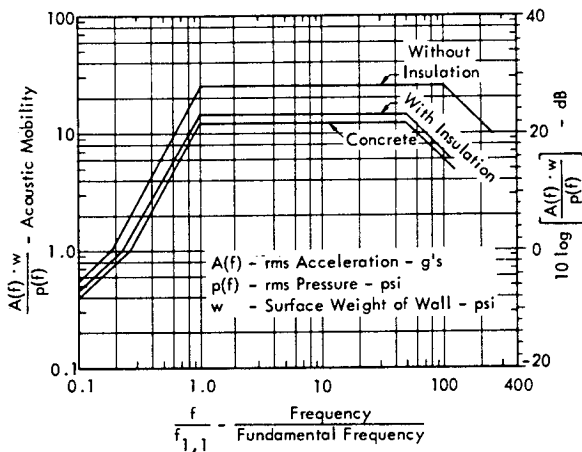


FIGURE 8.1.41 Design Envelope for Acoustic Mobility of Concrete and Corrugated Steel Industrial Walls, With and Without Insulation

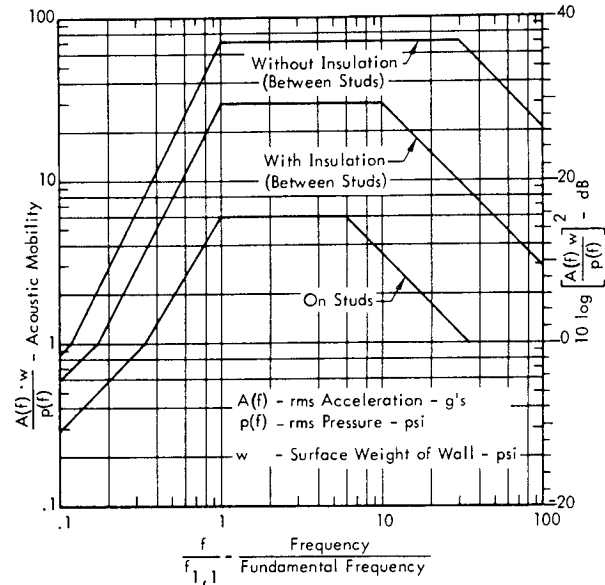


FIGURE 8.1.42 Design Envelope for Acoustic Mobility of Wood Residential Walls

- The maximum value of acoustic mobility at the fundamental frequency ( $f = f_{1,1}$ ) of the wall corresponds to an approximate upper bound of the measured data illustrated in Figures 8.1.35-8.1.39 for the corresponding type of building structure.
- Below the fundamental natural frequency mode, the acoustic mobility is assumed to be proportional to  $f^2$  based on the decrease in the sinusoidal transfer function  $(f/f_{mn})^2 |H_{mn}(f)|$  for acceleration response.
- Above the fundamental frequency, the acoustic mobility, shown in Figure 8.1.41 or 8.1.42, is extended at a constant value to an upper limiting frequency  $f_U$  and then decreased at a rate  $\propto 1/f$ . The upper limiting frequency is assumed to be at least 5 times the fundamental frequency  $f_{1,1}$ , or higher, as indicated by the experimental data.

Application of these design curves is illustrated for the following case.

- Given an acoustic environment in terms of one-third octave band sound pressure levels, or 1/3 OBL, find the rms acceleration in g's at the fundamental frequency of a steel wall with a surface weight  $w$  of 0.1 psi.
- ▲ Find the rms pressure  $p(f)$  in the one-third octave band at the fundamental frequency of the panel using the conversion chart in Chapter 12. If the one-third OBL is 160 dB, the rms pressure is 0.3 psi.

- ▲ For the steel plate, use the value of acoustic mobility  $[A(f) w/p(f)]$  given in Figure 8.1.41 for corrugated steel. At  $f/f_{1,1} = 1$ , this is 25.
- ▲ Compute the rms acceleration  $A(f)$  at the fundamental frequency by the expression

$$A(f) \approx \left[ \frac{A(f) w}{p(f)} \right] \cdot \left[ \frac{p(f)}{w} \right] - g's \text{ (rms)} \tag{8.1.48}$$

From the values given

$$A(f) = \frac{(25) (.3)}{(.1)} = 75 \text{ g's (rms)}$$

This would be the rms acceleration measured at the fundamental frequency by a system with a bandwidth greater than the resonant bandwidth of the panel (i.e., one-third octave band).

Statistical Variation in Acoustic Mobility

To provide some degree of statistical confidence for a result computed by the preceding methods, the statistical variation in acoustic mobility of structure should be considered.

The statistical distribution in the acoustic mobility observed for the full scale and model scale tests reviewed in the preceding sections is illustrated in Figure 8.1.43. Comparable values for the acoustic mobility observed for other types of structure are also indicated in this figure for the sake of comparison (Reference 8.1.21). Due to the greater quantity of data available, the latter tend to illustrate more clearly the systematic statistical distribution that is apparent in this vibro-acoustic response parameter. It should be recognized that a number of sources of variation are involved.

- Variation in the type of acoustic field (i.e., plane progressive to diffuse)
- Diffraction effects not accounted for in the definition of the acoustic pressure spectrum.
- Structural configuration and boundary conditions.
- Degree of damping, both internal and external.

The general similarity of these statistical distributions is surprising considering the number of possible sources of variation. The significance of these data may be illustrated by indicating the approximate probability of exceedance for any given acoustic mobility factor,  $M_A$ , relative to its mean value. This is illustrated in Figure 8.1.44 by a plot of the cumulative distribution of relative acoustic mobility from an extensive collection of measurements on rocket vehicles. The data show that approximately 95 percent of the time, the acoustic mobility will be less than four times the mean value.

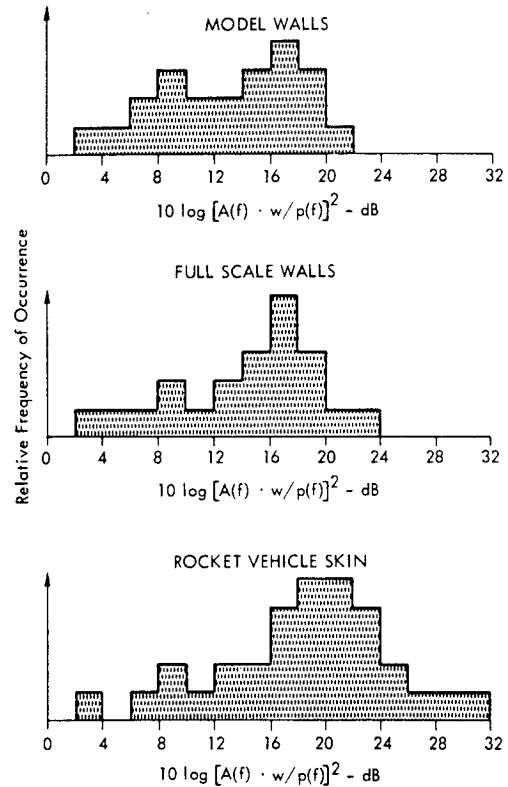


FIGURE 8.1.43 Distribution of Acoustic Mobility (dB) at the Fundamental Mode for Model and Full Scale Walls and Rocket Vehicle Skin (Data from References 8.1.1 and 8.1.2)

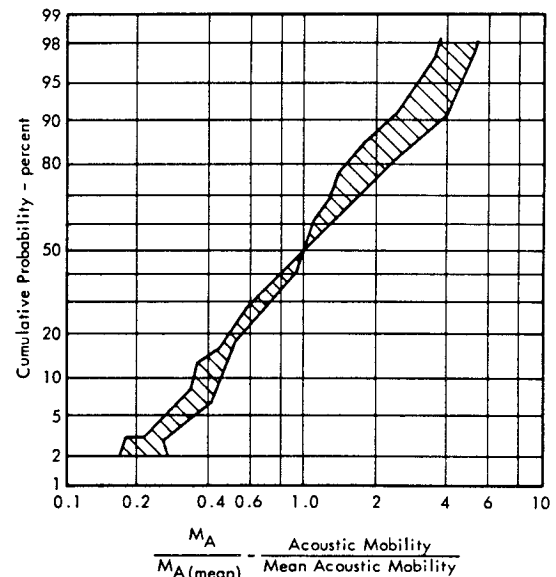


FIGURE 8.1.44 Cumulative Probability of Acoustic Mobility Relative to Mean Value Based on Data Measured on Rocket Vehicle Structure (Data from References 8.1.21-8.1.23)

8.1.5.1 Dynamic Stresses in Structure Subjected to Acoustic Loads

In the example worked out in Section 8.1.3.4, page 8-26, approaches for predicting dynamic stresses were utilized. The first was based on the classical method which is simply an extension of basic static stress analysis techniques. This technique is discussed in more detail in Section 3.3.6 of Chapter 3. It will generally involve the prediction of the peak displacement for at least the fundamental mode of a wall or roof panel under acoustic loading. The dynamic deflection can then be used to compute the stress directly or can be used to define an equivalent static load which would produce the same peak stress. The latter technique will often provide the most convenient approach for the structural analyst since the capability of a given building design to withstand given static loads is usually well defined.

The second general approach was based on the relationship between peak dynamic stress in a structure vibrating in a harmonic mode definable by sinusoidal mode shapes and the peak modal velocity (Reference 8.1.25).

Each of these equivalent techniques are considered here but the principal emphasis will be placed on the second method. It offers a simpler approach which provides a practical approach for dynamic stress analysis of building

8.1.5.2 Classical Method for Dynamic Stress Analysis

The Direct Approach

By combining the basic equations for bending stresses in plates (see Equation 3.364, page 3-145), with the equations for the resonance frequency of plates (see Section 3.3.5.6, page 3-130), the expression for the peak dynamic stress in the m<sup>th</sup> mode of a simply-supported plate with a modal acceleration amplitude  $\bar{a}_{mn}$  can be shown to be

$$\sigma_{max} = \frac{6}{\pi^2} \frac{\left[ \left( \frac{m}{a} \right)^2 + v \left( \frac{n}{b} \right)^2 \right]}{\left[ \left( \frac{m}{a} \right)^2 + \left( \frac{n}{b} \right)^2 \right]^2} \frac{w}{h^2 g} F_c \bar{a}_{mn} \quad (8.1.49)$$

where

m, n = mode numbers for plate along sides a and b (a < b), respectively

v = Poisson's ratio

w/g = surface mass of plate

F<sub>c</sub> = stress concentration factor

h = true total thickness of plate.

This maximum fiber stress is at the center of the plate in a direction parallel to the short side (a).

Combining the theory reviewed earlier in this chapter for the acceleration response of structure in its normal modes with the theory for the response of single degree-of-freedom systems to random excitation (see Section 3.2.3, Chapter 3), it can be shown that for excitation by a wide band random noise, the peak modal acceleration is

$$\bar{a}_{mn(max)} \approx 12 \left[ \frac{\pi}{\sqrt{2}} \right]^{1/2} \frac{F_p J_{mn} \sqrt{Q_{mn}} p(f_{mn})}{w/g} \quad (8.1.50)$$

where

F<sub>p</sub> = effective peak to rms ratio for random noise  
 ≈ 2.2 to 3

J<sub>mn</sub> = joint acceptance (to first power) for m<sup>th</sup> mode

Q<sub>mn</sub> = resonant amplification factor for m<sup>th</sup> mode

p(f<sub>mn</sub>) = rms pressure in one-third octave band at the m<sup>th</sup> natural frequency.

(The approximation indicated involves only a rounding error of 1.3 percent in the constants involved in converting a random noise pressure spectral density to an rms one-third octave band pressure.) Combining these two expressions, the peak dynamic stress in the m<sup>th</sup> mode of a simply-supported plate under a random acoustic load is

$$\sigma_{max} = 11.0 \frac{\left[ 1 + v \left( \frac{a/m}{b/n} \right)^2 \right] F_c F_p J_{mn} \sqrt{Q_{mn}} \cdot \left( \frac{a}{h} \right)^2 p(f_{mn})}{\left[ 1 + \left( \frac{a/m}{a/n} \right)^2 \right]^2 m^2} \quad (8.1.51)$$

where the constants involved are defined in the preceding equations. The important points indicated by this expression are:

- A decrease in stress with mode number m beams evident indicating that the maximum stress will tend to be greatest in the fundamental mode.
- The span to thickness ratio a/h pertains to the geometric dimensions so that the expression is still valid for honeycomb or other nonhomogeneous (but isotropic) plates.
- The peak stress for random loads varies as the square root of Q instead of the first power as for sinusoidal excitation.

For the case of a square steel plate vibrating in its first mode under a normally incident acoustic wave, then a = b, v = 0.3, J<sub>mn</sub> = 4/π<sup>2</sup>, m, n = 1 so that, with g = 386 in/sec<sup>2</sup>, the simple expression obtained is

$$\sigma_{max} = 1.45 F_c F_p \sqrt{Q_{1,1}} \left( \frac{a}{h} \right)^2 p(f_{1,1}) \quad (8.1.52)$$

8.1.4.4 Acoustic Excitation of Bending Vibrations of Buildings

The vibro-acoustic response of structure considered up to this point has been concerned only with lateral bending vibrations of individual building wall or roof panels. One example of the acoustic excitation of bending vibrations of an entire building has been noted (Reference 8.1.24).

During static test firings of a large multi-million pound thrust rocket, displacement amplitudes were measured on the top of a nearby nine-story building, as illustrated in Figure 8.1.45. The observed and computed results for this situation are summarized below.

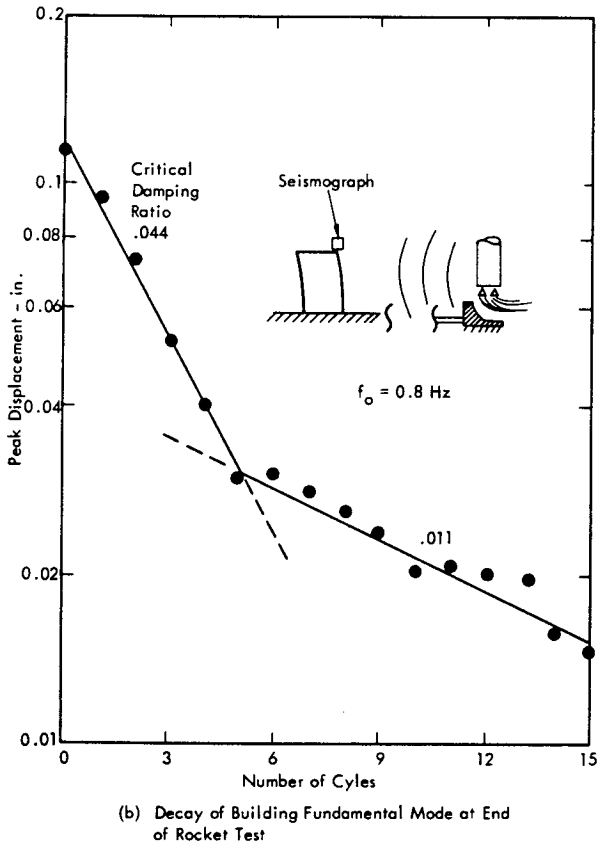
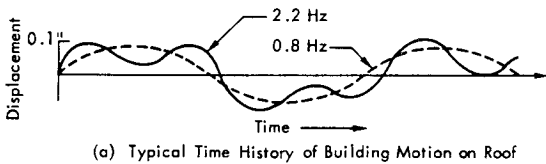


FIGURE 8.1.45 Observed Bending Vibration of Nine-Story Building Due to Acoustic Excitation (Data from Reference 8.1.24)

Observed Motion (Measured with Seismograph)

- Peak Displacement at Top of Building in Direction of Source  
0.04 to 0.11 in. at 0.8 Hz  
0.01 in. at 2.2 Hz

- Peak Velocity 0.14 in/sec at 2.2 Hz

Predicted Motion

- Estimated Octave Band SPL at 0.8 Hz = 76 dB
- Diffraction Correction (Figure 8.1.11)  
Building Width (Approx.) = 100 ft  
Width/Wavelength Ratio ≈ 0.07  
 $20 \log [\text{Effective Force/Incident Force}] \approx -3 \text{ dB}$
- Joint Acceptance Correction (Figure 8.1.18)  
Building Height (Approx.) = 100 ft  
"Beam" Length/Wavelength Ratio ≈ 0.07  
 $10 \log [J_o^2(f)] = -6 \text{ dB}$
- Building Mass =  $0.84 \times 10^6 \text{ lb-sec}^2/\text{ft}$   
Generalized Mass Fraction ≈ 1/4
- Displacement Spectral Density -  $W_x(f) = 0.21 \text{ in}^2/\text{Hz}$
- Resonant Amplification Factor (Figure 8.1.45)  $Q = 11$
- rms Displacement

$$\tilde{X} = \left[ \frac{\pi}{2} W_x(f) \cdot \frac{f_o}{Q} \right] = 0.15 \text{ in.}$$

- Peak Displacement Amplitude at 0.8 Hz

$$\tilde{X}_{\text{max}} \approx \sqrt{2} \tilde{X} = 0.22 \text{ in.}$$

The 2 to 1 difference between predicted and observed peak motion at the fundamental mode of 0.8 Hz is not unreasonable for this situation due to the difficulty of accurately predicting the true sound pressure levels at such low frequencies (see Chapters 6 and 7).

This problem is considered here principally to illustrate a potential hazard that could be encountered at a future rocket test or launch site involving very high energy at low frequencies. However, at least an order of magnitude increase in the vibration observed in this case would probably be required before any light structural damage would be expected. However, it should be pointed out that the observed levels illustrated in Figure 8.1.45 were definitely noticeable subjectively.

8.1.5 EVALUATION OF ACOUSTIC FATIGUE OF BUILDING STRUCTURE

A primary application of this section of Chapter 8 on acoustic loads on buildings is the evaluation of potential fatigue damage to structure resulting from the imposed acoustic loads. This evaluation process involves two principal steps.

- Prediction of the peak dynamic stress, and
- Prediction of cumulative fatigue damage.

Each of these steps is considered in this section.



With these expressions, the critical rms one-third octave band pressure (or equivalent rms octave band pressure  $p_{ob}(f) = 3.04 p(f)$ , can be determined which will cause excessive stresses in a vibrating structure whose geometry and stress capability are known.

The Equivalent Static Load Approach

An alternate form of the classical method simply equates the static and dynamic loads for a structure which give the same peak stress. Consider the case of a simply-supported plate vibrating in its first mode under a normal incidence wide-band random noise. The result to be given also applies when the acoustic wavelength is much greater than two times the largest panel dimension, regardless of the angle of incidence. Then it can be shown that the equivalent uniform static pressure on the panel  $p_s$  which produces the same peak stress as the wide band acoustic pressure is given by

$$p_s = 1.23 K' F_c F_p \sqrt{Q_{1,1}} p(f_{1,1}) \quad (8.1.53)$$

where

$K'$  = a constant dependent on the panel aspect ratio and Poisson's ratio

$Q_{1,1}$  = resonant amplification factor for first mode

$F_c$  = stress concentration factor  $\approx 1.5-2$

$F_p$  = effective peak/rms ratio  $\approx 2.2-3$

$p(f_{1,1})$  = rms pressure in one-third octave band of noise centered at fundamental frequency  $f_{1,1}$ .

The constant  $K'$  has the following values for a Poisson's ratio of 0.3.

a/b	0	0.2	0.4	0.6	0.8	1.0
$K'$	4.83	4.60	4.15	3.77	3.91	4.11

8.1.5.3 The Modal Velocity Method for Predicting Dynamic Stresses

As discussed in detail in Section 3.3.6.6, page 3-156, the peak dynamic stress in a plate vibrating in a sinusoidal mode mn can be given by

$$\sigma_{mnmax} = K_s E \frac{\bar{q}_{mn}}{c_L} \quad (8.1.54)$$

where

$\bar{q}_{mn}$  = modal velocity amplitude for mnth mode

$K_s$  = shape factor which varies from 1.2 to 1.8 for sinusoidal-like mode shapes of plates (see Figure 3.110, page 3-158)

$E$  = modulus of elasticity of plate material

$c_L$  = longitudinal wave velocity =  $\sqrt{E/\rho}$ .

Note that all the constants involved except  $\bar{q}_{mn}$  are dependent only on material properties and shape of the structure and are independent of size.

A basic reason for employing this convenient form is that it tends to confirm extensive practical experience with damaging dynamic stresses in buildings subjected to various forms of ground motion such as quarry blasts, and earthquakes. The criteria for building damage, in this case, is approximately defined by a critical velocity of the structure equal to approximately 2 in/sec. This is illustrated by the extensive summary of data in Figure 8.1.46 on damaging displacement amplitudes versus frequency of the building vibration (Reference 8.1.26). Lines sloping down at 45 degrees through the data correspond to lines of constant velocity. The line for a velocity of 2 in/sec provides a consistent demarcation between no damage and damage.

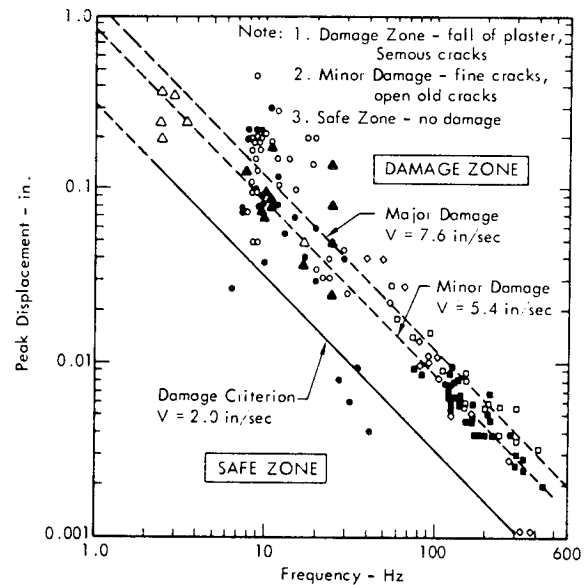


FIGURE 8.1.46 Correlation of Peak Velocity of Building Structure with Damage Due to Quarry Blasts and Earthquakes (Adopted, in part, from Reference 8.1.26)

LEGEND

- ◇ Martin Company - 135dB Sinusoidal
  - Bureau of Mines
  - Langefors
  - △ Edwards and Northwood
  - Bureau of Mines
  - Langefors
  - ▲ Edwards and Northwood
- { Major Damage Data  
 { Minor Damage Data

With this expression, a critical modal velocity can be defined for a given critical stress. This velocity response can then be related to the excitation through Equation 8.1.50. In this way, it can be shown that for simply-supported plates, the critical one-third octave band pressure  $p(f)_c$  for a given critical modal velocity  $\bar{q}_{mn_c}$  can be given by

$$p(f)_c \approx \frac{3}{2} \frac{\pi}{g} \left[ \frac{\sqrt{2}}{\pi} \right]^{1/2} \frac{f \cdot w}{F_c F_p J_{mn} \sqrt{Q_{mn}}} \bar{q}_{mnc} \tag{8.1.55}$$

where the constants are the same as defined earlier.

For example, for the first mode of a simply-supported plate, setting  $F_c = 1$ ,  $F_p = 3$ , and  $J_{mn} = 4/\pi^2$ ,

$$p(f)_c \approx 0.0068 \frac{f \cdot w \cdot \bar{q}_c}{\sqrt{Q_{1,1}}}$$

Thus, for a given value for the critical modal velocity  $\bar{q}_c$  and assuming a reasonable value for the resonant amplification factor  $Q_{1,1}$ , the critical one-third octave band pressure is readily defined in terms of the product of frequency times surface weight of the wall. This provides a simple method for developing criteria for acoustic damage for various types of wall structure. These criteria are illustrated in more detail in Chapter 5. Values for design stresses for a wide variety of building materials are specified in the tables of material properties in Chapter 12.

8.1.5.4 Fatigue Damage for Acoustic Loads on Ground Structure

Ground facilities located near static test or launch sites for high energy rocket vehicles will be exposed to a varying time-history acoustic loading. Thus, as illustrated conceptually in Figure 8.1.47, for a building located next to frequently used static test stands, an exterior wall can accumulate a large number of fatigue cycles in a relatively short period of time. In constant, a structure located very close to a launch site may receive much exposure in terms of time but the intensity of acoustic loading may be much greater so that fatigue damage accumulated in either case may be comparable.

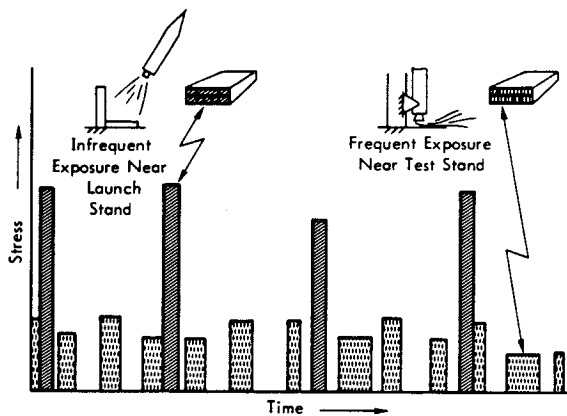


FIGURE 8.1.47 Variation in Duration, Frequency and Level of Acoustic Fatigue Loads on Ground Facilities Near Launch and Static Test Sites

If the useful fatigue life of the structure exposed to this type of loading is of the order of  $10^7$  cycles or more, it is ordinarily sufficient to design the structure so that the peak stress  $\sigma_{max}$  defined by Equation 8.1.51, 8.1.52 or 8.1.54 will not exceed the so-called endurance limit stress  $\sigma_e$ . Ratios of the endurance limit stress to the ultimate tensile strength for a number of materials are listed in Table 12.13, Chapter 12. Values for the endurance limit stress may also be estimated from the fatigue curves for a variety of materials in Figure 12.6, Chapter 12. In the absence of any data,  $\sigma_e$  is frequently taken as 1/2 the ultimate stress.

Fatigue of Concrete

A more detailed evaluation of the fatigue of concrete under random and sinusoidal loading is reported in detail in Reference 8.1.1. The results reported were obtained from fatigue tests conducted on a number of model scale concrete beams. The data provide basic information, previously unavailable from the literature, on random and sinusoidal reverse cycle loading of concrete with standard and light reinforcement. The basic results of the study may be summarized as follows.

- An endurance limit stress could not be clearly established by  $10^6$  cycles of vibration.
- The minimum fatigue strength for reinforced and lightly reinforced beams (i.e., roof planks) is comparable to previously determined values (~ 50 percent of ultimate strength) for zero-to-maximum cyclic loading (see Figure 12.6, Chapter 12).
- For random loading, the fatigue strength appears to be lower by a factor of about 2 at  $10^6$  cycles than for the equivalent fatigue strength with zero to maximum loading.
- The resonant amplification factor and natural frequency for reinforced concrete beams decreases rapidly for random vibration in excess of  $10^5$  cycles with loads which are comparable to the fatigue strength. This is attributed to the accumulation of finite cracks in the concrete.

When the peak stress cannot be limited to less than the endurance limit, then a more sophisticated method of fatigue design is required. This is based on accounting for the accumulation of fatigue damage for a varying stress. There are several theoretical approaches for defining the accumulation of fatigue damage for such variable cycle loading. However, the simplest version is commonly identified as the Palmgren-Miner theory (References 8.1.27 and 8.1.28). This has been designated the linear law and defines damage D as

$$D = \sum_i \frac{n_i}{N_i} \tag{8.1.56}$$

where

$n_i$  = the number of cycles actually occurring at stress amplitude  $S_i$

$N_i$  = the number of cycles necessary to cause failure in fatigue at a constant stress amplitude  $S_i$ .

The damage index  $D$  is a dimensionless number having the value  $0 < D < 1$ , where failure is assumed to occur at  $D = 1$ . Actual experimental fatigue data shows that a mean value of  $D$  at failure is, in fact, roughly equal to 1 (Reference 8.1.29). However, appreciable variation exists for individual cases. This point is considered shortly in more detail. If an appropriate S-N curve is within the limits of data scatter, a straight line on a log-log scale, then

$$N_i = \frac{K}{S_i^\alpha} \tag{8.1.57}$$

where the constant  $K$  is determined from the upper limit of the straight line, i.e.,

$$K = \frac{1}{N_i S_i^\alpha} \tag{8.1.58}$$

and  $1/\alpha$  is the slope of the line. This linear damage scale is indicated in Figure 8.1.48 for random excitation which shows the spread of random stress peaks.

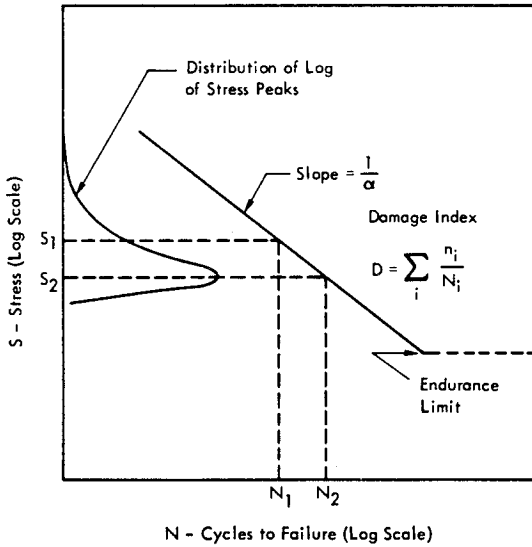


FIGURE 8.1.48 Illustration of Random Stress S-N Curve for Linear Accumulation of Damage

Now if the structure under investigation can be approximated as a linear single degree-of-freedom system with a natural frequency  $f_n$  and with Gaussian white noise excitation, then the average value of damage  $D$  in time  $T$  is

$$D = f_n T K (\tilde{\sigma} \sqrt{2})^\alpha \Gamma \left( 1 + \frac{\alpha}{2} \right) \tag{8.1.59}$$

where

$\tilde{\sigma}$  = overall rms stress, and

$\Gamma (1 + \alpha/2)$  = the standard gamma function of  $(1 + \alpha/2)$ .

The rms stress may be found from Equation 8.1.51 or 8.1.52 by dividing the peak stress  $\sigma_{max}$  by the peak to rms ratio factor  $F_p$ . Assuming failure will occur when  $D = 1$ , then the time to failure is (from Reference 8.1.59)

$$T = \frac{1}{f_n K (\tilde{\sigma} \sqrt{2})^\alpha \Gamma \left( 1 + \frac{\alpha}{2} \right)} \tag{8.1.60}$$

A typical value of  $\alpha$  for most building wall materials is 20 (from Figure 12.6, Chapter 12). Thus,

$$T = \frac{2.7 \times 10^{-10}}{f_n K \tilde{\sigma}^{20}} \tag{8.1.61}$$

Due to the random nature of the excitation and variances between fatigue specimens, experimental fatigue life exhibits a scatter of results along the N axis. An illustration of this scatter is shown in Figure 8.1.49 which indicates various degrees of scatter for 460 fatigue tests. Also, Figure 8.1.50 shows actual fatigue data taken from aluminum specimens. Figure 8.1.51 indicates observed fatigue damage of various building materials exposed to acoustic excitation. Other theories of fatigue in structures are indicated in References 8.1.30-8.1.34.

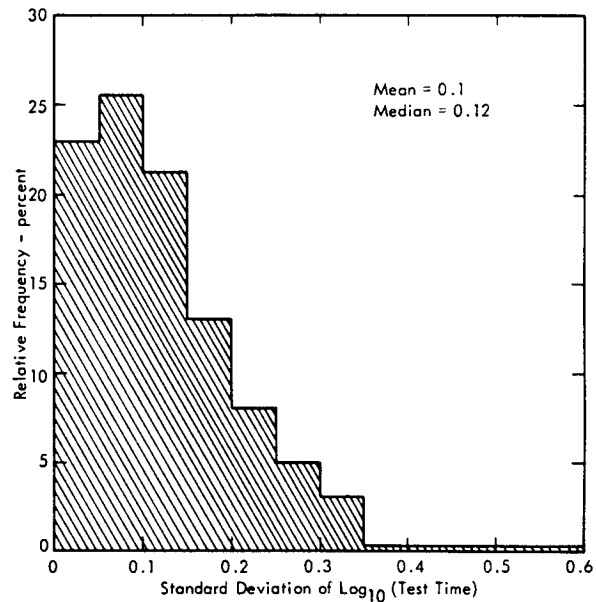


FIGURE 8.1.49 Standard Deviations of Fatigue Data Scatter Based on Fatigue Tests of 460 Test Specimens (Data from Reference 8.1.29)

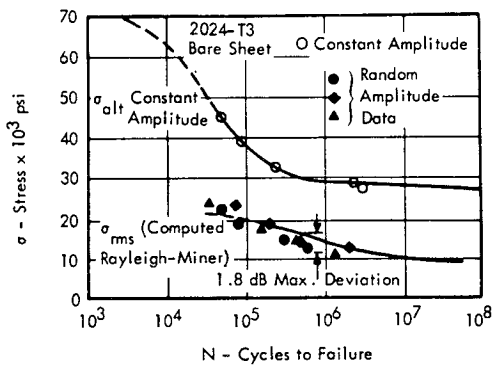
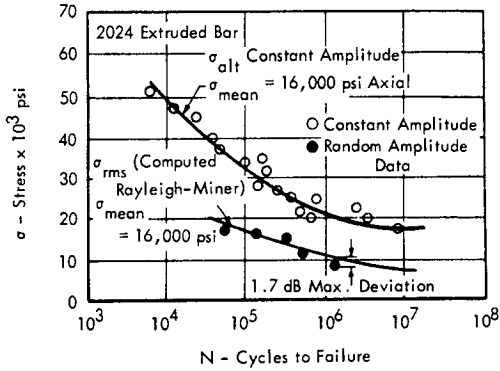
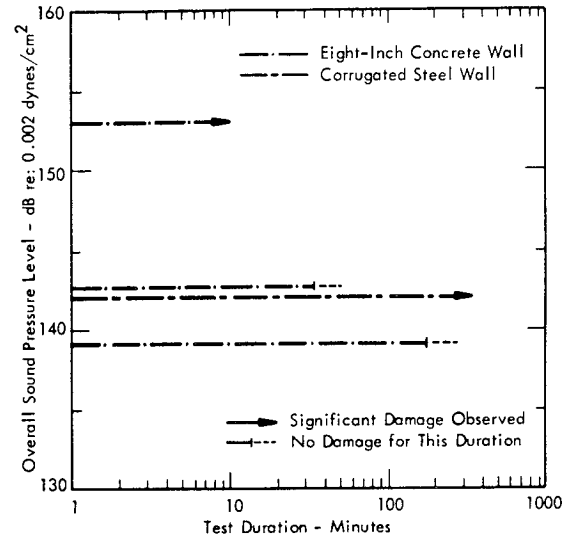


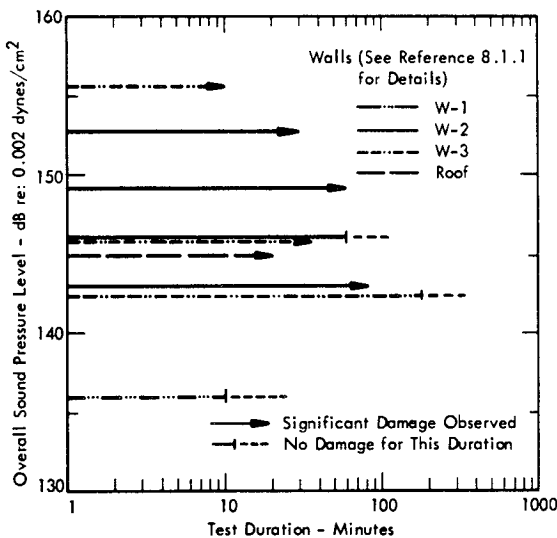
FIGURE 8.1.50 Typical S-N Curves for Aluminum Specimens (Reference 8.1.30)



(b) Eight-Inch Concrete Wall and Steel Industrial Wall

FIGURE 8.1.51 Summary of Fatigue Damage Results from Acoustic Tests of Residential and Steel Industrial Walls (Data from Reference 8.1.1)

Many structures exhibit somewhat nonlinear trends in vibration. The stress response in conventionally mounted windows show these nonlinearities. Figure 8.1.52 (from Reference 8.1.35) indicates this nonlinear stress trend as the acoustic level is increased.



(a) Wood-Frame Residential Walls and Roof Section

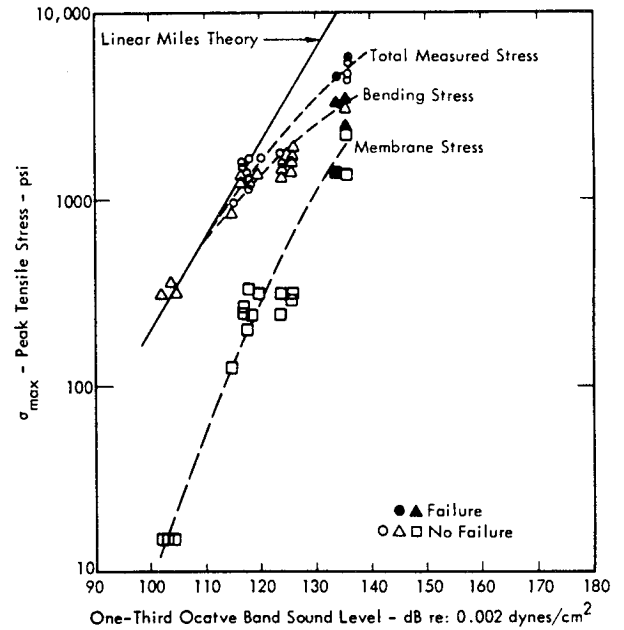


FIGURE 8.1.52 Experimental Data Indicating Nonlinear Trends for Acoustic Fatigue of Windows (Data from Reference 8.1.35)

## 8.2 EXTERNAL BLAST LOADS ON BUILDINGS

### INTRODUCTION

The purpose of this section is to summarize the methods for predicting the response of a building subject to a shock wave due to rocket explosions. The methods considered are based on the extensive literature written on the effects of nuclear blast waves on structures, (References 8.2.1, 8.2.2, 8.2.10, and others). Key elements of this material (primarily from Reference 8.2.1) are included within this section for the sake of completeness of the manual. Accordingly, some repetition cannot be avoided. However, long theoretical discussions will not be included. A list of references is presented in which the reader can find more detailed theory.

The topics to be considered on blast loading will be:

- 1) Determination of the load acting on different types of buildings.
- 2) Idealization of the load in order to simplify the response calculations.
- 3) Representation of the actual building by a spring-mass system having one or more degrees of freedom according to the number of stories of the building.
- 4) Methods of computing the response by the classical and other approximate techniques.
- 5) Comparison of the results obtained by the various response analysis methods.
- 6) Comparison of the various loading function simplifications.
- 7) A method for the rapid verification of the resistance of a building subject to a given overpressure.

At the end of this section, a numerical example, applied to a three-story building, will be developed in order to clarify the analysis procedures presented in the text.

### 8.2.1 DETERMINATION OF BLAST LOADS

The blast loads on building structure, developed in this section, are based on the air blast parameters covered in detail in Chapter 6. Since a blast load consists of a diffraction phase and a drag phase, the computation of a blast load acting on a structure varies according to the following types of structures (Reference 8.2.3):

- a) Structures with resistant walls but without openings or with openings less than 5 percent of the area of the walls.
- b) Structures with openings more than 5 percent and less than 50 percent of the area of the walls.

- c) Structures with openings more than 50 percent of the area of the walls.

Structures to be studied will be oriented with one face normal to the direction of propagation of the shock wave, because this is the most severe loading case. Furthermore, no distinction will be made between structures located in the region of regular reflection and those located in the region of Mach reflection (Section 6.2). The reasons for this simplification are: a) very few data are available within the region of regular reflection, b) the Mach stem results from the fusing of two shock fronts and the single shock front, so formed, has a higher overpressure and a greater destructive potential to structures located in its path; therefore, this simplification leads to conservative results.

#### 8.2.1.1 Loading on Rectangular Structures Without Openings

##### Incident Overpressure and Positive Phase Duration

An illustration of the behavior of a blast wave which reaches a closed rectangular structure is given in Figure 8.2.1. Assume that the overpressure-versus-time function acting on the structure be represented by Figure 8.2.2, where  $p_{so}$  indicates the peak incident overpressure and  $t_p^+$  indicates the duration of the positive phase. The prediction of the later parameter has been covered in Section 6.2.5. However, due to the obvious significance of this parameter for dynamic analysis, it is desirable, to re-examine its magnitude and suggest improvements that may be possible for design. The values for the positive phase durations of overpressure and dynamic pressure presented in this manual are based on limited data from propellant explosions and are not complete or entirely consistent. For both the overpressure and dynamic pressure, two questions are therefore pertinent.

- What is the true value of the positive phase duration for a propellant explosion?
- What is a suitable effective value to use for simplified design analysis. (e.g. - a value equal to the duration of a triangular pulse with the same positive phase impulse)?

##### Overpressure Positive Phase Duration

Figure 8.2.3 compares values of positive phase overpressure duration for TNT explosions predicted analytically (Reference 8.2.7), measured (Reference 8.2.8) and commonly used for design (Reference 8.2.1). The most recent values proposed by the Naval Ordnance Laboratory (Reference 8.2.8) agree well with previous results and appear to be the most reliable estimates of the true value of positive phase duration,  $t_p^+$ . For blast load analysis, a useful simplification is to treat the time history of the pressure as a triangular pulse with the same peak overpressure  $p_{so}$ , and positive phase impulse  $I_p^+$ . The duration of this trian-

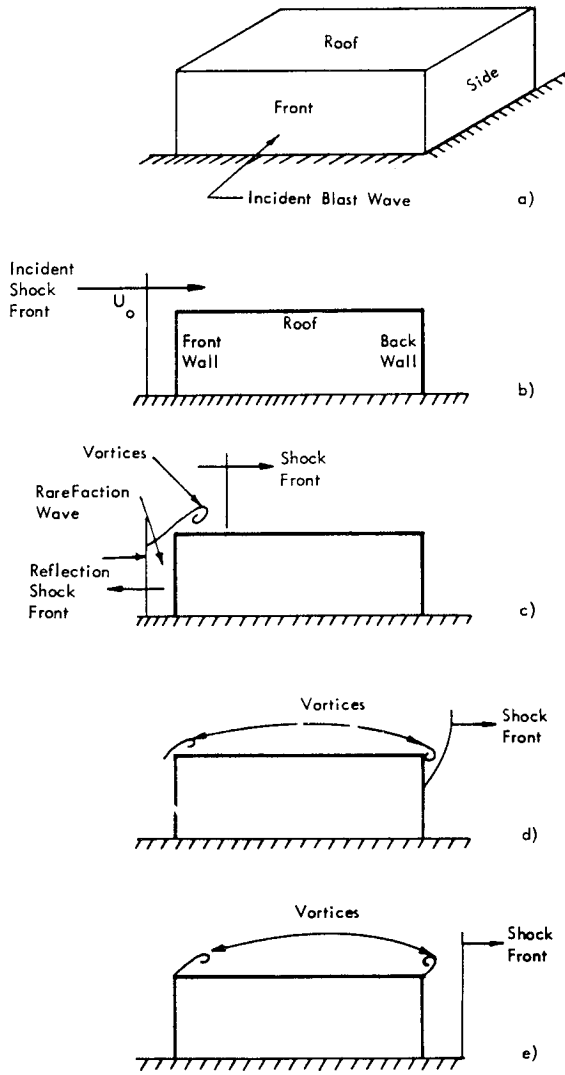


FIGURE 8.2.1 Behavior of Blast Wave Along Center Portion of Closed Rectangular Structure

gular pulse can be considered as an effective value  $t_{pe}$  of the duration given in scaled form by the expression:

$$t_{pe} W_T^{1/3} = 2 \left[ I_p^+ W_T^{1/3} \right] p_{so} \quad (8.2.1)$$

Three estimates of this effective duration are also shown on Figure 8.2.3. The first is based on current estimates of overpressure (see Figure 6.26 in Chapter 6) and positive phase impulse (Figure 6.39 and Reference 8.2.8) for TNT explosions. The second is based on a graphical analysis of the theoretical time histories for overpressure proposed by Brode (Reference 6.18) for TNT and shown in Figure 6.42. The third, shown as a shaded area, is an estimate for pro-

pellant explosions based on the estimated overpressure and positive phase impulse shown in Figures 6.26 and 6.29 of Chapter 6.

As expected, the effective duration for propellant explosions exceeds that for TNT at small values of the scaled distance.

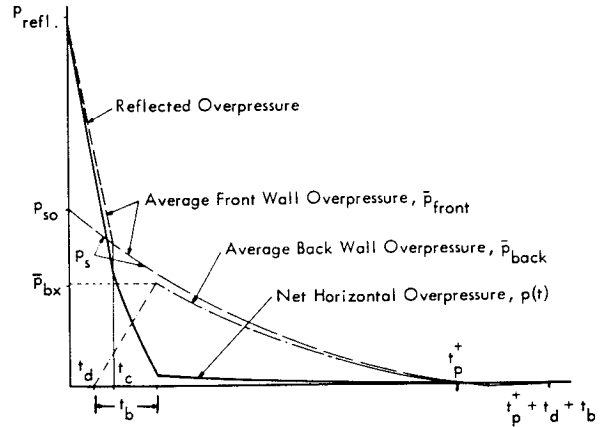
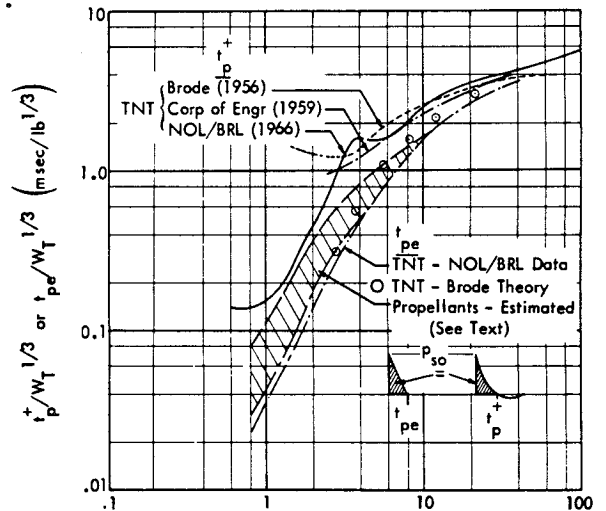


FIGURE 8.2.2 Front Wall - Back Wall - Net Overpressure versus Time



$$\text{Scaled Distance, } Z = \frac{R}{W_T^{1/3}} \left( \frac{ft}{lb^{1/3}} \right)$$

FIGURE 8.2.3 Duration of Positive Overpressure Phase - Actual and Effective Values for TNT and Propellant Explosions

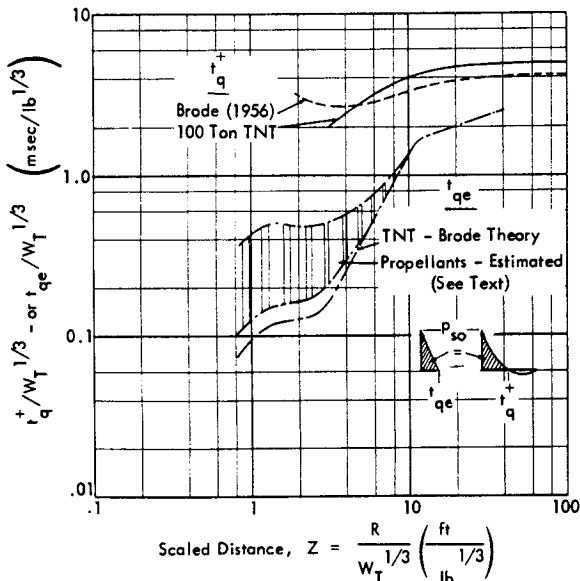


FIGURE 8.2.4 Duration of Positive Dynamic Pressure Phase - Actual and Effective Values for TNT and Propellant Explosions

Dynamic Pressure Positive Phase Duration

Figure 8.2.4 compares values of the duration of the positive phase dynamic pressure for TNT explosions predicted analytically (Reference 8.2.7) and measured (Reference 8.2.15). Values of the effective duration are also shown for TNT and for propellant explosions. The values for TNT are based on a modification of Brode's result in Reference 8.2.7. The ratio of his predicted values of dynamic pressure impulse  $l_q^+$  to overpressure impulse  $l_p^+$  was multiplied by the recently measured values of  $l_p^+$  to obtain a better estimate of the dynamic pressure impulse for TNT. From this corrected value, (20-100 percent higher than Brode's predicted values in 1956) the effective dynamic pressure duration was expressed in the form

$$t_{qe}^+ / W_T^{1/3} = 2 \left[ l_q^+ / W_T^{1/3} \right] \cdot q_{so} \quad (8.2.2)$$

where  $q_{so}$  is the maximum dynamic pressure at the same scaled distance used for the dynamic pressure impulse. The estimates of effective dynamic pressure duration for propellants are based on the corrected theoretical values of impulse for TNT and the estimated dynamic pressures for propellants shown in Figure 6.35 in Chapter 6. Various methods are suggested in the literature to estimate the actual or effective value of dynamic pressure duration. Their accuracy is limited. The values shown in Figure 8.2.4 obtained from Brode are suggested as suitable for design. However, additional data are clearly desired for verification.

The use of an effective duration is suggested as suitable for structural analysis; it is also readily computed from the peak pressure and positive phase impulse. A more detailed

definition of the time history seems unwarranted due to the inherent uncertainty in the total energy released by a propellant explosion.

Average Overpressure on Front Wall

As the shock front strikes the wall of the building a reflected blast wave is formed and the overpressure on this wall is raised to a value,  $p_{refl.}$ , called reflected overpressure and is given in terms of  $p_{so}$  by

$$p_{refl.} = 2 \times p_{so} \left[ \frac{7 \times 14.7 + 4 p_{so}}{7 \times 14.7 + p_{so}} \right] \quad (8.2.3)$$

Figure (8.2.5) illustrates this relationship.

At the instant the reflected shock front is formed, the lower overpressure existing in the incident blast wave adjacent to the top edge of the front wall initiates a rarefaction wave (Figure 8.2.1(c)). This rarefaction wave travels with the speed of sound in the reflected blast wave toward the bottom of the front wall. Within a short time, called the clearing time, the rarefaction wave reduces the overpressure to the value  $p_s(t_c)$  (Figure 8.2.2). This clearing time is given by the relation:

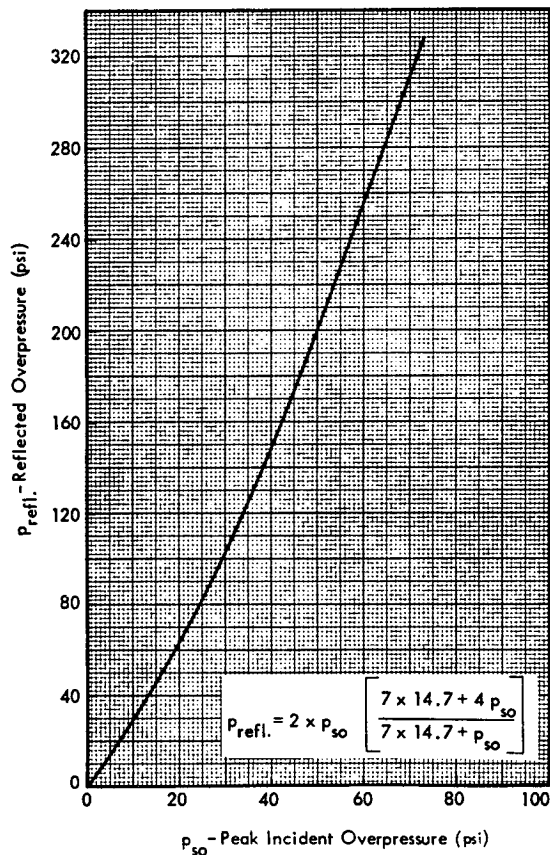


FIGURE 8.2.5 Reflected Overpressure versus Peak Incident Overpressure for Normal Reflection

$$t_c = \frac{3h'}{c_{refl.}} \quad (8.2.4)$$

where  $h'$  = clearing height, taken as the full height of the front face or half its length whichever is the smaller.

$c_{refl.}$  = speed of sound in the reflected region given by the relation (Reference 8.2.1)

$$c_{refl.} = 422 \sqrt{\frac{1.088 p_{so}^2 + 70 p_{so} + 720}{102.9 + 6 p_{so}}} \text{ ft/sec.} \quad (8.2.5)$$

This is illustrated in Figure 8.2.6.

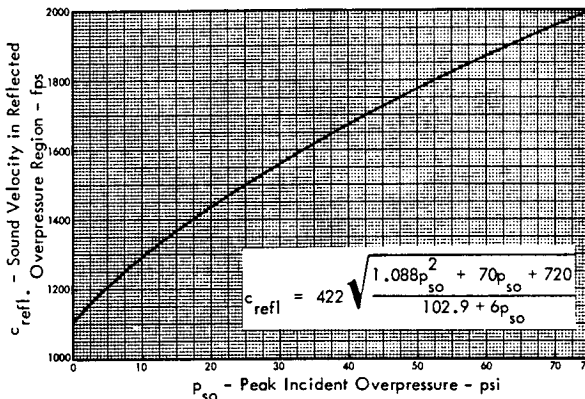


FIGURE 8.2.6 Velocity of Sound in Reflected Overpressure Region versus Peak Incident Overpressure

Therefore the average overpressure time history acting on the front of the building between  $t=0$  and  $t=t_c$  is given by:

$$\bar{p}_{front} = P_{refl.} - \left[ P_{refl.} - p_s(t_c) \right] \frac{t}{t_c} \quad (8.2.6)$$

and for  $t_c < t < t_p^+$ ,  $p_{front} = p_s$

$$\text{and } p_s = p_{so} (1 - t/t_p^+) e^{-t/t_p^+} \quad (8.2.7)$$

Average Pressure on Back Wall

Consider now the time ( $t_d$ ) required for the shock front to reach the back wall. The value of  $t_d$  will be given by:

$$t_d = \frac{L}{U_o} \quad (8.2.8)$$

where  $L$  is the length of the building in the direction of the shock and  $U_o$  is the shock front velocity given by (Reference 8.2.1)

$$U_o = 1117 \sqrt{1 + \frac{6 p_{so}}{7 \times 14.7}} \text{ ft/sec.} \quad (8.2.9)$$

Figure 8.2.7 illustrates this relationship.

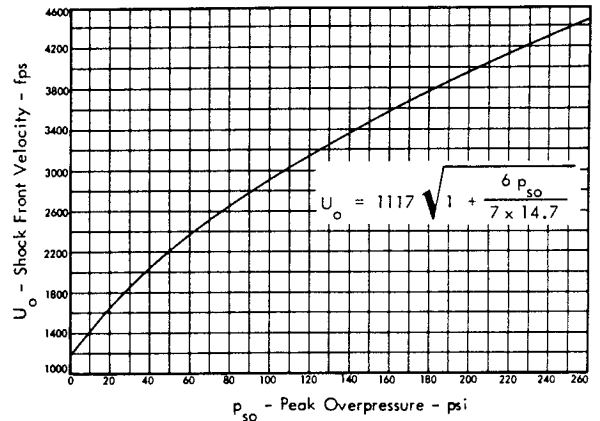


FIGURE 8.2.7 Shock Front Velocity versus Peak Overpressure

When the shock front crosses the rear edge of the structure, the foot of the shock spills down the back wall. The overpressure on the back wall behind this diffracted wave, because of the vortices developed at the top and traveling down the wall, requires a period of time ( $t_b$ ) before reaching its peak value.

The value of  $t_b$  is given by the relation:

$$t_b = \frac{4h'}{c_o} \quad (8.2.10)$$

where  $h'$  = clearing height of the back wall

$c_o$  = velocity of sound in undisturbed air (= 1117 fps.)

Considering the average overpressure on the back wall, the peak value, reached at time  $t = t_d + t_b$ , is given by (Reference 8.2.1)

$$\bar{p}_{bx} = \frac{p_{sb}}{2} \left[ 1 + (1 - \beta) e^{-\beta} \right] \quad (8.2.11)$$

where  $p_{sb} = p_s(t_d + t_b)$  is the incident blast wave overpressure at the back wall at time  $t = t_d + t_b$

$$\text{and } \beta = \frac{0.5 p_{so} (\text{psi})}{14.7} \quad (8.2.12)$$



For times in excess of  $t = t_d + t_b$ , the average overpressure at time  $t$ , ( $\bar{p}_{\text{back}}(t)$ ), on the back wall is given by (Reference 8.2.1)

$$\bar{p}_{\text{back}}(t) = p_s \left\{ \frac{p_{\text{bx}}}{p_{\text{sb}}} + \left[ 1 - \frac{\bar{p}_{\text{bx}}}{p_{\text{sb}}} \right] \left[ \frac{t - (t_d + t_b)}{t_p^+ - t_b} \right]^2 \right\} \quad (8.2.13)$$

Now, considering all overpressures exerted on the structure and directed toward the interior, as positive, the average net horizontal overpressure is given by the relation

$$p(t) = \bar{p}_{\text{front}} - \bar{p}_{\text{back}} \quad (8.2.14)$$

#### Negative Phase

For most structures, it is justifiable to neglect the negative phase of the blast beyond  $t_p^+$ . However, if more accuracy is required by the designer, the net negative overpressure, given by the following relations, can be included.

$$\text{For } t_p^+ \leq t \leq (t_p^+ + t_d) \quad p_s = p_{\text{so}} \left( 1 - \frac{t}{t_p^+} \right) e^{-\frac{t}{t_p^+}} \quad (8.2.15)$$

$$\text{For } (t_p^+ + t_d) \leq t \leq (t_p^+ + t_d + t_b) \quad p_s(t) = p_{\text{so}} \left( 1 - \frac{t}{t_p^+} \right) e^{-\frac{t}{t_p^+}} - \frac{t - t_p^+ - t_d}{t_b} p_N \quad (8.2.16)$$

where

$$p_N = p_{\text{so}} \left( 1 - \frac{t_p^+ + t_d + t_b}{t_p^+} \right) e^{-\frac{t_p^+ + t_d + t_b}{t_p^+}} \quad (8.2.17)$$

#### Net Pressure Load in Horizontal Direction

The previous considerations can be summarized into the following relations which define the behavior of the net average pressure acting on the front wall of the building. The loading is obtained by multiplying this pressure by the area of the front wall. (See Figure 8.2.2.)

$$\text{For } 0 \leq t \leq t_d \quad p(t) = p_{\text{refl.}} - \left[ p_{\text{refl.}} - p_s(t_c) \right] \frac{t}{t_c} \quad (8.2.18)$$

$$\text{For } t_d < t \leq t_c \quad p(t) = p_{\text{refl.}} - \left[ p_{\text{refl.}} - p_s(t_c) \right] \frac{t}{t_c} - \frac{p_{\text{bx}}(t - t_d)}{t_b} \quad (8.2.19)$$

$$\text{For } t_c < t \leq (t_d + t_b) \quad p(t) = p_{\text{so}} \left( 1 - \frac{t}{t_p^+} \right) e^{-\frac{t}{t_p^+}} - \frac{p_{\text{bx}}(t - t_d)}{t_b} \quad (8.2.20)$$

$$\text{For } (t_d + t_b) < t \leq t_p^+ \quad p(t) = \left\{ p_{\text{so}} \left( 1 - \frac{t}{t_p^+} \right) e^{-\frac{t}{t_p^+}} \right\} \left\{ 1 - \left[ \frac{p_{\text{bx}}}{p_{\text{sb}}} + \left( 1 - \frac{p_{\text{bx}}}{p_{\text{sb}}} \right) \left( \frac{t - t_d - t_b}{t_p^+ - t_b} \right)^2 \right] \right\} \quad (8.2.21)$$

$$\text{For } t_p^+ < t \leq (t_p^+ + t_d) \quad p(t) = p_{\text{so}} \left( 1 - \frac{t}{t_p^+} \right) e^{-\frac{t}{t_p^+}} \quad (8.2.22)$$

$$\text{For } (t_p^+ + t_d) < t \leq (t_p^+ + t_d + t_b) \quad p(t) = p_{\text{so}} \left( 1 - \frac{t}{t_p^+} \right) e^{-\frac{t}{t_p^+}} - \frac{t - t_p^+ - t_d}{t_b} p_N \quad (8.2.23)$$

In these equations it has been assumed  $p_{so}$  is  $\leq 10$  psi in which case the time variation of the wave overpressure

is given by  $p_s = p_{so} \left(1 - \frac{t}{t_p}\right) e^{-\frac{t}{t_p}}$ . If  $p_{so}$  will be

$> 10$  psi, Figure 6.43 must be used to determine the overpressure time history and the expression

$p_s = p_{so} \left(1 - \frac{t}{t_p}\right) e^{-\frac{t}{t_p}}$  in the above formulas must be corrected accordingly.

Average Roof Overpressure

The value of the average roof overpressure,  $\bar{p}_{roof}$ , varying with the time can be obtained from Figure 8.2.8 where the variation of the ratio of  $\bar{p}_{roof}$  and  $p_s$  vs time is illustrated (Reference 8.2.1)

This behavior is due to the fact that during the passage of the blast wave across the structure, low pressure areas develop on the roof and side walls due to vortex formation. In Figure 8.2.8 the values of  $p'$  and  $p''$  are given by the following relationships:

$$p' = \frac{p_{roof}}{p_s} = 2 - \left(\frac{p_{so}}{14.7} + 1\right) \left(\frac{h'}{L}\right)^{1/3} \quad (8.2.24)$$

or

$$p' = 0.5 + 0.125 \left(2 - \frac{p_{so}}{14.7}\right)^2 \quad (8.2.25)$$

whichever is smaller; except  $p'$  may not be less than zero

$$p'' = \frac{p_{roof}}{p_s} = 0.9 + 0.1 \left(1.0 - \frac{p_{so}}{14.7}\right)^2 \quad (8.2.26)$$

A restriction which must be imposed is due to the importance of the lateral variation of overpressures on the roof. If the width of the structure, normal to the direction of travel of the shock wave, is greater than twice the structural length, the average roof overpressures determined by Figure 8.2.8 are satisfactory. For a structure whose width is less than its length, the average roof overpressure for times greater than time  $t = (L/U_o)$  is more correctly given by the relation (Reference 8.2.1)

$$\bar{p}_{roof} = p_s \quad (8.2.27)$$

For the first case, in order to have the expression for  $\bar{p}_{roof}$  as a function of time,  $p_s$  must be computed for various values of time. After doing this, the  $\bar{p}_{roof}$  vs time curve is drawn as in Figure 8.2.9. The load is obtained by multiplying  $\bar{p}_{roof}$  by the area of the roof.

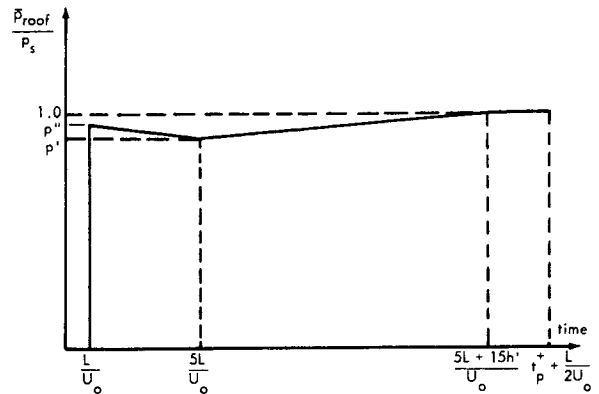


FIGURE 8.2.8 Average Roof Overpressure,  $\bar{p}_{roof}$  Divided by  $p_s$  versus Time

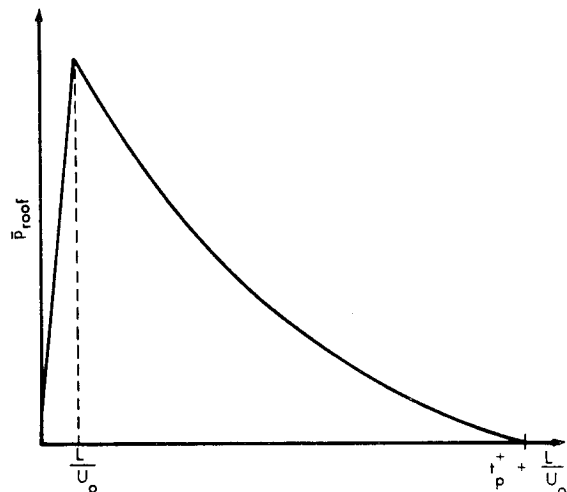


FIGURE 8.2.9 Average Roof Overpressure versus Time

8.2.1.2 Loading on Rectangular Structures with Openings More than 5 Percent and Less than 50 Percent of the Area of the Walls.

Structures with openings will be considered as those structures having open interiors free of walls and other obstructions which could hinder the propagation of the blast wave.

Structures having interior walls and other obstructions can be studied as closed structures.

Average Exterior Front Wall Overpressure  $\bar{p}_{ex}$  - front

In this case as well as for closed structures, the shock wave, after reaching the front wall, reflects and rises to the reflected overpressure. Rarefaction waves move in from the edges of the wall and of the openings (it is assumed that windows and door will be broken under the reflected overpressure), clearing the reflected overpressures.

The time required to clear the front face  $t'_c$ , can be evaluated from the relation

$$t'_c = \frac{3h'_f}{c_{refl.}} \tag{8.2.28}$$

where

$c_{refl.}$  is given by Equation (8.2.5) and Figure 8.2.6.

$$h'_f = \sum \frac{\delta_n h_n A_n}{A_F} \tag{8.2.29}$$

In order to obtain the value of  $h'_f$ , the front wall must be subdivided, as shown in Figure 8.2.10 into convenient areas of equal size. The symbols of Equation (8.2.29) can be evaluated as follows:

- $A_F$  = Net area of front face ( $w \times h$  less openings)
- $A_n$  = Area of each portion of the subdivided front face, except openings
- $h_n$  = For areas 2, the average distance between the openings or sides for which clearing occurs
  - = For areas 1 and 4, the average height or width, whichever is smaller
  - = For areas 3, the average distance between the side from which clearing occurs and the side opposite
- $\delta_n$  = 1/2 for areas 2
  - = 1.0 for areas 1, 3, 4

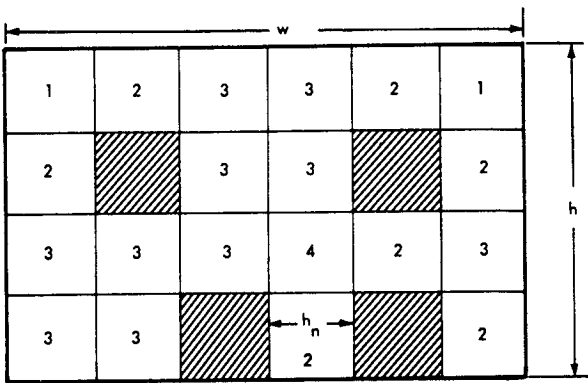


FIGURE 8.2.10 Subdivision of the Front Wall of a Structure with Openings

- Area 1, All Areas Cleared from Two Adjacent Sides
- Area 2, All Areas Cleared from Two Opposite Sides
- Area 3, All Areas Cleared from One Side
- Area 4, All Remaining Areas

The time curve of the average front wall overpressure on the net wall area can be constructed as it has been done for closed structures but using the clearing time  $t'_c$  computed from Equation 8.2.28 (see Figure 8.2.11).

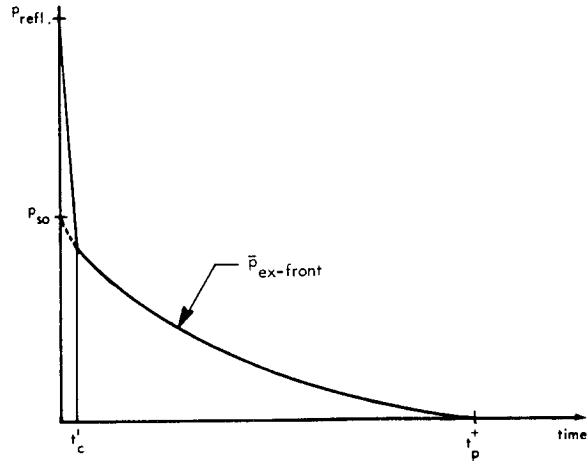


FIGURE 8.2.11 Average Exterior Front Wall Overpressure,  $\bar{P}_{ex-front}$

Average Interior Front Wall Overpressure  $\bar{P}_i$  - front

The behavior of the average interior front wall overpressure is illustrated in Figure 8.2.12 (for a small rectangular structure) or 8.2.13 (for a large rectangular structure), where the new symbols used have the following meanings: (Reference 8.2.1).

$h'_{if}$  = Weighted average build up height of the interior front computed from Equation (8.2.29) but with all the quantities interpreted as applying to the interior surface of the front wall

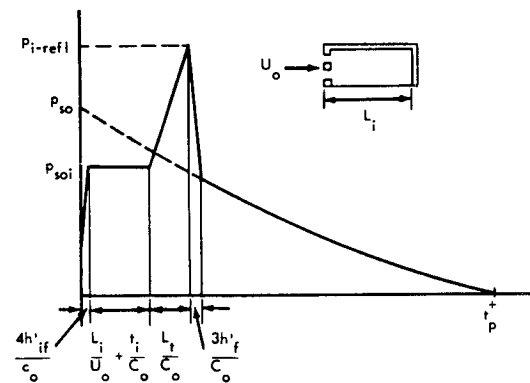


FIGURE 8.2.12 Average Interior Front Wall Overpressure versus Time When  $L_i/U_o \leq 0.1 t_p^+$

- $L_i$  = Distance from the outside of the front wall to the inside rear face
- $p_{soi}$  = Peak overpressure of the interior shock wave is plotted in Figure 8.2.14 and 8.2.15 as functions of  $p_{so}$  and  $\frac{A_{of}}{A_{gf}}$  (where  $A_{of}$  = area of openings in the front face and  $A_{gf}$  = gross area of the front face).
- $p_{i-refl.}$  = Reflected internal overpressure value given by

$$p_{i-refl.} = 2 \times p_{soi} \left[ \frac{7 \times 14.7 + 4p_{soi}}{7 \times 14.7 + p_{soi}} \right] \quad (8.2.30)$$

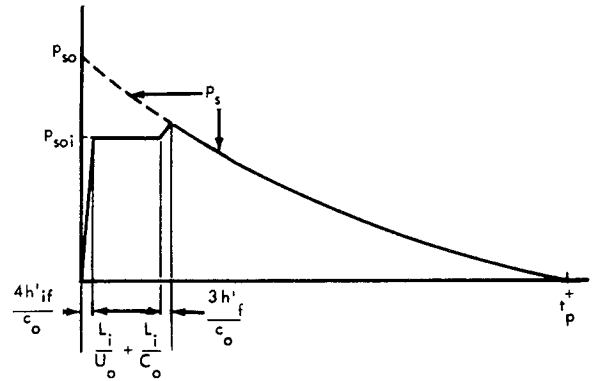


FIGURE 8.2.13 Average Interior Front Wall Overpressure versus Time When  $L_i/U_o \geq 0.1 t_p^+$

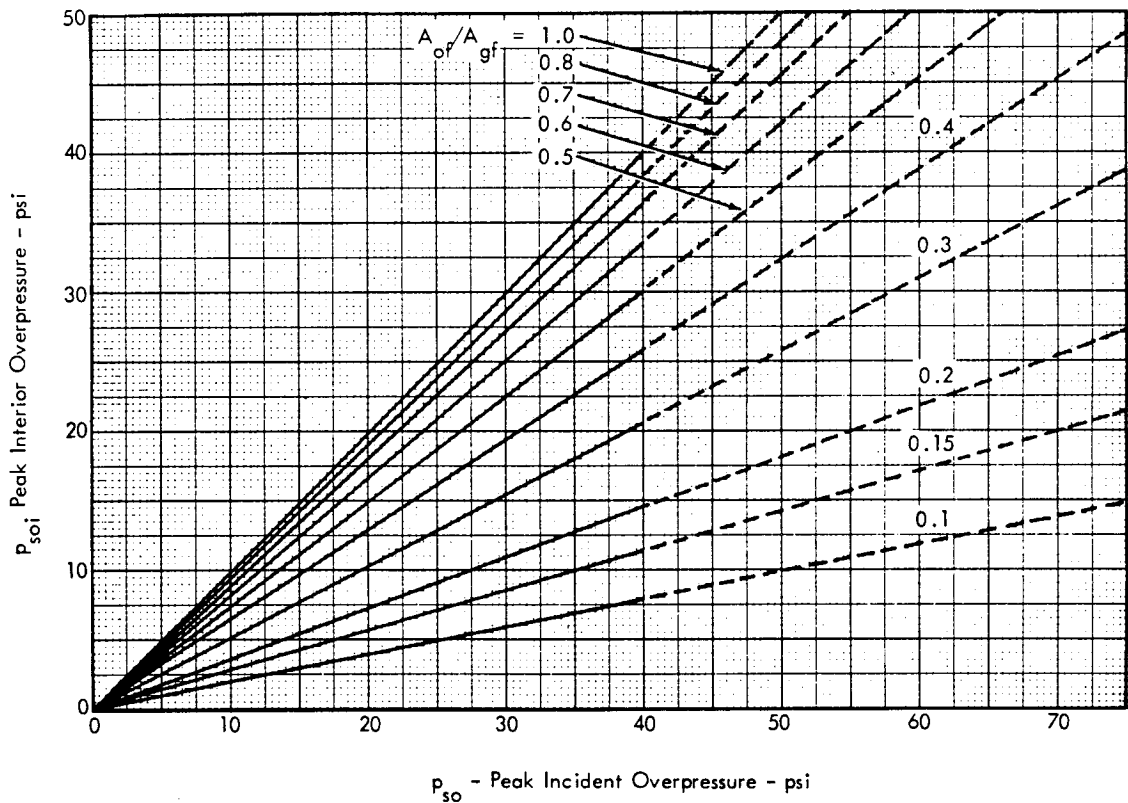


FIGURE 8.2.14 Peak Interior Overpressure versus Peak Incident Overpressure for Various Percentages of Front Wall Openings, (Validity of Dashed Portions of Curves Uncertain)

Average Net Front Wall Overpressure  $\bar{p}_{f-net}$

The average net front wall overpressure can be obtained by subtracting the interior front wall overpressure from the

exterior front wall overpressure on a common time basis. The variation of  $\bar{p}_{f-net}$  ( $= \bar{p}_{ex-front} - \bar{p}_{i-front}$ ) with time is illustrated in Figure 8.2.16.

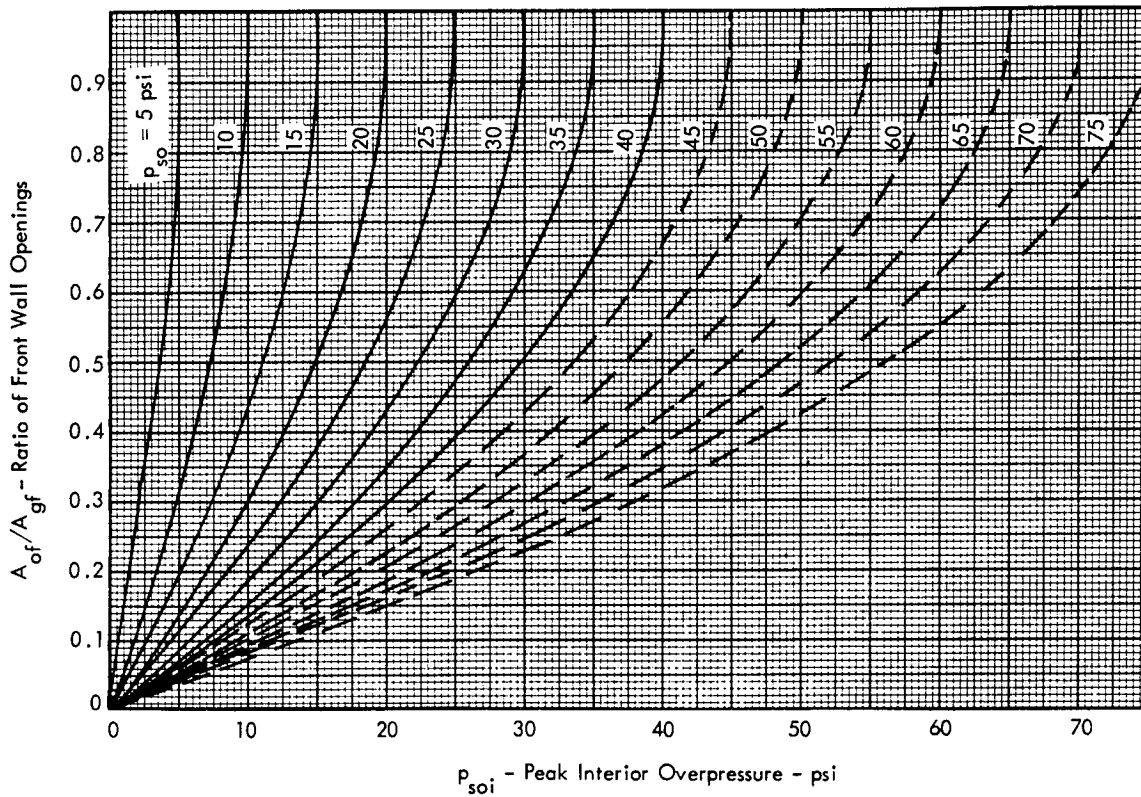


FIGURE 8.2.15 Peak Interior Overpressure Versus Percentage of Front Face Openings for Various Peak Incident Overpressures. (Validity of Dashed Portions of Curves Uncertain)

Average Exterior Back Wall Overpressure  $\bar{p}_{ex-back}$

The variation with time of the average exterior back wall overpressure is illustrated in Figure 8.2.17 where the new symbols used have the following meanings:

$h'_b$  = Weighted average build up height of the rear face defined by:

$$h'_b = \sum \frac{\delta_n h_n A_n}{A_R} \tag{8.2.31}$$

where:

$A_R$  = Net area of the back wall

$\delta_n h_n A_n$  = As defined in previous section

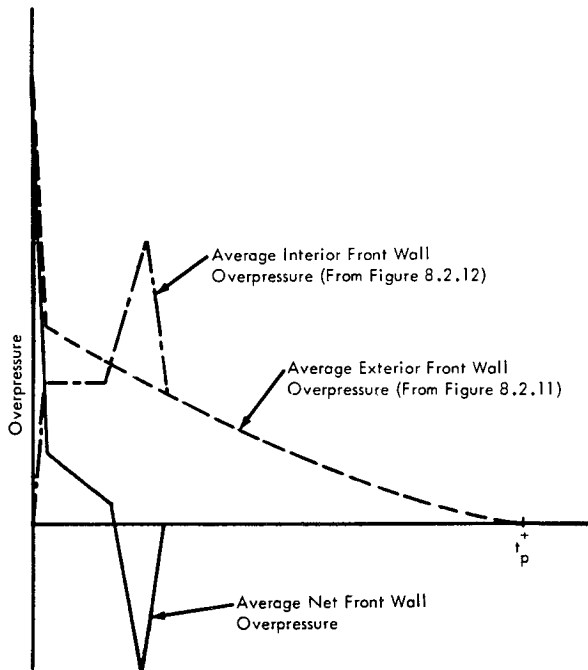


FIGURE 8.2.16 Average Net Front Wall Overpressure versus Time

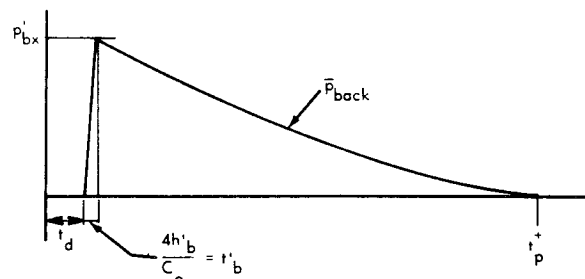


FIGURE 8.2.17 Average Exterior Back Wall Overpressure  $\bar{p}_{ex-back}$

$$p'_{bx} = \frac{p'_{sb}}{2} \left[ 1 + (1 - \beta) e^{-\beta} \right] \quad (8.2.32)$$

where:

$p'_{sb}$  = The incident blast wave overpressure at the back wall at time  $t'_{b'}$ , where

$$t'_{b'} = t_d + \frac{4h'_b}{c_o} = t_d + t'_b \quad (8.2.33)$$

where

$t_d$  is given by Equation (8.2.8)

and

$$\beta = \frac{0.5 p_{so} \text{ (psi)}}{14.7} \quad (8.2.34)$$

For times in excess of  $t = t_d + \frac{4h'_b}{c_o}$ , the average overpressure on the external back wall is given by

$$\bar{p}'_{ex-back} = p_s \left\{ \frac{p'_{bx}}{p'_{sb}} + \left[ 1 - \frac{p'_{bx}}{p'_{sb}} \right] \left[ \frac{t - (t_d + t'_b)}{t'_p - t'_b} \right]^2 \right\} \quad (8.2.35)$$

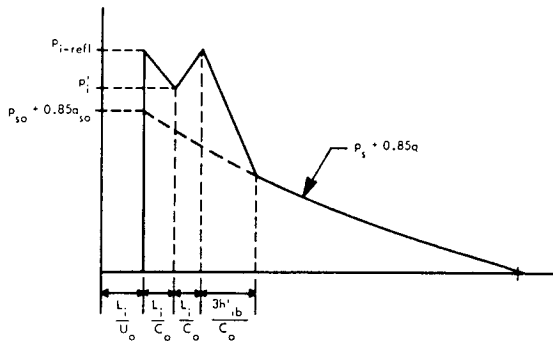


FIGURE 8.2.18 Average Interior Back Wall Overpressure  $\bar{p}'_{i-back}$  versus Time  $L_i/U_o \leq 0.1 t'_p$

Average Interior Back Wall Overpressure  $\bar{p}'_{i-back}$

The variation with time of the average interior back wall overpressure is illustrated in Figure 8.2.18 (for small rectangular structure) or Figure 8.2.19 (for large rectangular structure) where the new symbols used have the following meanings:

$h'_{ib}$  = Weighted average build up height of the interior back wall computed from Equation (8.2.31) but with all quantities interpreted as applying to the interior surface of the rear wall

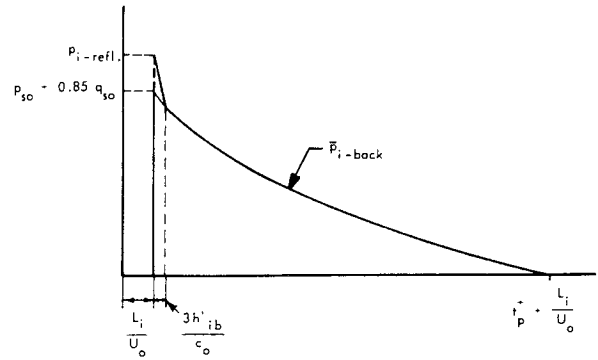


FIGURE 8.2.19 Average Interior Back Wall Overpressure  $\bar{p}'_{i-back}$  versus Time ( $L_i/U_o > 0.1 t'_p$ )

$$p'_i = p_{soi} + \left( 1 - \frac{A_{of}}{A_{gf}} \right)^2 (p_{i-refl} - p_{soi}) \quad (8.2.36)$$

where  $p_{soi}$  and  $p_{i-refl}$  are obtained from Figure 8.2.14 and equation 8.2.30 respectively.

Average Net Back Wall Overpressure

The average net back wall overpressure is obtained by subtracting the interior back wall overpressure from the exterior back wall overpressure on a common time basis. The variation of  $\bar{p}_{b-net} (= \bar{p}_{ex-back} - \bar{p}_{i-back})$  with time is illustrated in Figure 8.2.20.

Total Load Acting on the Structure

The total load acting on the structure is easily found by means of the following relation

$$L_T = \bar{p}_{f-net} \times A_f - \bar{p}_{b-net} \times A_b \quad (8.2.37)$$

where:

$A_f$  = Net front wall area

$A_b$  = Net back wall area.

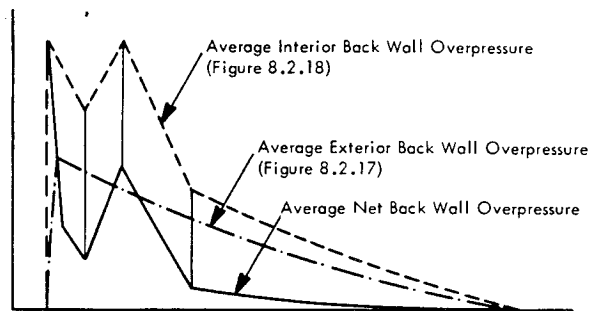


FIGURE 8.2.20 Average Net Back Overpressure versus Time,  $\bar{p}_{b-net}$

8.2.1.3 Loading on Rectangular Structures with Openings More than 50 Percent of the Area of the Walls

When the area of the openings is more than about 50 percent of the area of the walls one should consider the building as a drag type building. The reflected overpressure load is neglected due to the very short clearing time. The areas subject to drag are then the net areas of the parts of the structure.

The total load on the structure due to the drag forces can be obtained by computing the load on all the individual elements of the building, and adding them together on a common time basis.

The total drag pressure is obtained from the formula:

$$\text{Drag pressure} = C_d q \tag{8.2.38}$$

where:

$C_d$  = Drag coefficient (see Table 8.2.1)

$q$  = Dynamic pressure due to the air velocity is given by Figure 6.43. For  $q_{so} \leq 10$  psi, the following equation (from Reference 8.2.1) can be used for  $q$  versus time.

$$q = q_{so} \left( 1 - \frac{t - t_d}{t_p} \right) e^{-3.5 \frac{t - t_d}{t_p}}$$

$$t_d = \frac{L}{U_o}$$

$L$  = The distance from the front face of the structure to the element for which the load is being computed.

The peak dynamic pressure,  $q_{so}$ , given by

$$q_{so} = 14.7 \left[ \frac{5}{14} \left( \frac{P_{so}}{14.7} \right) \right]^2 \left/ \left[ 1 + \frac{1}{7} \left( \frac{P_{so}}{14.7} \right) \right] \right. \tag{8.2.39}$$

is plotted in Figure 8.2.21.

The load acting on each element is obtained by multiplying the drag pressure by the projected area of the member transverse to the direction of travel of the blast wave.

The total load is given by the summation, on a common time basis, of the loads acting on all the individual elements.

Figure 8.2.22 a illustrates the computation of loading acting on the 1st, 2nd, 3rd, and 4th row of columns of an assumed structure of four rows of columns. Figure 8.2.22b illustrates the variation with time of the total load active on the structure. The symbols used have the following meanings:

- $L_i$  = Loading on the  $i^{\text{th}}$  row of columns
- $A_i$  = Projected area of the  $i^{\text{th}}$  row of columns transverse to the direction of travel of the blast wave.
- $t_i$  = Time required for the blast wave to reach the  $i^{\text{th}}$  row after striking the first row.
- $t_p$  = Duration of the positive phase of the drag pressure.

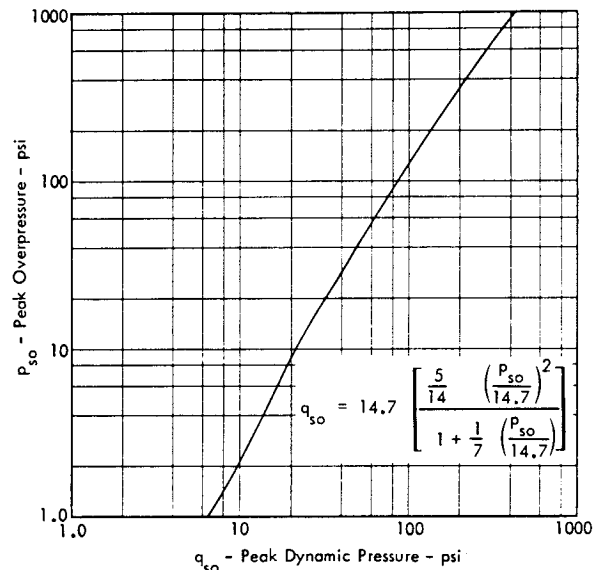


FIGURE 8.2.21 Peak Dynamic Pressure versus Peak Incident Overpressure

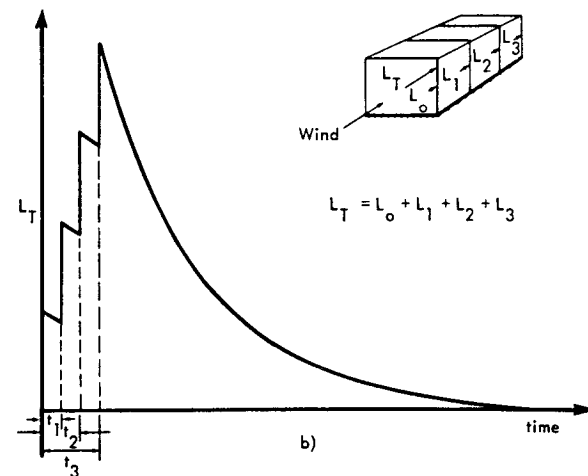
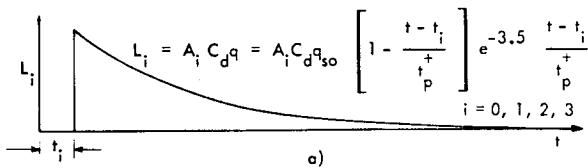


FIGURE 8.2.22 Example of a Loading versus Time Function Due to Drag Pressures Acting on a Structure Having Four Rows of Columns.

TABLE 8.2.1  
DRAG COEFFICIENTS (Reference 8.2.5)

Flow from Left to Right. For High Reynolds Numbers.

Bodies of Revolution

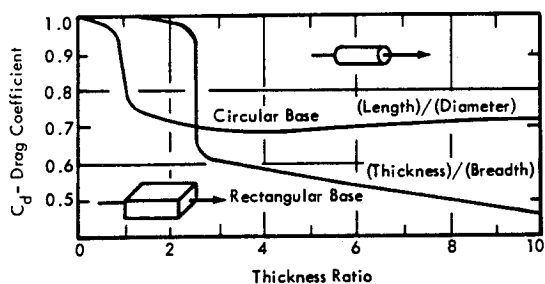
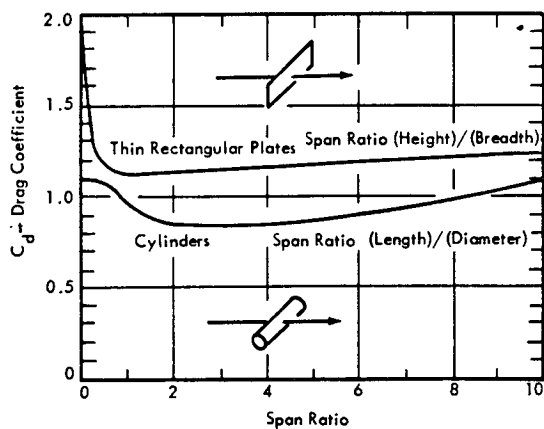
	$C_d$		$C_d$
Sphere	0.10	Circular Plate	1.17
Half Sphere	0.42	60° Cone	0.5
Half Sphere	1.42		

Structural Shapes (Long Members, Without end Effects)

$C_d$	$C_d$	$C_d$
2.0	1.45	1.55
1.65	2.2	2.0
2.05	1.2	1.05
1.8	2.3	1.2

Protuberances (With end Effects)

$C_d$	$C_d$
0.80	1.03
1.20	1.00
1.25	1.28



8.2.1.4 Loading on Structures with Gabled Roofs

Average Roof Overpressure for Structures Having Ridge Line Perpendicular to Wave Travel Direction

When the shock wave strikes a roof surface, because of the reflection, the overpressure rises to an average peak value,  $p'_{rf}$ , given by the following expression (Figure 8.2.23).

$$p'_{rf} = p_{sL} + K\theta (p_{r-\alpha} - p_{sL}) \quad (8.2.40)$$

where

$p_{sL}$  = Overpressure in the incident shock wave at time  $t = t_d + \frac{L}{4U_o}$

$L$  = Length of one gabled roof span

$t_d$  = Time Displacement Factor (=  $L/4U_o$  for front slope of first bay; =  $\frac{L}{U_o} + \frac{L}{4U_o}$  for front slope of 2<sup>nd</sup> bay; =  $\frac{2L}{U_o} + \frac{L}{4U_o}$  for 3<sup>rd</sup> bay and so forth)

$K\theta$  = Constant for a given angle of inclination of the roof plotted in Figure 8.2.24

$p_{r-\alpha}$  = Reflected pressure-function of the incidence angle,  $\alpha$ , and of the peak incident overpressure,  $p_{so}$ . The ratio  $\frac{p_{r-\alpha}}{p_{so}}$  as a function of  $\alpha$  is plotted in Figure 8.2.25.

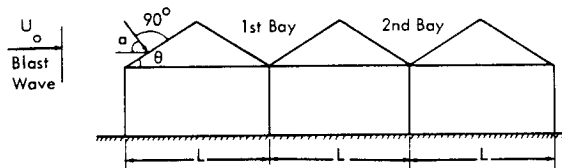


FIGURE 8.2.23 Structure with Gabled Roof Reached by a Blast Wave

The average overpressure on the front slope of the roof builds up linearly from zero at time  $t = t_d - \frac{L}{4U_o}$  to  $\bar{p}'_{rf}$  at time  $t = t_d + \frac{L}{4U_o}$ . The average overpressure then clears at time  $t = t_d + \frac{3L}{4U_o}$  to the value  $\bar{p}_{rf}$  given by

$$\bar{p}_{rf} = p_s + C_d q \quad (8.2.41)$$

where:

$p_s$  = Overpressure in the incident shock wave

$q$  = Dynamic pressure given by Equation 8.2.39

$C_d$  = Drag coefficient plotted in Figure 8.2.26 as a function of  $\theta$ .



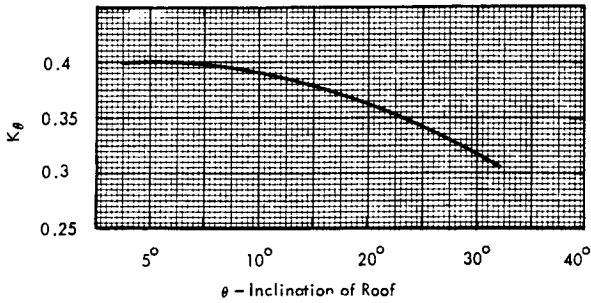


FIGURE 8.2.24 Values of  $K_\theta$  as Function of  $\theta$

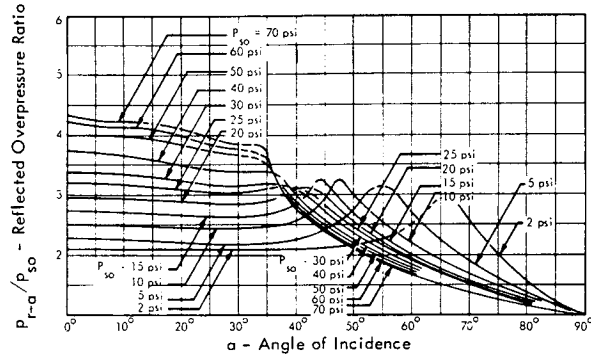


FIGURE 8.2.25 Reflected Overpressure Ratio versus Angle of Incidence

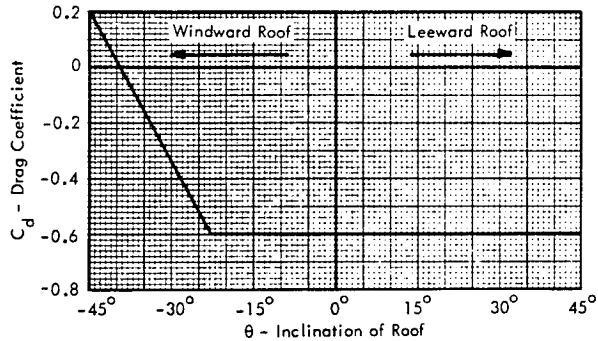


FIGURE 8.2.26 Drag Coefficient for Gabled Roofs versus Slope Angle of Roof

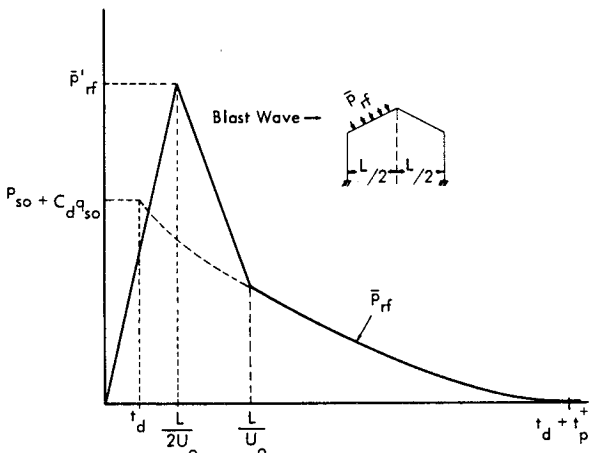


FIGURE 8.2.27 Average Overpressure  $\bar{p}_{rf}$  on Windward Slope of a Gabled Structure versus Time

Figure 8.2.27 and 8.2.28 illustrate graphically the variation with time of the average overpressure  $\bar{p}_{roof}$ , acting on the windward roof slope of the first and of any other bay of a gabled structure.

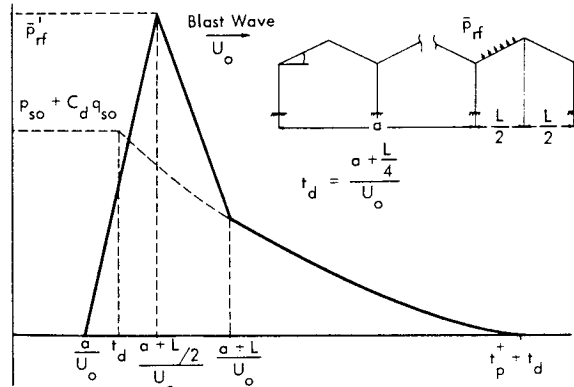


FIGURE 8.2.28 Average Overpressure  $\bar{p}_{rf}$  on Windward Roof Slope of Any Bay of a Gabled Structure versus Time

Average Rear Slope Overpressure  $\bar{p}_{rf-R}$  For Structures Having Ridge Line Perpendicular to Wave Direction

No reflection takes place on the rear roof slope. The variation of  $p_{rf-R}$  with time is illustrated in Figure 8.2.29. The symbols used have been defined above. The time  $t_d$  is equal to the time required by the wave to travel from the front edge of the structure to the point at which it is necessary to determine the local overpressure, (therefore,

$$t_d = \frac{3L}{4U_o} \text{ for the first bay, } t_d = \frac{(a + \frac{3L}{4})}{U_o} \text{ for any other bay)}$$

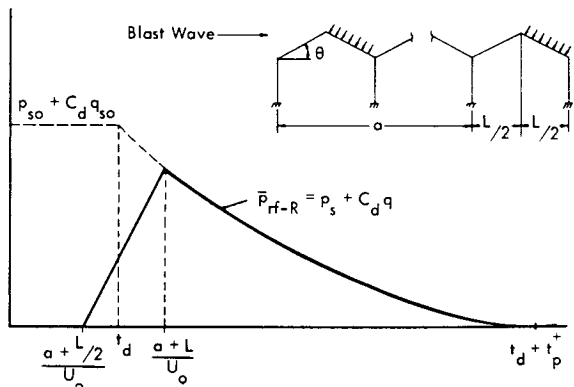


FIGURE 8.2.29 Average Overpressure  $\bar{p}_{rf-R}$  on Leeward Roof Slope of Any Bay of Gabled Structure versus Time

Total Load Acting on the Roof of a Gabled Roof Structure

The total load acting on the roof resolved in its horizontal and vertical components, is easily found by multiplying the overpressures by the areas of slopes and by adding on a

common time basis these products multiplied by  $\sin \theta$  and  $\cos \theta$  respectively. The expressions for  $L_{TH}$ , total horizontal load, and for  $L_{TV}$ , total vertical load, are:

$$L_{TH} = \left[ \sum_k^{1..n} (\bar{p}_{rf}^{(k)} - \bar{p}_{rf-R}^{(k)}) A_k \right] \sin \theta \quad (8.2.42)$$

$$L_{TV} = \left[ \sum_k^{1..n} (\bar{p}_{rf}^{(k)} - \bar{p}_{rf-R}^{(k)}) A_k \right] \cos \theta \quad (8.2.43)$$

where

- $\bar{p}_{rf}^{(k)}$  = Average overpressure on windward roof slope of  $k^{th}$  bay
- $\bar{p}_{rf-R}^{(k)}$  = Average overpressure on leeward roof slope of  $k^{th}$  bay
- $A_k$  = Area of slope of  $k^{th}$  bay
- $\theta$  = Inclination of the roof - (see Figure 8.2.23).

Total Loading Acting on a Gabled Roof Structure

The total blast loading acting on a gabled roof structure is given by adding the total horizontal load,  $L_{TH}$ , acting on the roof to the net load acting on the front and back wall calculated as in previous sections.

8.2.1.5 Loading on Cylindrical Structures

Structures of this category consist of exposed arch structures and surface structures of various shapes covered by an earth fill. If the arch or earth fill surface is not truly circular, it is approximated by an arc of a circle.

Cylindrical Arch Overpressure  $p_{cyl}$ , Axis Parallel to Shock Front. (Reference 8.2.1)

In the procedures of this section for computing the blast loading as a function of time, zero time is the instant at which the incident shock front first strikes the cylindrical arch surface at its intersection with the horizontal ground surface, along the line defined by  $\theta = \theta'$ . (Figure 8.2.30)

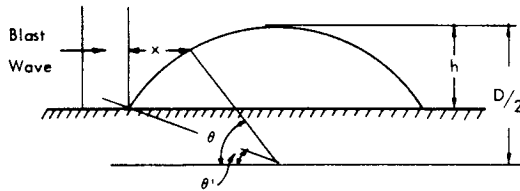


FIGURE 8.2.30 Sketch for Cylindrical Arch Notation

The clearing time determines two different ranges of  $\theta$  values and for each of them the overpressures are defined as follows:

For  $0^\circ \leq \theta' < \theta < 90^\circ$  Figure 8.2.31 is valid. The overpressure rises instantaneously from zero to  $p_{r-\theta}$  (given in Figure 8.2.25 putting  $\alpha = \theta$ ) at time  $t_d = \frac{x}{U_o}$ .

The clearing time is given by

$$t_c = \frac{4h}{c_{refl}} \quad (8.2.44)$$

where  $c_{refl}$  is given by Equation (8.2.5) and Figure 8.2.6. The local overpressure at any point after the clearing of reflection effects is given by:

$$p_{cyl} = C_d q + p_s \quad (8.2.45)$$

where

$q$  is the dynamic pressure given by Equation (8.2.39) (for  $q_{so} \leq 10$  psi) or by Figure 6.43.

$p_s$  = Overpressure in the incident blast wave at anytime.

$C_d$  = The local drag coefficient which is a function of  $\theta$  and is obtained from Figure 8.2.32, 8.2.34, 8.2.35, 8.2.36, and 8.2.37 as discussed hereafter.

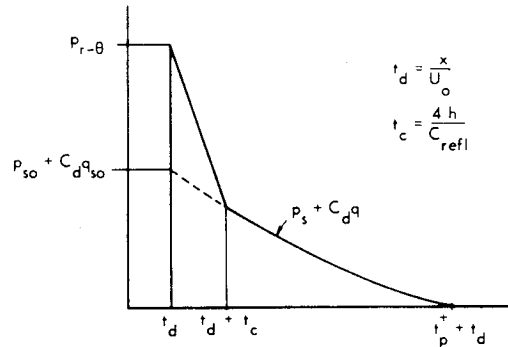


FIGURE 8.2.31 Local Overpressure on Front Surface of Cylindrical Arch versus Time

The distribution of dynamic pressure about an arch is a function of both the Reynolds Number,  $Re$ , and the Mach number,  $M$ , of the high-velocity wind in the blast wave.

The Mach number is given by:

$$M = \frac{1.89 \left[ 1 - \frac{1}{\frac{p_{so}}{14.7} \left( \frac{p_s}{p_{so}} \right) + 1} \right]}{\left[ 1 + \frac{6}{\frac{p_{so}}{14.7} \left( \frac{p_s}{p_{so}} \right) + 1} \right]^{1/2}} \quad (8.2.46)$$

and it is plotted in Figure 8.2.32.

The Reynolds number can be obtained from Figure 8.2.33. Figures 8.2.34 and 8.2.35 give the dynamic pressure coefficient,  $C_d$  as a function of  $\theta$  for  $M > 1$  and  $.4 < M < 1$ .

Figure 8.2.36 gives the dynamic pressure coefficient  $C_d$ , for  $M < .4$  and  $Re > 5 \cdot 10^5$ .

For  $M < .4$  and  $Re < 5 \cdot 10^5$   $C_d$  is given by

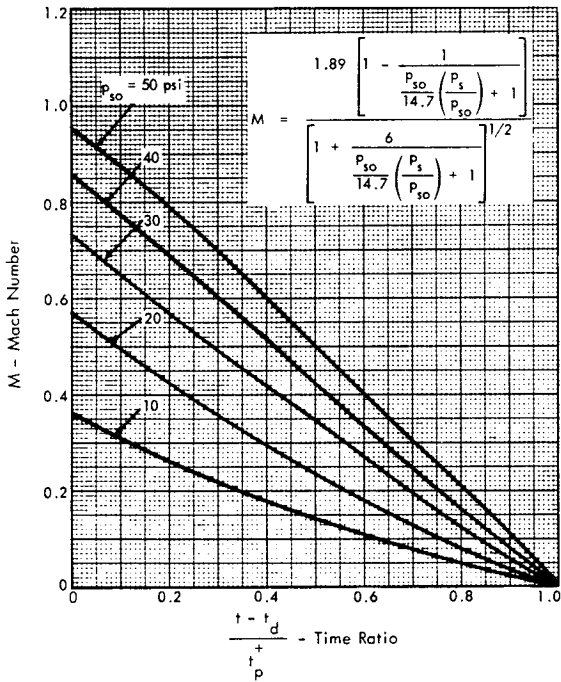


FIGURE 8.2.32 Mach Number of Undisturbed Stream versus Time Ratio for Various Peak Overpressures

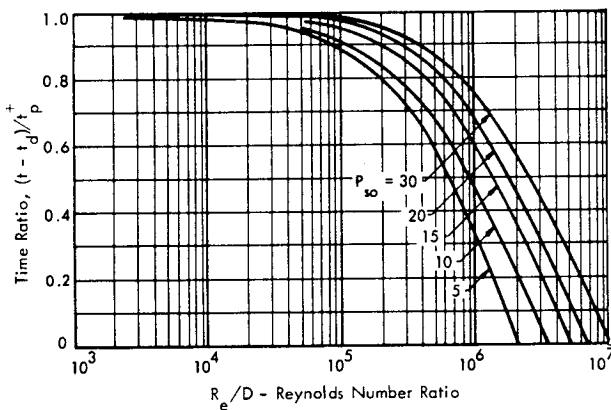


FIGURE 8.2.33 Reynolds Number Ratio of Undisturbed Stream versus Time Ratio for Various Peak Overpressures

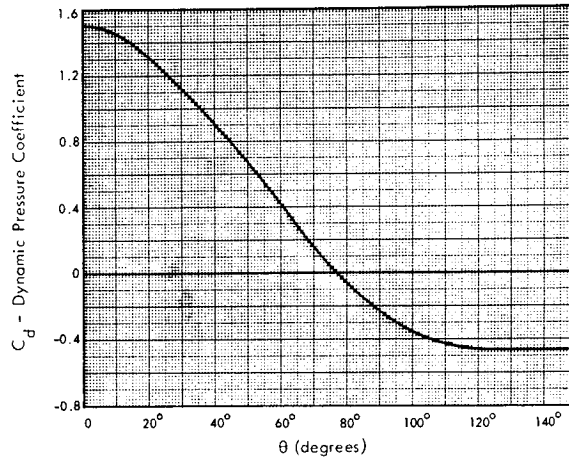


FIGURE 8.2.34 Local Dynamic Pressure Coefficient for Cylindrical Arch-Axis Parallel to Shock Front - Supersonic Mach Numbers ( $M > 1$ )

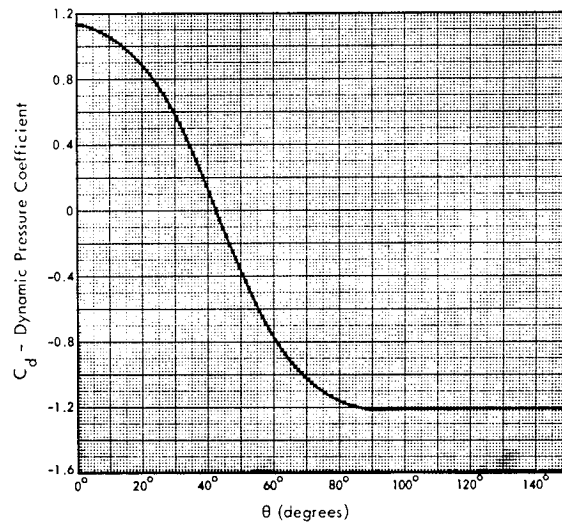


FIGURE 8.2.35 Local Dynamic Pressure Coefficient for Cylindrical Arch-Axis Parallel to Shock Front-High Subsonic Mach Numbers ( $0.4 < M < 1$ )

$$C_d = \frac{C'_d}{1.2} \left[ 0.7 + 0.5 \sqrt{1 - 4/(L/D)^2} \right] \quad (8.2.47)$$

where

$C'_d$  is given by Figure 8.2.37 as a function of  $\theta$

$D$  is the diameter of the arch

$L$  is the length of the axis of the arch.

For  $90^\circ < \theta < 180^\circ$  Figure 8.2.38 gives the variation with time of  $p_{cyl.}$  for a given value of  $\theta$ . In this figure, the overpressure rises at time  $t_d$  instantaneously from zero to a value given by

$$p_{cyl.} = p_{so} \left( 1.5 - \frac{\theta}{180} \right) \quad (8.2.48)$$

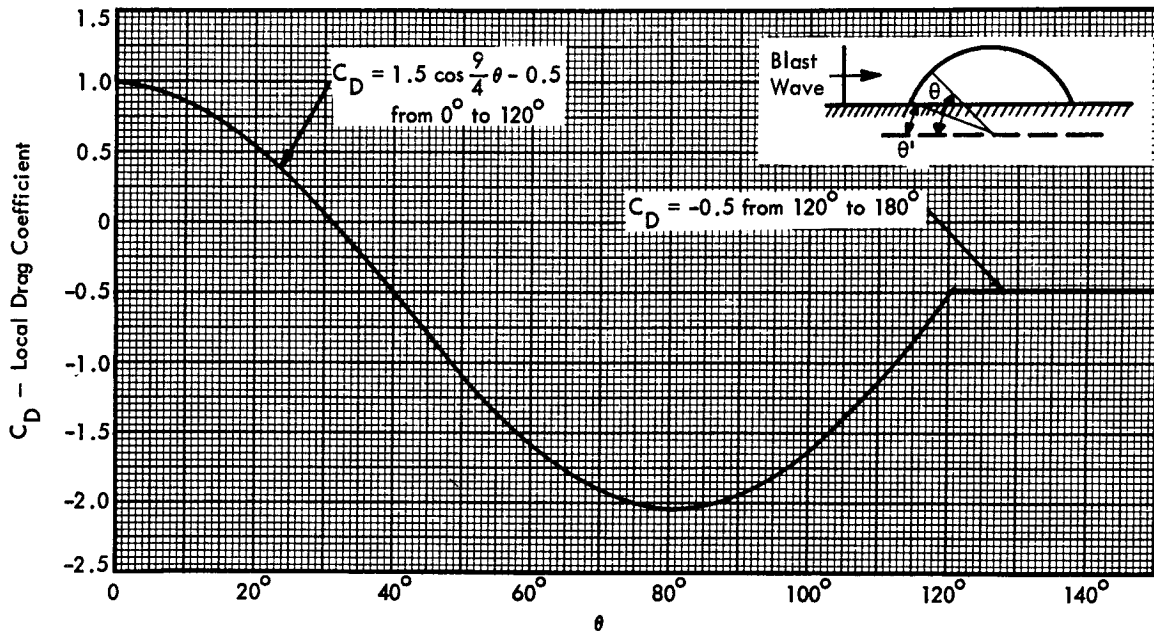


FIGURE 8.2.36 Local Dynamic Pressure Coefficient for Cylindrical Arch-Axis Parallel to Shock Front [ $R > 5(10)^5$  and  $M < 0.4$ ]

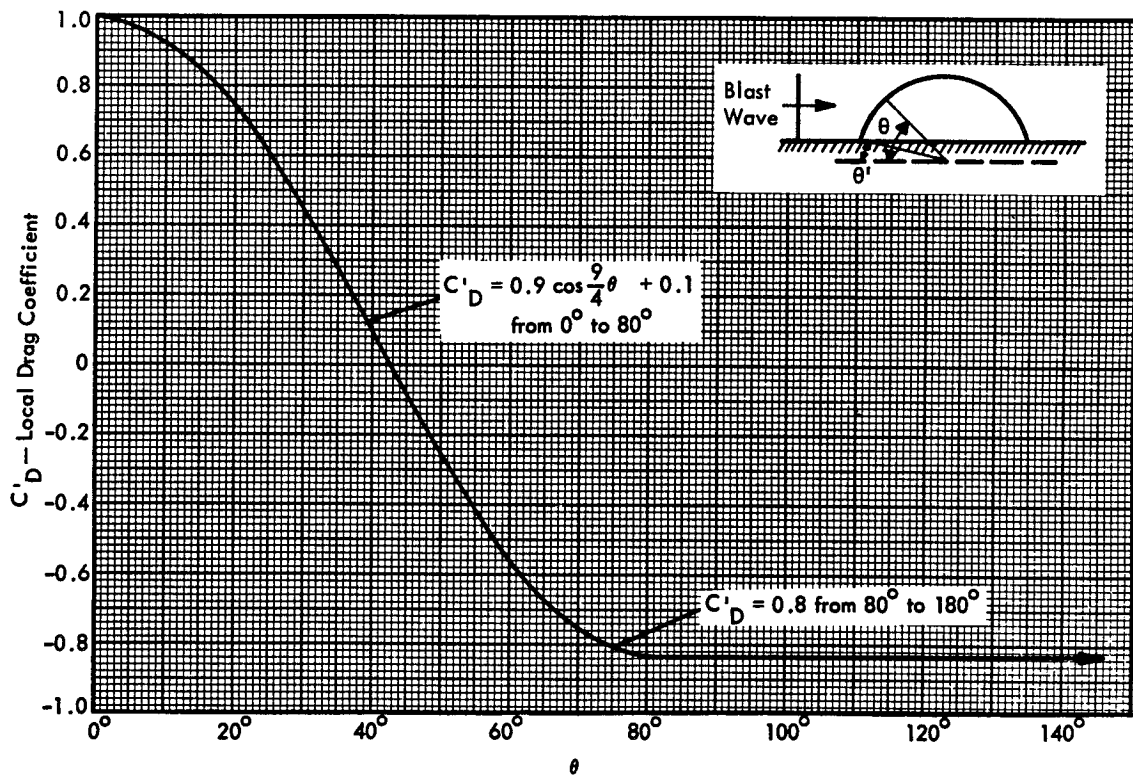


FIGURE 8.2.37 Local Dynamic Pressure Coefficient for Infinitely Long Cylindrical Arch-Axis Parallel to Shock Front [ $R < 5(10)^5$  and  $M < 0.4$ ]

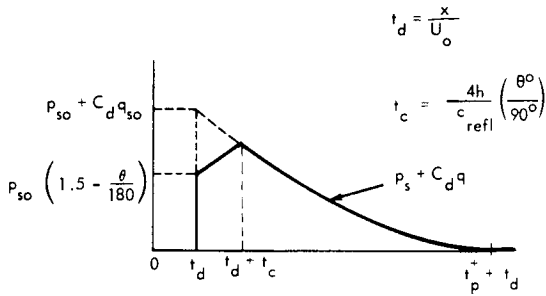


FIGURE 8.2.38 Local Overpressure on Leeward Surface of Cylindrical Arch versus Time for  $90 < \theta < 180$

After this, the initial overpressure clears to the value given by Equation 8.2.45 at time  $t = t_d + t_c$ , where

$$t_c = \left( \frac{4h}{c_{refl.}} \right) \left( \frac{\theta^{\circ}}{90^{\circ}} \right) \tag{8.2.49}$$

Average End Wall Overpressure  $\bar{p}_{end}$ , Axis Parallel to Shock Front

Figure 8.2.39 illustrates the time variation of the average end wall overpressure  $\bar{p}_{end}$ . It is assumed that the variation of incident overpressure, in the time required for the shock wave to travel across the cylinder, is linear and that the average overpressure on the ends is equal to the overpressure in the incident blast wave with the time displacement factor  $t_d$  given by

$$t_d = \frac{D \cos \theta'}{2 U_o} \tag{8.2.50}$$

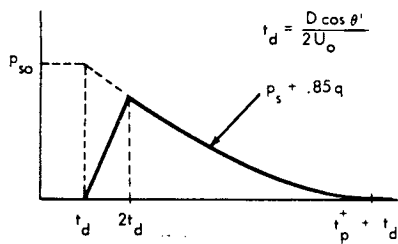


FIGURE 8.2.39 Average Overpressure on Closed Ends of Cylindrical Arch versus Time

Local Cylindrical Arch Overpressure, Axis Perpendicular to Shock Front.

The local overpressure at any point on the structure is the overpressure in the incident blast wave  $p_s$  with a time displacement factor  $t_d = L'/U_o$  where  $L'$  is the distance from the front end to the point at which the overpressure is desired.

As far as the average overpressure is concerned, it can be computed as outlined in Section 8.2.1.1.

Computation of the Total Load on Arches with Axis Parallel to Wave Front

After having predicted the overpressures acting on the structure, the next step is to construct the total load vs time curve. This can be done, in an approximate way, as follows: (see Figure 8.2.40)

- a) Divide the arch into a certain number of  $n$  sections (for instance,  $10^{\circ}$  wide).
- b) Compute the overpressure, vs time curve, according to the above mentioned procedures, for the middle point,  $x_m$  of each section
- c) Assume overpressure to be equal on every point of each section and construct the curves of overpressure multiplied by  $\cos \theta$  (horizontal component) and by  $\sin \theta$  (vertical component) versus time for each section
- d) Add, on a common time basis, the various overpressure curves multiplied by the area of each section.

The two resulting curves will represent the time variation of the horizontal and vertical total load acting on the structure.

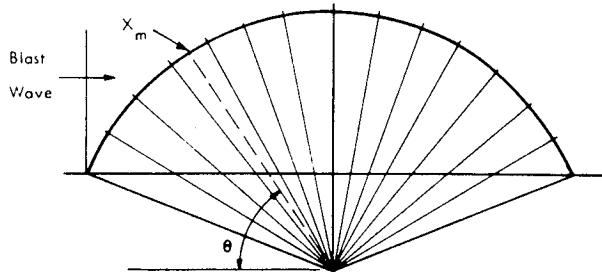


FIGURE 8.2.40 Example of Subdivision for Computation of Total Horizontal and Vertical Load on Arches

8.2.1.6 Loading on Domes

Figure 8.2.41 illustrates the notation convention used to designate a point on the surface of a dome. (Reference 8.2.1). With that notation, any point on a spherical dome is located by the two angles  $\theta$  and  $\phi$ . Denoting by  $p$  any point on the sphere,  $\theta$  is the angle between the horizontal diameter parallel to the direction of travel of the shock and the radius  $Op$  joining the surface point to the geometrical center of the sphere. The elevation of the point  $p$  above a horizontal plane through the center of the sphere is  $R \sin \theta \sin \phi$ , where  $\phi$  is the angle between the horizontal plane through the center of the sphere and the inclined plane containing points  $O, O',$  and  $p$ .

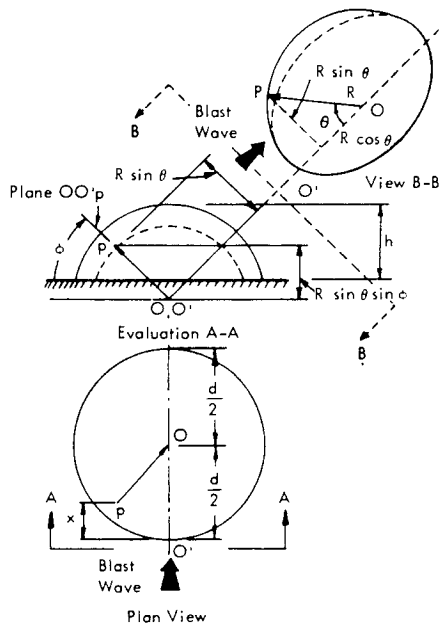


FIGURE 8.2.41 Definition Sketch for Spherical Dome Notation

The variation with time of the local overpressure  $p_{dome}$  normal to the surface of the dome is similar to that for a cylinder as shown in Figures 8.2.31 and 8.2.38. The overpressure at a given point rises instantaneously from zero to  $P_r - \theta$  given on Figure 8.2.25 (for  $\theta < 90^\circ$ ) or by (for  $\theta > 90^\circ$ ):

$$p_{dome} = \left(1.5 - \frac{\theta}{180}\right) p_{so} \quad (8.2.51)$$

Furthermore:

$$t_d = \frac{x}{U_o} = \frac{\frac{d}{2} - R \cos \theta}{U_o} \quad (8.2.52)$$

where

- $x$  = Distance shown in Figure (8.2.41)
- $d$  = Distance across the dome at its base (Figure 8.2.41)
- $R$  = Radius of the sphere
- $U_o$  = Shock front velocity Equation (8.2.9).

The clearing time is given by:

$$t_c = \frac{3h}{c_{refl.}} \quad (\text{for } \theta < 90^\circ) \quad (8.2.53)$$

$$t_c = \left(\frac{3h}{c_{refl.}}\right) \left(\frac{\theta}{90}\right) \quad (\text{for } \theta > 90^\circ) \quad (8.2.54)$$

where

$h$  is the height of the dome above its base (Figure 8.2.41)

$c_{refl.}$  is given by Equation (8.2.5).

The local overpressure at any point after the clearing of reflected overpressure is given by:

$$p_{dome} = C_d q + p_s \quad (8.2.55)$$

where

$q$  = Drag pressure given by Figure 6.43 or, for  $q_{so} \leq 10$  psi, by Equation (8.2.39).

$C_d$  = Local Drag Coefficient plotted as a function of  $\theta$  in Figures 8.2.42 and 8.2.43. The ratio of the Reynolds number of the air blast wind to the diameter of the sphere is plotted in Figure 8.2.33.

To predict the total load, the procedure indicated for cylindrical structures can be used.

### 8.2.1.7 Loading on Buried Structures

An air blast wave impinging upon the surface of the ground induces an underground pressure wave which is propagated at the seismic velocity  $C_s$  given in Table 8.2.2.

If the ground surface above the structure is in the regular reflection region, the induced ground pressure wave is assumed to be horizontal and moving downward through the soil with a vertical velocity  $C_s$ .

TABLE 8.2.2

#### TYPICAL SEISMIC VELOCITIES FOR SOILS AND ROCKS (REFERENCE 8.2.6)

Material	Seismic Velocity, $C_s$ Hz
Loose and Dry Soils	600 - 3,300
Clay and Wet Soils	2,500 - 6,300
Coarse and Compact Soils	3,000 - 8,500
Sandstone and Cemented Soils	3,000 - 14,000
Shale and Marl	6,000 - 17,500
Limestone - Chalk	7,000 - 21,000
Metamorphic Rocks	10,000 - 21,700
Volcanic Rocks	10,000 - 22,600
Sound Plutonic Rocks	13,000 - 25,000
Jointed Granite	8,000 - 15,000
Weathered Rocks	2,000 - 10,000

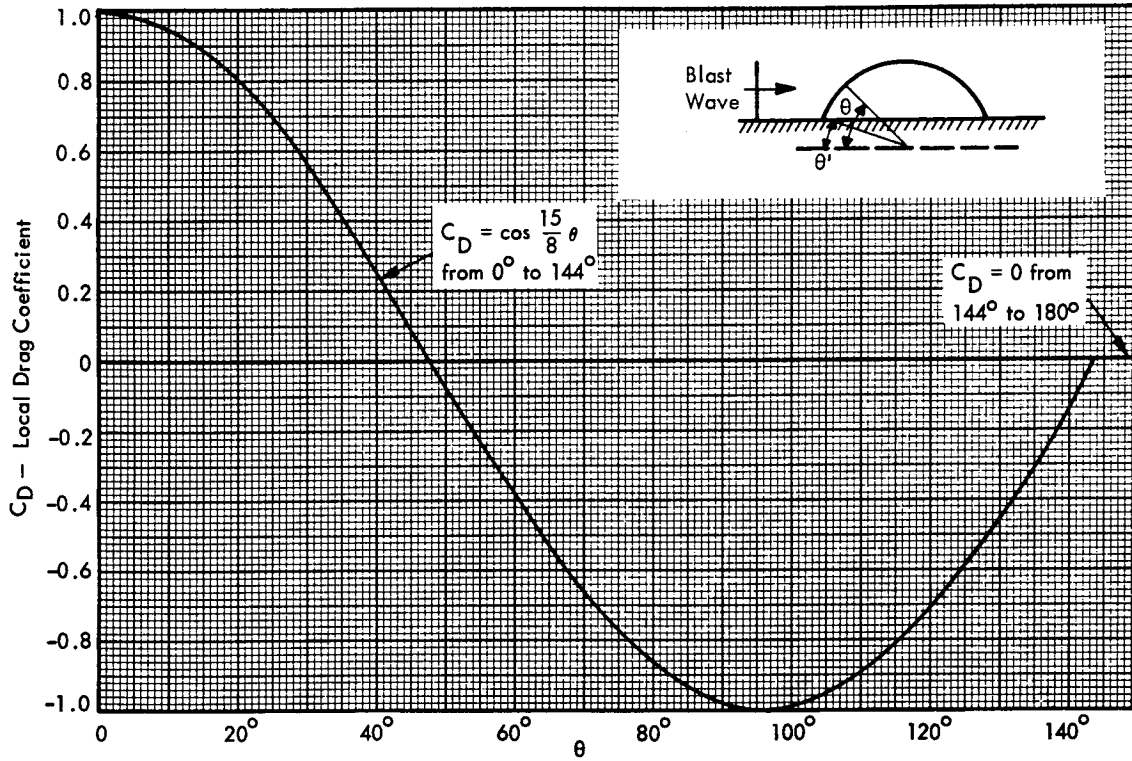


FIGURE 8.2.42 Local Drag Coefficients for Spherical Dome,  $R_e > 10^5$

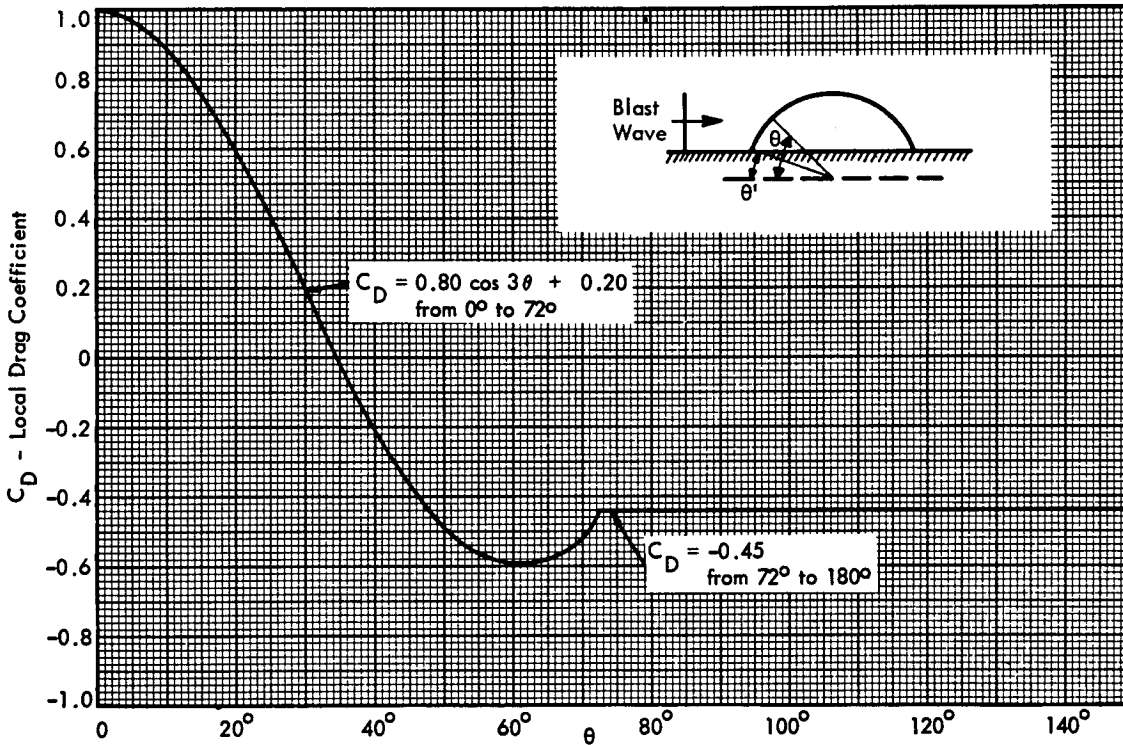


FIGURE 8.2.43 Local Drag Coefficients for Spherical Dome,  $R_e < 10^5$

If the structure is under the region of Mach reflection, the induced ground pressure wave is assumed to behave as illustrated in Figure 8.2.44.

The local overpressure on the roof is approximately equal to the overpressure of the air blast wave on the ground surface  $p_s$ .

The lateral overpressure varies according to soil characteristics. The ratios of lateral to vertical pressure for several types of soil are given in Table 8.2.3.

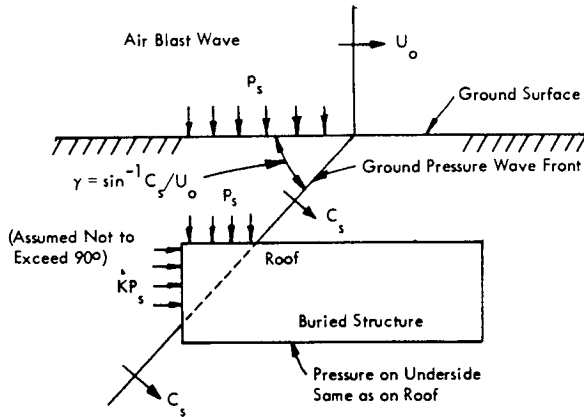


FIGURE 8.2.44 Ground Pressure Wave Induced by Air Blast Wave in Region of Mach Reflection

Local Roof Overpressure  $p_{B-roof}$

Figure 8.2.45 gives the time variation of the local roof overpressure  $p_{B-roof}$  for the buried structures located in regions of regular and Mach reflection. In that figure,  $L'$  is the distance from the point on the roof where the pressure is desired to the upper front corner of the structure and  $U_o$  is given by Equation (8.2.9).

TABLE 8.2.3

RECOMMENDED COEFFICIENT OF LATERAL TO VERTICAL SOIL PRESSURE (STRESS ON VERTICAL SURFACES OF STRUCTURES) (REFERENCE 8.2.14)

Soil Type	Stress Coefficient K
Cohesionless Soil, Damp or Dry	1/4
Unsaturated Cohesive Soils of Stiff Consistency	1/3
Unsaturated Cohesive Soils of Medium Consistency	1/2
Unsaturated Cohesive Soils of Soft Consistency	3/4
All Saturated Soils With the Water Table at the Surface	1

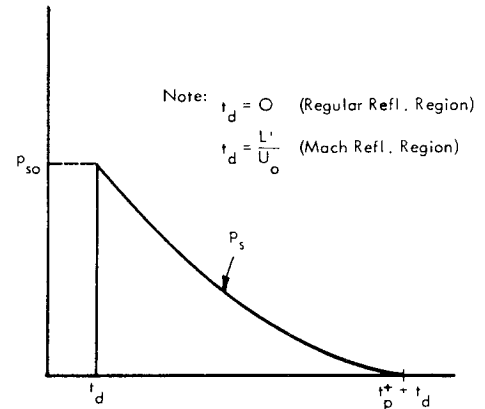


FIGURE 8.2.45 Local Roof Overpressure versus Time for Buried Structures Located in Regions of Regular and Mach Reflection

Average Roof Overpressure  $\bar{p}_{B-roof}$

Regular reflection region:  $\bar{p}_{B-roof}$  is identical with the local roof overpressure.

Mach reflection region: Figure 8.2.46 gives the time variation of the average roof overpressure; in this Figure,  $L$  is the length of roof in the direction of travel of the air shock wave.

Overpressure on Underside of Buried Structure

The overpressures exerted on the underside of buried structures with an integral floor are approximately the same as on the roof and the above mentioned procedure for predicting them can be used.

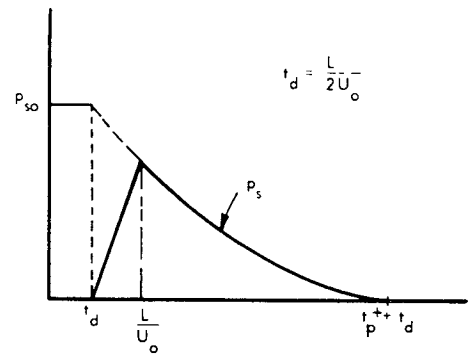


FIGURE 8.2.46 Average Roof Overpressure versus Time for Buried Structure Located in Region of Mach Reflection



Average Front Wall Overpressure  $\bar{p}_{B-front}$

Figure 8.2.47 illustrates the time variation of the average front wall overpressure,  $\bar{p}_{B-front}$  for buried structures located in regions of regular or Mach reflection. In this figure,  $t_d$  is given by:

$$t_d = \frac{h}{2U_o \tan \gamma} \tag{8.2.56}$$

where

- h is the height of the front wall of the structure
- L is the length of roof in direction of travel of air shock wave
- $U_o$  is the shock front velocity given by Equation (8.2.9)
- $\gamma$  is the angle whose sine is  $C_s/U_o$  (see Figure 8.2.44)
- K is given in Table 8.2.3

Average Back Wall Overpressure  $\bar{p}_{B-back}$

Regular reflection region: The average back wall overpressure is identical with the average front face overpressure.

Mach reflection region: The average back wall overpressure is illustrated in Figure 8.2.48 where the symbols used have the same meaning as for Figure 8.2.47.

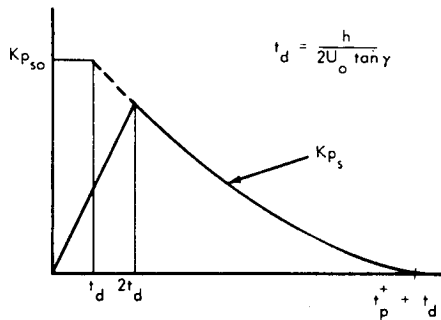


FIGURE 8.2.47 Average Front Wall Overpressure versus Time for Buried Structure Located in Regions of Regular and Mach Reflection

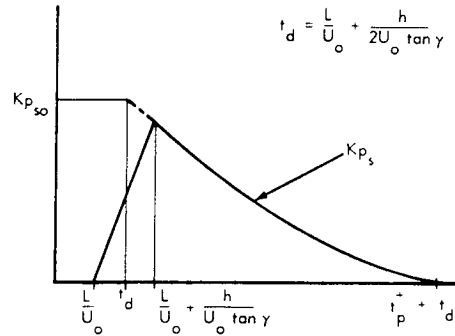


FIGURE 8.2.48 Average Back Wall Overpressure versus Time for Buried Structure Located in Region of Mach Reflection

Average Side Wall Overpressure  $\bar{p}_{B-side}$

Regular reflection region: The average side wall overpressure is identical with the average front face overpressure.

Mach reflection region: The average side wall overpressure is illustrated in Figure 8.2.49 where the symbols used have the same meaning as for Figure 8.2.47.

Total Load on Buried Structure

Once the average overpressures have been predicted, the total load due to a shock wave, acting on a buried structure can be calculated as previously shown in this section for surface structures.

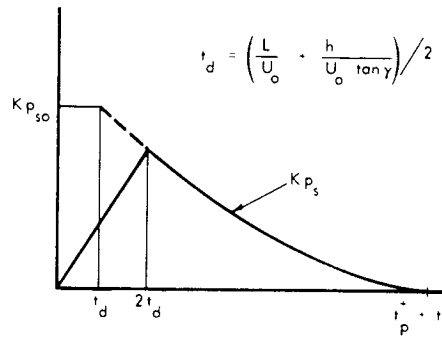


FIGURE 8.2.49 Average Side Wall Overpressure versus Time for Buried Structure Located in Region of Mach Reflection

8.2.2 COMPUTATION OF DYNAMIC STRUCTURAL RESPONSE

The steps required for predicting the response of a structure are the following: (Reference 8.2.4)

- a) Substitution of the actual building with an analytical model as a spring-mass system (having one or more degrees of freedom according to the number of stories of the real building).
- b) Replacing of the actual load vs time function with either a triangular or bilinear load to simplify calculations (it will be shown that very small errors result from this simplification).
- c) Computation of mass-displacement vs time function by using rigorous or approximate methods.

8.2.2.1 Substitution of the Actual Building with a Spring-Mass System

The objective of the analysis would be to predict the displacement of each point of the structure during the duration of the blast, but such analytical prediction would involve lengthy and difficult calculations so that certain simplifications would be required.

One way of approaching the problem is by replacing the actual building with a spring-mass system having one or more degrees of freedom according to the number of the building stories. Essentially, a distributed mass-load-spring system is replaced by a lumped mass-load-spring. In other words, the masses are assumed to be lumped at the top of the columns of each floor and the loads are considered to be acting on the lumped masses.

The next step is to simulate the actual building, by applying the principles of dynamic similarity, with a spring-mass system.

Computation of the Resistance Function and Equivalent Spring Constant

The simulation of the structure with a mass-spring system requires the computation of the resistance function and consequently of the spring constant to be applied to the analytical model.

Because of the importance of the resistance function and of the spring constant, it is necessary to clarify here the way to predict them.

The resistance of an element is defined as the internal force tending to restore the deflected element to its equilibrium condition; at a given deflection, the restoring force (or resistance) is defined as numerically equal to the static load required to produce the same deflection.

In order to simplify the calculations, the resistance-displacement function is always idealized to the elasto-plastic function as shown in Figure 8.2.50. The criteria to be used for such a replacement are:

- 1) The energy absorbed by the element subject to a deflection following the elasto-plastic resistance function must be equal to the energy absorbed in the case of strain-hardening or decaying resistance functions for a given value of the maximum response. This implies that the area under the elasto-plastic function must be equal to the area under the real resistance function for a given value of the maximum response (see Figure 8.2.50 where Area "A" is equal to Area "B").
- 2) The initial slope,  $K$ , of the elasto-plastic resistance must be equal to the initial slope of the real function.

Now, it is known that the distortion of structural elements when subjected to dynamic loads depends on the stiffness of the element; on spatial distribution of the loads; on the time variation of the loads and on the support conditions of the element. Any impulsively-loaded element having distributed masses vibrates in an infinite number of modes of vibration. It is hard to predict the exact behavior of such an element and, for all practical purposes, the problem can be simplified by utilizing a spring-mass system and assuming a deflected shape for the element. The deflected shape assumed for the element under the dynamic load is identical to the deflected shape due to a static load with the same distribution. An example will clarify this.

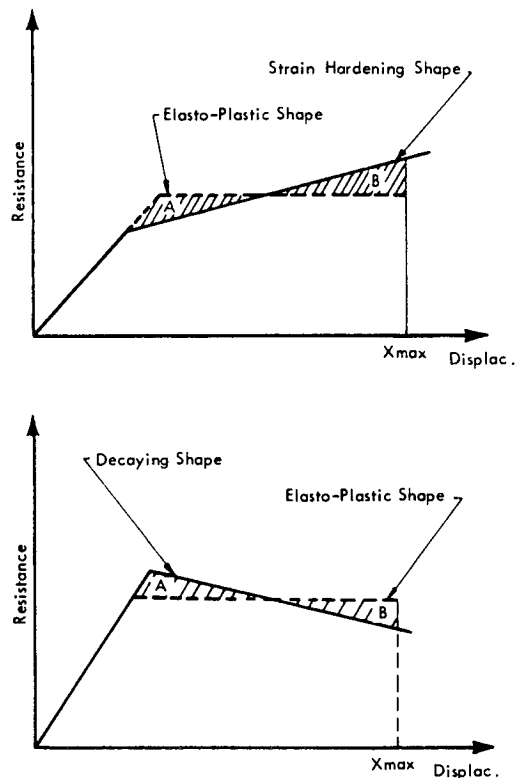


FIGURE 8.2.50 Simplification of the Resistance Function

Consider now, simultaneously, the beam of Figure 8.2.51a and the spring-mass system of Figure 8.2.51b which will substitute for the beam. The displacement,  $y$ , for the beam shown in Figure 8.2.51a, is given as a function of the load per unit of length ( $p$ ) and as a function of the distance  $h$  from the end B, by the familiar expression

$$y = \frac{1}{EI} \left( \frac{pL^4}{24} + \frac{ph^4}{24} - \frac{pL^2h^2}{12} \right) \quad (8.2.57)$$

where

$E$  = Young's Modulus

$I$  = Moment of inertia of the beam section with respect to the centroidal axis normal to the load plane

$p$  = Loading per unit of length

$P$  = Total load.

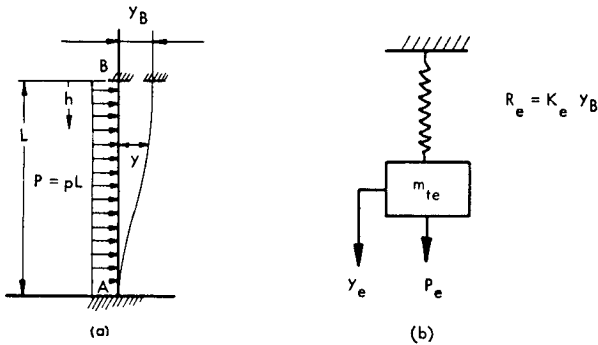


FIGURE 8.2.51 Uniformly loaded Clamped Sliding Beam (a) and the Equivalent Single Degree System (b).

It will be assumed that the displacement  $y_e$  of the mass  $m_{te}$  of Figure 8.2.51b represents the displacement of the beam at the point B. In the following discussion,  $y_B$  will represent the displacement of floor B of the building as shown by:

$$y_B = \frac{pL^4}{24EI} = \frac{PL^3}{24EI} = y_e \quad (8.2.58)$$

and the true stiffness of the beam  $K$  will be

$$K = \frac{P}{y_B} = \frac{24EI}{L^3} \quad (8.2.59)$$

Note that the boundary conditions used in this example are commonly employed to represent end-fixity of building columns. The last column of Table 8.2.4 gives the equivalent spring constant for other boundary conditions.

In order to define correctly the equivalent spring constant  $K_e$ , it is necessary to equate the strain energy of the structural element, as computed from the assumed deflection shape, and the strain energy of the equivalent spring-mass system.

Consider, now a resistance factor,  $K_R$ , defined by the equation

$$K_R = \frac{R_e}{R} \quad (8.2.60)$$

where

$R$  = Computed resistance of the structural element

$R_e$  = Resistance of the equivalent system.

The strain energy,  $SE$ , of the real beam is given by:

$$(SE)_{\text{beam}} = \int_0^L \frac{M^2}{2EI} dh \quad (8.2.61)$$

where  $M$  is the bending moment at any point.

$$\text{Since } M = \frac{pL^2}{6} - \frac{ph^2}{2} \quad (8.2.62)$$

$$\begin{aligned} (SE)_{\text{beam}} &= \frac{1}{2EI} \int_0^L \left( \frac{p^2L^4}{36} + \frac{p^2h^4}{4} - \frac{p^2h^2L^2}{6} \right) dh \\ &= \frac{p^2L^5}{2EI} \frac{1}{45} \end{aligned} \quad (8.2.63)$$

which may also be written in the following form, where

$$\begin{aligned} y_B &= \text{deflection of the point B} = \frac{pL^3}{24EI} \\ (SE)_{\text{beam}} &= \frac{1}{2} y_B^2 \frac{24^2}{45} \frac{EI}{L^3} \end{aligned} \quad (8.2.64)$$

$$\text{Equating } (SE)_{\text{beam}} = (SE)_{\text{spring}} = \frac{1}{2} K_e y_e^2$$

$$\frac{1}{2} K_e y_e^2 = \frac{1}{2} y_B^2 \frac{24^2}{45} \frac{EI}{L^3} \quad \text{gives}$$

$$K_e = \frac{24^2}{45} \frac{EI}{L^3} \quad (8.2.65)$$

Therefore, with Equation (8.2.59), the resistance factor is

$$K_R = \frac{K_e}{K} = \frac{24}{45} = 0.53 \quad (8.2.66)$$

In the plastic range, a different way must be used to find the resistance factor. This is due to the development of plastic hinges at the fixed end. In this case, assume that the beam is initially supported as in Figure 8.2.52, to avoid an unstable condition.

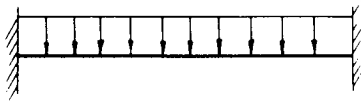


FIGURE 8.2.52 Uniformly Loaded Fixed-End Beam.

After the moment has reached the value at which the plastic range starts, the moment restraint at the ends is lost.

In this range, called elasto-plastic, the resistance factor is equal to that of a simply supported beam and can be shown to be equal to 0.64.

In the plastic range, which is reached after the deflection has exceeded the point  $y_{2m}$  of Figure 8.2.53; the resistance factor is calculated as follows.

The strain energy absorbed in the actual beam during the distortion indicated in Figure 8.2.54 may be written:

$$(SE)_a = 2M_c \theta_c \quad (8.2.67)$$

where  $M_c$  is the bending moment at the plastic "hinge" in the center of the beam and  $\theta_c$  is the slope of the beam at this point.

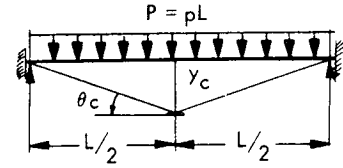


FIGURE 8.2.54 Uniformly Loaded Fixed-End Beam; Plastic Range.

The strain energy stored in the equivalent plastic system is

$$(SE)_e = R_{me} y_e \quad (8.2.68)$$

In other words, it is equal to the work done by the resistance  $R_{me}$  of the equivalent system over the deflection  $y_e$ . Equating the strain energies of the equivalent and actual systems,

$$R_{me} y_e = 2M_c \theta_c \quad (8.2.69)$$

$$\text{But } M_c = R_m L/8 \quad (8.2.70)$$

$$\text{and } \theta_c = 2y_c/L. \quad (8.2.71)$$

Thus, setting  $y_c = y_e$

$$R_{me} = \frac{R_m}{2} \quad (8.2.72)$$

and

$$K_R = \frac{R_{me}}{R_m} = 0.5 \quad (8.2.73)$$

For any other loading or support conditions in the plastic range, the procedure for determining  $K_R$  is the same.

Resistance factors for other cases are shown in Table 8.2.4.

### Load Factor

In order to obtain an equivalent system which could replace the actual beam, the actual load and mass must be reduced by means of two factors called the load factor and the mass factor.

The load factor  $K_L$  is defined as the ratio between the equivalent load  $P_e(t)$  and the actual load  $P(t)$

$$K_L = \frac{P_e(t)}{P(t)} \quad (8.2.74)$$

It can be derived by equating the external work done by the equivalent load on the equivalent system and the external work done by the actual load on the actual beam to the assumed deflected shape (Figure 8.2.55).

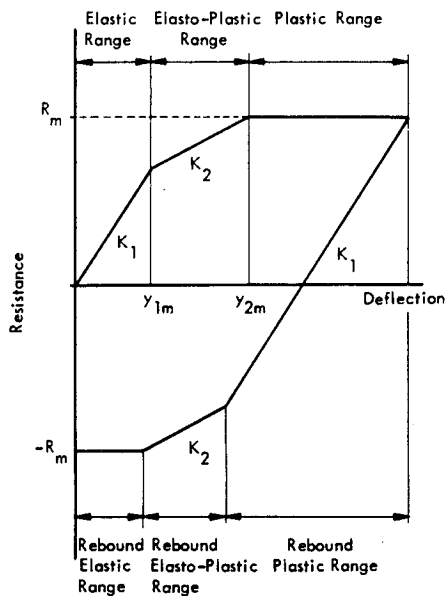


FIGURE 8.2.53 Idealized Resistance Function for Fixed-End Beams.

Assume that the space and time variations of the deflection,  $y = f(h, t)$  are separable into two functions as:

$$y = f_1(h) \cdot f_2(t) \quad (8.2.75)$$

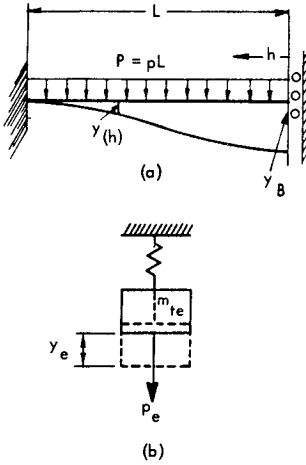


FIGURE 8.2.55 Uniformly Loaded Clamped Sliding Beam (a) and the Equivalent Single Degree System (b)

The work done for a unit length of the beam by the actual load in time  $dt$  is:

$$dW = p(t) \frac{\partial y}{\partial t} dt = p f_1(h) \frac{df_2(t)}{dt} dt \quad (8.2.76)$$

and the work done up to time  $t$  is:

$$\int_0^t dW = \int_0^L f_1(h) dh \int_0^t p \frac{df_2(t)}{dt} dt \quad (8.2.77)$$

The displacement of the spring-mass system represents the displacement of the point B of the actual beam:

$$y_e = y_B = f_1(0) f_2(t) \quad (8.2.78)$$

The work done on the equivalent system by the equivalent load,  $P_e(t)$  up to any time,  $t$ , must be:

$$W_e = f_1(0) \int_0^t P_e \frac{df_2(t)}{dt} dt \quad (8.2.79)$$

Equating the work done for each system and differentiating with respect to time gives

$$K_L = \frac{P_e}{P} = \frac{\int_0^L f_1(h) dh}{L f_1(0)} \quad (8.2.80)$$

In this example,  $K_L$  is given by:

$$K_L = \frac{\int_0^L \frac{1}{EI} \left( \frac{pL^4}{24} + \frac{ph^4}{24} - \frac{pL^2 h^2}{12} \right) dh}{L \cdot \frac{pL^4}{24EI}} = \frac{8}{15} = 0.53 \quad (8.2.81)$$

The load factor for the plastic range is computed in the same manner as was done previously for the resistance factor, but equating the work done.

From this example, it can be seen that  $K_L$  is equal to  $K_R$ .

#### Mass Factor

The mass factor,  $K_M$ , is defined as the ratio between the mass of the equivalent system,  $m_{te}$ , and the mass of the actual element,  $m_t$ .

The mass factor can be obtained by equating the kinetic energies of the beam and the equivalent system for any time.

Referring to the Figures 8.2.55, a, b, the kinetic energies are given by:

$$(KE)_{\text{actual}} = \int_0^L \frac{1}{2} m \left( \frac{dy}{dt} \right)^2 dh \quad (8.2.82)$$

where  $m = \frac{m_t}{L}$

$$(KE)_{\text{equiv.}} = \frac{1}{2} m_{te} \left( \frac{dy_e}{dt} \right)^2 \quad (8.2.83)$$

Equating the energy expressions as shown above, gives:

$$K_M = \frac{m_{te}}{m_t} = \frac{1}{L} \int_0^L \frac{\left( \frac{dy}{dt} \right)^2}{\left( \frac{dy_e}{dt} \right)^2} dh \quad (8.2.84)$$

But, as shown previously,

$$y = f_1(h) f_2(t) \text{ and } \frac{dy}{dt} = f_1(h) \frac{df_2(t)}{dt} \quad (8.2.85)$$

$$y_e = f_1(0) f_2(t) \text{ and } \frac{dy_e}{dt} = f_1(0) \frac{df_2(t)}{dt} \quad (8.2.86)$$

TABLE 8.2.4

DYNAMIC DESIGN FACTOR (Reference 8.2.1)

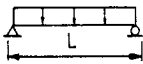
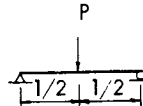
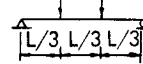
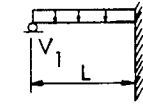
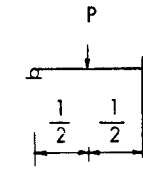
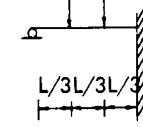
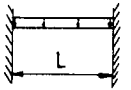
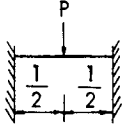
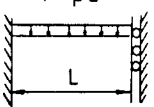
Loading Diagram	Strain Range	Load Factor $K_L$ or Resistance Factor $K_R$	Mass Factor $K_M$		Maximum Resistance $R_m$	Spring Constant $K$
			Concentrated Mass*	Uniform Mass		
$P = pL$ 	Elastic	0.64		0.50	$\frac{8 M_p}{L}$	$\frac{384 EI}{5L^3}$
	Plastic	0.50		0.33	$\frac{8 M_p}{L}$	0
	Elastic	1	1.0	0.49	$\frac{4 M_p}{L}$	$\frac{48 EI}{L^3}$
	Plastic	1	1.0	0.33	$\frac{4 M_p}{L}$	0
$P/2 \quad P/2$ 	Elastic	0.87	0.76	0.52	$\frac{6 M_p}{L}$	$\frac{56.4 EI}{L^3}$
	Plastic	1	1.0	0.56	$\frac{6 M_p}{L}$	0
$P = pL$ 	Elastic	0.58		0.45	$\frac{8 M_{ps}}{L}$	$\frac{185 EI}{L^3}$
	Elasto-Plastic	0.64		0.50	$\frac{4}{L} (M_{ps} + 2M_{pm})$	$\frac{384 EI}{5L^3}$
	Plastic	0.50		0.33	$\frac{4}{L} (M_{ps} + 2M_{pm})$	0
	Elastic	1.0	1.0	0.43	$\frac{16 M_{ps}}{3L}$	$\frac{107 EI}{L^3}$
	Elasto-Plastic	1	1.0	0.49	$\frac{2}{L} (M_{ps} + 2M_{pm})$	$\frac{48 EI}{L^3}$
	Plastic	1	1.0	0.33	$\frac{2}{L} (M_{ps} + 2M_{pm})$	0
$P/2 \quad P/2$ 	Elastic	0.81	0.67	0.45	$\frac{6 M_{ps}}{L}$	$\frac{132 EI}{L^3}$
	Elasto-Plastic	0.87	0.76	0.52	$\frac{2}{L} (M_{ps} + 3M_{pm})$	$\frac{56 EI}{L^3}$
	Plastic	1	1.0	0.56	$\frac{2}{L} (M_{ps} + 3M_{pm})$	

TABLE 8.2.4 (CONTINUED)

	Elastic	0.53		0.41	$\frac{12 M_{ps}}{L}$	$\frac{384 EI}{L^3}$
	Elasto-Plastic	0.64		0.50	$\frac{8}{L} (M_{ps} + M_{pm})$	$\frac{384 EI}{5L^3}$
	Plastic	0.50		0.33	$\frac{8}{L} (M_{ps} + M_{pm})$	0
	Elastic	1	1.0	0.37	$\frac{4}{L} (M_{ps} + M_{pm})$	$\frac{192 EI}{L^3}$
	Plastic	1	1.0	0.33	$\frac{4}{L} (M_{ps} + M_{pm})$	0
	Elastic	0.53		0.41	$\frac{3 M_{ps}}{L}$	$\frac{24 EI}{L^3}$
	Plastic	0.50		0.35	$\frac{8}{L} (M_{ps} + M_{pm})$	0

\*Concentrated mass is lumped at the concentrated load.

So that equation 8.2.84 gives

$$K_M = \frac{1}{L} \int_0^L \left( \frac{f_1(h)}{f_1(0)} \right)^2 dh$$

$$= \frac{1}{L} \int_0^L \left[ \frac{\frac{1}{EI} \left( \frac{pL^4}{24} + \frac{ph^4}{24} - \frac{pL^2 h^2}{12} \right)}{\frac{pL^4}{24EI}} \right]^2 dh$$

$$= 0.41 \tag{8.2.87}$$

The procedure would be the same for beams with different support and load conditions.

As far as the plastic range is concerned, the procedure is the same as for the resistance factor except that kinetic energies are equated. In this case, a value of 0.35 will be found.

The dynamic design factors derived above are summarized in Table 8.2.4 for a variety of typical beam configurations. Corresponding values for the maximum resistance in the elastic, elasto-plastic, and plastic range are also

given. With these factors, an equivalent mass-spring model can be defined for each type of beam and utilized in a lumped mass model of building response to a blast. A specific example of this application is given at the end of this section. All these factors are defined as follows:

$$K_L = \text{Load Factor} = \frac{\text{Load on Equivalent System}}{\text{Total Load on Beam}}$$

$$K_R = \text{Resistance Factor} = \frac{\text{Spring Constant of Equivalent System}}{\text{Actual Stiffness of the Beam}}$$

$$K_M = \text{Mass Factor} = \frac{\text{Mass of Equivalent System}}{\text{Mass of the Beam}}$$

$R_m$  = Maximum resistance in terms of:

$$M_p = \text{plastic resisting moment (elastic range);}$$

$$M_{ps} = \text{plastic support moment, and}$$

$$M_{pm} = \text{plastic hinge moment at midspan (elasto-plastic and plastic range).}$$

$K$  = Stiffness of the Beam

$$K_e = \text{Equivalent Spring Constant} = K \cdot K_R$$

8.2.2.2 Idealization of the Load Acting on Structures

In the previous section the computation of the load acting on structures due to blast waves has been analyzed and theoretical expressions have been found applicable to various types of structures. These expressions are rather complicated and a simplification would be very desirable in order to reduce the time required for predicting the behavior of structures subject to blast waves. To indicate the convenience of using approximate expressions of load instead of exact ones, the results of a numerical example are presented in this section.

Figure 8.2.56 illustrates how a typical load function can be simplified:

- a) The continuous curve represents a close approximation of the actual loading.
- b) The two dashed lines represent a first approximation of loading, that is the complicated curve is approximated by two lines giving more severe conditions of loading and the negative phase is not considered.
- c) In this case, the load is a triangular pulse (dash dot line) having the same impulse as the positive phase of line a) (Area A is equal to Area B.)

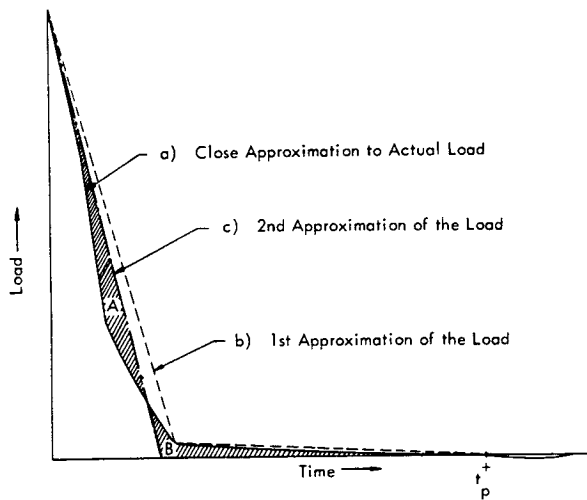


FIGURE 8.2.56 Idealizations of a Typical Blast Load Acting on the Building

To obtain an idea of the accuracy achieved by using the simplified loading, a numerical example has been carried out. (see Section 8.2.3). In this example a rigorous method of calculation has been applied to a three-story building subject to a blast wave.

The displacement of each floor, called  $x_1, x_2, x_3$ , has been plotted in Figures 8.2.57, 8.2.58 and 8.2.59 where:

- 1) The dashed curve represents the floor displacement vs time according to the first approximation of loading.
- 2) The dash-dot curve represents the floor displacement vs time according to the triangular impulse.

The maximum positive and negative displacements computed for each floor in the example worked out in Section 8.2.4, using the two idealizations of the load, differed by the percentages indicated in Table 8.2.5.

TABLE 8.2.5

PER CENT DIFFERENCE BETWEEN RESPONSE WITH BILINEAR LOAD APPROXIMATION AND TRIANGULAR PULSE APPROXIMATION

	1st Floor	2nd Floor	3rd Floor
Maximum Positive Displacement	+10.8%	+11%	+12%
Maximum Negative Displacement	+ 5.0%	+ 4.8%	+7.5%

The triangular pulse has the same impulse but a shorter duration, while the bilinear loading has a larger impulse but the same duration. The results shown in Table 8.2.5 indicate that the maximum difference between the response for the two types of loadings is 12 percent. The exact value of the response would, in fact, be expected to fall between the two results.

Since there are so many other approximations made in blast analysis, these differences are not considered significant and the simpler triangular pulse is justified for general response calculations.

A more detailed comparison of the computed responses for the two different types of load idealization will be made in Section 8.2.3 along with a comparison of the responses computed by the various analysis methods covered in the next section.

8.2.2.3 Methods of Analyzing Dynamic System Response to Blast Loads

Once the structure has been replaced with an analytical model, that is with a spring-mass system, the response of this model can be predicted by several means. In this section, one classical and two approximate methods will be presented and applied to a general N-degree of freedom system. Therefore, the following parameters will be involved:

- N masses:  $m_1; m_2; \dots; m_N$
- N absolute displacements:  $x_1; x_2; \dots; x_N$
- N external forcing functions:  $f_1(t); f_2(t); \dots; f_N(t)$
- N resisting forces:  $R_1(t); R_2(t); \dots; R_N(t)$

Depending on the type of construction, two cases are considered for the determination of the resisting forces, that is the shear wall building case and the frame building case.



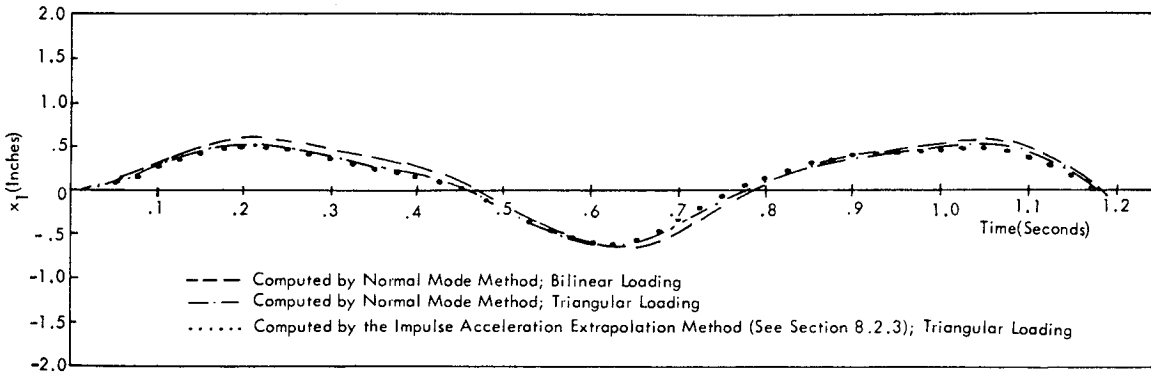


FIGURE 8.2.57 First Floor Absolute Displacement,  $x_1$ , vs Time Curve

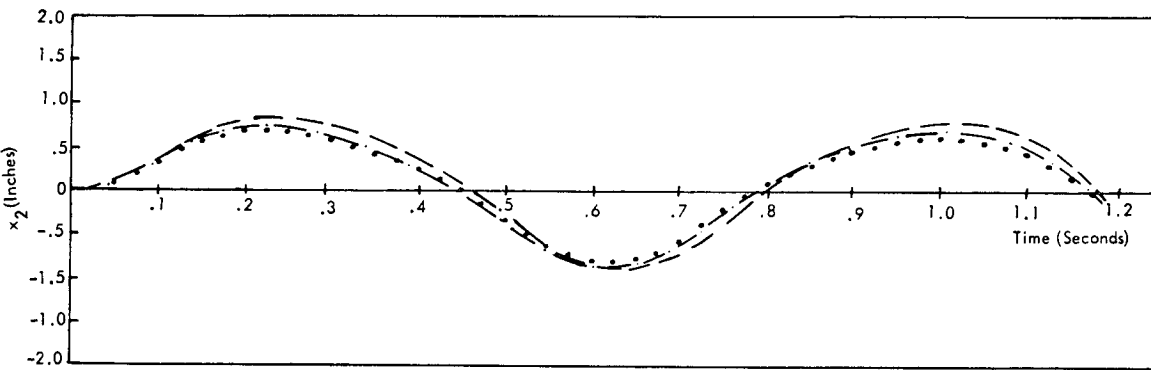


FIGURE 8.2.58 Second Floor Absolute Displacement,  $x_2$ , vs Time Curve

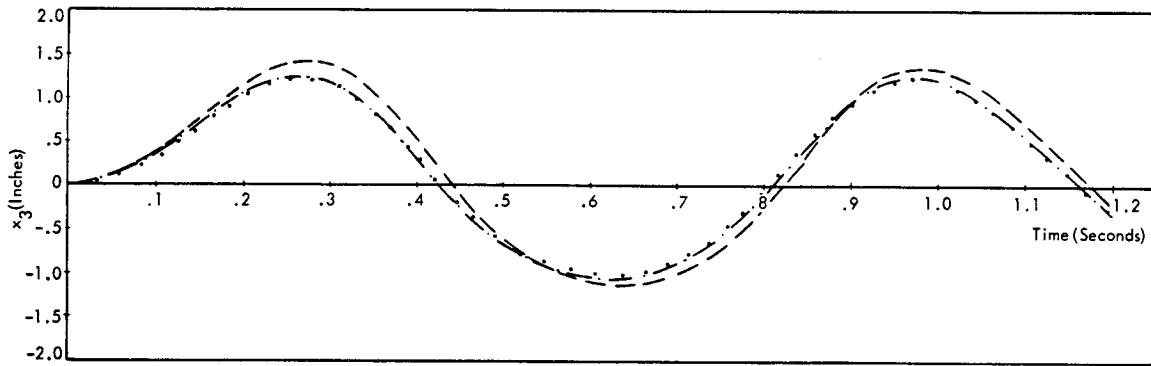


FIGURE 8.2.59 Third Floor Absolute Displacement,  $x_3$ , vs Time Curve

a) **Shear Wall Buildings.** In this case the resisting forces acting on any floor depend on the displacement of all floors. (See Figure 8.2.60). The resisting force, due to their relative displacement ( $x_g - x_i$ ), is given by:

$$R_{gi} = K_{gi} (x_g - x_i) \quad (8.2.88)$$

where  $K_{gi}$  is the coupling spring constant.

The expression for the total resisting force,  $R_g$ , acting on the  $g$ -th floor is:

$$R_g = \sum_{i=0}^N R_{gi} \quad (8.2.89)$$

or,

$$R_g = \sum_{i=0}^N K_{gi} (x_g - x_i) \quad (8.2.90)$$

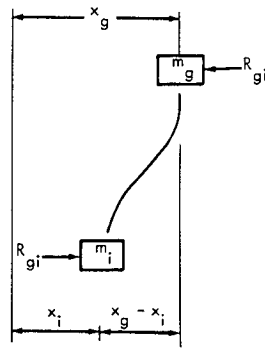


FIGURE 8.2.60 Any Two Floors of a Multi-Story Building

- b) Frame Buildings. In this case, most of the resistances,  $R_{gi}$ , in Equation (8.2.89) are negligible except for the resistances  $R_{g,g+1}$  and  $R_{g,g-1}$ , which are the resistances developed between adjacent masses. Therefore  $R_g$  is given by (using the simplified notations  $K_{g,g-1} = K_g$ )

$$R_g = K_g(x_g - x_{g-1}) - K_{g+1}(x_{g+1} - x_g) \quad (8.2.91)$$

Classical Normal Mode Method

The equation of motion of mass,  $m_g$ , is given by the equation:

$$m_g \ddot{x}_g + R_g(t) = F_g(t) \quad (8.2.92)$$

For an  $N$ -th degree dynamic system, there are  $N$  separate equations of the same type as Equation (8.2.92) which can be written (for the frame building case), for the  $g$ -th mass, in the form,

$$m_g \ddot{x}_g + (K_g + K_{g+1})x_g - K_g x_{g-1} - K_{g+1}x_{g+1} = f_g(t) \quad (8.2.93)$$

Setting the external forces to zero,

$$f_1(t) = f_2(t) = \dots = f_N(t) = 0 \quad (8.2.94)$$

and assuming solutions for the free vibration of the form

$$\begin{aligned} x_1 &= A_1 \sin(\omega t + \theta) \\ x_2 &= A_2 \sin(\omega t + \theta) \\ x_N &= A_N \sin(\omega t + \theta) \end{aligned} \quad (8.2.95)$$

and substituting into Equation (8.2.93), the following set of equations are obtained

$$\begin{aligned} A_1 \omega^2 m_1 - A_1(K_1 + K_2) + A_2 K_2 &= 0 \\ A_2 \omega^2 m_1 - A_2(K_2 + K_3) + A_1 K_2 + A_3 K_3 &= 0 \\ \dots \\ A_g \omega^2 m_g - A_g(K_g + K_{g+1}) + A_{g-1} K_g \\ &\quad + A_{g+1} K_{g+1} = 0 \\ \dots \\ A_N \omega^2 m_N - A_N K_N + A_{N-1} K_N &= 0 \end{aligned} \quad (8.2.96)$$

The system (8.2.96) has solutions for  $\omega^2$ , if the determinant of the coefficient  $A_N$  is equal to zero. From this condition, the values of the square of natural frequencies  $\omega_1^2; \omega_2^2; \dots; \omega_N^2$  can be found and accordingly the values of the coefficients,  $A_1, A_2 \dots A_N$  as a function of  $\omega$  can be determined.

The normal mode method consists of defining each of the displacements  $x_g(t)$  of the system as the sum of its responses in its  $N$  normal modes as given by:

$$x_g(t) = \sum_{n=1}^N A_{gn} q_n(t) \quad (8.2.97)$$

where  $A_{gn}$  is the  $n$ -th modal amplitude of the  $g$ -th mass and  $q_n(t)$  is the amplitude of the  $n$ -th normal mode. The magnitudes of the modal coefficients  $A_{gn}$  are found by Equation (8.2.96) and may be tabulated according to the following table:

Table of Modal Coefficients -  $A_{gn}$

	$\omega_1$	$\dots \omega_n \dots$	$\omega_N$
$A_1$	$A_{11}$	$\dots A_{1n} \dots$	$A_{1N}$
$\vdots$	$\vdots$	$\vdots$	$\vdots$
$A_g$	$A_{g1}$	$\dots A_{gn} \dots$	$A_{gN}$
$\vdots$	$\vdots$	$\vdots$	$\vdots$
$A_N$	$A_{N1}$	$\dots A_{Nn} \dots$	$A_{NN}$

The various amplitudes,  $A_{gn}$ , must be normalized to the largest amplitude for each mode.

Now, the following steps are carried out to define the response:

- i) Determine the generalized mass for each mode using the following expression:

$$M_n = \sum_{g=1}^N m_g A_{gn}^2 \quad (8.2.98)$$

- ii) Determine the generalized force for each mode by means of the following expression:

$$F_n(t) = \sum_{g=1}^N f_g(t) A_{gn} \quad (8.2.99)$$

- iii) Solve the following characteristic equation for the one degree of freedom system for each mode: (Damping is neglected)

$$\ddot{q}_n(t) + \omega_n^2 q_n(t) = \frac{F_n(t)}{M_n} \quad (8.2.100)$$

where:

$q_n(t)$  = contribution of the  $n$ -th mode

$F_n(t)$  = generalized force for the  $n$ -th mode

$M_n(t)$  = generalized mass for the  $n$ -th mode.

Comparison of these last three equations with the equations for the single degree of freedom system in Chapter 3 shows that they have the same form, except for the use of generalized or effective values of force and mass. This is also essentially the same form as was shown for the response of a distributed system such as a plate. The only difference now is that the present system consists of lumped elements instead of a continuous system so that the generalized forces and masses are found by summations over the  $N$  lumps instead of integration over the system.

Equation (8.2.100) for loading by a triangular pulse of duration  $T$  and peak value  $F_0$ , simulating a blast, has been shown to have the solution, for forced response during the pulse, equal to: (See Chapter 3)

$$q_n(t) = \frac{F_n(0)}{\omega_n^2 M_n} \left[ 1 - \frac{t}{T} + \sqrt{1 + (1/\omega_n T)^2} \sin(\omega_n t - \tan^{-1} \omega_n T) \right]_{t < T} \quad (8.2.101)$$

After the pulse, the residual or free motion solution is

$$q_n(t-T) = q_n(t=T) \cos \omega_n(t-T) + \dot{q}_n(t=T) \frac{\sin \omega_n(t-T)}{\omega_n}$$

where  $\dot{q}_n(t=T)$  is the velocity at the end of the pulse, so that the solution can be written as:

$$q_n(t-T) = \frac{F_n(0)}{\omega_n^2 M_n} \left[ 1 - \frac{2 \sin \omega_n T}{\omega_n T} + \frac{\sin^2 \omega_n T/2}{(\omega_n T/2)^2} \right]^{1/2} \sin(\omega_n t - \theta_n) \quad (8.2.102)$$

$$\theta_n = \tan^{-1} \frac{\omega_n T - \sin \omega_n T}{1 - \cos \omega_n T}$$

Evaluate the total displacement of the  $g$ -th mass by summing over all the normal modes to give,

$$x_g(t) = \begin{cases} \sum_{n=1}^N A_{gn} q_n(t), & t \leq T \\ \sum_{n=1}^N A_{gn} q_n(t-T), & t \geq T \end{cases} \quad (8.2.103)$$

#### Approximate Methods

One of the best approximate methods for computing the dynamic response of a multi-degree of freedom system has been presented by Newmark (Reference 8.2.10) and it is called the  $\beta$ -method. This method defines the displacement and the velocity of a mass,  $m$ , at time  $t_{n+1}$  as follows:

$$x(t_{n+1}) = x(t_n) + \dot{x}(t_n) \Delta t + \left( \frac{1}{2} - \beta \right) \ddot{x}(t_n) \Delta t^2 + \beta \ddot{x}(t_{n+1}) \Delta t^2 \quad (8.2.104)$$

$$\dot{x}(t_{n+1}) = \dot{x}(t_n) + \left[ \frac{\ddot{x}(t_{n+1}) + \ddot{x}(t_n)}{2} \right] \Delta t \quad (8.2.105)$$

where

- $x(t_n)$  = displacement of the mass at time  $t_n$
- $x(t_{n+1})$  = displacement of the mass at time  $t_{n+1}$
- $\dot{x}(t_n)$  = velocity of the mass at time  $t_n$
- $\ddot{x}(t_n)$  = acceleration of the mass at time  $t_n$
- $\Delta t$  = interval time between  $t_n$  and  $t_{n+1}$
- $\beta$  = a parameter which can have the following values: 1/4; 1/6; 1/8 and smaller.

The three values of  $\beta$  correspond to three assumptions made for the time history of the acceleration and are categorized as follows: (see Figure 8.2.61).

$\beta = 1/4$  - the acceleration during the time interval  $\Delta t$  is constant but has a value which is the average of the values at the beginning and the end of the interval.

$\beta = 1/6$  - the acceleration varies linearly during the time interval from the initial to the final value.

$\beta = 1/8$  - the acceleration has a constant value equal to the initial value for the first half of the time interval and a constant value equal to the final value for the second half of the time interval.

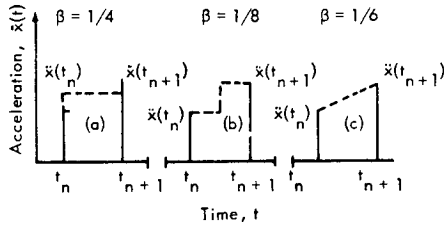


FIGURE 8.2.61 Variation in Acceleration During Interval, Consistent With Particular Values of  $\beta$

The recurrence formulas (8.2.104) and (8.2.105) can be used to predict the displacements and the velocities of an N-degree of freedom system. The expression for the acceleration is given, in general, by

$$\ddot{x}(t) = \frac{f(t) - R}{m} \quad (8.2.106)$$

where:  $f(t)$  is the forcing function  
 $m$  is the mass to which  $f(t)$  is applied  
 $R$  is the resistance function given by Equations (8.2.90) and (8.2.91).

Equations (8.2.104) and (8.2.105) for the  $g$ -th mass can now be written, using the expression (8.2.106) for  $\ddot{x}(t)$ , as follows:

$$\begin{aligned} x_g(t_{n+1}) &= x_g(t_n) + \dot{x}_g(t_n) \Delta t \\ &+ \left\{ \left( \frac{1}{2} - \beta \right) \left[ f_g(t_n) - R_g(t_n) \right] \frac{\Delta t^2}{m} \right. \\ &+ \left. \beta \left[ f_g(t_{n+1}) - R_g(t_{n+1}) \right] \right\} \frac{\Delta t^2}{m} \quad (8.2.107) \end{aligned}$$

$$\begin{aligned} \dot{x}_g(t_{n+1}) &= \dot{x}_g(t_n) \\ &+ \left[ f_g(t_n) - R_g(t_n) + f_g(t_{n+1}) - R_g(t_{n+1}) \right] \frac{\Delta t}{2m_g} \quad (8.2.108) \end{aligned}$$

Equations (8.2.107) and (8.2.108) can now be used for predicting the response of a spring-mass model of a shear wall or frame building using Equations (8.2.90) or (8.2.91), respectively, to define the resistance terms  $R_g(t_n)$  and  $R_g(t_{n+1})$ . In either case,  $R_g(t_{n+1})$  will involve knowing  $x_g(t_{n+1})$ , the quantity to be determined. Hence,

a trial and error procedure has to be adopted. As a first trial, for example,  $x_g(t_{n+1})$  can be assumed to be  $x(t_n) + \dot{x}(t_n) \Delta t$ . Using this in Equation (8.2.107), a new value  $x_g(t_{n+1})$  can be computed and compared with the assumed value. This procedure is repeated until the assumed and computed values of  $x_g(t_{n+1})$  converge. In the plastic region the resistance is a constant and the trial and error procedure is subject to some problems which are:

- 1) Divergence, or increasing difference between the assumed and computed values of  $x_g(t_{n+1})$
- 2) Instability that is due to an accumulation of errors causing the response to become infinitely large.

In order to prevent these possibilities, the following values of  $\beta$  and  $\Delta t/T$  (from Reference 8.2.10) should be used, where  $T$  is the period of the highest mode to be analyzed.

	$\beta = 1/4$	$\beta = 1/6$	$\beta = 1/8$	
$\frac{\Delta t}{T} \leq$	inf.	.551	.450	← Stability Limit
$\frac{\Delta t}{T} \leq$	.318	.389	.450	← Convergence Limit

As far as the choice of  $\beta$  is concerned, the values of  $\beta = 1/6$  should give the best results, due to the fact that the external loading is almost always assumed to vary linearly.

If stability problems arise, the use of  $\beta = 1/4$  is more convenient.

If convergence problems arise, a value of  $\beta = 1/8$  or less must be used.

Acceleration Impulse Extrapolation Method  
 (Reference 8.2.1)

In this method, the actual acceleration curve is replaced by a train of equally spaced impulses having a magnitude of:

$$I_g(t_n) = \ddot{x}_g(t_n) \Delta t \quad (8.2.109)$$

where

$I_g(t_n)$  is the acceleration impulse magnitude of time  $t_n$  (see Figure 8.2.62).

If  $t_n^-$  and  $t_n^+$  are the times immediately before and after the application of the impulse, the velocities at these times are related by:

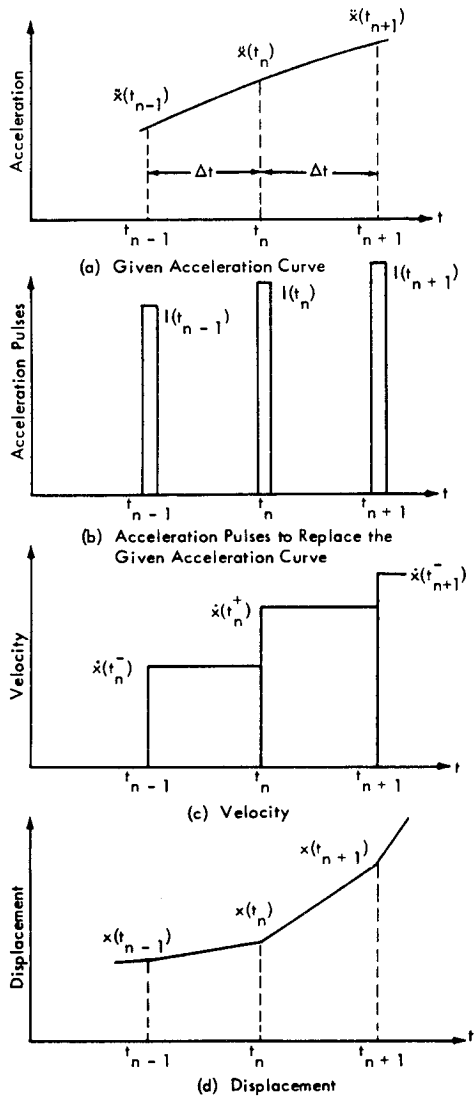


FIGURE 8.2.62 Acceleration Impulse Extrapolation Method

$$\dot{x}_g(t_n^+) = \dot{x}_g(t_n^-) + \ddot{x}_g(t_n) \Delta t \quad (8.2.110)$$

The relationships between  $x_g(t_{n-1})$  and  $x_g(t_n)$ , and between  $x_g(t_n)$  and  $x_g(t_{n+1})$  are given by:

$$x_g(t_n) = x_g(t_{n-1}) + \dot{x}_g(t_n^-) \Delta t \quad (8.2.111)$$

$$x_g(t_{n+1}) = x_g(t_n) + \dot{x}_g(t_n^+) \Delta t$$

Combining Equations (8.2.110) and (8.2.111),  $x_g(t_{n+1})$  is given by:

$$x_g(t_{n+1}) = 2x_g(t_n) - x_g(t_{n-1}) + \ddot{x}_g(t_n) \Delta t^2 \quad (8.2.112)$$

Equation (8.2.112) can be expanded as follows:

$$x_g(t_{n+1}) = 2x_g(t_n) - x_g(t_{n-1}) + \frac{\Delta t^2}{m} [f_g(t_n) - R_g(t_n)] \quad (8.2.113)$$

where the term  $R_g(t_n)$  may be replaced by Equation (8.2.90) or (8.2.91) according to the type of structure to be studied.

Equation (8.2.113) is the basic recurrence formula for the impulse acceleration method which does not require a trial and error procedure. As will be shown by an example for relatively simple systems, this simple method provides good accuracy.

Computation of the Maximum Response from a Design Chart.

Single-Degree-of-Freedom System

In Reference 8.2.11 a design chart (Figure 8.2.63) has been developed for rapid computation of the maximum response of an elasto-plastic spring-mass system subjected to a triangular blast load. The symbols used in this chart are the following:

- $p_{50}$  = peak pressure
- $\sigma_y$  = yield resistance pressure = maximum resistance divided by the loading area
- $x_y$  = yield deflection
- $T$  = load duration (=  $t_{pe}$  or  $t_{qe}$ )
- $f$  = natural frequency of vibration
- $x_{max}$  = maximum displacement reached by the mass at time  $t_{max}$ .

Knowing these values, the use of Figure 8.2.63 is very simple and is self-explanatory. However, it must be noticed that this chart gives values of  $x_{max}/x_y$  greater than 1.0. Thus, it is good for predicting maximum response in the plastic range or for checking that the maximum displacement falls in the elastic or in the plastic range. This can be useful in many design cases because, in general, structures located near rocket test facilities are designed to avoid permanent deformation under blast loads.

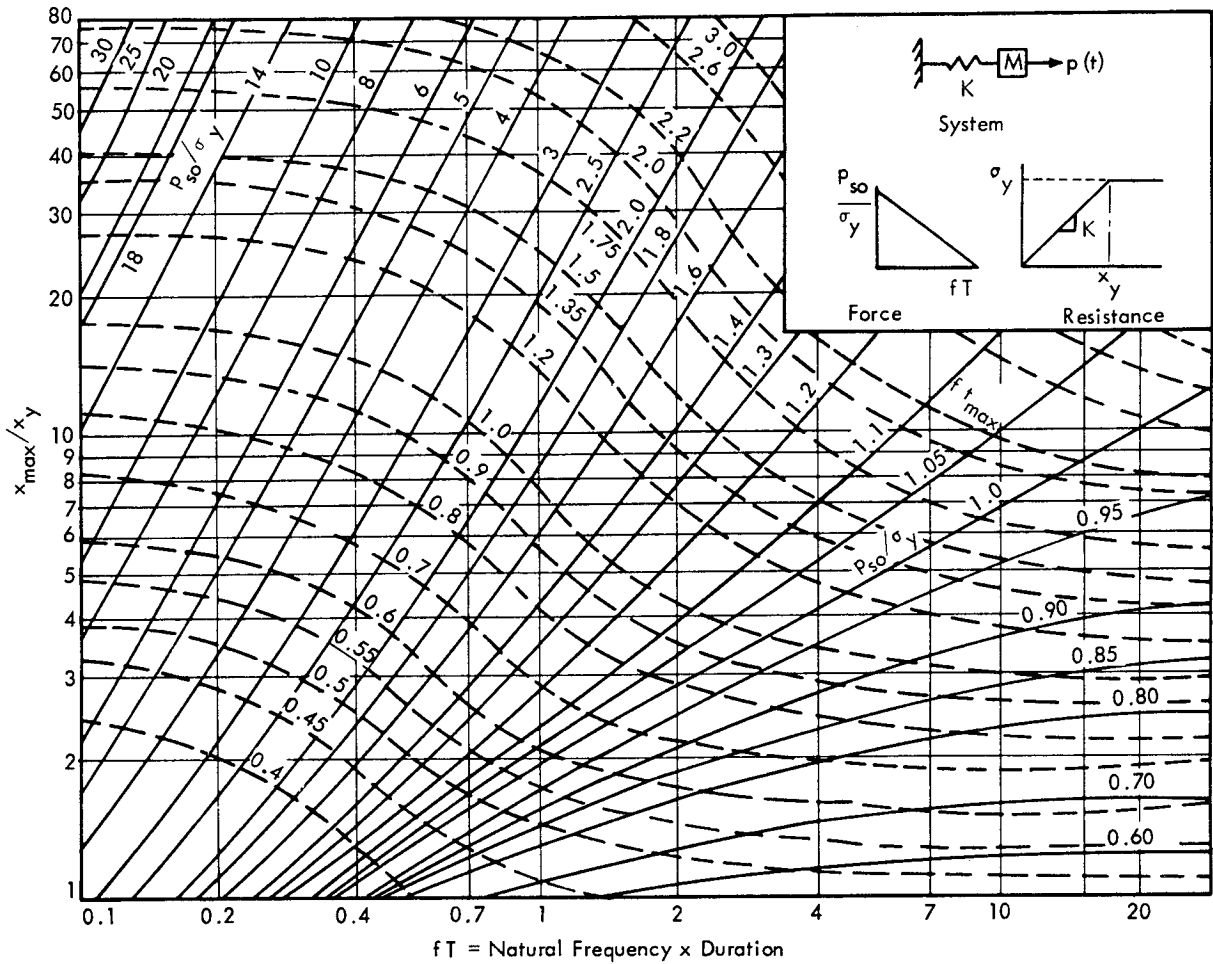


FIGURE 8.2.63 Maximum Response of Simple Spring-Mass System to Initially Peaked Triangular Force Pulse (Reference 8.2.11)

Multi-Degree-of-Freedom Systems

To predict the maximum displacement of each mass of a multi-degree-of-freedom system, Figure 8.2.63 can be used with the following modified notations:

$\sigma_{iy}$  = yield strength factor of the  $i$ -th mass given by maximum resistance  $R_{mi}$  divided by the loading area above the  $i$ -th story.

$\frac{1}{f^i}$  = pseudo period corresponding to a static collapse configuration and obtained as follows:

A uniform lateral static load is placed on the structure such that the weakest story yields, according to its  $\sigma_{iy}$ . Under this load, the relative displacement of each mass is computed with the exception of the "yielded" story. This "yielded" story is displaced, with the static load constant, to a collapse displacement. Then using this resulting configuration, the pseudo period  $1/f^i$  is determined using the following equation:

$$\frac{1}{f^i} = 2\pi \left[ \frac{\sum_{i=1}^{0..n} m_i x_i^2}{\sum_{i=1}^{0..n} K_i y_i^2} \right]^{1/2} \quad (8.2.114)$$

where:

$x_i$  is the absolute displacement resulting from the "collapse configuration" explained above.

$y_i = x_i - x_{i-1}$  is the corresponding relative displacement.

$m_i$  = the  $i$ -th mass.

$K_i$  = the stiffness of the  $i^{\text{th}}$  story

An example in Section 8.2.3 will clarify the computation. This procedure for predicting the response of multi-degree of freedom systems is not as accurate as the other methods

and its reliability is about  $\pm 30\%$  (Reference 8.2.11). For very small relative displacements, the error can reach very high values (up to 100%).

However, this method is very useful to rapidly evaluate the damage pressure level for a given structure and can be used for a rapid verification of the resistance of a designed building.

Note that the intersection of the parameter lines, labeled  $p_{so}/\sigma_y$ , with the abscissa axis ( $x_{max}/x_y = 1$ ), defines the peak value of the triangular load which will just cause a maximum deflection equal to the yield deflection. The resulting ratio of  $p_{so}/\sigma_y$  as a function of  $fT$ , corresponds to the shock spectrum defined in Chapter 3 for the elastic response of a single degree of freedom system to a triangular pulse.

### 8.2.3. NUMERICAL EXAMPLE

The procedures for predicting the dynamic response of structures are applied in this section to the building shown in Figure 8.2.64. This numerical example, besides clarifying the theory, will evaluate the approximations in the simplified analysis methods.

**Given:** The frame building of Figure 8.2.64 is located at a distance of 5800 feet from  $5 \times 10^6$  lb TNT Equivalent Rocket Explosion. Assume the building has no openings and the external walls are made of bricks.

**Find:** The response of the building to the blast wave in terms of the time variation of the displacement of the tops of the three stories.

**Solution:** Calculations made in Section 6.2.6 furnish the time variations of overpressure and dynamic pressure which are illustrated in Figure 6.44. Since the building is without openings, the dynamic pressure can be neglected. To be conservative, assume the time variation of overpressure be represented by the upper curve having a peak value,  $p_{so}$ , of 1.6 psi and a positive phase duration,  $t_p^+$ , of 0.865 sec.

As  $p_{so}$  is smaller than 10 psi, Equation 8.2.15 can be used to express the time variation of overpressure,  $p_s(t)$ , that is:

$$p_s(t) = 1.6 \left( 1 - \frac{t}{0.865} \right) e^{-t/0.865} \quad (8.2.115)$$

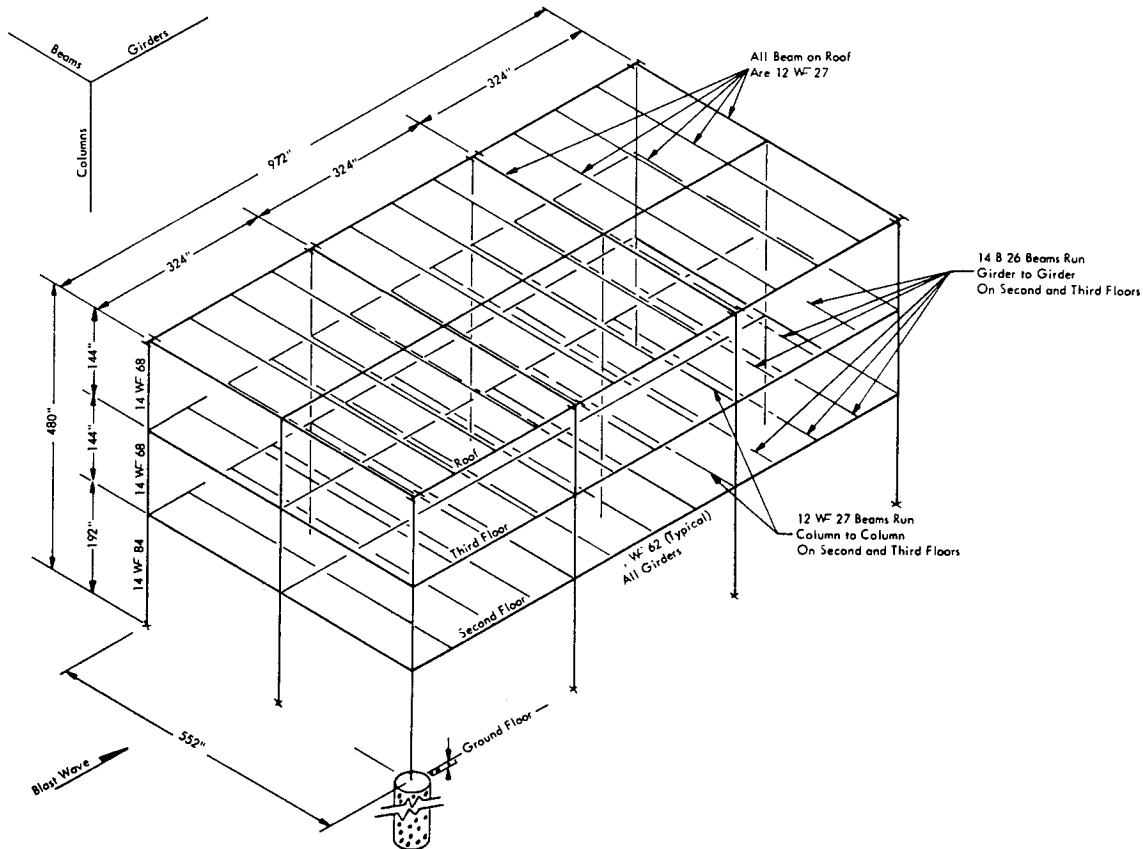


FIGURE 8.2.64 Frame Three-Story Building Used for Numerical Example

The reflected peak pressure is given by (Equation 8.2.3)

$$P_{refl.} = 2 \times 1.6 \left[ \frac{7 \times 14.7 + 4 \times 1.6}{7 \times 14.7 + 1.6} \right] = 3.14 \text{ psi}$$

The velocity of sound,  $c_{refl.}$ , is found (from Figure 8.2.6 or Equation 8.2.5) to be

$$c_{refl.} = 1130 \text{ Hz}$$

Therefore, the value of the clearing time,  $t_c$ , is (Equation 8.2.4)

$$t_c = \frac{3 \times 40}{1130} = .106 \text{ sec.}$$

The value of shock velocity,  $U_o$ , is (Equation 8.2.9 or Figure 8.2.7)

$$U_o = 1150 \text{ Hz}$$

The displacement factor,  $t_d$ , is given by (Equation 8.2.8)

$$t_d = \frac{81}{1150} = .054 \text{ sec.}$$

The time required by the pressure to build up on the back wall is given by (Equation 8.2.10)

$$t_b = \frac{4 \times 40}{1115} = .139 \text{ sec.}$$

The peak value of the average overpressure on the back wall is given by (Equation 8.2.11).

$$P_{bx} = \frac{P_{sb}}{2} \left( 1 + (1 - \beta) e^{-\beta} \right) = .915$$

where  $P_{sb}$  and  $\beta$  are obtained from (Equation 8.2.12) as

$$P_{sb} = 1.6 \left( 1 - \frac{.193}{0.865} \right) e^{-\frac{.193}{0.865}} = 1.02 \text{ psi}$$

$$\beta = \frac{.5 \times 1.6}{14.7} = .055$$

The time variation of the back wall overpressure is given by (Equation 8.2.13) (for  $t > t_d + t_b = .193 \text{ sec.}$ )

$$\bar{P}_{back}(t) = P_s(t) \left[ .9 + .172 (t - .193)^2 \right] \quad (8.2.116)$$

The net pressure acting on the building is

$$p(t) = \bar{P}_{front}(t) - \bar{P}_{back}(t) \quad (8.2.117)$$

( $\bar{P}_{front}(t)$  can be calculated by using Equation 8.2.6)

and the net total loads are given by:

$$\begin{aligned} L'_{T1} &= S'_1 p(t) \\ L'_{T2} &= S'_2 p(t) \\ L'_{T3} &= S'_3 p(t) \end{aligned} \quad (8.2.118)$$

where

$$\begin{aligned} L'_{T1} &= \text{Total load acting on the 1}^{st} \text{ floor} \\ L'_{T2} &= \text{Total load acting on the 2}^{nd} \text{ floor} \\ L'_{T3} &= \text{Total load acting on the 3}^{rd} \text{ floor} \\ S'_1 &= \text{Loaded area of the 1}^{st} \text{ floor} = 105900 \text{ inch}^2 \\ S'_2 &= \text{Loaded area of the 2}^{nd} \text{ floor} = 79480 \text{ inch}^2 \\ S'_3 &= \text{Loaded area of the 3}^{rd} \text{ floor} = 79480 \text{ inch}^2 \end{aligned}$$

The total masses lumped at each floor are:

$$\begin{aligned} m'_1 &= 4640 \text{ lb sec}^2/\text{in} \text{ for the 1st floor} \\ m'_2 &= 3750 \text{ lb sec}^2/\text{in} \text{ for the 2nd floor} \\ m'_3 &= 4160 \text{ lb sec}^2/\text{in} \text{ for the 3rd floor} \end{aligned}$$

The resistance functions, plotted in Figure 8.2.65, are calculated as follows:

1st Floor Consider the column supported as shown in Figure 8.2.6. The maximum bending moment  $M_{max}$  is given by:

$$M_{max} = \frac{QL}{3}$$

The stress due to this moment,  $\sigma$ , is given by

$$\sigma = \frac{Q_1 L_1 y}{3 I_1 n} = .041 Q$$

where:

$$\begin{aligned} I_1 &= \text{Area moment of inertia of each column of the first floor} = 928 \text{ in}^4 \\ y &= 7.09 \text{ (see Figure 8.2.65)} \\ L_1 &= \text{Height of the first floor} = 192 \text{ in.} \\ Q_1 &= \text{Loading on the first floor} \\ n &= \text{Number of columns} = 12. \end{aligned}$$

Assuming a yield stress,  $\sigma_y$ , of 3800 psi, the maximum resistance is given by:

$$R_{1m} = \sigma_y Q / \sigma = \frac{38,000}{.041} = 930,000 \text{ lbs}$$



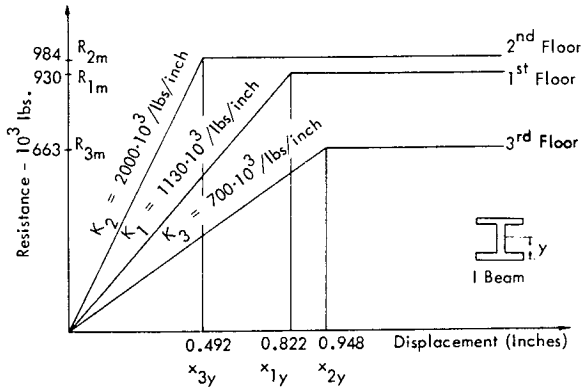


FIGURE 8.2.65 Resistance Functions for a Three Story Frame Building

The corresponding yield displacement is given by:

$$x_{1y} = \frac{R_{1m}}{K_1} = \frac{930,000}{1130 \cdot 10^3} = .822 \text{ in.}$$

where  $K_1'$  is the spring constant given by (Table 8.2.4).

$$K_1' = \frac{24 \times E_1 (I_1 \times 12)}{L_1^3} = \frac{24 \times 30 \times 10^6 \times 928 \times 12}{192^3} = 1130 \cdot 10^3 \frac{\text{lb}}{\text{inch}}$$

The maximum resistance, spring constant and yield displacement of the 2<sup>nd</sup> and 3<sup>rd</sup> floor are the following: (Figure 8.2.65)

$$\begin{aligned} R_{2m} &= 984 \cdot 10^3 \text{ lb} \\ K_2' &= 2000 \cdot 10^3 \text{ lb/in.} \\ x_{2y} &= .948 \text{ in.} \\ R_{3m} &= 663 \cdot 10^3 \text{ lb} \\ K_3' &= 700 \text{ lb/in.} \\ x_{3y} &= .492 \text{ in.} \end{aligned}$$

At this point the building must be replaced with a spring-mass model having the equivalent parameters. These are given by the following values according to Table 8.2.4.

$$\begin{aligned} m_1 &= m_1' K_M = 4640 \times .41 = 1900 \text{ lb sec}^2/\text{in.} \\ m_2 &= m_2' K_M = 3750 \times .41 = 1540 \text{ lb sec}^2/\text{in.} \\ m_3 &= m_3' K_M = 4160 \times .41 = 1710 \text{ lb sec}^2/\text{in.} \\ K_1 &= K_1' K_R = 1130 \cdot 10^3 \times .53 = 600 \cdot 10^3 \text{ lb/in.} \\ K_2 &= K_2' K_R = 2000 \cdot 10^3 \times .53 = 1060 \cdot 10^3 \text{ lb/in.} \\ K_3 &= K_3' K_R = 700 \cdot 10^3 \times .53 = 371 \cdot 10^3 \text{ lb/in.} \end{aligned}$$

Figures 8.2.66 and 8.2.67 illustrate the equivalent loading functions (the negative phase has been neglected) to be applied to the spring-mass model, obtained by multiplying Equation (8.2.118) by the load factor  $K_L$  from Table 8.2.4 as follows:

$$\begin{aligned} L_{T1} &= L_{T1}' K_L = S_1' p(t) K_L = 56170 p(t) \text{ lbs.} \\ L_{T2} &= L_{T2}' K_L = S_2' p(t) K_L = 42120 p(t) \text{ lbs.} \\ L_{T3} &= L_{T3}' K_L = S_3' p(t) K_L = 42120 p(t) \text{ lbs.} \end{aligned}$$

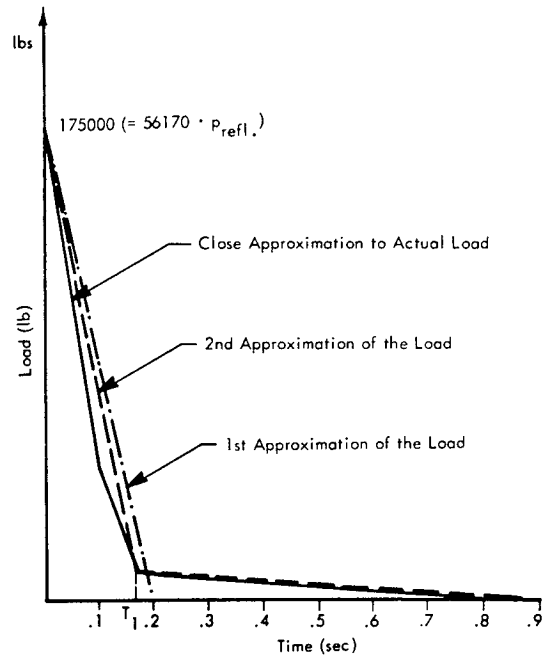


FIGURE 8.2.66 Equivalent Load Versus Time Curve for the First Floor

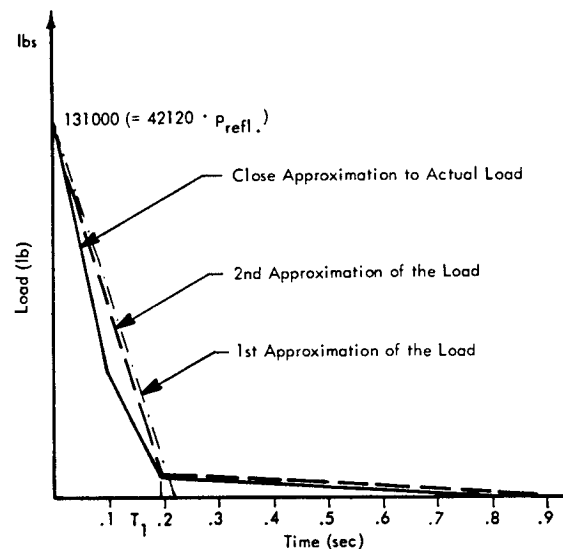


FIGURE 8.2.67 Equivalent Load Versus Time Curve for the Second and Third Floor

Now, the various methods from Section 8.2.2.3 can be used to predict the response.

a) Classical Method.

The equations of motion are:

$$\begin{aligned} m_1 \ddot{x}_1 + (K_1 + K_2)x_1 - K_2 x_2 &= L_{T1} \\ m_2 \ddot{x}_2 + (K_2 + K_3)x_2 - K_2 x_1 - K_3 x_3 &= L_{T2} \\ m_3 \ddot{x}_3 + K_3 x_3 - K_3 x_2 &= L_{T3} \end{aligned} \quad (8.2.119)$$

From Equation (8.2.96), replacing the symbols with their values, the following relationships are obtained:

$$\begin{aligned} 1900 A_1 \omega^2 - 1660 \cdot 10^3 A_1 + 1060 \cdot 10^3 A_2 &= 0 \\ 1540 A_2 \omega^2 - 1431 \cdot 10^3 A_2 + 1060 \cdot 10^3 A_1 \\ &+ 371 \cdot 10^3 A_3 = 0 \\ 1710 A_3 \omega^2 - 371 \cdot 10^3 A_3 + 371 \cdot 10^3 A_2 &= 0 \end{aligned} \quad (8.2.120)$$

Setting the determinant of the coefficients,  $A_1, A_2, A_3$  equal to zero, the following values of  $\omega$  (rad/sec) are found

$$\begin{aligned} \omega_1^2 &= 73.05 & \omega_2^2 &= 382.2 & \omega_3^2 &= 1461.34 \\ \omega_1 &= 8.53 & \omega_2 &= 19.55 & \omega_3 &= 38.3 \end{aligned}$$

Putting these values into Equation (8.2.120), the following table of modal coefficients can be written:

	$\omega_1 = 8.55$	$\omega_2 = 19.55$	$\omega_3 = 38.3$
$A_1$	$A_{11} = .453$	$A_{12} = 1.0$	$A_{13} = .875$
$A_2$	$A_{21} = .65$	$A_{22} = .844$	$A_{23} = -1.0$
$A_3$	$A_{31} = 1.0$	$A_{32} = -.995$	$A_{33} = .166$

From Equation (8.2.98), the generalized masses can be evaluated as follows:

$$\begin{aligned} M_1 &= 1900 (.453)^2 + 1540 (.65)^2 + 1710 (1.0)^2 \\ &= 2711 \text{ lb sec}^2/\text{in.} \\ M_2 &= 1900 (1.0)^2 + 1540 (.844)^2 + 1710 (-.995)^2 \\ &= 4669 \text{ lb sec}^2/\text{in.} \\ M_3 &= 1900 (.875)^2 + 1540 (-1.0)^2 + 1710 (.166)^2 \\ &= 3043 \text{ lb sec}^2/\text{in.} \end{aligned}$$

From Equation (8.2.99) the generalized force for each mode can be found.

$$\begin{aligned} F_1(t) &= .453 L_{T1} + .65 L_{T2} + L_{T3} \\ F_2(t) &= L_{T1} + .844 L_{T2} - .995 L_{T3} \\ F_3(t) &= .875 L_{T1} - L_{T2} + .166 L_{T3} \end{aligned}$$

For the triangular load (dash-dot line of Figures 8.2.66 and 8.2.67), which has the same impulse as the exact load

$$\begin{aligned} \text{for } 0 < t < .2, & \quad L_{T1} = 175,000 - 875,000 t \\ \text{for } t > .2, & \quad L_{T1} = 0 \\ \text{for } 0 < t < .2, & \quad L_{T2} = L_{T3} = 131,000 - 655,000 t \\ \text{for } t > .2, & \quad L_{T2} = L_{T3} = 0 \end{aligned}$$

Now, using Equations, 8.2.101, 8.2.102 and 8.2.103, the displacements  $x_1, x_2, x_3$  of the three masses, that is of the three stories of the building, can be computed. These values have been plotted vs time in Figures 8.2.57-58-59 (dash-dot curve). The same values have been tabulated in Table 8.2.6 along with the relative displacements which must be known for design purposes.

Response of the building was also computed based on a bilinear model of the blast load. The results, plotted as dashed lines in Figures 8.2.57-58-59, show that the different shape of the bilinear load has only a small effect on the response.

The values of  $x_1, x_2, x_3, x_2 - x_1$  and  $x_3 - x_2$  calculated for this kind of load are also tabulated on Table 8.2.6.

b)  $\beta$  - Method

Equations 8.2.107, 8.2.108 and 8.2.91 can be used to calculate the value of  $x_1, x_2,$  and  $x_3$ .

To avoid stability problems, values of  $\beta = 1/4$  and  $\Delta t = .005$  seconds were used.

The results obtained by applying this method to the three story frame building (Figure 8.2.64) subject to a triangular load are also tabulated on Table 8.2.6. The calculations have been made by means of a high speed Digital Computer requiring 0.5 hours of machine time.

c) Impulse Acceleration Extrapolation Method

Equations 8.2.113 and 8.2.91 must be used. The results obtained by applying this method to the example of this section, have been tabulated on Table 8.2.6.

These calculations were also made on the same high speed Digital Computer and required 0.12 hours of machine time.

Some useful conclusions can be drawn from the example made in this section using various methods and approximations.

As indicated earlier, a triangular load can be used to simulate a blast load on a conventional building structure.

Furthermore, the impulse acceleration extrapolation method is recommended to analyze the response to this load. This method avoids long calculations and gave sufficiently accurate results for the example selected. This can be seen by comparing results tabulated in Table 8.2.6 and by examination of Figure 8.2.57 - 58 - 59 where the dotted curves illustrate the results obtained using this simple method.

Rapid Verification of Critical Blast Loads for the Three Story Building

Given: The building of Figure 8.2.64 and the triangular loads of Figures 8.2.66 and 8.2.67.

Find: Damage pressure level to avoid plastic deformations.

First of all, the building must be replaced with a spring-mass system as shown in the previous example. The yield shear strengths are:

$$\sigma_{1y} = \frac{R_{m1}}{S_1 + S_2 + S_3} = \frac{930,000 \times .53}{140,410} = 3.4 \text{ psi}$$

$$\sigma_{2y} = \frac{R_{m2}}{S_2 + S_3} = \frac{984,000 \times .53}{84,240} = 6.1 \text{ psi}$$

$$\sigma_{3y} = \frac{R_{m3}}{S_3} = \frac{66,300 \times .53}{42,120} = 8.3 \text{ psi}$$

The static displacement produced by a uniform load of 3.4 psi is as shown in Figure 8.2.68.

The pseudo period corresponding to this configuration is Equation (8.2.114).

$$\frac{1}{f'} = 2\pi \left[ \frac{1900(.822)^2 + 1540(1.107)^2 + 1710(1.514)^2}{.53 [1130(.822)^2 + 2000(.285)^2 + 700(.407)^2]} \right]^{\frac{1}{2}}$$

$$= .825$$

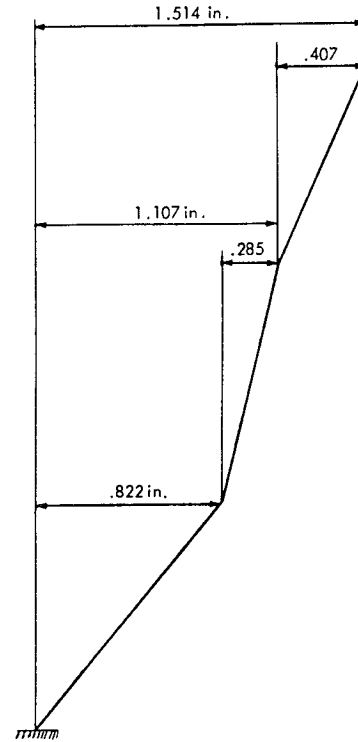


FIGURE 8.2.68 Displacement Produced by a Uniform Load of 3.4 psi

Therefore, the ratio of load duration to pseudo period is

$$f' T = \frac{.865}{.825} = 1.04$$

From Figure 8.2.63, it can be seen that this corresponds to a value of  $p_{so}/\sigma_y = 0.6$  for a response within the limit ( $x_{max}/x_y = 1$ ).

For the weakest story,  $\sigma_y$  is given by (Figure 8.2.65).

$$\sigma_y = \frac{930,000 \times .53}{56,170} = 8.75 \text{ psi}$$

Therefore, the damage pressure level is given by

$$p_{so} = \sigma_y \times .60 = 5.2 \text{ psi}$$

TABLE 8.2.6  
ABSOLUTE AND RELATIVE DISPLACEMENTS PREDICTED BY MEANS OF VARIOUS METHODS

Time Sec.	Analysis Method	$x_1$	$x_2$	$x_3$	$x_2 - x_1$	$x_3 - x_2$
.1	1	.300	.346	.330	.046	-.016
	2	.309	.357	.340	.068	-.012
	3	.295	.344	.330	.049	-.014
	4	.295	.345	.330	.05	-.015
.2	1	.531	.736	1.024	.205	.288
	2	.589	.809	1.104	.220	.295
	3	.529	.732	1.020	.203	.288
	4	.530	.732	1.022	.202	.290
.3	1	.370	.607	1.177	.237	.570
	2	.470	.748	1.379	.278	.631
	3	.373	.605	1.172	.232	.567
	4	.272	.605	1.172	.233	.567
.4	1	.194	.238	.301	.044	.063
	2	.283	.372	.529	.089	.147
	3	.188	.235	.297	.047	.062
	4	.189	.234	.295	.045	.061
Maximum Value	1	.532 (.205)*	.740 (.210)*	1.247 (.265)*	.238 (.290)*	.581 (.285)*
	2	.597 (.220)*	.832 (.230)*	1.417 (.275)*	.278 (.300)*	.635 (.290)*
	3	.529 (.205)*	.738 (.215)*	1.241 (.265)*	.234 (.285)*	.578 (.290)*
	4	.530 (.200)*	.737 (.215)*	1.241 (.265)*	.235 (.290)*	.578 (.280)*

- 1 Triangular load, classical method  
 2 Bi-linear load, classical method  
 3 Triangular load,  $\beta$ -Method  
 4 Triangular load, impulse acceleration method  
 \* Time of occurrence (sec.)

### 8.3 RESPONSE OF GROUND STRUCTURE TO SONIC BOOM LOADS

Aircraft traveling at supersonic speeds generate an overpressure wave called a sonic boom. It propagates away from the aircraft at sonic velocity and, upon reaching the ground, results in an N shaped transient pressure load on ground structures. Section 1.3 of Chapter 1 gives a detailed outline of the general characteristics of this sonic source of dynamic loading. The dynamic load imposed on buildings by this overpressure wave is illustrated in Figure 8.3.1. The incident overpressure wave will be modified by diffraction effects in the same manner as for the loads developed by blast waves. Thus, the methods outlined in the preceding section of this chapter could be applied if it were necessary to make a detailed investigation of the dynamic loading on a building. Such an approach has been reported in Reference 8.3.2, and includes both the positive and negative phases of the transient load. This complex loading will consist, initially, of a pressure loading on the wall facing the shock wave, and will have an initial value of approximately twice the free-field overpressure. Then the entire building will be loaded, first by a positive pressure, then by a negative pressure. Finally, a negative pressure load will appear on the back wall of the building.

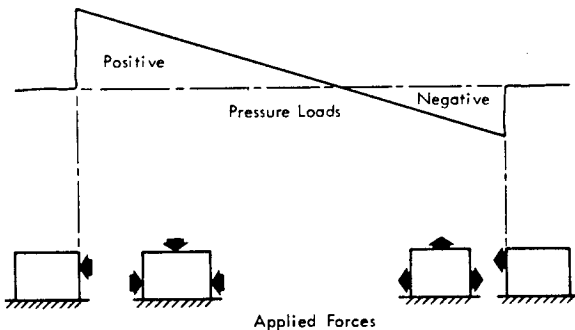


FIGURE 8.3.1 Basic Characteristics of Load Imposed on Buildings by a Sonic Boom (from Reference 8.3.1)

The sonic boom load on ground structures differs from blast overpressure loads in three important aspects

- The sonic boom wave travels along the ground with an approximately constant intensity, covering a path, as wide as 10 to 40 miles. (See Figure 6.48, page 6-40.) This contrasts with the relatively rapid reduction in overpressure as a function of distance from a fixed explosion source.
- The maximum overpressure in a sonic boom wave can be controlled, within a factor of approximately 2, by imposing specific operational procedures for flight speed and altitude on the aircraft. For example, proposed regulations to be placed on the SST commercial jet transport would limit sonic boom overpressures to a nominal value of  $2.5 \text{ lb/ft}^2$  during transition to cruise conditions. (Reference 8.3.3).

- For the same positive phase duration and peak overpressure, in an ideal sonic boom or blast wave striking a wall face on, the maximum dynamic displacement of the structure in any single mode will be greater for the sonic boom N-wave than for the blast wave. This is illustrated in Figure 8.3.2 by the displacement shock spectrum for the N-wave and a triangular pulse simulating the blast waves. (The effects of reflected overpressure are assumed to be the same in each case.) The displacement shock spectrum represents the peak dynamic response of a single mode relative to its static displacement for the same peak overpressure. This relative response varies with the product of the natural frequency of the mode  $f_n$  and the duration  $T$  of the positive phase.

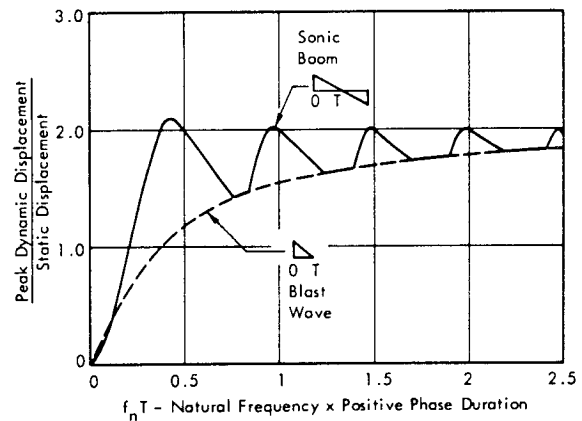


FIGURE 8.3.2 Displacement Shock Spectrum for Sonic Boom N-Wave and Triangular Blast Wave (See Figures 3.10 and 3.34 in Chapter 3)

#### 8.3.1 TYPE OF BUILDING DAMAGE CAUSED BY SONIC BOOMS

The sonic boom exposure from normal operations of supersonic aircraft must necessarily be controlled in order to prevent widespread building damage.

##### 8.3.1.1 Primary Structure for Industrial Buildings

It will not be necessary to consider a sonic boom as a source of significant design loads on primary load-carrying members of industrial-type structures. In one reported case, for example, an accidental exposure of an aircraft terminal building to a high intensity sonic boom from a close fly-by of a fighter aircraft did not cause any measurable permanent damage to the primary structure of the building. (Reference 8.3.4.) However, very extensive damage resulting in repair costs of about \$3,00,000 was incurred on the secondary structure. This secondary type of damage included:

- Shattering of all glass panes facing the on-coming aircraft.
- Dislodging of curtain wall panels and distortion of attachment brackets.

- Dislodging of various components of the built-up roofing.
- Permanent distortion of doorways and transoms.
- Extensive cracking and dislodging of sections of plaster in external soffits.
- Permanent distortion of aluminum grid-work in a large part of the conventional suspended-ceiling system.

This extreme example illustrates the principal concern for sonic boom loads on buildings - the potential damage to structural elements, particularly those of a brittle nature. Normally this type of damage is more likely to occur in residential structure. The conclusions developed in the following sections relative to residential structure will apply, in general, to industrial type structure. One exception occurs for acceleration loads imposed on roof-mounted equipment in industrial buildings with large flat roof structure. This problem is treated in Section 11.7.5, page 11-28.

8.3.1.2 Residential Structure

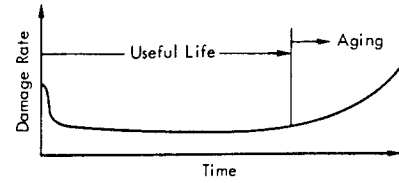
Because of the less stringent design requirements for lateral loads on residential walls, and the corresponding methods of construction, this type of structure is more susceptible to damage from sonic booms. However, minimum wind load design requirements generally exceed 10 lb/ft<sup>2</sup>, corresponding to a nominal 55 mile per hour wind. (Reference 8.3.5.) Thus, except for uncontrolled exposure to a sonic boom, major sonic boom damage to a residential building in good repair, is not expected.

However, the type of wood frame construction which is so widely used for residences is susceptible to deterioration over a long period of time due to:

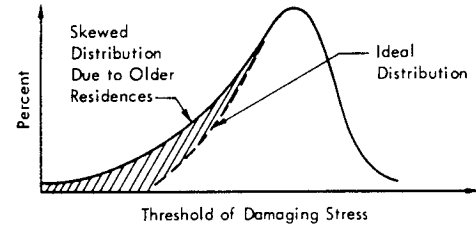
- Foundation setting
- Swelling or warping due to humidity changes
- Frame distortion due to changing temperature.

Thus, as suggested in Figure 8.3.3, there will be a certain percentage of residences in such a condition that any significant, dynamic load (even a thunderclap) would be sufficient to cause at least minor damage. Such structure would, therefore, be subject to damage by sonic booms of almost any measurable intensity. However, this type of damage is generally uncontrollable and, as suggested, inevitable.

The most common type of damage claimed to be caused by sonic booms is shown by the data in Figure 8.3.4 based on experience by the U.S. Air Force. (Reference 8.3.1). The ability to validate such damage claims, however, is severely limited without more basic and objective information on dynamic response characteristics of buildings to sonic booms.



(a) Hypothetical Increased Damage Rate of Residences Due to Aging



(b) Hypothetical Distribution, Due to Aging, of Threshold Levels for Damaging Stress

FIGURE 8.3.3 Illustration of Susceptibility of Older Residential Structure to Damage by Any Significant Stress

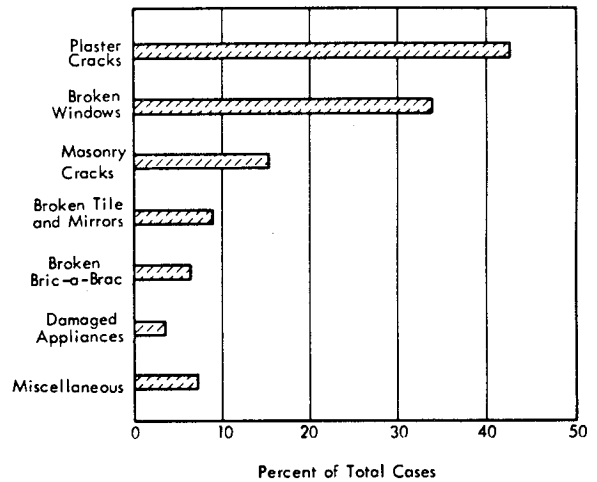


FIGURE 8.3.4 Classification of about 3000 complaints Due to Sonic Booms as Recorded in Air Force Files. (The damage reported in the complaints was not necessarily validated). (Data from Reference 8.3.1)

8.3.2 CORRELATION OF MEASURED AND PREDICTED DYNAMIC STRESSES IN RESIDENTIAL STRUCTURE

Results from measurements of structural response to normal sonic booms have been reported in References 8.3.1 and 8.3.7. These included stress measurements in residential frame structures exposed to sonic boom overpressures (from about 0.7 to about 4.8 lb/sq.ft) generated by a supersonic aircraft. The duration T of the N-wave for these tests ranged from about 0.06 to 0.10 seconds.

Typical strain time-histories measured at various locations on a wood-frame structure, as reported in Reference 8.3.1, are illustrated in Figure 8.3.5. The strain measurements rafter and vertical stud, indicated in the figure have the approximate appearance of a single-degree-of-freedom system response to excitation by a transient N-wave. Additional complexity in the time history is due to response in higher modes.

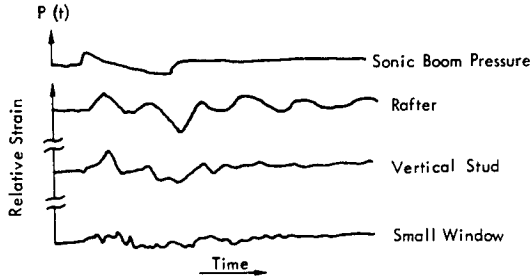


FIGURE 8.3.5 Typical Strain Time-Histories Measured in Residential Structure Exposed to a Sonic Boom from a Bomber Aircraft. ( $T \approx 0.1$  second). (Data from Reference 8.3.1)

The multi-modal response is even more apparent for the strain record measured on a small window. A thorough analytical study of the multi-modal response of panels to a sonic boom N-wave has been reported in Reference 8.3.8.

8.3.2.1 Correlation of Measured Strain With Theoretical Shock Spectrum

Assuming a single degree-of-freedom model can be applied, the following method is used to provide a rough estimate of the peak dynamic strain in structures exposed to sonic booms. The method is based on the peak dynamic response of a single degree-of-freedom system to a transient N-wave.

- As shown in Table 12.15, Chapter 12, the ultimate static load for failure of a typical wood frame wall is about 1.5 psi. Identify this failure as  $P_{sc}$ .
- From this same table, two additional parameters are obtained for typical wood framing materials:
  - Fiber strength in Bending,  $\sigma_u \approx 6000$  psi
  - Youngs Modulus (minimum)  $E = 1.2 \times 10^6$  psi
- Assume a stress concentration factor  $F_c$  of 2 for static failure of such a wall by a uniform lateral load.
- Assume the strain  $\epsilon_{sc}$  for ultimate static failure, is given by

$$\epsilon_{sc} = \frac{\sigma_u}{F_c E} = C p_{sc} \tag{8.3.1}$$

where  $C =$  the proportionality constant relating strain to pressure load.

$$= \frac{\sigma_u}{F_c E p_{sc}} = \frac{6000}{(2)(1.2 \times 10^6)(1.5)}$$

$$= 0.0017/\text{psi}$$

- Thus for a transient N-wave load with a peak side on pressure (including reflection)  $p_o$ , assume the peak dynamic stress  $\sigma_{max}$  is given by (neglecting Poisson coupling effects)

$$\sigma_{max} \approx S(f_1 t) \cdot C E p_o \tag{8.3.2}$$

where  $S(f_1 t) =$  the displacement shock spectrum for the N-wave illustrated in Figure 8.3.2. This defines the peak dynamic response for a single degree-of-freedom system relative to its static response for the same peak pressure  $p_o$  (See Figure 8.3.2)

- Thus, the ratio of peak stress  $\sigma_{max}$  to peak pressure  $p_o$  in the reflected N-wave is estimated to be

$$\frac{\sigma_{max}}{p_o} \approx S(f_1 T) C E =$$

$$\approx 2 \times 10^3 \cdot S(f_1 T) \tag{8.3.3}$$

The measured peak strain data reported in Reference 8.3.7 were converted to a peak stress by multiplying by an  $E$  of  $1.2 \times 10^6$  psi. The resulting values are shown in Figure 8.3.6 by the non-dimensional ratio  $\sigma_{max}/p_o$  as a function of the product  $f_1 T$ . The predicted value for  $\sigma_{max}/p_o$ , based on equation 8.3.3, is also shown in this figure and forms an approximate upper bound for the measured data. Thus, this semi empirical method appears to offer a reasonable basis for initial estimates of the maximum peak stress in residential structure for sonic boom loads. The proportionality constant  $C$  can be estimated from equation 8.3.1 for other types of wall or roof structure using appropriate values for the ultimate failure load  $p_{sc}$ , maximum bending stress  $\sigma_{sf}$ , modulus of elasticity  $E$ , and stress concentration factor  $F_c$ . Values for the first three parameters are given for a wide variety of building wall configurations in Table 12.13, Chapter 12.

For typical wood frame structure, the maximum dynamic stress for sonic boom loads is estimated from equation 8.3.3 as follows:

For  $C \approx 2000/\text{psi}$

and  $S(f_1 T)_{max} \approx 2$  for  $(f_1 T) > 0.4$

$$\text{then } \sigma_{\max} \approx 4000 p_o - \text{psi} \quad (8.3.4)$$

for  $p_o$  in units of  $\text{lb/ft}^2$ , this is

$$\sigma_{\max} = 28 p_o (\text{lb/ft}^2) - \text{psi} \quad (8.3.5)$$

It must be recognized that this can only be considered a rough estimate of the upper bound for bending stresses in the structural frame. Nevertheless, this estimated maximum value indicates that the stresses induced by controlled sonic boom loads will be well below normal live-load design stresses of approximately 1000 psi for framing members. It will be shown later that light damage can occur to ceiling and wall panels for sonic booms only slightly higher than the expected maximum operational limits for an SST aircraft.

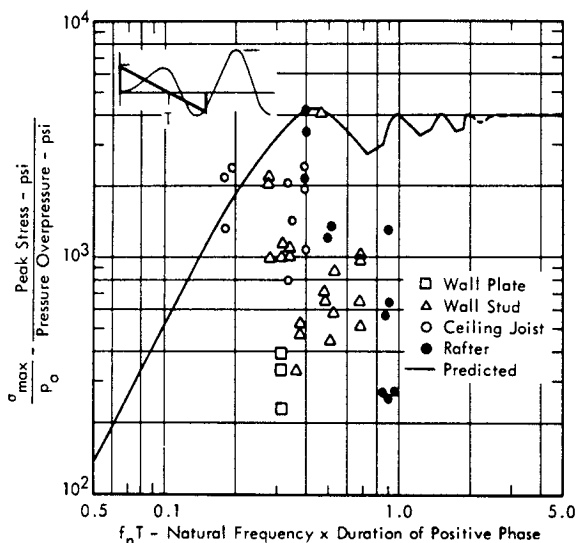


FIGURE 8.3.6 Correlation of Measured and Predicted Value for Stress Observed in Residential Structure When Exposed to a Sonic Boom N-Wave (Data from References 8.3.1 and 8.3.7)

### 8.3.2.2 Correlation of Measured Strain and Pseudo-Velocity

As shown earlier in this Chapter and in Section 3.3.6.6 of Chapter 3, the peak modal strain in a structure vibrating harmonically with a sinusoidal-like mode shape is

$$\epsilon_{n(\max)} = K_s \frac{\bar{a}_n}{c_L} \quad (8.3.6)$$

- where
- $\bar{a}_n$  = modal velocity amplitude
  - $K_s$  = shape factor varying from 1.2 to 1.8 for plates
  - $c_L$  = longitudinal wave velocity.

This expression might also be used to provide a rough estimate of the peak dynamic stress for a transient load in terms of a pseudo-velocity  $\bar{a}_n(\max)/2\pi f_n$  where  $\bar{a}_n(\max)$  = peak transient acceleration amplitude of the rig mode with a natural frequency  $f_n$ . This is not an exact expression for velocity since the motion is not a steady state harmonic motion, hence the term pseudo-velocity. Experimental data were available from Reference 8.3.7 to check this hypothesis. Values of peaks from strain and peak acceleration increased at five locations in a residential structure under a sonic boom load are shown in Figure 8.3.7. For a typical value of  $c_L$  in wood of  $1.5 \times 10^5$  in/sec, the proportionality constant  $K_s$  relating strain and pseudo-velocity varied from 0.55 to 0.88, which is approximately 1/2 the theoretical value for sinusoidal vibration of a plate (see Section 3.3.6.6.) Considering the many simplifying assumptions made in this case, this order of agreement is reasonable. Without additional supporting data, the results shown in Figure 8.3.7 are considered as indicating only approximate trends in the relationship between peak stress and pseudo-velocity of structure.

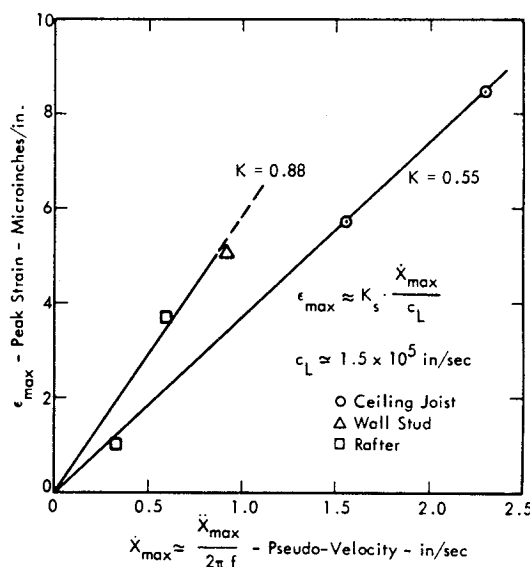


FIGURE 8.3.7 Correlation of Maximum Strain and Pseudo-Velocity Measured for Three Sonic Boom Tests at Five Locations on a Residential Structure (Data from Reference 8.3.7)

### 8.3.2.3 Correlation of Predicted and Observed Damage In Residential Structure For Sonic Boom Loads

Test data are reported in Reference 8.3.9 on light damage thresholds for sonic boom overpressures for residential structure. These are summarized in Table 8.3.1. The tests were conducted with a supersonic bomber aircraft generating sonic boom pressures up to  $30 \text{ lb/ft}^2$  with a typical positive phase duration  $T$  of about 0.16 seconds.



TABLE 8.3.1

THRESHOLD LEVELS OF SONIC BOOM OVERPRESSURES FOR MINOR DAMAGE TO RESIDENTIAL STRUCTURAL WALLS AND CEILINGS (1)

Type of Damage	Overpressure lb/ft <sup>2</sup>
Cracks in Plaster on Wood Lathe (Poor Quality Construction)	6.5 - 10
Nail Popping - 1/2 inch Gypsumboard	10.3
Paint Flecks on Old Gypsumboard	9.0
Falling Bric-a-Brac and Rattling Dishes	6 - 11

(1) Data from Reference 8.3.9

Sonic Boom Positive Phase Duration

Based on typical frequencies for residential walls and ceilings of 8 to 15 Hz (Reference 8.3.1), the characteristic parameter  $fT$  would range from about 1.3 to 2.4, well above a  $n$  value of 0.4. Thus, a dynamic response factor  $[S(f_n T)]$  of 1.5 to 2 times the static response is expected. Assuming a minimum reflected pressure of 6.5 lb/ft<sup>2</sup> (i.e., grazing incidence across a roof), applying Equation 8.3.5, an estimated peak stress  $\sigma_{max}$  in the wood frame structure would be

$$\sigma_{max} \approx (28)(6.5) = 180 \text{ psi}$$

For a modulus of elasticity of  $1.2 \times 10^6$  psi, this would correspond to a strain on the frame members of

$$\epsilon_{max} \approx \sigma_{max} / E = 150 \times 10^{-6} \text{ in/in}$$

Data are available on static failure stress in gypsum plasters and cement mortars from a series of carefully controlled tests on laboratory samples, as reported in Reference 8.3.10. These data are summarized in Table 8.3.2. Assuming the same magnitude of strain estimated above is applicable to the cement or mortar in plaster or gypsum board, the estimated peak stresses would be given by  $\sigma_{max} \approx \epsilon_{max} (E_{plaster})$ . In this way, the following values of stress are estimated.

- For ordinary Portland Cement Mortar -  $\sigma_{max} = 740$  psi
- For early high strength Portland Cement Mortar -  $\sigma_{max} \approx 810$  psi
- For Ultracal 60 gypsum plaster -  $\sigma_{max} \approx 290$  psi
- For Hydrostone gypsum plaster -  $\sigma_{max} = 360$  psi

TABLE 8.3.2

STATIC AND DYNAMIC PROPERTIES OF GYPSUM PLASTERS AND CEMENT MORTARS. (1)

Material	Density lb/in <sup>3</sup>	Modulus of Elasticity (2) 10 <sup>-6</sup> lb/in <sup>2</sup>	Static Tensile Strength (3) lb/in <sup>2</sup>
Ordinary Portland Cement Mortar	0.0813	4.93	546
High Early Strength Portland Cement Mortar	0.0830	5.41	654
Ultracal 60 Gypsum Plaster	0.0570	1.90	602
Hydrostone Gypsum Plaster	0.0609	2.40	981

(1) Data from Reference 8.3.10

(2) Calculated from dynamic tests of pulses transmitted through Bar of Material,  $E = \rho c_L^2$

(3) Based on 42 to 60 test specimens per material. Deviation of results was 18.5 - 23% of mean values. Dynamic strength for a load duration of 0.2 milliseconds was approximately the same as static strength for Portland Cement mortars and 63 to 70% greater than the static value for Ultracal and Hydrostone.

Comparing these numbers with the measured static failure stresses noted in the last column of Table 8.3.2, it appears that failure would be expected in 2 out of the 4 materials. At best, these order of magnitude results indicate that estimated values for a predicted damage stress for plaster and gypsum board fall in a range where the type of damage noted in Table 8.3.1 is feasible. The actual failure stress for such materials, in-place, is known to vary widely due to a large number of factors involving construction methods, states of repair, temperature, humidity, etc. (Reference 8.3.1.)

To conclude this section on wall damage by sonic booms,

- Available experimental data on dynamic stresses are roughly predictable by simple theory
- The combined experimental evidence and theoretical predictions indicate that for houses in good construction, sonic boom overpressures within the proposed limit, would not cause dynamic stresses in excess of failure stresses for residential wall and ceiling materials
- A certain percentage of homes of low quality construction or in disrepair may be expected to suffer noticeable damage from any significant sonic boom exposure.

### 8.3.3 WINDOW DAMAGE BY SONIC BOOMS

The failure of windows by a sonic boom represents the most critical form of probable damage due to the danger of secondary injury effects by falling glass. (See Section 10.6.3, page 10-20 for a discussion of injury criteria for glass missiles. The principal results from these studies are briefly summarized in this section.

#### 8.3.3.1 Static Failure Strength of Glass Windows

Glass is classified as a brittle material with a yield strength very nearly equal to its ultimate strength. The term, breaking strength, is commonly used to identify the failure stress on glass. This breaking strength varies over a range of about 3000 to 30,000 psi depending on the type of glass, age surface condition, and load duration. Typical values are listed in Table 8.3.3 for large panes with normal surface quality for several types of loads.

TABLE 8.3.3

TYPICAL BREAKING STRENGTH OF LARGE PANES OF GLASS WITH NORMAL (AS GLAZED) SURFACE QUALITY AS A FUNCTION OF THE TYPE OF LOADING. ( $10^3$  PSI)

Type of Loading	Load Duration	Regular		Heat Strengthened	Fully Tempered
		Plate	Window		
Sonic Boom	~0.1 sec	6.0	6.6	15.0	30.0
Wind Gusts	5-10secs	5.5	6.05	13.75	27.5
Fastest Mile Wind (1)	1 min	4	4.4	10	20
Long Term	2 hrs-Indef.	3	3.3	7.5	15

- 1) Fastest mile wind is average wind velocity over 1 minute period.
- 2) Data from Reference 8.3.5

The important point brought out by this table is that glass will tend to break at a lower stress for longer duration loads with the same intensity. The net result is that "fastest mile" wind loads (i.e. - the steady dynamic pressure for the average wind velocity over a 1 minute period) will generally represent the design load condition for large windows. Minimum design wind loads normally exceed  $10 \text{ lb/ft}^2$ . Assuming a maximum probable sonic overpressure of  $5 \text{ lb/ft}^2$  and a 2 to 1 dynamic magnification factor, an approximate upper bound for the equivalent static load would be  $10 \text{ lb/ft}^2$ . However, according to Table 8.3.3 the breaking strength of glass for this type of load will normally exceed that for a  $10 \text{ lb/ft}^2$  wind load.

Under laboratory conditions, the breaking strength of the same type of glass having the same surface quality will vary in the manner shown in Figure 8.3.8. The actual breaking strength for window panes, as installed, will be

lower than indicated by Figure 8.3.8 due to effects of superimposed in-plane loads or stress concentrations around surface defects. In fact, the location, number, and nature of surface defects is generally the controlling factor which, limits the breaking strength of windows. (Reference 8.3.5.)

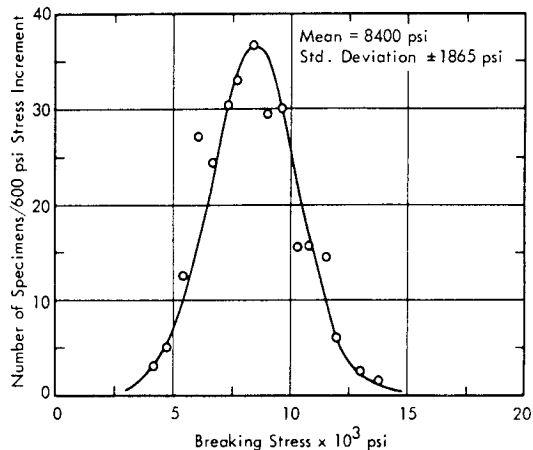


FIGURE 8.3.8 Distribution of Breaking Strength of 1/4" Polished Plate Glass Revealed by Concentric Ring Bending Tests Carried to Destruction (Data from Reference 8.3.5)

#### 8.3.3.2 Failure Strength of Windows for Sonic Boom Loads

The inherent variability of the breaking strength of glass, coupled with random variations in the sonic boom N-wave for a given aircraft, result in an appreciable variation in sonic boom damage for a given type of window design. This is illustrated by Figure 8.3.9 by the data from one series of controlled tests of sonic boom damage for conventional 3ft x 3ft window panes employing double strength (1/8th in.) and single strength (~0.09 in.). No failures were observed for overpressures less than 20 lb/sq.ft. Even at overpressures in the range of 80-100 lb/sq.ft., approximately 35% of the windows survived without failure. On the other hand, results from other tests have shown that windows which were intentionally

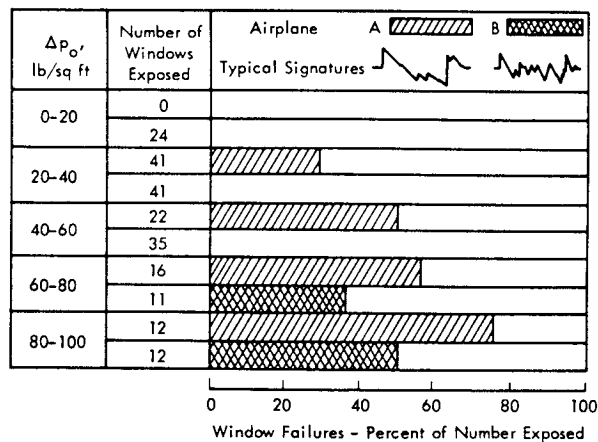


FIGURE 8.3.9 Summary of Results from Window Breakage Tests (Data from Reference 8.3.10)

cracked before exposure to a sonic boom would fail at overpressures as low as 7.6 lb/sq.ft. (Reference 8.3.9).

Correlation of Sonic Boom Window Damage With Theory

Results from a number of different test programs on sonic boom damage of windows have been summarized in Reference 8.3.11. The results are shown in Figure 8.3.10 by a plot of a normalized loading parameter  $p_o(a/h)^2$  as a function of the product  $f_{1,1}T$  where  $a/h$  is the panel span to thickness ratio,  $f_{1,1}$  is the fundamental natural frequency, and  $T$  is the duration of the positive phase. A theoretically predicted value for the boundary between damage and no damage, derived in Reference 8.3.2, is also shown. This is similar to the inverse of the shock spectrum curve for the N-wave, shown in Figure 8.3.2, with the one variation that the curve in Figure 8.3.10 is derived for an unsymmetrical N-wave with a positive phase equal to 1/6 th total duration. (Reference 8.3.11). A critical examination of the data and test procedures for the results shown in Figure 8.3.10 indicate that a more conservative value is desired for this damage criteria line. This is derived as follows.

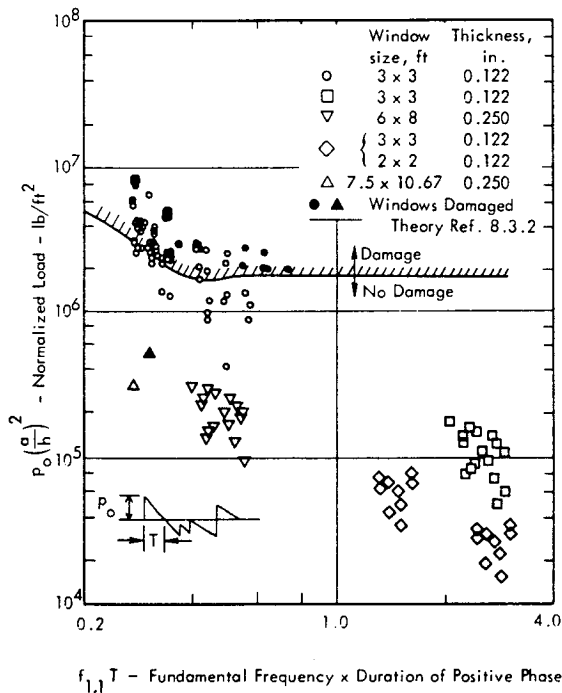


FIGURE 8.3.10 Summary of Window-Glass Breakage Experienced Due to Sonic Booms. Load Specified by the Normalized Parameter  $p_o(a/h)^2$  where  $a/h$  is the Ratio of a Side Length ( $a$ ) to Thickness ( $h$ ). (Data from a Summary in Reference 8.3.11)

Revised Criteria For Sonic Boom Damage For Windows

For the tests involving failure by sonic boom, identified in Figure 8.3.10 by the filled data points, a static load test was also reported in Reference 8.3.11. The resulting non-linear load-deflection curve is shown in Figure 8.3.11 where failure is again identified by the filled data points.

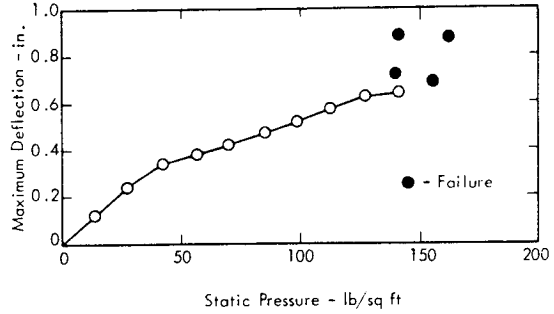


FIGURE 8.3.11 Static Load - Deflection Curve for 3ft x 3ft x 1/8 in Window Pane (Data From Reference 8.3.11)

According to the procedures outlined in Reference 8.3.12, the stress at failure for this non-linear static response is estimated to be about 8000 psi. The recommended design value for breaking strength for regular window and plate glass for sonic boom loads is about 6300 psi, according to Table 8.3.3. Thus, one reduction factor to be applied will involve reducing the criteria to allow for a more conservative breaking strength.

Further examination of the procedures employed for the sonic boom tests reveals that a 16 cu.ft. sealed cavity was placed behind the panel to insure a positive pressure differential across the window pane. However, this has the effect of increasing effective stiffness of the panel due to the added "acoustic stiffness" of the back-up panel. The computed relative change in effective panel stiffness is 1.77 with the cavity. A similar stiffening effect was experimentally in Reference 8.3.13. The net effect of this added stiffness would have been to require a correspondingly higher overpressure to achieve the expected failure stress. This, then, provides a second correction factor which would tend to reduce the damage criteria level indicated in Figure 8.3.10.

Combining these two corrections, the original criteria for the parameter  $p_o(a/h)^2$  at  $1.8 \times 10^6$  lb/sq.ft. (for values of  $f_{1,1}T > 0.6$ ) is reduced to the following.

No Sonic Boom Damage For Windows Expected For

$$p_o(a/h)^2 \leq 0.8 \times 10^6 \text{ lb/sq.ft.}$$

and  $f_{1,1}T > 0.6$

where  $p_o$  = sonic boom overpressure - lb/sq.ft.

$a$  = characteristic side of approximately square window

$h$  = glass thickness

$f_{1,1}$  = fundamental frequency - Hz

$T$  = duration of positive phase.

For values of sonic boom overpressure within the proposed limits for the SST and for windows whose length to thickness ratio meets standard building code requirements. This criteria indicates that normal quality windows should not be damaged.

#### 8.3.4 VALID DAMAGE CLAIMS FOR SONIC BOOM DAMAGE

So far, the conclusion would be that sonic boom damage would not be expected to occur, either for residential structure or windows, in good repair.

This last qualification, however, can not always be met so that, in fact, some claims for sonic boom damage have been judged valid by the United States Air Force. This experience is summarized in Table 8.3.4 and shows that every sonic boom generated approximately one valid claim per 300,000 houses exposed. This is a small percentage indeed in terms of the usual engineering accuracy for estimating the probability of damage and tends to validate the conclusion stated above.

TABLE 8.3.4  
DAMAGE CLAIMS RESULTING FROM  
SONIC BOOMS (1)

Test Areas: Chicago, Pittsburgh, Milwaukee St. Louis, Oklahoma City St. Louis (2nd Exposure)	
Number of Claims Directly Proportional to Number of People Hearing Boom and Number of Booms	
a.	Average claim per 100,000 people per boom varied from 1.2 in Pittsburgh to 0.77 in Oklahoma City.
b.	Census shows three people per residence; therefore, there was about one claim per 30,000 houses.
c.	Personal investigation of claims by engineers indicates that 5% to 10% of claims reflect true "trigger" effects from sonic booms; therefore, one sonic boom caused one valid damage claim per 300,000 houses.
d.	For each 100 valid claims the damages were as follows:
	Structural damage 0
	Wallboard and nail popping 1
	Plaster cracking and crack aggravation 5
	Fallen sections of plaster ceiling 10
	Bric-a-brac damage 34
	Glass window damage 50

(1) From Reference (8.3.14). Based on information furnished by Engineering Services, Air Force Logistics Command, Wright-Patterson Air Force Base, Ohio. These results are primarily for B-58 Overflights with mean peak overpressures of about 1.7 psf (altitude 42,500 feet).

#### REFERENCES SECTION 8.1.1

- 8.1.1 Sutherland, L., Chan, G. and Andriulli, J., "Experimental Tests on the Response of Industrial and Residential Structure to Acoustic Excitation," Wyle Research Staff Report WR 68-2, Mar. 1968.
- 8.1.2 Sivian, L. J. and O'Neil, H. T., "On Sound Diffraction Caused by Rigid Circular Plate, Square Plate and Semi-Infinite Screen," J. Acoust. Soc. Am. 3, Apr. 1938, pp. 483-510.
- 8.1.3 Muller, G. G., Black, R. and Davis, T. E., "The Diffraction Produced by Cylindrical and Cubical Obstacles and by Circular and Square Plates," J. Acoust. Soc. Am. 10, Jul. 1938, pp. 6-13.
- 8.1.4 Schaar, P., "Some Promising Techniques for Calculating the Scattering of Sound by Buildings," Wyle Research Staff Report WR 65-4, April 1965.
- 8.1.5 Morse, P. M., "Vibration and Sound," McGraw-Hill Book Co., N. Y., 1948.
- 8.1.6 Lindsay, R. M., "Mechanical Radiation," McGraw-Hill Book Co., N. Y., 1960.
- 8.1.7 Reschevkin, S. N., "A Course of Lectures on the Theory of Sound," Pergamon Press, The MacMillan Co., N. Y., 1963.
- 8.1.8 Wenzel, A., "Surface Pressure Correlation Function for a Cylinder in a Diffuse Reverberant Sound Field," Wyle Research Staff Report WR 66-14, Mar. 1966.
- 8.1.9 Powel, A., "On the Fatigue Failure of Structures Due to Vibrations Excited by Random Pressure Fields," J. Acoust. Soc. Am. 30, Dec. 1958, pp. 1130-1135.
- 8.1.10 Bozich, D. J., "Spatial Correlation in Acoustic-Structural Coupling," J. Acoust. Soc. Am. 36, Jan. 1964, pp. 52-58.
- 8.1.11 White, R. W., "Vibration Characteristics of Beams and Plates Mounted on Elastic and Inertial Supports," Wyle Research Staff Report WR 64-2, Aug. 1964.
- 8.1.12 White, R. W., "Predicted Vibration Responses of Apollo Structure and Effects of Pressure Correlation Lengths on Response," Wyle Research Staff Report WR 67-4, Mar. 1967.
- 8.1.13 Abramowitz, M. and Stegun, I., ed., "Handbook of Mathematical Functions with Formulas, Graphs, and Mathematical Tables," National Bureau of Standards, Applied Mathematics Series 55, Jun. 1964.

- 8.1.14 Dyer, I, et al., "Sonic Fatigue Resistance of Structural Designs," ASD Tech. Report 61-262, Oct. 1961.
- 8.1.15 Crandal, S. H., ed., "Random Vibration," The Technology Press of M.I.T., Cambridge, Mass., 1958.
- 8.1.16 Lyon, R. H., "Random Noise and Vibration in Space Vehicles," The Shock and Vibration Information Center Monograph SVM-1, United States Department of Defense.
- 8.1.17 The South Florida Building Code, Board of County Commissioners, Dade County, Florida, 1965 edition.
- 8.1.18 Hanks, B. R. and Stephens, D. G., "Mechanisms and Scaling of Damping in a Practical Structural Joint," The Shock and Vibration Bulletin, No. 36, Part 4, Jan. 1967.
- 8.1.19 Morse, P. M. and Ingard, K. V., "Theoretical Acoustics," McGraw-Hill Book Co., N. Y., 1968.
- 8.1.20 Barrett, R. E., "Structural Damping Investigations of Saturn Structure," M-P&VE-STA-TR-1-06, May 1963.
- 8.1.21 Barrett, R. E., "Statistical Techniques for Describing Localized Vibratory Environments of Rocket Vehicles," NASA TN D-2158, Jul. 1964.
- 8.1.22 Eldred, K. McK., Roberts, W. and White, R. W., "Structural Vibrations in Space Vehicles," WADD Tech. Report TR 61-62, 1961.
- 8.1.23 Sutherland, L. C., "Preliminary Acoustics and Vibration Environment - Saturn S-1B," The Boeing Co., Report D2-12955, Dec. 1961.
- 8.1.24 Sutherland, L. C. and Eldred, K. McK., "Estimating the Acoustic Loading on Building Structures Near Launch Sites," Paper Before 69th Meeting of Acoust. Soc. of Am., Washington, D. C., Jun. 1965.
- 8.1.25 Hunt, F. V., "Velocity-Strain Ratio for Vibrating Elastic Bodies," J. Acoust. Soc. Am. 32, Sept. 1960, pp. 1123-1128.
- 8.1.26 Peverly, R. W., "Determination of Rocket Engine Noise Damage to Community Dwellings New Launch Sites," The Martin Co., Report CR-64-65, Vol. 1, Dec. 1964.
- 8.1.27 Palmgren, A., "Die Lebensdauer van Kugellagern," Ziet. des. Vereines, Inc., Vol. 58, 1924.
- 8.1.28 Miner, M. A., "Cumulative Damage in Fatigue," J. Appl. Mech., Trans. ASME, Vol. 12, No. 3, 1945.
- 8.1.29 Butler, J. P., "Fatigue Scatter and a Statistical Approach to Fatigue Life Prediction," Proc. of Sym. on Fatigue of Aircraft Structures, WADC TR 59-507, AD-227-788, Aug. 1959.
- 8.1.30 Eshleman, A. L. and van Dyke, J. D., "A Rational Method of Analysis by Matrix Methods of Acoustically Loaded Structure for Prediction of Sonic Fatigue Strength," Chapter 35, "Acoustical Fatigue in Aerospace Structures," Syracuse Univ. Press, 1965.
- 8.1.31 Swanson, S. R., "An Investigation of the Fatigue of Aluminum Alloy Due to Random Loading," Univ. of Toronto Inst. of Aero., Report 84, Feb. 1963.
- 8.1.32 Corten, H. T. and Dolan, T. J., "Cumulative Fatigue Damage," Inst. Conf. on Fatigue of Metals, Inst. of Mech. Eng., London, 1956.
- 8.1.33 Freudenthal, A. M. and Heller, R. A., "On Stress Interaction in Fatigue and a Cumulative Damage Rule," J. Aero. Space Sci., Vol. 26, No. 7, Jul. 1959.
- 8.1.34 Gatts, R. R., "Application of a Cumulative Damage Concept to Fatigue," J. Basic Eng., Trans. ASME, Vol. 83, Dec. 1961.
- 8.1.35 Freynik, H. S., "Response of Windows to Random Noise," SOUND, May-Jun. 1963, p. 31.

## SECTION 8.1.2

- 8.2.1 Corps of Engineers, U. S. Army, "Design of Structures to Resist the Effects of Atomic Weapons." EM 1110 - 345 - 413 Weapons Effects Data.  
414 Strength of Materials and Structural Elements.  
415 Principles of Dynamic Analysis and Design.  
416 Structural Elements Subjected to Dynamic Loads.  
417 Single - Story Frame Buildings.  
418 Multi - Story Buildings.  
419 Shear Wall Structures.  
420 Arches and Domes.  
421 Buried and Semi-Buried Structures, 1957-1958.
- 8.2.2 Special Projects Division of Holmes and Narver, Inc., "Design Manual AEC Test Structures".  
Vol. 1 Nuclear Weapons Effects and Blast Loading.  
Vol. 2 Structural Response Characteristics Under Dynamic Loads.  
Vol. 3 Design of Blast Resistant Structures. TID 16347 December 1961.
- 8.2.3 Newmark, N.M., "An Engineering Approach to Blast Resistant Design." A.S.C.E. Transactions Paper No. 2786, 1956.

- 8.2.4 Norris, C.H., et al, "Structural Design for Dynamic Loads." McGraw-Hill Book Company, Inc., 1959.
- 8.2.5 M.I.T., "Structural Design for Dynamic Loads." McGraw-Hill Book Company, Inc., 1959.
- 8.2.5 Kinney, G.F., "Explosive Shocks in Air". Macmillan, N.Y., 1962.
- 8.2.6 Evorslev, J., "Subsurface Exploration and Sampling of Soils for Civil Engineering Purposes." A.S.C.E. Research Report printed by Waterways Experimental Station, Vicksburg, Miss., 1948.
- 8.2.7 Brode, H.L., "Point Source Explosions in Air." The Rand Corp. Research Memo RM-1824-AEC., 1956.
- 8.2.8 Keefer, J.H., "Air Blast Predictions for Operation Distant Plain." BRL Tech. Note 1612, Ballistic Research Laboratories, 1966.
- 8.2.9 Bracco, F.V., "A Method for Predicting the Air Blast Parameters from Liquid Propellant Rocket Explosions." Wyle Laboratories Report 64-11, Huntsville, Alabama, 1965.
- 8.2.10 Newmark, N.M., "Analysis and Design of Structures to Resist Atomic Blast." Papers presented at the V.P.I. Conference on New Developments in Engineering Design, August 1954 - Bulletin of the Virginia Polytechnic Institute, January 1956.
- 8.2.11 Melin, J.W. and Sutcliffe, S., "Development of Procedures for Rapid Computation of Dynamic Structural Response." Univ. of Illinois, Urbana, Illinois, January 1959.
- 8.2.12 Armour Research Foundation. "A Simple Method for Evaluating Blast Effects on Buildings," July 1954.
- 8.2.13 Newmark, N.M. and Hansen, R.J., "Design of Blast Resistant Structures." Harris, C.M. and Crede, C.E. (Editors): "Shock and Vibration Handbook." Vol. 3, Chapter 49. McGraw-Hill Book Company, Inc., 1961.
- 8.2.14 Merritt, J. L., and Newmark, N. M., Nuclear Geoplosics, Part V, "Effects on Underground Structures and Equipment," DASA 1285(V), May 1964.
- 8.2.15 Smith H.D., Clark W.R., Mayor R.P., "Evaluation of Model Techniques for the Investigation of Structural Response to Blast Loads." M.I.T. Report No. R6316 - February, 1963.
- SECTION 8.1.3
- 8.3.1 Mayes, W. H. and Edge, P. M., Jr., "Response of Ground Buildings to Sonic Booms," Materials Research and Standards, Vol. 4, Nov. 1964, pp. 588-593.
- 8.3.2 ARDE Associates, "Response of Structures to Aircraft Generated Shock Waves," WADC Tech. Report 58-169, U.S. Air Force, Apr. 1959.
- 8.3.3 Kryter, K. D., et al., "Definition Study of the Effects of Booms from the SST on Structure, People and Animals," Stanford Research Institute, Tech. Report 1, Jun. 1966.
- 8.3.4 Ramsay, W. A., "Damage to Ottawa Air Terminal Building Produced by a Sonic Boom," Materials Research and Standards, Vol. 4, Nov. 1964, pp. 612-616.
- 8.3.5 McKinley, R. W., "Response of Glass in Windows to Sonic Booms," Materials Research and Standards, Vol. 4, Nov. 1964, pp. 594-600.
- 8.3.6 Andrews Associates, Inc. and Hudgins, Thompson, Ball and Associates, "Structural Response to Sonic Booms," FAA Report SST 65-1, Vol. 2 - Appendix Feb. 1965.
- 8.3.7 Power, F. K., "Sonic Boom Effects on Light Aircraft, Helicopters, and Ground Structures," FAA Paper Before Am. Soc. Testing Materials, Chicago, Jun. 1964.
- 8.3.8 Crocker, M. J., Multi-Mode Response of Panels to Sonic Boom," Wyle Research Staff Report WR 66-1, Jan. 1966.
- 8.3.9 "Preliminary Data, Sonic Boom Structural Response Program," White Sands Missile Range, New Mexico, Mar. 1965.
- 8.3.10 Martin, C. W., "Fracture of Gypsum Plasters and Cement Mortars by Dynamic Loading," Air Force Weapons Laboratory, Tech. Report AFWL-TR-65-140, Dec. 1965.
- 8.3.11 Parrott, T. L., "Experimental Studies of Glass Breakage Due to Sonic Booms," SOUND, May-Jun. 1962.
- 8.3.12 Roark, R. J., "Formulas for Stress and Strain," McGraw-Hill Book Co., N. Y., 1954.
- 8.3.13 Freynik, H. S., Jr., "Response of Windows to Random Noise," SOUND, May-Jun. 1963.
- 8.3.14 Kryter, K. D. et al., "Definition Study of the Effects of Booms from the SST on Structures, People and Animals," Stanford Research Institute, Tech. Report 1, Jun. 1966.

**CHAPTER 9**  
**ARCHITECTURAL ACOUSTICS**  
**AND VIBRATION CONTROL**  
**FOR GROUND FACILITIES**

TABLE OF CONTENTS

SECTION	PAGE
9.1	INTRODUCTION . . . . . 9-1
9.2	ABSORPTION . . . . . 9-2
9.2.1	ROOM ABSORPTION . . . . . 9-2
9.2.1.1	Reflection and Absorption . . . . . 9-2
9.2.2	ABSORPTION MECHANISMS . . . . . 9-3
9.2.2.1	The Porous Absorber . . . . . 9-3
9.2.2.2	Panel Absorbers . . . . . 9-5
9.2.2.3	Resonant Absorbers . . . . . 9-6
9.2.3	RATING OF ABSORPTION COEFFICIENTS . . . . . 9-9
9.2.4	WAVE ACOUSTICS APPROACH . . . . . 9-10
9.2.4.1	One-Dimensional Enclosure . . . . . 9-10
9.2.4.2	Three-Dimensional Enclosure . . . . . 9-11
9.2.5	STATISTICAL APPROACH . . . . . 9-14
9.2.5.1	Sabine Equations . . . . . 9-14
9.2.5.2	Reverberation Time . . . . . 9-15
9.2.5.3	Air Absorption . . . . . 9-16
9.3	TRANSMISSION LOSS . . . . . 9-17
9.3.2	DEFINITIONS . . . . . 9-17
9.3.3	MEASUREMENT OF TRANSMISSION LOSS . . . . . 9-18
9.3.4	TRANSMISSION LOSS FOR A STRUCTURE . . . . . 9-19
9.3.5	INFINITE LIMP WALL . . . . . 9-19
9.4	DUCTS . . . . . 9-27
9.4.1	THEORETICAL ATTENUATION OF A LINED DUCT . . . . . 9-28
9.4.2	PRACTICAL VALUES OF ATTENUATION IN DUCTS . . . . . 9-28
9.5	NOISE REDUCTION . . . . . 9-30
9.5.1	DETERMINATION OF NOISE LEVELS . . . . . 9-31
9.5.2	INTERNAL SOURCE . . . . . 9-32
9.5.3	SAMPLE CALCULATION . . . . . 9-33
9.6	APPLICATION OF DAMPING TREATMENT FOR NOISE AND VIBRATION CONTROL . . . . . 9-35
9.6.1	APPLICATION OF VISCOELASTIC MATERIALS FOR DAMPING OF PANELS . . . . . 9-35
9.6.2	DESIGN THEORY FOR SINGLE LAYER AND TWO LAYER DAMPING TREATMENT . . . . . 9-36
9.6.2.1	Unconstrained (Free) Layer Damping Treatment . . . . . 9-36
9.6.2.2	Constrained Layer Damping Treatment . . . . . 9-38
9.6.3	VISCOELASTIC DAMPING MATERIALS . . . . . 9-45
9.6.3.1	Terminology of Viscoelastic Damping and Adhesive Materials . . . . . 9-46
9.6.3.2	Properties of Viscoelastic Materials . . . . . 9-47
9.7	STRUCTURAL VIBRATION CONTROL . . . . . 9-51
9.7.1	EFFECT OF DAMPING TREATMENT ON STRUCTURALLY TRANSMITTED VIBRATION . . . . . 9-51
9.7.2	VIBRATION ISOLATION . . . . . 9-51
9.7.2.1	Isolation of a Single Degree-of-Freedom System . . . . . 9-52
9.7.2.2	Isolation of Two Degree-of-Freedom System . . . . . 9-53
	REFERENCES . . . . . 9-56



## CHAPTER 9

# ARCHITECTURAL ACOUSTICS AND VIBRATION CONTROL FOR GROUND FACILITIES

### 9.1 INTRODUCTION

An essential step in the design of buildings to be located near high intensity noise sources is to provide adequate protection for both personnel and delicate equipment against excessive noise levels. It is a well known fact that high levels of noise can be harmful to people, but even if the harmful level is not exceeded, the proper function of the building can often not be realized. This is certainly the case where speech communication between personnel is concerned and, more seriously, where audible working systems are in operation. In addition, there are some tasks which involve concentration that require low levels of noise in order to obtain high efficiency. To satisfy these requirements, it is necessary to incorporate acoustical treatments in the design of building. If this is not done from the outset, remedial treatments may be needed which are frequently ineffective and costly.

The same problems are encountered if a noise source, such as a launch site, is placed in the vicinity of residential housing where the major problem is one of annoyance to a community. It is not safe to assume that if the houses are far removed from the source there will be no noise problems, because climatic effects can radically alter the situation. Therefore, noise intrusion into homes must also be considered when evaluating a site location for rocket test facilities.

Another important consideration concerns the housing of equipment near to a launch site. It is often the case that delicate and essential components are situated in very intense noise fields, where the resulting high level of vibration can easily cause damage and jeopardize the

complete launch procedure. This equipment has therefore to be carefully mounted on antivibration supports and shielded from direct acoustical fields.

#### The System Approach

A noise control problem can essentially be divided into three sections:

- (a) The source of the noise where all airborne and structureborne vibrations are initiated,
- (b) The path of noise propagation from the source, and
- (c) The receiver, which includes personnel and any other objects that are affected by the noise.

Sections (a) and (b) have been discussed elsewhere in this manual; this particular chapter concentrates on the local transmission of sound and vibration within a receiver. The receiver system can be most analyzed by means of the schematic diagram as shown in Figure 9.1.

Here, the source, paths and receivers are designated as impedances, the flow of acoustical power being analogous to electrical power. The direction of power flow is shown by arrows. With such a diagram, it is possible to eliminate some of the transmission paths by inspection. For example, if the effective impedance offered by the walls is increased, less power may reach the receiver. However, since this is in parallel with the flanking paths, which may have a lower effective impedance, the net result may be negligible. If the approach is continued in this manner, the important sections may be pin-pointed prior to any practical alterations.

The following sections in this Chapter are concerned with the above importances and include an investigation into the effects of absorbent materials on sound levels, the transmission loss of structures, the attenuation of ducts and the isolation of vibrations. To complete the subject, sections on noise and vibration control are included, in which the results from previous sections are combined in the analysis of some practical situations.

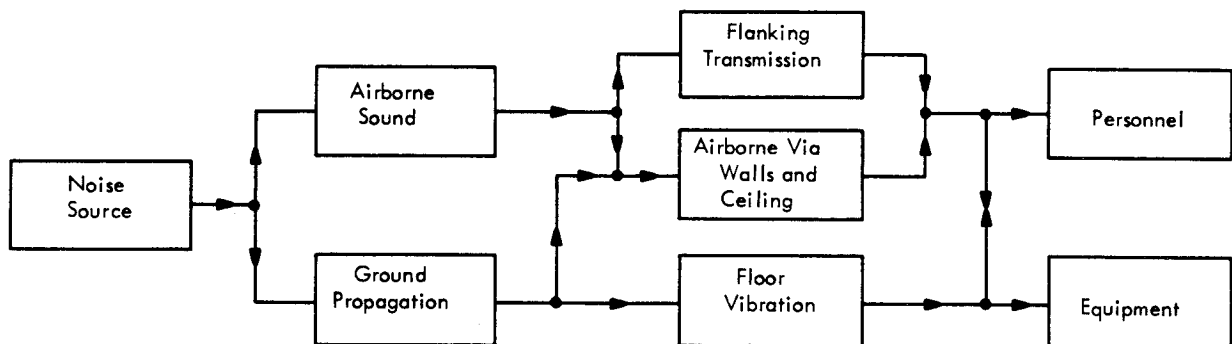


FIGURE 9.1 Schematic Diagram of the Transmission of Sound to a Receiver by Various Paths

## 9.2 ABSORPTION

In order to determine the sound levels produced in buildings, it is necessary to have a knowledge of the mechanism of sound transmission through structures together with the effects of absorption. Both factors must be considered together in design optimization for noise control; sound absorption determining the level of sound in the room for a given sound power input, and transmission loss controlling the fraction of external sound which enters the room. This section develops the basic factors related to the sound absorption properties of various material configurations, and their utilization in controlling the sound level in a room.

### 9.2.1 ROOM ABSORPTION

The main action of an absorbent material is to reduce the sound energy that is reflected by a surface. The application of such a material to the surfaces of an enclosure will reduce the sound energy inside the enclosure, but the magnitude of the reduction depends on the type and quantity of material used together with the manner and position of mounting. Thus, for a given sound energy source, either inside or outside the enclosure, the noise level and hence the interference with personnel activities is reduced by room absorption. This can result in improved safety levels for personnel, reduced noise levels in equipment rooms, and an improved work environment for speech communication.

In practice, all materials used in buildings absorb a certain proportion of the incident energy, but to obtain the optimum acoustic conditions requires a knowledge of the absorption mechanism so that the correct material can be chosen.

The absorbing material is usually placed on the surfaces of the enclosure, although this is not mandatory nor is it always the best solution. For example, in an extremely large enclosure with an abundance of wall fittings, or where a suspended ceiling is impractical, it is often better to use suspended absorbers closer to the source of sound. They are also extensively used in ventilating and heating ducts for attenuation purposes, and in certain wall constructions to increase the transmission loss. These two applications will be discussed more fully later in this Chapter.

#### 9.2.1.1 Reflection and Absorption

At a sufficient distance away from a noise source situated in free space (i.e., beyond the near field) the sound waves propagate radially. If an obstacle of infinite lateral dimensions is placed in the path of these waves then a part of the energy incident will be reflected, the object acting as an acoustic mirror and the waves obeying the same laws as met in optics. It is simpler for the analysis at this point to place the obstacle at a distance from the source such that the radiated waves can be assumed to be plane waves. The principle of the conservation of energy can then be applied at the obstacle resulting in the following expression:

$$E_i = E_r + E_t + E_A \quad (9.1)$$

where  $E$  represents the energy in the incident (i), reflected (r) and transmitted (t) waves and  $E_A$  represents the energy lost in transit through the obstacle. This can be re-written as

$$1 = \frac{E_r}{E_i} + \frac{E_t}{E_i} + \frac{E_A}{E_i}$$

With the definitions

$$r^2 = \frac{E_r}{E_i}$$

where  $r$  is the amplitude reflection coefficient, for normal incidence,

$$\tau = \frac{E_t}{E_i}$$

where  $\tau$  is the energy transmission coefficient (the transmittivity), for normal incidence

and 
$$\alpha = \frac{E_A}{E_i}$$

then 
$$1 = r^2 + \tau + \alpha \quad (9.2)$$

$\alpha$  is then termed the normal incidence absorption coefficient for the obstacle and is defined as the ratio of absorbed to incident energy. Equation (9.2) can be applied to any absorbent material. In most cases the absorbent is placed in the vicinity of a fairly rigid structure so that the transmission coefficient is very small. Under these conditions,

$$\alpha = 1 - r^2 \quad (9.3)$$

It is obvious from the definition of  $\alpha$  that it can never be greater than unity. This is a general expression since the mechanism of absorption is immaterial.

From the above expressions, it can be seen that

$$E_r = (1 - \alpha) E_i$$

In an enclosure, the reverberant sound energy is dependent on the strength of the reflections from the surfaces. Thus, the energy, and hence the sound level, can be reduced by placing an absorbent material on the surfaces; the reduction in level being dependent on the value of  $\alpha$ .

9.2.2 ABSORPTION MECHANISMS

What actually happens when a sound wave is incident on an absorbing surface depends on the mechanism of absorption. However, all absorbers have one thing in common in that they convert the sound energy into heat. It is now necessary to see how this transformation is obtained for various types of treatment.

9.2.2.1 The Porous Absorber

The porous type of absorber is a material which has a multitude of small interconnecting pores. In passing through these pores, the kinetic energy of the sound wave is partly transformed into heat due to frictional and viscous resistance. As the particle velocity increases with frequency, the energy lost due to friction also increases, together with the absorption. The general character of the absorption curve is shown in Figure 9.2 where it can be seen that low values are obtained at the lower frequencies.

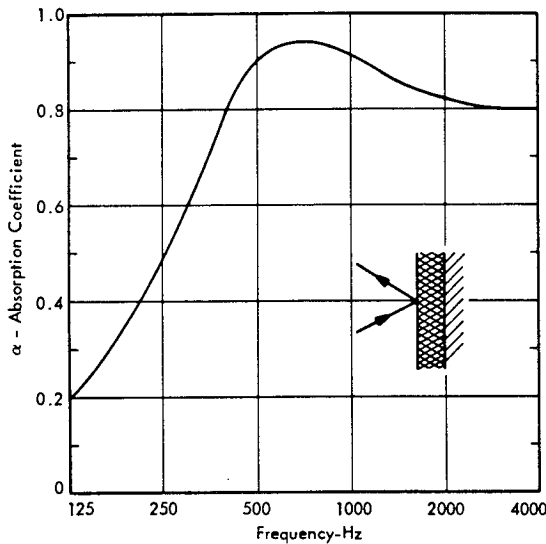


FIGURE 9.2 Absorption Characteristic of 2" Fiberglass with Rigid Backing

Flow Resistance

One of the important factors determining the amount of absorption available is the so-called "flow resistance" of the material to a direct air-flow, defined as the ratio of the pressure drop across the sample to the velocity of the air passing through it, and measured in rayls. The relationship between flow resistance and absorption coefficient is shown in Figure 9.3. If the flow resistance is too high, energy will not flow through the material, if too low, the absorption in the interior will be reduced, necessitating a thick layer. There is thus an optimum value of the flow resistance for each thickness of the material, as shown in Figure 9.3. If a thick layer of porous absorber is placed in contact with a rigid wall then the absorption coefficient is determined mainly by the amount of energy reflected at the front surface, since all other energy is

absorbed in the material. In the case of a thin layer, however, the coefficient is reduced by the reflection of energy from the rigid surface. Thus, to obtain high absorption at the low frequencies requires a thick material having low flow resistance. This is demonstrated in Figure 9.4 where the influence of thickness on the absorption coefficient can be seen. In order to minimize reflections at the front surface of the absorber, it is preferable to choose the flow resistance to be the same as the impedance of the sound field present (see Chapter 4).

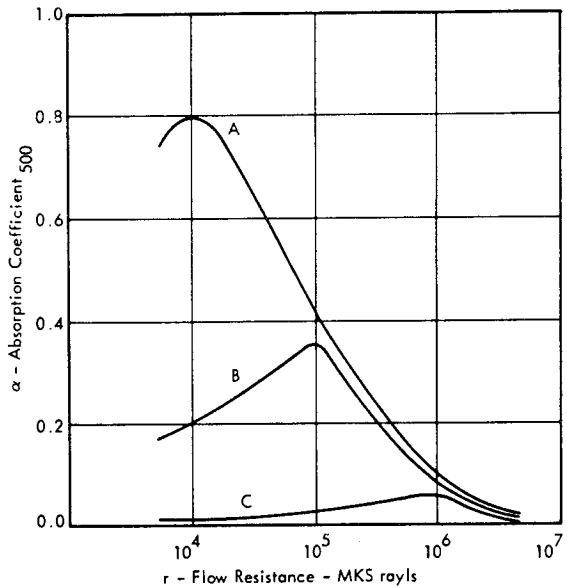


FIGURE 9.3 The Dependence of the Measured Absorption Coefficient at 500 Hz of a Porous Material on the Flow Resistance. (From Reference 9.1)  
A: 10 cm. thick layer  
B: 3 cm. thick layer  
C: 1 cm. thick layer

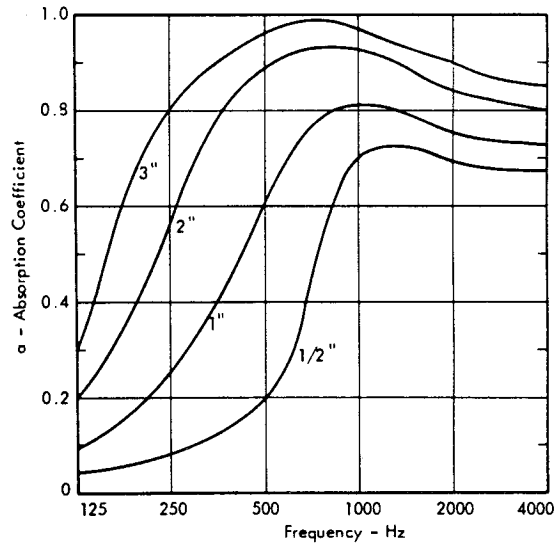


FIGURE 9.4 Effect of Thickness of a Porous Material on the Absorption Coefficient. (Data from Reference 9.2)

Effect of Spacing

The absorption coefficient of a porous material can be increased in the low frequency range by spacing it away from the surface to which it is attached. Since the absorption depends on the particle velocity, the maximum effectiveness will be obtained at a distance a quarter wavelength from the wall, as at this point, the particle velocities of the incident and reflected waves are a maximum. Thus, if the material is assumed to be thin, the absorption coefficient at a particular frequency as a function of the separation from the wall, will be as shown in Figure 9.5. Conversely, if the material is placed a distance  $d$  from the wall, the frequency at which the maximum absorption is obtained is given by

$$f_m = \frac{c}{4d} = \frac{280}{d}$$

where  $c$  is the velocity of sound in ft./sec. and  $d$  is measured in feet. In the usual application, the material of thickness  $t$ , is placed in contact with the wall. Thus, at frequencies given by

$$f > \frac{280}{t}$$

there is absorbent material at a position of maximum particle velocity. The thickness therefore determines the lower frequency limit at which a high absorption coefficient is obtained. Figure 9.6 shows measured results of the absorption coefficient of rock-wool spaced away from a rigid surface.

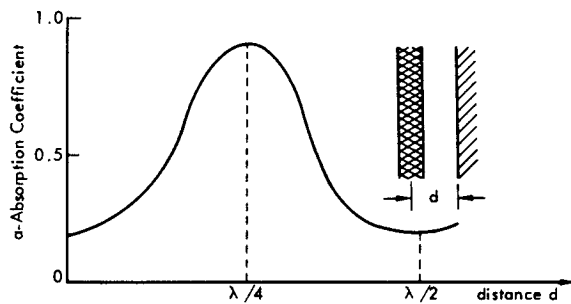


FIGURE 9.5 The Effect of an Air Space on the Absorption Coefficient of a Porous Material at Low Frequencies

One important point to remember in the use of porous materials is that great care or advice should be taken prior to treating or covering the exposed surface in any manner. Any interference with the system of pores may adversely affect the flow resistance and hence the absorption.

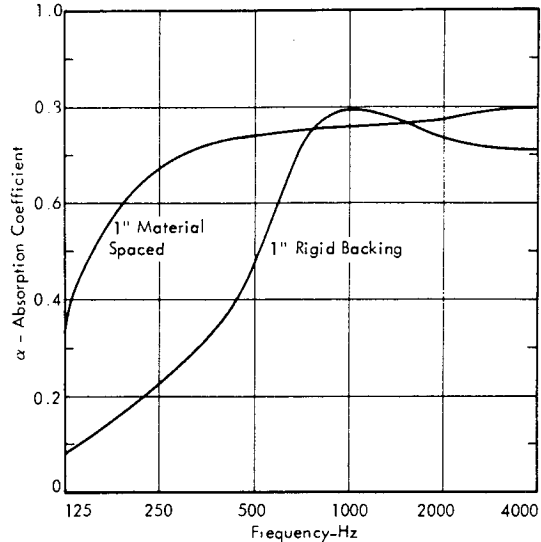


FIGURE 9.6 The Effect of Spacing on the Absorption of a Typical Porous Material (Data from Reference 9.2)

Porous Absorbers at Low Frequencies

The impedance of a layer of porous material, having a flow resistance greater than about  $5 \times 10^3$  mks rayls, can, in the low frequency region, be expressed approximately as (Reference 9.3)

$$z = \frac{Rt}{3} \left\{ 1 + \left( \frac{3p_o c}{Rt} \right)^2 \right\} + j \left\{ \frac{4\omega t}{9c} - \frac{p_o}{\omega t p_o c} \right\}$$

where  $R$  is the flow resistance (mks rayls/m)

$t$  is the material thickness (m)

$p_o$  is the atmospheric pressure (newtons/m<sup>2</sup>)

It can be seen that a resonance occurs when the imaginary part is zero, or when

$$\omega = \frac{3}{2t} \sqrt{\frac{p_o}{\rho_o}}$$

For a sample of fibreglas 3" thick, this leads to a resonant frequency of 900 Hz which agrees well with the maximum in the corresponding curve of Figure 9.4. At this frequency

$$z = \frac{Rt}{3} \left[ 1 + \left( \frac{3p_o c}{Rt} \right)^2 \right]$$

The maximum of the normal incidence absorption coefficient can thus be calculated using

$$\alpha_o = 1 - \left( \frac{z - \rho_o c}{z + \rho_o c} \right)^2$$

provided the flow resistance of the material is known.

Below the resonant frequency, the capacitive part of the impedance  $z$  becomes dominant, and the reactive part approaches

$$-j \frac{\rho_o}{\omega t \rho_o c}$$

Denoting  $z = r + jx$

it follows that

$$\alpha_o = \frac{4 \rho_o c r}{(r + \rho_o c)^2 + x^2}$$

At low frequencies,  $x \gg (r + \rho_o c)$  and thus in this region

$$\alpha_o = \frac{4 \rho_o c r}{x^2} \tag{9.4}$$

The theoretical absorption coefficient at normal incidence is thus proportional to  $\omega^2$ , since  $r$  is independent of frequency. However, in practice, this proportionality is not obeyed and the coefficient is approximately proportional to  $\omega^{3/2}$ .

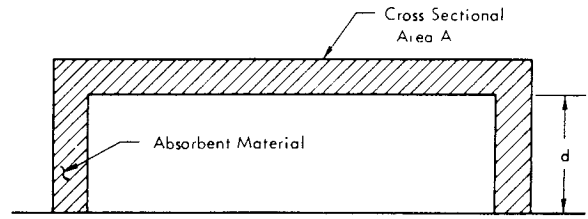
Using the above expressions, the absorption coefficient can be calculated at low frequencies, the value being slightly smaller than that averaged over all angles. However, if it is required to calculate  $\alpha_o$  at the higher frequencies, recourse should be made to the general expression for impedance given in Reference 9.3.

### 9.2.2.2 Panel Absorbers

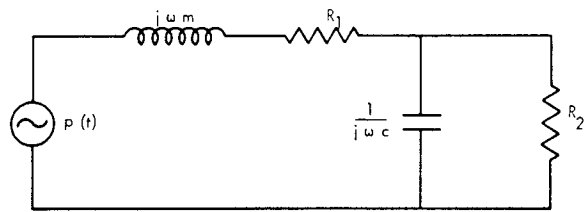
The second type of absorber depends for its action on the resonance between the mass of a thin panel and the stiffness of an enclosed amount of air (Figure 9.7).

The definition of acoustic capacitance is

$$C = \frac{\text{volume displacement}}{\text{pressure}} = \frac{dV}{p}$$



(a) Resonator Panel Absorber



(b) Electrical Analogue

(a) Resonator Panel Absorber

(b) Electrical Analogue

FIGURE 9.7 Configuration and Equivalent Analog of Resonant Panel Absorber

From the results of Chapter 4, this can be written as

$$C = \frac{V}{\rho_o c^2}$$

where  $V$  is the enclosed volume,  $\rho_o$  is the equilibrium density of air and  $c$  is the velocity of sound in air. This can also be expressed as

$$C = \frac{V}{K}$$

where  $K = \rho_o c^2$  is the Bulk Modulus of air, and is equal to 2923 lbs./ft.<sup>2</sup>. Thus, if the cross-sectional area is  $A$  and the depth of the resonator  $d$ ,

$$C = \frac{dA}{K}$$

If the panel is sufficiently thin for the stiffness to be negligible, the resonant frequency is

$$f_{res} = \frac{1}{2\pi} \sqrt{\frac{K}{md}} \quad (9.5)$$

where  $m$  is the mass of the panel per unit area. Thus any incident sound wave having a frequency of, or in the vicinity of  $f_{res}$  will excite the system resonance. The bandwidth of resonance and the energy absorbed will depend on the losses in the system and can both be increased by the addition of a porous material in the cavity. The analogous electrical circuit, as discussed in Chapter 4, can be drawn as shown in Figure 9.7, where  $m$  is the mass of the panel,  $C$  is the capacitance, and  $R_2$  represents the losses in the absorbent placed in the air-space. A practical example in the absorption spectrum obtained from a freely vibrating panel mounted on battens is shown in Figure 9.8.

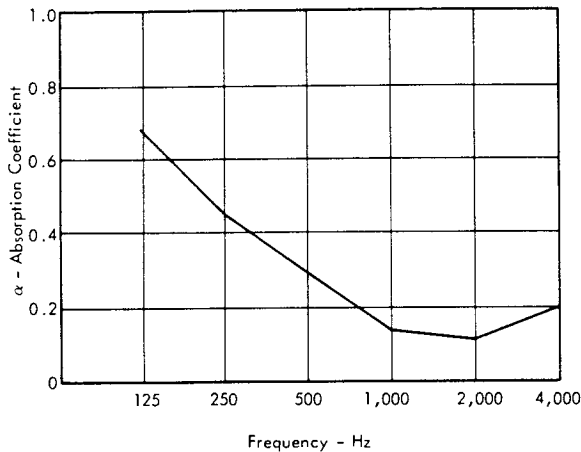


FIGURE 9.8 Absorption Characteristic of a Resonating Panel (from Reference 9.1)

This type of absorber can be extremely useful since it takes up little room, can be treated and painted, and gives a high absorption at the low frequencies where porous material gives poor results. The range of operation can also easily be altered.

9.2.2.3 Resonant Absorbers

An absorbing system similar to that discussed in the previous section but having a much narrower bandwidth of useful absorption is known as the Helmholtz resonator. This consists of a chamber of air in the room via a neck; a good example being a jug or bottle. In operation, the mass of air in the neck together with the stiffness of the enclosed air in the chamber forms a resonant system. At resonance, the frictional drag experienced in the neck provides the absorption and this can be usefully increased by placing a porous material across the mouth. In a manner similar to Section 9.2.2.2, it can be shown that the resonant frequency of such a system is given by

$$f_{res} = \frac{1}{2\pi} \sqrt{\frac{KA}{\rho_0 LV}} \quad (9.6)$$

- where  $A$  = the cross-sectional area of the neck.
- $L$  = the effective length of the neck.
- $V$  = the volume of the chamber.
- $\rho_0$  = the density of air.

It is not essential for the chamber to be spherical; indeed, more often than not, this is not the case in practice since other shapes are usually more convenient. The analogous electrical circuit in this case is as shown in Figure 9.9a

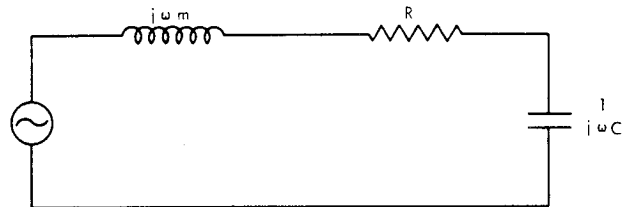
where

$$m = \rho_0 / S$$

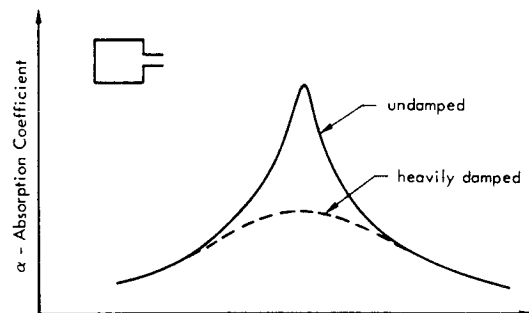
$$C = \frac{V}{K}$$

and  $R$  represents the total losses in the circuit including the energy radiated by the resonator. As in the previous case the bandwidth of the absorption curve depends on the internal losses. (Figure 9.9b.)

This type of absorber is very useful when only a few discrete frequencies must be damped.



(a) Electrical Analog



(b) Absorption vs Frequency

FIGURE 9.9 Typical Wide and Narrow Band Characteristics of a Helmholtz Resonator and Electric Analog

At very low frequencies, it is possible for a room having an opening or a connecting corridor to behave as a Helmholtz resonator. Under these conditions, a very high sound level that extends over a narrow frequency range will be produced in the room in the absence of absorption. This is particularly true if the room is subject to rocket noise which contains some very low frequency components.

Alternative Types of Absorber

The previous three sections have dealt with the basic types of absorbing mechanisms. There are other types in common use which are combinations of these, which will now be described.

Resonator-panels

The basis of the resonator panel type of absorber is a perforated panel mounted a certain distance away from a rigid surface, as illustrated in Figure 9.10.

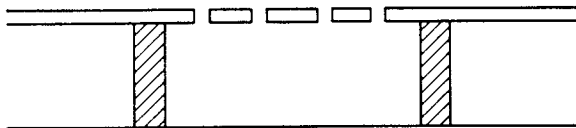


FIGURE 9.10 Resonator Panel Absorber.

This in effect produces a series of Helmholtz resonators, the resonant frequency of which can easily be altered by varying either the separation  $d$  or the size of the perforations. In most cases the perforations are circular and regularly spaced, but they can be randomly spaced or in the form of slits.

The absorption characteristics can be made to cover a wider frequency range by incorporating a porous material in the cavity. In this manner the porous material is protected from contamination, yet the passage of sound waves into the interior is not unduly affected. Figure 9.11 shows the type of characteristic obtained.

The absorption decreases at higher frequencies due partly to increased flow resistance, but the turnover point can be varied by choosing the appropriate percentage of perforation. (The greater the exposed area, the higher will be the frequency at which the absorption begins to fall.) This procedure however, also affects the low frequency absorption, so a compromise has to be made. The design of such absorbers is complicated by many factors, but design charts have been published (Reference 9.3) to facilitate the procedure.

In order to design a panel absorber to specification, consider a perforated panel spaced a distance  $d$  from a rigid wall, the intervening space being filled with a porous material.

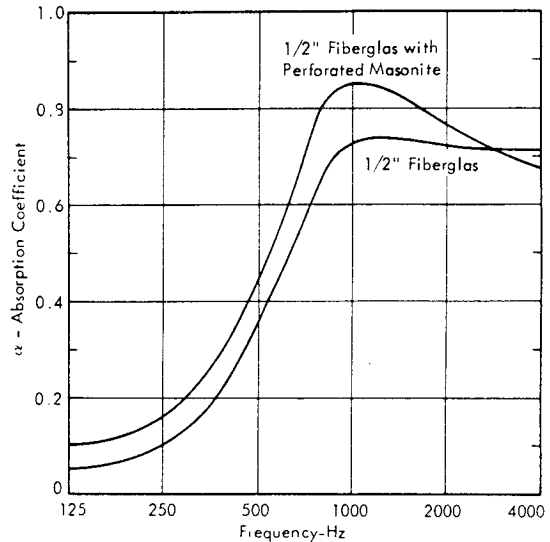


FIGURE 9.11 Typical Absorption Characteristic of Porous Material with Perforated Facing (Data from Reference 9.2)

- Let  $V$  be the volume per perforation
- $n$  the number of perforations per unit surface area
- $G$  the conductivity of one hole
- $R$  the flow resistance of one hole (including that of the porous material insert).

If the specific acoustical impedance of the surface per unit area is  $z$ , then the absorption at normal incidence is

$$a_o = 1 - \left( \frac{z - \rho_o c}{z + \rho_o c} \right)^2$$

The impedance  $z$  is comprised of resistance, mass and capacitance where

$$m = \frac{\rho_o}{G}$$

$$C = \frac{V}{K}$$

where  $K$  is the bulk modulus of air.

Hence

$$z = \frac{1}{n} \left\{ R + j\omega \frac{\rho_o}{G} + \frac{K}{j\omega V} \right\}$$

since the volume displacement is  $n$  times that per unit hole.

The frequency of resonance is given

$$f_{res} = \frac{1}{2\pi} \sqrt{\frac{KG}{\rho_o V}} = \frac{c}{2\pi} \sqrt{\frac{G}{V}}$$

at which the impedance is

$$z_f = f_{res} = \frac{R}{n}$$

Thus at resonance

$$a_o = \frac{4\mu}{(1+\mu)^2}$$

where

$$\mu = \frac{R}{\rho c n}$$

The resonance curve has a bandwidth (defined in this case only as the frequency difference between the 50 percent absorption points) whose upper and lower frequencies are given by the equation

$$f - \frac{1}{f} = \pm n \sqrt{GV} \left( \frac{R}{nW_o} + 1 \right)$$

It can be shown (Reference 9.3) that the number of octaves between these two frequencies ( $f_1$  and  $f_2$ ) is given by

$$O = \frac{1}{2} \left( \frac{c_o}{f_{res}} \right)^2 1.44 (1 + \mu) g$$

where

$$g = \frac{nG}{\lambda_{res}}$$

The chart in Figure 9.12 enables the values of

$$\frac{nV}{\lambda_{res}}, \frac{R}{n\rho c} \text{ and } nG\lambda_{res}$$

to be determined. Thus, if one parameter is set (either  $n$ ,  $V$ ,  $R$  or  $G$ ) the others can be determined.

If the perforations are cylindrical holes with diameter  $d$  and length  $L$ , then

$$G = \frac{S}{L + 0.8d}$$

where  $S$  is the cross-sectional area.

For small diameters

$$G \sim \frac{S}{L}$$

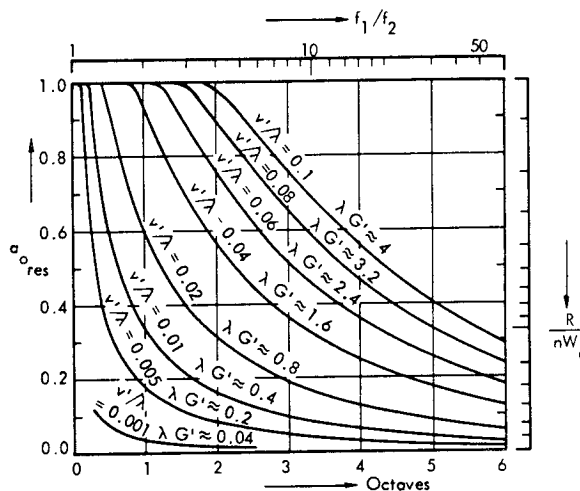


FIGURE 9.12 Design Chart for Perforated Panels. (From Reference 9.3)

As an example, assume that an absorber is required to provide an absorption coefficient of 0.6 ranging over a one octave frequency band from 50 to 100 Hz (center frequency 70 Hz).

From the design chart,

$$nV = 0.094 \text{ (= air space in meters)}$$

$$\frac{R}{n} = 1750$$

and  $nG = 0.17$

It is now necessary to set one of the parameters, say,  $n = 200$  per meter<sup>2</sup>.

Thus  $R = 3.5 \times 10^5$  rays

and  $G = 0.9$  mm.



If the thickness of the perforated panel is 1 cm, the diameter of the perforations is thus 3.5 mm, and the percentage of open area is 0.2 percent. It is often more convenient however, to start the calculation by setting the flow resistance  $R$  and calculating the hole dimensions.

It is recommended that tests be performed to evaluate any unique absorber configurations, although in practice it is found that the results from these calculations agree reasonably well with those measured, the absorption bandwidth being wider in the latter case due to extra damping of the system. If the bandwidth must be increased yet further, it is possible to combine two resonators in series (Reference 9.3).

Acoustic Tiles

The acoustic tile consists of a slab of compressed wood or mineral fibers having perforations extending from the front surface to a distance of perhaps three-quarters of the slab thickness. This is an example of the way that materials having a high flow resistance can be used as absorbers by the introduction of openings in the surface. The characteristics of such tiles are shown in Figure 9.13 with and without an air gap and the peaked nature of the latter is clear. These are probably the most commonly used absorbents today, partly because they can be installed easily by non-skilled persons without fear of poor results.

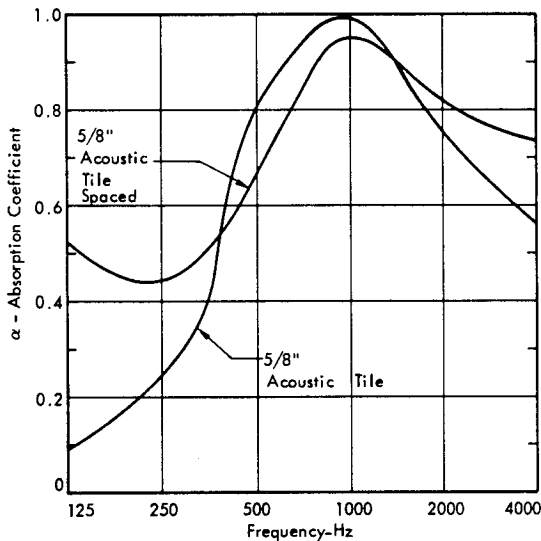


FIGURE 9.13 Absorption Characteristics of a Typical Acoustic Tile with and without an Air-Gap (Data from Reference 9.4)

Suspended Absorbers

As mentioned previously, there are some occasions when it is undesirable to mount the absorbent at a surface of an enclosure. In these cases it is usual to suspend the absorbent in the vicinity of the noise source (if it is also in the

enclosure). The characteristics of such an absorber show extremely high efficiencies due to diffraction effects at the edges and the fact that sound energy is incident on both sides. This is shown in Figure 9.14 for a perforated absorber.

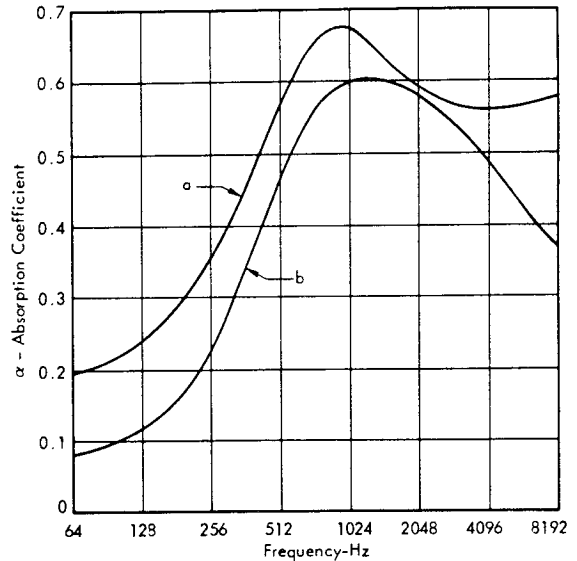


FIGURE 9.14 Absorption Characteristic for Perforated Sheet Metal with Muslin Covering (a) with Both Sides Exposed to the Sound, and (b) Mounted 2" from a Rigid Wall (From Reference 9.8)

Sometimes the suspended absorber is made in the shape of a cone out of a material such as shredded wood, and can have absorption coefficients of up to 1.8. From what has been said, a figure, such as this, appears to violate the basic laws of physics, but this point will be discussed in a later section.

9.2.3 RATING OF ABSORPTION COEFFICIENTS

In order that engineers can design acoustical systems, tables of the absorption coefficients of building materials should be readily available in a compact and yet comprehensive form. Accomplishment of this requirement is complicated by the fact that the coefficients vary greatly with both frequency and angle of the incident sound energy. A complete statement of the coefficients of any one material would be exceedingly complex and difficult to understand, and thus various standard methods of measurement and presentation have had to be put forward.

Variation With Angle of Incidence

There are two methods by which the absorption coefficient can be measured: (i) using an impedance tube, in which case only the coefficient at normal incidence is obtained; (ii) the reverberation chamber method which results in a coefficient averaged over all angles of incidence (see Section 9.2.5).

In this section and in Chapter 12, all values quoted have been measured using method (ii), and these averaged results are usually greater than the normal incidence values, sometimes by a factor of two

#### Variation With Frequency

The absorption coefficients are averaged over a band of frequencies one-third octave in width, with center frequencies of 125, 250, 500, 1000, 2000 and 4000 Hz. Thus six numbers are stated to define the coefficient under a particular condition. In some cases the values are given at centerfrequencies spaced one-third of an octave apart, i.e., 100, 125, 160, 200 Hz et cetera, so that more detailed information can be obtained. This information is necessary for materials where the absorption varies rapidly with frequency. However, there are some designs (e.g., the resonator type) that have usable absorption over such a narrow frequency range that even this detail is not sufficient, and a continuous curve of performance vs frequency should be given in this case.

#### Single Figure Rating

However, with the above method of stating the absorbing properties of a given material it is still difficult to compare the effectiveness with that of a different material - one may have less absorption at the low frequencies and higher absorption at high frequencies. Therefore, for noise reduction purposes, a single figure is often given, this being the mean of the values at 250, 500, 1000 and 2000 Hz. This figure is known as the noisereduction coefficient (NRC). However, since the NRC does not include values of the absorption coefficient at frequencies below 250 Hz, care must be taken in the selection of materials on this basis, especially if low-frequency absorption is required. Table 9.1 shows values of  $\alpha$  for various common materials - a more comprehensive table can be found in Chapter 12.

TABLE 9.1

A LIST OF THE ABSORPTION COEFFICIENTS FOR A FEW COMMON MATERIALS

	125	250	500	1000	2000	4000
Brick Wall, Unpainted	.02	.02	.03	.04	.05	.07
Brick Wall, Painted	.01	.01	.02	.02	.02	.02
Concrete, Unpainted	.01	.01	.02	.02	.02	.03
Carpet on Concrete	.09	.08	.21	.26	.27	.37
Wooden Floor	.04	.04	.03	.03	.03	.02
Glass Pane 1/8"	.03	.03	.03	.03	.02	.02
Plasterboard, Plastered	.02	.05	.06	.08	.04	.06

### 9.2.4 WAVE ACOUSTICS APPROACH

The previous section has been devoted to the mechanism of various absorbing systems. It is now necessary to investigate the effect that absorbent systems have on the sound field in an enclosure. The type of absorbent will not be defined as it is immaterial for this section.

#### 9.2.4.1 One-Dimensional Enclosure

The type of enclosure to be considered at first is one-dimensional, in other words, a tube of length  $L$  terminated at both ends. It is assumed that the diameter of the tube is smaller than the wavelength at all frequencies considered. The equation for the propagation of plane waves along the tube is

$$\frac{\partial^2 p}{\partial x^2} = \frac{1}{c^2} \frac{\partial^2 p}{\partial t^2} \quad (9.7)$$

If the harmonic time dependence of frequency  $\omega$  is assumed, a solution to (9.7) can be written

$$p = p_0 \phi(x) \sin \omega t \quad (9.8)$$

where  $\phi(x)$  is given by

$$\phi(x) = \cos\left(\frac{\omega}{c} x\right) + j \sin\left(\frac{\omega}{c} x\right) \quad (9.9)$$

and  $p_0$  is a constant.

In the absence of dissipation, the particle velocity  $u$  will be zero at the boundaries  $x = 0$  and  $L$ . Introducing the first of these conditions, Equation 9.8 can be written

$$p = p_0 \cos\left(\frac{\omega}{c} x\right) \sin \omega t \quad (9.10)$$

An extra boundary condition is that the pressure  $p$  is a maximum at  $x = 0$  and  $L$ .

$$\text{Thus} \quad \cos\left(\frac{\omega}{c} L\right) = 1$$

$$\therefore \quad \frac{\omega}{c} L = n\pi, \quad n = 0, 1, 2, \dots$$

$$\text{or} \quad f_n = \frac{nc}{2L} \quad (9.11)$$

$$\text{Thus } \cos(k_x L_x) \cos(k_y L_y) \cos(k_z L_z) = 1.$$

The maximum values are obtained when  $x=L_x$ ,  $y=L_y$  and  $z=L_z$ . Hence

$$\left. \begin{aligned} k_x L_x &= n_x \pi \\ k_y L_y &= n_y \pi \\ k_z L_z &= n_z \pi \end{aligned} \right\} \begin{aligned} n_x &= 0, 1, 2 \dots \\ n_y &= 0, 1, 2 \dots \\ n_z &= 0, 1, 2 \dots \end{aligned} \quad (9.22)$$

If these values are then substituted in (9.22) it is found that the characteristic frequencies of a rectangular room are given by

$$f = \frac{c}{2} \left[ \left( \frac{n_x}{L_x} \right)^2 + \left( \frac{n_y}{L_y} \right)^2 + \left( \frac{n_z}{L_z} \right)^2 \right]^{1/2} \quad (9.23)$$

For example, the first few modes of two rooms of size 30' x 20' x 15' and 15' x 13' x 10' are:

$n_x$	$n_y$	$n_z$	$f_n$ Hz	$f_n$ Hz
0	0	0	0	0
1	0	0	18.3	37.3
0	1	0	27.5	43.1
0	0	1	37.3	56.0
1	1	0	33.0	57.0
1	0	1	41.7	67.3
0	1	1	46.6	70.7
1	1	1	50.3	80.0

There are thus three types of modes,  $(j, 0, 0)$ ,  $(j, k, 0)$  and  $(j, k, l)$  where  $j, k$ , and  $l$  are any integers, called respectively the axial, tangential and oblique modes. In some cases, the dimensions of an enclosure are such that standing waves having different values of  $(j, k, l)$  give rise to the same frequency. These are called degenerate modes and at these frequencies the room responds strongly to excitation. The situation is worst in a cubical room where even sixfold degeneracies can be obtained at the low frequencies. This must obviously be avoided, if an even distribution of modes is required, by correctly proportioning the sides of the enclosure. This can be achieved by making the enclosure

with sides of length  $L_x$ ,  $qL_x$  and  $\frac{L_x}{q}$  where  $q$  is a number such as  $\sqrt{2}$ , or even better  $3\sqrt{5}$ . This technique is employed in the design of reverberant test chambers for acoustic tests of structures and equipment.

Modal Density

One of the most important quantities that can be calculated using wave acoustics is the spacing of the characteristic frequencies or the modal density (defined as the number of modes per cycle). This can be achieved by examination of Equation 9.23 where it can be seen that  $k$  can be considered as a vector having components  $k_x$ ,  $k_y$  and  $k_z$ . Transforming from  $k$  to frequency space gives the components as

$$\frac{n_x c}{2L_x}, \frac{n_y c}{2L_y}, \text{ and } \frac{n_z c}{2L_z}$$

the length of the vector being the frequency of the mode and the direction being that required to sustain the mode. A lattice can therefore be constructed in frequency space with lattice spacings of

$$\frac{c}{2L_x}, \frac{c}{2L_y} \text{ and } \frac{c}{2L_z}$$

as shown in Figure 9.15. The volume of frequency space

occupied by one mode is therefore  $\frac{c^3}{8V}$  where  $V = L_x \cdot L_y \cdot L_z$  is the total volume of the enclosure (in real space), and the number of modes having frequencies less than  $f$  is given by

$$\begin{aligned} N &\doteq \frac{\text{volume of } 1/8 \text{ of a sphere of radius } f}{\text{volume occupied by one mode}} \\ &\doteq \frac{\pi f^3}{6} \cdot \frac{8V}{c^3} \doteq \frac{4\pi V}{3c^3} f^3 \quad (9.24) \end{aligned}$$

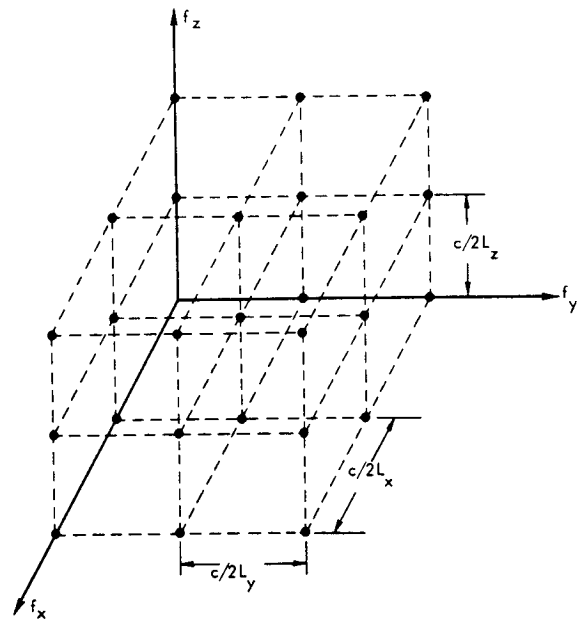


FIGURE 9.15 Characteristic Points in Frequency Space (From Reference 9.5)

The result of a standing wave in the form given by Equation 9.10 is to limit the values of  $\left(\frac{\omega}{c}\right)$  and hence frequency. Equation 9.11 thus gives the characteristic frequencies corresponding to the allowed normal modes of vibration. These frequencies, as can be seen, are equally spaced, the fundamental ( $n = 1$ ) being determined by the length of the tube. If the tube is short, then the spacing between the modes (i.e.,  $\frac{c}{2L}$ ) is large; if it is long, the fundamental frequency is low and the spacing small. The next step is to replace the rigid terminations with an absorbent material, thus damping the standing wave. This can be incorporated by assuming a time variation of  $(\omega - j\beta)t$ , where  $\beta$  is the damping constant, showing that the amplitude decreased with time. In this case, the pressure maximum may not lie at  $x = 0$  and  $L_x$ , so a phase constant  $\phi$  has also to be included. With these modifications, Equation 9.10 becomes

$$p = p_o \cosh \left[ \left( \frac{\beta - j\omega}{c} \right) x + \phi \right] \sin \omega t \quad (9.12)$$

However, no mention has yet been made of the absorption coefficient of the terminations, only of the decay constant  $\beta$ . It is found, in fact, that it is more convenient to consider the energy lost in terms of the acoustic impedance of the surfaces, defined as the complex ratio of sound pressure to the normal velocity into the surface.

Since  $u = -\frac{1}{\rho_o} \int \frac{dp}{dx} dt$ , it can be shown that the normal acoustical impedance  $z$  is given by

$$z = \rho_o \coth \left[ \left( \frac{\beta - j\omega}{c} \right) x + \phi \right] \quad (9.13)$$

which may have both real and imaginary parts.

In the one-dimensional case being considered, the term absorption coefficient has little meaning (as will be seen later in this chapter). It is also not a suitable property to use because it is a value averaged over all angles of incidence. For the one-dimensional model the energy impinges only normally on the surfaces at the end of the tube.

If the real part of the impedance is much greater than the imaginary part, then the characteristic frequency will be the same as in the undamped case. If it is not, they will differ slightly.

The one-dimensional standing wave case, considered above, leads to a method of measuring the normal acoustic impedance and the absorption coefficient of a material. If the incident and reflected sound pressure at the surface of the sample placed in a tube are denoted by  $p_i$  and  $p_r$ , and the respective normal velocities  $u_i$  and  $u_r$  then the following relationships can be written:

$$p_i + p_r = p = \text{total pressure at the surface of the sample} \quad (9.14)$$

$$u_i - u_r = u = \text{the resultant particle velocity at the surface} \quad (9.15)$$

$$u_i = \frac{p_i}{\rho_o c} \quad \text{and} \quad u_r = \frac{p_r}{\rho_o c} \quad (9.16)$$

and

$$z = \frac{p}{u} = \text{impedance at the surface} \quad (9.17)$$

then

$$r = \frac{p_r}{p_i} = \frac{z - \rho_o c}{z + \rho_o c} \quad (9.18)$$

The ratio of maximum and minimum values of pressure in the standing wave is

$$\frac{p_i + p_r}{p_i - p_r} = \text{SWR} = \frac{1+r}{1-r} \quad (9.19)$$

Thus, if the SWR in the tube is measured,  $z$  can be calculated. Also, since  $\alpha = 1 - r^2$ , the absorption coefficient can also be obtained. However, the value is for normal incidence only, and should be used with reservation in any design.

#### 9.2.4.2 Three-Dimensional Enclosure

In order that the basic knowledge from the previous section can be applied, it is now necessary to extend the treatment to three-dimensions. In this case, the solution of the general wave equation has the form

$$p = p_o \phi(x) \phi(y) \phi(z) \sin \omega t \quad (9.20)$$

where  $\phi(x)$ ,  $\phi(y)$  and  $\phi(z)$  are the mode shapes in the  $x$ ,  $y$  and  $z$  directions, and the boundaries are assumed to be rigid. Inserting the boundary conditions, as before, produces the standing wave equation.

$$p = p_o \cos(k_x x) \cos(k_y y) \cos(k_z z) \sin \omega t \quad (9.21)$$

where  $k_x$ ,  $k_y$  and  $k_z$  are the components of  $\left(\frac{\omega}{c}\right)$  in the  $x$ ,  $y$  and  $z$  directions. As before,  $p$  is a maximum at the boundaries  $x = 0$  and  $L_x$ ,  $y = 0$  and  $L_y$ ,  $z = 0$  and  $L_z$ .

This result is not strictly correct because a part of the volume occupied by the lattice points in the  $x$ - $y$ ,  $y$ - $z$  and  $x$ - $z$  planes lies outside the octant  $\frac{\pi f^3}{6}$  which has not been included. A more exact expression is (Reference 9.6).

$$N = \left(\frac{4\pi V}{3c^3}\right) f^3 + \left(\frac{\pi A}{4c^2}\right) f^2 + \left(\frac{L}{8c}\right) f \quad (9.25)$$

where

$$V = L_x L_y L_z$$

$$A = 2(L_x L_y + L_y L_z + L_x L_z) \text{ - the total surface area}$$

$$L = 4(L_x + L_y + L_z) \text{ - the sum of the length of the sides}$$

The number of modes  $dN$  in a frequency band of width  $df$  is given by

$$dN = \left[ \left(\frac{4\pi V}{c^3}\right) f^2 + \left(\frac{\pi A}{2c^2}\right) f + \left(\frac{L}{8c}\right) df \right] \quad (9.26)$$

$$\text{or } dN = G(f) df$$

where  $G(f)$  is the modal density of the enclosure. It can be seen from Equation 9.26 that  $G(f)$  increases approximately with the square of the frequency as opposed to the one-dimensional case where it remains constant.

#### Modal Response

It can be shown (Reference 9.6) that the expression for the mean square pressure in an enclosure can be written

$$p_{rms}^2 = \frac{p_o^2 c^4 Q_o^2}{2V^2} \sum_N \frac{E_n(s)}{\left[1 - \left(\frac{\omega_n}{\omega}\right)^2\right]^2 + \left[2 \frac{\omega_n}{\omega} \beta_n\right]^2} \quad (9.27)$$

where  $Q_o$  is the strength of the source,  $V$  is the volume of the enclosure,  $\beta_n$  the damping constant for the  $n^{\text{th}}$  mode, and  $E_n(s)$  is a function of the position of the source of sound.

Examination of Equation 9.13 shows that the introduction of a resistive term into the impedance  $z$  of a material results in energy being dissipated and a gradual decrease

in amplitude ( $e^{-\beta t}$ ) of the standing wave. From the fundamentals of vibration (Reference 9.6) it can be shown that the energy damping constant  $2\beta$  (since  $\beta$  is the amplitude damping constant) is given by

$$2\beta = \frac{\text{power dissipated per cycle}}{\text{power stored}}$$

The power can only be dissipated at the surfaces, so if the resistive part of the specific wall impedance is  $r$ , and the sound pressure  $p$ ,

$$2\beta \sim \frac{\text{average } \frac{p^2}{r} \text{ over the surfaces}}{\text{average } p^2 \text{ over the volume}}$$

where  $p^2$  is taken from Equation 9.21.

Thus if the average of  $\frac{p^2}{r}$  over the surfaces is large, the damping constant will be large, corresponding to a high absorption. In order to obtain a large average value, it is necessary to place the absorption material, of resistance  $r$  at positions where  $p^2$  is large i.e., in the corners, in order to obtain a high damping constant. It can also be seen, that it is inadvisable to place an absorbent material only at positions where the pressure is maximum for one particular mode, since it will be less effective in damping other modes. In order to obtain adequate damping of all modes, it is necessary to scatter the absorption material over all the surfaces.

If  $\beta_n$  is small, it can be seen that only when  $\omega$  is very close to  $\omega_n$  is the coefficient of any importance. In other words, the only allowed frequencies are those lying close to the normal modes. The situation is changed when  $k_n$  is not small, and a larger range of frequencies is allowed.

At low frequencies where the spacing between normal modes ( $\omega_{n+1} - \omega_n$ ) is large, there will be large regions where no coefficient is large. For high frequencies, there are several modes close together so that they can all be excited by a single frequency source. In this case, the pressure will be more or less constant throughout the room. It can be shown (Reference 9.6) that the bandwidth (defined as the frequency range between points 3 dB below the maximum value) of the resonance curve for the sound pressure is

$$\Delta f = \frac{c\alpha}{8\pi V} \text{ Hz}$$

where  $a$  is the absorption constant for the mode considered. If the condition for a uniform room response (and hence a diffuse sound field) is that neighboring modes intersect at the -3 dB point, then the frequency at which this occurs is given by

$$\frac{ca}{8\pi V} = \frac{1}{G(f)}$$

where  $G(f)$  is the modal density. Using the approximate form for  $G(f)$  gives the result that above a frequency given by

$$f_{lim} = c \sqrt{\frac{2}{a}} \text{ Hz} \tag{9.28}$$

the room response can be considered to be uniform and the behavior can be treated by using statistical methods. If two rooms of different volumes are considered, each having concrete floors, brick walls and tiled ceiling, this frequency turns out to be

Room 1 (30' x 20' x 15')  $f_{lim} = 86 \text{ Hz}$

Room 2 (15' x 13' x 10')  $f_{lim} = 158 \text{ Hz}$

Below this limiting frequency, the sound level in an enclosure has to be determined using Equations 9.12, 9.13 and 9.27. If the impedance of the walls are known, together with the phase constant  $\phi$ , then the decay constant  $\beta$  can be determined. The sound pressure  $p$  can then be determined.

To summarize, the statistical approach can only be employed when the sound energy distribution is uniform and independent of the boundary conditions. These conditions are approximately obeyed at high frequencies and in irregularly shaped rooms. In all other situations, the wave analysis approach should be employed.

9.2.5 STATISTICAL APPROACH

A statistical approach to the problem of sound waves in enclosures is possible if the sound field can be considered to be diffuse. The definition of a diffuse field is that the sound pressure, and hence the energy density, is constant throughout the volume and that all directions of propagation are equally probable. The lower frequency limit for the application of this method has been discussed in the last section. It is of course necessary to assume that the source of sound consists of a band of frequencies; otherwise standing wave patterns will predominate. Under these conditions, the relationship between the intensity  $I$  at any point in the room and the energy density  $E$  is

$$I = \frac{1}{4} c E \tag{9.29}$$

At the surfaces therefore, the energy absorbed is  $\alpha I$  per unit area, where  $\alpha$  is the random incidence absorption coefficient and

$$\alpha = \frac{\int_0^{\pi/2} \alpha(\theta) \sin 2\theta d\theta}{\int_0^{\pi/2} \sin 2\theta d\theta}$$

or

$$\alpha = \int_0^{\pi/2} \alpha(\theta) \sin 2\theta d\theta \tag{9.30}$$

where  $\alpha(\theta)$  is the absorption coefficient for angle of incidence  $\theta$ .

The total energy absorbed per unit time is therefore

$$I \iint_S \alpha(S) dS$$

If  $\alpha(S)$  is constant, this reduces to  $I\alpha S$  where  $S$  is the total surface area of the enclosure. This is usually written as  $Ia$  where  $a = \alpha S$  is the total amount of absorption present. The quantity  $a$  has the dimensions of an area, and if the area is in square feet, the unit of  $a$  is called a "sabin."

9.2.5.1 Sabine Equations

With these facts, an equation for the energy in the enclosure having a source of power  $W$  can be set up as follows:

$$W(t) = \alpha I(t) + \frac{d}{dt} (VE(t))$$

or, using 9.29

$$W(t) = \alpha I(t) + \frac{4V}{c} \frac{dI(t)}{dt} \tag{9.31}$$

Introducing conditions that

$$\left. \begin{aligned} W(t) &= W & t < 0 \\ &= 0 & t > 0 \end{aligned} \right\}$$

results in the expression for the decay of the steady-state sound field

$$I(t) = I_o \exp\left(-\frac{\alpha c t}{4V}\right) \quad (9.32)$$

where  $I_o = \frac{W}{a}$

The steady-state intensity is thus dependent on the room absorption, as would be expected, but not on the volume or shape of the enclosure.

Since  $E = \frac{p^2}{\rho c^2}$  for a diffuse sound field as well as a plane wave, and using 9.29, the steady-state mean square pressure  $p_r^2$  can be written

$$p_r^2 = \frac{4W \rho_o c}{a} \quad (9.33)$$

This then is a simple expression for the mean square sound pressure (constant throughout the enclosure) at any point.

### 9.2.5.2 Reverberation Time

Equation 9.32 shows one method of measuring the amount of absorption in a room, as long as the power output of the source is known. A much more convenient method, however, is to use Equation 9.30, which can be written

$$\frac{I(t)}{I_o} = e^{-\frac{\alpha c t}{4V}}$$

or  $10 \log \left[ \frac{I(t)}{I_o} \right] = -\frac{4.34 \alpha c t}{4V}$

A measure of the decay rate is taken as the time for the intensity to decrease by 60 dB from the initial steady-state value. This time is called the reverberation time and is given by

$$T = \frac{27.7 V}{\alpha c} \text{ seconds}$$

If the lengths are measured in feet, then the familiar Sabine equation is obtained

$$T = \frac{0.049 V}{a} \quad (9.34)$$

For example, if the same enclosures as before (Section 9.2.3.2) are considered with absorption coefficients given as

	100 Hz	1000 Hz
Concrete floor	0.01	0.02
Brick walls	0.02	0.04
Tiled ceiling	0.50	0.80

the reverberation times of two rooms are

	100 Hz	1000 Hz
Room 1 (30'x 20'x 15')	1.3 secs	0.79 secs
Room 2 (15'x 13'x 10')	0.86 secs	0.52 secs

The absorption  $a (= \alpha S)$  can be calculated by measuring the slope of the decay curve and using 9.34. If the walls are covered with different amounts of absorption then

$$a = \sum \alpha_i S_i \quad (9.35)$$

Thus, if the sound source level fluctuates slowly, the sound pressure level will follow closely; if it changes rapidly (i.e., in a time less than the reverberation time), the pressure level will remain reasonably constant and not follow the fluctuations. This is of importance in speech communication where the fluctuations are rapid, and supports the everyday experience that one has to speak more slowly and distinctly in a reverberant space. A method of improving the intelligibility is to reduce the reverberation time by adding extra absorption to the enclosure, the result of which is also to reduce the sound pressure produced by a given sound source level.

In the case of a conference room where good speech communication is essential, the reverberation time should not be greater than 1 second at the low frequencies, and preferably slightly less at high frequencies. However, T should not be too low, since this implies high absorption and hence a low sound level in the enclosure, making communication difficult over large distances.

### Sound Pressure Distribution

If a source of sound is inside an enclosure, it has been shown that the reverberant sound pressure is given by Equation 9.33. However, in the vicinity of the source, but beyond the near field, the intensity decreases according to the inverse-square law,

$$I_x = \frac{W}{4\pi x^2} = \frac{p_x^2}{\rho_o c}$$

Hence

$$p_x^2 = \frac{W \rho_o c}{4 \pi x^2} \quad (9.36)$$

At some distance  $r$  this pressure, in what is termed the direct field, will equal that in the reverberant field.

In other words,

$$\frac{W \rho_o c}{4 \pi r^2} = \frac{4W \rho_o c}{a}$$

This equality occurs at a distance given by

$$r = \sqrt{\frac{a}{16\pi}} \quad (9.37)$$

which increases with the absorption  $a$  and thus with frequency.

For example, in the rooms considered in Section 9.2.3.2, the values of  $r$  at which the direct and reverberant sound intensities are equal are given by

	100 Hz	1000 Hz
Room 1 (30'x 20'x 15')	2.6 ft	3.3 ft
Room 2 (15'x 10'x 13')	1.5 ft	1.9 ft

In order to compute the pressure at any position, it should first be ascertained whether the position is in the direct or reverberant field before using the appropriate expression 9.33 or 9.36.

#### Eyring's Expression

Examination of Equation 9.34 shows that the correct result is obtained when  $a \rightarrow 0$ , i.e.,  $T \rightarrow \infty$ , but that the reverberation time is finite when the absorption coefficient for all the surfaces is unity. This is because the sound field in an enclosure having highly absorbent surfaces is not diffuse as was assumed in the derivation of Equation 9.34. An approach to the theory of highly absorbent enclosures has been made by Eyring (Reference 9.7) by considering the image sources instead of the surface reflections. The resultant expression is identical to the previous one except for the value of  $a$ , which is then given by

$$a = -S \log_e (1 - \bar{\alpha}) \quad (9.38)$$

where  $S$  is the total surface area of the enclosure and  $\bar{\alpha}$  is the average absorption coefficient

$$\bar{\alpha} = \frac{\sum \alpha_i S_i}{\sum S_i} \quad (9.39)$$

It can be shown that 9.38 reduces to the same value as 9.35 when  $\bar{\alpha}$  is small, and gives the correct value of  $T$  when  $\bar{\alpha} = 1$ . However, the treatment only gives the correct result when the absorption coefficients of the surfaces are of similar magnitude.

This expression has the same limitations as the previous one, that is only strictly true for low absorption, since the sound field becomes less diffuse as the absorption is increased.

#### 9.2.5.3 Air Absorption

So far, only absorption at the boundaries of an enclosure have been discussed. While this is sufficient in small spaces, in large volumes, atmospheric absorption must be accounted for. This absorption loss is due primarily to molecular relaxation in moist air and is thoroughly treated in Chapter 7.

The intensity of a plane wave will decrease during its passage through the atmosphere by an amount given by

$$I(x) = I(0) e^{-m x} \quad (9.40)$$

where  $m$  is the attenuation constant of the medium and depends mainly on the humidity and the frequency. Values of this constant are shown in Figure 7.11 in dB per 1000 ft. In order to convert these figures to the units for  $m$  (1/ft), multiply dB/1000 ft. by  $2.3 \times 10^{-4}$ , (See Table 12.10).

Incorporating this attenuation in Equation 9.3 gives

$$I(r) = I_o \exp \left[ - \left( \frac{a}{4V} + m \right) c t \right] \quad (9.41)$$

and the reverberation time is

$$T = \frac{0.049 V}{a + 4 m V} \quad (9.42)$$

It can be seen that the effect of air absorption in an enclosure is only of importance when the volume is large.

#### Relationship Between Impedance and Absorption Coefficient

If the damped standing wave Equation 9.12 is extended to three-dimensions, then it can be shown (Reference 9.6)



that the decay constant, in say the x-direction,  $\beta_x$  is approximately for  $r_n \gg 1$

$$\beta_x \doteq \frac{2c}{r_n L_x}$$

where  $r$  is the real part of the normal acoustic impedance. Thus, the decay of intensity in an enclosure can be written

$$\begin{aligned} I &= I_o e^{-2\beta t} \\ &= I_o e^{-\frac{4ct}{r_n L_x}} \end{aligned} \tag{9.43}$$

the factor of 2 being introduced since  $\beta$  is the amplitude decay constant. Comparing this with Equation 9.30 shows that

$$\frac{4c}{r_n L_x} = \frac{ac}{4V}$$

or

$$\begin{aligned} r_n &= \frac{16V}{aL_x} \\ &= \frac{16L_y L_z}{a} \end{aligned}$$

or since  $a = 2\alpha S_{yz} = 2\alpha L_y L_z$

$$r_n \approx \frac{8}{\alpha} \tag{9.44}$$

which is the relationship between the normal acoustic impedance and the equivalent absorption coefficient. However, the same conditions apply to 9.44 as to Sabine's equation; that they are only correct for low absorption, i.e., high values of  $r_n$ .

### 9.3 TRANSMISSION LOSS

The preceding section has dealt with the methods of reducing the level of noise inside an enclosure, but in noise control it is also necessary to prevent external noise from entering the enclosure. In this section, the emphasis is wholly on the transmission of sound through walls. First of all, it must be appreciated that there are several different paths by which sound waves are transmitted from the outside to the interior of a structure, some of which are shown in Figure 9.16.

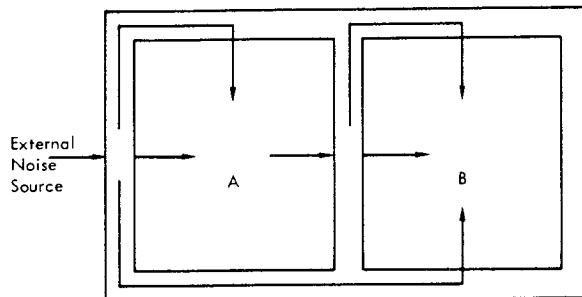


FIGURE 9.16 Paths by which Transmission of Sound Occurs Between Two Rooms

The sound level in the rooms is usually made up of contributions from all these paths, the relative amounts depending on the structure, and the frequency. Paths of sound between rooms A and B other than the direct one through the common wall are termed flanking paths, which will be discussed later in the chapter.

Basically, the mechanism of sound transmission is that the incident waves excite the wall into vibration, causing energy to be radiated on the other side. To a certain extent, the amount of radiation depends on the mass of the wall except under the special circumstances to be discussed. Some of the incident energy is reflected (in most cases the majority), some absorbed and the remainder transmitted, therefore, Equation (9.1) is still applicable.

$$E_i = E_r + E_t + E_a$$

or

$$\tau = 1 - r^2 - \alpha \tag{9.45}$$

#### 9.3.2 DEFINITIONS

Before beginning the discussion on methods of achieving high transmission loss, terms used and definitions must be explained. The factor  $\tau$  in Equation (9.45) is the fraction of the incident energy that is transmitted, where  $\tau$  is called the transmission coefficient or transmissivity.

$$\tau = \left( \frac{P_t}{P_i} \right)^2 \tag{9.46}$$

Since this is always less than unity, it is usual to use the term  $1/\tau$  in the expression for transmission loss, defined as transmission loss or insulation =

$$TL = 10 \log \frac{1}{\tau} \tag{9.47}$$

The value of  $\tau$  in this expression is of course a function of  $\theta$ . To account for random incidence, the value of  $\tau$  used must be averaged over all angles of incidence as for the absorption coefficient (see Equation 9.30).

$$\tau_{av} = \int_0^{\pi/2} \tau(\theta) \sin 2\theta \, d\theta \quad (9.48)$$

Also, as laboratory measurements of TL are usually carried out using bands of random noise one-third of an octave wide, then (Equation 9.48) must be averaged over frequency,

$$\langle \tau_{av} \rangle = \frac{1}{\omega_2 - \omega_1} \int_{\omega_1}^{\omega_2} \int_0^{\pi/2} \tau(\theta) \sin 2\theta \, d\theta \cdot d\omega \quad (9.49)$$

where

$$\omega_2 = 1.12 \omega_0$$

$$\omega_1 = 0.89 \omega_0$$

and  $\omega_0$  is the center of the appropriate one-third octave band.

### 9.3.3 MEASUREMENT OF TRANSMISSION LOSS

In the standard laboratory procedure for measuring the transmission loss, the panel or structure of interest is situated in the common wall between two reverberant chambers, as shown in Figure 9.17. The source of sound is then placed in one chamber and the measuring system in the other. In terms of the energy density therefore, the intensity  $I_1$  in room 1

$$I_1 = \frac{E_1 c}{4} \quad (\text{See 9.29})$$

Thus, the power flowing through the panel is

$$\begin{aligned} W &= \tau I_1 S \\ &= \tau \frac{E_1 c S}{4} \end{aligned} \quad (9.50)$$

where  $S$  is the area of the panel. The intensity in room 2 due to this influx of energy is

$$\begin{aligned} I_2 &= \frac{W}{a} = \frac{\tau E_1 c S}{4a} \quad (\text{see 9.32}) \\ &= \frac{E_2 c}{4} \end{aligned}$$

where  $a$  is the total amount of absorption in room 2.

Hence,

$$\tau = \frac{E_2}{E_1} \cdot \frac{a}{S} \quad (9.51)$$

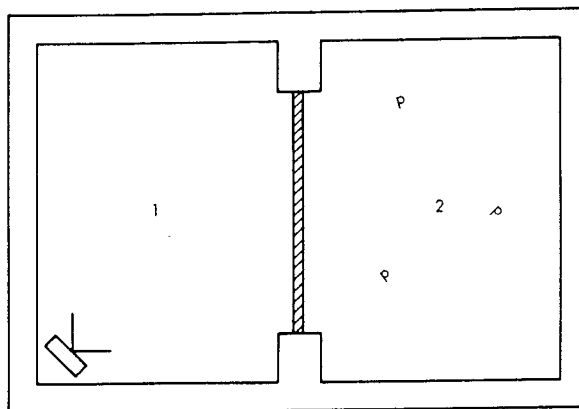


FIGURE 9.17 Transmission Loss Measurement Set-Up

The transmission loss according to (Equation 9.47) is

$$TL = 10 \log \left( \frac{E_1}{E_2} \right) + 10 \log \left( \frac{S}{a} \right) \quad (9.52)$$

Since the energy density is proportional to the square of the sound pressure  $p$ ,

$$\begin{aligned} TL &= 20 \log \frac{P_1}{P_2} + 10 \log \left( \frac{S}{a} \right) \\ &= SPL_1 - SPL_2 + 10 \log \left( \frac{S}{a} \right) \end{aligned} \quad (9.53)$$

where  $SPL_1$  and  $SPL_2$  are the respective sound pressure levels in room 1 and 2. These levels, together with the receiving room absorption and the panel area, are thus required to measure the transmission loss.

The measurements are made using one-third octave bands of random noise having center frequencies from 125 Hz to 4000 Hz. In some cases the 100 Hz band is also included. There is also a single figure rating called the sound transmission class (STC) that can be used in comparing different structures in a similar manner to the NRC figure. However, this rating is only used for internal walls because it is based on the subjective impressions of the sound insulation provided against the normal sounds experienced internally. For external walls, where the sound is due to such sources as rockets and airplanes, it is necessary to make use of the more detailed information. The determination of the STC figure is more complicated than for the NRC and is fully described in Reference 9.9. A comprehensive list of transmission loss charts for common materials is given in Chapter 12.

9.3.4 TRANSMISSION LOSS FOR A STRUCTURE

To determine a general expression for the transmission loss of a panel, it is assumed that a plane wave is incident normally on an infinite panel as shown in Figure 9.18. If the normal impedance  $z$  of the panel is defined as the ratio of net pressure acting on the panel to the panel velocity  $u$ , the equation of motion for the panel is then (assuming  $x = 0$  at the panel and the thickness is negligible)

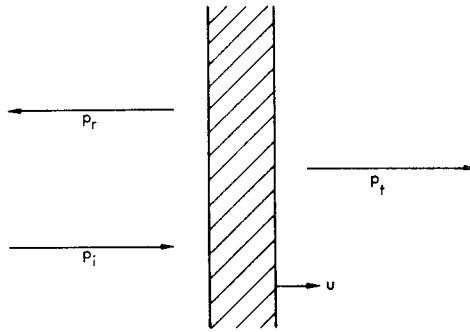


FIGURE 9.18 Transmission of Sound through a Single Panel

$$(p_i + p_r) - p_r = zu = \frac{z p_t}{\rho_o c} \quad (9.54)$$

Since

$$p = \rho_o c u \text{ for a plane wave}$$

or

$$p_i + p_r = \left[ 1 + \frac{z}{\rho_o c} \right] p_t$$

Since the medium always remains in contact with the panel

$$u_i - u_r = u$$

or

$$p_i - p_r = p_t \left( \frac{p}{u} = \rho_o c \right) \quad (9.55)$$

Combining (9.54) and (9.55) results in

$$\tau = \left( \frac{p_t}{p_i} \right)^2 = \left[ 1 + \frac{z}{2 \rho_o c} \right]^{-2} \quad (9.56)$$

and

$$TL = 20 \log \left[ 1 + \frac{z}{2 \rho_o c} \right] \quad (9.57)$$

This is then the general expression for a single, infinite panel of impedance  $z$ . If the sound wave is incident at an angle  $\theta$  with the normal, (9.57) becomes

$$TL_\theta = 20 \log \left[ 1 + \frac{z \cos \theta}{2 \rho_o c} \right] \quad (9.58)$$

remembering that  $z$  possibly is a function of  $\theta$ .

This expression shows that the transmission loss is zero for grazing incidence ( $\theta = 90^\circ$ ). However, at this angle, there is no normal component of the plate velocity and hence no transmission. It is also found in a reverberation room that there is little sound energy incident at grazing angles above approximately  $78^\circ$ . Therefore, the expression (9.48) for the mean transmissivity should read

$$\tau_{av} = \frac{\int_0^{78^\circ} \tau(\theta) \sin 2\theta \, d\theta}{\int_0^{78^\circ} \sin 2\theta \, d\theta} \quad (9.59)$$

9.3.5 INFINITE LIMP WALL

If the panel mentioned in the previous section has a low bending stiffness, i.e., it is limp, then the impedance is due entirely to its inertia or mass, assuming it to be a loss-free structure. Thus, for a panel having a mass  $m$  per unit area,

$$z_m = j \omega m \quad (9.60)$$

where

$$m = \rho h$$

$\rho$  = density of the panel

$h$  = thickness of the panel

and (9.50) becomes (with the angular dependence)

$$\tau_\theta = \left[ 1 + \frac{j \omega m \cos \theta}{2 \rho_o c} \right]^{-2} = \left[ 1 + \left( \frac{\omega m \cos \theta}{2 \rho_o c} \right)^2 \right]^{-1}$$

Thus for high values of mass and/or frequency

$$(TL)_\theta \approx 20 \log \left[ \frac{\omega m \cos \theta}{2 \rho_o c} \right]$$

The transmission loss (TL) can now be calculated under various limitations of angle  $\theta$ .

(a) For  $0^\circ < \theta < 90^\circ$  (random incidence)

$$(TL)_{\text{random}} \approx (TL)_0 - 10 \log [0.23 (TL)_0] \quad (9.61)$$

where

$$(TL)_0 \approx 20 \log \left[ \frac{\omega m}{2 \rho_0 c} \right] = \text{normal incidence transmission loss.}$$

(b) For  $0^\circ < \theta < 78^\circ$  (field incidence)

$$(TL)_{\text{field}} \approx (TL)_0 - 5 \text{ dB} \tag{9.62}$$

(c) For  $\theta = 45^\circ$

$$(TL)_{45^\circ} \approx 20 \log \left[ \frac{\omega m}{2 \rho_0 c} \right] - 3 \text{ dB}$$

$$= (TL)_0 - 3 \text{ dB} \tag{9.63}$$

For limp constructions, it is found that the field incidence curve (b) produces results that are in reasonable agreement with measurements and is recommended for initial approximation of TL.

Thus, the transmission loss increases linearly with frequency if plotted on a logarithmic scale, the slope being 6 dB per octave. Figure 9.19 shows this graphically for normal and random incidence and also for what is known as field incidence (0 to 78°). If the mass is increased the TL rises also, the rate being 6 dB per doubling of the mass. The latter curve is known as the "mass law", a term which is often mistakenly used for the increase with frequency.

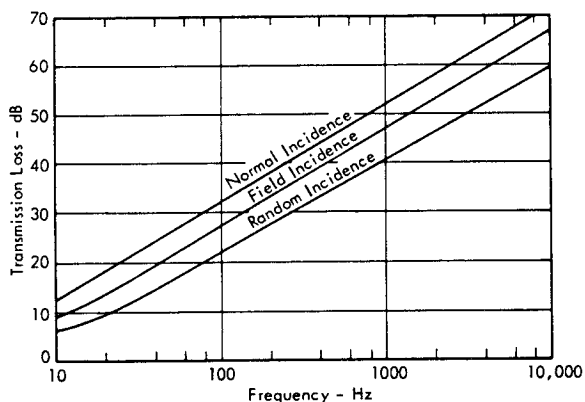


FIGURE 9.19 Theoretical Curves of Transmission Loss for a Limp Wall of Surface Weight 10 lb/ft<sup>2</sup>

However, for practical constructions that are finite and not limp, this simple theory predicts incorrect values at low and high frequencies.

Transmission Loss for Finite Panels

If the panel considered in the previous section is reduced to a finite size, and the boundaries are supported in some way, it will exhibit stiffness characteristics at the lower frequencies. First of all, the case of a stiff panel having negligible mass is considered. The impedance will be a pure reactance (in the absence of damping) given by

$$z_s = - \frac{k}{j \omega} \tag{9.64}$$

where k is the stiffness of the panel defined as the ratio of applied (static) pressure to average deflection. In this case, the transmission loss will be

$$TL_s = 10 \log \left[ 1 + \left( \frac{k \cos \theta}{2 \omega \rho_0 c} \right)^2 \right]$$

which for high stiffness or low frequencies approximates to

$$TL_s \approx 20 \log \left( \frac{k \cos \theta}{2 \omega \rho_0 c} \right) \tag{9.65}$$

Thus the TL due to stiffness alone, decreases with increasing frequency, the rate being 6 dB per octave. Combining (9.60) and (9.64) given an expression for the impedance over a wider range of frequencies

$$Z = j \omega m + \frac{k}{j \omega} \tag{9.66}$$

As with other systems having both mass and stiffness, a resonance occurs at a frequency given by

$$f_0 = \frac{1}{2\pi} \sqrt{\frac{k}{m}} \tag{9.67}$$

At this frequency, the impedance and hence the transmission loss of the panel is zero, assuming that there are no internal losses. The form of the curve is shown in Figure 9.20. The ordinate of the graph at the point where the two slopes meet is given by

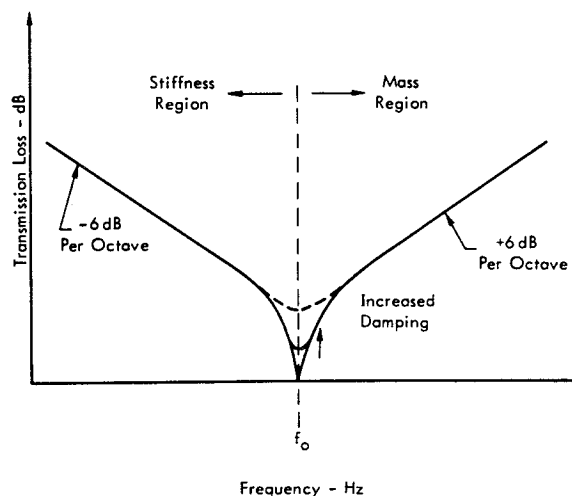


FIGURE 9.20 Showing the Form of the Transmission Loss Curve in the Stiffness and Mass Controlled Regions in Absence of Panel Resonances. The effect of Increased Damping is also Demonstrated.

$$20 \log \frac{\sqrt{mk} \cos \theta}{2 \rho_0 c}$$

In practice, however, very few materials in the form of a plate exhibit a transmission loss controlled by stiffness in the audible frequency range, but the effect can be extremely important and useful at frequencies below 50 Hz.

The Natural Frequencies of Finite Panels

If the panel is of finite size, then, the boundary conditions will produce a series of normal modes occurring at the characteristic frequencies of the plate in a similar manner to the tube and the enclosure. These frequencies for a simply supported panel are given by

$$f_{n,m} = 0.45 c_L' h \left[ \left(\frac{n}{a}\right)^2 + \left(\frac{m}{b}\right)^2 \right] \quad (9.68)$$

where  $c_L'$  is the velocity of longitudinal waves in the panel,  $h$  is the panel thickness,  $a$  and  $b$  the lateral dimensions and  $m, n = 0, 1, 2, 3, \dots$

In terms of the longitudinal wave velocity in a bar  $c_L$ ,

$$c_L' = \frac{c_L}{\sqrt{1 - \nu^2}}$$

where  $\nu$  is Poisson's ratio for the material of the plate.

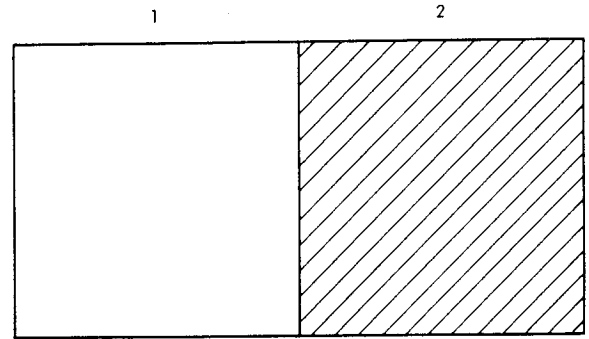
The lowest such frequency, other than  $n$  or  $m = 0$ , is

$$f_{1,1} = 0.45 c_L' h \left[ \frac{1}{a^2} + \frac{1}{b^2} \right]$$

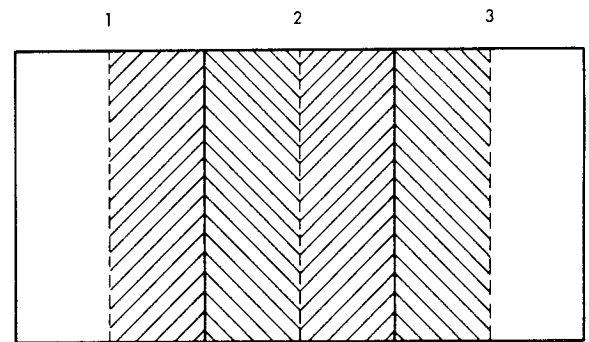
in which all parts of the panel vibrate in phase, but with different amplitudes.

In this case, the transmission loss is low as the radiated energy is high. Keeping  $m$  constant, the next highest mode is  $f_{2,0}$  in which the panel is effectively split into two halves, each half vibrating in anti-phase with the other, as shown in Figure 9.21(a). The result is to merely push the air from a high to a low pressure area and little radiation takes place, i.e., the radiation load is reactive. Figure 9.21(b), shows the modal system for  $f_{3,0}$  and it can be seen that the panel is now effectively split into three sections, the only radiation coming from the points on the panel near the edges. This effect is repeated for all modes, even numbers of either  $m$  or  $n$  canceling completely out, odd numbers of both  $m$  and  $n$  only partially canceling. If the panel is damped, then the modal shapes and the characteristic frequencies will be altered, the new values being quoted in Section 3.3.5.6.

From the above qualitative treatment, it follows that for  $m$  or  $n$  even, the radiation will be minimal and the transmission loss high. Conversely, for  $m$  and  $n$  odd, the transmission loss will be lower. The total effect therefore is as shown in Figure 9.22.



(a)



(b)

FIGURE 9.21 Modal Shapes of a Vibrating Plate. (a) the Two Halves of the Plate Vibrate in Antiphase and Cancellation is Complete (in Theory). Here the Plate is Divided into Three Sections, hence the only Radiated Energy is from the Edges.

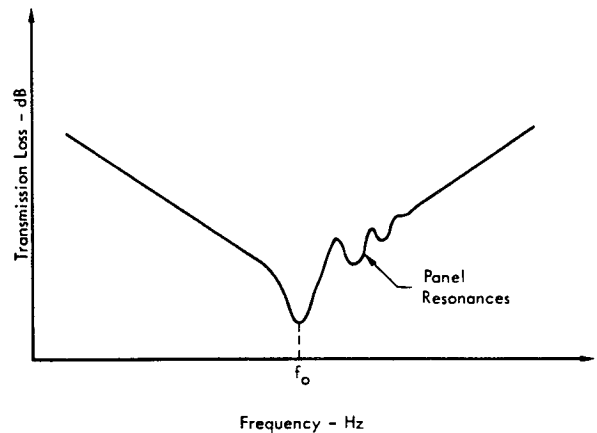


FIGURE 9.22 The Form of the Transmission Loss Curve for a Panel Exhibiting Natural Resonances

If there is any form of damping present, then the curve will move closer to the 6 dB/octave mass law line. In practice, there is always a certain degree of damping present in all building materials and only the first few resonances are of importance, except with small panels.

The Coincidence Effect

There is still one more effect of apparent stiffness which must be considered, known as the coincidence effect. This effect is due to the coincidence of the bending wave vibration and the airborne vibration in space and time. This effect is not associated with the normal modes of a panel.

Figure 9.23 shows an airborne wave incident at an angle  $\theta$  to the normal of a panel. The velocity of the wave in the direction of propagation is of course  $c$ . However, the velocity at which the wave normal travels along the panel (the trace velocity) is  $c/\sin\theta$ . This wave traveling at this speed produces a forced wave on the panel. The velocity  $c'_B$  of free bending waves on a panel is given by

$$c'_B = \sqrt[4]{\frac{D}{m}} \sqrt{\omega}$$

where  $D$  is the bending stiffness of the panel,  $m$  is the mass per unit area, and  $\omega = 2\pi f$ . Thus at low frequencies  $c'_B < c$ , at high frequencies  $c'_B > c$ . At some intermediate frequency, there will be a situation where  $c'_B = c/\sin\theta$ , or

$$\sqrt[4]{\frac{D}{m}} \sqrt{\omega} = \frac{c}{\sin \theta}$$

i.e.,

$$f = \frac{c^2}{2\pi \sin^2 \theta} \sqrt{\frac{m}{D}} \tag{9.69}$$

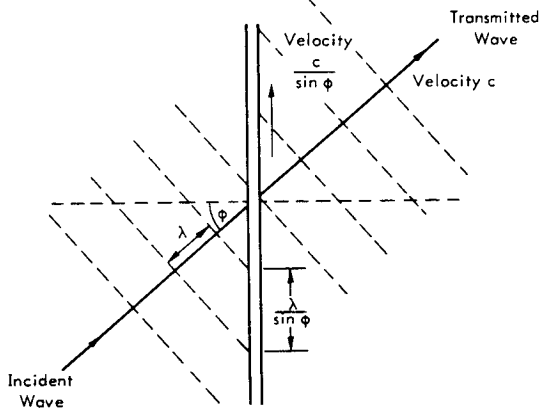


FIGURE 9.23 Schematic Diagram of a Plane Wave Incident at Angle  $\phi$  onto a Panel, Indicating the "Trace Velocity"  $\frac{c}{\sin \phi}$

At this frequency, a wave incident at an angle  $\theta$  will have a trace velocity equal to the free bending wave velocity on the panel. Energy is thus easily transferred from the wave to the panel and radiated on the other side, resulting in a low transmission loss. From (9.69), it can be seen that the lowest frequency at which this occurs is when  $\theta = 90^\circ$  i.e., grazing incidence, and is given by

$$f = f_c = \frac{c^2}{2\pi} \sqrt{\frac{m}{D}} \tag{9.70}$$

This frequency is known as the "critical frequency" being the result of the coincidence effect.

$$\left. \begin{aligned} \text{Since, } & m = \rho h \\ \text{and } & D = \frac{E h^3}{12(1-\nu^2)} \end{aligned} \right\} \tag{9.71}$$

- where
- $\rho$  = density of panel,
  - $h$  = thickness of panel,
  - $E$  = Young's modulus of the material constituting the panel,
  - $\nu$  = Poisson's ratio

Figure 9.24 shows the critical frequency of various materials as a function of the thickness.

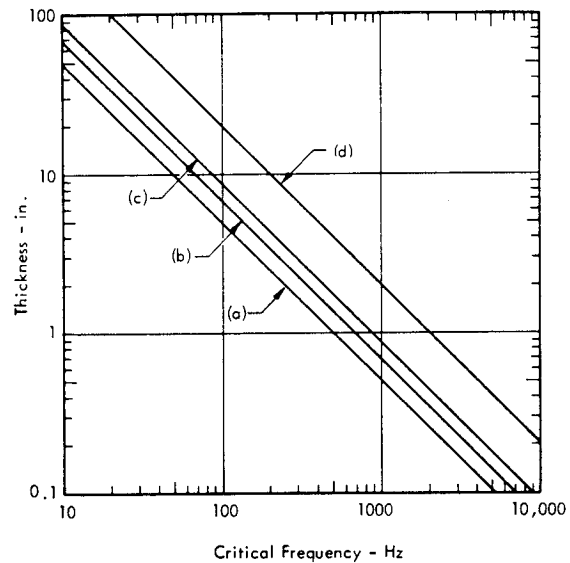


FIGURE 9.24 Graph Showing the Critical Frequency of Various Materials as a Function of Thickness. (a) Steel, (b) Concrete, (c) Plywood, (d) Porous Concrete (Data from Reference 9.15)

(9.70) can be written as

$$f_c = \frac{6.9 \times 10^5}{h} \sqrt{\frac{\rho(1-\sigma^2)}{E}}$$

when the parameters are measured in f.p.s., units. The critical frequency therefore depends on  $h^{-1}$ ,  $\rho^{1/2}$  and  $E^{-1/2}$ , the factor  $(1-\sigma^2)$  being approximately equal to unity for most materials.

Infinite Panels

It can be shown (Reference 9.10), or can be deduced from (9.69), that the impedance of an infinite panel undergoing bending vibrations in response to a plane wave incident at angle  $\theta$  is given by

$$z_B = j \left( \omega m - \frac{BK^4}{\omega} \sin^4 \theta \right) \quad (9.72)$$

where  $K = \omega/c$

in the absence of internal losses. This has to be used in conjunction with (9.58) and (9.49) to obtain a value for the mean transmission loss. The form of the result which holds for any solid material is shown in Figure 9.25. Above the critical frequency, the term in (9.72) relating to the bending stiffness rapidly assumes maximum importance and the mass term can be ignored. In practice, the slope in this region is approximately 9-10 dB per octave.

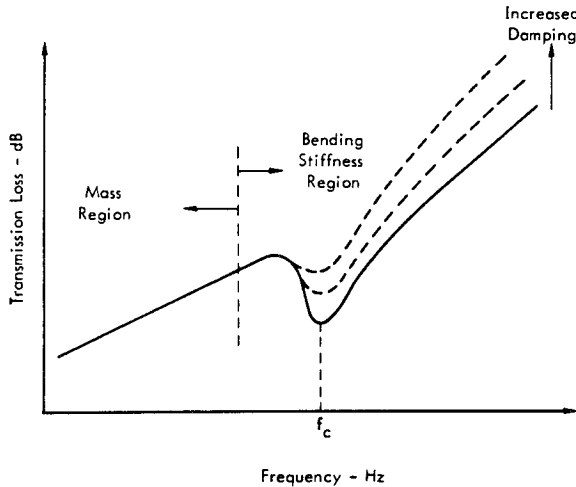


FIGURE 9.25 The Form of the Transmission Loss Curve in the Coincidence Region, with the Effect of Increasing the Internal Losses.

It has so far been assumed that the internal losses in the panel were negligible, whereas this is certainly not so with building materials in common use. The effect of damping can most easily be incorporated by assuming a complex Young's modulus  $E^*$  given by

$$E^* = E (1 + j \eta) \quad (9.73)$$

where  $\eta$  is the loss factor for the material of the panel if a time variation of  $e^{j\omega t}$  is assumed. This makes the bending stiffness complex

$$D^* = D (1 + j \eta) \quad (9.74)$$

and the bending impedance becomes

$$z_B = \eta \frac{\omega^3 D}{c^4} \sin^4 \theta + j \left\{ \omega m - \frac{\omega^3 D}{c^4} \sin^4 \theta \right\} \quad (9.75)$$

At coincidence, the impedance is not zero but given by

$$z_{B(\omega=\omega_c)} = \eta \frac{\omega_c^3 D}{c^4} \sin^4 \theta$$

where  $\omega_c = 2\pi f_c$ .

The effect of damping is also shown in Figure 9.25 where it can be seen the importance it assumes at and above the critical frequency.

The radiation from a panel depends greatly on the coincidence effect and whether the panel is considered to be infinite or finite. If a plane wave is incident at an angle  $\theta$  with the normal to an infinite panel, a forced bending wave will propagate along the panel to infinity. The radiation from the panel will be directed at an angle  $\theta$  to the normal on both sides of the panel as shown in Figure 9.26.

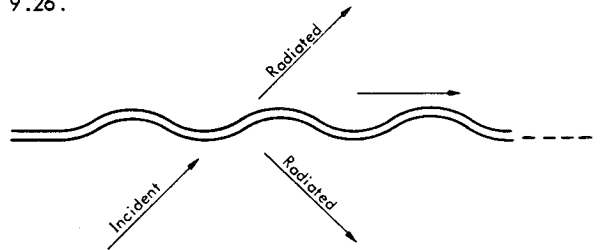


FIGURE 9.26 Radiation from an Infinite Panel

The amount of radiation will of course be greatest at the coincidence frequency corresponding to angle of incidence  $\theta$ , because the vibration amplitude will be greatest at this frequency.

Finite Panels

It has been shown (by Westphal) that the power  $W$  radiated by a panel undergoing free bending vibrations is proportional to the mean square velocity and to a term  $S$  called the radiation factor

$$W \sim u^2 S$$

where

$$S = \left[ 1 - \left( \frac{c}{c_T} \right)^2 \right]^{1/2} \quad (9.76)$$

and  $c_B^i$  is given by Equation 9.68 at frequencies such that  $c_B^i > c$ ; i.e., above the critical frequency, the value of  $S$  soon becomes unity and  $W \sim u^2$ . Below the critical frequency,  $c_B^i < c$  and  $S$  becomes imaginary, hence no power will be radiated. However, if internal damping of the panel is included, there will be an imaginary part to the velocity  $u$  and some energy will be radiated. This increases with increasing damping but decreases with decreasing frequency as can be seen from Equation 9.76.

If the panel is subjected to plane wave excitation at an angle  $\theta$  there will always be radiation on both sides of the panel also at angle  $\theta$ . However, above the coincidence frequency for this angle of incidence the free standing waves that are produced by reflection of the forced waves at the boundaries will radiate at an angle  $\phi$  given by

$$\phi = \sin^{-1} \frac{c}{c_B^i}$$

as shown in Figure 9.27.

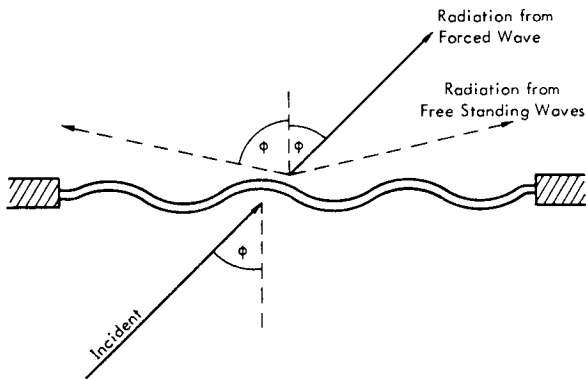


FIGURE 9.27 Radiation from a Finite Panel at a Frequency Less Than the Critical Frequency. For Clearness, only the Radiation on One Side of the Panel has been Shown.

The radiated waves coincide when  $\theta = \phi$  or  $\sin \theta = c/c_B^i$  from which the frequency can be calculated. In any case, however, a typical curve of transmission loss versus frequency for a solid, thin panel is shown in Figure 9.28. This curve is expanded and shifted along the frequency axis by an amount depending on the elastic parameters and dimensions of the panel. It is obviously a disadvantage for the coincidence effect to lie in the particular frequency range of interest in any practical application, so it should be arranged that it lies either above or below this range. In the former case, thin, dense and limp materials are required so that the mass law is obeyed, whereas, the reverse is required for the bending stiffness region to be applicable.

Figure 9.29 shows the transmission loss characteristics of three materials having different elastic parameters but the same lateral dimensions and weight. It can be seen that the resonance and coincidence effects vary considerably between the materials.

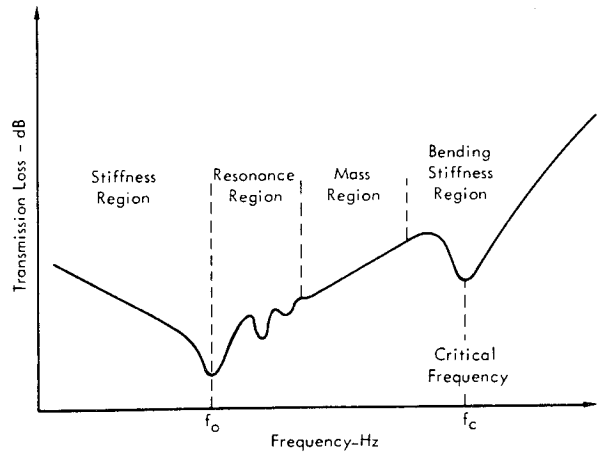


FIGURE 9.28 The Form of the Transmission Loss Curve for a Solid, Thin Panel Clamped at the Edges

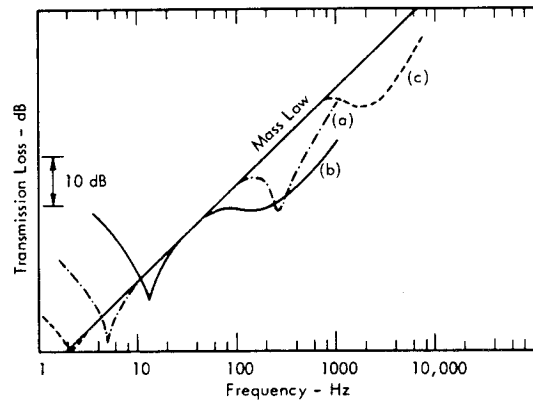


FIGURE 9.29 Theoretical Curves of Transmission Loss for Steel (1.8"), Concrete (6"), and Lead (1.2"). The mass/unit area is the same in each case, and the area is 10 ft by 20 ft. The natural resonances are excluded from this diagram.

### Double Walls

One of the most common ways of increasing the transmission loss is to add another single panel a certain distance away from the original. The total mass of the combined structure is thus doubled if the panels are identical, so an increase of 6 dB in the insulation would be expected in the mass-law region. However, the problem is complicated with the introduction of an air gap and extra resonances occur resulting in a lower TL than would at first be realized. This type of structure does have one big advantage in that the critical frequency is as for one of the individual leaves, and not half of this (see Equation 9.70) as would be the case if the two panels were fixed firmly together. If an analysis is made on an infinite double wall construction in a similar manner to that of Section 9.3.4, the expression for the transmittivity can be found to be

$$\frac{1}{\tau} = 1 + \frac{z_1 + z_2}{2 \rho_o c} \cos \theta + \frac{z_1 z_2 \cos^2 \theta}{4 \rho_o^2 c^2} (1 - e^{-j\gamma}) \tag{9.77}$$



where  $z_1$  and  $z_2$  are the impedances of the two panels,  $\theta$  is the angle of incidence of a plane wave, and  $\gamma$  is given as

$$\gamma = \frac{2\omega d \cos \theta}{c}$$

where  $d$  is the separation of the panels. If  $d = 0$ , then Equation 9.77 is identical to that for a single panel, Equation 9.56. The value of the impedances  $z_1$  and  $z_2$  are given by Equation 9.60, 9.64 or 9.72, whichever frequency range it is desired to investigate. If the two panels are limp then

$$z_1 = z_2 = j\omega m$$

for two identical panels. In this case, assuming normal incidence

$$\begin{aligned} \frac{1}{\tau} &= \left[ 1 + \frac{j\omega m}{\rho_0 c} - \left( \frac{\omega m}{2\rho_0 c} \right)^2 (1 - e^{-j\gamma}) \right]^2 \\ &= \left[ 1 - \left( \frac{\omega m}{2\rho_0 c} \right)^2 (1 - \cos \gamma) \right]^2 + \left[ \frac{\omega m}{\rho_0 c} \left( 1 - \frac{\omega m}{4\rho_0 c} \sin \gamma \right) \right]^2 \end{aligned} \quad (9.78)$$

In this expression, the second part is zero when

$$\sin \gamma = \frac{4\rho_0 c}{\omega m}$$

If  $\gamma = (2\omega d/c)$  is small, which it is at low frequencies, and normal separation (less than 1 ft) then

$$\sin \gamma \approx \gamma = \frac{2\omega d}{c} = \frac{4\rho_0 c}{\omega m}$$

or

$$\omega_0 = \sqrt{\frac{2\rho_0 c^2}{md}} \quad (9.79)$$

This is thus a resonant frequency of the system and can be looked upon as a mass-spring-mass resonance, the stiffness of the air gap being  $\rho_0 c^2/d$ . At this frequency it can be seen from Equation 9.78 that

$$\frac{1}{\tau} \approx 1 \quad \text{or} \quad \text{TL} = 0 \text{ dB}$$

At higher frequencies, another minimum occurs when

$$\cos \gamma = 1$$

or

$$f = \frac{nc}{2d}, \quad n = 1, 2, 3, \dots \quad (9.80)$$

This occurs when the separation is a multiple of the half wavelength; therefore, there will be an infinite number of these resonances having a relative spacing of  $c/2d$  Hz. The form of the transmission loss curve is thus as shown in Figure 9.30. (It should be pointed out that the TL at the high frequency resonances is only equal to the total mass law value as shown if they lie below the critical frequency. If this is not the case, the TL may well be zero at these points.)

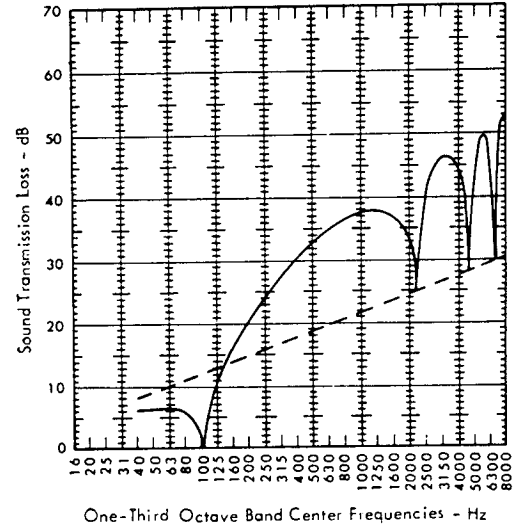


FIGURE 9.30 Theoretical Transmission Loss for a Double Wall at Normal Incidence, Each Wall Having a Surface Mass of 2 lb/ft<sup>2</sup>, and an Air Gap of 3". The Dashed Line Represents the Mass-Law Values at Normal Incidence for a Limp Wall of Mass Equal to the Total Mass of the Double Wall (i.e. 4 lb/ft<sup>2</sup>)

If the two panels are of mass  $m_1$  and  $m_2$  per unit area, then

$$z_1 = j\omega m_1$$

$$z_2 = j\omega m_2$$

If these values are inserted into Equation 9.77, the mass-spring-mass resonance at normal incidence is

$$\omega_0 = \sqrt{\frac{\rho_0 c^2 (m_1 + m_2)}{m_1 m_2 d}} \quad (9.81)$$

The cavity resonances are the same as before.

In addition to the resonances mentioned above, each individual panel responds in the same manner as explained in the last section. In other words, each panel exhibits the mass-stiffness resonance, the natural resonances (if it is of finite size) and the coincidence effect, making the complete characteristic extremely complicated. It is usually impossible to separate all these resonances, but care should always be taken to ensure that the most important do not coincide. To these ends, it is good practice to use individual leaves of different thicknesses or elastic parameters.

Despite these precautions, however, it is common for double wall constructions to have a lower TL than that provided by one of the leaves independently at the low frequencies. This situation is reversed at medium and high frequencies. The variation of insulation with separation is shown in Figure 9.31.

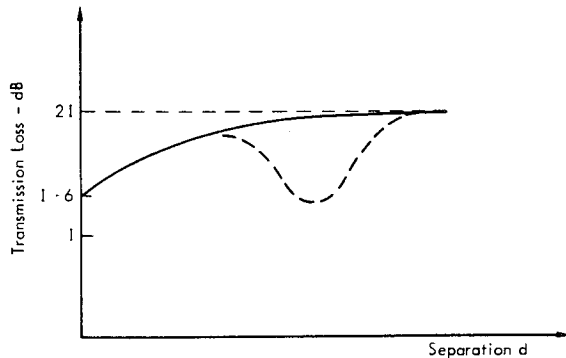


FIGURE 9.31 Effect of Separation of Leaves in a Double Wall on the Transmission Loss (Averaged Over the Frequency Range 125 Hz to 4000 Hz)

If  $l$  is the TL provided by one of the leaves, then the theoretical (mass-law) TL for two leaves is approximately  $l + 6$  dB. The TL then increases with separation eventually reaching a value 21 when the leaves are several wavelengths apart. However, if at a certain separation, the associated cavity resonance coincides with the critical frequency, then the TL will decrease as shown in the dashed curve. The introduction of damping into the panels will of course have the same effects as in the case of the single panel. However, the effect of the mass-spring-mass resonance will be reduced.

Despite these disadvantages, however, the TL that can be obtained from carefully designed double wall structures can far exceed that for a single panel at the high frequencies. In this region, it can also be advantageous to utilize triple walls to good effect.

#### Mechanical Isolation of Double Walls

An important point to remember when designing and constructing double walls, is that the two leaves must be completely isolated from each other. Any structural ties connecting the leaves effectively reduce the structure to a single panel and hence lower the TL. If ties have to be provided, as with the double brick wall, they should be light and flexible. The addition of an absorbent in the cavity can have beneficial effects as long as the leaves are separated. If they are not, this measure has no effect except when the leaves are light and the absorbent thick, when an increase in the mass may be apparent. The absorbent should preferably have a high flow resistance, yet not be so stiff as to act as a structural tie, when it may even reduce the insulation. Because of the complexity of this type of structure, and because the finite panels are, in practice, usually joined at the edges, calculations of the TL give results that tend to be rather optimistic. Hence, the design is usually based on experimental work.

If multiple panels are employed with air-gaps, then it is essential to have different thicknesses and separations and to minimize coincidence effects in the frequency range of interest, otherwise the high TL that could be obtained will be drastically reduced due to resonances.

#### Subdivided Partitions

In many practical cases, a wall may be subdivided into different sections, such as doors and windows. These sub-sections usually have lower values of TL, hence the complete structure will itself provide less insulation. However, the new value for the transmissivity can be calculated providing that the individual values for the sub-sections are known.

If  $\tau_i$  is the transmissivity of the  $i$ th subsection, having area  $S_i$ , then the average transmissivity for the complete structure  $\tau$  is given by

$$\tau = \frac{\sum \tau_i S_i}{\sum S_i} \quad (9.82)$$

If the transmission loss of the material constituting the  $i$ th section is  $TL_i$ , then

$$\tau_i = 10^{-(TL_i/10)}$$

and

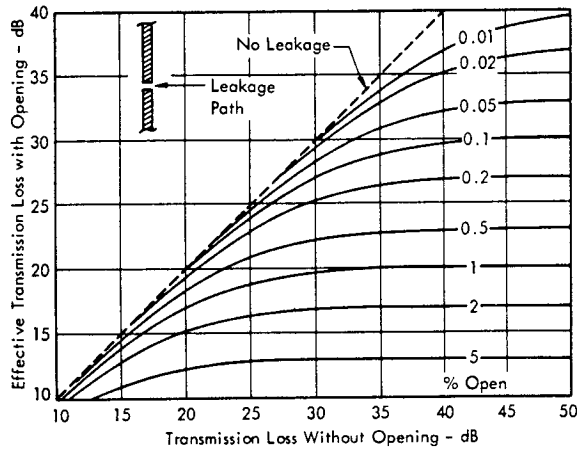
$$\tau = \frac{\sum S_i 10^{-(TL_i/10)}}{\sum S_i} \quad (9.83)$$

and

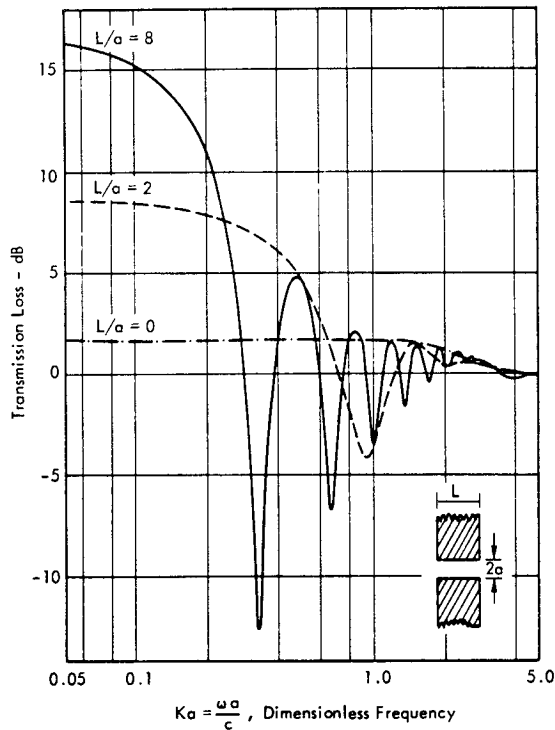
$$TL = 10 \log \left( \frac{1}{\tau} \right)$$

This method is useful in many cases but it should be used with care if there are any gaps or cracks in the structure. An example of how damaging to the insulation a door can be is shown in the following example and in Figure 9.32(a).

Consider a wall of size 10 ft by 10 ft having a door 8 ft by 4 ft with insulations of 50 dB and 40 dB, respectively. Combination of the two using Equation 9.83 results in a TL of 44 dB; i.e., a drop of 6 dB on the wall alone. This type of calculation can be carried out to show the influence of air gaps on the TL of a structure. Assume that the door in the last example is situated in a wall having an extremely high transmission loss, and that there is an air gap of 1/16" between the door and the wall. If the transmission loss of the door is, say 30 dB, then by using Equation 9.82 it can be shown that the combined loss is only 24 dB. In other words, the effect of this small air gap is to reduce the TL by 6 dB. It should be mentioned, however, that diffraction and tube effects make this calculation only approximate.



(a) Low Frequency Transmission Loss Through Walls Versus Percent Opening



(b) Transmission Loss Through Circular Aperture Versus Frequency and Length to Radius Ratio L/a

FIGURE 9.32 Transmission Loss Through (a) Leakage Paths in Walls and (b) Through Circular Apertures (Part (a) from Reference 9.15, Part (b) from Reference 9.19)

Transmission Through an Aperture

The case of the transmission of sound through a circular aperture is complex and has been dealt with fully in References 9.18 and 9.19. In this section, only the more important results will be quoted, using the following nomenclature,

$a$  = radius of the aperture

$L$  = length of the aperture

$K = 2\pi f/c$ , where  $f$  is the frequency and  $c$  is the speed of sound.

It is assumed that the circular aperture is situated in a plane wall and is subjected to a plane wave incident along the normal to the wall. Under these conditions it is found that the curve for transmission loss as a function of frequency is of the form shown in Figure 9.32(b). Experimental verification of the theory is given in Reference 9.19 and shows that the results also apply for a diffuse incident field. The theoretical curve can be divided into three sections:

- At very low frequencies, ( $Ka < 0.1$ ), the transmission loss is always positive and if  $L/a > 20$ , then

$$TL = 20 \log (L/a) - 3 \text{ dB}$$

Thus the TL is dependent on the ratio  $(L/a)^2$ . In the case when  $L/a < 20$ , the transmission loss is slightly higher than that calculated using the above expression.

- At high frequencies ( $Ka > 4$ ) the transmission loss is approximately unity.
- In the intermediate region ( $0.1 < Ka < 4$ ) the TL curve exhibits several maxima and minima, the number and the sharpness of which are determined by the factor  $L/a$ . If this is large, the resonances are sharp and numerous. When  $L/a$  is small, the transition from the low to high frequency region is smooth as shown in Figure 9.32(b).

9.4. DUCTS

One of the most important aspects of the acoustics of enclosures is the acoustic attenuation provided by ventilating and heating ducts. In order to provide good sound insulation from external noise, open windows and doors are of course out of the question. Thus, artificial ventilation systems have to be incorporated into the structure, providing an extra path for sound transmission. It is essential, therefore, not only for ducts to provide high attenuation of external noise but also of their self-made noise due to fans etc.

The majority of ducts consist of a rectangular tube of metal sheeting which is lined with an absorbent material. This material must obviously be fireproof and fairly secure so as not to be damaged by air currents, and must attenuate sound waves without impeding the direct air flow. Many different methods have been reported in the literature for determining the effectiveness of a lined duct, but the most convenient one is to state the attenuation in decibels per unit length.

9.4.1 THEORETICAL ATTENUATION OF A LINED DUCT

If the duct is rectangular in cross-section with the x-axis corresponding to the main axis an expression for the sound pressure traveling in the positive x-direction can be written as (see 9.12)

$$p = A \cosh(K_y y) \cosh(k_z z) e^{j(K_x x - \omega t)} \tag{9.84}$$

where  $K_x, K_y$  and  $K_z$  are the components of the propagation constant  $K$  in the  $x, y$  and  $z$  directions.

This expression can then be inserted into the three dimensional wave equation, and a relationship between  $K, K_x, K_y$  and  $K_z$  obtained. If the admittance of the duct lining is introduced, the propagation constants  $K_y$  and  $K_z$  can be determined and hence  $K_x$ , which represents the propagation of sound waves along the duct. From this analysis (which is explained in more detail in Reference 9.6) it turns out that the wave along the duct has a damping term associated with it, given by

$$\exp\left[-\frac{L\epsilon}{2A} x\right]$$

where  $L$  is the length of the duct perimeter,  $A$  the duct area, and  $\epsilon$  the susceptance of the duct lining. This demonstrates that the pressure decreases with distance  $x$  along the duct. The attenuation in dB per unit length is thus

$$A' = 4.34 \frac{L\epsilon}{S} \tag{9.85}$$

Expression 9.85 has been derived, however, assuming plane wave motion along the duct. At higher frequencies, there will be wave motion perpendicular to the x-axis and in these cases the attenuation is approximately

$$A' = 8.68 \frac{L\epsilon}{S\tau} \text{ dB per unit length}$$

where

$$\tau = \left[ 1 - \left(\frac{\lambda n_y}{2L_y}\right)^2 - \left(\frac{\lambda n_z}{2L_z}\right)^2 \right]^{1/2} \tag{9.86}$$

$L_y$  and  $L_z$  are the lateral dimensions of the duct,  $\lambda$  is the wavelength and  $n_y, n_z = 1, 2, 3 \dots$  are the mode numbers for the transverse waves. For a square duct with  $L_y = L_z$ , it can be seen that  $\tau$  becomes imaginary for a particular mode number  $n = n_y = n_z$ , and thus no true wave motion can occur.

The radiation from the end of the duct into an enclosure, depends, to a certain extent, on whether it is flush with the wall. Figure 9.33 shows that the acoustical radiation resistance at the end of a tube is (for  $k_z < 1$ ) 3 dB less for a tube in free space than it is for flush mounting. Thus, the power radiated will also be approximately 3 dB less, the remaining energy being reflected back along the duct.

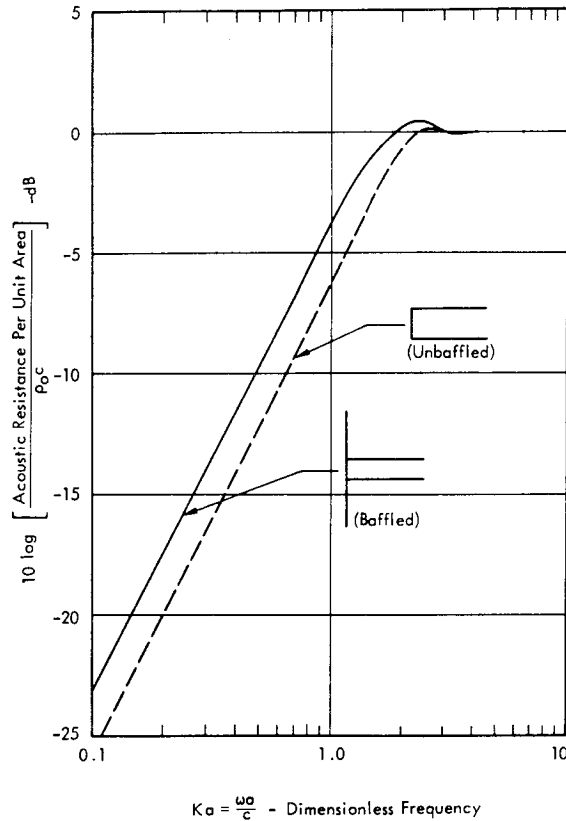


FIGURE 9.33 Acoustical Resistance at the Exit of a Duct for Baffled and Unbaffled Combinations where  $a$  is the Effective Radius

The attenuation at the end of ducts having various cross-sections is shown in Figure 9.34. The values from this should be added to the attenuation due to the duct absorption.

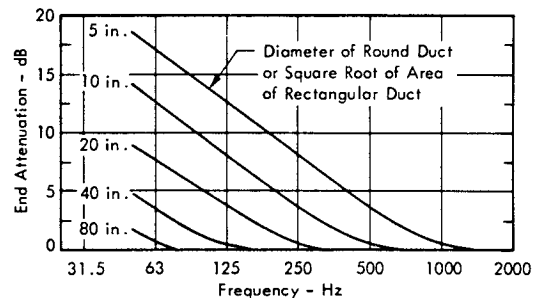


FIGURE 9.34 Attenuation at End of Ducts of Various Cross-Sectional Areas when Mounted Flush with a Wall (from Reference 9.13)

9.4.2 PRACTICAL VALUES OF ATTENUATION IN DUCTS

A qualitative approach to the attenuation of sound in a duct shows that it is proportional to the absorption of the

lining only at frequencies where the distribution of pressure is approximately uniform, i.e., at low frequencies. Thus, with a porous absorber (see Section 9.2.2.1) the attenuation at low frequencies increases with the frequency. At high frequencies, the sound is directed more towards the center of the duct and hence, the attenuation will be less. Combination of these two effects results in a band-stop frequency response, the position of the maximum depending on the duct dimensions and the type of absorber.

The walls of the duct are usually of thin metal sheeting, as mentioned previously. Since the transmission loss of such sheets is low at low frequencies, some of the sound energy will be transmitted out of the duct. This increases the effective attenuation, but may prove disadvantageous unless the duct is insulated from any enclosures.

Since the absorption provided by a porous material depends partly on the flow resistance (see Section 9.2.2.1), this will also have an effect on the attenuation. In Figure 9.35 design curves are shown for a duct having only two lined walls with flow resistance and open-area percentage as parameters. This clearly demonstrates the maxima occurring when  $L_y = \lambda$  for all values of flow resistance.

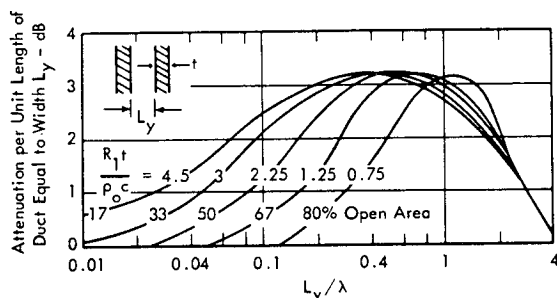


FIGURE 9.35 The Effect of Flow Resistance  $R_1$  (Expressed by the Dimensionless Parameter  $R_1 t / \rho_0 c$ ) on the Attenuation of a Duct with Absorbent Lining on Two Sides Only. The attenuation is expressed in dB per length of duct equal to the width (from Reference 9.11).

In practice, the expression for the attenuation given in Equation 9.85 and 9.86 proves to give optimistic results. A simpler, empirical formula that can be used for design purposes under certain circumstances is

$$\text{attenuation} = 12.6 \frac{L}{S} \alpha^{1.4} \text{ dB/unit length} \quad (9.87)$$

where  $\alpha$  is the absorption coefficient of the duct lining.

This is found to be correct within 10% for ducts having height to width ratios of between 1:1 and 1:2, absorption coefficients in the range 0.25 to 0.5 and for frequencies 200 - 1500 Hz. Figure 9.36 shows a comparison between experimental and calculated results. At the higher frequencies, the attenuation is greater than expected for short distances along the duct, but becomes constant at larger distances, where flanking transmission along the surfaces is the dominating factor.

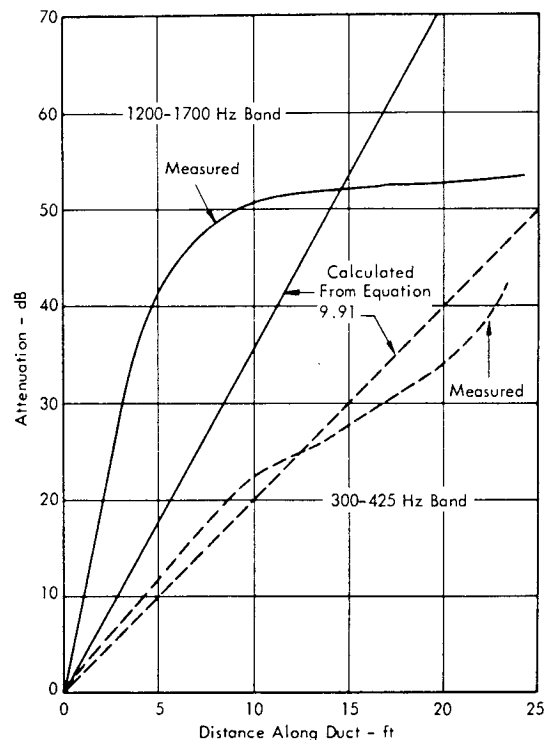


FIGURE 9.36 Comparison of Measured and Calculated Attenuation in a Duct 1 Foot Square Lined with 1 Inch Blanket (Data from Reference 9.13)

### The Effect of Bends

Because of the beaming of the high frequencies along the center of the duct, increases in boundary absorption have little effect on the attenuation in this range. However, it can be increased by the introduction of a bend in the duct, which becomes effective at frequencies above that where the wavelength is smaller than the duct dimensions. If the bend is unlined, then the action will be one of pure reflection giving perhaps an attenuation of 3 to 4 dB at the high frequencies. More attenuation can of course be gained by lining the bend with absorptive material, as shown in Figure 9.37, which is drawn for the lining in different positions. Only little excess attenuation is noticed at low frequencies where the wavelength is greater than the duct dimensions and diffraction around the bend occurs. Thus a compromise has to be made between cost and low frequency attenuation, since cost is proportional to the lateral dimensions. It should be pointed out that these results are only valid strictly when the lining extends a distance of at least two duct widths after the bend, otherwise a correction should be subtracted from the total.

At the sudden discontinuity caused by the introduction of a bend, turbulence and hence, noise is produced, which will be greater the sharper the bend and the larger the duct (Figure 9.38). It is inadvisable, however, to use rounded bends, as the attenuation is extremely low (Figure 9.37). Therefore, a further compromise has to be made between duct size and noise.

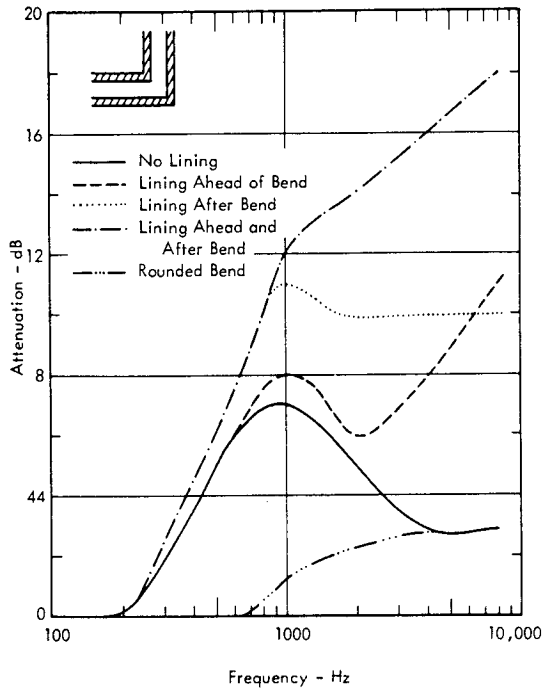


FIGURE 9.37 Attenuation of Right-Angled Bends in a Duct 10" Wide (Data from Reference 9.13)

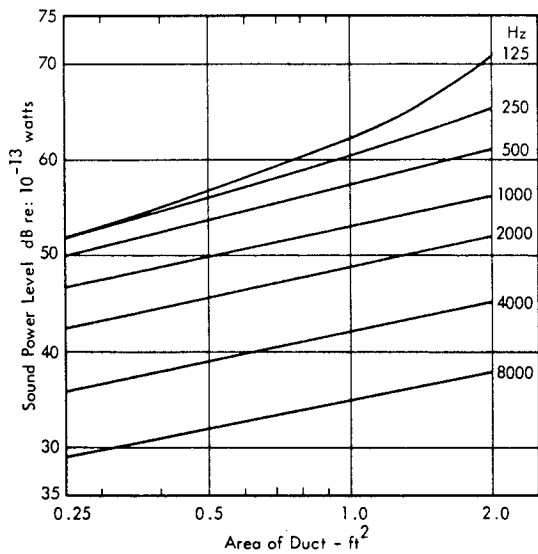


FIGURE 9.38 Approximate Sound Power Levels Generated by Air Flowing Around Duct Bends at 2000 fpm (Data from Reference 9.13)

**Resonators**

The attenuation of a lined duct is poor at very low frequencies, because of the characteristics of porous absorbers, unless the lining is made extremely thick. Since the effect of bends is also small at these frequencies, tuned resonators (see Section 9.2.2.3) are sometimes employed to increase the attenuation. These are placed in the side of the duct and are useful in the frequency range 20 - 100 Hz.

The positioning of the resonator along the length of the duct can be important if the duct is small (laterally) and a substantial amount of energy is reflected at the exit. In this case, standing waves will be set up, and care should be taken to ensure that the resonator mouth is at a pressure antinode.

**Splitters**

In some cases, more absorption than that due to a simple lined duct is required. This can be achieved by increasing the area of the absorbent material while retaining the same percentage open area as shown in Figure 9.39.

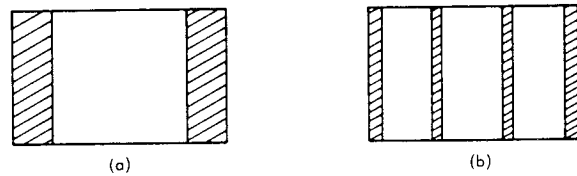


FIGURE 9.39 Illustration of the Use of "Splitters" to Increase the Effective Absorbing Area of a Duct. The shaded portions represent absorbent materials.

Attenuation curves for ducts with splitters are shown in Figure 9.40, in the case of 50% open area. The high values at the higher frequencies can only be attained if flank-transmission is kept under control.

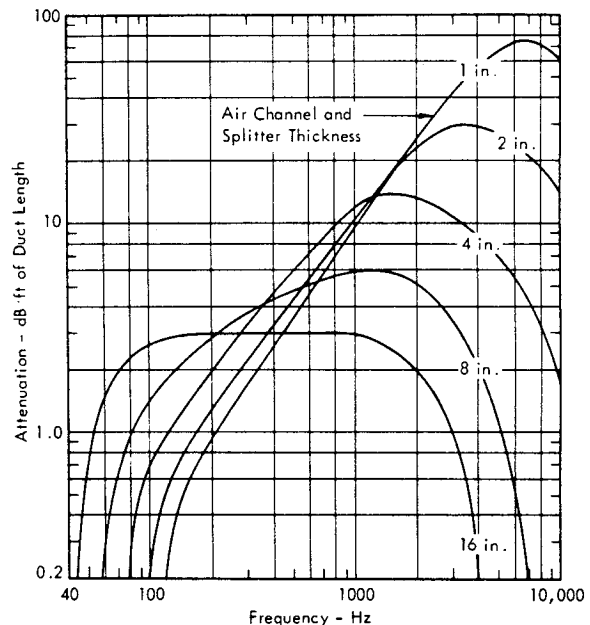


FIGURE 9.40 Attenuation of a Duct with Splitters of Different Thicknesses. The percentage open cross-sectional area in each case is 50 percent (from Reference 9.13).

**9.5 NOISE REDUCTION**

The basic acoustical theory of absorbers, insulators and ducts have been described in the preceding sections of this chapter. In this section, the idea is to combine the knowledge thus gained and apply it to the problem of reducing the noise inside enclosures, the aim being to provide an environment with the lowest possible annoyance, and that permits the full utilization of the enclosure as originally planned.

To begin with, it is necessary to define the term "noise reduction" (NR). This is simply the reduction in energy density level or sound pressure level produced by the application of a certain acoustical treatment.

Consider two adjacent rooms separated by a wall, one room containing a source of noise that produces an energy density of  $E_1$ . If the energy density in the second room due to this source is  $E_2$ , then the noise reduction is defined as:

$$NR = 10 \log \left( \frac{E_1}{E_2} \right)$$

which from Equation 9.52 can be written:

$$NR = TL - 10 \log \left( \frac{A}{a} \right)$$

where TL is the transmission loss of the dividing wall. Thus, the noise reduction depends on the absorption in the second room, as opposed to the transmission loss which depends solely on the properties of the dividing wall. It also depends on the area A of the wall, the smaller this is, the higher the noise reduction.

If a noise source inside an enclosure produces an energy density  $E_1$ , and acoustical treatment is applied reducing the density to  $E_2$ , then the noise reduction is given by:

$$NR = 10 \log \left( \frac{E_1}{E_2} \right) = SPL_1 - SPL_2$$

where  $SPL_1$  and  $SPL_2$  are the sound pressure levels existing before and after the treatment respectively.

### 9.5.1 DETERMINATION OF NOISE LEVELS

#### External Source

Consider an enclosure which is situated in the sound field of a noise source such that only one surface is directly exposed. Figure 9.41(a) This case is encountered with a sunken building where perhaps only the roof is visible. The incident sound pressure level at the point x on the exposed surface can be calculated using the results of Chapters 6 and 7. Let the incident level be  $SPL_1$ . The required maximum level inside the enclosure  $SPL_2$  depends mainly on the purpose for which it is used, and can be determined from Chapters 10 and 11. Thus, the required TL of the wall can be calculated in the following manner, assuming that the energy falls on one wall only. At high frequencies, when the wavelength is smaller than the dimensions of the enclosure, there will be negligible diffraction at the edges. If the enclosure is, say, 20 ft x 20 ft, this occurs for frequencies above approximately 50 Hz. Common experience tells us that noise will be heard in this acoustic shadow, but compared to the level in the direct field, this will have a negligible effect on the internal sound level. The situation is different and much more complicated, if there are reflecting surfaces, i.e., other

buildings in the vicinity. The incident mean square sound pressure will be

$$p_i^2 = p_{ref}^2 \cdot 10^{SPL/10}$$

The mean square pressure transmitted is given by

$$p_t^2 = \tau p_i^2$$

and the power radiated by this wall, having area A, is

$$W = IA = \frac{p_t^2}{\rho c} A$$

Using the fact that the mean square sound pressure in a reverberant room, having a source of power W, is

$$p^2 = \frac{4W \rho c}{a}$$

where a is the total absorption in the room, it can be shown that the TL required is

$$TL = SPL_1 - SPL_2 + 10 \log \frac{A}{a} + 6 \text{ dB} \tag{9.88}$$

where  $SPL_2$  is the reverberant level in the enclosure. This is a useful expression since it contains both the TL for the wall and the total absorption "a". However, this is only the case when one wall is subject to impinging sound waves. If the noise source is situated as in Figure 9.41(b), then the transmission through two of the walls has to be calculated. The incident levels being taken at the center of each wall.

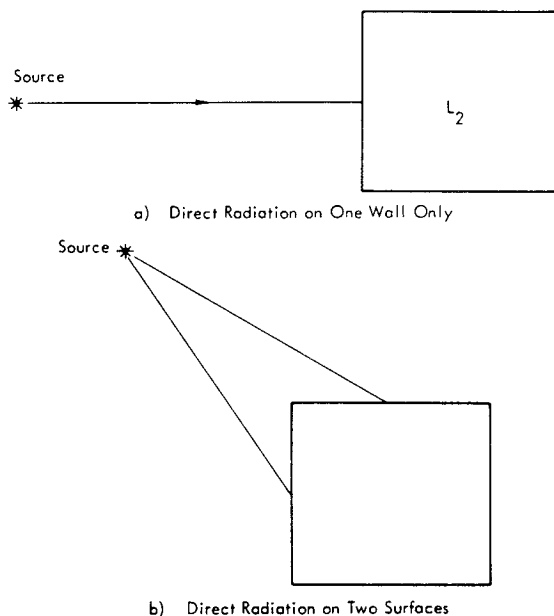


FIGURE 9.41 External Source Driving One or More Surfaces of an Enclosure

9.5.2 INTERNAL SOURCE

If a noise source is situated inside an enclosure and away from the surfaces of the enclosure, it produces a direct mean square pressure at a distance  $r$  given by (Chapter 7)

$$p_d^2 = \frac{W \rho_o c}{4 \pi r^2}$$

The reverberant field as shown in Equation 9.33 will be

$$p_r^2 = \frac{4 W \rho_o c}{a}$$

If there are  $N$  sources each of power  $W$ , then

$$p_r^2 = \frac{4 N W \rho_o c}{a}$$

and the SPL is increased by an amount  $10 \log N$ . In this case,  $p_d^2$  has to be calculated for each source.

At any point, therefore, the mean square pressure will be

$$p^2 = p_d^2 + p_r^2 = \rho_o c W \left[ \frac{1}{4 \pi r^2} + \frac{4}{a} \right]$$

or

$$SPL \approx PWL + 10 \log \left[ \frac{1}{4 \pi r^2} + \frac{4}{a} \right] \text{ dB} \tag{9.89}$$

where the power level reference is taken as  $10^{-13}$  watts and the distances in feet. Examination of 9.89 shows that for small values of  $r$ , the first term in the bracket assumes most importance (unless  $a$  is also very small) and the SPL decreases by 6 dB per doubling of  $r$ . In this direct field region, an operator receives no benefit from any absorption on the walls of the enclosure. To protect this person, therefore, the power level has to be reduced, either by quieting the source or by the introduction of an intervening barrier, although the latter precaution will not offer protection from the reverberant sound level.

When  $r > \frac{a}{16 \pi}$ , the sound field is dominated by the reverberant field and the SPL can be decreased by quieting the source or by the addition of absorption. Figure 9.42 shows the actual SPL in the presence of a source in an enclosure for various amounts of absorption.

If the noise level is too high in an enclosure, then it is common practice to provide small partition offices for noise control. These are usually constructed of lightweight materials and hence if the interior noise level needs to be

predicted, it should be done so at octave or 1/3 octave intervals. A single figure value is not sufficient. If the original enclosure has a total absorption " $a$ ", and a source of power  $W$  watts is producing a reverberant sound pressure level SPL then

$$SPL = 10 \log \frac{p^2}{p_{ref}^2} = 10 \log \left( \frac{4 W \rho_o c}{a} \right) + 74 \text{ dB} \tag{9.90}$$

where the reverberant mean square sound pressure is given by

$$p^2 = \frac{4 W \rho_o c}{a}$$

If the introduction of the partitions having a total area  $A$  increases the absorption by an amount " $a_1$ ", then the sound pressure in the enclosure will decrease to

$$p_1^2 = \frac{4 W \rho_o c}{a + a_1}$$

and the SPL to  $SPL_1$

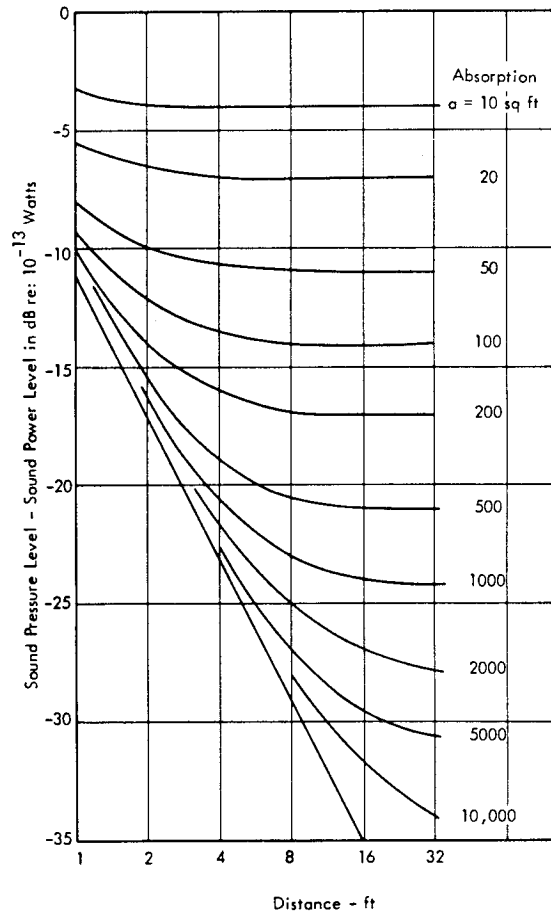


FIGURE 9.42 Sound Pressure Level in a Room Relative to the Sound Power Level at Various Distances from the Source for Varying Absorption.



Different parts of the partitions will have different transmission characteristics and so the average transmission coefficient  $\tau$  has to be calculated from Equation 9.82. Hence, the sound pressure level  $SPL_2$  inside the office will be

$$SPL_2 = SPL_1 - (TL) + 10 \log \left( \frac{A}{a_2} \right) \quad (9.91)$$

where

$$(TL) = 10 \log \left( \frac{1}{\tau} \right)$$

and  $a_2$  is the total absorption inside the office, assuming that the sound fields inside and outside the office are diffuse.

Thus, approximate calculations of noise levels can be carried out simply and quickly by using the few formulae mentioned in this and previous sections.

In a building which is subdivided into several parts, such as laboratories, offices and machine rooms, the above calculations have to be carried out in stages, considering one part at a time. If a prediction of the noise level in a particular room is required, then the calculation begins at the source. On the other hand, a building may need to be designed acoustically to provide a certain minimum noise requirement. In this case, the calculation is begun with these final requirements and worked in reverse to determine the required transmission and absorption characteristics. To specify the acoustic properties fully, it has to be repeated at every 1/3 - octave or octave band as required.

### 9.5.3 SAMPLE CALCULATION

Consider a building that is to be situated in the vicinity of a rocket launch site. It will be assumed that it is sufficiently far removed from the site so as not to require any protection from blast, which, from Chapter 6, fixes the minimum distance at around 17,000 ft for the Rocket Number 3 as defined in Table 6.1, page 6-9.

Suppose that it is required to determine the acoustical properties of the exterior walls and interior materials so as to meet a certain noise level criterion. In this example, one room of the building will be considered, with one of its surfaces being the exterior wall. It will be assumed that this surface is to be of dimensions 20 ft x 10 ft and will have one window included, 4 ft x 5 ft; the length of the room being 20 ft.

At the above distance from the site, the approximate sound pressure levels in octave bands are shown in Table 9.2. These figures are taken from data in Chapter 6, the levels being produced by the rocket 20 seconds after take-off.

In order to set a limit on the noise level inside the room, it is useful to use the speech interference level (SIL) concept discussed in Chapter 10. The required SIL figure depends on the purpose of the room but assuming that in this case the room houses equipment and personnel, a convenient figure to take corresponds to the NCA 60 curve (Reference 9.11) which is shown in Table 9.2.

In order to fulfill this noise criterion, it may not be possible to gain ventilation via the windows, and so a separate system will be required. The resultant noise level in the room will therefore be composed of the level transmitted from outside and that from the ventilation system; this total noise level should not exceed the level set down in the criterion.

First of all, the ventilation system will be considered. If this is assumed to consist of a 1/4 h.p. vaneaxial fan together with a lined duct of length 15 ft., the SPL produced in the room can be calculated. The power level produced by such a fan is given in Table 9.3, and by using Equation 9.89, assuming that all the power is transmitted into a reverberant field, the attenuation required of the duct can be determined. Assuming a square duct of side 18", lined on all sides with 1" absorber with the absorption coefficient as shown, the attenuation due to a length of 15 ft is shown according to Equation 9.87. Thus, the required TL of the wall can be written.

$$TL = SPL_1 - SPL_2 + 10 \log \left( \frac{A}{a} \right) + 6 \text{ dB} \quad (9.92)$$

where  $SPL_1$  is the exterior level,  $SPL_2$  is the maximum possible interior, reverberant level to fulfill the criterion, and  $A$  is the area of the exterior wall. The required transmission loss as shown in Table 9.4 does not appear excessive, but it is to be noticed that reasonably high values are required at extremely low frequencies. Also, there is the effect of the windows to be considered.

Now that the required transmission loss of the exterior wall is known, the requirement for the windows can be calculated if the TL of the wall is assumed. In this case, if the wall is 4" of reinforced concrete or 9" brick, the window requirements are as shown in Table 9.4.

TABLE 9.2

COMPARISON OF THE CALCULATED EXTERNAL SPL DUE TO THE SOURCE TOGETHER WITH THE REQUIRED SPL INSIDE THE BUILDING

Octave band Description Frequency - Hz	16	32	64	128	250	500	1000	2000	4000
SPL at a Distance of 17,000ft from a Rocket Source (dB)	111	110	108	106	103	98	95	90	85
NCA - 60 Curve	107	97	87	78	71	65	62	59	58

TABLE 9.3  
CALCULATION OF THE SPL IN A ROOM DUE TO A VENTILATION SYSTEM

Octave Band Description Frequency in Hz	16	32	64	128	250	500	1000	2000	4000
Power Level Produced by Vaneaxial Fan - dB re $10^{-13}$ watts	79	84	86	88	88	87	85	84	81
$10 \log a$ - where $a$ is the Total Absorption in the Room in $\text{ft}^2$	15	18	21	23	24	25	27	27	26
SPL in Room = $\text{PWL} - 10 \log a + 6 \text{ dB}$	70	72	71	71	70	68	64	63	61
Absorption Coefficient for the Material in the Duct	-	-	0.1	0.23	0.48	0.78	0.73	0.71	0.68
Attenuation Due to 15' of Lined Duct - Calculated in dB from Equation 9.87	-	-	3	6	9	23	20	18	17
SPL in Room in dB	70	72	68	65	61	45	44	45	44

TABLE 9.4  
CALCULATION OF REQUIRED TL OF AN EXTERIOR WALL WITH WINDOW INCLUDED

Octave Band Description Frequency in Hz	16	32	64	128	250	500	1000	2000	4000
$10 \log \left( \frac{A}{a} \right)$ in dB $A$ = Area of Wall in $\text{ft}^2$ $a$ = Absorption in Room $\text{ft}^2$	8	5	2	0	-2	-2	-4	-4	-3
Required TL for Wall from Equation 9.92	18	24	29	34	36	37	35	33	30
TL for 4" Reinforced Concrete Wall in dB	23	29	35	37	37	45	52	60	65
Requirement for Window in 4" Concrete Wall to Meet NCA 60 in dB	10	16	20	27	32	27	26	22	19
TL for 9" Brick Wall with 1/2" plaster on Both Sides	30	34	37	41	45	49	56	57	58
Requirement for Window in 9" Brick Wall to Meet NCA 60	12	15	20	25	27	28	25	23	20
TL of 1/4" Plate Glass	13	17	21	25	28	30	34	25	36
TL of 6" Concrete Wall	30	34	37	40	44	52	56	62	66

Inside the room it is expected that the walls will be painted brick, two of them having half their areas covered with acoustic tiles mounted in the Standard No. 7 position (Chapter 12). The floor will be assumed to be concrete and the ceiling tiles mounted directly onto concrete. Using the tables in Chapter 12, the total room absorption in each octave band can be calculated. These values will of course be lower than the absorption in the completed room, because of the presence of personnel and equipment. Thus, using Equation 9.89, the SPL due to the ventilation system can be calculated. This then has to be added (logarithmically) to the SPL due to the noise transmittal from outside, the resultant level meeting the criterion mentioned above. This calculation can also determine the maximum SPL allowable due to transmission through the exterior wall.

In this case the SPL due to the ventilation system is negligible compared to the values of the NCA criterion, and can be ignored, these values having been determined using Equation 9.82. With the reinforced concrete construction, a simple window such as a 1/4 in. plate glass, is not sufficient for the requirements. A double window, consisting of two 1/4 in. plates could be used, but the resonance at low frequencies might well reduce the TL below that for the signal plate. This is important since the low frequency region contains a major part of the sound energy. The combination of the 9 in. brick wall with the 1/4 in. plate glass provides sufficient TL to satisfy the internal noise requirements. Examination of the TL values for a 6 in. concrete wall shows that this is also sufficient for the purpose, and may well be cheaper and easier to construct.

## 9.6 APPLICATION OF DAMPING TREATMENT FOR NOISE AND VIBRATION CONTROL

The minimum sound transmission loss through a wall at its lower natural frequencies  $f_n$  and at the coincidence frequency  $f_c$ , has been shown to be strongly dependent upon the loss factor  $\eta$  of the wall. Any increase in this loss factor will obviously be beneficial for maximizing the sound transmission loss. However, very important additional benefits are realized when damping of the wall is increased. All of these effects may be summarized as follows.

- Increased sound transmission loss at lower order wall resonances and at coincidence.
- Reduction in vibratory stresses in wall. (For walls subject to sonic fatigue, this can result in very large increases in fatigue life.)
- Reduction in reaction forces at wall boundaries for lower order wall resonances and hence a reduction in structurally transmitted vibration.

Since the beneficial effects are significant for both acoustic and vibration environments transmitted into the interior of buildings, the application of damping treatment to reduce the vibration of walls or panels is considered in detail at this point. Other specific methods for the isolation or control of structurally transmitted vibration will be discussed later in this chapter.

### 9.6.1 APPLICATION OF VISCOELASTIC MATERIALS FOR DAMPING OF PANELS

The stress in a viscoelastic material under a dynamic load depends on both the average strain and rate of strain. Such materials are therefore capable of absorbing appreciable amounts of energy when subjected to vibratory loads. This energy absorption represents a form of damping called Dynamic Hysteresis Damping (see Table 3.19, page 3-161). For harmonic motion, this type of damping can be conveniently described in terms of a complex elastic modulus  $E^*$  and a material loss factor  $\eta$ . For a continuous structural element such as a bar, the loss factor  $\eta$  represents the relative value of the imaginary part of the elastic modulus of the material. Thus, for a viscoelastic material under-

going a sinusoidal extensional strain, the corresponding complex elastic modulus is given by

#### Extensional Strain

$$E^* = E (1 + j \eta)$$

where

$E$  = real elastic or storage modulus of elasticity.

For viscoelastic materials under a shear load, the corresponding loss factor is designated by  $\beta$  and the complex modulus of rigidity is given by

#### Shear Strain

$$G^* = G (1 + j \beta)$$

where

$G$  = storage modulus of rigidity.

#### Optimum Damping Material

Since the stress-strain characteristics of viscoelastic materials depend on average strain as well as strain rate, their stiffness and damping properties exhibit a marked sensitivity to temperature and the frequency of vibration. This is illustrated conceptually in Figure 9.43 to show that for a constant frequency, the real or storage modulus changes from a high to low value as temperature is increased. The loss factor passes through a "temperature resonance" peak at the temperature where this change in stiffness is most rapid. Conversely, for a constant temperature, the modulus increases as frequency increases and a "frequency resonance" peak appears in the loss factor.

This "resonance" in the loss factor corresponds to a relaxation process in the material (Reference 9.34). Roughly speaking, for vibration at frequencies below the characteristic peak in the loss factor frequency curve, the viscoelastic material has a rubber-like quality. At frequencies well above this transition point, the material tends to become brittle or glass-like. Thus, the design of viscoelastically damped structure involves the choice of a material which has its optimum or maximum value of loss factor in the temperature and frequency range for which it is to be employed. Some practical guidelines covering this point

will be covered later. It is sufficient, for now, to emphasize that the temperature-frequency characteristics are properties of the damping material and that selection of an optimum viscoelastic material is an important part of the design of viscoelastically damped structure.

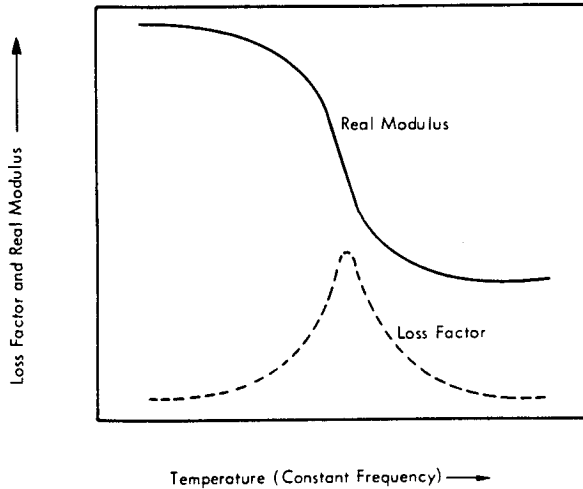


FIGURE 9.43 Illustration of Trend in Loss Factor and Real Modulus of Elasticity (or Rigidity) of Typical Viscoelastic Materials as a Function of Temperature and Frequency (From Ref. 9.20)

Optimum Geometry of Damping Configurations

For relatively low values of dynamic strain, the damping characteristics of viscoelastic materials are linear. This is illustrated in Figure 9.44 by the change in loss factor of a typical elastomer (a rubber-like viscoelastic material) as a function of the dynamic strain. Therefore, the damping characteristics of a composite structure, employing part metal and part viscoelastic materials can be carried out by a linear theory. The following section reviews this basic theory for two common geometrical forms of a composite structure which employ viscoelastic materials to increase the damping of vibrating plates. Practical design charts are given for application to a variety of basic configurations of uniform plates. Application of some of these concepts to equipment structure is illustrated in Section 11.8.2.1, pages 11-31 to 11-38.

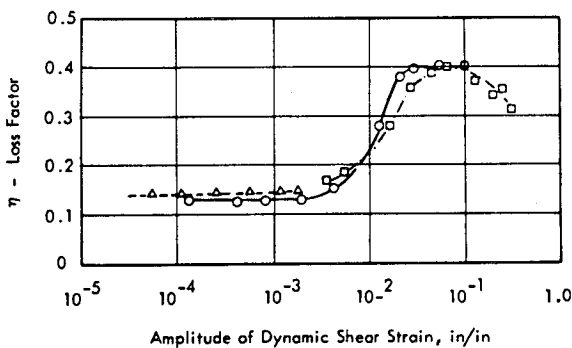


FIGURE 9.44 Illustration of the Dynamic Strain Sensitivity of the Damping Loss Factor of a Typical Elastomeric Material in Dynamic Shear (From Ref. 9.21)

It will be convenient to define the damping of a composite structure in terms of a combined loss factor  $\eta$  which is equal to  $1/Q$  where  $Q$  is the resonant amplification factor.

9.6.2 DESIGN THEORY FOR SINGLE LAYER AND TWO LAYER DAMPING TREATMENT

A general analysis of the overall loss factor for a composite structure consisting of elastic and viscoelastic components has been reported by Ungar in Reference 9.22. Based on this analysis, the following design methods are given for the two special cases 1) a two element system consisting of an unconstrained damping element on an elastic element and 2) a three element system with a damping element constrained between two elastic elements. For the latter case, the theory in Reference 9.22 has been used to develop a new and simplified design method specifically for this manual.

9.6.2.1 Unconstrained (Free) Layer Damping Treatment

Based on the usual assumptions that a) the extensional stiffness of the free damping layer is small relative to the extensional stiffness of the metal layer, b) the loss factor of the damping layer does not significantly exceed one, and c) the elastic element has no material damping, then the loss factor,  $\eta$  of the composite structure illustrated in Figure 9.45 is, to a very good approximation, given by

$$\eta = \frac{\eta_2 k_2' \left[ r_2^2 + h_{12}^2 \alpha^2 \right]}{k_1 r_1^2 + k_2' \left[ r_2^2 + h_{12}^2 \alpha \right]} \quad (9.93)$$

where

- $\eta_2$  = Extensional loss factor of damping layer
- $k_2'$  = Elastic stiffness of damping layer  
=  $E_2 A_2$  = Storage Modulus of Elasticity of Damping Layer x Cross Sectional Area, (Area per unit width for plates).
- $k_1$  = Elastic stiffness of metal base  
=  $E_1 A_1$  - Modulus of Elasticity of Undamped Element x Cross Sectional Area, (Area per unit width for plates)
- $h_{12}$  = Distance between neutral planes of each component
- $r_1, r_2$  = Radius of gyration of respective cross sections  
=  $h_1 / \sqrt{12}$ ,  $h_2 / \sqrt{12}$  for uniform treatment of a uniform beam or plate.
- $\alpha$  =  $k_1 / (k_1 + k_2')$

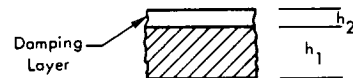


FIGURE 9.45 Two - Element Damping Configuration

The approximation is valid providing

$$\eta_2 k_2' / (k_1 + k_2') < 0.3$$

which will be true for the great majority of cases, particularly for any uniform damping treatment of a metal structure with currently available damping materials. Simpler formulations have been commonly used in the past for cases where the stiffness of the damping layer is negligible ( $\alpha \approx 1$ ,  $k_2' \ll k_1$ ). However, recent advances in the development of very stiff damping materials dictate the need for the above more accurate formulation for the general case.

For a given plate and damping material,  $h_1$ ,  $E_1$ ,  $E_2$ , and  $\eta_2$  are fixed. It is only necessary, then, to define the thickness  $h_2$  to determine the desired damping.

The thickness of the damping layer can be determined from Figure 9.46 which is a plot of Equation 9.93 for the case of a uniform unconstrained damping layer on uniform plates or beams. In this case, the combined loss factor, relative to the extensional loss factor of the material, may be expressed as

$$\eta / \eta_2 = \frac{e_2 H_2 \left[ H_2^2 + 3(1 + H_2)^2 / (1 + e_2 H_2)^2 \right]}{1 + e_2 H_2 \left[ H_2^2 + 3(1 + H_2)^2 / (1 + e_2 H_2)^2 \right]} \tag{9.94}$$

where

$$e_2 = E_2 / E_1$$

$$H_2 = h_2 / h_1$$

In practice, the maximum damping indicated in Figure 9.46 is seldom achieved. Practical limitations on damping materials and application thickness usually limit the combined loss factor to less than about 0.3. A comparison of observed loss factors and values calculated from Equation 9.94 for damping treatment of steel beams and plates is shown in Figure 9.47. The observed results were obtained from a manufacturer's published test data. In general, the theoretical results appear to be conservative. However, the agreement between theory and observation for plates is quite good, indicating the validity of the theory.

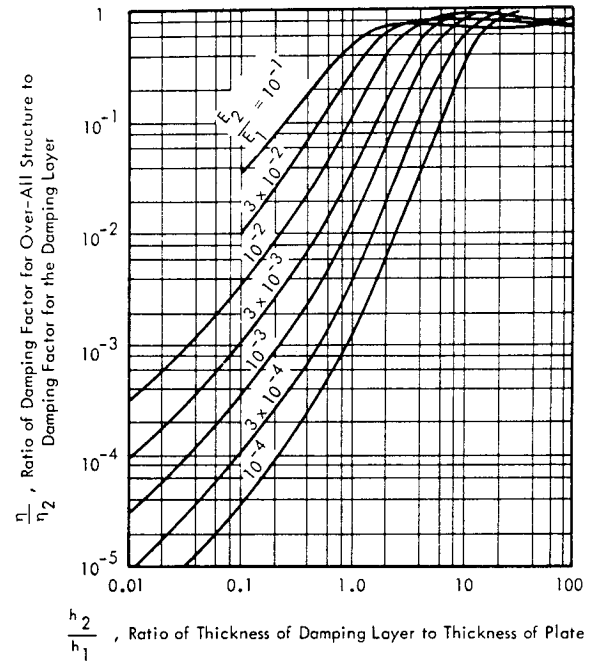


FIGURE 9.46 Loss Factor ( $\eta$ ) of Uniform Unconstrained Layer Damping Configuration Relative to Loss Factor of Damping Material ( $\eta_2$ ) as Function of the Thickness Ratio (Data from Reference 9.28)

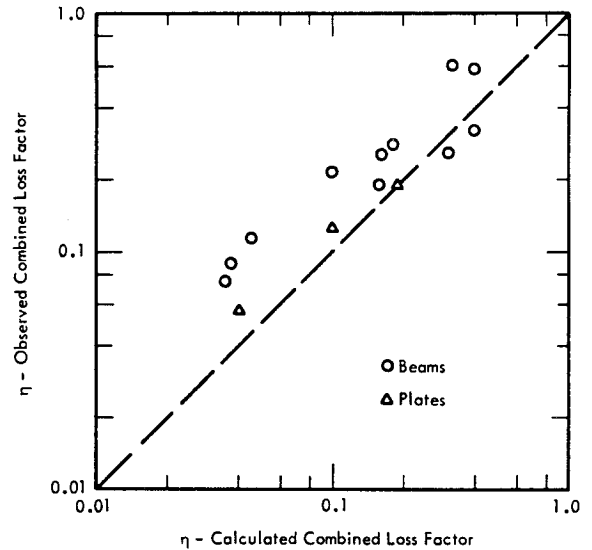


Figure 9.47 Comparison of Observed and Calculated Combined Loss Factors for Unconstrained Layer Damping Treatment of Beams and Plates

Typical loss factors that can be realized at room temperature with various types of commercially available high damping unconstrained layer treatment on aluminum panels are shown in Figure 9.48 as a function of the weight of the damping layer,  $W_2$ , divided by the weight  $W_1$ . A wide variety of other materials are available with similar or lower loss factors and suitable for temperatures from about 30° to 150°F (See Section 9.6.3). As indicated by the figure, the variation of loss factor over the practical range of weight ratios varies with the first to second power of this ratio. The lower power law is characteristic of some recently developed damping materials with a very high elastic modulus. Due to this wide variation in damping characteristics, simplified design equations can not be developed for the general case. Rather, it is necessary to determine the extensional loss factor,  $\eta_2$ , and storage modulus of elasticity  $E_2$ , at the operating temperature for the particular damping material being considered and then with Equation 9.93 or 9.94, construct curves such as in Figure 9.48. It is important to note that the damping achieved is independent of the densities of the damping or base layer. However, weight ratio, instead of thickness ratio of treatment, has been used in Figure 9.48 for convenience in estimating the cost of representative damping treatment.

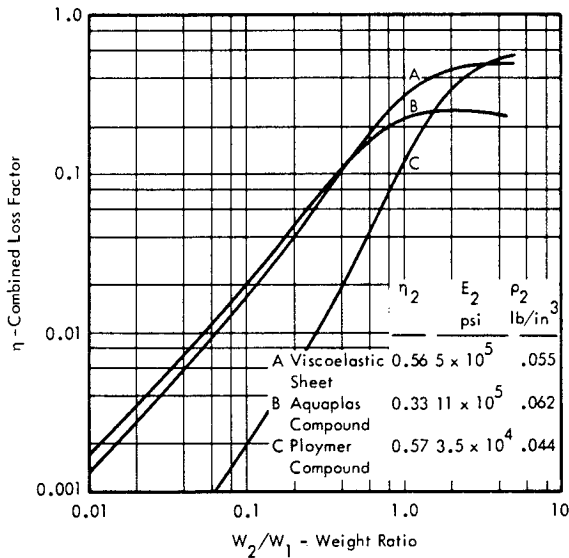


Figure 9.48 Calculated Combined Loss Factors for Three Typical Commercial Damping Materials Applied, at Room Temperature, to a Uniform Aluminum Plate in an Unconstrained Damping Layer. Frequency  $\approx$  75 Hz

To illustrate the effect this type of damping treatment has on panel stiffness, the effect of varying the thickness of the base layer on both combined loss factor and stiffness for damping treatment of an aluminum base plate is shown in Figure 9.49. The damping material is a current type of Aquaplas. As shown, for a constant thickness of the base element, the overall stiffness increases rapidly for thickness ratios greater than 1 but for a constant overall weight, the stiffness is nearly constant.

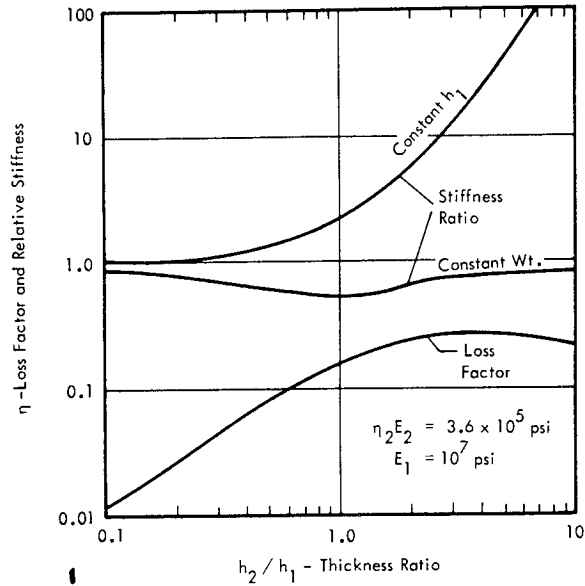


Figure 9.49 Combined Loss Factor and Relative Stiffness of Aluminum Plate Treated with Current Brand of Aquaplas Unconstrained Damping Layer. Stiffness Shown for Constant Weight (Varying Thickness of Base Layer) and Constant Thickness of Base Layer (From Reference 9.23)

9.6.2.2 Constrained Layer Damping Treatment

Constrained layer damping treatment, which includes laminated panels with built-in damping, is a more recent development which has demonstrated a capability for very high damping with less added weight than for unconstrained layer damping treatment. For this reason and also because of the more complex design procedures required, the subject is treated in some detail in this section for the benefit of equipment and structural designers.

The theory developed in Reference 9.22 for damping of a three element configuration is applicable to complex geometries such as illustrated in Figures 11.38 and 11.39, page 11-33 as well as for uniform laminated plates or treatment of a solid panel by foil-backed damping tapes. The basic assumptions made are:

- a) The metal elements are perfectly elastic
- b) The loss factors of the damping element in tension and in shear are the same.
- c) The extensional and flexural stiffnesses of the damping element are small relative to either of the metal elements.
- d) The thickness of the damping element is essentially constant and much less than the bending wavelength.

The resulting general expression for the combined loss factor of the structure, illustrated in Figure 9.50 is

$$\eta = \frac{\beta \times Y}{1 + (2 + Y) X + (1 + Y) (1 + \beta^2) X^2} \quad (9.95)$$

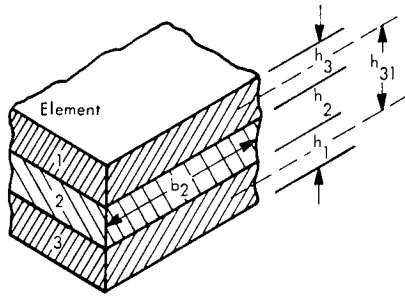


FIGURE 9.50 Cross Section of Typical Constrained Damping Layer

where

$$Y = \text{Structural Parameter} = \frac{h_{31}^2}{(D_1 + D_3) \left( \frac{1}{k_1} + \frac{1}{k_3} \right)}$$

$$X = \text{Shear Parameter} = G_2 b_2 / h_2 k_b^2 \left[ \frac{1}{k_1} + \frac{1}{k_2} \right]$$

$h_{31}$  = Distance between Neutral Planes of the two metal elements

$D_1, D_3$  =  $\left\{ \begin{array}{l} \text{Bending Stiffness of each metal element} \\ E_1 I_1, E_3 I_3 \end{array} \right.$

$k_1, k_3$  =  $\left\{ \begin{array}{l} \text{Extensional stiffness of each metal element} \\ E_1 A_1, E_3 A_3 \end{array} \right.$

$E_1, E_3$  = Young's Modulus of each metal element

$I_1, I_3$  = Area Moment of Inertia of each metal element (per unit width if element is a uniform plate)

$A_1, A_3$  = Cross Section of each metal element (per unit width if element is a uniform plate)

$G_2$  = Storage Modulus of Rigidity of damping element (Real part of complex modulus of rigidity)

$b_2$  = Mean length of cross section of damping element

$h_2$  = Average Thickness of damping element

$K_b$  =  $\left\{ \begin{array}{l} \text{Bending Wavenumber of composite system} \\ \sqrt{2\pi f [m/D]}^{1/4} \end{array} \right.$

$m$  = Mass per unit length for beams or per unit area for plates

$D$  = Bending stiffness of composite system.

$f$  = frequency of vibration.

Assumptions (c) and (d), upon which Equation 9.95 is based,

$$E_2 A_2 \left( \frac{1}{k_1} + \frac{1}{k_b} \right) \ll (K_b h_2)$$

and

$$(K_b h_2)^2 \ll 1$$

where  $E_2$  is the storage modulus of elasticity of the damping element and  $A_2$  is the cross-sectional area of the damping element (per unit width if the element is a uniform plate).

For typical damping materials applied uniformly with an optimum configuration to aluminum or steel plates, these

$$\frac{E_2}{E_1} \left( \frac{1}{h_1} + \frac{1}{h_3} \right) \ll 0.01 \sqrt{\frac{f}{h_1}} \ll 1$$

where  $f$  is the frequency of vibration in Hz and  $h_1, h_3$  are the thicknesses of the metal elements in inches.

These criteria are ordinarily satisfied for most practical cases. If very stiff damping materials were used with a thin constraining layer ( $h_3 \ll h_1$ ), on thick plates ( $h_1$  large), at low frequencies, the criteria may be violated and a more exact theory, developed in Reference 9.22 would be required. However, the improved accuracy would seldom justify the additional complexity of the more exact solution and it is recommended that Equation 9.95 be used for design purposes. A simpler formulation carried out in Reference 9.24 is restricted to the case of thin damping tapes applied to plates or beams.

Before considering the design process in more detail, the physical significance of the parameters  $X$  and  $Y$  should be clarified. The shear parameter  $X$  is a frequency dependent quantity which defines the basic configuration of the damping element. The more complex design procedures required for laminated or constrained layer damping configurations are primarily due to the importance of this frequency dependent parameter. It has also been shown that  $X^{1/2}$  is proportional to the ratio of the bending wavelength  $\lambda_b$  to the distance within which a local shear disturbance decays to  $1/e$ , (or 37 percent of its original value) (Reference 9.24). For the structural parameter,  $Y$ , a more useful physical significance exists. This may be expressed as

$$Y = \frac{D(\text{coupled})}{D(\text{uncoupled})} - 1 \quad (9.96)$$

where  $D(\text{coupled})$  would be the bending stiffness of the system if the damping material were infinitely rigid - that is, the metal elements would be rigidly connected together as one unit.  $D(\text{uncoupled})$  is just the opposite. It is the bending stiffness of the system if the damping material were absent entirely so that the stiffness would be just the sum of the stiffnesses for each metal element.

Typical values of  $Y$  are shown in Figure 9.51 for a variety of structural systems. For uniform layers in a laminated structure,  $Y$  can be expressed in a simpler form as

$$Y = \frac{3e_3 H_3 (1 + 2H_2 + H_3)^2}{(1 + e_3 H_3^3) (1 + e_3 H_3)} \quad (9.97)$$

where

$$H_2 = h_2 / h_1 - \text{Damping Layer/Base Plate, Thickness Ratio}$$

$$H_3 = h_3 / h_1 - \text{Top Plate/Base Plate, Thickness Ratio}$$

$$e_3 = E_3 / E_1$$

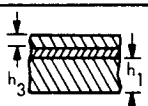



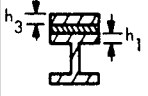


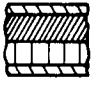
Structure	Structural Parameter $\gamma$
Plate with thin tape of same material 	$\gamma \approx 3 \frac{h_3}{h_1}$
Plates with thickness ratio of 2 to 1 	2.0
Two identical plates or thin-core sandwich 	3.0
Three identical plates with thin cores 	8.0
Highly asymmetric composites 	$\gamma \approx \frac{h_3}{2h_1}$
I-beams with equal flanges and depth ratio of 2 to 1 	0.75
Identical I-beams 	1.0
Thick-core sandwich 	> 3

FIGURE 9.51 Typical Values of Structural Damping Parameter  $\gamma$  for Several Structural Cross Sections (From Ref. 9.25 and 9.26)

This equation is plotted in Figure 9.52 for a wide range of values of  $h_2/h_1$  and  $h_3/h_1$  and for  $e_3 = 1$ . This shows that for a uniform laminated three element structure with the same material in the outer layers the maximum value of  $\gamma$  occurs for a value of  $h_3/h_1$  close to 1. Consider now the variation in the combined loss factor,  $\eta$ , given by Equation 9.95, with changes in the three parameters,  $X$ ,  $Y$ , and  $\beta$ .

The change in  $\eta$  with  $X$  is shown in Figure 9.53 for  $\beta = 1$  and for  $Y = 0.2$  (typical for a thin damping tape treatment) and  $Y = 3$  (typical for a symmetrical laminated panel). The important result to note is that there is an optimum value for the shear parameter,  $X$ , for any given  $\beta$  and  $Y$ , which maximizes the overall damping. Fortunately, however, this maximum is very broad so that a nearly optimum value of  $X$  is not difficult to achieve. A deviation of the actual shear parameter realized, for a given configuration, by a factor of 2 from the optimum value, will only reduce the combined loss factor by about 15 percent below its maximum value.

The required optimum value of  $X$  can be readily shown to be given in terms of  $Y$  and  $\beta$  as:

$$X_{opt} = 1 / \sqrt{(1 + Y)(1 + \beta^2)} \quad (9.98)$$

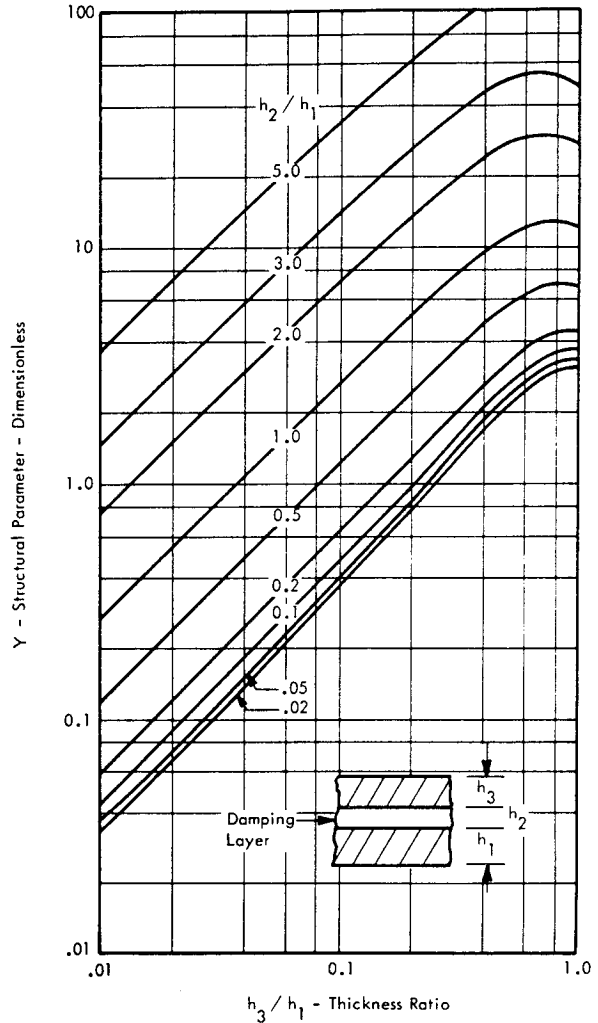


FIGURE 9.52 Variation in Structural Parameter  $\gamma$  as a Function of Thickness Ratios for Uniform Constrained Layer Damping Configuration

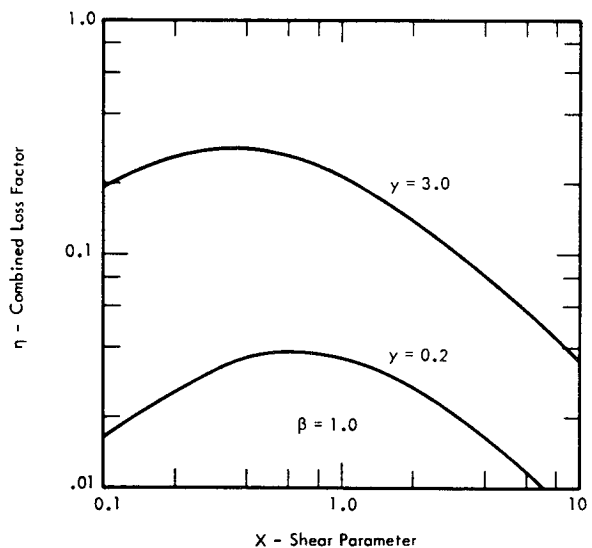


FIGURE 9.53 Illustration of Optimization of Damping of Laminated Panels for a Particular Value of the Shear Parameter



and the resulting maximum damping obtained is

$$\eta_{\max} = \beta Y / \left[ 2 + Y + 2 \sqrt{(1 + Y)(1 + \beta^2)} \right] \quad (9.99)$$

The maximum loss factor, predicted by Equation 9.99, is plotted in Figure 9.54 as a function of Y and  $\beta$ . Note that increasing either Y or  $\beta$  increases the maximum loss factor. For values of Y or  $\beta$  below 1, the loss factor is approximately proportional to the product of Y $\beta$  but for higher values of either quantity, the increase in the combined loss factor is less rapid. In general, however, increasing Y will be equally or more effective than increasing  $\beta$  (Reference 9.25).

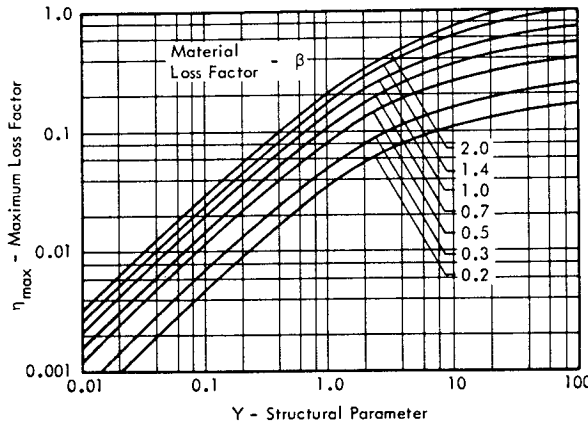


Figure 9.54 Maximum Combined Loss Factor of Three Element Laminated, Structures Structural Parameter and Material Shear Loss Factor (from Reference 9.25)

The process of optimizing the design of a laminated or constrained layer configuration may be carried out in a number of ways, depending on the constraints on the geometry or choice of damping materials. The current method discussed in the literature involves selecting a suitable high loss factor material, i.e., large  $\beta$ , for the required temperature range and then selecting a value for the structural parameter Y from Figure 9.54 (to meet the desired combined loss factor) or from Figure 9.52 for a predetermined configuration). The desired optimum value of the shear parameter,  $X_{\text{opt}}$ , is then computed from Equation 9.98 and the thickness of the damping and constraining layer adjusted until the actual shear parameter obtained, as defined for Equation 9.95, is close to the optimum value. This may involve a trial and error process to achieve the optimum design.

A simpler and more direct method has been developed for this manual which reduces the trial and error process to a minimum. This method, to be explained subsequently, is based on the use of a modified shear parameter which is independent of the thickness of the damping layer. First, however, it is desirable to consider the stiffness and resonance frequency of the laminated configuration since these parameters may impose additional constraints on the design. They are also required for both of the design procedures.

Dynamic Bending Stiffness of Laminated Structure

From Reference 9.22 it can be shown that the real bending stiffness,  $D$ , of a three-element laminated structure is given by

$$D = (D_1 + D_3) \left[ 1 + \frac{X + (1 + \beta^2) X^2}{1 + 2X + (1 + \beta^2) X^2} \cdot Y \right] \quad (9.100)$$

where

$D_1 + D_3$  = Bending stiffness of the structure if the intermediate layer were absent entirely. (i.e. - the uncoupled bending stiffness)

Assuming the optimum value of X is obtained, Equation 9.98 is substituted into Equation 9.100 to give the elastic bending stiffness for optimum damping,  $D_{\text{opt}}$ , in terms of the uncoupled bending stiffness as

$$\frac{D_{\text{opt}}}{D_1 + D_3} = 1 + \frac{1 + Y + \sqrt{(1 + Y)(1 + \beta^2)}}{2(1 + Y) + (2 + Y) \sqrt{(1 + Y)(1 + \beta^2)}} \cdot Y \quad (9.101)$$

This is plotted in Figure 9.55 for 3 values of  $\beta$  representative of "easily obtainable (0.5), "probable" (1.0) and "possible" (2.0) damping materials (Reference 9.27). For a symmetrical laminated panel, (Y = 3), the dynamic stiffness is approximately twice the uncoupled stiffness. Note that if the damping layer were infinitely stiff, the shear parameter approaches infinity and, as indicated by Equation 9.100, the bending stiffness of the composite structure would be

$$D_{\text{coupled}} = (D_1 + D_3) (1 + Y) \quad (9.102)$$

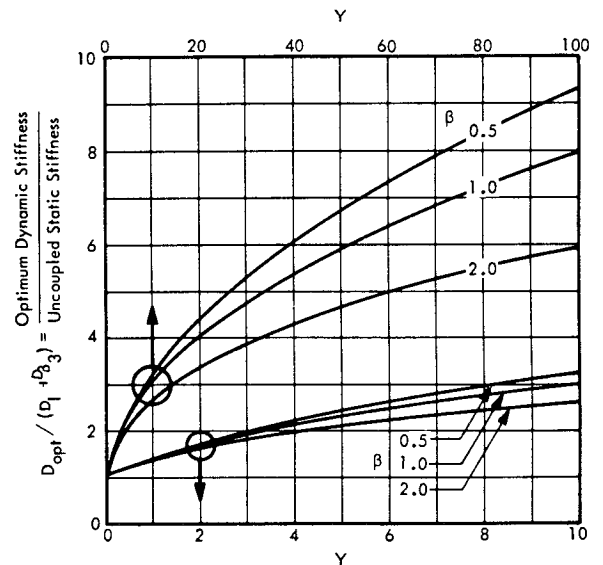


FIGURE 9.55 Ratio of Dynamic Bending Stiffness to Uncoupled Static Bending Stiffness for Optimally Designed ( $x = x_{\text{opt}}$ ) Three-Element Laminated Structure

The relative decrease in bending stiffness due to the finite shear stiffness of the damping layer is equal to the ratio  $D_{opt}/D_{coupled}$ . According to Equations 9.101 and 9.102, this is equal to the ratio

$$\frac{D_{opt}}{D_{coupled}} = \frac{D_{opt}}{D_1 + D_3} \cdot \frac{1}{1 + Y} \quad (9.103)$$

Thus, the decrease in bending stiffness of the laminated structure below what it would be if the outer metal layers were rigidly attached can be determined by dividing the ordinate values in Figure 9.55 by the quantity  $(1 + Y)$ . For example, for a symmetrical laminated panel, ( $Y=3$ ), designed to have optimum damping, the dynamic stiffness will be about 48 percent of the stiffness of a solid plate with the same total metal thickness but will be 190 percent stiffer than the uncoupled stiffness of the two metal layers.

Resonant Frequencies of Laminated Structure

It is important to recognize that the essential objective of damping treatment is to reduce response at resonance, hence, only resonant frequencies are significant for evaluation of frequency effects on damping. The  $n$ -th resonance frequency of a laminated beam or plate may be expressed in terms of the bending wave number  $K_{bn}$  for this frequency, the real part of the complex bending stiffness of the composite structure,  $D$ , and the unit mass  $m$ . The equation is:

$$f_n = K_{bn}^2 \sqrt{\frac{D}{m}} \quad (9.104)$$

where  
 $K_{bn}$  = Bending wave number for the  $n^{th}$  mode  
 $m$  = Mass per unit area for a plate or per unit length for a beam

Assuming an optimum design, Equation 9.101 can be used to define the dynamic bending stiffness,  $D = D_{opt}$ . For laminated plates, the terms  $D_1$  and  $D_3$  are expressed in terms of stiffness/unit area (i.e. -  $Eh^3/12(1 - \nu^2)$ ) while for laminated beams, they are given in terms of the stiffness per unit length (i.e. -  $Ebh^3/12$ ) where  $b$  is the beam width and  $h$  is the plate or beam thickness. The bending wave number for the  $n$ -th resonance mode,  $K_{bn}$ , of a vibrating beam or plate is a constant for a given plate or beam size with specified end conditions and can be given terms of the frequency parameter,  $C_n$ , used in Tables 3.27 and 3.31 of Chapter 3 to define the resonant frequencies of beams and plates. The expressions are:

For plates,

$$K_{bn}^2 = \frac{2\pi \sqrt{12(1 - \nu^2)} C_n K_m \cdot 10^4}{a^2 c_L} \approx 1.03 \frac{C_n}{a^2} \quad (9.105)$$

where  
 $\nu$  = Poissons ratio  
 $a, C_n$  = Plate span and frequency constant given in Table 3.31, page 3-176  
 $c_L$  = Longitudinal speed of sound in material  
 $K_m$  = Material constant in Table 3.39, page 3-188.

(Note that  $K_{bn}$  is not actually dependent on the material since the ratio  $c_L/K_m$  is a constant equal to the speed of sound in steel at room temperature - the reference condition for the values of  $C_n$ )

For beams,

$$K_{bn}^2 = \frac{2\pi C_n K_m \cdot 10^4}{L^2 c_L} = 0.311 \frac{C_n}{L^2} \quad (9.106)$$

where  
 $L, C_n$  = Beam length and frequency constant given in Table 3.27, page 3-170.

Combining the above relationships with Equation 9.102 and 9.104, the resonant frequency of a laminated plate, with optimum damping, can be given by

$$f_n = \frac{C_n h_1 K_m \cdot 10^4}{a^2} \left[ \frac{(1 + H_3^3)(D_{opt}/(D_1 + D_3))}{1 + H_2 \rho_2/\rho_1 + H_3} \right]^{1/2} \quad (9.107)$$

where  
 $H_2, H_3 = h_2/h_1$  and  $h_3/h_1$ , respectively.  
 $\rho_2, \rho_1$  = density of damping and elastic layers, respectively

and  
 $D_{opt}/(D_1 + D_3)$  = normalized dynamic stiffness found from Figure 9.6.

Equation 9.107 is the same for beams except that  $h_1$  is replaced by  $r_1$ , the radius of gyration of the base element and  $a$  is replaced by  $L$ , the beam length. In both cases, the top and bottom elastic elements are assumed to have the same elastic modulus and mass density.

Thus, the resonant frequency calculation reduces to calculating the resonance of the base element alone, using the charts presented in Tables 3.27 and 3.31 of Chapter 3, and multiplying the result by the correction factor in brackets in Equation 9.107. The numerator of this factor

accounts for the increased stiffness of the composite beam while the denominator accounts for the increase in mass. For optimum damping, this factor is a function of the parameter  $h_2$ ,  $h_3$ ,  $\beta$ , and  $\rho_2/\rho_1$ . This correction factor is plotted in Figure 9.56 as a function of  $h_3/h_1$  for representative values of  $h_2/h_1$  and for  $\beta = 1$  and  $\rho_2/\rho_1 = 0.3$ . For typical configurations consisting of thin damping tape applied to a base plate or a symmetrical laminated sandwich, the increase in resonance frequency will be 20 to 40 percent.

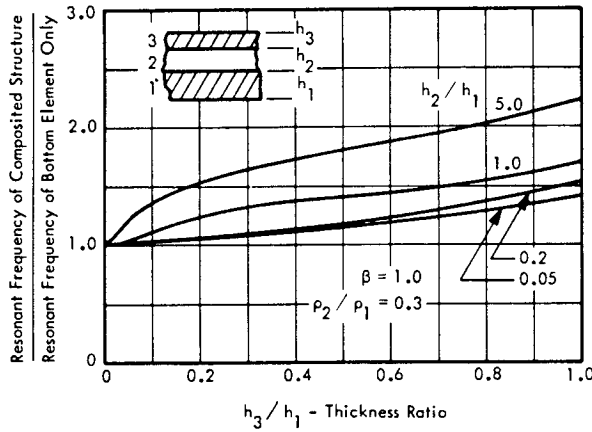


FIGURE 9.56 Resonant Frequency of Laminated Structure Relative to Resonant Frequency of Base Layer Alone (For Optimum Damping Configuration)

**Simplified Design Method**

The shear parameter  $X$ , defined for Equation 9.95, can now be expressed in a modified form, using the expressions in Equations 9.105 and 9.106 for the bending wave number of the  $n$ th resonance. The result for a laminated plate, with uniform treatment, is

$$X = \left[ \frac{G_2}{1.03 C_n E_1} \left( \frac{a}{h_1} \right)^2 \right] \left[ \frac{h_1}{h_2} \cdot \left( 1 + \frac{E_1 h_1}{E_3 h_3} \right) \right] \quad (9.108)$$

If this is equated to the expression for the optimum value of the shear parameter  $X_{opt}$  in Equation 9.98, and the terms rearranged, a reduced shear parameter,  $\gamma$ , is obtained which relates the damping and elastic properties of the system to its geometry. The resulting criteria for optimum design can then be reduced to the single equation

$$\frac{\sqrt{1 + Y} (1 + e_3 H_3)}{e_3 H_3 H_2} = \gamma \quad (9.109)$$

where

$\gamma$  = the reduced shear parameter, and

$$e_3 = E_3/E_1$$

$H_2, H_3 = (h_2/h_1)$  and  $(h_3/h_1)$ , respectively.

For uniform plates,

$$\gamma = \frac{1.03 C_n}{\sqrt{1 + \beta^2}} \cdot \frac{E_1}{G_2} \left( \frac{h_1}{a} \right)^2 \quad (9.110)$$

Note that the left side of Equation 9.109 is solely a function of the variables,  $e_3$ ,  $H_3$  and  $H_2$  since  $Y$  is also determined by these same variables. They, in turn, are related by Equation 9.109 to the value of the reduced shear parameter  $\gamma$  required for optimum damping. The latter depends on the frequency constant for the configuration,  $C_n$ , the ratio of the elastic modulus of the base layer,  $E_1$ , to the magnitude of the complex shear modulus  $[G_2 \sqrt{1 + \beta^2}]$  of the damping layer, and the thickness to span ratio  $(h_1/a)$  of the base plate.

For laminated beams, Equation 9.110 still applies except that the constant 1.03 is replaced with 0.311,  $C_n$  becomes the appropriate frequency constant for the beam configuration, and the plate side  $a$  is replaced with the beam span  $L$ .

Using Equation 9.109, the relationship between  $H_2$ ,  $H_3$ , and  $\gamma$  for the same material on the outer layers ( $e_3 = 1$ ) is given in Figure 9.57. This figure is applicable to optimum damping treatment for either a plate or a beam. For a given value of the shear loss factor,  $\beta$ , the maximum combined loss factor  $\eta_{max}$  can also be established in terms of  $H_2$  and  $H_3$  using Equations 9.97 and 9.99. Contours of constant  $\eta_{max}$  are therefore shown in Figure 9.8 for  $\beta = 1$ . For other values of  $\beta$ , the maximum combined loss factor varies approximately as  $\beta^{0.7}$  for values of  $\beta$  from 0.5 to 2. Thus, a single design chart is provided which relates the geometric, elastic and damping parameters. For a symmetric laminated panel, where  $E_3/E_1$ , and  $h_3/h_1 = 1$ , the optimum thickness ratio of the damping layer can be specified in terms of the reduced shear parameter as

$$\frac{h_{2opt}}{h_1} = \left[ \frac{1 + \sqrt{\gamma^2 - 3/3}}{(\gamma^2/12) - 1} \right] h_3 = h_1 \quad (9.111)$$

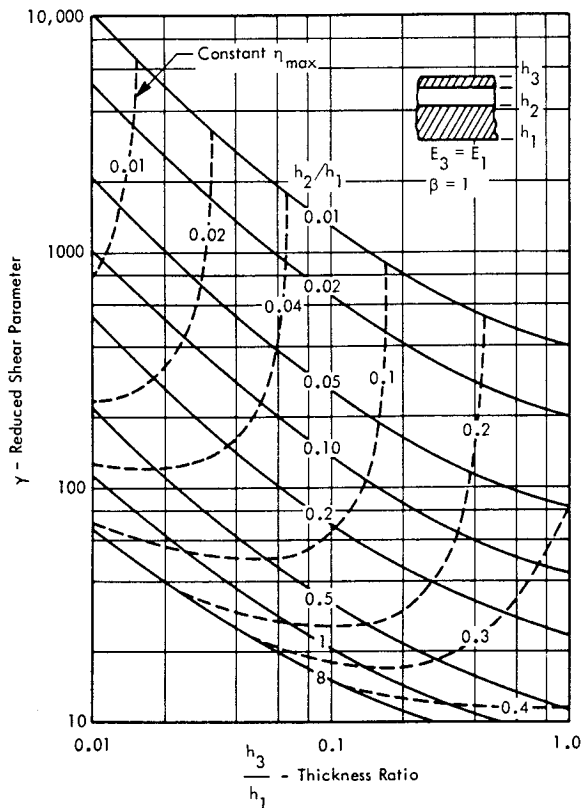


Figure 9.57 Design Chart for Optimum Constrained Layer Damping Treatment Based on Reduced Shear Parameter  $\gamma$  as a Function of Constraining Layer Thickness Ratio ( $h_3/h_1$ ) with Damping Layer Thickness Ratio ( $h_2/h_1$ ) and Maximum Combined Loss Factor ( $\eta_{max}$ ) as Parameters

The corresponding maximum combined loss factor for the symmetrical panel is

$$\eta_{max} = \frac{3\beta(1 + H_{2o})^2}{2 + 3(1 + H_{2o})^2 + \sqrt{1 + \beta^2} \gamma H_{2o}} \quad (9.112)$$

where

$$H_{2o} = h_{2opt}/h_1 \text{ as defined by Equation 9.111.}$$

The optimum thickness ratio  $h_{2opt}/h_1$  and the corresponding maximum value of the combined loss factor, given by Equations 9.111 and 9.112 are shown in Figure 9.58 as a function of the reduced shear parameter,  $\gamma$ , for four values of  $\beta$ . For practical laminated structure, the optimum thickness ratio is approximately equal to  $4/\gamma$ , and the the maximum combined loss factor is practically independent of  $\gamma$  and is roughly equal to 0.3 of  $\beta$ , the material loss factor in shear.

Due to practical considerations, such as fabrication techniques, the optimum thickness of the damping layer may not always be realized. The change in combined loss factor with variation in the thickness ratio,  $h_2/h_1$ , is

shown in Figure 9.59 for  $\beta = 1$  and a typical value of the reduced shear parameter  $\gamma = 100$ . As expected, considerable latitude is possible in the damping layer thickness without a serious decrease in the combined loss factor.

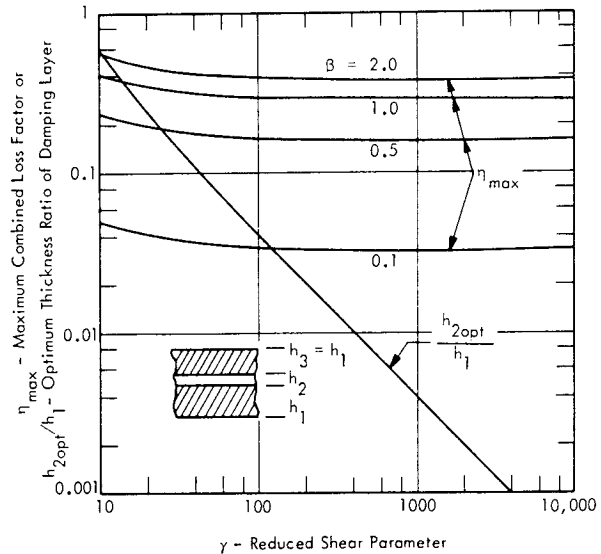


Figure 9.58 Maximum Combined Loss Factor and Optimum Thickness of Damping Layer for Symmetrical Laminated Panels or Beams

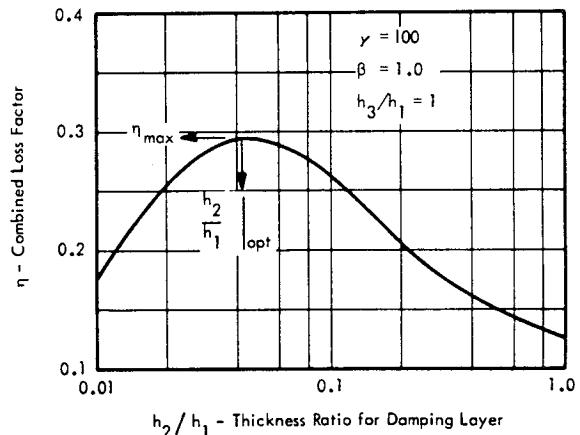


Figure 9.59 Variation in Combined Loss Factor for Change in Thickness Ratio of Damping Layer Above and Below Optimum Value for a Symmetrical Laminated Panel

### Weight of Constrained Layer Damping Treatment

For constrained layer damping treatment of uniform aluminum plates, the additional weight of treatment, relative to the weight of the untreated plate is shown in Figure 9.60 for three different values of the relative thicknesses of the damping and constraining layer. A shear loss factor of 1 and density of  $0.05 \text{ lb/in}^3$  is assumed for the damping material. Optimum design for the damping layer thickness  $h_2$ , is assumed in each case. Since this optimum

thickness depends on the damping material and base panel configuration, only one optimum set of values of the thickness ratios,  $h_2/h_1$  and  $h_3/h_1$  are possible for a given configuration. Thus, Figure 9.60 illustrates the probable range of the added weight for various constrained layer damping treatments using a damping material with the density assumed. A similar evaluation of weight versus maximum combined loss factor is shown in Figure 9.61 for constrained layer damping treatment of steel plates. In both cases, the constraining layer and base layer are assumed to be the same material. For aluminum plates, a combined loss factor of 0.2 requires a damping treatment weight of about 40 percent of the base plate weight while for steel plates, the added weight is about 25 percent for the same loss factor.

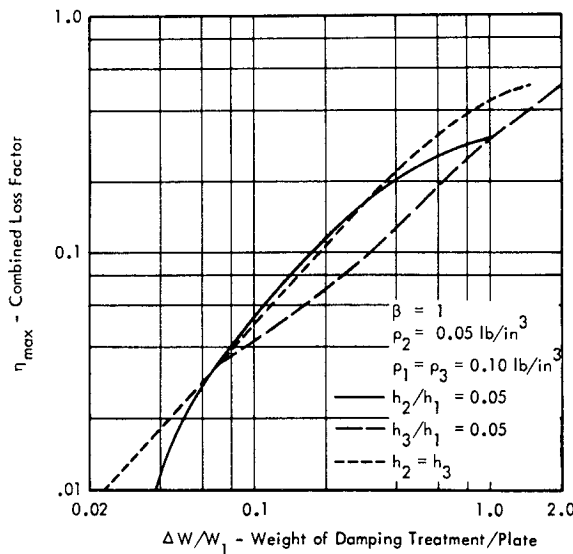


Figure 9.60 Weight of Constrained Layer Damping Treatment Applied to Aluminum Plates for Three Thickness Ratios of Damping Configuration

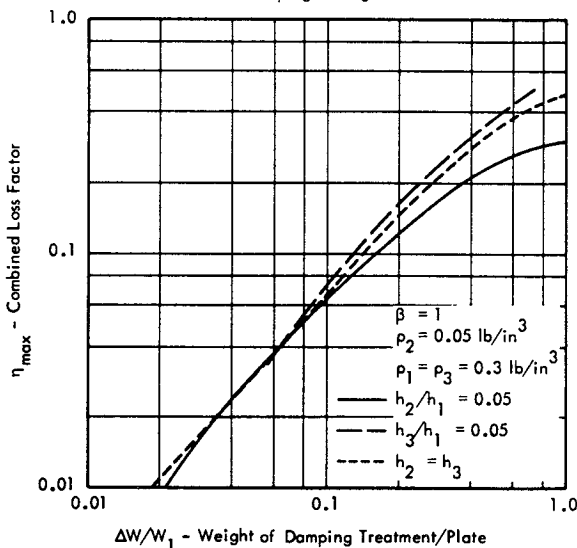


Figure 9.61 Weight of Constrained Layer Damping Treatment Applied to Steel Plates for Three Thickness Ratios of Damping Configuration

Practical Applications of Constrained Layer Damping Treatment

From a comparison of typical design curves for two and three layer damping treatment, (e.g., Figure 9.46 and Figure 9.60, see also Figure 11.42 - 11.44, page 11-37), it is clear that the three layer configuration can achieve higher damping factors. There are, in general, two basic types of these three layer configurations (Reference 9.28).

- Panels with a thick damping layer constrained by a thin metal foil
- Laminated panels fabricated with thin self-adhesive damping layers

The first type of treatment can be readily applied to existing structure, although the cost would generally be very high for any application requiring treatment over very large surface areas. However, this method of treatment can be easily applied to irregular structure. It is widely used in the damping treatment of aircraft fuselage panels.

The second type of treatment employing panels laminated with thin adhesive layers combines the maximum capability for high damping with convenient fabrication techniques and varying degrees of static strength. Thus, it is receiving wide usage for the fabrication of highly damped equipment mounting structure. An increase in the availability of load carrying structural stock such as plates, and beams (see Figure 11.38, page 11-33) can be expected in the future as the benefits of incorporating damping into load carrying structure becomes more important. Critical structural elements of ground facilities could be fabricated from such damped elements.

9.6.3 VISCOELASTIC DAMPING MATERIALS

As pointed out earlier in this section, the development of an optimum layered damping configuration depends on the selection of a suitable viscoelastic damping material. Unlike the more common building materials, the names and physical properties of these materials are less familiar to the structural designer. Space does not permit more than a brief review of the subject in this manual for, as with all organic materials, the variations in types and properties of these materials are numerous. As a minimum guide for design applications, the following topics are considered.

- Terminology for viscoelastic damping and adhesive materials
- General characteristics and examples of these materials
- Variations in loss factor with temperature and frequency.

Viscoelastic adhesive materials are included in this review since they are used for fabrication of laminated structural elements requiring modest strength capability and high damping. Additional practical details covering application of viscoelastic adhesives to equipment packages are given in Section 11.8.2.1, page 11-31.

### 9.6.3.1 Terminology of Viscoelastic Damping and Adhesive Materials.

The following pertinent terminology for viscoelastic materials has been compiled from References 9.25, 9.28, 9.30, 9.33, and 9.34. The terms are grouped conveniently into four categories

- Types of Material
- Processing Modifiers
- Qualitative Characteristics
- Physical Parameters.

#### TYPES OF MATERIAL

Viscoelastic - A material for which the stress under load is dependent on both the strain and the rate of strain.

Adhesives - Thermoplastic, thermosetting, elastomer polymers or combinations thereof which are used for bonding materials together. Structural adhesives for high strength bonding of metal parts usually consist of thermo setting plastics, while adhesives with maximum damping capability employ elastomers or mixtures of elastomers and plastics.

Branched Polymer - Polymer with branched molecular chains.

Cross-linked Polymer - Polymer with chemical links at intervals along the chain.

Elastomer - A polymeric material which, at room temperature, can be stretched, to at least twice its original length and will return quickly to approximately its original length. This property is attributed to chemical cross-connecting bonds (vulcanizing) between the basic carbon chain molecules which provides the rubbery quality. Most elastomers can accept elongations of 500 to 1000 percent.

Linear Polymer - Polymer consisting basically of a linear or amorphous chain molecule.

Plastics - General name for thermoplastics and thermosetting plastics.

Polymer - Organic material consisting of long carbon molecule chains to which are attached one or more of seven other elements - hydrogen, oxygen, nitrogen, chlorine, fluorine, sulfur, and silicon. Also used to designate raw or uncompounded rubber-like material.

Thermo-elastomers - A cross between plastics and elastomers with the properties of both. Can be molded or remolded like a thermoplastic and will stretch, elastically, like an elastomer. While not chemically linked like elastomers or like thermosetting polymers, the nature and structure of the chemical bonds provides a rubber-like quality.

Thermoplastic (resin) - A polymer which undergoes no permanent chemical change during moderate heating, and can be remolded or liquified upon reapplication of heat.

Thermosetting Polymer - A polymer which undergoes permanent chemical change by heating, can be molded but does not revert to liquid form upon reapplication of heat.

Thixotropic Paste - Substance whose properties are affected by mechanical action (i.e., flows only under pressure).

Vulcanizate - A vulcanized elastomer compound.

#### PROCESSING MODIFIERS

Additives - Materials added to a viscoelastic material to modify its damping or structural properties. (e.g., addition of carbon black to rubber and addition of organic fibers to an adhesive polymer.)

Copolymerization - Chemical linking together of two polymeric materials.

Filler - An inert additive, such as vermiculite, which replaces some of the viscoelastic material tending to change the loss factor and stiffness. This change is generally not as dependent on temperature or frequency as for a plasticizer.

Gum Stock - Basic ingredients of an elastomer necessary for vulcanizing only; without any plasticizer or filler.

Plasticizer - An organic fluid additive which serves to increase the flexibility of a polymer by diluting the polymer.

Polyblending - Mechanical blending of two polymers.

Polymerizing - Linking together of single molecules or monomers into long chains called polymers.

#### QUALITATIVE CHARACTERISTICS

Aging - The tendency for rubber to increase its stiffness with time.

Creep - Continued elongation under steady load - characteristic primarily of thermoplastics and elastomers, thus precluding their use when high loads must be sustained for long times.

Crystallinity - Property of stretched elastomers where molecules are highly oriented like crystals leading to a much higher stiffness of the material.

Durometer - A relative measure of the hardness of a rubber compound - the higher the Durometer, the harder the rubber. It is obtained with a simple handle-held spring actuated indenter with a conical tip of standard dimensions.

Transition, First Order - Temperature at which an elastomer starts to increase its stiffness rapidly.

Transition, Second Order - Temperature at which an elastomer becomes brittle like glass.

## PHYSICAL PARAMETERS

Dynamic Modulus – Mean ratio of stress to strain under dynamic loading – of the order of 1.3 to 2.2 times the static modulus.

Loss Factor in Extension – Ratio of loss modulus to storage modulus of elasticity – equal to tangent of phase angle between tensile stress and strain.

Loss Modulus of Elasticity – Imaginary part of dynamic modulus of elasticity (ratio of stress to component of strain which lags stress by  $90^\circ$ ).

Loss Modulus of Rigidity – Imaginary part of dynamic modulus of rigidity.

Modulus of Elasticity – Modulus in tension or compression – complex when measured dynamically.

Modulus of Rigidity – Modulus in shear – complex when measured dynamically.

Shape Factor – Ratio of area of surface under load to area of free surface (applied to rubber isolators).

Static Modulus – Ratio of stress to strain under steady load.

Storage Modulus of Elasticity – Real part of a dynamic modulus of elasticity (ratio of stress to component of strain in phase with stress).

Storage Modulus of Rigidity – Imaginary part of dynamic modulus of rigidity.

### 9.6.3.2 Properties of Viscoelastic Materials

Based on the definitions given in the previous section, the following general characteristics can be defined for basic types of viscoelastic damping materials. These have varying degrees of adhesive and damping properties and are used for laminated damped structure or for surface application with unconstrained-layer damping treatments.

#### Plastics

- Thermoplastics
  - Usually requires careful pre-bonding surface treatment
  - Subject to creep under static loads
  - With proper mixture and/or additives can provide very high damping and good bonding strength
  - Examples
    - Vinylchloride copolymer  
Damping Foil  
Spray-on Surface Layer
    - Vinylacetate copolymer  
Self-adhesive bonding layer

- Thermosetting Plastics
  - Requires minimum pre-bonding surface treatment for adhesive application
  - Very low creep
  - Maximum strength and temperature capability but lower damping
  - Examples
    - Epoxy – Shear strength to 8000 psi at  $70^\circ\text{F}$   
– Usable to  $180^\circ\text{F}$
    - Epoxy Phenolics – Shear strength to 3000 psi at  $70^\circ\text{F}$   
– Usable to  $500^\circ\text{F}$
    - Epoxy Silicones – Shear strength to 2000 psi at  $70^\circ\text{F}$   
– Usable to  $900^\circ\text{F}$
- Thermo-Elastomers
  - Combines high strength of plastics with varying flexibility of elastomers, depending on mixture
  - Examples
    - Polyurethanes – Shear strength to 6000 psi at  $70^\circ\text{F}$   
– Usable from  $-100$  to  $+200^\circ\text{F}$
    - Phenolic Nitrites – Shear strength to 4600 psi at  $70^\circ\text{F}$   
– Usable to  $500^\circ\text{F}$

#### Elastomers

- Adhesive Type
  - Pre-bonding requirements vary from minimum removing oil and grease to maximum of adding primer coating
  - Lowest strength and highest flexibility of adhesive viscoelastic materials
  - Examples
    - Silicones – Shear strength to 200 psi at  $70^\circ\text{F}$   
– Temperature range –  $90^\circ\text{F}$  to  $+600^\circ\text{F}$
- Non-Adhesive Type
  - Widely used for vibration isolators
  - Intermediate between liquid and solid (isovolumetric like liquid and stability of shape like a solid, Poisson's ratio 0.5)
  - Examples
    - Natural Rubber (Hevea)
    - Neoprene
    - Butyl Rubber
    - Polyurethanes

Detailed information on physical properties of these materials may be found in the following references

- General physical properties - References 9.33, 9.34, and 9.36.
- Damping properties - References 9.20, 9.28, 9.30, and 9.32.
- Adhesive Properties - References 9.37 and 9.38.

Temperature - Frequency Variation in Damping Properties

Practical design configurations which employ viscoelastic damping materials will often be exposed to a significant change in ambient temperature. The typical "temperature bandwidth" for a number of common viscoelastic materials is illustrated in Figure 9.62. As shown, the combined loss factor of typical configurations is within 1/2 its maximum value for a total temperature range of about 35 to 90° F. The operating temperature for maximum damping for these data lies between 50° to 140° F. (Reference 9.29).

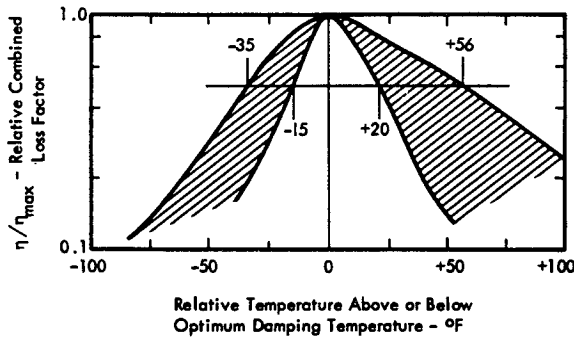


FIGURE 9.62 Typical Temperature "Bandwidth" of Loss Factor for Viscoelastic Damping Materials (From data in Ref. 9.29)

Optimum frequency temperature operating zones of maximum damping for six typical viscoelastic polymer materials are shown in Figure 9.63. This illustrates the boundaries of frequency and temperature for which the shear loss factor  $\beta$  or the material is equal to or greater than 1. The data has been selected from values given in Reference 9.30 to illustrate the relatively wide temperature range that can be covered by selected damping materials. From the analytical results in section 9.6.2.2 on constrained layer damping configurations, it was shown that the maximum combined loss factor,  $\eta$  for an optimum design, was about 0.3 times the shear loss factor  $\beta$ . Thus, by proper choice of materials, the data in Figure 9.63 indicate that a maximum combined loss factor of approximately 0.3 (i.e.,  $Q \approx 3$ ) would be possible for an optimally designed configuration at operating temperatures from about -40° C (-40° F) to 120° C (+248° F) in the frequency range from 100 to 1000 Hz.

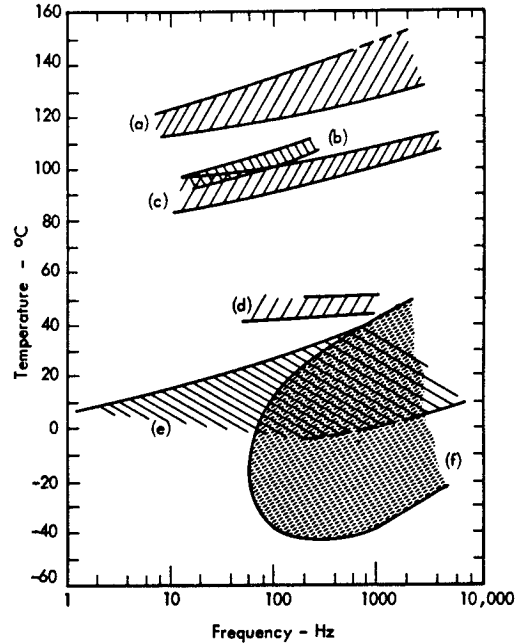


FIGURE 9.63 Frequency and Temperature Zones for Shear Loss Factor,  $\beta$ , Equal or Greater Than 1.0 for Six Viscoelastic Polymer Damping Materials Covering a Wide Range of Operating Temperatures. a) Polystyrene, b) Polyester, c) Polyvinyl Chloride, (PVC) d) Plasticized PVC e) Plasticized Polyvinyl Acetate f) Polyisobutylene (Data from Reference 9.30)

Similar data on temperature-frequency zones for the maximum shear loss of several common elastomer materials are shown in Figure 9.64. In this case, the maximum shear loss factor varies from 0.2 to over 1.0. These materials are representative of the type commonly used for rubber-in-shear vibration mounts. (see Figure 11.54, page 11.49).

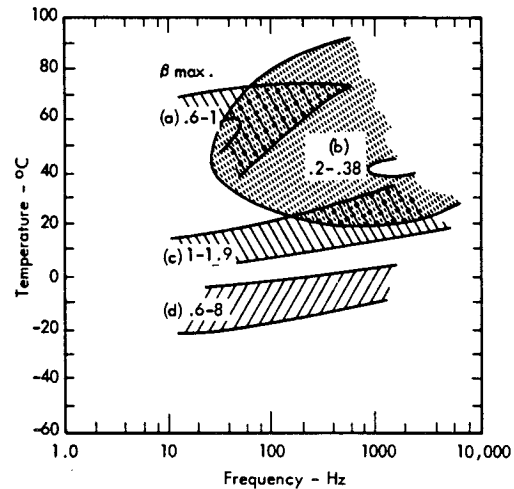


FIGURE 9.64 Frequency and Temperature Zones for Maximum Shear Loss Factor,  $\beta$ , for Elastomer Damping Materials Covering a Wide Range of Operating Temperatures. a) Hard Rubber, b) Aquaplas c) Urethane Rubber-Shore 80A, d) Polysulfide Rubber (Data from Reference 9.30)



Extended Temperature Range for Mixtures of Viscoelastic Compounds.

One method for extending the operating temperature range of a viscoelastic material is to mix two or more compounds. The results from one investigation which used this method are shown in Figure 9.65. This shows the variation with temperature of the loss factor  $\eta$  and dynamic elastic modulus  $E$  for 1, 2, and 3 compound mixtures. It is apparent that by a proper choice of mixtures, the usable temperature range for high damping can be increased. This is also accompanied by a more gradual decrease in the dynamic modulus.

Range of the Loss Factors and Elastic Modulus for Polymer Compounds and Elastomers

From the data presented so far in this section, it is obvious that a wide variety of damping characteristics are possible for various types of viscoelastic materials. This is shown more clearly in Figure 9.66. Approximate envelopes of the storage modulus  $E_1$  and loss modulus  $E_2$  of elasticity for a large number of polymer (thermoplastic and thermosetting plastic) materials and elastomer (rubber-like) materials have been plotted based on the extensive data summary contained in Reference 9.32. The material loss factor  $\eta$  in extension is represented on this graph by lines representing a constant value of the ratio

$$\frac{E_2}{E_1} = \eta$$

The data indicate that for extensional strains, the loss factor for polymer or plastic type materials generally lie in the range of 0.01 to 1.0 and for elastomer materials, in the range of 0.1 to 1.0.

A similar set of envelopes for the storage modulus  $G_1$  and loss modulus  $G_2$  of rigidity is shown in Figure 9.67 for the same two general types of viscoelastic materials. In this case, the loss factor  $\beta$  in shear, where

$$\frac{G_2}{G_1} = \beta$$

is close to 1 for the softer polymer materials, with decreasing values of  $\beta$  for materials with a high storage modulus. For elastomer materials, the loss factor in shear lies roughly between 0.1 and 1 with some extreme materials (such as Butyl rubber) having a loss factor much greater than 1.

Considering all the data shown, these indicate that viscoelastic materials have loss factors 1 to 2 orders of magnitude greater than typical loss factors for metallic materials. In summary, methods for applying viscoelastic materials to increase the damping of conventional metallic wall structure has been demonstrated. This increased damping will have the following effects:

- Increased sound transmission loss
- Reduction in structural vibration environments generated by vibrating walls
- Improved fatigue life for such walls.

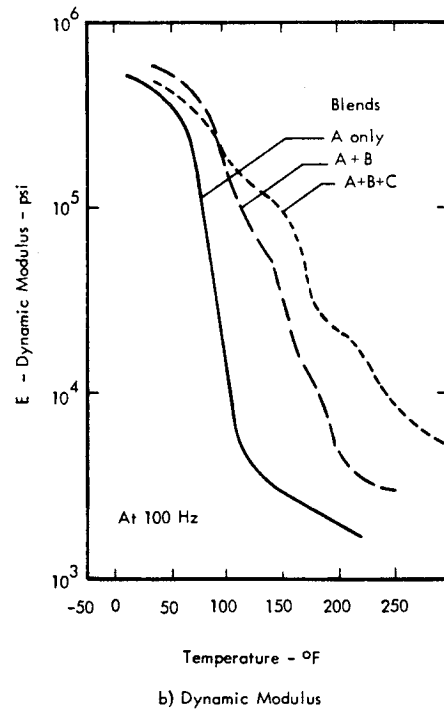
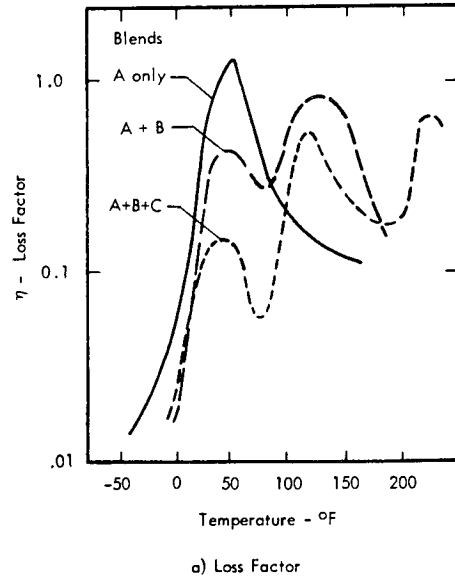


FIGURE 9.65 Improvement in Loss Factor and Dynamic Modulus of High Temperatures for 2 and 3 Element Blends of Viscoelastic Compounds. (Data from Ref. 9.31)  
 A - Nitrile-Butadiene Vulcanizate  
 B - Polyvinyl Acetate  
 C - Polystyrene

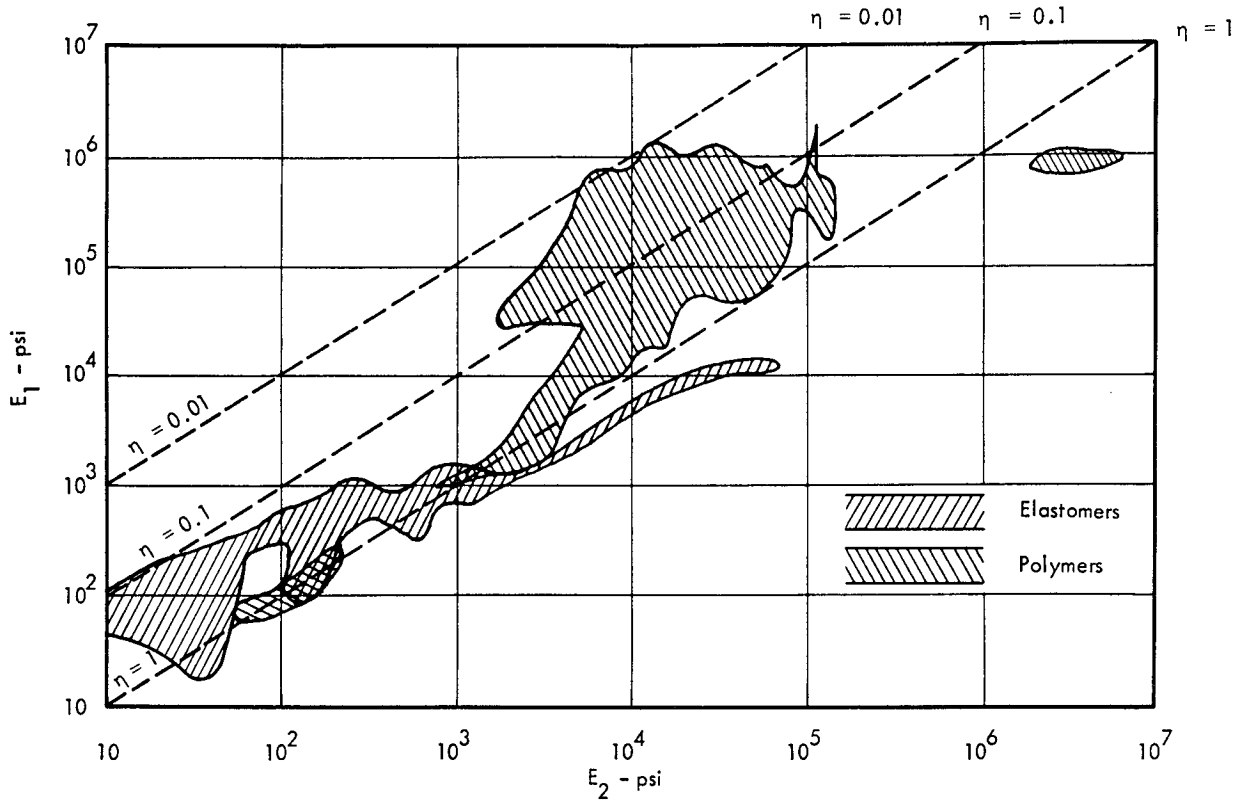


FIGURE 9.66 Storage Modulus of Elasticity  $E_1$ , versus Loss Modulus of Elasticity  $E_2$ , For Various Polymers and Elastomers (Data from Ref. 9.32)

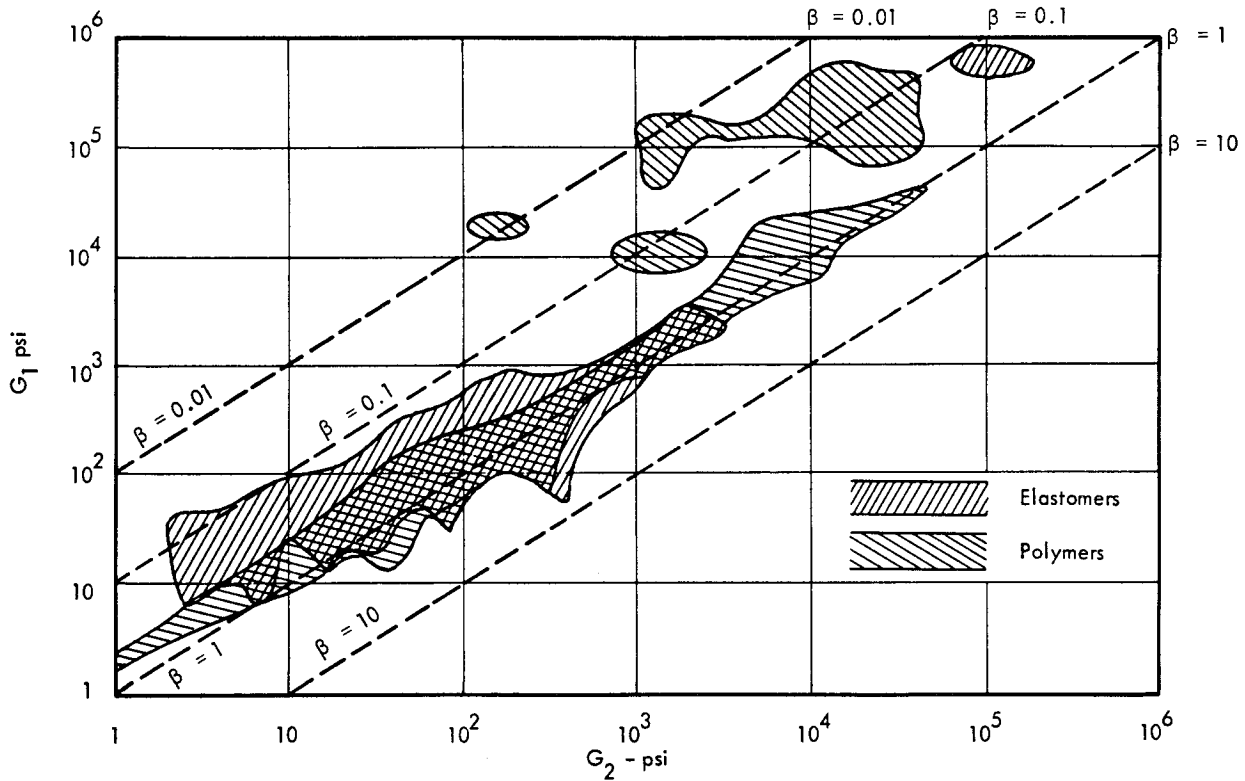


FIGURE 9.67 Storage Modulus of Rigidity  $G_1$ , versus Loss Modulus of Rigidity  $G_2$ , For Various Elastomers and Polymers (Data from Ref. 9.32)

## 9.7 STRUCTURAL VIBRATION CONTROL

Vibration energy can be transmitted into interior sections of a building which is exposed to a high intensity noise field by two basic paths:

- Direct transmission through the structural framework of the building.
- Indirect acoustic transmission into the interior of the building and subsequent acoustically induced vibration of the structure.

Methods of control of the second path have been covered in the preceding sections of this chapter. Consider now the control methods applicable to the first path - the direct transmission.

### 9.7.1 EFFECT OF DAMPING TREATMENT ON STRUCTURALLY TRANSMITTED VIBRATION

From the review of transmission of damped structural waves in Section 3.3.7.2, page 3-161, it was shown that the attenuation per wavelength of plane longitudinal waves and lateral bending waves in beams was defined by

- Longitudinal waves

$$\mu_L \approx 8.68 \pi \eta - \text{dB/wavelength} \quad (9.113)$$

- Lateral bending waves

$$\mu_B \approx 4.34 \pi \eta - \text{dB/wavelength} \quad (9.114)$$

where

$\eta$  = material loss factor.

This attenuation loss is directly proportional to the material loss factor  $\eta$  so that any increase in the latter provides a proportional increase in attenuation of structural vibration.

According to the results presented in Section 9.6.2, loss factors of damped configurations of the order of 0.2 are not difficult to achieve. Thus, the attenuation rate of longitudinal waves and lateral bending waves for heavily damped structure would be approximately

$$\mu_L (\text{Damped}) \sim 5.5 \text{ dB/wavelength}$$

$$\mu_B (\text{Damped}) \sim 2.7 \text{ dB/wavelength}$$

For the fundamental frequency of a typical beam, the longitudinal or bending wavelength will be of the order of twice the length of the beam so that the total attenuation of longitudinal or bending waves, at the fundamental frequency, would be of the order of 2.7 and 1.4 dB, respectively over the length of the beam. To be more specific, for the  $n$ th mode, the total attenuation  $A$  over the length of a beam for a combined loss factor of  $\eta$  would be

- Longitudinal waves

$$A_L \sim 13.6 \eta n - \text{dB}$$

- Lateral bending waves

$$A_B \sim 6.8 \eta n - \text{dB}$$

Therefore, for a given loss factor, this total attenuation over the length of the element increases directly with mode number but is independent of its size. Thus, significant attenuation of structurally transmitted vibration can be achieved for higher modes of vibration of heavily damped structural elements. A more exact analysis of this problem is not attempted here. The problem is complicated by the types of modes involved, the method of coupling of connected structural elements in any structure, the frequency variation in the loss factor, and the frequency of vibration of the various modes of the structure. It is sufficient to point out, at least qualitatively, trends for the effect of structural vibration. The concept could have important applications in cases where excessive structurally-transmitted vibration could only be reduced by increasing the attenuation of the transmission path.

### Damping of Joints

The major part of the damping achieved in conventional structural framework is due to various forms of energy loss at the joints. Several techniques are being investigated which would further increase this joint damping (References 9.28, 9.39-9.41). These include

- Use of oil-films between joints
- Use of viscoelastic inserts between joints
- Optimization of frictional or viscous losses in riveted or bolted joints.

While design applications have not been standardized for these techniques, they offer promise for application in the future to special cases, such as rocket facility structure, where improved structural damping is desirable.

### 9.7.2 VIBRATION ISOLATION

One of the last stages in the control of vibratory motion from external sources is accomplished by employing vibration isolation for sensitive equipment. This can also be one of the initial stages for control of vibratory forces from internal sources such as rotating machinery. In either case, the basic method is the same. In the simplest form, this consists of inserting one or more isolator spring elements between the equipment and its mounting structure. The spring element is designed to insure that the natural frequency  $f_o$  of the combined equipment mass  $m$  and isolator stiffness  $k$  is well below some critical frequency  $f_c$ . This may be expressed by

$$f_o = \frac{1}{2\pi} \sqrt{\frac{k}{m}} \ll f_c \quad (9.115)$$

For isolation of vibration from external sources, this critical frequency may simply be a characteristic peak frequency in the excitation or it may be the natural frequency of a critical internal part within the equipment item which must be protected.

For isolation of internal sources, the critical frequency  $f_c$  will be the predominant frequency of the driving source (e.g., the rotational speed of a compressor system).

The vibration attenuation of an isolator system is specified by its motion or force transmissibility as follows.

Motion Transmissibility

- The ratio of the amplitudes of the vibratory motion (displacement  $x_2$ , velocity  $\dot{x}_2$ , or acceleration  $\ddot{x}_2$ ) of the isolated mass to the corresponding motion ( $x_1$ ,  $\dot{x}_1$ , or  $\ddot{x}_1$ ) at the input to the isolator system.

Force Transmissibility

- The ratio of the force  $P_T(t)$  transmitted through the isolator to the driving force  $P(t)$  of the isolated machinery.

9.7.2.1 Isolation of a Single Degree-of-Freedom System

The basic theory for vibration of a single degree of freedom has been covered in Section 3.2.1, Chapter 3. From Equation 3.29, page 3-7, it can be shown that the transmissibility for an undamped single degree-of-freedom mass-spring isolation system is given by

$$T(\omega) = \frac{1}{1 - (\omega/\omega_0)^2} \tag{9.116}$$

where

$$\omega = 2\pi f, \text{ the excitation frequency}$$

$$\omega_0 = 2\pi f_0, \text{ the natural frequency of the isolator defined by Equation 9.115.}$$

This expression is plotted in Figure 9.68. Note that for excitation frequencies greater than  $2\omega_0$ , the transmissibility is always less than 1. This still holds true for damped single degree-of-freedom isolators, as shown in Figure 3.7, page 3-8.

The natural frequency of a lumped mass single degree-of-freedom system can be determined from Figure 9.69. This is a graphical evaluation of Equation 9.115 in a convenient form for design calculation.

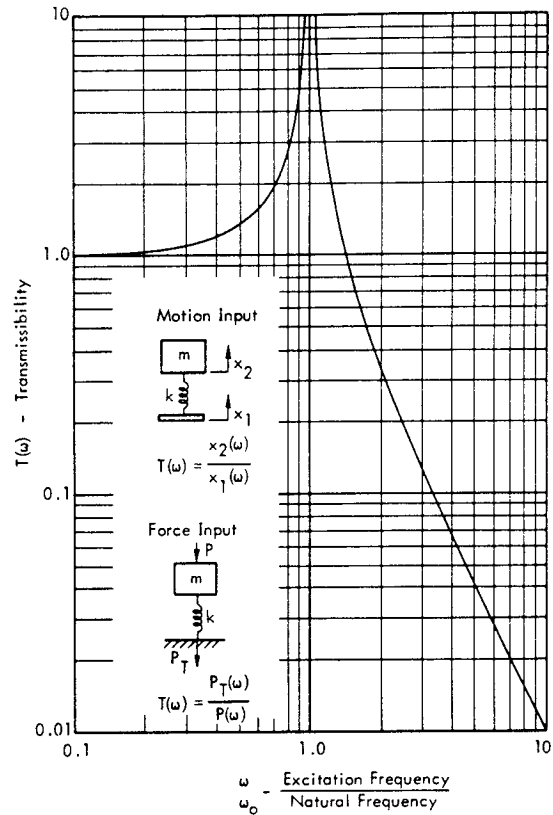


FIGURE 9.68 Transmissibility for Motion or Force Excitation of an Undamped Single Degree-of-Freedom System

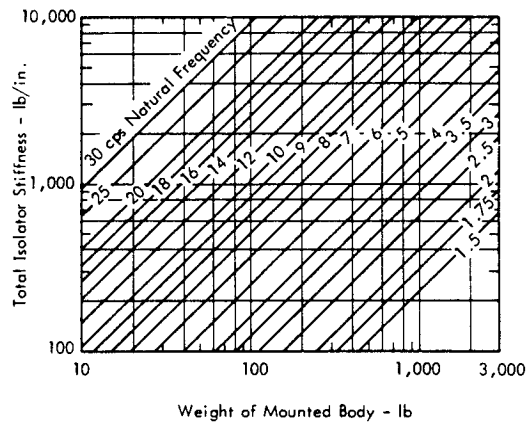


FIGURE 9.69 Natural Frequency of a Single-Degree-of-Freedom System as a Function of Weight of Mounted Body and Isolator Stiffness. ( from Reference 9.35)

Lower Limit for Natural Frequency of Isolator

A practical lower limit for the natural frequency of the isolation system is imposed by the maximum static deflection  $\epsilon_s$  relative to the base or the peak dynamic deflection  $\epsilon_{max}$  (relative to the base) at the resonance frequency  $f_o$ .

For a linear spring, the static deflection can be specified in terms of  $f_o$ , as shown graphically in Figure 9.70. This relationship is obtained from the equation

$$f_o = \frac{1}{2\pi} \sqrt{\frac{k}{m}} = \frac{1}{2\pi} \sqrt{\frac{k g}{W}} = 3.13 \sqrt{\frac{1}{\epsilon_s}} \quad (9.117)$$

where

$W = mg$ , the weight of the equipment

$g = 386 \text{ in/sec}^2$

$\epsilon_s =$  static deflection, inches.

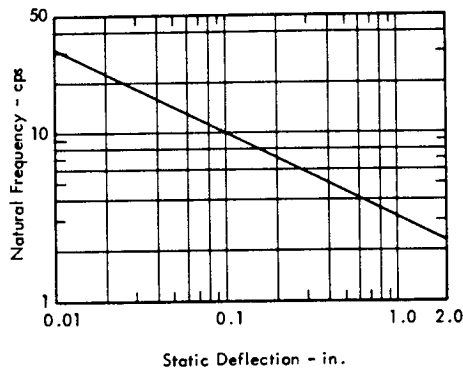


FIGURE 9.70 Relation Between Natural Frequency and Static Deflection for a Linear, Single-Degree-of-Freedom System (from Reference 9.35)

Isolation systems which employ materials such as rubber, fiberglass, or cork have nonlinear load-deflection characteristics so that the above expression is no longer valid. Typical data relating  $f_o$  to the static deflection for such cases are illustrated in Figure 11.55, page 11-50.

The peak (relative) dynamic deflection,  $\epsilon_{max}$  defines the envelope of additional clearance needed for the isolated equipment, relative to the mounting structure, to permit full dynamic response without impacting adjacent structure. For a sinusoidal input displacement, with an amplitude  $X_1(f_o)$  at the natural frequency  $f_o$ , the isolated system,  $\epsilon_{max}$  is given by

$$\epsilon_{max} = Q X_1(f_o) \quad (9.118)$$

where

$Q =$  resonant amplification factor of isolator

$= c/c_c$  or  $1/\eta$ .

For random excitation with a constant input acceleration spectral density, the peak relative dynamic deflection for a linear system can be determined from the design chart in Figure 3.46, page 3.46. Additional practical details of vibration isolation of equipment, based on a single degree-of-freedom model, are covered in Section 11.8.2.4, page 11-48.

9.7.2.2 Isolation of Two Degree-of-Freedom System

The application of a single degree-of-freedom model for design of vibration isolators is not adequate for many cases which involve motion in two or more directions. In fact, good engineering practice would usually dictate that at least two degrees of freedom be considered when designing an isolation system for any but the simplest lightweight equipment. In recognition of this, most manufacturers of vibration isolators specify the stiffness of standard vibration isolators in two directions - longitudinally along the axis of the isolator and perpendicular to this axis. Some of the basic design principles involved for two degree-of-freedom isolators are considered in this section (Reference 9.35).

Force Excitation

Consider the system illustrated in an elevation view in Figure 9.71. The mass  $m$  is assumed to have four equal linear spring isolators located at the four corners. Let this mass represent a unit of rotating machinery with an unbalance force  $P_y \sin \omega t$  acting vertically through the center of gravity and a force  $P_x \cos \omega t$  acting in the horizontal direction at a distance  $e$  above the center of gravity. For the sign convention illustrated, forces and translational displacements are positive when up or to the right, and moments and rotational displacements are positive when counterclockwise. Vertical distances from the X axis through the center of gravity are also positive in the up direction.

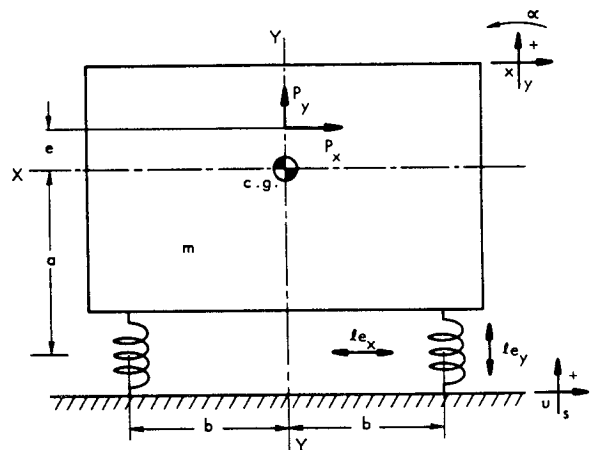


FIGURE 9.71 Elevation View of Rigid Body Mounted on Isolators Located at Four Lower Corners, and Excited by Harmonic Forces  $P_x, P_y$  applied to Mounted Body in XY Plane. Excitation May Also Result from Motion  $u_s$  of Support where  $P_x = P_y = 0$  (Adapted from Reference 9.35)

For motion in the vertical direction, only one equation of motion is involved since the applied vertical force is through the center of gravity. In this case, the system is statically decoupled in the vertical direction and motion in this direction cannot excite vibration in any other mode for equal stiffness of the vertical springs (see Section 3.3.2.6, page 3-56 for discussion of statically and dynamically coupled systems).

Applying the methods discussed in Section 3.3.2, page 3-50, the equation of motion for the y direction can be given by

$$m \ddot{y} + 4 k_y = P_y \sin \omega t \quad (9.119)$$

where

$k_y$  = vertical stiffness of each spring.

The two equations of motion for translation along the X axis and rotation about the Z axis (the axis perpendicular to the plane of the paper) are

$$m \ddot{x} + 4 k_x - 4 k_y a \alpha = P_x \cos \omega t \quad (9.120)$$

$$I_z \ddot{\alpha} - 4 k_x a x + 4 k_x a^2 \alpha + 4 k_y b^2 \alpha = - P_x e \cos \omega t$$

where

$k_x$  = horizontal stiffness of each spring

$a$  = vertical distance from CG to mid-point of isolators

$\alpha$  = angular rotation

$I_z$  = mass moment of inertia of body about Z axis

$b$  = horizontal distance from CG to vertical axis through springs.

These two equations of motion define the dynamic response of the mass as a two degree-of-freedom system for the coordinates  $x$  and  $\alpha$ . A complete solution for the forced response of this system is carried out in Reference 9.35 along the same general lines discussed in Section 3.3.3. Transmissibilities for forced response in each of the two directions  $x$  and  $\alpha$  can be obtained in a similar fashion.

For design purposes, the primary problem is similar to that for the single degree-of-freedom system - to design the isolator stiffnesses so that the natural frequencies of the system fall below (or outside) the range of critical fre-

quencies. In this case, the disturbing frequency is internally set by the rpm of the rotating machinery.

The two natural frequencies of the two degree-of-freedom system are obtained by a solution of Equation 9.120 in the same manner outlined in Section 3.3.2.2. The resulting expression can be given in a convenient nondimensional form as (Reference 9.35)

$$\frac{\omega_c}{\omega_y} \frac{\rho}{b} = \left[ \frac{R}{2} \pm \frac{1}{2} \sqrt{R^2 - 4S} \right]^{1/2} \quad (9.121)$$

where

$\omega_y = \sqrt{4 k_y / m}$  - the natural frequency for vertical translation

$\rho = \sqrt{I_z / m}$  - the radius of gyration with respect to the Z axis

$$R = \left( \frac{k_x}{k_y} \right) \left( \frac{\rho}{b} \right)^2 \left[ 1 + \left( \frac{a}{\rho} \right)^2 \right] + 1$$

$$S = \frac{k_x}{k_y} \left( \frac{\rho}{b} \right)^2$$

$a, b$  = dimensions defined for Equation 9.120, and

$\omega_c$  = the two natural frequencies of the coupled system.

This expression is shown graphically in Figure 9.72 in terms of the nondimensional parameters used in the above equation. For a given value for the stiffness parameter

$$\frac{\rho}{b} \sqrt{\frac{k_x}{k_y}}$$

the two natural frequencies of the system are found by the intersection of a vertical line through this abscissa value and the two parameter lines for a given value of  $a/\rho$ .

For a case where the stiffness parameter  $(\rho/b) \sqrt{k_x/k_y}$  is close to 1/2 and the distance ratio  $a/\rho$  is much less than 1, the two natural frequencies approach the one value  $\omega_c = \omega_y (b/\rho)$ . In this case, to avoid excessive coupling between the two modes, it is common practice to attach the isolators to the mass in a plane which passes approximately

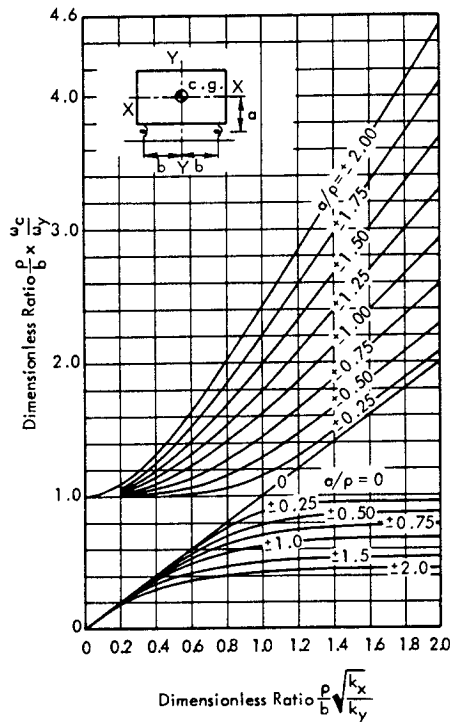


FIGURE 9.72 Curves Showing Ratio of Two Coupled Natural Frequencies  $\omega_c$  in XY Plane to Decoupled Natural Frequency  $\omega_y$  in Translation along Y Axis. The Isolator Stiffness in the X and Y Directions are Indicated by  $k_x$  and  $k_y$ , Respectively, and the Radius of Gyration with Respect to the Z Axis through the Center of Gravity is Indicated by  $\rho$ . (from Reference 9.35)

through the center of gravity. In this way, just as for vertical translation, dynamic coupling between horizontal motion and rotation is eliminated or reduced.

Equation 9.121 defines two of the natural frequencies of the rigid mass for motion in the XY plane. A third is given by the natural frequency  $\omega_y = \sqrt{4k_y/m}$  which is the solution of Equation 9.119 for vertical translation in this plane. Two more coupled natural frequencies are obtained for motion in the YZ plane. Equation 9.121 still applies except that the dimension b becomes the corresponding dimension c, illustrated in the plane view in Figure 9.73, and  $I_z$  is replaced by  $I_x$ , the mass moment of inertia about the X axis.

One more natural frequency remains to define the six degrees of freedom for a rigid body - the natural frequency for rotation in the XZ plane about the Y axis. Again, for equal stiffness of the four springs in the X direction ( $k_x$ ), and in the Z direction ( $k_z$ ), the system reduces to a single

degree-of-freedom model with the equation of motion given by

$$I_y \ddot{\beta} + 4\beta b^2 k_z + 4\beta c^2 k_x = 0$$

where

$I_y$  = mass moment of inertia about the Y axis

$\beta$  = angular rotation about Y axis.

The last natural frequency obtained from this equation is given by

$$\omega_\beta = 2 \sqrt{\frac{b^2 k_z + c^2 k_x}{I_y}} \tag{9.122}$$

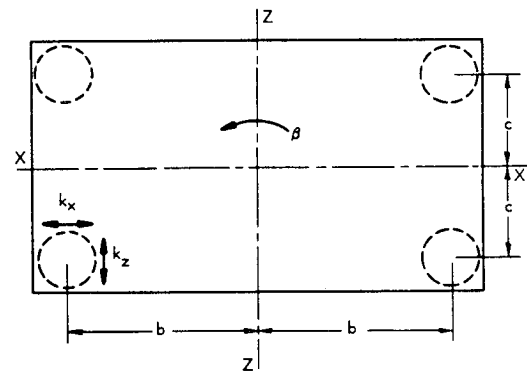


FIGURE 9.73 Plan View of Rigid Body Mounted Upon Isolators Located at Four Lower Corners. The Stiffnesses of the Isolators in the Directions of the X and Z axes are Indicated by  $k_x$  and  $k_z$ , respectively. (From Reference 9.35)

Thus, each of the natural frequencies of the idealized system are defined so that the spring stiffnesses can be designed to achieve the desired minimum transmissibility of the driving force into the foundation. For constant-speed rotating machinery, this may involve having some of the natural frequencies of the isolator system well above the driving frequency.

Motion Excited Systems

The same principles outlined above apply for motion excitation of the base. In this case, with a wide band random input, it is usually desirable to have all the natural frequencies as low as possible, and well separated unless center-of-gravity mounting is employed.

## REFERENCES

- 9.1 Furrer, W., "Room and Building Acoustics and Noise Abatement," Butterworths, London, 1946.
- 9.2 "Solutions to Noise Control Problems in the Construction of Houses, Apartments, Motels and Hotels," AIA File No. 39-E, Owens-Corning Fiberglas Corporation, Toledo, Ohio, 1963.
- 9.3 Zwikker, C., and Kosten, C.W., "Sound Absorbing Materials," Elsevier Publishing Co., N.Y. 1949.
- 9.4 "Architectural Acoustical Materials," Acoustical Materials Association Bulletin No. XXXVII, N.Y.
- 9.5 Kinsler, L.E., and Frey, R.F., "Fundamentals of Acoustics," John Wiley & Sons, N.Y., 1967.
- 9.6 Morse, P.M. "Vibration and Sound," McGraw-Hill Book Co., N.Y., 1948.
- 9.7 Eyring, C.F., "Reverberation Time in Dead Rooms," J. Acoust. Soc. Am. 1, 1930, 217.
- 9.8 Knudsen, V.O., and Harris, C.M., "Acoustical Designing in architecture," John Wiley & Sons, N.Y., 1950.
- 9.9 "Laboratory Measurement of Airborne Sound Transmission Loss of Building Partitions," American Society for Testing and Materials, Philadelphia, Pa. Designation E90-66T, Revised 1966.
- 9.10 Cremer, L., "The Propagation of Structure-Borne Sound," D.S.I.R. Sponsored Research (Germany), Report No., 1, Series B.
- 9.11 Beranek, L.L., "Noise Reduction," McGraw-Hill Book Co., N.Y., 1960
- 9.12 Gosele, K., "Radiation Behavior of Plates," *Acustica*; Vol. 6, No. 45, 1946.
- 9.13 ASHRAE Guide and Data Book, Systems and Equipment, Published by American Society of Heating, Refrigerating and Air Conditioning Engineering, N.Y., 1957.
- 9.14 Bolt, Beranek and Newman, "Handbook of Acoustic Noise Control," WADC Technical Report 52-104, Vol. 1, 1952.
- 9.15 Lukasik, S.J., and Nolle, A.W., ed., "Handbook of Acoustic Noise Control," Bolt, Beranek and Newman, WADC Technical Report 52-204, Vol. 1, Supplement 1, 1955.
- 9.16 Bolt, Beranek and Newman, "Methods for Improving the Noise Insulation of Houses with Respect to Aircraft Noise," Report 1387, Submitted to FHA Nov., 1966.
- 9.17 Beranek, L.L., "Acoustics", McGraw-Hill Book Co., N.Y., 1954.
- 9.18 Comperts, M.C., "The Sound Insulation of Circular and Slit-Shaped Apertures," Fourth Int. Congress on Acoustics, Copenhagen, 1962.
- 9.19 Wilson, G.P. and Soroka, W.W., "Approximation to the Diffraction of Sound by a Circular Aperture in a Rigid Wall of Finite Aperture," J. Acoust. Soc. Am. 37, No. 1, Feb. 1965, p. 287.
- 9.20 Lazan, B.J., and Goodman, L.E., "Material and Interface Damping" Chap. 36, Shock and Vibration Handbook, Harris, C.M. and Creede, C.E., ed., McGraw-Hill Book Co., N.Y., 1961.
- 9.21 Crede, C.E., "Application and Design of Isolations," Chap. 32, Shock and Vibration Handbook, Harris, C.M., and Crede, C.E., ed., McGraw-Hill Book Co., N.Y., 1961.
- 9.22 Ungar, E.E., "Loss Factors of Viscoelastically Damped Beam Structures," *Acoust. Soc. Am.* 34, Aug., 1962, pp. 1082-1089.
- 9.23 Mead, D.J., "The Damping of Stiffened Plate Structures," Chap. 26, Acoustical Fatigue in Aircraft Structures, Trapp, W.J., Forney, D.M., ed., Syracuse University Press, N.Y., 1965.
- 9.24 Kerwin, Jr., E.M., "Damping of Flexural Waves by a Constrained Viscoelastic Layer," *J. Acoust. Soc. Am.* 31, Jul. 1959, pp. 952-962.
- 9.25 Ungar, E.E., "A Guide to Designing Highly Damped Structures," *Machine Design*, Feb. 14, 1963.
- 9.26 Ruzicka, J.E., "Vibration Response Characteristics of Viscoelastic-Damped Structures," *Shock and Vibration Bulletin*, Part 5, Feb. 1965.
- 9.27 Ross, D., et al, "Design Study of Damping Techniques - Quarterly Progress Report," Bolt, Beranek and Newman Report No. 591, USN BuShips Contract NObs-72452, Oct. 20, 1958.
- 9.28 Ruzicka, J.E., ed., "Structural Damping" American Society of Mechanical Engineers, N.Y., 1959.



- 9.29 Oberst, H. and Schommer, A. "Optimization of Viscoelastic Damping Materials for Specific Structural Composite Applications," Chap. 29, "Acoustical Fatigue in Aerospace Structures," Trapp, W. J. and Forney, D.M. Jr., ed., Syracuse University Press, Syracuse, N.Y., 1965.
- 9.30 Ungar, E.E., and Hatch, D.K., "Your Selection Guide to High-Damping Materials," Product Engineering, April 17, 1961.
- 9.31 Owens, F.S., "Elastomers for Damping Over Wide Temperature Ranges," Shock and Vibration Bulletin, Jan 1967.
- 9.32 Chi, S.H., "Bibliography and Tabulation of Damping Properties of Non-Metallic Materials," WADD TR 60-540, Sept. 1962.
- 9.33 Rondeau, H.F., "Synthetic Materials," Machine Design, July 21, 1966.
- 9.34 Ferry, J.D., "Viscoelastic Properties of Polymers" John Wiley & Sons, N.Y., 1961.
- 9.35 Crede, C.E., "Vibration and Shock Isolation," John Wiley & Sons, N.Y., 1951.
- 9.36 Frye, W. A., "Rubber Springs," Chapter 35, "Shock and Vibration Handbook," Harris, C. M. and Crede, C. E., ed., McGraw-Hill Book Co., N. Y., 1961.
- 9.37 Sharpe, L. H., "Assembling with Adhesives," Machine Design, Apr. 18, 1966.
- 9.38 Guttman, W. H., "Concise Guide to Structural Adhesives," Reinhold Publishing Co., N. Y., 1961.
- 9.39 Hanks, B. R. and Stephens, D. G., "Mechanisms and Scaling of Damping in a Practical Structural Joint," Shock and Vibration Bulletin, Part 4, Jan. 1967.
- 9.40 Maidanik, G., "Energy Dissipation Associated with Gas-Pumping in Structural Joints," J. Acoust. Soc. Am. 40, No. 5, 1966, pp. 1064-1072.
- 9.41 Eaton, D. C. G., "Interface Damping at Riveted Joints," ASD TR 61-467, Part II, Air Force Materials Laboratory, Aug. 1965.

**CHAPTER 10**  
**EFFECTS OF NOISE,**  
**VIBRATION AND BLAST**  
**ON PERSONNEL**

TABLE OF CONTENTS

<u>SECTION</u>	<u>PAGE</u>
10.1	<u>EFFECTS OF ACOUSTIC NOISE ON PERSONNEL</u> . . . . . 10-1
10.2	<u>PHYSIOLOGICAL EFFECTS OF ACOUSTIC NOISE</u> . . . . . 10-1
10.2.1	PAIN . . . . . 10-1
10.2.2	HEARING DAMAGE . . . . . 10-2
10.2.3	NON-AUDITORY EFFECTS . . . . . 10-5
10.3	<u>SUBJECTIVE REACTION TO ACOUSTIC NOISE</u> . . . . . 10-5
10.3.1	LOUDNESS . . . . . 10-6
10.3.2	NOISINESS . . . . . 10-7
10.3.3	AGE . . . . . 10-10
10.3.4	ANNOYANCE . . . . . 10-10
10.4	<u>OBJECTIVE INFLUENCE OF ACOUSTIC NOISE</u> . . . . . 10-10
10.4.1	SPEECH COMMUNICATION . . . . . 10-10
10.4.2	EFFECTS OF NOISE ON BEHAVIOUR AND EFFICIENCY . . . . . 10-12
10.5	<u>COMMUNITY REACTION</u> . . . . . 10-13
10.6	<u>EXPOSURE OF PERSONNEL TO BLAST</u> . . . . . 10-18
10.6.1	GENERAL DISCUSSION . . . . . 10-18
10.6.2	PRIMARY EFFECTS . . . . . 10-18
10.6.2.1	Effects of Duration on Lethal Limits for Blast . . . . . 10-18
10.6.2.2	Analytical Model for Predicting Effects of Duration . . . . . 10-20
10.6.3	SECONDARY EFFECTS . . . . . 10-20
10.6.4	TERTIARY EFFECTS . . . . . 10-21
10.6.5	SUMMARY OF BLAST EFFECTS . . . . . 10-22
10.7	<u>EXPOSURE OF PERSONNEL TO SONIC BOOM</u> . . . . . 10-22
10.7.1	THE BOOM INDOORS AND OUTDOORS . . . . . 10-22
10.7.2	THE EFFECTS OF SPECTRAL CONTENT UPON NOISINESS . . . . . 10-23
10.7.3	DAMAGE LEVELS . . . . . 10-24
10.8	<u>EFFECTS OF VIBRATION ON PERSONNEL</u> . . . . . 10-24
10.8.1	MECHANICALLY INDUCED VIBRATION . . . . . 10-24
10.8.1.1	Mechanical Effects . . . . . 10-24
10.8.1.2	Physiological Effects . . . . . 10-25
10.8.1.3	Psychological Effects . . . . . 10-25
10.8.1.4	Pathological Effects . . . . . 10-26
10.8.2	ACOUSTICALLY INDUCED VIBRATION . . . . . 10-26
10.8.2.1	Sonic Vibration of the Head . . . . . 10-26
10.8.2.2	Sonic Vibration of Whole Body . . . . . 10-26
10.8.2.3	Sonic Vibration of the Thorax/Abdomen System . . . . . 10-27
10.9	<u>HEARING PROTECTION</u> . . . . . 10-28
10.9.1	PROTECTION DEVICES . . . . . 10-28
10.9.1.1	Earplugs . . . . . 10-28
10.9.1.2	Semi-Inserts . . . . . 10-29
10.9.1.3	Earmuffs . . . . . 10-29
10.9.1.4	Helmets . . . . . 10-29

TABLE OF CONTENTS (Continued)

<u>SECTION</u>		<u>PAGE</u>
10.9.2	COMPARISON OF EAR PROTECTION DEVICES .....	10-29
10.9.3	SUMMARY OF EAR PROTECTION DEVICES .....	10-32
10.9.4	ACOUSTIC SHELTERS FOR PERSONNEL .....	10-34
10.10	<u>BLAST PROTECTION FOR PERSONNEL</u> .....	10-34
10.10.1	PROTECTION OF THE EARDRUM .....	10-34
10.10.2	PROTECTION AGAINST BLAST-GENERATED MISSILES .....	10-35
10.10.3	PROTECTION BY BLAST-PROOF BUILDINGS .....	10-36
10.11	<u>SHOCK AND VIBRATION PROTECTION FOR PERSONNEL</u> .....	10-37
10.11.1	PROTECTION FROM GROUND VIBRATION .....	10-37
10.11.2	PROTECTION FROM DIRECT ACOUSTICALLY INDUCED VIBRATION OF BUILDINGS ..	10-38
10.11.3	PROTECTION FROM GROUND SHOCK DUE TO EXPLOSIONS .....	10-38
	REFERENCES .....	10-39

## CHAPTER 10

### EFFECTS OF NOISE, VIBRATION, AND BLAST ON PERSONNEL

Basic criteria for maximum noise and vibration environments that are acceptable to man have been briefly summarized in Chapter 5. A more extensive background of the basis for these criteria is developed in this chapter.

By definition, noise is considered as an undesirable stimulus. In this case, it is convenient to consider both acoustical and mechanical excitation as "noise". Furthermore, acoustical noise may be defined to include consideration of transient overpressures such as blast or sonic boom. Thus, this chapter presents, in sequence, a detailed review of the effects on man of acoustical noise, blast and sonic boom overpressure and mechanical vibration and concludes with the discussion of devices for protecting man against these environments.

#### 10.1 EFFECTS OF ACOUSTIC NOISE ON PERSONNEL

Consider first, the effects of acoustic noise. The main factors which determine its effects upon personnel are its intensity and its frequency spectrum. In general, the effects increase in number and magnitude as the intensity increases. The listener's behaviour depends almost entirely upon his previous experience, and his initial reaction to noise stimuli may be to identify the noise as a warning of danger. His further reaction, as the noise increases in level, is one of disturbance and annoyance, particularly, if it interferes with sleep or rest. The next most important effect of the noise is its interference with speech communication. At this point, the noise has become a definite handicap which is measured by the extent to which speech is masked by the noise. Further increases of intensity cause temporary hearing loss to a degree which depends upon the spectrum of the noise and its duration. Upon cessation of the sound, hearing is gradually restored although the cumulative effects of numerous temporary losses of hearing can cause permanent damage over a period of time. As the intensity becomes still greater, the noise actually becomes uncomfortable. Such sound levels can excite physiological reactions such as tension, which in turn leads to fatigue, the cumulative effects of which could become dangerous. Although the pain sensation is obviously indicative of dangerously high sound levels, it does not necessarily accompany ear damage. Unfortunately, the converse is also true; that ear damage is not always accompanied by a warning sensation of pain. There is also evidence that very high sound levels can cause nausea, dizziness, and inhibit performance of motor tasks.

These subjective and objective effects of noise may be

divided into two distinct areas. The first is the effect of the launch site noise environment on personnel who must work in the area for which the noise is "part of the job" and the second is "community response," defining the effects of the noise upon a nearby population for which the noise may be either a distinct nuisance or a necessary part of a working environment.

Existing data applicable to effects of rocket noise on man are incomplete and show a large degree of scatter. This is primarily due to the difficulty of measuring the effects of rocket engine noise. Many of the results which are available for the lower frequencies are not accurate, having been obtained from experiments utilizing earphones. These are inadequate at low frequencies since, at these frequencies, the entire body becomes an important receptor for sound waves. Fortunately, one series of tests have been conducted with whole body exposure down to 1 Hz. and can be used to estimate an upper bound of physiological effects of infrasonic noise.

Figure 10.1 illustrates a qualitative model for the overall response of man to noise. The community response problem is conceived as an amalgam of four major factors, which are, roughly, in order of importance:

- (1) Physiological effects of acoustic noise.
- (2) Objective influence of acoustic noise.
- (3) Subjective response to acoustic noise.
- (4) Community socio-economic factors.

The noise itself, in this particular case, comprises two components, the ambient noise environment and the additional stimulus due to the booster exhaust noise. The effects of the total noise are thus dependent on both the sum and difference of the two components that represent the total level of exposure and the all-important increment, of short duration, which gives rise to the noise problem at a rocket launch or test site. The four factors will now be discussed in detail.

#### 10.2 PHYSIOLOGICAL EFFECTS OF ACOUSTIC NOISE

##### 10.2.1 PAIN

Auditory or aural pain is normally identified as an aching sensation which is located "deep in the ear" and a threshold of pain can be defined as the sound pressure level which causes the onset of this sensation over and above the discomfort associated with excessive loudness and an intermediate tickling sensation.

Figure 10.2 shows the threshold of pain produced by both pure tones and broadband noise according to three sources (References 10.1, 10.2, and 10.3). The Benox report (Reference 10.1) describes experiments conducted using five subjects with some experience in high intensity noise exposure. These were exposed to (i) static pressures,

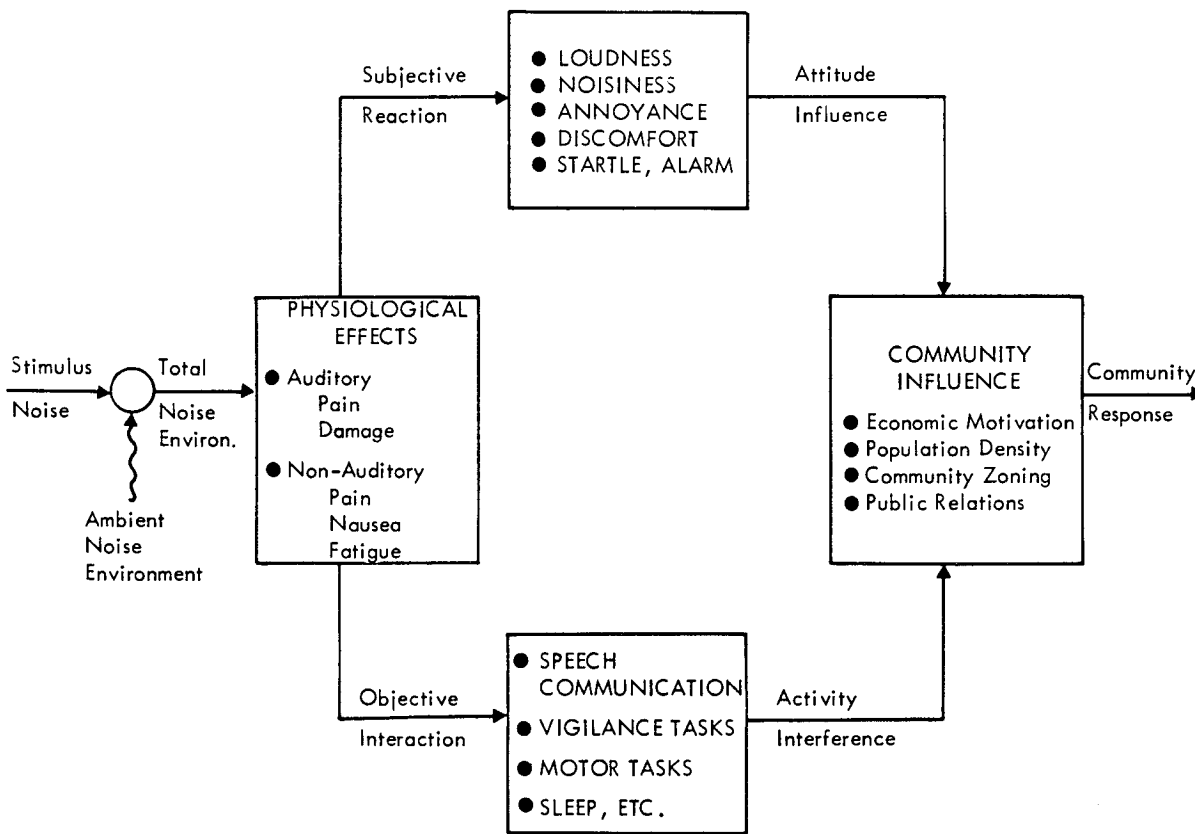


FIGURE 10.1 Model for Overall Response of Man to Acoustic Noise

(ii) discrete frequencies, and (iii) jet noise. It was found that below 50 Hz., pain was felt with little or no "loudness," and the subjects noted only a "rhythm of overtones" at the pain threshold. In the higher frequency range between 800 and 2,000 Hz., the sound was found to be uncomfortably loud at levels well before the pain threshold was reached. Between 15 and 2,000 Hz., the pain threshold is very close to 140 dB, a result which is corroborated by the measurement of von Békésy (Reference 10.2). Below 15 Hz., the pain threshold for sounds presented by earphones rises rapidly to 175-180 dB at very low frequencies approaching quasi-static pressure changes. At frequencies higher than 2,000 Hz., the pain threshold may begin to rise again, but the measurements do not extend into this region. For jet engine noise from small jet fighter aircraft, the pain threshold was found between the overall levels of 134 and 140 dB.

Superimposed on Figure 10.2 are the envelopes of sound pressure levels to which subjects were exposed during the tests of Reference 10.3. These experiments were conducted to discover the effects of low frequency and infrasonic noise and no attempt was made to determine thresholds of any kind. The results are discussed more fully below and it is sufficient to state here that the pure tone levels between 40 and 100 Hz. represent the limits of voluntary tolerance.

### 10.2.2 HEARING DAMAGE

Exposure to high intensity sound causes a loss of hearing which may be permanent, or temporary with normal hearing acuity returning gradually after the noise ceases. It is now recognized that some degree of permanent hearing loss can result from a single exposure to excessive noise, or from the cumulative effect of repeated cases of temporary loss. Hearing loss is detected by a shift in the threshold of hearing.

The most complete study of hearing damage criteria to date is reported in Reference 10.4, which is a review of available research material conducted by the NAS-NRC Committee on Hearing, Bioacoustics, and Biomechanics. Figures 10.3 and 10.4, taken from Reference 10.4, show damage risk contours for narrow bands of noise and pure tones, respectively. These curves are based either upon direct measures of temporary threshold shifts or permanent noise induced losses in hearing and extrapolations from such data. The data points and extrapolations have been verified to a reasonable extent by one or more independent investigations, although some relations are based upon less evidence than others. In particular, the maximum pure tone levels to be allowed regardless of duration (i.e., the top curve of Figure 10.4) are estimates which are not supported by experimental data, and, in fact, all the pure

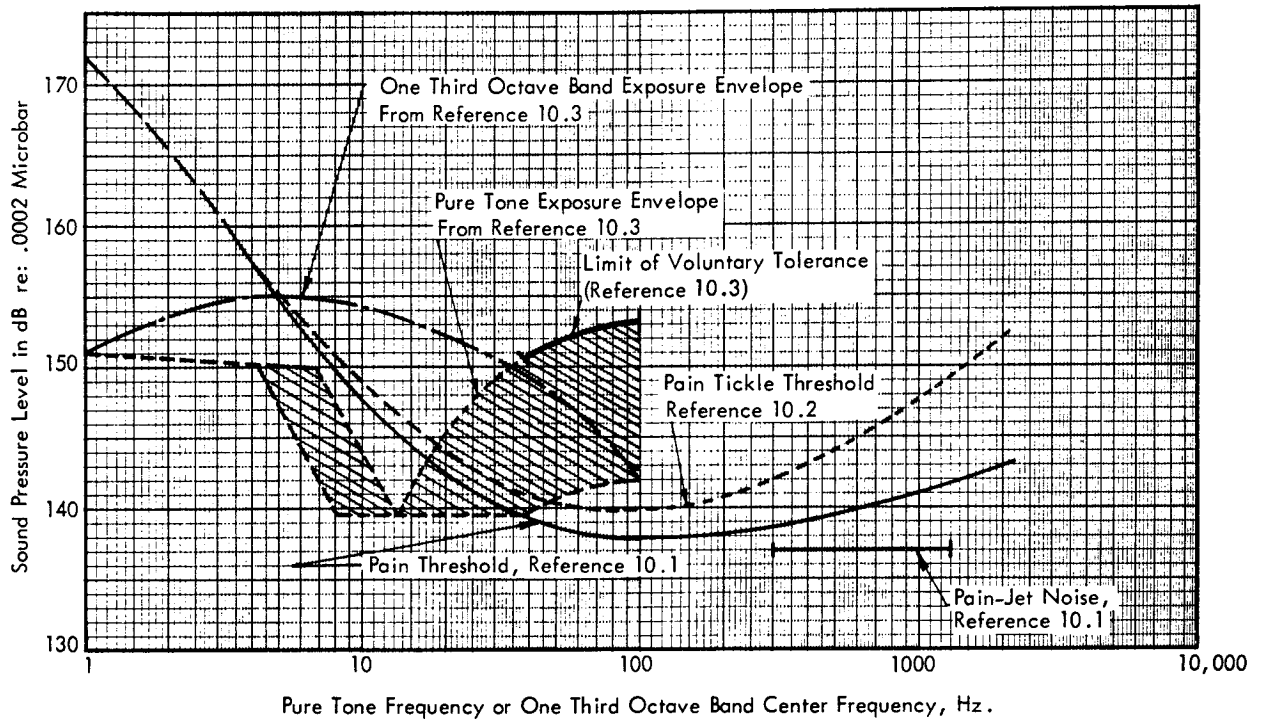


FIGURE 10.2 Aural Pain Thresholds and Noise Exposure Limits

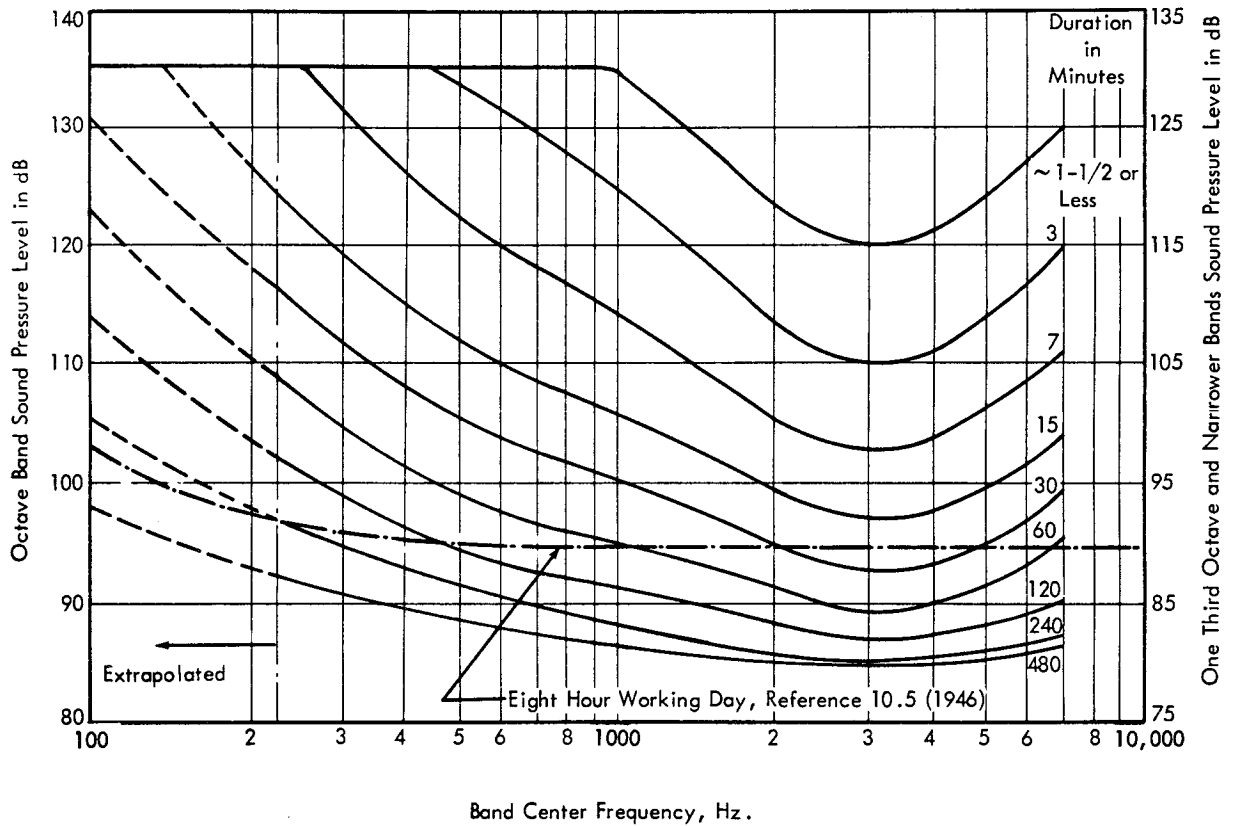


FIGURE 10.3 Damage Risk Contours for one Exposure Per Day to Octave (Left-Hand Ordinate) and One Third Octave or Narrower (Right-Hand Ordinate) Bands of Noise, (From Reference 10.4)

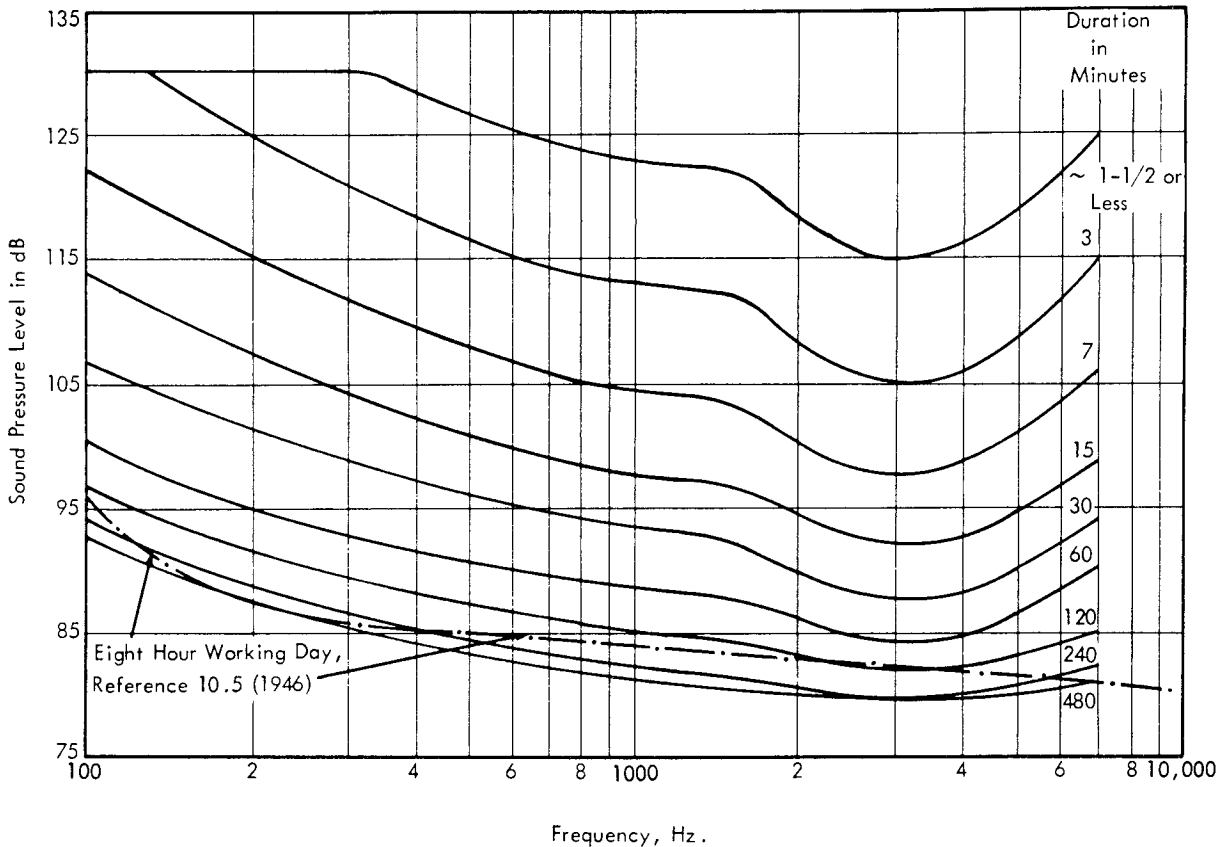


FIGURE 10.4 Damage Risk Contours for one Exposure Per Day to Pure Tones, (From Reference 10.4)

tone results are not so well substantiated by experiment as are the equivalent results for bands of noise. However, because of the similarity of Figures 10.3 and 10.4, it is felt that the results are valid. Also, there is very little data showing effects at frequencies below 100 Hz. and it was concluded that there is insufficient evidence to warrant extrapolating the results into that region.

Permanent damage risk is predicted from observations of temporary threshold shifts from the generally acknowledged belief that temporary shifts become permanent after repeated occurrence, once per day, five days per week, for ten years. The specification of sound levels which constitute a damage risk, utilized in producing Figures 10.3 and 10.4, is that "exposure to sound may be deemed excessive if it will cause ears of normal hearing (that of an average young adult) to experience an average temporary threshold shift in pure tone auditory acuity measured two minutes after exposure, of 10 dB or more at 1,000 Hz. or below, 15 dB at 2,000 Hz. or 20 dB at 3,000 Hz."

Shown for comparison in Figures 10.3 and 10.4 are damage criteria curves proposed in 1946 in Reference 10.5. These levels were claimed to cause negligible damage for continuous daily exposure during 8 hour working days. It can

be seen that for the random noise case in particular, the level is significantly higher than the more recently proposed criteria, especially at the higher frequencies.

Another comparison can be made with a more recent and widely used criteria for hearing damage. Since 1956, a general hearing damage risk criteria, embodied in Air Force Regulation No. 160-3 "Hazardous Noise Exposure", has been in use at many government facilities. This criteria specifies a damage risk in terms of an Equivalent Exposure Time (EET) for exposure each working day for 25 years to a wide band noise spectrum with a constant octave band level of 85 dB in the frequency range of 300 to 4800 Hz. The equivalent exposure time is based on the assumption that equal hearing damage results from equal energy (intensity times duration) of exposure. A Limiting Equivalent Exposure Time (LEET) at the specified constant octave band level is used to define an acceptable risk criteria, beyond which ear protection is recommended, or mandatory, depending on the particular LEET chosen. Thus, ear protection is recommended if the EET exceeds a LEET of 480 minutes (8 hours per day) at a constant octave band level of 85 dB from 300 to 4800 Hz. Ear protection is mandatory, if the EET exceeds a LEET of 4800 minutes at the same band level. Based on the energy equivalence



concept, the LEET of 4800 minutes at 85 dB is considered equally damaging as 480 minutes at 95 dB. This criteria can now be compared with those specified in Figure 10.3 for wide band noise exposure.

First, it is clear that the minimum LEET of 480 minutes at a constant band level of 85 dB, beyond which ear protection is recommended, agrees very well with the more recent data shown in Figure 10.3. In the latter, the hearing damage risk contour for 480 minutes per day has an octave band level varying from 89 dB in the 300-600 Hz band to 85 dB in the 2400-4800 Hz band. To compare the two criteria at higher levels, the 300-600 Hz band is chosen as more representative for low frequency rocket noise. Allowable exposure levels for a range of exposure time are listed in the following brief table, based on the two damage criteria.

Exposure Time Per 8 Hour Day	Allowable Octave Band Level (300-600 Hz)	
	Figure 10.3	AF Reg 160-3
480 min	89 dB	85 dB
120 min	96 dB	91 dB
30 min	107 dB	97 dB
7 min	125 dB	103 dB
1 1/2 min	135 dB	110 dB

Clearly, the Air Force Regulation is much more conservative at higher levels than the more recent data in Figure 10.3. At the particular frequency band chosen, the latter indicate that an equal damage criteria is roughly equivalent to a constant product of sound pressure times exposure time in contrast to the equal damage criteria assumed for the Air Force Regulation of a constant product of pressure squared times exposure time (i.e. - constant energy). However, the two criteria do agree on one further point - in both cases, an octave band level of 135 dB is specified as the maximum allowable exposure level without ear protection, regardless of the time duration. (According to the more recent criteria in Figure 10.3, this is only true below 1000 Hz.) Furthermore, the Air Force Regulation specifies a maximum exposure level at 150 dB under any condition, with ear protection. This maximum level is consistent with the results discussed in the following section.

### 10.2.3 NON-AUDITORY EFFECTS

Many reports suggest that intense sound can cause nausea, dizziness, and vomiting in certain individuals. Some of the symptoms resemble those of sea sickness and probably depend, in part at least, on the stimulation of the sense of spatial orientation, a process whereby the non-auditory part of the inner ear, the "labyrinth," plays a part. This supposition is supported by the fact that the symptoms can be suppressed by plugging the ears.

Mohr, et al. (Reference 10.3) report particular effects sustained by subjects with considerable experience in ex-

posure to high noise levels during low frequency tests at sound pressure levels up to 153 dB. The tests were conducted in the NASA Langley Low Frequency Noise Facility using both narrow band noise and discrete frequencies. The envelopes of the test points are shown superimposed on Figure 10.2. Exposures were made with ear protection in the majority of cases and no threshold shifts were detectable after one hour's exposure. However, the most prominent effects were found, as would be expected, when ear protection was removed for brief periods. The main features of the effects noted by the subjects, in addition to the aural sensations described above, were as follows.

At frequencies in the range of 5 to 50 Hz., some subjects felt nostril vibration, chest and abdominal wall vibration, hypopharyngol fullness (gagging) and perceptible visual field vibration. However, these experienced subjects thought these exposures were well within tolerance limits. For discrete frequency sounds, the effects were very similar although subjective sensations rose very rapidly above levels of 145 dB. At higher frequencies, the limits of voluntary tolerance, with ear protection, were reached and are shown in Figure 10.2. Decisions concerning these limits were made upon observation of certain alarming responses. These included mild nausea, dizziness, chest discomfort, skin tingling at 100 Hz., coughing, choking respiration, salivation, pain on swallowing, hypopharyngol discomfort, and headache. All subjects suffered a temporary loss in visual acuity. Most symptoms disappeared immediately after the test, although there was a marked degree of post exposure fatigue. No evidence of permanent damage was observed as a result of these tests.

### 10.3 SUBJECTIVE REACTION TO ACOUSTIC NOISE

The two attributes of a sound which are commonly used to evaluate the reaction of a listener are its "loudness" and its "noisiness". In principle, the distinction between the two properties is clearly defined. "Loudness" is the subjective magnitude of a sound, i.e., the absolute level or strength of a sound as assessed by the listener. Noisiness, on the other hand, can be defined as a measure of the unacceptability of the sound. It is therefore possible for two sounds of equal loudness to have entirely different noisiness values depending upon the quality of a sound.

Generally speaking, a sound can be described quantitatively by its sound pressure level, frequency spectrum and duration, and it might be expected that this information could be utilized to define both its loudness and its noisiness. Unfortunately, this task is difficult due to the extremely complex mechanisms involved in the human hearing processes. Not only does judgment of a single noise vary between listeners, but also the judgment of a single listener may vary, being influenced by such factors as his environment, emotional state, activity, fitness, and hearing acuity among many others. Also it may be difficult, in a given situation, to distinguish between the loudness and the noisiness of a sound, since the two properties are strongly interrelated. In fact, as will later be seen, subjective judgments of the two quantities are closely similar. In spite of the obvious difficulties of measuring individual subjective reaction to noise, it has been shown by many

workers that collective judgment is sufficiently uniform to justify the development of quantitative rules for evaluation of loudness and noisiness. Current methods, in fact, show good consistency in the prediction of subjective response to broadband noise. However, these methods are continuously being refined to account for factors such as duration, rate of onset and decay, and discrete frequency content.

10.3.1 LOUDNESS

The loudness, or subjective magnitude of noise, is a relative property, and the first step to be taken in its definition and measurement is to specify a scale of units. Fletcher and Munson (Reference 10.7) suggested a 1,000 Hz tone as a standard sound against which others should be judged for loudness. Stevens (Reference 10.8) later proposed the unit of loudness be called the sone, and gave a value of 1 sone to the loudness of a 1,000 Hz tone with a sound pressure level of 40 dB. The sone scale is such that a sound "twice as loud" as 1 sone is given a value of 2 sones and so on.

An alternative dimension is that of "loudness level" which is measured in phons and is, by definition, equal to the sound pressure level, in dB, of the 1000 Hz. pure tone which has equal loudness. Thus this scale is more closely related to the conventional logarithmic scale of sound intensity, and for this reason is generally used for the definition of loudness values. Nevertheless, the sone scale forms a more convenient basis for the rating of subjective judgments, and it has been necessary to find the relationship between sones and phons. It is now generally accepted that a doubling of loudness, that is a factor of two increase in loudness, corresponds to an increase in loudness level of 10 phons for a loudness level greater than 40 phons. This relationship applies at all frequencies and is fundamental for the establishment of the equal loudness contours which are discussed below. It is important to note however, that this result represents the mean of measured data, some of which are presented in Figure 10.5. The scatter is considerable, and is partly the result of the different methods of loudness estimation used.

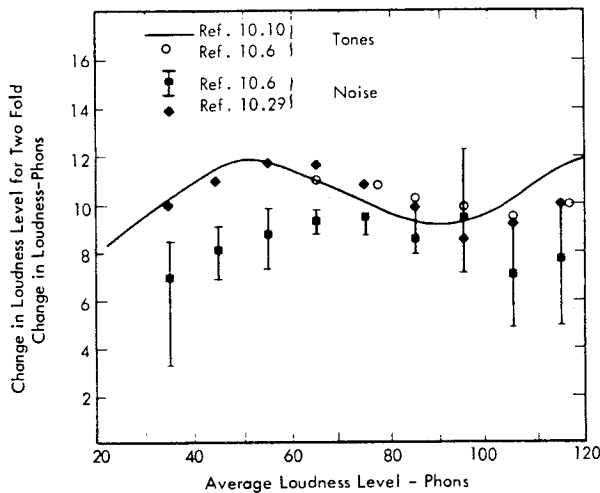


FIGURE 10.5 Slope of Loudness Functions for Tones and Bands of Noise

Now to predict the loudness of a complex sound of known frequency spectrum one needs to know (i) how loudness varies with frequency, (ii) how loudness varies with bandwidth, and (iii) what is the rule for adding the loudness of different bands of noise. The loudness of pure tones is reviewed first since the results prove useful for extrapolation of loudness of bands of noise to low frequencies and high levels.

Numerous "equal loudness contours" for a pure tone have been produced which show the variation of judged loudness with frequency. Notable among these are those of Fletcher and Munson, 1933 (Reference 10.7), Churcher and King, 1937 (Reference 10.9), and Robinson and Dadson, 1956 (Reference 10.10) examples of which are shown in Figure 10.6. Differences among the three sets of data are apparent, especially towards the lower frequencies. Of the three sets, that of Robinson and Dadson, being the most recent, is considered the most reliable.

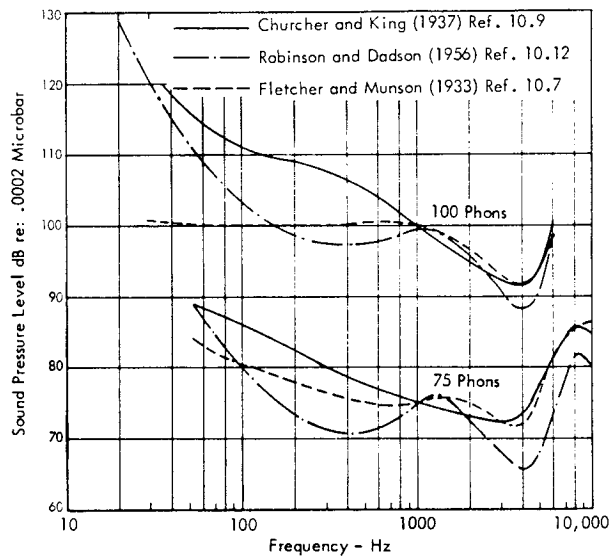


FIGURE 10.6 Comparison of Equal Loudness Contours for Pure Tones for Two Different Loudness Levels

Investigations similar to the earlier pure tone experiments have been carried out using bands of noise, the first of which was made by Stevens (Reference 10.11) using octave bands. Stevens found that loudness contours for bands of noise differed from the pure tone contours although exhibiting the same general trends. The loudness of a given band of noise was still measured in sones, relative to the 1,000 Hz. pure tone standard, and it was found that, for a reasonably smooth spectrum, the rule for adding together the loudness of a number of adjacent bands is approximately

$$S_t = S_m + F (\sum S - S_m)$$

This states that the total loudness, in sones,  $S_t$  is equal to the loudness of the loudest band,  $S_m$ , plus some fraction,  $F$ , of the sum of the loudness of the remaining bands. For the value of  $F$ , Stevens recommended 0.3 for octave bands, 0.2 for half octaves and 0.15 for one third octaves. From the sone summation, the overall loudness level in phons (LL) is obtained from the overall loudness in sones  $S_t$  by the following expression

$$LL = 40 + 33.3 \log_{10} S_t, \quad (S_t > 1 \text{ sone})$$

Robinson and Whittle (Reference 10.12) performed a careful and extensive study of the available data on loudness contours for bands of noise, in addition to compiling an additional set, and recommended that the most valid result could be obtained by simply averaging the contours given by Stevens (Reference 10.11), Cremer et al. (Reference 10.13), Robinson and Whittle (Reference 10.12) and Zwicker (References 10.14 and 10.15). A comparison of the results obtained by this averaging process and the pure tone contours of Robinson and Dadson (Reference 10.10) is made in Figure 10.7 where the boundaries designating the measurement limits are also shown.

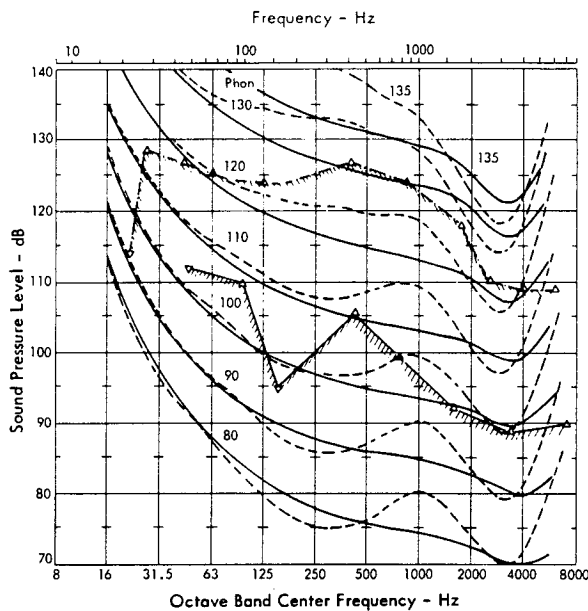


FIGURE 10.7 Average Loudness Contours for Pure Tones and For Noise (After Reference 10.12)

These subjective judgments have one major shortcoming for application to the noise field of large rocket boosters in that the extent of the contours in level and frequency is inadequate. The pure tone results of Reference 10.10 cover loudness values up to 120 phons and the composite broadband contours are limited to about 100-110 phons. In addition there are few results below 50 Hz. The reasons for this deficiency are clear enough; it is difficult to perform accurate experiments in the low frequency range and the physiological dangers of high sound pressures, discussed in paragraph 10.2, make large scale testing at such levels impractical.

Robinson and Dadson made a detailed analysis of their pure tone loudness contours and found that at each frequency the loudness could be accurately expressed as a quadratic function of sound pressure level. From the data which they provide, the contours have been extrapolated to 135 phons as shown in Figure 10.7. Using these results as a guide, the broadband equal loudness contours have been extended in a similar way. It must be mentioned at this point that in deriving the average contours shown in Figure 10.7, Robinson and Whittle corrected all data to equivalent diffuse field conditions, using the relationships presented as Figure 10.8 which may therefore also be used when applying these curves to normally incident plane wave conditions.

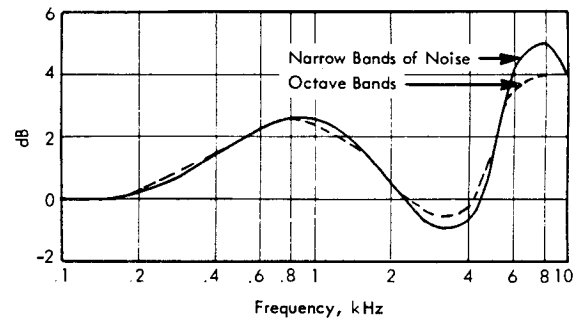


FIGURE 10.8 Difference Between Sound Pressure Levels of Frontally Incident and Diffuse Sound Fields At Equal Loudness (From Reference 10.12)

### 10.3.2 NOISINESS

In attempts to develop simple methods by which the loudness of sounds could be physically measured, standard sound level meters have been provided with A, B, and C scales. These scales utilize filter networks which weigh the measured sound spectrum in accordance with the Fletcher-Munson loudness contours. The A, B, and C scales correspond approximately to the compliment of the 40, 70, and 100 phon contours respectively. When these instruments were used to measure the sound of jet aircraft and observers were simultaneously asked to rate the "acceptability" of the noise, it was found that the correspondence between the two ratings was not as good as might be desired. This led to the notion that loudness and noisiness

are not necessarily the same thing. Figure 10.9 from Kryter and Pearsons, (Reference 10.16) illustrates a recent measurement of the difference between judged noisiness and loudness for bands of noise. Based on such data, Kryter modified the existing equal loudness contours of Stevens and established a set of noisiness contours to account for the effects of annoyance of a noise. (Reference 10.16). A unit of noisiness, was also proposed, called a noy, which is analagous to the sone as a loudness unit. One noy is defined as the noisiness of a band of random noise centered at 1000 Hz and having a sound pressure level of 40 dB. The actual bandwidth of the reference standard was not fixed but could vary appreciably above or below approximately one octave. To illustrate the resulting noisiness contours, Figure 10.10 compares the 40 and 160 noy noisiness contours proposed by Kryter (Reference 10.16) with the corresponding 40 and 160 sone loudness contours for octave bands of noise of Stevens (Reference 10.11) upon which the former are based. Also shown are the 40 and 160 sone loudness contours for octave bands of noise from Robinson and Whittle interpolated from Figure 10.7. The general trend of all three curves at both levels is similar. However, the differences in absolute level are indicative of the degree of accuracy inherent in any subjective rating scale.

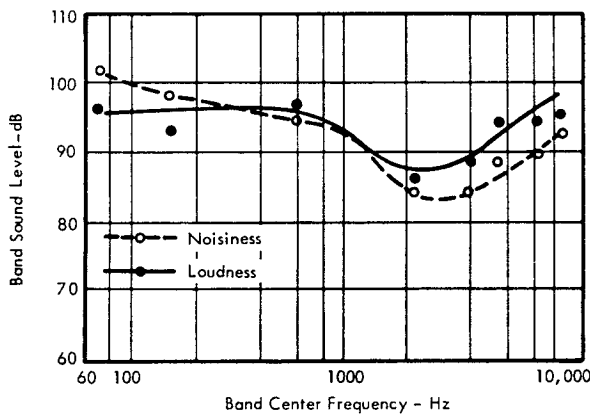


FIGURE 10.9 Equal Loudness and Equal Noisiness Judgements of Bands of Noise (From Kryter and Pearsons, Ref. 10.16).

The perceived noisiness of a sound is calculated in much the same way as its loudness in phons, using noys instead of sones. The summation formula for wide band spectra is

$$N = n_{max} + F (\sum n - n_{max})$$

where N = total noisiness in noys,  $n_{max}$  is the noisiness of the noisiest band and F is a factor which takes values 0.3 for octave bands, 0.15 for one-third octave bands and 0.07 for one-tenth octave bands. Figure 10.11, prepared for use in the calculation of perceived noisiness, represents a complete set of noisiness contours (in noys) obtained from Reference 10.16 and extrapolated to 20 Hz. and 750 noys. Given the sound pressure level in each octave or third octave band, the noy value for each can be read from these curves. The overall noisiness is then calculated according to one of the summation formulae

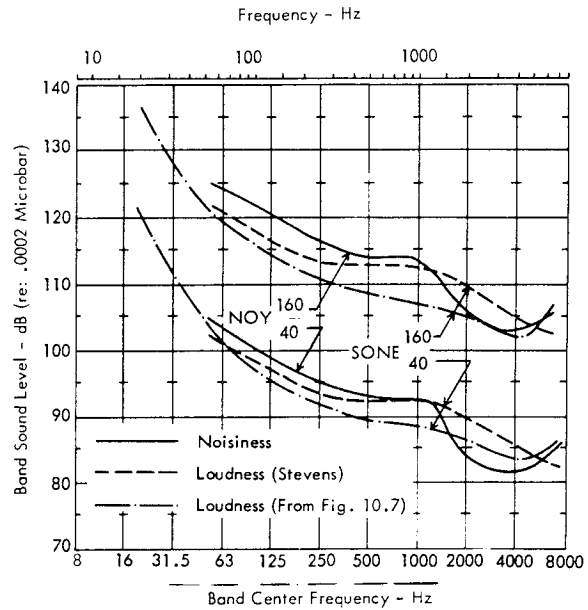


FIGURE 10.10 Comparison of Equal Noisiness Contours and Equal Loudness Contours for an Octave Band of Noise

$$N = n_{max} + 0.3 (\sum n - n_{max}) \quad [\text{octave}]$$

or

$$N = n_{max} + 0.15 (\sum n - n_{max}) \quad [1/3 \text{ octave}]$$

The perceived noise level in PNdB is defined as the sound pressure level corresponding to the overall noisiness, N, at 1000 Hz., and can therefore be obtained directly from Figure 10.11.

#### Effects of Duration

Both rate of onset and decay of a sound, together with its duration have significant effects upon an observer's evaluation of both loudness and noisiness. Garner (Reference 10.18) has shown that the loudness of a tone or a band of noise increases with duration for periods measured in fractions of seconds. For longer periods the loudness stays constant and actually begins to decrease during extended exposures. In contrast, noisiness continues to increase with increased duration. Kryter and Pearsons (Reference 10.16) investigated the effects of both duration and rise and decay times and found that judged noisiness was relatively insensitive to the latter. The effect of duration, however, was important; an increase in duration resulted in an increase in noisiness. Specifically, it was found that the sound pressure level for equal noisiness of a given sound spectrum decreases approximately 4.5 dB per doubling of duration. However their tests were performed at sound pressure levels of around 100 dB and the applicability of this result to other levels is unknown. Also the durations used in these tests were between one and one-half and twelve seconds. Pearsons (Reference 10.19) extended these tests to durations of 64 seconds and found that the dependence of perceived noisiness on duration appears to be a

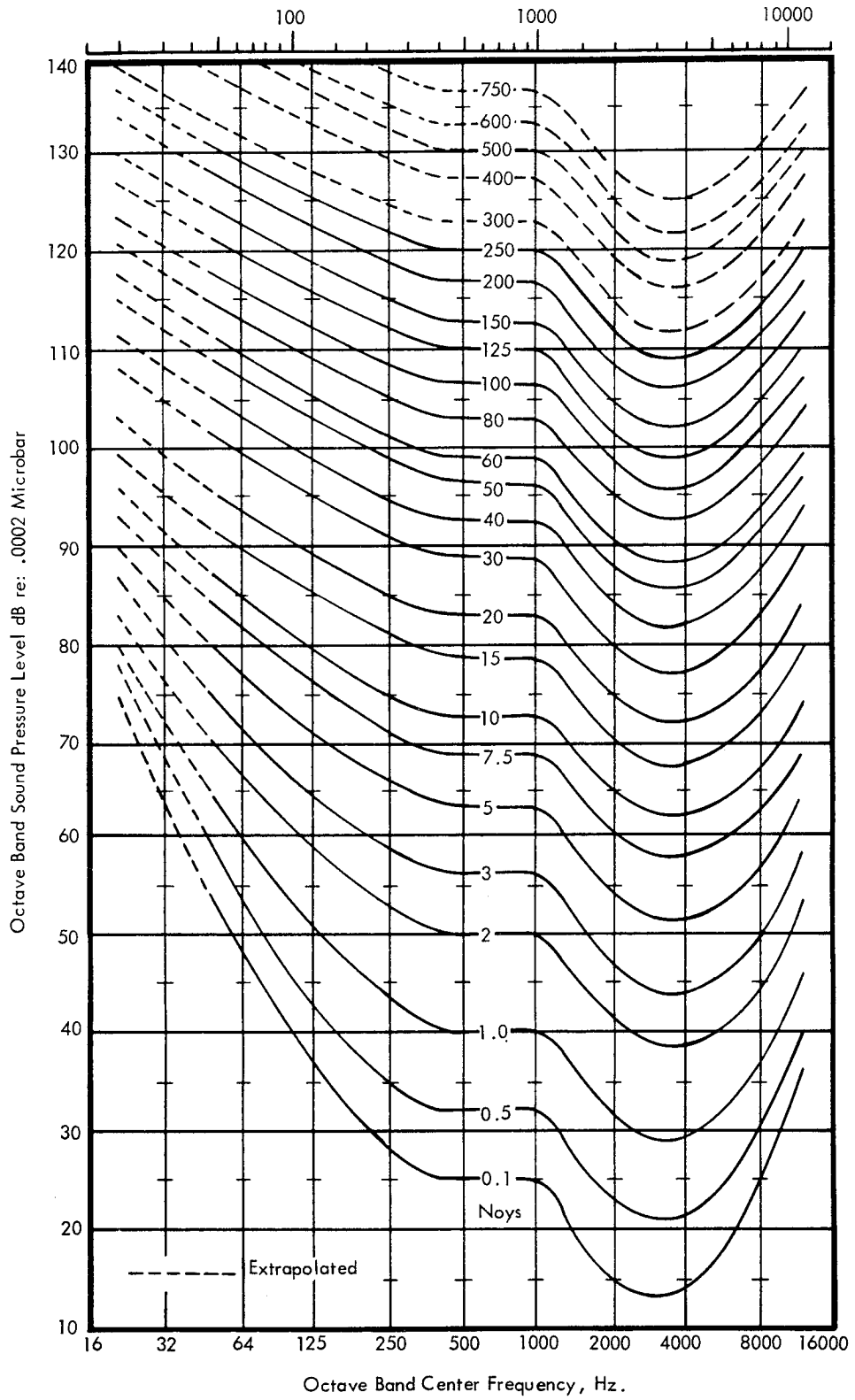


FIGURE 10.11 Equal Noisiness Contours for Bands of Noise After Kryter and Pearsons (Reference 10.16)

continuously varying function. Figure 10.12 taken from Reference 10.19, shows the combined set of results for the two tests. Three straight line segments have been fitted to the data, arbitrarily broken at durations of one and one-half, four, sixteen, and sixty-four seconds. Within the three ranges, the perceived noise level increases by 6.0, 3.5, and 2.0 PNdB per duration doubling respectively. For application to rocket launch and static tests, a duration of exposure equal to or greater than 16 seconds will be typical, and the 3 PNdB correction per doubling of duration may be expected to apply.

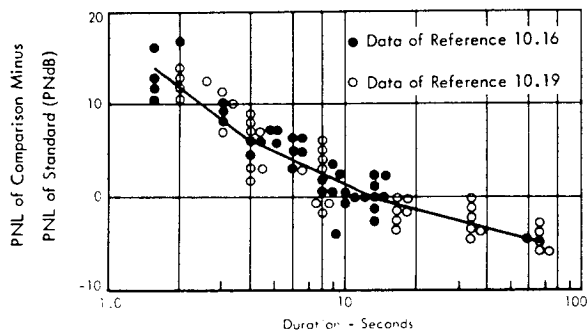


FIGURE 10.12 Summary of Equally Acceptable Noises of Various Durations

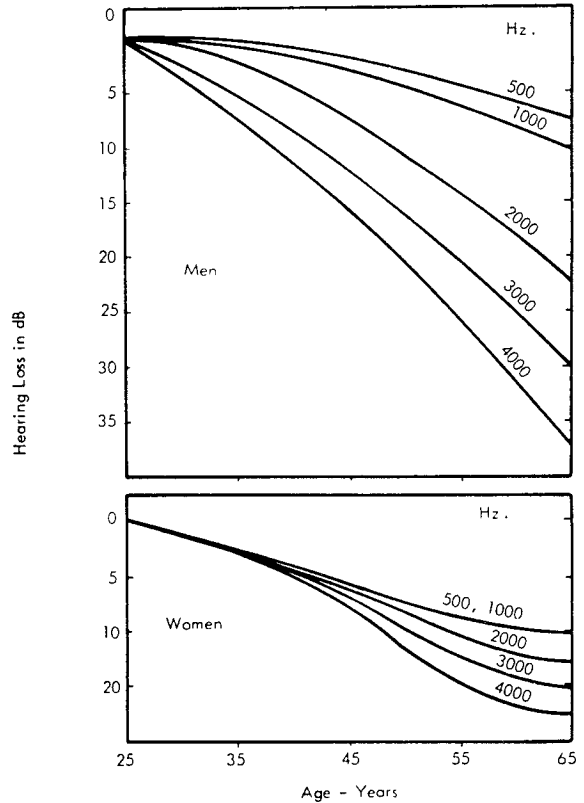


FIGURE 10.13 Presbycusis. Average Hearing Losses to be Expected With Age (From Reference 10.20)

### 10.3.3 AGE

One factor which should be taken into consideration during both subjective judgment tests and the later application of the results is the normal loss of hearing with increasing age, presbycusis. Statistically averaged figures for the increase in hearing loss level with age for various frequencies are plotted in Figure 10.13. Unfortunately the data are limited and the relationships between threshold deficiencies and subjective evaluation of noise are not defined.

### 10.3.4 ANNOYANCE

Under actual day-to-day conditions, an individual's judgment of the annoyance of a sound will depend upon many factors. It is extremely difficult to categorize sounds into annoyance ratings and each individual case must be treated upon its merits. Some typical factors which affect the annoyance of sound are: (i) the observer's activity and degree of concentration upon it, (ii) whether or not the noise is necessary for any practical purposes, (iii) the frequency with which the sound is heard and the degree of the listener's conditioning to it and, (iv) his emotional state of mind.

## 10.4 OBJECTIVE INFLUENCE OF ACOUSTIC NOISE

### 10.4.1 SPEECH COMMUNICATION

The most immediate objective effect of excessive noise on people is the interference with voice communication due to masking. Due to the low frequency content of rocket noise and the relative high frequency content of speech sounds, this interference would seldom be a significant factor in a community area around a launch or test site. However, for operating personnel, in control centers or exposed areas close to a rocket firing, noise levels which interfere with voice communication can be a serious operational handicap. As a rough initial guide, voice communication can become impaired when the average octave band sound level of the noise in the frequency range of 600 to 4800 Hz exceeds levels ranging from 40 dB for normal voice communication at distances of 8 to 10 ft to 55 dB for voice communication of 3 to 4 ft (Reference 10.21). Such levels may often be reached in operating areas where voice communication is critical.

To evaluate the resulting degree of interference with voice communication, methods have been developed which relate a weighted ratio of the speech-to-noise intensity to communication efficiency. This relationship is quantified in a single number called the articulation index.

One method, frequently used for detailed evaluation of communication systems, in lieu of actual operational tests in noise, is based on the following concepts: (Reference 10.21, 10.22).

- The effective intensity range of the speech signal lies within a 30 dB spread equal to + 12 dB above and -18 dB below the long time average rms pressure spectrum level of the speech signal.
- Limiting lower and upper values for this effective intensity range are specified respectively by the threshold of hearing and an overload limit beyond which, speech communication is not improved by further increases in the speech signal.
- The effective frequency spectrum of the speech signal, between about 200 and 6000 Hz, can be divided into 20 unequal frequency bands which contribute an equal amount of intelligence.

These first three concepts are illustrated in Figure 10.14 which is from Reference 10.21. This shows the range of the effective pressure spectrum level for normal speech at a distance of 1 meter from a speaker. This spectrum is plotted on a non-linear frequency scale established by letting the frequency bands of equal intelligence have equal width on the abscissa.

The overload limit is shown in Figure 10.14 as a constant pressure spectrum level of 95 dB. This value is from Reference 10.21 and is chosen for simplicity in lieu of the more complex and somewhat higher values in Reference 10.22. It corresponds approximately to a speech sound level of about 115 dB at the ear and would rarely be exceeded in most communication systems employed at rocket firing areas.

To compute the articulation index, the actual peak speech spectrum levels received by a listener are determined by adjusting the spectrum levels in Figure 10.14 for the acoustic gain-versus-frequency characteristics of the system. If the adjusted spectrum exceeds the overload limits in any band, the latter level is used as the effective peak speech spectrum level in that band. The rms pressure spectrum level of the noise at the ear, corrected for any noise rejection by headsets etc., is then plotted on the same graph. The area between the speech peaks and the rms noise spectrum divided by the area of the effective speech spectrum without noise is called the articulation index. It is normally expressed as a percentage.

Additional refinements to this procedure, covered in detail in Reference 10.22, include corrections to the noise spectrum to account for non-linear growth in masking at high noise levels and effective growth in masking of the spectrum above and below its predominant peak frequency. The validity of applying these corrections to low frequency rocket noise spectra is not known.

Since the peak spectrum level of speech is usually below 95 dB, the articulation index can ordinarily be expressed as

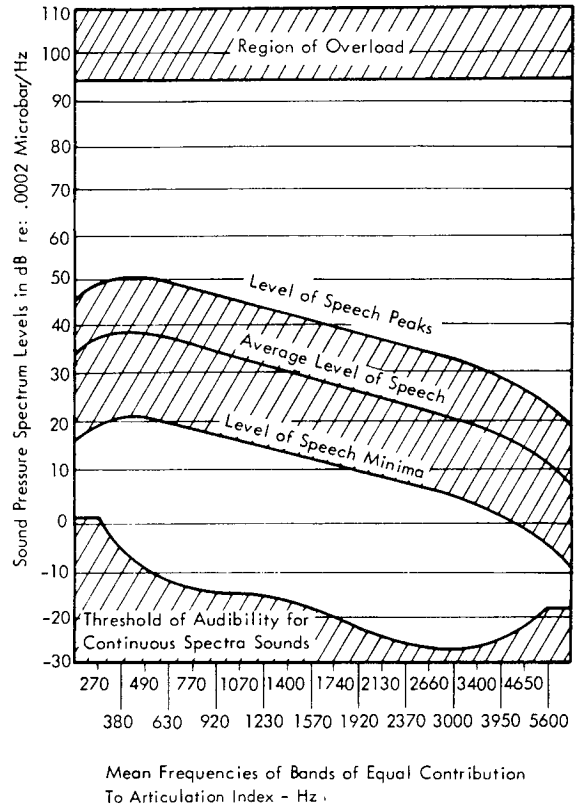


FIGURE 10.14 Basis for Calculation of Speech Articulation Index, Showing Audibility Threshold, Region of Speech Level, and Overload Region (From Beranek, Ref. 10.21).

$$AI = 100 \sum_{i=1}^{20} (S_i - N_i)/600$$

where

$S_i$  = peak speech spectrum level in dB in  $i^{th}$  band

$N_i$  = rms noise spectrum level in dB in the  $i^{th}$  band (including any corrections from Reference 10.22)

and

$$(S_i - N_i) = \begin{cases} 0 & \text{when } N_i > S_i \\ 30 & \text{when } N_i < S_i - 30 \end{cases}$$

Thus, the computation reduces to summing the peak signal to rms masking noise ratio, in dB, in each band, with the limitation that the values cannot be negative and cannot exceed 30 dB. Additional corrections to the value of the articulation index itself can be made to account for acoustic reverberation at the receiving end, relative vocal effort of the talker and visual cues. (See Reference 10.22). In general, however, these refinements would not apply in the analysis of communication systems around rocket launch areas.

Numerous investigators have verified the general validity of this analytical process for predicting the efficiency of a communication system by actual tests. For test material consisting of sentences, the percent correctly understood is related to the computed articulation index as follows.

Articulation Index - %	10	20	30	40	50	60
Sentence Intelligibility - %	18	54	80	90	94	97

Thus, as a rough guide, a system with an articulation index of less than 30 percent will generally be unsatisfactory while 60 percent will provide nearly perfect transmission of information.

A less precise but more easily calculated parameter which is widely used for estimating speech interference is the Speech Interference Level (SIL). This is related to the articulation index, in that the spectrum is divided into three bands which make equal contribution to speech intelligibility, but in this case convenient bands are chosen which coincide with the filter bands of commercial sound analyzers. These three bands are chosen as 300-1200 Hz., 1200-2400 Hz., and 2400-4800 Hz. (see Figure 10.14) where the first of these is represented in analyzers by the two octave bands 300-600 and 600-1200 Hz. If the level in the 300-600 Hz. band is not more than 10 dB above that in the 600-1200 Hz. band, the SIL is defined as the arithmetic average of the sound pressure levels in the three bands 600-1200, 1200-2400, and 2400-4800 Hz. However if the levels in the 300-600 Hz. band are more than 10 dB higher than those in the 600-1200 Hz. band, then the average in the four bands between 300 and 4800 Hz. must be used. If the speech spectrum is known, an approximation to the articulation index can be made as follows:

- (i) Using the damped meter circuit of an octave band analyzer, measure the octave band sound pressure levels of the ambient noise to derive the SIL as defined above.
- (ii) Using the undamped meter circuit, measure the peak sound pressure levels of the speech signal (with the ambient noise removed or reduced to a level which causes no interference) in the same bands and average in the same way to yield an "adjusted peak level of speech." It is advisable to add about 4 dB to the final answer to compensate for the inertia of the standard sound level meter movement.
- (iii) The difference between the adjusted peak level and the speech interference level, when divided by thirty, approximates the articulation index.

As a guide to the direct effects of SIL upon voice communication, Table 10.1, taken from Chapter 13 of Reference 10.21, shows the SIL's which barely permit reliable speech intelligibility at various talker-listener distances and voice levels. For more details on the calculation and use of both Articulation Index and Speech Interference Level the reader is referred to Chapter 13 of Reference 10.21.

TABLE 10.1

SPEECH-INTERFERENCE LEVELS (IN DECIBELS RE 0.0002 MICROBAR) THAT BARELY PERMIT WORD INTELLIGIBILITY AT THE DISTANCES AND VOICE LEVELS INDICATED. NO REFLECTING SURFACES TO AID THE DIRECT SPEECH ARE ASSUMED (AFTER L.L. BERANEK REFERENCE 10.21)

Distance, ft	Voice Level (Average Male)			
	Normal	Raised	Very Loud	Shouting
0.5	71	77	83	89
1	65	71	77	83
2	59	65	71	77
3	55	61	67	73
4	53	59	65	71
5	51	57	63	69
6	49	55	61	67
12	43	49	55	61

10.4.2 EFFECTS OF NOISE ON BEHAVIOUR AND EFFICIENCY

It has been noted previously that high intensity noise and sudden unexpected noise can cause undesirable physical reactions in the body of minor or negligible significance. It might also be expected that noise which does not cause such direct reactions might reduce the efficiency of a subject performing his normal activities. This could be a significant factor for defining an acceptable environment for manned ground stations near launch or test sites where the efficiency of control or test operators is vitally important. Unfortunately, the direct physiological effects of noise are extremely difficult to isolate, being masked to a great extent by psychological effects such as annoyance and distraction. Thus, changes of external influences on subjects during a test, together with consequent changes of mental attitude, play an important part in their reaction to a given situation. Industrial surveys are particularly prone to this type of unknown factor, and therefore, yield poor results. Laboratory experiments are limited by the number of subjects and results are of correspondingly less statistical value. Nevertheless, the results are of value in helping to specify tolerable noise limits. The main conclusions are discussed below.

Noise does interfere with efficiency to some extent, and it can broadly be stated that, for simple tasks, the more unfamiliar the noise or the more unfamiliar the work, the more serious will this interference be. It is found that for simple tasks, efficiency declines when the subject is first exposed to the noise but that efficiency is gradually regained as the subject becomes familiar with the sound. However, the magnitude of the effect is always small and



the main conclusion is that familiar noises of short duration do not represent a serious threat to efficiency. When the average rate of work over a fair period of time is taken there is no consistent decline in performance and there may even be some increase.

Similar results are found when the work is of a more complex and intellectual nature. In this case, the net effect of noise is normally found to be an increase in errors. Speed and output are apparently not affected significantly. A subject performing a complex task is much more susceptible to distraction and annoyance and steps to reduce the noise or loudness level of infrequent, though familiar, noises are desirable if efficiency is to be maintained.

More significant effects of noise have been found on vigilance tasks which include visual watch-keeping and continuous work over extended periods. A typical example of such work is the monitoring of warning signals (e.g. pressure gauges). Definite deterioration of performance on this specific task has been found over periods of one and one-half hours. Detailed analysis has shown a sudden decline in performance at the onset of the noise and then an improvement, sometimes followed by a further decline. This suggests that the subject initiates additional effort in a noisy environment which he cannot maintain. Noise appears to have an even more marked effect upon tasks which require continuous activity and concentration. Errors begin to increase rapidly after a short time (10 minutes or so) and further increase with an increase in noise level.

A study of particular relevance to the problem of launch or test site operation was made by Woodhead (Reference 10.30) who investigated the effects of short bursts of noise on a group of subjects performing a complex visual search task. The task involved the identification of printed numbers presented in random sequence at the rate of five per second. The total period of performance in each case was fifteen minutes and the subjects were exposed to bursts of recorded rocket noise, of one second duration, at various intervals during the task. In a quiet environment it was found that of the total errors made, 44 percent occurred during tests when the bursts of noise were at a level of 110 dB, 27 percent when the noise was at 70 dB, and 29 percent when there were no noise stimuli. A detailed analysis of performance during the 30 second periods following each noise burst showed that the errors induced by the loud noise were of a particular type, i.e., failure to notice a warning signal. The continuous activity involved in the task was not appreciably affected.

Extensive tests have uncovered no significant effects of noise upon sensory and motor functions with the exception of a recent experiment (Reference 10.23) which included a study of the effect of different sound pressure levels at each ear. With a difference of 20 dB between ears (80 dB and 100 dB of random noise), some loss of balance was noted among the subjects. Although the effect was slight, it was considered of potential significance in motor task performance. Such an unbalanced exposure could occur with a communicator wearing a headset.

Practical conclusions which can be drawn from the results of the many studies are that

- 1) The direct effects of noise on human performance are far less significant than the annoyance it causes,
- 2) there is no effect on efficiency at sound pressure levels less than 90 dB. At higher levels, power of concentration may be impaired,
- 3) familiar noises are less likely to reduce efficiency than unfamiliar ones.

## 10.5 COMMUNITY REACTION

Predicting likely community reaction to a noise stimulus involves several steps. Three factors are of prime importance. First, "likely reaction" is a statistical problem. Annoyance by sound at any particular instant is a function of current activity. Secondly, the annoyance created by a particular sound is a relative matter. It depends on the extent to which the sound compares with the ambient noise environment to which the listener may be accustomed. Thirdly, there is the problem of how "community reaction" is to be measured. A commonly used index is the level at which complaints are received. However, it is an obvious reality that for every complaint registered many more people will be annoyed and disturbed, but do not make a formal complaint.

Considerable effort has been directed, therefore, towards developing methods for predicting community reaction to noise based on a knowledge of the physical parameters of the noise weighted by due consideration of other subjective elements. While each community noise problem must be evaluated carefully on its own merits, such prediction methods provide a valuable guide for site planning of potential noise sources and a guide for defining operational controls on such sources to avoid adverse community reaction.

A major advance in the development of reliable methods for assessing community reaction to noise was made by Stevens, Rosenblith, and Bolt (Reference 10.24) who proposed the concept of a composite noise rating (CNR). They suggested that the measured or computed loudness of the noise could be modified by increments which take account of additional subjective response factors. These include background noise, temporal and seasonal factors, character of the noise and previous exposure. The modified result, the CNR, could then be related directly to an expected scale of community response based upon observations of the reactions of typical residential communities. While their method for allocation of numerical values to the various factors was necessarily crude, correlation between prediction and observation for a series of subsequently studied case histories was sufficient to justify use of this method in most cases. Figure 10.15 taken from Reference 10.24 is a graphical representation of the results, showing the range of responses which can be expected from communities exposed to noise of varying CNR. A method for relating the CNR to physical characteristics of the noise will be covered later on in this section.

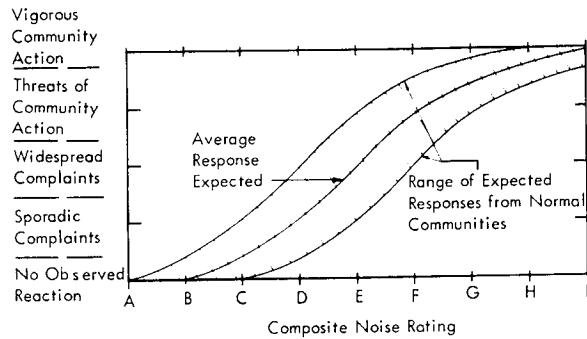


FIGURE 10.15 Variation of Expected Community Response With Severity of Noise Intrusion (From Reference 10.24)

Later studies have modified, simplified, improved and adapted this initial work (References 10.25, 26, and 27) with particular emphasis on the airport noise problem. Reference 10.27, gives comprehensive instructions for predicting community reactions in the vicinity of airports from a knowledge of aircraft types and operation schedules, and has been recommended as a standard procedure for evaluating airport noise problems (Reference 10.28). Unfortunately the technique is not suitable for direct application to the community noise problem at rocket operation centers for a number of obvious reasons. The operation schedules, noise time histories and noise characteristics are different from those at an airport. Also, communities in the immediate vicinity of rocket test centers are likely to be much more tolerant, since a high percentage of the population will be motivated economically and professionally towards acceptance of, and indeed interest in, the noise. This is a very important difference between noise intrusion from rocket tests or launch operations and airport noise. It can be worth up to 15 dB in noise level for the same community acceptance.

A suggested method for the prediction of noise response outlined in this section is believed to be a realistic approach, and is developed from those of Reference 10.27 and the earlier more comprehensive techniques of Reference 10.24. The final result of the suggested calculations can be left in the form of that of Reference 10.27, namely one of three levels of community reactions which can be predicted within a certain area. Alternatively, however, a more detailed method can be used which gives estimated numerical values for areas of known population density which may be subsequently integrated to give a measure of the average complaint reaction of the entire community. Although complaint density does not necessarily indicate the true intrusion value for a given noise disturbance, it does provide a useful numerical rating which can be compared with observed complaints to validate or improve the prediction methods. This alternate proposed method assumes that sound pressure level spectra can be calculated at relevant points in any community by methods outlined in Chapters 6 and 7 of this manual. Additional factors which are then taken into consideration are,

- Time histories of noise stimulus exposure.
- Background noise.
- Temporal factors; time of day, time of year.
- Frequency of firings.
- Previous exposure.
- Population distribution.

The step-by-step procedure which accommodates these aspects of community reaction will now be detailed.

#### Step 1 Launch or Test Operation Data

The first step is to collect pertinent data on the expected launch or test operations for extended periods of time. For each launch or test firing, this comprises information on the type of vehicle launch or test sequence, pad location and likely acoustic propagation conditions at the time of firing. This information should then be divided into two groups corresponding to firings occurring between the hours of 0700 and 2200 and those between 2200 and 0700. Table 10.2 shows a suggested format for gathering this information. It is recommended that the vehicle specification be represented by one of 5 different categories, each defined by an approximate thrust range ratio of 3 to 1 which corresponds to an approximate overall sound power ratio of 5 dB.

#### Step 2 Sound Level Contours

Typical ground noise contours can then be defined for each vehicle thrust class and for each propagation condition. The time period within which average frequencies of rocket firings are to be computed, should be chosen to cover a period when both firing frequency and weather conditions are reasonably uniform. For the larger rockets, it is anticipated that the distances between launch pads will be important for community areas at a great distance from the launch center. For smaller rockets, inter-pad distances will tend to be small enough so that all tests can be assumed to originate from a central point in the middle of a test complex.

For each firing category (defined by thrust class and weather conditions) and each community location, the time variation of the stimulus sound pressure level and octave band spectrum in each community area of interest is calculated according to the methods described in Chapters 6 and 7.

#### Step 3 PNdB Calculations

A perceived noise level, in PNdB, is then calculated with the data of paragraph 10.3.2 using the maximum sound pressure level in each octave band from Step 2.

It is recognized that the equal noisiness contours of Figure 10.11, even in their extrapolated form, are not entirely adequate for the perceived noise calculations for the classes of large launch vehicles which have spectrum peaks at sub-audible frequencies. However, the upward trend

TABLE 10.2  
SUGGESTED FORMAT FOR GATHERING LAUNCH OR STATIC TEST SCHEDULE DATA

TIME PERIOD: . . . . to . . . .										
VEHICLE THRUST (LB)	0700-2200				2200-0700					
	TOTAL FIRINGS	PAD				TOTAL FIRINGS	PAD			
		1	2	3	4		1	2	3	4
< 100,000										
100,000 to 330,000										
330,000 to 1,000,000										
1,000,000 to 3,300,000										
3,300,000 to 10,000,000										
OVER 10,000,000										

of the contours at the low frequencies, together with the loudness contours of Figure 10.7 and the pain threshold curves of Figure 10.2 illustrate that these frequencies are not likely to cause auditory disturbances. A further important influence of the sub-audible part of the spectrum occurs through building vibration which adds to the annoyance and general fear reaction. The particular fear of possible property damage and depreciation may also be especially significant. However, it may be expected that launchings of these very large vehicles will be relatively infrequent, and when they do occur, of considerable interest to the local communities. This factor will play a large part in countering the adverse effects of the lower frequencies and may even weigh public reaction in a favorable direction. For this reason it seems justifiable to ignore the sub-audible part of the spectrum for launch sites. For static test sites, however, community motivation factors will not necessarily be so great and infrasonic effects, which include direct physiological factors and indirect effects such as window rattle may be approximately accounted for by applying the following increments to the calculated perceived noise level.

Correction Factor to CNR for Infrasonic Effects		
Octave Band Level 5 - 20 Hz	Below 115 dB	0
	115 to 125 dB	+ 5 PNdB
	Above 125 dB	+10 PNdB

A more detailed consideration is made of infrasonic vibration effects in Section 10.8.

Step 4 Corrections for Operational Factors

Table 10.3 lists the additional correction increments, in PNdB, as functions of the operational factors discussed below.

It will be noticed that all the increments listed are multiples of 5 PNdB. The reason for this is that in most cases more resolution is not justifiable in the light of current knowledge of the effects of the various factors. Also it is doubtful whether public reaction scales could be specified to a greater degree of accuracy.

(i) Duration of Stimulus

For each community area and each vehicle category, an equivalent exposure time is defined as the period within which the overall sound pressure level is within 10 dB of its maximum value.

The duration corrections listed in Table 10.3 are based on the assumption that the perceived noise level scale is valid for durations of around 20 seconds. The results shown in Figure 10.12 indicate that for test signal durations greater than 16 seconds the perceived noise level should be increased by 3 PNdB for each doubling of duration, and the 5 PNdB increments are suggested to accommodate duration effects.

(ii) Time of Day

During the daytime, many people are away from their residences, working in an area with a higher noise level.

TABLE 10.3  
OPERATIONAL CORRECTION FACTORS TO CNR

Factor		Correction	
Exposure Time (Minutes)	Less Than 0.5	0	
	0.5 to 3	+ 5	
	More Than 3	+ 10	
Time of Day	0700 - 2200	0	
	2200 - 0700	+ 10	
Number of Firings	0700 - 2200	2200 - 0700	
	5 or Less		3 or Less
	More Than 5	More Than 3	+ 5
Firing Type	Test Firing (Ground)		0
	Launch		- 10
Seasonal Effects *	Winter - With Sound Focusing Effects		+ 5
	Winter - No Sound Focusing Effects		- 5
	Summer		0
Background Noise	PNdB	Class of District	
	≤ 50	Very Quiet Suburban	+ 5
	51 - 60	Suburban	0
	61 - 70	Residential Urban	- 5
	71 - 80	Urban Near Industry	- 10
> 80	Heavy Industry	- 15	
Previous Exposure *	None		+ 5
	Some		0

\* Optional  
(See Text)

This factor could be accommodated in two ways. The population survey can be divided into two parts, day and night, with the daytime estimation based on place of work rather than place of residence. However, the additional effects due to increased activity, and consequently decreased noise sensitivity, are difficult to take into account. The alternative procedure is to ignore population movement during the daytime and merely allow for the increased disturbance at nighttime by applying the 10 PNdB correction for night firings.

(iii) Number of Firings

From the total firing schedule defined for a long period under Step 1, the average number of firings per daily time period can be calculated. In doing so, consideration should be given to any known and regular periods of increased activity. For example, if the majority of firings are confined to the Monday to Friday period each week, then weeks should be taken as five, rather than seven days.

(iv) Firing Type

It is a known fact that the motivation factor in communities adjacent to a launch center is very high and the population has a very favorable attitude towards noise intrusion. It is also likely that the bigger and noisier the vehicle, the more informed and interested the public will be. In the vicinity of static test areas, however, motivation is not so high. Static firings command much less glamour and public interest with the result that tolerance is lower. A 10 PNdB decrement is then proposed for application in the case of launch operations.

(v) Seasonal Variations

The validity of this correction is wholly dependent upon climatic conditions. In regions where seasonal variations do not significantly influence community habits, applicability is certainly doubtful. However, if winter temperatures cause residents to spend appreciably greater proportions of their time indoors, the average noise levels to which they are exposed will be reduced. On the other hand, sound focussing problems are likely to be more severe in winter time so that a 5 PNdB increase relative to summer conditions may be justifiable.

(vi) Background Noise

Prime interest is in the reaction of people to the stimulus noise due to the rocket firing itself. However, some of the sound energy reaching a community will originate from other, more local sources, which contribute to a general background level. Generally, residents accept this background noise as part of their daily environment and the effect of the stimulus is really measured by how it compares with this reference level.

The perceived noise level (PNdB) of the appropriate background noise is calculated by the standard methods and the corresponding correction factor can then be found from Table 10.3.

(vii) Previous Exposure

A person's reaction to a sound is dependent upon whether

or not he has heard it before (See paragraph 10.3.4) and the degree of his adaptation to it. The noise of an occasional aircraft overhead is now very familiar to the majority of people who may therefore be considered to be completely adapted to it. Unfortunately, this adaptation is unstable and can be upset by events such as accidents which are associated with the noise. In such circumstances, corrections should be reconsidered but Table 10.3 indicates the increment which should be applied in cases of no previous exposure. In fact, this is an unlikely situation among the residents near rocket firing centers and it is anticipated that no such correction need be applied, except in the event of introduction of particularly powerful noise sources which radiate to previously insignificant areas.

**Step 5** Calculation of the Composite Noise Rating (CNR)

The composite noise rating is calculated for each firing category by adding algebraically the total of the correction numbers derived from Table 10.3 to the perceived noise

level in PNdB determined in Step 3. From the various values applying to each category, an overall effective CNR must then be evaluated for each community area of interest. Only those CNR's which are within three units of the maximum need be considered. If there are three or more CNR's which satisfy this requirement, then 5 units must be added to the highest one to give the overall CNR. If there are less than three, the highest CNR applies.

**Step 6** Estimation of the Area Community Response

The relationship between three different scales of community reaction to the PNdB Composite Noise Rating is shown in Figure 10.16. The first, shown on the far left of the ordinate scale, is the same as presented earlier in Figure 10.15. It predicts 5 levels of community reaction in terms of an alpha numeric CNR scale. The later is shown on the abscissa PNdB CNR scale.

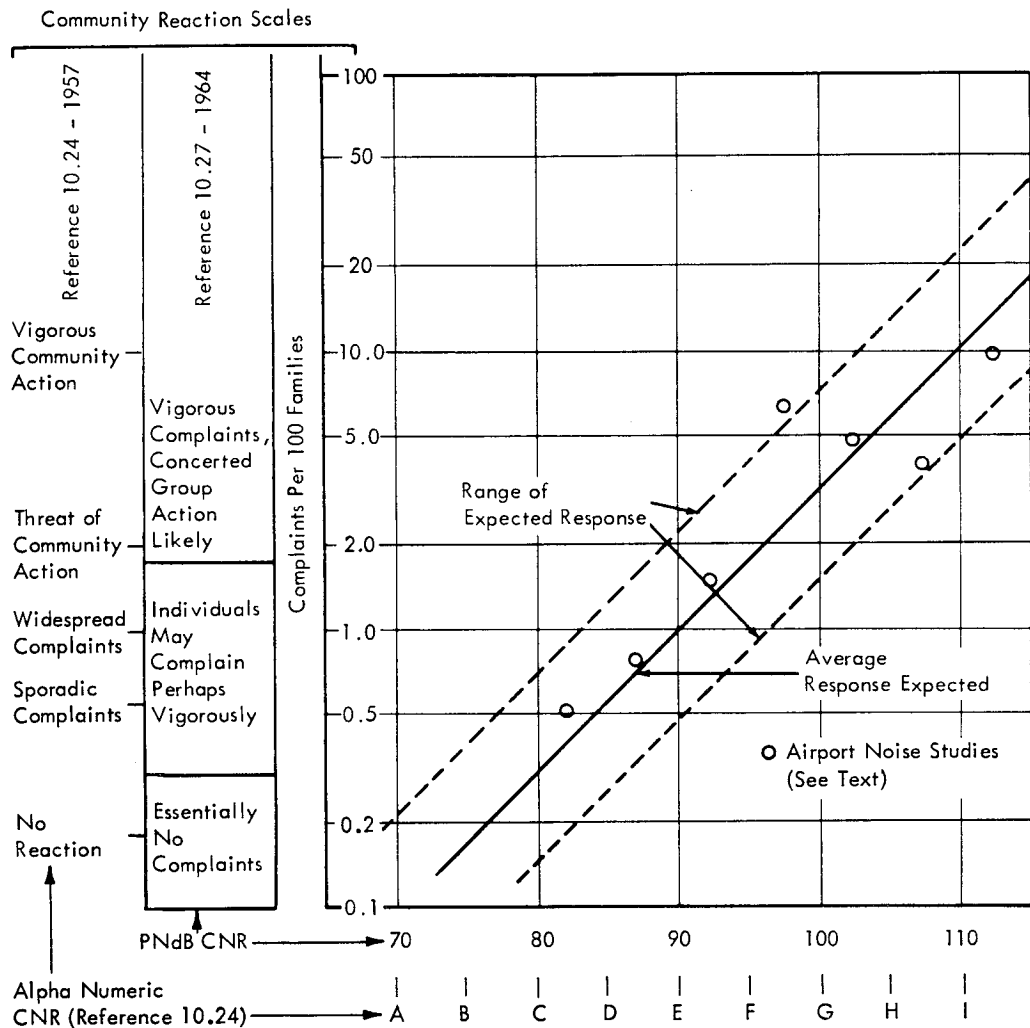


FIGURE 10.16 Relationships Between Expected Community Reaction to Noise and Composite Noise Rating

The second reaction scale on the ordinate axis is taken from Reference 10.27, and involves only 3 reaction ranges which are predicted by the corresponding PNdB CNR range.

Finally, a new quantitative scale of community reaction is constructed which correlates the number of complaints per 100 families with the PNdB CNR. This scale is based on previously unpublished data obtained during community reaction studies around a major airport. These data are also plotted in Figure 10.16 along with the mean line through the data and two "confidence bands" thus relating all three community reaction scales on a single graph. This new scale provides a valuable tool for quantifying community reaction with a parameter (complaint density or per cent complaints) which is a measurable and realistic gauge of community reaction. The correlation of this quantitative ordinate scale with the other qualitative rating groups is considered as a preliminary but useful tool for interrelating available data on community response to noise intrusion.

It is worth noting that the slope of the mean line on Figure 10.16 is equivalent to a 6 PNdB increase in level for a two-fold increase in complaint response. This compares with the slope of the subjective loudness function, shown in Figure 10.5 which shows a 10 dB increase in level for a two-fold increase in judged loudness. It is recognized that all these scales are based on jet noise and spectra which peak at higher frequencies than typical rocket noise. (Reference 10.28). However, assuming community reaction to be dominated by the noisiness of the sound intrusion, the perceived noisiness concept should automatically compensate for this frequency shift and it is proposed that Figure 10.16 can be used with reasonable confidence to classify likely community reaction by any one of the three scales.

#### Step 7 Estimation of the Average Community Response

Use of the first five steps to estimate a likely complaint density in a particular community region can be extended to define an average complaint density or likely mean reaction for an entire community. This additional step is based on the supposition that a district can be conveniently divided into a number of regions within which the various reaction factors can be regarded as uniform. After calculating the expected complaint density for each of these regions the mean community complaint density is simply the sum of the product of the complaint density and number of families for each region, divided by the total number of families. Thus, if an entire community is divided up into  $N$  zones of Area  $A_N$ , not necessarily equal, with population density  $P_N$  in each zone and a complaint density  $C_N$  is estimated for each zone on the basis of its average community noise rating  $CNR_N$ , then the total complaints  $C_o$ , from the community, can be estimated by the expression

$$C_o = \sum P_N \cdot A_N \cdot C_N (CNR_N)$$

## 10.6 EXPOSURE OF PERSONNEL TO BLAST

### 10.6.1 GENERAL DISCUSSION

The basic concern for personnel exposed to the blast wave from a propellant explosion is to prevent anybodily injury. Non-injurious subjective reactions to explosions are not considered significant factors for siting criteria. While such subjective reactions could be very marked, in this case, it is not considered justifiable to base site locations or distances on such reactions.

Extensive studies have been carried out by White and Richmond at the Lovelace Foundation for biological effects of blast. They have shown that bodily injury due to a blast can be categorized as follows (References 10.31, 10.32, 10.33, and 10.56).

#### Primary Effects (Tolerance to Transient Overpressure)

- Eardrum Rupture
- Lung Damage
- Lethality

#### Secondary Effects (Tolerance to Impact by Missiles)

- Skin Lacerations
- Serious Puncture Wounds
- Concussion
- Skull Fracture

#### Tertiary Effects (Tolerance to Physical Displacement)

- Body Displacement
- Skull Fracture From Impact

The maximum allowable overpressure for each of these effects is specified in the following sections.

### 10.6.2 PRIMARY EFFECTS

The criteria listed in Table 10.4 have been suggested for the maximum incident overpressure for injurious primary effects. Two values of incident overpressure are given; the lower value holds for a subject located near a reflecting wall where, due to reflection, the effective overpressure is equal or greater than the incident overpressure.

The criteria for lethal blast overpressures have been estimated by Richmond and White (Reference 10.56) by extrapolation of data obtained on animals.

#### 10.6.2.1 Effects of Duration on Lethal Limits for Blast

The criteria for lethal exposure given above apply only to blast waves with actual durations greater than 0.1 second. Figure 10.17 shows the estimated overpressures ( $LD_{50}$ ) for 50 percent fatality of man versus duration of the blast pulse. The data points represent smoothed values reported by Richmond and White for the observed 50 percent mortality overpressure versus duration for 6 different types of mammals scaled up to a 70 Kg man (Reference 10.33).

TABLE 10.4

THRESHOLD BLAST PRESSURES FOR PRIMARY EFFECTS  
OF FAST RISE TIME - LONG DURATION BLAST PULSE

Effect	INCIDENT PRESSURE	
	No Reflection,psi	With Reflection,psi
• Ear drum Rupture	5	2.3
• Lung Damage Threshold	10-12	4.4-5.1
• Lethality % Fatalities	30-42	11-15
( $t_p^+ > 0.1$ sec) 50% "	42-57	15-18
99% "	57-80	19-24

[  $t_p^+$  is the duration of the positive phase of the blast ]

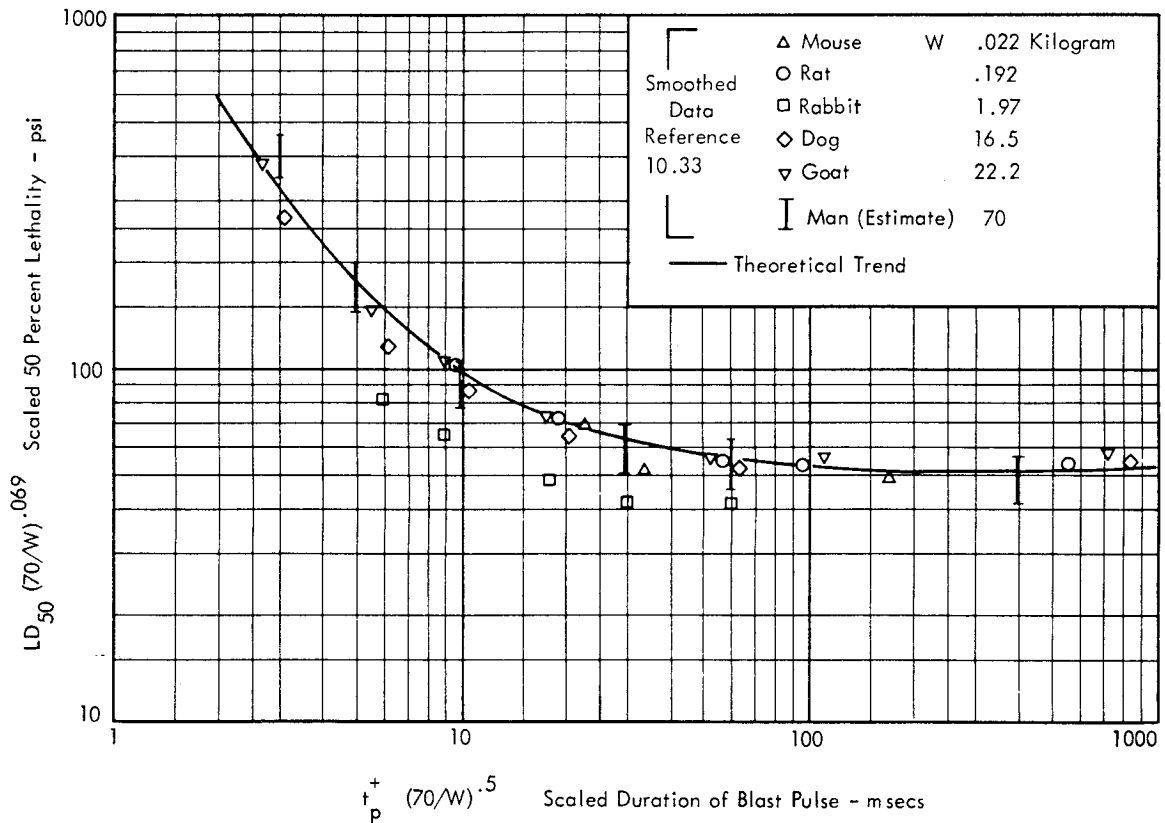


FIGURE 10.17 Fifty Percent Lethality Incident Overpressures versus Blast Duration For Mammals, Scaled by Weight to 70 Kilogram Mammal (man), Compared to Theoretical Trend Expected for Shock Response to Classical Blast Pulse of Simple Oscillator with 36 Hz. Resonance Frequency. (Data from Reference 10.33)

The weight of the test animals covered a range of 1,000 to 1 and scaling was accomplished by the following steps:

- 1) Following Reference 10.33, the overpressure peak causing 50 percent fatalities ( $LD_{50}$ ) was multiplied by  $(70/W)^{.069}$  where  $W$  is body weight in Kg.
- 2) The measured duration of the positive phase of the blast,  $t_p^+$  was multiplied by the ratio  $(70/W)^{1/2}$ .

The choice of a square root scaling law between body weight and characteristic time is at variance with a cube root scaling law expected for a linear dynamic model of the body. The latter scaling concept is, in fact, proposed by von Gierke (Reference 10.34). The scaling laws were chosen, in this case, on the basis of a "best fit" to the experimental data.

Justification for the use of these scaling laws is apparent from the good collapse of the data, and it is thus believed that the results can be used for the prediction of the effects of blast on humans with reasonable confidence. The scaling laws themselves imply that an increase of body weight increases the tolerable level of overpressure and increases a characteristic response time.

#### 10.6.2.2 Analytical Model for Predicting Effects of Duration

The increase in allowable overpressure for shorter duration blasts suggests that the response of the body to a blast may be a function of the impulse of the blast wave for durations much less than some characteristic reaction time. Thus, it is reasonable to use, as an analytical model, the response of a single degree of freedom system to a blast wave, to attempt to explain this duration effect. This simple model can only be considered as a rough approximation (i. e., representing a critical normal mode) of a complex bio-dynamic nonlinear system.

A significant application of this model can be for semi-empirical analysis of blast protection methods for personnel. For example, the allowable rate of blast pressure increase inside a personnel shelter can be estimated from the known ramp-step response of a simple oscillator.

To apply this model, the mirror image of the shock response spectra for a classical blast wave (see Chapter 3) has been fitted to the data in Figure 10.17. The theoretical curve is adjusted for a best fit to the scaled data and the fit indicates that the "critical single degree of freedom system" has a characteristic frequency of about 36 Hz. It is interesting to compare this result with the findings of von Gierke (Reference 10.34). He associated blast tolerance with lung response on the assumption that equal maximum compression of the lungs in response to blast (or pressure in the lungs) produces equal injury patterns. Using a thorax resonant frequency of 45 Hz. (see paragraph 10.8.1), which is somewhat higher than the above result, curves of equal thorax compression in response to sawtooth blast waves were calculated and showed a strong similarity to the data of Richmond and White (Reference 10.33).

It is also important to note that the critical dynamic mode

involved in lung damage or lethal injury will not necessarily be the same as that involved in noninjurious reaction to low frequency sound or overpressure. For the former, excessive pressure differentials within the body are a major source of physical damage (Reference 10.32). For the latter, noninjurious phenomena such as dynamic distortions of internal organs may be the cause of nonauditory subjective sensation.

#### 10.6.3 SECONDARY EFFECTS

Secondary effects of blast injury to humans are associated with injury by missiles. Such missiles can be fragments of an exploded vehicle or secondary missiles generated at some distance from the explosion by excessive overpressure (i. e., glass fragments from windows). The first category is not considered further in this chapter since normal safety requirements for operating personnel will dictate adequate protective housing to prevent injury.

For secondary missiles generated by failure of structure remote from the explosion, the degree of possible human injury is dependent on

- Weight and Shape of Missile
- Distance Traveled Before Impact
- Velocity and Angle at Impact
- Location of Impact on Body and Degree of Penetration (if any).

Detailed investigations on this topic have been conducted by the Lovelace Foundation (see References 10.32, 10.35, and 10.36). Some of their results are summarized in Table 10.5 which lists proposed criteria for threshold of injury by secondary effects. Reference 10.37 outlines an analytical method for predicting the required overpressure and yield to achieve the missile velocities indicated in Table 10.5.

However, experimental data is preferred due to the particular significance of the hazard from glass fragments. Experimental data on the distribution of mass and velocity of glass fragments from blast-failed windows is shown in Figure 10.18. The measurements were made during tests at the Nevada Proving Ground and were reported in Reference 10.35. Also shown, from the same reference, is the criteria for the threshold mass and velocity for glass fragment puncture wounds in the abdomen of a dog. The glass fragments were trapped at a distance of 10-12.75 feet from the windows which were located at various distances from the blast center.

The mean overpressure at each window location is shown beside the mean velocity and mass of the glass fragments. The wide range of missile velocities and masses for a given overpressure is very apparent. Although the mean velocities decrease with overpressure, the mean fragment mass increases so that over the range of incident pressures studied, a trend relative to the injury criteria is not clear. However, it is reasonable to assume that for blast pressures just sufficient to break a window, a serious wound could be inflicted on a person by any large fragment within a few feet of the window. With this in mind, it is recommended



TABLE 10.5  
TENTATIVE CRITERIA FOR THRESHOLD  
OF INJURY BY MISSILES

Effect	Missile	Velocity ft/sec
Skin Laceration	10gm Glass	50
Serious Puncture Wounds	10gm Glass	100
Lung Hemorrhage - (1)	0.4 lb Object	80
Lung Hemorrhage	0.8 "	40
Rib Fracture - (1)	0.4 "	120
Rib Fracture	0.8 "	60
Fatality - (1)	0.4 "	170
Fatality	0.8 "	155
Cerebral Concussion or Skull Fracture	10 lb Object	15

(1) Non Penetrating Missile Impact on Chest Wall of Dogs  
(Reference 6.30)

that, for siting criteria for rocket test facilities, overpressures required for window breakage alone be used as a basis for establishing criteria for secondary effects of blast on man.

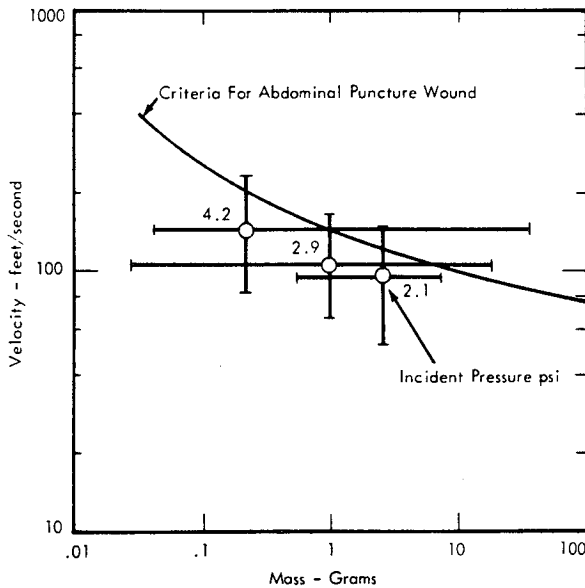


FIGURE 10.18 Distribution of Glass Fragments at 10 to 12 Feet From Windows Failed by Blast Compared to Criteria for Threshold of Abdominal Puncture Wounds in Dogs by Glass Fragments (Data From Reference 10.35)

10.6.4 TERTIARY EFFECTS

Persons exposed to a blast are subjected to injury by being blown down by the blast wind and impacting a hard surface. Again, criteria from the studies reported by the Lovelace Foundation can be used as a guide for this type of injury.

These criteria are listed in Table 10.6.

TABLE 10.6  
TENTATIVE CRITERIA FOR THRESHOLD OF  
INJURY BY BODILY DISPLACEMENT

Effect	Impact Velocity ft/sec
Whole Body Displacement	
Mostly "Safe"	10
Lethality Threshold	20
Skull Fracture	
Mostly "Safe" Threshold	13

Although analytical methods are available for correlating blast parameters with the required velocities listed above, (Reference 10.36), pertinent experimental data will be used instead. Experimental studies have been conducted by the FAA with a simulated blast wind to determine the dynamic pressure required to cause a man to lose his

balance, (Reference 10.38). The dynamic pressure required for unbalance varied with the position of the man. The minimum value, for which no recovery was possible, varied from 0.103 to 0.165 psi for a man walking with one side facing the blast wind. The minimum value would correspond to an incident overpressure of 2.2 psi at a scaled ground distance ( $R/W_T^{1/3}$ ) of 27 ft/lb<sup>1/3</sup>. The highest dynamic pressure required was 0.2 psi for a man standing with his back to the blast.

10.6.5 SUMMARY OF BLAST EFFECTS

In summary, the most critical effect of blast exposure for man will be injury by glass missiles. Siting criteria involving blast hazards to personnel in uncontrolled areas should therefore be based on minimum risk of window breakage. For personnel in controlled areas where glass fragments are not involved, maximum incident overpressures must be limited to less than 2 psi to avoid injury by impact of the head or eardrum rupture.

10.7 EXPOSURE OF PERSONNEL TO SONIC BOOM

A further source of community disturbance is the "sonic boom". At large distances from the aircraft, it takes the form of an impulsive acoustic pressure disturbance, having a time history which can be approximated by an N-wave, and having a duration between approximately .04 second for a fighter type aircraft to approximately 0.4 second for a commercial supersonic transport. Details of the sonic boom N-wave are covered in Chapter 6, Section 3. For very low flying aircraft it can reach levels around 150 pounds per square foot, but for normal supersonic flight of fighter through SST aircraft, overpressures at the ground would rarely exceed 5 pounds per square foot.

10.7.1 THE BOOM INDOORS AND OUTDOORS

Outdoors, the progressive shock wave diffracts around the

human body and leads to a pressure doubling for the higher frequencies on the side facing the oncoming wave. Von Gierke (Reference 10.39) suggests this could be responsible for the common subjective sensation of being "hit" by the boom. Indoors, the effect of a boom is quite different. The building itself acts as a filter which removes much of the high frequency energy. The transmitted pressures and particle velocities are lower but reverberation extends the duration of the disturbance and essentially eliminates its directional character. The building vibrations result in rattling noises which add to the general stimulus. Airborne shock waves also give rise to a ground shock. However, magnitude of the ground shock is not considered to be a major contributing factor to subjective response to a sonic boom.

Pearsons and Kryter (Reference 10.40) performed laboratory experiments to determine the relationships between the judged "acceptability" of subsonic jet aircraft and simulated sonic booms as heard indoors, and their results are shown as Table 10.7. These results indicate that:

- 1) When the building is "rattle free", the sonic boom is less noisy indoors than outdoors by about 11 PNdB.
- 2) When the boom causes the building to rattle, it is judged 2 to 3 PNdB more noisy indoors than outdoors.
- 3) In the latter case, the sonic booms considered, which could be expected from high altitude flight of fighter type aircraft, were considered to be as noisy as a subsonic airliner take-off heard indoors about 1.5 miles from the airport. Thus, it is clear that the degree of sonic boom exposure expected in communities near commercial air routes, where large SST aircraft fly at frequent intervals, represents a very significant form of community noise.

TABLE 10.7

COMPARISON OF JUDGED NOISINESS OF SUBSONIC JET AIRCRAFT AND SIMULATED SONIC BOOMS (AFTER PEARSONS AND KRYTER, REFERENCE 10.40)

Location	Typical Sonic Boom Measured (lb/sq ft)		PNdB Values From Subsonic Jet Aircraft That Would be Judged Equally Acceptable			Typical PNdB Values Actually Present 1.5 Miles From Airport After Takeoff of Subsonic Jet Aircraft	
	Outdoors	Indoors	Outdoors	Indoors		Outdoors	Indoors
				No Rattle	Window Rattle		
Under Flightpath	2.3	0.5	95.5	84.5	98	112	95
4 Miles to Side of Flightpath	2.0	0.45	94.5	83.5	97	70	55
8 Miles to Side of Flightpath	1.6	0.36	92.5	81.5	95	...	...

10.7.2 THE EFFECTS OF SPECTRAL CONTENT UPON NOISINESS

Considerable insight into the subjective effects of the sonic boom has been gained from studies of the loudness of acoustic impulses performed at the University of Southampton, England (References 10.41 and 10.42.) Subjects were asked to judge the loudness of acoustic impulses (N-waves) having different rise times, amplitudes and total duration, as compared to a steady 400 Hz. pure tone. Both were played through special earphones. The main results of these studies are that:

- (i) rise time has a significant effect upon loudness but duration does not.
- (ii) N-waves having durations longer than 50 milliseconds were heard as double impulses, and
- (iii) filtering out energy below 40 Hz. did not affect the loudness.

But probably the most significant finding, by Zepler and Harel (Reference 10.42), was that the loudness of an N-wave is highly correlated with its spectrum, which is dependent to a large extent upon the rise time. The power spectrum of the N-waves was calculated and weighted according to the 80 phon equal-loudness contour of Robinson and Whittle (Reference 10.12) extrapolated to 40 Hz. The integrated area under this weighted spectrum gave a measure of loudness and Figure 10.19 shows excellent agreement between calculated and judged loudness for different rise times.

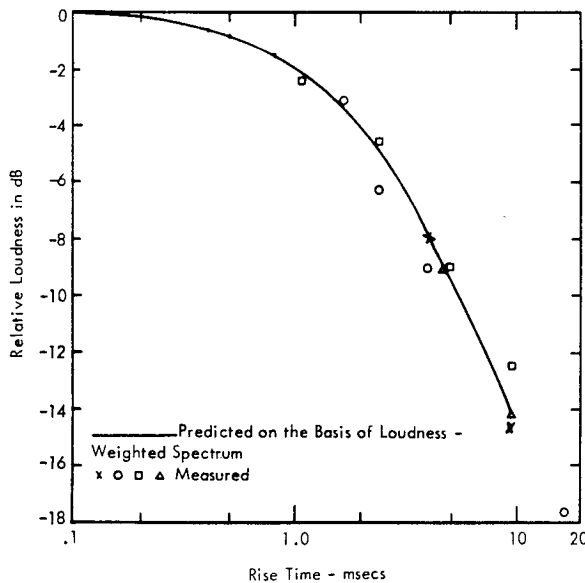


FIGURE 10.19 Relative Loudness of Simulated Sonic Booms As a Function of Rise Time. (From Reference 10.42)

It might be expected that the same reasoning would apply equally well to both loudness and noisiness, as discussed in Section 10.3, but when Pearsons and Kryter applied

their Perceived Noise Level calculations to both the sonic boom spectra and the spectra of the subsonic aircraft which were judged to be equally noisy (Reference 10.40), they found that the booms were computed to be noisier by some 12 dB. Although this discrepancy may possibly be explained as a duration phenomenon, the duration corrections discussed in paragraph 10.3.2 would be greatly excessive, being of the order of 40 dB. A much more likely explanation is that the noisiness increment is the effect of the low, and particularly the infrasonic, frequency content of the boom signature. The earphone tests of Reference 10.14 preclude the very important acoustic wave reception by the whole body, particularly by the thorax/abdomen system which doubtlessly play an important part in the subjective judgment of low frequency sounds. It is useful, therefore, to consider the form of the energy spectrum of a sonic boom N-wave. (See Section 6.3.2 of Chapter 6).

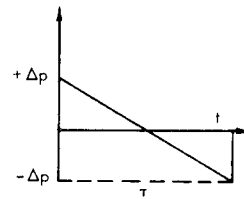


FIGURE 10.20 Ideal N Wave

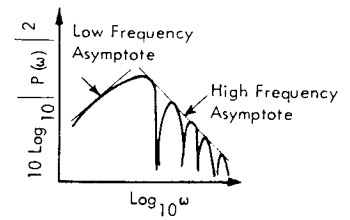


FIGURE 10.21 Energy Spectrum of N-Wave

Figure 10.20 shows the time history of an idealized N wave. The energy spectral density, defined as the square of the absolute value of the Fourier Spectra for this time history, is illustrated conceptually in Figure 10.21. The effects on the energy spectrum of the two independent parameters, the peak overpressure,  $\Delta p$ , and the time duration  $\tau$ , are shown in Figure 10.22. For a constant  $\Delta p$ , it is clear, from Figure 10.22, that the audible part of the spectrum is essentially constant for varying  $\tau$ . However, the infrasonic energy increases rapidly with aircraft size. It is to be expected that the larger aircraft, although judged equally noisy by the ear, will be considerably more disturbing due to non-auditory effects of the low frequency content of the longer N wave.

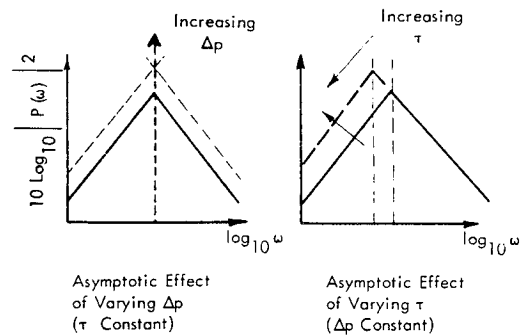


FIGURE 10.22 Scaling of Energy Spectral Density of Sonic Boom N Wave (Ref. 10.43)

10.7.3 DAMAGE LEVELS

Due to the impulsive nature of sonic booms, their most significant effect on observers is to induce a startle reaction. The actual level of the pressure disturbance is very much lower than that which may cause any damage to the hearing mechanism. For example, no temporary hearing loss has been measured in subjects,

- (i) immediately after exposures to booms up to 30 lb/ft<sup>2</sup>, or
- (ii) 3 to 4 hours after exposure to booms up to 120 lb/ft<sup>2</sup>. (Reference 10.39)

Further, no damage to the eardrum is expected below 720 lb/ft<sup>2</sup> and certainly none has been found at pressures up to 144 lb/ft<sup>2</sup>.

Therefore, no acoustic protective measures for personnel exposed to high level sonic booms at flight test centers is considered necessary.

10.8 EFFECTS OF VIBRATION ON PERSONNEL

10.8.1 MECHANICALLY INDUCED VIBRATION

From a subjective point of view, vibration may be defined as any fluctuating mechanical force which man perceives by senses other than hearing, although in the majority of practical cases, vibration at frequencies within the hearing range will be accompanied by sound. At all frequencies, the whole body is a receptor for acoustic waves but their reception becomes particularly important at infrasonic frequencies, since the sound is felt purely as a vibration. High levels of vibration can make people uncomfortable although it does not necessarily follow that all levels interfere with the performance of manual or mental tasks. Sensory detection of vibration involves differential motion between the body and its point of contact with the vibration source, and the elastic response of the body itself. The body is an extremely complex dynamic structure which has equally complex resonance modes. At low frequencies, roughly in the range 1 to 30 Hz., these involve whole body resonances due to the elastic coupling of the various limbs whereas in a higher frequency range, between 30 and 100 Hz., the tissue responds like a fairly uniform visco-elastic medium. At higher frequencies still, vibrations are strongly attenuated at the body surface and, subjectively, become insignificant in comparison with the associated acoustic stimulation. The frequency ranges of some of the more important body resonance phenomena are shown in Figure 10.23.

10.8.1.1 Mechanical Effects

Von Gierke (Reference 10.34) has developed a simplified mechanical model which simulates the response of the human body to vibratory excitation and this is shown diagrammatically in Figure 10.24. This combines the essential response characteristics of the thorax-abdomen system, and upper torso for longitudinal force applications

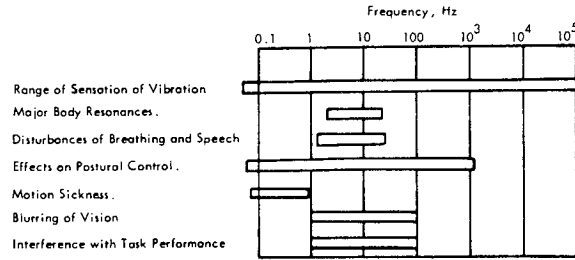


FIGURE 10.23 Frequency Ranges of Subjective Vibration Effects

and pressure, accounting for the motions of the mass of the upper torso on the elastic structure of the spine and the motion of the abdominal wall, the diaphragm and the lung plus thorax.

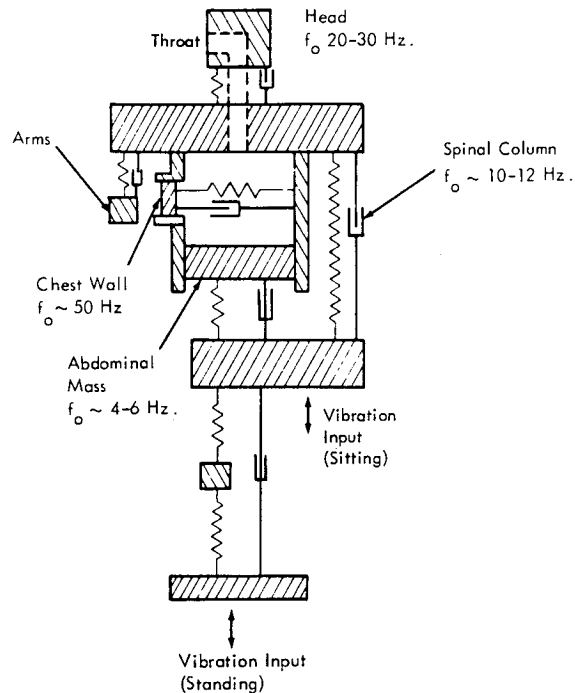


FIGURE 10.24 Mechanical Model of Human Body Exposed to Vibration (Reference 10.34)

This model helps to illustrate the mechanical effects of low frequency vibration on the body. The dominant mode of vibration, either standing or sitting, occurs around 4-6 Hz. This involves mainly the abdominal mass and structures inside the chest and an important effect is its interference with the respiratory mechanisms as it causes increased pumping of air to the lungs. An important secondary mode is the longitudinal oscillation of the spinal column which occurs around 10 to 12 Hz. and a third is one in which

the head oscillates with respect to the torso between 20 and 30 Hz. At frequencies below about 4 Hz. the body moves as a single mass, without resonance.

The mass, stiffness, and damping coefficients of the mechanical model shown in Figure 10.24 were determined by comparing theoretical and measured body responses. The coefficients of the thorax-abdomen system yielded a theoretical resonance peak for the chest wall around 45 Hz. (Reference 10.34), which helps to explain the responses of subjects exposed to high intensity, low frequency sound (Sections 10.6.2 and 10.8.2). Also, an identical model was used by Holladay and Bowen (Reference 10.61) to calculate the lung pressures in rabbits exposed to blast. By estimating the coefficient values from a consideration of physical dimensions, they were able to mathematically simulate measured lung response with great precision.

#### 10.8.1.2 Physiological Effects

Vibration certainly constitutes an environmental stress which contributes to fatigue, but also causes a number of specific physiological disturbances. These include interference with breathing and speech, particularly in the range 3 to 15 Hz. and widespread effects upon the nervous system. Low frequency vibrations affect the organs of balance and other receptors involved in the regulation of posture, and increased effort is required to maintain both balance and posture. In severe cases, unsteadiness can persist for some time after the vibration has ceased.

Whole body vibration at frequencies lower than 4 Hz. and acceleration amplitudes greater than 0.03 g can cause motion sickness, the effect being maximal around 0.3 Hz.

#### 10.8.1.3 Psychological Effects

Figure 10.25 taken from Reference 10.45 shows various sinusoidal vibration exposure criteria, which define limits of perception, unpleasantness and intolerability. Subjective tolerance is at a minimum at frequencies between 5 and 10 Hz., primarily due to abdominal response. Within that range, the threshold of vibration perception is approximately 0.005 g, the threshold of discomfort is about 0.1 g and the ultimate limit of voluntary tolerance is around 2g.

Although these criteria were derived from experiments using purely sinusoidal excitation, the work of Reference 10.46 indicates that the effects of narrow band random vibration are equivalent to those of sinusoidal vibration having the same mean frequency and the same rms level.

Task performance is reduced by vibration through its direct effects upon the body, interfering with muscular action, vision, and communication. For example, the legibility of instruments is reduced, particularly at frequencies between 2 and 20 Hz due to excitation of body resonances and involvement of the eye movement systems.

A tentative criterion for the effects of vibration on task performance is shown in Figure 10.26, based on a comparison of the data reviewed in Reference 10.47 and the subjective response data of Figure 10.25.

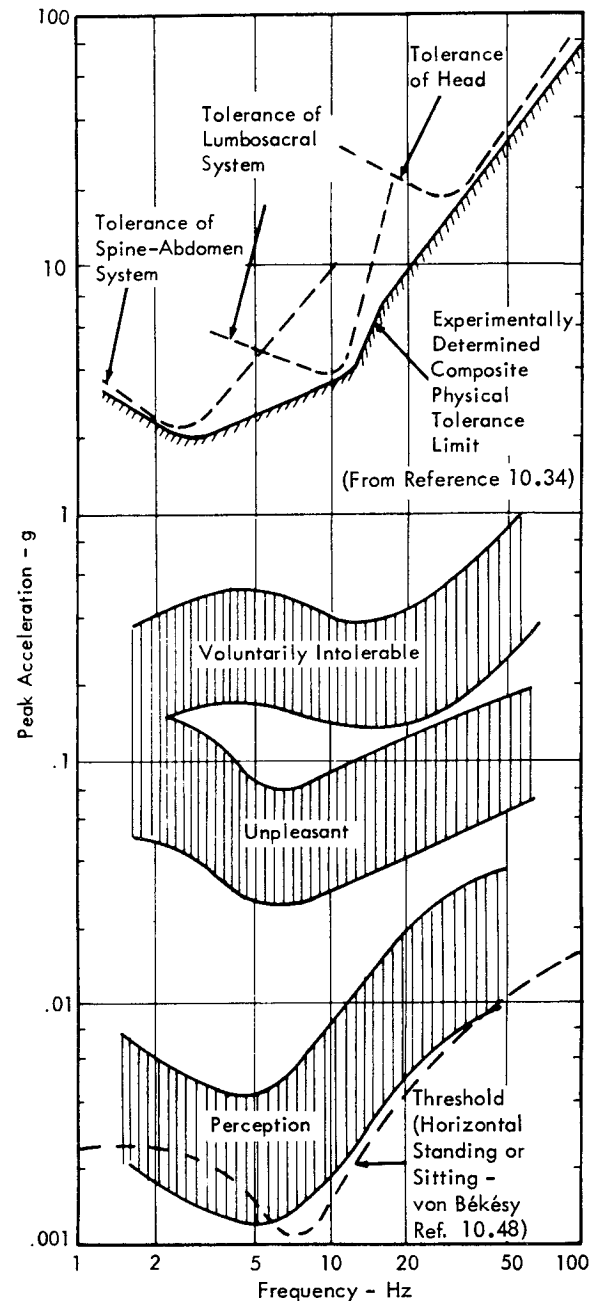


FIGURE 10.25 Sinusoidal Vibration Exposure Criteria. (From Goldman and von Gierke, Ref. 10.45). The Widths of the Bands Indicate  $\pm 1$  Standard Deviation.

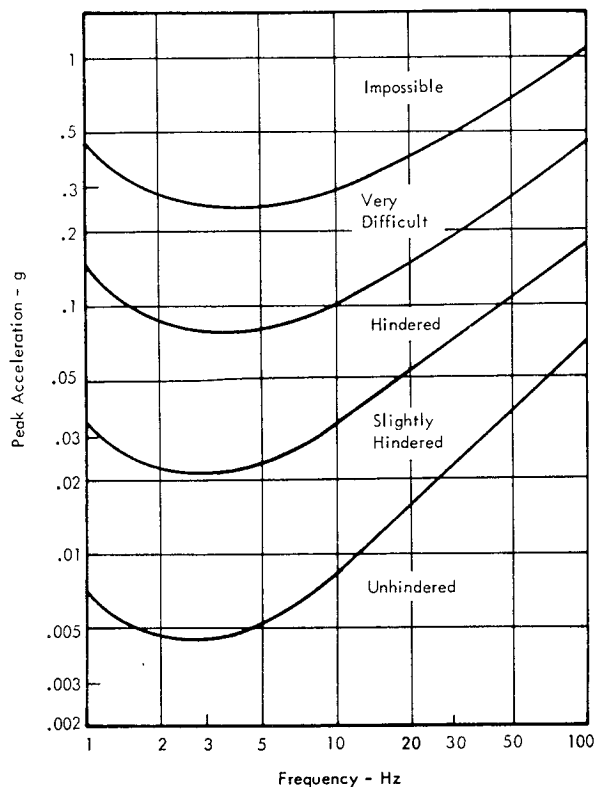


FIGURE 10.26 Tentative Criteria for the Effects of Vibration on Task Performance

10.8.1.4 Pathological Effects

Exposure to moderate vibration levels for long periods can cause medical disorders such as backache although there are no published criteria for these effects. Acceleration amplitudes exceeding 2g in the frequency range 2 to 10 Hz. are likely to cause injury if sustained for more than a few seconds and very high levels, greater than 5g, can cause hemorrhage of the lungs and intestines, and spinal injury. Superimposed on Figure 10.25 is an experimentally measured limit for physical tolerance of sinusoidal vibration. (Reference 10.34). Higher vibration levels than these are known to cause physical damage to tissue and bone. A further example of the usefulness of the mechanical model discussed above is to be found in the individual tolerance curves of the various subsystems, (head, spine, etc.,) which are plotted for comparison. These curves were computed using the mechanical analogy and represent lines of constant critical displacement.

It should be noted that levels at which vibrations become intolerable to the subject are considerably lower than levels which cause damage, particularly at higher frequencies.

10.8.2 ACOUSTICALLY INDUCED VIBRATION

It has been pointed out that infrasonic or subaudible acoustic levels will evoke subject reactions due to sensation of vibration induced by the noise. It is desirable to attempt

to relate the criteria for mechanical vibration to low frequency acoustic levels which will generate low frequency vibrations of the body. Three estimates are made to provide some approximate criteria for subjective response to subaudible noise.

10.8.2.1 Sonic Vibration of the Head

A controlled experiment was conducted by von Békésy (Reference 10.48) involving measurements of the motion of the human head in a 134 dB sound field. Over the frequency range of 100-500 Hz, the observed motion, expressed in terms of peak acceleration, can be defined by

$$A \approx 2 \times 10^{-4} f, \text{ peak g's}$$

where  $f$  = frequency of the incident wave - Hz.

The data indicates a linear extrapolation to lower frequencies is reasonable. As shown in Section 8.1.1.3 of Chapter 8, the rms net force  $\tilde{P}$  on a sphere of diameter  $d$  in a plane wave sound field with an rms pressure  $\tilde{p}$  is,

$$\tilde{P} = \frac{\pi d^2}{4} \tilde{p} \left[ \frac{2\pi f d/c}{\sqrt{1 + 4(\pi f d/2c)^4}} \right]$$

where  $c$  = speed of sound.

It has been shown that first resonances of the human skull occur between 500 and 1000 Hz. (Reference 10.49) and that the head-neck mass-spring system has a resonance around 2 Hz. (Reference 10.50). Thus, it is reasonable to consider the head as approximating a free rigid sphere in the frequency range of about 5-250 Hz.

With the above expression for the net force, assuming a weight of 7.5 lb and an average diameter of 6.5 in., then such a sphere, in a sound field with an rms sound level of 134 dB would have a peak acceleration over the range of 5 - 250 Hz of

$$A' \approx 2.8 \times 10^{-4} f, \text{ peak g's}$$

The remarkable agreement between the predicted and observed head vibration justifies the use of the latter data as a predictor for sonically induced head vibration in the range of 5 to 250 Hz. The estimated and measured acceleration amplitude is plotted as a function of frequency in Figure 10.27 for a 134 dB sound field.

10.8.2.2 Sonic Vibration of Whole Body

Below a frequency of about 4 Hz. the body will behave approximately as a rigid system. Assuming the theory for net acoustic force on a rigid cylinder may be applied, an estimated sonic vibration level of the body is predicted by the expression (see Chapter 3):

$$A \approx \frac{dL\tilde{p}}{W} [\pi^2 f d/c]$$

where  $L$  = Length of "cylinder" - in.  
 $W$  = Weight of "cylinder" - lb  
 $\tilde{p}$  = rms pressure in incident wave - psi, and  
 $d$  = Diameter of cylinder.

Based on  $d=12$  in.,  $L=70$  in.,  $W=150$  lbs, the acceleration is roughly

$$A \approx .05 \tilde{p} f - g's \quad f < 5 \text{ Hz.}$$

This relationship is also shown in Figure 10.27 for a 134 dB sound field.

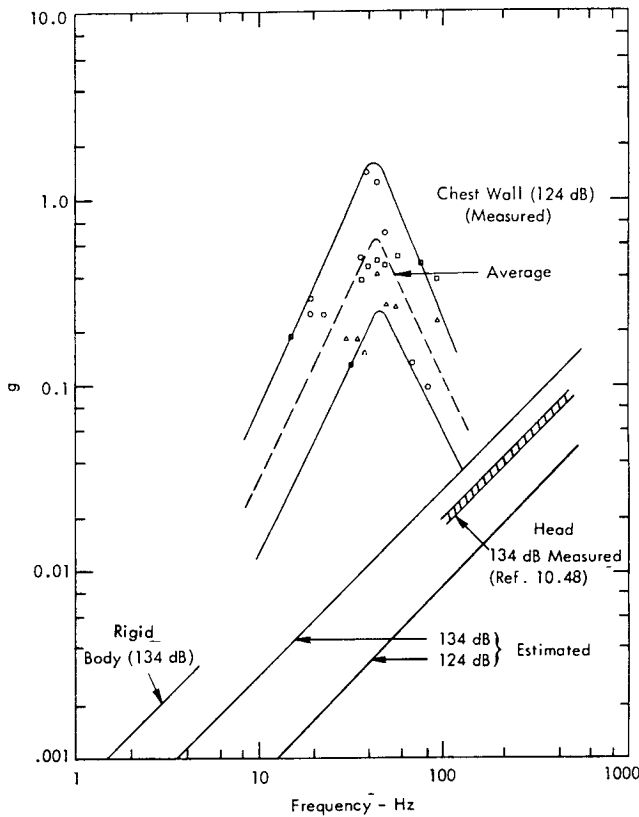


FIGURE 10.27 Acceleration Amplitude of Various Body Responses to Discrete Frequency Acoustic Excitation

10.8.2.3 Sonic Vibration of the Thorax/Abdomen System

Studies of the mechanical model of the human body, which were discussed in paragraph 10.8.1.1, suggested that a chest wall resonance should occur at a frequency around 45 Hz, for acoustic excitation, with the air volume in the lungs oscillating through the throat. Mohr and von Gierke (Reference 10.34) in fact, observed this resonance close to 60 Hz. From unpublished test results (Reference 10.51), which are compared in Figure 10.27 with the "rigid body" acceleration responses of the head and torso, a resonance of around 45 Hz is apparent. The comparison shows that

chest acceleration amplitudes, measured in a semi-reverberant sound pressure level of 124 dB are considerably greater than the predicted "rigid body" responses for this same sound level.

It seems likely then that these chest motions will play an important part in subjective sensations of low frequency sound, and it is interesting to relate these results to the data on subjective response to vibration discussed in paragraph 10.8.1.3. Figure 10.25 shows a region of acceleration versus frequency which is judged to be "unpleasant". Although this region represents acceleration levels applied to the body at various points and in various directions, Figure 10.28 has been prepared, which shows the estimated range of discrete frequency sound pressure levels which would be required to produce the same acceleration levels at the chest wall. No attempt has been made to account for possible attenuation between the point of application of the accelerating force and the thorax, which may have been a significant factor in the results of Figure 10.25. Also it has been assumed that chest acceleration are linearly related to sound pressure level in calculating equivalent sound pressure levels from Figure 10.27.

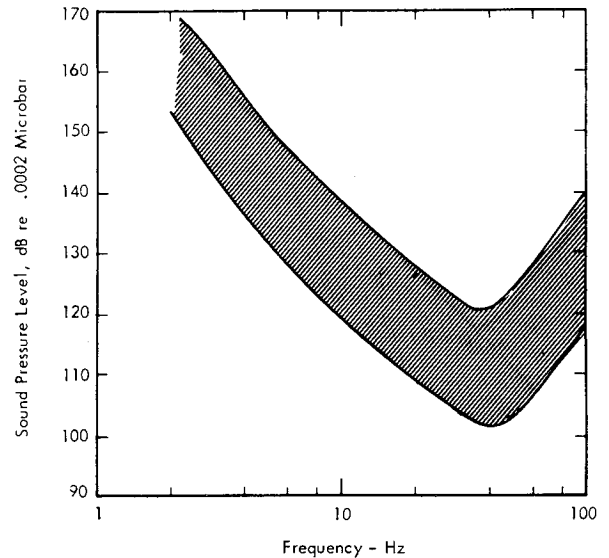


FIGURE 10.28 Discrete Frequency Sound Pressure Levels Estimated to Cause Chest Wall Vibration Levels Corresponding to "Unpleasant" Acceleration Region of Figure 10.25

Provided these assumptions are reasonable, Figure 10.28 represents an estimate of the non-auditory subjective effects of low frequency sound which are additional to the normal judgements of loudness and noisiness (section 10.3). The tests of Reference 10.51 were performed with the subjects wearing ear protection and it was noted that their sensations were dominated by chest vibrations. However, they were exposed to constant sound pressure levels of 124 dB and it was only in the immediate vicinity of the chest resonance (around 40-50 Hz.) that the levels were regarded as uncomfortable. Figure 10.28 shows "unpleasant levels" at somewhat lower sound pressures. This apparent discrepancy

could be attributed to differences in the definitions of "uncomfortable" and "unpleasant" and attenuations of mechanically excited vibrations through the body may also be important. Nevertheless, in the absence of other sources of information, this data was used to compile the table of infrasonic noise corrections to the PN dB calculations in section 10.5 and again it must be stressed that the values are tentative.

## 10.9 HEARING PROTECTION

In situations where it is impossible to shield personnel from excessive noise levels which are potentially damaging to hearing, it is necessary to provide some direct protection of the ears. Biological problems make it difficult to devise convenient methods which provide complete hearing protection against sound of any frequency or level and current devices compromise cost, comfort and convenience to yield sound attenuation at the ear of the order of 30 dB in the

mid-frequency range. The main problem is that sound does not reach the inner ear through the ear canal alone, and sound received by any part of the body is transmitted, admittedly via a high transmission loss, to the hearing mechanism. By exposing very small areas of the body to sound radiation, von Gierke, et al (Reference 10.52) found that the thresholds of hearing for body absorbed sound were approximately 60 dB, 70 dB and 85 dB above the air conduction threshold for the forehead, chest and abdomen respectively. For free field exposure, these figures are reduced appreciably and bone conducted sound, especially that received by the head, becomes a controlling factor which limits the maximum sound attenuation that can be provided by ear protective devices.

Devices currently available for hearing protection include earplugs, semi-inserts, earmuffs, and helmets and an example of each type is illustrated in Figure 10.29. Before making a direct comparison of their relative merits, each will be described in terms of its mode of operation.

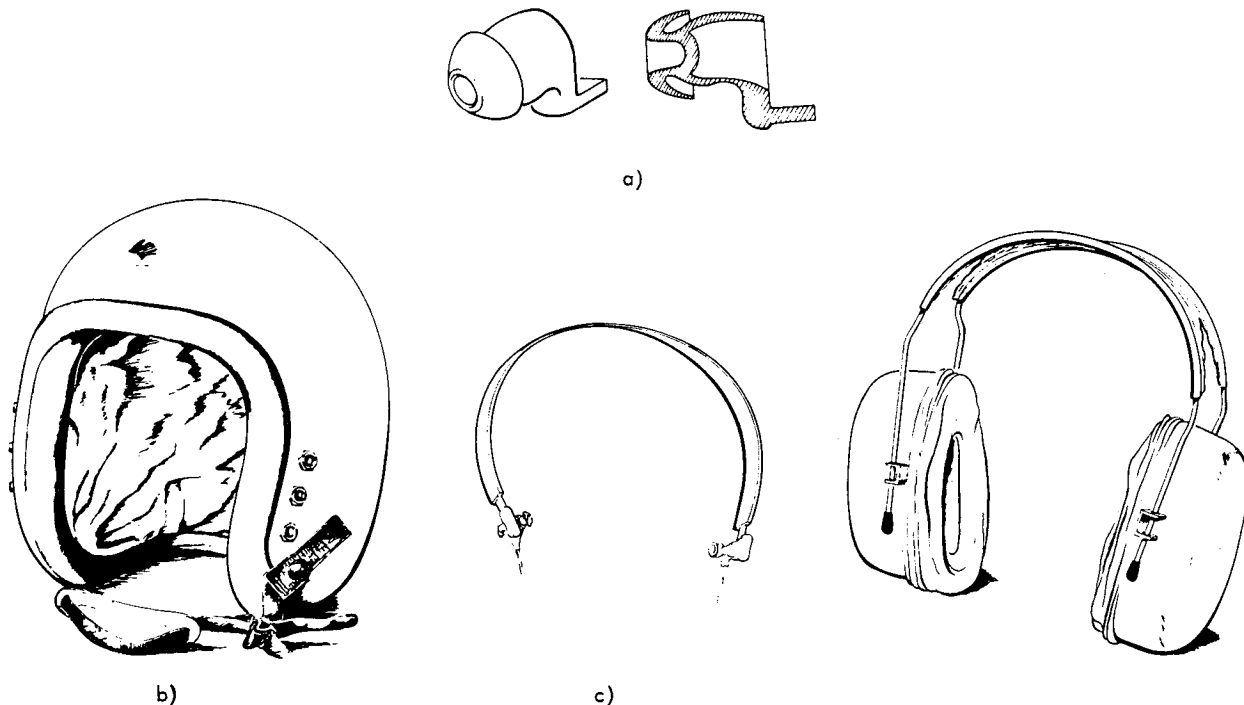


FIGURE 10.29 Types of Hearing Protectors. a) earplugs, b) helmet, c) semi-inserts, d) earmuffs

### 10.9.1 PROTECTION DEVICES

#### 10.9.1.1 Earplugs

Earplugs are made of a pliable material and are inserted directly into the ear canal. A simple physical model of the inserted plug, is shown in Figure 10.30.

An ideal earplug would be completely rigid, precluding all sound transmission. This ideal cannot be achieved in practice. There are three ways in which an earplug transmits sound to the eardrum. These are 1) by vibrating as a rigid

body, 2) directly, through air leaks, or 3) through longitudinal elastic vibrations of the plug material.

Of these, the third can practically be ignored since the impedance mismatch reduces excitation and transmission to a very low level, and the second can be minimized through good plug design. The first, however, is unavoidable since a completely solid plug will still be free to vibrate due to the compliance of the skin lining the ear canal. In fact, assuming a plug weight of 0.5 gm. which is typical, the best attenuation which can possibly be achieved at frequencies below 200 Hz. is less than 30 dB, although at



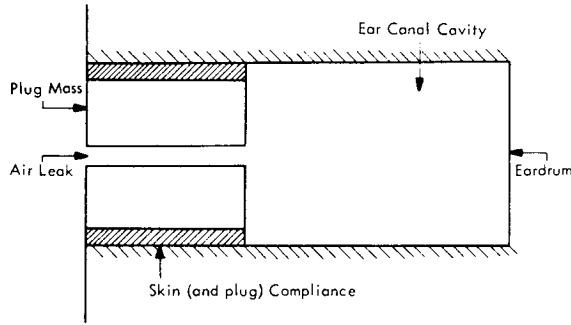


FIGURE 10.30 Simple Model of Ear Plug Inserted in the Ear Canal

high frequencies, the attenuation theoretically increases by 6 dB per octave. Further transmission reductions could be gained by using heavier plugs but comfort would be sacrificed and external support may be necessary. Unfortunately, practical plugs fall well short of this ideal limit, mainly due to the difficulty of achieving a good airtight seal. Figure 10.31 compares the noise attenuation of a practical earplug with the ideal. The measured data indicate that practical earplugs show approximately 12 dB less attenuation than the ideal plug at frequencies below 1000 Hz. At higher frequencies the deficiency increases sharply. This is because sound can reach the eardrum indirectly via routes other than the ear canal and even with the ears completely occluded, bone conducted sound reduces the maximum attenuation to approximately 30 dB at 1000 Hz.

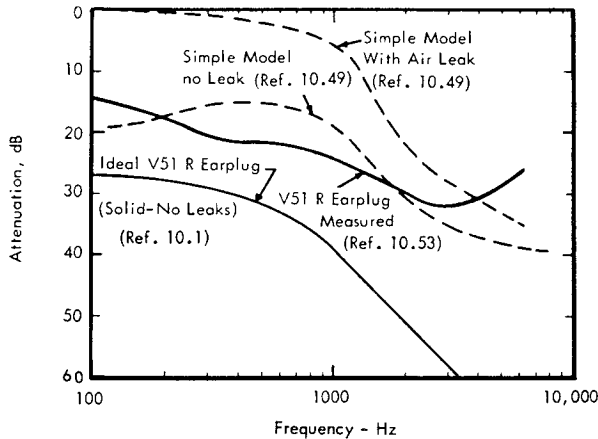


FIGURE 10.31 Earplug Transmission Loss

10.9.1.2 Semi-Inserts

Semi-inserts close the entrance to the ear canal without being inserted into it and must be supported by a headband. Their prime use is with earphone systems rather than ear protectors, and they usually carry small hearing-aid type earphones in their outer ends. Although they attenuate sound in much the same way as earplugs, they are generally not as efficient, mainly due to the problem of achieving a good seal to the ear canal. Substantial improvements are

undoubtedly possible, but plugs and muffs are much more popular and very little data on semi-inserts are available.

10.9.1.3 Earmuffs

Earmuffs cover the entire outer ear, being supported by a headband and cushioned against the side of the head. They are the most conveniently fitted of all ear protection devices and a satisfactory seal can be achieved on almost any head. At high frequencies, their sound attenuation characteristics are good but the large contact area can cause appreciable air leakage which reduces their performance at low frequencies. The attenuation at the ear is given by an equation of the form (Reference 10.49, Chapter 8).

$$\frac{p_i}{p_o} = \frac{S_o}{S_i} \left( \frac{Z_{bm}}{Z_m + Z_{bm}} \right)$$

where  $S_o$  is the effective outer area, approximately equal to the area encompassed by the outer cushion perimeter,  $S_i$  is the area enclosed by the inner cushion perimeter,  $Z_m$  is the parallel impedance of the earmuff mass and its compliant cushion and  $Z_{bm}$  is the impedance of the air cavity enclosed by the earmuff.  $p_i/p_o$  is the ratio of the sound pressures inside and outside the muff. Thus to maximize the protection,  $S_o/S_i$  and  $Z_{bm}$  must be as small as possible.

Many factors govern the choice of these various parameters and a compromise is necessary. A small value of  $S_o/S_i$  implies a small cushion area which is uncomfortable; typical values for this area ratio are approximately 2. The impedance of the muff,  $Z_m$ , is restricted by the need to limit the weight and maintain a pliable cushion necessary for a good fit against the head. Current designs attempt to increase the damping of this "spring-mass" impedance by filling the cushions with material of extremely high viscosity, such as oil, putty or wax. The impedance of the cavity,  $Z_{bm}$ , varies inversely as the air volume of the muff and directly as the square of the cross-sectional area leading to it ( $S_i$ ). These requirements lead to a deep earmuff, since  $S_i$  is governed by the dimensions of the outer ear.

10.9.1.4 Helmets

Helmets cover a large proportion of the head surface with either a rigid plastic shell or a non-rigid fabric material. The latter type is not effective, by itself, for good sound attenuation. However, if the ears are protected by some other means, such as earplugs, to the extent that bone conducted sound becomes significant, the fabric helmet can provide additional transmission loss. Rigid helmets, on the other hand, can provide good ear protection with enclosed earmuffs and also materially reduce the bone transmission through the skull.

10.9.2 COMPARISON OF EAR PROTECTION DEVICES

Available data on the amount of sound attenuation provided by the various types of hearing protection devices show a high degree of scatter. The effectiveness of any one model of any type varies from person to person and, on one person,

depends on the care taken to fit it. Also, different models of the same type of device vary considerably in their characteristics. Finally, the measurements of various investigators show large differences.

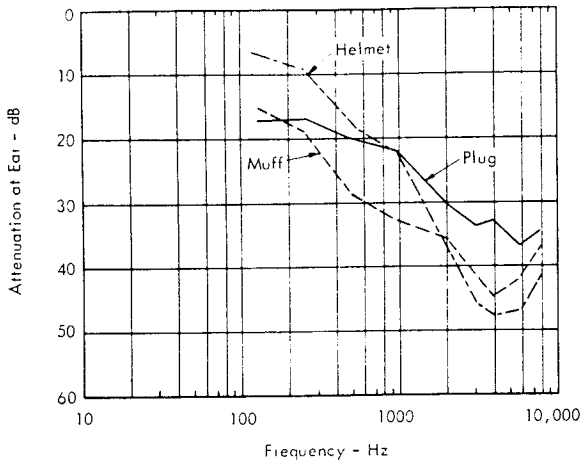


FIGURE 10.32 Comparison of the Attenuations Produced by Earplugs, Earmuffs and Helmets. (Data from Reference 10.52)

Figure 10.32 compares the mean sound attenuation curves for earplugs, earmuffs and helmets taken from Reference 10.52. The numerical data corresponding to these results are presented in Table 10.8. The distribution of the performance of the various models about the mean is illustrated as plus or minus one standard deviation in Figure 10.33. Although these results disagree to some extent with the data from other sources they do constitute a useful comparison of the three devices, since they should be self-consistent. Figure 10.32 shows that at frequencies below about 200 Hz, the earplug provides the best protection, whereas at high frequencies, above 1500 Hz, the helmet appears best. In the mid-frequency range the earmuff has clearly superior characteristics.

An interesting concept which this comparison suggests is that of using earplugs, earmuffs and a helmet in combination, to provide maximum protection throughout the frequency range. Figure 10.34 represents an analogous circuit of such a system showing the two major sound transmission paths, through the ear canal and through the bone structure, with the various impedance elements affecting each. It is seen that bone conducted sound can stimulate the hearing sense in two ways, either directly, or through excitation of the air volume between the earplug and the eardrum, and consequently, the eardrum. The diagram illustrates that, although the individual transmission loss of each device may be substantial, they are not additive when all three are used in combination. No experimental data is available for the sound attenuation of this combination but Figure 10.35 shows the effect of using earplugs in conjunction with earmuffs for one particular model of each. These curves, from Reference 10.53, show the mean results of measurements using five different subjects. The bands on either side of the mean attenuation line represent the experimental scatter expressed at  $\pm 1$  s.d. of the five tests. No data scatter figures were presented for the plug/muff combination.

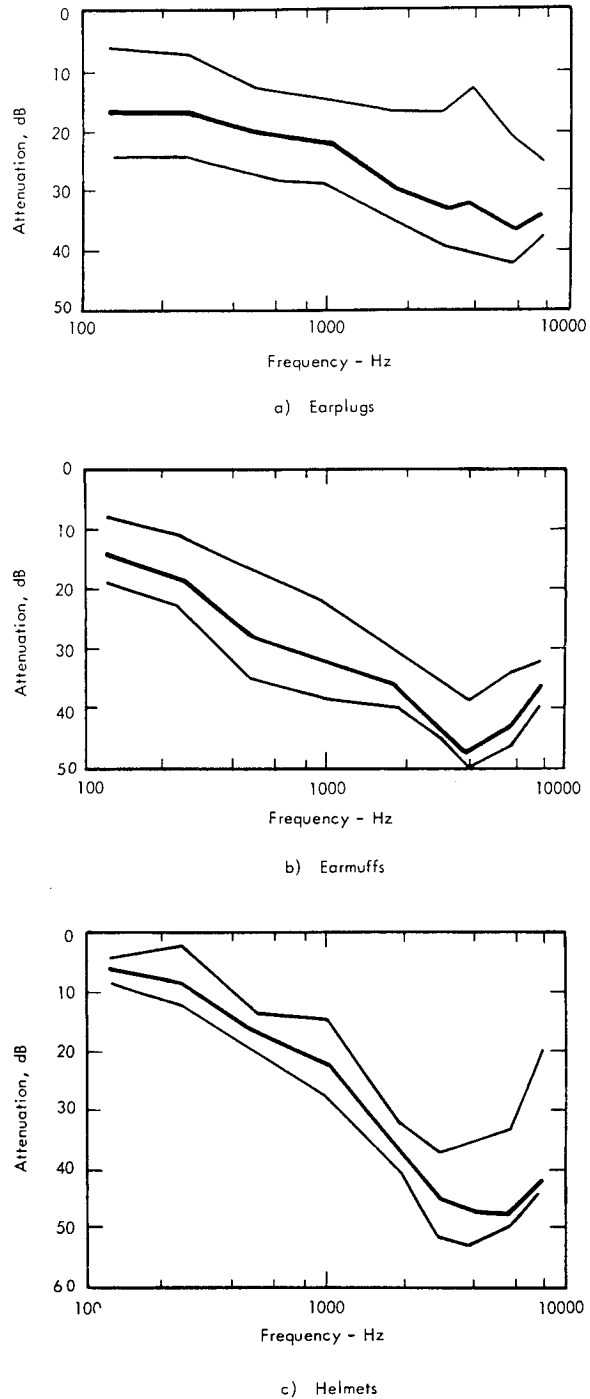


FIGURE 10.33 Attenuation Produced by Various Types of Ear Protectors. The Boundaries on Either Side of the Mean Lines Represent  $\pm 1$  S.D. of the Scatter of Results Found for a Number of Different Makes (data from Reference 10.52).

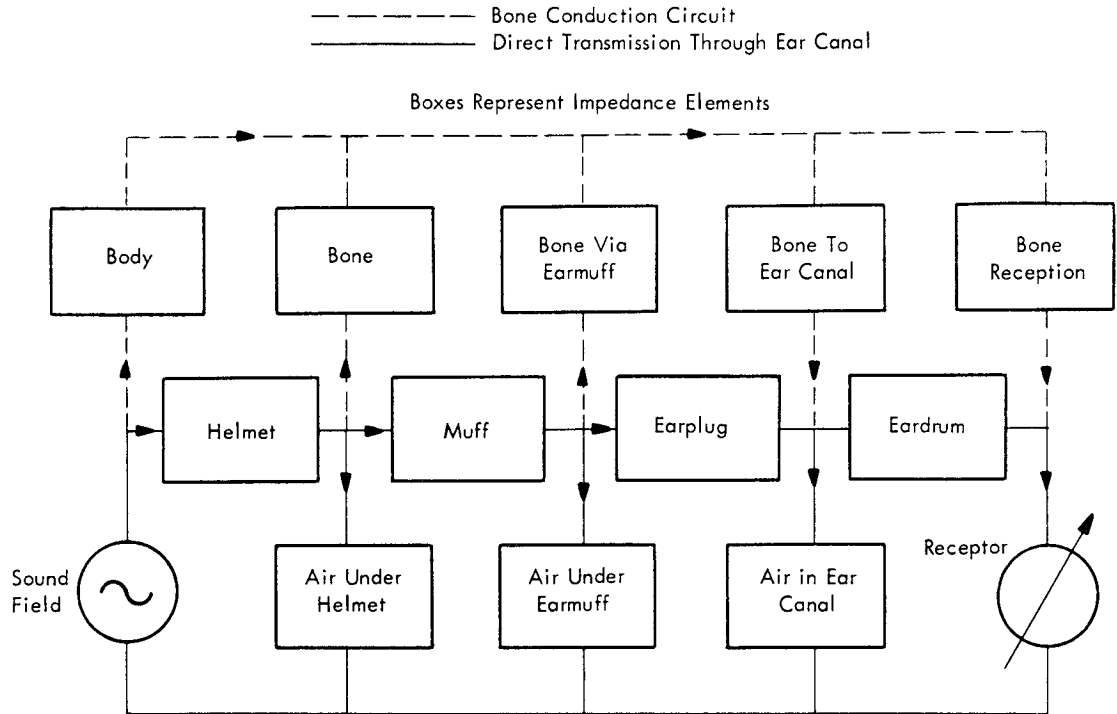


FIGURE 10.34 Conceptual Analog Circuit of Sound Transmission Paths for Simultaneous Use of Earplugs, Earmuffs, and Helmet

Also shown for comparison in Figure 10.35 is a curve showing the bone conduction threshold relative to the air conduction threshold, taken from von Gierke et al (Reference 10.1). The latter reports results of experiments conducted to measure the bone conduction threshold for sound transmitted through various parts of the body. It was concluded, as may be expected, that the maximum attenuation is limited by bone conduction from sound impinging upon the head. The curve shown in Figure 10.35 was calculated from data for bone conducted sound received by the forehead. Bone conduction explains to a large extent the result, apparent in this figure, that the additional presence of earplugs does not appreciably increase the transmission loss above that of ear muffs alone, at frequencies above about 500 Hz. In fact, for a range of frequencies around 1000 Hz, the converse is true, the earplugs actually decrease the attenuation. However, this phenomenon is associated with a coupled resonance of the air volumes in the ear canal and under the earmuff. The fact that earmuffs yield a transmission loss greater than the maximum predicted by bone conduction considerations, again at frequencies around 1000 Hz., is attributed to the shielding effect of the muffs. They cover an appreciable surface area at the side of the head where bone transmission effects may be expected to be most significant.

It is emphasized that the results presented in this section

are susceptible to practically the same degree of experimental variation as the subjective response data discussed in previous sections of this chapter. This is basically due to the variation of physical characteristics from subject to subject. With earplugs especially, the attenuation will depend very largely on the fit of the earplug to the ear canal. Superimposed on Figure 10.31 are two curves showing the effects of an air leak upon attenuation. These were obtained experimentally using a cylindrical tube 0.15 cm in diameter and 1 cm long (Reference 10.54). The leak in this case is rather higher than would be likely in practice but the example does serve to show how sensitive earplugs are to the degree of fit.

In reality, the highest attenuation of sound to the ear is achieved by pressing the thumbs against the entrance to the ear canal. The resulting attenuation closely approaches the maximum limit imposed by the bone-conduction threshold.

Unfortunately, no data are available for the efficiency of the various ear protectors at frequencies below 100 Hz. However, it may be expected that due to air leakage, the attenuation of each type will fall to zero at low frequencies as shown by the air leakage curve of Figure 10.31. On this basis, tentative extrapolations are indicated in Figure 10.35.

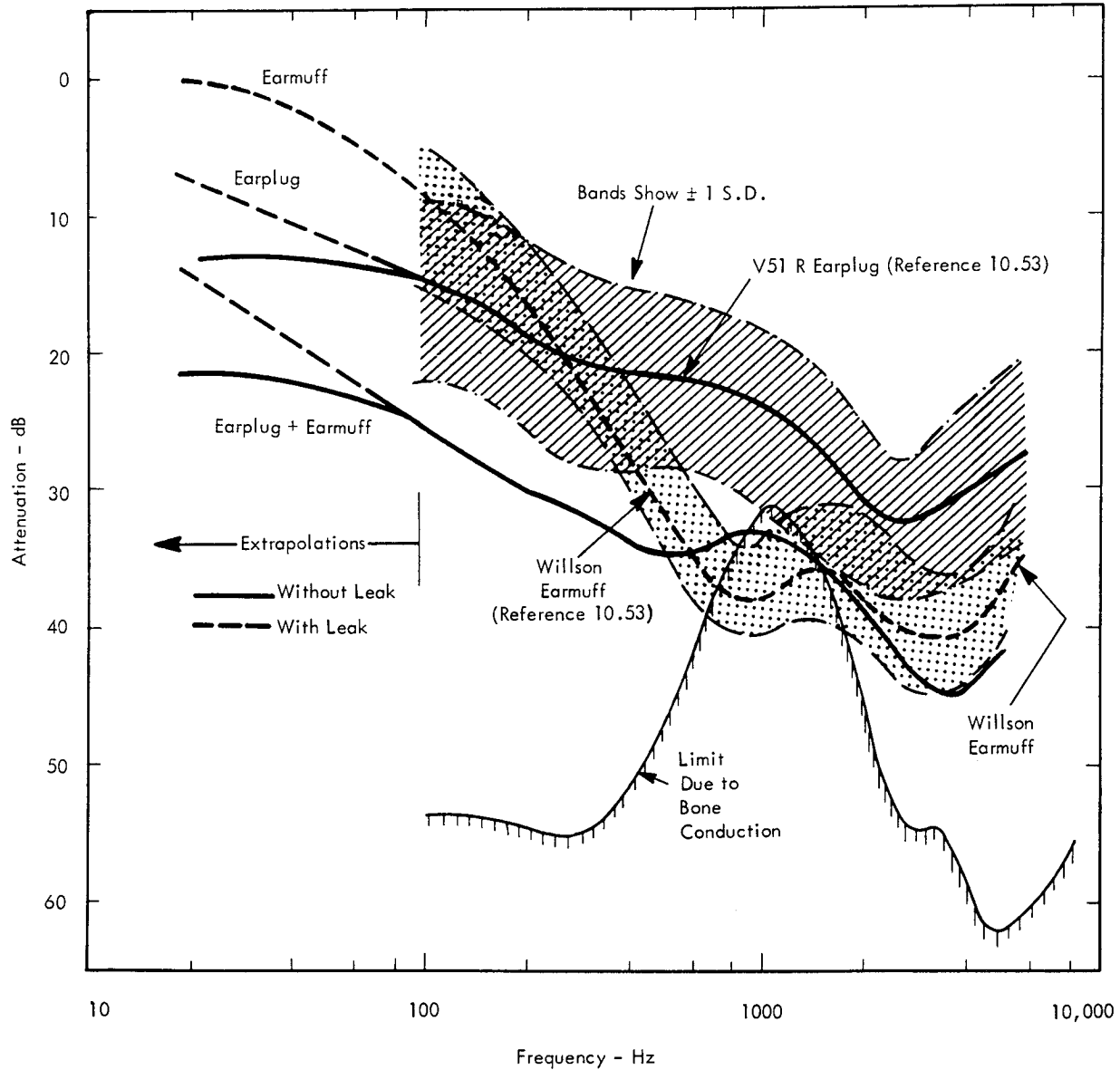


FIGURE 10.35 The Use of Earplugs and Earmuffs in Combination (Bone conduction curve obtained by calculation, using data on sound transmission through forehead. Plugs and Muff tested by method of threshold shift in 1/2 octave bands of noise).

### 10.9.3 SUMMARY OF EAR PROTECTION DEVICES

The data presented in this section indicate that:

- The best sound attenuation possible, using available ear protection devices, ranges from around 25 dB at 100 Hz to about 45 dB at 4,000 Hz. This can be achieved using earplugs and earmuffs in combination.
- Earmuffs alone give roughly the same protection at frequencies above 500 Hz where earplugs alone are less efficient by approximately 10 dB.
- It is essential that hearing protectors be adjusted or selected to fit well in order to minimize leakage effects.
- Additional attenuation can be gained by the use of large rigid helmets which can effectively reduce the conduction of sound by the skull. However, there would be large penalties of expense and comfort to achieve the gain in attenuation.
- At frequencies below 100 Hz., no measured data are available but, because of leakage, the best protection will be limited to 0 to 25 dB at these low frequencies.

TABLE 10.8  
SUMMARY OF EAR PROTECTOR ATTENUATION IN DB (FROM REFERENCE 10.52)

EAR PROTECTORS	FREQUENCY IN Hz								
	125	250	500	1000	2000	3000	4000	6000	8000
<u>Earplugs</u>									
V-51R	25	24	26	28	36	38	34	40	38
SMR	29	29	32	30	33	41	46	46	42
Flents	25	23	26	29	35	42	40	39	36
Selectone A	21	20	22	27	37	41	43	44	39
Selectone K	9	11	14	17	32	37	39	42	34
Relaxor	6	8	9	14	18	17	14	15	20
Lee Sonic Ear Valve	2	3	11	10	16	17	12	30	29
CM-1 (representative custom molded)	19	17	19	21	32	34	34	37	36
<u>Earmuffs</u>									
Clark 372-8A(a)	12	18	33	40	40	44	46	41	39
Clark 372-8A(b)	20	24	42	36	35	43	43	44	35
Clark 372-8A(c)	19	23	38	37	31	41	40	46	35
Clark X-372-4	12	20	30	38	40	41	47	43	38
Clark Experimental 31X	19	22	35	30	35	41	42	41	36
Clark Experimental 32X	18	21	28	31	35	45	42	41	38
Clark Experimental 33X	14	17	28	28	28	36	40	40	37
Clark 248	19	26	36	44	43	48	53	46	39
Clark 124	5	9	21	21	30	42	46	45	37
RH-2 Sta-Safe Soundmaster	3	4	6	13	25	30	34	39	32
MSA Earsaver	8	10	9	22	38	39	55	46	46
Willson Safe-T-Earmuff (early model)	19	20	30	37	41	38	40	38	34
Willson Safe-T-Earmuff (present model)	21	26	34	39	41	47	52	41	39
RCA Prototype Quiet Ear (initial)	14	15	25	39	34	35	44	36	31
RCA Prototype Quiet Ear (refined)	16	18	26	35	37	37	39	29	31
<u>Helmets</u>									
Bill Jack Flite Sound Helmet	8	9	22	25	37	50	50	50	44
Bill Jack Sound Absorb Helmet (comfortable fit)	4	12	17	26	36	48	52	48	44
Bill Jack Sound Absorb Helmet (tight fit)	9	14	18	30	43	55	57	49	44
High Alt. MB-5 Flying Helmet	4	12	15	22	39	42	52	53	55
Pilot Protective DH-5 Helmet	8	4	21	21	36	43	44	47	42
AF P-4 Helmet	5	1	10	9	28	32	30	33	20
<u>Ear Protector Combinations</u>									
Clark 372-8A(c) and V-51R	37	35	40	40	39	48	56	48	40
Clark 372-8A(a) and V-51R	29	33	38	38	45	52	55	49	44
MSA Noisefoe and V-51R	27	33	32	41	42	43	51	45	38
Willson Safe-T-Earmuff and V-51R	36	33	37	40	40	44	49	49	40
AF Ear Cushion MX-2088 and V-51R	24	29	37	40	43	41	48	49	43
Bill Jack Flite Sound Helmet and V-51R	29	35	44	45	49	53	58	53	45

#### 10.9.4 ACOUSTIC SHELTERS FOR PERSONNEL

For locations very near a launch or test site, the hearing protection that can be provided by the personal protection devices discussed so far in this section would be inadequate. In such regions, it is necessary, therefore, to provide additional attenuation of noise by having the personnel located inside shelters or buildings with adequate sound transmission loss. Such steps are even more important for protection from blast, which is discussed in the following section.

Additional requirements can also exist for acoustic protection of personnel. For example, operating positions near sources of high intensity noise, other than the rocket exhaust itself, may require such additional protection to be provided during various types of ground check-out testing operations.

Design of such acoustic shelters follows the concepts discussed in more detail in Chapter 9 under architectural acoustics. Whenever possible, such shelters are designed into the basic building in anticipation of high noise levels near operating personnel or at locations where communication interference is critical.

Prefabricated shelters can also be employed, when necessary, to provide required noise attenuation at temporary locations or in permanent locations which are not suitable for integrally designed acoustic treatment. A typical example of such a shelter is shown in Figure 10.36. These units can be readily assembled on-site using a custom or standard configuration which utilize modular construction concepts. A representative range of the noise reduction

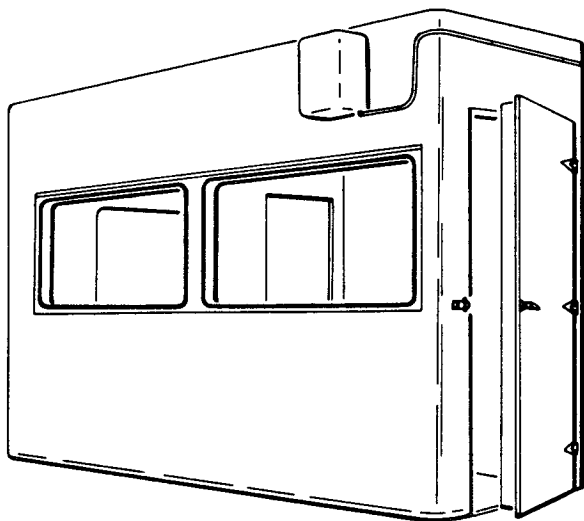


FIGURE 10.36 Typical Pre-Fabricated Acoustic Shelter for Personnel Protection

available for such units is shown in Figure 10.37. These units will be particularly effective near sources of high frequency noise such as turbines or high speed pumps but will not materially reduce overall sound levels generated by current and future high thrust rocket boosters due to the relatively low noise reduction achieved at low frequencies. Vibration isolation of such shelters, however, can assist in improving their performance in this range.

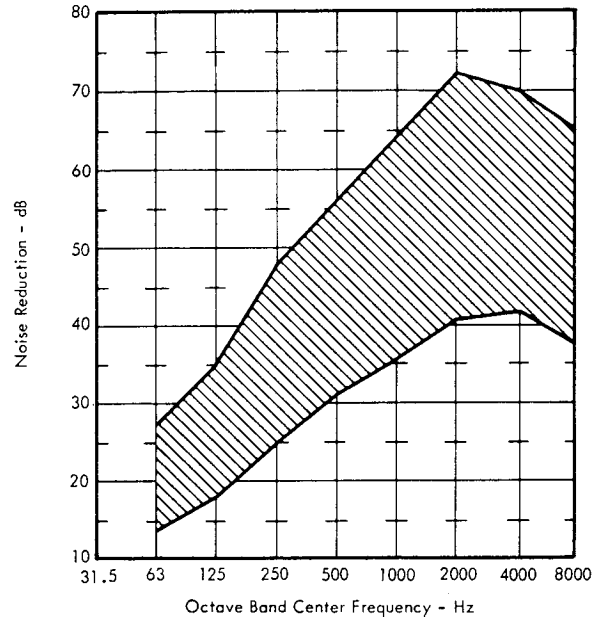


FIGURE 10.37 Typical Range of Noise Reduction Provided by Pre-Fabricated Sound Reduction Shelters

#### 10.10 BLAST PROTECTION FOR PERSONNEL

Methods for protecting personnel from blast hazards consist primarily of separating exposed personnel a sufficient distance from a firing pad or, protecting them inside blast-resistant buildings. No standard equipment is available which would allow exposed personnel to be protected from blast overpressures significantly greater than about 2 psi (Reference 10.45). If impact for exposed personnel due to bodily displacement or injury to missiles could be reduced or eliminated by special emergency procedures, the principle remaining hazard would be that associated with the blast overpressure.

##### 10.10.1 PROTECTION OF THE EARDRUM

Some protection can be provided against eardrum rupture due to blast overpressure by the use of hearing protection devices. This can be illustrated as follows. The average attenuation characteristics of hearing protection devices, illustrated in Figure 10.33 and 10.35 indicates that the attenuation, when extrapolated to low frequencies, may have either a finite value, such as for earplugs, or will decrease to zero, as for earmuffs, depending on leakage into the ear canal. The amount of attenuation of a blast

overpressure pulse provided by ear protectors may be estimated, theoretically, by a Fourier analysis technique. (Reference 10.55). The time history of the blast wave is transformed into a frequency spectrum which is then multiplied by the predicted frequency response (or attenuation) of the ear protector. This modified spectrum is then transformed back into a time history of the resulting response. Typical analytical results are illustrated in Figure 10.38 and 10.39. The first figure shows the Fourier spectrum of a classical blast wave with a duration of 0.1 seconds (typical for possible explosion of current boosters). Also shown is the attenuation versus frequency for a typical earmuff. The theoretical time histories of the attenuated and unattenuated blast pulses are shown in Figure 10.39. The attenuation for the ear protector is based on a simplified analog model of a typical earmuff or earplug with a small leak which reduces the attenuation loss to zero below 100 Hz.

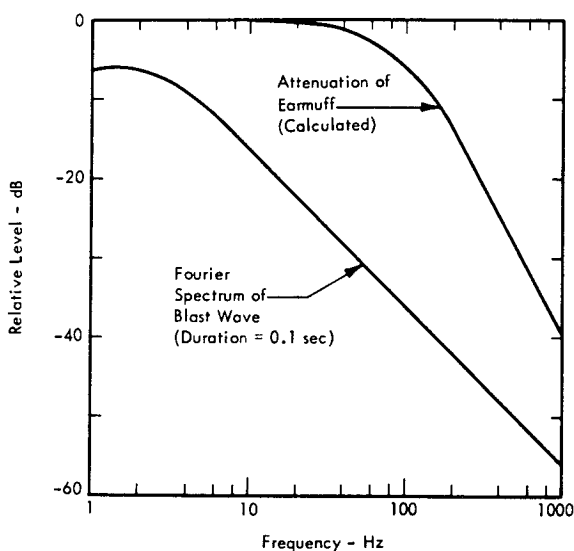


FIGURE 10.38 Relative Fourier Spectrum of Classical Blast Wave and Low Frequency Attenuation of Typical Ear Protection.

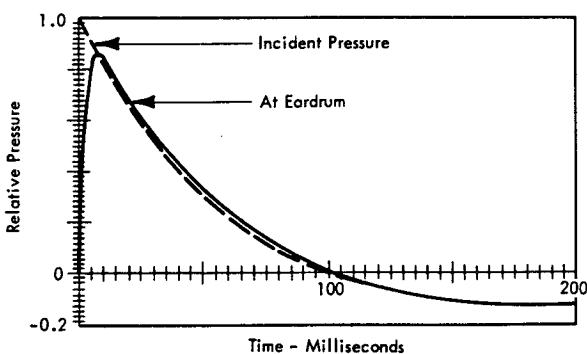


FIGURE 10.39 Calculated Time History of Incident and Attenuated Overpressure at Eardrum for Typical Earmuff with Low-Frequency Cutoff at 100 Hz Due to Leakage

The equivalent analog circuit of an earmuff, which exhibits this attenuation characteristic, is shown in Figure 10.40a. The circuit consists of a mass and resistance, representing the air leak, in series with the compliance of the air cavity between the ear protector and the eardrum.

For earplugs which can be fitted without an air leak, the equivalent circuit shown in Figure 10.40b, represents the impedance of the mass of the earplug in series with the compliance and resistance of the skin around the earplug, all in series with the compliance of the ear canal cavity. In this case, a constant attenuation at low frequencies is provided by the two compliance elements in series.

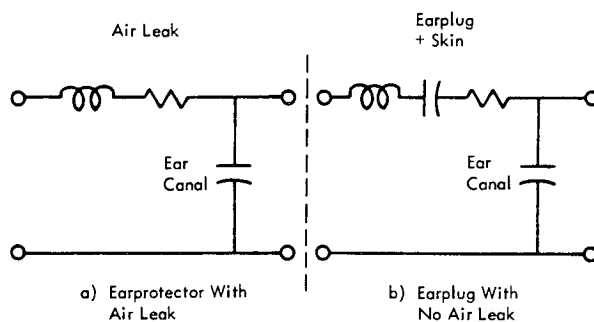


FIGURE 10.40 Simplified Equivalent Analog Circuit of Ear Protectors (Reference 10.49).

Considering typical field use of ear protection devices, the expected attenuation characteristics would tend to be closely represented by the model which accounts for the effect of an air leak. In this case, a significant reduction in blast pressure at the eardrum can be achieved for blast waves with durations less than about 0.1 seconds. For longer durations, the low frequency content of the blast wave is not appreciably reduced by typical ear protection devices.

Practical limits also exist on how much benefit can be realized by such ear protection, from the standpoint of avoiding eardrum rupture. For exposed personnel not subject to injury by missiles or glass fragments, lung injury due to the stresses imposed by the blast wave can appear at overpressures in excess of 4.4 psi, with reflection (Reference 10.31). Thus, for long duration blast waves from large rockets, protection provided for the eardrum would tend to be of limited practical significance. For shorter duration blasts, however, protection for the ears would be beneficial, not only to avoid eardrum rupture but to avoid discomfort, pain, or hearing damage.

### 10.10.2 PROTECTION AGAINST BLAST-GENERATED MISSILES

For exposed personnel, protection against missiles originating from the blast site can only be safely provided by

adequate separation distance. Figure 10.41 illustrates the approximate range of such missiles as a function of equivalent explosive weight. The estimated range is based on correlation of measured data as discussed in more detail in Chapter 8. The maximum blast overpressure, corresponding to the equivalent explosive weight and missile range, is also shown on this figure. These overpressures are appreciably less than the maximum values discussed earlier for primary effects of blast. This illustrates the fact that separation distances dictated by possible blast-generated missiles will ordinarily be much greater than distances dictated by injury from overpressure alone. Because of the wide range of possible sizes and trajectories of blast generated missiles, any such missile must be considered a source of potential injury to exposed personnel.

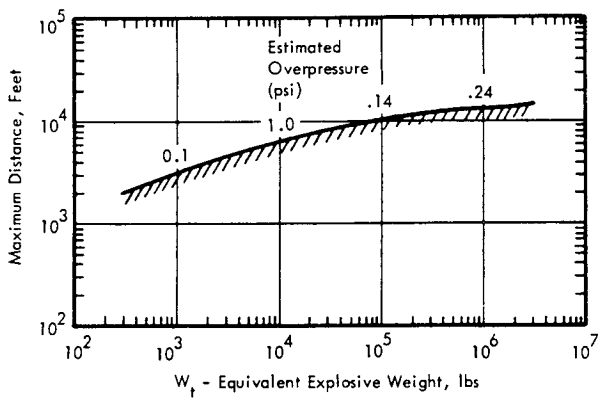


FIGURE 10.41 Equivalent Explosive Weight vs Maximum Fragment Distance. (From Ref. 10.60)

10.10.3 PROTECTION BY BLAST-PROOF BUILDINGS

When it is necessary to locate personnel closer to a rocket firing pad than would be allowed by missile or overpressure criteria, blast-designed protective housing must be employed. A detailed discussion of blast design procedures is given in Chapter 8. Since such buildings cannot always be completely sealed against intrusion of any incident overpressure wave, it is desirable to consider the damage criteria for exposure to any resulting internal transient pressure pulse. In this case, it is possible to utilize the analytical model discussed in Section 10.6.2, which relates effects of blast duration on blast injury, to predict possible injury by an internal pressure rise inside a building.

The overpressure environment inside a building will generally consist of a slowly rising pulse. A typical example of such a pulse, measured during nuclear weapons tests inside a small 5 ft. by 7 ft. concrete shelter, is shown in Figure 10.42 (Reference 10.56). A conservative analytical model of such a pulse can be described as a ramp-step change in pressure with a rise time  $T$  and a maximum value  $P_{max}$ . The response of the human lung to just such a pressure change has been analyzed by von Gierke using

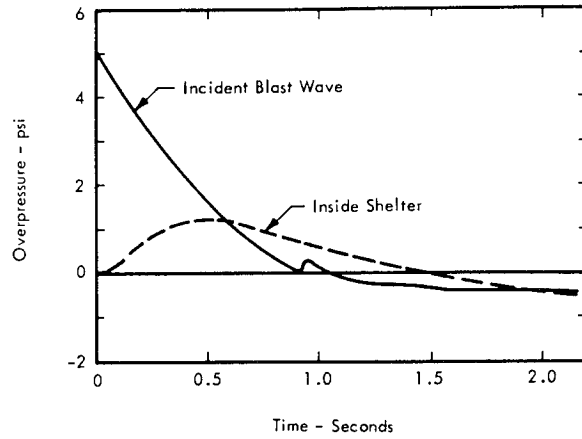


FIGURE 10.42 Typical Blast Overpressure Measured Inside 5 ft x 7 ft Shelter at 4700 ft from 29 KT Nuclear Test. (From Ref. 10.56)

the detailed dynamic model illustrated in Figure 10.24 based on a characteristic resonance frequency of the lung of 45 Hz. (Reference 10.34). These results have been utilized to define an approximate upper limit of overpressure as a function of rate of rise which would produce equal damage to the lung. For a fast rising pressure step, for which the dynamic response of the lung would be comparable to a long duration blast pulse, the maximum overpressure was set equal to 4.4 psi, the lower limit for threshold of injury to the lung (See Table 10.4). The results are shown in Figure 10.43 and clearly indicate the potential improvement in maximum allowable internal blast pressure inside a building providing the rate of change of pressure is less than 1000 psi/second. Note that the maximum rate of change of pressure inside a building will be essentially a characteristic of the building design and will be independent of the external environment.

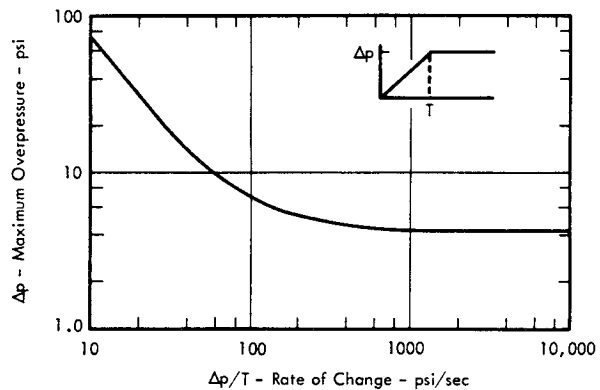


FIGURE 10.43 Calculated Maximum Overpressure vs Rate of Change for Ramp-Step Pressure Pulse Which Would Correspond to Threshold of Lung Injury by a 4.4 psi Fast-Rise Step. (Based on Dynamic Model of Lung in Ref. 10.34 and Blast Injury Criteria in Ref. 10.56)



However, the maximum value of the internal pressure will depend on both the external pressure transient and the characteristic pressure change rate for the structure. The latter can be effectively determined with the use of models in shock tube facilities. Given a requirement for definite venting to the atmosphere from inside a building a lower response rate to pressure changes can be achieved by incorporating bends or baffles in the venting passages. In fact, as shown in Reference 10.57, by simply incorporating constrictions in venting ducts, significant reductions in the transmitted blast pressure can be achieved. The use of rock-filled filters, followed by an expansion plenum, has also been evaluated as an effective means of blast attenuation through venting ducts (Reference 10.58).

## 10.11 SHOCK AND VIBRATION PROTECTION FOR PERSONNEL

In the close vicinity of rocket launch or test stands, personnel working inside structures exposed to severe ground vibration from blast, acoustic, or rocket exhaust environments, may require special shock and vibration protection. The design of such protective measures will be dependent on the specific loads anticipated and upon location. This section, which is restricted to a brief discussion of vibration isolation concepts, explains how material presented in other chapters of this manual may be used to design protection facilities in cases where the loading can be defined.

### 10.11.1 PROTECTION FROM GROUND VIBRATION

Ground vibrations are excited indirectly during rocket firings through the transmission of test stand vibrations which result from fluctuating thrust forces. They are also caused by the fluctuating pressures in the turbulent exhaust stream when it impinges on the blast deflectors on the ground. However, in both these cases, the vibrations are confined to a relatively small area near the stand, since propagating ground waves are very highly damped. However, high intensity acoustic waves propagating away from the exhaust, continue to excite ground motions at significantly greater distances.

As a rough guide, acoustically-excited ground vibration levels that are potentially hindering to performance of tasks (See Figure 10.26) may be expected at distances from the firing which are less than:

$$210 \left[ \text{Thrust-lbs}/10^6 \right]^{0.4} - \text{ft}$$

In the event that operational factors require personnel to be stationed within such distances from the rocket firing pad, vibration protection may be required in working areas. For any particular case, the amount of vibration required can be estimated by using the methods outlined in Chapter 9 to predict the ground vibration input to the building and then comparing this with the criteria specified in Figure 10.26. This protection can be provided, for ex-

ample, by vibration-isolated modular floors utilizing a common type of spring isolation system such as illustrated in Figure 11.11 of Chapter 11. The design resonant frequency of such an isolation system should decrease inversely with engine thrust, due to the increased low frequency content of the acoustic energy of the higher thrust rocket. Again, as a rough initial estimate, the resonant frequency of the loaded spring isolation system should satisfy the following criterion:

$$f_0 < 15 \left[ 10^6 / \text{Thrust} - \text{lbs} \right]^{0.4} - \text{Hz}$$

Note that for rocket thrusts much less than one million pounds, the above expression indicates that the resonant frequency (or low pass cut-off frequency) of the isolation system can be higher than 15 Hz. However, frequencies in this range coincide with the natural frequencies of typical building structures so that, except for the ground floor, inherent vibration isolation will tend to be provided by the normal vibration characteristics of the building itself. Thus protection for ground vibration induced by acoustic excitation will not generally be required except for areas very close to high thrust rockets.

### 10.11.2 PROTECTION FROM DIRECT ACOUSTICALLY INDUCED VIBRATION OF BUILDINGS

Structures located above ground very close to rocket firing sites will experience appreciable vibration due to direct acoustic excitation of external walls. Again, as for ground vibration, only occupied buildings located very close to a large rocket firing pad would require provisions for vibration protection of personnel. Protection methods would consist of the same type of vibration isolated floors discussed earlier. Building vibration levels, in this case, will generally equal or exceed those induced by ground motion, particularly on floor levels well above the ground. The relationships stated in the last section may be used, with the following corrections, to estimate the approximate radius and isolation frequency requirements, for protection of personnel, to reduce vibration below hinderance levels.

- 1) Increase radius of protection zone by 50 percent over that indicated in Section 10.11.1.
- 2) Decrease resonant frequency of isolation system by 50 percent from that indicated in Section 10.11.1.

A more exact analysis of protection requirements requires a detailed analysis of the building response to acoustic excitation following the methods of Section 8.1.

### 10.11.3 PROTECTION FROM GROUND SHOCK DUE TO EXPLOSIONS

Incorporated in the launch pad facility for the Saturn V vehicle is a "blast shelter" for pad personnel or flight crews. This is an example of shelters which can be provided at a rocket launch pad for personnel safety in the event of an anticipated vehicle explosion. A typical shelter, illustrated conceptually in Figure 10.44, must provide protection from very high blast pressures (of the order of 100 psi) as well as protection from the resulting severe ground shock. The protection against blast pressures

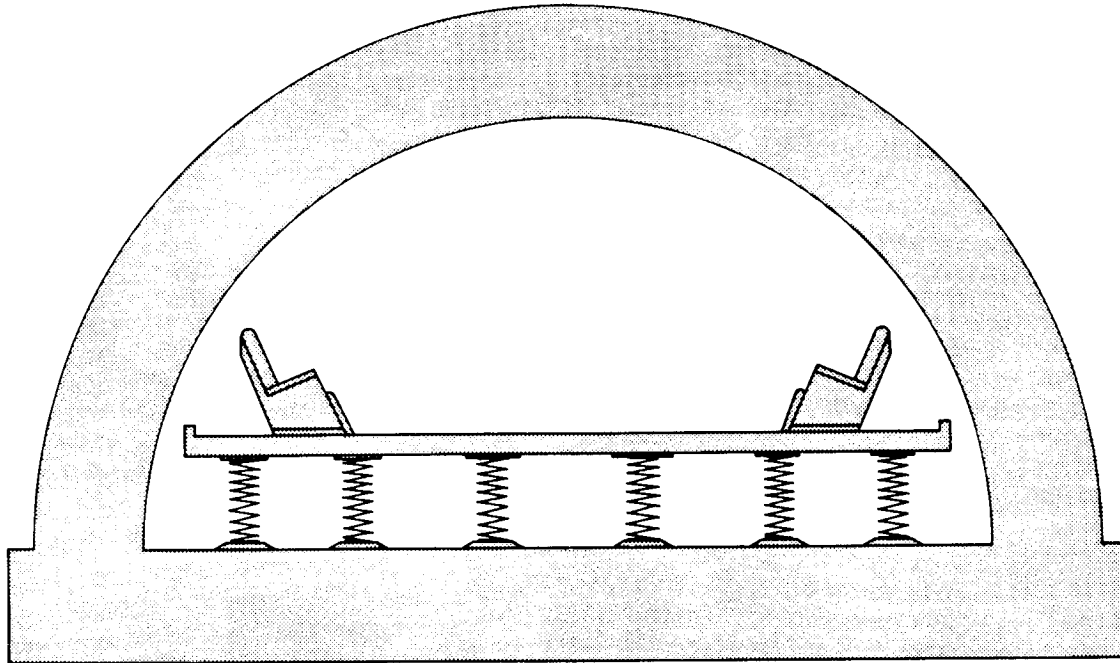


FIGURE 10.44 Typical Blast Proof Shelter for Personnel Near Rocket Launch Site

is efficiently and readily achieved through the use of blast resistant dome structures such as illustrated. Blast loads on such structures are discussed in detail in Section 8.2 of Chapter 8.

For protection against injury by the ground shock, it is necessary to provide some means of secure retention of the personnel in chairs which are, in turn, mounted on a shock-isolated floor. The severity of the ground shock environment that could occur, in a typical case, and the resulting protection criteria are illustrated in Figure 10.45. This shows the estimated ground shock spectrum at 315 ft from a propellant explosion with a TNT equivalent of  $10^6$  lb. (comparable to the TNT equivalent for a fully loaded Saturn V). The incident blast is estimated to have a peak pressure of 100 psi and an equivalent positive phase duration of 65 milliseconds. The ground motion has been estimated by the methods outlined in Chapter 9 using a typical seismic velocity of 1000 ft/sec and a soil elastic modulus of 25,000 psi.

Also shown in Figure 10.45 are criteria for human tolerance to a single vertical acceleration pulse (up or down) and criteria for tolerance to short time sinusoidal vibration. The actual ground motion will generally consist of a short burst of approximately sinusoidal oscillations which would, in turn, excite a number of damped oscillations of the isolated floor. Thus, a criterion for tolerance to ground shock would be expected to fall between the criterion for single acceleration pulses and the short-time vibration

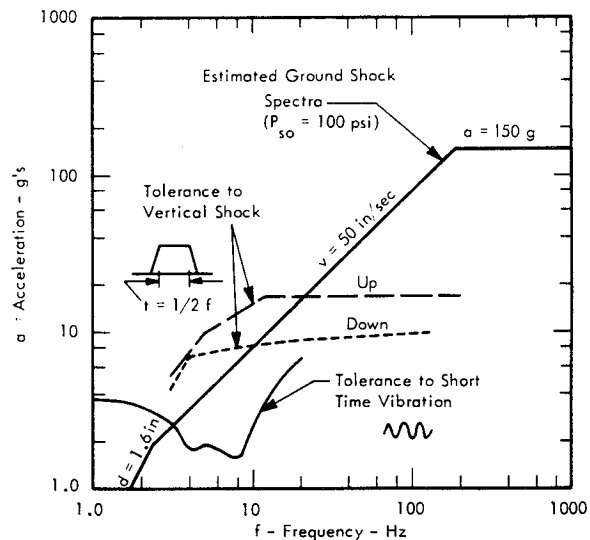


FIGURE 10.45 Comparison of Estimated Ground Shock Environment at 315 Ft From Explosion of Saturn V ( $W_T \approx 10^6$  TNT) With Criteria for Voluntary Tolerance to Shock or Vibration (Data From Reference 10.45 and 10.50)

criteria. With this in mind, and allowing for the displacement amplifications near resonance, it is estimated that for the case illustrated in Figure 10.43 a resonant frequency of 2 to 3 Hz would be required for the isolation system. This corresponds to a static deflection of the isolation system, under its own weight, of 1.1 to 2.5 inches.

The blast shelter illustrated in Figure 10.44 is designed to accommodate a number of personnel on one spring-mounted platform. In this case, the weight of the platform would be appreciably greater than the total weight of the personnel. Thus, any dynamic response of the human body will tend to have little effect on the shock response of the isolated floor. Another type of shock protection system could consist of an individually isolated chair for each person with a weight comparable to the body weight. In this case, the mechanical impedance (or dynamic mass) of the human should be considered in the design of the suspension system for each chair. As shown in Figure 10.46, the average mechanical input impedance measured for a seated man is roughly approximated by a simple mass-spring-damper system with a mass equal to the static mass of the body and a resonant frequency of about 5 Hz (Reference 10.59). The effect of this dynamic input impedance will be to reduce the effective shock input to the man at frequencies near the fundamental resonance of 5 Hz.

## REFERENCES

- 10.1 The Benox Report, Prepared Under Contract N6 ori-020 Task Order 44. ONR Project NR 144079. The University of Chicago. December 1953.
- 10.2 Von Békésy, G., "Über die Horschwelle und Fühlgreuge Rangsame Sinusformiger Luftdruckschwankungen," (The Threshold of Hearing and Feeling for Slow Sinusoidal Pressure Variations), *Ann. Physik*, Vol. 26, pp 554 - 566, 1936.
- 10.3 Mohr, G.C., et al., "Effects of Low-Frequency and Infrasonic Noise on Man." AMRL-TR-65-69. September 1965.
- 10.4 Kryter, K.D., "Hazardous Exposure to Intermittent and Steady State Noise," NAS-NRC Committee on Hearing, Bioacoustics and Biomechanics, Rept. of Working Group 46, January 1965.
- 10.5 McFarland, R.A., "Human Factors in Air Transport Design," McGraw-Hill Book Company Inc., New York, 1946.
- 10.6 Stevens, S.S., "The Measurement of Loudness," *J. Acoust. Soc. Am.*, Vol. 27, pp 815-829, 1955.
- 10.7 Fletcher, H. and Munson, W.A., "Loudness, its Definition, Measurement and Calculation." Part 1, - Audio 41:53+, No. 11, 1957. Part II, - Audio 41:40+, No. 12, 1957.
- 10.8 Stevens, S.S., "A Scale for the Measurement of a Psychological Magnitude: Loudness," *Psychol. Rev.*, Vol. 43, pp 405-416, 1936.
- 10.9 Churcher, B.G. and King, A.L., "The Performance of Noise Meters in Terms of the Primary Standard." *J. Inst. Elect. Engrs.* Vol. 81, pp 59 - 90, 1937.
- 10.10 Robinson, D.W. and Dadson, D.S., "A Redetermination of the Equal - Loudness Relations for Pure Tones," *Brit. J. Appl. Phys.*, Vol. 7, pp 166 - 181, May 1956.
- 10.11 Stevens, S.S., "The Calculations of the Loudness of Complex Noise," *J. Acoust. Soc. Am.*, Vol. 28, pp 807-832, September, 1956.
- 10.12 Robinson, D.W. and Whittle, L.S., "The Loudness of Octave Bands of Noise," *Acustica*, Vol. 14, Number 1, pp 24 - 35, 1964.
- 10.13 Cremer, L., et al., "Kurven Gleicher Lautstärke mit Oktav-gefiltertem Rauschen im Diffusen Schallfeld." (Equal Loudness Contours for Octave Band Noise in a Diffuse Sound Field). *Acustica* Vol. 9, pp 65-75, 1959.
- 10.14 Zwicker, E., "Über Psychologische und Methodische Grundlagen der Lautheit," (Psychological and Methodical Foundations of Loudness), *Acustica* Vol. 3, pp 237 - 258, 1958.
- 10.15 Zwicker, E., "Ein Graphisches Verfahren zur Bestimmung der Lautstärke und der Lautheit aus dem Terzpegeldiagramm." (Graphic Evaluation of Loudness from One-Third Octave Band Sound Pressure Level Curves). *Frequenz*, Vol. 13, pp 234 - 238, 1959.
- 10.16 Kryter, K.D. and Pearsons, K.S., "Some Effects of Spectral Content and Duration on Perceived Noise Level," *J. Acoust. Soc. Am.*, Vol. 35, pp 866-833, June, 1963.
- 10.17 Kryter, K. D. "Scaling Human Reactions to the Sound from Aircraft," *J. Acoust. Soc. Am.*, Vol. 31, pp 1415 - 1429, November 1959.

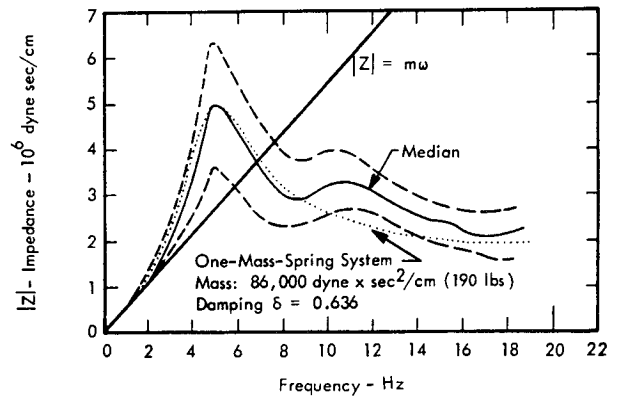


FIGURE 10.46 The Median and the Twentieth and Eightieth Percentile of the Modulus of Impedance of 8 Different Subjects Sitting Erect, Compared with the Impedance of a Pure Mass and a One-Mass-Spring System with Damping.

- 10.18 Garner, W.R., "The Loudness and Loudness Matching of Short Tones," *J. Acoust. Soc. Am.*, Vol. 21, pp 398-403, 1949.
- 10.19 Pearsons, K.S., "The Effects of Duration and Background Noise Level on Perceived Noisiness," FAA-ADS-78, April 1966.
- 10.20 American Standards Association, "The Relations of Hearing Loss to Noise Exposure," ASA, Z24 - X - 2.
- 10.21 Beranek, L.L., "Acoustics." McGraw-Hill Book Company, Inc., New York, 1954.
- 10.22 Kryter, K.D., "Methods for Calculation and Use of the Articulation Index", *J. Acoust. Soc. Am.*, Vol. 34, pp 1689-1697, November, 1962.
- 10.23 Nixon, C.W., et al., "Rail Test to Evaluate Equilibrium in Low Level Wideband Noise," AMRL-TR-66-85, July 1966.
- 10.24 Stevens, K.N., Rosenblith, W.A. and Bolt, R.H., "A Community's Reaction of Noise: Can it be Forecast?", *Noise Control*, pp 63-71, January 1955.
- 10.25 Stevens, K.N. and Pietrasanta, A. C., et al., "Procedures for Estimating Noise Exposure and Resulting Community Reaction from Air Base Operations," WADC Tech. Note 57-10, April 1957.
- 10.26 Clark, W., "Reaction to Aircraft Noise," ASD Tech. Report, 61 - 610, November 1961.
- 10.27 Bolt, Beranek and Newman Inc., Technical Report, "Land Use Planning Related to Aircraft Noise," October 1964.
- 10.28 Green, T.H., "Discussion of the Utility of Available Techniques for Measuring Aircraft Noise and Predicting Community Response," FAA Report, Number RD-66-31, May 1966.
- 10.29 Stevens, S.S., "Procedure for Calculating Loudness: Mark VI," *J. Acoust. Soc. Am.*, Vol. 33, pp 1577-1585, November, 1961.
- 10.30 Woodhead, M., "Searching a Visual Display in Intermittent Noise," *J. Sound Vib.* Vol. 1, pp 157 - 161, 1964.
- 10.31 White, C.S., "Tentative Biological Criteria for Assessing Potential Hazards from Nuclear Explosions," Lovelace Foundation, DASA Report - 1462, December 1963.
- 10.32 White, C.S. and Richmond, D.R., "Blast Biology" Lovelace Foundation, TID-5764, September 1959.
- 10.33 Richmond, D.R. and White, C.S., "A Tentative Estimation of Man's Tolerance to Overpressures from Air Blast," Lovelace Foundation, DASA - 1335, November 1962.
- 10.34 Von Gierke, H.E., "Biodynamic Response of the Human Body," *Appl. Mech. Rev.* Vol. 17, Number 12, pp 951-958, December 1964.
- 10.35 Goldizen, V.C. et al., "Missile Studies with a Biological Target," Operation Plumbob, Lovelace Foundation, WT-1470, January 1961.
- 10.36 White, C.S., et al., "A Comparative Analysis of Some of the Immediate Environmental Effects at Hiroshima and Nagasaki," Lovelace Foundation. Printed in *Health Physics*, Vol. 10, 1964.
- 10.37 Bowen, I.G., et al., "A Model Designed to Predict the Motion of Objects Translated by Classical Blast Waves," USAEC Civil Test Operations Report, CEX-58.9, 1961.
- 10.38 Swearingen, J. J. and McFadden, E. B., "Studies on Air Loads on Men," FAA, Civil Aeromedical Research Institute, Oklahoma City, AD 602207.
- 10.39 Von Gierke, H.E., "Effects of Sonic Boom on People: Review and Outlook," *J. Acoust. Soc. Am.*, Vol. 39, Number 5, pp 543-550, May, 1966.
- 10.40 Pearsons, K. and Kryter, K.D., "Laboratory Tests of Subjective Reactions for Sonic Boom," NASA Contractor Report, CR-187, 1964.
- 10.41 Ellis, R.M., "A Subjective Reaction to Simulated N-Waves," M. Sc. Thesis, University of Southampton, England, 1964.
- 10.42 Zepler, E.E. and Harel, J.R., "The Loudness of Sonic Booms and Other Impulsive Sounds," *J. Sound Vib.* Vol. 2, Number 3, pp 249-256, 1965.
- 10.43 Kryter, K.D., et al., "Definition of the Effects of Booms from the SST on Structures, People and Animals," Stanford Research Institute Report for the National Sonic Boom Evaluation Office, Department of the Air Force, Under Contract AF 49(638) - 1696, June 1966.
- 10.44 Guignard, J.C., "Effects of Vibration on Man," *Jour. Environmental Sci.* pp. 29-32, August 1966.
- 10.45 Goldman, D.E. and von Gierke, H.E., "Shock and Vibration Handbook," eds. Harris, C.M. and Crede, C.E., Vol. 3, Chapter 44, McGraw-Hill, New York, 1961.
- 10.46 Weisz, A.Z., et al., "Human Performance Under Random and Sinusoidal Vibration," AMRL-TR-65-209, December 1965.

- 10.47 Buckmann, E., "Criteria for Human Reaction to Environmental Vibration on Naval Ships," David Taylor Model Basin Report 1635, June 1962.
- 10.48 Stevens, S.S., (ed) Handbook of Experimental Psychology, Chapter 7, John Wiley and Sons, 1962.
- 10.49 Harris, C.H., (ed) Handbook of Noise Control, McGraw-Hill Book Company, 1957.
- 10.50 Goldman, D. E., et al., "The Biological Effects of Vibration," Report of Working Group 39 of the Armed Forces-National Research Council Committee on Hearing and Bio-Acoustics. Office of Naval Research Contract Number NONR 2300 (05), 1961.
- 10.51 Wyle Laboratories. Unpublished Test Data.
- 10.52 Nixon, C. W., et al., "Performance of Several Ear Protectors," WADC Technical Report 58-208, May 1958.
- 10.53 Webster, J. C., and Rubin, E. R., "Noise Attenuation of Ear Protective Devices," Sound, Volume 1, Number 5, pp 34-46, October 1962.
- 10.54 Zwislocki, J., "Acoustic Filters as Ear Defenders", J. Acoust. Soc. Am., Vol. 23, pp 36, 1951.
- 10.55 Crocker, M.J. and Sutherland, L.C., "The Effects Upon Shock Measurements of Limited Frequency Response Instrumentation", Wyle Laboratories Research Staff Report WR 65-1, January, 1965.
- 10.56 Richmond, D.R., White, C.S., "Biological Effects of Blast and Shock", Lovelace Foundation, DASA Report-1777, April, 1966.
- 10.57 Swatosh, J.J. and Birukoff, R., "Blast Effects on Tunnel Configurations", SWC TR-59-48, Air Force Special Weapons Center, Kirtland AFB, New Mexico, October, 1959.
- 10.58 Crist, R.A., "The Use of Rock Filters to Attenuate Air Shocks", Air Force Special Weapons Center, AFSWC-TDR-63-27, March, 1963.
- 10.59 Coermann, R.R., "The Mechanical Impedance of the Human Body in Sitting and Standing Position at Low Frequencies", ASD Tech. Report, 61-492, September, 1961.
- 10.60 Anderson, T.O. et al., "Blast, Fragmentation and Damage", Preliminary Report, Naval Ordnance Laboratory, November, 1966.
- 10.61 Holladay, A., and Bowen, I. G., "A Mathematical Model of the Lung for Studies of Mechanical Stress," Proceedings of the San Diego Symposium for Biomedical Engineering, 1963.

**CHAPTER 11**  
**VIBRO-ACOUSTIC CONTROL**  
**FOR EQUIPMENT**

## TABLE OF CONTENTS

SECTION	PAGE
11.1	INTRODUCTION . . . . . 11-1
11.2	<u>LOCATION OF SENSITIVE GROUND SUPPORT EQUIPMENT</u> . . . . . 11-2
11.2.1	ENVIRONMENTAL ZONES . . . . . 11-2
11.3	<u>TYPES OF GROUND SUPPORT EQUIPMENT</u> . . . . . 11-3
11.4	<u>RELIABILITY OF GROUND SUPPORT EQUIPMENT</u> . . . . . 11-4
11.4.1	SERIES SYSTEM . . . . . 11-4
11.4.2	PARALLEL OR REDUNDANT SYSTEM . . . . . 11-4
11.4.3	SERIES - PARALLEL SYSTEM . . . . . 11-5
11.4.4	ANALYSIS OF SYSTEM RELIABILITY AND ENVIRONMENTAL PROTECTION . . . . . 11-5
11.5	<u>RESPONSE OF EQUIPMENT TO ACOUSTIC ENVIRONMENTS</u> . . . . . 11-5
11.5.1	GENERAL DISCUSSION . . . . . 11-5
11.5.2	SUMMARY OF ACOUSTIC TESTS AND FAILURE DATA . . . . . 11-5
11.5.2.1	Estimated Reliability of Exposed Ground Support Equipment . . . . . 11-10
11.5.3	ACOUSTIC EXCITATION OF EQUIPMENT MOUNTING STRUCTURE . . . . . 11-11
11.5.3.1	Analytical Method . . . . . 11-11
11.5.3.2	Experimental Data on Acoustic Mobility of Cabinet Mounted Equipment . . . . . 11-12
11.5.4	ACOUSTIC SENSITIVITY OF SPECIFIC EQUIPMENT COMPONENTS . . . . . 11-18
11.5.5	SOURCES FOR ADDITIONAL INFORMATION ON ACOUSTIC SENSITIVITY . . . . . 11-20
11.5.5.1	Interservice Data Exchange Program . . . . . 11-20
11.5.5.2	Manufacturer Specifications and Environmental Design and Test Specifications . . . . . 11-21
11.5.5.3	Evaluation of Acoustic Sensitivity from Vibration Environment Specifications . . . . . 11-21
11.6	<u>RECOMMENDED ACOUSTIC ENVIRONMENT CRITERIA FOR EQUIPMENT</u> . . . . . 11-22
11.6.1	CRITERIA FOR RELIABILITY ANALYSIS . . . . . 11-22
11.6.2	CRITERIA FOR ACOUSTIC DESIGN ENVIRONMENT . . . . . 11-22
11.7	<u>RESPONSE OF EQUIPMENT TO OVERPRESSURE FROM BLAST AND SONIC BOOM</u> . . . . . 11-24
11.7.1	INTRODUCTION . . . . . 11-24
11.7.2	OVERPRESSURE LOADS ON EQUIPMENT MOUNTING STRUCTURE . . . . . 11-24
11.7.2.1	Force of Blast Overpressure and Dynamic Pressure on Exposed Equipment . . . . . 11-24
11.7.3	TRANSIENT OVERPRESSURE EFFECTS ON EQUIPMENT . . . . . 11-26
11.7.4	ACCELERATION LOADS ON EQUIPMENT DUE TO BLAST RESPONSE OF MOUNTING STRUCTURE . . . . . 11-26
11.7.5	ENVIRONMENTAL EFFECTS ON EQUIPMENT DUE TO SONIC BOOMS . . . . . 11-28
11.7.5.1	Direct Effects . . . . . 11-28
11.7.5.2	Indirect Effects . . . . . 11-28
11.8	<u>DESIGN METHODS FOR ENVIRONMENTAL PROTECTION OF EQUIPMENT</u> . . . . . 11-29
11.8.1	SELECTION OF COMPONENTS . . . . . 11-29
11.8.2	PROTECTIVE PACKAGING DESIGN . . . . . 11-30
11.8.2.1	Damping Treatment of Component Mounting Structure . . . . . 11-31
11.8.2.2	Protective Potting of Components . . . . . 11-38
11.8.2.3	Acoustic Isolation of Equipment . . . . . 11-41
11.8.2.4	Vibration Isolation of Equipment . . . . . 11-48
	REFERENCES . . . . . 11-51

## CHAPTER 11

### VIBRO-ACOUSTIC CONTROL FOR EQUIPMENT

#### 11.1 INTRODUCTION

The most complex and, frequently, most costly part of a launch pad facility or engine test stand is the ground support equipment. This consists of the broad spectrum of electronic, electromechanical, hydraulic, and pneumatic equipment used to measure, control, and record all of the checkout and test functions of the facility. The success of the firing or launch may very well depend on proper operation of this equipment. Thus, test facility structure has a major function to provide the protective housing necessary to keep the internal vibration and acoustic environment below failure levels for critical ground support systems.

To define the vibro-acoustic design requirements for equipment, it is necessary to consider the following questions:

- Where is the equipment located and what is its normal unprotected environment?
- What type of equipment is involved?
- What role does it play in the testing sequence?
- What is an acceptable failure risk?
- What is the probable equipment failure or response level in the normal acoustic environment?
- What additional protection or equipment hardening is required?
- How is this protection or hardening provided?

Each of these questions will be considered in the rest of this chapter.

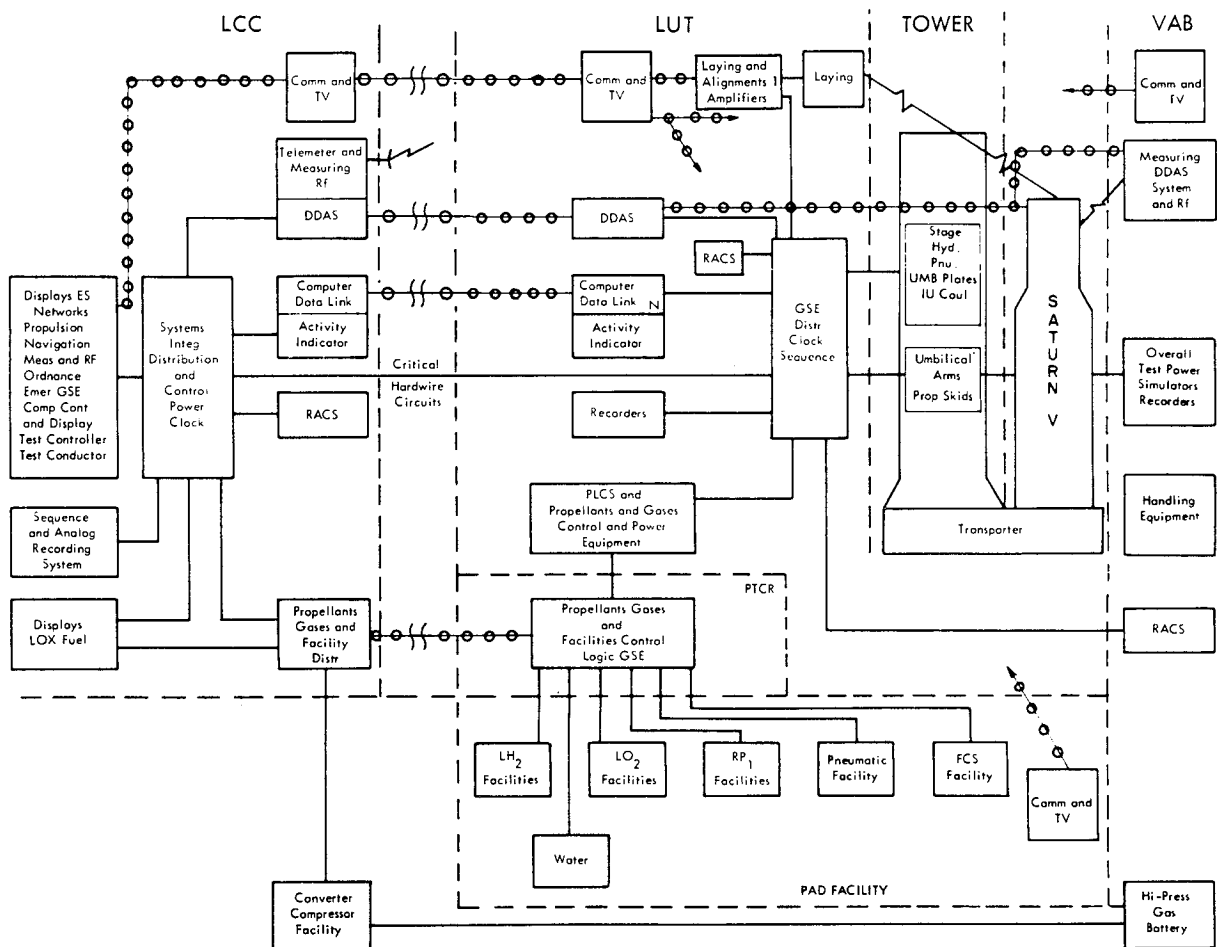


FIGURE 11.1 General Location of Ground Support Equipment for SATURN V Launch Facility (Reference 11.1)



## 11.2 LOCATION OF SENSITIVE GROUND SUPPORT EQUIPMENT

A representative distribution of ground support equipment (GSE) for a major launch facility is shown in Figure 11.1. This illustrates the general arrangement of the GSE for the Saturn V launch facility. The significant point in this layout is the amount of sensitive equipment which is located at the launch site inside the launch/umbilical tower. In contrast to this type of arrangement, engine test facilities will generally have a minimum of sensitive equipment located immediately adjacent to the test stand to minimize requirements for protective housing. A trade-off is clearly indicated between the cost of the protective housing for equipment versus the cost of remote operations with the equipment. Both quantities depend on the distance from the engine test stand so that an optimum distance could be chosen as indicated conceptually in Figure 11.2.

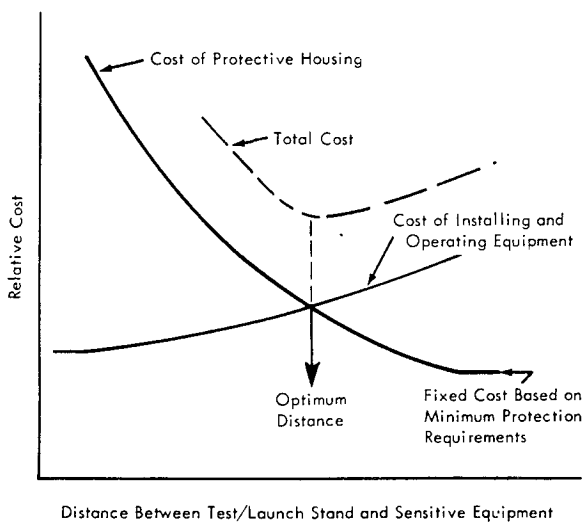


FIGURE 11.2 Optimizing Equipment Location At Test/Launch Site

The purpose of this chapter is to provide necessary information on environmental effects on equipment to assist a facility designer in conducting such a cost study. There are, of course, many other systems operation factors that would be involved in this trade-off study.

### 11.2.1 ENVIRONMENTAL ZONES

To provide a scale for measuring the severity of acoustic environment problems with ground equipment, it will be convenient to establish the following zones.

**ZONE 1** - Areas exposed to the high temperature and/or high velocity flow induced by the engine exhaust. This zone extends

out to a radius of about 10 nozzle diameters for an undeflected rocket flow. Sound levels will be of the order of 165 dB in this zone so that only very rugged equipment can be located in this region.

**ZONE 2** - Areas protected from exhaust flow but exposed to overall sound levels of 150 dB to 165 dB. Such an area would extend out to approximately 75 nozzle diameters from the jet axis for an undeflected rocket flow. Within this zone, special construction techniques will be necessary to house sensitive equipment.

**ZONE 3** - Areas exposed to overall sound levels from 130 dB to 150 dB. Such an area would extend from about 75 to 750 nozzle diameters for an undeflected rocket exhaust. Protection of sensitive equipment within this zone could be provided by more conventional industrial construction.

**ZONE 4** - Areas exposed to overall sound levels below 130 dB will extend from about 750 nozzle diameters from the rocket and beyond. Little or no protection for equipment will be necessary in this zone.

These approximate zones are based on acoustic environment levels for a typical advanced vehicle launch facility. For a better definition of the limits of the zone for the on-pad condition at a launch site or for a static test site, see Chapter 6.

Associated with the acoustic environments for each of these zones would be a potential blast hazard environment. Although the blast overpressure at the boundaries of these zones can not be predicted as easily as the acoustic pressures, it is possible to define approximate values for preliminary design purposes. The estimates are based on the criteria for TNT blast equivalents of 10 percent for LOX/RP-1 propellants and 60 percent for LOX/LH<sub>2</sub> propellants as discussed in Chapter 6. Applying these criteria to typical large boosters in the Saturn and Post Saturn class, the following approximate values of potential blast pressure and nominal acoustic pressures at the boundaries of the above zones can be defined in Table 11.1A.

Note that for a multi-engine booster, one nozzle diameter is the diameter of an equivalent single nozzle with the same thrust as the cluster, that is, it is equal to the exit diameter per nozzle times  $\sqrt{\text{Number of Engines}}$ . As shown in the last column, the possible blast pressure exceeds the rms sound pressure by one to two orders of magnitude. Even though the dynamic magnification factor for structural response to continuous acoustic noise will be higher than the dynamic response to a transient blast pulse, the design load for nonexpendable types of structure near a launch site will ordinarily be based on blast loads rather than

acoustic loads. Thus, the basic structural design features required for blast protection of ground equipment must be incorporated first before considering any acoustic protection. It must be emphasized, however, that the blast overpressures presented in Table 11.1A are applicable only for a launch site or flight configuration engine test stand. Other types of test stands, such as engine development test stands, may have a much lower blast hazard so that acoustic protection requirements may be controlling factors for structural design of equipment rooms.

### 11.3 TYPES OF GROUND SUPPORT EQUIPMENT

Ground support equipment may be identified, according to its functional characteristics, as follows:

Electronic or Electrical  
Hydraulic  
Pneumatic  
Mechanical

The major problems associated with acoustic and vibration effects will involve the first three categories and the emphasis in this chapter will be placed accordingly.

However, since all types of equipment may appear in any of the basic zones outlined above, a more useful breakdown can be made by dividing all equipment into two general groups according to the consequences of failure occurring during a test. These groups are:

- A. Equipment which must be operational before and during the firing sequence of a rocket engine for launch or static tests. This type of equipment requires the highest degree of environmental protection or rugged design since the equipment must not malfunction during a test. Four subdivisions within this group can be defined in descending order of criticality according to the type of failure involved.

- A-1 Equipment failure which would cause a catastrophic failure of the engine or launch vehicle.  
-2 Equipment failure which would cause an immediate shutdown of an engine test sequence or delay initiation of a vehicle launch.  
-3 Equipment failure which would result in loss of critical control or test data.  
-4 Equipment failure which would result in loss of desired test data.

- B. Equipment which is required during pre-firing check-out to verify the readiness of the test or vehicle system. The acoustic environment protection required, in this case, need only prevent equipment damage during the firing of a launch.

While other breakdowns can be made, the arrangement above will be suitable for purposes of this chapter.

Before proceeding, it should be pointed out that some of the equipment on a launch or test stand is considered expendable and is usually replaced after every launch or test firing. However, if the item falls in category A, it has a function to perform during the initial part of the firing so that environmental design is still an important consideration. A list of typical components which were damaged during a launch is given in Table 11.1B. These data, from Reference 11.2, show that most of the components would fall in the A-1 and A-2 category identified above. Therefore, they would have to be evaluated for their operational reliability during the initial engine noise and vibration environment that exists prior to the high temperature exposure.

TABLE 11.1A

BOUNDARIES OF TYPICAL LAUNCH ENVIRONMENTS

Zone	Radius (Nozzle Diameters)	Sound Pressure dB	Sound Pressure psi-rms	Blast Pressure psi	Blast Pressure Sound Pressure
1	0	—	—	—	—
2	10	165	0.5	≥100	>200
3	75	150	0.1	3.5	35
4	750	130	0.01	0.15	15
	>750	<130	<.01	<0.15	-

TABLE 11.1B

TYPICAL LAUNCH DAMAGE OF AUXILIARY GROUND SUPPORT EQUIPMENT DURING  
LAUNCH OF RANGER SPACECRAFT (DATA FROM REFERENCE 11.2)

Quantity	Item	Damage	Cause
1	Air Conditioning Duct to Vehicle	Covering Torn Away	Flame and Blast
1	Air Conditioning Blanket for Vehicle	Destroyed	Flame
24	Propellant and Pressurized Gas Quick Disconnect Components	Overheated	Flame
3	Air Ducts to Thrust Section and Instrument Pod	Overheated	Flame
3	Propellant Check and Drain Valves	Overheated	Flame
2	Propellant Flexible Ducts and Harnesses	Overheated	Flame
2	Microswitches	Overheated	Flame
8	Umbilical Cables	Overheated	Flame
6	Hold-Down Release Components	Overheated	Flame
16	Miscellaneous Harnesses and Hoses	Excess Heat and Blast	Flame and Blast
2	Duct and Tubing Support Brackets	Excess Blast	Blast

#### 11.4 RELIABILITY OF GROUND SUPPORT EQUIPMENT

A brief review of system reliability concepts is desirable at this point (Reference 11.10).

The reliability  $R$  over a lifetime  $t$  of a single component whose failure rate is  $\lambda$  failures per unit time is

$$R = e^{-\lambda t} \quad (11.1)$$

For example, if  $\lambda = 1$  failure per 1,000 hours, the reliability over a lifetime of 10 hours (probability that the component would still be operational) would be

$$R = e^{-10/1000} = 0.990$$

Thus, there is a 99 percent chance that the component will be operational throughout the period of 10 hours.

##### 11.4.1 SERIES SYSTEM

In a series system, all components must operate for the system to function. Its reliability  $R_s$  is given by the product of the component reliabilities. For a system with  $K$  components,

$$R_s = R_1 \cdot R_2 \cdot R_3 \cdots R_K \quad (11.2)$$

$$= e^{-\lambda_s t} \quad (11.3)$$

where  $\lambda_s$  = system failure rate =  $\lambda_1 + \lambda_2 + \lambda_3 \cdots + \lambda_K$   
For example, for two components each with the same

failure rate of one failure per 1000 hours, the system failure rate would be two failures per 1000 hours and the system reliability for a 10 hour lifetime would be 0.9802.

##### 11.4.2 PARALLEL OR REDUNDANT SYSTEM

If any one of the components can operate the entire system, the system is called parallel or redundant. For  $K$  redundant components, the system reliability is

$$R_s = 1 - Q_s \quad (11.4)$$

where

$$Q_s = \begin{cases} \text{Parallel System Unreliability} \\ Q_1, Q_2, Q_3 \dots Q_K \end{cases} \quad (11.5)$$

Thus, for a redundant system, the unreliability (i.e., one minus the reliability) is equal to the product of the component unreliabilities. Therefore, the redundant system reliability is

$$R_s = 1 - (1 - R_1)(1 - R_2)(1 - R_3) \cdots (1 - R_K) \quad (11.6)$$

where  $R_K$  is the  $K$ -th component reliability defined by equation (11.1).

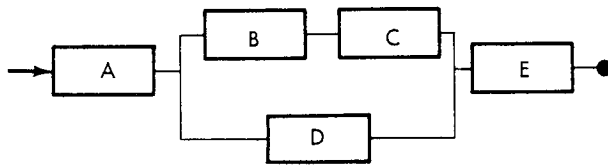
For example, if two components are in parallel and each has the same failure rate (1 in 1000 hours) as before, the system reliability over a 10 hour life will be

$$\begin{aligned} R_s &= 1 - (1 - 0.99)(1 - 0.99) \\ &= 0.999 \end{aligned}$$

This is equivalent to a system failure rate of one failure per 100,000 hours.

#### 11.4.3 SERIES - PARALLEL SYSTEM

The usual system consists of a combination of series and parallel operations as indicated by the schematic diagram of a typical Saturn V launch facility subsystem in Figure 11.4. A simplified diagram of such a system is shown in Figure 11.3. This system will operate through either ABCE or ADE. As shown, the system reliability is established by defining first the reliability of the redundant subsystem BC and D using Equation 11.6, and then using Equation from 11.2 for the rest of the system.



$$R_s = R_A R_E \left[ 1 - (1 - R_B R_C) (1 - R_D) \right]$$

FIGURE 11.3 Reliability of Series-Parallel System

#### 11.4.4 ANALYSIS OF SYSTEM RELIABILITY AND ENVIRONMENTAL PROTECTION

In the initial planning stages of a new launch or test facility, the facility designer must examine the basic reliability requirements for the major support systems. The specific objective would be to establish a clear definition of the degree of environmental protection required for various components of each system. The analysis might be carried out in the following steps:

- 1) Identify the failure category for the system according to the breakdown in the last section (i.e., A-1 category for any system whose failure would result in a catastrophic failure of the launch or test vehicle.)
- 2) Establish an overall reliability target for the system based on this category.
- 3) Identify the major components of the system and their general physical arrangement.
- 4) Estimate the basic reliability of each of the major components neglecting for the moment any effects of the actual environment.

- 5) Compute the "laboratory environment reliability" of the overall system.
- 6) Optimize the decrease in reliability (e.g., increase in failure rate) allowable for each component which will still meet the overall reliability goal of Step 2.
- 7) Estimate the maximum allowable environment for each component which can cause this decrease in reliability.
- 8) Compare this allowable environment with the normal external environment to establish the degree of environmental protection required.

Unfortunately, the currently available information on effects of high intensity acoustic environments on equipment reliability is not sufficient to make Step 7 practical at this time. However, the available information on this subject, covered in the remainder of this chapter, can be used for preliminary estimates of reliability effects.

### 11.5 RESPONSE OF EQUIPMENT TO ACOUSTIC ENVIRONMENTS

#### 11.5.1 GENERAL DISCUSSION

The dynamic response of equipment in a high level acoustic environment will consist of one or more of the following forms:

- a) Vibration of the equipment mounting induced by acoustic excitation of the support structure.
- b) Vibration of the equipment as a rigid body on its mounting due to the net acoustic forces on the equipment surface.
- c) Vibration of portions of the external housing of the equipment due to acoustic loading.
- d) Vibrational or compressional stresses of internal equipment elements due to the internal acoustic environment.

The first two types of response depend critically on the equipment mounting structure while the last two depend solely on the equipment design. While the complexity of response modes makes it difficult to determine with great precision the acoustic effects on equipment, useful data and analysis methods will be presented which are sufficiently accurate for evaluating environmental protection requirements.

#### 11.5.2 SUMMARY OF ACOUSTIC TESTS AND FAILURE DATA

Before considering the various response modes in detail, the available acoustic test data on equipment malfunction will be briefly reviewed. A malfunction is defined as any momentary out-of-tolerance performance of the equipment such as excessive noise, contact chatter, etc. Except for

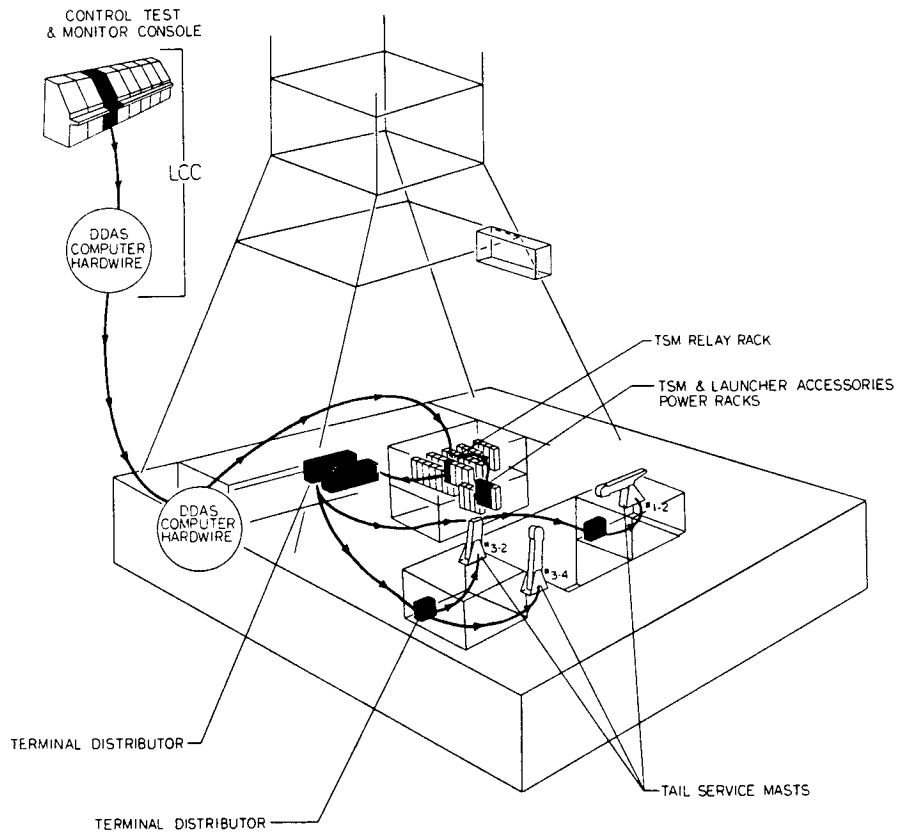


FIGURE 11.4 Tail Service Masts Subsystem, SATURN V Launch Facility

the case of vacuum tubes, no report has been found of irreversible damage to equipment due solely to acoustic excitation. This excludes, of course, the many cases of structural damage due to acoustically induced vibration. Table 11.2 summarizes available acoustic environment test data on equipment reported in References 11.3-11.7. Also shown are some data from Reference 11.8 on mean failure rates of the same type of components under a laboratory environment. The first column indicates the number of types of the component tested. The second column shows the minimum octave band level in the frequency range of 200-2000 Hz for which a malfunction occurred. This frequency range was chosen as representative of the range of fundamental resonant frequencies of internal parts of the various components. The next column shows the maximum octave band level, over the same frequency range, for any test which did not show a malfunction. For certain types of equipment, a sufficient variety were tested acoustically to provide a statistically significant measure of minimum sensitivity levels.

These items include accelerometers, capacitors, coaxial cable, meters, potentiometers, relays, and vacuum tubes. Further details for these will be given later.

Additional data on failure rate of equipment, is given in Reference 11.8. It must be emphasized that the failure rate, called the generic failure rate, applies only for a laboratory environment. According to Reference 11.8, the generic failure rate must be corrected for more severe environments to obtain a service failure rate by multiplying by the following factor:

Usage	Multiply Generic Failure Rate By
Laboratory	1
Ground Equipment	10
Trailer-Mounted Equipment	25
Rail-Mounted Equipment	30
Aircraft Equipment-Bench Test	50
Missile Equipment-Bench Test	75
Aircraft Equipment-In Flight	100
Missile Equipment-In Flight	1000

These factors are not entirely applicable to ground support equipment for launch or test facilities due to the wide range of possible environments. Some indication of the average failure rate for ground equipment may be determined from the data in Table 11.2. These were analyzed to show the distribution in percent malfunction as a function of the average octave band sound level in 6 dB intervals for frequencies of 200-2000 Hz. A careful examination of the results where a malfunction occurred shows that the data fell into two groups - items that failed at a level of less than 145 dB (Group I) and items that failed at higher levels (Group II). For tests which did not exhibit a malfunction, it was assumed that an increase of 6 dB in level (doubling of sound pressure) would have resulted in a malfunction. These hypothetical "malfunction" data coincided with the actual malfunction data in Group II. These two distributions are plotted in Figure 11.5 on a probability graph for the 65 different types of equipment

tested. The two groups of data fall roughly on one of two straight lines indicating a log normal distribution in each case. Note that the three points at the lower end of the Group II data fall outside this group by definition. Data on vacuum tubes were excluded in this analysis due to their exceptionally high acoustic sensitivity.

The data used for this analysis included results ranging from a test of only one specimen of a type up to tests of five specimens for one out of 30 varieties of a single type. The equipment mounting configurations for these acoustic tests also vary considerably from components freely suspended in the sound field through components mounted on a rigid block to items mounted on a chassis. The latter situation was in the minority, however, so that the results are considered representative of acoustically induced malfunctions which were not the result of acoustic vibration of support structure.

Clearly, the malfunction probability curves in Figure 11.5 can not be used for predicting the acoustic sensitivity of any one type of ground equipment. However, one attempt was made to categorize the equipment tested by possible response mode as a basis for predicting acoustic sensitivity. Each equipment item in Table 11.2 is identified in the first column, by one of the three categories given below (Reference 11.3).

- a) Components whose function involves motion of flexible parts (i.e., relays, pressure switches, etc.
- b) Components which are nominally stationary but contain structural elements which are relatively flexible (i.e., vacuum tubes, coaxial cable, etc.).
- c) Components with relatively rigid parts and support structure (i.e., solid state components, capacitors, resistors, etc.).

An analysis of the data in Table 11.2 according to this breakdown did not show significant differences among the three categories.

The observed probability of malfunction can be utilized to predict a failure rate from the expression

$$\text{Probability of Malfunction} = P = 1 - R \quad (11.7)$$

where R is the reliability defined by equation 11.1. The corresponding failure rate,  $\lambda$ , is found by substituting equation 11.7 in 11.1 and solving for  $\lambda$  to give

$$\lambda = \frac{\log [1/(1 - P)]}{t \log e} \quad (11.8)$$

where t is the time to failure.

Assuming a time to failure (or malfunction) for the acoustic tests of 0.1 hours, the failure rates shown in Figure 11.6 were calculated from the data in Figure 11.5. A single datum point is also shown which represents a measurement of component failure from a four-hour sonic fatigue test of

TABLE 11.2

ACOUSTIC TEST LEVELS FOR EQUIPMENT MALFUNCTION AND MEAN FAILURE RATES OF  
EQUIPMENT IN A LABORATORY ENVIRONMENT

CLASS		ACOUSTIC TEST LEVEL (1)			Mean Failure Rate (2) Failures/10 <sup>6</sup> hr
Type (3)	Electrical and Electronic Components	No. of Types Tested (4)	Minimum Failed dB	Maximum Passed dB	
c	Accelerometer	8		145-168 (8)	2.8
c	Amplifier, Audio			150	
b	Amplifier, Decade, Lab. Type		120		
c	Amplifier, Magnetic	2		157	2
b,c	Amplifier, Servo			157	2.0
c	Capacitors	11		184 (7)	
b	Coaxial Cable	8	138	157	0.02
a	Commutators		142		
c	Computer, Analog	3	165		
c	Connectors			155	0.2/pin
c	Current Repeater		134		
c	Diode Module			168	0.2
b	Heater, Electrical, 100 watt			140	0.02
c	Inductor			160	
c	Inverter			155	
c	Junction Box			155	
a	Limit Switch			166	0.5/cs (5)
a	Moving Coil Meters	8		155	
b	Oscillator, Lab. Type		135		
b	Oscilloscope, Lab. Type		130		
b	Phase Shifter			149	
a	Potentiometer	13	138	160	0.13
c	Power Supply, 400 Hz			156	
a	Recorder, Strip Chart		139		
c	Rectifier	2	130		
a	Relays	30	131	160	0.25/cs
a	Relay Module, Solid State		156		
a	Relay, Time Delay			150	
c	Resistance to Current Convertor		139		
c	Resistors	3		165 (7)	0.25
c	Signal Conditioner, Power			160	
a	Switch, Solenoid		128		
a	Switch, Fluid Pressure, Electrical		142		0.5/cs (5)
b	Television Camera			133	
b	Telemetry Data System			155	
c	Thermal Sensors	2	134	160	0.6
b,c	Timer Control			155	1.2
c	Transducer, Temperature			148	
c	Transistors	2		151	0.61
b,c	Transmitter, Telemetry		140		2
b	Vacuum Tubes	40	110	150 (6)	0.80
c	Voltage Regulator		130		
c	Voltage to Current Convertor		160		
b	Voltmeter, Lab. Type		130		

TABLE 11.2 (CONTINUED)

CLASS		ACOUSTIC TEST LEVEL (1)			Mean Failure Rate (2) Failures/10 <sup>6</sup> hr
Type (3)	Pneumatic and Hydraulic Components	No. of Types Tested (4)	Minimum Failed dB	Maximum Passed dB	
a	Computer, Pneumatic			134	
a	Controller, Pressure		134		2.14
a	Control Panel, Pneumatic			159	2.4
a	Gas Volume and Analysis Meter			120	
a	Gauge, Pressure 0-5000 psi			162	4.0
a	Indicator, Controller			134	
a	Indicating Switch, Pressure		159		0.5/cs (5)
a	Regulator, Hydraulic			155	2.14
a	Regulator, LO <sub>2</sub>			155	3.00
a	Recorder, Pneumatic			134	
a	Switch, Pressure Activated	10	135	150	
c	Thermometer Bulb			160	1
b	Transmitter, Pressure	4	134	160	
b	, Temperature		160		15
a	Valve Pressure			155	5
a	Valve, Solenoid		163	156	
a	Valve, Vent and Relief			155	5.7
Pyrotechnic Components					
c	Ejector Cartridges			151	
c	Explosive Cartridges			175	
c	Igniters			151	
c	Pyrotechnic Squibbs			151	

- (1) Octave Band Sound Level in dB re: 0002 microbars from 200 - 2000 Hz - Minimum at which malfunction occurred - Maximum for which no malfunction occurred for a different variety of the same type (References 11.3-7).
- (2) Mean Generic Failure Rate in laboratory environment (Reference 11.8).
- (3) Equipment Response Category - see text.
- (4) Only one type tested except as noted.
- (5) Failures per 10<sup>6</sup> cycles.
- (6) Maximum Failure Level.
- (7) Octave Band Sound Level to produce 1 mv output with 300 volt bias on capacitor.
- (8) Octave Band Sound Level producing a 1 g output.



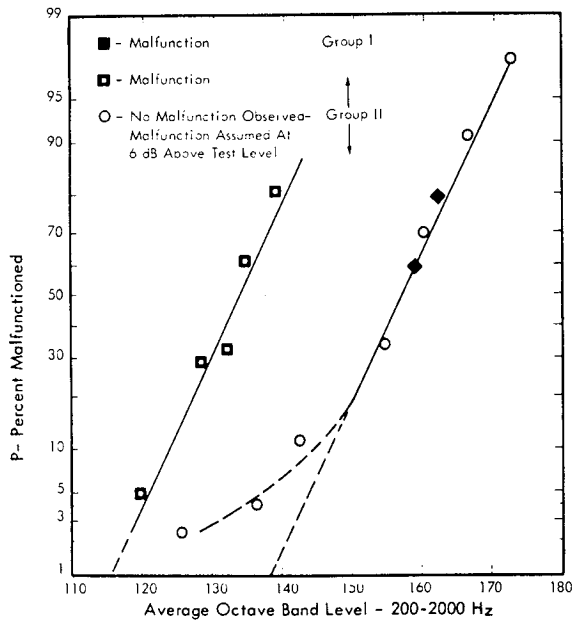


FIGURE 11.5 Malfunction Distribution from Acoustic Tests of 65 Different Types of Electrical, Pneumatic, Hydraulic and Pyrotechnic Equipment and Components - Vacuum Tubes Excluded. (From References 11.3 - 11.7)

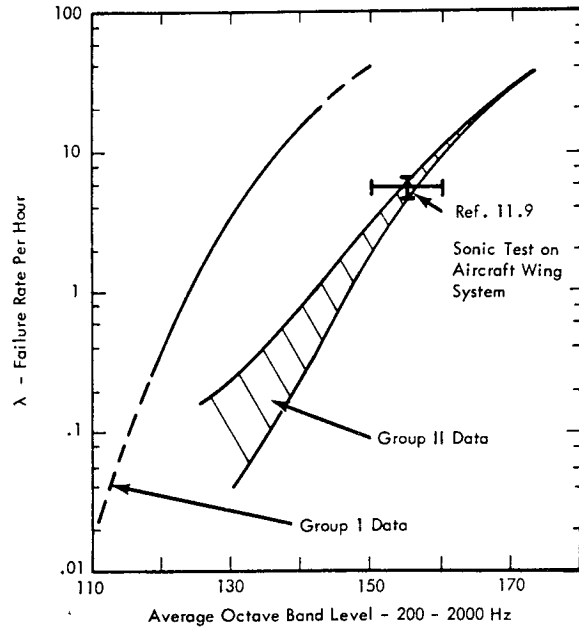


FIGURE 11.6 Failure Rate Calculated From Acoustic Test Data in Figure 11.5 Assuming A Test Failure Time of 0.1 Hour

a complete jet aircraft wing system (Reference 11.9). The significance of this single point is that it represents direct measurement of the acoustically induced failure on a complex structural-equipment system with a large number of component parts. The statistical significance of the point is therefore very high. It applies only to the observed functional or structural failures of the various hydraulic, and electrical systems. It does not include any failures of wing structure components.

The surprising agreement between this datum point and the estimated failure rate for the Group II equipment indicates that the latter is representative for hardened equipment used near a rocket launch or test facility. Thus, as indicated in Section 11.4.4, a preliminary method is available for estimating ground support equipment reliability as a function of acoustic environment.

11.5.2.1 Estimated Reliability of Exposed Ground Support Equipment

The average reliability of hardened equipment due only to exposure to the launch acoustic environment can be estimated from Figure 11.6 and equation 11.1. This estimate is shown in Figure 11.7 for an exposure time of 10 seconds and 200 seconds, typical for a launch and test stand, respectively. The failure rate used for these estimates was obtained from the maximum value of the Group II data in Figure 11.6. The very high probability of malfunction indicated by Figure 11.7, particularly for exposed equipment near a test stand, must be considered as a preliminary conservative estimate. However, for a given required reliability, the estimate does provide a basis for defining a maximum acoustic isolation requirement for protective housing.

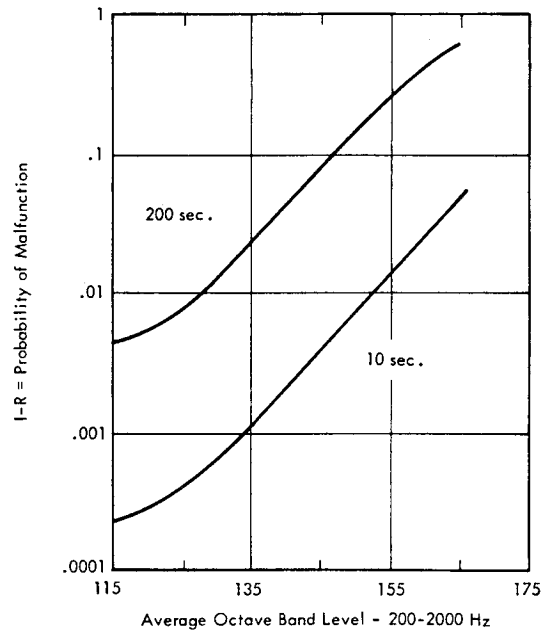


FIGURE 11.7 Estimated Probability of Malfunction of Exposed Acoustically-Sensitive Equipment For Launch Stand (Duration = 10 Seconds) and Test Stand (Duration = 200 Seconds). Based on Group II Data, Figure 11.6

11.5.3 ACOUSTIC EXCITATION OF EQUIPMENT MOUNTING STRUCTURE

11.5.3.1 Analytical Method

For most equipment, the most significant effect of a high intensity acoustic environment is the acoustic excitation of the equipment mounting structure. This is particularly true for equipment mounted on large lightweight panels. The acceleration response of structural panels due to acoustic excitation may be estimated empirically by the expression

$$A(f) = \frac{P(f)}{w} \cdot M_A \quad (11.9)$$

where

$A(f)$  = space average rms acceleration at a frequency  $f$  - g's

$P(f)$  = rms pressure at the same frequency -psi

$w$  = panel surface weight-psi

$M_A$  = acoustic mobility of panels.

The theoretical development and related experimental data for acoustic mobility of panels has been covered in Chapter 8. The recommended design value for  $M_A$  for equipment loaded panels is shown in Figure 11.8. This represents an upper bound to the experimentally derived factor relating acceleration response of a panel of a given weight to the acoustic driving force. The expected higher damping for panels supporting bolt- or rivet-mounted equipment is reflected in this curve. The surface weight will be the total weight of the panel plus equipment. The fundamental mode of the panel, which is the normalizing factor for the frequency scale in Figure 11.8, can be determined from the charts presented in Chapter 3. For panels which are not enclosed on the back side or mounted in a large stiff baffle, a correction must be made to Figure 11.8 to account for the decrease in net acoustic loading due to diffraction of sound waves around the back of the panel.

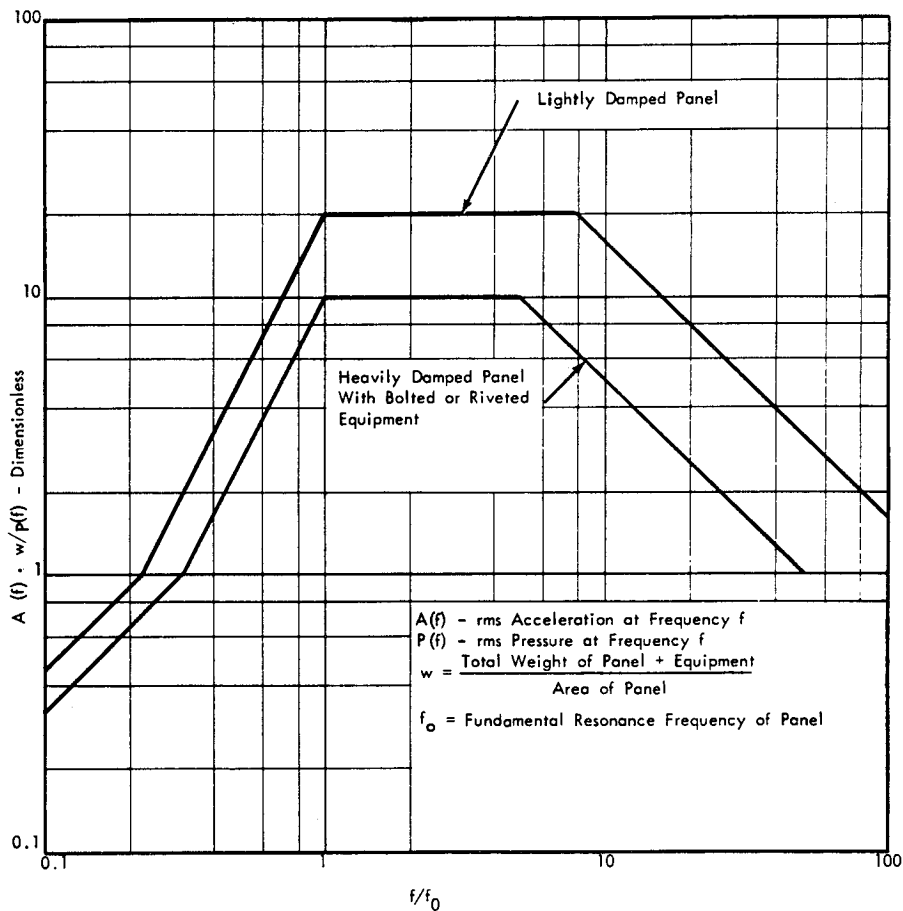


FIGURE 11.8 Design Envelope for Acoustic Mobility of Baffled Flat Panel with Mounted Equipment

This correction factor, shown in Figure 11.9, depends on the ratio of a geometric mean panel dimension  $S$  to the acoustic wavelength  $\lambda$ . For values of  $S/\lambda < .5$ , the net acoustic driving force on the panel is assumed equivalent to that on a rigid sphere (see Section 11.5.4). For  $S/\lambda > .5$ , the random phasing of the diffracted waves around the back of the panel provides an effective "acoustic" baffle. Experimental data, shown in the curve, were measured on a 2" x 10" panel with and without a baffle; the data indicates the theoretical estimate is conservative.

As an illustration of the above analysis method, the vibration response of a typical unbaffled panel with low damping is calculated in the following example:

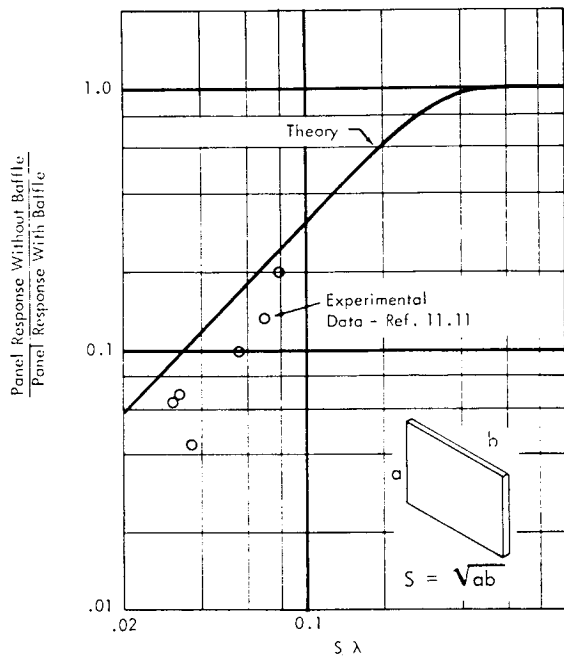


FIGURE 11.9 Correction for Acoustic Response of Panel Due to Lack of Baffle or Back Enclosure

Example:

Panel Size -  $a = 24$  in,  $b = 34.5$  in,  $h = 1/8$  in

Panel Material - Steel

Bare Panel Surface Weight =  $(1/8 \text{ in})(.3 \text{ lb/in}^3) = .038 \text{ lb/in}^2$

Equipment Weight Distributed over Panel =  $.012 \text{ lb/in}^2$

Total Surface Weight =  $.050 \text{ lb/in}^2$

Panel Edge

Conditions - 24 in side - simply supported  
 - 34.5 in side - free

First Resonance Frequency (Bare Panel)  $-f_{1,0} = 9.6 h \cdot 10^4 / b^2$   
 $= 10 \text{ Hz}$

Assume mass and stiffening effect of equipment cancel each other out so that panel resonance is not changed.

$$S/\lambda = f \sqrt{ab}/13,400 = f/465.$$

The response acceleration spectral density (APSD) and overall rms acceleration is calculated in Table 11.3 for a hypothetical acoustic environment near a launch stand. A suitable vibration test spectrum for equipment mounted on the panel can be defined by an envelope of the calculated points.

### 11.5.3.2 Experimental Data on Acoustic Mobility Of Cabinet Mounted Equipment

A large part of the ground support equipment for a launch or test facility is mounted in standard equipment racks such as illustrated in Figure 11.10. The acoustically induced vibration of equipment mounted in such racks is not readily predictable by analytical means. However, experimental data are available from two different tests of equipment racks located in a high intensity acoustic environment. These data have been analyzed to provide an estimate of the acoustic mobility of rack mounted equipment.

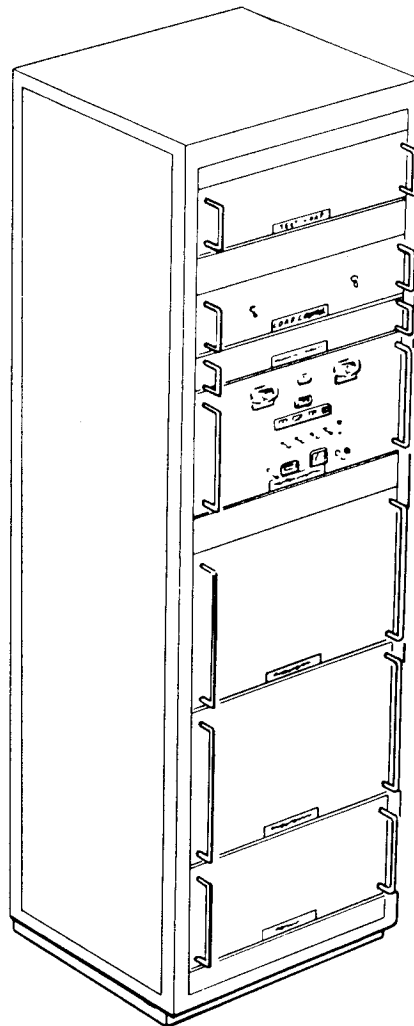


FIGURE 11.10 Typical Power Distribution Rack

TABLE 11.3  
CALCULATION OF VIBRATION RESPONSE OF UNBAFFLED  
EQUIPMENT PANEL TO ACOUSTIC EXCITATION

Frequency (f) - Hz	10	40	80	320	1280
Octave Band Level - dB	138.0	146.0	150.0	143.5	139.0
P (f) - lb/in <sup>2</sup> - rms (in Octave Band)	0.023	0.058	0.092	0.044	0.026
s/λ	0.022	0.086	0.17	0.69	2.8
No Baffle Correction (Figure 11.9)	0.064	0.26	0.52	1.0	1.0
Effective Pressure lb/in <sup>2</sup>	0.0015	0.015	0.048	0.044	0.026
f/f <sub>o</sub>	1.0	4.0	8.0	32.0	128.0
A (f) · w/P (f)	20.0	20.0	20.0	5.0	1.25
P (f)/w	0.03	0.3	0.96	0.88	0.52
A (f) - g's - rms	0.6	6.0	19.2	4.4	0.65
A <sup>2</sup> (f) - g <sup>2</sup>	0.36	36.0	368.0	19.3	0.42
Δf - Hz (Octave Band)	7.1	28.0	56.5	226.0	905.0
APSD - g <sup>2</sup> /Hz	0.051	1.3	6.5	0.085	0.00046
Overall G's = $\left[ \sum A^2 (f) \right]^{1/2} = 20.6g \text{ rms}$					

Saturn V Ground Computer Environmental Test

The first test, described in detail in Reference 11.12, was conducted on a portion of the SATURN V ground computer system to be located in Level A of the Saturn V Launcher/Umbilical tower approximately 100 feet from the vehicle centerline. Separate acoustic and vibration tests were conducted providing a separate measure of the relative acoustic and mechanical mobility of the equipment racks, (Reference 11.12). In both cases, an array of equipment cabinets was mounted on a section of the shock-isolated floor designed to reduce mechanical input to the base of the cabinets. The isolation was provided by coil springs, illustrated in Figure 11.11, which were designed for a 4 Hz. resonance frequency of the floor system. The average acoustic and vibration test levels are shown, in Figures 11.12 and 11.13 respectively, in terms of one-third octave band levels. These represent the highest test levels employed during a series of successively more severe test levels. The response data for two typical cabinets have been analyzed in one-third octave bands to determine their acoustic and vibration mobilities, respectively.

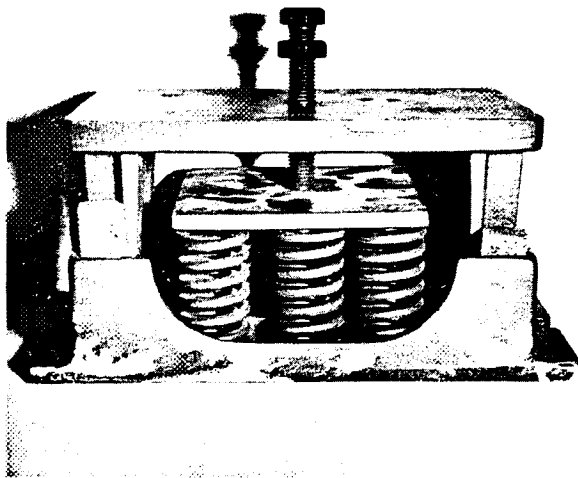


FIGURE 11.11 Typical Floor Isolation Springs Employed With Saturn V Ground Computer Acoustic Vibration Test

For the acoustic test data, the acceleration response, measured in one-third octave bands, was normalized by the one-third octave band sound level to obtain a vibro-acoustic transfer function or acoustic mobility. For presentation of the data, this function is expressed in the form,

$$10 \log \left| \frac{A(f)}{P(f)} \right|^2 = A.L. - SPL + 170.7 \text{ dB} \text{ re: } 1 \text{ g/psi} \quad (11.10)$$

where

- A(f) = rms acceleration at frequency f - g's
- P(f) = rms pressure at frequency f - psi
- A.L. = Band acceleration level in dB re: 1 g
- SPL = Band sound level in dB re: 0.0002 microbar.

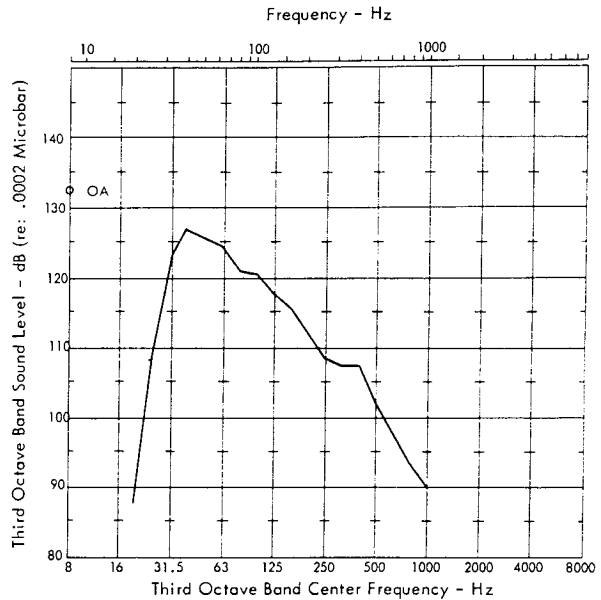


FIGURE 11.12 Average Acoustic Test Spectrum for SATURN V Ground System Computer Cabinet (Ref. 11.12)

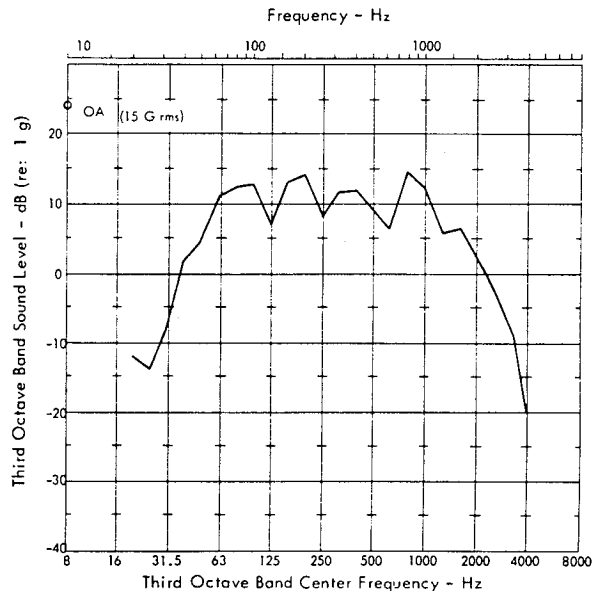


FIGURE 11.13 Average Vibration Test Spectrum for SATURN V Ground System Computer Cabinet (Ref. 11.12)

A typical plot of this acoustic mobility, measured at one point at different sound levels, is shown in Figure 11.14. The frequency range of the data is limited due to the low signal to noise ratio encountered at the higher frequencies where acoustic excitation and the resulting acceleration levels were low.

The maximum acoustic mobilities were computed from the data for horizontal motion and vertical motion. The results are shown on Figures 11.15 and 11.16 respectively. For the horizontal motion, (i.e., motion normal to the surface of the cabinet walls), a predicted upper bound for the data

is shown. This was computed from Figure 11.8 using, for a surface weight, a total cabinet weight of 1800 pounds divided by the total surface area for the 34" x 36" x 80" cabinets. A typical fundamental resonance of 100 Hz for a stiffened section of the 1/16 inch steel cabinet wall was estimated.

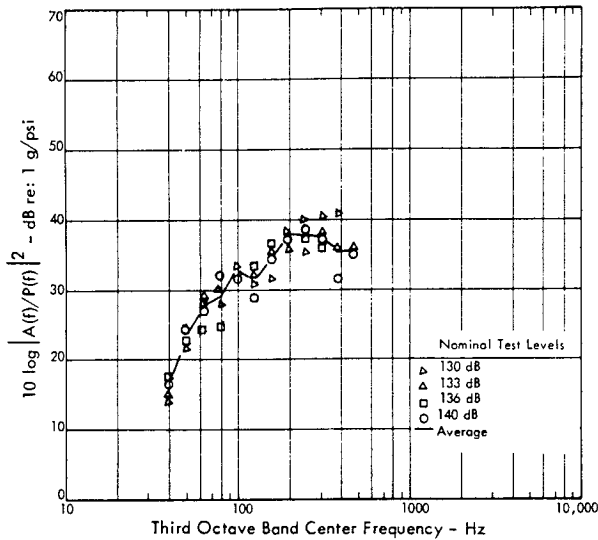


FIGURE 11.14 Acoustic Mobility Measurement in Third Octave Bands at Four Test Levels on One Location of the SATURN V Ground Computer.  
Cabinet - Horizontal Motion of Cabinet Structure (Ref. 11.12)

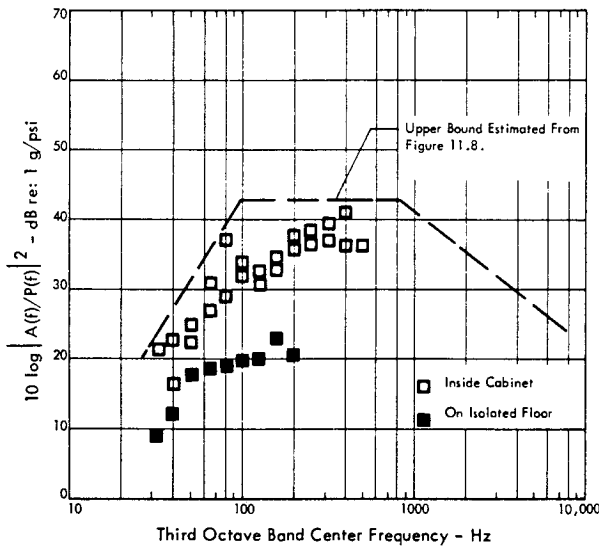


FIGURE 11.15 Maximum Acoustical Mobility Measured in Third Octave Bands in Horizontal Direction From Acoustic Test of SATURN V Ground Computer System (Ref. 11.12)

For the vertical direction, the acoustic excitation of the isolated floor results in much higher vibration levels than in the horizontal direction for frequencies below about 40 Hz. This will be a significant feature of the acoustically generated vibration environment for equipment mounted on an isolated floor. While structural vibration transmission to the floor will be reduced by the isolation system, acoustic

energy transmitted into the room through the walls or ceiling will act as an additional and direct driving force for the floor.

Another important result should be noted in Figures 11.15 and 11.16. In both cases the maximum acoustic mobility or response of the cabinet structure is about 10 dB higher than the corresponding floor response. This is not due to resonant amplification of structurally borne vibration from the base of the cabinet. Rather it is due to the local acoustic excitation of the lighter cabinet structure.

A general design method for predicting the acoustic vibration of equipment cabinet cannot be developed from the limited data given above. This is attributed partly to the lack of sufficient data to establish a valid analytical or empirical model and partly to the complex vibration response characteristics of a typical equipment cabinet. This is illustrated by the following estimates of the fundamental vibration modes for the cabinet tested.

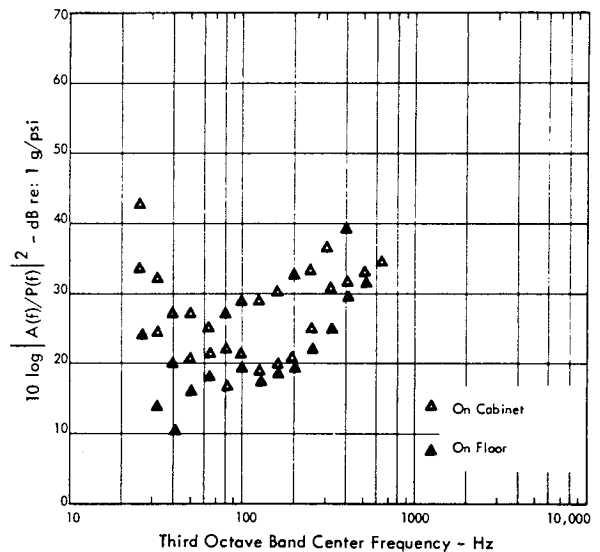


FIGURE 11.16 Maximum Acoustic Mobility Measured in Third Octave Bands in Vertical Direction From Acoustic Test of SATURN V Ground Computer System (Ref. 11.12)

Estimated Vibration Modes of Equipment Cabinet

- a) Unstiffened Panel Lateral Vibration - (Simply Supported)

$$f_{1,1} = \frac{\pi c_L h}{2\sqrt{12(1-\mu^2)}} \left[ \frac{1}{a^2} + \frac{1}{b^2} \right]$$

where

- $c_L = 2 \times 10^5$  in/sec - speed of sound in steel
- $a = 33$  in - average panel width
- $b = 80$  in - panel height
- $h = 1/16$  in - panel thickness
- $\mu =$  Poisson's ratio = 0.3

so that

$$f_{1,1} \approx 6.4 \text{ Hz.}$$

For the torsional, longitudinal and bending modes of the cabinet, it is assumed that the equipment mass adds no stiffness. The modes can be estimated as follows.

b) Cabinet Torsional Mode - (Fixed-Free)

$$f_1 = \frac{1}{4} \sqrt{\frac{k_r}{I_p}}$$

$$k_r = \frac{a^3 h G}{L} \text{ - Torsional stiffness of square box beam of length } L, \text{ side } a, \text{ and thickness } h < a.$$

$$G = \text{Modulus of Rigidity} = 12 \times 10^6 \text{ psi}$$

$$I_p = \frac{W a^2}{6 g} = \text{Polar mass moment of inertia of solid with square cross section.}$$

$$W = 1800 \text{ pounds - weight of cabinet with equipment}$$

so that  $f_1 = 158 \text{ Hz.}$

c) Cabinet Longitudinal Mode - (Free-Free)

$$f_1 = \frac{1}{2} \sqrt{\frac{E A g}{W b}}$$

where  $E = \text{Young's Modulus} = 30 \times 10^6 \text{ psi}$

$A = 4 a h$  - cross sectional area

so that  $f_1 = 407 \text{ Hz.}$

d) Cabinet Lateral Bending Mode - (Free-Free)

$$f_1 = 3.56 \sqrt{\frac{E I g}{W b^3}}$$

where

$$I \approx \frac{2}{3} a^3 h \text{ - area moment of inertia for thin square box section}$$

so that  $f_1 = 491 \text{ Hz.}$

The significant point indicated by these estimates is the very low frequency of the fundamental modes of the cabinet side panels relative to the cabinet mode. The estimated modes of the cabinet would therefore have limited validity due to lateral bending modes of the side panels which exist at much lower frequencies.

Limited measurements were also made during this test on sound transmission through the cabinet walls. Between 30 and 100 Hz, the internal sound level varied from 5 to 10 dB higher than the external level and then dropped sharply below the external level at higher frequencies. This region of transmission gain coincides with the frequency range near the lower modes of the cabinet walls

and the region where structurally transmitted vibration from the base was higher than the input at the base. This is considered representative of the combined structural and acoustic transmission into this type of equipment cabinet. Typical results from the vibration test are summarized in Figures 11.17 and 11.18. The first figure shows the transmission loss or relative acceleration response, as measured in one-third octave bands between the vertical input to the bottom of the floor isolators, and the top of the floor and cabinet. As shown, a theoretical prediction of transmission loss based on a simple single degree of freedom isolator does not properly account for the degraded loss due to standing waves in the isolator and structural resonances in the floor and cabinet structure. The amplification between the top of the floor and internal locations in the cabinet in the frequency range of 20 to 125 Hz is also evident.

Figure 11.18 shows the cross-axis response between the vertical acceleration at the base of the floor and horizontal motion within the cabinet. The minimum value of in-axis response in the vertical direction, between the floor and cabinet is also shown. The amplification for both directions is very evident in the low frequency range. Equally significant for definition of internal vibration levels in the cabinet is the amplification above 700 to 1500 Hz between the cabinet base or floor and points inside the cabinet. In other words, for the particular cabinets analyzed, the design vibration environment for components within the cabinet will exceed the design environment at the base of the cabinet.

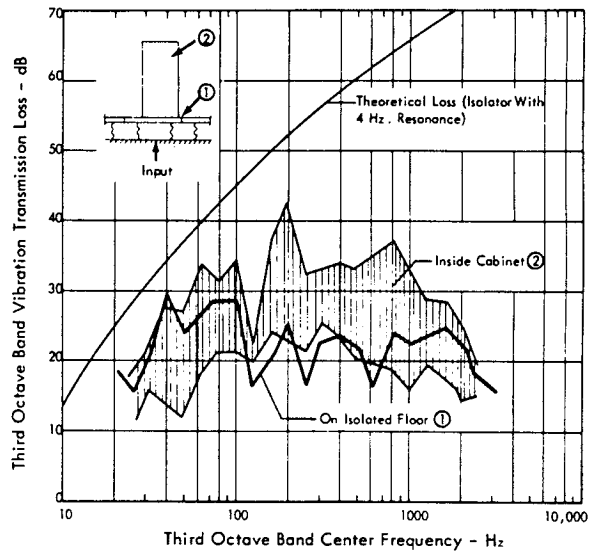


FIGURE 11.17 Vibration Transmission Loss in Vertical Direction Between Input to Shock Isolated Floor and SATURN V Ground Computer Cabinet

Equipment Cabinet Response During Saturn I Launch

As a comparison with the above laboratory test, data were obtained from a test conducted by NASA on the vibration response of a standard equipment rack used for mounting relay modules (Reference 11.13). The measurements were obtained during the period  $T - 1 \frac{1}{2}$  to  $T + 2$  sec. of a

Saturn I launch. The rack was located in level B of Pad 34 at the Kennedy Space Flight Center. The raw vibration data were analyzed with a fixed 10 Hz bandwidth filter and have been converted to equivalent one-third octave band levels for purposes of this analysis. The acoustic environment measured in this area was reported in Reference 11.14 and is shown in Figure 11.19. The average and maximum response levels observed at 30 locations on the rack in the vertical and lateral directions are shown in Figure 11.20. For this test, the rack was bolted directly to a 3/8 inch steel floor. Lacking any data on the floor, its vibration level was estimated using a resonant frequency of 20 Hz, and the acoustic mobility curve in Figure 11.8. This estimate, also shown in Figure 11.20, indicates that the floor vibration would be slightly less than the cabinet vibration at the lower frequencies as expected. The apparent acoustic mobility of the cabinet, based on the above data, has been computed and is shown in Figure 11.21. The maximum mobility is 20 to 40 dB higher than observed for the Saturn V Ground Computer System. This higher mobility is attributed to the combined effects of: a) lack of an isolated floor mounting, b) structurally transmitted building vibration, and c) lower rack weight.

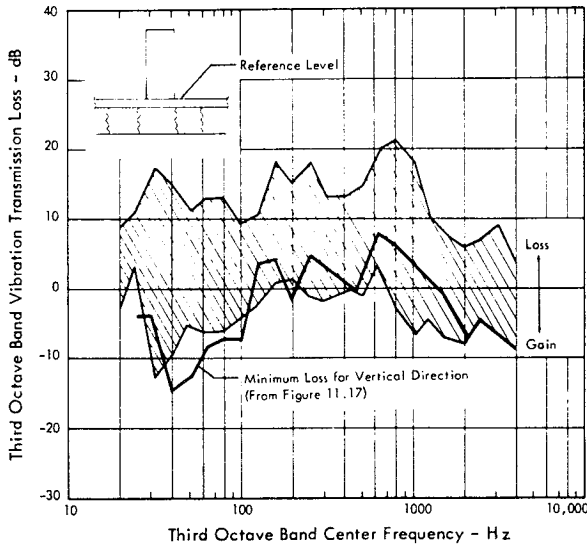


FIGURE 11.18 Vibration Transmission Loss Between Horizontal Response Inside Cabinet and Vertical Input at Base of Isolated Floor. Measured During Vibration Test of SATURN V Ground Computer System (Ref. 11.12)

As shown in Figure 11.21, vertical motion of the rack structure is higher than the horizontal motion at low frequencies as expected due to coupling with the floor vibration. Above about 150 Hz, however, the difference in levels in either direction is not significant.

Due to the wide range of maximum values of acoustic mobility noted in these two experiments, a general model for predicting internal vibration levels of equipment cabinets located in high intensity noise areas cannot be established. Further testing is required to more clearly define the relative significance of structurally borne acoustically induced vibration for this type of structural assembly.

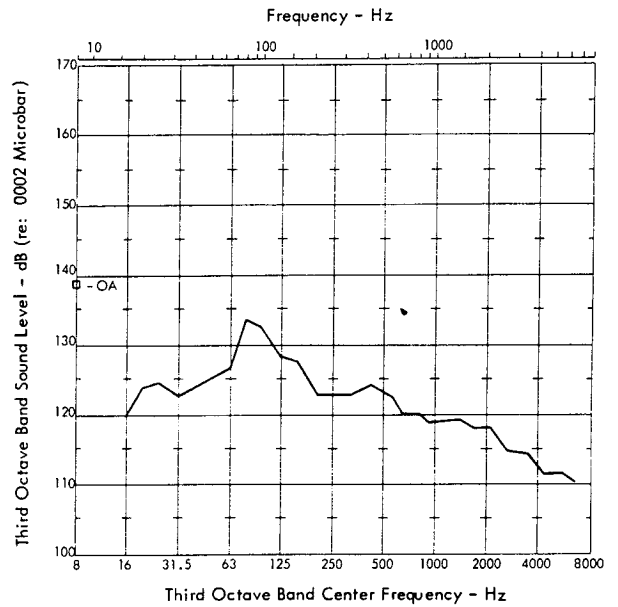


FIGURE 11.19 Internal Acoustic Environment at Level B, Pad 34 Umbilical Tower During Saturn Launch for Period  $T - 1 \frac{1}{2}$  to  $T + 2$  seconds (Ref. 11.14)

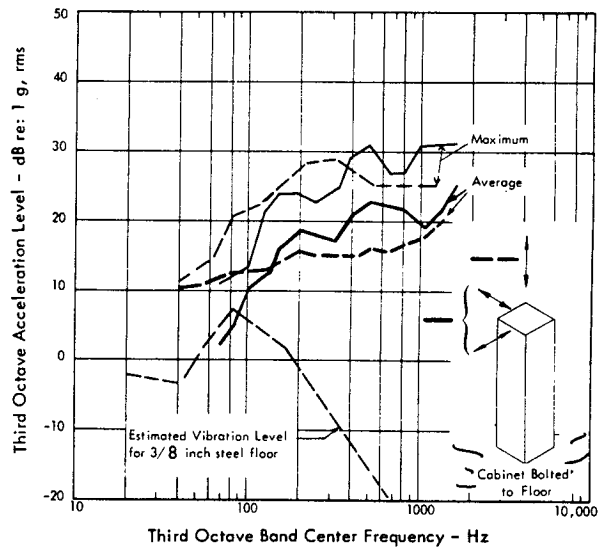


FIGURE 11.20 Acceleration Response Level at 30 Points Inside Standard Equipment Rack During SATURN I Launch KSC, Pad 34, Level B ( $T - 1 \frac{1}{2}$  to  $T + 2$  Secs) (Ref. 11.13)



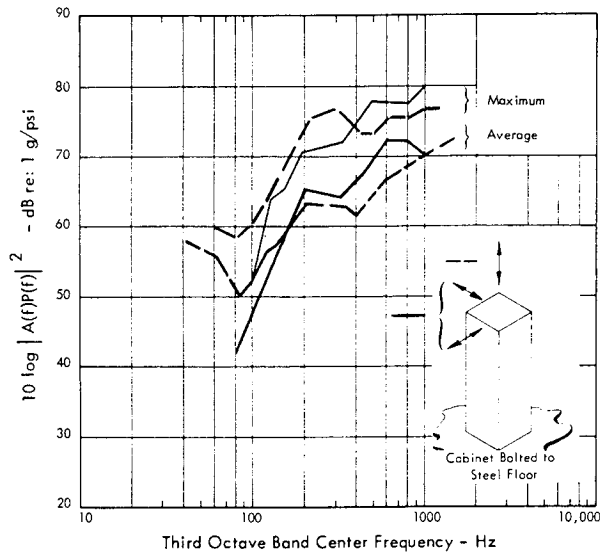


FIGURE 11.21 Apparent Vibro-Acoustic Mobility Calculated From Acceleration Response Levels in Figure 11.20 and Sound Levels in Figure 11.19

#### 11.5.4 ACOUSTIC SENSITIVITY OF SPECIFIC EQUIPMENT COMPONENTS

Acoustic sensitivity test results of some of the components included in Table 11.2 are briefly reviewed in more detail below. Results are given only for those components for which sufficient tests were conducted to provide some degree of statistical confidence. Acoustic test environments are given in terms of the minimum octave band levels for which components or equipment malfunctioned or the maximum levels used in a test.

The curves shown in Figure 11.22 - 11.25 cover the following types of components and equipment:

- Hydraulic Regulator
- Inverter
- LO<sub>2</sub> Regulator
- Potentiometers
- Pressure Switches
- Pressure Valve
- Relays and Relay Panels
- Sensitive Moving Coil Meters
- Timer Control
- Vacuum Tubes
- Vent and Relief System

Additional details which have been observed during acoustic tests of specific types of components are given below. These effects were observed while the item was suspended in a wide band random reverberant noise field with a spectrum centered about 500 Hz. (Reference 11.4).

**Capacitors** - Polarized units generate electrical noise levels of the order of 50 microvolt/microfarad in a 160 dB sound field.

**Coaxial Cable** - No electrical noise output above 0.3

millivolt for sound levels less than 133 dB. At 160 dB, the following noise signals were observed for 4 different types of coaxial cable.

5 ft of RG 59/U	- 0.85 mv
27 ft of RG 58/U	- 0.65 mv
13.5 ft of RG 58/U	- 0.44 mv
5 ft of RG 8A/U	- 2.5 mv
5 ft of RG 62A/U	- 1.3 mv

Length of the sample was not necessarily significant. The highest electrical noise output was observed for the largest cable (RG 8A/U) with a loosely woven braided shield. In general, the electrical noise spectrum coincided approximately with the acoustic spectrum. It is important to note that these results represent only acoustically induced noise. Electrical noise is also commonly generated in coaxial cables by mechanical vibration of the cable supports.

**Accelerometers** - Two barium titanate accelerometers tested did not generate any output within the normal frequency range of the acoustic test signal at levels up to 160 dB. However, at the resonant frequency of the accelerometers, (15-18 kHz), the two units generated an electrical output equivalent to a 11-13 g acceleration when exposed to a 100 dB noise field at these frequencies.

**Thermistor** - A 10°C temperature rise was observed on a thermistor mounted in a small electronic package exposed to a 158 dB sound field for 5 minutes.

**Transistor Amplifier** - A two-stage amplifier with 43 dB gain employing 2N333 transistors exhibited a negligible increase of electrical noise output when exposed to a 160 dB sound field.

**Vacuum Tubes** - Vacuum tubes tested were very sensitive to acoustic excitation particularly at the resonant frequencies of the internal grid elements and their supports. These resonances fall in the range of 200 to 13,000 Hz. Suggested acoustic sensitivity criteria for vacuum tubes are,

- 110 dB - malfunction threshold for low signal level vacuum tube circuits
- 130 dB - malfunction threshold for ruggedized vacuum tubes
- 150 dB - mechanical damage possible.

#### Miscellaneous Laboratory Equipment

Two sensitive vacuum tube AC voltmeters and a decade amplifier tested showed marked increases in electrical noise floor levels for octave band sound levels over 120 dB in the frequency range of 300 - 1200 Hz. For one of the voltmeters, internal resonances were excited by octave band levels as low as 97 dB. Based on the approximate linear relationship observed between electrical noise output and acoustic excitation level, the electrical noise to acoustical noise transfer functions ranged from -140 dB to -168 dB re: 1 v/0.0002 microbars. Thus, for octave band levels of the order of 140 to 168 dB, the corresponding electrical noise output from these units would be about 1 volt.

Two cathode ray oscilloscopes tested exhibited picture distortion at a 130 dB octave band level.

A precision differential AC-DC voltmeter began to show disturbance of the meter reading when exposed to 130 dB octave band level.

A precision phase meter showed no noticeable effect at an octave band level of 140 dB.

An RC vacuum tube audio oscillator exhibited noticeable disturbance to the output wave form at an octave band level of 140 dB.

Tests of resistors, inductors, capacitors, dry cell batteries, connectors, and transistors exhibited little or no effect at octave band levels up to 160 dB in the range from 150 to 600 Hz.

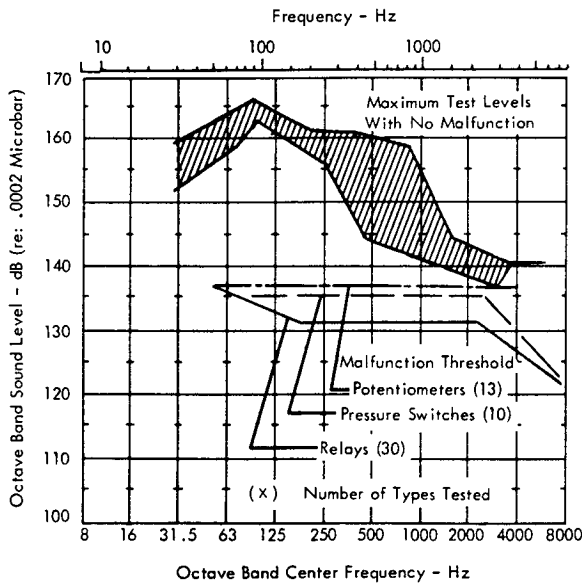


FIGURE 11.22 Acoustic Test Environment For Electronic Components With Moving Parts (Type a) Which Exhibited Contact Chatter. (Ref. 11.3 and 11.4)

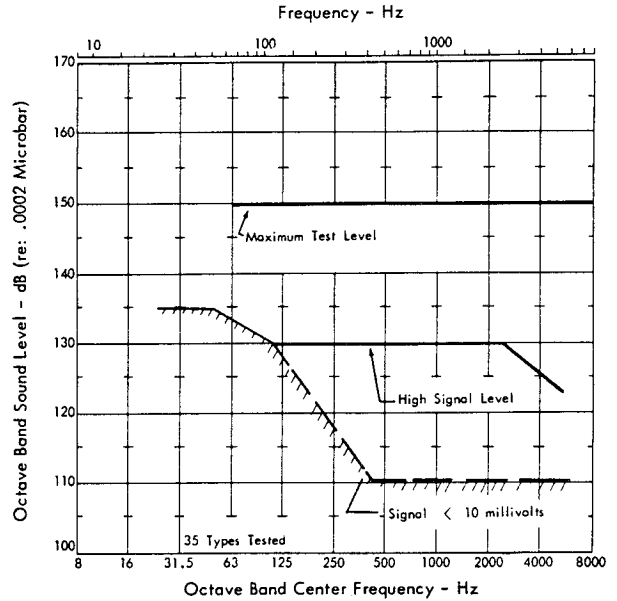


FIGURE 11.24 Minimum Acoustic Test Environment for Observed Malfunction of Vacuum Tubes. (Type b) All Types Tested Within These Bounds Malfunctioned or Failed. (Ref. 11.3 and 11.4)

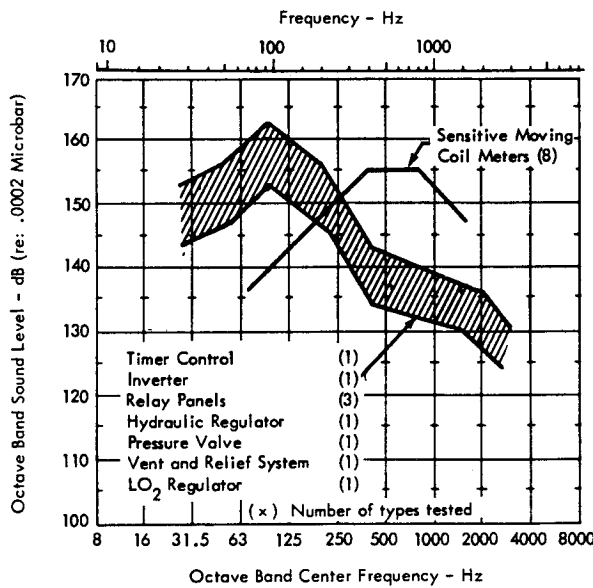


FIGURE 11.23 Maximum Acoustic Test Environment for Electronic, Hydraulic, and Pneumatic Flight Vehicle Components With Moving Parts (Type a) Which Did Not Malfunction. (Reference 11.3)

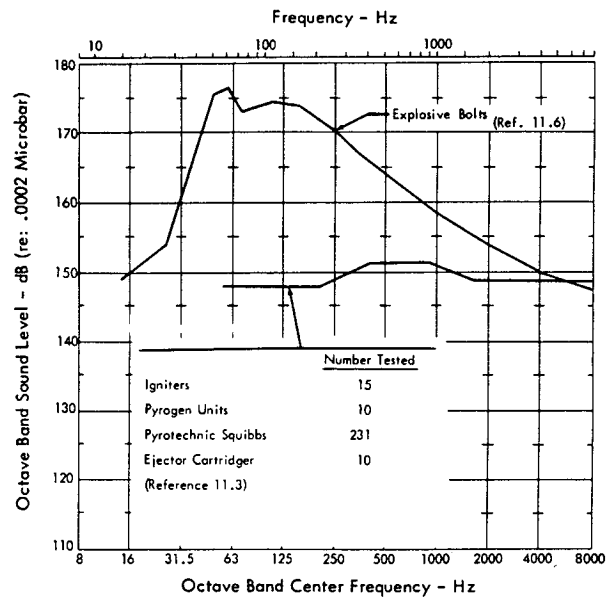


FIGURE 11.25 Acoustic Test Environment for Pyrotechnic Components (Type c) Which Do Not Malfunction

11.5.5 SOURCES FOR ADDITIONAL INFORMATION ON ACOUSTIC SENSITIVITY

For analysis of environmental design requirements of specific equipment, it may be desirable to review available acoustic test data for similar items.

11.5.5.1 Interservice Data Exchange Program

One source of information is available through the Interservice Data Exchange Program (IDEP). This is a cooperative activity between the three military services to provide

automatic interchange of environmental test data for equipment and components. Over 165 defense contractors and Government research facilities participate in this data exchange program. Copies of environmental test reports generated by the participants are submitted to the IDEP Office of the cognizant service where they are microfilmed and duplicate film copies attached to summary cards. (See Figure 11.26.) These cards are then automatically distributed to all full participating contractors and agencies which have contractual interests in the subject area covered by each report. Coded listings of the available reports are also published for assistance in identifying pertinent test data according to the type of component and type of environmental tests conducted.

REPORT SUMMARY SHEET												
1 COMPONENT PART NAME PER GENERIC CODE Transducers, Temperature, Voltage				7 PROGRAM OR WEAPON SYSTEM Saturn				White				
4 ORIGINATOR'S REPORT TITLE Design Evaluation, Qualification Test of Thermoelectric Calorimeter Transducer				5 ORIGINATOR'S REPORT NO. SM-46703				TEST COMPL. DATE MO YR 10 10 64				
7 THIS TEST (SUPERSEDES) (APPROXIMATE) REPORT NO.: 552.74.85.00-07-06-P1				6 TEST TYPE, ETC. Evaluation and Qualification								
8A PART TYPE, SIZE, RATING, LOT, ETC.			9 VENDOR			10 VENDOR PART NO.			11 IND./GOV. STD. NO.			12 TOTAL TESTS
Heat sensing, 200°F max. oper. temp., 5/8 dia x 1 5/8 length, S/N 11931 & 11936, 13.5 mv output for max. heat flux input.						C 1161-A-03						2
13 INTERNAL SPECS ETC. REQ'D TO UTILIZE REPT. ENCL.				SENT WITH REPORT NO.				14 MIL SPECS/STDS REFERENCED IN ISC				
A none								D none				
15A TEST OR ENVIRONMENT	C REF. SPEC.	D SPEC. PARAGRAPH METHOD/CONDITION	E TEST LEVELS, DURATION AND OTHER DETAILS					F NO. TESTS	G PASS	H FAIL	I TOTAL	
1A Acoustical Noise			S/N 11931, 30 minutes random noise, 153.2 db overall SPL, 37.5 to 9600 cps.					1	0			
1A Acceleration			S/N 11931, 7g for 12 minutes in both directions in each axis.					1	0			
1A Random Vibration			S/N 11931, 1 1/2 minutes 0.15 g/cps max. in each axis followed by 16 minutes in each axis at 3 db less.					1	0			
1A Shock			3 sawtooth shocks in each axis, 35g 0-peak, 1 millisecc. S/N 11931					1	0			
1B Humidity			Ten 24 hour cycles, 84° to 160° to 84° F with 95% RH. S/N 11936					1	0			
1 Operational Heat Flux			8 minute exposure to 200°F at heat flux of 3 BTU/ft <sup>2</sup> sec.					2	0			
16 SUMMARY OF REPORT, NATURE OF FAILURES AND CORRECTIVE ACTIONS TAKEN												
<p>This transducer is considered adequate to perform the intended function on the Saturn S4 stage.</p> <p>Photo pages were not microfilmed-poor contrast. Available from originator.</p>												
17 TESTED BEYOND VENDOR CATALOG SPECIFICATIONS												
18 VENDOR INFORMED OF TEST RESULTS												
19 SIGNED												
20 CONTRACTOR												
21 SUPPLEMENTARY CONTRACTOR												

REPRODUCTION OR DISPLAY OF THIS MATERIAL FOR SALES OR PUBLICITY PURPOSES IS PROHIBITED.

FIGURE 11.26 Sample Format of IDEP Environmental Test Data Reports

11.5.5.2 Manufacturer Specifications and Environmental Design and Test Specifications

A survey of manufacturers of typical ground support equipment employed on current rocket vehicle test stands was conducted in preparation of this manual. The response to this survey was limited and did not provide significant information for evaluating the acoustic sensitivity of ground support equipment. However, as the acoustic environments increase for the larger launch and test facilities, and as reliability requirements increase for man-rated systems, it can be expected that more manufacturers will be required to specify equipment compatibility with high intensity noise environments. The imposition of standard Military Environmental Test Specifications as design requirements for equipment will assist in providing information on environmental integrity to the equipment designer.

An example of a typical acoustic test requirement for such a specification is shown in Figure 11.27. Although the test spectrum is not necessarily typical of a low frequency rocket noise spectrum, it provides a reasonable acoustic test environment for many ground support equipment items. This is based on the fact that acoustically induced malfunction will frequently be due to internal resonant responses of the equipment. The test spectra shown in Figure 11.27 encompass the frequency range of internal resonances for most equipment items so that sensitivity to direct acoustic excitation can frequently be established on the basis of these tests. Two important exceptions can occur.

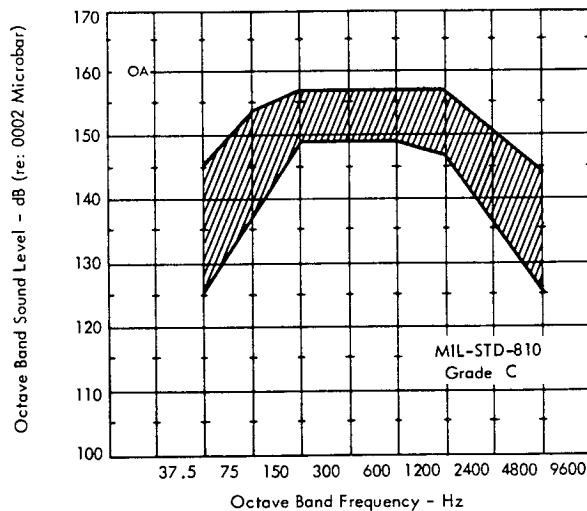


FIGURE 11.27 Typical Example of Standard Acoustic Test Specification for Equipment

- 1) A more accurate simulation of an expected service environment containing intense high frequency energy may be required for evaluation of items (i.e., accelerometers) whose internal resonant responses fall above the range of the standard test specifications

- 2) A better simulation of the low frequency content of rocket noise may be very necessary to properly evaluate the acoustically induced vibration sensitivity of equipment mounted on large low-surface-density mounting structure.

It must be stressed, however, that reliance on a standard test specification is not a replacement for accurately defining the acoustic design environment. Typical acoustic design environments for the Saturn V launch facility are shown on Figure 11.28. (Reference 11.15.) Clearly these expected service environments differ significantly from the standard test spectra shown on Figure 11.27. It is always necessary, therefore, to evaluate the expected equipment response to the real environment before compromising by using a standard environmental test specification.

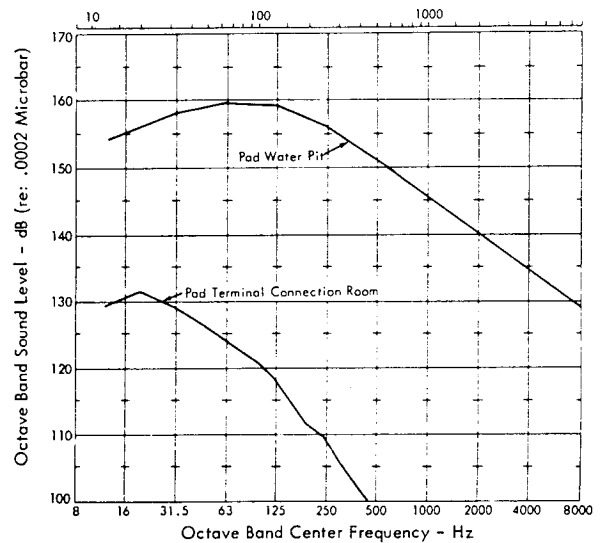


FIGURE 11.28 Typical Acoustic Design Environments for NASA Launch Complex 39, SATURN V

11.5.5.3 Evaluation of Acoustic Sensitivity from Vibration Environment Specifications

Vibration qualification test data for equipment are more commonly available than acoustic test data. This can be helpful in evaluating equipment sensitivity to acoustic excitation for certain types of equipment. For example, equipment which has a heavy, damped enclosure and is capable of withstanding high acceleration levels will tend to be insensitive to direct acoustic excitation. Quantitative estimates of the acoustically induced vibration input for such equipment, mounted on large metal panels, may be estimated by the methods discussed in Section 11.5.3.1. If the acoustically induced vibration levels, estimated for a particular acoustic environment, is well below the known vibration environment capability of the equipment, it is reasonable to assume that the item will withstand this acoustic environment. This is not a safe assumption for equipment with light metal enclosures as shown by the experimental data for the vibro-acoustic response of the ground computer cabinet discussed in Section 11.5.3.2. To emphasize this point, these data have been replotted in Figure 11.29 to show the maximum equipment cabinet

vibration relative to the vibration at the top of the isolated floor for both the vibration test and the acoustic test. Although the acoustic test data cover a limited frequency range, it is clear that the local acoustic response of the cabinet structure exceeds the structurally transmitted vibration response by 10 to 15 dB for the same vibration level at the base of the cabinet.

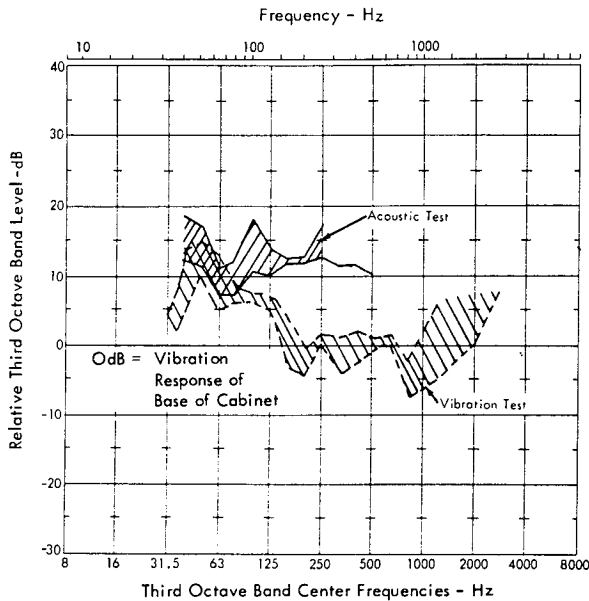


FIGURE 11.29 Maximum Response of Equipment Cabinet Structure Relative to Response at Base for Vibration and Acoustic Tests of a SATURN V Ground Computer Equipment Cabinet

11.6 RECOMMENDED ACOUSTIC ENVIRONMENT CRITERIA FOR EQUIPMENT

Although the available data on acoustic response of ground equipment is relatively limited, the information presented in this chapter is sufficient for establishing a preliminary environmental design criteria for such equipment. Once this criteria is defined, and the ambient acoustic environment near the equipment is determined, the amount of additional acoustic or vibration protection or hardening required can be defined.

Based on the preceding discussion in this chapter, it would be desirable to establish an environmental criteria on the basis of the following three key variables.

- 1) Reliability requirements
- 2) Equipment type
- 3) Mounting or installation configuration

A general requirement for equipment reliability while operating in an acoustic environment would require an analysis of system criticality and system reliability as outlined in Sections 11.3 and 11.4.

11.6.1 CRITERIA FOR RELIABILITY ANALYSIS

In lieu of a general reliability design requirement, the following method is suggested for preliminary design.

- 1) Establish the generic failure rate of the equipment in a laboratory environment. Values for some equipment types are listed in Table 11.2.
- 2) Multiply this failure rate by a factor of 100 to establish an operating failure rate providing the maximum environments listed in Table 11.4 are not exceeded. This factor of 100 is an order of magnitude higher than the factor suggested for ground equipment in Section 11.5.2.1. It is considered a more realistic multiplier for operational acoustic environments near rocket launch or test sites.
- 3) Multiply this failure rate by additional factors as necessary to account for environments other than acoustics.
- 4) If the operating acoustic environment exceeds the levels indicated in Table 11.4, further increase the failure rate by the following factors.

Change in Sound Level Above Design Environments in Table 11.4	Multiply Failure Rate By
5 dB	3
10	10
15	30
20	100

- 5) Using the corrected failure rate estimate the equipment reliability as outlined in Section 11.4.

The additional multiplying factors in Step 4 for sound levels in excess of the following design environments are based on the approximate slope of the curves in Figure 11.6. These show the estimate of failure rate versus sound level for a wide range of equipment.

It must be emphasized that this suggested procedure is a tentative one and will require additional validating data on failure rate of equipment in an acoustic environment.

11.6.2 CRITERIA FOR ACOUSTIC DESIGN ENVIRONMENT

The recommended acoustic design environments for ground support equipment are given in Table 11.4. The sound levels specified are the maximum octave band levels in the frequency range 200 - 2000 Hz or in the octave band closest to the internal resonance frequency of the equipment. These represent conservative estimates of maximum design environments for ground equipment with normal malfunction or failure rates.

For equipment mounted inside a typical thin gauge equipment cabinet, the levels specified in the first column may be assumed to be the design environments on the outside

surface of the equipment cabinet.

For equipment mounted inside a blast proof enclosure or similar thick metal enclosure with appreciable damping, the allowable external design environments outside the enclosure, specified in the second column, are 10 dB higher, based on a nominal 10 dB noise reduction for such an enclosure.

The design environments listed in Table 11.4 must be applied with discretion. For example, the levels suggested for pneumatic and hydraulic equipment are conservative estimates based on the limited data available. In many cases, equipment components in this category can be exposed without malfunction to higher levels. However, such items should be examined on an individual basis to establish more accurate design environments.

TABLE 11.4  
RECOMMENDED ACOUSTIC DESIGN ENVIRONMENT FOR GROUND  
SUPPORT EQUIPMENT

(Maximum Octave Band Sound Levels in the 200 - 2000 Hz  
frequency range or at the frequency of internal  
equipment resonances - dB re: 0.0002 Microbar)

TYPE OF EQUIPMENT	MOUNTING	
	Cabinet or Shock Mtd.	Rigid Mtg. or Blast Proof Enclosure
<u>Electronic Equipment</u>		
Accelerometers		
Isolated Bending Type	—	140
Compression Type		145
Isolated Compression Type		155
Heavy Duty Relays, Switches	130	140
Sensitive Relays Potentiometers Commutators	120	130
Solid State Components Resistors Capacitors	145	155
Vacuum Tubes Signal < 10 mv Signal > 10 mv	100 120	110 130
Laboratory Electronic Equipment not Covered Above	100	110
Ruggedized Electronic Equipment not Covered Above	120	130
<u>Pneumatic, Hydraulic Equipment</u>		
Low Pressure Components (< 10 psi)	130	140
High Pressure Components (> 10 psi)	140-150	150-160
Pyrotechnic Components	—	150-160

11.7 RESPONSE OF EQUIPMENT TO OVERPRESSURE FROM BLAST AND SONIC BOOM

11.7.1 INTRODUCTION

Exposed ground equipment near rocket launch and test stands is subject to damage from blast by an explosion of the propellants. Facilities located near aircraft flight research centers such as Edwards Air Force Base are also subject to sonic booms loads generated by supersonic aircraft.

Peak overpressures from these two phenomena can range from .001 psi (2 psf) for normal sonic boom overpressures to over 100 psi near a propellant explosion. The effects of such loads and criteria for protective design will clearly vary considerably for such a wide range of overpressures. Due to the lack of definitive data on transient overpressure effects on equipment, it is necessary to use analytical or semi-empirical means for evaluation of the problem.

Effects of blast or sonic overpressures may be categorized as follows:

- 1) Overpressure loads on secondary mounting structure which supports exposed equipment.
- 2) Transient overpressure effects on the equipment itself.
- 3) Transient acceleration loads on the equipment or its mounting structure due to the dynamic response of primary building structure induced by the overpressures.

Each of these effects is briefly analyzed in the following.

11.7.2 OVERPRESSURE LOADS ON EQUIPMENT MOUNTING STRUCTURE

For exposed equipment near a rocket launch or test stand, potential blast pressures may far exceed the damage limits for the equipment itself. If a blast-proof protective housing cannot be provided for the equipment, it must be considered as expendable. However, assuming the expected blast damage will not destroy the basic primary structure on which the equipment is mounted, it may be necessary to insure that the equipment is not torn loose from its mounting to become a missile. This would be particularly important for exposed equipment at a static test site located near inhabited areas or secondary propellant storage tanks. In this case, the equipment mounting structure should be designed to withstand the blast loads. The normal blast load analysis for building structure, covered in Chapter 8, is used with some simplifications for analysis of this problem.

11.7.2.1 Force of Blast Overpressure and Dynamic Pressure on Exposed Equipment

Considering the wide variety of possible configurations of an exposed equipment package, a simple cube can be used as a model to represent the equipment. The blast load on the equipment is the sum of the diffraction load on the

front face due to the incident overpressure and the net drag load due to the dynamic pressure of the blast wind.

Diffraction Load

The duration of the diffraction load will ordinarily be very short relative to the duration of the positive phase of the overpressure or dynamic pressure. In this case, for a cubical obstacle, the diffraction load can be assumed to consist of a triangular pulse with a peak pressure equal to the peak reflected overpressure,  $P_{ro}$ .

The effective duration  $t_c$  of the triangular pulse on the cube with one side face on to the blast front can be shown to be approximately

$$t_c = 3a/C_{refl} \tag{11.11}$$

where  $a$  = 1/2 the width or the full height of the obstacle, whichever is smaller,

$C_{refl}$  = velocity of sound in reflected overpressure region (see Chapter 8),

and  $t_c$  is much less than the blast duration.

Figure 11.30 shows the value of  $P_{ro}$  and  $t_c/a$  versus scaled distance  $R/W_T^{1/3}$  for a cube with side  $2a$ . The discussion in Chapter 3 on response to a triangular load may be used to estimate the response to this diffraction load. As an example, consider the following.

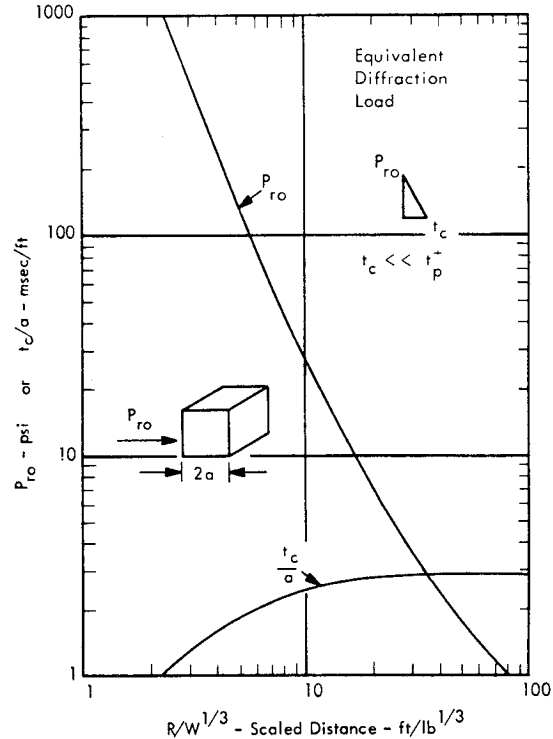


FIGURE 11.30 Peak Reflected Overpressure and Effective Duration for Diffraction Load on a Cube

**Example**

Equipment "Cube"	- a	= 1/2 ft
Equipment Weight	- W	= 6.1 lb
Mounting Structure Stiffness	- k	= 10 <sup>5</sup> lb/in.
Resonant Frequency of Package on Mounting Structure	- f <sub>o</sub>	= 3.13√k/W 400 Hz
Location of Equipment	- R	= 1000 ft
Equivalent TNT Weight of Propellant	- W <sub>T</sub>	= 10 <sup>6</sup> lb
Scaled Distance	- R/W <sub>T</sub> <sup>1/3</sup>	= 10 lb/ft <sup>1/3</sup>
Peak Diffraction Load (Figure 11.30)	- P <sub>ro</sub> (2a) <sup>2</sup>	= 28 psi x 1 x 144 = 4030 lb
Effective Duration of Load(Figure 11.30)	- t <sub>c</sub>	= 1/2 x 2.4 = 1.2 msec
Resonant Frequency x Duration	- f <sub>o</sub> t <sub>c</sub>	= 0.48
Dynamic Load Factor for Triangular Pulse	- $\frac{x_{max}}{x_s}$	= 1.17
Static Equivalent of Diffraction Load	- 1.17 x 4030	= 4550 lb
Peak Dynamic Deflection	- x <sub>max</sub>	= 4550/10 <sup>5</sup> = 0.045 in.
Time of Maximum Deflection	- t <sub>max</sub>	= .44/f <sub>o</sub> ≈ 1.1 msec

Drag Load

The drag load may be assumed to be a triangular pulse with a peak value given by

$$F = q_{so} C_D A \tag{11.12}$$

- where  $q_{so}$  = Peak Dynamic Pressure  
 $C_D$  = Drag Coefficient  
 $A$  = Frontal Area

The estimated maximum peak dynamic pressure for propellant explosions, discussed in Chapter 6, is shown in Figure 11.31 as a function of scaled distance. The drag coefficient will vary with the exact shape of the equipment. A value of 1.3 is typical for a rectangular structure.

The effective duration  $t_{qe}$  of the actual dynamic pressure load is also shown in Figure 11.31, normalized by the cube root of the equivalent TNT yield in pounds. For the same example considered earlier, the maximum dynamic response to this load can be estimated as follows.

Scaled Distance	R/W <sub>T</sub> <sup>1/3</sup>	= 10 lb/ft <sup>1/3</sup>
TNT Equivalent	W <sub>T</sub>	= 10 <sup>6</sup> lb
Peak Dynamic Pressure	q <sub>so</sub>	= 1.9 psi

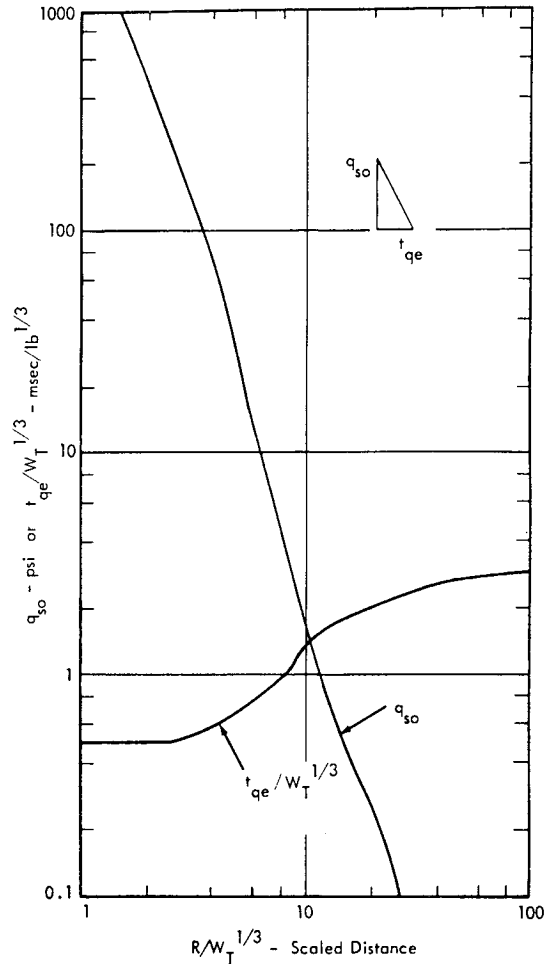


FIGURE 11.31 Peak Dynamic Pressure and Effective Duration for Drag Load on a Cube

Scaled Effective Duration	t <sub>qe</sub> /W <sub>T</sub> <sup>1/3</sup>	= 1.4 msec/lb <sup>1/3</sup>
Effective Duration	t <sub>qe</sub>	= 140 msec
Resonant Frequency x Duration	f <sub>o</sub> t <sub>qe</sub>	= 56
Dynamic Load Factor		≈ 2
Static Equivalent of Drag Load		= 2 x 1.9 x 1.3 x 144 = 710 lbs

In this case, the dragload is much less than the diffraction load and may be neglected. For smaller equipment packages closer to the blast, the drag load would frequently be predominant. The methods developed in this section for computing the blast loads on small exposed equipment packages are considered suitable for design purposes. While approximate, they are based on simplified versions of standard blast load analysis methods discussed in Chapter 8. Full advantage of plastic design concepts should be used where necessary to avoid an overly conservative design.



11.7.3 TRANSIENT OVERPRESSURE EFFECTS ON EQUIPMENT

For equipment which must function during an explosion or for which internal damage must be prevented, an approximate criteria for direct effects of transient overpressure can be estimated based on the acoustic design criteria in Section 11.6. This extrapolation of acoustic criteria to blast criteria is necessary due to the lack of any data on direct effects of overpressure on equipment.

It is assumed that malfunction or failure of equipment under acoustic excitation is caused by resonant responses. The peak value of the response  $x_n$  for a single resonance at a modal frequency  $f_n$  can be defined by;

$$x_n = 3\beta_n \left[ \frac{\pi}{\sqrt{2}} P_{ob}^2 \cdot Q \right]^{1/2} \quad (11.13)$$

where  $\beta_n$  = modal response parameter relating the static value of the response parameter  $x_n$  (i.e.-stress, acceleration, etc.) to pressure.

$P_{ob}$  = rms pressure in the octave band centered around the resonant frequency  $f_n$

$Q$  = dynamic magnification factor.

The factor of 3 in the above expression accounts approximately for the effective peak value of the random response. Fatigue effects are not considered.

For excitation by a blast wave, the peak response  $x'_n$  in the same mode is obtained from a shock response spectrum  $S$  in the form

$$x'_n = \beta_n P_{ro} S(f_n t_{pe}) \quad (11.14)$$

where  $\beta_n$  = the same response parameter as above

$P_{ro}$  = peak reflected overpressure

$S(f_n t_{pe})$  = Shock Response Spectrum - a function of the modal frequency  $f_n$  times the effective blast duration  $t_{pe}$ .

If it is further assumed that the same degree of equipment malfunction or failure occurs for the same peak response, for both acoustic and blast overpressures, then the peak reflected overpressure  $P_{ro}$  which will cause the same response as the acoustic environment is given by

$$P_{ro} = \frac{3 P_{ob} \left[ \frac{\pi Q}{\sqrt{2}} \right]^{1/2}}{S(f_n t_{pe})} \quad (11.15)$$

For blast pulse durations ranging from 10 to 500 milliseconds and internal resonant frequencies of equipment ranging from 200 to 2,000 Hz, the shock spectrum parameter for the triangular pulse will range from 1.77 to 2. Based on a conservative value of 2, the ratio of peak reflected blast overpressure to rms octave band acoustic pressure for equal peak response is

$$\frac{P_{ro}}{P_{ob}} = \frac{3}{2} \left[ \frac{\pi}{\sqrt{2}} Q \right]^{1/2} \approx 2.5 \sqrt{Q} \quad (11.16)$$

A range of incident blast overpressures for malfunction or damage levels of equipment based on the above expression is listed in Table 11.5.

These estimated overpressure damage levels for equipment can provide a guide for blast overpressure protection requirements for sensitive ground support equipment which is not considered expendable in a blast environment.

11.7.4 ACCELERATION LOADS ON EQUIPMENT DUE TO BLAST RESPONSE OF MOUNTING STRUCTURE

The last effect of blast loads on equipment to be considered is the acceleration load on equipment induced by blast response of its mounting structure. Consider the example of a rigid equipment package mounted to a large panel exposed face-on to a blast load as illustrated in Figure 11.32. The overall blast load on the panel is represented by the superposition of two equivalent triangular pulses as shown in Figure 11.32. In this case, the back of the plate is assumed enclosed by a sealed cabinet so that the incident overpressure is effective for its full duration.

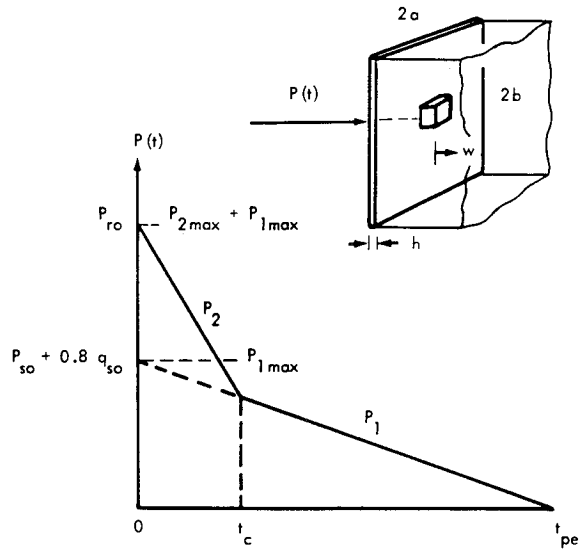


FIGURE 11.32 Approximate Time History of Blast Load on Panel Mounted Equipment

The first pulse, which excludes the diffraction load due to the reflected overpressure, has a peak pressure  $P_{1max}$  equal to the sum of the peak incident overpressure  $P_{so}$  plus 0.8 times the peak dynamic pressure  $q_{so}$ . The duration is equal to the effective positive phase duration,  $t_{pe}$ , of the incident overpressure wave.

TABLE 11.5  
ESTIMATED BLAST OVERPRESSURE CRITERIA FOR EQUIPMENT

	Octave Band Level at Equipment Resonance dB re: 0.0002 microbar	Equivalent Incident Blast Overpressure psi	
		Q = 5	25
MALFUNCTION (Sensitive Equipment)	130	.01	.023
DAMAGE (Sensitive Equipment) / MALFUNCTION (Rugged Equipment)	150	.11	.23
DAMAGE (Rugged Equipment)	170	1.0	2.2
	190	8.0	15.0

The second pulse which accounts for the diffraction load has a peak pressure  $P_{2max}$  equal to the peak reflected overpressure  $P_o$  minus  $P_{1max}$ . The duration, for side a less than side  $b$ , is equal to  $t_c = 6a/c_{ref}$ . These four quantities are shown in Figure 11.33. The clearing time  $t_c$  is given for a square plate with  $a = 1$  foot (panel width = 2 feet). The effective duration  $t_{pe}$ , scaled by the cube root of the TNT equivalent  $W_T$ , is also shown. The response of the mounting panel to these two triangular pulses can be determined from the shock spectra for a triangular pulse given in Chapter 3 in terms of the peak dynamic displacement  $x_{max}$  relative to the static displacement  $x_s$ . The resonant frequencies of the mounting panel with its equipment and the panel stiffness can be estimated by the methods presented in Chapter 3.

As an example, consider the following case of a 60-pound equipment package centrally mounted on a 40-inch x 40-inch x 1/2-inch steel plate located at the same position considered in the example in Section 11.7.3.

EXAMPLE

Static Stiffness at Center -  $k_p = 33.4$  psi/lb  
 Resonance Frequency of Bare Panel -  $f_{1,1} = 60$  Hz  
 Resonance Frequency -  $f_o = f_{1,1} \sqrt{1 + \frac{4(\text{Equip. Wt.})}{(\text{Panel Wt.})}} = 42$  Hz  
 Blast Load:  $P_{1max} = 11.5$  psi  $t_{pe} = 170$  msec  
 (From Figure 11.33)  $P_{2max} = 17.5$  psi  $t_c = 4$  msec

Dynamic Response to  $P_{1max}$  (See Chapter 3)

Resonance Frequency x Duration -  $f_o t_{pe} = 7.15$   
 Dynamic Mag. Factor -  $x_{max}/x_s = 1.97$   
 Static Deflection -  $x_s = P_{1max}/k_p = 0.344$  in.  
 Max. Dynamic Deflection -  $x_{max} = 0.68$  in.  
 Time of Max. Deflection -  $f_o t_{max} = 0.50$

(Max. occurs during pulse)

∴ Max. Acceleration -  $\ddot{x}_{max} \approx \frac{(2\pi f_o)^2 x_s}{g} = 62$  g  
 (For  $f_o t_{pe} \gg 1$ )

Dynamic Response to  $P_{2max}$

Resonance Frequency x Duration -  $f_o t_c = 0.168$   
 Dynamic Mag. Factor -  $x_{max}/x_s = 0.53$   
 Static Deflection -  $x_s = P_{2max}/k_p = 0.52$  in.  
 Max. Dynamic Deflection -  $x_{max} = 0.28$  in.  
 Time of Max. Deflection -  $f_o t_{max} = 0.31$

(Max. occurs after pulse)

∴ Max. Acceleration -  $\ddot{x}_{max} = \frac{(2\pi f_o)^2 x_{max}}{g} = 50$  g

For this case, a conservative acceleration load could be defined as the sum of the peak responses to each input. However, in this case, the time of occurrence for each peak is such that coincidence of the peak responses will not occur. A better approximation to the net peak response is obtained if it is taken to be the square root of the sum of the squares of the peak response for each input. Thus, for this example, the equipment would experience a transient peak acceleration of about 80 g's. Note that this also represents an acceleration load on the equipment attachment points which is in addition to any blast loading on the equipment container itself, discussed in Section 11.7.2. A similar analysis can be made for other cases to define transient acceleration or shock loads on panel-mounted equipment.

Application of this type of loading to ground equipment near a potential propellant explosion will depend on the design philosophy of preventing damage to the equipment or simply preventing failure of its attachment structure. For the latter case, a more economical design will be possible by allowing for plastic deformation of the attachment structure. In this case, the more detailed blast response methods outlined in Chapter 8 should be used.

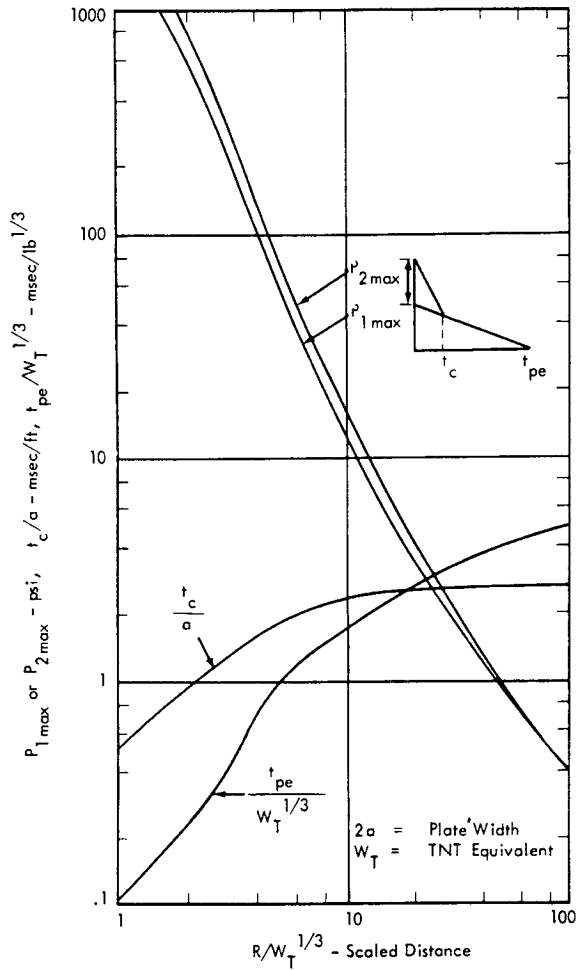


FIGURE 11.33 Estimated Maximum Load Parameters for Propellant Blast Load (Face-On) for a Square Equipment Mounting Plate

11.7.5 ENVIRONMENTAL EFFECTS ON EQUIPMENT DUE TO SONIC BOOMS

11.7.5.1 Direct Effects

The upper range of incident overpressures associated with sonic booms from supersonic aircraft is generally less than 10 lbs/ft<sup>2</sup> (.07 psi). The dynamic magnification factor for response of a single degree of freedom system by a sonic boom N wave has a maximum value between 1.8 and 2 for the parameter  $f_o T = 1/2$  (Resonance Frequency) x Duration of N wave)  $\geq 2.5$ . Since the duration will range from .08 to 0.4 seconds, and internal equipment resonance frequencies will usually fall above 100 Hz,  $f_o T$  will exceed 2.5 and a value of 2 for the dynamic magnification is reasonable for consideration of direct effects of the N wave on equipment. From equation 11.16, it can be shown that the peak responses of equipment resonances to a sonic boom can be expected to be no more than comparable momentary peak responses caused by acoustic excitation having an octave

band sound level of 132 to 138 dB (Q = 5 - 25). This falls in the range of possible malfunction of sensitive equipment but below the range of any probable damage.

11.7.5.2 Indirect Effects

More significant effects are expected for sonic boom excitation due to building responses. These are considered in more detail in Chapter 8. It will be sufficient here to point out one of the major problems associated with equipment, or more specifically, mechanical or electrical systems mounted to building walls and ceilings.

Vibration of a roof or wall, which is caused by sonic boom loading, will impose acceleration or inertia loads on equipment attachment points.

The magnitude of such acceleration loads may be estimated as follows:

- 1) Assume the total static design load on the roof is 75 lbs/ft<sup>2</sup>.
- 2) Assume design practice requires that the static deflection to the load not exceed 1/360th of the roof span.
- 3) For a peak normal incident pressure of 10 lb/ft<sup>2</sup>, a reflection factor of 2, and a dynamic magnification factor of 2 (the normal range will be from about 1.6 to 2.1 for typical building resonance frequencies), the peak dynamic load would result in  $2 \times 2 \times 10/75$  or 53 percent of the peak deflection under the design static load, assuming only the fundamental mode of the roof responds significantly.
- 4) The fundamental resonance can be estimated by assuming the roof has just the required stiffness to pass the static load design criteria. The fundamental resonance of the roof is then given by: (See Chapter 3)

$$f_{1,1} = 3.93 \sqrt{\frac{\beta}{b} (1 + W_e/W)} \quad (11.17)$$

- where
- $\beta$  = ratio of span to center deflection
  - $b$  = shortest span - in.
  - $W_e$  = external static design load - lb.
  - $W$  = weight of roof plus dead load - lb.

For  $\beta = 360$ ,  $b = 300$  inches,  $W_e = 35$  lb/ft<sup>2</sup>,  $W = 40$  lbs/ft<sup>2</sup>, the fundamental would be

$$f_{1,1} = 5.9 \text{ Hz.}$$

- 5) The maximum incremental static displacement at the center of the panel which would occur for an additional static load equal to the peak sonic boom reflected overpressure would be

$$x_s = \frac{2 \times 10 \times 300}{75 \times 360} = 0.22 \text{ in.}$$

- 6) The maximum acceleration of the center of the panel, for response to a sonic boom has been shown to be

$$\frac{\ddot{x}_{\max}}{g} = \frac{2\pi f_o x_s}{g T} \sqrt{1 + (2\pi f_o T)^2} \text{ g's} \quad (11.18)$$

where  $f_o = f_{1,1} = 5.9 \text{ Hz.}$   
 $T = 1/2 \text{ duration of N wave - sec.}$

For  $T = 0.1 \text{ sec.}$ , this gives a value for the peak acceleration at the center of the roof of  $0.84 \text{ g.}$  Allowing for the effect of response in the higher modes, a reasonable design estimate for the added load on equipment mounted at the center of the roof is  $1 \text{ g.}$

Thus, the net load for equipment mounted near the center of the roof would be at least  $2 \text{ g.}$  This would normally be within the design margin for equipment mounting structure. A more detailed analysis would be required, however, for buildings routinely exposed to such high sonic boom loads. For inhabited buildings, it would be desirable to isolate any light fixtures or other roof-supported equipment to reduce the startling effects of motion induced by the sonic boom.

## 11.8 DESIGN METHODS FOR ENVIRONMENTAL PROTECTION OF EQUIPMENT

The final aspect of effect of noise on equipment to be considered is the application of various environmental protection techniques. This is the logical final phase in the environmental design process once the environment at the equipment location and its potential effects have been evaluated.

If a requirement for additional environmental protection is indicated to insure overall reliability of a ground system, the designer may consider one or more of the following steps.

- Selection of more rugged components
- Protective packaging design employing:
  - Damping treatment of component mounting structure
  - Protective potting of components
  - Acoustic isolation of equipment
  - Vibration isolation of equipment

Each of these steps is reviewed in the following sections. No attempt is made to present a complete review of equipment design. The reader is referred to References 11.8 and 11.10 and 11.16 for additional information.

### 11.8.1 SELECTION OF COMPONENTS

As indicated earlier in this chapter, the sensitivity of a given type of component to acoustic excitation varies appreciably. For example, relays can have a malfunction threshold at sound pressure levels ranging from 130 to more than 170 dB, depending on the particular type, function, and construction. While a smaller range of malfunction thresholds may be expected for relays which are designed to perform the same function, nevertheless appreciable variations in acoustic sensitivity may still be expected. What then, are the criteria for selection of the most rugged type of component for a given functional requirement?

#### Simplicity of Design

Clearly, the simpler the design, in particular, the fewer the parts, the higher is the inherent reliability of the component. The exception to this rule occurs when complexity is added to provide redundant or alternate functional modes for the component, thus increasing its reliability. (See Section 11.4).

#### Absence of Moving Parts

Perhaps more significant, in the case of resistance to acoustic excitation, is the number and type of moving parts. For example, a solid state electronic switch will tend to be much more resistant to acoustic noise than a functionally comparable mechanical relay. This is even more dramatically true in the case of electronic equipment employing transistors in place of vacuum tubes. In fact, given the current state of the art of solid state circuitry, it would seldom be necessary or desirable to employ vacuum tube type electronic equipment in areas close to rocket launch or test sites when noise levels around the equipment would exceed 110 dB.

#### Size and Surface Weight Density of Equipment

All other things being equal, the smaller the volume and the higher the weight per unit surface area of a given type of equipment, the higher the threshold of acoustic sensitivity. This may be explained by the following simple qualitative analysis.

In the frequency range of equipment resonances, the acoustic pressure spectrum will decrease roughly inversely with the first to second power of frequency or

$$P(f) \propto f^{-m}$$

$$\text{where } m = 1 \rightarrow 2.$$

The vibro-acoustic coupling factor,  $J(f)$  or ratio of effective acoustic pressure to actual acoustic pressure can increase or decrease with frequency depending on the mounting of the equipment and its size relative to the acoustic wavelength. Thus, let

$$J(f) \propto f^n,$$

where  $-1 < n < +1$ .

Malfunction or failure of the equipment may be assumed to occur at a characteristic resonance  $f_0$  which, for similar shapes, will vary roughly inversely as a characteristic dimension  $L$  of the equipment, or

$$f_0 \propto L^{-1}$$

Consider first that malfunction occurs due to an excessive acceleration response at this resonance frequency.

The acceleration response,  $A(f_0)$  will vary as

$$A(f_0) \propto P(f_0) \cdot J(f_0)/w$$

where  $w$  = surface weight density of equipment.

Thus, from the above relationships

$$A(f) \propto L^r/w$$

where  $r = m - n = 0 \rightarrow 3$ .

Thus, at one extreme the acceleration response would tend to be independent of size and vary inversely as the surface weight and, at the other extreme, the response would vary directly as the third power of size and inversely as the surface weight.

Now assume that the malfunction occurs due to an excessive displacement  $D(f_0)$  at the characteristic resonance. In this case the response will vary as

$$D(f_0) \propto A(f_0)/f_0^2$$

$$\text{or } D(f_0) \propto L^S/w$$

where  $S = 2 \rightarrow 5$ .

Thus, the displacement response will vary from the second to the fifth power of the size and inversely as the surface weight.

Thus the inherent variation in acoustic response magnitude with size and weight of an equipment package is clearly demonstrated and shows that the smaller and more densely packaged the equipment, the lower will be its acoustic response.

#### Preferred Components

Lists of preferred components are published by various government centers for use by equipment designers. Selection of components from such lists takes advantage of the previous experience accumulated with their satisfactory use. Providing their application to new equipment will involve similar acoustic environments, the element of "proven experience" is a significant advantage. However,

such "preferred components" lists are subject to two shortcomings. 1) They can easily become outdated as new components or modifications are used. 2) They seldom provide sufficient information for evaluation of equipment sensitivity in severe acoustic environments.

#### Optimum Mechanical Design

For equipment subject to malfunction or damage induced by acoustically generated vibration, a number of general design guidelines exist for carrying out good mechanical design practice. (References 11.16, 11.17).

Some of these guidelines are summarized below in the form of a check-list which may be used for selecting equipment which will tend to be insensitive to acoustically-induced vibration.

- Minimum use of cantilevered mounting for parts.
- Use of chassis-clamps for wire lead-connected components larger than about 0.4 in. in diameter.
- Wire lead connections made to minimize fatigue failure (e.g., short leads with some slack plus insulation covering to provide damping).
- Internal and external wiring laced into a cable and secured to chassis at frequent intervals to prevent conductor vibration fatigue.
- Use of close-fitting alignment pins or guides to bear shock and vibration loads between chassis, assemblies and enclosures.
- Heavier parts located as close as possible to load bearing structure.
- Maximum rigidity of mounting chassis without excessive weight.
- Adequate reinforcement at corners of mounting structure and at other stress concentration points.
- Proper bend radii of sheet metal parts.
- Minimum unsupported spans of circuit cards.
- Static balance of rotating or pivoting parts.
- Minimum use of large unsupported cabinet walls for component mounting.
- Proper choice and application of shock mounts to achieve desired isolation with minimum cross-coupling between modes of vibration.
- Adequate "rattle" space to avoid shock loads.

#### 11.8.2 PROTECTIVE PACKAGING DESIGN

In addition to the general guidelines for low sensitivity to vibration given in the preceding check-off list, more

specific protection design techniques can be employed which are particularly suitable for reducing sensitivity of equipment to acoustic excitation. These techniques have been discussed in general conceptual form in Chapter 5. Specific examples of the application of these techniques for protective packaging design will be considered in this section.

Optimum choice of any given packaging technique can best be illustrated by reviewing again the multiple paths for vibro-acoustic excitation of equipment. This is illustrated in Figure 11.34. The transmission of vibro-acoustic energy through the multiple paths illustrated can be reduced by:

- Damping treatment of equipment mounting structure
- Protective potting of components
- Acoustic isolation of equipment
- Vibration isolation of equipment

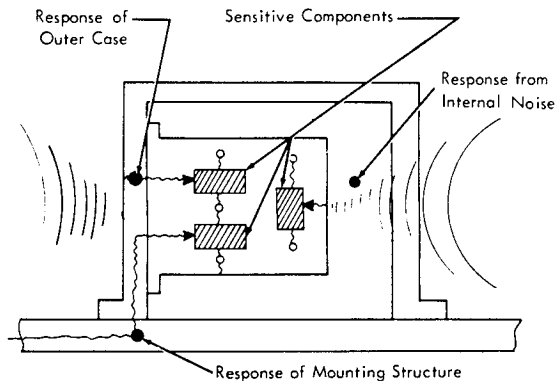


FIGURE 11.34 Structural and Acoustic Paths for Vibro-Acoustic Excitation of Equipment Components

Note that these four steps are not listed in the logical sequence of a source-transmission path-receiver concept. Rather they are given in an approximate order of maximum effectiveness for application to existing equipment. The logical order for new facilities under design might very well put the last two on top of the list.

#### 11.8.2.1 Damping Treatment of Equipment Mounting Structure

As discussed in Chapter 3, the maximum response of a single degree of freedom system to random excitation, such as noise from rocket engines, varies directly as the square root of the dynamic magnification factor  $Q$ . Thus any method of fabrication or assembly of equipment structure which reduces the " $Q$ ", by increasing damping, will tend to reduce the dynamic environment for internal components. Exceptions to this rule can occur for discrete resonant modes of a structural assembly when application of damping alters the dynamic response character-

istics in such a way as to increase the response level at certain frequencies. Such a situation is illustrated in Figure 11.35 which shows a comparison of the measured transmissibilities for a damped and undamped structural chassis (Reference 11.18). While the damped chassis has a much lower overall transmissibility, (i.e.-ratio of response acceleration to input acceleration), higher responses do occur, with damping, at frequencies below about 120 Hz and in the range of 550-720 Hz. In general, however, such situations can be easily remedied and do not compromise the advantages of incorporating damping in structural design of equipment packages.

Damping treatment for protective packaging of equipment may be grouped into two broad categories: 1) treatment designed as an integral part of the structure, and 2) externally applied treatment.

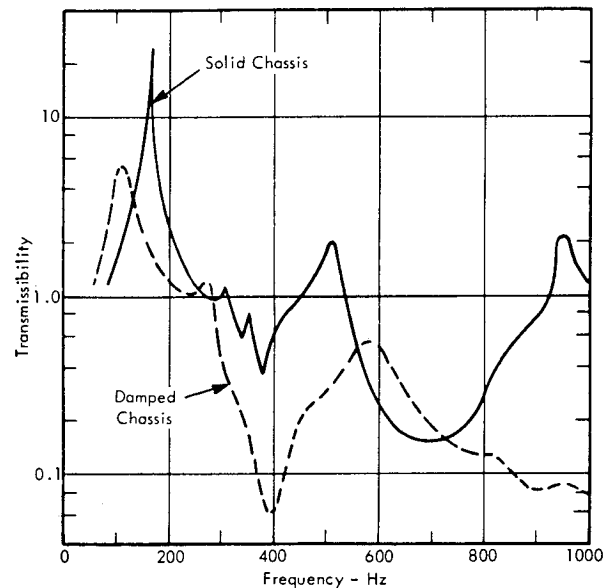


FIGURE 11.35 Transmissibility Curves for Typical Solid and Viscoelastic-Damped Chassis. (From Ref. 11.18)

#### Integrated Damping Treatment

Design techniques for incorporating damping within a structural configuration may range from modifications of conventional metal chassis fabrication techniques to the use of specially designed viscoelastic-damped laminated panels. Typical values for dynamic magnification factors for different types of construction can be specified, as shown in Table 11.6. This table provides an approximate degree of improvement in damping (lower  $Q$ ) that can be expected in changing from one structural concept to another. It must be emphasized, however, that variations on the actual values for  $Q$  of  $\pm 100$  percent may be expected for different models of the same basic structural

concept. For conventional fabrication techniques, the use of bolted joints generally offers the highest potential damping. The damping is due to coulomb friction at the joints and damping due to air-pumping between surfaces of the unbolted sections. (Reference 11.19). It has also been shown that the use of lubricants or thin viscoelastic films on the joints can be used to increase joint damping by a factor of 2 to 4 (See Chapter 9).

The use of high-strength structural adhesives employing various thermoplastic and thermosetting polymeric resins provides an efficient fabrication technique which offers damping capability roughly comparable to bolted joints. The information on damping characteristics of such materials discussed in Chapter 9, indicates that available structural adhesive materials which have the required high shear and elastic strength tend to have a damping loss factor of the order of 0.1 (Reference 11.8, 11.19).

TABLE 11.6

TYPICAL VALUES OF DYNAMIC MAGNIFICATION FACTORS FOR VARIOUS TYPES OF STRUCTURAL FABRICATION

(Data from Reference 11.16, 11.18)

Method of Construction	Typical Q
One-piece metal structure	50
Welded assembly	24
Riveted assembly	12.5
Bolted assembly	10
Adhesively bonded metal structure	8
Viscoelastic-damped laminated structure	5

The highest damping capability that can be built-in to structural materials is achieved with laminated or sandwich panels employing relatively low-strength, high-loss factor viscoelastic materials. Loss factors of the order of 1.0 are typical for such materials.

An example of improved damping that can be achieved with such materials is shown in Figure 11.36. This figure illustrates measured transmissibilities for a basic chassis design that was fabricated by three different methods ranging from solid construction through simple 2-layer viscoelastic damped panels to 2-layer damped panels with additional viscoelastic damping provided at corner joints (Ref. 11.18). Maximum transmissibilities were reduced from about 15 for the solid construction to 2 for the damped-panel with damped-corner construction.

In the succeeding discussion in this section, it will be convenient to consider the effectiveness of various types of damping treatment in terms of the combined (or specimen) loss factor,  $\eta$ , of the assembly. This loss factor is essentially equal to the reciprocal of the dynamic magnification factor,  $Q$ , and depends on the damping and elastic properties of the materials used in the assembly as well as its geometry.

The same concept of sandwich or laminated construction can also be applied to component circuit boards. A typical example of the results of such an application is illustrated in Figure 11.37. This shows a comparison between the dynamic response of a solid circuit board and a damped circuit board consisting of a layer of viscoelastic shear-damping material bonded to the underside of a conventional circuit board and constrained on the outside by a thin fiberglass sheet (Reference 11.18). The use of integrated damping in this case, shows a reduction in peak transmissibility from over 40 without damping to about 4 with damping treatment.

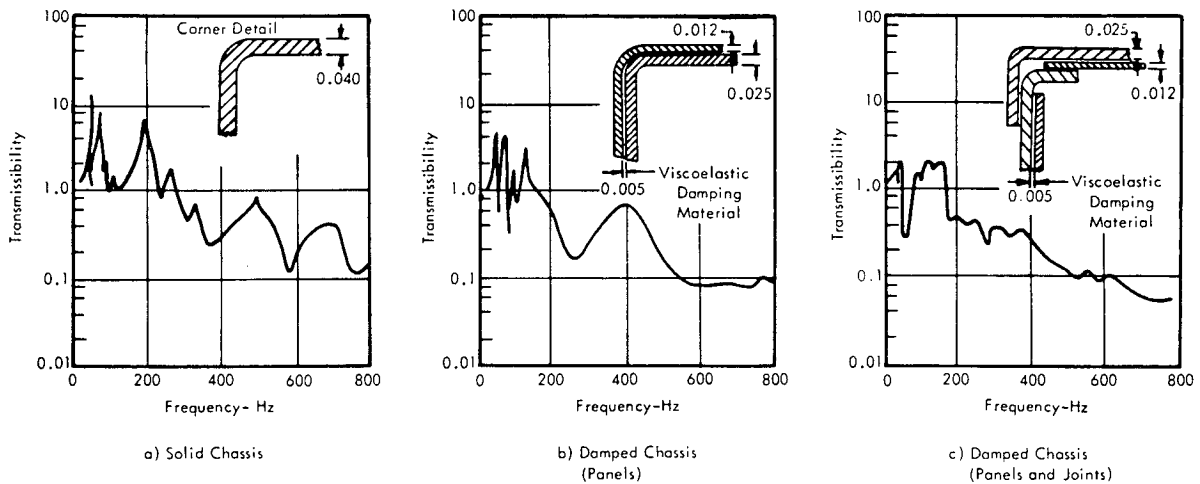


FIGURE 11.36 Transmissibility Curves for Solid and Viscoelastic Damped Box Chasses Loaded with Multiple Mass Elements to Simulate Components (From Ruzicka, Reference 11.18)

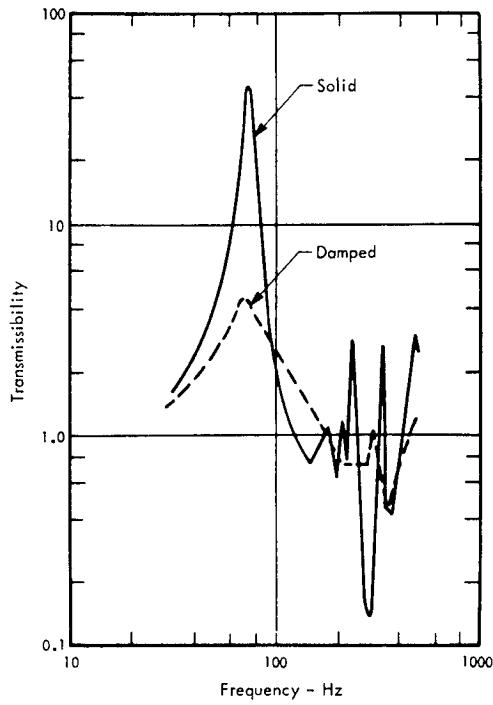


FIGURE 11.37 Transmissibility Curve for Solid and Viscoelastically Damped Circuit Boards (From Ruzicka, Reference 11.18)

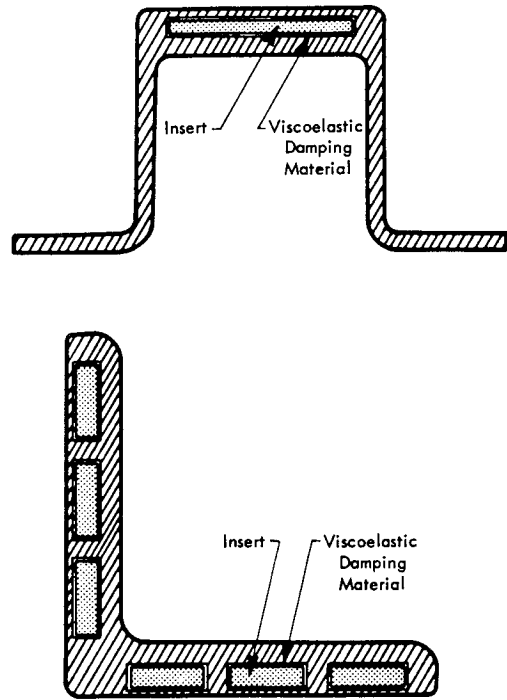


FIGURE 11.39 Cross Sections of Cell-Insert Damped Structural Shapes (From Reference 11.18)

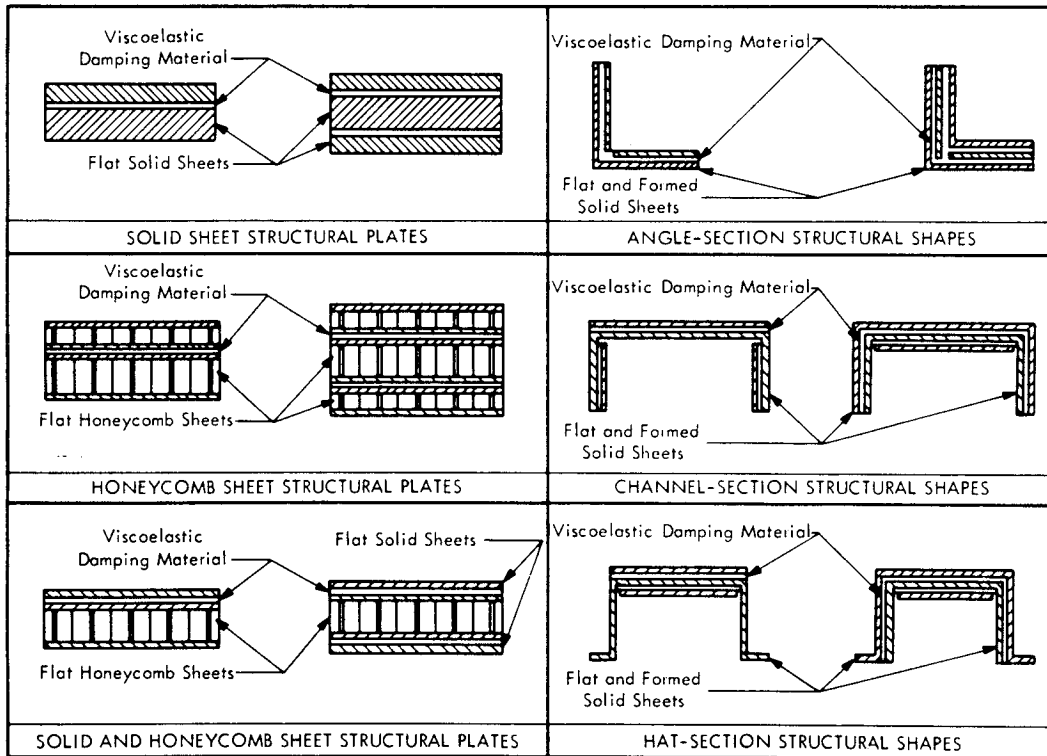


FIGURE 11.38 Cross Section of Typical Viscoelastic Shear-Damped Structural Plates and Shapes. (From Ruzicka, Reference 11.18)



The application of integrated damping treatment to the fabrication of new equipment structural assemblies may be accomplished by using commercially available materials or by custom design and fabrication. Some of the types of commercially available structural shapes, which incorporate internal damping treatment, are illustrated in Figures 11.38 and 11.39. These illustrate fabricated structural materials consisting of

- Laminated structural plates
- Honeycomb plates, laminated or with external solid plates
- Formed laminated structural shapes
- Formed structural shapes with damping inserts

In each of the structural assemblies illustrated, damping is achieved primarily by dissipation of thermal energy within the viscoelastic damping materials in shear, as the result of mechanical vibration of the structure.

The design and fabrication of such structure involves the following key steps:

- Selection of an optimum structural configuration to achieve the desired damping characteristics and structural strength (See Chap. 9).
- Selection of suitable viscoelastic damping material which has the required shear loss factor  $\beta$  and shear storage modulus,  $G'$  (See Chapter 9 for review of applicable viscoelastic materials).
- Use of proper pre-bonding and bond curing procedures to insure maximum structural integrity of the laminated structure.

The importance of this last step can not be overemphasized. However, all three steps are interrelated since the entire process of design and fabrication of laminated damped structure must be considered from the system's standpoint.

Some of the more significant practical aspects associated with the use of laminated or bonded structure for design of protective packaging systems may be outlined as follows. (From References 11.8, 11.20-11.23)

- Maximum structural strength is ordinarily achieved at the expense of reduced damping.
- Maximum bonding strength is obtained with thermoplastic and thermosetting plastic adhesives (structural adhesives).
- Bonding strength of structural adhesives tends to increase with a decrease in thickness of the bond while bonding strength and damping capability of non-structural or elastomer adhesives will generally increase with an increase in thickness of the bond.
- Equipment mounted to laminated panels should be attached, if possible, to the outer lamination only, to avoid short circuiting the damping effect achieved by relative-shear motion between the laminations.

- Bonded joints offer the advantage of sealing, electrical and thermal insulation, and potentially higher reliability than bolted or welded joints
- An optimum design for a bonded joint will usually have a different configuration and require more careful design than a mechanical joint. Jigs and fixtures may be required for assembly to realize a potential advantage of faster and cheaper fabrication over bolted or welded structure.
- In practice, bonded joints should be designed to be loaded in shear rather than in tension. Although ideally stronger in tension, viscoelastic bonded joints do not ordinarily realize the higher strength in pure tension due to eccentric loading.
- An increase in impact resistance of joints bonded with elastomer adhesives will generally result in lower shear strength of the joints.
- Bonded joints tend to be weak under peel and cleavage stresses (stress concentrations at the edge of a joint) and should be designed accordingly. (See Reference 11.20)
- For lap joints of equal area, a joint with the greater length, normal to the load, is stronger.
- Some joints are subject to weakening under stress combined with excessive temperature, moisture, and certain gaseous vapors, depending on the type of bonding material.
- Some adhesives contain volatile gases which, under confinement or under heat, can condense on critical components causing corrosion, or fouling of electrical contacts and sensitive mechanical parts. For example, epoxy adhesive, processed with curing agents containing amines, can be extremely corrosive to copper, especially in the presence of moisture.

#### Externally Applied Damping Treatment

Prior to the development of bonded multilayer structure incorporating built-in damping, damping of equipment packages was limited to externally applied treatment. This method is still used effectively (in some cases, more effectively than built-in damping) and is particularly convenient for application to existing equipment packages of complex shape. The types of externally-applied treatment can be grouped into the following three general categories according to the mechanism for energy loss. Some specific configurations within these categories are also listed. (Reference 11.22, 11.23).

- Constrained Layer Damping Treatment (Energy Loss by Hysteresis in Shear Strain)
  - Viscoelastic layer with outer rigid panel
  - Damping tape with outer metal foil
  - Multiple layer variations of first two types

- Unconstrained (Free) Layer Damping Treatment (Energy Loss by Hysteresis in Extensional Strain)
  - Flexible viscoelastic sheet
  - High polymer mastic compound
  - Water soluble mastic compound
  - Asphalt base mastic compound
  
- Frictional and Inertial Damping Treatment (Energy Loss by Friction and Viscous Effects)
  - Fibrous blankets, spot-cemented between panel and loading septum
  - Passive mass dampers applied locally to large panels

The three general categories are listed roughly in decreasing order of damping effectiveness and cost. However, wide variations are possible in damping performance of the various types of treatment so that a precise quantitative ranking cannot be made. The choice of any one type of treatment for application to protective packaging of single equipment packages will tend to be based primarily on its damping characteristics, durability, and ease of application. Unless a large number of units are to be treated, cost will be secondary. Other factors such as; weight, ease of removal, flammability, and thermal conductivity may also be considered. A qualitative comparison of the various types of treatment, based on such factors, is shown in Table 11.7.

For the first two general categories, damping effectiveness is strongly influenced by ambient temperature and the damping material must be chosen to achieve optimum results for any design temperature range. In general, single compounds or mixtures of viscoelastic compounds are available which can achieve their maximum damping at temperatures ranging from about  $-40^{\circ}\text{F}$  to  $280^{\circ}\text{F}$ . The more common types of viscoelastic damping materials, however, are most effective in the range from about  $30^{\circ}\text{F}$  to  $150^{\circ}\text{F}$ . Water soluble and asphalt base mastic materials are generally effective over the temperature range of  $0$  to  $80^{\circ}\text{F}$ . For the third category of damping treatment, variations in damping with temperature are not ordinarily significant. In fact, these fibrous materials can provide thermal insulation, in addition to the damping, and are frequently used effectively in situations requiring both characteristics. The frequency of vibration also has an important effect on damping characteristics of externally applied damping treatment. Examples of temperature and frequency effects are illustrated in the following.

A typical example of the effect of temperature on damping of a constrained layer configuration is shown by the measured data in Figure 11.40 for several variations of the thickness of the top layer of a laminated panel configuration (Reference 11.24). Note that the maximum (or optimum) loss factor for each configuration occurs at a temperature of  $20 - 30^{\circ}\text{C}$  ( $68 - 86^{\circ}\text{F}$ ). Other damping materials are available with a broader "temperature bandwidth" or one centered about a lower or higher temperature (See Chapter 9). The lower two curves in Figure 11.40 are representative of the loss factor obtainable with self adhesive damping foils with a thin metal constraining layer. Figure 11.41 illustrates the typical

variation in loss factor with frequency for such damping foils. The data shown were measured for damping tape with 3 different foil thicknesses applied to a  $1/8$ th inch aluminum bar as reported in Reference 11.25. The measured data have been shown to be predictable by the theory discussed in Chapter 9.

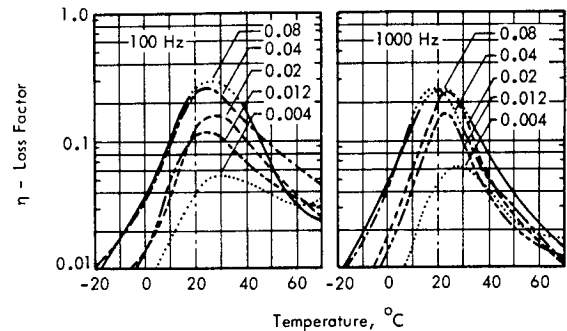


FIGURE 11.40 Variation in Combined Loss Factor with Temperature of a Constrained Layer Damping Configuration Consisting of a  $0.08$ " Steel Panel with a  $0.008$ " Damping Layer of a Modified Vinyacetate Copolymer Material with Varying Thicknesses (in inches) of the Steel Constraining Layer (Data from Reference 11.24)

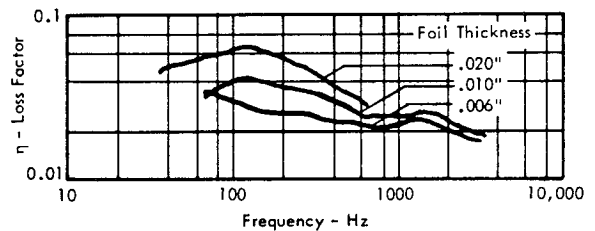


FIGURE 11.41 Loss Factor vs Frequency for Constrained Layer (Damping Foil) Treatment of an Aluminum Bar with Bar Thickness =  $0.125$ " and Damping Layer Thickness =  $0.01$ " (Data from Reference 11.25)

The same general effect of ambient temperature also occurs for unconstrained or free damping treatments as shown in Figure 11.42. This shows the variation of combined loss factor for several types of treatment. The importance of carefully selecting the proper damping material for a given temperature range is clearly illustrated. For the sake of comparison, the combined loss factor obtained for a well designed laminated panel (i.e.—a special case of a constrained layer configuration) is also shown in Figure 11.42. This illustrates the improvement in overall loss factor obtainable with optimum constrained layer damping configurations over that of the free or unconstrained configuration. It is also important to note that constrained layer damping treatment, while just as sensitive to temperature variations, can provide effective damping over a wider temperature range due to its inherently higher peak loss factor. Nevertheless, the achievement of combined loss factors of  $0.1-0.2$  with unconstrained damping treatments offers a very significant reduction in vibro-acoustic response of equipment packages. Furthermore, the relative ease of application and ready availability of a wide variety of materials for this type of treatment will continue to provide an incentive for its effective application.

TABLE 11.7  
 QUALITATIVE CHARACTERISTICS OF EXTERNALLY APPLIED DAMPING TREATMENT  
 (DATA COMPILED FROM REFERENCE 11.22 AND MANUFACTURERS LITERATURE)

Type of Treatment	Damping Characteristics			Ease of Application ⑦	Physical Durability	Resistance to Oil, Water, Acids, Etc.	Availability in Wide Varieties ⑩	Density lb/in <sup>3</sup> (lb/ft <sup>2</sup> )	Cost \$/lb. ⑨ (\$/ft <sup>2</sup> )	Thermal Conductivity BTU/hr/ft <sup>2</sup> /°F
	Effectiveness	Frequency Sensitivity	Temperature Sensitivity							
Constrained Layer										
Viscoelastic Layer With Outer Rigid Panel	Excellent	Variable Effect	Highly Sensitive	Fair ①	Excellent	Good	Good	-	-	-
Damping Tape	Good	Usually shows increased damping at lower frequencies	Requires Selecting Material for maximum damping within +20°F of operating temp.	Excellent (Self-Adhesive)	Good	-	Excellent	0.1 (0.1-.3)	\$ 3.00 (\$ 0.4-\$ 0.8)	-
Spaced Layer	Excellent			Poor ①	Excellent	Good		-	-	-
Unconstrained Layer										
Viscoelastic Sheet	Fair to Excellent	Critical frequency tuning usually not required		Good to Excellent ②	Good ⑧	Good	Excellent (Variable Thickness)	.046-.055 (0.16-1)		-
High Polymer Water Emulsion Compounds	Dependent on Configuration and Material			Good ③	Good ⑧	Good	Excellent			-
Epoxy-Base Compounds				Good	Excellent	Excellent	Good	.052-.055	\$ 2.50	.075
Asphalt-Base Compounds	Fair			Fair ⑥	Fair ⑪	Good	Good ⑫	(0.5)	Low	Low
Frictional and Inertial Damping										
Felt Layers	Fair	Low	Low	Fair		Poor	Fair	(0.2-1.0)	Medium	-
Fiber Blankets	Fair	Low	Low	Fair	Fair	Poor	Good	.002-.006 (.14-1.0)	Medium	Low
Passive Mass Dampers Tuned to Resonance	Excellent at tuned frequency	High ④	Low	Poor		Fair	Poor ⑤		-	NA

① Usually requires special design or fabrication

② Some require separate bonding process

③ Requires careful mixing and preparation

④ Effective only at tuned resonance

⑤ Usually custom made

⑥ Optimum treatment requires baking

⑦ Compounds require 1-4 days cure

⑧ Flame pt 400°F

⑨ Approximate only for 100 lb or 100 sq. ft lots

⑩ Most varieties suited for 50-100°F

⑪ Flammable

⑫ Primarily designed for auto industry

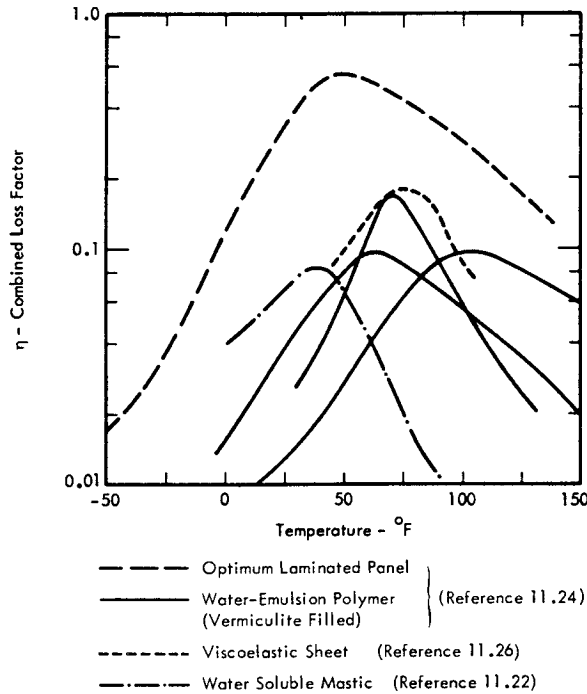


FIGURE 11.42 Typical Variation of Combined Loss Factor for Different Types of Unconstrained Layer Damping Treatment with Damping Layer: Base Layer Thickness Ratio  $\approx 1$ . Loss Factor for Well Designed Laminated Panel Shown for Comparison. (Frequency - 75-160 Hz)

Application of externally applied damping treatment to ground equipment packages is not generally critical from the standpoint of additional weight. The criteria for optimum design is more likely to be the reduction of response and the cost of treatment. Sophisticated structural design methods would, in fact, allow a trade-off study to be made between the added cost of damping treatment versus cost savings due to lower vibro-acoustic design environments, increased structural integrity, or equipment reliability. While such a trade-off study could be made within the current state of the art, it is more likely that design objectives would be limited to achievement of some desired damping or loss factor for minimum cost.

For a given type of damping treatment, the damping material costs will tend to be a function of the total added weight of the treatment so that weight increment, while not necessarily a critical design factor, is a useful parameter for trade-off studies.

The approximate range of added weight for constrained and unconstrained layer damping treatment of aluminum and steel plates is shown in Figures 11.43 and 11.44 respectively. The range of weight ratio versus combined loss factor for each type of treatment is based on an envelope of the typical damping configurations considered in more detail in Chapter 9. For example, the range for constrained layer treatment encompasses configurations where the thickness of the damping layer is 5 percent of the base layer thickness (i.e., very thin constrained layer) to configurations where the constraining layer thickness is 5 per-

cent of the base layer (i.e., very thin or no damping layer). Based on the highest performance damping configurations indicated by the upper bounds of the shaded areas in Figures 11.43 and 11.44, the minimum absolute weight of damping treatment required to achieve a design goal of 0.2 for the combined loss factor ( $Q = 5$ ) can be estimated. For example, for 0.1 inch thick plates with an area of 1 square foot, the minimum weight of damping treatment would be about 0.5 to 1 lb for aluminum plates, and 1 to 1.2 lbs for steel plates. The lower value, in each case, corresponds to the weight for constrained layer damping treatment.

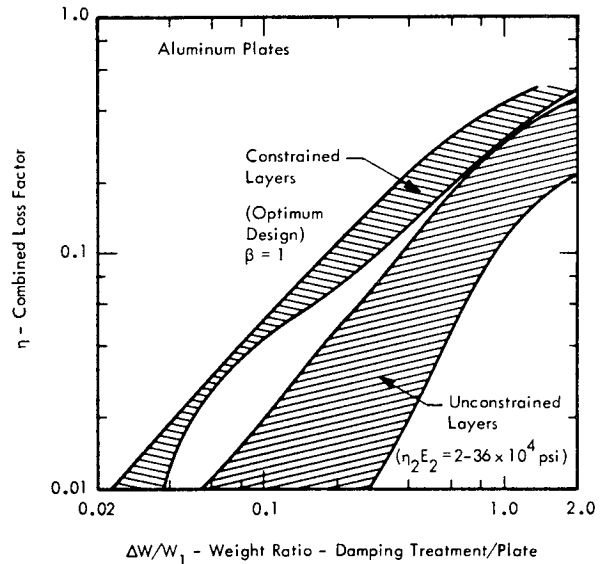


FIGURE 11.43 Comparison of Additional Weight of Constrained and Unconstrained (Free Layer) Damping Treatment of Aluminum Plates. Based on Typical Damping Configurations and Materials Analyzed in Chapter 9.

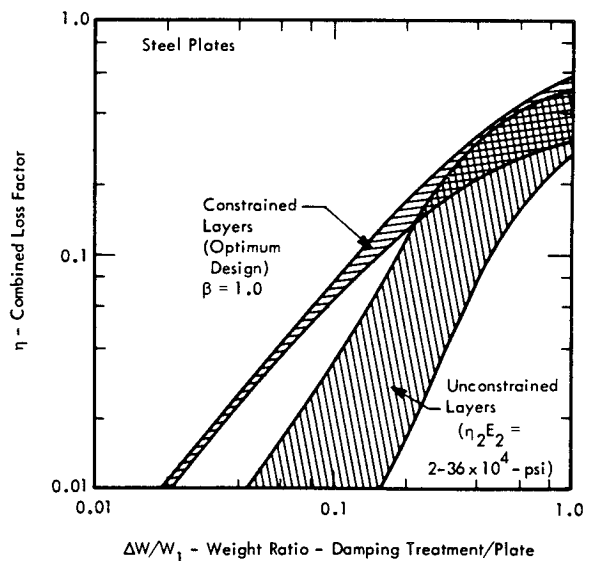


FIGURE 11.44 Comparison of Additional Weight of Constrained and Unconstrained (Free Layer) Damping Treatment of Steel Plates. Based on Typical Damping Configurations and Materials Analyzed in Chapter 9.

To minimize cost of damping treatment for large areas, less than 100 percent coverage can be used to advantage, providing the localized treatment is properly located. While no quantitative methods have been developed to predict overall damping achieved with reduced coverage, a reasonable design estimate, based on empirical data, is provided in Figure 11.45. The optimum location for the reduced treatment is at the regions of the highest plate vibration (or antinodes) at the resonance frequencies to be damped. A mixed treatment can also be used employing lightweight damping over the entire panel with heavier concentration at antinode positions. These positions can be readily determined for the first few resonance modes of a panel by simple vibration tests. The antinodes for low order modes will not deviate appreciably with variation in production tolerances between various units of the same equipment package.

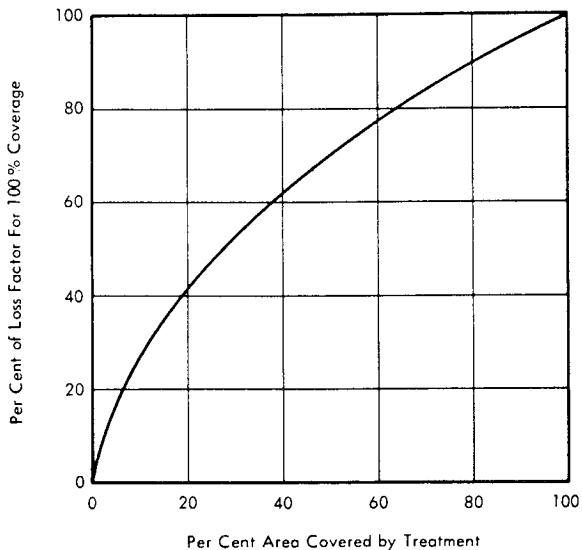


FIGURE 11.45 Relative Damping Effectiveness for Partial Coverage of Plate

Reference 11.22 provides a useful guide for design of the third category of externally applied damping treatment - fibrous blankets or tuned mass dampers. This last category of damping treatment is not as widely employed for aerospace ground equipment and, hence, is not covered in detail in this manual.

#### 11.8.2.2 Protective Potting of Components

An effective and widely used method for protecting and improving the reliability of electronic components mounted inside equipment packages involves the use of potting compounds. This process can take the form of simply coating the component and its adjacent support structure with a rigid or flexible potting compound or completely encapsulating the components inside the equipment package. An obvious additional benefit of such treatment, when properly applied, is the potential ability to reduce vibro-

acoustic response of the equipment by damping or attenuation of vibro-acoustic energy. The two qualifications; "proper application," and "potential ability" can best be illustrated by examining data reported in Reference 11.5 on the effects of potting treatment on the vibro-acoustic response of a 1/16" x 2" x 10" glass epoxy circuit board supporting an array of electrically polarized capacitors. Two types of capacitors (type A and B) were used in each of two configurations (capacitor mounted parallel and perpendicular to the long side of the circuit board) with two different types of potting treatment applied to the board. The acceleration at the center of the board and the electrical noise output of the capacitors were monitored while the circuit board, mounted at its corners, was exposed on one side to high intensity sinusoidal acoustic noise. The results of these tests are summarized in Table 11.8 in terms of the decrease (in decibels) of the acceleration and electrical noise output for the two types of damping treatment; aquaplas and epoxy. A negative entry signifies an increase in response. Also listed are the number of capacitors which failed, mechanically, during tests at sound levels above 140 dB.

The significant results of these tests may be summarized as follows.

- With one important exception, damping treatment with either an epoxy compound or aquaplas damping compound resulted in about 10 dB reduction in acceleration response. The exception occurred for configuration 2B treated with epoxy. In this case, the acceleration increased accompanied by a corresponding decrease in damping. The fundamental resonance frequency of this configuration increased only 9 percent with epoxy treatment over the untreated configuration. The reduced damping, in this case, may be due to elimination of coulomb friction losses between the capacitor and circuit board by the epoxy bonding action. Some evidence for this is found in the fact that the electrical noise output of the capacitors generally decreased, when the epoxy treatment was employed, even though the vibration response increased. This is attributed to a reduction in relative motion or impact between the capacitors and circuit board which would be a source for electrical noise output. For all the tests, the electrical noise from the capacitors ranged from about 1 to 40 microvolts per g acceleration.
- In several cases, the electrical noise output from the capacitors increased for a reduced vibration response. This is attributed to one of two anomalies: 1) the breaking of the bond between the capacitor and damping compound causing increased impact noise to be generated, or 2) increased bending or shear stresses imposed on the capacitors by their bonding to the vibrating circuit board. The latter effect was noted for configuration 1B coated with epoxy and was accompanied by a 57 percent increase in resonance frequency over the uncoated configuration. This required an increase in stiffness of 146 percent for

TABLE 11.8

EFFECT OF POTTING TREATMENT ON ACOUSTICALLY INDUCED ACCELERATION AND ELECTRICAL NOISE RESPONSE OF CAPACITORS MOUNTED ON A GLASS EPOXY CIRCUIT BOARD (DATA FROM REFERENCE 11.5)

Config-uration	Sound Level dB	Average Decrease In Response (in dB) Due to Potting				No. of Capacitors Mechanically Failed		
		Aquaplas (5)		Epoxy (6)		No Treatment	Aquaplas	Epoxy
		Accel.	Elect. Noise	Accel.	Elect. Noise			
1A (1)	140 150 160 165	12 dB 10	16 dB 10			3	4 Fracture	
2A (2)	140 150 165	9 4	-5 -9			1 2	11 (7)	
1B (3)	97-126 140 150 162	13 7	8 4	7	-4(-5to-22)	0 11		0 1 3(7)
2B (4)	97-126 140 150 155 165 170	14 1	6 -2	-7	3.5 (-5to16)	0 3	4 11 (7)	0 1 10(7)
<p>(1) 5 rows of 3 parallel capacitors (Type A) each with axis parallel to 10 inch side of 1/16" x 2" x 10" circuit board</p> <p>(2) 11 parallel capacitors (Type A) each with axis perpendicular to 10 inch edge</p> <p>(3) Same as 1A except Type B capacitors</p> <p>(4) Same as 2A except Type B capacitors</p> <p>(5) Thickness - slightly less than diameter of capacitors</p> <p>(6) Thickness - 0.0375 in.</p> <p>(7) Circuit Board Failed Completely</p>								

this configuration where the capacitors were aligned with the long dimension of the circuit board and would hence carry part of the bending stress for the fundamental mode of the treated circuit board.

- Mechanical failure of the capacitors commenced at sound levels of about 140 dB for the untreated board and about 150 dB for the potted units.

In general, these limited results suggest that to optimize damping effects without imposing added bending stresses on sensitive components, potting treatment should consist of thick coatings of a material with a low elastic modulus. Components should be oriented in such a way as to minimize curvature or bending strain along the sensitive axis of the potted component. In any event, bonding strength of the potting compound should be sufficient to insure that

bond separation does not occur under the most adverse environmental conditions so that impact effects are eliminated.

More specific quantitative criteria for designing potting treatment, from the standpoint of vibro-acoustic protection are difficult to establish. This is due to the wide variety of complex mounting configurations and the importance of other characteristics of the potting treatment. Some of these characteristics are (Reference 11.27)

- Resistance to corrosion, moisture, fungus, etc.
- Electrical resistivity
- Thermal conductivity
- Resistance to high temperature
- Ease of removal for repairs

However, some guidelines are offered by considering the potting treatment of component mounting boards as equivalent to an unconstrained or free damping layer.

TABLE 11.9  
TYPICAL PROPERTIES OF POTTING COMPOUNDS\* AND PLASTIC LAMINATES USED FOR  
CIRCUIT MOUNTING BOARDS (DATA FROM REFERENCES 11.8, 11.23, 11.28-30)

Material	Loss Factor	Freq. Hz	E × 10 <sup>3</sup> psi	ρ lb/in <sup>3</sup>	Max. Temp. °F	Tensile Strength × 10 <sup>3</sup> psi
<b>POTTING COMPOUNDS</b>						
Epoxy Polymers	.2 - .3	-	10 - 100	.04 - .075	500	2 - 12
Silicone Rubber	.2 - .25	-	.021 - .68	.038 - .053	300 - 500	.2 - 1.0
" "	.37	100	.021	.04	-	-
" "	.34	400	.035	↓	-	-
" "	.47	1000	.036	↓	-	-
Silicone Rubber Foam	-	-	.005 - .01	.0072	-	.02
Thiokol Rubber	.15 - 1.9	-	.2 - 10	.048	170	1.3
" "	.56	10	.30	↓		
" "	.83	40	.33	↓		
" "	1.29	100	.36	↓		
Polyurethane	.5 - 2.6	3600	4.5 - 8.7	.046	250	6 (shear)
<b>PLASTIC LAMINATES</b>						
Phenolic	.02		400-1200	.047		6 - 9
Acrylic	.02		350-450	.039-.043		6 - 10.5
Fiber Laminated Plastics	.022		2700-7900	.048-.062		40

\*Representative values - subject to wide variation depending on formulation.

Typical damping and elastic properties of some of the more common type of potting compounds and plastic laminates for circuit boards are listed in Table 11.9. Due to the wide range of properties inherent in such materials and the lack of readily available detailed data, a detailed listing is not possible. Thus the table provides only a representative range of the significant dynamic characteristics for common potting compounds and also gives typical test data on single samples for the sake of illustration.

These data may be used with the theory for unconstrained damping layers covered in Chapter 9 to estimate the damping or combined loss factor for component mounting boards treated with a layer of potting compound. Since most of these compounds have a relatively low elastic modulus, the combined loss factor may be roughly estimated by the equation: (Reference 11.22)

$$\eta \approx 14 \eta_2 \left( \frac{E_2}{E_1} \right) \left( \frac{h_2}{h_1} \right)^2 \quad (11.18)$$

where

- $\eta_2$  = loss factor of potting compound
- $E_2, E_1$  = elastic modulus of potting compound and mounting board respectively.
- $h_2, h_1$  = thickness of potting layer and mounting board respectively.

Estimates of damping made with this expression are likely to be conservative due to the more complex geometry and the tendency for the potted components themselves to increase the effective stiffness of the "damping" layer.

When the potting treatment involves complete encapsulation of components within an equipment container, resonant vibration response of the components, relative to their mounting structure, will be virtually eliminated due to damping and bonding action. Vibro-acoustic excitation reduces to rigid body motion of the component due to vibration of the entire package or to dynamic stresses imposed by compressional or shear waves transmitted from the walls of the equipment package through the potting compound to the component. The former type

of excitation will generally be significant only for components, such as sealed relays, which contain internal sensitive elements inside a separate housing. In this case, vibration isolation of the entire equipment package may be necessary. For the latter type of direct excitation through the potting medium, a rough estimate of the amount of attenuation can be made as follows.

The attenuation in decibels per unit distance of a longitudinal stress wave in a lossy medium is given by

$$a = 8.68 \pi \eta f / C_L \quad \text{dB/unit distance}$$

where

$$\begin{aligned} \eta &= \text{extensional loss factor in medium} \\ f &= \text{frequency - Hz} \\ C_L &= \begin{cases} \text{speed of plane longitudinal waves} \\ \sqrt{E/\rho} \end{cases} \end{aligned}$$

If the small difference between velocity of longitudinal waves and compressional or dilatational waves in the medium is ignored, then the above expression provides a rough estimate of attenuation of the latter type of waves in a three dimensional lossy medium. This expression has been used with the data in Table 11.9 and additional, more detailed data in Reference 11.28, to estimate the attenuation rate for typical potting compounds. Typical results, given on Figure 11.46 show that an attenuation of 10-20 dB per inch of thickness could be expected at frequencies above 1000 Hz. The benefit of such attenuation would be significant for electronic components which are very sensitive to compressive stresses. It should be pointed out, however, that the magnitude of such stresses will normally be very low for most equipment packages, even without any attenuation. The stresses would not generally exceed the acoustic pressures on the outside of the equipment package. Also, an even greater reduction in compressional stresses on components could be achieved, depending on the configuration, by acoustic isolation. This topic is considered in the next section.

To summarize, the primary vibro-acoustic protection offered by potting treatment is to reduce or eliminate secondary vibration of components relative to their mounting structure and provide increased damping of the mounting structure itself. Potting treatment should be applied with careful consideration of the sensitivity of components to induced bending stresses resulting from more rigid bonding to the mounting. Application of protective coatings to circuit boards and modules is increasing due, primarily, to improvements obtained in circuit reliability by elimination of arcing, corrosion, etc. Further improvements in the vibro-acoustic protection resulting from such treatment can be made by optimizing the dynamic properties of these potting materials. Development tests should be conducted on any new configurations to insure that optimum vibro-acoustic protection is achieved. This is likely to be particularly important for potting treatment of solid state circuits which may be more sensitive to induced bending stresses imposed by the potting treatment.

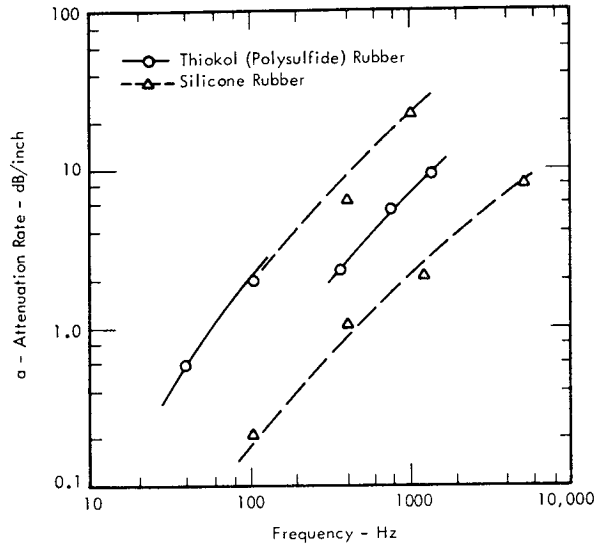
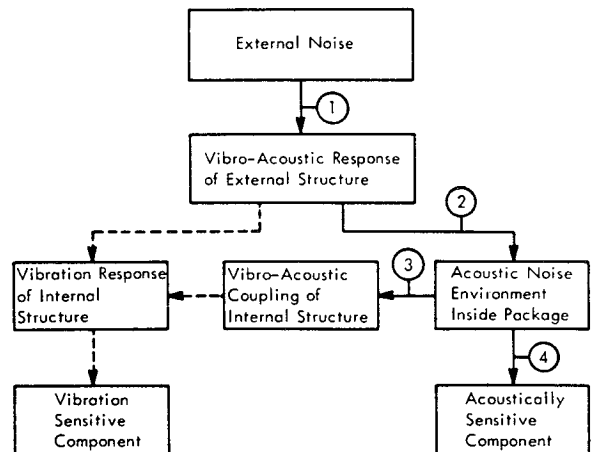


FIGURE 11.46 Estimated Attenuation Rate of Compression Waves for Typical Potting Compounds (Data from Reference 11.28 and Table 11.8)

### 11.8.2.3 Acoustic Isolation of Equipment

Protective packaging design concepts discussed so far have been concerned with reducing the vibration response of the equipment structure and its contents by various forms of damping or potting treatment. However, reduction of the acoustic environment for the equipment may also be desirable or necessary. It will be necessary if internal components are sensitive to direct acoustic excitation (e.g.-See Table 11.4, page 11-23) and desirable if acoustically-induced vibration response of the equipment is more efficiently reduced by decreasing the acoustic input rather than by applying damping treatment. The design objectives and methods for acoustic isolation will not necessarily be the same in each case. To clarify these differences, a brief review of the significant paths for flow of acoustic energy to equipment components inside a package is again in order. This is illustrated in the following diagram. Flow of acoustic energy is represented by solid lines and flow of vibration energy by dashed lines.





There are four links involving flow of acoustic energy. The first link represents the path between the source of external noise and the equipment package itself. Noise control in this link can range from local acoustic shielding of a single equipment package by a single protective enclosure to noise reduction within the room, building, or test area where the original source is located. These latter noise reduction concepts are treated elsewhere in this manual (Chapter 7 and 9) and are not repeated here. For a single protective enclosure, the theoretical design objective for noise reduction would depend on the relative significance of the subsequent excitation paths within the enclosed package. If internal vibration response of the protected equipment package is the critical path, then noise reduction of the protective housing should be effective at frequencies starting with the first structural resonance of the equipment. If noise transmission to the inside of the protected package is critical, then the design objective may be either the same as for the vibration path, if structural resonances control the internal noise, or be limited to achieving effective noise reduction at the internal acoustic resonance frequencies when the latter control the internal noise. A practical design objective would tend to ignore this distinction and would be based on achieving an effective transmission loss at frequencies starting with the lowest structural resonances.

The second link in the diagram represents the overall acoustic noise reduction between the outside and inside of the equipment package itself. A similar evaluation of design objectives can be made for this path as for the first path except that now the objectives can be based on the relative significance of direct acoustic excitation of the component (path 3) or acoustically induced vibration of internal structure, (path 4). Specific examples and design concepts for these first two paths will be given shortly.

The third path represents the direct excitation of a component by the internal noise field. Some acoustic isolation in this path may be achieved by potting treatment, as discussed in Section 11.8.2.2, or by hermetically sealed containers for individual components. Such measures will generally only be effective at frequencies above about 1000 Hz. Noise reduction will be limited to about 10-15 dB and would ordinarily be only a secondary benefit of the protective housing or coating.

Finally, path 4 represents the vibro-acoustic coupling of internal noise resulting in a vibration response of internal structure. In most compact, hardened, ground equipment packages, this will be a relatively ineffective path compared to direct mechanical or acoustical excitation of external structure. Such a situation is illustrated by the data in Figure 11.47. This illustrates the results of an experiment reported in Reference 11.5, on the structural vibration transmitted from the front to back wall of a simulated equipment package driven mechanically. The test was conducted, first, at normal atmospheric pressure and then in a vacuum chamber. No significant differences were encountered in vibration transmission between the two tests thus clearly demonstrating, for this case, the predominance of direct structural transmission instead of

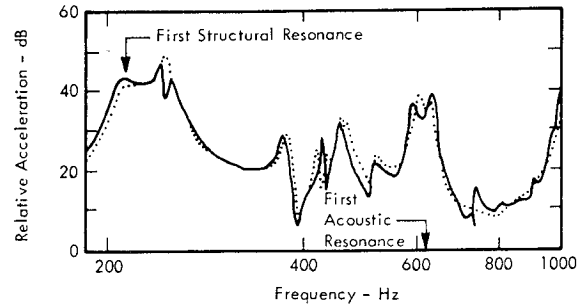


FIGURE 11.47 Relative Vibration Response of One Wall of a Chassis with Mechanical Vibration Excitation on the Opposite Wall. One Line for Test at Atmospheric Pressure and Other Line at Less than 1mm Hg. (Data from Reference 11.5)

internal acoustic excitation. Exceptions can occur, however, when internal component mounting structure is effectively vibration isolated. In this case, internal acoustic noise may be a more significant source of internal vibration response. An approximate upper bound of the effectiveness of this path can be specified by a simplified form of the analytical methods discussed in Section 11.5.3.1. Based on an analysis of the acoustic tests of component-laden circuit boards, reported in Reference 11.5, the maximum acceleration,  $A(f_o)$ , at the fundamental frequency ( $f_o$ ) of the circuit board could be predicted by the expression:

$$A(f_o) \approx \frac{P(f_o)}{w} \cdot Q - g's \quad (11.20)$$

where

- $P(f_o)$  = rms acoustic pressure near circuit board at frequency  $f_o$  - psi
- $w$  = surface weight of circuit board plus components - psi
- $Q$  = resonant amplification factor of board

Observed resonant amplification factors for this test varied from 23 to 100; the average was 40.

Consider, now, the noise control design procedures for the first two paths. Both involve essentially the same three basic elements:

- Maximize the structural impedance of the outer walls to reduce their vibration response and corresponding noise transmission
- Minimize acoustic leaks through the outer wall to prevent "short circuits" of the basic noise attenuation through these walls
- Minimize resonant response of internal acoustic modes by providing internal acoustic absorption

### Estimating Noise Reduction

The types of enclosures used for equipment may be grouped roughly into the following three categories according to their characteristic noise reduction capability.

- Conventional Cabinet Racks
  - Low Frequency Noise Reduction - Low
  - High Frequency Noise Reduction - Low to Average
- Specially designed Large Cabinets or Walk-In Enclosures
  - Low Frequency Noise Reduction - Low to Average
  - High Frequency Noise Reduction - Average to High
- Small Sealed Enclosures for Exposed Equipment
  - Low Frequency (Below 100 Hz) Noise Reduction - High
  - High Frequency (Above 100 Hz) Noise Reduction - Average

Methods for predicting noise reduction for these three categories vary, depending largely on their size and degree of venting to the surrounding atmosphere.

For example, for the first category, vents or air conditioning systems are usually necessary so that noise attenuation will normally be limited to very low values. A rough estimate of the noise reduction (NR) could be made, in this case, with the following expression.

$$NR \approx 10 \log \frac{\text{Total Surface Area of Cabinet}}{\text{Vent Area}} - \text{dB}$$

This assumes that the vent area has zero transmission loss and effectively cancels any transmission loss provided by the rest of the structure. Thus, a cabinet with a vent area of five percent would have a sound transmission loss of about 13 dB. The actual noise reduction, or difference between external and internal sound levels, would be about 6 dB less than this figure at low frequencies and 0 to 4 dB higher at high frequencies (above 200 Hz). Further refinements to this type of estimate would usually not be practical for this type of enclosure.

For the second category, conventional methods for estimating noise reduction for rooms, discussed in Chapter 9, can be employed. Typical noise reduction obtainable for this type of enclosure has been shown in Figure 10.37, page 10.34.

These prediction methods are based on statistical concepts for the structural response and internal noise field and are not entirely applicable to the third category of equipment packages due to their size and corresponding low density of structural and acoustic modes. This is illustrated by the measured noise reduction of a small simulated equipment package shown in Figure 11.48. The lowest acoustic re-

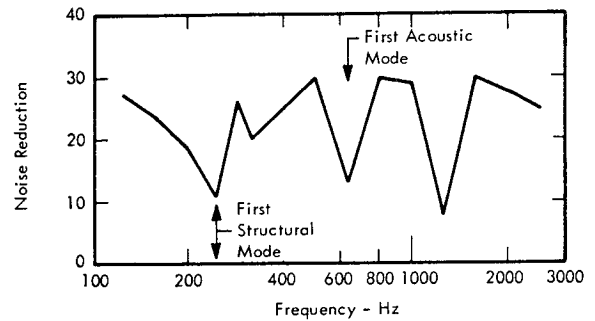


FIGURE 11.48 Example of Noise Reduction Through 1/16" Walls of a 5" x 7" x 11" Aluminum Container Simulating an Equipment Package (Data from Reference 11.5)

sonance of the 5" x 7" x 11" enclosure occurs at a frequency of 610 Hz which is well above the lowest structural mode (~250 Hz in this case). Thus, resonant response of discrete structural and acoustic modes of these small equipment containers will usually control the maximum internal noise levels. This makes it difficult to accurately predict noise transmission for such enclosures due to uncertainties in estimates of damping and absorption of the discrete modes. Nevertheless, a simplified prediction method can be usefully employed to estimate noise reduction for these enclosures. It can also provide a guide for improving noise reduction design particularly at frequencies below the lowest structural mode.

Such a prediction method is outlined in self-explanatory fashion in Figure 11.49. The chart has been simplified to include both the transmission loss through the enclosure walls and the internal effects of the sound absorption inside the enclosure. The chart has been developed, in part, from concepts outlined in Reference 11.31. A graph similar to Figure 11.49 can be constructed for a given equipment container using a semi-log graph paper and following the procedures indicated.

The graph should be started by plotting the mass law line using the equation indicated and then the fundamental frequency of the largest panel,  $f_1$ , located on the abscissa.

The design charts in Table 3.11 of Chapter 3 may be used for estimating the resonance frequencies of the panels. Between this frequency and the frequency  $f_2$ , (the lower bound of the coincidence region), the noise reduction will fall well below the mass law transmission loss at discrete structural and acoustic modes of the enclosure. The estimated minimum noise reduction in this range is located 10 dB below the mass line and is based on average conditions. Deviations as much as 10 dB near the lower order panel resonance frequencies can be expected. (See Reference 11.32 for a more detailed analysis of sound transmission in this frequency range).

Between the frequency  $f_2$ , which is found by construction on Figure 11.49, and  $4f_2$ , the noise reduction will be controlled largely by coincidence effects. The estimated minimum noise reduction in this range is specified by the

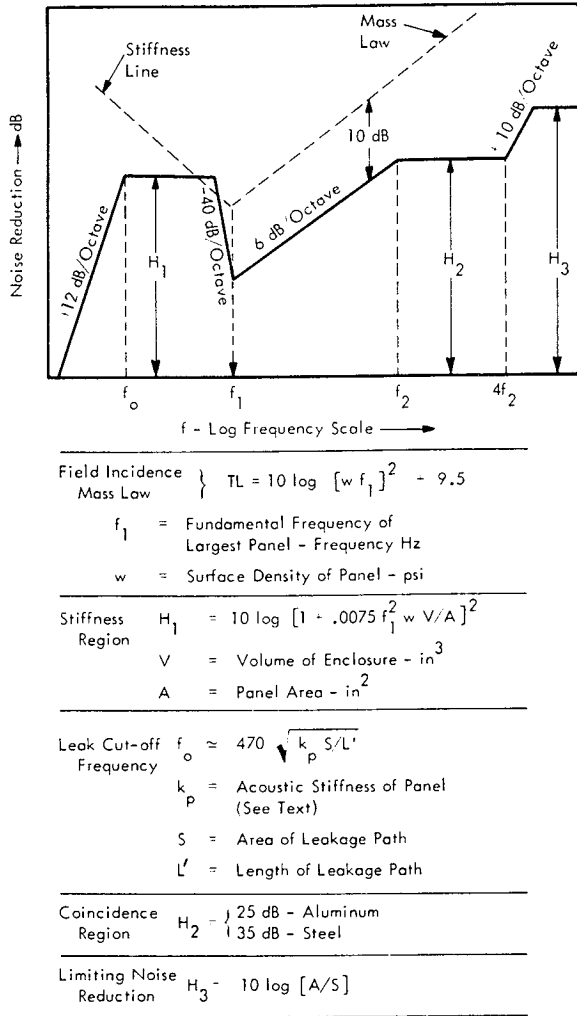


FIGURE 11.49 Design Chart for Estimating Noise Reduction Through Small Equipment Enclosures with Simply Supported Side Walls

parameter  $H_2$  in Figure 11.49. This corresponds to the frequency range where bending wavelengths in the panel walls are equal to the trace wavelengths of the acoustic waves impinging on the walls. The lowest frequency at which this condition can occur is called the critical frequency,  $f_c$ , and in typical metal walls of thickness  $h$  inches, is equal to

$$f_c = 470/h \text{ Hz}$$

In this frequency range, as in the last one, acoustic absorption helps to limit the maximum sound transmission. However, structural damping, while beneficial, is not as important as in the lower range. In this higher frequency region, the panel tends to act more like a lumped mass. According to the above criteria, this frequency range will tend to fall near the upper frequency range of interest for most equipment containers.

The estimated noise reduction in the stiffness region is based on the ratio of effective stiffnesses of a panel and the enclosure. The largest panel of the enclosure is selected as the controlling element for predicting noise reduction. The effective stiffness (or ratio of static pressure load to net volume displacement) for a typical side panel is given, with sufficient accuracy for this analysis, by the first term in a normal mode expansion of the deflection of a simply supported panel to a static load. For any consistent system of units, this is given by:

$$k_p = \frac{\pi^8 D h^3}{64 A^3} \left[ \frac{b}{a} + \frac{a}{b} \right]^2 \quad (11.21)$$

where

- $D$  = Bending Stiffness =  $Eh^3/12(1 - \nu^2)$
- $E$  = Modulus of Elasticity
- $h$  = Panel Thickness
- $\nu$  = Poisson's Ratio
- $a, b$  = Panel sides
- $A$  =  $ab$

The error incurred by neglecting higher order terms in the modal expansion is conservative and entirely negligible for normal panel aspect ratios. This stiffness is more conveniently expressed in terms of the fundamental frequency,  $f_1$ , and surface weight  $w$  of the panel in the form

$$k_p = \frac{\pi^6 f_1^2 w}{16 g A} \quad (11.22)$$

where

- $g$  = Acceleration of gravity.

The corresponding effective or acoustical stiffness of the enclosure is given by

$$k_c = \frac{\rho c^2}{V} = \frac{\gamma P_o}{V} \quad (11.23)$$

where

- $\rho$  = Density of Air
- $c$  = Velocity of sound in air
- $V$  = Volume of enclosure
- $\gamma$  = 1.4 for air
- $P_o$  = Atmospheric pressure

The volume taken up by the contents inside the enclosure can usually be neglected. However, it may be desirable to modify the predicted fundamental frequency of the panel, to account for the added stiffness of the enclosure, when plotting the noise reduction curve. In this case, the frequency is increased by the ratio  $\left[ 1 + k_c/k_p \right]^{1/2}$  where  $k_p$  and  $k_c$  are given by Equations 11.22 and 11.23, respectively.

The noise reduction in this region is defined by

$$NR = 10 \log \left[ 1 + k_p/k_c \right]^2 \quad (11.24)$$

which reduces to the term  $H_1$  given in Figure 11.49 for an ambient pressure of  $P_o = 14.7$  psi and an inch-lb-sec. system of units.

For panel boundary conditions other than simply supported, the following corrections apply to Equation 11.22, assuming changes in resonant frequency due to different boundary conditions have already been applied.

- Clamped Edges - Multiply  $k_p$  by 1.5
- Supported on one Edge Clamped on Other Edge - Multiply  $k_p$  by 1.2

The decrease in noise reduction at the lowest frequencies is due to leakage through joints or penetrations of the enclosure walls. The loss in this region has been estimated with the use of the lumped parameter analog of the enclosure which is illustrated in Figure 11.50. A typical transmission curve is also shown indicating the cut-off frequency  $f_o$ . The model is applicable for frequencies well

below the fundamental structural and acoustic modes of the enclosure. The stiffness elements are the same as defined in Equations 11.22 and 11.23. The leakage path, shorted across the plate stiffness, is represented by the acoustic mass  $m_l/S^2$  where

$$m_l = \rho L'S \quad (11.25)$$

$\rho$  = Mass density of air =  $1.4 \times 10^{-7}$  lb. sec<sup>2</sup>/in.<sup>4</sup> at 59°F

$L'$  = Effective length of leakage path-in.

$S$  = Cross-sectional area of leakage path-in<sup>2</sup>.

The effective length of the path can be assumed to be equal to the actual length plus an end correction  $1.7\sqrt{S/\pi}$ . Although a more accurate representation of the leakage path could be made to account for viscous and heat conduction losses (Reference 11.33), this refinement would only be justified in cases where extreme requirements exist for minimizing low frequency sound transmission into a critical enclosure. Such a situation could exist for a protective enclosure of sensitive equipment located very close to a launch or rocket test stand. In this case, an intentional leak could be built into the unit for pressure relief purposes which could still provide high sound attenuation. If necessary, the leak could be calibrated by imposing a small but rapid change in pressure differential on the enclosure and observing the internal pressure change with time. Under such conditions, a small leak will act like a pure acoustic resistance and the differential pressure time history can be roughly described by the simple expression

$$\Delta P(t) = \Delta P_o e^{-t/T} \quad (11.26)$$

where

$\Delta P_o$  = Initial differential pressure

$T$  = Acoustic time constant

$$= \frac{8\pi \mu L' V}{S^2 \gamma P_o} \text{ - sec.}$$

where

$\mu$  = Viscosity of air =  $27 \times 10^{-10}$  lb. sec./in.<sup>2</sup>

$\times \left( \frac{T^\circ R}{526} \right)^{0.7}$

$V$  = Volume of enclosure - in<sup>3</sup>

$\gamma$  = 1.4 for air

$P_o$  = Ambient pressure - psi

As an example, for a 10-inch cubical enclosure with a leakage path consisting of a 0.02-inch diameter hole through a 0.1-inch plate, the time constant  $T$  would be 3.9 sec. This would be the time required for a sudden differential pressure change to decrease to 37 percent of

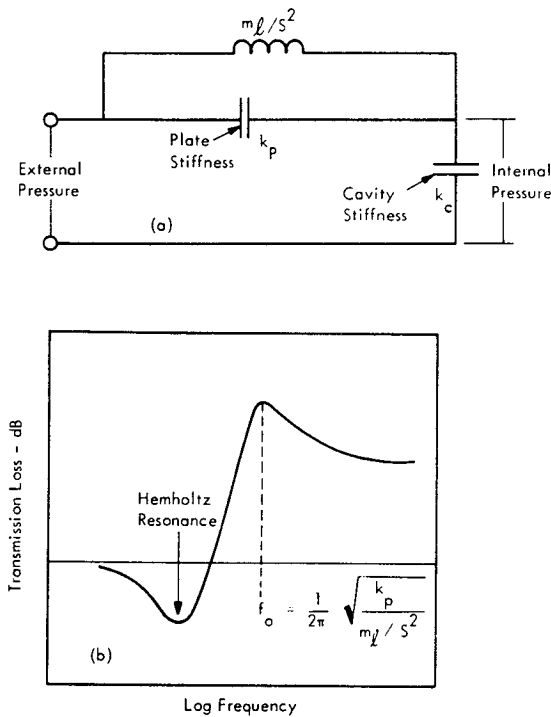


FIGURE 11.50 (a) Equivalent Analog Circuit and (b) Acoustic Transmission Curve, with Damping, Through Leakage Path into Small Equipment Enclosure at Frequencies Well Below the Fundamental of Structural and Acoustic Modes

its initial value. If the enclosure were made of aluminum, the stiffness controlled noise reduction would be 31 dB but would drop rapidly to zero for frequencies below 18 Hz.

#### Summation of Noise Reduction For All Panels of the Enclosure

For larger, more complex enclosures, it may be desirable to compute the noise reduction for each major panel to determine an overall composite noise reduction for the enclosure. The effective acoustic stiffness  $k_p$  of the outside walls is equal to: one over the sum of the compliance (1/stiffness) of each wall or

$$\bar{k}_p = 1 / \left[ 1/k_{p1} + 1/k_{p2} + \dots + 1/k_{pn} \right] \quad (11.28)$$

Then using Equation 11.22 and Figure 11.49 or Equations 11.22 - 11.24, the stiffness-controlled noise reduction can be computed for the composite structure. In this frequency range, it is assumed that the acoustic wavelength is greater than the circumference of the enclosure. At higher frequencies, the net displacement of air inside will decrease due to the out-of-phase action of the various panels.

At frequencies above the first structural resonance, the overall noise reduction through all sides of the enclosure can not be readily computed by the usual methods applicable in architectural acoustics due to the low modal density. However, some guidelines can be provided to assist in design improvements. At frequencies near the lower panel modes, opposing symmetrical panels will tend to vibrate in-phase causing approximately a 6 dB decrease in noise reduction. In this same frequency range, the additional noise transmission through the other walls which vibrate out-of-phase will tend to smooth out the transmission curve since each panel will contribute its own independent modes to the transmission of sound energy. As a rough guide, the initial estimate of noise reduction based on the largest single panel could be reduced by 6dB at frequencies where in-phase motion will occur and by the following correction factor,  $\Delta$ , at intermediate frequencies above the lowest panel modes.

$$\Delta = -10 \log \left[ \sum_{i=2}^n \frac{r \cdot A_i}{A_1} \right] - \text{dB} \quad (11.29)$$

where

$A_i$  = area of each of the other  $n$  panels

$A_1$  = area of largest panel

$r$  = empirical weighting factor  $\leq 1$

The factor  $r$  would be used to weight the relative area  $A_i/A_1$  of the other panels according to an engineering estimate of the relative damping or vibration characteristics of the other panels. Thus,  $r$  could have the value of 1 for any undamped panel not supporting any equipment components and 0.1 for any panels which are

well damped or heavily loaded with components. Additional refinements could include identification of the fundamental modes of the other panels. Further improvements in noise reduction estimates would require experimental tests.

#### Methods for Design Improvement

Methods for increasing the noise reduction through small equipment enclosures have now become clear and may be summarized as follows.

Transmission through the leakage paths is accomplished by reducing the ratio-leakage area/path length. Very small leakage areas are required to maintain high noise reduction at low frequencies encountered around rocket test sites.

In the stiffness controlled region, increasing panel stiffness is the only effective solution for increasing noise reduction for a given enclosed volume. Addition of stiffeners, and use of corrugated or honeycomb panels can be used to provide such stiffening. Note that increasing structural damping is ineffective in this range since the panel impedance is stiffness controlled. Although lightweight, stiff materials can provide high noise reduction in this range, this will be at the expense of reduced transmission loss at high frequencies.

In the frequency range of low order structural resonances, selective application of damping treatment, such as discussed in Section 11.8.2.1, will be the single most effective means for reducing internal noise levels. A typical example of improved noise reduction achieved for a small equipment container with the use of laminated structure in place of solid panels is illustrated in Figure 11.51. Note the marked reduction of the dip in noise reduction at the first panel mode for the laminated panel. It is also worth noting the high noise reduction achieved at lower frequencies with both configurations. A predicted noise reduction of 41 dB agrees very well with the observed results. As expected, structural damping has no effect on noise reduction in this stiffness controlled region.

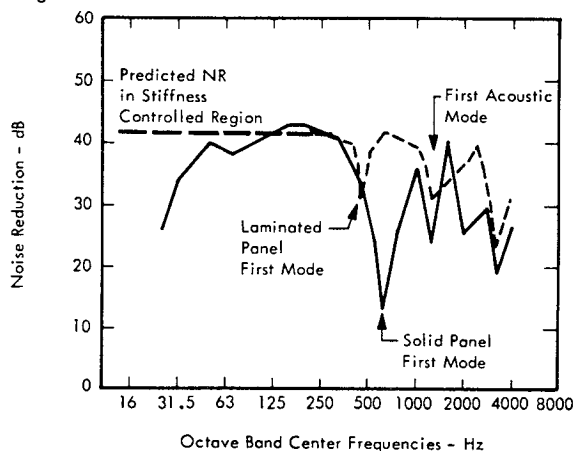


FIGURE 11.51 Comparison of Measured Noise Reduction for Solid and Laminated Panel Equipment Enclosure (0.08" x 4.5" x 6.5" x 6.5" Aluminum)

In the frequency range of internal acoustic resonances, treatment of the interior with acoustic absorption material will help to maximize noise reduction. Such material can also provide an indirect source of damping for panel vibration by increasing the acoustic radiation resistance load for the vibrating panels. One type of treatment, available commercially from suppliers of damping materials, incorporates unconstrained layer damping treatment on one side of a two layer composite with a layer of open cell, foamed plastic material on the other side to provide high acoustic absorption. Typical acoustic absorption coefficients for one type of treatment are listed in Table 11.10.

TABLE 11.10

TYPICAL ACOUSTIC ABSORPTION COEFFICIENTS OF FOAMED PLASTIC SHEETS FORMING EXPOSED SIDE OF A COMBINED STRUCTURAL DAMPING\* AND ACOUSTIC ABSORPTION TREATMENT

Foam Thickness	Frequency Hz					
	125	250	500	1000	2000	4000
1/4"	0.05	0.06	0.10	0.20	0.45	0.82
1/2"	0.06	0.10	0.25	0.60	0.90	0.99
1"	0.12	0.30	0.66	0.90	0.99	0.96

\*Loss factor of 0.05 in thick damping layer was 0.017 at 160 Hz on 0.25 in. steel plate (Geiger Plate Test).

The potential benefits of this type of combined structural and acoustic damping for interior lining of small equipment containers are obvious.

A wide variety of conventional acoustical materials are also available for interior acoustic treatment of enclosures. Materials to be considered should have a very high absorption coefficient at the lower order internal acoustic resonances for maximum effectiveness. An extensive table of absorption coefficients of such materials is given in Table 12.13, page 12.23. Radiation damping of the walls and low frequency acoustic absorption can be increased by adding a thin impervious membrane to the outside surface of the treatment. Maximum effectiveness of any acoustic treatment can be achieved by placing it at pressure antinodes. For example, a minimum cost treatment for damping internal acoustic resonances would consist of an acoustic lining on three adjacent walls forming one corner of the enclosure.

Structural design changes can be made which can also reduce noise transmission. These include the avoidance of large unsupported opposing walls, breaking up symmetry of the wall structure, and use of adhesively bonded joints. Finally, a desirable design concept would minimize the ratio of unsupported area to thickness for the walls of the enclosure since this ratio controls the modal density of the structure and the noise reduction will vary inversely to modal density at high frequencies (Reference 11.32).

In the frequency range where coincidence effects become significant, the same design improvement concepts involving structural damping, acoustic absorption, and structural design are beneficial. However, one additional factor becomes significant in this range. At coincidence frequencies much greater than the fundamental mode, damping of the bending waves in the finite panel causes it to behave as if it had no boundaries, and hence standing waves are suppressed. Then, as shown in Reference 11.31, the sound transmission loss (in linear units) is proportional to the square of the quantity:

$$\text{where } \rho_p \eta / c_L$$

$\rho_p$  = material density  
 $\eta$  = material loss factor, and  
 $c_L$  = speed of sound in material.

While the above expression indicates that material thickness is not important for sound transmission at coincidence, the total surface mass, and hence panel thickness does control sound transmission at frequencies near coincidence. Nevertheless, maximizing this quantity will tend to reduce coincidence dips in the noise reduction curve. The ratio  $\rho_p / c_L$  is listed below for a few materials in descending order of relative magnitude, based on a value of 1 for steel. Available data on the loss factor,  $\eta$ , for these materials is also listed and indicates a similar trend is followed.

## "Coincidence" Parameters

Material	$\rho_p / c_L$ (relative to steel)	$\eta$
Lead	6.1	.015
Plywood	2.18	.01
Brass	1.66	-
Copper	1.63	-
Cast Iron	1.36	.10
Steel	1.00	.0047
Plexiglass	0.85	.002
Titanium	0.58	.0012- .0037
Aluminum	0.34	.000045 at 1500 Hz to .003 at 15 Hz
Magnesium	0.23	.0032

On the basis of these parameters, steel is clearly preferable among the more common materials used for equipment containers. The inherent difference in noise reduction for steel and aluminum indicated by the above data is reflected in Figure 11.49. Brass and copper alloys offer further possible improvements where strength is not critical. Unfortunately, comparable data are lacking for the wide variety of structural plastics which are frequently employed for equipment packages. Although optimum material selection appears to offer definite benefits in maximizing noise reduction of high frequencies, it should not be overemphasized. In other words, the most effective means for reducing noise transmission through equipment enclosures is through optimum application of structural damping, acoustic absorption and good vibro-acoustic design practices.

11.8.2.4 Vibration Isolation of Equipment

As indicated earlier in this chapter, vibration isolation is one of the important methods for reducing acoustically-induced environmental loads on equipment. As shown in Figure 11.34, page 11-31, structurally transmitted vibration can originate at a point remote from the equipment package due to acoustic vibration of the basic mounting structure or originate at the package structure itself by direct acoustic excitation of the container walls. When other means of reducing this acoustically generated vibration have been exhausted, such as noise reduction or damping treatment, then vibration isolation may be called for to provide adequate equipment protection. It is desirable to conclude this chapter, therefore, with a brief review of practical methods for protecting ground support equipment from such vibration. Only the use of vibration isolators, as a part of protective packaging design, is considered in this section. A more general discussion of methods for vibration control is given in Chapter 9. The theoretical background for vibration isolation is reviewed in Chapter 3 and is also extensively covered in engineering texts and handbooks (e.g. Reference 11.34-35).

Basic Principles

If an equipment package is represented as a rigid mass with a weight  $W$ -lbs, then a linear spring with a stiffness  $k$ -lb/in, inserted between the package and its support structure will attenuate frequency components of the support motion which exceed a cut-off frequency  $f_c$  equal to  $\sqrt{2}$  times the resonant frequency of the spring-mass. That is

$$f_c = \sqrt{2} f_o \quad (11.30)$$

where

$$f_o = \frac{1}{2\pi} \sqrt{\frac{k}{W/g}} = 3.13 \sqrt{k/W}$$

The absolute transmissibility  $T$ , which is equal to the ratio of the absolute motion of the mass to motion of the support, varies with the frequency ratio  $f/f_o$ , as plotted in Figure 11.52 for a linear damped vibration isolator. The motion may be specified as the amplitude of the displacement, velocity or acceleration. Note in Figure 11.52 that for  $f/f_o > 1.4$ , the transmissibility increases (i.e., higher vibration transmission) as the amplification factor,  $Q$ , of the isolator decreases. This is just opposite to the change in transmissibility at resonance which is approximately equal to the dynamic magnification factor  $Q$ . At frequencies well above resonance, the transmissibility is equal to

$$T_{f > f_o} \approx \sqrt{(1 + (f/f_o Q)^2) / (f/f_o)^2} \quad (11.31)$$

which approaches  $f_o/fQ$  for low values of  $Q$ , or  $(f_o/f)^2$  for high values of  $Q$ . Thus, the idealized model for an isolator indicates low damping is desired for isolators to achieve maximum vibration attenuation at high frequencies

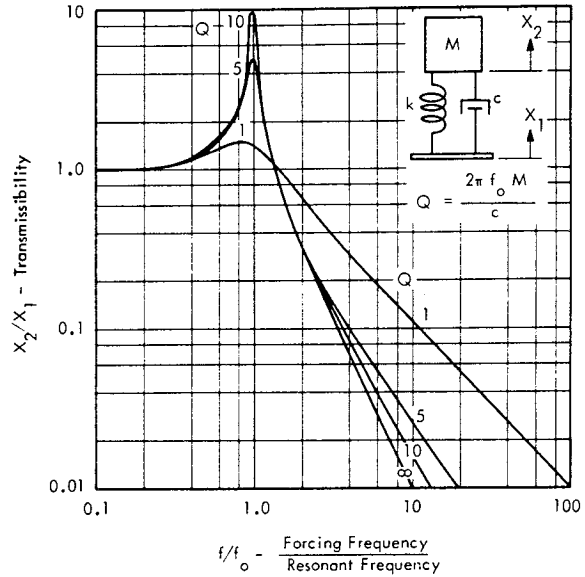


FIGURE 11.52 Transmissibility of a Linear Viscous Damped Isolator

well above the resonant frequency. However, an additional effect occurs in vibration isolators at high frequencies which dictates a compromise is desired in selection of an isolator material for optimum high frequency transmissibility. This is the phenomena of wave motion in the isolator which acts to increase the transmissibility at frequencies corresponding to one-half wavelength resonances in the isolator spring (Reference 11.34). These resonant peaks may be very pronounced for isolators, such as steel springs, with low damping properties. A suitable compromise is provided by the use of rubber vibration isolators with intermediate values of damping ( $Q$ 's of the order of 5 to 20). A comparison of typical transmissibilities for three different types of isolator materials is shown in Figure 11.53. This illustrates the variation in high frequency transmissibility with damping discussed above. The curves for the rubber and Hycar isolator materials are based on measured data. The curve for the steel coil spring was calculated on the basis of the theory in Reference 11.34.

The peaks in the transmissibility curve above the cut-off frequency occur at the standing wave resonance frequencies,  $f_{sn}$  given by

$$f_{sn} = n\pi f_o \sqrt{W_E/W_I} \quad (11.32)$$

where

- $f_o$  = resonance frequency of ideal isolator (Equation 11.30)
- $W_E$  = weight of equipment supported by isolator
- $W_I$  = weight of isolator
- $n$  = 1, 2, 3, .....

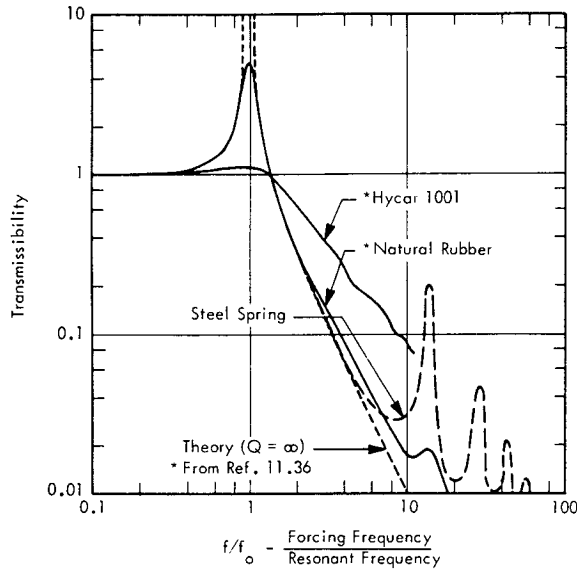


FIGURE 11.53 Comparison of Transmissibilities of Vibration Isolator Using Three Different Types of Isolator Material

It is important that these standing wave effects be considered when evaluating high frequency vibration transmission of isolators. Due to these standing waves and the additional influence of the flexibility of the equipment package itself, minimum transmissibility of an isolator is usually limited to .01 to .1 (20 to 40 dB) at frequencies greater than 10 times the resonant frequency.

Selection of Vibration Isolator Configuration

The types of vibration isolators most frequently used for equipment packages are

- Rubber (in shear or compression) vibration isolators
- Steel coil compression springs
- Wire mesh compression springs
- Foam rubber compression pads

Typical examples of these isolators are illustrated in Figure 11.54. Other types of material such as cork, fiberglass and felt are also used for vibration isolation along with pneumatic cylinders or air bags. However, these types are more frequently employed for isolating large structures or heavy machinery.

Selection of a particular isolator configuration may require the evaluation of several design parameters, in addition to the obvious ones of resonant frequency and damping. The significance of these parameters will increase with the size and complexity of the equipment package and its ambient environment.

- Resonant frequency to achieve required transmissibility in the frequency range of the input motion

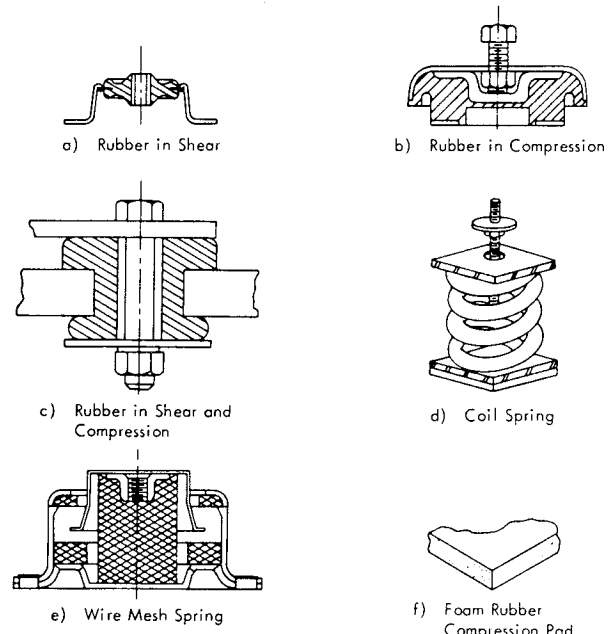


FIGURE 11.54 Typical Vibration Isolators for Ground Support Equipment

- Damping
- Maximum static load
- Maximum allowable deflection
- Maximum operating temperature
- Mounting position on package to minimize coupling of multiple modes of isolation system
- Effect of non-rigid equipment package

Resonant Frequency Under Load

Most rubber materials exhibit non-linear characteristics under static loads. In this case, the resonant frequency estimated for the linear spring by Equation 11.30 or by its equivalent,

$$f_o = 3.13 \sqrt{1/\delta_{st}} \tag{11.33}$$

where

$$\delta_{st} = \text{static deflection under load - inches}$$

is not valid. The effective or dynamic stiffness of a non-linear spring for a given static load is the local slope of the force-deflection curve at the static equilibrium point. For isolators using rubber in compression, this dynamic stiffness is greater than the static stiffness (hard spring) so that the resonant frequency is higher than predicted by Equation 11.33. This is illustrated in Figure 11.55 which shows the typical relationship between resonance frequency and static deflection for several types of vibration isolators under full load. For steel springs, the actual resonance frequency is closely approximated by theory. Rubber



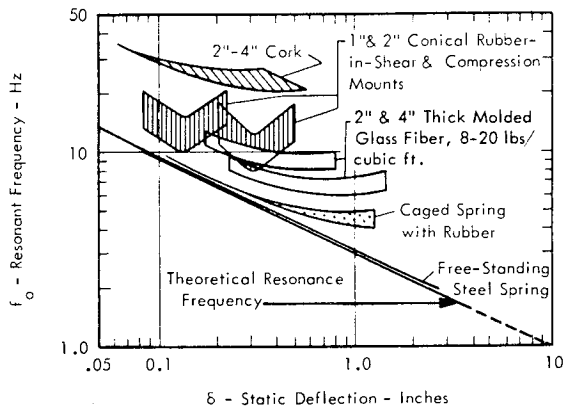


FIGURE 11.55 Resonant Frequency Versus Static Deflection for a Variety of Vibration Isolator Materials (From Reference 11.38)

isolators loaded well below their full capacity also behave in a nearly ideal fashion.

This figure also illustrates the fact that for the materials shown, resonance frequencies below 6 Hz are achieved only with coil springs. Thus, for maximum attenuation of low frequency vibration induced by noise of rockets, coil spring isolators, or equivalent mechanical or pneumatic springs, are generally required.

Damping

Typical values for resonant amplification factors of several types of vibration isolator materials are given in the following (References 11.34 and 11.36).

Material	Q
Natural Rubber (50 parts, Carbon Black)	5-25
GR-S Rubber (Krylene)	4.5
Polyisobutylene	1.7-3.3
Steel	100

These represent approximate values which are subject to appreciable variation depending on the amount of additional friction damping provided by the isolator configuration.

Maximum Static Load

The maximum static load capacity of conventional vibration isolators ranges from less than 1 pound to over 10,000 lbs per unit. The resonance frequencies, under full load, fall in the range from 6 to over 30 Hz. Detailed performance characteristics of specific units should be obtained from manufacturers specifications. A summary of maximum load capacity, stiffness and size of a wide variety of commercially available rubber and coil spring isolators is contained in Reference 11.34.

Maximum Allowable Deflection

The maximum deflection of a vibration isolated package must be considered to insure that: 1) the isolator does not bottom-out under peak dynamic loads or 2) the rattle space, or envelope of maximum displacement of the package, is sufficient to prevent any impacts with adjacent hard surfaces. The result, in either case, would be to generate a shock input to the package which can be more severe than the environment of the mounting structure. This is particularly true for any shocks resulting from inadequate rattle space. Shocks due to bottoming out of the isolator are frequently attenuated by a gradual "hardening" of the load-deflection characteristics of the isolator spring, thus eliminating any sudden changes in acceleration. However, specific "bottoming" characteristics vary widely with the design of the isolator and must be determined from detailed manufacturers specifications.

The determination of rattle space requirements will depend on the frequency spectrum of the input motion to the isolator. Since the source of vibration at rocket test sites will be random acoustic noise, the vibration spectrum of the equipment foundation will generally consist of a complex spectrum of random noise with peaks in the spectral content corresponding to the vibration modes of the supporting structure. When the random input spectrum can be described by a constant acceleration spectral density,  $W(f)$ , (See Chapter 3 for definition of acceleration spectral density) over a bandwidth appreciably wider than the resonant bandwidth,  $f_0/Q$ , of the isolator, then the root rms deflection,  $\tilde{X}_r$ , of the package, relative to its mounting surface, can be estimated by

$$\tilde{X}_r \approx \frac{386}{(2\pi f_0)^2} \sqrt{\frac{\pi}{2} W(f) Q f_0} \quad (11.34)$$

where

$$Q \approx \text{Maximum Transmissibility at Resonant Frequency } f_0$$

If the input acceleration spectral density can not be assumed to be constant, or is known from measurements, then a more accurate estimate of the rms relative deflection can be made by integrating, graphically, the product of the input acceleration spectrum  $W(f)$  in  $g^2/Hz$  times the square of the absolute transmissibility curve and multiplying the square root of the resulting area by  $386/(2\pi f_0)^2$  for a deflection in inches. This graphical process is illustrated in Figure 11.56. The method is approximate but is sufficiently accurate for design purposes.

The peak deflection  $X_{pr}$  of the package, relative to its support, can be stated statistically; the deflection will exceed 3 times the rms value about 1 percent of the time, or 4.3 times the rms value 0.01 percent of the time.

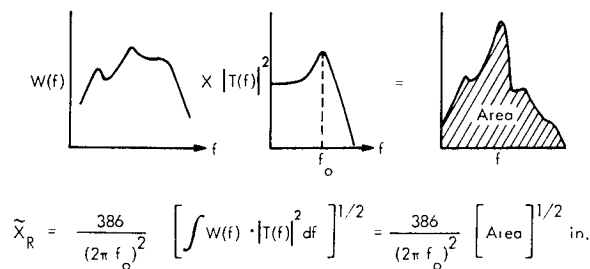


FIGURE 11.56 Graphical Determination of rms RELATIVE DEFLECTION of Vibration Isolated Mass Excited by Wide-Band Random Noise

### Maximum Operating Temperature

Conventional rubber isolators are generally limited to a temperature range of  $-65^{\circ}\text{F}$  to  $175^{\circ}\text{F}$  or, with special materials, to  $250^{\circ}\text{F}$ . Metal coil springs or wire mesh springs can be used up to  $500^{\circ}\text{F}$  to  $1000^{\circ}\text{F}$ , depending on the design and material.

### Mounting Position

The vibration isolated package can vibrate in 6 degrees of freedom, that is along 3 translational axes and about 3 rotational axes. The optimum mounting arrangement for the vibration isolators is one which minimizes coupling of vibration from a translational direction to a rotation. This has the advantage of simplifying the analysis of the isolation characteristics to that of a single degree of freedom system and reduces the rattle space requirements. This "uncoupled" mounting arrangement can be accomplished by arranging the isolators so that no rotation of the package occurs when it is displaced by a force directed through its center of gravity. Methods of designing such mounts are treated in detail in Reference 11.35. The methods require knowledge of the in-axis and lateral stiffnesses of the isolator units as well as their mounting positions and the mass moments of inertia of the package about its axes at rotation.

### Effect of Non-Rigid Equipment Package

The vibration isolation concepts considered so far have assumed a rigid equipment package. In reality, most packages exhibit a dynamic mass which changes with frequency due to their flexibility or non-rigidity. The effect of this is to reduce the maximum isolation that can be achieved. An example of this effect was shown by the measured vibration isolation of a spring mounted floor assembly in Figure 11.17, page 11-16. In this case, maximum transmission loss was limited to about 20 dB.

To briefly summarize, proper application of vibration isolation systems to sensitive equipment packages provides a useful and efficient means of reducing the vibration loads due to acoustic excitation of the package or its mounting structure by 20 to 40 dB. However, if the acoustic excitation is applied directly to the package, vibration isolation must be applied to internal components to be effective.

### REFERENCES

- 11.1 Anonymous, "Saturn IB/V Program - Launch Site Support Equipment", Systems Operation Equipment Design Branch, M-ASTR-ES (no date).
- 11.2 "NASA/AGENA-B Ranger Program Launch Pad Damage Report for Spacecraft RA-4, Complex 12, AMR", Lockheed Missiles and Space Co., SSQ-592-T62-1, April, 1962.
- 11.3 Sugamele, J., "Response of Electronic Equipment to Acoustic Noise Environments", The Boeing Co. Document D6-9492, May, 1965.
- 11.4 Murray, F., "The Effects of Acoustic Noise On Electronic Equipment", The Boeing Co. Document No. D2-7791.
- 11.5 Noiseux, P.U., et al., "Response of Electronics to Intense Noise Fields", ASD Technical Report 61-391, November, 1961.
- 11.6 Wyle Laboratories Acoustic Qualification Test Reports, 1964-1966.
- 11.7 Interdepartmental Data Exchange Program (IDEP) Reports.
- 11.8 Rothbart, H.A., editor "Mechanical Design and Systems Handbook", McGraw-Hill Book Co., N.Y., (1964).
- 11.9 Unpublished Test Data, Wyle Laboratories
- 11.10 Winlund, E.S. et al., "Reliability and Maintainability Training Handbook", Prepared for U.S. Navy, BuShips by General Dynamics/Aeronautics Co., NAVSHIPS 0900-002-3000, Dec., 1964.
- 11.11 Noiseux, D.U., "Response of Electronics to Intense Sound Fields", WADD TR 60-754, January, 1961.
- 11.12 Bozich, D., "Investigations of the Vibratory Response of an RCA 110A Saturn Ground Computer System to Acoustic and Vibration Test Requirements", Wyle Laboratories Research Staff Report WR-65-23, September, 1965.
- 11.13 Saunders, B., Marshall Space Flight Center, NASA (Personal Communication).
- 11.14 Dorland, W.D., and Tedrick, R.N., "Results of Acoustic Survey of SA-1 Launch", NASA Report MTP-Test-62-2, March, 1962.
- 11.15 Acoustic and Vibration Environments and Test Specification Levels - Ground Support Equipment Launch Complex 39 NASA, J.F.K. Space Center Report SP-4-38-D, July, 1964.

- 11.16 Harris, C.M. and Crede, C.E., "Shock and Vibration Handbook", Chapters 42 and 43, McGraw-Hill Book Co., 1961.
- 11.17 "Suggestions for Designers of Electronic Equipment", Naval Electronics Laboratory, 1960.
- 11.18 Ruzicka, J.E., "Vibration Response Characteristics of Viscoelastic-Damped Structures", Shock and Vibration Bulletin, Part 5, Feb. (1965).
- 11.19 Maidanik, G., "Energy Dissipation Associated with Gas-Pumping in Structural Joints", Journ. Acoust. Soc. Amer. 40: 1064-1072, Nov. (1966).
- 11.20 Sharpe, L.H., "Assembling with Adhesives", Machine Design, Aug. 18, (1966).
- 11.21 Guttman, W.H., "Concise Guide to Structural Adhesives", Academic Press, New York, (1961).
- 11.22 (Reference 11.16, Chapter 37).
- 11.23 Ruzicka, J.E., (Ed), "Structural Damping" Applied Mechanics Division of ASME, Dec. (1959).
- 11.24 Oberst, H., and Schommer, A., Chapter 29, "Acoustical Fatigue in Aircraft Structures", Edited by W.J. Trapp and D.M. Forney, Syracuse Univ. Press.
- 11.25 Kerwin, E.M., "Damping of Flexural Waves by a Constrained Viscoelastic Layer", Journ. Acoust. Soc. Am. 31: pp 952-962, (1959).
- 11.26 "Special Report on LD-400 Damping Material", Lord Manufacturing Co., (1965).
- 11.27 Licari, J.J., and Brands, E.R., "Organic Coatings for Metal and Plastic Surfaces", Machine Design, pp 176-194, May 25, (1967).
- 11.28 Chi, S.H., "Bibliography and Tabulation of Damping Properties of Non-Metallic Materials", WADD-TR-60-540, Sept. (1962).
- 11.29 Rondeau, H.F., "Synthetic Materials, Machine Design, July 21, (1966).
- 11.30 Misc. Technical Data Sheets, Silicone Products Department, General Electric Company.
- 11.31 Beranek, L.L., "Noise Reduction", McGraw-Hill Book Co., (1960).
- 11.32 Lyon, R.H., "Noise Reduction of Rectangular Enclosures with one Flexible Wall", Journ. Acoust. Soc. Am. 35: 1791-1797, Nov., (1963).
- 11.33 Beranek, L.L., "Acoustics", McGraw-Hill Book Company, (1954).
- 11.34 (Reference 11.16 - Chapters 30 and 32).
- 11.35 Crede, C.E., "Vibration and Shock Isolation", John Wiley and Sons, N.Y., (1951).
- 11.36 Snowdon, J.C., "Dynamic Mechanical Properties of Rubber-Like Materials with Reference to the Isolation of Mechanical Vibration", Noise Control, 6: 18-23, March, (1960).
- 11.37 Harris, C.M., (Ed), "Handbook of Noise Control", McGraw-Hill Book Co., N.Y., (1957).

**CHAPTER 12**  
**CONVERSION TABLES AND**  
**MATERIAL PROPERTIES**

## TABLE OF CONTENTS

<u>SECTION</u>		<u>PAGE</u>
12.1	<u>INTRODUCTION</u> .....	12-1
12.2	<u>CONVERSION TABLES AND CHARTS</u> .....	12-1
12.3	<u>DATA ON BASIC MATERIALS</u> .....	12-13
12.4	<u>DATA ON ACOUSTIC ABSORPTION COEFFICIENTS AND SOUND TRANSMISSION LOSS</u> ...	12-25
	REFERENCES FOR SECTIONS 12.3 And 12.4 .....	12-40
	BIBLIOGRAPHY FOR TABLE 12.5 .....	12-42

## CHAPTER 12

### CONVERSION TABLES AND MATERIAL PROPERTIES

#### 12.1 INTRODUCTION

This chapter consists of conversion tables, charts and material data compiled from various sources, for this manual. Section 12.2 gives the conversion factors with particular emphasis on conversions among the MKS, CGS, and the English Engineering systems, Tables 12.1 through 12.10. Conversion charts are also included in this Section to convert decibels (dB) to corresponding power and pressure ratios, Chart 12.1; to convert sound pressure level to intensity, Chart 12.2, and to pressure, Chart 12.3; and to convert pressure spectral density to octave and one-third octave band levels, Chart 12.4. Table 12.11 provides corrections for the addition of Sound Pressure Level in dB. Table 12.12 lists the preferred frequencies, intervals and band numbers for acoustic measurements. Section

12.3 contains a collection of the physical properties of the commonly used building construction materials. In particular, Table 12.13 represents an extensive effort of technical and literature review. Nevertheless, many no-entries are due to the lack of published information. Figures 12.3.1 through 12.3.6, and Table 12.14 are supplementary data on glass and woods, and the stress-cycles curves of a few representative building materials. In Section 12.4 the acoustic absorption coefficients of various materials commonly found in buildings and residences are listed alphabetically in Table 12.15. Most absorption coefficient values are given in terms of a probable range rather than a single value, to cover the wide range of similar materials or products encountered. Sources for these absorption coefficient data are mainly from literature published in the United States. Data from foreign sources, obtained from laboratory tests with different test standards, were excluded. Figures 12.7a through 12.7f show the sound transmission loss through representative partitions, walls, doors, windows, and floor-ceiling assemblies. References and bibliography of data sources are listed for Sections 12.3 and 12.4 at the end of this chapter.

#### 12.2 CONVERSION TABLES AND CHARTS

TABLE 12.1a CONVERSION FACTORS FOR UNITS OF LENGTH

From X Equals	cm	m	in.	ft
1 cm	1	0.01	0.3937	0.032808
1 m	100.	1	39.37	3.2808
1 in.	2.5400	0.02540	1	0.08333
1 ft	30.480	0.30480	12.	1

TABLE 12.1b CONVERSION FACTORS FOR UNITS OF AREA

From X Equals	cm <sup>2</sup>	m <sup>2</sup>	sq.in.	sq.ft
1 cm <sup>2</sup>	1	10 <sup>-4</sup>	0.15500	1.0764 · 10 <sup>-3</sup>
1 m <sup>2</sup>	10 <sup>4</sup>	1	1550.0	10.764
1 sq.in.	6.4516	6.4516 · 10 <sup>-4</sup>	1	6.9444 · 10 <sup>-3</sup>
1 sq.ft	929.03	0.09290	144.	1

TABLE 12.1c CONVERSION FACTORS FOR UNITS OF VOLUME

From X Equals	cm <sup>3</sup>	cu in.	cu ft	m <sup>3</sup>
1 cm <sup>3</sup>	1	0.061023	$3.5315 \cdot 10^{-5}$	$10^{-6}$
1 cu in.	16.387	1	$5.7870 \cdot 10^{-4}$	$1.6387 \cdot 10^{-5}$
1 cu ft	28317.0	1728.	1	$2.8316 \cdot 10^{-2}$
1 m <sup>3</sup>	$10^6$	$6.1023 \cdot 10^4$	35.315	1
1 gal	3785.4	231.	0.13368	$3.7854 \cdot 10^{-3}$

TABLE 12.2 CONVERSION FACTORS FOR UNITS OF MASS

From X Equals	g	kg	lb	slug
1 g	1	$10^{-3}$	$2.2046 \cdot 10^{-3}$	$6.8522 \cdot 10^{-5}$
1 kg	$10^3$	1	2.2046	$6.8522 \cdot 10^{-2}$
1 lb	453.59	0.45359	1	$3.1081 \cdot 10^{-2}$
1 slug	14594.	14.594	32.174	1

TABLE 12.3 CONVERSION FACTORS FOR UNITS OF FORCE

From X Equals	dyne	newton	kg (wt)	lb (wt)
1 dyne	1	$10^{-5}$	$1.0197 \cdot 10^{-6}$	$2.2481 \cdot 10^{-6}$
1 newton	$10^5$	1	0.10197	$2.2481 \cdot 10^{-1}$
1 kg (wt)	$9.8067 \cdot 10^5$	9.8067	1	2.2046
1 lb (wt)	$4.4482 \cdot 10^5$	4.4482	0.45359	1

TABLE 12.4 CONVERSION FACTORS FOR UNITS OF DENSITY

From X Equals →	$\text{g/cm}^3$	$\text{kg/m}^3$	lb/cu in.	lb/cu ft
1 $\text{g/cm}^3$	1	1000.	0.036128	62.428
1 $\text{kg/m}^3$	$10^{-3}$	1	$3.6128 \cdot 10^{-5}$	$6.2428 \cdot 10^{-2}$
1 lb/cu in.	27.680	27680.	1	1728.
1 lb/cu ft	0.016018	16.018	$5.7870 \cdot 10^{-4}$	1

TABLE 12.5 CONVERSION FACTORS FOR UNITS OF PRESSURE

From X Equals →	$\text{dyne/cm}^2$	bar	atm	$\text{newton/m}^2$
1 $\text{dyne/cm}^2$	1	$10^{-6}$	$9.8692 \cdot 10^{-5}$	0.1
1 bar	$10^6$	1	0.98692	$10^5$
1 atm	$1.0133 \cdot 10^6$	1.0133	1	$1.0133 \cdot 10^5$
1 $\text{newton/m}^2$	10	$10^{-5}$	$9.8692 \cdot 10^{-4}$	1
1 mm Hg (0°C)	1333.2	$1.3332 \cdot 10^{-3}$	$1.3158 \cdot 10^{-3}$	133.32
1 in. Hg (0°C)	33864.	0.033864	0.033421	3386.4
1 lb(wt)/sq in.	68947.	0.068947	0.068046	6894.7

TABLE 12.5 CONVERSION FACTORS FOR UNITS OF PRESSURE (CONTINUED)

From X Equals →	mm Hg (0°C)	in. Hg (0°C)	lb(wt)/sq in.	in. $\text{H}_2\text{O}$ (4°C)
1 $\text{dyne/cm}^2$	$7.5006 \cdot 10^{-4}$	$2.9530 \cdot 10^{-5}$	$1.4504 \cdot 10^{-5}$	$4.0148 \cdot 10^{-4}$
1 bar	750.06	29.530	14.504	$4.0148 \cdot 10^2$
1 atm	760.	29.921	14.696	406.78
1 $\text{newton/m}^2$	$7.5006 \cdot 10^{-3}$	$2.9530 \cdot 10^{-4}$	$1.4504 \cdot 10^{-4}$	$4.0148 \cdot 10^{-3}$
1 mm Hg (0°C)	1	0.03937	0.019337	0.5352
1 in. Hg (0°C)	25.400	1	0.49116	13.595
1 lb(wt)/sq in.	51.715	2.0360	1	27.673



TABLE 12.6a CONVERSION FACTORS FOR UNITS OF ENERGY

From X Equals →	joule	erg.	Btu	ft-lb(wt)
1 joule, newton-m	1	$10^7$	$0.94805 \cdot 10^{-3}$	0.73756
1 erg, dyne-cm	$10^{-7}$	1	$9.4805 \cdot 10^{-11}$	$7.3756 \cdot 10^{-8}$
1 Btu	1054.80	$1.0548 \cdot 10^{10}$	1	778.16
1 ft-lb(wt)	1.3558	$1.3558 \cdot 10^7$	$1.2851 \cdot 10^{-3}$	1

TABLE 12.6b CONVERSION FACTORS FOR UNITS OF POWER

From X Equals →	Watt	ft-lb/sec	Hp	Btu/min
1 watt, joule/sec	1	0.7378	$1.341 \cdot 10^{-3}$	0.05688
1 ft-lb/sec	1.3558	1	$1.818 \cdot 10^{-3}$	0.07712
1 Hp	745.7	550.0	1	42.44
1 Btu /min	17.57	12.96	0.02356	1

TABLE 12.7 CONVERSION FORMULAS FOR UNITS OF TEMPERATURE

To Convert to From, Use →	°F	°C	°R	°K
°F	1	$\frac{5}{9}(\text{°F} - 32)$	$\text{°F} + 459.67$	$\frac{5}{9}\text{°F} + 255.37$
°C	$\frac{9}{5}\text{°C} + 32$	1	$\frac{9}{5}\text{°C} + 491.67$	$\text{°C} + 273.15$
°R	$\text{°R} - 459.67$	$\frac{5}{9}\text{°R} - 273.15$	1	$\frac{5}{9}\text{°R}$
°K	$\frac{9}{5}\text{°K} - 459.67$	$\text{°K} - 273.15$	$\frac{9}{5}\text{°K}$	1

TABLE 12.8 a CONVERSION FACTORS FOR TRANSLATIONAL VELOCITY AND ACCELERATION

From X Equals $\rightarrow$ $\downarrow$	g-sec, g	ft/sec ft/sec <sup>2</sup>	in./sec in./sec <sup>2</sup>	m/sec m/sec <sup>2</sup>
g-sec, g	1	32.16	386	9.80
ft/sec ft/sec <sup>2</sup>	0.0311	1	12.0	0.3048
in./sec in./sec <sup>2</sup>	0.00259	0.0833	1	0.0254
cm/sec cm/sec <sup>2</sup>	0.00102	0.0328	0.3937	0.010
m/sec m/sec <sup>2</sup>	0.102	3.28	39.37	1

TABLE 12.8 b CONVERSION FACTORS FOR ROTATIONAL VELOCITY AND ACCELERATION

From X Equals $\rightarrow$ $\downarrow$	rad/sec rad/sec <sup>2</sup>	degree/sec degree/sec <sup>2</sup>	Hz. Hz./sec	rev/min rev/min/sec
rad/sec rad/sec <sup>2</sup>	1	57.30	0.1592	9.549
degree/sec degree/sec <sup>2</sup>	0.01745	1	0.00278	0.1667
Hz. Hz./sec	6.283	360	1	60
rev/min rev/min/sec	0.1047	6.00	0.0167	1

TABLE 12.9 CONVERSION FACTORS FOR SIMPLE HARMONIC MOTION

From X Equals $\rightarrow$ $\downarrow$	Amplitude	Average Value	Root-Mean- Square Value (rms)	Peak-to-Peak Value
Amplitude	1	0.637	0.707	2.000
Average Value	1.571	1	1.111	3.142
Root-Mean-Square Value (rms)	1.414	0.900	1	2.828
Peak-to-Peak Value	0.500	0.318	0.354	1

TABLE 12.10 CONVERSION FACTORS FOR EXCESS ACOUSTIC ATTENUATION RATE CONSTANT

From X Equals	Attenuation Constant $\alpha$			Pressure Attenuation Constant $\alpha^*$	
	dB/1000 ft.	dB/mile	dB/m	nepers/ft	nepers/m
dB/1000 ft.	1	5.280	$3.281 \cdot 10^{-3}$	$1.151 \cdot 10^{-4}$	$3.777 \cdot 10^{-4}$
$\alpha$ dB/mile	0.1895	1	$6.214 \cdot 10^{-4}$	$2.182 \cdot 10^{-5}$	$7.158 \cdot 10^{-5}$
dB/m	304.8	1609.	1	$3.509 \cdot 10^{-2}$	0.1155
$\alpha$ $\frac{\text{nepers}}{\text{ft}}$	8686.	$4.586 \cdot 10^4$	28.50	1	3.281
$\frac{\text{nepers}}{\text{m}}$	2648.	$1.398 \cdot 10^4$	8.686	0.3048	1

\*  $e^{-\alpha(x_2 - x_1)} = (\text{Pressure at } x_2)/(\text{Pressure at } x_1)$   
 $\alpha = (\text{Intensity Decay Constant})/2 = m/2$   
 $e^{-m(x_2 - x_1)} = (\text{Intensity at } x_2)/(\text{Intensity at } x_1)$

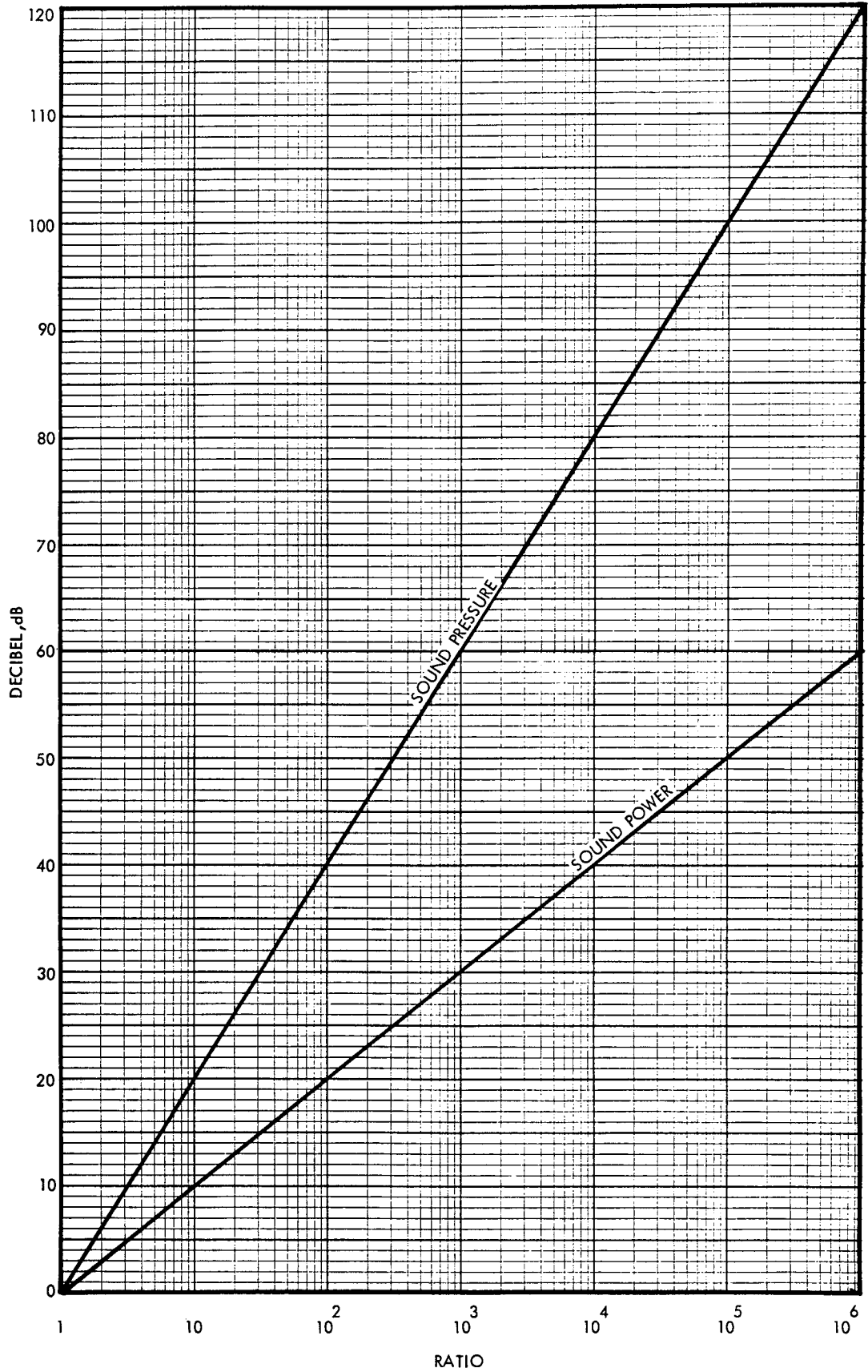


Chart 12.1 Conversion of Decibels to Sound Power Ratio and Sound Pressure Ratio

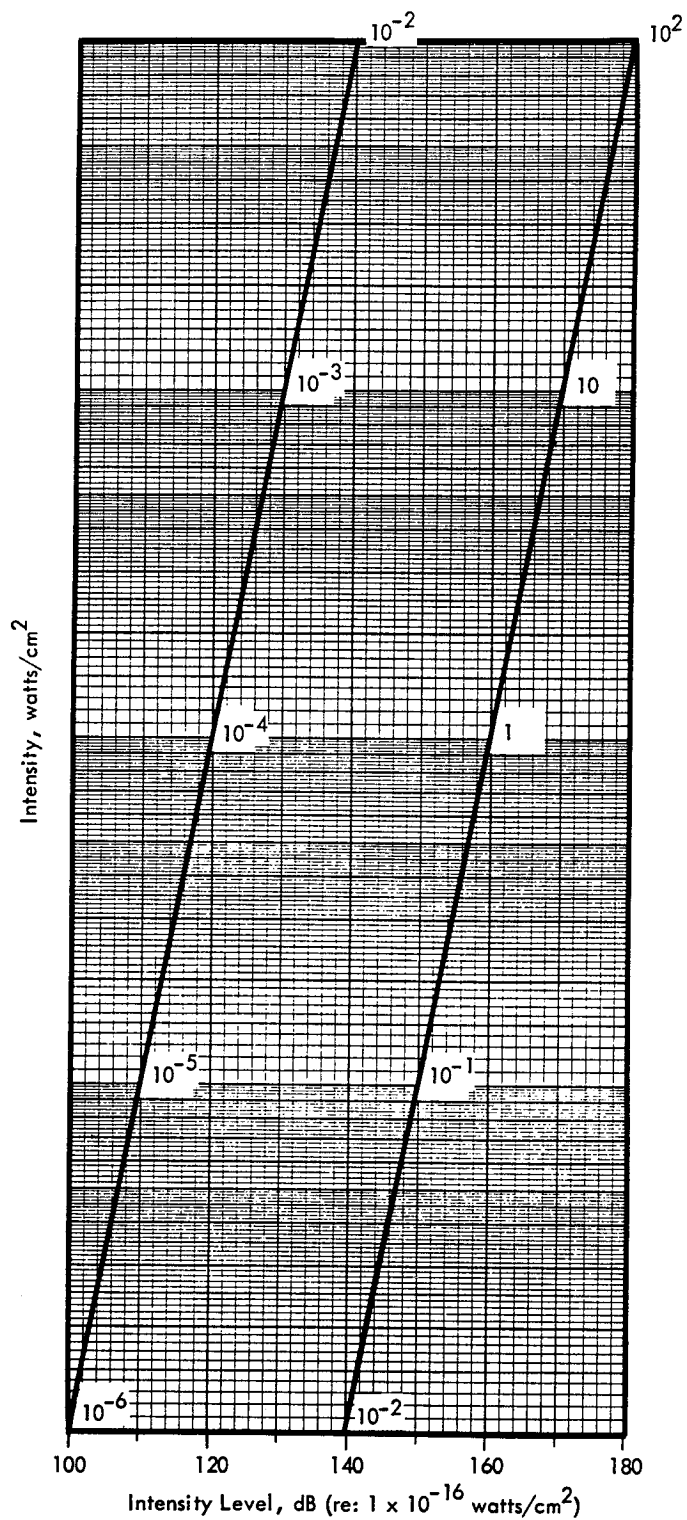


CHART 12.2 Conversion from Intensity Level (dB) to Intensity (watts/cm<sup>2</sup>)

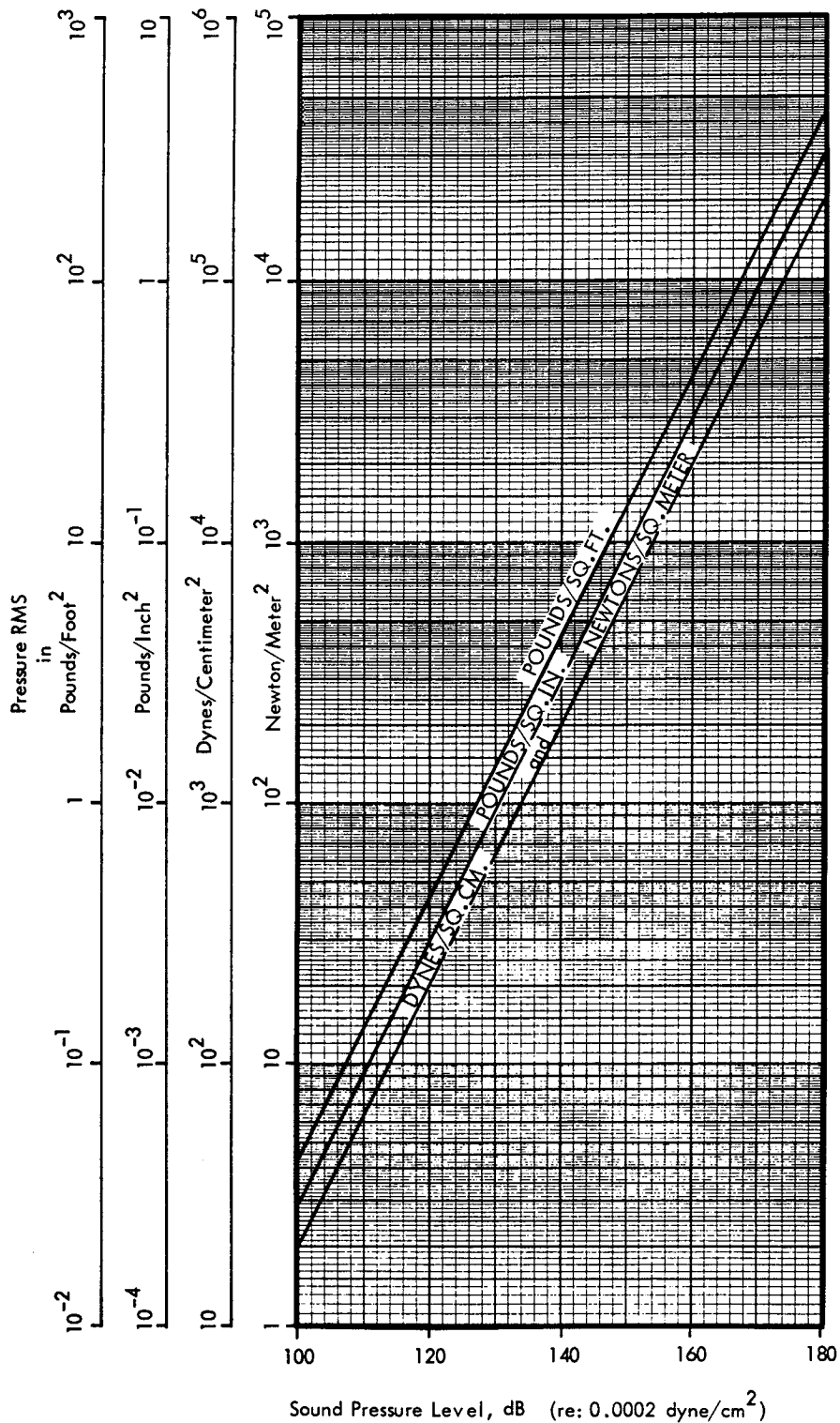


CHART 12.3

Conversion From Sound Pressure Level (dB) To Pounds/Foot<sup>2</sup>, Pounds/Inch<sup>2</sup>, Dynes/Centimeter<sup>2</sup>, and Newton/Meter<sup>2</sup>.

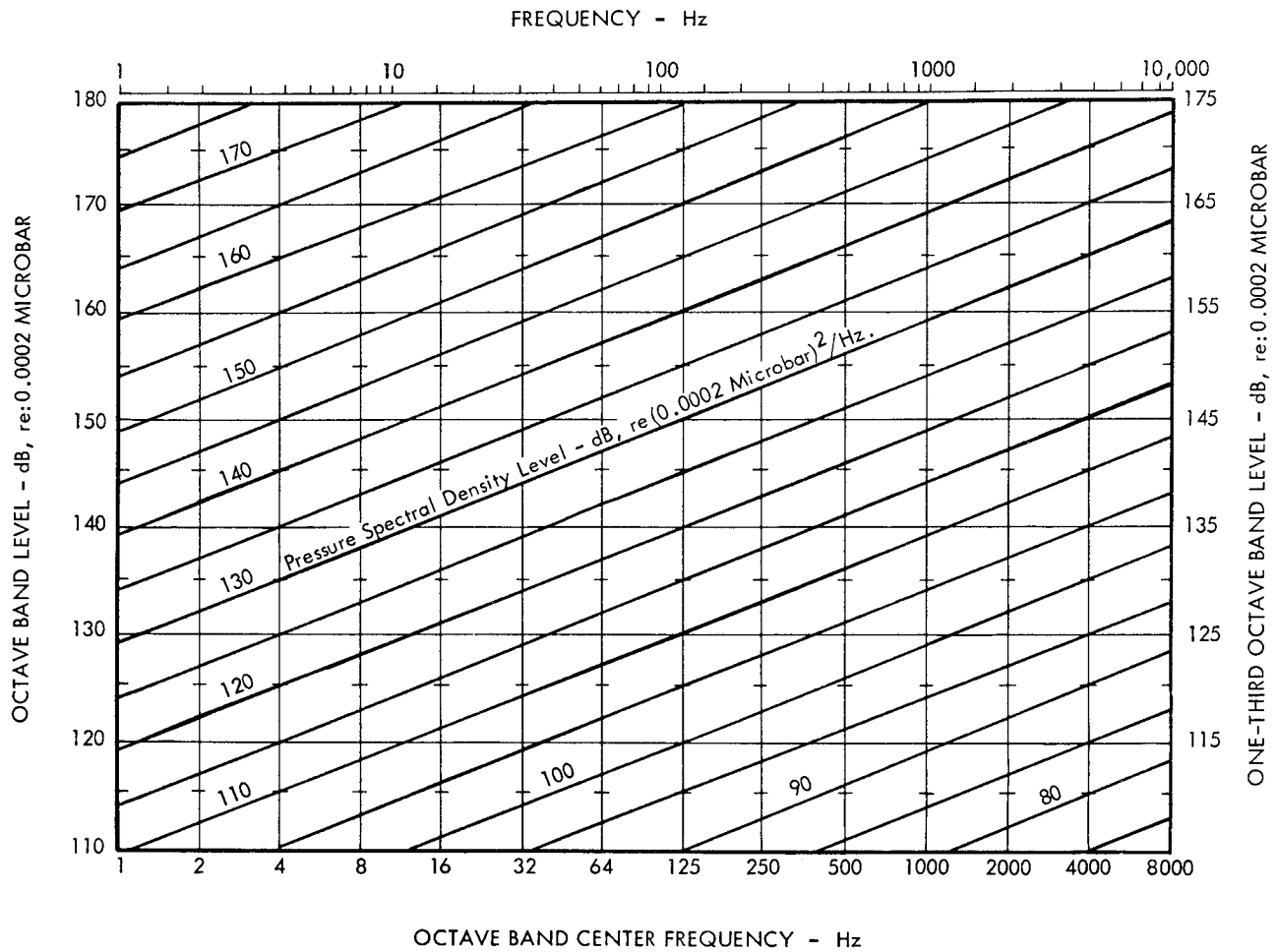


CHART 12.4 Conversion of Pressure Spectral Density Level to Octave and One-Third Octave Band Levels

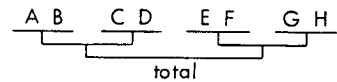
TABLE 12.11  
DIFFERENCES CORRECTIONS FOR USE IN THE ADDITION OF SOUND PRESSURE LEVELS

dB	0	0.1	0.2	0.3	0.4	0.5	0.6	0.7	0.8	0.9
0	3.01	3.06	3.11	3.16	3.22	3.27	3.32	3.38	3.43	3.48
1	3.54	3.60	3.65	3.71	3.77	3.83	3.88	3.94	4.00	4.06
2	4.13	4.19	4.25	4.31	4.37	4.44	4.50	4.57	4.63	4.70
3	4.76	4.83	4.90	4.97	5.04	5.10	5.17	5.24	5.31	5.39
4	5.46	5.53	5.60	5.67	5.75	5.82	5.89	5.97	6.04	6.12
5	6.19	6.27	6.35	6.42	6.50	6.58	6.66	6.74	6.81	6.89
6	6.97	7.05	7.13	7.22	7.30	7.38	7.46	7.54	7.63	7.71
7	7.79	7.87	7.96	8.04	8.13	8.21	8.30	8.38	8.47	8.55
8	8.64	8.73	8.81	8.90	8.99	9.07	9.16	9.25	9.34	9.43
9	9.52	9.60	9.69	9.78	9.87	9.96	10.05	10.14	10.23	10.32
10	10.41	10.50	10.60	10.69	10.78	10.87	10.96	11.06	11.15	11.24
11	11.33	11.42	11.52	11.61	11.70	11.80	11.89	11.98	12.08	12.17
12	12.27	12.36	12.46	12.55	12.64	12.74	12.83	12.93	13.02	13.12
13	13.21	13.31	13.40	13.50	13.60	13.69	13.79	13.88	13.98	14.07
14	14.17	14.27	14.36	14.46	14.56	14.65	14.75	14.84	14.94	15.04
15	15.14	15.23	15.33	15.43	15.52	15.62	15.72	15.82	15.91	16.01
16	16.11	16.21	16.30	16.40	16.50	16.60	16.69	16.79	16.89	16.99
17	17.09	17.18	17.28	17.38	17.48	17.58	17.68	17.77	17.87	17.97

**Method:** Compute the numerical difference between two sound pressure levels. Add the correction from the Table to the smaller of the two levels to get the final level.

**Addition of more than two levels**

Take the levels successively in pairs and perform the above operations i.e.



**Example:** To add 85 dB, 83.4 dB, 74 dB and 89.6 dB

For the first pair, the Diff. = 85 - 83.4 = 1.6 dB  
 Corr. from table = 3.88 dB  
 Total = 83.4 + 3.88 = 87.28 dB

For the second pair the Diff. = 89.6 - 74 = 15.6 dB  
 Corr. from table = 15.72 dB  
 Total = 74 + 15.72 = 89.72 dB

Using the two totals from the two pairs, we obtain  
 Diff. = 89.72 - 87.28 = 2.44 dB  
 Corr. from table = 4.40 dB  
 Final total = 87.28 + 4.40 ≈ 91.7 dB

**Note:** When the difference between two levels is more than 18 dB, use the higher level as the final value without correction.



TABLE 12.12

PREFERRED FREQUENCIES IN HERTZ, AT VARIOUS INTERVALS, AND BAND NUMBERS FOR  
ACOUSTICAL MEASUREMENTS AND FOR CENTER FREQUENCIES OF FILTER PASSBANDS  
(FROM UNITED STATES OF AMERICA STANDARDS INSTITUTE S 1.6-1967)

Preferred Frequencies	Band No.	1 octave	1/2 octave	1/3 octave	Preferred Frequencies	Band No.	1 octave	1/2 octave	1/3 octave	Preferred Frequencies	Band No.	1 octave	1/2 octave	1/3 octave
<u>16</u>	12	X	X	X	160	22			X	1600	32			X
18	12.5				180	22.5		X		1800	32.5			
20	13			X	200	23			X	<u>2000</u>	33	X	X	X
22.4	13.5		X		224	23.5				2240	33.5			
25	14			X	<u>250</u>	24	X	X	X	2500	34			X
28	14.5				280	24.5				2800	34.5		X	
<u>31.5</u>	15	X	X	X	315	25			X	3150	35			X
35.5	15.5				355	25.5		X		3550	35.5			
40	16			X	400	26			X	<u>4000</u>	36	X	X	X
45	16.5		X		450	26.5				4500	36.5			
50	17			X	<u>500</u>	27	X	X	X	5000	37			X
56	17.5				560	27.5				5600	37.5		X	
<u>63</u>	18	X	X	X	630	28			X	6300	38			X
71	18.5				710	28.5		X		7100	38.5			
80	19			X	800	29			X	<u>8000</u>	39	X	X	X
90	19.5		X		900	29.5				9000	39.5			
100	20			X	<u>1000</u>	30	X	X	X	10000	40			X
112	20.5				1120	30.5				11200	40.5		X	
<u>125</u>	21	X	X	X	1250	31			X	12500	41			X
140	21.5				1400	31.5		X		14000	41.5			
160	22			X	1600	32			X	<u>16000</u>	42	X	X	X

12.3 DATA ON BASIC MATERIALS

TABLE 12.13  
PHYSICAL PROPERTIES OF VARIOUS BASIC BUILDING CONSTRUCTION MATERIALS

Building Material	Ultimate strength, psi <sup>①</sup> [Allowable Strength, psi]			Modulus of Rupture psi <sup>②</sup>	Endurance Limit <sup>③</sup>	Young's Modulus [Mod. of Rigidity] x 10 <sup>-6</sup> psi <sup>④</sup>	Poisson's Ratio $\mu$	Loss Factor $\eta$ <sup>⑤</sup>	Density lb/cu. ft [lb/sq. ft]	Reference
	Comp.	Tension	Shear							
<b>ASBESTOS-CEMENT</b>										
Corrugated Sheet										28
Type A (Std.) 3/8"				13,000					[3.7-4.0]	
Type B (Light Wt.) 3/16"				5,300					[1.7-2.0]	
Flat Sheet and Fiberboard Insulating Panel										
Type F (Flexible) 1/8" to 5/8"				9,600 - 10,800						
Type U (Utility) 3/16" to 5/8"				7,600						
<b>BOARD</b>										
Beaverboard, 1/2"						0.175	0.027	[0.8]		13
Cellulose Insulation Board, 1/2"		145-270						[0.7-1.7]		39
Masonite, 3/16"						0.61	0.017	[0.9]		13
Paper Board										3
Asbestos Board, 3/16"		1,250		3,000				[1.36]		
Asphalt-Saturated Sheathing, 25/32"		185		38						
Cellulose Insulation Building Board, 1/2"		650		1,100				[1.0]		
Under Floor Insulation Board, 25/32"		650		1,100				[1.53]		
Sheathing Insulation Board, 25/32"		200		300				[1.40]		
Wallboard, Panel Board Hardboard, 11/32"		930-2,030						[0.95]		
Plasterboard, 27/32"						0.035	0.009	[3.9]		13
Sheetrock, 1/2"						0.31	0.098	[2.0]		13
Transite, 1/4"						0.68	0.007	[2.3]		13
<b>BRICK</b>										
70% of U.S. made Clay, Shale, and Sand-Lime Bricks	2,500 - 15,000	500 - 9,000		450 - 1,500		0.75-1.8 [0.3-0.6]	0.01	110-130		1, 2, 5, 6, 10, 28, 29
25% of U.S. made Clay, Shale, and Sand-Lime Bricks	15,000 - 22,500			1,500 - 3,500		0.75-1.8 [0.3-0.6]	0.01	110-130		
Brick						0.75-1.8	0.01	100-130		
Grade SW	2,500 - 3,000 M									
MW	2,000 - 1,500 M									
NW	1,250 - 2,500 M									
Concrete Building Brick	1,250 - 2,500 M					0.75-1.8	0.01	100-125		
SCR Brick (Manufactured by Structural Clay Product Research Foundation)	11,140			458				106		10
<b>BLOCK CONCRETE</b>										
Load Bearing, Hollow	600 - 1,000 M						0.005	80-90		18
Load Bearing, Solid	1,000 - 1,800 M						0.012	90-120		18
Non-Load Bearing, Hollow	300 - 350 M						0.005	80-90		

TABLE 12.13 (Continued)  
 PHYSICAL PROPERTIES OF VARIOUS BASIC BUILDING CONSTRUCTION MATERIALS

Building Material	Ultimate Strength, psi <sup>①</sup> [Allowable Strength, psi]			Modulus of Rupture psi <sup>②</sup>	Endurance Limit <sup>③</sup>	Young's Modulus [Mod. of Rigidity] <sup>④</sup> x 10 <sup>-6</sup> psi	Poisson's Ratio $\mu$	Loss Factor $\eta$ <sup>⑤</sup>	Density [lb/cu.ft] [lb/sq.ft]	Reference
	Comp.	Tension	Shear							
<b>CONCRETE (28 Day Strength)</b>	Add 20 to 30% for Dynamic Strength.									
Plain Concrete	[750-900]	[80-160]	[80-160]		0.5-0.6	2.0-2.2 [0.07-0.1]	0.07-0.1	0.06-0.12	145-160	1, 7, 5, 16, 27, 43
Am. Concrete Institute (Command Building):						4.0-4.2D <sup>⑥</sup>				14
Type I	2,800 - 3,500	350								
Type II	2,800 - 3,500	325								
Type III	2,200 - 3,000	325								
Type IV	2,000	300								
Type V	3,000	325								
U.S. Military Spec.										24
Class AAA	5,000									
AA	3,750									
A	3,000									
B	2,500									
C	1,500									
Lightweight Aggregate Concretes:					0.5-0.55		0.07-0.1	0.06-0.1		
Expanded Slag	350 - 2,100			120-600		0.8-2.5			90-130	
Haydite	1,500 - 7,000			250-600		1.8-3.0			90-125	
Vermiculite and Perlite	90 - 1,100			20-70		0.8-2.9			35-80	
Precast Concrete										
Floor Slab	1,500 - 7,000	[2-7]							50-120	
Insulating Roof Tile (Reinforced)	400 - 600								35-55	
Roof Slab	1,500 - 2,500	[2-3]							50-70	
Reinforced Concrete (Ordinary 1 to 2% of Tensile Reinforcement)	2,500 - 7,500 [750 - 1,000]	1,500 - 3,000 M [500 - 750]	1,500 - 3,000 M [500 - 750]		0.45-0.55	2.3-3.4	0.07-0.1	0.06 - 0.12	155-170	
	3,000 - 9,000 D <sup>⑥</sup>									
<b>GLASS</b>										2,3,25
Annealed Plate Glass and Window Glass	36,000 [1,000] <sup>⑧</sup>	6,500 [1,000] <sup>⑦</sup>		6,500 <sup>⑦</sup>	0.45-0.50 <sup>⑧</sup>	10 12.5 D [3.6]	0.17 - 0.27	0.002 - 0.03	120-180	
Laminated Glass				3,500					120-180	
Tempered Plate Glass	90,000 - 180,000	20,000 - 30,000		20,000 - 30,000					120-180	
Glass Block Panel (with 100 psi Band Strength)	400 - 600	10.4 <sup>⑨</sup>		10						

TABLE 12.13 (Continued)  
 PHYSICAL PROPERTIES OF VARIOUS BASIC BUILDING CONSTRUCTION MATERIALS

Building Material	Ultimate strength , psi <sup>①</sup> [Allowable Strength, psi]			Modulus of Rupture psi <sup>②</sup>	Endurance Limit <sup>③</sup>	Young's Modulus [Mod. of Rigidity] x 10 <sup>-6</sup> psi <sup>④</sup>	Poisson's Ratio $\mu$	Loss Factor $\eta$ <sup>⑤</sup>	Density lb/cu. ft [lb/sq. ft]	Reference
	Comp.	Tension	Shear							
<b>GYPSUM PRODUCTS</b>										
Lath 3/8" to 1/2"				700-750 <sup>⑩</sup> 280-335 <sup>⑪</sup>		1.0		0.005	60-80	2, 4, 7, 26, 18
Ready Mixed Plaster	400 M							108		
Plaster (Neat, Wood-Fibered, Bond, and Ganging)	1,200 - 2,200	50 - 2,200						60		
Wallboard 1/4" to 3/8"				990 - 1,400 <sup>⑩</sup> 420 - 670 <sup>⑪</sup>			0.035	0.01-0.03	43-62	
1/2" to 5/8"				670 - 770 <sup>⑩</sup> 270 - 350 <sup>⑪</sup>					70-85	
Sheathing Board				770 <sup>⑩</sup> 350 <sup>⑪</sup>						
Formboard, 1/2"				1,120 <sup>⑩</sup> 420 <sup>⑪</sup>						
Gypsum-Concrete Class A	500 M [125]	[100]	[10]			1.2-1.8 0.2 D			55-65	
Class B	1,000 M [220]	[165]	[20]			1.2-1.8 0.6 D				
Gypsum-Cement	5,000 - 9,000	600 - 1,000		900 - 2,400		1.2-1.8			80-115	7
Gypsum Hollow Tile	75 M									
<b>METALS</b> (Commonly Used in Building Structures)										
<b>Aluminum Alloys</b>										
Annealed (1100-0, 2014-0, 3003-0, 3004-0, 5052-0, 5154-0, and 6061-0)	3,500 - 11,000	11,000 - 30,000	8,000 - 19,000		0.6 <sup>⑫</sup>	10 [3.8]	0.33	0.003	165	30, 44, 49
Heat Treated (2014-T3, T4, T6)	32,000 - 58,000	55,000 - 60,000	34,000 - 40,000		0.5 <sup>⑫</sup>	10.6 [4.0]	0.33	0.003	165	
(6061-T4, T6, T62)	14,000 - 26,000	26,000 - 35,000	16,000 - 22,000		0.5 <sup>⑫</sup>	10 [3.8]	0.33	0.003	165	
Brass	25,000 [12,000]	65,000 [12,000]	15,000 [7,000]		0.35 - .5	13.5 [4.8]	0.33		525	32, 49

TABLE 12.13 (Continued)  
PHYSICAL PROPERTIES OF VARIOUS BASIC BUILDING CONSTRUCTION MATERIALS

Building Material	Ultimate strength, psi <sup>①</sup> [Allowable Strength, psi]			Modulus of Rupture psi <sup>②</sup>	Endurance Limit <sup>③</sup>	Young's Modulus [Mod. of Rigidity] <sup>④</sup> x 10 <sup>-6</sup> psi	Poisson's Ratio $\mu$	Loss Factor $\eta$ <sup>⑤</sup>	Density lb/cu. ft [lb/sq. ft]	Reference
	Comp.	Tension	Shear							
<b>METALS (Continued)</b>										
Copper					0.35-0.5	13-17 [6.4]	0.33	0.003	555	32, 49
Annealed	30,000	33,000 36,700 D	23,000							
Cold Rolled	38,000 [19,000]	45,000 - 53,000 60,000 D [19,000]	23,000 - 28,000 [11,000]							
Gray Cast Iron # 20	75,000 [10,000]	20,000 [3,000]	[3,000]		0.35-0.5	12 [5]	0.25		450	50
# 40		40,000				18 [7]				
Structural Steel	30,000 - 41,000 [21,000]	52,000 - 75,000 [21,000 33,000 46,000 <sup>⑬</sup>	37,000 - 52,000 [14,000]		0.65	29 [12]	0.33	0.001 - 0.003	490	31
<b>MORTAR</b>										
General Mix (Cement:Lime:Sand) By Volume 1 : 1 : 6	900 - 2,800 100 - 750 M	165 - 350	45 - 70			0.8-1.3 2.3 <sup>⑨</sup>			45-70	9, 29
1 : 1/2 to 1 : 4-1/2	2,100 - 3,600 1,800 M	270 - 400	55 - 70							
1 : 1/4 : 2-1/4 to 3.0 (Type A-1)	4,800 - 5,500 2,500 M	420 - 460								
1 : 1/4 to 1/2 : 2-1/4 to 3.0 (Type A-2)	2,100 - 2,800 1,800 M	260 - 300								
High Bond Mortar 1:0:2-1/2 to 3.0 (with 15% to 20% Saran Polymer)	5,000 - 10,000	460 - 1,100	140 - 260			1.0 - 1.8				
Stucco 1:1/4:3-1/4	1,500 - 2,800									
<b>STONE, Building</b>										
Granite	7,700 - 60,000	600 - 1,000	2,000 - 4,800	1,400 - 5,200		5.7-8.2			160-190	2, 5
Limestone	2,600 - 28,000	280 - 900	800 - 4,600	500 - 2,000		7.5 - 12.4			150-170	
Marble	8,000 - 50,000	150 - 2,300	1,300 - 6,500	600 - 5,000		7.2 - 14.5			160-180	
Sandstone	5,000 - 20,000	280 - 500	300 - 3,000	700 - 2,300		1.9-7.7			135-160	
Slate		3,000 - 4,300	2,000 - 3,600	6,000 - 15,000		9.8-18			170-180	
<b>SYNTHETIC MATERIAL</b>										
Acrylic (Plexiglass)	18,000	10,500		16,000		0.45		0.002	75	48, 18

TABLE 12.13 (Continued)  
PHYSICAL PROPERTIES OF VARIOUS BASIC BUILDING CONSTRUCTION MATERIALS

Building Material	Ultimate strength, psi <sup>①</sup> [Allowable Strength, psi]			Modulus of Rupture psi <sup>②</sup>	Endurance Limit <sup>③</sup>	Young's Modulus [Mod. of Rigidity] <sup>④</sup> x 10 <sup>-6</sup> psi	Poisson's Ratio $\mu$	Loss Factor $\eta$ <sup>⑤</sup>	Density lb/cu.ft [lb/sq.ft]	Reference
	Comp.	Tension	Shear							
<u>TILE</u> , Clay									45-75	1,7,28
Floor, Tile	850 - 3,000									
Wall Tile, Load Bearing End Construction	1,000 - 5,000									
Side Construction	700 - 2,500 M 700 - 1,300 500 - 700 M									

Building Material	Ultimate Load [Allowable Strength]				Endurance Limit <sup>③</sup>	Young's Modulus [Mod. of Rigidity] <sup>④</sup> x 10 <sup>-6</sup> psi	Poisson's Ratio $\mu$	Loss Factor $\eta$ <sup>⑤</sup>	Density lb/cu.ft [lb/sq.ft]	Reference
	Comp. <sup>⑭</sup>	Trans. <sup>⑮</sup>	Racking <sup>⑯</sup>	Impact <sup>⑰</sup>						
<u>WALL</u>										2,7-10 13,29 33-42
Brick Wall with Ordinary Mortar Mix and Commercial Workmanship: Bearing Wall, Vertical Load	600 - 800 M [150-200]					0.9-3.7	0.1	0.1		
Non-Bearing or Filler Wall	300 - 350 M [100-150]									
6" Brick Wall 1:1:6 Mortar, Medium Strength Brick	500	0.15	40	1.2					[41.4]	10
6" Single Wythe SCR Brick Wall with 1:1:6 Mortar	1,450	2.19	113	1.58					[56]	10
with 1:1/4:3 Mortar		2.28							[58]	10
with 1:1/2:4-1/2 Mortar		4.34							[58]	10
6" Concrete Block Wall with 1:1:6 Mortar	330	0.08	25	1.5						
8" Brick Wall with Ordinary Brick and 1:1:6 Mortar	900 - 1,200	0.16 - 0.18	75	3.0 - 3.7					[79-89]	8,37
8" Tile or Stone Concrete Wall with 1:1:6 Mortar	250 - 500 [100-300]	0.2 - 0.5	25 - 45	1.2 - 1.3					[43-55]	8
8" Brick-Block Wall	350-410	0.25 - 0.34	52	4-4.3					[61]	38

TABLE 12.13 (Continued)  
PHYSICAL PROPERTIES OF VARIOUS BASIC BUILDING CONSTRUCTION MATERIALS

Building Material	Ultimate load [Allowable Strength]				Endurance Limit (3)	Young's Modulus [Mod. of Rigidity] x 10 <sup>-6</sup> psi (4)	Poisson's Ratio μ	Loss Factor η (5)	Density lb/cu. ft. (lb./sq. ft.)	Refer- ence
	Comp. (14)	Trans. (15)	Racking (16)	Impact (17)						
<b>WALL (Continued)</b>										
10" Brick-Brick Cavity Wall	520 [80-110]	0.17	50 [5]	2.8					[67]	36
10" Brick-Tile Cavity Wall	238	0.20	53	3.0					[62]	37
10" Block-Block Cavity Wall	315	0.35	50	3.0					[44]	34
Solid Concrete Unit Masonry, with Ordinary Mortar	[100-140]		[6]				0.1	0.012		2
Hollow Concrete Unit Masonry, with Ordinary Mortar	[70]		[5]				0.1	0.007		2
Reinforced Solid Concrete Unit Masonry	[250-300]		[30-50]			0.3-0.4 0.75-0.9D	0.1	0.012		7, 20
Reinforced Hollowed Concrete Unit Masonry	[225]		[30-50]							7
Wood Frame Wall, or Partition, 8 Ft. High Conventional Construction:										
- Wall Using 2x4 Studs; 16" o.c.; 5/16" Plywood Sheathing; 1/4" Plywood or 1/4" to 1/2" Wall-board Inside Face; with Siding or Shingle; Total Wall Thickness 5-1/4" to 5-7/8"	92-140	1.5-2	20-38	10					[4.5-5.5]	39, 40 41, 44 45
- Wall Using 2x4 Studs; 16" o.c.; 25/32" Sheathing Board, Level Siding or Shingle Outside Face; Lath and Plaster Inside Face; Total Thickness 6" to 7"	90-157	2.1-2.4 0.4-0.6 (18)	19-24	3-4					[9-10.5]	45, 39
- Wall Using 2x4 Studs; 16" o.c.; 25/32" Sheathing Board and Brick Veneer Outside Face; Lath and Plaster Inside Face; Total Thickness 10-1/4"	52.5	2.2 0.83 (18) 0.52 (19)	51	6.5					[50.5]	45
- Wall Using 2x4 Studs; 16" o.c.; 25/32" Sheathing Board; Metal Lath and Stucco Outside Face; Lath and Plaster Inside Face; Total Thickness 6-3/4"	83.5	2-36 0.6 (18)	26	5.7					[20]	45
- Wall, or Partition, Using 2x4 Studs; 16" o.c.; Fiberboard Sheets Both Faces; Total Thickness 4-1/2"	116	2.5	10.5	6.5					[3.6]	47
- Same as above Except Sidewings are Added to the Outside Face; Total Thickness 5-1/2"	68-78	1.7-2.3	11.4-2.1	10					[4.5]	39, 47

TABLE 12.13 (Continued)  
 PHYSICAL PROPERTIES OF VARIOUS BASIC BUILDING CONSTRUCTION MATERIALS

Building Material	Ultimate load [Allowable Strength]				Endurance Limit (3)	Young's Modulus [Mod. of Rigidity] $\times 10^{-6}$ psi (4)	Poisson's Ratio $\mu$	Loss Factor $\eta$ (5)	Density lb/cu.ft [lb/sq.ft]	Refer- ence
	Comp. (14)	Trans. (15)	Racking (16)	Impact (17)						
<b>WALL (Continued)</b>										
- Partition, Using 2x4 Studs; 16" o.c.; Wall Board on Both Faces; Total Thickness 4-5/8"	88	0.95	13	6.8					[5.4]	40
- Wall Using 1x3 Studs; 15" o.c.; 3/8" Outside and 1/4" Inside Plywood Faces; Total Thickness 3-1/8"	280	2.1	5.0	10					[3.0]	41
- Partition, Same Construction as Above Except 1/4" Plywood Faces on Both Faces; Total Thickness 3"	250	1.9	48	7.0					[2.6]	41
<b>Metal Panel Wall:</b>										
- Sheet-Steel Wall, Using 3" Steel Channel Studs; 10" o.c.; Sheet-Steel on Both Faces; 18 gage Steel; Total Thickness 3"	225	1.7	37	7.0					[7.5]	33
- Sheet-Steel Wall, Using 16" Wide Outside Channel Shaped Sheet Steel Panel; 16" Wide Inside Sheet Steel Panel; Wood Strip and Key Construction in Joining Panels; 18 Gage Steel; Total Thickness 3"	230	1.2	21	10					[6.8]	42
- Sheet-Steel Partition, Using 3" Steel Channel Studs; 16" o.c., or Using 16" Inside Channel Shaped Steel Panel; Wallboard on Both Faces.				1.3-1.7					[4.0]	33,42
<b>ROOF</b>										
Steel Roof Deck; 18 to 22 Gage Steel	[18,000]								[1.9-3]	19
Sheet-Steel Roof with Joist, Angle, Zee, Insulation Board, and Built-up Roofing		1.1-1.3							[10.5-12]	33
Wood Frame Roof; 1x4 Joist, 11-1/4" o.c.; Bridging, 25" o.c.; 3/8" Plywood Sheathing; 1/4" Plywood Ceiling		1.0-1.5							[7.2]	41



TABLE 12.13 (Continued)  
 PHYSICAL PROPERTIES OF VARIOUS BASIC BUILDING CONSTRUCTION MATERIALS

Building Material	Density lb ft <sup>3</sup>	Fiber Strength at Proportion Limit, x 10 <sup>-3</sup> psi [Allowable Strength in Bracket]						Ultimate Static Bending x 10 <sup>-3</sup> psi			Max. Compression Crushing Strength x 10 <sup>-3</sup> psi		End- urance Limit	
		Compression		Tension		Bending (Tension Parallel to grain)		Max. Horiz. Shear	Mod. of Rupture Parallel to Grain	Young's Modulus		Par. to Grain		Perp. to Grain
		Par. to Grain	Perp. to Grain	Par. to Grain	Perp. to Grain	Static	Impact			Par. to Grain	Perp. to Grain			
(References: 1, 2, 3, 4, 5, 7, 17, 18, 21, 22, 23, 54)														
<b>WOOD, TIMBER AND PLYWOOD</b> (20)														
Douglas Fir	26-30	4.6 - 6.45 [1.05- 1.70]	0.82 0.95 [0.20- 0.28]	(22)	(23)	6.3- 8.1 [1.6- 2.6]	11.8 12.7	[0.12- 0.15]	6.8- 9.6	1,400- 1,900		6.06- 7.42	1.07- 1.19	0.3
(See Legend (24) for Poisson's Ratio, Elastic Ratio, Rigidity Ratio and Material Loss Factor of Douglas Fir.)														
Balsam Fir and White Fir	22-24	3.87- 3.97 [0.95]	0.38- 0.61 [0.11- 0.22]	(22)	(23)	5.2- 6.3 [1.3- 1.6]	7.8- 11.2	[0.1]	7.6- 9.3	1,230- 1,470		4.53- 5.38	0.71- 0.93	
Hemlock (Eastern and Western)	25-26	4.02- 5.34 [0.95- 1.20]	0.68- 0.8 [0.22]	(22)	(23)	6.1- 6.8 [1.6- 1.9]	10.7- 12.4	[0.10- 0.11]	8.9- 10.1	1,200 1,450		5.41- 6.21	1.06- 1.17	
Pine (Lodgepole, North- ern White, Western White and Ponderosa)	22-25	3.68- 4.48 [0.95- 1.05]	0.54- 0.75 [0.16- 0.19]	(22)	(23)	6.0- 6.7 [1.3- 1.6]	9.5- 11.9	[0.09- 0.12]	9.2- 9.5	1,260- 1,510		4.84- 5.62	0.8- 1.16	
Pine (Southern Yellow and Norwegian)	30-32	4.82- 6.15 [1.05- 1.70]	0.83- 1.19 [0.16- 0.28]	(22)	(23)	7.7- 9.4 [1.6- 2.6]	12.1- 15.9	[0.16- 0.19]	12.5- 14.7	1,760- 1,990		7.08- 8.44	1.23- 1.50	
Spruce (Eastern)	25	4.16 [1.05]	0.59 [0.19]	(22)	(23)	6.5 [1.6]	11.4	[0.12]	10.1	1,440		5.59	1.07	0.3
Plywood (Douglas Fir)	30	[1.8- 2.5]	1.94 [0.35- 0.41]	6.18	3.91	9.34 [2.0- 3.0]		[0.15- 0.17]		1,530	126			
Plywood (White Fir)	25		1.81	5.67	3.70	9.2				1,580	160			
Plywood (White Pine)	26	[1.3- 1.45]	2.05 [0.24- 0.28]	5.72	3.34	10.13 [1.6- 2.0]		[0.1 - 0.14]		1,570	111			
Plywood (Southern Pine)		[2.0- 2.35]	[0.35- 0.41]			[2.75- 3.20]		[0.18- 0.22]		1,800				
Plywood (Hemlock)	29	[1.65- 2.0]	1.96 [0.33- 0.35]	6.8	4.58	9.25 [2.0- 2.4]		[0.13 0.15]		1,580	112			

## LEGEND

- ① Strength in  $\text{lb}/\text{in}^2$ , on gross area if applicable. Values may be given as average values or as ranges. Values followed by letter 'M' indicate minimum strength as approved by American Standards Association. Values followed by letter 'D' indicate dynamic strength. Values in square brackets indicate allowable strength commonly recommended.
- ② Modulus of Rupture is defined as the stress given by the formula  $Mc/I$ , where  $M$  is the maximum bending moment in a beam specimen loaded to rupture,  $c$  is the distance from the neutral axis to extreme fiber, and  $I$  is the area moment of inertia. It is also known as flexural tensile strength.
- ③ Fraction of ultimate tensile strength at  $10^6$  cycles of loading. The S-N curves of some common materials are shown in Figure 12.3.6.
- ④ Both Young's Modulus of elasticity and modulus of rigidity are determined by static tests, except those values followed by a letter 'D', which indicates from dynamic tests. Values of modulus of rigidity are given in square brackets.
- ⑤ This material damping term is defined as  $\eta = 1/Q = 2\xi$  where  $Q$  is the dynamic magnification factor at resonance, and  $\xi$  is the critical damping ratio  $C/C_c$ . Values of  $\eta$  are given for a frequency range of 100 to 1000 cps.
- ⑥ Determined by shock wave propagation method, a very fast rate of loading.
- ⑦ Strength also depends on size of glass plate.
- ⑧ Strength also depends on load duration, rest period, aspect-ratio and nature of loading. See Figures 12.3.1 through 12.3.5 for various service conditions.
- ⑨ Lateral loading for glass block; or perpendicular loading for the case of mortar.
- ⑩ Bending parallel to fiber of surfacing.
- ⑪ Bending across fiber of surfacing.
- ⑫ Based on  $10^8$  cycles of loading.
- ⑬ Yield strength of structural steel.
- ⑭ Vertical compression load on wall sample. Values in psi.
- ⑮ Transverse load,  $\text{lb}/\text{in}^2$  of surface area, based on equivalent uniform lateral loading on outside face.
- ⑯ A measurement of diagonal tension and shear strength,  $\text{lb}/\text{in}^2$ , based on cross-sectional area of wall.
- ⑰ Maximum drop height, in feet, of a 60 lb sandbag that causes specimen failure. Wall span 7-1/2 ft; supported along top and bottom edges of interior face. Drop-load on exterior face.
- ⑱ Plaster cracks on interior side of wall.
- ⑲ Mortar cracks on exterior brick veneer.
- ⑳ Small clear specimen, free of defect, average moisture 12 percent for wood and timber, or 9 percent for plywood. For various service conditions, see Table 12.14
- ㉑ For clear material under long-time service at maximum design load and dry condition use.
- ㉒ Strength much higher than the corresponding compressive strength.
- ㉓ Approximately three times the corresponding values of the compressive strength.
- ㉔ Douglas fir:

<u>Poisson's Ratio</u>	<u>Elasticity Ratio</u>	<u>Rigidity Ratio</u>
$\mu_{LR} = 0.229$	$E_T/E_L = 0.050$	$G_{LR}/E_L = 0.064$
$\mu_{LT} = 0.450$	$E_R/E_L = 0.068$	$G_{LT}/E_L = 0.078$
$\mu_{RT} = 0.390$		$G_{RT}/E_L = 0.007$
$\mu_{RL} = 0.036$		
$\mu_{TL} = 0.029$	<u>Loss Factor</u>	
$\mu_{TR} = 0.374$	$\eta = 0.006 -$	
	$= 0.013$	

where subscripts L, R, and T indicate longitudinal, radial, and tangential respectively.

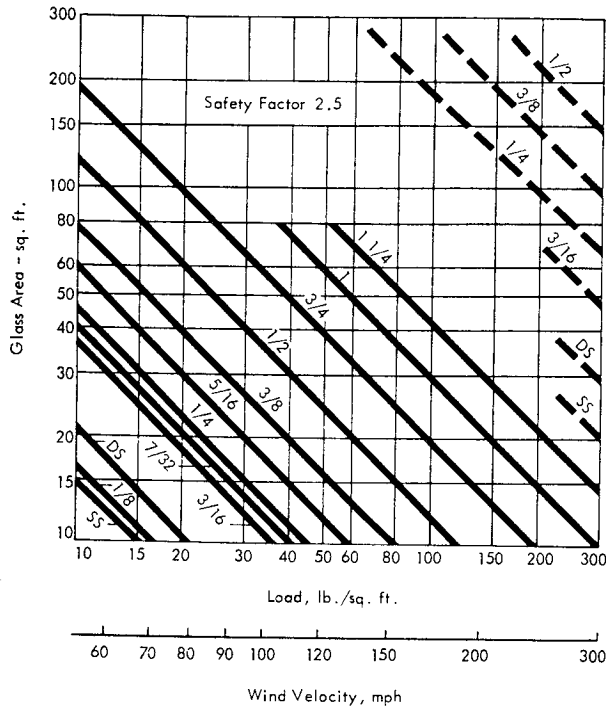


FIGURE 12.1 Allowable Loads for Minimum Thickness of Rectangular Plate and Window Glass, Four Sides Supported, Subjected to Wind Load (Solid Lines) and Sonic Boom (Dashed Lines), or their Equivalents. One Minute Uniform Loading, Representative of "Fastest Mile Wind." Where Short Side/Long Side  $\leq 1/3$ , Adjust Glass Area By Using Figure 12.2.

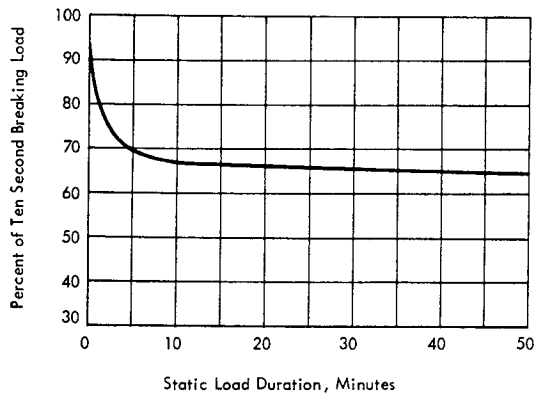


FIGURE 12.3 Strength of Glass as Function of Load Duration

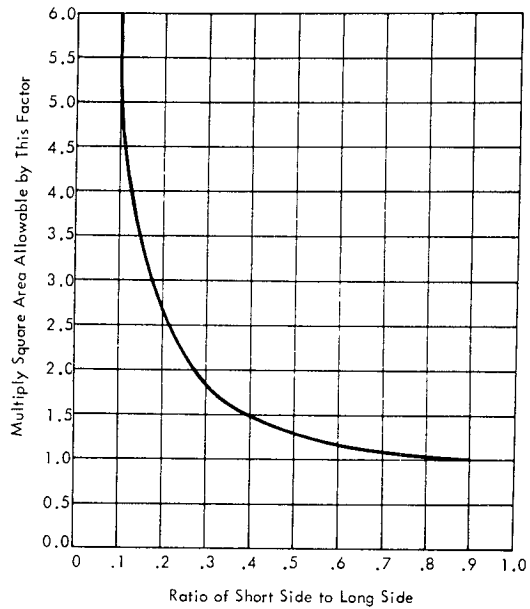


FIGURE 12.2 Aspect-Ratio (Short Side/Long Side) Correction Factors for Rectangular Glass Panels.

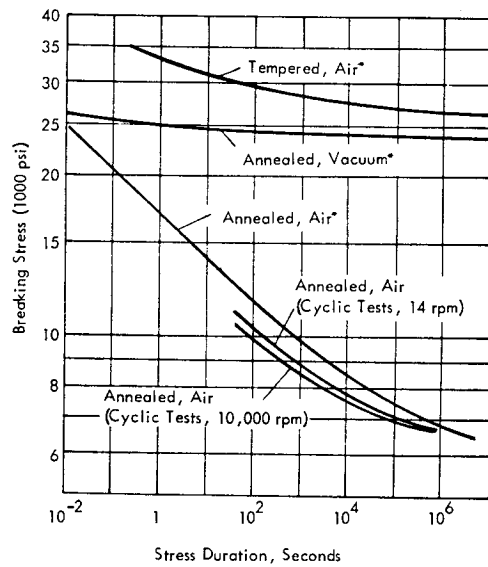


FIGURE 12.4 Stress-Time Characteristics and Dynamic-Fatigue Characteristics of Glass at Room Temperature.

\*Indicates Static Test.

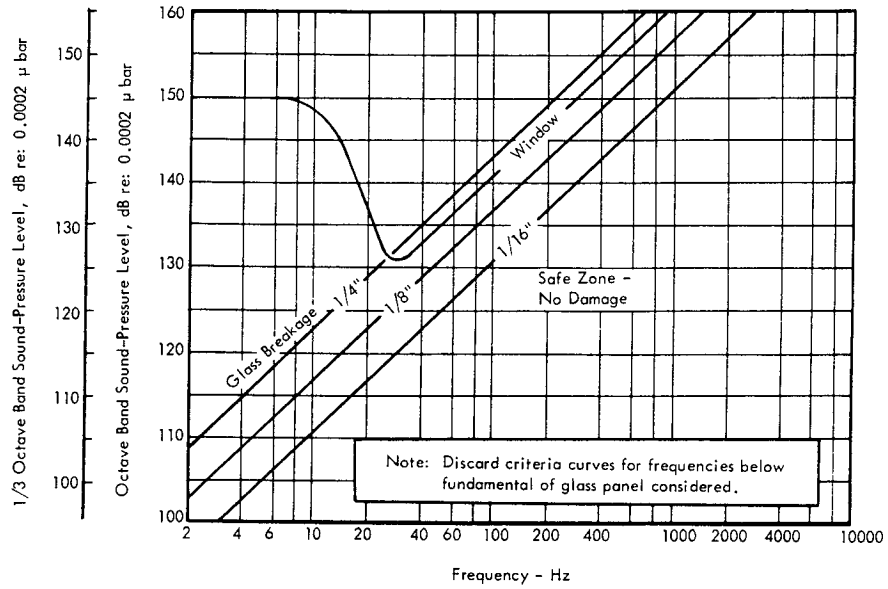


FIGURE 12.5 Tentative Damage Criteria for Glass Panes of Various Thicknesses and Window Exposed to Random Acoustic Noise. Adopted from Regier, et al, "Noise Control," 4, 13-19, 1959.

TABLE 12.14 Strength Variations of Wood and Lumber Under Various Service Conditions.

Strength Variations of Wood and Lumber Under Various Service Conditions, in Percentage Increase (+), or Decrease (-) from Small Clear Test Specimen as Defined in (20)	Density $\frac{\text{lb}}{\text{ft}^3}$	Fiber Strength at Proportion Limit [Allowable Strength in Bracket]				Ultimate Static Bending			Maximum Compression Crushing Strength	
		Compression		Bending		Max. Horiz. Shear	Young's Modulus		Par. to Grain	Perp. to Grain
		Par. to Grain	Perp. to Grain	Static	Impact		Mod. of Rupture Parallel to Grain	Par. to Grain		
Slope of Grain with Respect to Straight Grain Load Application Slope - 1:5				0 -21 -48 -68	0 -10 -38 -64		0 -7 -19 -45	0 -4 -11 -33		
Full Size Common Grade Lumber with Ordinary Defects		0 to -40	0 to -50	0 to -50	0 to -50		0 to -60	0 to -50	0 to -50	0 to -50
Increase of Specimen's Moisture Content by 1%		-5	-5.5	-5	-3		-4	-2	-6	-3
Possible Variation of an Individual Piece from Species Average	+ 8	+ 18	+ 21	+ 16	+ 13		+ 12	+ 16	+ 13	
Temperature Effect, °F (Douglas Fir)	- 20 0 40 70 100 140	[+ 32] [+ 25] [+ 10] [0] [- 11] [- 25]		[+ 25] [+ 15] [+ 8] [0] [- 10] [- 25]			15 to 40 10 to 35 5 to 15 0 -7 to -15 -14 to -38	3 to 18 3 to 15 1 to 10 0 -3 to -8 -8 to -28	20 to 50 10 to 40 5 to 15 0 -5 to -18 -10 to -40	
Effect of Use Under Continuously Wet Condition or when Moisture Exceeds 16%		[0 to -20]	[0 to -20]	[0 to -20]		[0]				
Effect of Load Duration, in Days (Douglas Fir)	10 <sup>-4</sup> 10 <sup>-2</sup> 1 10 <sup>2</sup> 10 <sup>4</sup>						+ 8 - 6 - 18 - 31 - 42			

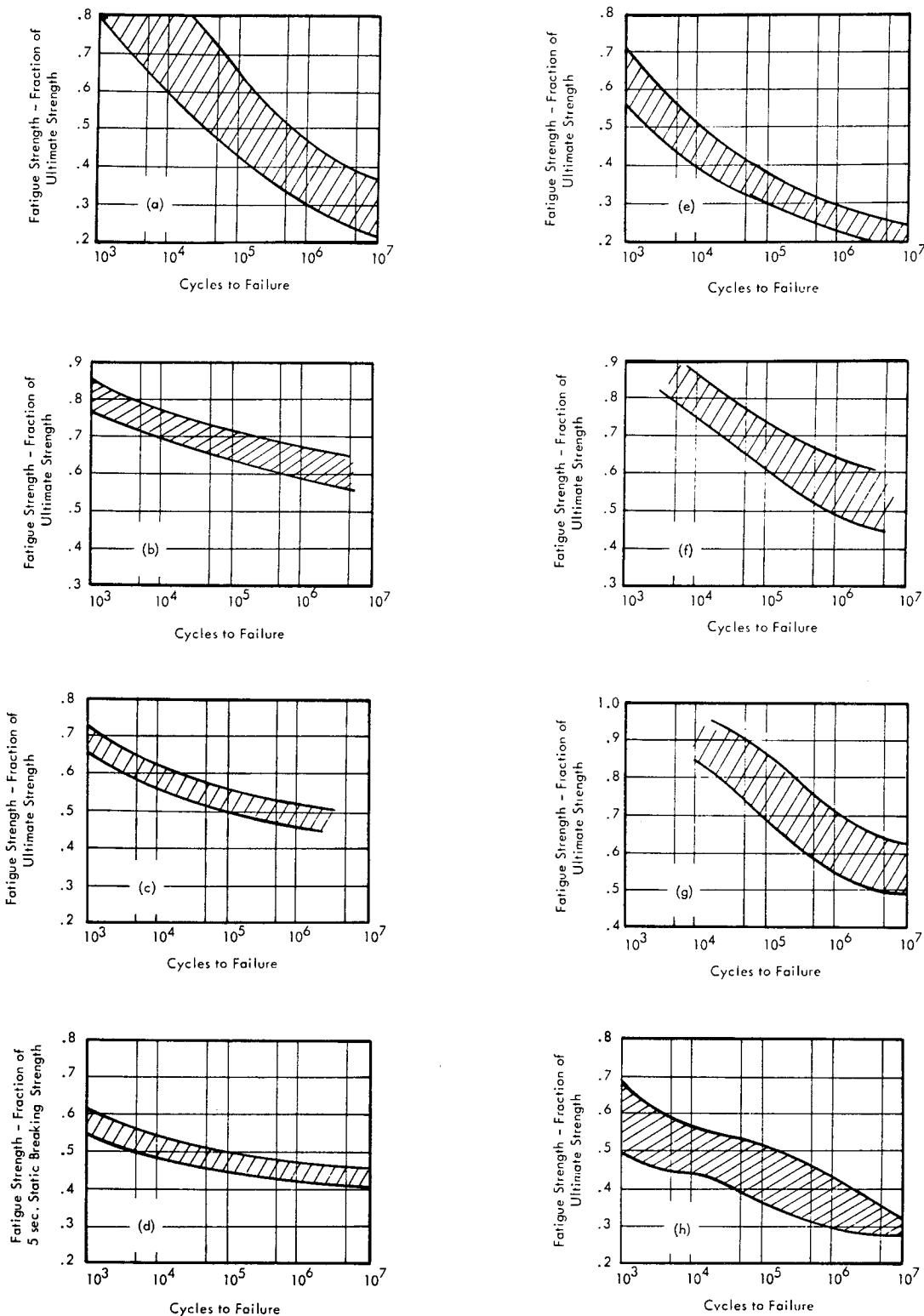


FIGURE 12.6

Composite Stress-Cycle (S-N) Curves For Some Building Construction Materials, Subjected to Complete-Reversal-Repeated Loads Except Indicated. (a) Aluminum Alloys, Ref. 52, (b) Plain Concrete, Ref. 16,27, (c) Reinforced Concrete, Ref. 16,27, (d) Annealed Glass, Ref. 25, (e) Glass-Fiber Reinforced Plastic Laminates, Ref. 25,54, (f) Wrought Steels, Ref. 51,54, (g) High-Strength Low-Alloy Steels, Ref. 53,54, and (h) Natural and Laminated Woods, (Solid Sitka, Spruce and Douglas Fir, and 5-Ply Yellow Birch and Yellow Poplar). (b) and (c) are Subjected to Zero-To-Maximum Repeated Loads.

## 12.4 DATA ON ACOUSTIC ABSORPTION COEFFICIENTS AND SOUND TRANSMISSION LOSS

TABLE 12.15

SOUND ABSORPTION COEFFICIENTS OF GENERAL BUILDING MATERIALS AND FURNISHINGS<sup>†</sup>

MATERIALS	THICK- NESS	COEFFICIENTS					
		125 Hz.	250 Hz.	500 Hz.	1000 Hz.	2000 Hz.	4000 Hz.
<u>ASBESTOS</u>							
Sprayed, Solid Backing	3/4"	.10	.25	.60-.70	.85-.90	.90-.95	.85-.90
Sprayed, on Metal Lath	3/4"	.40-.50	.75-.90	.90-.97	.80-.88	.80-.90	.81-.88
Panel with Glass or Mineral Wool							
Backing, 2" to 3" Pad		.66	.79	.99	.99	.89	.81
Same, 1-1/4" Pad		.07-.46	.32-.70	.73-.89	.66-.99	.63-.75	.33-.58
<u>ASHES</u>							
Damped, Loose (2.5 lb Water per ft. <sup>3</sup> )	11"	.90	.90	.75	.80		
	3"	.25	.55	.65	.80	.80	
<u>BRICK</u>							
Brick, Unglazed		.03	.03	.03	.04	.05	.07
Brick, Unglazed, Painted		.01	.01	.02	.02	.02	.03
<u>CARPET</u>							
Carpet,		.05-.10	.05-.15	.15-.25	.20-.30	.25-.35	.30-.40
Carpet, on Concrete		.02-.11	.06-.14	.14-.24	.25-.40	.25-.50	.30-.60
Carpet, Rubber or Felt Underpad, on Concrete		.10-.20	.20-.27	.35-.65	.34-.70	.48-.80	.60-.75
<u>CONCRETE</u>							
Poured Concrete, Unpainted		.01	.01	.02	.02	.02	.03
Same, Painted		.01	.01	.01	.02	.02	.02
Concrete Block, Coarse		.36	.44	.31	.29	.39	.25
Same, Painted		.10	.05	.06	.07	.09	.08
Porous Concrete Block, with Mortar		.15	.21	.43	.37	.39	.51
<u>CORK</u>							
Cork Board	1"		.08	.30	.31	.28	
<u>DRAPERIES</u>							
Draperies, Hung Straight, in Contact with Wall, 10 to 18 oz/yd <sup>2</sup>		.03-.05	.04-.12	.11-.35	.17-.45	.24-.40	.35-.44
Same, Draped to Half Area, 14 to 18 oz/yd <sup>2</sup>		.07-.14	.31-.35	.49-.55	.72-.75	.70	.60-.65
18 oz/yd <sup>2</sup> Velour, Hung Straight, 4" from Wall		.09	.33	.45	.52	.50	.44

TABLE 12.15 (Continued)

MATERIALS	THICK- NESS	COEFFICIENTS					
		125 Hz.	250 Hz.	500 Hz.	1000 Hz.	2000 Hz.	4000 Hz.
<u>DUCT-LINING MATERIAL</u>							
Duct-Lining Material	1/2"	.05-.10	.30-.45	.30-.50	.50-.75	.75-.85	.80-.85
	1"	.30-.35	.40-.45	.50-.75	.75-.90	.80-.95	.80-.85
<u>FELT</u>							
Felt, All Hair, Contact with Wall	1"	.13	.41	.56	.69	.65	.49
Felt, Scott, Firmness 1 to 3	1"		.24-.32	.36-.52	.54-.87	.74-1.0	.97-1.0
Same, Firmness 4 to 8	1"		.35-.40	.54-.69	.71-.91	.78-1.0	.92-1.0
<u>FIBER GLASS</u>							
Bonded Fiber Glass Board, (PF Board) #4 Mounting*							
2 to 3-1/4 lb/cu .ft.	1/2"	.03	.06	.12-.19	.60-.68	.67	.62-.65
	1"	.08	.23	.42-.53	.77-.80	.73	.71
	2"	.19	.51-.54	.79-.85	.93	.82	.79
	3"	.29	.75-.78	.92-.95	.96	.88	.84
	4"	.38	.90	.97	.98	.92	.88
	5"	.45	.96	.99	.99	.95	.91
4-1/4 to 7-3/4 lb/cu .ft.	1/2"	.04	.08	.20 .31	.71	.69	.68
	1"	.09	.25	.60-.70	.81-.86	.76	.75
	2"	.21	.57	.89-.94	.94	.84-.87	.81
	3"	.31	.81	.97	.97	.91	.86
	4"	.40	.92	.99	.99	.93-.96	.87
	5"	.48	.97	.99	.99	.96	.92
9 to 10-1/2 lb/cu .ft.	1/2"	.05	.10	.36	.73	.71	.71
	1"	.10	.26	.72	.87	.79	.76
	2"	.22	.60	.95	.96	.88	.82
	3"	.32	.83	.99	.98	.93	.86
	4"	.41	.93	.99	.99	.96	.90
	5"	.50	.97	.99	.99	.97	.93
Fiber Glass Ceiling Board, #7 Mounting	3/4"	.67-.69	.76-.77	.81-.92	.81-.88	.82-.88	.60-.88
	1" and 1-1/4"	.65-.85	.74-.78	.85-.91	.93-.95	.96-.97	.93-.97
Fiber Glass Tile, #7 Mounting	3/4"	.57-.72	.64-.84	.66-.85	.65-.88	.66-.92	.50-.90

TABLE 12.15 (Continued)

MATERIALS	THICK- NESS	COEFFICIENTS					
		125 Hz.	250 Hz.	500 Hz.	1000 Hz.	2000 Hz.	4000 Hz.
<u>FIBER GLASS (Continued)</u>							
Unbonded Fiber Glass; rolls or or Batts, #4 Mounting 2 to 3 lb/cu.ft.	1"	.24-.27	.30-.35	.57-.68	.69-.77	.70-.76	.71
	2"	.38-.44	.49-.61	.84-.96	.91-.93	.76-.77	.86
4 to 6 lb/cu.ft.	2.5"-3"	.47-.68	.59-.78	.93-.99	.90-.94	.79-.86	.60-.87
	1"	.33-.35	.44-.51	.76-.89	.88-.93	.77-.87	.73
	2"	.54-.62	.68-.85	.99	.99	.86-.91	
<u>FLOORS</u>							
Slate on Solid Base		.01	.01	.01	.02	.02	.02
Concrete or Terrazzo		.01	.01	.015	.02	.02	.03
Wood on Solid Base		.04	.04	.03	.03	.03	.02
Wood Block, Pitch Pine		.05	.03	.06	.09	.10	.22
Cork, Linoleum, Gypsum, or Rubber Tile on Concrete	3/16"	.02-.04	.03	.03-.04	.03-.04	.03	.02
Cork Flooring Slabs, Glued Down	3/4"	.08	.02	.08	.19	.21	.22
Same, Waxed and Polished	3/4"	.04	.03	.05	.11	.07	.02
<u>FOAM</u>							
Polyurethane Form							
20 ppi* *	1"		.09	.11	.13	.18	.37
45 ppi	1"		.12	.20	.23	.44	.52
60 to 93 ppi	1"		.17	.34-.38	.32-.64	.58-.89	.64-.84
80 ppi	1/4"		.10	.18	.15	.18	.38
	1/2"		.13	.25	.25	.37	.60
	3/4"		.20	.27	.37	.64	.88
	1"		.24	.36	.54	.74	.88
	1-1/4"-2"		.27-.37	.44-.68	.62-.94	.84-1.0	.97-.99
	3"-4"		.61-.77	.96-1.0	1.00	1.00	1.00
	5"-6"		.88-.95	1.00	1.00	1.00	1.00
<u>GLASS</u>							
Large Panes of Heavy Glass		.18	.06	.04	.03	.02	.02
Ordinary Window Glass		.35	.25	.18	.12	.07	.04
Glass Pane	1/8"	.03	.03	.03	.03	.02	.02
	1/4"	.04	.04	.03	.03	.02	.02



TABLE 12.15 (Continued)

MATERIALS	THICK- NESS	COEFFICIENTS					
		125 Hz.	250 Hz.	500 Hz.	1000 Hz.	2000 Hz.	4000 Hz.
<u>GYPSUM</u>							
Board, Nailed to 2 x 4's 16"oc	1/2"	.29	.10	.05	.04	.07	.09
<u>GRAVEL SOIL</u>							
Gravel Soil, Loose and Moist	4"	.25	.60	.65	.70	.75	.80
	12"	.50	.65	.65	.80	.80	.75
<u>MARBLE</u>							
Marble, or Glazed Tile		.01	.01	.01	.01	.02	.02
<u>OPENING</u>							
Window, Open				1.0			
Grills, Ventilating				.15-.50			
Deep Balcony, Upholstered Seats				.50-1.0			
Stage				.25-.75			
<u>PLASTER</u>							
Gypsum or Lime Plaster							
Smooth Finish, on Tile or Brick		.013	.015	.02	.03	.04	.05
Sand Finish, on Metal Lath		.02	.02	.03	.04	.04	.03
Rough Finish, on Lath		.02	.03	.04	.05	.04	.03
Scratch Finish, on Metal Lath		.02	.03	.04-.06	.06-.09	.04-.06	.03-.06
Acoustic Plaster	3/8"		.03	.07	.11	.20	.34
<u>PLYWOOD</u>							
Plywood Paneling	3/8"	.28	.22	.17	.09	.10	.11
	3/4"	.10	.11	.10	.08	.08	.11
<u>SAND</u>							
Sand (Sharp), Dry	4"	.15	.35	.40	.50	.55	.80
	12"	.20	.30	.40	.50	.60	.75
Sand (14 lb water/cu.ft.)	4"	.05	.05	.05	.05	.05	.15

TABLE 12.15 (Continued)

MATERIALS	THICK- NESS	COEFFICIENTS					
		125 Hz.	250 Hz.	500 Hz.	1000 Hz.	2000 Hz.	4000 Hz.
<b>TILES, PANELS AND CEILING BOARDS</b>							
Regular Perforated Cellulose							
Fiber Tiles:							
# 1 Mounting *	1/2"	.03-.05	.16-.20	.56-.58	.82-.95	.87-.93	.71-.74
	3/4"	.04-.09	.26-.29	.77-.81	.88-.99	.81-.85	.51-.64
# 2 Mounting *	1/2"	.12-.13	.57	.54-.56	.74-.85	.84-.95	.71-.79
	3/4"	.08-.23	.55-.67	.64-.68	.87-.99	.86-.87	.55-.71
# 7 Mounting *	1/2" to 3/4"	.25-.41	.38-.47	.54-.67	.83-.99	.82-.92	.54-.75
Randomly Perforated Cellulose							
Fiber Tiles :							
# 1 Mounting	1/2"	.08-.25	.18-.30	.62-.68	.58-.79	.59-.84	.56-.75
	3/4"	.07-.24	.23-.42	.66-.79	.67-.86	.59-.83	.42-.73
# 2 Mounting	1/2"	.08-.17	.50-.67	.46-.61	.52-.70	.57-.85	.55-.81
	3/4"	.22-.33	.61-.71	.51-.64	.63-.84	.59-.87	.47-.78
# 7 Mounting	1/2"	.33-.65	.33-.39	.43-.50	.57-.69	.65-.79	.67-.81
	3/4"	.32-.56	.36-.45	.54-.58	.69-.83	.66-.86	.49-.69
Cellulose Fiber Lay-in Panels,							
# 7 Mounting	1/2"	.23-.41	.28-.50	.41-.61	.54-.92	.49-.82	.30-.61
	3/4"	.38-.50	.32-.33	.43-.48	.54-.62	.56-.69	.57-.78
	1"	.29-.44	.33-.49	.44-.56	.62-.77	.67-.79	.78-.83
Perforated Mineral Fiber Tile :							
# 1 Mounting	1/2"	.03-.14	.11-.26	.20-.64	.65-.99	.64-.95	.58-.77
	5/8"	.03-.20	.15-.35	.56-.79	.71-.99	.74-.95	.41-.78
	3/4"	.03-.20	.19-.38	.70-.85	.95-.99	.72-.87	.51-.75
# 2 Mounting	1/2" to 5/8"	.01-.11	.36-.40	.68-.84	.97-.99	.85-.86	.56-.62
# 7 Mounting	5/8"	.44-.73	.38-.81	.59-.76	.82-.99	.72-.97	.50-.72
	3/4"	.53-.77	.44-.76	.64-.81	.89-.99	.79-.93	.47-.75
Fissured Mineral Fiber Tile :							
# 1 Mounting	1/2"	.03-.14	.16-.23	.65-.71	.82-.93	.77-.80	.51-.74
	3/4"	.03-.14	.19-.41	.67-.96	.84-.99	.74-.92	.61-.90
# 2 Mounting	1/2"	.12-.18	.52-.62	.58-.61	.74-.89	.81	.70-.74
# 7 Mounting	1/2" to 5/8" 3/4"	.44-.79	.34-.86	.50-.72	.71-.93	.81-.86	.59-.92
		.30-.87	.38-.81	.51-.80	.73-.99	.70-.99	.60-.98

TABLE 12.15 (Continued)

MATERIALS	THICK- NESS	COEFFICIENTS					
		125 Hz.	250 Hz.	500 Hz.	1000 Hz.	2000 Hz.	4000 Hz.
<u>TILES, PANELS AND CEILING</u>							
<u>BOARDS (Continued)</u>							
Mineral Fiber Lay-in Panels, #7 Mounting	1/2"	.24-.60	.23-.50	.50-.67	.57-.96	.56-.93	.41-.81
	3/4"	.30-.94	.33-.93	.71-.83	.85-.99	.79-.99	.42-.94
	1"	.39-.84	.45-.86	.79-.84	.93-.99	.62-.97	.44-.76
	2"	.53-.94	.66-.86	.65-.94	.75-.95	.56-.80	.37-.75
	3"	.84-.91	.84-.87	.95-.99	.85-.87	.56-.58	.30-.34
Perforated Metal Pans with Mineral Fiber Pads or Blankets, #7 Mounting	1"	.65-.69	.56-.72	.57-.71	.73-.88	.66-.73	.54-.55
	1-1/4"	.34-.91	.37-.91	.66-.95	.99	.75-.98	.60-.80
Same, Pads Rated as Part of Fire Resistive Assemblies (Mineral Fiber Pad 1-1/4")	1-9/16"	.81-.91	.89-.91	.88-.93	.99	.77-.84	.60-.80
	2-13/16"	.66	.72	.96	.99	.83	.67
Mineral Fiber Tile Rated as Part of Fire Resistive Assemblies, #7 Mounting	1/2" to 5/8"	.26-.83	.26-.73	.39-.72	.50-.99	.49-.98	.36-.91
	3/4"	.45-.85	.44-.75	.55-.77	.80-.99	.67-.97	.44-.99
Mineral Fiber Lay-in Panels Rated as Part of Fire Resistive Assemblies, #7 Mounting	1/2"	.19-.42	.23-.53	.34-.68	.42-.96	.44-.93	.46-.85
	5/8"	.07-.68	.25-.56	.41-.80	.49-.99	.46-.97	.31-.82
	1"	.76	.76	.83	.99	.98	.92
Perforated Asbestos Cement Board Panels with Mineral Fiber Pads, #7 Mounting	13/16" to 15/16" 23/16"	.75-.77	.64-.66	.60-.62	.75-.78	.65-.68	.42-.44
		.18	.55	.98	.98	.58	.44
<u>WALLS AND CEILING</u>							
Concrete, Unpainted		.01	.01	.02	.02	.02	.03
Concrete, Painted		.01	.01	.01	.02	.02	.02
Brick, Plastered		.01	.01	.02	.02	.03	.03
Brick, Unpainted	18"	.02	.02	.03	.04	.05	.07
Brick, Painted	18"	.01	.01	.02	.02	.02	.02
Plasterboard, Plastered		.02	.05	.06	.08	.04	.06

TABLE 12. 15 (Continued)

MATERIALS	THICK- NESS	COEFFICIENTS					
		125 Hz.	250 Hz.	500 Hz.	1000 Hz.	2000 Hz.	4000 Hz.
<u>WALLS AND CEILING (Continued)</u>							
Plywood, 5/8", on Battens (1.6"):							
Non-Perforated Board		.18	.12	.10	.09	.08	.07
Board Perforated with Slits		.04	.05	.14	.32	.20	.24
Board Perforated with Slits and 1" Slagwool Blanket in Air Space		.05	.30	.65	.68	.60	.56
Board Perforated with Slits and a Layer of Plywood Nailed to the Back of Board		.08	.27	.27	.27	.37	.70
Plywood, 3/8", on Battens, 2"		.28	.22	.17	.09	.10	.11
Wood-Wool Slab, 1", on Solid Wall		.18	.11	.19	.39	.95	.56
<u>WATER</u>							
Water Surface, as in a Swimming Pool		.008	.008	.013	.015	.020	.025
<u>WOOD</u>							
Wood, Solid and Polished	2"	.1		.05		.04	.04
Wood, Paneling, 2 to 4 in. Air Space Behind	3/8" to 1/2"	.30	.25	.20	.17	.15	.10
Wood Veneer, on 2"x 3" Wood Studs, 16" o.c.	7/16"	.11		.12		.10	
Wood Sheathing, Pine	3/4"	.10	.11	.10	.08	.08	.11
Wood Platform with Large Space Beneath		.40	.30	.20	.17	.15	.10
<u>ABSORPTION OF SEATS AND AUDIENCE</u>							
(Values given are in Sabins per sq.ft. of Floor Area, or per Unit)							
Adult							
Seated in Upholstered Seats Per sq.ft. of Floor Area		.60	.74	.88	.96	.93	.85
Per Person (Add to Absorption of Chair)		.70	.60	.60	1.0-1.3	1.0-1.6	1.0-2.0

TABLE 12.15 (Continued)

MATERIALS	COEFFICIENTS					
	125 Hz.	250 Hz.	500 Hz.	1000 Hz.	2000 Hz.	4000 Hz.
<u>ABSORPTION OF SEATS AND AUDIENCE (Continued)</u>						
Standing, Per Person	2.0-2.5	3.2-3.5	4.2-4.8	4.5-4.6	5.0	4.0-5.0
Child						
Seated, Per Person	1.8-2.2		2.8-3.8		3.5-4.5	
Seats, Unoccupied						
Chair, Upholstered, per Unit	2.0-3.5	2.5-3.5	3.0-3.5	3.0-3.5	3.0-3.5	2.5-3.5
per sq.ft. of Floor Area	.44-.49	.54-.66	.60-.80	.62-.88	.58-.82	.50-.70
Chair, Wood or Metal per Unit	.10-.15	.15-.19	.20-.22	.35-.39	.38-.50	.30-.60
Pews, Wooden, per sq.ft. of Floor Area	.57	.61	.75	.86	.91	.86

‡ Sources of information are listed in the bibliography. These data sources are mainly from literature published in the United States. Foreign sources, obtained from laboratory tests with different test standards, are excluded.

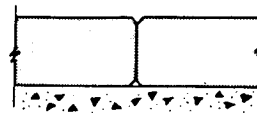
\*\* Pores per linear inch

\* For Nos. 1, 2, 4 and 7 mountings, (laboratory tests) see figures below:



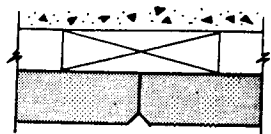
No. 1 MOUNTING

Cemented to plaster board with 1/8" air space. Considered equivalent to cementing to plaster or concrete ceiling.



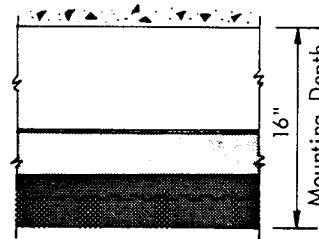
No. 4 MOUNTING

Laid directly on laboratory floor.



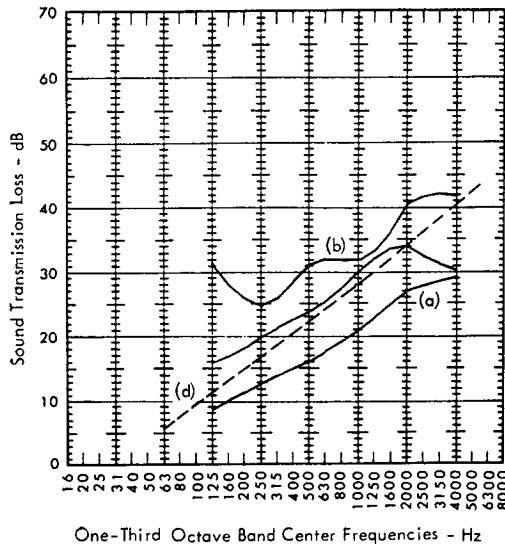
No. 2 MOUNTING

Nailed to nominal 1" x 3" (3/4" x 2 - 5/8" actual) Wood furring 12" o.c.

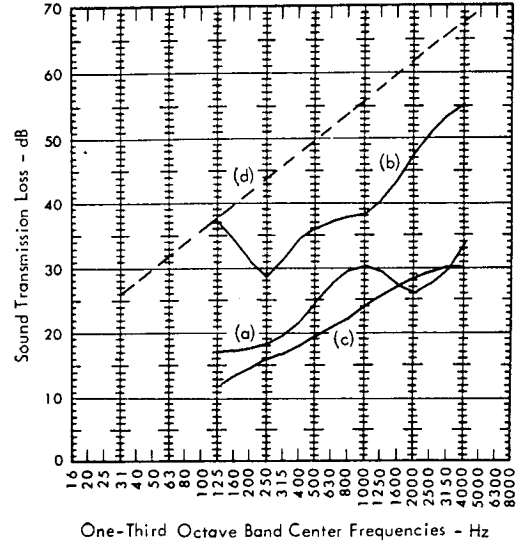


No. 7 MOUNTING

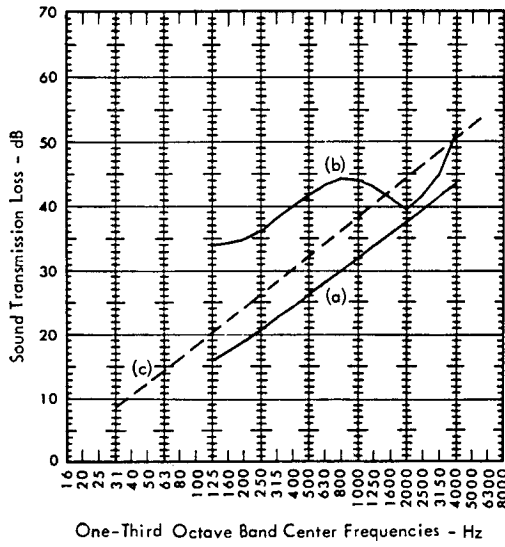
Mechanically mounted on special metal supports.



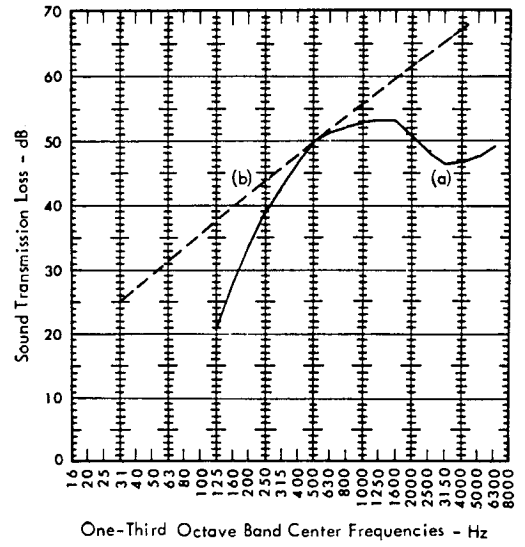
- (a) 1/4 in. Plywood on Wood Framework. Surface Density 0.7 lb/sq.ft. From Reference 60. (STC = 20 dB)
- (b) Wood-Shaving (Portland-Cement Binder) Board Core, 2 in. Thick 3/4 in. Gypsum Plaster on Both Sides. Surface Density 16 lb/sq.ft. From Reference 57. (STC = 33 dB)
- (c) 3/8 in. Plasterboard on Wood Frame. Surface Density 1.9 lb/sq.ft. From Reference 55. (STC = 29 dB)
- (d) 0.7 lb/sq. ft. Mass Line



- (a) 3/4 in. Chipboard on Wood Framework. Surface Density 3.2 lb/sq.ft. From Reference 60. (STC = 26 dB)
- (b) 2 in. Solid Plaster With Expanded Metal-Lath Core. Surface Density 18.4 lb/sq.ft. From Reference 57. (STC = 39 dB)
- (c) 3/8 in. Laminated Building Board on Wood Frame. Surface Density 0.78 lb/sq.ft. From Reference 55. (STC = 27 dB)
- (d) 18.4 lb/sq. ft. Mass Line

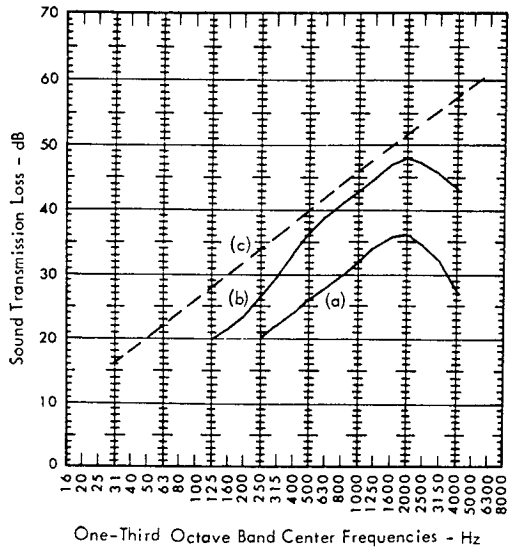


- (a) 16 Gage (1/16 in.) Steel Plate in Steel Frame. Surface Density 2.5 lb/sq.ft. From Reference 55. (STC = 30 dB)
- (b) 3/8 in. Steel Covered on One Side With 1/4 in. Lino on 1/2 in. Cork Bonded to Surface. Surface Density 20 lb/sq.ft. From Reference 60. (STC = 42 dB)
- (c) 2.5 lb/sq.ft. Mass Line

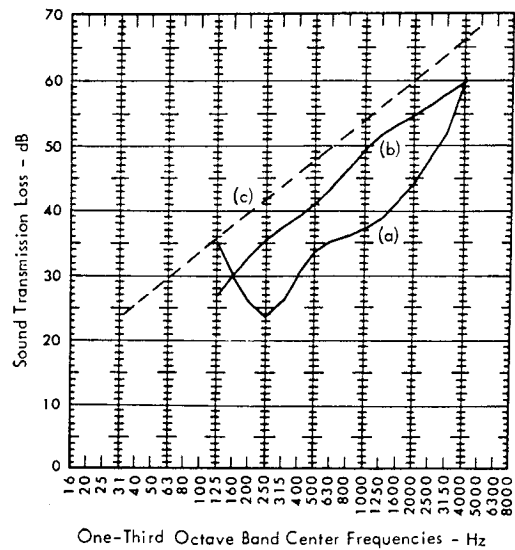


- (a) 2-1/2 in. Sandwich Panel - 0.04 in. Lead, 1.96 in. Resin Bond Wood-Wool, and 0.5 in. Compressed Shavings. Surface Density 6.1 lb/sq.ft. (STC = 46 dB)
- (b) 6.1 lb/sq.ft. Mass Line

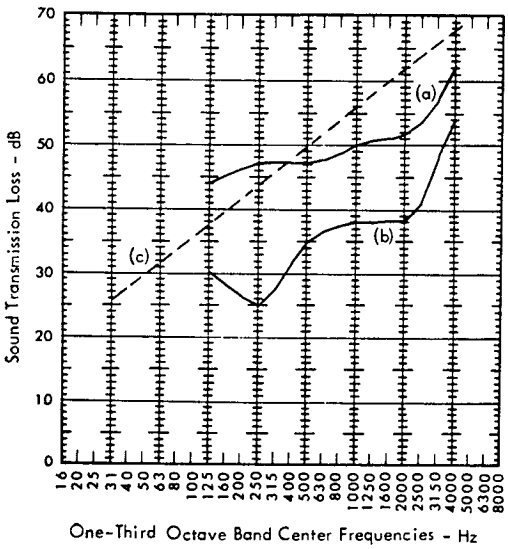
FIGURE 12.7a Sound Transmission Loss Through Single Partitions



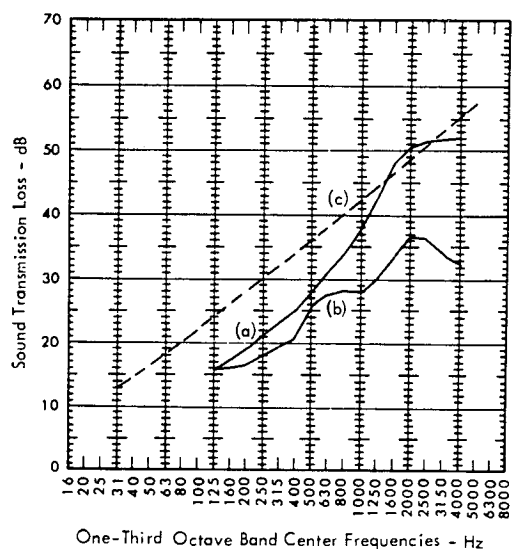
- (a) 1/2 in. Gypsum Board Nailed on One Side of 2 x 4 Wood Studs, 16 in. o.c. Total Thickness 4-1/2 in. Surface Density 5.9 lb/sq.ft. From Reference 57. (STC = 37 dB)
- (b) 1/2 in. Gypsum Wallboard, on Both Sides of 2 x 4 Wood Studs, 16 in. o.c. Total Thickness 4-1/2 in. Surface Density 5.9 lb/sq.ft. From Reference 57. (STC = 37 dB)
- (c) 5.9 lb/sq.ft. Mass Line



- (a) 1/2 in. Gypsum Plaster on Wood Lath; 2 x 4 Wood Studs, 16 in. o.c. Surface Density 17.1 lb/sq.ft. From Reference 55. (STC = 35 dB)
- (b) 1/2 in. Lime Plaster on Wood Lath; 2 x 4 Wood Studs, 16 in. o.c. Surface Density 15.6 lb/sq.ft. From Reference 55. (STC = 44 dB)
- (c) 15.6 lb/sq.ft. Mass Line

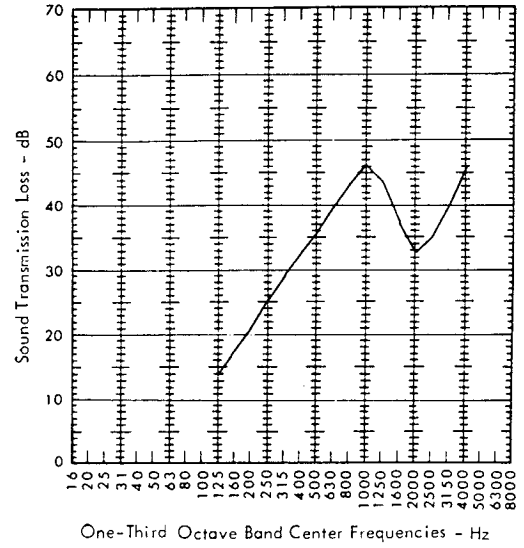
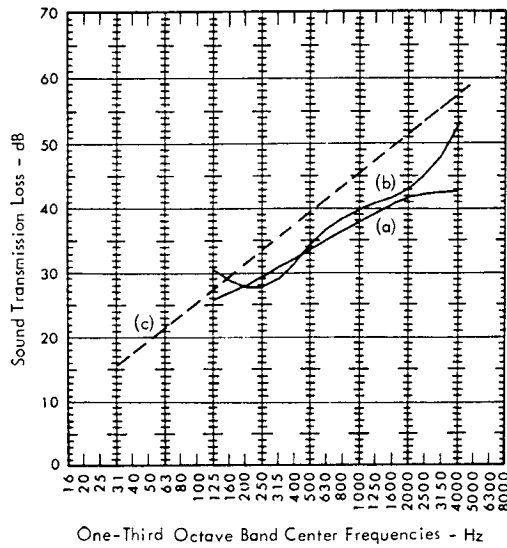


- (a) 7/8 in. Gypsum Plaster on Metal Lath; 2 x 4 Wood Studs, Staggered. Surface Density 19.8 lb/sq.ft. From Reference 55. (STC = 51 dB)
- (b) 3/4 in. Gypsum Plaster on Paper-Backed Wire-Mesh Lath; 2 x 4 Wood Studs, 16 in. o.c. Surface Density 12.6 lb/sq.ft. From Reference 55. (STC = 36 dB)
- (c) 19.8 lb/sq.ft. Mass Line



- (a) Dense Fiberboard on Both Sides of 2 x 4 Wood Studs, 16 in. o.c., Fiberboard Joints at Studs. Total Thickness 4-1/2 in. Surface Density 3.8 lb/sq.ft. (STC = 31 dB)
- (b) 1/4 in. Plywood Glued to Both Sides of 1 x 3 Studs, 16 in. o.c. Total Thickness 3 in. Surface Density 2.5 lb/sq.ft. From Reference 57. (STC = 27 dB)
- (c) 3.8 lb/sq.ft. Mass Line

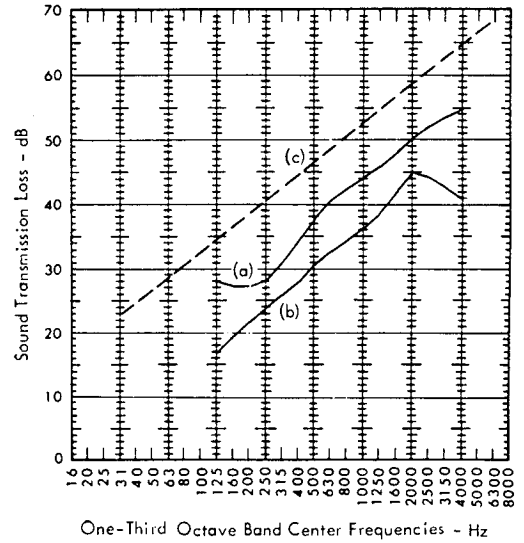
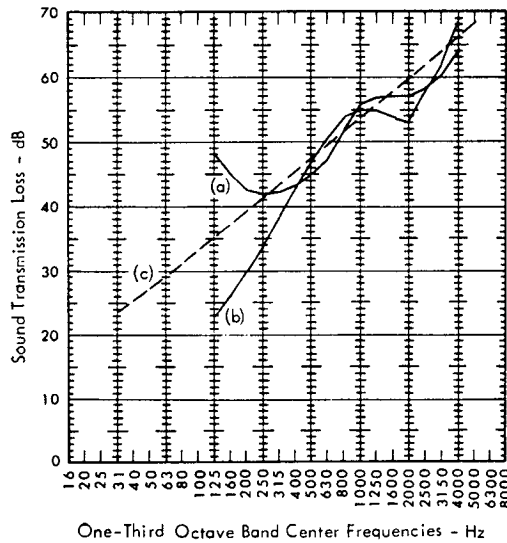
FIGURE 12.7b Sound Transmission Loss Through Wood and Metal Partitions



- (a) 1/16 in. Lead Core Faced Each Side With 3/16 in. Wood Between 2 x 4 Vertical Wood Studs. Surface Density 5.1 lb/sq.ft. From Reference 60. (STC = 38 dB)
- (b) 7/8 in. Gypsum Plaster on Expanded Metal Lath on Both Sides of 3-1/4 in. Metal Studs, 16 in. o.c. Total Thickness 5 in. Surface Density 19.6 lb/sq.ft. From Reference 57. (STC = 37 dB)
- (c) 5.1 lb/sq.ft. Mass Line

Steel Stud Partition - 5/8 in. Gypsumboard on Both Sides of 2-1/2 in. Steel Stud, 24 in. o.c. Joints Taped (STC = 35 dB)

FIGURE 12.7b Sound Transmission Loss Through Wood and Metal Partitions (Continued)

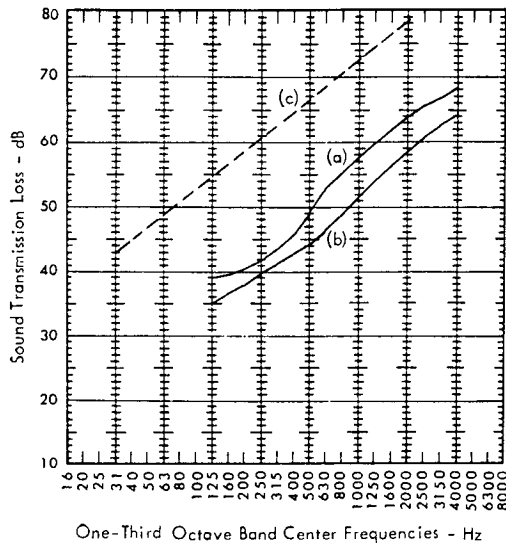


- (a) 4 in. Reinforced Concrete Floor Isolated From Support Structure With Fiverglass. Surface Density 53.2 lb/sq.ft. From Reference 57. (STC = 49 dB)
- (b) 2 x 8 Joists, 16 in. o.c.. Floor: 1 in. Pine Subfloor, 1 in. Pine Finish Floor. Ceiling: 1/2 in. Fiberboard, 1/2 in. Gypsum Plaster. Surface Density 14.3 lb/sq.ft. From Reference 57. (STC = 45 dB)
- (c) 14.3 lb/sq.ft. Mass Line

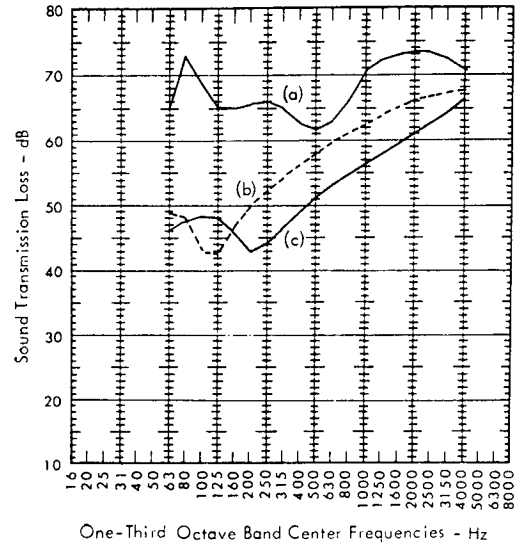
- (a) 9 in. Wood-Joist Floor, Plaster Ceiling, 7/8 in. T and G Wood Floor Boards. Total Thickness 10-1/4 in. Surface Density 12.5 lb/sq.ft. From Reference 59. (STC = 39 dB)
- (b) 8 in. Wood-Joist Floor, 3/8 in. Plaster Board Ceiling, 7/8 in. T and G Wood Floor Boards. Total Thickness 9-1/4 in. Surface Density 7 lb/sq.ft. From Reference 59. (STC = 33 dB)
- (c) 12.5 lb/sq.ft. Mass Line

FIGURE 12.7c Sound Transmission Loss Through Floor and Ceiling

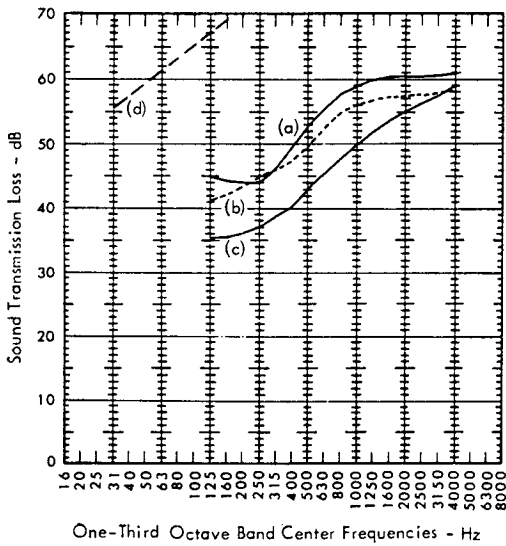




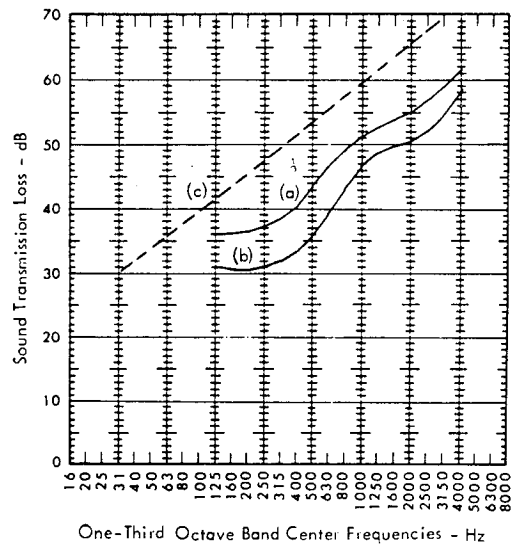
- (a) Solid Concrete 6 in. 1/2 in. Plaster on Both Sides. Surface Density 80 lb/sq.ft. (STC = 52 dB)
- (b) Solid Concrete 3 in. All Surface Cavities Sealed With Mortar Mix. Surface Density 39 lb/sq.ft. (STC = 47 dB)
- (c) 39 lb/sq.ft. Mass Line



- (a) Double Concrete Wall, 12 in. - 4 in. - 12 in. (STC = 67 dB)
- (b) Concrete Wall, 12 in. (STC = 62 dB)
- (c) Concrete Wall, 6 in. (STC = 54 dB)

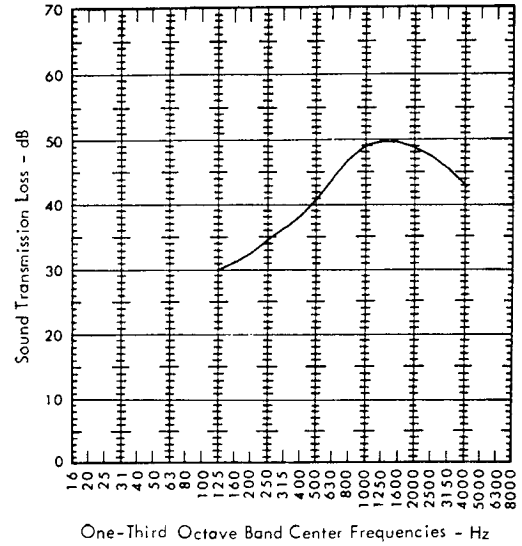
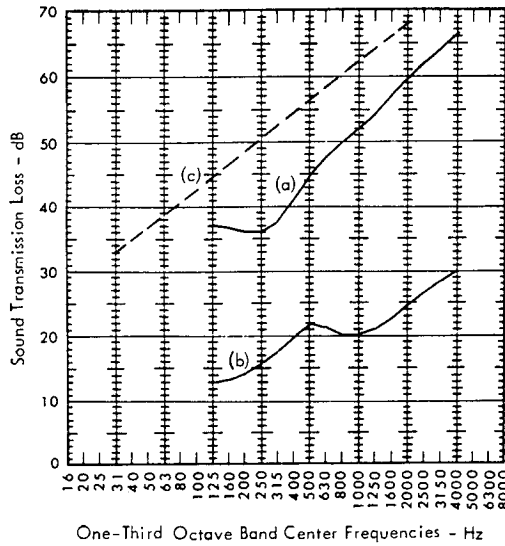


- Solid Brick Walls.**
- (a) 12 in. Thick. Surface Density 121 lb/sq.ft. From Reference 57. (STC = 54 dB)
  - (b) 10 in. Thick. Surface Density 100 lb/sq.ft. From Reference 59. (STC = 53 dB)
  - (c) 4-1/2 in. Brick, 1/2 in. Plaster on Both Sides. Total Thickness 5-1/2 in. Surface Density 55 lb/sq.ft. From Reference 59. (STC = 35 dB)
  - (d) 55 lb/sq.ft. Mass Line



- (a) Cinder Block, Hollow, 4 in. x 8 in. x 16 in., 5/8 in. Gypsum Plaster on Both Sides. Total Thickness 5-1/4 in. Surface Density 35.8 lb/sq.ft. From Reference 57. (STC = 46 dB)
- (b) Clay Tile, Hollow, 4 in. x 12 in. x 12 in., 5/8 in. Gypsum Plaster on Both Sides. Total Thickness 5-1/4 in. Surface Density 27.5 lb/sq.ft. From Reference 57. (STC = 39 dB)
- (c) 27.5 lb/sq.ft. Mass Line

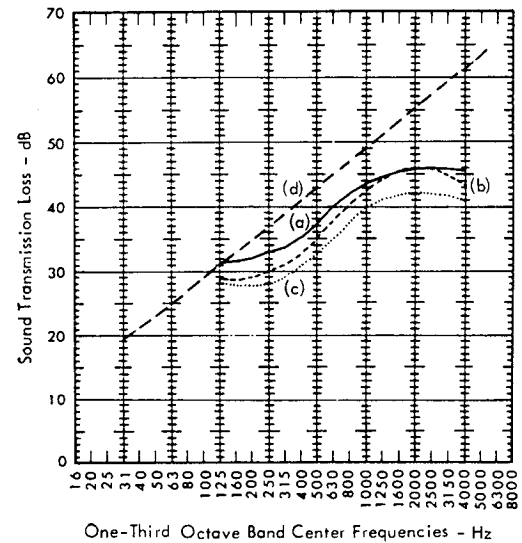
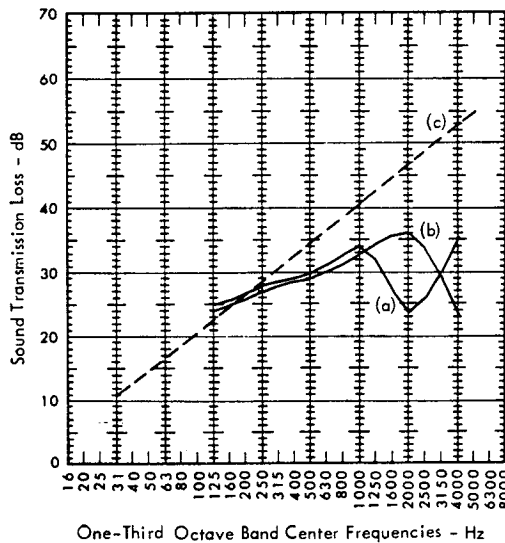
FIGURE 12.7d Sound Transmission Loss Through Bricks, Concrete, Tiles, and Glass Blocks



- (a) 4 in. Reinforced Concrete Slab. From Reference 57. (STC = 46 dB)
- (b) Lightweight Aggregate, Pumice and Portland Cement Tile, Hollow. 12 in. Thick. Surface Density 38.7 lb/sq.ft. From Reference 57. (STC = 22 dB)
- (c) 38.7 lb/sq.ft. Mass Line

3-3/4 in. Glass Brick Partition. 3-3/4 in. x 4-7/8 in. x 8 in. Brick. From Reference 58. (STC = 43 dB)

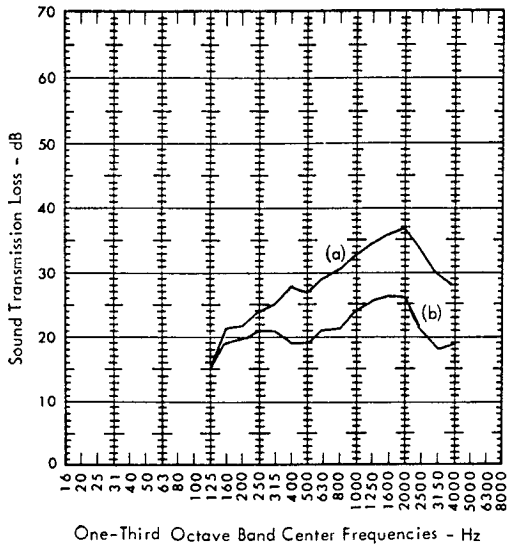
FIGURE 12.7d Sound Transmission Loss Through Bricks, Concrete, Tiles, and Glass Blocks (Continued)



- Plate Glass. From Reference 57.
- (a) 1/4 in. Thick. Surface Density Approximately 3.2 lb/sq.ft. (STC = 30 dB)
  - (b) 1/8 in. Thick. Surface Density Approximately 1.6 lb/sq.ft. (STC = 30 dB)
  - (c) 3.2 lb/sq.ft. Mass Line

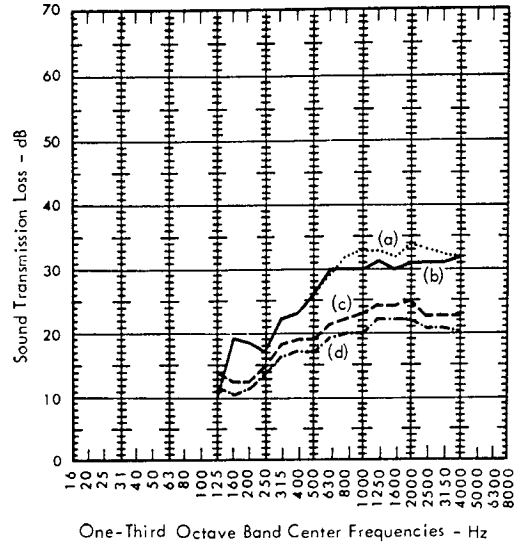
- Laminated Glass. From Reference 57.
- (a) 0.80 in. Thick, 4 Ply. Surface Density Approximately 10 lb/sq.ft. (STC = 41 dB)
  - (b) 0.62 in. Thick, 4 Ply. Surface Density Approximately 8 lb/sq.ft. (STC = 39 dB)
  - (c) 0.45 in. Thick, 3 Ply. Surface Density Approximately 5.5 lb/sq.ft. (STC = 37 dB)
  - (d) 8 lb/sq.ft. Mass Line

FIGURE 12.7e Sound Transmission Loss Through Glass and Windows



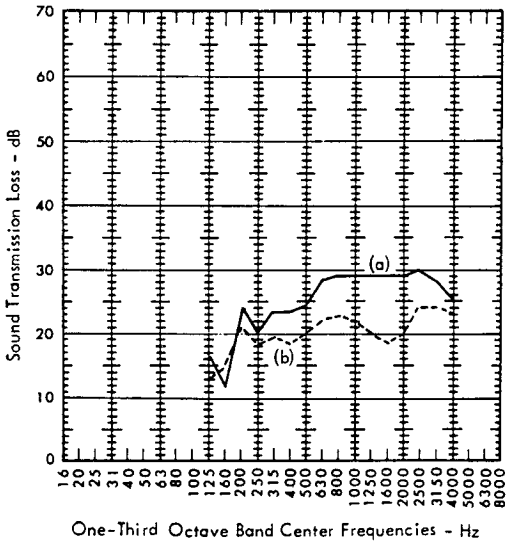
Wood Frame Double Hung Windows

- (a) With Storm Window, Screen. (STC = 32 dB)
- (b) Modern, With 3/8 in. Insulating Glass. (STC = 24 dB)

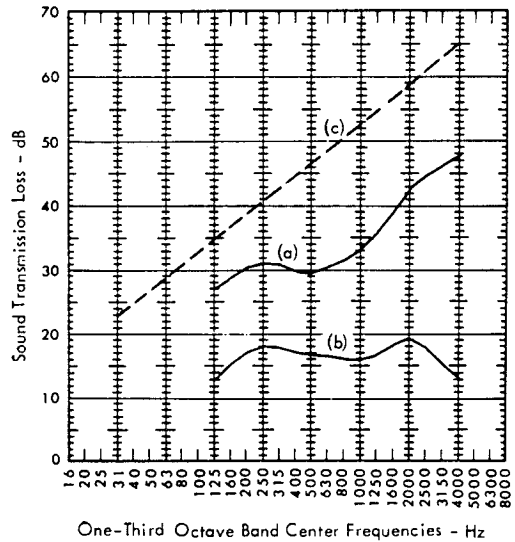


Wood Frame Old Double Hung Window With 3/32 in. Glass.

- (a) With Caulked Storm Window. (STC = 30 dB)
- (b) With Storm Window. (STC = 29 dB)
- (c) Locked. (STC = 23 dB)
- (d) Unlocked. (STC = 21 dB)

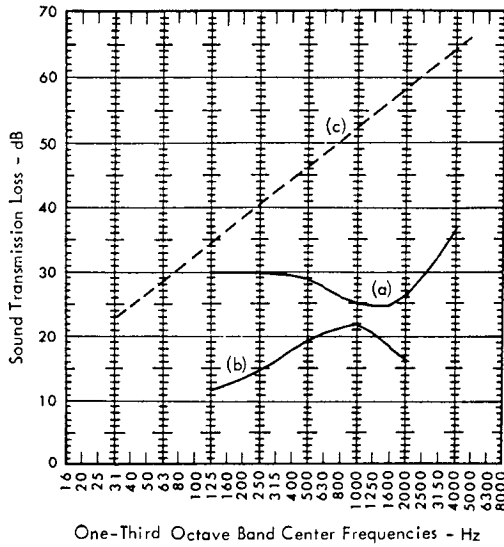


- (a) Steel Frame Casement Window With 3/32 in. Glass Caulked in Place. (STC = 29 dB)
- (b) Steel Frame Casement Window With 3/32 in. Glass Normal Installation (STC = 21 dB)

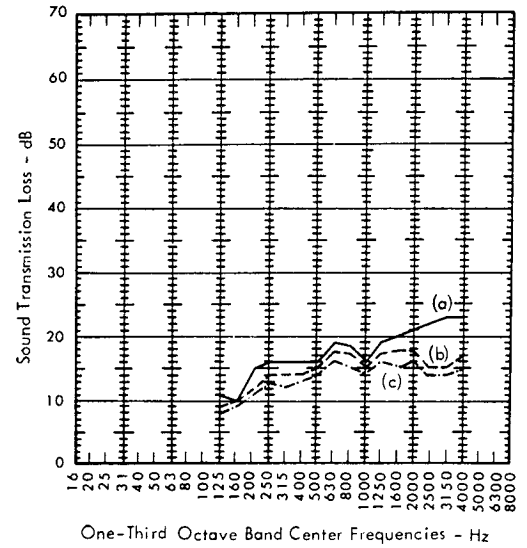


- (a) 1 in. Glass in Wood Frame. Surface Density 13 lb/sq.ft. From Reference 60. (STC = 34 dB)
- (b) Aluminum Frame Jalousie Window, 1/4 in. Window Glass. From Reference 56. (STC = 17 dB)

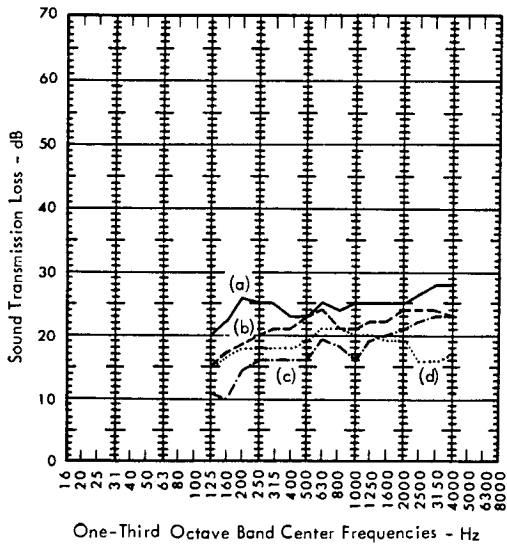
FIGURE 12.7e Sound Transmission Loss Through Glass and Windows (Continued)



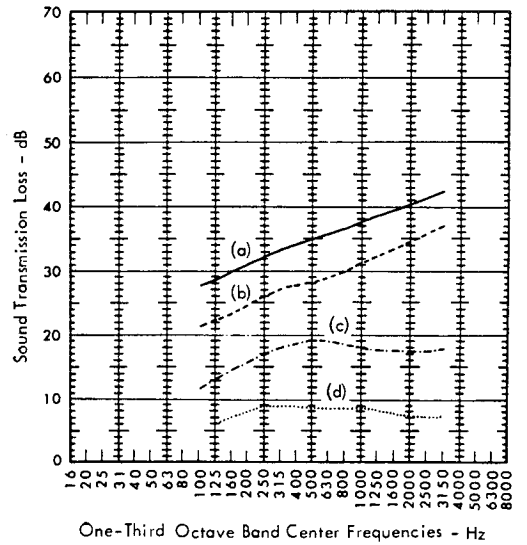
- (a) Wood, Heavy, Approximately 2-1/2 in. Thick, Rubber Gaskets Around Sides and Top; Special Felt Strip Pushed Down as Door Closes, Eliminating Any Crack Under Door. Surface Density 12.5 lb/sq.ft. From Reference 57. (STC = 26 dB)
- (b) 1-3/4 in. Solid Oak Door, With Cracks, as Ordinarily Hung. From Reference 55. (STC = 20 dB)
- (c) 12.5 lb/sq.ft. Mass Line



- 1-3/4 in. Hollow-Core Flush Wood Doors
- (a) Weatherstripped. (STC = 19 dB)
  - (b) 1/16 in. Undercut. (STC = 17 dB)
  - (c) 5/16 in. Undercut. (STC = 16 dB)



- Weatherstripped Wood Doors
- (a) 1-3/4 in. Solid-Core Flush, 95 lbs. (STC = 26 dB)
  - (b) Solid Panel, Wood Frame, 60 lbs. (STC = 23 dB)
  - (c) 1-3/4 in. Hollow-Core Flush, 30 lbs. (STC = 19 dB)
  - (d) Same as (a) except without Weatherstripping, 1/16 in. Undercut (STC = 19 dB)



- From Reference 58.
- (a) Solid Core Door, Gasketed (STC = 39 dB)
  - (b) Hollow Core Door, Gasketed (STC = 33 dB)
  - (c) Ungasketed Door (STC = 18 dB)
  - (d) Door Open (STC = 9 dB)

FIGURE 12.7f Sound Transmission Loss Through Doors

## REFERENCES FOR SECTIONS 12.2 and 12.4

1. Abbett, R.W., "American Civil Engineering Practice," Vol. III, Wiley and Sons, 1957.
2. Merritt, F.S. Ed., "Building Construction Handbook," McGraw-Hill, 1958.
3. Miner, D.F. and Seastone, J.B., Editors, "Handbook of Engineering Materials," Wiley and Sons, 1955.
4. Mills, G. C. and Hayward, H. W., "Materials of Construction," 3rd Edition, Wiley and Sons, 1926.
5. Moor, H. F., "Materials of Engineering," 7th Edition, McGraw-Hill, 1947.
6. Davidson Brick Co., "Steeltyd and Modular Grouted Reinforced Brick Masonry Structural Design Manual," Los Angeles 22, Calif., 1956.
7. International Conference of Building Offices, California, "Uniform Building Code," Vols. I and III, 1964.
8. Whittemore, H.L. Ambrose, H.S. and Parsons, D.E., "Structural Properties of Six Masonry Wall Constructions," Building Materials and Structures Report BMS 5, National Bureau of Standards, 1938.
9. Monk, C. B., Jr., "Testing High Bond Clay Masonry Assemblages," from the Symposium on Masonry Testing Special Technical Publication, Number, 3201, Am. Soc. for Testing and Materials, 1962.
10. Monk, C. B., Jr., "SCR Brick Wall Tests," A Research Report by Structural Clay Products Research Foundation, 1965.
11. Chi, S.H., "Bibliography and Tabulation of Damping Properties of Non-Metallic Materials," University of Minnesota, 1962.
12. Parrott, T.L., "Experimental Studies of Glass Breakage due to Sonic Booms," Sound, Its Uses and Control, Vol. I, Number 3, pp. 18-21, Acoustical Soc. of Am., 1962.
13. Clary, R.R. and Leadbette, S.A., "Experimental Investigation of the Vibratory Responses and Structural Characteristics of Some Simulated Wall Panels," NASA Langley Working Paper 41, 1964.
14. Goldsmith, W., Polivka, M. and Yang, T., "Dynamic Behavior of Concrete," J. of Soc. for Experimental Stress Analysis, Vol. 6, Number 2, 1966.
15. "Significance of Tests and Properties of Concrete and Concrete Aggregates," ASTM Special Technical Publication, Number 169, 1956.
16. Am. Concrete Institute, "Fatigue of Concrete," ACI Bibliography 3, 1960.
17. Brady, G.S., "Material Handbook," 9th Edition, McGraw Hill, 1963.
18. Beranek, L.L., "Noise Reduction," McGraw-Hill, 1960.
19. F.W. Dodge Corp., "Sweet's Catalog Service," New York.
20. Norris, C.H., Hansen, R.J., Holly, M.J., Jr., Biggs, J.M., Namyet, S. and Minami, J.K., "Structural Design for Dynamic Loads," McGraw-Hill, 1959.
21. Dietz, A. G. H., "Materials of Construction, Wood, Plastics, Fabrics," Van Nostrand, 1949.
22. Forest Products Laboratory, "Forest Products Journal," Vol. XI, Number 9, U.S. Government Printing Offices, 1961.
23. Forest Products Laboratory, "Wood Handbook," Agriculture Handbook, Number 72, U.S. Government Printing Offices, 1955.
24. Engineering Manuals for Military Construction.
25. Shand, E. B., "Glass Engineering Handbook," McGraw-Hill, 1958.
26. A.S.T.M., "Cement; Lime; Gypsum," Part 9, ASTM Standards, Am. Soc. for Testing and Materials, 1965.
27. A.S.T.M., "Cement and Concrete," Am. Soc. for Testing and Materials, 1956.
28. A. S. T. M., "Mortars, Clay and Concrete Pipe and Tile; Masonry Units; Asbestos-Cement Products," Part 12, ASTM Standards, Am. Soc. for Testing and Materials, 1965.
29. Plummer, H. C. and Blume, J. A., "Reinforced Brick Masonry Lateral Force Design," Structural Clay Product Institute, Washington D.C., 1953.
30. ALCOA Structural Handbook, Al. Co. of Am.
31. A.I.S.C., "Steel Construction Manual," Am. Inst. of Steel Construction, 6th Edition.
32. Rothbart, H. A., Ed., "Mechanical Design and Systems Handbook," McGraw-Hill, 1964.
33. Whittemore, Stang, and Phelan, Building Materials and Structures Report BMS 9, National Bureau of Standards, 1938.

34. Whittemore, Ambrose, and Parsons, Building Materials and Structures Report BMS 21, National Bureau of Standards, 1939.
35. Whittemore, Stang, and Parsons, Building Materials and Structures Report BMS 22, National Bureau of Standards, 1939.
36. Whittemore, Stang, and Parsons, Building Materials and Structures Report BMS 23, National Bureau of Standards, 1939.
37. Whittemore, Stang, Fishburn, Building Materials and Structures Report BMS 24, National Bureau of Standards, 1939.
38. Whittemore, Stang, and Parsons, Building Materials and Structures Report BMS 32, National Bureau of Standards, 1939.
39. Whittemore, Stang, and Wilson, Building Materials and Structures Report BMS 42, National Bureau of Standards, 1940.
40. Whittemore, Stang, and Wilson, Building Materials and Structures Report BMS 47, National Bureau of Standards, 1940.
41. Whittemore, Stang, and Luxford, Building Materials and Structures Report BMS 104, National Bureau of Standards, 1945.
42. Whittemore, Stang, and Phelan, Building Materials and Structures Report BMS 46, National Bureau of Standards, 1940.
43. Chan, G. C., "Fatigue of Reinforced Concrete Due to Sinusoidal and Random Loadings," Wyle Laboratories Report WR 66-40, Huntsville, Alabama, 1966.
44. Grover, H. J. and Gordon, S. A., "Fatigue of Metals and Structures," U.S. Government Printing Offices, 1960.
45. Whittemore, Stang, and Wilson, Building Materials and Structures Report BMS 31, National Bureau of Standards, 1939.
46. Whittemore, Stang, and Wilson, Building Materials and Structures Report BMS 30, National Bureau of Standards, 1939.
47. Whittemore, Stang, and Wilson, Building Materials and Structures Report BMS 48, National Bureau of Standards, 1940.
48. Machine Design, Vol. 38, Number 14, "Plastics," A Penton Publication, Cleveland, June 16, 1966.
49. Machine Design, Vol. 35, Number 22, "Non-ferrous Metals Book," A Penton Publication, Cleveland, 1963.
50. Machine Design, Vol. 37, Number 21, "Metals," A Penton Publication, Cleveland, 1965.
51. Lipson, C. and Juvinall, R. C., "Application of Stress Analysis to Design and Metallurgy," Handbook of Stress and Strength, MacMillan, 1963.
52. Gover, H. J., Gordon, S. A. and Jackson, L. R., "Fatigue of Metals and Structures," U.S. Government Printing Offices, 1960.
53. Information from McLouth Steel Corp., Detroit, Michigan.
54. Cummings, H. N., "Some Quantitative Aspects of Fatigue of Materials," WADD Technical Report 60-42, 1960.
55. Knudsen, V. O. and Harris, C. M. "Acoustical Designing in Architecture," John Wiley and Sons, New York, September 1965.
56. "Methods for Improving the Noise Insulation of Houses with Respect to Aircraft Noise," Bolt, Beranek and Newman, Inc., Report 1387, for the F.H.A., November 1966.
57. "Sound Insulation of Wall and Floor Constructions," Staff of Sound Section, Nat. Bur. Standards (U.S.) Report No. BMS 144, February, 1955. Supplement: NBS Monograph No. 77, November 1964.
58. "Solutions to Noise Control Problems in the Construction of Houses, Apartments, Motels and Hotels," Owens Corning Fiberglas Corp., AIA File No. 39-E, March 1965.
59. Parkin, P. H. et al., "Field Measurements of Sound Insulation Between Dwellings," Her Majesty's Stationery Office, London, 1960.
60. Bagley, E. N., "The Airborne Sound Insulation of Partitions," National Physical Laboratory, 1966.

## BIBLIOGRAPHY FOR TABLE 12.15

Knudsen, V.O., and Harris, C.M., "Acoustical Designing in Architecture," Wiley and Sons, 1950.

Beranek, L.L., "Noise Reduction," McGraw-Hill, 1960.

Acoustical Materials Association, "Architectural Acoustic Materials," A.I.A. Number 39-B, Bulletin Number XXV, 1965.

Bolt, R.H. and Newman, R.B., "Architectural Acoustics," Architectural Record, April, June, September and November, 1950.

Beranek, L.L., "Music, Acoustics and Architecture," John Wiley and Sons, 1962.

Burris-Meyer, H. and Goodfriend, L., "Acoustics for the Architect," Reinhold, N.Y., 1957.

Olsen, H.F., "Acoustical Engineering," Van Nostrand, 1957.

Celotex Acoustical Products, A.I.A. Number 39-B.

Owens-Corning Fiberglass Co., "Noise Control Products," A.I.A. File Number 37.

United States Gypsum Co., "USG Gypsum Plastics," A.I.A. File Number 21-A, 39-B, 1964.

Data Obtained from Scott Paper Co., Form Division, Chester, Pennsylvania.